

FOURTH INTERNATIONAL CONFERENCE ON SELF-HEALING MATERIALS



CONFERENCE PROCEEDINGS

Proceedings of ICSHM2013
FOURTH INTERNATIONAL CONFERENCE ON SELF-HEALING MATERIALS
Ghent, 16-20 June 2013

Edited by: Nele De Belie
Sybrand van der Zwaag
Elke Gruyaert
Kim Van Tittelboom
Brenda Debbaut

Organizing committee of ICSHM2013
Magnel Laboratory for Concrete Research
Department of Structural Engineering
Ghent University
Technologiepark Zwijnaarde 904
9052 Ghent
Belgium
T: +32 9 264 55 18
F: +32 9 264 58 45

Publisher: Magnel Laboratory for Concrete Research
Technologiepark Zwijnaarde 904
9052 Ghent
Belgium

ISBN: 9789082073713

TABLE OF CONTENTS

Welcome	5
Day 1	
Plenary session – Bio-inspired materials	7
Keynote: P. Fratzl	8
Session 1 – Self-healing cementitious materials	11
Session 2 – Self-healing polymeric materials	29
Session 3 – Bio-inspired materials	47
Session 4 – Self-healing cementitious materials	59
Session 5 – Self-healing polymeric materials	83
Session 6 – Self-healing metallic and ceramic materials	96
Session 7 – Self-healing cementitious materials	109
Session 8 – Modelling and numerical analysis tools	129
Session 9 – Self-healing coatings and paints	151
Poster session	
Advanced characterization methods for self-healing	163
Bio-inspired materials	176
Self-healing bituminous materials	186
Self-healing cementitious materials	191
Self-healing fiber-reinforced composite materials	259
Self-healing metallic and ceramic materials	269
Self-healing coatings and paints	291
Self-healing thermoplastic/thermoset polymeric materials	332
Self-healing supramolecular materials	373
Microvascular systems	387
Regional / national / international projects on self-healing materials	392
Day 2	
Session 10 – Self-healing cementitious materials	405
Keynote: K. Van Tittelboom	406
Session 11 – Self-healing supramolecular polymers	431
Keynote: F. Tournilhac	432
Session 12 – Self-healing materials for functional applications	449
Keynote: G. J. M. Koper	450
Session 13 – Self-healing polymeric materials	471
Session 14 – Self-healing bituminous materials	483

Session 15 – Self-healing fiber-reinforced composite materials	502
Session 16 – Self-healing coatings and paints	518
Session 17 – Self-healing metallic and ceramic materials	543
Session 18 – Microvascular systems	564
Session 19 – Self-healing metallic and ceramic materials	572
Day 3	
Plenary session – Self-healing polymeric materials	585
Keynote: J. S. Moore	586
Session 20 – Self-healing cementitious materials	587
Session 21 – Self-healing polymeric materials	615
Session 22 – Self-healing coatings and paints	624
Plenary session – Modelling and numerical analysis tools	637
Keynote: A. C. Balazs	638
Session 23 – Self-healing cementitious materials	647
Session 24 – Modelling and numerical analysis tools	664
Session 25 – Self-healing supramolecular polymers	678
Session 26 – Self-healing fiber-reinforced composite materials	692
Session 27 – Self-healing polymeric materials	712
Session 28 – Advanced characterization methods for self-healing	721

WELCOME TO ICSHM2013 !

Materials play an extremely important role in our lives. These materials may be of a very different nature ranging from metals over concrete to polymers and composite materials. They all have in common to carry loads, to cope with forces and especially to be durable, because maintenance, repair or replacement may be difficult, costly or in some cases nearly impossible. With a continuous drive for better materials with lower weights that are costing less, materials may be positioned at the edge of their performance. On the contrary when safety and reliability are extremely important factors, materials usually are over-dimensioned for the added safety.

All strategies developed over the past 20 centuries to improve the strength and reliability of materials, are ultimately based on the paradigm of “damage prevention”, i.e. the materials are designed in such a way that the damage as a function of load and/or time is postponed as much as possible. The level of damage will here never go down spontaneously. In recent years, however, it has been realized that an alternative strategy can be followed to make materials effectively stronger and more reliable, and that is by “damage management”, i.e. these materials have a built-in capacity to repair the damage incurred during use. When cracks form, the material itself is capable of “self-healing” the crack and restoring the functionality of the material.

This approach, inspired by nature, captures the imagination of scientists and laymen alike. Biological systems such as bones, skin or plants have the capacity to detect damage very quickly and have moreover the unique feature to repair the damage efficiently. We would like to translate this concept to our engineering materials.

With the series of International Conferences of Self-Healing Materials, we want to offer participants a full overview of the developments in this exciting and rapidly evolving field. The mission of ICSHM is to attract a diverse and multidisciplinary group of scientists and engineers coming from academia, industry and government agencies, managers, and policy makers, from all over the world.

After successful ICSHM events organised in Noordwijk (The Netherlands, 2007), Chicago (USA, 2009) and Bath (UK, 2011), we are proud to host the Fourth International Conference on Self-Healing Materials in Ghent. We hope that you will enjoy this opportunity to share your latest experiences, to discover new avenues for exploration, to meet colleagues, and of course to savour the beautiful historic city of Ghent.



Professor
Nele De Belie

Ghent University
Belgium



Professor
Sybrand van der Zwaag

Delft University of Technology
the Netherlands

PLENARY SESSION – BIO-INSPIRED MATERIALS

BIO-INSPIRATION FROM NATURALLY HEALING TISSUES

P. Fratzl¹, W. Wagermaier¹, R. Weinkamer¹, J.W.C. Dunlop¹ and M.J. Harrington¹

¹ Max Planck Institute of Colloids & Interfaces, Department of Biomaterials, 14424 Potsdam, Germany – e-mail: matt.harrington@mpikg.mpg.de; wolfgang.wagermaier@mpikg.mpg.de; richard.weinkamer@mpikg.mpg.de; john.dunlop@mpikg.mpg.de; peter.fratzl@mpikg.mpg.de

ABSTRACT

In the course of evolution, load-bearing biological materials have generally not evolved towards perfection and maximum strength, but instead developed high defect tolerance and adaptability [1]. Adaption occurs at various levels, see figure 1. While evolution leads to adaptation of entire species, each individual has mechanisms which confer some self-repair properties even at smaller scales to cope with a variety of environmental challenges. Healing and regeneration occur at the level of organs, but many biological materials are damage-tolerant at the supra-molecular level or have (passive) self-repair properties.

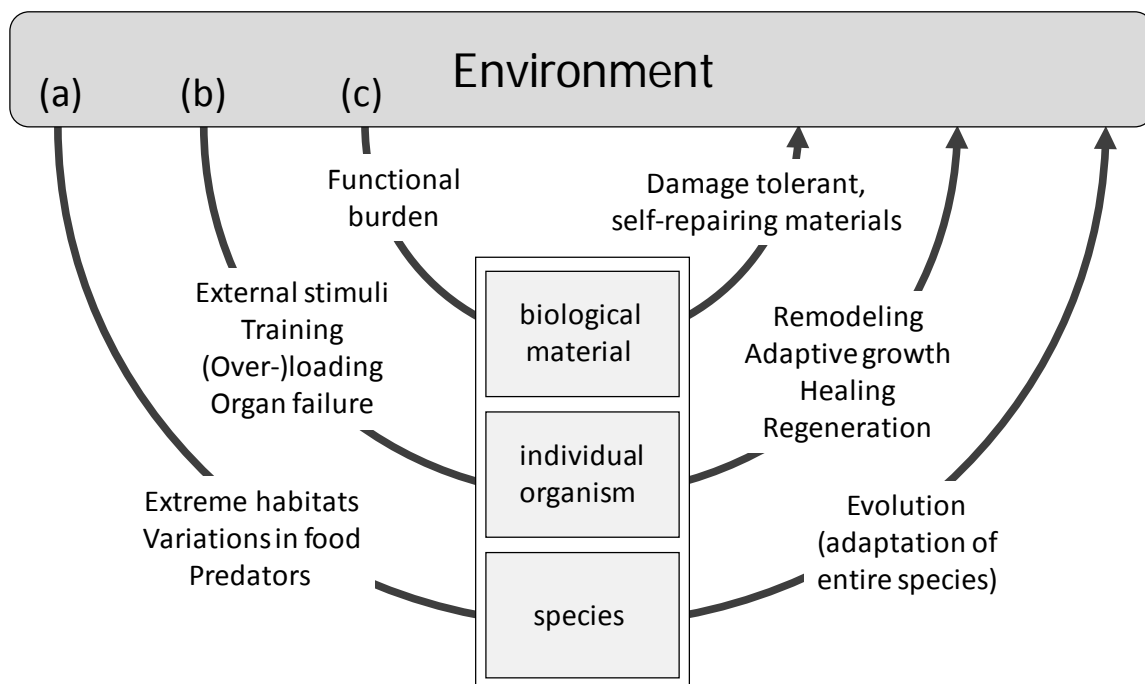


Figure 1: Three levels of natural adaptation to environmental influences [1]. (a) Darwinian evolution acts on the species level to adapt to long-term challenges, such as habitat, food type or predators. (b) Remodeling, healing or regeneration operate at the organ level within an individual organism. (c) Biological materials, such as bone, extracellular tissue or protein fibers are damage tolerant and often have self-repair mechanisms that operate on the supra-molecular level.

The lecture discusses some aspects of self-repairing natural tissues on the levels (b) and (c), as outlined in figure 1. Repeated loading, such as side-winds in trees leads to adaptive growth of the plant to better withstand these loads. Similarly, training in

humans not only leads to an increase in muscle mass but also of bone mass and architecture through a remodeling process. The interesting difference between adaptive growth in woody plants and bone remodeling lies in the fact that bone can not only be synthesized but also be resorbed by cells, while wood growth is only additive. This results in different adaptation strategies [2].

Bone remodeling is also a process by which damaged tissue is continuously replaced by newly synthesized material and, thus, an interesting case to inspire self-repairing artificial materials. Bone remodeling generally depends on a dense network of mechanosensitive cells, called osteocytes. This network is such that all mineralized tissue in bone is not further away from the next osteocyte canaliculum than about one micron, making the network an extremely effective transport system [3]. While bone continuously repairs damage through remodeling, it needs a more complicated process to heal after a fracture occurred. The healing process is a matter of intensive research and we will report new data showing that both natural [4] and scaffold-supported [5] healing requires a mechanical interaction between the growing tissue and its surrounding, which can be rationalized by *in-vitro* experiments [6]. This is also true for the rapid re-growth of the deer antler, which is another interesting case study for natural material regeneration [7].

While bone remodeling and healing are processes operating at the organ level (similarly to many kinds of wound healing in animals or plants), there are also intrinsic material properties which provide damage tolerance and self-repair. Examples are deformable interfaces connecting stiff protein or polysaccharide fibers or mineral platelets and capable of absorbing large deformations in tissues, such as tendons or plant cell walls [8]. In some cases, damage is fully recovered over a short [9] or a longer [10] period of time, thus providing some type of self-repair. In this context, we will briefly mention pseudo-elastic properties of whelk egg capsules [9] and a self-healing protein system in the mussel byssus [10].

Nature has evolved a wide range of mechanisms to cope with damage and imperfection in general. They exist as passive mechanisms within the material itself or they are controlled (at a much larger scale) by cells which add and/or remove material as needed. We are only beginning to unravel some of those principles. This lecture can only cover a very small selection of examples, based primarily on the authors' own research interests.

REFERENCES

- [1] R. Weinkamer, J.W.C. Dunlop, Y. Bréchet, P. Fratzl, All but diamonds: Biological materials are not forever, *Acta Materialia* 61 (2013) 880-889.
- [2] R. Weinkamer, P. Fratzl, Mechanical adaptation of biological materials – The examples of bone and wood, *Materials Science and Engineering C* 31 (2011) 1164-1173.
- [3] M. Kerschnitzki, P. Kollmannsberger, M. Burghammer, G.N. Duda, R. Weinkamer, W. Wagermaier, P. Fratzl, Architecture of the osteocyte network correlates with bone material quality, *Journal of Bone and Mineral Research* (2013) [Epub ahead of print] doi: 10.1002/jbmr.1927.

- [4] M. Kerschnitzki, W. Wagermaier, Y. Liu, P. Roschger, G.N. Duda, P. Fratzl, Poorly Ordered Bone as an Endogenous Scaffold for the Deposition of Highly Oriented Lamellar Tissue in Rapidly Growing Ovine Bone, *Cells Tissues Organs* 194 (2011) 119-123.
- [5] W.A. Woodruff, C. Lange, F. Chen, P. Fratzl, D.W. Hutmacher, Nano- to macroscale remodeling of functional tissue-engineered bone, *Advanced Healthcare Materials* 2 (2013) 546-551.
- [6] C.M. Bidan, K.P. Kommareddy, M. Rumpler, P. Kollmannsberger, P. Fratzl, J.W.C. Dunlop, Geometry as a factor for tissue growth: towards shape optimization of tissue engineering scaffolds, *Advanced Healthcare Materials* 2 (2013) 186-194.
- [7] S. Krauss, W. Wagermaier, J.A. Estevez, J.D. Currey, P. Fratzl, Tubular frameworks guiding orderly bone formation in the antler of the red deer (*Cervus elaphus*), *Journal of Structural Biology* 175 (2011) 457-464.
- [8] J.W.C. Dunlop, R. Weinkamer, P. Fratzl, Artful interfaces within biological materials, *Materials Today* 3 (2011) 70-78.
- [9] M.J. Harrington, S.S. Wasko, A. Masic, F.D. Fischer, H.S. Gupta, P. Fratzl, Pseudoelastic behaviour of a natural material is achieved via reversible changes in protein backbone conformation, *Journal of the Royal Society Interface* 9 (2012) 2911-2922.
- [10] M.J. Harrington, H.S. Gupta, P. Fratzl, J.H. Waite, Collagen insulated from tensile damage by domains that unfold reversibly: In situ X-ray investigation of mechanical yield and damage repair in the mussel byssus, *Journal of Structural Biology* 167 (2009) 47-54.

SESSION 1 – SELF-HEALING CEMENTITIOUS MATERIALS

DESIGN OF MICROCAPSULE SYSTEM USED FOR SELF-HEALING CEMENTITIOUS MATERIAL

M. Zhang ¹, N. Han ¹, F. Xing ¹, X. Wang ¹ and E. Schlangen ²

¹ Guangdong Provincial Key Laboratory of Durability for Marine Civil Engineering; Shenzhen Durability Centre for Civil Engineering; College of Civil Engineering, Shenzhen University, Shenzhen, P.R. China – e-mail: xingf@szu.edu.cn

² Faculty of Civil Engineering and GeoSciences, Delft University of Technology, Delft, The Netherlands

Keywords: self-healing, microcapsule, in situ polymerization, activation energy, reaction order, curing kinetics

ABSTRACT

For a microcapsule based self-healing system in the cementitious material, a fundamental issue is to find and facilitate a suitable microcapsule system, concerning either the material selection or design and manufacture process. In this study, urea formaldehyde resin is used for the shell of microcapsule, and bisphenol – an epoxy resin E-51 diluted by n-butyl glycidyl ether (BGE) is adopted as the heal-agent inside the microcapsule. The production process mainly includes pre-polymerization preparation, emulsification, acidification and curing stage. The fundamental reaction mechanisms with respect to the synthesis process and the properties of the obtained microcapsule are discussed in this paper. Meanwhile, the healing mechanism by means of catalyst MC120D is further explored. Results show that the microcapsule obtained with the adopted production process can be used for the self-healing system in the cementitious materials.

1. INTRODUCTION

Using organic microcapsules in making cementitious composites with a self-healing function is a novel technology. Considering the self-healing mechanism, microcapsules should not only store healing agent during period of storage, but also provide driving force during self-healing process when trigger is excited (e.g. the cement matrix cracks and the microcapsules broke). In addition, microcapsules should owe enough external sensibility; the healing agent should have high fluidity with low viscosity; the reaction energy of curing reaction of healing agent system should reach its minimum value. Thus as the trigger is turned on, the healing agent flows out from microcapsule and is cured quickly. In this study, an optimized proportion of healing agent with minimum activation energy is investigated with the help of differential thermal analysis and infrared analysis.

2. MATERIALS

Experimental materials in this study include: the healing agent - epoxy resin E-51 and diluent BGE; the catalyst MC120D.

3. METHODS

The thermal gravimetric analyzer (STA 409 PC) was adopted in order to carry out differential thermal analysis. The rate of temperature-rising was taken as 5 K/min, 10K/min, 15 K/min, 20 K/min, respectively. Spectrum BX II was used for Fourier transform infrared spectroscopy (FTIR) analysis.

4. RESULTS

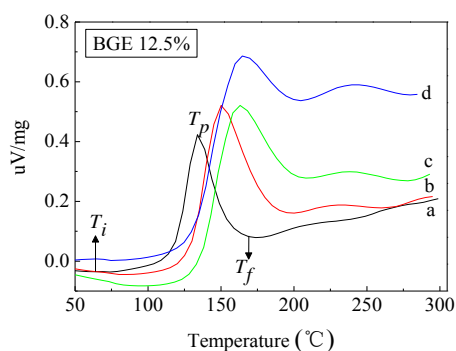
According to Kissinger equation [1] (eq. (1)) and Crane equation [2] (eq. (2)), the relation among the temperature-rising rate, the exothermic peak temperature with the activation energy and the reaction order are:

$$\frac{d(\ln(\beta/T_p^2))}{d(1/T)} = -\frac{E}{R} \quad (1)$$

$$\frac{d(\ln \beta)}{d(1/T_p)} \approx -\frac{E}{nR} \quad (2)$$

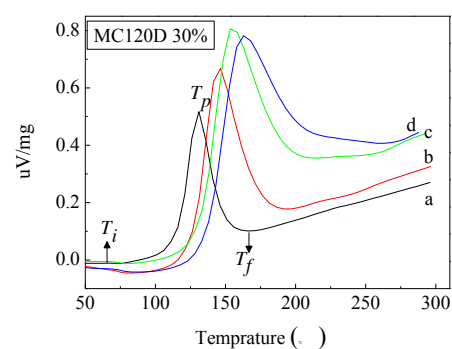
where β is the temperature-rising rate, T is the reaction temperature, T_p is the exothermic peak temperature, E is the activation energy, n is the reaction order.

Figure 1 shows differential thermal curves of a healing system with 20% MC120D and 12.5% of BGE. As seen from the figure, the curing reaction shows two exothermic peaks, which indicates that the curing-reaction proceeds step-wisely [1, 2, 3]. As the rate of temperature-rising increases, the initial temperature (T_i), the peak temperature (T_p) and the final temperature (T_f) of the healing agent system increase too. The total generated heat (the area under the exothermic peak temperature curve) increases with the increase of the rate of temperature-rising, which indicates that the curing reaction speed also goes up. Figure 2 illustrates the differential thermal curves of a healing system with 30% MC120D and 17.5% of BGE. As seen from the figure, the differential thermal curve only has one exothermal peak, which means that when MC120D content is higher than 30%, the curing reaction of healing agent is entirely dependent on the catalyst's functionality.



a. 5k/min, b. 10k/min, c. 15k/min, d. 20k/min

Figure 1: Differential thermal analysis of healing system with 12.5% BGE



a. 5k/min, b. 10k/min, c. 15k/min, d. 20k/min

Figure 2: Differential thermal analysis of healing system with 30% MC120D

Results related to the activation energy and the reaction order are shown in Table 1, which were obtained by using different contents of BGE and MC120D was kept at 20%. As seen from the table, activation energy and reaction order reach their

minimum values when BGE content is 17.5%. In Table 2 results of the activation energy and the reaction order are shown which were obtained by using different contents of MC120D and BGE content was kept at 17.5%. As seen from the table, the activation energy and reaction order reach their minimum values when MC120D content is 20%. Based on systematic tests it was found that the optimal proportion of the healing agent system is: MC120D content 20% and BGE content 17.5%.

Table 1: Activation energy and reaction order for different diluents mass fraction

BGE fraction (%)	$-\ln(\beta/T_p^2) \sim 1000/T_p$ fitting	Relative coefficient R^2	Activation energy E (KJmol ⁻¹)	Reaction order n
	$-\ln\beta \sim 1000/T_p$ linear fitting			
10.0	$y = -3.65469 + 5.72375x$	0.998	47.59	0.870
	$y = -17.76639 + 6.57637x$	0.999		
12.5	$y = -5.68331 + 6.55079x$	0.969	54.47	0.885
	$y = -19.78786 + 7.40054x$	0.976		
15.0	$y = -4.4576 + 6.06282x$	0.998	50.41	0.877
	$y = -18.56654 + 6.91445x$	0.999		
17.5	$y = -3.36634 + 5.61983x$	0.998	46.73	0.868
	$y = -17.4921 + 6.47836x$	0.998		
20.0	$y = -3.32175 + 5.62768x$	0.998	46.79	0.868
	$y = -17.44446 + 6.48505x$	0.998		

Table 2 : Activation energy and reaction order for different mass fraction of catalyst

MC120D fraction (%)	$-\ln(\beta/T_p^2) \sim 1000/T_p$ fitting	Relative coefficient R^2	Activation energy E (KJ·mol ⁻¹)	Reaction order n
	$-\ln\beta \sim 1000/TP$ linear fitting			
10	$y = -4.81416 + 6.36782x$	0.985	52.94	0.880
	$y = -18.96889 + 7.23911x$	0.989		
20	$y = -3.36634 + 5.61983x$	0.998	46.73	0.868
	$y = -17.4921 + 6.47836x$	0.998		
30	$y = -6.91955 + 6.99507x$	0.991	58.16	0.892
	$y = -21.00677 + 7.83769x$	0.993		
40	$y = -5.98578 + 6.53037x$	0.999	54.30	0.888
	$y = -20.03786 + 7.35817x$	0.999		
50	$y = -11.31952 + 8.65504x$	0.981	71.96	0.913
	$y = -25.37057 + 9.48248x$	0.984		

Figure 3 shows the Fourier transform infrared spectroscopy (FTIR) analysis of curing products by using different contents of BGE. It can be seen the main absorption peaks of epoxy resin, 771cm⁻¹, 1035cm⁻¹, 1184cm⁻¹, 1361cm⁻¹, 2928cm⁻¹ are disappeared. The same phenomenon was observed for BGE, 913cm⁻¹, 844cm⁻¹, 761cm⁻¹, which indicates the participation of BGE in the curing reaction [4, 5, 6].

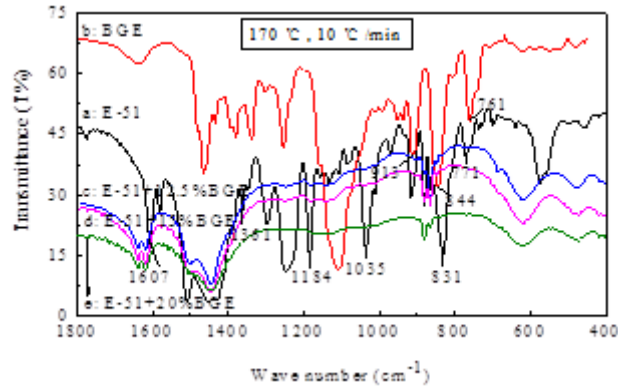


Figure 3 : FTIR spectra of cured epoxy resin E-51 (20%MC120D)

5. CONCLUSIONS

From this study, optimal proportion of healing agent is obtained. Results show that the microcapsule obtained with the adopted production process can be used for the self-healing system in the cementitious materials.

ACKNOWLEDGEMENTS

Financial support from the NSFC (Project No. 51120185002; No. 51078238, No. 50925829) is gratefully acknowledged.

REFERENCES

- [1] Adalbert Farkas, Paul F. Strohm. Imidazole catalysis in the curing of epoxy resins. *Journal of Applied Polymer Science*, 1968, 12(1): 159-168.
- [2] Yang Yanxu, Deng Guangqi, Pang Yaohua, et al. Study on the Curing Process of Epoxy Resins by FT-IR-the Curing Behavior and Kinetics of the E-51/2, 4 EMI System [J]. *Journal of Xi'an Jiaotong University*. 1989, 23(5): 65-70.
- [3] F Ricciardi, W A Romanchick, M M Joulie. Mechanism of imidazole catalysis in the curing of epoxy resins[J]. *Polymer Science*. 1983, (21): 1475-1481.
- [4] Junwei Gu, Qiuyu Zhang, Jing Dang, et al. Preparation and mechanical properties researches of silane coupling reagent modified β -silicon carbide filled epoxy composites[J]. *Polymer Bulletin*, 2009, 62(5): 689-697.
- [5] Abdelkader, AF, White, JR. Curing characteristics and internal stresses in epoxy coatings: Effect of crosslinking agent[J]. *Journal of Materials Science*, 2005, 40(8): 1843-1854.
- [6] Weng Shifu. *Analysis of Fourier Transform Infrared Spectrometer* [M], 2nd edition, Beijing : Chemical Industry Press 2010,389.

EXPERIMENTAL STUDY ON SELF-HEALING CAPABILITY OF FRCC WITH DIFFERENT FIBER TYPES AND SHAPES

M. Yamada¹, T. Nishiwaki¹, S. Kawakami², H. Mihashi¹ and T. Kikuta³

¹ *Tohoku University, Department of Architecture and Building Science, Sendai, Japan – e-mail: makotoyamada@hjogi.pln.archi.tohoku.ac.jp*

² *Daiwabo Polytec Co.,Ltd., Osaka, Japan*

³ *Nippon Institute of Technology, Faculty of Engineering, Saitama, Japan*

Keywords: FRCC, Self-healing, calcium carbonate crystallization

ABSTRACT

To maintain the global environment and build a sustainable society, highly durable and long-life concrete structures are strongly required. However, cracks in concrete cause various problems of not only aesthetic aspect but also durability, i.e. ingress of active substances.

On the other hand, even normal concrete has potential for self-healing of crack with small crack width in the presence of moisture. This self-healing process is induced by the precipitation of calcium carbonate crystals, which combine the dissolved CO_3^{2-} and Ca^{2+} in water with each other. The precipitated crystals cover and close the crack surface.

According to the author's previous studies, FRCC (Fiber Reinforced Cementitious Composite) has a great potential for self-healing than the normal concrete. That is because FRCC has mechanical characteristics which can control propagation of a crack width in the cement matrix through bridging with fibers. Additionally, it has been revealed that some types of synthetic fibers can accelerate the self-healing capability of FRCC due to its chemical properties. The FRCC reinforced by fibers with polar groups, such as polyvinyl alcohol (PVA) with hydroxy group, showed better performance of self-healing than fibers without polarity, such as polypropylene (PP). However, such self-healing phenomena have been experimentally confirmed only in the unrealistic condition, i.e. specimens were completely immersed in water. Therefore, observation of self-healing effects in a practical condition, i.e. a wet-dry cyclic condition will be valuable to develop it to practical application.

In this study, experimental studies were carried out under the wet-dry cyclic condition using different types of fibers, e.g. PVA, PP and PP with a deformed section (D-PP). As a result, it was confirmed that self-healing products filled up the crack with a width of 50 μm in specimen of PVA and D-PP, even in wet-dry cyclic condition.

MICROFIBRES AND HYDROGELS TO PROMOTE AUTOGENOUS HEALING IN CEMENTITIOUS MATERIALS

D. Snoeck¹, P. Dubruel² and N. De Belie¹

¹ *Magnel Laboratory for Concrete Research, Ghent University, Technologiepark-Zwijnaarde 904, 9052 Ghent, Belgium – e-mail: didier.snoeck@ugent.be, nele.debelie@ugent.be*

² *Polymer Chemistry and Biomaterials Group, Ghent University, Krijgslaan 281, 9000 Ghent, Belgium – e-mail: peter.dubruel@ugent.be*

Keywords: concrete, self-sealing, self-healing, superabsorbent polymers

ABSTRACT

Cementitious materials are sensitive to crack formation and it would be beneficial if the material could stop the crack propagation, repair the damage and reach again the original liquid-tightness and/or strength. Therefore, a cementitious material with synthetic microfibres and superabsorbent polymers (SAPs) is proposed. Upon crack formation, the microfibres will become active and due to the bridging action, they will stop the opening of a crack, forcing the cementitious material to crack somewhere else. There, other fibres will become active. In this way, not one large crack, but several small healable cracks are formed.

Further cement hydration and calcium carbonate precipitation will seal the crack if sufficient building blocks and water are present. The building blocks are available through the well-designed mixture with a low water-to-binder (W/B) ratio and water is available through the inclusion of SAPs. These polymers are able to extract moisture from the environment and to provide it to the cementitious matrix for autogenous healing. This healing will lead to the regain in mechanical properties.

In this paper, the formed products are studied by means of optical and scanning electron microscopy. The healing efficiency was evaluated by reloading cracked and healed specimens and by comparing the new mechanical properties with the original properties.

The crack width was limited to 50 μm at 1% strain. While specimens without SAPs showed a regain of mechanical properties of 40-55% in wet/dry cycles, specimens with SAPs showed a total regain of 80-95%. Even in humid air, those specimens show partial healing of 35-55%. SAP B, a cross-linked potassium salt polyacrylate, showed better healing properties compared to SAP A, a copolymer of acrylamide and sodium acrylate. The smart material with SAP B thus is an excellent material to use in future building applications.

1. INTRODUCTION

Concrete cracks give an unsafe feeling and are aesthetically unwanted. Manual repair of these cracks is not only time-consuming, it is also very expensive. It would thus be beneficial if the material could self-heal. Human bones have the ability to detect damage, to stop its propagation, to repair the damage and to reach again the original strength. These features are also available in cementitious materials with synthetic microfibres and superabsorbent polymers (SAPs) as additives.

2. MATERIALS

The mortar mixtures contained CEM I 52.5 N, Class F fly ash (FA/CEM = 1), fine silica sand M34 from Sibelco (M34/B = 0.35), water (W/B = 0.30), polycarboxylate superplasticizer Glenium 51 (Spl/B = 0.0097), 2 volume-% of Polyvinyl-alcohol (PVA) fibres from Kuraray, and a varying amount of SAP expressed as mass-% (m%) relative to the cement weight. **Additional water** was used to compensate for the loss in workability. The composition of all mixtures used, is shown in Table 1.

Table 1: Mixture composition of the used test series (kg/m³).

	CEM	FA	M34	W	Spl	PVA	SAP A	SAP B
REF	608	608	426	365	11.8	26	-	-
0.5A	554	554	388	332 +85	10.7	26	2.77	-
0.5B	590	590	413	354 +26	11.4	26	-	2.95
1B	572	572	400	343 +51	11.1	26	-	5.72

Two types of SAPs from BASF were used: SAP A being a copolymer of acrylamide and sodium acrylate (particle size $100.0 \pm 21.5 \mu\text{m}$) and SAP B, a cross-linked potassium salt polyacrylate ($476.6 \pm 52.9 \mu\text{m}$). The absorption capacity (Table 2) was determined by means of a filtration test and the moisture uptake by dynamic vapor sorption tests. The cement filtrate was obtained by mixing 10 g CEM I 52.5 N in 100 ml de-mineralized water for 6 h and subsequent filtration. All SAPs were vacuum dried with silica gel in a desiccator with a relative humidity (RH) of 3% prior to testing.

Table 2: Swelling capacities of SAP A and SAP B (g/g SAP).

	SAP A	SAP B
De-mineralized water (pH = 6.5)	305 ± 4	283 ± 2
Cement filtrate (pH = 12.8)	61 ± 1	58 ± 2
at 60/90/98% RH	0.26/0.83/3.94	0.28/0.84/3.94

3. METHODS

Cracks were created by means of a four-point-bending test (Walter+Bai DB 3) at the age of 28 days until 1% of strain was reached (1 $\mu\text{m/s}$). After cracking, samples were cured at $20 \pm 2^\circ\text{C}$ by applying wet/dry cycles (alternatively 1 h stored in water and 23 h at 60% RH), or by placing them in a climate chamber with a RH > 90% or 60%. After another 4 weeks, the specimens were reloaded under four-point-bending and the mechanical properties during the first and second loading cycle were compared.

$$\text{regain in } \sigma_{fc} = \frac{\sigma_{fc, \text{reloading}} - \sigma_{\text{unloading}}}{\sigma_{fc, \text{loading}} - \sigma_{\text{unloading}}} \quad [\%] \quad (1)$$

where σ_{fc} = the first-cracking-strength and $\sigma_{\text{unloading}}$ = the residual strength [MPa]. Microscopic observations were performed both on specimens and on thin sections perpendicular to the crack plane, to study the new-formed products. Scanning Electron Microscopy (SEM) equipped with an EDS (Energy Dispersive Spectroscopy) detector was used for elemental analysis of the formed autogenous healing products.

4. RESULTS

The first-cracking-strength of the different series is not significantly different (Figure 1). A higher amount of SAPs, however, would lead to a lower strength [2]. Therefore, in this study, the amount of SAPs was limited to 0.5 and 1% respectively.

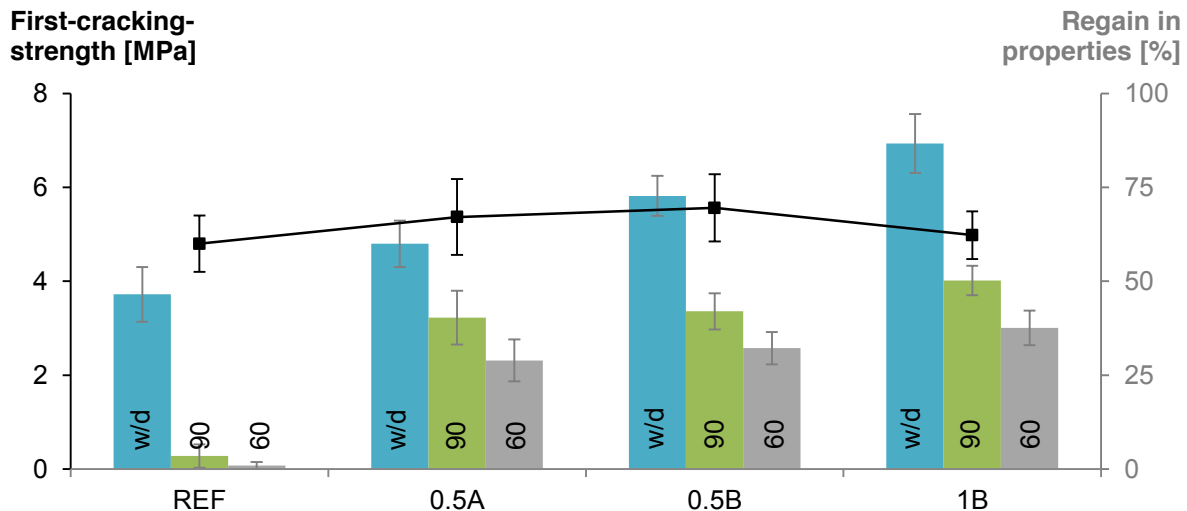


Figure 1: First-cracking-strength (—■—) and the autogenous regain (■ ■ ■). “wd” stands for wet/dry cycles, “90” for a RH > 90% and “60” for a RH = 60%.

Specimens without SAPs showed a regain of mechanical properties of 40-55% in wet/dry cycles, and almost no healing in standard laboratory conditions (RH > 90% and RH = 60%). As the storage condition of 1 h in water and 23 h in air is very strict, this amount of autogenous healing could be anticipated.

Specimens containing SAPs, however, showed a total regain of 55-95%. SAPs hold the water and release it steadily to the cementitious matrix for autogenous healing. Even in humid air, those specimens with SAPs show partial healing of 25-55%. SAPs manage to take moisture out of the humid environment and then they provide it to the cementitious matrix for crack healing. In that way, partial healing occurs.

A higher amount of SAPs, without impairing the strength, leads to a higher amount of healing due to more available water. Series with SAP B showed more healing compared to series with SAP A. This is mainly due to the different particle size.

As the strain was limited to 1%, only small cracks were formed. The crack width was always limited to 50 μm for all test series. These cracks are able to heal completely in wet/dry cycles which caused the regain in mechanical properties.

In the deeper crack region of specimens containing SAPs and stored in standard laboratory conditions (RH > 90% and RH = 60%), further hydration occurred. At the crack mouth, the crack was still open. Only at some distinct places, the formed products were able to bridge a crack. These bridging products were not strong enough and only the inner further hydration was responsible for the measured healing capacity.

Microscopic measurements on a thin section taken from specimens in wet/dry cycles and with SAPs (Figure 2a) revealed that the outer 400 μm of the crack was filled with a whitish product. EDS spectra (Figure 2b) showed that this material was mainly composed of calcium carbonate (CaCO_3). In the inner crack less CaCO_3 was formed, but, further hydration occurred, especially at the crack tip. This led to a regain of

tightness and a regain in the available cross-sectional area and thus mechanical properties.

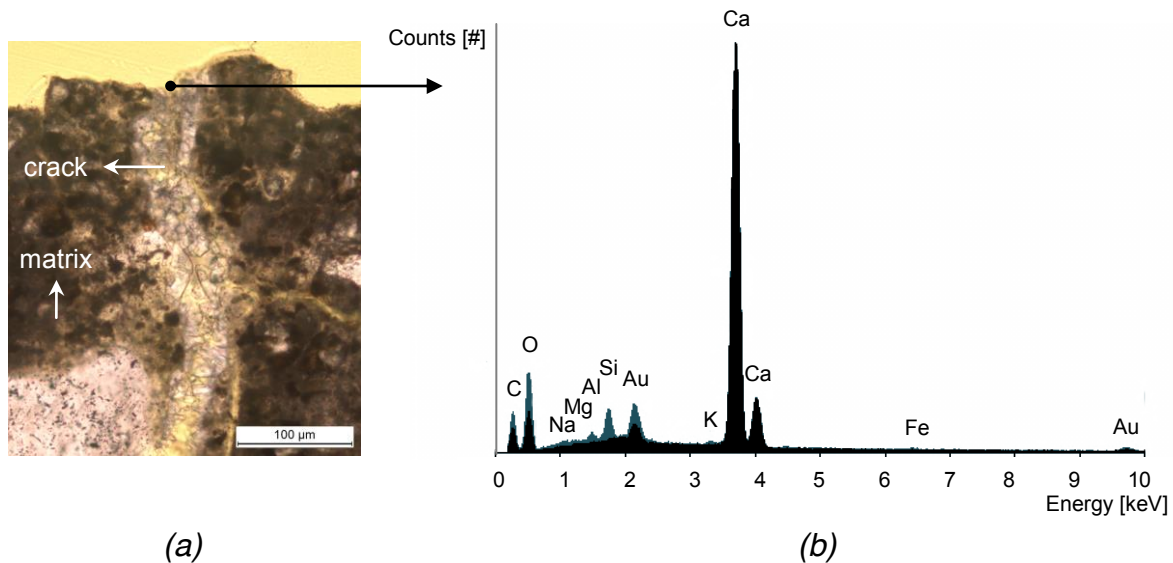


Figure 2: Thin section of healing products in an autogenously healed crack (a) and an EDS spectrum of the formed healing products at the crack face (b).

5. CONCLUSIONS

The combination of microfibres and superabsorbent polymers enhances the autogenous healing capacity. The material is able to recover its mechanical properties, even in standard laboratory conditions.

SAPs are able to extract moisture from the environment and provide the moisture to the matrix for self-healing. SAP B showed the best healing properties and showed a total strength regain of 80-95% in wet/dry cycles and a partial healing of 35-55% in humid air.

ACKNOWLEDGEMENTS

As a Research Assistant of the Research Foundation-Flanders (FWO-Vlaanderen), D. Snoeck wants to thank the foundation for the financial support. The authors also want to thank Dr. G. Herth from BASF for providing SAP A and SAP B.

REFERENCES

- [1] V.C. Li, Engineered Cementitious Composites (ECC) – Material, Structural and Durability Performance, in: E. Nawy (ed.), Concrete Construction Engineering Handbook, CRC Press (2008) 78 p.
- [2] D. Snoeck, K. Van Tittelboom, S. Steuperaert, P. Dubruel, N. De Belie, Self-healing cementitious materials by the combination of microfibres and SAPs, Journal of Intelligent Material Systems and Structures, DOI: 10.1177/1045389X12438623.

EXPERIMENTAL STUDIES OF SELF-HEALING CEMENTITIOUS MATERIALS INCORPORATING MINERAL ADMIXTURES

K. Olivier^{1,2}, A. Darquennes¹, F. Benboudjema¹ and R. Gagné²

¹ ENS Cachan / LMT-CNRS UMR8535 / UPMC / PRES-UniverSud Paris – e-mail: kelly.olivier@ens-cachan.fr

² Centre de recherche sur les infrastructures en béton (CRIB), Université de Sherbrooke, Québec, Canada

Keywords: self-healing, cementitious material, blast-furnace slag, cracking, X-Ray tomography

ABSTRACT

In order to limit the release of CO₂ produced in cement manufacturing, clinker (the major cement component) is often partially replaced by mineral admixtures like blast-furnace slag. The use of mineral admixtures presents different advantages such as the recycling of industrial waste and the improvement of different material properties (workability, sulfate resistance, compressive strength at long term...). Nevertheless, several civil engineering constructions made with blast-furnace slag cement presented cracking at early age due to restrained shrinkage (autogeneous, thermal and drying shrinkage) that affects significantly the material transfer properties and their durability in aggressive environments (chloride, CO₂). Under certain conditions however, it is known that cementitious materials present a self-healing capacity. The purpose of this research work is to study the beneficial influence of the natural self-healing capacity of mortars with blast-furnace slag cement on the lifetime of civil engineering constructions.

A new experimental device has been designed in order to understand the self-healing capacity of mortars at early age. The novel apparatus allows developing micro-cracks in a mortar ring specimen by restrained shrinkage and monitoring the evolution of self-healing by gas permeability and effective diffusivity measurements. The effects of different slag contents (0%, 50%) and curing conditions (air conditioned room at 25±1°C and 45±5% R.H., in tap water) on the self-healing kinetics are studied. Optical measurements in 2D (optical microscope, SEM) and 3D (tomography), chemical analyses of the self-healing products and quantification of the properties of cement with blast-furnace slag (compression and tensile strength, autogenous and drying shrinkage, heat release) complete the study.

1. INTRODUCTION

Modern cementitious materials can nowadays be designed with improved properties (strength, durability...) and lesser environmental negative effects. For example clinker, whose industrial production releases important amounts of CO₂, is sometimes partially replaced with mineral admixtures like blast-furnace slag. But some constructions realized with this new material showed cracking at early age reducing their durability performance. The self-healing capacity of these materials (by activation of the hydration of the anhydrous cement close to crack) could act as a counterpart. The latent hydraulic properties of slag could present interest to improve the self-healing phenomenon.

2. MATERIALS AND METHODS

In this work, two mortar compositions are used: the first using a Portland cement CEMI 52.5 N CP2 NF and the second where 50% of the cement is substituted by blast-furnace slag. The two compositions are defined hereafter as CEMI and 50%BFS and are characterized by a Water/Binder (W/B) ratio equal to 0.50 and 0.52 respectively (the quantity of binder is the same for the two compositions). The sand used has a normalized size.

Two methods are adopted to follow the kinetics of the self-healing phenomenon at early age. The first consists in monitoring the decrease in the cracking size of the mortar samples (diameter $\varnothing = 4\text{cm}$ and height $h = 10\text{cm}$) by means of tomography. A crack characterized by a width equal to about $100\ \mu\text{m}$ was obtained on seven days old specimens by using a splitting test. Specimens were confined with a bi-composant resin reinforced with a glass fiber band to avoid breaking in two parts (method proposed by Van Tittelboom et al., [1]). The analysis by tomography was performed at different ages. Between the different steps, the samples were stored in individual boxes filled with tap water.

The second method consists in following the self-healing phenomenon at early age on a crack due to restrained shrinkage [2] using an optical microscope (measuring the crack width) and performing gas permeability tests. Cylindrical specimens ($\varnothing = 15\text{cm}$ and $h = 5\text{cm}$) were tested and their deformations were restricted by a brass cylinder core located at their center. A crack appeared after about 10 days ($\sim 100\mu\text{m}$) and was detected by Digital Image Correlation. The samples were submitted to different curing conditions (kept in tap water and in an air-conditioned room at $25\pm 1^\circ\text{C}$ and $45\pm 5\%$ R.H). The self-healing phenomenon was monitored at 7, 14, 21 and 28 days after the crack formation. Before the gas permeability tests, the samples stocked in tap water were dried during 24 h at 35°C to allow the gas flow through the crack.

Moreover, and in parallel of the above study, the compression and tensile strengths, the autogenous and drying shrinkage of the two mortar compositions were characterized on prismatic samples ($4\text{cm}\times 4\text{cm}\times 16\text{cm}$). Semi-adiabatic calorimetry tests were also realized in order to assess the hydration rate.

3. RESULTS

The tomography allows observing in 3D the evolution of the crack characteristics (density, length, opening, percolation..., see Figure 1), for a crack larger than the voxel size (here about $20\ \mu\text{m}$). To quantify the cracking density, a specific program was developed in Matlab. It analyses the gray level of each radiography picture (256 gray levels), the quantity and the size of the voxels and allows determining the empty volume. In figure 1, we can clearly see that the crack and porosity have the same gray levels. To distinguish these two types of voids, the program was adapted to only determine the connected (percolated) voxels with the same gray scale using a "burning" algorithm. An example is presented in figure 2 for the 50%BFS specimen just after cracking and 28 days later. We note the decrease in the crack width. Moreover, the crack does not follow the same pattern as of the previous image. This is evidence of the self-healing phenomenon acting in this sample.

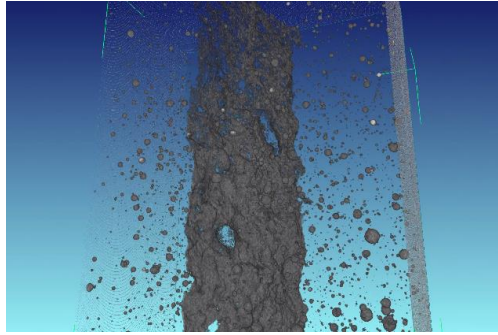


Figure 1: 3D reconstruction by tomography: Crack and porosity

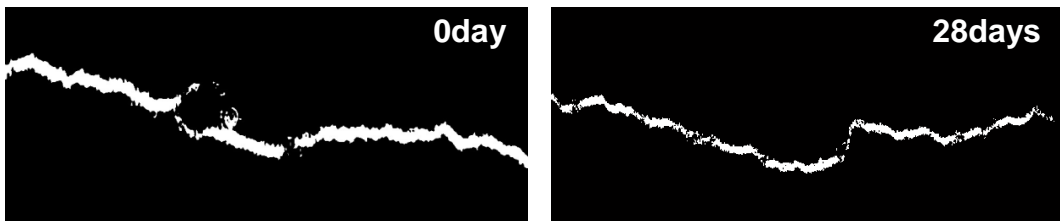


Figure 2: Evolution of the crack size on the 50%BFS sample just after cracking and 28 days later (percolated cluster in 3D)

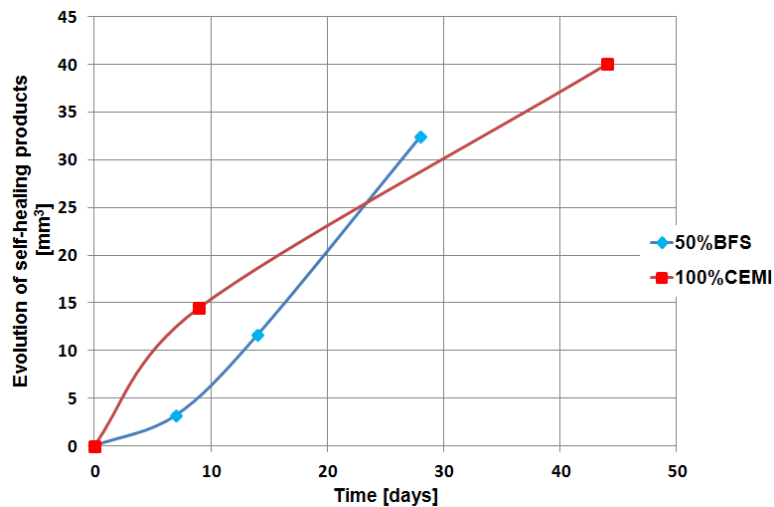


Figure 3: Evolution of self-healing products in the crack (after a splitting test)

In figure 3, the evolution of the self-healing products formed in the crack over several weeks confirms the decrease of crack size. We can also observe a different behavior between the two cementitious materials (CEMI and 50%BFS). At early age, the formation of the self-healing products is three times faster for the CEMI than for the 50%BFS. After 22 days, this behavior changes and the 50%BFS sample seems to have a greater self-healing capacity at long term. This is well correlated with the hydration degree presented in figure 4. At early age, the hydration of the CEMI specimen is faster and reaches a degree close to 0.6 at 7 days. The hydration degree of the 50%BFS specimen is less significant but it increases progressively. This is due to the latent hydraulic behavior of the slag. The 50%BFS sample needs the formation of portlandite to activate its hydration. During the first few days, the hydration of the anhydrous cement in the CEMI sample is activated by water contact. The chemical reaction is quick and the crack can self-heal. In the same period, the

cement and thus portlandite quantities are less important in the 50%BFS specimen. After this period however, slag hydration is activated and the self-healing capacity is progressively increasing.

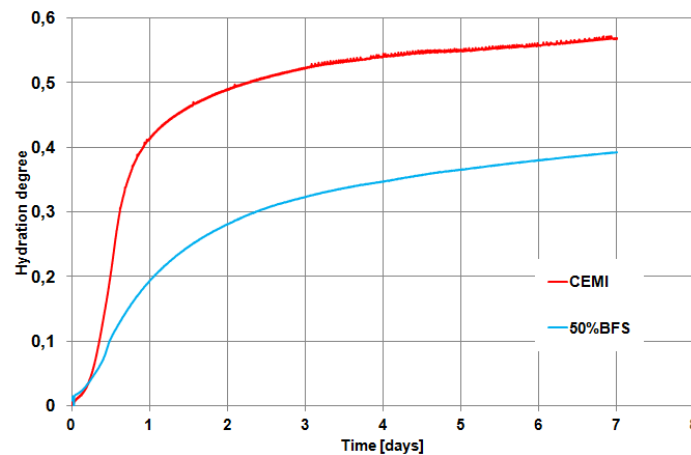


Figure 4: Evolution of the hydration degree by semi-adiabatic calorimetry

4. CONCLUSIONS

Thanks to the use of tomography it was possible to observe and quantify the self-healing capacity of two types of cementitious materials. If a formulation with 50% slag has the tendency to a slower self-healing in an early age than a formulation with 100% portland cement, its latent hydraulic behavior is critical to its self-healing in long term. Future work will be focus on validating this behavior at very long term.

REFERENCES

- [1] K. Van Tittelboom, N. De Belie, W. De Muynck, W. Verstraete, Use of bacteria to repair cracks in concrete , Cement and Concrete Research Vol.40 (2010) 157-166.
- [2] M. Briffaut, F. Benboudjema, J.-M. Torrenti, G. Nahas, "A thermal active restrained shrinkage ring test to study the early age concrete behaviour of massive structures", Cement and Concrete Research, Volume 41, Issue 1, January 2011, Pages 56-63.

THE SMART RELEASING BEHAVIOR OF A MICROCAPSULE BASED ON CHEMICAL SELF-HEALING SYSTEM CAUSED BY CHEMICAL TRIGGER ACTIVATION

B. Dong¹, Y. Wang¹, N. Han¹, F. Xing¹

¹ School of Civil Engineering, Guangdong Province Key Laboratory of Durability for Marine Civil Engineering, Shenzhen University, Shenzhen, P.R.China. 518060 - e-mail: incise@szu.edu.cn; wang.ys1988@gmail.com; nxhan@szu.edu.cn; xingf@szu.edu.cn

Keywords: Microcapsule; Chemical self-healing; Smart releasing behavior; EDTA

ABSTRACT

A novel chemical self-healing system based on microcapsule technology for cementitious composites is established in Guangdong Key Laboratory of Durability for Coastal Civil Engineering, Shenzhen University. The key issue of this system is how to release the healing material and how to activate the healing mechanism. In this paper, the study is focused on the releasing behavior. The smart releasing behavior of healing material in the microcapsule is characterized by EDTA (Ethylene Diamine Tetraacetic Acid) titration method. The experimental results show that releasing procedure of the corrosion inhibitor covered with PS is a function of the time, and is controlled by the wall thickness of the microcapsule. Moreover, the pH value affects the release rate of corrosion inhibitor. With the increasing of pH value, the releasing rate will increase greatly.

1. INTRODUCTION

Concrete is a basic material used for modern construction. Due to concrete creep, the humidity change and non-homogeneous settlement of buildings, concrete structures may generate a lot of cracks during service period. These cracks will affect the safety of the buildings and even cause severe accidents [1]. Self-healing technology then has been introduced to repair the cracks in a concrete structure automatically, resulting in an improvement of concrete structure performance. This technology does not require external monitoring because the cement matrix itself acts as a sensor. And practical requirements of self-healing concrete material are low cost, passive smart and easily to be distributed uniformly [2-3]. An acceptable work that initiates an engineering approach for self-healing cement composite with microcapsules is first developed in Shenzhen University, China. Even so, existing efforts are focusing on the crack repair and mechanical performance recovery. It is not an effective method to deal with the degradation of the concrete structure, which caused by the ions erosion (such as Cl^- , SO_4^{2-} , CO_3^{2-} etc.). For this reason, a chemical trigger mechanism is proposed and a chemical self-healing system with microcapsule based corrosion inhibitor is designed. In this study, a polystyrene resin (PS)/sodium monofluorophosphate ($\text{Na}_2\text{PO}_3\text{F}$) microcapsule is fabricated and studied. And its releasing behavior is measured under a simulated concrete environment with improved EDTA that is designed for microcapsule mentioned above [4]. Moreover, an alterative pH value condition is design to characterize the smart releasing performance of the microcapsule. Further, micro-morphology of the microcapsule is studied to observe the damage pattern variation with pH value alteration.

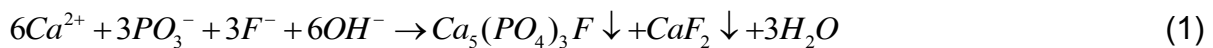
2. MATERIALS AND METHODS

For preparation of the microcapsule, sodium monofluorophosphate and microcrystalline cellulose are mixed into Polysorbate 80. Then the small spherical particles are molded by extrusion method. After that, the microcapsules are fabricated through the spray drying method. In the study, three types of microcapsules with different amount of capsule wall materials are fabricated, which can be seen in Table 1. The weight percentage of the microcapsule wall materials are 10%, 20% and 43% (Respectively, The samples are labeled as N_a , N_b and N_c).

Table 1: The formulation used for microcapsule fabrication

Ingredients	Capsule core materials	N_a	N_b	N_c
Na_2PO_3F	500g	0	0	0
Microcrystalline cellulose	500g	0	0	0
Polysorbate 80	50g	0	0	0
Talc powder	0	35g	70g	146g
Polystyrene resin	0	50g	100g	150g
Chloroform	0	500mL	1000mL	1500mL
Pure water	50g	50g	50g	50g

Since microcapsule will be used in concrete structure for self-healing, understanding the releasing behavior of the microcapsules under the cementitious environment will be our best interests. In order to simulate the cementitious environment, $Ca(OH)_2$ solutions with different pH levels are designed. Microcapsules are then added into $Ca(OH)_2$ solutions for the measurement with different periods. The releasing behavior is studied by EDTA titration method. And the chemical reaction involved is shown as the following chemical equation:



Since Ca^{2+} reacts with PO_3^- and F^- that released from sodium monofluorophosphate inside the microcapsules to form $Ca_5(PO_4)_3F$ and CaF_2 , and turns solution into cloudy, the amount of Ca^{2+} consumption can be calculated and the amount of sodium monofluorophosphate is also deduced. The micro-morphology of the microcapsule samples is observed by Scanning Electronic Microscopy (SEM) (SU-70; Hitachi, Japan) and the particle size distribution of the microcapsule samples is measured by Laser Particle Analyzer (S3500; Microtrac, USA).

3. RESULTS AND DISCUSSION

The size of microcapsule samples is at the level of hundreds of micrometer. According the particle size distribution, the diameter of the capsules is mainly ranged from $400 \mu m$ to $1200 \mu m$. The mean diameter of the capsule core is $405.3 \mu m$ and the mean diameter of the capsule with formula from N_a to N_c is $694.9 \mu m$, $720.1 \mu m$ and $772.0 \mu m$ respectively. Based on the size distribution results, the average wall thickness of the microcapsules with different formula can be calculated with the equation $T = \frac{D - D_0}{2}$ (where, T is the wall average thickness; D is the particle diameter of capsule and D_0 is the particle diameter of capsule core) [5].

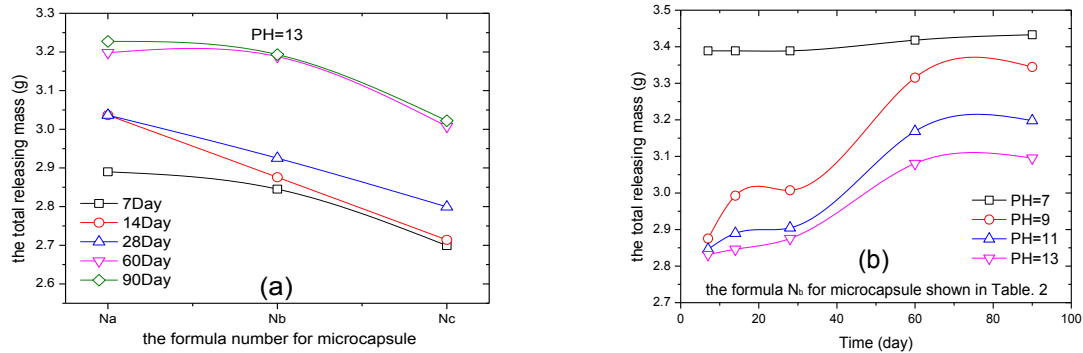


Figure 1: The total releasing mass of microcapsules with different conditions

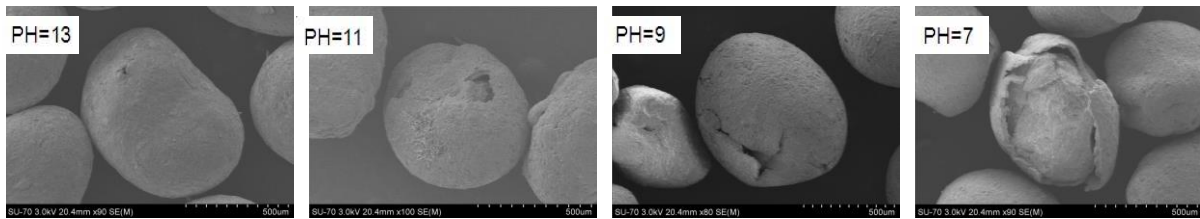


Figure 2: The SEM images of microcapsules after soaked in the solutions with different pH values for the same soaking time

The correlation of the releasing amount of microcapsules changing with the releasing time in the simulated cementitious environment is shown in Figure 1(a). It can be found that the releasing amount with different capsule wall thicknesses are all increased with increasing of the releasing time when pH value is 13. Moreover, for three different microcapsules with different wall thicknesses, it is obvious that the releasing amount has the pattern as $N_c < N_b < N_a$, which tells that the releasing amount decreases with the increasing of the wall thickness of the microcapsules. This is the strong evidence proving that the releasing rate of core materials inside the microcapsules can be controlled effectively by controlling the wall thickness of the microcapsules. The influence of pH value on the releasing behavior of the microcapsule is shown in the Figure 1(b). It is obvious that the largest releasing amount happens at value of pH=7. With increasing the pH value, the releasing amount of the microcapsules decreases. It is well know that polystyrene resin can be swelled in the environment with water existing. The swelling could cause micro-cracks or pinholes on the surface of the microcapsules. On the other hand, microcrystalline cellulose has strong capability of absorbing the water while $\text{Na}_2\text{PO}_3\text{F}$ can be easily dissolved in the water. Moreover, there is a concentration gradient of core material existing between inside and outside of the microcapsules. As the result, the core material of microcapsule can be released from the micro-cracks or the pinholes when the water exists. At first beginning, the releasing rate should be slow since there is only little damage on surface of the microcapsules. With the time increasing, the number and size of cracks or pinholes increase. This directly results in a dramatically increasing amount of the core material releasing is obtained in experiment duration between 28 days to 60 days. Regarding to different pH values, the higher pH value stands the higher concentration of Ca^{2+} in the simulating solution. As mentioned in formula (1), Ca^{2+} can react with PO_3^- and F^- to form $\text{Ca}_5(\text{PO}_4)_3\text{F}$ and CaF_2 as the precipitates. These precipitates can deposit on the surface of the microcapsules and

fill the micro-cracks and pinholes, which eventually hinders the core material releasing. This is the reason that the core material releasing amount is larger when pH value is smaller. Under the neutral condition when pH value is 7, there is no Ca^{2+} existing and reaction of formula (1) can't happen. As the result, the releasing amount is big at the first beginning. The results shown in Figure 1(b) indicate that the designed microcapsules in this experiment are the good candidates for working at alkaline environment to fulfill the smart releasing control, especially during the carbonation process of the concrete materials, the releasing amount of the microcapsules will increase with the reduced pH value. Further study is carried out by SEM observation to understand the surface damaging of microcapsules at different pH values. Figure 2 shows the SEM images of microcapsules after soaked in the solutions with different pH values for the same periods. For pH=13, it is found that there is no obvious surface damage for the soaked microcapsules. With the reduced pH value, the damage of the soaked surface is getting more and more obvious. When it reaches neutral environment with pH=7, the microcapsule surface has been totally destroyed after soaking. This further approves the result that different pH value has tremendous effect on microcapsule releasing behavior and can be used for smart controlling of the core material releasing.

4. CONCLUSION

The wall thickness of the microcapsules can be controlled by the weight percentage of the wall materials. Under the simulated cementitious environment, the releasing amount of the microcapsule core material increases with the increasing of the releasing time in disregard of the different wall thickness of the microcapsules. The core material releasing amount increases with the reduced pH values, which indicates that the designed microcapsules are the good candidates to be used under alkaline cementitious environment with smart releasing control. SEM images further approve that different pH values can be used to control the microcapsule releasing behavior.

ACKNOWLEDGEMENTS

The authors would like to acknowledge financial support provided by Natural Science Foundation for the team project of Guangdong Province (No. 9351806001000001), National Key Basic Research Program funded by MOST (Project No. 2011CB013600; Issue No:2011CB013604) and National Natural Science Foundation of China (No. 50925829/51120185002/51272160)

REFERENCES

- [1] S.J. Jaffer, C.M. Hansson. The influence of cracks on chloride-induced corrosion of steel in ordinary Portland cement and high performance concretes subjected to different loading conditions. *Corrosion Science*. 2008, 50(12): 3343-3355
- [2] M. R. Kessler, N. R. Sottos and S. R. White. Self-healing structural composite materials. *Applied Science and Manufacturing*. 2003, 34(8): 743-753
- [3] S.R.White, N.R.Sottos, P.H.Geubelle. Autonomic healing of Polymer Composites. *Nature*. 2001, 409: 794-797
- [4] Zhou KH, Zhang LF and Zhang YM. Determination of calcium oxide in rare earth ore by EDTA titration method. *Metallurgical Analysis*. 2012,32(1): 64-67
- [5] Joseph D. Rule, Nancy R. Sottos and Scott R. White. Effect of microcapsule size on the performance of self-healing polymers. *Polymer*. 2007, 48(12): 3520-3529

SESSION 2 – SELF-HEALING POLYMERIC MATERIALS

EFFECTS OF NA NEUTRALIZATION LEVEL ON THE SH BEHAVIOUR AFTER BALLISTIC TESTS OF EMAA BASED IONOMERS

A. M. Grande¹, L. Castelnovo¹, I. Quadrio¹, S. Zaffaroni¹ and L. Di Landro¹

¹ *Dipartimento di Scienze e Tecnologie Aerospaziali, Politecnico di Milano, via La Masa 34, 20156, Milano, Italy – e-mail: grande@aero.polimi.it; castelnovo@aero.polimi.it; ivan.quadrio@mail.polimi.it; stefano.zaffaroni@mail.polimi.it; luca.dilandro@polimi.it*

Keywords: self-healing, ballistic impact, EMAA, ionomer, mechanical properties

ABSTRACT

Ethylene-co-methacrylic acid (EMAA) based ionomers have thermo-mechanical properties strongly dependent on neutralization level of acid groups. Research revealed also how these materials are able to heal after ballistic impacts. In order to better understand the role of neutralization level on the Self-Healing (SH) behaviour, mechanical and ballistic tests on EMAA copolymers, neutralized with different amount of Na ions, were performed in different experimental conditions.

The SH capability was studied by shooting bullets at low velocity (180 m/s) and mid velocity (400 m/s); different testing conditions such as sample thickness and bullet diameter were examined. In all impact tests, spherical projectiles were used. These experiments allowed to define a critical ratio between sample thickness and bullet diameter below which the SH behaviour does not appear.

After ballistic damage, the healing efficiency was evaluated by applying a pressure difference through tested samples. Subsequently, morphology analysis of the impacted areas was made observing all tested samples by Scanning Electron Microscope (SEM). These analysis revealed different characteristic features in the damaged zones of tested polymers impacted at different projectile speed.

Obtained results show how the Na ions content influences the SH capability; in particular the EMAA copolymer with the highest Na neutralization level does not show a complete hole closure after low velocity impact test. Conversely, increasing projectile speed, all the polymers exhibit nearly the same SH behaviour.

1. INTRODUCTION

Ionomeric polymers, developed in the early sixties, contain a certain percentage of ions (usually up to 20%) along the polymer chains [1]. Ionomers based on ethylene-co-methacrylic acid copolymer (EMAA) are one of the first classes of polymeric materials which have been found to exhibit such SH capability. The SH behaviour of these polymers after high energy impact has been studied and described in several references [2-5]. The repair of damages is autonomous and instantaneous without any external intervention. On the other hand, SH is observed in relatively limited range of temperature and bullet speed conditions. In view of an extension of the properties and operative ranges required in different potential applications, self-healing blends based on ionomers with the addition of different crystalline or elastomeric polymers and modifiers have also been prepared and investigated [6-9]. In this work, the SH behaviour of ionomers with different neutralization levels,

exhibited in diverse testing conditions, such as bullet speed and material thickness, is presented and compared.

2. MATERIALS

EMAA based copolymers and ionomers are available on the market with different trade names (e.g. Nucrel® and Surlyn®). In this research an EMMA copolymer and two sodium ionomers were analysed. Pellets of polymers were supplied by DuPont®. All studied materials have the same acid part content, 5.4 mol%, with 0% (EMAA - Nucrel 960), 30% (EMAA30Na - Surlyn 8940) and 60% (EMAA60Na - Surlyn 8920) of the acid groups neutralized by Na ions. After drying pellets in vacuum at 60 °C for 5 hours, square samples (120x120 mm) of 0.5, 1, 2, 3 (± 0.1) mm thickness were produced by compression moulding at 180 °C. Prior to testing, flat specimens were stored in a controlled environmental chamber at 23 °C for 30 days in order to achieve non-variable and stable mechanical properties due to aging.

3. METHODS

Two different types of ballistic tests were carried out. The first set of tests investigated SH ability of studied materials after a low velocity impact, while the second set explored the ability to repair a damage following an impact at mid velocity. The low velocity tests were performed by shooting steel balls (diameter from 2.5 to 14.4 ± 0.15 mm) on target samples with thickness varying from 0.6 to 2.6 ± 0.2 mm. The air gun firing system allows to obtain a bullet velocity of 180 ± 5 m/s. Tests at mid velocity speed were carried out in a shooting lab; steel spheres with a diameter ranging from 1.5 to 7.5 ± 0.1 mm were fired with a shotgun on samples with thickness of 0.5, 1, 2 and 3 ± 0.2 mm. The actual speed of spheres varied between 380 m/s and 440 m/s. The healing efficiency after ballistic tests was evaluated using two different techniques: microscopic observation and leakage test [10].

4. RESULTS

Low velocity impact tests allowed to identify a critical ratio between sample thickness (t) and bullet diameter (d) below which full repair was not observed. This ratio is often recognized as a peculiar parameter to discriminate the impact behaviour of flat panels [11]. Results presented in Table 1 show how above a 0.2 t/d ratio a complete SH behaviour is well maintained for EMMA30Na; on the other hand, below this specific ratio, an effective hole closure did not occur. Similar results were obtained for EMMA copolymer. Conversely, EMMA60Na does not show a complete hole closure after low velocity impact test for all t/d ratios.

Microscope analysis after low velocity ballistic tests highlighted different morphologies of the impacted areas. In the bullet entry side (Figure 1.a), radial striations originating at the impact point can be evidenced, which are caused by plastic deformation both in healed and no healed samples. However, a significant difference in the response of these materials after impact was detected; the morphology of the damaged area in healed samples presented petaling phenomenon (Figure 1.a) with a melted zone at the apex of the petals. These melted areas, even if small, are responsible for the sealing of the hole caused by the bullet, thus becoming a crucial factor for the global SH behaviour exhibited by the studied material. On the

other hand, non-healed samples present a circular hole with clearly defined edges (Figure 1.b), which evidence removal of material preventing the repair.

Table1: Low velocity impact test results for EMAA30Na (no SH for gray cells);
t = sample thickness [mm], d = sphere diameter [mm].

<i>t/d</i>	2.35	3	5	6.34	8	10	12	14.27
0.6	0.26	0.20	0.12	0.09	0.08	0.06	0.05	0.04
1.0	0.43	0.34	0.2	0.16	0.13	0.1	0.09	0.07
1.9	0.79	0.62	0.37	0.29	0.23	0.19	0.16	0.13
2.6	1.11	0.87	0.52	0.41	0.33	0.26	0.22	0.18

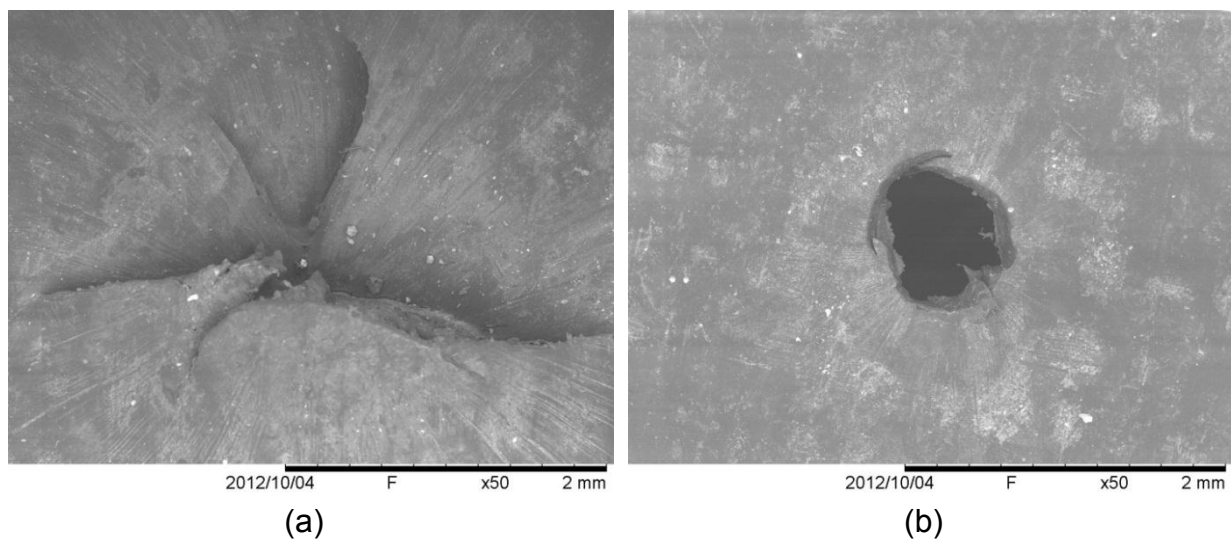


Figure 1: Entry side in a EMAA30Na repaired sample (a), t = 2.6 mm, d = 10 mm, and unrepaired sample (b), t = 0.6 mm, d = 3 mm, tested at low velocity.

In mid velocity impact tests, as in the previous case, steel spheres of different diameter were fired. Obtained results show how all tested polymer exhibited an efficient SH behaviour after impact at this projectile speed range. However, also in these tests critical *t/d* ratios can be identified, below which SH behaviour did not appear. For repaired samples, SEM analysis again revealed a morphology of the impact sites with a clear melted zone in the centre of the crater and radial striations due to extensive deformation. Unrepaired samples present clear-cut holes similar to those obtained after low velocity impacts; however, in some cases a competition between these two failure modes occurred.

5. CONCLUSIONS

SH behaviour after ballistic puncture tests of EMAA based copolymer and Na ionomers were investigated under different experimental conditions. Impact tests were carried out firing spherical projectiles at different speeds ranging from 180 m/s, up to 400 m/s.. At low velocity impact a clear SH behaviour is not detectable for EMAA60Na; other tested polymers show instead an efficient SH ability. Mid velocity impact tests revealed instead a SH behaviour for all studied polymers allowing to identify critical *t/d* ratios.

ACKNOWLEDGEMENTS

The sponsorship of Regione Lombardia - projects STIMA and SMAT - is gratefully acknowledged. The authors wish to thank the company DuPont (Italy) for providing the polymeric materials.

REFERENCES

- [1] Holiday L. Ionic Polymer. London: Applied Science Publisher, 1975.
- [2] Kalista SJ, Ward TC, Oyetunji Z. Self-healing of poly(ethylene-co-methacrylic acid) copolymers following projectile puncture. *Mech Adv Mater Struct* 2007;14(5):391-397.
- [3] Kalista SJ, Ward TC. Thermal characteristics of the self-healing response in poly(ethylene-co-methacrylic acid) copolymers. *J R Soc Interface* 2007;4(13):405-411.
- [4] Varley RJ, van der Zwaag S. Towards an understanding of thermally activated self-healing of an ionomer system during ballistic penetration. *Acta Mater* 2008;56(19):5737-5750.
- [5] Varley RJ, van der Zwaag S. Autonomous damage initiated healing in a thermo-responsive ionomer. *Polym Int* 2010;59(8):1031-1038.
- [6] Penco M, Rahman MA, Spagnoli G, Janszen G, Di Landro L. Novel system with damage initiated autonomous healing property based on heterogeneous blends of ethylene-methacrylic acid ionomer. *Mater Lett* 2011;65(14):2107-2110.
- [7] Rahman MA, Penco M, Spagnoli G, Grande AM, Di Landro L. Self-Healing Behavior of Blends Based on Ionomers with Ethylene/Vinyl Alcohol Copolymer or Epoxidized Natural Rubber. *Macromol Mater Eng* 2011;296(12):1119-1127.
- [8] Rahman MA, Penco M, Peroni I, Ramorino G, Grande AM, Di Landro L. Self-Repairing Systems Based on Ionomers and Epoxidized Natural Rubber Blends. *ACS Appl Mater Interfaces* 2011;3(12):4865-4874.
- [9] Varley RJ, Shen S, van der Zwaag S. The effect of cluster plasticisation on the self healing behaviour of ionomers. *Polymer* 2010;51(3):679-686.
- [10] Grande AM, Coppi S, Di Landro L, Sala G, Giacomuzzo C, Francesconi A, Rahman MA. An experimental study of the self-healing behavior of ionomeric systems under ballistic impact tests. *Proc SPIE* 2012;8342.
- [11] Francesconi A, Giacomuzzo C, Grande AM, Mudric T, Zaccariotto M, Etemadi E, Di Landro L, Galvanetto U. Comparison of self-healing ionomer to aluminium-alloy bumpers for protecting spacecraft equipment from space debris impacts. *Adv Space Res* 2013; Volume 51, Issue 5, 1 March 2013, Pages 930-94.

INVESTIGATION OF AUTOCATALYTIC CROSSLINKING REACTIONS BASED ON ROOM TEMPERATURE “CLICK” CHEMISTRY AS VERSATILE TOOL FOR DESIGNING SELF-HEALING POLYMERS

D. Döhler¹, P. Michael¹ and W. H. Binder¹

¹ Institute of Chemistry, Chair of Macromolecular Chemistry, Faculty of Natural Sciences II (Chemistry, Physics and Mathematics), Martin-Luther-University Halle-Wittenberg, von-Danckelmann-Platz 4, Halle (Saale) 06120, Germany – e-mail: diana.doehler@chemie.uni-halle.de; philipp.michael@chemie.uni-halle.de; wolfgang.binder@chemie.uni-halle.de

Keywords: autocatalysis, click chemistry, poly(isobutylene), room temperature, self-healing polymer

ABSTRACT

Fast crosslinking and post-crosslinking reactions based on catalytic reactions acting at room temperature are a major focus of materials scientists as highly reliable toolbox for the design of self-healing polymeric materials. While applying liquid and reactive polymeric precursors with different architectures as well as reactions with autocatalytic behavior, the efficiency and thus the self-healing performance of the associated network formation, determined via melt rheology, can be optimized.

We therefore investigated the network formation of multivalent polymeric alkynes and azides, namely poly(acrylate)s and poly(isobutylene)s (PIB's) via the copper(I)-catalyzed alkyne-azide "click" cycloaddition reaction (CuAAC) as well as the corresponding crosslinking kinetics via *in situ* melt rheology.

Due to the formation of 1,3-triazole rings acting as internal ligands during the catalytic process an acceleration of subsequent "click"-reactions up to a factor of 4.3 (increase of rate constant) was observed. Thus efficient crosslinking within several hours could be enabled at room temperature dependent on the molecular weight while linking the starting viscosity of the polymer mixture as well as molecular mobility to changes in the CuAAC-reactivity.

Based on the deeper understanding of CuAAC-catalysis and the optimization of the reaction rate of CuAAC we subsequently have expanded our crosslinking concept to hyperbranched PIB's prepared via living carbocationic inimer (initiator-monomer) type polymerization. Accordingly, we created a new crosslinking system based on CuAAC in order to improve the resulting network strand densities and therefore the stiffness of the final crosslinked material.

1. INTRODUCTION

Crosslinking as well as post-crosslinking reactions and their associated network formation are in major focus of materials scientists to create unique self-healing materials with various architectures or to improve existing materials regarding their thermomechanical and physicochemical properties. Accordingly, the quest for such types of reactions proceeding under ambient reaction conditions like low temperature as well as for reactive and liquid reactants generating an efficient amount of network points is very high. We therefore investigated the CuAAC[1-2] as one of the most

prominent “click”-type reactions and valuable as well as versatile tool for the design of self-healing polymers due to its substrate insensitivity and high efficiency even under mild reaction conditions. Thus, we explored the crosslinking reaction of various poly(acrylate)s and PIB’s bearing alkyne- respectively azide-groups and the corresponding reaction kinetics via *in situ* melt rheology.[3-5]

2. MATERIALS AND METHODS

Rheological measurements were performed on an oscillatory plate rheometer MCR 501/SN 80753612 from Anton Paar (Physica). For all measurements a PP08 measuring system (parallel plated, diameter 8 mm) was used. Measurements were performed at 20 °C. For evaluation of data the RheoPlus/32 software (V 3.40) and OriginPro7 was used. For sample preparation a 1: 1 mixture of an azido-functionalized polymer was used. The frequency sweep of the pure polymer mixture which was used as basic measurement was performed with a strain γ of 10.0% and with an angular frequency ω ranging from 100 to 1 rad/s. $\text{CuBr}(\text{PPh}_3)_3$ (0.1 equiv per functional group) was dissolved in CHCl_3 (40.0 μL) and was added as a stock solution to all investigated polymer mixtures. Subsequently, the reaction mixture was mixed with a spatula and was immediately put on the rheometer plate. Measurements were performed with a strain γ of 0.1% or 0.5% and with an angular frequency ω ranging from 100 to 1 rad/s. A frequency sweep was performed every 20 minutes.

3. RESULTS AND DISCUSSION

Three-arm-star azido-telechelic PIB’s were synthesized with molecular weights from 5500 g/mol to 30000 g/mol and were crosslinked with three-arm-star alkyne-telechelic PIB with a molecular weight of 6300 g/mol via CuAAC at 20 °C in order to study the influence of the correlated decreasing concentration of the reactive functional groups from 0.238 to 0.076 M on the crosslinking kinetics. Accordingly, the gelation time, determined via *in situ* melt rheology, increased from 290 to 855 minutes with increasing molecular weight respectively decreasing functional group density. This observation was in line with the starting viscosity of the polymer mixtures which increased as well with increasing molecular weight respectively decreasing functional group density while linking reactivity and molecular mobility of the polymer chains. Thus, an autocatalytic effect of the CuAAC of multivalent PIB’s could be observed as illustrated in figure 1 showing the correlation of the rate constants k vs time t for crosslinking PIB’s with azide- respectively alkyne-groups and applying bromotris(triphenylphosphine)copper(I) as catalyst.[3]

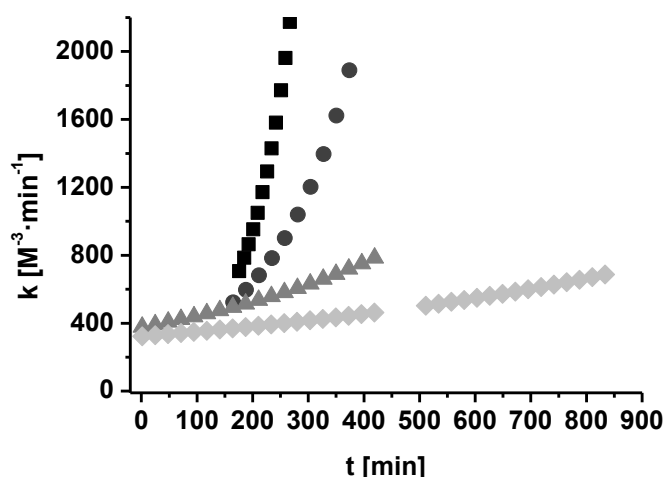


Figure 1: Correlation of the rate constants k vs time t at 20 °C for crosslinking PIB's with azide- respectively alkyne-groups applying bromotris(triphenylphosphine)copper(I) as catalyst.

In accordance with the development of the gelation times the strongest autocatalytic effect could be observed for crosslinking the polymer mixture with the lowest molecular weights and thus with the highest concentration of functional groups. Consequently the increase of the rate constants k became less prominent for crosslinking polymer mixtures with higher molecular weights.

The observed autocatalytic effect could be explained due to different functionalities of the formed triazole rings during CuAAC which can act as internal ligand while forming the corresponding copper(I)-acetylide/ligand complex or which can preorientate the functional groups next to the catalytically active copper(I) center and thus, promoting further click reactions. [3]

Due to the autocatalysis of the CuAAC of polymeric azides and alkynes enabling efficient crosslinking reactions at room temperature we subsequently have expanded the crosslinking concept to hyperbranched PIB's. For the synthesis a living carbocationic inimer (initiator-monomer) type polymerization was used according to Puskas et al.[6] as illustrated in figure 2.

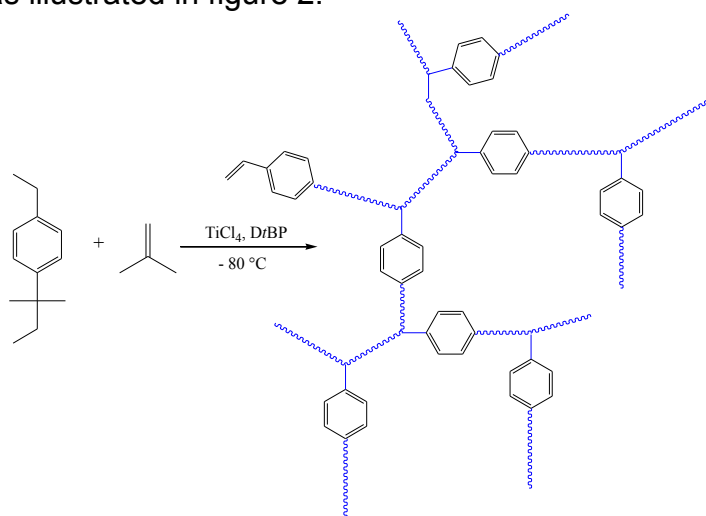


Figure 2: Synthesis of hyperbranched PIB's via living carbocationic inimer (initiator-monomer) type polymerization.

Due to the architecture of the hyperbranched PIB's and the higher amount of functional groups per molecule even shorter gelation times could be observed in comparison to star-shaped PIB's while crosslinking azide- respectively alkyne-functionalized polymers at room temperature and using $\text{CuBr}(\text{PPh}_3)_3$ as catalyst.

4. CONCLUSION

The crosslinking of various reactive polymeric alkynes and azides via CuAAC was investigated at room temperature while studying the autocatalytic behavior of the reaction via *in situ* melt rheology. Due to the triazole rings acting as internal ligands during the crosslinking process an acceleration of the rate constant up to a factor of 4.3 dependent on the reactivity of functional groups could be observed enabling the design of polymeric networks for self-healing applications without the need of any external stimuli like elevated temperature. Thus, a highly efficient crosslinking system suitable for the processing of self-healing materials based on polymeric alkynes and azides could be highlighted due to strong and designable autocatalytic effects.

ACKNOWLEDGEMENTS

We are grateful for the grant DFG BI 1337/8-1 (within the SPP 1568 "Design and Generic Principles of Self-Healing Materials") and the EU-project IASS for financial support.

REFERENCES

- [1] W. H. Binder, R. Sachsenhofer, 'Click' Chemistry in Polymer and Materials Science, *Macromol. Rapid Commun.* (2007) 15-54.
- [2] W. H. Binder, R. Sachsenhofer, 'Click' Chemistry in Polymer and Material Science: An Update, *Macromol. Rapid Commun.* (2008) 952-981.
- [3] D. Döhler, P. Michael, W. H. Binder, Autocatalysis in the Room Temperature Copper(I)-Catalyzed Alkyne-Azide "Click" Cycloaddition of Multivalent Poly(acrylate)s and Poly(isobutylene)s, *Macromolecules* (2012) 3335-3345.
- [4] M. Schunack, M. Gragert, D. Döhler, P. Michael, W. H. Binder, Low-Temperature Cu(I)-Catalyzed "Click" Reactions for Self-Healing Polymers, *Macromol. Chem. Phys.* (2012) 205-214.
- [5] M. Gragert, M. Schunack, W. H. Binder, Azide/Alkyne-"Click"-Reactions of Encapsulated Reagents: Toward Self-Healing Materials, *Macromol. Rapid Commun.* (2011) 419-425.
- [6] C. Paulo, J. E. Puskas, Synthesis of Hyperbranched Polyisobutylenes by Inimer-Type Living Polymerization. 1. Investigation of the Effect of Reaction Conditions, *Macromolecules* (2001) 734-739.

PROTON-COUPLED MECHANOCHEMICAL TRANSDUCTION – MECHANOGENERATING ACIDS

C.E. Diesendruck¹ and J.S. Moore¹

¹ *Department of Chemistry and Beckman Institute for Advanced Science and Technology, University of Illinois at Urbana-Champaign, 405 N. Mathews Avenue, 61801 Urbana, Illinois, USA - e-mail: diesendr@illinois.edu; jsmoore@illinois.edu*

Keywords: mechanochemistry, self-healing, mechanoacid, self-reinforcing, photoacid generator, cross-linking

ABSTRACT

Biological structural materials have the intrinsic capability to self-reinforce, self-heal or remodel in response to macroscopic damage. Incorporation of these features in synthetic polymers could lead to materials with service lifetimes well beyond current generation materials, circumventing costly repairs. Acid catalyzed reactions can be used to promote the remodeling of a polymer backbone and/or side chains because the catalyst is simple, stable and can diffuse in the solid state, allowing it to reach high turnover. Using known photochemically and thermally-promoted acid-producing reactions, unique mechanically sensitive chemical functionalities (mechanophores) with acid-releasing capability were designed to produce a simple catalyst that can induce numerous chemical transformations in materials under mechanical stress. The development of these new mechanophores is a first step towards force-induced remodeling of stressed polymeric materials that will potentially enable the development of smart, autonomic self-healing polymers and composite materials.

INTRINSIC SELF-HEALING OF POLYMER SOLID WHILE KEEPING INTEGRITY AND LOAD-BEARING CAPABILITY

M. Z. Rong¹, M. Q. Zhang¹, C. E Yuan², F. Wang²

¹ Key Laboratory for Polymeric Composite and Functional Materials of Ministry of Education, School of Chemistry and Chemical Engineering, Sun Yat-sen (Zhongshan) University, Guangzhou 510275, P. R. China – e-mail: cesrmz@mail.sysu.edu.cn, ceszmq@mail.sysu.edu.cn

² Materials Science Institute, Sun Yat-sen (Zhongshan) University, Guangzhou 510275, P. R. China – e mail: chaneyuan@yahoo.com.cn, hdwfei@163.com

Keywords: polymer solid, intrinsic self-healing, alkoxyamines moieties, thermally dynamic reversible, load-bearing capability

ABSTRACT

Generally, intrinsic self-healing polymers based on reversible covalent bonds scission and reconnection would lose their load bearing capability as a result of molecular cleavage during healing process. This shortcoming also results in creep deformation of the products. To solve the problem, we introduce a novel healing mechanism by using dynamically reversible C-ON bonds. Upon heating to a certain homolysis temperature, C-ON bonds in alkoxyamines moieties frequently cleave but immediately recombine. When alkoxyamines are incorporated into polymer chains, C-ON covalent bonds fission and recombination synchronously take place with very high frequency, and the equilibrium tends to the combination side. Cracked parts can thus be restored through chemical exchange reaction of alkoxyamine moieties. More importantly, because a large amount of C-ON bonds remain connection, the possible material deformation in the course of crack remending could be avoided.

Here, crosslinked polystyrenes and epoxy with alkoxyamine moieties are synthesized as model polymers to prove feasibility of the above considerations. It is shown that the polymers can repeatedly self-heal cracks without deformation induced by chain scission, and provides the polymer with mechanical stability at elevated temperature as well. Moreover, the healing can be conducted within a wide temperature range when different alkoxyamines moieties are used.

Molecular structures of alkoxyamines moieties, as well as thermodynamic behavior of C-ON bonds scission and recombination, etc., are studied in detail to optimize self-healing behavior of the polymers. Full reversibility can be acquired when only one type of C-ON bond is included in the polymers. Accordingly, synthesis routes, molecular structures, thermally reversible characteristics, self-healing performance and self-healing mechanism, thermal stability and thermal-mechanical properties, etc, have been studied in detail.

1. INTRODUCTION

To remend damaged polymer intrinsically, thermally reversible covalent bonds, typically like Diels-Alder (DA) bonds, were introduced to polymer chains [1]. Cracks in polymers can be repeatedly restored via fission and reconnection processes of reversible covalent bonds upon heating. However, the polymers should inevitably lose their functions as a result of molecular cleavage during healing processes. Here we show the feasibility of using dynamically reversible C-ON bond as the healing chemistry, which combines the aforesaid covalent bond breakage and re-connection into one step. The possible material deformation in the course of crack remending would thus be avoided.

2. MATERIALS

4-Hydroxy-2,2,6,6-tetramethylpiperidinyloxy (4-OH-TEMPO, 98%) and methacryloyl chloride (98%) were purchased from Aldrich and used as received. Styrene (99%) was obtained from Alfa Aesar and purified by distillation under reduced pressure in the presence of calcium hydride. Linear PS (GPPS 685D) was provided by Dow Chemical. All the other reagents and solvents were commercial products and used without further purification.

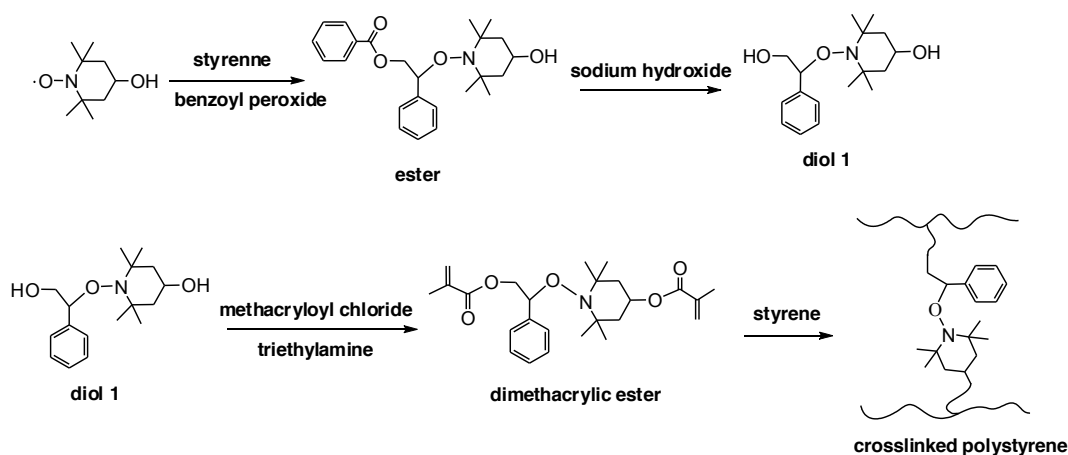
3. METHODS

Starting from 4-OH-TEMPO, a diol containing alkoxyamine unit was obtained. Then, two alkoxyamine-based monomers, which were functionalized with bi-C=C (dimethylacrylic ester) and bi-epoxy group (diEPO), were prepared from this diol respectively. Their molecular structures were confirmed by FTIR, NMR and MS. Crosslinked polystyrenes were prepared through bulk polymerization of styrene and dimethylacrylic ester (Scheme 1). Epoxy was prepared via curing the mixture of diEPO and Epo828 using diethylenetriamine (DETA) as hardener. Healing efficiency of the materials was evaluated by double cleavage drilled compression (DCDC) tests [2], using a SANS CMT 6000 universal tester. Healing efficiency was calculated from the ratio of the fracture toughness of the healed specimen over that of the virgin specimen. To conduct the calculation, for a measured critical stress of the virgin specimen at a certain crack length, the corresponding critical stress of the healed specimen at the same crack length was estimated by interpolation from the fitted crack length dependence of the measured critical stress of the healed specimen.

4. RESULTS

The resultant crosslinked PS possesses similar mechanical properties as conventional crosslinked PS with ethyleneglycol dimethacrylate (EGDMA) as crosslinking agent. When the molar feeding ratio of styrene over cross-linker is fixed at 10/1, for example, flexural strength and modulus of the former are 99.4 MPa and 5.0 GPa, while those of the latter are 93.0 MPa and 5.2 GPa. Thermal reversibility of C-ON bonds for all the polymers was carefully studied by temperature dependent ESR spectroscopy. The data show that with a rise in temperature homolytic C-ON bonds in the system increased until a homolysis-recombination equilibrium is reached (Figure 1). Crosslinking density and chain flexibility are main factors that influence reversibility of C-ON bonds. Lower crosslinking density and flexible chains give better

reversibility of C-ON bonds, and thus offer higher healing performance. Dynamic mechanical behavior of the polymers during repeated heating and cooling cycles were studied by DMA. The results show that the alkoxyamines-based polymers exhibit reversibly dynamic equilibriums after several heating-cooling cycles. Even at higher temperatures, the C-ON bonds at crosslinking points can still help to maintain shape and integrity of materials. Thermal stabilities of the polymers were investigated by TGA. The initial weight loss temperatures of these alkoxyamines-based polymers are lower than the counterparts excluding alkoxyamines, owing to the fact that the radicals generated from alkoxyamine moieties induce decomposition of materials.



Scheme 1: Synthesis route of alkoxyamine-based crosslinked polystyrene.

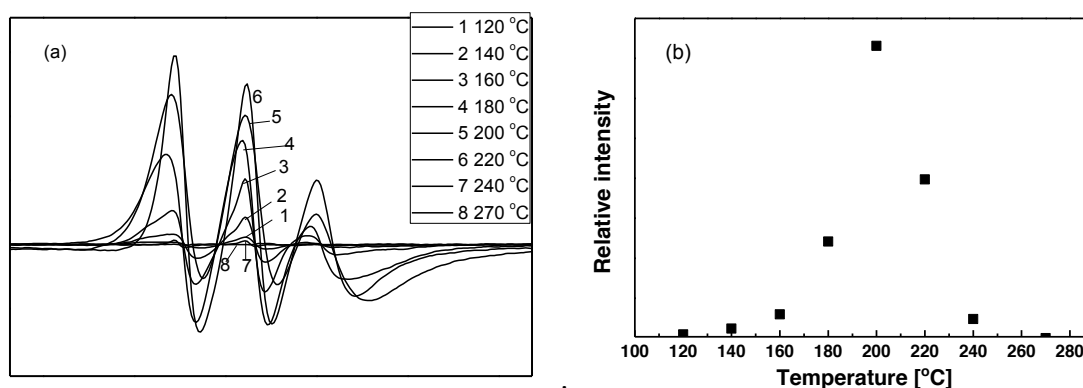


Figure 1: (a) ESR spectra of PS with the molar feeding ratio of styrene over cross-linker 7.5/1 measured at various temperatures. (b) Relative ESR signal intensities calculated from integral area of the normalized absorption lines.

Healing efficiency was defined as the ratio of strength property of the healed specimen over that of the virgin one. Different methods were employed depending on the polymers' mechanical characteristics: DCDC test for the hard and brittle crosslinked polystyrene, while Izod impact test for the tough epoxy. The experimental results show that all the polymers are characterized by repeatable self-healing ability, with healing efficiency ranging from 50% to 75% (Table 1 and 2). In general, the higher concentration of alkoxyamines in the polymers and the greater reversibility of C-ON bonds, the higher healing efficiency.

Table 1: Healing efficiencies of polystyrene with the molar feeding ratio of styrene over cross-linker 7.5/1, healed at 130 °C for 2.5 h.

	virgin	Healing 1	healing 2	healing 3	healing 4	healing 5
K_c [MPa m ^{1/2}]	0.54	0.41	0.40	0.37	0.39	0.35
η [%]	-----	75.9	74.1	68.5	72.2	64.8

Table 2: Healing efficiencies of polystyrene with the molar feeding ratio of styrene over cross-linker 5/1 healed at (a, 130 °C, b, 145 °C) for 2.5 h and 10/1 healed at 130 °C for 2.5 h.

	5/1			10/1	
	virgin	healed a	healed b	virgin	healed
K_c [MPa m ^{1/2}]	0.57	0.15	0.40	0.46	0.15
η [%]	-----	26.4	70.1	-----	32.6

5. CONCLUSIONS

In this work, alkoxyamine moieties are introduced into crosslinked polystyrene, polyurethane and epoxy, respectively, providing the polymers with self-healing ability. Under ceratin homolysis temperature, alkoxyamines undergo a reversible radical reaction and there exists a fast dynamic equilibrium between dissociation and association. By taking advantage of this behavior, possible material deformation in the course of crack remending would thus be avoided even when the healing is carried out above its glass transition temperature.

ACKNOWLEDGEMENTS

The authors thank the support of the Natural Science Foundation of China (Grants: 51273214, 20874117, 51073176 and U0634001), the Science and Technology Program of Guangdong Province (Grant: 2010B010800021, 2010A011300004), and the Basic Scientific Research Foundation in Colleges and Universities of Ministry of Education of China (Grant: 12lgjc08).

REFERENCES

- [1] X. X. Chen, M. A. Dam, K. Ono, A. Mal, H. Shen, S. R. Nutt, K. Sheran, F. Wudl, A thermally re-mendable cross-linked polymeric material, *Science* 295 (2002) 1698-1072.
- [2] A. P. Thomas, N. N. Sia, Quantitative evaluation of fracture, healing and re-healing of a reversibly cross-linked polymer, *Acta Materialia* 55 (2007) 5684~5696.

RESPONSE OF SOLVENT-BASED SELF-HEALING SMART MATERIALS UNDER FATIGUE

S. Neuser¹, V. Michaud¹

¹ *Laboratoire de Technologie des Composites et Polymères (LTC), Institut des Matériaux, Ecole Polytechnique Fédérale de Lausanne (EPFL), CH-1015 Lausanne, Switzerland*

Keywords: self-healing polymer, smart composite, SMA, fatigue testing

ABSTRACT

Self-healing of epoxy matrix could prove essential in increasing the reliability and service life of fiber-reinforced polymers. The principle of encapsulated liquid healing agents dispersed in the matrix has been demonstrated successfully using different chemistries and different testing setups. In addition, progress has been made in the field of smart composites regarding crack detection and closure, using for example fiber optics and shape memory alloy fibers. An active response is given to a detected and localized damage event by the combined action of crack closure and local heating.

We report here on encapsulated EPA solvent based epoxy materials with embedded SMA fibers tested in fatigue loading of TDCB sample geometries. Healing in solvent-based capsule systems occurs through solvent diffusion, swelling of the polymer on the crack faces thus enabling further reaction of residual monomer and bonding crack faces which are in contact.

Epoxy samples loaded with EPA microcapsules fared substantially better than samples without capsules or samples with inactive control solvent microcapsules. This behavior is attributed to a crack blunting effect: as the EPA diffuses into the matrix, the modulus decreases while the epoxy becomes more ductile. As a result, complete crack arrest at relatively high stress intensities K_{Ic} was observed.

TDCB samples containing capsules and embedded SMA wires were tested statically until complete fracture, activated through the SMA wires for healing and finally tested in fatigue after healing. Such healed samples exceeded the virgin properties in fatigue response. Secondly, samples with or without SMA wires were tested in fatigue for 20'000 cycles at high stress intensities, followed by a rest period (with SMA wire activation, if applicable) for different durations and further tested in fatigue. Sample response was improved by SMA wire activation and longer healing rest periods.

Overall, EPA solvent capsules are beneficial to the fatigue life of an epoxy matrix, by combined effects of crack blunting during loading and crack healing at rest periods.

1. INTRODUCTION

Fatigue cracks are an important damage scenario in the service life of composite materials. In this work, an epoxy matrix with a solvent-filled capsule healing system based on Caruso et al.'s work [1], combined with embedded shape memory alloy (SMA) fibers was investigated under dynamic testing [2]. The effect of solvent on the epoxy during fatigue testing is analyzed through both continuous experiments, as well as with rest periods and SMA activation.

2. MATERIALS

The epoxy resin was Epon 828, a DGEBA resin (Brenntag) which was cured with diethylenetriamine (DETA, Sigma Aldrich) in the stoichiometric ratio of 100:12. Curing took 24h at ambient temperature followed by post-curing 24h at 35°C (PC1). The SMA wire used in this study was a martensitic NiTiCu alloy with respective composition of 44.86/45.08/10.06 and a diameter of 150 μ m (Furukawa Techno Material).

3. METHODS

TDCB samples were cast in silicone molds and spacers were used to minimize the amount of microcapsules per sample by casting in two steps: first the surrounding matrix consisting of pure epoxy resin, then the self-healing capable, 15wt% microcapsule loaded resin. The microcapsules were produced using the urea-formaldehyde (UF) microencapsulation protocol established by Blaiszik et al. [3] using a stirring rate of 400rpm and retaining only the microcapsule fraction between 125 and 355 μ m of diameter. For samples with integrated SMA wires, knots were introduced at their ends and these were aligned using free-hanging 50g weights before the silicone molds were closed, thereby clamping the SMA wires at 3 equally spaced locations (as done previously [2]).

Fatigue testing involved a tension-tension triangular wave form with an stress intensity ratio of $R=K_{min}/K_{max}=0.1$ a frequency of 5Hz and for active healing in samples with integrated SMA wires, an electrical current of 0.5A per wire was applied during the break.

4. RESULTS

In the first instance, we specifically compared plain epoxy to the well-known DCPD/Grubbs self-healing epoxy and the EPA solvent-loaded epoxy. Representative results are presented in Fig.1. At constant 0.47MPa $m^{1/2}$ loading, a crack in the plain sample progresses rapidly while in the DCPD/Grubbs sample, crack progression was slower. EPA solvent microcapsule loaded TDCB samples also showed a reduced crack progression rate as compared to the plain epoxy, but after about 4h for this sample, complete crack arrest at these relatively high loading conditions was observed. This behavior was observed for samples loaded with solvent microcapsules even if the time until crack arrest varied.

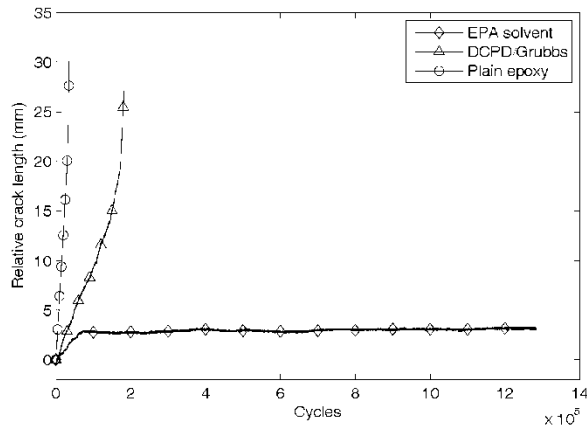


Figure 1: In plain epoxy, crack progression is fast while in the DCPD/Grubbs sample crack progression is slower. In the EPA solvent microcapsule loaded TDCB sample, crack arrest occurred after 4h ($\Delta K=0.47\text{MPam}^{1/2}$).

Based on the observations above, we investigated the solvent effect on stress and strain distribution around the crack tip using the finite element method (FEM). The analysis was performed using ANSYS and a simple 2D crack tip model was generated. Fig.2 shows the chosen geometry: the crack tip protruded by $100\mu\text{m}$ into the $400\mu\text{m}$ wide geometry. The crack tip was modeled by a simplified circular notch of $1\mu\text{m}$ of diameter, surrounded by a solvent-weakened layer of $4\mu\text{m}$ thickness ($\pm 2h$ of solvent diffusion). Using the symmetry of this problem, the bottom boundary was clamped while a stress of 1MPa was applied to the top boundary.

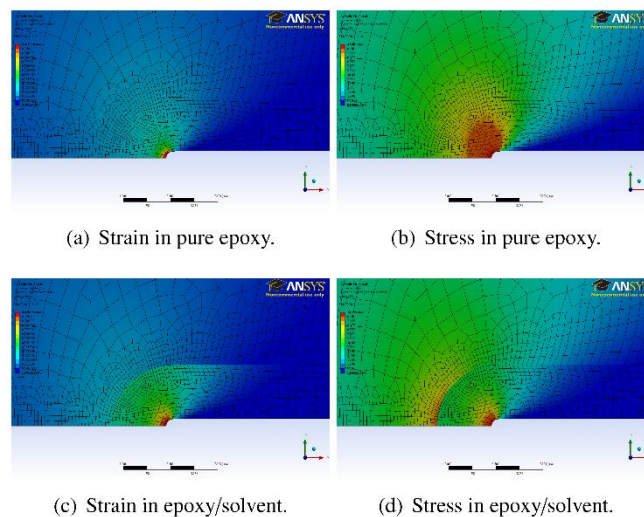


Figure 2: Equivalent von Mises stress and strain distribution around the crack tip for the pure epoxy case as well as the solvent-affected epoxy.

The model showed a slight increase in the strains and a substantial decrease of the stress in the crack tip. Knowing that the solvated epoxy showed an almost threefold increased elongation at break (5.7% vs. 2.0% in plain epoxy), the observed crack arrest is therefore due crack blunting.

After investigating continuous fatigue testing on virgin and healed samples, we also characterized the effect of resting periods during low-cycle fatigue tests. The tests were conducted on samples with or without SMA wires at a stress intensity of $0.50\text{MPa}\sqrt{\text{m}}$ and the resting periods were 10min, 2h and 24h. Fig.3 shows a representative results for a 10min rest period is shown. The rest period on samples without SMA wires had no significant effect on the overall trend of the crack progression while in samples with SMA wires, crack arrest occurred.

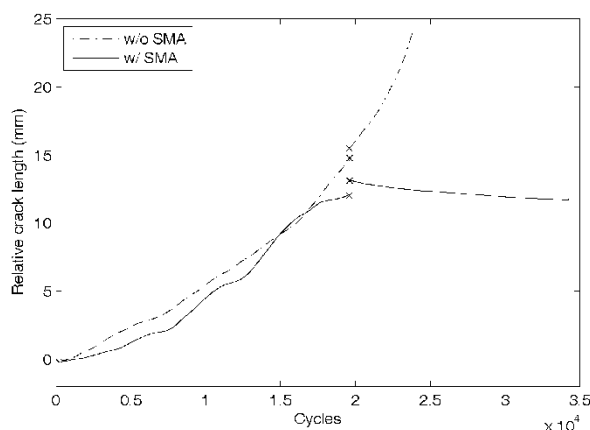


Figure 3: For 10min rest periods, no effect was observed unless the SMA wires were activated, which led to crack arrest.

5. CONCLUSIONS

Fatigue performance of a self-healing epoxy with EPA solvent-filled UF microcapsules and SMA wires was investigated. Complete crack arrest for very high loading conditions was observed and this phenomenon is due to the reduced stresses in the crack tip due to the solvent. Furthermore, SMA activation led to crack arrest during low-cycle fatigue tests, which was not observed in samples without SMA wires.

ACKNOWLEDGEMENTS

The authors gratefully acknowledge the financial support of the Swiss National Science Foundation (FNRS 511482), the Laboratory of Applied Mechanics and Reliability Analysis (LMAF) at EPFL for using their fatigue testing device and M. G. Sahini, E. Rotterman and S. Clerc for their technical assistance.

REFERENCES

- [1] Caruso MM, Blaiszik BJ, White SR, Sottos NR, Moore JS. Full recovery of fracture toughness using a nontoxic solvent-based self-healing system. *Advanced Functional Materials* 2008;18(13):1898–904.
- [2] Neuser S, Michaud V, White SR. Improving solvent-based self-healing materials through shape memory alloys. *Polymer* 2012;53(2):370–8.
- [3] Blaiszik BJ, Caruso MM, McIlroy DA, Moore JS, White SR, Sottos NR. Microcapsules filled with reactive solutions for self-healing materials. *Polymer* 2009;50(4):990–7.

SESSION 3 – BIO-INSPIRED MATERIALS

PLANTS AS CONCEPT GENERATORS FOR BIOMIMETIC SELF-HEALING AND SELF-ADAPTIVE MATERIALS, STRUCTURES AND SURFACES

T. Speck^{1,2,3}, O. Speck^{1,2}, T. Masselter^{1,2}, H. Bohn¹ & R. Mülhaupt³

¹ Plant Biomechanics Group Freiburg, Botanic Garden, University of Freiburg, Schänzlestr. 1, 79104 Freiburg, Germany and ² Competence Networks BIONIK international, BIONIK and Biomimetics – e-mail: thomas.speck@biologie.uni-freiburg.de, olga.speck@biologie.uni-freiburg.de, tom.masselter@biologie.uni-freiburg.de, holger.bohn@biologie.uni-freiburg.de
³ Freiburg Materials Research Center (FMF), Stefan-Meier-Straße 21, 79104 Freiburg, Germany – e-mail: rolf.muelhaupt@makro.uni-freiburg.de

Keywords: biomimetics, bio-inspiration, self-x-materials, self-healing, self-adaptation

ABSTRACT

Plants have inspired the development of numerous novel (self-)adaptive and self-healing materials, structures and surfaces over the last decade. Examples include: (1) self-repairing elastomers for sealing gaskets and dampers inspired by self-healing processes in latex bearing plants, (2) self-adaptive biomimetic attachment systems inspired by permanent attachment organs of plants, (3) adaptive biomimetic anti-adhesion surfaces inspired by leaf surfaces, and (4) (self-)adaptive elastic façade shading systems inspired by the bird of paradise flower.

1. INTRODUCTION

Many biological materials, structures and surfaces possess in addition to their excellent mechanical functions self-healing- and other self-x-properties (e.g. self-organization, self-adaptability, self-cleaning). The entity of these properties allows them to interact very efficiently with their respective environment. These biological solutions are cost- and energy-efficient, multi-functional and environmentally friendly. And with several billion test runs, they have surely stood the test of time. Novel sophisticated methods for quantitatively analysing and simulating the form-structure-function-relationship on various hierarchical levels allowed over the last decade new fascinating insights in the functional principles of biological materials, structures and surfaces. On the other hand, new production methods allow for the first time the transfer of many outstanding properties of the biological role models into innovative biomimetic products [1,2]. However, the transfer of characteristic functions of life, as self-healing, self-adaptation, self-organization, and self-cleaning still represents a major challenge for materials research. Using current R&D-projects, the process sequences in biomimetic research applied for the development of hierarchically structured biomimetic self-x-materials, structures and surfaces are presented [3].

2. MATERIALS AND METHODS

Materials and methods used within the research topics presented, are described in detail in the literature cited in the respective section.

3. RESULTS AND DISCUSSION

Self-healing bio-inspired elastomers: Over the last decade plants have proved to be a promising source of inspiration for the development of self-healing biomimetic materials and structures [2,4]. Inspired by self-healing processes found in latex bearing rubber plants, self-healing elastic polymers for sealing gaskets and dampers were developed. Rubber plants of the genera *Ficus*, *Hevea* and *Euphorbia* contain latex emulsions in micro-tubes (laticifers) that are released after injury and seal the fissure by coagulation. In *Ficus* we could prove that the laticifers are under high overpressure (up to 15 bar) [5]. After injury the membranous vesicles burst due to the pressure drop, proteins are set free and, mediated by Ca^{2+} ions, cause the coagulation of latex particles which possess protein binding sites on their surface [4]. Based on these results, two approaches were used for producing novel bio-inspired self-healing elastomers. Inspired by the function of Ca^{2+} ions, ionomeric self-healing elastomers were designed by the project partner Fraunhofer UMSICHT, Oberhausen. In the second approach bio-inspired multiphase blends of Nitrile butadiene rubber (NBR) with liquid polymers (hyperbranched polyethyleneimine, PEI) as self-sealing and self-healing agent were developed [6]. The latter represent an alternative to micro-encapsulation of self-healing agents, avoiding the micro-encapsulation by phase separation. In the micro-phase separated domains the liquid polymer is under a high internal pressure. If a micro-crack propagates into such a domain the self-healing agent seals the crack. We found considerable self-healing efficiencies (measured as %-recovery of tensile strength) after cutting strips of the self-healing elastomers in half and rejoining them under controlled conditions. For carboxylated NBR ionomers a self-healing efficiency of 50% in the non-vulcanized state and of 15% in the vulcanized state were found (rejoining and annealing for 24h at 55°C). For vulcanized NBR/PEI blends (PEI: 2000 g mol⁻¹) the self-healing efficiency amounts to 44% (annealing under compression for 12h at 100°C and subsequent storing at room temperature without compression for 12h) [2,4,6].

(Self-)adaptive permanent biomimetic attachment systems: Climbing plants evolved different types of permanent attachment structures. In plants with adhesive pads and adventitious roots efficient attachment is caused by a combination of structural form-closure on the micrometre scale and/or organic glue allowing the plants to climb even flat and smooth supporting structures [7]. Attachment pads were studied in Boston Ivy (*Parthenocissus tricuspidata*), Monkey's Comb (*Amphilophium crucigerum*) and *Passiflora discophora*. In all three species the pads represent highly efficient and reliable permanent attachment structures. Boston Ivy secretes an adhesive fluid and is able to attach to a wide range of smooth and rough substrates [7]. The Monkey's Comb does not secrete glue and requires (micro-)rough surfaces for attachment in which its pads grow and produce an excellent form-closure. In all tested species the pads can sustain high mechanical loads. A single lignified pad of Boston Ivy shows on plaster a maximum normal force at failure of 7.6±2.5 N, i.e. it fails at normal stresses of ca. 4 MPa [7].

As root climbing species English Ivy (*Hedera helix*), Trumpet Vine (*Campsis radicans*), Climbing Fig (*Ficus pumila*), and two Vanilla species (*Vanilla* ssp.) were investigated. In addition to an excellent form-closure caused by root hairs that grow into (micro-)cavities of the climbing substrate all species secrete adhesive fluids for further increasing adhesion. A typical root cluster at a 2 cm long stem segment of English Ivy grown on bark fails at a maximum normal force of 3.8±2.4 N. Root

clusters at nodes of the Trumpet vine grown on wood show a maximum normal force at failure of 18.3 ± 6.0 N [7]. An additional feature interesting for the development of bio-inspired attachment materials is the self-adaptive form-closure found in English Ivy. After chemical adhesion in a (micro-)cavity, initiated by desiccation processes and due to the arrangement of cellulose micro-fibrils in the cell wall, the root hairs form an apical hook and spirally curl up. Thereby the root hairs shorten and self-adaptively improve the form-closure of the root with the climbing substrate [8]. Based on the various types of permanent attachment structures in plants several approaches for novel bio-inspired attachment materials and structures using a combination of physical and chemical anchoring methods are currently developed.

Adaptive biomimetic anti-adhesion surfaces: Some plant surfaces are known to strongly reduce insect adhesion. The anti-adhesive effect can be caused by different types of hierarchically structured plant surfaces. The most well known ones are double structured leaf surfaces with cuticular wax crystals, famous for their self-cleaning properties technically used in so called biomimetic Lotus-Effect[®] surfaces. By quantitatively analysing the ability of Colorado Potato Beetles (*Leptinotarsa decemlineata*) to walk successfully on a variety of differently structured leaf surfaces, we found even higher anti-adhesive effects in leaves with special types of cuticular folds. The traction forces of walking beetles tethered to the force sensor were determined by using a high-resolution force sensor (resolution ± 50 μ N). Our results proved that compared to a smooth glass surface, cuticular folds can reduce the traction force by a factor of 20 or more [9]. The lowest traction forces were found for leaves with smooth surfaces and medium cuticular folds possessing a height and width of ca. 0.5 μ m and a spacing between 0.5 and 1.5 μ m. Such structures are found e.g. on adaxial leaf surfaces of *Hevea brasiliensis* and *Cyclamen persicum*. A similar reduction of traction forces is also found for untreated and hydrophobized replicas of such plant surfaces produced with epoxy resin by using a moulding technique. This proves that the anti-adhesive effect is mainly controlled by the micro-structuring of the surfaces and not by the surface chemistry [10]. This together with the high stability of cuticular folds and their replicas makes these structures promising candidates for developing bio-inspired technical anti-adhesive surfaces.

(Self-)adaptive bio-inspired elastic façade shading systems: The biological concept generator is the perch in the flower of *Strelitzia reginae* (Bird-Of-Paradise). Birds landing on this perch to feed on nectar induce by their bodyweight two lamina flaps to bend sideways, which enables pollination by first exposing the stamens and in a later phase of blooming the stigma. The elastic bending of the structure is fully reversible, fail-safe, very reliable and can be repeated over 3.000 times with almost no sign of fatigue. The deformation of the perch has been quantitatively analysed, abstracted, simulated and transferred into a (self-)adaptive bio-inspired façade shading system which undergoes a major shape change by only a minute deformation of its backbone. The avoidance of local hinges, which need a lot of maintenance and are prone to failure, is together with the high reliability and the fail-safe behaviour the main benefit of the patent-registered façade-shading system Flectofin[®] [11]. Flectofin[®] is a biomimetic technical structure with a flapping system based on the elastic opening mechanism found in the perch of *Strelitzia reginae* that was developed by using glass fibre-reinforced polymers. The good scalability of this biomimetic structure is of high importance as it allows developing of individual façade shading elements in various sizes from several centimeters up to 20 m. The high

potential of this structure is proven by the actual advanced prototype status and by being an inspiration for the development of another bio-inspired shading system that was used in the Thematic Pavilion at the World Expo 2012 in Yeosu, Korea [12].

4. CONCLUSION

Plants have proven to be increasingly important role models for the development of novel self-adaptive and self-healing bio-inspired materials, structures and surfaces. With their high reliability, their fail-safe behaviour and their high potential for sustainability these bio-inspired technical products become more and more interesting in many fields of industrial production and application.

ACKNOWLEDGEMENTS

We thank the German Federal Ministry of Education and Research (BMBF), the MWK Baden-Württemberg and the Baden-Württemberg Stiftung for financial support.

REFERENCES

- [1] T. Masselter, W. Barthlott, G. Bauer, J. Bertling, F. Cichy, P. Ditsche-Kuru, F. Gallenmüller, M. Gude, T. Haushahn, M. Hermann, H. Immink, J. Knippers, J. Lienhard, R. Luchsinger, K. Lunz, C. Mattheck, M. Milwich, N. Mölders, C. Neinhuis, A. Nellesen, S. Poppinga, M. Rechberger, S. Schleicher, C. Schmitt, H. Schwager, R. Seidel, O. Speck, T. Stegmaier, I. Tesari, M. Thielen, T. Speck, Biomimetic products, in: Y. Bar-Cohen (Ed.), Biomimetics: nature-based innovation, CRC Press, Boca Raton, London, New York, 2012, pp. 377-429.
- [2] T. Speck, G. Bauer, F. Flues, K. Oelker, M. Rampf, A.C. Schüssele, M. v. Tapavicza, J. Bertling, R. Luchsinger, A. Nellesen, A.M. Schmidt, R. Mülhaupt, O. Speck, Bio-inspired self-healing materials, in: P. Fratzl, J.W.C. Dunlop, R. Weinkamer (Eds.), Materials design inspired by nature: function through inner architecture, RSC Smart Materials No. 4, The Royal Chemical Society, London, 2013, pp. 359-389.
- [3] T. Speck, O. Speck, Process sequences in biomimetic research, in: C.A. Brebbia (Ed.), Design and nature IV, WIT Press, Southampton, 2008, pp. 3-11.
- [4] T. Speck, R. Mülhaupt, O. Speck, Self-healing in plants as bio-inspiration for self-repairing polymers, in: W. Binder (Ed.), Self-healing materials, Wiley-VCH, Weinheim, 2013, pp. 69-97.
- [5] G. Bauer, T. Speck, Restoration of tensile strength in bark samples of *Ficus benjamina* due to coagulation of latex during fast self-healing of fissures, *Annals of Botany* 109 (2012) 807-811.
- [6] A.C. Schüssele, F. Nübling, Y. Thomann, O. Carstensen, G. Bauer, T. Speck, R. Mülhaupt, Self-healing rubbers based on NBR blends with hyperbranched polyethylenimines, *Macromolecular Materials and Engineering* 297 (2012) 411-419.
- [7] T. Steinbrecher, E. Danninger, D. Harder, T. Speck, O. Kraft, R. Schwaiger, Quantifying the attachment strength of climbing plants: a new approach, *Acta Biomaterialia* 6 (2010) 1497-1504.
- [8] B. Melzer, T. Steinbrecher, R. Seidel, O. Kraft, R. Schwaiger, T. Speck, The attachment strategy of English Ivy: a complex mechanism acting on several hierarchical levels, *Journal of The Royal Society Interface* 7 (2010) 1383-1389.
- [9] B. Prüm, R. Seidel, H.F. Bohn, T. Speck, Plant surfaces with cuticular folds are slippery for beetles, *Journal of The Royal Society Interface* 9 (2012) 127-135.

- [10] B. Prüm, R. Seidel, H.F. Bohn, S. Rubach, T. Speck, Microscopical surface roughness: a relevant factor for slipperiness of plant surfaces with cuticular folds and their replica, *Acta Biomaterialia* (2013) DOI.org/10.1016/j.actbio.2013.01.030.
- [11] J. Lienhard, S. Schleicher, S. Poppinga, T. Masselter, M. Milwich, T. Speck, J. Knippers, Flectofin: a nature based hinge-less flapping mechanism, *Bioinspiration and Biomimetics* 6 (2011) DOI:10.1088/1748-3182/6/4/045001.
- [12] J. Knippers, T. Speck, Design and construction principles in Nature and Architecture, *Bioinspiration and Biomimetics*, 7 (2012) DOI:10.1088/1748-3182/7/1/015002.

SELF-HEALING PROCESSES IN PLANTS – A TREASURE TROVE FOR BIOMIMETIC SELF-REPAIRING MATERIALS

O. Speck¹, M. Schlechtendahl¹, F. Schmich¹ and T. Speck¹

¹ Plant Biomechanics Group Freiburg, Botanic Garden, Faculty of Biology, University of Freiburg, Schänzlestr. 1, 79104 Freiburg, Germany - e-mail: olga.speck@biologie.uni-freiburg.de, marksmail@gmx.de, Florian.Schmich@gmx.de, thomas.speck@biologie.uni-freiburg.de

Keywords: Biomimetics, *Delosperma*, Plants, Self-Healing, Self-Sealing

ABSTRACT

After an artificial injury in succulent leaves of *Delosperma cooperi* and *Delosperma ecklonis* rapid wound sealing by deformation of the entire leaf takes place within approximately 90 minutes. On the basis of comparative anatomical and biomechanical analyses of the closely related species conclusions can be drawn on necessary boundary conditions allowing self-sealing by leaf deformation and movement. An analytical model of the underlying principle found in *D. cooperi* has been developed as basis for the transfer into bio-inspired self-repairing materials.

1. INTRODUCTION

In the course of 3.8 billion years plants have evolved the amazing capacity to seal and heal wounds. In all plants examined we identified firstly a self-sealing phase and secondly a self-healing phase. The rapid self-sealing prevents the plants from desiccation and from infection by pathogenic germs. This gives time for the subsequent self-healing of the injury which in addition to wound closure also results in the (partly) restoration of mechanical properties of the plant organ.

Based on a variety of self-sealing and self-healing processes in plants different functional principles were successfully transferred into bio-inspired self-repairing materials [1,2]. Inspired by rapid self-sealing processes in the twining liana *Aristolochia macrophylla* and related species a biomimetic PU-foam coating for pneumatic structures was developed [3]. With respect to low coating weight and thickness of the foam layer maximum repair efficiencies of 99.9 % have been obtained [4-6]. Other role models are the weeping fig (*Ficus benjamina*) and the rubber tree (*Hevea brasiliensis*), in which the coagulation of latex is involved in the sealing of lesions [7]. Different self-sealing strategies for elastic materials are developed showing significant mechanical restoration after a macroscopic lesion [8,9].

In this study, three main aspects of self-repairing mechanisms are addressed: (1) the underlying principles and boundary conditions necessary for self-sealing in *Delosperma* leaves, (2) the evolutionary interaction between self-repair abilities of closely related *Delosperma* species and their respective ecological niches, and (3) the translation of the results into a reasonable concept for bio-inspired technical self-repairing materials

2. MATERIALS AND METHODS

Plant material — Both, *Delosperma cooperi* (Hook f.) L. Bolus and *Delosperma ecklonis* (Salm-Dyck) Schwantes are members of the Aizoaceae family, native to South Africa (Fig. 1). They are perennial plants forming dense lawns. *D. cooperi* reaches sizes of approximately 20-40 cm in height, with fleshy leaves and a trailing stem that hangs down. *D. ecklonis* grows to a height of approximately 25 cm having also succulent leaves. Test plants of *D. cooperi* and *D. ecklonis* were obtained from greenhouse cultivations in the Botanical Garden of the University of Freiburg (Germany).



Figure 1: (a) *Delosperma cooperi*: flowering plants in the open field of the Botanic Garden Freiburg, (b) *Delosperma ecklonis* in the greenhouses of the Botanic Garden Freiburg.

Anatomical analyses — Thin sections of leaves were cut with a microtome from embedded material. Toluidinblue staining was used for discrimination between different leaf tissues. Parameters of cells and tissues were determined with the image analysis software IMAGEJ.

Mechanical analyses — Biomechanical properties of the entire leaves and of single tissue layers were studied in tensile tests performed on a custom-made micro-tensile-testing device (Fig. 2).

Self-repair mechanisms — Leaves were injured artificially with a razor blade. Tests were carried out with different cutting depth damaging various numbers of tissue layers. Three types of injuries were examined: longitudinal, transversal, and circular cuts.

Self-repair efficiency — In order to quantify the self-repair properties by leaf movement maximum bending angle and maximal angle velocity were measured at different air humidity.

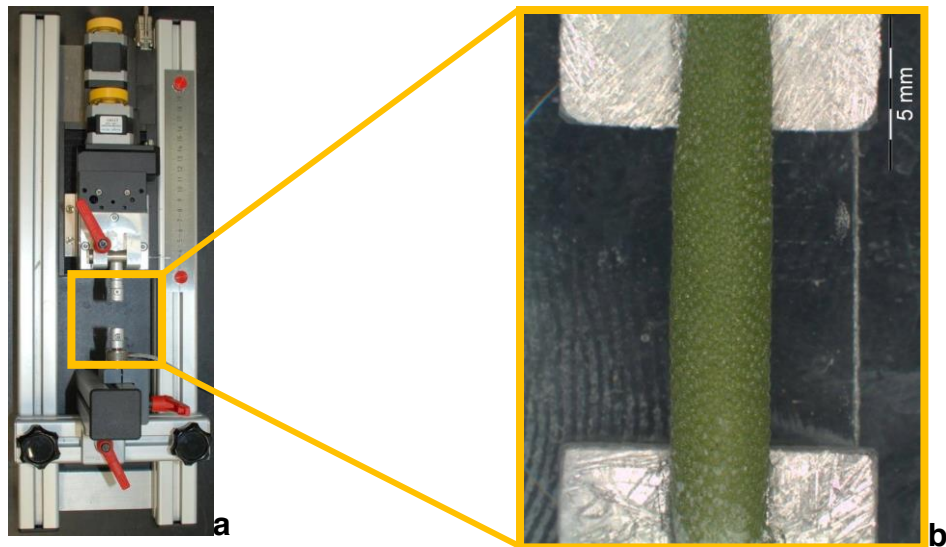


Figure 2: (a) Custom-made experimental set-up for tensile tests of small samples, (b) detailed view showing an entire leaf of *D. cooperi* glued on the measuring stage.

3. RESULTS AND DISCUSSION

Anatomical analyses —The form of leaf cross-sections in *D. cooperi* range from oval to round, whereas leaf form of *D. ecklonis* is three-cornered. Cross-sections of leaves of both species reveal a centripetal arrangement of five tissue types consisting of an outer layer of epidermis with window cells, a peripheral ring of chlorenchyma, a thin net made of vascular bundles, an inner ring of parenchyma and a strand of vascular bundles in the leaf centre. The vascular tissue consists in part of wide-band tracheids, a specialized type of tracheids that prevent cell collapse under water stress.

Mechanical analyses — Mechanical properties of the entire leaf and of single tissue layers were measured in tensile tests which render the basis for calculating Young's modulus and tensile strength [1,2].

Self-repair mechanisms — After an artificial injury wound sealing takes place by deformation and movement. Two principles are involved: (1) rolling in of the fringes of the lesion within a few minutes, and (2) curvature or contraction of the entire leaf within a time span of up to 90 minutes. Subsequent wound healing leads to a callus formation in the wound region [1,2].

Self-repair efficiency — Significant differences in maximum bending angle can be found at different air humidity. Dynamics of motion can be described by at least two characteristic curve shapes if bending angles are plotted over time [1,2].

Analytical model — An analytical model describing the self-sealing process in *D. cooperi* is developed. Based on geometrical and mechanical data of the entire leaf and its tissue layers the model describes stress-states of intact leaves and self-sealing of wounded leaves with regard to elastic and to visco-elastic behavior [10].

4. CONCLUSION

Quantitative anatomical and mechanical analyses and the development of models of the self-repairing process found in model plants are prerequisites for a successful transfer into innovative biomimetic self-repairing materials. In cases where mainly physical-chemical processes are involved a transfer is especially promising.

ACKNOWLEDGEMENTS

This project is funded by the German Federal Ministry of Education and Research (FKZ 0313778 A).

REFERENCES

- [1] T. Speck, R. Mülhaupt, O. Speck, Self-healing in plants as bio-inspiration for self-repairing polymers, in: W. Binder (Ed.), Self-healing materials, Wiley-VCH, Weinheim, 2013, pp. 69-97.
- [2] T. Speck, G. Bauer, F. Flues, K. Oelker, M. Rampf, A.C. Schüssele, M. v. Tapavicza, J. Bertling, R. Luchsinger, A. Nellesen, A.M. Schmidt, R. Mülhaupt, O. Speck, Bio-inspired self-healing materials, in: P. Fratzl, J.W.C. Dunlop, R. Weinkamer (Eds.), Materials design inspired by nature: function through inner architecture, RSC Smart Materials No. 4, The Royal Chemical Society, London, 2013, pp. 359-389.
- [3] T. Speck, R. Luchsinger, S. Busch, M. Rüggeberg, O. Speck, Self-healing processes in nature and engineering: self-repairing biomimetic membranes for pneumatic structures. In: C.A. Brebbia (Ed.), Design and Nature III, WIT Press, Southampton, 2006, pp. 105-114.
- [4] M. Rampf, O. Speck, T. Speck, R. H. Luchsinger, Investigation of a fast mechanical self-repair mechanism for inflatable structures, International Journal of Engineering Science, 63 (2013) 61-70.
- [5] M. Rampf, O. Speck, T. Speck, R. H. Luchsinger, Structural and mechanical properties of flexible polyurethane foams cured under pressure, Journal of Cellular Plastics, 48 (2012) 49- 65.
- [6] M. Rampf, O. Speck, T. Speck, R. H. Luchsinger, Self-repairing membranes for inflatable structures inspired by a rapid wound sealing process of climbing plants, Journal of Bionic Engineering, 8 (2011) 242-250.
- [7] G. Bauer, T. Speck, Restoration of tensile strength in bark samples of *Ficus benjamina* due to coagulation of latex during fast self-healing of fissures, Annals of Botany, 109 (2012) 807-811.
- [8] A. Nellesen, M. von Tapavicza, J. Bertling, A. Schmidt, G. Bauer, T. Speck, Pflanzliche Selbstheilung als Vorbild für selbstreparierende Elastomerwerkstoffe, GAK — Gummi, Fasern, Kunststoffe 64/8 (2011), 472-475.
- [9] A.C. Schüssele, F. Nübling, Y. Thomann, O. Carstensen, G. Bauer, T. Speck, R. Mülhaupt, Self-healing rubbers based on NBR blends with hyperbranched polyethylenimines, Macromolecular Materials and Engineering 297 (2012) 411-419.
- [11] W. Konrad F. Flues, F. Schmich, T. Speck, O. Speck, An analytic model of the self-sealing mechanism of the succulent plant *Delosperma cooperi*, Journal of Theoretical Biology (submitted).

PROTEIN METAL COMPLEXES AS REVERSIBLE SACRIFICIAL BONDS IN SELF-HEALING BIOPOLYMERS

C.N.Z. Schmitt¹, Y. Politi¹, P. Fratzl¹ and M.J. Harrington¹

¹ Max Planck Institute of Colloids and Interfaces, Department of Biomaterials, 14424 Potsdam, Germany – e-mail: clemens.schmitt@mpikg.mpg.de, yael.politi@mpikg.mpg.de, peter.fratzl@mpikg.mpg.de, matt.harrington@mpikg.mpg.de

Keywords: biomaterials, self-healing, metal coordination, Raman, EXAFS

ABSTRACT

Protein-metal coordination complexes often play an active role in the mechanisms of enzymatic catalysis, as well as signal transduction, gas transport, and hormones. Recent investigations reveal that these complexes can also act as load-bearing bonds in biological materials such as the jaws of Nereis worms[1] and mussel byssal threads.² Byssal threads are protein fibers that mussels use to attach to substrates at the seashore. These threads dissipate large amounts of mechanical energy by extending up to ~100% of their initial length and subsequently self-healing to regain initial mechanical properties. Complexes between histidine residues in thread proteins and transition metal ions have been suggested as suitable candidates for reversible sacrificial bonds for this self-healing behavior [2]. However, the existence of histidine-metal coordination in mussel byssal threads and their role in thread mechanics remains to be substantiated in situ.

In this study we combine in-situ Raman spectroscopy and X-ray absorption spectroscopy (XAS) to probe the coordination environment of zinc in *Mytilus californianus* byssal threads during stretching and subsequent healing. Analysis of the extended X-ray absorption fine structure (EXAFS) shows stress-induced perturbations in the coordination environment of zinc and recovery to near initial coordination geometry after healing. While EXAFS sheds light on the species of the nearest neighboring atoms of zinc and the coordination geometry, Raman spectroscopy investigates transitions in histidine vibration modes due to binding of metal ions such as zinc. The combination of both in-situ techniques provides important insights into the role of histidine-zinc coordination in mussel byssal thread mechanics and healing behavior.

Extracted biochemical concepts from the byssal threads have already inspired the development of metallopolymeric hydrogels exhibiting self-repair behavior [3].

REFERENCES

- [1] C.C. Broomell, M.A. Mattoni, F.W. Zok, Critical role of zinc in hardening of Nereis jaws, *The Journal of Experimental Biology* 209 (2006) 3219-3225.
- [2] M.J. Harrington, H.S. Gupta, P. Fratzl, J.H. Waite, Collagen insulated from tensile damage by domains that unfold reversibly: In situ X-ray investigation, *Journal of Structural Biology* 167 (2009) 47-54.
- [3] D.E. Fullenkamp, L. He, D.G. Barrett, W.R. Burghardt, P.B.D. Messersmith, Mussel-inspired histidine-based transient network metal coordination hydrogels, *Macromolecules* 46 (2013) 1167-1174.

SEMI-CRYSTALLINE FRAMEWORK PROVIDES ELASTIC RECOVERY IN SELF-HEALING BIOLOGICAL FIBERS

S. Krauss^{1,2}, H. Metzger¹, P. Fratzl¹ and M. J. Harrington¹

¹ Max Planck Institute of Colloids and Interfaces, Dept. of Biomaterials, Research Campus Golm 14424 Potsdam, Germany – e-mail: stefanie.krauss@mpikg.mpg.de, hartmut.metzger@mpik.mpg.de, peter.fratzl@mpikg.mpg.de, matt.harrington@mpikg.mpg.de

² BAM Federal Institute of Materials Research and Testing, Division 5.4 - Ceramic Processing and Biomaterials, Unter den Eichen 44-46 D-12203 Berlin – e-mail: stefanie.krauss@bam.de

Keywords: bio-inspiration, metal coordination, SAXS, molecular healing

ABSTRACT

Supramolecular polymers based on reversible metal coordination cross-linking have recently shown promise as self-healing materials. However, these materials are for most part entirely unstructured. In contrast, nature's self-healing metallopolymers exploit anisotropic and hierarchical arrangements of molecular building blocks to enhance mechanical properties and increase healing efficacy. Mussel byssal threads, for example, are tough fibrous biopolymers with the ability to autonomously and intrinsically heal following damage. Healing behavior involves molecular repair of reversible metal-protein complexes embedded in extensible protein domains. Here, we present in situ X-ray diffraction data suggesting that the spatial organization of these cross-links strongly influences the mechanics and healing behavior of byssal threads.

X-ray diffraction of native threads reveals a highly organized semi-crystalline framework of protein building blocks with long-range axial and lateral order. When threads are stretched past mechanical yield, the framework deforms completely due to the rupture of sacrificial protein-metal cross-links and unfolding of hidden protein length. The semi-crystalline protein framework recovers elastically immediately following unloading; however, mechanical healing requires longer time-scales, suggesting that ruptured bonds are slower to reform. In light of these observations, we propose a two-stage molecular repair mechanism in which elastic recovery of the protein lattice is a prerequisite for reformation of reversible metal cross-links, presumably by bringing binding partners back into spatial register following damage. This mechanism allows not only precise damage localization at the molecular level, but a recoil mechanism for reuniting sacrificial bonds. Our results suggest that nanoscale order should, perhaps, be a principal design consideration for the next-generation of self-healing polymers.

SESSION 4 – SELF-HEALING CEMENTITIOUS MATERIALS

NON-DESTRUCTIVE TESTING TECHNIQUES FOR THE OBSERVATION OF HEALING EFFECTS IN CEMENTITIOUS MATERIALS – AN INTRODUCTION

C. U. Grosse ¹, K. Van Tittelboom ² and N. De Belie ²

¹ Chair of Non-destructive Testing, Technische Universität München, Baumbachstr. 7, 81245 München, Germany – e-mail: grosse@tum.de

² Magnel Laboratory for Concrete Research, Ghent University, Technologiepark-Zwijnaarde 904, 9052 Ghent, Belgium – e-mail: kim.vantittelboom@ugent.be

Keywords: Non-destructive testing, structural health monitoring, ultrasound, acoustic emission, vibration analysis

ABSTRACT

To develop an appropriate method of self-healing for cementitious materials including the right composition and amount of suitable healing agents it is required to investigate the healing efficiency for certain material mixtures. While some researchers evaluate the regain in compressive strength by means of destructive load tests, this method is obviously second best in particular for field applications. In a large EU project the best candidates among the non-destructive testing methods are investigated to be applied in small and large laboratory experiments as well as at real structures in-situ. The paper is giving an introduction to these techniques and addresses also issues of structural health monitoring used for example to monitor the healing effects on a long term basis and to assess the condition of the structure, where self-healing techniques are applied.

1. INTRODUCTION

Developing healing techniques for cementitious materials the self-healing efficiency should be evaluated to observe the usually time and space dependent healing effect. Up to now, the self-healing efficiency has mostly been evaluated based on the amount of regain in mechanical properties after a certain period. Most of the work done so far in this field is referenced in [1] and in the HealCon proposal (see below). While some researchers evaluate the regain in compressive strength, most evaluate the regain in strength, stiffness and/or energy when performing a tensile or bending test. Regain in mechanical properties is then determined by reloading the previously loaded and thus damaged sample and by comparing the mechanical properties gained during reloading at a certain time, with the original properties.

Non-destructive testing methods have – compared to this – obvious advantages. Granger et al. [2] derived the amount of regain in energy due to autogenous crack healing from acoustic emission measurements. The authors conducted several acoustic emission experiments to evaluate the crack healing efficiency. In the case of Van Tittelboom et al. [1] encapsulated healing agents were provided inside the matrix to obtain autonomous crack healing. With the used equipment it was not possible to prove crack healing by the released polyurethane-based healing agent, although capsule breakage was clearly noted from the captured acoustic events. Also resonance frequency measurements have been proposed to evaluate the healing efficiency [3]. This technique, however, has only been used when autogenous

healing was the mechanism causing crack repair. Little information is available up to now about the regain of permeability properties related to cementitious materials working as a barrier against gases and fluids (air- and liquid-tightness). Nishiwaki et al. [4] reported the use of a funnel which was glued onto the cracked surface to measure the water permeability at low water pressure. In Van Tittelboom et al. [5] regain in water tightness is measured using a test setup based on the low pressure water permeability setup of Aldea et al. [6] and Wang et al.[7]. Measurements at high water pressure were performed by Jonkers [8] to evaluate the efficiency of bacterial self-healing concrete. The air permeability of cracked concrete has been measured by Yang et al. [9].

In this paper we focus on the use of non-destructive testing techniques being applied to cementitious materials investigating either the effect of healing agents over time in laboratory experiments or to determine the healing efficiency in-situ at large structures. Before the individual techniques are addressed we want to describe one of the most developed technique with the potential of both, laboratory and in-situ applications.

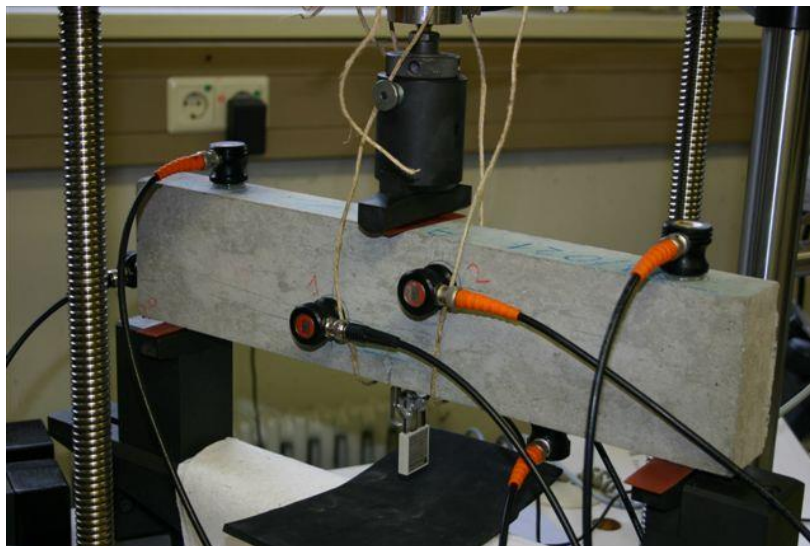


Figure 1: Acoustic emission measurements during a crack width controlled three-point bending experiment at the University of Stuttgart to test self-healing efficiency [1]

2. PREVIOUS ACOUSTIC EMISSION EXPERIMENTS

In a previous study experiments at the University of Stuttgart using acoustic emission (AE) techniques were conducted by Van Tittelboom et al.[1]. Acoustic emissions being released during a three-point bending experiment at concrete beams with polymer capsules as healing agents have been recorded by an 8-channel transient recorder and acoustic emission broadband transducers (fig. 1). The crack formation before and after healing has been recorded continuously during loading and unloading of the specimens and the events were localized in 3D (fig. 2). The signals (AE events) have been divided in arbitrarily chosen classes based on the AE events energy. It was supposed that AE events belonging to the highest classes were caused by capsule breakages. However, further research is needed to confirm this and eventually define more correct energy classes belonging to crack formation in the cementitious matrix, capsule breakage, reopening of previously healed cracks

and so on. Optimization of the captured frequency range should also allow proving crack healing irrespective the type of used healing agent and the sample's size.



Figure 2: Acoustic emission activity recorded before (top) and after (bottom) healing of the specimen shown in fig. 1 [1]

3. NDT METHODS

In a collaborative project called HealCon (Self-healing concrete to create durable and sustainable concrete structures) sponsored by the European Commission in the Seventh Framework Programme healing concepts for concrete structures are investigated. The project started January 2013. It is the aim of HealCon's Workpackage 7 to develop reliable and suitable non-destructive testing and monitoring techniques and combine existing ones to characterize the effects of different self-healing mechanisms in small and full-size specimens and to enhance the variety of non-destructive testing (NDT) techniques since a combination of methods has to be used to get reliable results. Responsible for this workpackage are the Technical University of Munich (first author) and the company SmartMote in Stuttgart, Germany (www.smartmote.de).

AE techniques alone will certainly not be sufficient. The range of applications from small to larger lab scale tests and up to real constructions requires different NDT approaches making the selection and combination of techniques more difficult. There are generally two ways NDT techniques can contribute. One is the observation of healing mechanisms and successes during mechanical loading. This will be done in small lab-scale, large lab or in field tests. The other is to assess the condition of the structure, where self-healing is studied. This is important for tests at a larger scale, while for smaller lab tests this is of minor interest since the composition and condition of the specimen is well controlled. In particular this is of interest also to offer real data about material properties for the numerical simulation.

The application of NDT techniques ranging from several centimeters over several meters to large structures with several tens or hundreds of meters will require techniques and measuring devices being capable to cover these scales, providing detailed and reliable data and being applied later in an economically efficient way concerning applications in the field. A first task will be the categorization and description of all potentially suitable non-destructive and monitoring techniques.

The NDT methods that are candidates to be used for monitoring of self-healing are:

- a) Ultrasonic measurements in through-transmission and reflection
- b) Acoustic emission techniques
- c) Active Infrared-Thermography using thermally stimulated Lock-in techniques
- d) Microwave and RADAR techniques
- e) Resonance frequency measurements and modal analysis

Additional techniques are CT scanning, fiber optical measurement systems or displacement field mapping through Moiré fringes or optical image correlation. Measurements of e.g. strain, crack opening, temperature, humidity, electric impedance for salt and moisture determination can be integrated in small wireless sensor networks for long-term monitoring of large structures[10].

The characterization of the specimens or structural components at each scale in regard to their mechanical properties can be done by ultrasound, microwave/Radar and vibration measurements. These methods will deliver information about the elastic moduli, the wave velocities, the permittivity and about other material properties necessary to be determined for numerical simulations. Some of these fundamental values are in addition essential to be determined prior to NDT applications.

Ultrasonic and vibration (modal) analysis methods can further on be applied to characterize the material properties in a more global way. Ultrasound transmission and reflection methods will help to evaluate the healing efficiency by the observation of changes of the velocity (compressional and shear), amplitude and frequency. They can characterize the healing efficiency by investigating changes of e.g. Young's modulus.

Infrared thermography, microwave/RADAR and in particular acoustic emission techniques can deliver detailed data about the healing process. AE techniques can basically be applied in small and larger lab tests to study the occurrence and distribution of micro-fractures during the experiments. Using 3D localization techniques enables for a spatial and time resolution observation of fracture processes. If possible, more sophisticated AE methods can be applied including moment tensor inversion techniques to distinguish between opening and shear fractures [11]. Data about the fracture type can help to separate cracks in the cement matrix from fractures of the tubes. However, AE techniques have limits being applied in the field. Infrared thermography can be used in an active lockin way to observe the healing efficiency by detecting the release of resin. Microwave and RADAR techniques are as well sensitive to fluids and are able to detect released resin in a shallow (microwave) or deeper (RADAR) area underneath the surface of a structure.

Neutron and X-ray radiography can provide useful information about the regain in tightness due to autonomous crack healing. It was proven that both can be used to visualize and discriminate between the capillary water uptake of untreated and autonomously healed cracks. However, a quantitative evaluation of the amount of water uptake was only possible when neutron radiography was used. Filling of the crack with healing agent and release of the agent from the capsules was visualized using X-ray computed tomography [12]. However, in this study polyurethane was

used as encapsulated healing agent and it seemed to be difficult to discriminate between cracks filled with polyurethane and empty cracks (filled with air).

4. MONITORING

Monitoring is usually used as either a repetitive measurement in more or less small time intervals or as a continuous monitoring technique. For a continuous monitoring, AE and vibration analysis techniques are qualified. Some physical quantities (e.g. moisture content, temperature, and strain or crack width) that are related to self-healing investigations can be monitored by sensor nodes measuring more or less continuously [10]. Using such a device usually several different sensors are combined and data processing is done directly in the node.

5. CONCLUSIONS

The above mentioned non-destructive test methods (and certainly some more) have the potential being employed to find out whether self-healing approaches are able to show repeated healing actions. Possibly several non-destructive techniques have to be combined to increase the reliability. Reliability can be further enhanced by the application of verification techniques, among them are radiographic CT scans. However, this is true only for experiments on the laboratory level. In the HealCon project it will be in particular investigated which potential each of the described techniques has to check the efficiency of healing.

ACKNOWLEDGEMENTS

Financial support from the European Commission in the 7th Framework Program for project HealCon NMP3-SL-2012-309451 is gratefully acknowledged as well as the help of all HealCon partners and the colleagues of the University of Stuttgart during the preliminary AE experiments.

REFERENCES

- [1] Van Tittelboom K, De Belie N, Lehmann F, Grosse CU (2012) Acoustic emission analysis for the quantification of autonomous crack healing in concrete. *Construction and Building Materials* 28 (1), pp 333-341.
- [2] Granger S, Loukili A, Pijaudier-Cabot G, Chanvillard G (2007) Experimental characterization of the self-healing of cracks in an ultra high performance cementitious material: Mechanical tests and acoustic emission analysis. *Cement and Concrete Research* 37 (4), pp 519-527.
- [3] Yang Y, Lepech MD, Yang E-H, Li VC (2009) Autogenous healing of engineered cementitious composites under wet-dry cycles. *Cement and Concr.Res.* 39 (5), pp 382-390.
- [4] Nishiwaki T, Leite JPdB, Mihashi H (2004) Enhancement in durability of concrete structures with use of high-performance fibre reinforced cementitious composites. 4th International Conference on Concrete under Severe Conditions: Environment & Loading, pp 1524-1531.
- [5] Van Tittelboom K, De Belie N (2010a) Self-healing concrete: suitability of different healing agents. *International Journal of 3R's* 1 (1), pp 12-21.
- [6] Aldea C-M, Ghandehari M, Shah SP, Karr A (2000) Combined effect of cracking and water permeability of concrete. Paper presented at the 14th Engineering Mechanics Conference, Austin, Texas, 21-24 Mai 2000.

- [7] Wang K, Jansen DC, Shah SP, Karr AF (1997) Permeability study of cracked concrete. *Cement and Concrete Research* 27 (3), pp 381-393.
- [8] Jonkers HM (2011) Bacteria-based self-healing concrete. *Heron* 56 (1/2), pp 1-12.
- [9] Yang Z, Hollar J, He X, Shi X (2011) A self-healing cementitious composite using oil core/silica gel shell microcapsules. *Cement and Concrete Composites* 33 (4), pp 506-512.
- [10] Grosse CU, Glaser SD, Krüger M: *Initial development of wireless acoustic emission sensor nodes for civil infrastructure state monitoring*. *J. of Smart Structures & Systems* 6 (2010), No. 3, 197-209.
- [11] Grosse CU, Ohtsu M (Eds.): *Acoustic Emission Testing in Engineering - Basics and Applications*. Springer publ., Heidelberg (2008), ISBN: 978-3-540-69895-1, 404 p.
- [12] Van Tittelboom K, De Belie N, Van Loo D, Jacobs P (2011) Self-healing efficiency of cementitious materials containing tubular capsules filled with healing agent. *Cement and Concrete Composites* 33 (4), pp 497-505.

INTERACTION BETWEEN MICROCAPSULES AND CEMENTITIOUS MATRIX AFTER CRACKING IN A SELF-HEALING SYSTEM

X. Wang¹, F. Xing¹, M. Zhang¹, N. Han¹, and Z. Qian²

¹ Guangdong Provincial Key Laboratory of Durability for Marine Civil Engineering; Shenzhen Durability Centre for Civil Engineering; College of Civil Engineering, Shenzhen University, Shenzhen, P.R. China – e-mail: xingf@szu.edu.cn

² Faculty of Civil Engineering and GeoSciences, Delft University of Technology, Delft, The Netherlands

Keywords: self-healing concrete, organic microcapsules, interaction, crack, debonding.

ABSTRACT

A new type of self-healing cementitious composites by using organic microcapsules is designed in Guangdong Key Laboratory of Durability for Coastal Civil Engineering, Shenzhen University. For the organic microcapsules, the shell material is urea formaldehyde (UF), and the core healing agent is Epoxy.

The effect of organic microcapsules on mechanical behaviors of the composite specimens and the interaction between an organic microcapsule and an approaching crack is investigated in this study. The mechanical behaviors of bending and compression strengths for mortar specimens are tested. The results show that the strength may increase with a small amount of microcapsules and then decrease with increasing of microcapsules.

The FEM numerical simulation is carried out to study the interaction between a crack and a microcapsule in the concrete matrix. It is known that there exist two possibilities when a crack approaches a microcapsule, the microcapsule is ruptured or debonded from the matrix. The self-healing function is based on the rupture of microcapsules. Thus determination of judgment criterion (The physical trigger mechanism-cracking) that under what condition a microcapsule ruptures is necessary. For simplicity, a two-dimensional plane square area is considered, in which the side length is 1 cm. A microcapsule of radius 0.1mm is located at the center of the area. Left hand side is a line crack. The interface between the microcapsule and the mortar matrix, as well as the bonding behavior of the microcapsule shell wall is modeled using the cohesive traction-separation constitutive relationship. The actual parameters of the materials may lead to rupture or debonding of a microcapsule. Through numerical simulation, the criterion of the possible failure pattern for a microcapsule is obtained in terms of the intensity of microcapsule wall, the intensity of the interface, thickness of the microcapsule wall, location of the crack, and the microcapsule radius.

1. INTRODUCTION

It is known that crack formation is prone to present in concrete structures due to its low tensile strength, which may lead to deterioration and durability problem, and may also affect its serviceability. To prevent such deterioration, a self-healing strategy has been being developed in these years. van Breugel [1] summarized the research history of self-healing phenomena in cementitious materials. Wu et al [2], and Mihashi and Nishiwaki [3] present a review on self-healing in cementitious materials and engineered cementitious composite as a self-healing material.

Though there has been classification in the review papers, from the point of view of the authors, at present, there are two ways to achieve self-healing function for concrete structures. One is based on material level, such as making use of bacteria, microcapsules or expansive agents and mineral admixtures. Usually at this level, the self-healing is in passive way. That is, mix the healing agent uniform distributed into the concrete matrix and let it be. When a crack propagates to meet the healing agent, it will start to function and fill the crack faces. The other way to achieve self-healing is based on structural level, such as using of hollow fibers or shape memory material fibers et al. In this way, structural or location design is needed, independent or alliance sensor may also be arranged, the self-healing can be in both active and passive modes. In this study, a self-healing system of mortar is developed using organic microcapsules incorporating healing agent.

2. EXPERIMENTS

Standard prismatic mortar specimens with dimensions of 40 mm × 40 mm × 160 are prepared for the tests. To investigate the self-healing effect on the strength recovering rate, the experiments are designed for three factors: W/C, amount of organic microcapsules, preloading rate, in which preloading applied to the specimens is to obtain initial damage for investigating the self-healing phenomenon. The reference groups are tested to obtain the reference strengths, on which preloading rates are determined. In the experiments, 3 levels are considered for each factor, i.e. W/C: 0.45, 0.50, and 0.55; amount of microcapsules: 0%, 3% and 6%; preloading rate: 30%, 50% and 70%. An orthogonal test plan is set up and carried out to investigate the strength recovering rate due to self-healing. The strength recovering rate is defined by

$$\text{Recovering rate} = \frac{\text{strength after healing}}{\text{original strength}} \times 100\% \quad (1)$$

where the original strength denotes the specimen strength at 28 days, the strength after healing is obtained in the following steps: first, apply the prescribed preloading to the specimen at 28 days; then, leave the specimen curing for 3 days; finally, test the strength.

A plan of $L_9(3^4)$ array is used [4], in which column 4 is used for error analysis. The reliability of the test results and the role of each factor have been investigated by using variance analysis. The results show that the amount of microcapsules is the control factor, whereas W/C is the weakest one.

The curves of Intuitive analysis are given in Figure 1 for both bending and compressive tests. The horizontal axis represents different levels for corresponding factors, while the vertical axis denotes the average recovering rate K_{ij} .

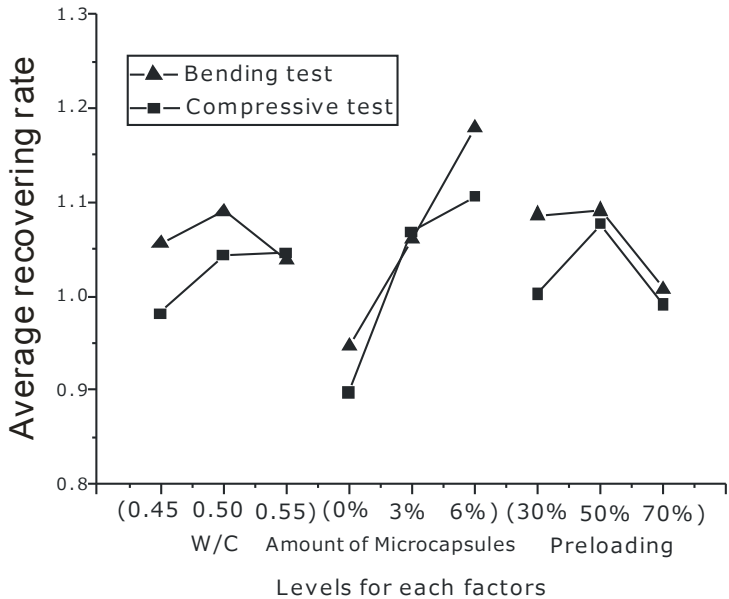


Figure 1: Relationship between the factors and strength recovering rate

3. NUMERICAL STUDY

It is known that there exist two possibilities when a crack approaches a microcapsule, the microcapsule is ruptured or debonded from the matrix. The self-healing function is based on the rupture of microcapsules. Thus determination of criterion that under what condition a microcapsule ruptures is necessary. In this study, a numerical model, as depicted in Figure 2, is setup to investigate this condition using Abaqus [5].

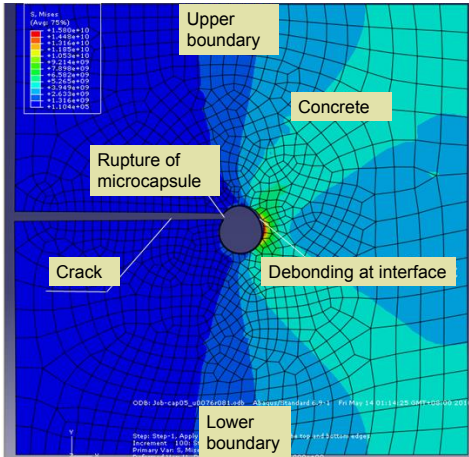


Figure 2: Computing model for a crack approaching a microcapsule

From the limiting status between a microcapsule rupture and debonding, a function is defined as follows:

$$Q = \frac{\sigma_c}{\sigma_D} - \frac{K_C}{K_D} \quad \left\{ \begin{array}{l} >0 \text{ Microcapsule rupture} \\ <0 \text{ Microcapsule debonding} \\ =0 \text{ limiting state} \end{array} \right. \quad (2)$$

where σ_c , σ_D are the effective stresses at microcapsule wall and the interface between the microcapsule and concrete matrix, respectively. K_C , K_D are the corresponding strengths. Then the criterion for a capsule rupturing or debonding can be expressed as in three normalized parameters t/R , h/R , and K_C/K_D :

$$Q = F\left(\frac{t}{R}, \frac{h}{R}\right) - \frac{K_C}{K_D} \quad (3)$$

where R and t represent the outer radius and the thickness of the microcapsule, respectively; h denotes the height coordinate of the crack. Using this model, varying t/R and h/R , forty points on the limiting surface are obtained. Then the following polynomial of 4th power is obtained by regression

$$\begin{aligned} Q &= F\left(\frac{t}{R}, \frac{h}{R}\right) - \frac{K_C}{K_D} \\ &= 110.8 + 539.5\left(\frac{h}{R}\right) - 5438\left(\frac{t}{R}\right) - 1774\left(\frac{h}{R}\right)^2 - 1823\left(\frac{h}{R}\right)\left(\frac{t}{R}\right) + 159900\left(\frac{t}{R}\right)^2 + 1701\left(\frac{h}{R}\right)^3 + \\ &26810\left(\frac{h}{R}\right)^2\left(\frac{t}{R}\right) - 249100\left(\frac{h}{R}\right)\left(\frac{t}{R}\right)^2 - 1296000\left(\frac{t}{R}\right)^3 - 419.8\left(\frac{t}{R}\right)^4 - 23770\left(\frac{h}{R}\right)^3\left(\frac{t}{R}\right) + 116000\left(\frac{h}{R}\right)^2\left(\frac{t}{R}\right)^2 \\ &+ 957100\left(\frac{h}{R}\right)\left(\frac{t}{R}\right)^3 + 3252000\left(\frac{t}{R}\right)^4 - \frac{K_C}{K_D} \end{aligned} \quad (4)$$

This is the criterion which means that, a point under the surface means $Q > 0$, corresponds to that a microcapsule ruptures, otherwise, the microcapsule is debonded. With this criterion, we can judge a microcapsule behavior using the parameters without need of simulation.

ACKNOWLEDGEMENTS

Financial support from the NSFC (Project No. 51120185002; No. 51078238, No. 50925829) is gratefully acknowledged.

REFERENCES

- [1] K Van Breugel, Is there a market for self-healing cement-based materials, Proceedings of the first international conference on self-healing materials, Noordwijk aan zee, the Netherland, 2007.
- [2] M. Wu, B. Johannesson, and M. Geiker, A review: Self-healing in cementitious materials and engineered cementitious composite as a self-healing material. *Construction and Building Materials*, 28 (2012) 571–583.
- [3] H. Mihashi, and T. Nishiwaki, Development of engineered self-healing and self-repairing concrete-state-of-the-art report, *Journal of Advanced Concrete Technology*, 10 (2012) 170-184.
- [4] Y. Cheng, Engineering experiment design method, Wuhan University of Technology Publisher, China, 2010.
- [5] ABAQUS/Standard User's Manual, ver. 6.9, Simulia, 2009.

IMPROVEMENT OF HARDENED CONCRETE DURABILITY BY NANOSILICA ELECTROMIGRATION

M. Sánchez-Moreno¹, M. C. Alonso¹, I Diaz² and R. González²

¹ *Research Centre on Safety and Durability of Structures and Materials, CSIC, Serrano Galvache 4, 28033, Madrid, Spain - e-mail: mercesanc@ietcc.csic.es, mcalonso@ietcc.csic.es*

² *Faculty of Civil Engineering, Universidad Autónoma de Nuevo León, Cd. Universitaria, San Nicolás de los Garza, N. L. México - e-mail: rhodio@hotmail.com*

Keywords: silica nanoparticles, hardened concrete, electromigration, repair

ABSTRACT

Application of nanotechnology in construction industry is a quite new field with many interesting and promising possibilities. Nanosilica self healing properties, based on the high reactivity of these particles with the calcium components of cement, are of great interest in rehabilitation treatments of hardened concrete. In present work, the application of nanosilica to hardened concrete is proposed as innovative technology to improve the effectiveness of electrochemical repair methods and to increase the durability of rehabilitated structures by sealing the concrete pores.

An accelerated methodology, compatible with the electrochemical repair treatments of concrete, is proposed to introduce nanosilica in hardened concrete by connecting an external electric field. Two different commercial products with SiO₂ of 7 nm and 12 nm in diameter have been analysed. Silica nanoparticles have been transported through a mortar sample under a 12 V electric field. The interaction between the SiO₂ nanoparticles and the concrete have been characterised by different techniques: resistivity measurements, mercury intrusion porosity, scanning electron microscopy.

The results show that the interaction concrete/nanosilica takes place in the first centimetre of concrete cover from the surface of the nanosilica application. A denser microstructure with higher content of capillary pores is obtained after the nanosilica penetration. Also the resistivity of the mortar increases due to the treatment with nanosilica.

1. INTRODUCTION

Nowadays application of nanotechnology to construction industry is one of the research areas with higher possibilities. Nanotechnology can be applied in several circumstances in the construction field, from the fresh state, added as additives to the concrete mix, to the hardened concrete, applied on the surface. Several studies reported with nanoparticles are based on the nano-silica (nano-SiO₂) addition to the fresh mix to improve the performance of concrete. Nano-SiO₂ is highly reactive with calcium hydroxide [1] and is able to act not only as a filler [2], blocking the concrete pores, but also as an activator to promote pozzolanic reaction [3]. In this sense, nano-SiO₂ is expected to be an active sealing with self-healing properties based on the high reactivity of these nanoparticles with the calcium hydroxide of solid phases

of concrete, blocking the transport of aggressive ions or refurbishing damaged or cracked concrete.

Nano-SiO₂ can also be considered in repair treatments in order to improve the performance of the repaired concrete structure. The application of nano-SiO₂ as a sealing in hardened concrete appears as an interesting option to block the pores in hardened concrete decreasing its permeability [4]. Repair of existing structures is nowadays one of the mayor concerns in construction. The trend is to minimize the amount of damaged concrete to be replaced during the reparation by developing more economic solutions, such as electrochemical repair methods, aiming on the removal of the aggressive agent (realkalisation or chloride removal) [5]. These techniques are based in the connection of an electric field between the reinforcement, acting as a cathode, and an external anode. Although the application of these electrochemical repair methodologies has already been standardized, several uncertainties concerning the long-term efficiency of the treatment remain.

Nowadays, new developments are emerging to improve the long-term performance of electrochemical repair treatments by modifying the procedure of application. The transport of nanoparticles, more particularly nano-SiO₂, through the concrete pores as the final stage of the electrochemical repair treatment is one of the most promising actuations [4, 6-7] hindering the further penetration of aggressive agents. The self-healing properties of the nano-SiO₂, as for instance by reacting with the calcium hydroxide of the cement paste like in a pozzolanic process, will promote the sealing of pores reducing the porosity of the concrete surface.

In this paper, the ability of colloidal silica nanoparticles to transport by electromigration through the concrete is analysed. The migration mechanism and the interaction between the concrete and the nano-SiO₂ have been assessed for two different commercial products.

2. MATERIALS

The study was carried out with mortar samples manufactured with Ordinary Portland Cement (OPC), normalized sand and deionized water. Cylindrical mortar samples of 7.5 cm were manufactured with a 0.5 w/c ratio and a 1:3 cement sand ratio. After 7 days of curing in chamber at 98±2% relative humidity and 21±2 °C of temperature, samples of 1 cm thickness were cut for migration tests. Before testing, mortar samples were saturated by immersion in water for 24 hours under vacuum conditions. Two different commercial colloidal silica suspensions lightly negatively charged were studied: the first one at 30% and the second one at 40% concentration by weight, with a particle size of 7 nm and 12 nm respectively.

3. METHODS

The cell employed in the migration tests is shown in Figure 1. The cell consists of two carbon steel electrodes, each one located to each side of the cell, and connected to a 12 V voltage supply. The mortar sample is located at the centre. The nano-SiO₂ suspension was placed in the compartment connected as cathode (catholyte) in order to promote its behaviour to the anode (anolyte), filled with distilled water. Samples were identified as 30% and 40%. To evaluate the effect of the electric field

on the mortar, a migration test using distilled water in both sides of the cell (sample named RH2O) was also carried out. Migration tests were carried out in 8 days approximately.

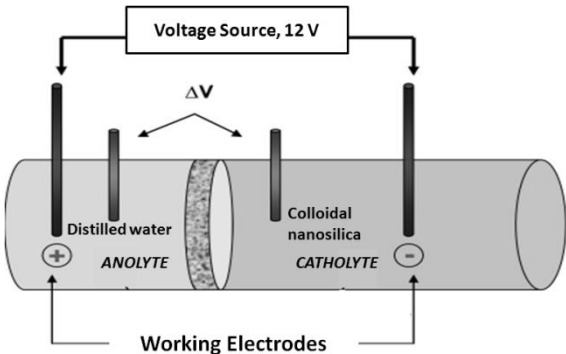
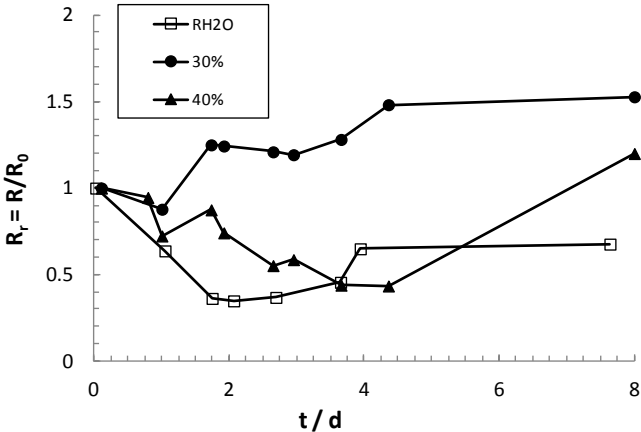


Figure 1: General scheme of the migration cell configuration.

Electrical and chemical measurements were periodically taken during the testing and at the end. Initial and post-treatment resistivity measurements were conducted in the mortar tested samples. After treatment, samples were dried at 40°C and mercury intrusion porosimetry tests, SEM observation and EDX analysis were carried out after 28 days.

4. RESULTS

The migration of colloidal silica nanoparticles to the interior of hardened mortar under the application of an external electric field shall be enhanced from the catholyte (negative pole) to the anolyte (positive pole) due to the negative charge of nanoparticle suspension employed. The mobility of the monodispersed colloidal silica particles may be affected both by the variables of the experimental process and by the electrochemical nature of the solution [8]. During the testing the electric response of the system was monitored by registering the voltage between both sides of the mortar sample and the current in order to estimate the evolution of the resistance values. In Figure 2 the evolution of the relative electric resistance (R_r), referred to the initial value (R_0) has been included. The influence of the type of nano-SiO₂ suspension can be deduced from these results.



Sample	Relative resistivity ($\rho_{final}/\rho_{initial}$)
30%	2.1
40%	2.0

Figure 2: Left - Evolution of the relative electric resistance (R_r) during the treatment at 12 V. Rigth – Relative resistivity in samples after the treatment at 12 V.

The application of the electric field without nano-SiO₂ (RH2O sample) promotes the decrease of the mortar relative resistance probably due to the extraction of different ions to the anolyte and to the catholyte depending of the ionic charge. In the case of nano-SiO₂ penetration, even though the decrease of the relative resistance also occurs during the first days of testing, after a certain period of time an increase of this parameter is registered: after two days of testing in the case of 30% and after 4 days of testing in the case of 40%. This increase of resistance could be associated with a reduction of the porosity in the mortar hindering the transport of ionic species. In this sense, also a significant increase on the mortar resistivity after the treatment with nano-SiO₂ was registered (table of Figure 2-Rigth) if comparing with the initial value of resistivity measured before the migration test.

The mercury intrusion porosimetry results also confirmed the efficiency of the nano-SiO₂ in sealing the mortar pores after an electromigration treatment, as can be deduced from Table 1, where the total porosity values as well as the percentage of pores of different size are resumed for the untreated mortar (R0) and the mortar samples after the different treatments.

Sample	% <0.1	% change	% 0.1-1	% change	% 1-10	% change	% >10	% change	Total poros.
R0	40.89		47.29		7.76		4.19		16.76
RH2O	38.62	-2.26	50.55	+3.26	4.55	-3.21	6.40	+2.21	16.64
30%	47.90	+7.01	33.82	-13.47	11.03	+3.27	7.40	+3.21	14.34
40%	38.02	-2.86	43.59	-3.70	12.81	+5.05	5.71	+1.52	15.06

If the total porosity is considered, only a minor decrease is measured after the treatment with the nano-SiO₂, slightly higher in the 30% sample. Furthermore, a significant decrease of the pores with size between 0.1 – 1 μm is observed when the nano-SiO₂ is transported through the mortar pores, and thus, it is expected that the nano-SiO₂ has been able to enter into the mortar matrix and to flocculate and react with the cement paste matrix.

EDX analysis conducted in cross-section of the study samples shows the reduction of the Ca/Si ration in the negative border of the sample when treated with nano-SiO₂ (values between 1.50 and 1.10 have been measured while a mean value of 1.80 can be considered for a conventional cement paste). Thus, the reaction of nano-SiO₂ with portlandite can be expected, in similar way than reported for studies with addition of nano-SiO₂ in fresh conditions [9], and self-healing properties of nano-SiO₂ added to hardened mortar by electromigration are confirmed.

5. CONCLUSIONS

Electromigration of colloidal silica nanoparticles to the interior of hardened mortar is possible under the action of an electrical field. The composition and nature of the nano-SiO₂ suspension influences the transport of the nanoparticles: it seems to be faster in the case of 30% with smaller size (7nm vs 12 nm). The sealing of capillary pores is expected to occur by reaction of nano-SiO₂ with calcium compounds of the cement paste.

ACKNOWLEDGEMENTS

Authors acknowledge to the Spanish Ministry of Economy and Competiveness for the economic support through project BIA 2011_22760. M. Sánchez also acknowledges her Juan de la Cierva Postdoctoral position (JCI-2011-09572).

REFERENCES

- [1] Y. Quing, Z. Zenen, K. Deyu, C. Rongshen, Influence of nano-SiO₂ addition on properties of hardened cement paste as compared with silica fume, *Construction and Building Materials* 21 (2007) 539-545.
- [2] H. Li, H. Xiao, J. Yuan, J. Ou, Microstructure of cement mortar with nano-particles, *Composites: Part B* 35 (2004) 185-189.
- [3] B.W. Jo, C.H. Kim, G. Tae, J.B. Park, Characteristics of cement mortar with nano-SiO₂ particles, *Construction and Building Materials* 21 (2007) 1351-1355.
- [4] H.E. Cardenas, L.J. Struble, Modeling Electrokinetic Nanoparticle Penetration for Permeability Reduction of Hardened Cement Paste, *J. Materials in Civil Engineering ASCE* 10 (2008) 683-691.
- [5] R. Polder, A. Raharinaivo, V. Pollet, Electrochemical maintenance methods, *Cost Action EU 521 Final Report Corrosion of steel in concrete*, Edt. R. Cigna, C. Andrade, U. Nürnberger, R. Polder, R. Weydert and E. Seitz EU, Chapter 3 (2003) 115-145.
- [6] H.E. Cardenas, L.J. Struble, Electrokinetic nanoparticle treatment of hardened cement psate for reduction of permeability, *J. Materials in Civil Engineering ASCE* 8 (2006) 554-560.
- [7] J.S. Ryua, N. Otsuki, Crack closure of reinforced concrete by electrodeposition technique, *Cement and Concrete Research* 32 (2001) 159-164.
- [8] C. Fernandez, M. Sanchez, M.C. Alonso, R. Gonzalez, Sealing of surface cover concrete by electromigration of SiO₂ nanoparticles, *proceedings NICOM 4 : 4th Int. Symp. on Nanotechnology in Construction, Crete (2012)*.
- [9] J.J. Gaitero, I. Campillo, A. Guerrero, Reduction of the calcium leaching rate of cement paste by addition of silica nanoparticles, *Cement and Concrete Research* 38 (2008) 1112-1118.

ATMOSPHERIC METHANE REMOVAL BY METHANE-OXIDIZING BACTERIA IMMOBILIZED ON POROUS BUILDING MATERIALS

G. Ganendra^{1,6}, W. de Muynck^{1,2}, A. Ho¹, S. Hoefman³, P. de Vos^{4,5}, P. Boeckx⁴, W. Verstraete¹, and N. Boon¹

¹ Laboratory of Microbial Ecology and Technology (LabMET), Ghent University, Coupure Links 653, B-9000 Gent, Belgium – e-mail: giovanni.ganendra@ugent.be ; Adrian.Ho@ugent.be ; Nico.Boon@ugent.be; Willy.Verstraete@ugent.be

² Magnel Laboratory for Concrete Research, Ghent University, Technologiepark-Zwijnaarde 904, 9052 Zwijnaarde, Belgium – e-mail: Willem.demuynck@ugent.be

³ Laboratory of Microbiology, Ghent University, K.L. Ledeganckstraat 35, B-9000 Gent, Belgium – e-mail: Sven.hoefman@ugent.be

⁴ Laboratory of Applied Physical Chemistry, Ghent University, Coupure Links 653, B-9000 Gent, Belgium – e-mail: Pascal.Boeckx@ugent.be

⁵ BCCM/LMG Culture Collection, K.L. Ledeganckstraat 35, B-9000 Gent, Belgium – e-mail: Paul.DeVos@ugent.be

⁶ SIM vzw, Technologiepark 935, BE-9052 Zwijnaarde, Belgium

Keywords: Biological methane mitigation, Methane-Oxidizing Bacteria, Building materials

ABSTRACT

Biological treatment using Methane Oxidizing Bacteria (MOB) immobilized on carrier materials is considered as the best solution to mitigate methane emission at low concentrations (e.g., in animal houses). The porosity of the support is one of the most important factors for an efficient removal of methane. In animal houses, building materials having a high porosity may provide a niche for MOB. In this study, we evaluated the methane removal capacity of MOB immobilized on porous building materials.

Six different types of building materials and MOB were chosen for the experiments. Building materials were immersed in an MOB liquid culture ($2 \cdot 10^8$ cells/ml) and after 24 hours the liquid were separated. The methane removal capacity of MOB was investigated by analyzing the evolution of the methane concentration in the headspace of a closed incubator containing the materials at starting concentrations of ~20 % (v/v) and ~50 ppmv.

MOB immobilized on Maastricht limestone and *Ytong* exhibited higher methane removal rates compared to when immobilized in other materials with *M. parvus* NCIMB 11129^T in Maastricht limestone ($0.1 \text{ mg CH}_4 (\text{m}^3 \text{air h})^{-1}$) exhibited the highest rate at ~50 ppmv and *M. trichosporium* NCIMB 11131^T in Maastricht limestone ($1451 \text{ mg CH}_4 (\text{m}^3 \text{air h})^{-1}$) at ~20 % (v/v). Both materials exhibited the highest macropores (i.e., pore diameter > 3 μm) volume. Therefore, they were likely to accommodate more bacteria and consequently higher methane removal rate by the MOB. *M. parvus* and *M. trichosporium* were able to remove methane for two months with decreasing activity. From this study it was shown that methane can be efficiently removed from the air by MOB immobilized on building materials.

1. INTRODUCTION

Biological treatment using immobilized Methane Oxidizing Bacteria (MOB) on carrier materials is considered the best solution to mitigate the emission of methane, one of greenhouse gasses, to the atmosphere. The porosity of carrier materials is considered one of the most important factors for a high removal of methane. In animal houses, where methane is emitted from the digestive system of ruminants, building structure comprised of materials having a high porosity may provide a niche for MOB. The objective of this study is to evaluate the methane removal capacity of MOB immobilized on porous building materials

2. MATERIALS

Ytong, Maastricht and Euville limestone were the selected building materials. Six different MOB were also selected: *Methylobacterium alcaliphilum* DSM 19304^T, *Methylobacterium kenyense* DSM 19305^T, *Methylosinus trichosporium* NCIMB 11131^T and *Methylocystis parvus* NCIMB 11129^T, *Methylomonas methanica* 11130^T and an MOB mixed culture. The methane removal capacity of each MOB immobilized in each of the building material was investigated.

3. METHODS

Building material blocks were cut into: 1 cm x 2 cm x 5 cm. Before tested, the porosity of materials was analyzed in triplicate by means of Mercury Intrusion Porosimetry (MIP) method according to Aligizaki, 2006 [1]. Each block was glued on the bottom of a 250 ml schott bottle using epoxy glue and autoclaved. The following procedure was performed under sterile condition except for the mixed cultures. MOB liquid culture (~150 ml) was poured into the schott bottle until the specimen was immersed. The schott bottle was closed and incubated at 28 °C under atmospheric air and at static conditions for 24 hours. The liquid was separated from the specimen afterwards. The schott bottle was sealed with a butyl rubber stopper and screwed with an aperture cap. Experiments were performed to investigate the methane removal capacity of MOB at high (~20% (v/v)) and low (~50 ppmv) methane concentration. Both concentrations were tested to study the potential application of this process (i.e., landfill for high concentration, animal house for low concentration).

Schott bottle containing building material inoculated with bacteria was injected with methane before measurements and incubated at 28 °C under static condition. Gas composition and pressure were measured to calculate the methane concentration over 100 (high concentration) or 200 hours (low concentration) of incubation. Gas composition was measured using a Compact GC (for high concentration) equipped with a Thermal Conductivity Detector and a Trace GC Ultra (for low concentration) equipped with a Flame Ionization Detector. Three types of additional experiments for each building material and methane concentration were performed to confirm the biological nature of the methane removal. These were activity tests using: (1) only building material, (2) sterile medium incorporated building material, and (3) autoclaved bacteria in building material. Each experiment was performed in triplicate.

4. RESULTS

MOB were capable to remove methane from the air when immobilized in each of the building material tested both at high and low concentrations (Table 1). Except *M. kenyense*, MOB exhibited higher methane removal rate in *Ytong* and Maastricht limestone than in Euville limestone at high concentration with *M. trichosporium* in Maastricht limestone being the highest ($1451 \text{ mg CH}_4 (\text{m}^3 \text{ air h})^{-1}$). Lower methane removal rates were exhibited by all MOB at low concentration compared to at high concentration. *M. parvus* in Maastricht limestone exhibited the highest methane removal rate ($0.1 \text{ mg CH}_4 (\text{m}^3 \text{ air h})^{-1}$) at low concentration. No methane removal could be observed from the control series.

Table 1: Methane removal rates ($\text{mg CH}_4 (\text{m}^3 \text{ air h})^{-1}$) of different MOB in different building materials at high and low concentrations. Bold font indicates the highest rate at each concentration.

	<i>M. alcaliphilum</i>	<i>M. kenyense</i>	<i>M. trichosporium</i>	<i>M. parvus</i>	Mixed culture
High concentration					
<i>Ytong</i>	1040	186	109	782	777
Maastricht limestone	1128	116	1451	836	850
Euville limestone	333	128	94	65	79
Low concentration					
<i>Ytong</i>	0.08	0.03	0.01	0.07	0.02
Maastricht limestone	0.05	0.02	0.09	0.10	0.03
Euville limestone	0.06	0.02	0.03	0.02	0.06

Among all building materials tested, *Ytong* and Maastricht limestone exhibited the highest macropores volume (i.e., pore with diameter $> 3 \mu\text{m}$) (red box in Figure 1). When incorporated inside building materials, higher amount of MOB are likely to reside within the material with higher macropores volume. With higher amount of MOB likely to be incorporated inside *Ytong* and Maastricht limestone, higher methane removal rates were exhibited by MOB in these materials (Table 1).

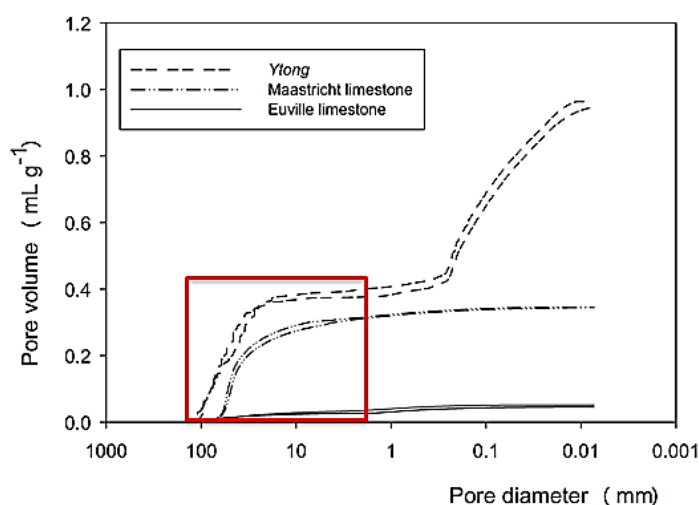


Figure 1: Pore size distribution of building materials from MIP analysis. The box indicates the area in which MOB are likely to reside inside the materials.

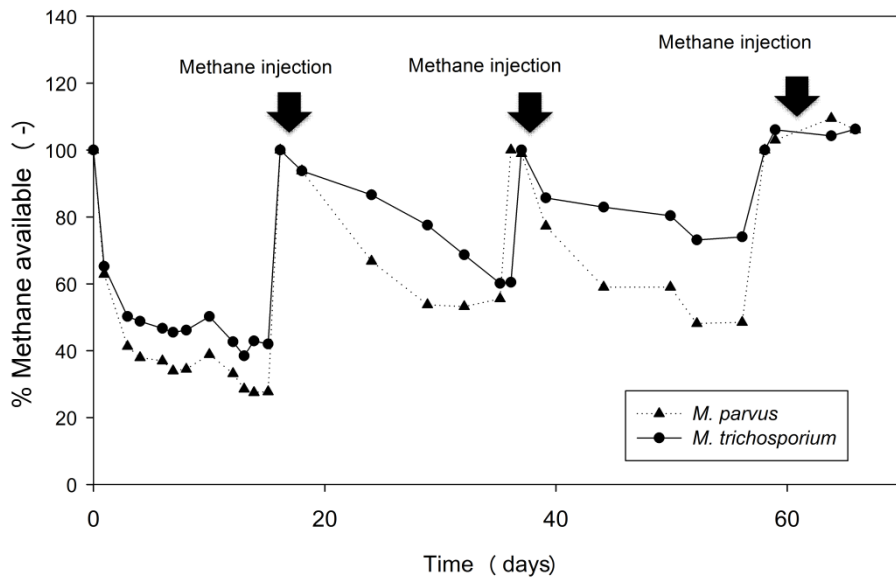


Figure 2: Period of methane removal by *M. trichosporium* and *M. parvus* in Maastricht limestone at low concentration

M. trichosporium and *M. parvus* could remove methane for approximately two months before they lost their methane removal capacity (Figure 2). After initial methane removal, additional methane was injected to the incubator. Both MOB could remove methane with decreasing rate after the first and second methane addition. After the third methane addition, no methane removal could be observed.

5. CONCLUSIONS

MOB could remove methane when immobilized on building materials at both high (~20 % (v/v)) and low (~50 ppmv) concentrations. MOB had higher methane removal when incorporated in building material with higher proportion of macropores volume. *M. trichosporium* and *M. parvus* could maintain their methane removal capacity for approximately two months with decreasing activity

ACKNOWLEDGEMENTS

The project is funded by SIM-SHE SECEMIN project (SIM 2009-1) and the Geconcerteerde Onderzoeksactie (GOA) of Ghent University (BOF09/GOA/005)

REFERENCES

[1] K. K. Aligizaki, Pore structure of cement-based materials: Testing, Interpretation, and Requirements, Taylor & Francis, London, 2006.

POSSIBILITY OF SELF-HEALING BY USING CAPSULES AND VASCULAR SYSTEM TO PROVIDE WATER IN CEMENTITIOUS MATERIALS

H. Huang¹, G. Ye¹

¹ *Microlab, Faculty of Civil Engineering and Geosciences, Delft university of Technology, the Netherland – e-mail: haoliang.huang@tudelft.nl; G.ye@tudelft.nl*

Keywords: self-healing, capsules, vascular system, cementitious materials

ABSTRACT

Since self-healing of cracks is able to improve the durability of concrete structures, it has attracted much attention in the recent years. As known, in concrete matrix there are large amounts of cement grains remaining unhydrated, particularly in high performance concrete. Further hydration of these unhydrated cement grains has potential to heal cracks when additional water is available.

By now, using capsules or vascular system are the main approaches to supply liquid healing agents inside the materials for self-healing. However, it is still uncertain about the possibility of these two approaches for the supply of water for self-healing in concrete. For this question, self-healing in concrete by using capsules or vascular system to provide water was investigated. Self-healing triggered by water was simulated and consequently, the filling fraction of a crack as a function of healing time was calculated. Moreover, the probability of the crack hitting capsules was calculated as well. Based on this information, the possibility of self-healing by using capsules to provide water was determined. Meanwhile, in the case of using vascular system, ultrasonic pulse velocity measurements were carried out to evaluate the self-healing efficiency in concrete.

From the results, it was found that using capsules to supply water for self-healing has very low efficiency. In comparison, the recovery of ultrasonic pulse velocity through the cracked sample can achieve 80% after supplying water for self-healing for 330 hours by vascular system. Thereby, using vascular system to supply water for self-healing is more feasible than using capsules.

1. INTRODUCTION

It is well known that there are large amounts of cement grains remaining unhydrated in concrete matrix, particularly in high performance concrete. Further hydration of these unhydrated cement grains has potential to heal cracks when additional water is available. By now, using capsules or vascular system are the main approaches to supply liquid healing agents inside the materials for self-healing. However, it is still uncertain about the possibility of these two approaches for supply of water to trigger self-healing in cementitious materials. In this paper, the possibility of self-healing in cementitious materials by using capsules and vascular system to provide water was compared. In previous study [1], the filling fraction of a crack as a function of healing time was determined when the cracked sample was cured in water for self-healing under sealed condition. Moreover, the probability of the crack hitting capsules was

calculated as well [2]. Based on this information, the possibility of self-healing by using capsules to provide water will be determined. For the case of using vascular system, ultrasonic pulse velocity measurements were carried out to evaluate the self-healing in concrete.

2. SELF-HEALING OF CRACKS BY USING CAPSULES

2.1 Amount of water released versus capsule dosage

Since the capsules are randomly dispersed inside the matrix, only some parts of them are ruptured by cracks and thereby only the water in the ruptured capsules can be released into cracks. The amount of water released as a function of capsule dosage was calculated in previous study [2], as present in Figure 1.

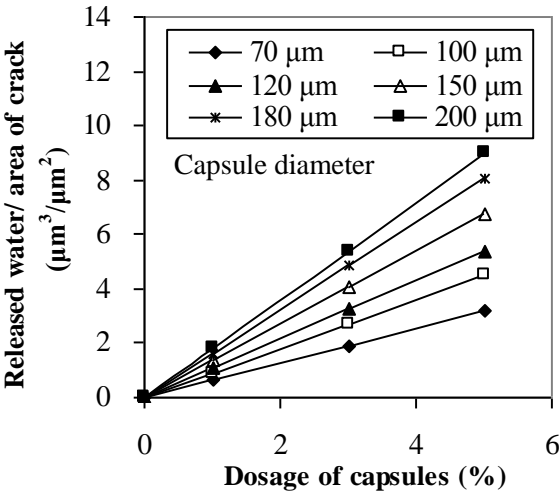


Fig. 1. Amount of water released versus dosage of capsules

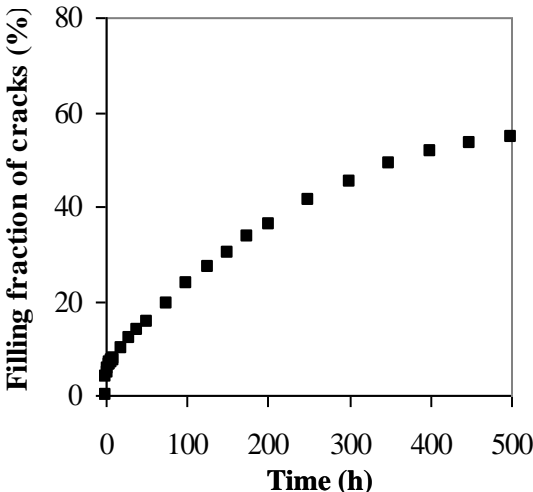


Fig. 2. Filling fraction of cracks versus healing time (10 µm crack)

2.2 Filling fraction of cracks versus capsule dosage

When certain amount of water is released from ruptured capsules, the water in cracks will be absorbed by the bulk cement paste matrix and the amount of water in the crack decreases. Once the water in cracks is consumed, the self-healing stops. Therefore, the period of crack saturation with water is actually the self-healing time. According to the water transport laws in porous media, the crack saturation time versus the amount of water provided was determined, as shown in Figure 2.

In previous study [1], self-healing of cracks due to further hydration as a function of healing time was simulated by a reactive transport model, which was based on ion diffusion and thermodynamic laws. As shown in Figure 3, the filling fraction of cracks by reaction products of self-healing is predicted. By coupling the results in Figure 2 and 3, the filling fraction of cracks versus amount of provided water is determined, which is displayed in Figure 4. As discussed in Section 2.1, the amount of water provided by capsules is governed by the capsule dosage added in matrix. Therefore, with the combination of Figure 1 and 4, the filling fraction of cracks by reaction products as a function of capsule dosage is addressed in Figure 5. As shown in Figure 5, the filling fraction increases with the increase of the dosage and the size of

capsules in cement paste matrix. Only 4% of the crack can be healed when dosage of capsules is 5% and the diameter of capsules is 200 μm . This value is even smaller when the size of capsules decreases. From the results, it can be learned that the efficiency of self-healing by using capsules to provide water is quite low.

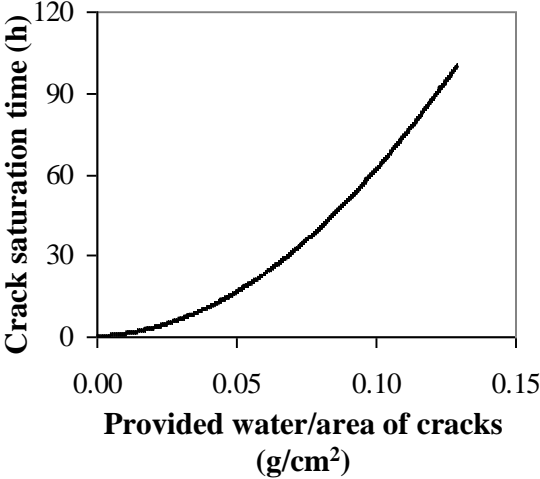


Fig. 3. Crack saturation time versus amount of water provided

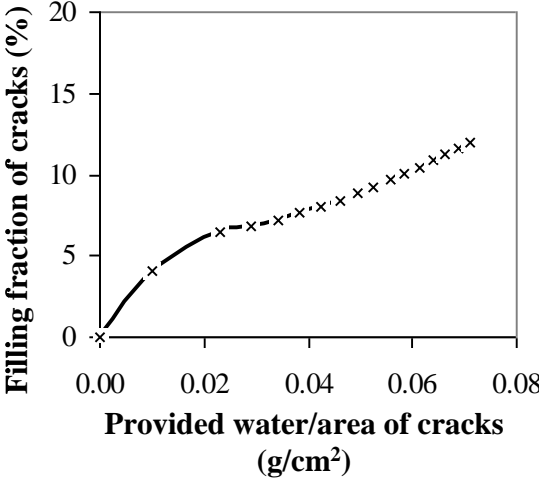


Fig. 4. Filling fraction versus amount of water provided

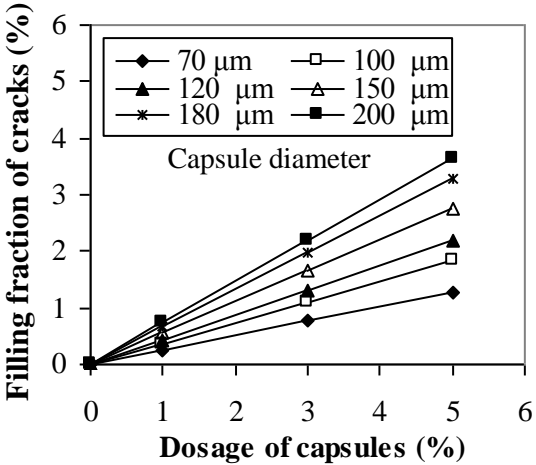


Fig. 5. Filling fraction of cracks due to self-healing by capsules

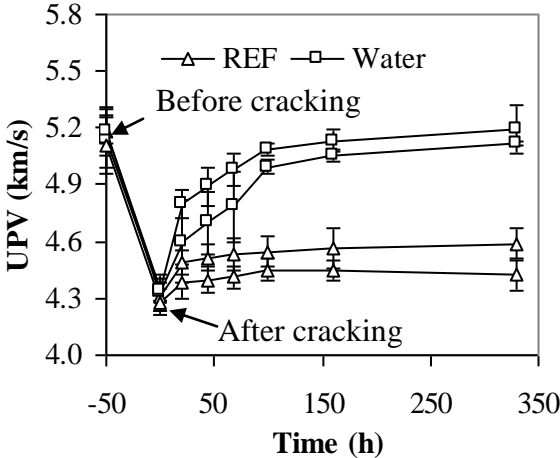


Fig. 6. Ultrasonic pulse velocity before/after self-healing by vascular

3. SELF-HEALING OF CRACKS BY USING VASCULAR SYSTEM

In addition to the capsules, it is also possible to use vascular system to provide healing agents for self-healing from the outside of the materials. In this section, the potential of self-healing by using vascular system to supply water was investigated. Reinforced concrete beams were cast and in each beam a glass tube with outside diameter of 5 mm and the wall thickness of 1 mm was embedded for the supply of water. At the age of 28 days, the initial ultrasonic plus velocity was measured. After that, the specimens were cracked by three-point bending until crack width ranged between 0.8 mm to 1 mm. The ultrasonic plus velocity was measured again after the cracking. Extra water was injected into cracks through the tubes for self-healing. In

comparison, the reference samples were cured without extract water.

Figure 6 shows the ultrasonic pulse velocity of the specimens at different stages: before cracking, after cracking and after healing. From Figure 6 it can be seen that the ultrasonic pulse velocity through the specimens decreases sharply after cracking. The reason is that the transmission of ultrasonic pulse through cracks is much slower than that through the concrete matrix. As being cured for a certain time after cracking, the ultrasonic pulse velocity increases gradually. The recovery of ultrasonic pulse velocity through the sample healed by water is much higher than the reference samples, which reaches almost 80% of the initial value before cracking. From the results, it is found that compared to the method of using capsules, using vascular system to supply water for self-healing is more efficiency.

4. CONCLUSIONS

In this paper, the possibility of self-healing in cementitious materials by using capsules or vascular system to provide water was compared. From the results, it can be learned that the capacity of self-healing by using capsules to provide water is very low. In comparison, the recovery of ultrasonic pulse velocity through the cracked sample can achieve 80% after supplying water for self-healing for 330 hours by vascular system. Thereby, using vascular system to supply water for self-healing is more feasible than using capsules. This principle can be applied when other liquid healing agents are used.

ACKNOWLEDGEMENTS

The authors would like to thank the China Scholarship Council (CSC) for the financial support for this work.

REFERENCES

- [1] Huang, H. and Ye, G. "Characterization and quantification of self-healing behaviors by further hydration in cementitious materials." *Cement and Concrete Research*, under reviewed.
- [2] Huang, H. and Ye, G., (2012). "The effects of capsules on self-healing efficiency in cementitious materials." In: G. Ye, K. van Breugel, W. Sun, and C. Miao, Eds. 2nd international conference on microstructural-related durability of cementitious composites. Amsterdam.

SESSION 5 – SELF-HEALING POLYMERIC MATERIALS

ONE-POT PREPARATION AND EVALUATION OF THERMO-REMENDABLE POLYURETHANES

F. Du Prez¹, G. Rivero², T. Nguyen¹, X. Hillewaere¹, G. Godier³

¹*Polymer Chemistry Research Group, Department of Organic Chemistry, Ghent University, Krijgslaan 281 S4bis, B-9000, Ghent, Belgium – e-mail: Filip.DuPrez@ugent.be*

²*Research Institute of Materials Science and Technology (INTEMA), National University of Mar del Plata, J.B. Justo 4302, 7600 Mar del Plata, Argentina – e-mail: grivero@fi.mdp.edu.ar*

³*Flamac, a division of SIM, Technologiepark 903, 9052 Zwijnaarde, Belgium.*

Keywords: polyurethane, shape memory, self healing, one-pot

ABSTRACT

In this presentation, the study of furan-based thermoset polyurethanes, which were prepared in a one-pot fashion and self-mended under mild temperature conditions, will be given. Diels-Alder thermoreversible covalent bonds were introduced as crosslinkers into a shape-memory polyurethane material, improving thereby the material mechanical properties. When a crack occurs, Diels-Alder bonds will preferentially break, regenerating free furan/maleimide functional groups. The shape memory effect favors the crack closure upon heating, resulting in a reformation of the reversible crosslinking bonds.

The preparation method involves an initial Diels-Alder reaction among a commercial bis-maleimide and a diol with a pendant furan moiety, easily synthesized on large scale. After the incorporation of polycaprolactone (PCL) as shape memory switching segments, the polyurethane formation reaction takes place in the same reaction vessel. Experimental conditions were chosen to optimize the reversibility and shape memory ability of the system. Different compositions were used to properly understand the role and influence of each component in the system.

The hard segment content does not only affect the physical/structural parameters such as crystallinity, toughness and transparency but also the self-healing characteristics in accordance with the resulting crosslinking degrees. Diels-Alder moieties are then proved to be the main responsible factor for the polyurethane thermo-remendability.

Polyurethanes heal at 50°C after mechanical damage induced by either the application of a large tensile deformation or by performing controlled macro/micro scratches. The PCL melting provides enough mobility to recover the shape in a couple of minutes, enabling the progressive Diels-Alder bonding reformation in this same condition. On-line FT-IR monitoring allowed the kinetic description of the system reversibility for numerous cycles. Furthermore, mechanical recovery was accomplished after multiple cycles of bulky deformation. Complete disappearance of microscratches was also achieved. The results were not only confirmed by scanning electron microscopy but also by instrumental recording of the cross-section profiles before and after healing as well as by confocal microscopic mapping.

SELF-HEALING AND MECHANOCROMISM OF DIARYLBIBENZOFURANONE-BASED DYNAMIC COVALENT POLYMERS

H. Otsuka^{1,2}, K. Imato², T. Kanehara², A. Irie², T. Ohishi¹ and A. Takahara^{1,2}

¹ Institute for Materials Chemistry and Engineering, Kyushu University, 744 Motooka, Nishi-ku, Fukuoka 819-0395, Japan – e-mail: otsuka@ms.ifoc.kyushu-u.ac.jp

² Graduate School of Engineering, Kyushu University, 744 Motooka, Nishi-ku, Fukuoka 819-0395, Japan

Keywords: polymer reactions, self-healing, dynamic covalent chemistry, mechanochromism, dynamic covalent polymers

ABSTRACT

Covalent bonds with the ability to reach an equilibrium state between combination and dissociation under certain conditions have been studied, and systematic method for controlling the structures of compounds and polymers based on these reversible covalent bonds has been spotlighted as dynamic covalent chemistry. In the present study, diarylbibenzofuranone (DABBF)-based dynamic covalent polymers were designed with two notable functionalities, self-healing of polymer gels cross-linked by DABBF and mechanochromism of DABBF-containing linear polyurethanes.

Cross-linked polymers with exchangeable dynamic covalent bond at room temperature were synthesized by polyaddition of DABBF-tetraol and tolylene diisocyanate terminated polypropylene glycol. The self-healing property of the DABBF-containing cross-linked polymer gel was investigated under air at room temperature. The gel samples were prepared and cut with a razor blade to expose fresh surfaces. The fresh surfaces were brought together immediately in the absence of external force. The in-contact samples were kept at room temperature under air. After 24 h, self-healing of the contacted samples could be observed and the scars had almost disappeared. Even after manually stretching the sample, no destruction occurred. Tensile tests were also performed to quantitatively evaluate self-healing properties. A recovery of 98 % of the original elongation at breaking was possible over periods of 24 h.

Stimuli-responsive polymers which show color change by mechanical stress were also synthesized and their mechanochromic behavior was investigated. Since the central C-C bonds in DABBF have lower bond dissociation energy, DABBF can reversibly cleave to the corresponding radicals with blue color. We employed DABBF as a mechanochromic unit. DABBF-containing polyurethane films were prepared and their elongation-induced color change was observed.

1. INTRODUCTION

Self-healing polymers attract much attention because they can repair their internal and/or external damage by themselves, thereby extending the lifetime and potential to be applied to many applications. Covalent bonds with the ability to reach an equilibrium state between combination and dissociation under certain conditions have been studied, and systematic method for controlling the structures of

compounds and polymers based on these reversible covalent bonds has been spotlighted as dynamic covalent chemistry [1,2]. Diarylbibenzofuranone (DABBF) derivatives show equilibrium between DABBF and arylbibenzofuranone (ABF) radicals even at room temperature (Figure 1), because the central C-C bonds in DABBF derivatives have lower bond dissociation energy. In the present study, DABBF-based dynamic covalent polymers were designed with two notable functionalities, self-healing of polymer gels cross-linked by DABBF [3] and mechanochromism of DABBF-containing linear polyurethanes.

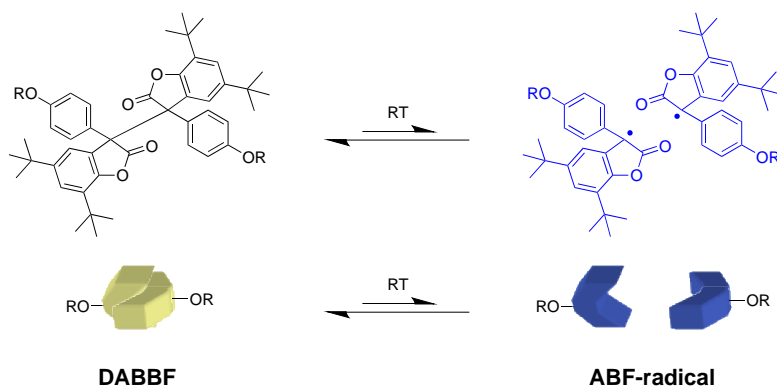


Figure 1: Equilibrium between DABBF and arylbibenzofuranone (ABF) radicals.

2. MATERIALS

As monomers for the synthesis of linear and cross-linked DABBF-based dynamic covalent polymers, we prepared **DABBF-diol** and **DABBF-tetraol** derivatives from 4-hydroxymandelic acid and 2,4-di-*tert*-butylphenol in three steps. As shown in Figure 2, DABBF-containing linear polyurethane (**DABBF-PU**) and cross-linked polymers (**DABBF-XL**) were prepared by polyaddition of **DABBF-tetraol** and a toluene-2,4-diisocyanate terminated poly(propylene glycol) (PPG, $M_n = 2400$), in the presence of di-*n*-butyltin dilaurate (catalyst) in *N,N*-dimethylformamide (DMF) or 1,4-dioxane. PPG was chosen as the main skeleton because of its high solubility and flexibility of its molecular chains and the resulting simplicity in using it in the reaction. In the case of linear polymer, the viscosity of the reaction mixture gradually increased during the course of the reaction. For the preparation of the cross-linking polymer, the fluidity of the reaction mixture decreased and finally gel was formed after 48 h, indicating that polymerization was successful. As a control sample, covalently cross-linked polymer (**BisA-XL**) was prepared from tetrahydric bisphenol A (**BisA-tetraol**) and diisocyanate-terminated PPG in a manner outlined for **DABBF-XL**.

3. METHODS

Self-healing experiment: Gel samples of cross-linked polymers (**DABBF-XL** and **BisA-XL**) were cut and contacted immediately. Healing process was performed in the dark under saturated vapor pressure of DMF at room temperature for different times.

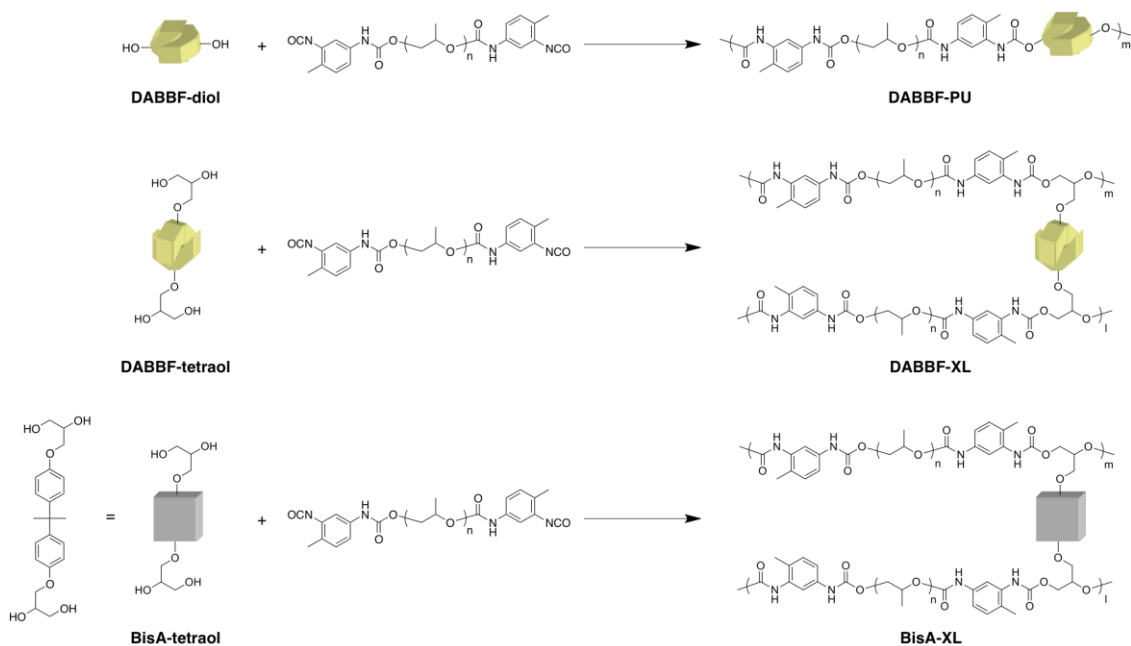


Figure 2: Preparation of DABBF-containing linear polyurethane (**DABBF-PU**) and cross-linked polymer (**DABBF-XL**), and bisphenol A-containing cross-linked polymer (**BisA-XL**).

Tensile tests: Gels of cross-linked polymers (**DABBF-XL** and **BisA-XL**) molded into ISO 37-4 specimens (dumbbell shape, 12 mm × 2 mm × 0.6-1 mm) and fixed at both ends on thin Al plates with glue and adhesion tape. The plates were pulled in tensile tests under air at room temperature by using a Shimadzu EZ graph equipped with a 50 N load cell at crosshead speed of 5 mm/min. The measurements were performed using more than six test pieces each healing times and each waiting times and three of them were chosen. Average values were determined by the three samples.

4. RESULTS AND DISCUSSION

Cross-linked polymers with exchangeable dynamic covalent bonds at room temperature were synthesized by polyaddition of **DABBF-tetraol** and tolylene diisocyanate-terminated PPG. The self-healing property of the **DABBF-XL** gel was investigated under air at room temperature. The gel samples were prepared and cut with a razor blade to expose fresh surfaces. The fresh surfaces were brought together immediately in the absence of external force. The in-contact samples were kept at room temperature under air. After 24 h, self-healing of the contacted samples could be observed and the scars had almost disappeared. Even after manually stretching the sample, no destruction occurred (Figure 3). Tensile tests were also performed to quantitatively evaluate self-healing properties. A recovery of 98 % of the original elongation at breaking was possible over periods of 24 h.

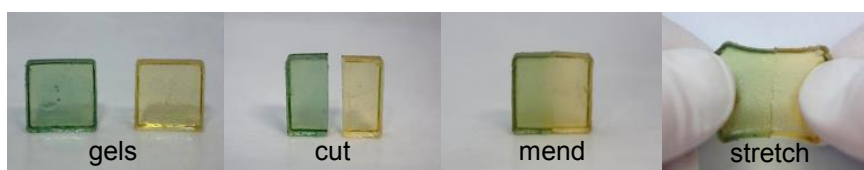


Figure 3: Self-healing behavior of **DABBF-XL** gel.

Stimuli-responsive polymers which show color change by mechanical stress were also synthesized and their mechanochromic behavior was investigated. Since the central C-C bonds in DABBF derivatives have lower bond dissociation energy, DABBF can reversibly cleave to the corresponding radicals with blue color. We employed DABBF as a mechanochromic unit. DABBF-PU films were prepared and their elongation-induced color change was clearly observed (Figure 4).

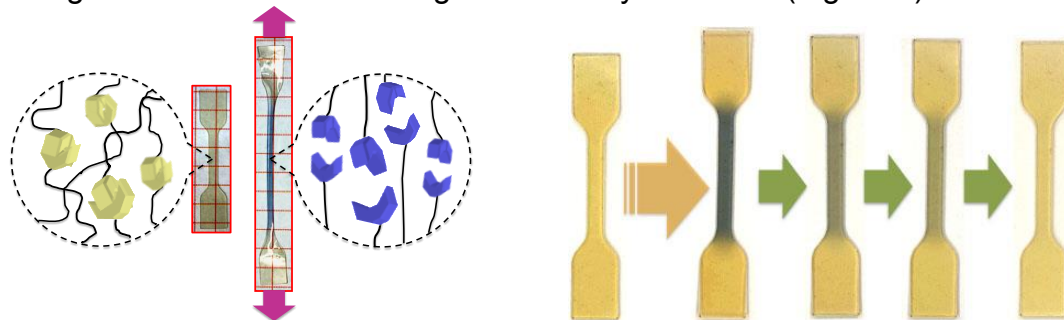


Figure 4: Mechanochromism of a DABBF-PU film.

5. CONCLUSIONS

We have demonstrated the autonomously self-healing nature of covalently cross-linked chemical gels under mild conditions. This system does not require any stimuli. Cross-linked polymers containing a DABBF unit, which is a novel dynamic covalent bond unit, were successfully prepared by polyaddition of diisocyanate compounds and a DABBF cross-linker. The autonomous structural transformation and the macroscopic mending of separated gel pieces under air at room temperature without any stimuli were accomplished by a dynamic covalent approach. Also, we have demonstrated mechanochromism of DABBF-PU.

ACKNOWLEDGEMENT

The authors gratefully acknowledge the financial support of Funding Program (Green Innovation GR077) for Next Generation World-Leading Researchers from Cabinet Office, Government of Japan.

REFERENCES

- [1] Rowan, S. J., Cantrill, S. J., Cousins, G. R. L., Sanders, J. K. M., Stoddart, J. F., *Dynamic Covalent Chemistry*, *Angew. Chem. Int. Ed.* 2002, 41, 898–952.
- [2] Maeda, T., Otsuka, H., Takahara, A., *Dynamic Covalent Polymers: Reorganizable Polymers with Dynamic Covalent Bonds*, *Prog. Polym. Sci.* 2009, 34, 581–604.
- [3] Imato, K., Nishihara, M., Kanehara, T., Amamoto, Y., Takahara, A.; Otsuka, H., *Room Temperature Self-healing Chemical Gels Cross-linked by Diarylbibenzofuranone-based Trigger-free Dynamic Covalent Bonds*, *Angew. Chem. Int. Ed.* 2012, 51, 1138–1142.

FOAMING SELF-HEALING AGENTS

S.I. Rae ¹, I.P. Bond ¹, R.S. Trask ¹, D.F. Wass ²

¹ *Advanced Composites Centre for Innovation and Science (ACCIS), Department of Aerospace Engineering, University of Bristol, University Walk, BS8 1TR, Bristol, UK – email: aesir@bristol.ac.uk; i.p.bond@bristol.ac.uk; r.s.trask@bristol.ac.uk*

² *School of Chemistry, University of Bristol, Cantock's Close, Bristol, UK, BS8 1TS – email: duncan.wass@bristol.ac.uk*

Keywords: self-healing, composites, foam, polymer

ABSTRACT

A new approach to self-healing systems is presented that aims to overcome the inherent drawbacks of conventional liquid resin based healing systems within composites. Finite embedded systems offer limited healing potential for small volume delaminations and as such cannot effectively heal large damage volumes often associated with shear damaged sandwich panel structures or debonding between skin and core. An expanding polymer based approach aims to overcome such limitations. The mechanical and physical properties of a prepared polyepoxide foam are investigated and how the inclusion of a carbon fibre reinforcement within the foam affects processability and performance. The healing efficiency of different polymer foams to heal damaged foam structures is also investigated.

1. INTRODUCTION

Fibre reinforced composites are becoming increasingly more prominent in both military and commercial aircraft structures due to the high specific strength and stiffness properties, low coefficient of thermal expansion and fatigue performance they exhibit compared to conventional metallic materials.¹⁻⁵ However, it is difficult to detect damage on the surface of a composite laminate due to an impact load, due to the absence of a mechanism for plastic deformation.⁵⁻⁷ The upper plies in a laminate stack will recover elastically after an impact event whilst lower plies can delaminate and develop interply cracks. Impact events, as well as static loading and fatigue, can also lead to damage in sandwich panel structures, with foam cores often failing in shear.⁸⁻¹⁰ There has been considerable success with self-healing systems with a substantial amount of research showing that a damaged piece of composite can recover its strength almost to its undamaged state using these systems.¹¹⁻¹⁴ Despite this, the vast majority of research to date has focussed on healing systems within a laminated FRP where cracks are small and the healing function is located nearby. However, it is possible to diversify the application of such self-healing approaches into sandwich structures, where damage distribution and volume are typically greater.^{8, 15, 16} Such a system would mitigate against potential shear damage and subsequent core/skin debonding in loaded sandwich panels.

Establishing a volume increasing self-healing system for a foam sandwich structure requires a new approach to the healing agent chemistry involved. Several factors had to be considered: the resultant post-reaction volume expansion must be rapid to avoid egress from the damaged area; the components must be stable over lengthy storage periods and still react without any retardation; expansion pressure must be

low enough to avoid exacerbating damage present but high enough to fill all voids as a result of the damage; the resulting polymer must be compatible with and adhere to the original structure. The two main classes of polymer investigated were polyurethanes and polyepoxides. Rate of expansion, density, cell size and mechanical properties of the polyurethane foams can be controlled by altering the relative amounts of reactants, blowing agents, surfactants, cross-linkers, catalysts and fillers. The investigation considered two aspects: the mechanical properties of the foams compared to conventional sandwich core polymer materials; the effectiveness of the foam system to act as a self-healing agent.

2. EXPERIMENTAL

Epoxy foams were made using a two part system consisting of a varied bisphenol diglycidyl ether and a varied polyamine hardener mixed in a 1:1 ratio. The foam was cast into a block and allowed to cure at ambient temperature for 5-6 hours before a post-cure overnight at 50°C. Epoxy foams were also cast with 1% wt. chopped carbon fibre distributed throughout the foam. Polyurethane foams were also prepared from two parts. Part A consisted solely of commercially available polymeric isocyanate. Part B contained a blend of polyols (relative amount dependant on functionality of polyol and isocyanate), n-pentane as a blowing agent, surfactant to control cell size and catalyst. Relative amounts of polyol and polymeric isocyanate were calculated based on the assumption that one alcohol group would react with one isocyanate group (in reality a slight excess of isocyanate was used to ensure complete reaction). The viscosity of Part B could be altered by varying the ratio of the polyol blend used; a higher proportion of hydroxyl terminated polybutadiene resulted in a lower viscosity premix and subsequently, a more elastomeric foam produced.

The mechanical properties of the epoxy foams were determined to ascertain their performance as a core material and provide benchmark data for healing efficiency of foaming self-healing agents. Due to the brittle nature of the foam samples, testing in axial tension was difficult due to complexities in gripping the samples and applying a uniformly distributed load. Therefore, measurement of the flexural strength of the foams was undertaken using a 4 point bend approach adapted from ASTM Standard C1161, "Standard Test Method for Flexural Strength of Advanced Ceramics at Ambient Temperature". The support span was set at 105 mm and the loading span at 35 mm. Testing was undertaken using an Instron 3343 single column load frame with a 1KN load cell.

3. RESULTS AND DISCUSSION

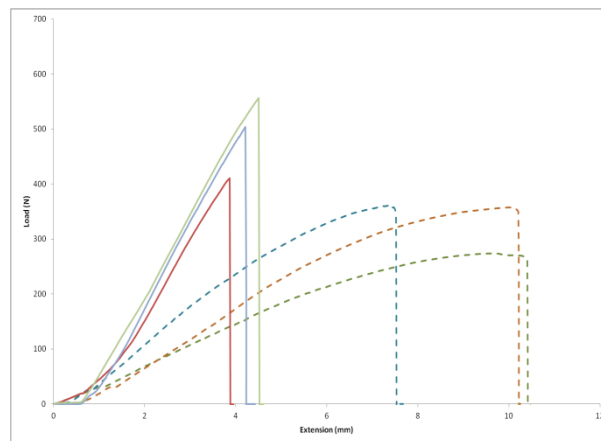


Figure 1: Stiffness comparison- foams with and without carbon fibre

There was typically significant extension with plain epoxy foam before brittle failure occurred at a mean load of $363 (\pm 73)$ N. This corresponds to a mean flexural strength of $3.21 (\pm 0.64)$ MPa. Addition of 1% wt. carbon fibre did not affect expansion of the foam, cure time or final foam structure. Foam samples were much stiffer with less displacement observed before failure when compared to the samples with no carbon fibre added (Fig. 1). Brittle failure occurred at a mean load of $448 (\pm 65)$ N which corresponds to a mean flexural strength of $3.96 (\pm 0.56)$ MPa. On average, the addition of 1% wt. carbon fibre increases the flexural strength of the epoxy foam by 23%.

Exploring the fracture surfaces of samples containing carbon fibre, it was clear that the fibres were distributed evenly throughout the thickness of the foam. On both fracture surfaces, examples could be found of fibre pull-out; holes with diameters closely corresponding to the diameter of the added fibres were observed along with fibres that were protruding from the surface (Fig. 2). We are confident that the inclusion of the fibres, through the failure mechanisms highlighted in the SEM images, are responsible for the increase in flexural strength observed.

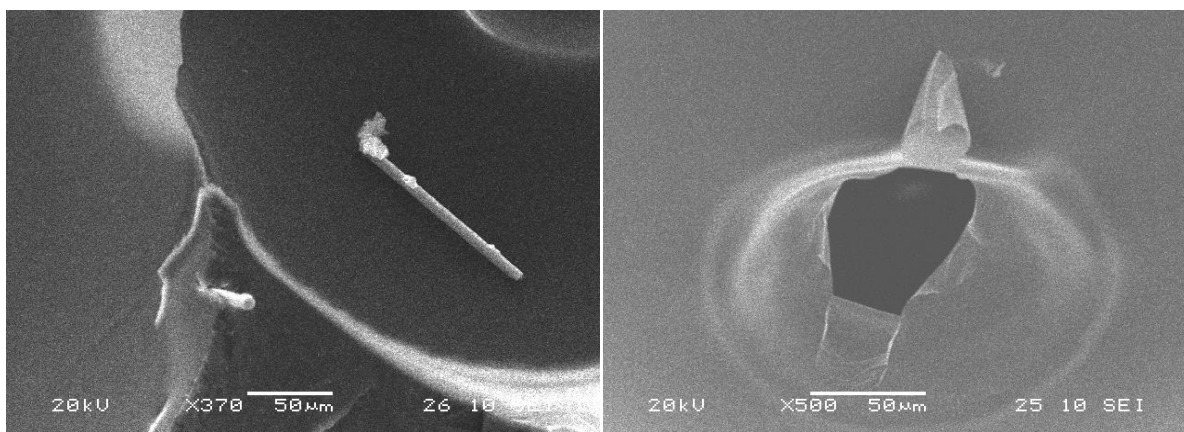


Figure 2: (Left) Carbon fibres exposed on fracture surface of foam. (Right) Example of damage left after flexural testing. Diameter of hole is of the same magnitude as the diameter of the fibres.

Fractured epoxy foam samples were used to investigate self-healing using the epoxy foam itself and a polyurethane foam healing agent. Polyurethanes offer an easier route to self-healing foams due to their lower viscosities and faster foaming/curing times compared to the polyepoxide foam systems. Healing agent was applied to the fracture surfaces of foam samples and allowed to cure before retesting. Samples cured with the polyurethane foam with high proportion of hydroxyl terminated polybutadiene exhibited the lowest average healing efficiency of 59 (± 10)%. These samples also consistently failed along the original fracture surface. Samples healed with the polyurethane with lower hydroxyl terminated polybutadiene content was only marginally more viscous but resulted in a much higher and consistent healing efficiency of 97 (± 5)%. These samples also failed in a different location to the original fracture line, consistently. Using the polyepoxide as a healing agent introduced drawbacks in terms of the higher viscosity and slower foaming/curing times but resulted in the highest average healing efficiency of 108 (± 9)%. Again, the samples cured with polyepoxide failed in a different area to the original fracture surface when re-tested.

4. CONCLUSIONS

The aim of this study was to diversify the application of self-healing systems in composite structures and characterise and develop potential chemical systems to do so. We have shown that it is possible to deliver healing agents that will expand to fill large areas of damage in a foam structure quickly. The addition of discontinuous carbon fibre to the healing agents has shown to increase the final foam properties in terms of its stiffness and flexural strength. We can attribute this effect due to fibre pull-out in the foam during flexural testing as indicated by the SEM images taken of the fracture surfaces. We also tested different foams abilities to heal damaged foam structures and measured high healing efficiencies highlighting the plausibility of diversifying self-healing to include systems in foam core sandwich panel structures.

REFERENCES

- [1] T. H. G. Megson, 2007. Aircraft Structures for Engineering Students. 4th ed. Oxford: Elsevier / Butterworth-Heinemann.
- [2] C. Soutis, Prog. Aerosp. Sci., 2005, 41, 143-151.
- [3] S. Seike, Y. Takao, W. X. Wang and T. Matsubara, Int. J. Fatigue, 2010, 32, 72-81.
- [4] J. P. Casas-Rodriguez, I. A. Ashcroft and V. V. Silberschmidt, Compos. Sci. Technol., 2008, 68, 2663-2670.
- [5] G. J. Appleby-Thomas, P. J. Hazell and G. Dahini, Compos. Struct., 2011, 93, 2619-2627.
- [6] R. O. Ochola, K. Marcus, G. N. Nurick and T. Franz, Compos. Struct., 2004, 63, 455-467.
- [7] C. Hochard, P. A. Aubourg and J. P. Charles, Compos. Sci. Technol., 2001, 61, 221-230.
- [8] J. F. Patrick, N. R. Sottos and S. R. White, Polymer, 2012, 53, 4231-4240.
- [9] A. Manalo, Compos. Struct., 2012 (in press), <http://dx.doi.org/10.1016/j.compstruct.2012.12.010>.
- [10] M. Kampner and J. L. Grenestedt, Compos. Struct., 2008, 85, 139-148.

- [11] B. J. Blaiszik, M. M. Caruso, D. A. Mcllroy, J. S. Moore, S. R. White and N. R. Sottos, *Polymer*, 2009, 50, 990-997.
- [12] M. M. Caruso, B. J. Blaiszik, S. R. White, N. R. Sottos and J. S. Moore, *Adv. Funct. Mater.*, 2008, 18, 1898 - 1904.
- [13] A. R. Hamilton, N. R. Sottos and S. R. White, *Adv. Mater.*, 2010, 22, 5159 - 5163.
- [14] E. N. Brown, S. R. White and N. R. Sottos, *J. Mater. Sci.*, 2004, 39, 1703 - 1710.
- [15] H. R. Williams, R. S. Trask and I. P. Bond, *Compos. Sci. Technol.*, 2008, 68, 3171-3177.
- [16] H. R. Williams, R. S. Trask and I. P. Bond, *Smart Mater. Struct.*, 2007, 16, 1198 - 1207.

ENCAPSULATION OF AN AMINE USING MICROFLUIDICS

P. W. Chen¹, S. Neuser², V. Michaud², A. R. Studart¹

¹ *Complex Materials, Department of Materials, ETH Zürich, Wolfgang-Pauli-Str. 10, 8093 Zürich, Switzerland – e-mail: philipp.chen@mat.ethz.ch; andre.studart@mat.ethz.ch*

² *Laboratoire de Technologie des Composites et Polymères, Institut des Matériaux, Ecole Polytechnique Fédérale de Lausanne, Station 12, 1015 Lausanne, Switzerland – e-mail: sam.neuser@epfl.ch; veronique.michaud@epfl.ch*

Keywords: microfluidics, encapsulation, amine, epoxy

ABSTRACT

The encapsulation of amines with traditional emulsification and interfacial polymerization techniques has been challenging due to their reactive nature and wide range of miscibility. In this study, we propose a new method where we encapsulate triethylenetetramine (TETA) within acrylate microcapsules using double emulsion templates made from microfluidics.

In this process, a 50 wt% solution of TETA in water is dripped from an emitting capillary into an acrylate monomer phase, which in turn is engulfed by another aqueous fluid and flow-focused into a collecting capillary, thereby forming double emulsions. The emulsions are collected downstream and irradiated with UV to form microcapsules via photopolymerization. The microfluidic approach allows for monodispersity in the size and properties of the capsules, which can be tuned through the fluid flow rates, capillary dimensions and monomer compositions.

To purify the amine, we exploit the extremely low volatility of TETA, which has a vapor pressure of only 0.01 mmHg at 20 °C. The capsules are washed with water and acetone and then dried in air. Thus, the water in the core is removed from the capsules through evaporation, leaving the amine inside.

The presence of TETA inside the capsules is confirmed with NMR spectroscopy. Despite the presence of some residual water, the amine is very reactive, which we verify by mixing and thereby curing epoxy with the contents of ruptured capsules. Current work is focused on combining amine and epoxy capsules to evaluate their performance in self-healing composites.

SELF-HEALING THERMOPLASTIC-TOUGHENED EPOXY

A. Jones¹, S. White^{2,3} and N. Sottos^{2,4}

¹ Department of Mechanical Science and Engineering, University of Illinois at Urbana-Champaign, 1206 W. Green St, Urbana, Illinois 61801, USA – e-mail: emnett1@illinois.edu

² Beckman Institute for Advanced Science and Technology, 405 N. Mathews, Urbana, Illinois 61801, USA – e-mail: swhite@illinois.edu; n-sottos@illinois.edu

³ Department of Aerospace Engineering, University of Illinois at Urbana-Champaign, 104 S. Wright St, Urbana, Illinois 61801, USA – e-mail: swhite@illinois.edu

⁴ Department of Material Science and Engineering, University of Illinois at Urbana-Champaign, 1304 W. Green St, Urbana, Illinois 61801, USA – e-mail: n-sottos@illinois.edu

Keywords: self-healing, thermoplastic-toughening, polymer-matrix composites, solvent

ABSTRACT

Microcapsule based self-healing strategies enable repair of matrix cracking and delamination in fiber reinforced composite materials. Most of the encapsulated healing systems reported to date lack stability at high temperatures and limit composite processing to relatively low cure temperatures. In prior literature, successful crack healing has been achieved in high temperature cured composites by incorporation of a thermoplastic phase in the matrix. These systems are not autonomous and require the application of heat to soften the thermoplastic phase and initiate healing. In this work, a thermoplastic resin is blended with a high performance epoxy matrix to simultaneously toughen and act as a healing agent in combination with encapsulated solvents.

Self-healing is achieved for a commercial Epon 828 epoxy resin cured with diamino diphenyl sulfone above 150°C. Based on early screening studies, two thermoplastic toughening agents, poly bisphenol A-co-epichlorohydrin and polysulfone, are identified as model thermoplastic/ epoxy systems to study. Each system is evaluated using a tapered double cantilever beam (TDCB) fracture specimen geometry. The effect of cure cycle, thermoplastic loading, thermoplastic type, and capsule loading on both phase separation and healing response is investigated. To achieve *in situ* healing, microcapsules containing a polymer co-dissolved in a solvent are added to the thermoplastic-epoxy blend. Key parameters for capsule stability, such as capsule core content, shell wall robustness, and maximum cure temperature, are identified.

Additionally, the optimized systems from the TDCB study are extended to repair of interfacial damage between the fiber and matrix. The effect on both healing performance and interfacial bond strength due to different fiber sizings and interfacial phase separation is investigated. Since interfacial debond of reinforcing fibers is one of the key failure mechanisms in composite materials, prevention of growth of these flaws could greatly extend the lifetime of the composite.

SESSION 6 – SELF-HEALING METALLIC AND CERAMIC MATERIALS

THE EFFECT OF SiC PARTICLE SIZE ON THE HEALING EFFICIENCY OF ALUMINA AT HIGH TEMPERATURES

L. Boatemaa¹, J. Zhou², S. van der Zwaag³ and W. G. Sloof¹

¹Department of Materials Science and Engineering, Delft University of Technology, Mekelweg 2, 2628 CD Delft, The Netherlands – e-mail: L.Boatemaa@tudelft.nl; w.g.sloof@tudelft.nl

² Department of Biomechanical Engineering, Delft University of Technology, Mekelweg 2, 2628 CD Delft, The Netherlands – e-mail: J.Zhou@tudelft.nl

³Novel Aerospace Materials, Delft University of Technology, Kluyverweg 1, 2629 HS Delft, The Netherlands – e-mail: s.vanderzwaag@tudelft.nl

Keywords: Self-Healing, Al₂O₃, SiC, High Temperature, Oxidation Kinetics

ABSTRACT

Structural ceramics like alumina are usually brittle and sensitive to flaws leading to a reduction in their mechanical properties. This situation is worsened by machining prior to service and during service by contact, which introduces micro cracks and hidden damages. Crack damage can easily be developed in such ceramics when loaded, which often leads to catastrophic failure. However, if sacrificial SiC healing particles are embedded into the matrix of alumina, then the cracks can be healed by exposure at high temperatures in an oxidizing environment. Then, the cracks are filled with SiO₂ restoring the strength of the composite and thereby prolonging its lifetime. Reducing the size of the SiC healing particles while keeping the volume fraction the same, will increase the efficiency and lowers the onset temperature of the oxidation induced crack healing.

1. INTRODUCTION

Structural ceramics such as alumina, mullite and zirconia are anticipated to be used as structural components operating at high temperatures because of their excellent heat, corrosion, chemical and wear resistance [1]. However, their application is restricted due to their brittleness, which makes them very susceptible to crack damage leading to a considerable decrease in strength. The reliability of these materials could greatly improve if inevitable cracks can be healed autonomously.

One way to make alumina a viable option as a structural ceramic is to embed SiC intermetallic particles into the matrix, so that when cracking occurs these sacrificial particles would react at high temperatures with oxygen. SiO₂ is expected to form, which fills the crack. To obtain a strong healed zone, the products of oxidation (i.e. SiO₂) must be mechanically strong in comparison with the base material, the volume between the two crack surfaces should be completely filled with the oxidation product and there should be a strong bond between oxidation product and matrix. Experiments have shown that it is possible to fully recover the fracture toughness of a cracked sample [2].

It has also been demonstrated that submicron sizing of these sacrificial healing agents enables faster healing at lower temperatures [3], but comprehensive information is lacking. In this work the crack healing behaviour as a function of the size of the sacrificial SiC particles is investigated.

2. MATERIALS AND METHODS

The crack healing in a ceramic with SiC as healing agent is schematically illustrated in Figure 1. Cracking allows SiC particles located on the crack walls to react with the oxygen in the atmosphere at high temperatures resulting in the formation of SiO₂, which fills the crack and recovers the structural integrity.

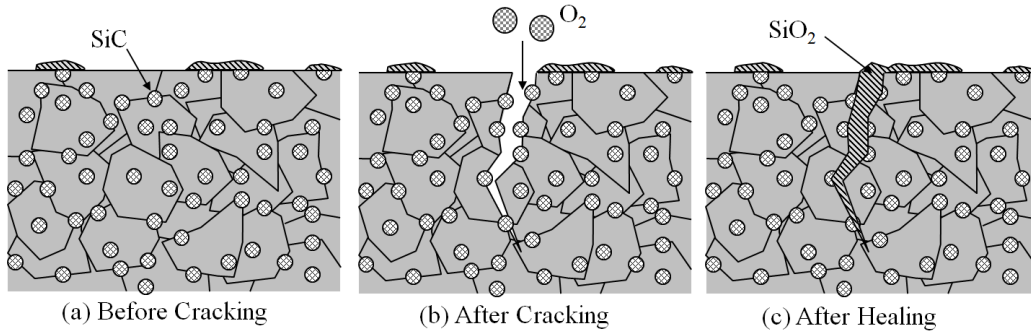


Figure 1: Schematic of crack healing with SiC particles, taken from [3].

SiC as healing agent is a viable option to regaining the strength of damaged ceramics because the reaction oxygen produces large exothermic heat, which bonds the product strongly to the matrix. In addition, SiO₂ has a higher volume expansion of 80% in comparison to SiC and this gives a good probability of completely fill a crack. Before embedding the SiC healing agent into the matrix a thorough understanding of the healing behaviour is necessary. To this end, the oxidation kinetics of SiC particles with different sizes (1, 2, 5 and 10 μm) was investigated with Thermogravimetric and Differential Thermal Analysis (TG-DTA) analysis.

The rate of transformation of SiC particles into SiO₂ by oxidation in Ar with 20 vol.% O₂ was studied at different but constant heating rates β , of 2, 5, 10 and 20 $^{\circ}\text{C}/\text{min}$ up to 1400 $^{\circ}\text{C}$. The size effect of SiC particles to heal crack damage is assessed through TG-DTA signal analysis.

3. RESULTS AND DISCUSSION

The oxidation rate of the SiC healing particles is obtained from the DTA signal whiles the TG signal shows mass gained during the reaction as shown in Figure 2. The activation energy E_a of the reactions can be evaluated using the Kissinger-Sunase-Akahira equation, which reads [3]:

$$\ln\left(\frac{\beta}{T_p^2}\right) + \frac{E_a}{RT_p} = \text{constant} \quad (1),$$

where, β is the heating rate, T_p is the peak temperature for the reaction, and R is the gas constant.

The peak temperature (T_p) for each reaction is determined by finding the region on the TG signal with the highest slope, which indicates the rate of oxidation. The temperature, at which the highest mass change occurs, usually correlates to a peak in the DTA signal. This temperature is taken as the peak temperature T_p .

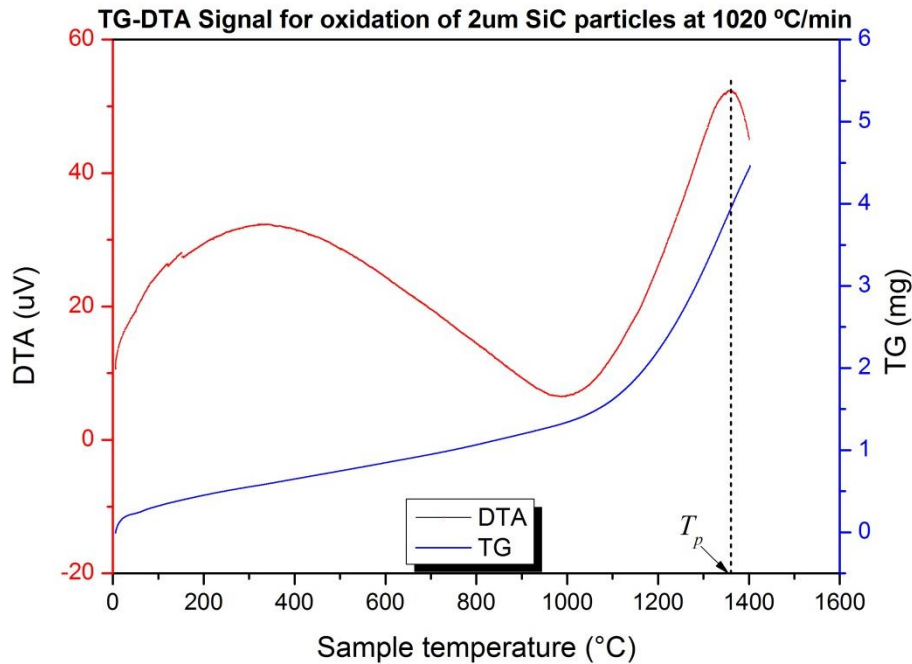


Figure 2: TG-DTA curves of 2 μm SiC oxidized in Ar with 20 vol,% O_2 recorded with a heating rate of 10 $^\circ\text{C}/\text{min}$.

The effect of the size of the SiC healing particles on the kinetics of oxidation induced crack healing is determined with TG-DTA. Evaluating the TG-DTA curves of the oxidation of SiC particles with different sizes recorded with different but constant heating rates and adopting Equation (1) gives the activation energy of the oxidation reaction. This activation energy increase with the size of the SiC particles. Moreover, the temperature decreases with decreasing SiC healing particle size considering the same oxidation induced crack healing kinetics.

4. CONCLUSIONS

The size of the SiC healing particles influences the kinetics of oxidation induced crack healing. The temperature at which these particles are capable to heal cracks decreases when smaller particles are applied.

AKNOWLEDGEMENTS

Financial support of the European Commissions 'Marie Curie International Training Network for Self-Healing Materials: from Concept to Market' (www.SHeMat.eu), project number 209308, is gratefully acknowledge.

REFERENCES

- [1] Nakao, W., K. Takahashi, and K. Ando, Threshold stress during crack-healing treatment of structural ceramics having the crack-healing ability. *Materials Letters*, 2007. 61(13): p. 2711-2713.
- [2] Ando K., et al., Self-crack-healing behavior and fracture strength of $\text{Al}_2\text{O}_3/\text{SiC}$ composites at the high temperature. *European Conference on Fracture Series 15*. Sweden, Aug. 11-13, 2004.

[3] Nakao, W. and S. Abe, Enhancement of the self-healing ability in oxidation induced self-healing ceramic by modifying the healing agent. *Smart Materials and Structures*, 2012. 21(2): p. 025002.

OXIDATION-INDUCED CRACK HEALING IN $Ti_2Al_{(1-x)}Sn_xC$ SOLID SOLUTIONS

G.P. Bei¹, J. Pedimonte¹, T. Fey¹ and P. Greil¹

¹ University of Erlangen-Nuernberg, Department of Materials Science (Glass and Ceramics), Martensstr. 5, D-91058 Erlangen, Germany - e-mail: Guoping.Bei@ww.uni-erlangen.de; Joana.Pedimonte@ww.uni-erlangen.de; Tobias.Fey@ww.uni-erlangen.de; Peter.Greil@ww.uni-erlangen.de

Keywords: MAX phase, solid solution, crack healing reactions

ABSTRACT

MAX phases such as Ti_2AlC and Ti_3AlC_2 show crack healing ability, which gives rise for recovery of the mechanical properties. Healing was attributed to high temperature oxidation-induced filling of the area between the disrupted crack surfaces by formation of adhesive $\alpha-Al_2O_3$ as well as TiO_2 rutile. After healing the mechanical properties can be fully recovered or even be higher than the virgin samples due to well-matched thermal expansion coefficients between adhesive $\alpha-Al_2O_3$ and Ti_3AlC_2 or Ti_2AlC . In this work, materials with multiple healing ability at low temperatures as well as fast healing rates were investigated using the $Ti_2Al_{(1-x)}Sn_xC$ MAX phase solid solution system. Substitution of Al with the lower melting element Sn enhances the mobility of the A element resulting in lower healing temperatures with higher rates of oxidation. TGA-DTA measurements show the onset of crack healing to be reduced from 600 °C ($x = 0$) to 400 °C ($x = 1$). Microstructure analysis of crack filling phases confirmed the formation of SnO_2 . Tailoring the MAX phase solid solution composition offers a high potential to crack healing ability in oxidizing atmosphere.

ENHANCING THE CREEP LIFE OF STEELS BY SELF-HEALING THROUGH DYNAMIC IN-SERVICE PRECIPITATION

G. Langelaan¹, S. Zhang¹, E. Brück¹, S. van der Zwaag² and N.H. van Dijk¹

¹ *Fundamental Aspects of Materials for Energy, Faculty of Applied Sciences, TU Delft, Mekelweg 15, 2629 JB Delft, the Netherlands – e-mail: G.Langelaan@TUDelft.nl; ShashaZhang@TUDelft.nl; N.H.vanDijk@TUDelft.nl; E.H.Bruck@TUDelft.nl*

² *Delft Center for Materials, TU Delft, Kluyverweg 1, 2629 HS Delft, The Netherlands – e-mail: s.vanderzwaag@tudelft.nl*

Keywords: Steel, grain boundary, precipitation, creep, cavities

ABSTRACT

Increasing the operating conditions in steam turbines is desirable to improve the efficiency of electricity generating stations. However, the operating temperature and pressure are limited by the creep lifetime of the steels used for the boilers and piping. In recent experiments we have aimed to develop a creep resistant steel that self-heals deformation damage by the in-service formation of second phase precipitates. To achieve self-healing, the precipitates should form preferentially on or near the surfaces of creep cavities to prevent their further growth.

In the experiments, we used a custom made binary alloy of iron with 2 weight % vanadium. This composition is normally a solid solution but by introducing nitrogen, vanadium nitride (VN) precipitates form readily. We have performed a series of interrupted creep tests to determine whether adding nitrogen by gas nitriding would allow the preferential formation of VN on the grain boundaries and on the creep induced cavities. We will present the results of the tensile creep tests as well as microscopy, which shows the concentration of creep cavities throughout the creep test as well as the distribution of the VN particles produced during the nitriding steps. The self-healing capabilities of this system will be discussed in detail.

INCREASE IN CRITICAL STRESS FOR CRACK-HEALING OF $\text{Si}_3\text{N}_4/\text{SiC}$ CERAMICS BY SHOT PEENING

K. Takahashi¹, S. Nakagawa², and T. Osada³

¹ Division of Materials Science and Engineering, Yokohama National University, 79-5, Tokiwadai, Hodogaya, Yokohama, 240-8501, Japan – e-mail: ktaka@ynu.ac.jp

² Graduate Student, Yokohama National University, 79-5, Tokiwadai, Hodogaya, Yokohama, 240-8501, Japan

³ Cooperative Research and Development Center, Yokohama National University, 79-5, Tokiwadai, Hodogaya, Yokohama, 240-8501, Japan – e-mail: tosada@ynu.ac.jp

Keywords: Ceramics, Crack-healing, Shot peening, Residual stress, Critical stress

ABSTRACT

The effects of shot peening on the critical stress for crack-healing of $\text{Si}_3\text{N}_4/\text{SiC}$ composite ceramics were investigated. Shot peening was carried out on a $\text{Si}_3\text{N}_4/\text{SiC}$ composite with a surface crack by using yttrium-stabilized zirconia beads. Shot-peened specimens were crack-healed at 1100 °C for 5 h under a tensile stress (σ_{app}) in the range 0–500 MPa. The results clearly showed that the surface cracks in shot-peened specimens were healed completely for $\sigma_{\text{app}} \leq 450$ MPa. Thus, the critical stress for crack-healing ($\sigma_{\text{app}}^{\text{C}}$) was determined to be 450 MPa. This $\sigma_{\text{app}}^{\text{C}}$ value was 2.3 times that for an unpeened specimen. Furthermore, the $\sigma_{\text{app}}^{\text{C}}$ values for both specimens showed a proportional relationship with the bending strength of the cracked specimen σ_{c} ($\sigma_{\text{app}}^{\text{C}} \approx 0.64\sigma_{\text{c}}$). Therefore, it can be concluded that the increase in $\sigma_{\text{app}}^{\text{C}}$ of the peened specimen is due to the compressive residual stress and the consequently increase in σ_{c} .

1. INTRODUCTION

Some structural ceramics have a self-crack-healing ability [1]. The utilization of this ability in ceramic components can afford the following great merits: (a) increase in reliability, (b) reduction in inspection, machining, polishing, and maintenance costs, and (c) increase in the lifetime of the ceramics.

However, the reliability of structural ceramics is considerably reduced by crack initiation during operation because their fracture toughness is not high. Thus, the reliability and lifetime of ceramic components for high-temperature applications such as micro-gas-turbine blades can be increased by healing cracks under service conditions, e.g., tensile stress and high temperatures.

The crack-healing behavior of $\text{Si}_3\text{N}_4/\text{SiC}$ under stress at 1100 and 1200 °C in air was investigated [2]. It was found that a surface crack of 100 μm , which reduced bending strength about 50%, could be healed completely in just 0.5–1 h even under cyclic stress at 1100 and 1200 °C in air. These results indicate that $\text{Si}_3\text{N}_4/\text{SiC}$ has an excellent crack-healing ability. In this study, the critical stress for crack-healing was as high as 200 MPa. The reliability of ceramics can be increased by further increasing the critical stress.

Takahashi et al. reported that shot peening on the surface of $\text{Si}_3\text{N}_4/\text{SiC}$ induces compressive residual stress [3]. This compressive residual stress prevents crack

propagation. In this study, the effects of shot peening on the critical stress for crack-healing of Si₃N₄/SiC composite ceramics were investigated.

2. MATERIALS

Hot-pressed SiC-reinforced Si₃N₄ containing 20 wt% SiC particles and 8 wt% Y₂O₃ as a sintering additive was used for preparing the specimens. The details of the material fabrication process are given in the literature [2,3]. The hot-pressed Si₃N₄ was cut into test specimens measuring 2 mm × 4 mm × 20 mm. Semi-elliptical surface cracks 100 μm in surface length and 45 μm in depth were induced at the center of the tension surface of the specimens by using a Vickers indenter. Shot peening (SP) was then carried out using a direct-pressure peening system. For this, commercial zirconium oxide (ZrO₂) shots with a diameter of 300 μm were used. The peening pressure and peening time were 0.2 MPa and 30 s, respectively. The specimens subjected and not subjected to SP are hereafter denoted as “SP” and “non-SP,” specimens, respectively.

3. METHODS

Crack-healing was carried out under constant bending stress by using an in-situ observation apparatus shown in Fig. 1. This apparatus consisted of an infrared image furnace, a three-point bending device, and an optical microscope equipped with a CCD camera. The pre-cracked specimens were crack-healed under a constant tensile stress (σ_{app}) in the range 0–500 MPa at 1100 °C for 5 h in air. After the crack-healing process, the bending strengths of the specimens were measured at room temperature in air. These tests were carried out using a universal monotonic testing machine.

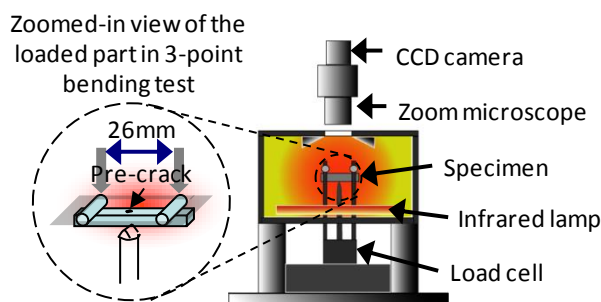


Figure 1: Schematic diagram of in-situ observation device

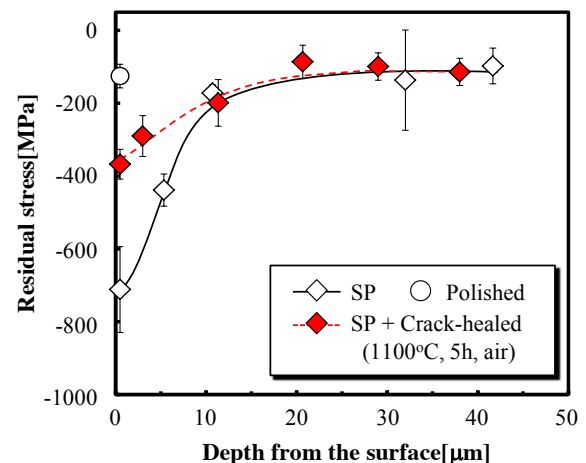


Figure 2: Relationship between residual stress and depth from the surface

4. RESULTS

Figure 2 shows the residual stress distributions for SP and SP + crack-healed specimens. A maximum compressive surface residual stress of 710 MPa was observed in the SP specimen. However, the compressive residual stress decreased in the depth direction. Moreover, a surface residual stress of 370 MPa was observed

in the SP + crack-healed specimen. Thus, some of the compressive residual stress induced by SP remained after the crack-healing process.

Figure 3 shows the relationship between the stress applied during crack-healing and bending strength at room temperature. The average value of the bending strength of smooth specimens was 780 MPa. The pre-cracks largely reduced the bending strength to 340 MPa. After SP, the bending strength of the pre-cracked specimens increased up to 580 MPa. The increase in the bending strength was attributed to compressive residual stress. The critical stress for crack-healing (σ_{app}^C) was defined as the maximum stress below which a crack-healed specimen recovered its bending strength and below which most specimens fractured outside the crack-healed zone. The σ_{app}^C values for pre-crack + crack-healed and pre-crack + SP + crack-healed specimens were determined to be 200 and 450 MPa, respectively. These results indicated that SP increased the σ_{app}^C value by 2.3 times.

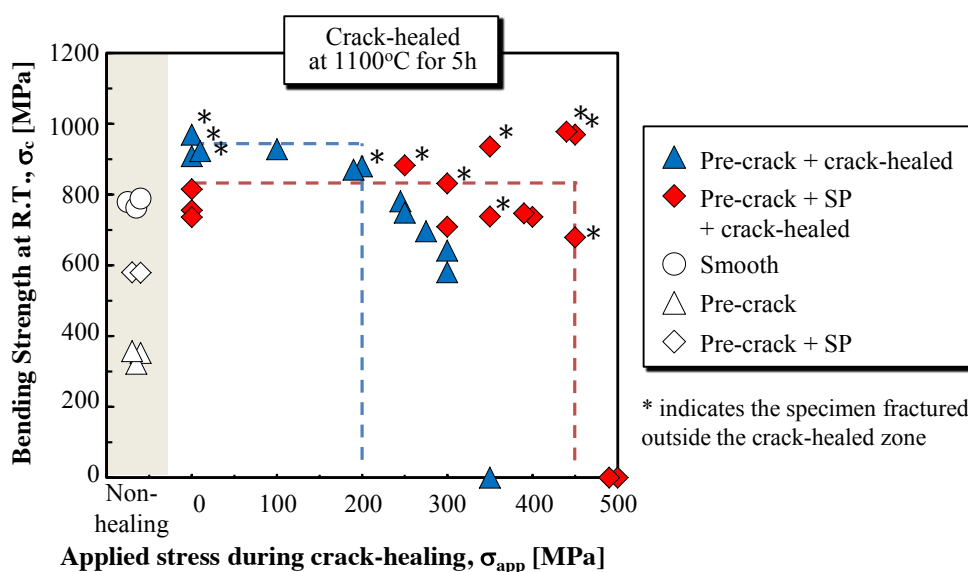


Figure 3: Bending strength of crack-healed specimens as a function of applied stress during crack-healing

Figure 4 shows σ_{app}^C as a function of the bending strength of pre-cracked specimens (σ_c). Nakao et al. have conducted similar tests on Al_2O_3/SiC particles, Al_2O_3/SiC whiskers, mullite/ SiC particles [4]. They reported that σ_{app}^C is proportional to σ_c . These results indicated that the increase in σ_{app}^C by SP was caused by an increase in σ_c . The proportional constant for the relationship between σ_{app}^C and σ_c (σ_{app}^C/σ_c) was approximately 64% for non-SP specimens in spite of the different material and crack-healing conditions. However, the value of σ_{app}^C/σ_c for the SP specimens was 78%. Figure 5 shows the specimen surface observed using an optical microscope and pre-cracked area observed using a scanning electron microscope. The crack opening displacement (COD) in the non-SP zone was 0.2 μm , whereas the COD in the SP zone was less than 0.1 μm . Moreover, the volume between crack surfaces in SP specimens was smaller than that in the non-SP specimens. Further, the volume of the healing substance, which is necessary to fill and bond surface cracks, in the SP specimens was smaller than that in the non-SP specimens. Thus, the crack-healing rate in the SP specimens was higher than that in the non-SP specimens. Therefore, the value of σ_{app}^C/σ_c was increased by subjecting the specimens to SP.

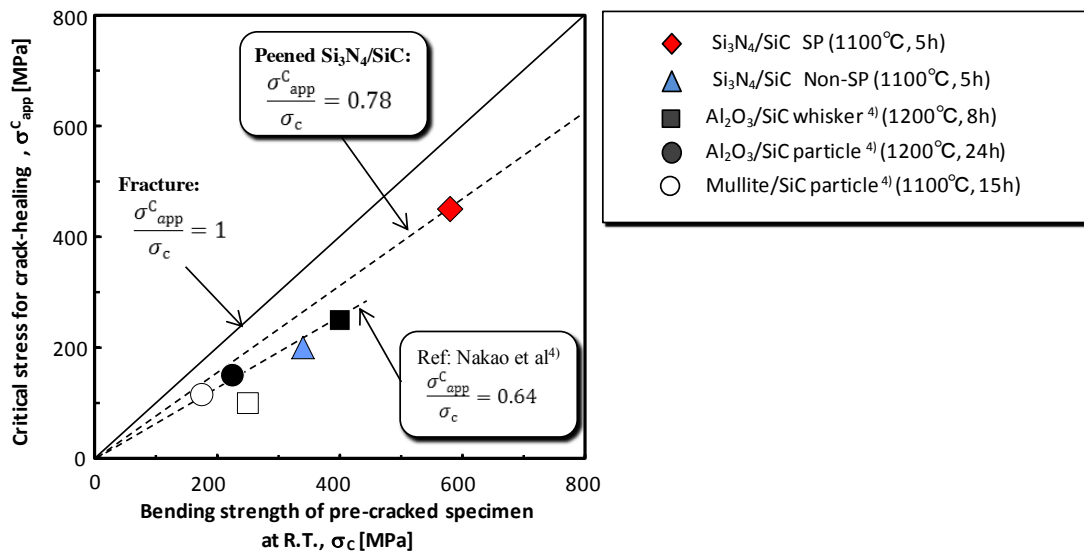


Figure 4: Relationship between critical stresses for crack-healing and bending strength of pre-cracked specimens

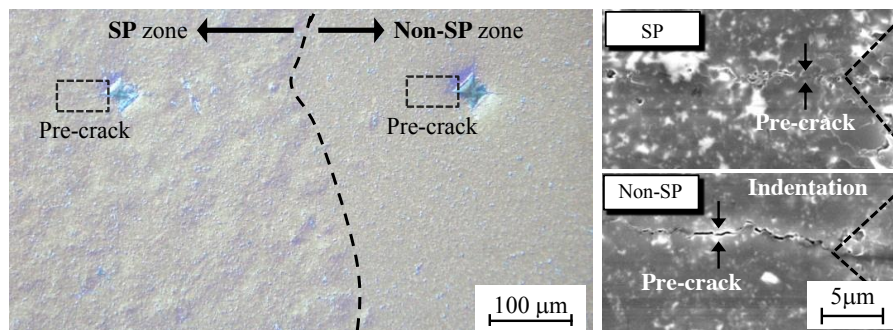


Figure 5: Crack closure by shot peening

5. CONCLUSIONS

The effects of shot peening on the critical stress for crack-healing (σ_{app}^C) in $\text{Si}_3\text{N}_4/\text{SiC}$ composite ceramics was investigated. Shot peening increased the σ_{app}^C value of $\text{Si}_3\text{N}_4/\text{SiC}$ by 2.3 times. The improved σ_{app}^C value of the peened specimen was due to the compressive residual stress. Thus, crack-healing combined with shot peening is a useful technique for increasing the structural integrity of ceramic components.

REFERENCES

- [1] W. Nakao, K. Takahashi and K. Ando, Self-Healing of Surface Cracks in Structural Ceramics, in S.K. Ghosh Ed.,: Self-healing Materials, Chapter 6, 183-217, WILEY-VCH, Weinheim, Germany, (2009).
- [2] K. Takahashi, K. Ando, H. Murase, S. Nakayama and S. Saito, Threshold Stress for Crack-Healing of $\text{Si}_3\text{N}_4/\text{SiC}$ and Resultant Cyclic Fatigue Strength at the Healing Temperature, *Journal of the American Ceramic Society*, 88 (2005) 645-651.
- [3] K. Takahashi, Y. Nishio, Y. Kimura and K. Ando, Improvement of Strength and Reliability of Ceramics by Shot Peening and Crack-healing, *Journal of European Ceramic Society*, 30 (2010) 3047-3052.

[4] W. Nakao, K. Takahashi and K. Ando, Threshold Stress during Crack-healing Treatment of Structural Ceramics having the Crack-healing Ability, *Materials Letters*, 61 (2007) 2711-2713.

DESIGN METHODOLOGY FOR LIQUID-ASSISTED SELF-HEALING METALS

C. R. Fisher¹, M. C. Wright², T. A. Wallace³, and M. V. Manuel¹

¹ *Materials Science & Engineering Department, University of Florida, 549 Gale Lemerand Drive, Gainesville, Florida 32611 USA – e-mail: cfisher@ufl.edu; mmanuel@mse.ufl.edu*

² *National Aeronautics and Space Administration – Kennedy Space Center, Florida 32899 USA – e-mail: m.clara.wright@nasa.gov*

³ *National Aeronautics and Space Administration – Langley Research Center, Hampton, Virginia 23665 USA – e-mail: terry.l.a.wallace@nasa.gov*

Keywords: Metal-matrix, aluminum, systems design, thermodynamics

ABSTRACT

Advanced metal-matrix composites reinforced with shape memory alloys (SMA) have the potential to demonstrate dramatic capabilities such as damage mitigation and repair. Investigations of liquid-assisted self-healing in metal-matrix composites have centered on developing a high specific-strength matrix possessing a low-melting eutectic for use as the healing material. A systems design approach motivated by thermodynamics was used to determine appropriate matrix alloying elements for increased strength while maintaining healing capabilities. Recent developments in aluminum-based alloys have shown potential healing across several ternary systems. This study will detail the prospective matrix alloy systems and establish the efficacy of the design approach through prediction of strength, fatigue properties, microstructure development, and SMA incorporation into the composite. In addition, improvements for future matrix alloy iterations will be outlined. This work has been supported by the National Science Foundation (CMMI-0824352) and the National Aeronautics and Space Administration (NNX12AQ42G and NNX12AP71A).

SESSION 7 – SELF-HEALING CEMENTITIOUS MATERIALS

LONG TERM STRESS RELAXATION BEHAVIOUR OF POLYETHYLENE TEREPHTHALATE SUBJECTED TO THERMALLY ACTIVATED RESTRAINED SHRINKAGE

T. Hazelwood¹, A. D. Jefferson¹ and R. J. Lark¹

¹ Cardiff School of Engineering, Cardiff University, Queen's Buildings, The Parade, CF24 3AA, Cardiff, Wales, United Kingdom – e-mail: hazelwoodt@cardiff.ac.uk; jeffersonad@cardiff.ac.uk; lark@Cardiff.ac.uk

Keywords: concrete, self-healing, shape memory polymer, thermo-mechanical behaviour, long-term stress relaxation.

ABSTRACT

Research has been carried out with the aim of better understanding the relevant properties of materials to be used in a new self-healing cementitious composite material system. The system consists of shape memory polymer tendons embedded within a cementitious matrix, upon heat activation these tendons undergo a shrinkage process which closes any cracks present. After this heat activation, autogenous healing of the cracks is enhanced by the ongoing application of pressure to the cracked faces.

In a previous study the build-up of stress in a restrained poly(ethylene terephthalate) specimen upon heat activation was investigated. In the current study, the long term stress relaxation behaviour of such a restrained specimen has been investigated so that its potential for use in the material system described above can be better understood. Both experimental and numerical approaches have been undertaken. A specimen of poly(ethylene terephthalate) was restrained against longitudinal shrinkage and a heat of 90°C applied for a duration of 10 minutes to simulate the conditions it would be subject to within the system. The stress in the specimen was continuously monitored during heat activation, cooling, and for approximately 6 months after this. This data was used to quantify the stress relaxation of the specimen.

The stress relaxation over the period studied was found to be very low; the peak stress was 32.80MPa, this fell to a minimum value of 30.84MPa after a period of approximately 97 days had elapsed. These low levels of stress relaxation are beneficial to the system since a larger shrinkage force will be applied for a longer period of time, which should also lead to improved autogenous healing of cracks.

1. INTRODUCTION

This study represents an extension of previous research carried out by this research group [1] into the behaviour of SMP tendons in the context of a new self-healing composite materials system. This system has been named LatConX and has been previously described by Jefferson et al [2].

Dunn et al [1] investigated stress development in pre-drawn PET during restrained shrinkage due to temperature activation using both experimental and numerical techniques. In the context of the LatConX system, the long term behaviour after stress development is also of significant importance as this will have an effect on the extent of any autogenous healing within the cementitious matrix. In light of this, the

current publication continues the work of Dunn et al [1] to include this long term aspect of the polymer's behaviour.

2. MATERIALS AND METHODS

All experiments have been carried out using the drawn polymeric material Aerovac Shrink Tite, in 32 mm × 0.046 mm tape form [3].

All test specimens consisted of 25 strips of the polymer tape approximately 400 mm long, clamped at both ends between grips consisting of two flat metal plates measuring approximately 60 mm × 23 mm × 2 mm. In reality it was impossible to have each specimen exactly 400 mm long due to the intricacies involved with assembling the multiple strips in the grips; the length of the specimens actually ranged from 400 mm to 402 mm.

Test specimens were held in the grips in a position so that they were just taut, a heat of 90°C was then applied to the specimen for a period of ten minutes, thus activating the shrinkage behaviour of the drawn polymer, and inducing a stress within the specimen. The stress and the ambient temperature were monitored and logged over time by a 2.5 kN load cell and 12 thermocouples respectively. The tests were carried out in a custom built rig consisting of an Instron oven fixed within a Mechtrix reaction frame; fixings were constructed to connect the grips holding the specimen to the top and bottom of the reaction frame with the specimen running through the middle of the oven.

3. RESULTS AND DISCUSSION

Five of these tests have been carried out; a typical set of results is presented in

Figure 1. From this it can be seen that the stress reaches a peak of 32.8 MPa at the start of the test before reducing over a period of approximately 100 days to an average plateau value 31.48 MPa. This value is an average as the stress continues to fluctuate between approximately 32 MPa and 31 MPa once the plateau is reached.

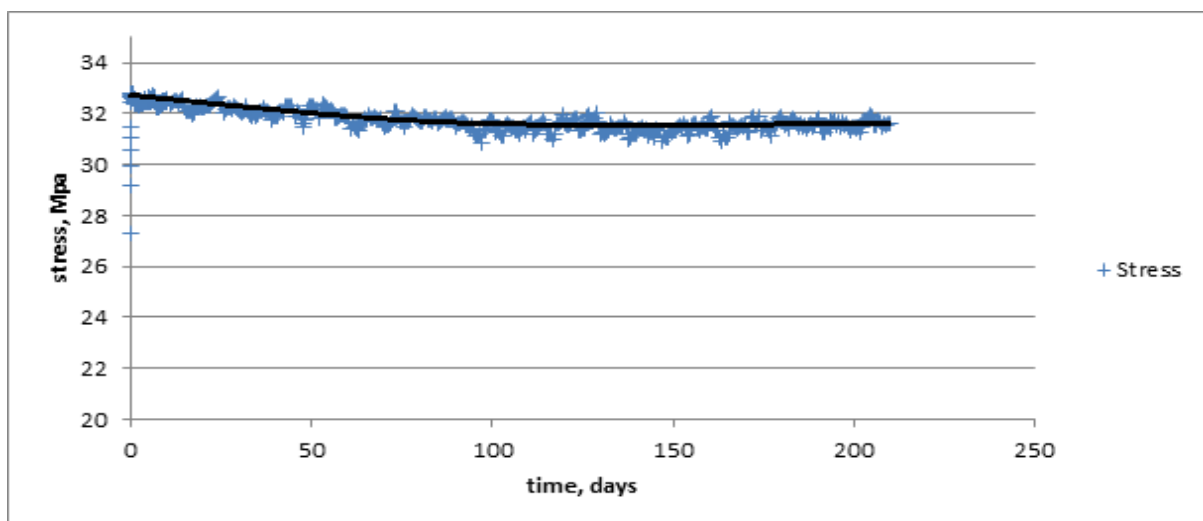


Figure 1: Stress vs time for heat activated stress relaxation test

The peak stress reached in the five tests has been observed to vary from a minimum of 25.95 MPa to a maximum of 32.80 MPa, one theory is that the value of the peak stress is closely linked to the age of the material as the locked in stress is thought to gradually release over time. The length of time that the material relaxed over was also seen to vary, the maximum period was approximately 100 days, and the minimum was approximately 1 day; this tended to be a shorter time in the older material. Finally the stress that the relaxation plateaued at also varied from a minimum of 96.4 % of the peak stress to a maximum of 98.6 % of the minimum. Due to the long time period required to carry out a test such as the one above, it was not possible to continue every test for this period. However four other shorter term tests were undertaken to confirm that a similar early trend was seen, these tests were found to show close agreement; they have been normalised to the peak stress and averaged to produce the results shown in Figure 2.

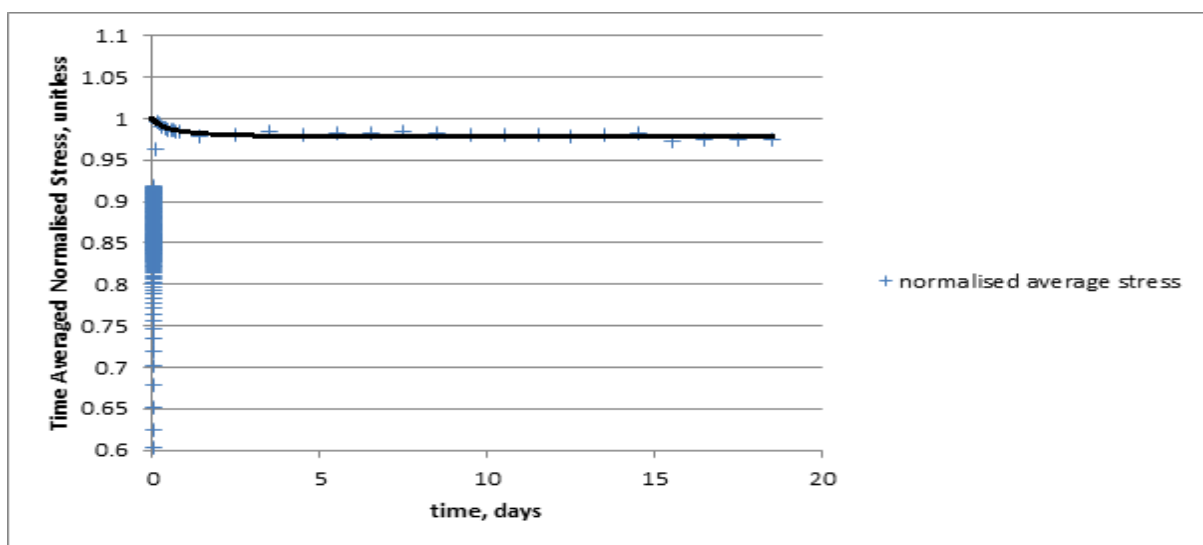


Figure 2: Normalised average stress vs time for 4 different heat activated stress relaxation tests

There was a concern regarding the tensile strength of the pre-drawn PET and whether any extension due to a crack crossing the material would induce a tensile stress close to failure. The authors have not carried out the relevant research themselves, however reference to other sources has yielded the following relevant values; the elongation at break ranges from 30 – 300 %, and the tensile strength at break ranges from 47 – 70 MPa [4], based on these figures we can be confident that the proposed application is comfortably within the safe operating limits of the material.

The set of experimental results presented above have good implications for the use of this material in the proposed LatConX system as they show very limited stress relaxation, so the force applied to the cracked faces of the cementitious material would remain high for an extended period of time giving more effective autogenous healing of the crack for a longer time.

4. CONCLUSION

An experimental study into the long term stress relaxation behaviour of the shape memory polymer Poly(ethylene terephthalate) has been presented here. Stress relaxation of this material has been monitored for periods of up to 6 months, following activation of the shape memory recovery process under restrained conditions. This study has been carried out in the context of the new LatConX material system. The findings of this study are considered to have good implications for the use of the material in the proposed LatConX system.

Further investigations into this and other related viscoelastic behaviour of this material have been undertaken in conjunction with the development of a numerical model capable of simulating this behaviour. The authors hope to present this further work in the form of a journal article in the near future.

REFERENCES

- [1] S. Dunn, A. Jefferson, R. Lark, B. Isaacs, Shrinkage behaviour of poly(ethylene terephthalate) for a new cementitious-shrinkable polymer material system. *Journal of Applied Polymer Science* 120 (2011) 2516-2526.
- [2] A. Jefferson, C. Joseph, R. Lark, B. Isaacs, S. Dunn, B. Weager, A new system for crack closure of cementitious materials using shrinkable polymers. *Cement and Concrete Research* 40 (2010) 795-801
- [3] <http://www.aerovac.com/> [Accessed: 17th May 2012]
- [4] <http://www.maropolymeronline.com/Properties/PET.asp#Tensile Strength at Break> [Accessed 8th March 2013]

CHARACTERISATION OF HEALING AGENTS FOR SELF-HEALING CEMENTITIOUS SYSTEMS

D. Gardner¹, D. Herbert¹, M. Jayaprakash¹ and A. Jefferson¹

¹ Cardiff School of Engineering, Cardiff University, Queen's Buildings, Newport Road, CF24 3AA, Cardiff, UK - e-mail: gardnerdr@cardiff.ac.uk; herbertdm@cardiff.ac.uk; jayaprakashM@cardiff.ac.uk; jeffersonad@cardiff.ac.uk

Keywords: Healing agents, Capillary flow, Cementitious materials, Self-healing

ABSTRACT

Recent developments in self-healing technology inspired by natural biological materials have the potential to dramatically improve the performance and durability of cementitious materials. These self-healing cementitious materials comprise artificial flow networks embedded within the cementitious matrix that upon damage release healing agents that are transported via capillary flow to macro-cracked and micro-cracked regions. However, the mechanisms of capillary flow in cementitious materials and the interactions between varying viscosity and surface tension are not well understood and there are few reported studies to date that have attempted to measure or simulate these for cementitious materials. This paper considers the flow characteristics of healing agents in macro-cracks formed as a result of material damage occurring during the early life of a structure and whose presence contributes to the deterioration processes that reduce the longevity of reinforced concrete structures. The ability to predict the capillary flow of healing agents within discrete cracks will further the development of efficient self-healing cementitious materials which will in turn deliver economic, environmental and social benefits, such as reduced maintenance and repair costs and reduced use of natural resources.

This paper presents the results from an experimental investigation into the Hagen-Poiseuille (H-P) flow characteristics of one autonomic (adhesive based) and one autogenic (pozzolanic based) healing agent. Particular attention is given to the time-viscosity and time-surface tension relationships of the healing agents when in contact with mortar. Additional benchmark experiments are currently being undertaken for the capillary flow of the two healing agents between glass plates and concrete plates of varying compressive strength. These studies provide data to validate a numerical model developed by the research group, in which terms are added to allow for stick-slip behaviour and frictional dissipation at the meniscus wall boundary. The initial results from these validations are promising and confirm the validity of the theoretical approach adopted.

1. INTRODUCTION

The presence of discrete cracks in a cementitious matrix, often formed as a result of thermal effects and plastic shrinkage during concrete hydration, contributes to deterioration processes such as freeze-thaw action, chloride ingress and carbonation. The independent or sometimes concurrent actions of these processes are partly responsible for reducing the service life of structures. Capillary flow, driven primarily by surface tension, has been frequently noted in the literature [1, 2] as one

of the primary transport mechanisms by which aggressive agents from the environment ingress concrete. Conversely, capillary flow also plays a role in the ability of a concrete to self-heal and recent work in the area of self-healing cementitious materials [3] has proved promising in enhancing the longevity of structures.

One variant of a self-healing cementitious material comprises artificial flow networks embedded within the cementitious matrix that upon damage release healing agents that are transported via capillary flow to macro-cracked and micro-cracked regions. However, the mechanisms of capillary flow in cementitious materials and the interactions between varying viscosity and surface are not well understood and there are few reported studies to date that have attempted to measure or simulate these for cementitious materials. The aim of this study is to therefore establish the Hagen-Poiseuille (H-P) flow characteristics of an autogenic and autonomic healing agent, through a series of experimental investigations, with particular attention given to the time-viscosity and time-surface tension relationships of the healing agents when in contact with mortar.

2. MATERIALS AND METHODS

The Lucas-Washburn equation for capillary flow is based on Poiseuille’s law for fluid motion in a circular capillary tube, the equation for which is provided in (1). The H-P flow characteristics were measured using the experimental arrangement presented in Figure 1(a). The test was performed on water and two healing agents; PC20 Cyanoacrylate (a low viscosity glue) and a 50:50 water/ground granulated blast furnace slag (GGBS) solution.

$$\Delta P = \frac{8\mu L Q}{\pi r^4} \tag{1}$$

Where L = capillary length (m); Q = flow rate (m³/s); r = capillary radius (m); μ = dynamic viscosity (Ns/m²) and ΔP= Pressure drop (N/m²).

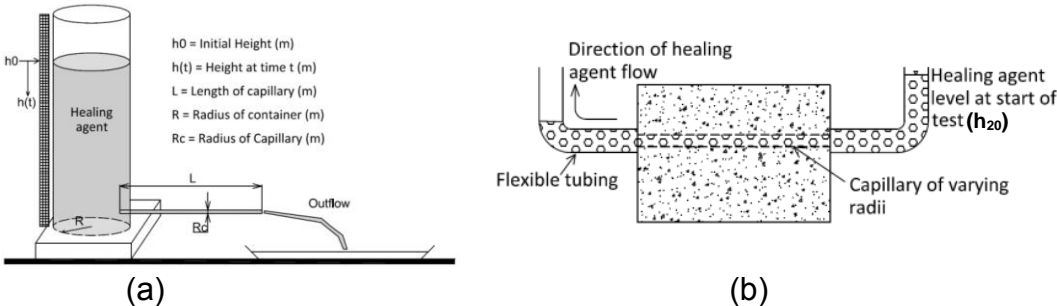


Figure 1. Measurement of H-P flow and time-viscosity characteristics

Glass capillary tubes with diameters of 0.8mm and 1.2mm and lengths of 100mm, 200mm and 300mm were used. The tests were conducted using pressure heads ranging from 750mm to 1600mm, dependent on the capillary radii and length. The flow rate and surface height (h(t)) was measured using a balance scale and AOS Motioneer high speed video camera respectively.

The time-viscosity relationship of the PC20 glue was further investigated via a bespoke test based on the principle of the Ostwald viscometer, as indicated in Figure

1(b). The flow of PC20 glue through a constricted channel section was observed. The channel was formed by drilling a circular 3mm diameter hole through a mortar prism. L-shaped pieces of flexible tubing were connected to the prism at both ends of the channel. One side of the mortar prism was raised and a stopper placed in the flexible tube. The specimen was then returned to the horizontal position and the stopper removed. The movement of the PC20 glue free surface (h_2) was recorded using high speed video and the test repeated at 10 second intervals for 30 seconds and then at 5 minute intervals for a further 15 minutes.

The method of measuring the time-surface tension relationship employed the sessile drop technique on glass plates and saturated and unsaturated high density mortar surfaces for water and the two healing agents. The technique was performed at regular intervals over a period of 1 hour. The contact angle between the drop and the solid surface and the profile of the surface was obtained using ImageJ with a DropSnake plug-in developed by Stalder et al. [4].

3. RESULTS

H-P flow was observed for the healing agents over the range of parameters identified in Section 2, as presented in Figure 2. The resulting viscosities of the healing agents were calculated as 1.2 cPs for water, 2.8 cPs for PC20 glue and 6.1 cPs for GGBS. The viscosities showed negligible change over the period of an hour. A numerical simulation of the time-viscosity relationship for the PC20 glue, as presented in Figure 2, yielded viscosities in the range of 7.4 to 8.2 cPs with insignificant change to viscosity over the experimental time scale. These viscosities are higher than those seen in the H-P flow experiments and demonstrate the influence of the alkaline environment on the viscosity. After 90 minutes a “skin” had formed on the cyanoacrylate surface, and after this time no flow of cyanoacrylate could be induced.

The wettability of a surface, as indicated by the contact angle, was found to be highly dependent on its moisture state and surface roughness, as indicated in Table 1 (for $t=0$ secs). This was true over the 1 hour period of the test.

The extent of flow will be governed by the contact angle and surface tension of the healing agent, whilst the viscosity of the healing agent will influence the rate of capillary rise. These investigations have provided data which would allow the accurate simulation of healing process which will be used to facilitate the future design of self-healing systems. Moreover, the data will be used to validate a numerical model in which terms are added to allow for stick-slip behaviour and frictional dissipation at the meniscus wall boundary. The initial results from these validations are promising and confirm the validity of the theoretical approach adopted.

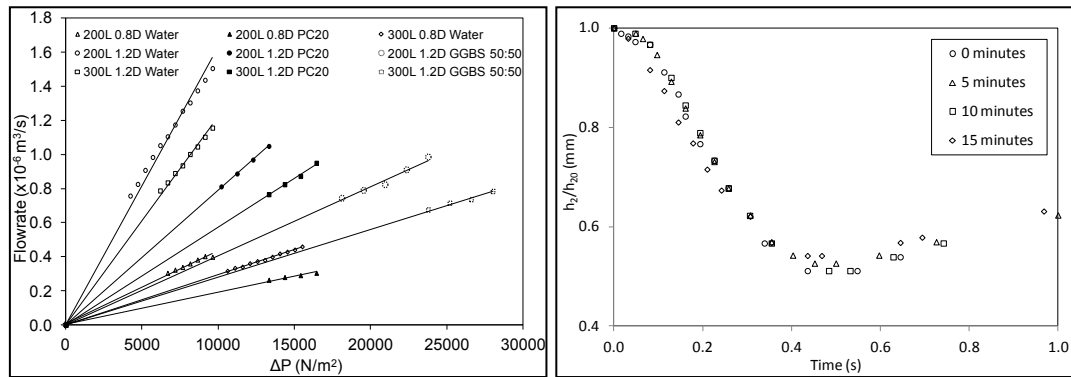


Figure 2. H-P flow characteristics and time viscosity relationship

Table 1. Contact angle measurements on a range of specimens (t= 0 secs)

Healing Agent	Contact angle measurements (°)		
	Glass	Saturated Mortar	Unsaturated Mortar
Water	10.5	36.5	18.8
PC20 Glue	9.5	15.6	14.1
GGBS 50:50	16.5	24.8	25.4

4. CONCLUSIONS

The experimental results indicate that the healing agents under consideration possess the necessary characteristics to allow flow into a discrete crack to enable self-healing. Numerical simulations of this process, using these experimental results for validation, are ongoing and will facilitate the future design of self-healing systems.

ACKNOWLEDGEMENTS

Financial support from the Engineering and Physical Sciences Research Council (EPSRC) for this study (Project No. EP/J021776/1) is gratefully acknowledged.

REFERENCES

- [1] M.D. Lepech, V.C. Li, Permeability of Cracked Engineered Cementitious Composites, *Cement and Concrete Composites*, 31 (10) (2009) pp. 744-753.
- [2] F. Collins, J. Sanjayan, Unsaturated Capillary Flow within Alkali Activated Slag Concrete, *Journal of Materials in Civil Engineering*, 20 (9) (2008) pp. 565-570.
- [3] C. Joseph, D. Gardner, A. Jefferson, R. Lark, B. Isaacs, Self-healing cementitious materials: A review of recent work, *Proceedings of the Institution of Civil Engineers, Construction Materials*, 164 (2010) pp. 29-41.
- [4] A.F. Stalder, G. Kulik, D. Sage, L. Barbieri, P. Hoffmann, A Snake-Based Approach to Accurate Determination of Both Contact Points and Contact Angles, *Colloids And Surfaces A: Physicochemical And Engineering Aspects*, 286 (1-3) (2006) pp. 92-103.

INJECTING A LIQUID BACTERIA-BASED REPAIR SYSTEM TO MAKE POROUS NETWORK CONCRETE HEALED

S. Sangadji¹, V. Wiktor¹, H. Jonkers¹, and E. Schlangen¹

¹ Delft University of Technology, Faculty of Civil Engineering & geosciences, Section of Materials & Environment – Microlab, Stevinweg 1 2628 CN Delft, the Netherland

Keywords: Porous network concrete, self-healing, concrete, liquid bacteria-based repair system.

ABSTRACT

Bacteria induced calcite precipitation has been proven to be effective in making concrete structure self-healing. In Microlab TU Delft, the concept has been enhanced by developing a liquid bacteria-based concrete repair system. The solution contains calcite precipitating bacteria, nutrients and buffer compound which may demonstrate high potential as healing agent to be injected into porous network concrete (PNC). This type of concrete has a porous core which can be used as a media to transport healing agents into the fracture zone.

The concept was tested in the 55×55×285 mm PNC prisms with 23×23×285 mm porous concrete core in the interior. Ø2 mm threaded steel rebar was installed below the core. A crack was formed by three-point bending loading and the solution was injected through porous network until it reached and flew out through the crack opening. The bacteria then precipitated calcium carbonate blocking the crack. The healing efficiency was measured by water permeability test before and after injection at several time intervals. Second cycle mechanical loading was carried out to assess regain of mechanical properties. Eventually, calcite precipitation in the crack wall was examined by polished section with ESEM.

Preliminary results showed more than 90% permeability reduction has been achieved at 11 days which appeared to be temporary since after 19 days permeability reduction drop to 70%. This could be attributed to the flushing of the solution after 11 days as the process could be not yet complete. However, bacteria imprints obtained from ESEM observation of polished section of Ø26-30 mm cylindrical porous core 21 days after injection with the solution provided strong evidence of bacterial activity and confirm the previous observation

The on-going research program has been devised implementing tap water and bacteria-based solution injected specimens with wet and dry curing. The results showed that wet cured bacteria series exhibited 99% permeability reduction while dry cured specimen only shows 60% reduction.

1. INTRODUCTION

The bacteria-based repair system has been developed recently by researchers at Microlab TU Delft [1]. This bio-based system is a liquid system containing alkaliphilic calcite precipitating bacteria, nutrients and transport solution leading to porosity reduction of concrete matrix. This system has been applied on concrete structure successfully as it yields to crack closure.

This paper investigates the feasibility to inject the solution into the fracture zone of concrete by means of porous network concrete (PNC). By mimicking bone shape,

PNC has porous (pervious/enhanced porosity) concrete in the interior of concrete structures [2]. This interconnected meso-size air void system constitutes an alternate means for distributing the healing agent to a crack or cracks in the main structure.

2. PRELIMINARY PROGRAM

The bacteria-based repair system consists of two types of solutions namely A which is composed of bacteria, feed and buffer compound and B containing a calcium source to promote massive calcium carbonate precipitation. The solutions were prepared based on Wiktor and Jonkers [1] meanwhile PNC was casted as described by Sangadji and Schlangen [2].

Initial falling head water permeability test (fig 1.a) was performed by flowing water from point (a) to the opposite point (b) prior to crack formation by means of strain controlled three point bending. Post-crack permeability test (fig 1.b) then was carried out by blocking the end connector (b) with water stop allowing water to flow out into container (c). This step then would also be used to measure post-healing permeability. After drying the excess water out from the porous core by blowing ± 0.7 bar pressurized air for ± 20 minutes, the solution was injected (fig 1.c) by means of syringe (d) which then flew out through the crack (e). Afterwards specimen was sealed with plastic for 24 hour. Then, to keep the porous core empty ± 0.7 bar pressurized air was blown through for ± 20 min. Specimen were cured under lab condition with RH $\pm 30\%$ and temperature $\pm 20^\circ\text{C}$ prior to after-healing permeability test and second mechanical three point loading.

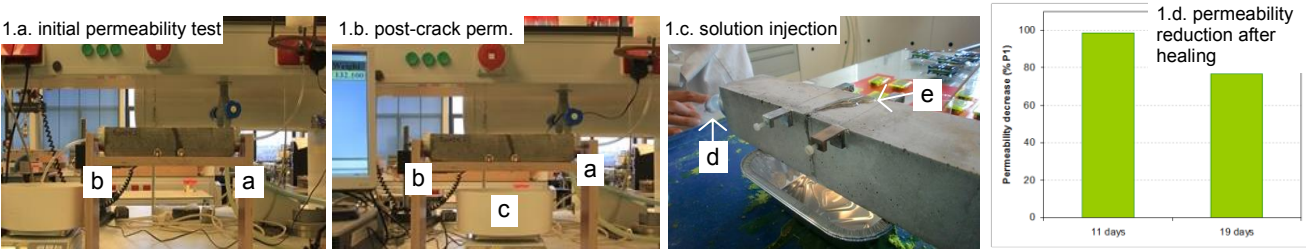


Figure 1: Preliminary experimental procedure and the result of the study

The result for permeability test after healing showed a very promising 98% reduction at 11 days assuming precipitation products were formed in the crack zone. However, lower percentage of permeability reduction was achieved after 19 days test on the same specimen, depicted in figure 1.d. This could be attributed to the flushing of the solution after 11 days. It was assumed that healing process have not yet completed. As temporary healing was observed, a preliminary investigation to assess sealing capacity of bio-based solution was conducted. The 4 ml same solution composition was then injected into $\varnothing 26\text{-}30$ mm cylindrical porous core covered with plastic film tightened with adhesive tape. One control (tap water injection) and four different series (bacteria-based solution injection) with two replicates were carried out. Bio-mineral precipitation was monitored 3, 7, 14, 21, and 28 days using several techniques; x-ray μCT Scan, water permeability test, and ESEM.

After 3 days, observations of polished sections under stereomicroscope and ESEM exhibited a cavity between porous concrete matrix and epoxy resin in the series comprising nutrients. This was attributed to the food dissolution during the grinding process with water. However, further higher magnification observation into this cavity

appears to be a good indicator for the location of bacteria-based solution and therefore to the presence of calcium carbonate precipitated due to bacterial activity. Bacteria imprints on Ca-based mineral (figure 2) observed in different spots provided the direct evidence of bacteria induced CaCO_3 precipitation. This result leads to the conclusion that bacteria-based repair solution can successfully be injected into porous network concrete as crack-healing agent.

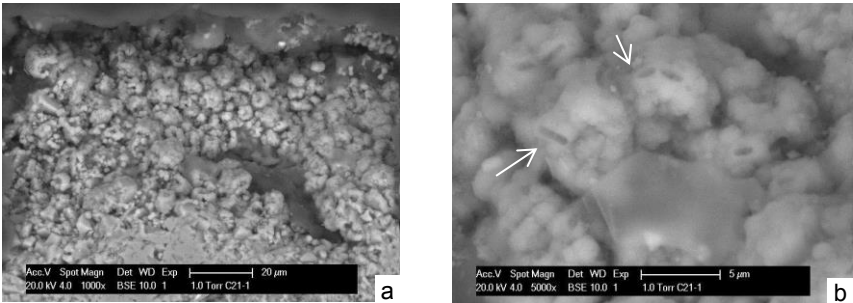


Figure 2: (a) Ca-based mineral formation of series ‘C’ at 21 days, (b) 5000x magnification shows bacteria imprints (white arrows) of spot (a).

3. ON-GOING RESEARCH PROGRAM

As a consequence of the preliminary results a research program (see table 1) has been devised to implement injection of bacteria based solution into 55×55×285 mm PNC specimen. Each specimen center interior is 23×23×285 mm porous concrete and Ø2 mm threaded steel rebar was installed under the core. The specimen was prepared as described by Sangadji and Schlangen [2]. Two type of treatment were implemented with 2 replicates. The ‘control’ series received injection of tap water and ‘bacteria’ series received injection of bacteria-based solution. Two different curing were conducted in which ‘wet’ series were cured in ± 95% RH and ± 20°C curing chamber while ‘dry’ series were cured under lab condition abovementioned.

Table 1: matrix of research program.

		Curing	
		Wet	Dry
Treatment	Control	CtrlW-1	CtrlD-1
		CtrlW-2	CtrlD-2
Bacteria		BactW-1	BactD-1
		BactW-2	BactD-2

Similar test procedure as described in preliminary program was performed. Initial crack width in the beam bottom side was achieved around ± 250 µm [2]. Then 30 ml water was injected into PNC ‘control’ series and solution A and B were injected into ‘bacteria’ series specimens. To improve CaCO_3 formation capacity, calcium salt has been changed. Crack closure has been monitored before and 7, 14, 21, and 28 days after injection under stereomicroscope. Quantification of crack-healing has been carried out using the method as described by Wiktor and Jonkers [3]. 28 days post-healing permeability test was executed to measure permeability reduction. The results showed that wet cured bacteria series exhibited 99% permeability reduction while dry cured specimen only shows 60% reduction. By the times this abstract is written, the first replicate specimen preparation for ESEM is in

progress meanwhile the second replicates is currently cured for on-going monitoring until 100 days.

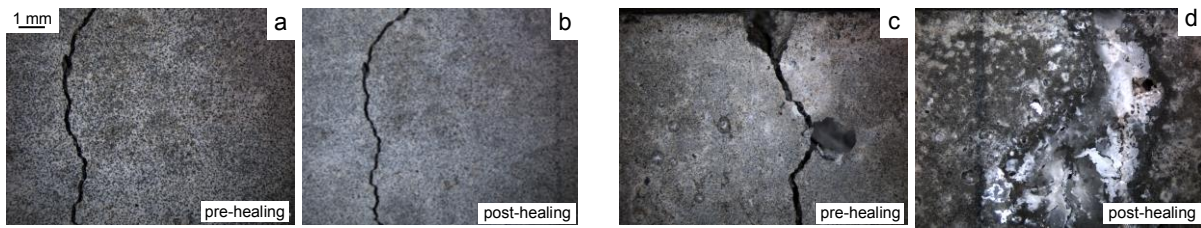


Figure 3: stereomicroscopic images of dry cured control before (a) and after (b) 28 days healing, and in wet cured 'bacteria' before (c) and after (d) 28 days healing.

Second cycle three-point loading was carried. The result was compared to the first cycle loading to assess regain of mechanical properties. The curves are presented in figure 4 which obviously showed limited strength and stiffness regain.

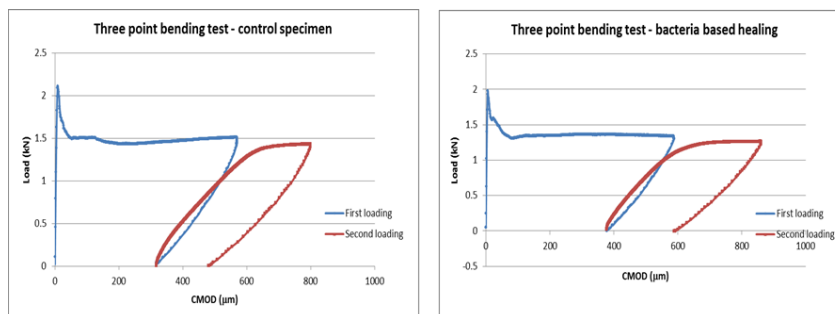


Figure 4: Load versus crack mouth opening displacement before and after healing.

4. CONCLUSIONS

As evidence of bacteria activity has been found with observation of bacteria imprints in the preliminary studies, the crack closure in the bacteria-based solution injected beam can then be allocated induced by bacteria. Even though mechanical regain in term of strength and stiffness of bacteria-based post-healing beam is quite limited, crack sealing works effectively and liquid tightness may be assured.

ACKNOWLEDGEMENTS

The authors acknowledge Mr. Ger Nagtegaal and Mr. Arjan Thijsen for their support, the Ministry of National Education, the Government of the Republic of Indonesia for scholarship for S. Sangadji and the Technology Foundation STW for the financial support for the project 11342.

REFERENCES

- [1] V. Wiktor, H.M. Jonkers, Application of bacteria-based repair system to damaged concrete structures, Proceedings of the 2nd International Workshop on Structural Life Management of Underground Structures, Daejeon, 2012, pp. 31-34.
- [2] S. Sangadji, E. Schlangen, Self-healing of Concrete Structures - Novel approach using porous network concrete, Journal of Advanced Concrete Technology, 10 (2012) 185-194.

[3] V. Wiktor, H.M. Jonkers, Quantification of crack-healing in novel bacteria based self-healing concrete, *Cement and Concrete Composite*, 33 (2011) 763-770.

INORGANIC POWDER ENCAPSULATED IN BRITTLE POLYMER PARTICLES FOR SELF-HEALING CEMENT-BASED MATERIALS

H. Dong¹, H. Huang¹ and G. Ye¹

¹ *Microlab, Faculty of Civil Engineering and Geosciences, Delft university of Technology, Stevinweg 1, 2628 CN Delft, The Netherlands - Email: H.Dong@tudelft.nl*

Keywords: cement-based material, healing agent, encapsulation, polystyrene, ECC

ABSTRACT

Many types of healing agents have been investigated. These agents are processed in different ways, such as adhesive polymer in capsules or hollow fibre glasses, bacteria in porous aggregates and geo-materials directly incorporated in the cement-based materials. In this study, sodium silicate powder is encapsulated in polystyrene particles (polystyrene particle containing sodium silicate is defined as PS particle in short).

The PS particles remain intact in the cement-based matrix before cracking. If water or moisture is available, the healing agent can be released into the crack provided that the crack passes through the PS particles. The dissolved sodium silicate reacts with calcium hydroxide in the matrix, and the healing products (C-S-H gel) can form in the crack. Furthermore, compared to the reference, for the cracked specimens with polystyrene particles, the recovery of flexural stiffness can be observed.

Different sizes and mass fractions, i.e. sodium silicate / cement ratios, of PS particles used in engineered cementitious composite (ECC) mixture are studied to see their influence on mechanical properties as well as their healing efficiency. When the mass fraction of polystyrene particles is 4% of cement and the polystyrene particles have a proper slender shape, the ECC show good results in terms of flexural strength, flexural deflection capacity and recovery of mechanical properties. Therefore, encapsulation of healing agent in polystyrene could be regarded as a promising way for realising self-healing of cement-based materials.

1. INTRODUCTION

Cracks are inevitable in concrete, possible resulting in further problems such as corrosion of reinforcement, thus accelerating the deterioration of concrete structures. To reduce the cost of repair and prolong the service life of concrete structures, self-healing of concrete has been regarded a promising solution. Many types of healing agents processed in different ways have been studied in the last decade, such as adhesive polymer in capsules or hollow fibre glasses [1], bacteria in porous aggregates [2] and geo-materials directly incorporated in cement-based materials [3].

In cement chemistry, $\text{Ca}(\text{OH})_2$ is one of the main hydration products in cementitious materials. Under certain conditions, $\text{Ca}(\text{OH})_2$ can facilitate the self-healing process. For example, $\text{Ca}(\text{OH})_2$ can be designed to react with sodium silicate solution that is encapsulated in polyurethane capsules [4]. However, for those capsules it is difficult to survive during casting in construction due to their weak shell. For self-healing, it is

of great importance that the healing agent should be well protected before the healing process is triggered by the crack. In general, polystyrene is widely used in the industry and it is one of the most brittle polymers. This characteristic of polystyrene facilitate its rupture in cementitious materials. In this study, concerning controlled release of the healing agent, sodium silicate powder is encapsulated in polystyrene matrix. The self-healing process of cementitious materials by using polystyrene particle (PS particle) is studied, the size and amount of polystyrene particles are optimized as well.

2. MATERIALS

Na_2SiO_3 powder (diameter: 500-700 μm) and polystyrene beans ($\text{Ø}2 \text{ mm} \times 3 \text{ mm}$, ultimate tensile capacity is 2%) are mixed at 170 $^\circ\text{C}$ by single screw extruder and pressed (170 $^\circ\text{C}$) into thin sheets (thickness: 1 mm). The amount of Na_2SiO_3 powder (36% by mass) used in the mixture is determined by the viscosity of the mixture. To improve the bond between PS particles and cementitious matrix, a coating of epoxy resin was applied on the PS sheets, and another layer of fine sand (diameter: 300-500 μm) is coated to the polystyrene sheets (After coating, mass fraction of Na_2SiO_3 is 20%). Then the sheets are cut into small particles with specified sizes, which are expected to rupture upon crack propagation in the cementitious materials (Fig 1).

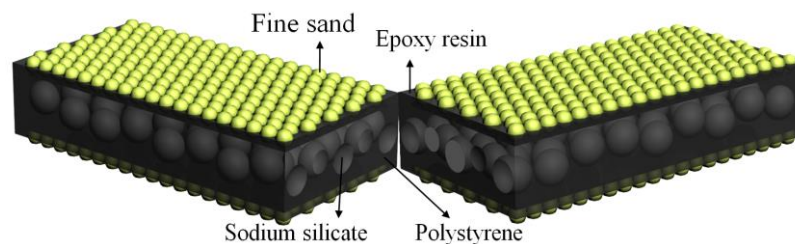


Figure 1: Rupture of PS particles ($3 \times 12 \times 2 \text{ mm}^3$)

Engineered cementitious composite (ECC) is adopted for the evaluation of healing efficiency of PS particles due to its good ductility with tight micro-cracks which are beneficial for self-healing process [5]. In this study, materials of thin ECC layers (size of $120 \times 30 \times 10 \text{ mm}^3$ or $120 \times 30 \times 5 \text{ mm}^3$) used for all tests consist of Portland cement CEM I 42.5 (PC), blast furnace slag (BFS), limestone powder as fine aggregate (LP), naphthalene based superplasticizer (SP) and PVA fiber (diameter: 39 μm , length: 8 mm).

2.1 Observation of self-healing process – proof of principle

A trial test to reveal the healing process is conducted by adding PS particles to a ECC mixture. The mix proportion (Kg) for 1m³ ECC is PC : PS particles : BFS : Water : SP : PVA fiber = 945 : 135 : 405 : 405 : 13.5 : 26. It is found that PS particles remain intact during mixing in the mixture. Then the mixture is poured into the mould with size of $240 \times 60 \times 10 \text{ mm}^3$ followed by sealed curing for 28 days at 20 $^\circ\text{C}$.

2.2 Optimization of PS particles and evaluation of healing efficiency

To evaluate the healing efficiency of PS particles in cementitious materials, different volume fractions and different sizes of PS particles are taken into account in the

mixtures (see table 1). 4-point bending tests are conducted. The volume fraction (v%) of PS particles is 0 (for reference), 3.45%, 6.9% and 10.35%, respectively (corresponding ratio of Na₂SiO₃ to cement as 0, 2%, 4% and 6%). In each series, PS particles with a size of 3 × 12 × 2 mm³ are used. M3 is designed for the evaluation of particle sizes, PS particle sizes of 5 × 5 × 2 mm³, 3 × 12 × 2 mm³, 3 × 20 × 2 mm³ and 5 × 20 × 2 mm³ are used in this series. After mixing, the mixture is cast into the mould (size: 240 × 60 × 5 mm³) followed by sealed curing for 28 days at 20 °C.

Table 1: Mix proportion of ECC (Kg/m³)

	V% of PS	PC	LP	PS particle	BFS	Water	SP	PVA fiber
M1	0	534	427	0	640	469.6	11.7	26
M2	3.45%	534	333.8	51.1	640	469.6	9.4	26
M3	6.9%	534	240.6	102.2	640	469.6	7.0	26
M4	10.35%	534	147.3	153.3	640	469.6	4.7	26

3. METHODS

In the trial test for self-healing in ECC, after 28 days curing, the specimen is cut into 120 × 30 × 10 mm³ and cracked by 4-point bending test (setup span is 110 mm, load span is 30 mm. Loading speed is 0.02 mm/s, and vertical deflection is controlled to 1 mm), the crack width obtained is in the range between 50 - 100 μm . The cracked specimens are subjected to 3 wet-dry cycles. One wet-dry cycle consists of 24h merging in the water (20 °C) and 24h drying in the air (20 °C, 50% relative humidity).

For the optimization of PS particles and evaluation of the healing efficiency, the specimens are cut to 120 × 30 × 5 mm³ for 4-point bending tests. Each series uses 8 specimens, which consist of:

- Three specimens for determination of ultimate flexural strength at 28 days.
- Two specimens (for reference) are preloaded to 3 mm deflection at 28 days. After 3 days curing in air (20 °C, 50% relative humidity), the specimens are reloaded to failure.
- Three specimens (for self-healing) are preloaded to 3 mm deflection at 28 days. After 3 days curing in 100% RH curing room (20 °C), the specimens are reloaded to failure.

In this test a loading speed of 0.02 mm/s is applied. For the calculation of flexural stiffness, stress from 1 MPa to 2 MPa (linear part) is specified (Fig 2). Ratio of flexural stiffness (R_S) is defined in equation (1). Higher R_S indicates a higher recovery of flexural stiffness after curing. For R_S it holds:

$$R_S = \frac{S_{Pre}}{S_{Re}} \quad (1)$$

where S_{Pre} is the flexural stiffness of specimen preloaded at 28 days, S_{Re} is the flexural stiffness of specimen reloaded at (28 + 3) days.

4. RESULTS

In the trial test for self-healing in ECC, after 3 wet-dry cycles, healing products are observed on the surface of cracks (Fig 3). From energy dispersive spectroscopy (EDS), it can be concluded that the healing products are mainly composed of C-S-H.

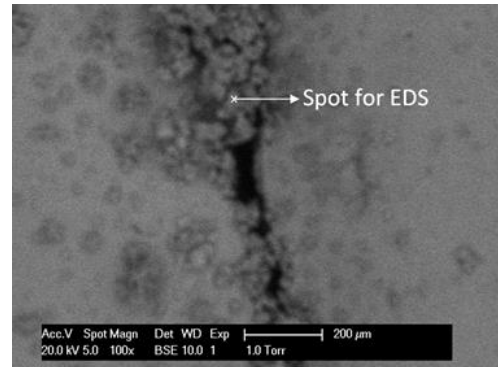
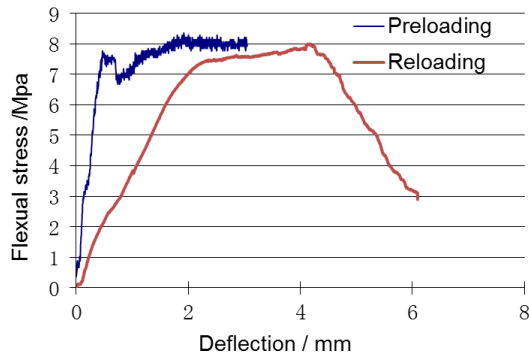


Figure 2: Stress-deflection curve of ECC Figure 3: Micrograph of crack after healing

Optimization of PS particles is studied to see their size and volume effect on the mechanical properties of cementitious materials. In this test, specimens with different sizes and volume fractions (v%) of PS particles are bended to failure at 28 days. The results of flexural strength and deflection capacity are shown in Fig 4 and Fig 5.

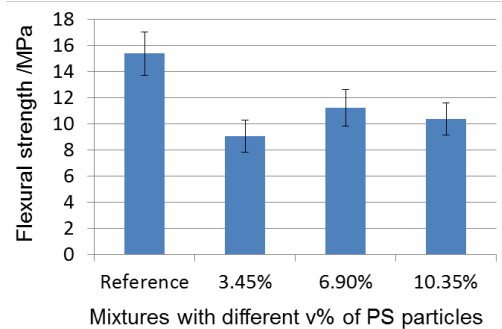
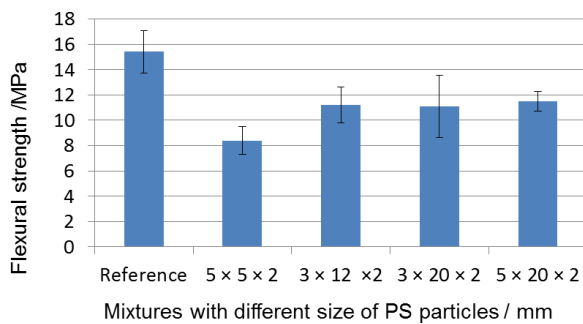


Figure 4: Flexural strength at 28 days

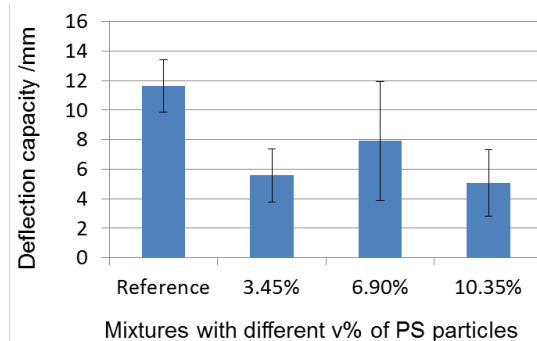
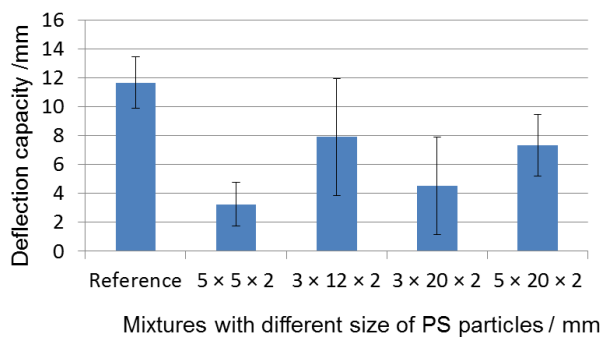


Figure 5: Flexural deflection capacity at 28 days

It can be seen that there is a lower reduction of flexural strength for the specimens with the PS particles in a slender shape, and PS particles with the size of $3 \times 12 \times 2$

mm³ has the lowest reduction of the deflection capacity. For the volume fraction of PS particles, it seems that 6.9% is the best one among 3 volume fractions incorporated in the specimens. In this test, PS particles are applied to replace a certain amount of limestone powder. Therefore, there is a delicate balance between the amount of PS particles and the total amount of binder.

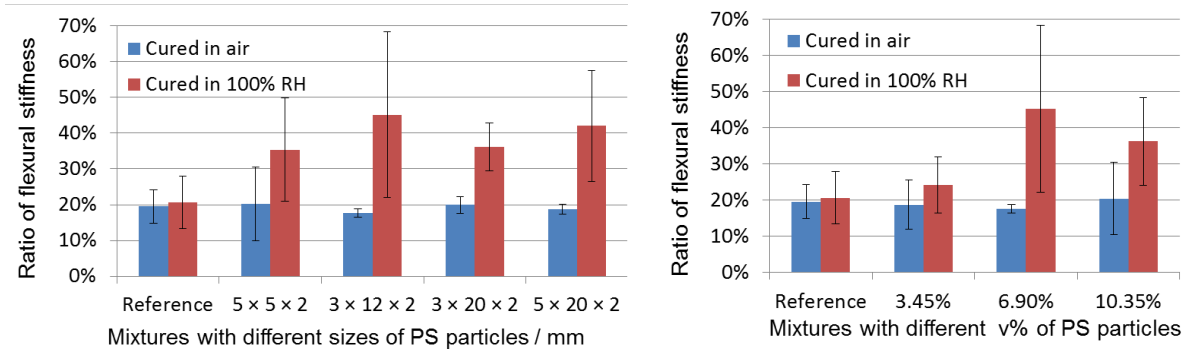


Figure 6: Ratio flexural stiffness (R_s) of specimens

To evaluate the healing efficiency of PS particles, after another 3 days curing (in air, or in 100% RH curing room) the ratio of flexural stiffness (R_s) of each specimen is calculated and plotted in Fig 6. Similar to the flexural strength and deflection capacity, PS particles with the size of $3 \times 12 \times 2$ mm³ and the volume fraction of 6.9% show the best results. From the results, high errors for the flexural stiffness ratio are observed which is in line with other results published in the article[6]. It is because of the presence of fibers and PS particles, and the flexural capacity and ratio of flexural stiffness (R_s) are dependent on the quantity and width of micro cracks. Nevertheless, the difference between different particle sizes and volume fractions are obvious.

5 CONCLUSIONS

A new self-healing agent, polystyrene particles containing Na₂SiO₃ is proposed. The polystyrene particles containing Na₂SiO₃ is proved to work well with cementitious materials. During mixing and casting, PS particles remain intact and can be ruptured upon the propagation of cracks. Then Na₂SiO₃ powder can be released into the crack when water or moisture is available. After moisture curing, the higher ratio of flexural stiffness (R_s) of ECC specimens with healing agent indicates a higher recovery of mechanical property than the reference. For particle dimensions, it shows that PS particles in a slender shape are preferable since they can bridge the cracks as fibers before failure of ECC.

ACKNOWLEDGEMENTS

Financial support by the Dutch Technology Foundation (STW) for the project 10981-“Durable Repair and Radical Protection of Concrete Structures in View of Sustainable Construction” is gratefully acknowledged.

REFERENCES

- [1] V.C.Li, Y.M.Lim, Y.W.Chan, Feasibility study of a passive smart self-healing cementitious composite, *Composites Part B: Engineering* 29 (1998), 819–827.
- [2] V.Wiktor, H.M.Jonkers, Quantification of crack-healing in novel bacteria-based self-healing concrete, *Cement and Concrete Composites* 33 (2011), 763–770
- [3] T.H.Ahn, T.Kishi, Crack self-healing behavior of cementitious composites incorporating various mineral admixtures, *Journal of Advanced Concrete Technology* 8 (2010), 171-186.
- [4] A.Bose, Self-healing concrete developed using sodium silicate microcapsules, *Advanced Composites Bulletin* 7 (2010), 8
- [5] Y.Yang, M.D.Lepech, E.H.Yang, V.C.Li, Autogenous healing of engineered cementitious composites under wet–dry cycles, *Cement and Concrete Research* 39 (2009) 382–390.
- [6] S.Z. Qian, J. Zhou, E. Schlangen, Influence of curing condition and precracking time on the self-healing behaviour of Engineered Cementitious Composites, *Cement and Concrete Composites* 32 (2010) 686-693.

SESSION 8 – MODELLING AND NUMERICAL ANALYSIS TOOLS

SELF-HEALING PHENOMENA IN POLYMERS BASED ON THE THEORY OF POROUS MEDIA

S. Specht¹, J. Bluhm¹, J. Schröder¹

¹ Faculty of Engineering, Department of Civil Engineering, Institute of Mechanics, University of Duisburg-Essen, Universitätsstr. 15, 45141 Essen, Germany – e-mail: steffen.specht@uni-due.de, joachim.bluhm@uni-due.de, j.schroeder@uni-due.de

Keywords: Multiphase Systems, Theory of Porous Media, Phase Transition, Healing Processes

ABSTRACT

Self healing materials are becoming more and more important for the construction of mechanical components due to their ability to detect and heal failures as well as cracks autonomously. Especially in polymers and polymer-composites, where the component can loose a high rate of strength and durability due to micro cracks, those damages are nearly impossible to repair from outside. Thus, self healing ability is a very effective approach to extend the lifetime of polymer-made components.

In view of the numerical simulation of such self healing effects we consider the microencapsulation approach [1] and develop a thermodynamically consistent macroscopic 5-phase model within the framework of the Theory of Porous Media (TPM) [2]. The model consists of the following different phases: solid, liquid, healed material, gas, and catalysts. The increase of damage, which is represented by the gas phase, is driven by a damage evolution equation. Furthermore, a mass exchange between the liquid-like healing agents and the solid-like healed material, i.e., the change of the aggregate state from liquid healing to solid healed material, describes the healing process. The onset of the healing process is associated with the break open of the microcapsules in connection with the subsequent motion of the liquid healing agents. Numerical examples of the simulation of healing processes in polymers and polymer-composites are presented in order to show the applicability of the model.

1. INTRODUCTION

The self healing system, which is analyzed in this contribution, is a polymer matrix with included microencapsulated healing agents and catalysts, see [1]. If a crack tip breaks through such a microcapsule, the healing agents flows into the crack, polymerizes due to reaction with the catalysts, and close the crack.

The multiphase system, modeled within the framework of the *Theory of Porous Media* (TPM) [2], consists of solid matrix material (S), liquid healing agents (L), solid healed material (H), catalysts (C), and a gas phase (G), which describes the damage of the structure. For simplification it will be assumed that the motion of the solid material and the solid-like healed material are all equal except at an initial solid motion. Furthermore, only isothermal processes are taken into consideration.

2. THEORETICAL FRAMEWORK

A porous media is composed of κ individual constituents φ^α ($\alpha = S, H, L, G, C$). Within the framework of the TPM it is assumed that all constituents are statistically distributed over a control space and that the system is in ideal disorder. The single constituents are smeared over the control space and occupy the whole volume of the control space simultaneously, see Fig. 1. Thus, all geometrical and physical quantities of the individual constituent such as motion, stress or deformation are defined as statistical averages of the real quantities of the corresponding constituent in the control space. In general, the control space is modeled by the solid phase. Furthermore, a real density $\rho^{\alpha R}$ as well as a volume fraction n^α are assigned to each phase. The real density of a constituent is the mass per unit volume dv^α , while the volume fraction $n^\alpha = dv^\alpha/dv$ represents the proportion of the total volume occupied by the constituent. The relation between the partial density ρ^α and the real density $\rho^{\alpha R}$ is given by $\rho^\alpha = n^\alpha \rho^{\alpha R}$. However, it is essential that the constituents of a porous medium can be easily identified at any time during a thermodynamic process with help of the volume fractions. For a detailed introduction and the historical development of the *Theory of Porous Media* the interested reader is referred to [3]. For the thermodynamically consistent simplified 5-phase macroscopic model some assumptions will be made: no consideration of dynamic effects; mass exchange occurs only between the liquid healing agents and the solid healed material ($\hat{\rho}^S = \hat{\rho}^G = 0$, $\hat{\rho}^H = -\hat{\rho}^L$); solid, healed material and liquid are incompressible ($\rho^{\beta R} = \text{const.}$ for $\beta = S, H, L$); and the motions of the solid and healed material phases are equal ($\mathbf{x}'_S = \mathbf{x}'_H$) except at an initial solid motion.

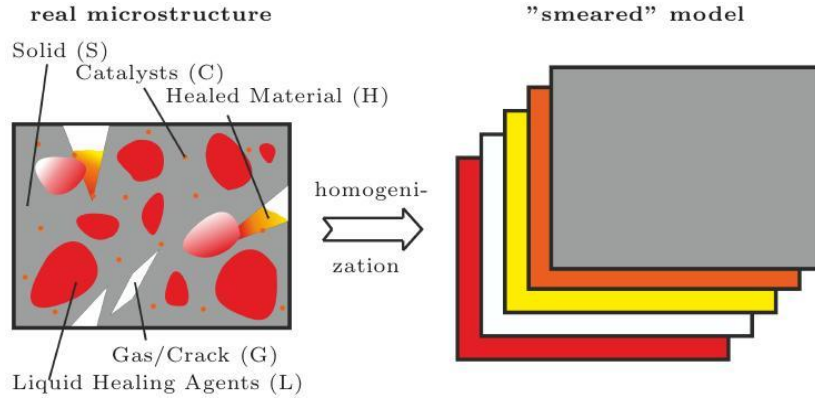


Figure 1: Homogenization of the real microstructure.

The simplified model for the simulation of healing processes is described by the local statements of the balance equations of mass,

$$\begin{aligned}
 (n^S)'_S + n^S \operatorname{div} \mathbf{x}'_S &= 0, & (n^H)'_S + n^H \operatorname{div} \mathbf{x}'_S &= \frac{\hat{\rho}^H}{\rho^{\text{HR}}}, \\
 (n^L)'_L + n^L \operatorname{div} \mathbf{x}'_L &= -\frac{\hat{\rho}^H}{\rho^{\text{LR}}}, & n^S (c^C)'_S - \operatorname{div} (n^S c^C \mathbf{w}_{\text{CS}}) &= \frac{\hat{\rho}^C}{\rho^{\text{CR}}}, \\
 (n^G)'_G + n^G \operatorname{div} \mathbf{x}'_G + \frac{n^G}{\rho^{\text{GR}}} (\rho^{\text{GR}})'_G &= 0,
 \end{aligned} \tag{1}$$

the balance equations of momentum for the mixture, liquid, gas, and catalysts,

$$\begin{aligned} \operatorname{div} \mathbf{T} + \rho \mathbf{b} &= -\hat{\rho}^H \mathbf{w}_{LS}, & \operatorname{div} \mathbf{T}^L + \rho^L \mathbf{b} &= -\hat{\mathbf{p}}^L, \\ \operatorname{div} \mathbf{T}^G + \rho^G \mathbf{b} &= -\hat{\mathbf{p}}^G, & \operatorname{div} \mathbf{T}^C + \rho^C \mathbf{b} &= -\hat{\mathbf{p}}^C, \end{aligned} \quad (2)$$

and the material time derivative of the saturation condition along the trajectory of the solid phase,

$$\operatorname{div} (n^L \mathbf{w}_{LS} + n^G \mathbf{w}_{GS} + \mathbf{x}'_S) + \frac{n^G}{\rho_{GR}} (\rho^{GR})'_G - \hat{\rho}^H \left(\frac{1}{\rho_{HR}} - \frac{1}{\rho_{LR}} \right) = 0. \quad (3)$$

In the equations above, $\mathbf{T} = \sum_{\alpha} \mathbf{T}^{\alpha}$ and $\rho = \sum_{\alpha} \rho^{\alpha}$ denote the Cauchy stress tensor and the density of the mixture. The mass production terms $\hat{\rho}^H$ and $\hat{\rho}^C$ depend on the concentration of catalysts. The production terms of momentum ($\hat{\mathbf{p}}^L, \hat{\mathbf{p}}^G, \hat{\mathbf{p}}^C$) are functions depending on the real pressures of the constituents and the vectors $\mathbf{w}_{\alpha S}$ are the relative velocities of the corresponding phase with respect to the solid. Values denoted by the symbol $(\dots)'_{\alpha}$ are the material time derivatives following the motion of φ^{α} . The vector \mathbf{b} denotes the gravity. For the derivation of the constitutive relations for the stresses and the production terms it is referred to [4].

3. RESULTS

To show the applicability of the model, the behavior of a self healing cantilever beam is shown in a numerical simulation. The beam, see Figure 2, is clamped on the left side. The boundaries are open for gas, but closed for the liquid phase, i.e., gas can flow in and out on every side and liquid can not flow out of the beam. The body is loaded with 64 kN in total over the whole length. The onset of healing starts after 2.0 sec. and only in areas where $n^G > 0.11$.

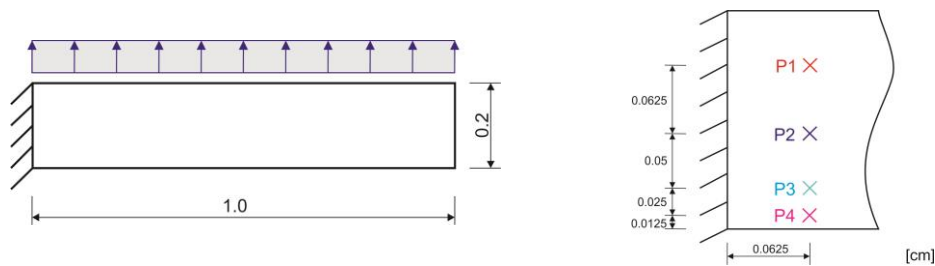


Figure 2: Boundary value problem and points of measurement.

	S	H	L	G	C	[-]
Young's modulus E^{α}	1.75e+7	1.75e+7	-	-	-	Pa
Poisson's ratio ν^{α}	0.2	0.2	-	-	-	-
real density $\rho^{\alpha R}$	1200.0	960.0	1000.0	1.0	-	kg/m ³
initial volume fraction n^{α}	0.6	0.0	0.3	0.1	-	-
initial concentration c^{α}	-	-	-	-	1.0	$\times 100\%$

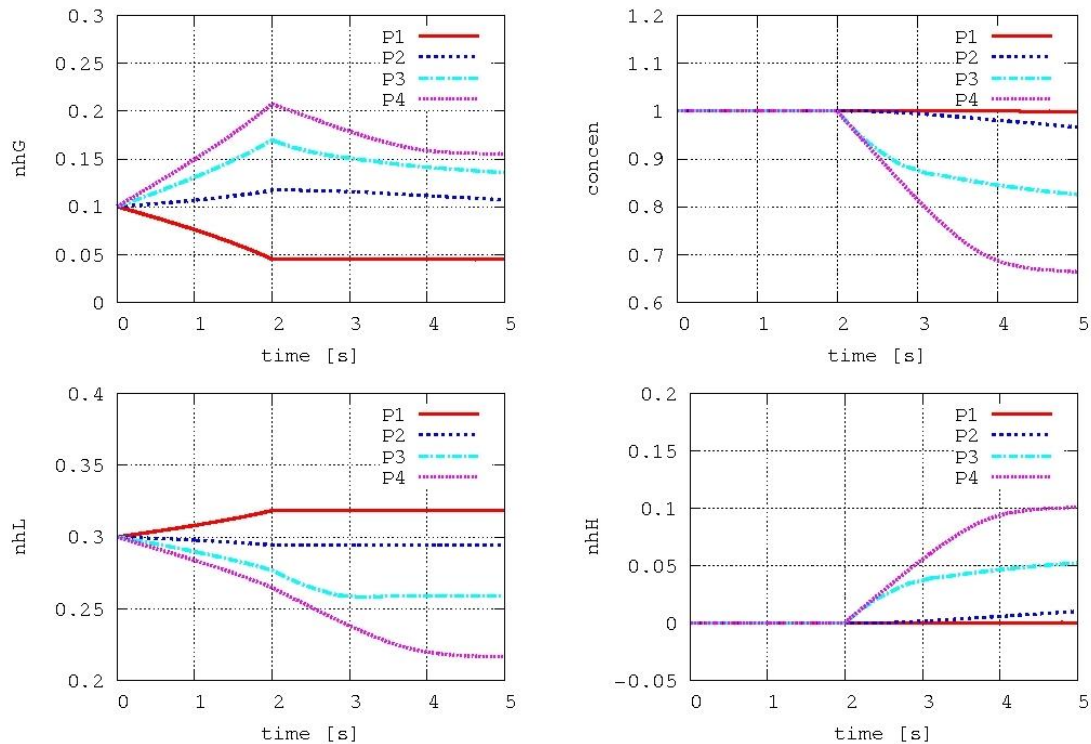


Figure 3: Evolution of different volume fractions during the simulation.

During the deformation, in the first 2 seconds, one can observe that the gas phase increase, i.e., an increase of damage, on the lower side of the beam where tension occur. After two sec. the healing process starts and liquid will be converted into healed material. This leads to an increase of healed material and simultaneously a decrease of gas. These effects describe the healing of the damaged material.

4. CONCLUSIONS

The presented five-phase model based on the TPM is applicable to simulate numerically self healing effects in a polymer matrix with embedded healing agents and catalysts. The simulation shows clearly the dependency of the healing and the concentration of catalysts.

ACKNOWLEDGEMENTS

This work has been supported by the German Research Society (DFG) SPP 1568.

REFERENCES

- [1] S.R. White, N.R. Sottos, P.H. Geubelle, J.S. Moore, M.R. Kessler, S.R. Sriram, E.N. Brown, and S. Viswanathan. Autonomic healing of polymer composites. *Nature*, 409 :794-797, 2001.
- [2] W. Ehlers and J. Bluhm. *Porous Media*. Springer, 2002.
- [3] R. de Boer. *Theory of Porous Media*. Springer, 2000.
- [4] S. Specht. *Self Healing Materials – A Continuum Mechanical Model Based on the Theory of Porous Media*. Masterthesis, 2012.

INTERACTIVE MATHEMATICAL MODEL OF SELF-HEALING IN CARBONATED CEMENTITIOUS MATERIALS

S.V. Zemskov¹, O. Copuroglu² and F.J. Vermolen¹

¹ Faculty of Electrical Engineering, Mathematics and Computer Science, Delft University of Technology, Mekelweg 4, 2628 CD Delft, The Netherlands – e-mail: zemskov01@gmail.com; F.J.Vermolen@tudelft.nl

² Faculty Civil Engineering & Geosciences, Delft University of Technology, Stevinweg 1, 2628 CN Delft, The Netherlands – email: O.Copuroglu@tudelft.nl

Keywords: numerical modeling, finite-element method, concrete, self-healing, carbonation

ABSTRACT

A mathematical model for the post-damage recovery of carbonated cement is described. The model is based on a two-dimensional initial-boundary value problem for a system of partial differential equations. The study is embedded within the framework of investigating the effect of using lightweight expanded clay aggregate, which is incorporated into the impregnation of the sodium mono-fluorophosphate (Na-MFP) solution. The model of the self-healing process is built under the assumption that the position of the carbonation front changes in time. Here the rate of diffusion of Na-MFP into the carbonated cement matrix and the reaction rates of the free phosphate and fluorophosphate with the components of the cement are comparable to the speed of the carbonation front. The main modeling results presented in the paper are related to the autonomous improvement of the structure of carbonated blast furnace slag cement. Nevertheless, the parameters of the model can be set for various types of cement paste and different conditions of the healing process (including both carbonation under natural conditions and accelerated carbonation). The governing diffusion-reaction equations are solved using a Galerkin finite-element method. For usage convenience, the model is completed as an interactive application on the basis of computer algebra system *Mathematica*.

1. INTRODUCTION

The microstructure of blast furnace slag cement (BFSC) is not too different from that of ordinary Portland cement (OPC) [1]. However, it has been found that cements containing a high amount of BFS have a poor resistance against carbonation. It is generally known that the content of calcium hydroxide ($\text{Ca}(\text{OH})_2$) in concrete plays an important role for carbonation resistance. However, BFSC concrete tends to suffer much more from carbonation than the OPC mixture does due to its significantly lower $\text{Ca}(\text{OH})_2$ content. One way to improve this disadvantage of BFSC concrete is to use sodium-monofluorophosphate (Na-MFP) as an addition to the cement mixture [2].

It is known that Na-MFP ($\text{Na}_2\text{PO}_3\text{F}$) hydrolyses into the solution to form $\text{H}_2\text{PO}_4^{2-}$ and F^- . These anions react with the certain components of the cement matrix (including products of carbonation reaction) to form fluorapatite ($\text{Ca}_5(\text{PO}_4)_3\text{F}$) and fluorite (NaF) [3] which are highly insoluble compounds. They improve the microstructure of BFSC and increase its tensile resistance.

In this paper we are going to consider a mathematical model for the post-damage improvement of the carbonated BFSC using expanded clay spherical capsules filled with Na-MFP.

2. THE MATHEMATICAL MODEL

To construct a mathematical model of the healing process, we consider one spherical capsule of radius R within a cement cube with side length $L \in [4R, 10R]$. The following assumptions are used:

- the cement cube is subject to carbonation and the ingress of gaseous carbon dioxide into the cement matrix takes place through the upper edge of the cube;
- the reaction of carbonation takes place in the narrow zone which can be approximated by a surface (a plane) referred to as the carbonation front; so, after some definite time, the cube is supposed to be divided by the carbonation front into two rectangular cuboids consisting respectively of carbonated and uncarbonated cement;
- both parts of the cement cube are penetrable for water to a different extent: the carbonated part possesses a higher effective porosity which implies, a higher permeability;
- the pores of both parts of the cement cube are filled with water, so diffusion of Na-MFP from the capsule through pores is facilitated assuming there is no diffusion transport through solid cement particles;
- the carbonation front position l is assumed to move downwards according to the relation $l(t) = L/2 - \kappa\sqrt{T+t}$ [4], where $l(0)$ is the initial z -coordinate of the horizontal carbonation front and T is the known time of carbonation process which is necessary to reach the position $l(0)$.

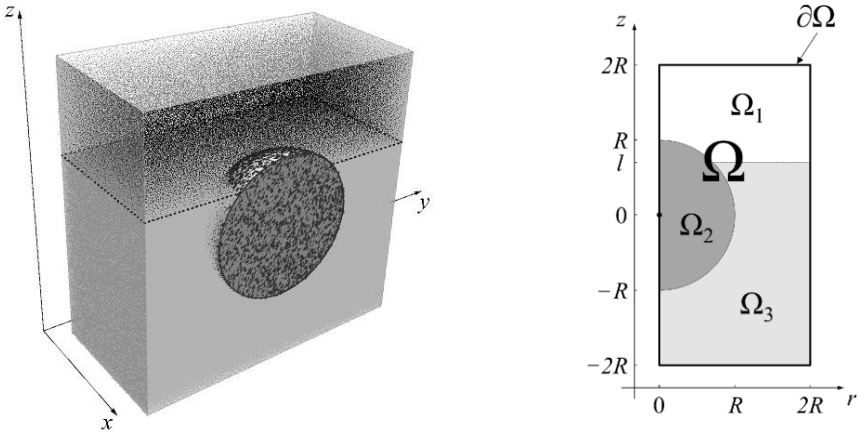


Figure 1: (left) Representation of a half of the concrete cube containing the capsule and consisting of uncarbonated (below) and carbonated (above) parts. (right) The computational domain for a two-dimensional mathematical model.

The vertical rectangular section of the cement cube passing through the center of the capsule provides us with a representation for the two-dimensional mathematical model (Figure 1 (left)). Due to symmetry reasons, we consider half of this cross-section (Figure 1 (right)).

The domain of computation Ω consists of three parts, Ω_1 , Ω_2 and Ω_3 , representing, respectively, the carbonated cement matrix, the capsule and the uncarbonated part of the cement matrix. The boundary $\partial\Omega$ of Ω is a rectangle of dimensions $L/2 \times L$. The center of the capsule section is assumed to have coordinates $(r, z) = (0, 0)$ in \mathbb{R}^2 . The z -coordinate of the horizontal carbonation front is denoted by l .

The content of the capsule (Na-MFP) dissolves and diffuses through water which fills the pores of both uncarbonated and carbonated parts of the cement cube. The chemical reaction between Na-MFP and certain components of the carbonated cement matrix (i.e. in the subdomains Ω_1 and Ω_3) takes place. Since the vast majority of the reacting chemicals in the cement are vaterite and aragonite, which are forms of CaCO_3 , we neglect the contribution of other cement components.

We denote the density of Na-MFP and CaCO_3 by $c_1 = c_1(r, z, t)$ and $c_2 = c_2(r, z, t)$, respectively. The following differential equations hold for c_1 and c_2 :

$$\frac{\partial c_1}{\partial t} = \nabla \cdot \left(\frac{D_0 \varepsilon_i}{1 - (\ln \varepsilon_i)/2} \nabla c_1 \right) - N_1 k c_1 \frac{1000 c_2}{M_{\text{CaCO}_3}}, \quad (r, z) \in \Omega_i, \quad i = 1, 2, 3; \quad (1)$$

$$\frac{\partial c_2}{\partial t} = -N_2 k c_2 \frac{1000 c_1}{M_{\text{Na}_2\text{PO}_3\text{F}}}, \quad (r, z) \in \Omega_1 \cup \Omega_3. \quad (2)$$

Here, D_0 is the actual diffusion coefficient of Na-MFP in water, $\varepsilon_i = \varepsilon_i(r, z, t)$ is the effective porosity of the i -th media, M_X are molar masses of corresponding chemicals, k is a proportionality factor defined experimentally, and N_1 , N_2 are the coefficients of the chemical equation.

No transport of Na-MFP is assumed through the boundary of Ω , hence we have a zero flux boundary condition. The initial densities of reacting chemicals are defined as follows:

$$c_1(r, z, 0) = \begin{cases} c_1^{\max}, & (r, z) \in \Omega_2; \\ 0, & (r, z) \in \Omega_1 \cup \Omega_3, \end{cases} \quad \text{and} \quad c_2(r, z, 0) = \begin{cases} c_2^{\Omega_1}, & (r, z) \in \Omega_1; \\ 0, & (r, z) \in \Omega_2; \\ c_2^{\Omega_3}, & (r, z) \in \Omega_3. \end{cases} \quad (3)$$

Equations (1), (2), zero flux boundary condition, and initial conditions (3) form an initial boundary value problem in Ω and for $t > 0$. After solving the boundary value problem on each time step, the density and the volume of fluoroapatite and fluorite formed in Ω_1 and Ω_3 as well as values of ε_1 and ε_3 are corrected with regard to amounts of reacted chemicals.

3. RESULTS AND DISCUSSION

Equations (1) and (2) are solved using Galerkin finite element method over a structured triangle grid. Some results obtained through a computer simulation are presented in Figure 2. In this example, we consider a half of the capsule section with the radius of 1 mm. The healing process proceeds under accelerated carbonation conditions.

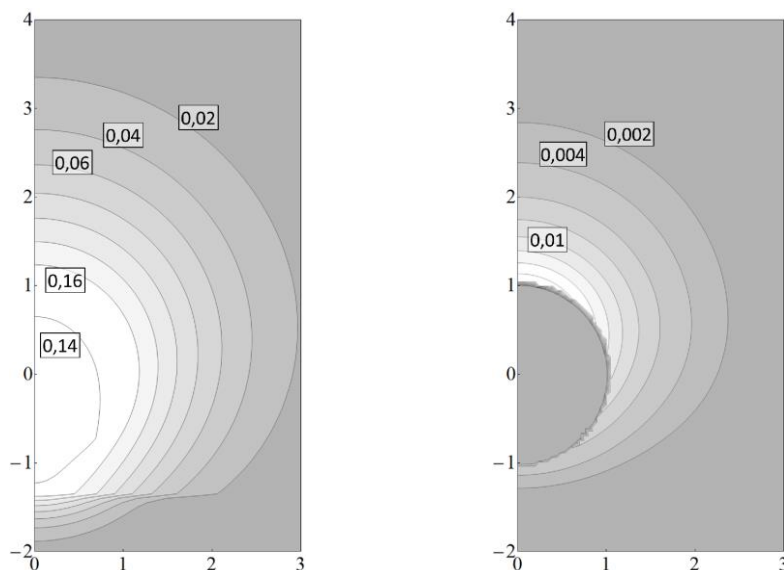


Figure 2: Concentration profile of Na-MFP (*left*) and total density profile of fluoroapatite and fluorite (*right*) after 100 days of healing process.

It can be seen how the movement of the carbonation front influences the process of diffusion of Na-MFP and, hence, forming of the reaction products. It is possible, in particular, to retrace the layer in which the density of the reaction product exceeds 0.01 g/cm^3 . This density is considered as sufficient to improve the cement structure. According to the results observed, one can make definite conclusions about necessary amount and concentration of Na-MFP in the capsule and the number of capsules per unit volume of cement.

A three-dimensional representation of this model can be obtained from symmetry considerations in a straight-forward manner. For usage convenience, the model is completed as an interactive application on the basis of computer algebra system *Mathematica*.

REFERENCES

- [1] I. Odler, *Special inorganic cements*, Taylor & Francis, New York, 2010.
- [2] O. Copuroglu, A.L.A. Fraaij, J.M.J.M. Bijen, Effect of sodium monofluorophosphate treatment on microstructure and frost salt scaling durability of slag cement paste, *Cem. Concr. Res.* 36 (2006) 1475-1482.
- [3] F. Farcas, T. Chaussadent, C. Fiaud, I. Mabilie, Determination of the sodium monofluorophosphate in a hardened cement paste by ion chromatography, *Anal. Chim. Acta* 472(1-2) (2002) 37-43.
- [4] T. Aiki, A. Muntean, Large time behavior of solutions to a moving-interface problem modeling concrete carbonation, *Comm. Pure Appl. Anal.* 9(5) (2010) 1117-1129.

BRIDGED CRACK APPROACH TO MODEL MATERIALS SELF-HEALING

M. Perelmuter¹

¹ Institute for Problems in Mechanics of RAS, Pr. Vernadskogo 101-1, 119526, Moscow, Russia - e-mail: perelm@ipmnet.ru

Keywords: self-healing, crack bridged model, stress intensity factors

ABSTRACT

The subject of this paper is the mathematical modelling of the crack self-healing process. For self-healing modeling of cracked structures the bridged crack approach is used. In the frames of this approach is assumed: 1) there is a crack in a structure after service loading; 2) there are bonds between surfaces of a crack (which are induced by a healing mechanism, the interface layer); 3) this layer is considered as a part of the crack with distributed nonlinear spring-like bonds between surfaces of crack (bridged zone). The bonds properties define the stresses at the crack bridged zone, its size and, hence, the fracture toughness of the material. The main goal of the modeling consists in the computational analysis of the bridging stresses distribution and in the computing of the stress intensity factors which are the main characteristics of self-healing efficiency. The mathematical background of the stress problem solution is based on the singular integral-differential equations method and the boundary elements method. Different self-healing methods (microcapsules filled with a self-healing agent, microvascular fibres, mendable polymers) with various mechanisms of self-healing are analyzed. The thermo-fluctuation kinetic Zurkov's model is used to evaluate the regeneration and formation of the crack bridged zone. The healing time and efficiency are dependent on the chemical reaction rate of the healing agent, crack size and the external loads. The non-local fracture criterion is used to evaluate the fracture toughness and the critical external loading in the frames of the bridged crack model. The model can be use for the evaluation of composite materials healing and durability.

1. THEORY BACKGROUND

We use the bridged crack approach for self-healing modeling of cracked structures. It is assumed that due to a healing process the crack surfaces interact in some zone starting from the crack tips. As a general case the plane elasticity problem on a crack at the interface of two dissimilar joint half-planes is considered. The crack surface interaction exists in the bridged zones, $\ell - d \leq |x| < \ell$. As a simple mathematical model of the crack surfaces interaction we will assume that the linearly elastic bonds act through out the crack bridged zones.

Denote by $\sigma(x)$ the stresses arising in the bonds

$$\sigma(x) = \sigma_{yy}(x) - i\sigma_{xy}(x), \quad i^2 = -1, \quad (1)$$

where $\sigma_{yy}(x)$ and $\sigma_{xy}(x)$ are the normal and shear components of the bond stresses. The crack opening, $u(x)$ at $\ell - d \leq |x| < \ell$ is determined as follows [1]

$$u(x) = u_y(x) - i u_x(x) = \frac{H}{E_b} (\phi_1(x) \sigma_{yy}(x) - i \phi_2(x) \sigma_{xy}(x)), \quad (2)$$

where $u_{y,x}(x)$ are the projections of the crack opening on the coordinate axes, H is a linear scale related to the thickness of the intermediate layer adjacent to the interface, E_b is the effective elasticity modulus of the bond and $\phi_{1,2}$ are dimensionless functions of the coordinate x .

By incorporating linearity of the problem one can represent the crack opening as follows

$$u(x) = u_o(x) - u_b(x), \quad (3)$$

where $u_o(x)$, $u_b(x)$ are the crack opening caused by the bond stresses $\sigma(x)$ and external loads, respectively.

By incorporating formulae (2)-(3) one can obtain a system of integral-differential equations relative to the bond stresses $\sigma(x)$.

Introduce the new variable, $s = x / \ell$, and differentiate the relations in (3) to obtain

$$\frac{H}{\ell} \frac{\partial}{\partial s} [\phi_1(s) \sigma_{yy}(s) - \phi_2(s) \sigma_{xy}(s)] + u'_b(s) E_b = u'_o(s) E_b, \quad (4)$$

where the right side is the given function of the coordinate.

Taking into account the results given in [2] one can obtain the following formula for the derivative of the function $u_b(x)$ [1]

$$u'_b(s) = iA(1 - \alpha)\sigma(s) - \frac{2A(1 + \alpha)}{\pi\sqrt{1 - s^2}} \left(\frac{1 - s}{1 + s} \right)^{-i\beta} \int_{1-d/\ell}^1 \frac{\sqrt{1 - t^2}}{t^2 - s^2} [sq_y(t) - itq_x(t)] dt \quad (5)$$

where

$$\sigma_{yy}(s) - i\sigma_{xy}(s) = (q_y(s) - iq_x(s)) \left(\frac{1 - s}{1 + s} \right)^{-i\beta}, \quad (6)$$

and parameters A , α and β depend on the elastic properties of the materials and bonds.

Finally, one can obtain the system of two singular integral-differential equations relative to the bond stresses $\sigma_{yy}(x)$ and $\sigma_{xy}(x)$ in the following form [1]

$$T_{ij}(s, \sigma) \frac{df_j(s)}{ds} + W_{ij}(s, \sigma) f_j(s) + \varepsilon \int_{1-d/\ell}^1 G_{ij}(s, t) f_j(t) dt = Z_i(s), \quad i, j = 1, 2 \quad (7)$$

where $f_j(s)$ are unknown function depending on bond stresses, $T_{ij}, W_{ij}, G_{ij}, Z_i$ are the equation kernels and the parameter ε depend on the materials and bond properties. For numerical solution of these equations we use a collocation scheme with piecewise quadratic approximation unknown of the bond stresses. See details in [1].

Having the distribution of the bond stresses $\sigma_{yy}(x)$ and $\sigma_{xy}(x)$ over the bridged zone one can calculate the stress intensity factors (SIF) K_I, K_{II} following to [3]

$$K_I + iK_{II} = \lim_{\delta \rightarrow 0} \sqrt{2\pi\delta} (\sigma_{yy}(\delta) + i\sigma_{xy}(\delta)) \delta^{-i\beta}, \quad (8)$$

where $\sigma_{yy}(\delta)$ and $\sigma_{xy}(\delta)$ are the stresses ahead the crack tip caused by the external loads and by the bonds stresses, δ represents the small distance to the crack tip.

On the other hand, the SIF can be written as follows

$$K_I + iK_{II} = (K_I^{ext} + K_I^{int}) + i(K_{II}^{ext} + K_{II}^{int}), \quad (9)$$

where $K_{I,II}^{ext}$ and $K_{I,II}^{int}$ are the SIF caused by the external loads and the bond stresses.

By incorporating the formula for the stress distribution ahead the interface crack tip under arbitrary loads [2] and using (8), (9) we obtain for the external tension load σ_0

$$K_I + iK_{II} = \frac{\sqrt{\pi\ell}}{(2\ell)^{i\beta}} \left[\sigma_0(1 + 2i\beta) - \frac{2 \cosh(\pi\beta)}{\pi} \int_{1-d/\ell}^1 \frac{(q_y(t) + itq_x(t))}{\sqrt{1-t^2}} dt \right] \quad (10)$$

The computation results for bonds stresses at the interface crack bridged zone and the crack opening over the crack for different combination of the materials parameters are presented. The dependencies of the SIF on bonds properties during the self-healing process were analyzed.

2. RESULTS of COMPUTATIONS

The above proposed approach was used for several problems analysis. A crack on the interface between different materials under the external tension σ_0 was considered. It was assumed that at the initial time instant (when the surfaces of a crack are free of constraints) some healing process is activated inside of a crack and bridges between the crack surfaces are built.

The numerical calculations were performed for plane strain conditions and the following elastic constants of the joint materials and bonds (Cu-epoxy polymer): $E_1 = 25GPa, E_2 = 135GPa; E_b = E_2, \nu_1 = \nu_2 = 0.35$. The purpose of calculations is the dependence analysis of the self-healing process efficiency (the measure of

efficiency is the level of SIF at the crack tip) on the bridged zone length (the crack filling with bonds) and on the bonds stiffness.

In Fig. 1 for different values of the relative bonds stiffness (see eq.(4)) $\kappa = \ell/H$ the dependencies of the SIF module (it can be obtained from eq. (10)) vs the relative bridged zone length are shown. For bonds with relative stiffness more than 10 the healing efficiency reaches the saturation if the crack has filled with bonds more than on the half of its length.

The evolution of the healing process as the dependence of SIF module vs relative bond stiffness (in logarithmic scale) is shown in Fig. 2. Saturation of the healing effect is observed for bonds with rather big stiffness.

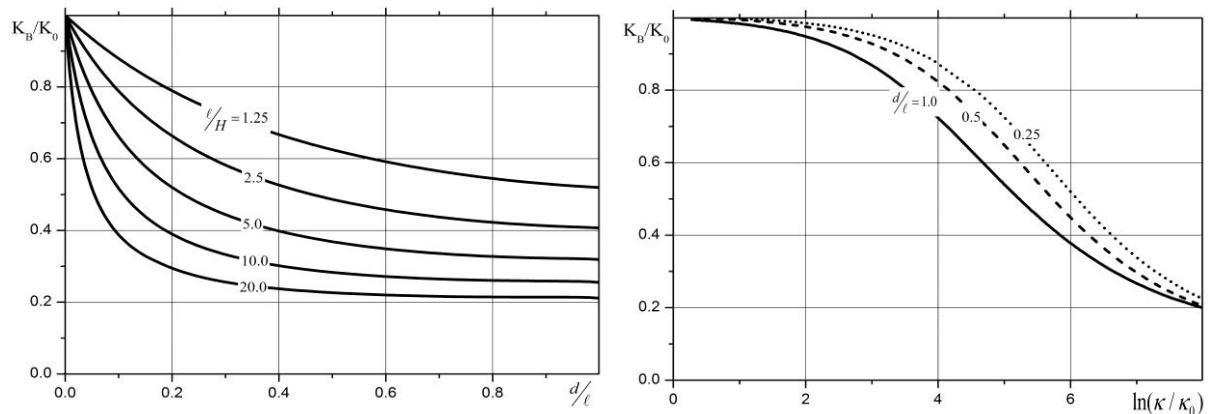


Figure 1: SIF module vs relative bridged zone length, $K_0 = \sigma_0 \sqrt{\pi \ell}$ Figure 2: SIF module vs relative bond stiffness, $K_0 = \sigma_0 \sqrt{\pi \ell}$

Analysis of the healing process in finite size structures can be performed by boundary elements method [4]. Growth prediction of healed cracks can be performed on the basis of the bridged cracks growth criterion [5].

ACKNOWLEDGEMENTS

This study was partially supported by Russian Foundation for Basic Research, research project No. 11-08-01243a

REFERENCES

- [1] R.V. Goldstein, M.N. Perelmuter, Modeling of bonding at the interface crack, Int. J. Fracture (1999) 99 (1-2) 53-79.
- [2] L.I.Slepjan, Crack Mechanics, Publ. "Sudostroenie", Leningrad, 1981 (in Russian).
- [3] J.R. Rice, Elastic fracture mechanics concepts for interface cracks, Trans. ASME. J. Applied Mech. (1988) 55 98-103.
- [4] M. Perelmuter, Boundary element analysis of structures with bridged interface cracks, Computational Mechanics (2012), P.1-12, DOI: 10.1007/s00466-012-0817-4 (online first paper).
- [5] M. Perelmuter, A criterion for the growth of cracks with bonds in the end zone, Journal of Applied Mathematics and Mechanics (PMM) (2007) 71 137-153 (in English).

MODEL BASED DESIGN OF SELF-HEALING EXPANDABLE COATINGS UNDER DIFFERENT ENVIRONMENTAL CONDITIONS

E. Javierre¹, V. Camañes², S.J. García³, S. van der Zwaag³ and J.M. García-Aznar²

¹ Centro Universitario de la Defensa, Academia General Militar, Ctra. Huesca s/n, 50090 Zaragoza, Spain – e-mail: etelvina.javierre@unizar.es

² Departamento de Ingeniería Mecánica, Universidad de Zaragoza, C/ María de Luna s/n, 50018 Zaragoza, Spain – e-mail: Victor.camanes@gmail.com, jmgaraz@unizar.es

³ Delft Center for Materials, TU Delft, Kluyverweg 1, 2629 HS Delft, The Netherlands – e-mail: s.j.garciaespallargas@tudelft.nl, s.vanderzwaag@tudelft.nl

Keywords: barrier protection, gap filling, coating, modelling, prediction

ABSTRACT

A long-lasting barrier protection at damaged sites of coated system can be achieved by means of an active response of the primer. This may be attained through the release of reactive liquids from dispersed containers, the increase of the local mobility of the polymeric network, or the expansion of (dispersed elements in) the primer [1]. Such self-healing mechanisms provide an excellent strategy towards repeated and sustained self-repair properties and, additionally, are not incompatible with the inclusion of passive elements within the primer to produce a corrosion inhibition response.

This work focuses on the modelling and simulation of expandable coatings resembling systems that contain thin clay-based interlayers [2]. However, a similar methodology could be applied to treat the hydraulic growth of inorganic grains in PPS coatings [3]. The expansion of a theoretical porous plastic primer is triggered by the ingress of environmental moisture. The volumetric growth of the primer into the crack is investigated under different humidity, temperature and atmospheric pressure conditions resembling different geographical locations (coastline vs. inland, changes in altitude and latitude, etc). Furthermore, the reversibility of the expansion process is investigated through hysteresis cycles resembling the change of the environmental conditions over a time lapse of several hours up to days.

The self-sealing capacity of the coating is estimated from the maximum crack width that can be filled. A full characterization of self-sealing efficiency is given in terms of key design parameters such as porosity, permeability, sorption behaviour, swelling range, shear modulus, layers widths and adhesion properties.

1. INTRODUCTION

Computational modelling and numerical simulation are powerful tools to aid and assist the design and optimization of self-healing materials. They can be used to evaluate design hypotheses prior to experimental setup and to perform throughout parameter analysis [4,5].

The goal of this work is to address the expansion process in a self-sealing clay-based coating [2,3]. By means of an analysis of fluid-flow in porous media we compute the

time-history deformation of the coating when it is exposed to different environmental conditions.

2. MATERIALS AND METHODS

We model the evolution of a coating consisting of a 7 μm thick poly-siloxane topcoat and a 15 μm thick montmorillonite primer [2]. The topcoat has water-repellent properties to prevent the ingress of moisture into the primer when the coating system is intact, whereas the montmorillonite primer expands by moisture ingress where damages in the topcoat occur. We will track the deformation of a damaged coating when it is exposed to fixed environmental conditions (temperature and relative humidity). In order to reduce the computational cost, we will consider a general cross-section of the damaged coating under plane strain hypotheses. Figure 1 shows the geometry of the damaged coating and the idealized computational domain with the boundary conditions.

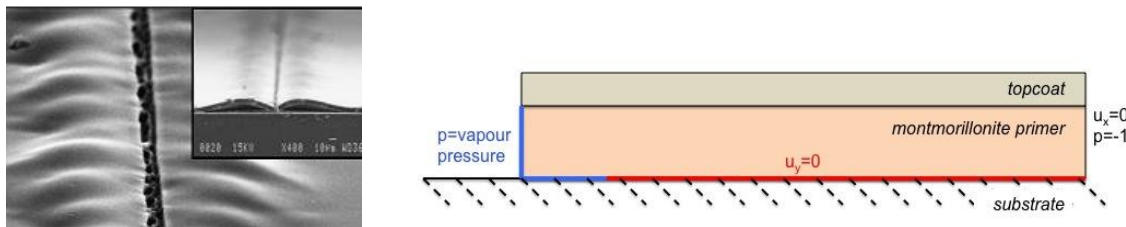


Figure 1: Damaged coating (taken from [2]) and computational domain.

The topcoat is modelled as a hyperelastic material. The montmorillonite primer is modelled as a permeable porous elastic material. Moisture sorption proceeds by capillary action through the exposed surfaces of the damaged coating (i.e. the left boundary of the primer and the left-bottom part of the primer where adhesion with the substrate is lost due to damage). Suction-saturation and permeability-saturation curves are defined accordingly to experimental results [6]. Moisture vapour pressure is obtained for different temperatures and relative humidity through psychrometric diagrams [7].

Table 1: Material properties of the coating.

Topcoat		Primer			
Shear modulus	50 MPa	Shear modulus	250 MPa	Permeability	10^{-10} m/s
Bulk modulus	1225 MPa	Swell range	0-300%	Porosity	0.4

3. RESULTS AND DISCUSSION

The self-sealing capacity of the coating is estimated from the maximum crack width that can be filled. The exposed coating expands gradually as moisture is adsorbed, and the free part of the coating bends slightly due to the restraining effect of the topcoat (see Figure 2), in agreement with experimental observations and previous numerical results [2,4].

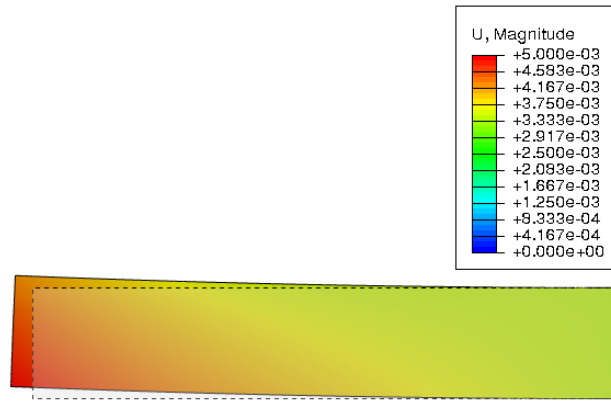


Figure 2: Initial and deformed coating after 10 min exposed to 30°C and 30% of relative humidity (close view of damaged area).

In order to study the performance of the coating at various geographical locations, we vary the environmental temperature and relative humidity. Vapour pressure, obtained from psychrometric charts, increases with both temperature and relative humidity (see Table 2).

Table 2: Vapour pressure (kPa) for different temperatures and relative humidity.

Temperature (°C)	Relative Humidity (%)		
	10	30	50
15	0.17	0.49	0.83
30	0.4	1.27	2.10

Taking as reference the response of the coating after 10 min of exposure to 15°C and 10% RH (i.e., the temperature and relative humidity that give the lowest vapour pressure), results show that the sealing capacity of the coating increases linearly with vapour pressure (see Figure 3). In terms of the environmental conditions, this means that the largest increment in the self-sealing capacity of the coating is obtained when both temperature and relative humidity are increased simultaneously.

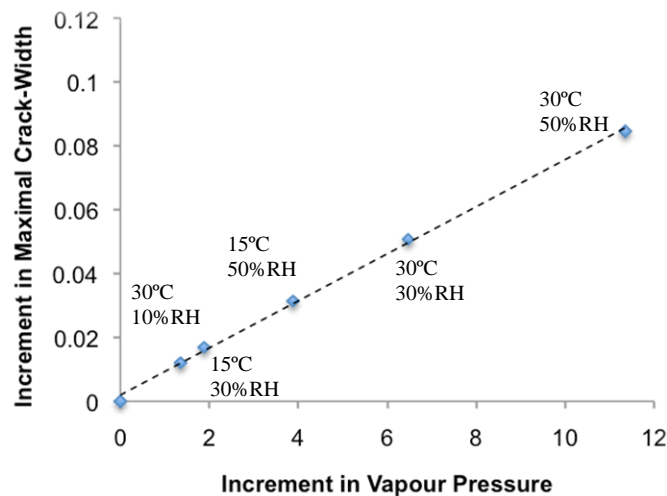


Figure 3: Increment in maximal crack-width sealed after 10 min of exposure to environmental conditions as function of the increment in vapour pressure. Results normalized with respect to the reference case.

4. CONCLUSIONS

The dependence of self-sealing capability of an expandable coating on the environmental conditions has been addressed. Results show that better performance is obtained under temperatures and relative humidity that yield a larger moisture vapour pressure.

However, thorough analyses of the material properties (both topcoat and primer) needs to be conducted in order obtain a full characterization of the self-sealing response of these types of coatings. A full set of results will be given in the presentation.

ACKNOWLEDGEMENTS

Financial support from the Spanish Ministry of Economy and Competitiveness for this study (Project No. DPI2012-32880) is gratefully acknowledged.

REFERENCES

- [1] S.J. García, H.R. Fischer, S. van der Zwaag, A critical appraisal of the potential of self healing polymeric coatings. *Progress in Organic Coatings*, 2011, 72, pp. 211-221.
- [2] F. Micciché, H. Fischer, R. Varley, S. van der Zwaag, Moisture induced crack filling in barrier coatings containing montmorillonite as the expandable phase. *Surface & Coatings Technology*, 2008, 202, pp. 3346-3353.
- [3] T. Sugama, K. Gawlik, Self-repairing poly(phenylenesulfide) coatings in hydrothermal environments at 200°C. *Mater. Letter*. 57 (2003) 4282.
- [4] R. Rey, E. Javierre, S.J. García, S. van der Zwaag, J.M. García-Aznar, Numerical study of the scratch-closing behavior of coatings containing an expansive layer. *Surface & Coatings Technology*, 2012, 206, pp. 2220-2225.
- [5] E. Javierre, S.J. García, J.M.C. Mol, F.J. Vermolen, C. Vuik, S. van der Zwaag, Tailoring the release of encapsulated corrosion inhibitors from damaged coatings: Controlled release kinetics by overlapping diffusion fronts. *Progress in Organic Coatings*, 2012, 75, pp. 20-27.
- [6] J.O. Lee, W.J. Cho and S. Kwon, Suction and water uptake in unsaturated compacted bentonite. *Annals of Nuclear Energy*, 2011, 38, pp. 520-526.
- [7] Hands Down Software, www.handsdownsoftware.com

MICROSTRUCTURAL SELF-HEALING OF BITUMINOUS MATERIALS: COMBINED EXPERIMENTAL AND NUMERICAL STUDY

A.Pauli^{1,2}, **A.J.M. Schmets**¹, C. Kasbergen¹, K. Varveri¹ and A. Scarpas¹

¹Structural Mechanics, Faculty of Civil Engineering & Geosciences, TU Delft. Stevinweg 1, 2628 CN, Delft, The Netherlands - e-mail: a.j.m.schmets@tudelft.nl; c.kasbergen@tudelft.nl; a.varveri@tudelft.nl; a.scarpas@tudelft.nl

²Western Research Institute, 365 North 9th St., Laramie, WY 82072-3380, USA - e-mail: tpauli@uwyo.edu

Keywords: Bitumen, microstructure, self-healing, finite element modeling, asphalt

ABSTRACT

Bituminous materials form a class of materials that possess the intrinsic ability to self-heal. This self-healing capability is evidenced by the observation that the service life of these materials ‘in the field’ exceeds the service life as predicted by standard mechanical laboratory tests. This mismatch between laboratory prediction and field service life is usually accounted for by applying a shift or healing factor.

In this contribution we demonstrate a model that is based on the observation that bitumen possesses a microstructure on the micrometre length scale, as can be observed by atomic force microscopy (AFM). On this scale bitumen can be regarded as a two-phase material, where the phases have a distinct stiffness. . One of the phases has a very typical appearance and is often referred to as ‘bee-phase’ [1-3]. The interface between the phases can be regarded as a manifold that is defined by stiffness gradient in the material. From mechanical considerations damage will initiate within this manifold. Modest variations in thermodynamic conditions (thus without melting the material) will already lead to rearrangement of phases, and a new damage initiation manifold, meanwhile the accumulated damage is erased.

Starting from two experimental microstructural arrangements, one before and one after phase rearrangement, a finite element mesh is produced. For both phases a viscoelastic constitutive model is implemented. The interface manifold is treated equally, but is allowed to acquire damage, as are the other phases, to a lesser extent. In this way, using experimental observations as a starting point, it is demonstrated that the effect of healing in bituminous materials can be treated micromechanically, and leads to quantitative results. This opens the way to quantify the healing potential of a bituminous material upon its microstructure. Optimal manifolds to accommodate the healing behaviour can then be derived. The experimental challenge will be to engineer the interface manifold in accordance with the desired healing potential of the material.

1. INTRODUCTION

Worldwide the most common pavement material is asphalt concrete. Asphalt is well known to display healing behaviour. The intrinsic healing characteristic of asphalt is utilized in asphalt pavement design. In the Netherlands healing factors are included for calculating the layer thickness of roads (higher healing factor, thinner layer). However,

this (design) healing factor happens to be a rather random property of mixes, and is therefore usually estimated conservatively.

This healing propensity of asphalt does depend on many parameters, a.o. temperature, maximum load levels, loading rates and it can be associated with an intrinsic healing property of one of the material's components. Usually this healing property is attributed to the bituminous binder, which is both the 'weakest link' in the asphalt concrete composite and the component that possesses the highest amount of 'physico-chemical mobility'. Mobility on the microscopic scales at service temperatures, is commonly regarded as a necessary condition for healing to occur.

AFM evidence indicates the presence 2 or 3 microstructural phases of bitumen [2]. Because the phases possess different mechanical stiffnesses, damage may originate at the interfaces between them, when subjected to mechanical loading. When bitumen undergoes relatively modest temperature changes (20-45 °C), the phases already tend to rearrange themselves into new configurations, Figures 1a and 1b. Phase rearrangements will then lead to 'erasure' of earlier damage, and hence improved service life characteristics. The necessary thermal variation of 25 °C for this to happen, is within the typical daily temperature variations experienced by real pavements.

2. MATERIALS AND METHODS

For this study the bitumen AAK from the SHRP bitumen library [4] was selected. Initially a 30×30 μm AFM (tapping mode) image was recorded at 20 °C, Figure 1a. Then the sample was slowly heated to 45 °C, cooled again to 20 °C and subsequently imaged again by AFM, Figure 1b. The AFM images were then digitally processed Figure 1c, displaying clearly the two phases and the interface (red) between them. Finally, finite element meshes consisting of three material types, were generated using Simpleware[®], Figure 1d.

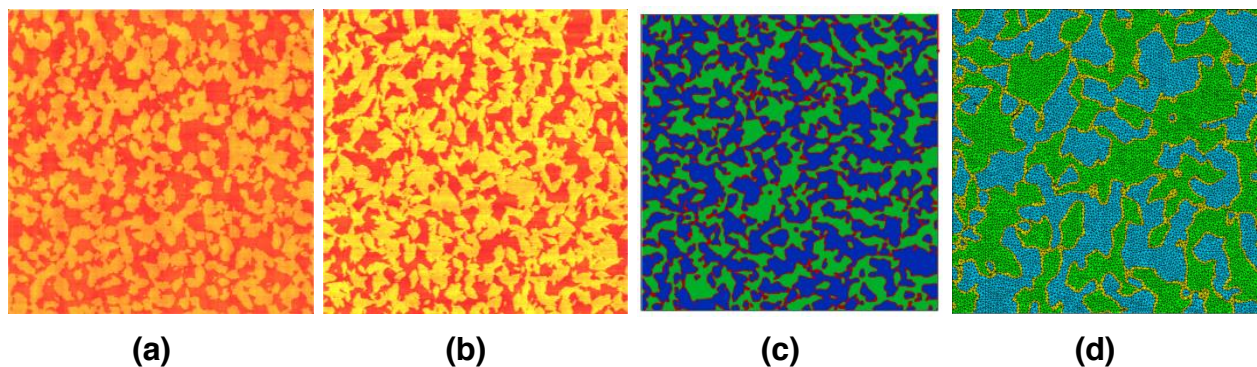


Figure 1 : AFM phase images (a and b), image-processed AFM image (c) and detail of the finite element mesh derived from the latter (d).

The viscoelastic Zener material model which consists of two parallel components, an elastic spring and a Maxwell component has been utilized for constitutive modelling. Additionally the standard model has been extended to include damage simulation. To allow for damage the second Piola-Kirchhoff stress S in the reference configuration is modified as:

$$S_{\text{eff}} = (1-d)S \quad (1)$$

where $d = 0$ in absence of damage and $d = 1$ for the case of complete damage. In this implementation damage is made a function of the total work W in the Zener component, and is expressed as:

$$d = 1 - \exp(-k W^r). \quad (2)$$

Here k and r are parameters, and the total W is the total work. This model is then implemented within the finite element framework CAPA-3D to simulate the response of bitumen to a triangular, stress controlled ($\sigma_{\max} = 2.5$ MPa, i.e. about 1% strain) repeated loading scenario with 15 load-unload cycles. The applied load was uniaxial in the vertical y -direction.

The material parameters like relaxation modulus E were derived from values obtained by dynamic shear rheometer (DSR) tests: the overall (averaged) parameters correspond to the DSR-derived values, whereas the range of properties 'per phase' were estimated from quantitative AFM measurements, Table 1. The damage parameter k was chosen to be in the range 1 to 5, while the parameter r was fixed to 1 for all simulations. The Poisson ratio is taken throughout as 0.4.

Table 1 : Parameter ranges as used in the FEM simulations for the 3 distinct phases. Between parentheses: the actual values used for the simulations of Figure 2.

	Bee-phase (‘green’ in Fig 1c)	Interface-phase	Continuous phase
E ($E_0=110$ MPa)	1-4 E_0 ($2E_0$)	1-2 E_0 ($1.45E_0$)	1-3 E_0 (E_0)
Viscosity ($\eta_0 = 5$ MPa.s)	$10\eta_0$	$5\eta_0$	η_0
Damage parameters $k ; r$	1-5 (3) ; 1	1-5 (5) ; 1	1-5 (1) ; 1

For the simulation presented in Figure 2, the damage parameters of the interface were chosen such as to make this phase to be most prone to developing early stage damage ($k = 5$). Furthermore, the continuous phase was given the lowest value ($k = 1$), with the ‘bee phase) in between these extreme values ($k = 3$). The order of magnitude of the damage parameters was selected such as to show a noticeable decrease of mechanical response within 15 load repetitions.

3. RESULTS AND DISCUSSION

In Figure 2 the results of the finite element simulation for one particular cyclic loading scenario is presented. After every full loading-unloading cycle, a value for the temporal stiffness was obtained by evaluating the ratio of total applied force and displacement. In Figure 2 surface displacements at 5 different surface locations (nodes) are shown. The stiffness shows a similar decreasing trend as a function of load cycle, with a maximum decrease of about 24% after 15 cycles. The spatial distribution of damage accumulated after 15 cycles is shown in the bottom right insert in Figure 2. Damage is most prominent in interface and bee phases. As the maximum strain is at the order of 1%, no discrete discontinuities are introduced into the material. Then the material was subjected to a temperature cycle of 25 °C.

At the end of the temperature cycle, phase rearrangement has erased damage (loss of memory). The response of the 'healed' material, Figure 1b, leads then to an increase in stiffness ('healing'), followed by a decrease with subsequent load cycles.

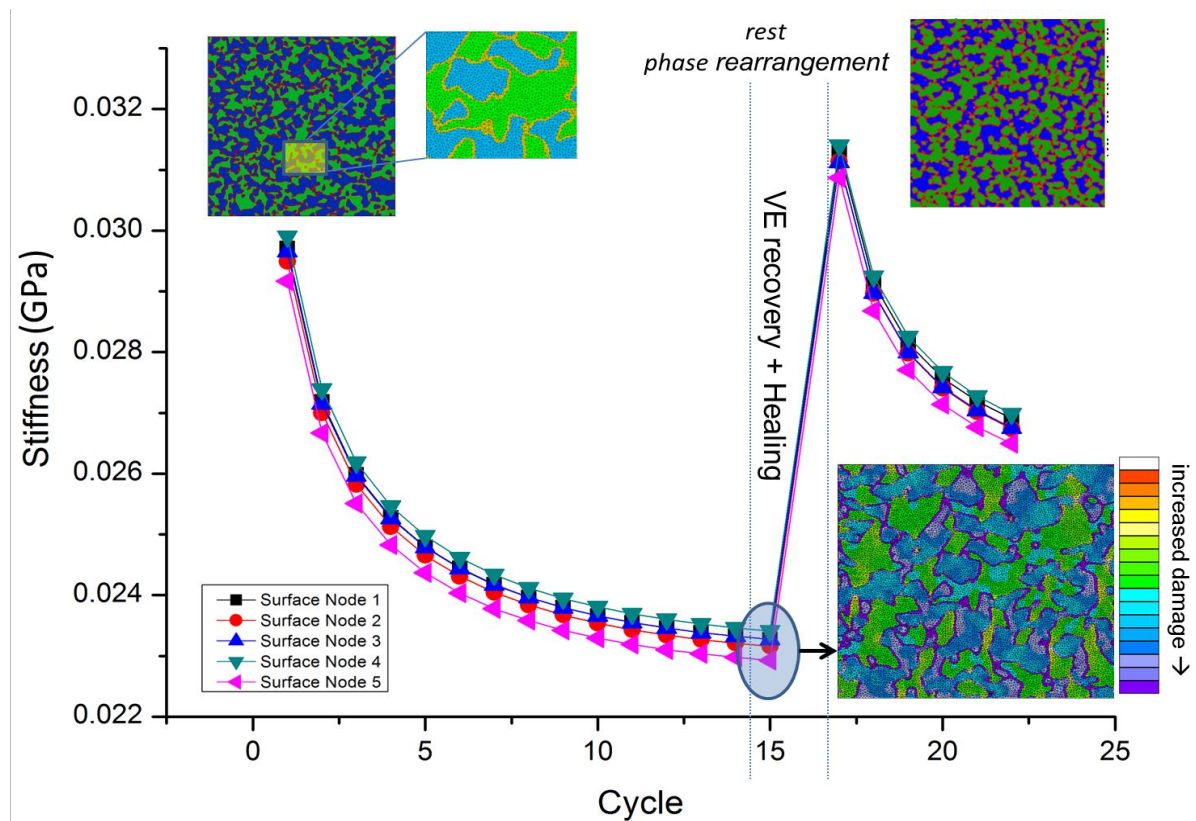


Figure 2 : Results of FEM simulations. Inserts show FEM meshes and damage after 15 stress controlled load cycles.

4. CONCLUSION

In a combined experimental and numerical study a possible scenario for the intrinsic healing phenomenon in bituminous materials is introduced. This scenario is based on the existence of microstructural phases in bituminous materials, and the AFM observation that moderate thermodynamic changes to the system lead to rearrangement of the phases and with accompanying loss of memory for moderate levels of straining. This was demonstrated by an increase of mechanical response of the material after moderate thermal cycling, leading to phase rearrangement.

REFERENCES

- [1] Loeber L, Sutton O, Morel J, Valleton JM, Muller G. New direct observations of asphalts and asphalt binders by scanning electron microscopy and atomic force microscopy. *Journal of microscopy*. 1996;182(1):32-39.
- [2] Pauli AT, Grimes RW, Beemer AG, Turner TF, Branthaver JF. Morphology of asphalts, asphalt fractions and model wax-doped asphalts studied by atomic force microscopy. *International Journal of Pavement Engineering*. 2011;12(4):291-309.

- [3] Schmets AJM, Kringos N, Pauli T, Redelius P, Scarpas T. On the existence of wax-induced phase separation in bitumen. *International Journal of Pavement Engineering*. 2010;11(6):555-563.
- [4] Branthaver, JF et. al, SHRP-A-368, Binder Characterization and Evaluation, Volume 2: Chemistry, Strategic Highway Research Program, National Research Council, Washington, DC, 1993.

SESSION 9 – SELF-HEALING COATINGS AND PAINTS

DEVELOPMENT OF A METHODOLOGY BASED ON ODD RANDOM PHASE ELECTROCHEMICAL IMPEDANCE SPECTROSCOPY TO EVALUATE CORROSION PROTECTION OF COATINGS

C. Cordioli^{1,2}, E. Bauters^{2,3}, T. Muselle¹ and A. Hubin¹

¹ *Vrije Universiteit Brussel, Department Materials and Chemistry, Research Group Electrochemical and Surface Engineering, Pleinlaan 2, B-1050 Brussels, Belgium - e-mail: ccordiol@vub.ac.be ; tmuselle@vub.ac.be ; ahubin@vub.ac.be*

² *SIM vzw, Technologiepark 935, B - 9052 Zwijnaarde, Belgium*

³ *FLAMAC, a division of SIM, Technologiepark 903, B - 9052 Zwijnaarde, Belgium*

Keywords: organic coating, HDG steel, ORP-EIS, self-healing

ABSTRACT

Commonly coatings are used to protect metals from corrosion. Different types of coatings are available and according to their characteristics they provide different levels of protection.

In order to evaluate the performance of the coating, it is fundamental to have a methodology that is reliable and efficient even when applied to different kinds of systems.

A good candidate technique to develop this methodology is the Electrochemical Impedance Spectroscopy (EIS). Among the advantages provided by this technique there are the ability to detect corrosion and the fact that the measurements are non-destructive. Recently Odd Random Phase Impedance (ORP-EIS) was developed. In comparison to classic Impedance, it allows for a reduction of measurement time by gathering information over a broad frequency range with a single measurement. In addition to that it is also possible to have direct information about the steady-state condition of the system by evaluating the recorded noise levels.

The methodology consists in the use of ORP-EIS combined with aging procedures. It is applied to different organic coated systems with different characteristics, including self-healing ones. Part of the coatings are applied on the same type of substrate, hot dipped galvanized (HDG) steel, in order to isolate the information uniquely linked with the protective layer.

1. INTRODUCTION

The use of organic coatings is one of the most common and cost effective choices for corrosion protection of metals [1].

In order to evaluate the protection properties of coatings, there is the need to evaluate their behavior under weatherable conditions. The most appropriate test is field exposure, which on the other hand is time consuming. To limit this problem several accelerated ageing methods have been developed over the years. One of the most commonly used in the industry is the ASTM B-117 or salt spray test. Unfortunately this method is not able to reproduce the real failure mechanism that will occur during field exposure and on top of that also usually the evaluation of the corrosion is made by a trained observer.

In order to have an early stage detection of corrosion Electrochemical Impedance Spectroscopy became a handy tool.

The advantages of this method are numerous. In particular it is non-destructive and it has the capability to detect ongoing corrosion already at an early stage. The downside of the technique is that it requires experts with some experience in coating evaluation to be able to model and evaluate the coating in a limited amount of time.

2. MATERIALS

In order to evaluate the capability of the methodology to be applied to different types of coatings, different type of materials were investigated.

Regarding the substrates, two different kinds were used in two different phases of the research. Initially an aluminum substrate was used and afterwards a hot dipped galvanized steel substrate was introduced.

On the aluminum (rolled sheet with purity 99.99%) a shape-memory segmented polyester-polyurethane block copolymer was applied. This was produced at the VUB according to the work of D'Hollander [2].

On the other hand on the HDG steel only commercially available epoxy based coatings were applied.

All the coatings were applied using the bar coating method. The thickness of the coatings varies according to the material applied.

3. METHODS

During this work the attention is concentrated to one specific technique for the evaluation of the coating, Odd Random Phase Electrochemical Impedance Spectroscopy (ORP-EIS) [3]. ORP-EIS is a technique that has all the traditional advantages of EIS with several specific additional features.

The main advantage is the capability to screen corrosion using the recorded noise levels. Through this noise it is possible to visualize both non-linear and non-stationar behavior. This allows the user to have immediate easy to detect information about the on-going corrosion processes. This information combined with the traditional evaluation of the impedance values becomes a very powerful tool. In fact, the noise levels are not only used as direct information about the system but they can also be used to optimize the equivalent circuit model used for the fitting of the system.

In addition to this, ORP-EIS also reduces sensibly the acquisition time of the impedance. In fact the ORP-EIS technique is based on multisines. The ability of reducing the acquisition time is due to the fact that instead of recording the impedance value linked with each applied frequency one at the time, the multisine technique is able to apply all the set of frequencies chosen at the same time and record the associated values simultaneously.

To evaluate the barrier properties of the coatings both ageing techniques (traditional methods such UV exposure) and induction of defects (scratches) were used.

4. RESULTS

So far it was possible to prove how ORP-EIS is capable of being a handy tool for several different aspects in evaluating and even choosing an appropriate new coating.

In fact from figure 1 it is possible to see how among different produced self-healing coatings with different content in polyurethane concentrations one of them had the better performance as can be deduced from their noise levels.

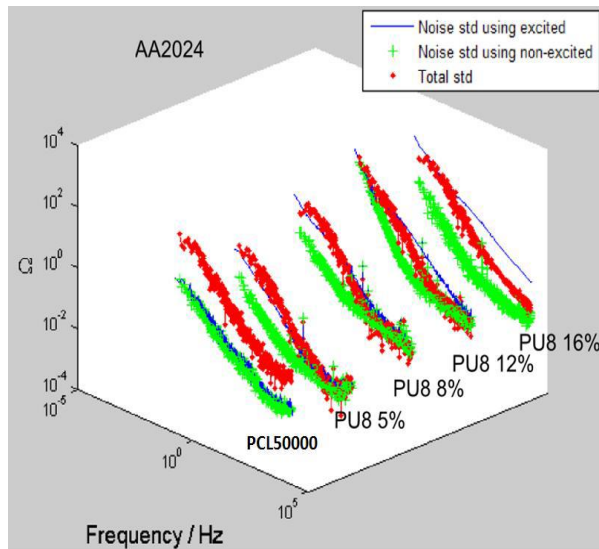


Figure 1: ORP-EIS performed on different self-healing coatings after 24h of immersion in Na_2SO_4 .

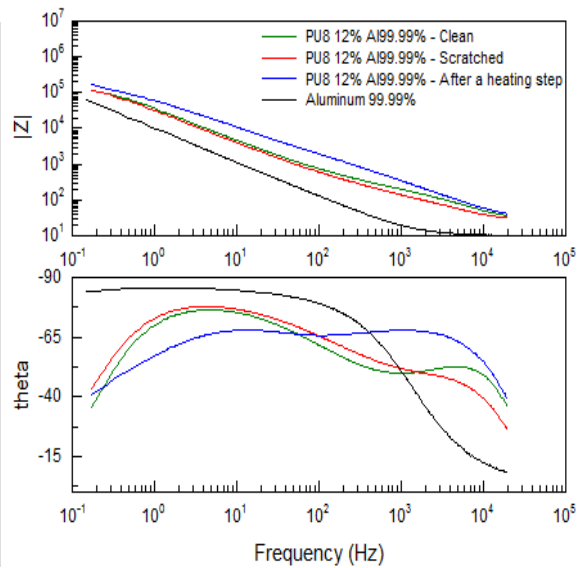


Figure 2: Prove of the complete recovery of the barrier properties of the SH coating.

In figure 2 on the other hand, using just the information about the impedance values it was possible to prove the full recovery of the barrier properties of the chosen SH coating after the application of a defect, in this case a scratch. On this sample an accelerated ageing test such as the ASTM B-117 was not performed, because the polycaprolactone(PCL) is biodegradable and thus it would not withstand the high humidity content of the atmosphere.

Regarding the other coatings applied on HDG steel, the accelerated ageing experiments are still on-going. However it is possible to present here the recorded ORP-EIS graphs linked with the coating as deposited.

Looking at figure 3 it is possible to evaluate the protection ability of the coating while in figure 4 the impedance linked with the coating after 1 week ageing in a climate chamber is presented.

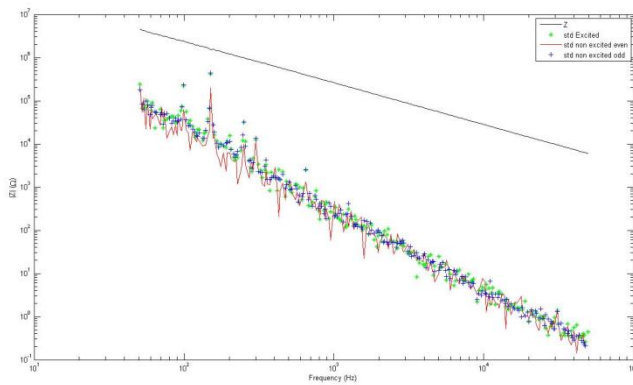


Figure 3 :Noise levels linked with the coated HDG steel.

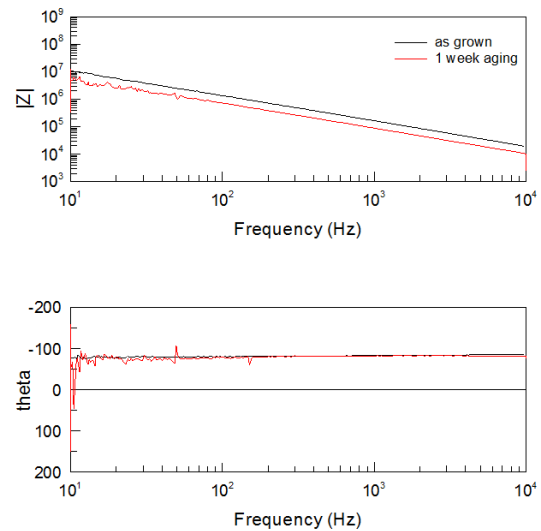


Figure 4 : Effect of 1 week ageing in a weathering chamber on the coating deposited on HDG steel.

5. CONCLUSIONS

Even if the ageing of the traditional coatings applied on HDG steel is still on-going, definitely we can say that the ORP-EIS can be applied successfully in the development of a methodology that can be used both for traditional coatings and self-healing ones.

ACKNOWLEDGEMENTS

Thanks to the Strategic Initiative Materials (SIM) to support this project and to CYTEC to be able to use their facilities to apply the coatings.

REFERENCES

- [1] G.P. Bierwagen, Reflections on corrosion control by organic coatings, Progress in organic coatings 28.1 (1996) 43-48.
- [1] S. D'Hollander, G. Van Assche, B. Van Mele, F. Du Prez, Modeling the morphology and mechanical behavior of shape memory polyurethanes based on solid-state NMR and synchrotron SAX/WAXD, Journal of Materials Chemistry (2010) 3475-3486.
- [2] T. Breugelmans, E. Tourwe', Y. Van Ingelgem, J. Wielant, T. Hauffman, R. Hausbrand, R. Pintelon, A. Hubin, Odd Random Phase multisine EIS as a detection method for the onset of corrosion of coated steel, Electrochemistry communications 12 (2010) 2-5.

SELF-HEALING CORROSION PROTECTIVE COATINGS BY TiO₂ PARTICLES AND A PH-SENSITIVE ORGANIC AGENT ON A MAGNESIUM ALLOY

A. Yabuki¹ and M. Sakai¹

¹ Graduate School of Engineering, Hiroshima University, 1-4-1 Kagamiyama, Higashi-Hiroshima, Hiroshima, 739-8527, Japan – e mail: ayabuki@hiroshima-u.ac.jp

Keywords: corrosion, coating, self-healing, pH-sensitive, magnesium

ABSTRACT

A self-healing corrosion protective coating was developed using TiO₂ particles and casein as pH-sensitive organic agents that is also environmentally friendly materials. A film structured of TiO₂ particles was formed on a substrate (magnesium alloy) by dip-coating followed by immersion in a casein solution. Casein was inserted and fixed in the particle film by changing the pH of the casein solution. The polarization resistance of the scratched specimen prepared by changing the pH of the solution from 12 to 5 increased with testing time, and a deposited film consisting of TiO₂ particles and casein was observed after the test.

1. INTRODUCTION

Corrosion-protective coatings are needed to improve the resistance of magnesium and its alloys, since these materials have limited application in corrosive environments because of their poor corrosion resistance [1-4]. An important requirement of these types of coatings is the ability to self-heal, so that if the coating suffers mechanical damage, and degradation of the bare metal surface by corrosive species in the environment begins, the damaged surface is automatically repaired. In the present study, a self-healing corrosion-protective coating for magnesium alloy AZ31 was developed using an environmentally friendly material. The coating used TiO₂ particles and casein as a pH-sensitive organic agent. Changes in the polarization resistance of the coatings, scratched by a knife-edge, were monitored, and the surface appearance of the specimen was observed after the corrosion test to elucidate the self-healing property of the coatings.

2. MATERIALS

A 12 x 12 x 1 mm magnesium alloy AZ31 substrate was used for the test. The substrate was cut from a plate material. The plate was abraded with emery paper #2000, followed by a thorough rinse in water, and air drying. TiO₂ particles of a rutile structure with a mean diameter of 270 nm (Tayca Co.) were dispersed in deionized water to prepare a 1 wt% TiO₂ particle solution. Casein from milk (α -casein) (Sigma-Aldrich Co.) was also dispersed in deionized water to prepare a 1 wt% casein solution. Either acetic acid (liquid, $\geq 99\%$) or sodium hydroxide (granular or saturated solution) was then added to adjust the pH of the casein solution. A polished substrate was dip-coated in the TiO₂ particle solution using a micro dip coater with a withdrawal speed of 10 mm s⁻¹. The TiO₂-coated specimen was calcined at 120 °C for 30 min in

air. The specimen was immersed in a casein solution, pH12, at 35 °C for 4 h, then the pH of the solution was changed to 7, 5 or 4.

3. METHODS

An artificial defect was created on the coated specimen using a knife-edge on a scratch tester (IMC-1552, Imoto Machinery Co., Ltd.). The load for the scratch was 10 g to expose the substrate. The scratched specimen was connected with a conductive wire on one side and mounted in a sample holder of polyvinylchloride with an exposure area 6 mm in diameter, then immersed in a 0.5 mM NaCl corrosive solution. The solution was air-saturated using an air pump, and maintained at 35 °C. The impedance of the specimen in the corrosive solution was measured at intervals of 4 h for 48 h using a platinum counter and Ag/AgCl reference electrodes connected to a potentiostat, a frequency response analyzer, and a personal computer. Sine wave voltages (10 mV rms) at frequencies from 20 kHz through 10 mHz were superimposed on a given electrode potential. The difference in impedance measured at low and high frequencies was used to measure the polarization resistance, since the phase shift was almost zero at low and high frequency ranges. The surface appearance of the specimens was observed after the corrosion test, using a field emission-scanning electron microscope (FE-SEM, JSM-6340F) at an accelerated voltage of 20 kV, to confirm the self-healing properties of the coatings. The scratched area of the specimen was analyzed after the corrosion test using an Energy Dispersive X-ray Fluorescence Spectrometer.

4. RESULTS

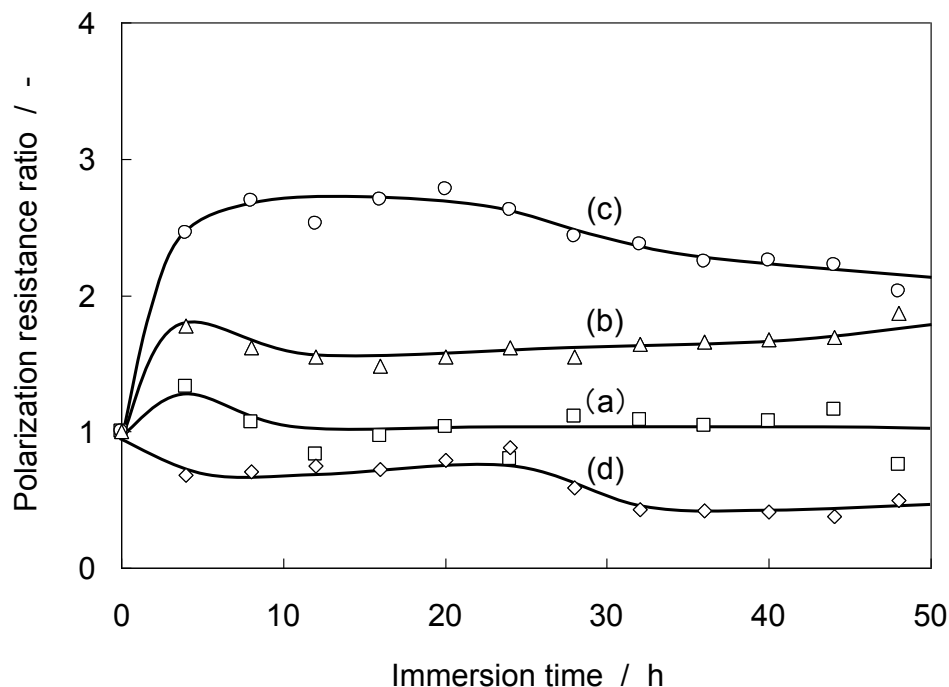


Figure 1: Polarization resistance ratio of scratched specimens coated with TiO₂ particle and TiO₂ particle-casein coatings prepared under various conditions; (a) TiO₂ particle coating, (b), (c) and (d) TiO₂ particle-casein coatings prepared by changing the pH from 12 to 7, 5, and 4, respectively.

The polarization resistance ratios of the scratched specimens coated with TiO₂ particles and casein, or with TiO₂ particles alone, are shown in Fig. 1. The resistance ratio of the scratched specimen coated with TiO₂ particles alone increased slightly, but it was almost the same as the initial resistance following the 8 h immersion (Fig. 1a). The resistance ratio of the TiO₂ particle-casein coating prepared by changing the pH from 12 to 7 increased soon after immersion, and was almost 1.5 after 8 h immersion, after which it was constant (Fig. 1b). The resistance of the scratched specimen prepared by changing the pH from 12 to 5 increased within the 4 h immersion, resulting in more than twice the initial resistance (Fig. 1c). On the other hand, the resistance ratio of the scratched specimen prepared by changing the pH from 12 to 4 decreased soon after immersion in corrosive solution, and the ratio was approximately 0.5 after 28 h immersion (Fig. 1d). As a result of polarization resistance, casein that was coated onto the TiO₂ particle coating, prepared by changing the pH from 12 to 7 and 5, increased the resistance, which was a self-healing effect.

The scratched portions of specimens coated with TiO₂ particle-casein — when the pH was changed from 12 to 5 — were observed. SEM images of the scratched area of the coating before the corrosion test, after 4 h immersion, and after 48 h immersion are shown in Figures 2a, b and c, respectively. A deposited film was observed in the scratched area of the specimens, and consisted not only of casein, but also of TiO₂ particles. The film was enhanced as immersion time increased. As Figure 2b shows, the TiO₂ particles seemed to move alone to the scratched area. However, a transparent film (thought to be casein) was observed at the edge of the scratched area shown in Figure 2c. The TiO₂ particles may have been taken along by the casein, since they were difficult to move because of their size. Thus, it is noteworthy that the TiO₂ particles moved to form a deposited film at the scratched area. It appears that TiO₂ particles have two roles: as a component of the healing film and as a reservoir for casein as the healing agent. On the other hand, casein also has two roles, since it serves as a component of the healing film and as a courier of TiO₂ particles as healing components. These materials thus play complementary roles, so the TiO₂ particle-casein coating has self-healing properties, as indicated in the increased polarization resistance (Fig. 1).

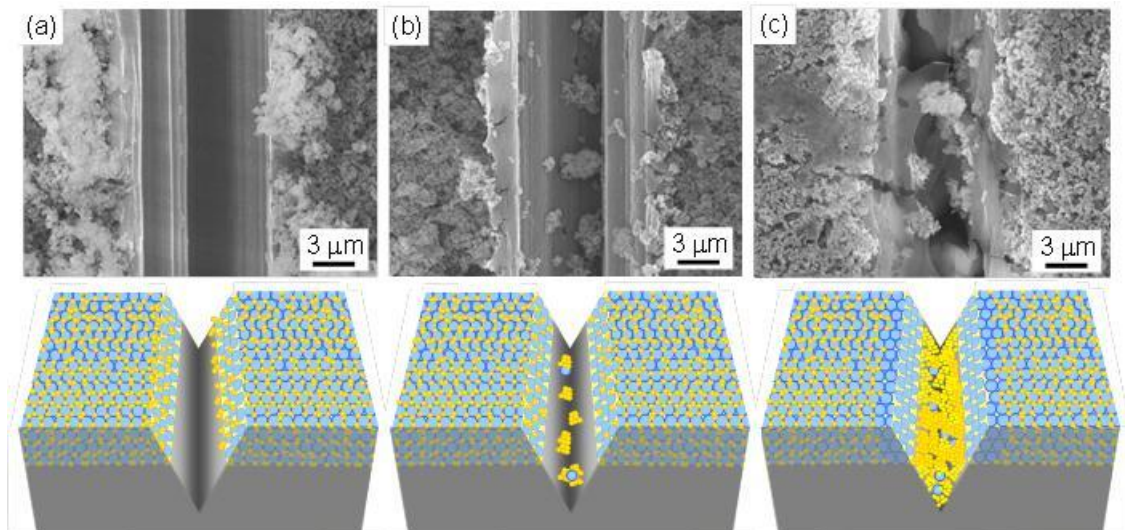


Figure 2: SEM images of the scratched area of specimens coated with TiO_2 particle-casein by changing the pH from 12 to 5 before the corrosion test (a), after 4 h immersion (b), and after 48 h immersion (c).

A schematic representation of the self-healing effect of the TiO_2 particle-casein coating is shown in Fig. 3. The self-healing effect is apparently due to the formation of a composite film that contains TiO_2 particles and casein. As a result of the defect in the coating, the bare magnesium alloy substrate was exposed to the corrosive solution, and then anodic dissolution occurred. The anodic process led to the generation of metal cations. Negatively charged OH^- ions were generated near the adherence between the coating and the substrate due to the cathodic reaction. Generated OH^- ions diffused in the coating and a local increase in pH near the TiO_2 particles promoted the release of casein from the surface of the TiO_2 particles. The released casein simultaneously took TiO_2 reservoir particles to the defect area. The casein and TiO_2 particles released from the coating gradually diffused onto the bare magnesium alloy substrate to form a barrier film, thereby repairing the defect.

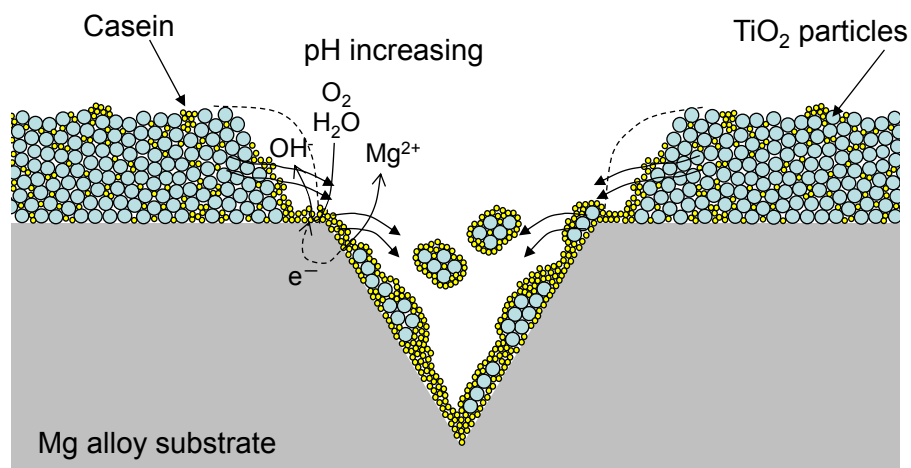


Figure 3: Self-healing mechanism of TiO_2 particle-casein coating.

5. CONCLUSIONS

The polarization resistance of the scratched specimen, coated with TiO₂ particles and casein by changing the pH from 12 to 5, increased with immersion time. A deposited film consisting of casein and TiO₂ particles was observed in the scratched area of the specimen. This was due to complementary roles: the TiO₂ particles acted both as a component of the healing film and a reservoir of casein, and the casein also acted as a component of the healing film and a courier of TiO₂ particles. The self-healing effect of the coating appears to be due to the release of the casein and TiO₂ particles due to the increase in pH, and the subsequent formation of a film on the defect.

ACKNOWLEDGEMENTS

This research was supported in part by a Grant-in-Aid for Scientific Research (C), Japan Society for the Promotion of Science (No. 17560635).

REFERENCES

- [1] G.L. Makar, J. Kruger, J. Electrochem. Soc. 137 (1990) 414-421.
- [2] G. Song, A. Atren, D. St. John, X. Wu, J. Nairn, Corros. Sci 39 (1997) 1981-2004.
- [3] R. Ambat, N.N. Aung, W. Zhou, Corros. Sci. 42 (2000) 1433-1455.
- [4] G. Song, A. Atrens, M. Dargusch, Corros. Sci. 41 (1999) 249-273.

SELF-HEALING COATINGS WITH MULTIPLE FUNCTIONALITIES FOR THE CORROSION PROTECTION OF METALS

I. De Graeve¹, A. Lutz^{1,2}, H. Verbruggen¹, O. van den Berg^{2,3}, F. Du Prez³ and H. Terryn¹

¹ *Research Group of Electrochemical and Surface Engineering, Vrije Universiteit Brussel, Pleinlaan 2, B-1050 Brussel, Belgium – e-mail: alexander.lutz@vub.ac.be*

² *SIM vzw, Technologiepark 935, 9052 Zwijnaarde, Belgium*

³ *PCR, Dep. of Organic Chemistry., Ghent University, Krijgslaan 281 S4-bis, 9000 Ghent, Belgium*

Keywords: inhibitor encapsulation, SVET, SIET, SECM

ABSTRACT

Lately different incorporation methods for inhibitors into organic coatings are described in literature [1,2]. Direct addition has several well-known drawbacks (incompatibility with the coating, uncontrollable inhibitor leaching, etc.). Alternatively inhibitors are accommodated in containers like Layered Double Hydroxides (LDH). In an encapsulation like this, not only the inhibitor release can be controlled and restricted depending on the pH, but also higher concentrations of insoluble substances in coatings can be achieved.

In this publication a comparison of different incorporation methods for corrosion inhibitors for hot dip galvanized steel into self-healing organic coatings will be presented. Firstly the self-healing ability of an Polyesterurethaneacrylate coating containing these inhibitor recipients will be shown. Secondly their leaching out process will be studied with advanced local electrochemical methods.

Scanning Vibrating Electrode Technique (SVET) allows the measurement of the electric field in solution by means of a vibrating microelectrode. As a result potential or – through calibration – ionic current density mappings can be recorded. Scanning Ion-selective Electrode Technique (SIET) is a micro-potentiometric technique which allows the local determination of individual ion concentrations. Other ions are avoided through an ion-exchange liquid in the tip of the microelectrode. With Scanning Electrochemical Microscopy (SECM) the local concentration of one selected electro-active species is monitored. By means of a redox reaction cycle between the ultra-microelectrode tip and the surface the discrimination of areas of different substrate activity is possible.

All these techniques enable one to follow the leaching out process in-situ and with high spatial resolution revealing information about its mechanism.

REFERENCES

- [1] S. K. Poznyak, et al., *Applied Materials & Interfaces* (2009), Vol. 1, 10, 2353-2362
- [2] F. Maia, et al., *Nanoscale* (2012), Vol. 4, 4, 1287-1298

SELF-HEALING COATINGS BASED ON ELECTROCHEMICAL POTENTIAL TRIGGERED RELEASE SYSTEMS

A. Vimalanandan¹, L.P. Lv², Y. Zhao², D. Crespy², K. Landfester² and M. Rohwerder¹

¹ Max-Planck-Institut für Eisenforschung GmbH, Max-Planck-Str. 1, 40237 Duesseldorf, Germany – e-mail: a.vimalanandan@mpie.de, m.rohwerder@mpie.de

² Max-Planck-Institut für Polymerforschung, Ackermannweg 10, 55128 Mainz, Germany, - e-mail: lv@mpip-mainz.mpg.de, d.crespy@mpip-mainz.mpg.de, y.zhao@mpip-mainz.mpg.de, k.landfester@mpip-mainz.mpg.de

Keywords: Corrosion, Polymerization, Inhibitor, Semi-conducting polymers, Scanning-Kelvin-Probe

ABSTRACT

For economical and ecological reasons corrosion protection of metals by functional coatings is an important research field in the chemical, steel and automotive industries. The first « self-healing » coatings were based on cancerogenic Cr(VI) compounds which are stepwise being abolished. This development initiated the introduction of alternative concepts regarding autonomous self-healing coatings to protect metals from corrosion once the coating is damaged and bare metal is exposed. The metal should be protected by intelligent release of corrosion inhibiting molecules and also of polymerization agents from micro- or nano-storage containers inside the coating. Until now the majority of concepts presented in this field are based on the release of the self-healing agents by mechanical damage of the coating, by pH-change inside the defect, by the change of ionic strength or a combination of these triggers.

Here we introduce a self-healing coating concept which can be used generally for any kind of metal. The release of self-healing agents in our concept is triggered by the change of the electrode potential at the defect site which is for all metals decreasing by several hundred millivolts in case of corrosion, while the change of pH and other triggers is usually different for different metals. Hence, potential is the best trigger [1-2].

The synthesis of suitable potential-sensitive nano-carriers, based on semi-conducting polymers and other redox-sensitive shell materials, and the mechanism of release of self-healing agents were investigated in depth to gain fundamental understanding of the coating system. The coating was applied and tested on iron as well as on zinc and the performance of the coating was investigated by advanced electrochemical techniques with local resolution, such as the Scanning-Kelvin-Probe (SKP).

REFERENCES

- [1] M. Rohwerder, S. Isik-Uppenkamp, C.A. Amarnath, Application of the Kelvin Probe method for screening the interfacial reactivity of conducting polymer based coatings for corrosion protection, *Electrochim. Acta* 56 (2011) 1889-1893.
- [2] M. Rohwerder, Le Minh Duc, A. Michalik, In situ investigation of corrosion localised at the buried interface between metal and conducting polymer based composite coatings, *Electrochim. Acta* 54 (2009) 6075-6081.

**ADVANCED CHARACTERIZATION METHODS FOR SELF-
HEALING**

POSTER SESSION

MONITORING THE RESTORATION OF INTERFACIAL CONTACT FOR SELF HEALING THERMAL INTERFACE MATERIALS FOR LED AND MICROELECTRONIC APPLICATIONS

U. Lafont^{1,3}, H. van Zeijl² and S. van der Zwaag³

¹ Material innovation institute, Mekelweg 2, 2600 GA, Delft, The Netherlands – email: U.Lafont@tudelft.nl

² DIMES, Electrical Engineering, Mathematics and Computer Science, Delft University of Technology, Mekelweg 4, 2628 CD, Delft, The Netherlands – email: H.W.vanZeijl@tudelft.nl

³ Novel Aerospace Materials, Aerospace Engineering, Delft University of Technology, Kluyverweg 1, 2629 HS, Delft, The Netherlands – email: S.vanderZwaag@tudelft.nl

Keywords: self-healing, in-situ characterization, thermal conduction, interfacial damage recovery

ABSTRACT

While conventional self healing materials focus on the restoration of mechanical properties, newer generations of self healing materials focus on the restoration of other functional (i.e. non-mechanical) properties. Thermal conductivity is an example of an important functional property of a Thermal Interface Material (TIM) for LED's and microelectronics devices. Current TIMs are optimized to provide thermal conductivity for as long a time as possible, yet these materials have no self healing potential and any crack formed will only lead to a decreased or lack of thermal conductivity and will dramatically reduce life time of the component.

In order to get a better insight on how, as function of time, self-healing TIM systems are able to recover structural (cracks) and interfacial (delamination, adhesion) damages, we have developed a new specific technique to monitor local heat conduction. This technique probes very locally the heat transfer through the material to monitor changes related to heat conduction. If the material is damaged (cracked), the cracking or delamination will result in a thermal impedance restricting the thermal transfer. If the material is self healing, the local thermal conduction paths will be restored in time. In order to probe the thermal transfer for conventional and our new self healing TIM materials, a dedicated silicon chip containing an array of 49 diodes spaced uniformly over a 1 cm² area has been fabricated. Using this device, it is possible to map with high spatial resolution the efficiency of the local thermal transfer and to relate it to the recovery of pre-imposed damage.

Such experiments will yield unique local and temporal insight into cohesion and adhesion recovery of our self-healing polymeric systems.

1. INTRODUCTION

Since the development of self-healing materials, some effort has been made to develop new characterisation techniques that lead to a quantification of a self healing response. The quantification of the recovery of the mechanical properties has been studied for many materials and is well established. However, the self healing concept also involve material able to recover other functionalities. Self-healing composites having the ability to recover their adhesion, cohesion and thermal conduction properties have been recently produced in our group [1, 2]. These new types of

material have potential application as thermal interface materials (TIM) for micro- and opto-electronic application. Failure of TIM usually involve bulk voiding, interfacial voiding or delamination and erosion [3]. These failures are non-reversible and always lead to a dramatic decrease of the overall system reliability or catastrophic failure. In this respect the use of a self-healing material as TIM will allow an increase in the system reliability and product life time in general [4]. There are several methods that are commonly used to characterize the performance of TIMs [5]. However none of them are suitable to *in-situ* characterize a recovery of property loss. In our study we are interested to quantify and investigate the effect of a multifunctional self healing composite on the recovery of interfacial thermal transfer. For this purpose a specific device has been developed that will allow us to monitor and quantify the recovery of thermal transfer as function of the “healing” of interfacial damages.

2. MATERIALS

In order to investigate the restoration of interfacial thermal transfer, a specific microelectronic device has been developed. This device consist of an array of 7*7 diodes on a 1 cm² silicon chip. The device dimensions are 1*2 cm² (W*L). The diodes use one common anode and each diode need its own cathode. In this configuration, 50 connections need to fan-out from the actual test area and be soldered on a print circuit board (PCB) for practical reasons. During the measurement, each diode will be connected to a current-voltage (IV) analyser via a multiplexer (Figure 1).

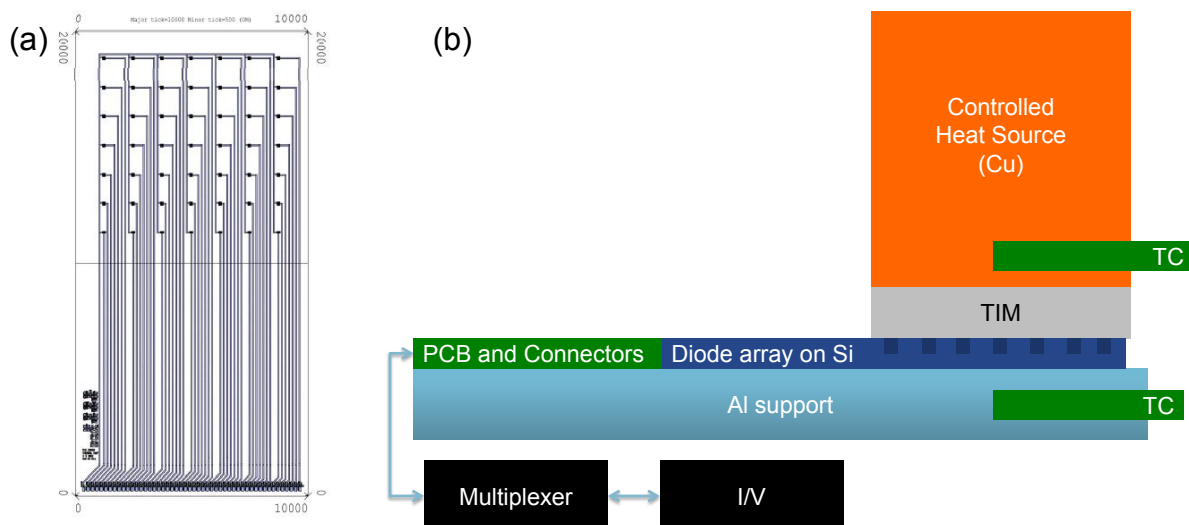


Figure 1: (a) Diode array with all connection and (b) measurement scheme including the controlled heat source, the self-healing material to be investigated (TIM) and the Si based sensor.

3. METHODS

The forward biased current through a silicon p-n junction is exponentially dependent on the temperature (equation 1). Hence the diode can be used as a thermo sensor and using micro electronic manufacturing technologies, large array of spatially small sensors are straightforward to fabricate.

$$I = I_0 \left(e^{\frac{V}{nkT}} - 1 \right) \quad (1)$$

$$\ln \left(\frac{I}{I_0} \right) = \frac{V}{nkT} \quad (2)$$

The logarithmic current-voltage plot of a diode is presented in Figure 2a. There are three main regions:

- at low forward bias voltage the current is related to the charge carrier recombination in the depletion region resulting in $n > 1$ (theoretically $n = 2$).
- a linear response at medium forward bias voltage. This is the so-called ideal region where the current is dominated by the diffusion of charge carriers over the p-n junction.
- a region where electrical resistance and high injection effects becomes dominant.

The voltage ranges at which the different regions can be identified is dependent on the diode area and the technology used to fabricate the diodes. To measure the temperature several strategies exist and need calibration step [6]. The chosen method do not require a calibration. Indeed, at medium forward bias voltages, the slope of a logarithmic current-voltage response is inverse proportional to the temperature (equation 2). Hence the temperature can be extracted from a current measurement at 2 different bias voltages. Particularly for large diode arrays, a no-calibration strategy is an advantage and can be applied if a common ideal region is found for all the diodes in the array.

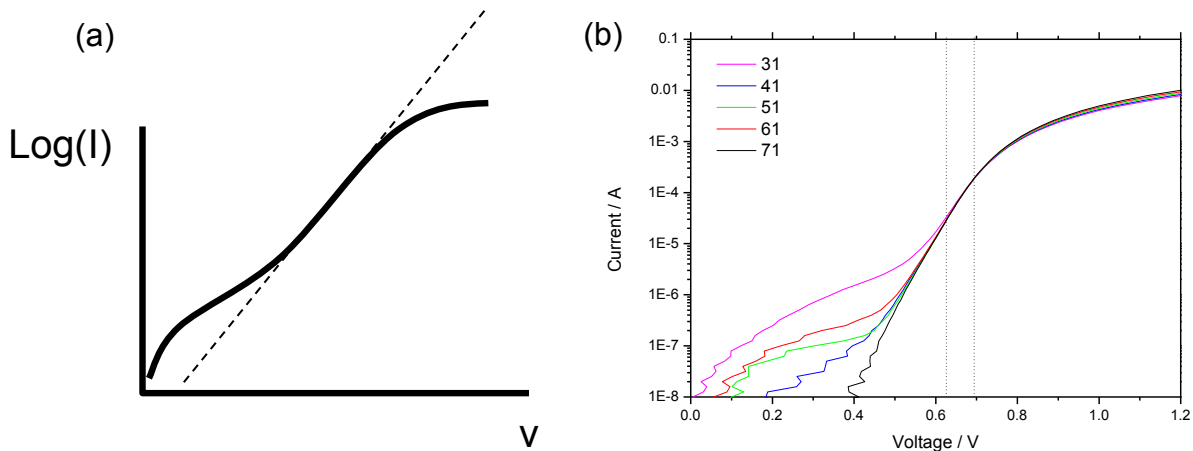


Figure 2: (a) Ideal Logarithmic IV response of a silicon diode showing the linear response. (b) IV response of several diode of the array measured at room temperature.

As each of the diodes in the array will act as singular thermal sensor, the changes in the temperature at the interface will be monitored as function of the position and as function of time. In comparison to an intact interface between the TIM and the diode array, interfacial damages will lead to a delay in thermal transfer. The recovery of the interfacial contact due to the self-healing ability of the TIM material use will be monitored in terms of temperature changes as function of time, i.e. as change in the delay time.

4. RESULTS

First, the IV response of the fabricated diode array has been investigated to look at the individual behaviour of each diodes. As it can be seen on Figure 2b, all diodes exhibit a linear response window that will be used for the temperature measurement. At 25°C the slope of the logarithmic response of each diode is equal to 0.001. For the temperature measurements, a forward bias voltage between 0.6 and 0.7 V will be used as it fit the linear voltage response region. Actual interfacial recovery results will be presented at the conference.

5. CONCLUSIONS

The use of silicon diode array in an integrated circuit configuration is a suitable strategy to construct a 2D heat-flow sensor. Besides having the ability to determine experimentally and in-situ the heat flow through a thermal interface material, it will be possible, in case of using a material with self-healing ability, to characterise the heat flow recovery after damage such as void or delamination. Finally, the direct correlation between the heat flow recovery and the interface or bulk healing of the thermal path can be translated in term of material healing efficiency.

ACKNOWLEDGEMENTS

This research was carried out under project number M71.9.10381 in the framework of the Research Program of the Material innovation institute (M2i) (www.m2i.nl). The authors would like to thanks Huaiyu Ye from DIMES/TU Delft for his help during the device production.

REFERENCES

- [1] U. Lafont, H. Van Zeijl, S. Van Der Zwaag, Influence of cross-linkers on the cohesive and adhesive self-healing ability of polysulfide-based thermosets, *ACS Appl. Mater. Interfaces*, 4 (2012) 6280-6288.
- [2] U. Lafont, C. Moreno-Belle, H. Van Zeijl, S. Van Der Zwaag, Self-healing Thermally Conductive Adhesives, *Journal of Intelligent Material Systems and Structures*, (2013) Submitted.
- [3] C. Feger, M. McGlashan-Powell, I. Nnebe, D.M. Kalyon, Rheology and stability of highly filled thermal pastes, in: *International Microelectronics and Packaging Society*, Scottsdale, Arizona, 2006.
- [4] U. Lafont, H.V. Zeijl, S.V.D. Zwaag, Increasing the reliability of solid state lighting systems via self-healing approaches: A review, *Microelectronics Reliability*, 52 (2012) 71-89.
- [5] A. Vass-Varnai, Z. Sarkany, C. Barna, M. Rencz, An approach for an industrial method for the in-situ characterization of thermal interface materials, in: *Electronics Packaging Technology Conference (EPTC), 2010 12th*, 2010, pp. 279-284.
- [6] N. Takashima, M. Kimura, Diode temperature sensor with the output voltage proportional to the absolute temperature and its application to the thin film Pirani vacuum sensor, in, 2007, pp. 2197-2202.

STUDYING THE HEALING BEHAVIOR AT A MICROSCOPIC SCALE

J. Brancart¹, G. Scheltjens¹, M. M. Diaz¹, B. Van Mele¹ and G. Van Assche¹

¹Physical Chemistry and Polymer Science, Vrije Universiteit Brussel, Pleinlaan 2, 1050 Brussel, Belgium - e-mail: jbrancart@vub.ac.be, gscheltj@vub.ac.be, mdiazace@vub.ac.be, bvmele@vub.ac.be, gvassche@vub.ac.be

Keywords: Self-Healing, Dynamic covalent bonds, Diels-Alder reaction, Atomic Force Microscopy, healing mechanism

ABSTRACT

Research in the field of smart materials that exhibit self-repair mechanisms has greatly expanded over the last few years. This is especially true for polymers and polymer composite materials. One class of self-healing polymer materials is the reversible polymer network systems that use dynamic covalent bonds as a means to repair sustained damage. Currently a range of different dynamic covalent bonds is considered, of which the reversible Diels-Alder chemistry has drawn the most attention. Reversible covalent bonds have been incorporated into polymer network structures based on the Diels-Alder reaction between a furan and a maleimide [1-2]. Repair of sustained damage can be established by means of heating-used self-healing in bulk materials as well as in coating applications.

The aim of this research is to study the healing mechanism and healing kinetics at the microscopic scale and to compare this healing mechanism for different polymer network structures and chemistries. The self-healing behavior is studied with local and surface analysis techniques, including Atomic Force Microscopy as an important tool. A better understanding of the healing mechanism at the microscopic level will lead to a better understanding of the macroscopic healing phenomena and ultimately to the adaptation of the polymer network structure to obtain the desired material properties, such as mechanical properties, healing conditions and additional functional properties. The research can then be extended towards self-healing polymer composites, with e.g. a reversible polymer matrix, to evaluate the recovery of the composite material properties [3].

1. INTRODUCTION

Covalently cross-linked polymer network structures exhibit superior mechanical and barrier properties compared to their linear and physically cross-linked analogues. These exceptional properties find numerous applications in e.g. glues, adhesives, coatings, molded products,... The main disadvantage of these material systems is the irreversibility of the network formation reaction. The addition of dynamic covalent bonds to the polymer network structure has proven to render the network formation reaction reversible and gives rise to a new type of materials: reversible or dynamic polymer network systems. These dynamic covalent bonds originate from chemical reactions that are reversible or dynamic upon application of a certain stimulus. This stimulus can be light for photoreversible reactions, heat for thermoreversible reactions, force for mechanoreversible reactions or other. Through application of the corresponding stimulus to the dynamic material a healing action can be triggered and

sustained damaged can be healed. When the external stimulus is removed the material will restore its initial properties and the material is considered to be repaired. In this work heat will be considered as the stimulus to trigger a healing action in a reversibly cross-linked covalent polymer network based on the reversible Diels-Alder cycloaddition reaction between a furan and a maleimide. In previous work [2-4] it was demonstrated that polymer network materials based on these dynamic covalent bonds showed the required reversibility to establish a successful healing of sustained damage, both on a microscopic and a macroscopic scale.

At each temperature an equilibrium exists between the reactants (furan and maleimide functions) and the Diels-Alder cycloadduct. As the temperature is increased, the Diels-Alder reaction equilibrium is pushed towards the breaking of the dynamic bonds to form the reactants. By incorporating these dynamic covalent bonds as cross-links into a polymer network structure, reversible covalent polymer network structures with different mechanical and thermal properties can be created. As the temperature of the network is increased, the reversible bonds are broken and the material becomes softer as more bonds are broken. Above a certain temperature so many bonds are broken that the material starts to behave like a fluid. When the material has gained enough mobility to fill a sustained defect, healing of the material can be established. Upon decreasing the temperature the equilibrium shifts toward the formation of bonds and the initial properties of the network are restored.

2. MATERIALS AND METHODS

A series of Jeffamine D hardeners (Poly(propylene glycol) bis(2-aminopropyl ether)) are functionalized with furan functional groups by means an irreversible epoxy-amine reaction with furfuryl glycidyl ether (FGE). The reaction is allowed to go to completion yielding a 4-functional furan compound that is then reversibly reacted with 1,1'-(methylenedi-1,4-phenylene)bismaleimide (DPBM) to create a reversible polymer network structure. All products were purchased from Sigma-Aldrich and used as received.

Reversible covalent polymer network structures are created with a wide range of properties going from rubbery materials with glass transitions of -65 to -55 °C to more glassy materials with glass transition temperatures of 56 and 64 °C. The equilibrium gel point temperatures range from 49 °C to 83 °C.

The reversible polymer network systems are applied as coatings on pure aluminium substrates by means of spin coating from a 10 w% chloroform solution. The solvent is evaporated and the coatings are allowed to cure at temperatures slightly above room temperature (50 – 60 °C). Coatings with a thickness of around 1 µm were created. Changing the concentration of the coating formulation yields coatings of different thicknesses.

3. RESULTS AND DISCUSSION

3.1. Local Thermal Analysis

The thermomechanical behavior of the dynamic covalently cross-linked polymer network systems is analyzed by means of Local Thermal Analysis (LTA). This technique combines the conventional Atomic Force Microscopy (AFM) with the option to heat up the probe to a certain temperature while maintaining contact with the studied material, providing thermomechanical information about the material.

Increasing the cross-link density of the network by altering the building blocks for the formation of the network structure, increases the toughness of the network and the glass transition temperature. Consequently the density or concentration of the Diels-Alder functional groups is also increased, influencing the equilibrium of the forward and reverse Diels-Alder reactions. The lower the cross-link density, the lower the equilibrium conversion becomes for the Diels-Alder reaction and the softer and more rubber-like the material becomes. In contrast, the higher the cross-link density, the harder and more glass-like the material becomes and the higher the equilibrium conversion becomes. Higher temperatures will be needed for the more cross-linked networks to break down a sufficient amount of bonds in the network structure to obtain efficient healing of sustained damage. It has been demonstrated that when the temperature is increased sufficiently and enough bonds are broken, a reversible gel transition is observed due to the reversible polymerization reaction. Above the gel point temperature the material behaves like a liquid.

3.2. Self-healing behavior

In order to create defects in a controlled and reproducible manner, the nano-lithography option on an Asylum Research MFP-3D™ Atomic Force Microscope (AFM) was used. Exerting a well-defined force on a rigid AFM probe allows the creation of defects such as scratches with very controllable and reproducible depth and width. In the case of nano-indentation elastic recovery of the material may interfere with the studied healing mechanism. Scratches and indentations can be made with varying width and depth to evaluate the effect of these parameters on the healing mechanism and its efficiency. The materials are heated in-situ in the AFM by means of a polymer heating stage. Damage was healed at different temperatures for different times to reveal the healing mechanism.

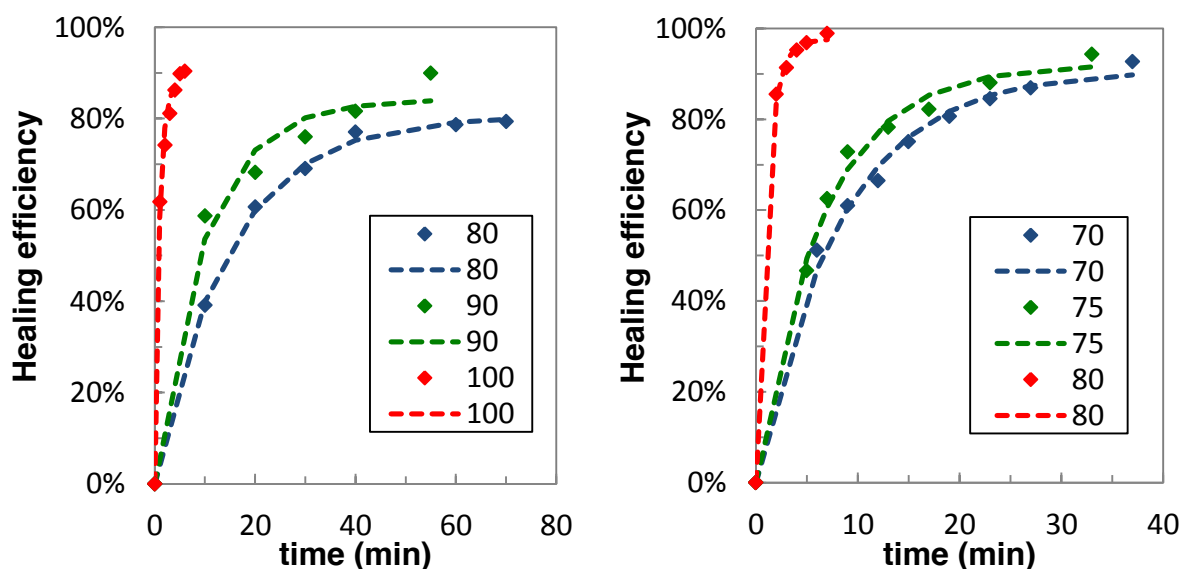


Figure 1: Local healing of defects in DPBM-FGE-J400 (left) and DPBM-FGE-J2000 (right) reversible covalent polymer network coating on pure aluminum substrate.

As the temperature is increased the equilibrium shifts towards the breaking of dynamic bonds and the reaction conversion decreases. The mobility in the material is increased and the healing action is facilitated. For both the rubbery and glassy

material systems the self-healing can only take place at temperature well above the glass transition temperature. The higher the healing temperature, the more mobility is created inside the material, hence the shorter the healing times and the more efficient the healing will be (Figure 1). Yet it was proven that healing of damage can be obtained at temperatures little below the gel point temperature, though very slowly and only to a certain extent. The size and geometry of the defect dictate the degree of mobility that is needed to efficiently heal the defect. To cover a microscopic defect the flexibility of the chains can be sufficient below the gel transition temperature. In this case the network structure can be retained and the material remains solid-like. For macroscopic defects a higher degree of mobility is needed and the network will need to be broken down to a higher extent to cover the bigger defects. For recycling purposes it may be even more interesting to go to even higher temperatures and lower conversions to obtain a liquid material, which then can be given a new shape.

4. CONCLUSIONS

Healing of sustained damage was achieved in different reversible polymer networks systems based on dynamic covalent bonds from the reversible Diels-Alder reaction between a furan and a maleimide functional group. Local thermal analysis was used to study the thermomechanical properties of the self-healing materials. It was demonstrated that not only the mechanical properties, but also the temperature window in which the healing of sustained damage can be established can be tailored by changing the building blocks in the reversible polymer networks structure.

Other reversible chemistries will be considered to optimize the healing circumstances and building blocks will be changed to alter the mechanical and thermal properties of the self-healing materials with regard to the intended applications.

REFERENCES

- [1] S. D. Bergman, F. Wudl, Mendable Polymers, *Journal of Materials Chemistry*, 18 (2008) 41-62.
- [2] G. Scheltjens, J. Brancart, I. De Graeve, B. Van Mele, H. Terryn, G. Van Assche, Self-healing property characterization of reversible thermoset coatings, *Journal of Thermal Analysis and Calorimetry*, 105 (2011) 805-809.
- [3] J. Brancart, G. Scheltjens, T. Muselle, B. Van Mele, H. Terryn, G. Van Assche, Atomic force microscopy-based study of self-healing coatings based on reversible polymer network systems, *Journal of Intelligent Material Systems and Structures*, published online (2012).
- [4] G. Scheltjens, M.M. Diaz, J. Brancart, G. Van Assche, B. Van Mele, A self-healing network based on reversible covalent bonding, *Reactive and Functional Polymers*, 73 (2012) 413-420.

Visualization of self-healing materials by X-ray Computed Micro-Tomography at UGCT

T. Bultreys^{1,5}, B. Masschaele^{2,3,5}, X. Hillewaere^{4,5}, M. Dierick^{2,3}, D. Van Loo³, L. Van Hoorebeke² and V. Cnudde¹

¹ Centre for X-ray Tomography (UGCT) – Dept. Geology and Soil Science, Ghent University, Krijgslaan 281, 9000 Ghent, Belgium – e-mail: Tom.Bultreys@UGent.be, Veerle.Cnudde@UGent.be

² Centre for X-ray Tomography (UGCT) - Dept. Physics and Astronomy, Ghent University, Proeftuinstraat 86, 9000 Ghent, Belgium – e-mail: Bert.Masschaele@UGent.be, Manuel.Dierick@UGent.be, Luc.VanHoorebeke@UGent.be

³ XRE, X-Ray Engineering BVBA, De Pintelaan 111, 9000 Gent, Belgium – e-mail: Denis.VanLoo@xre.be

⁴ Department of Organic Chemistry, Polymer Chemistry Research Group, Ghent University, Krijgslaan 281, S4-bis, B-9000 Ghent, Belgium – e-mail: Xander.Hillewaere@UGent.be

⁵ SIM vzw, Technologiepark Zwijnaarde 935, B-9052 Ghent, Belgium

Keywords: X-ray computed micro-tomography, self-healing

ABSTRACT

This work presents recent advancements in X-ray micro-computed tomography (XRMCT) of self-healing materials at Ghent University's Centre for X-ray Tomography (UGCT). Results of XRMCT imaging in a self-healing polymer system are shown to demonstrate the use of XRMCT in self-healing studies. Furthermore, two new XRMCT scanners are presented. The HECTOR scanner was designed for large samples and strongly attenuating samples, and is therefore well suited to study self-healing concrete. The EMCT scanner is well suited for dynamic self-healing experiments in a controlled environment.

1. INTRODUCTION

This work presents recent advancements in X-ray computed micro-tomography of self-healing materials made at Ghent University's Centre for X-ray Tomography (UGCT). UGCT designs and assembles its own scanners in room-sized bunkers to optimize flexibility and research possibilities. Furthermore, it develops CT reconstruction and analysis software and performs research into both the underlying physics as the advanced application of X-ray computed micro-tomography (XRMCT). XRMCT is a widely used, non-destructive, three-dimensional imaging technique with great potential for studying self-healing materials. As an example, we present results from self-healing polymers. Furthermore, we present two new set-ups, named HECTOR and EMCT, well suited for respectively the study of self-healing concrete and (dynamic) self-healing processes in a controlled environment.

2. X-RAY COMPUTED MICRO-TOMOGRAPHY

X-ray computed tomography can provide a fully three-dimensional image of the interior of an object by reconstructing slices using two-dimensional radiographs of the object, made from a large number of different angles. In each voxel (three-dimensional pixel) of the three-dimensional image the local X-ray attenuation

coefficient is obtained, which depends on local densities and effective atomic numbers. As such, it is possible to visualize the internal structure of the sample. A laboratory-based XRMCT set-up consists out of three main parts : an X-ray tube, a rotation stage to mount the sample on and an X-ray detector.

3. SELF-HEALING POLYMERS

As an example of the use of XRCMT for the study of self-healing materials, we show some results from a capsule-based self-healing polymer system. Microcapsules containing healing agents are embedded in an epoxy thermosetting matrix to provide the self-healing property. The microcapsules break upon rupture of the matrix and release the healing agents in the crack, where these react to form a new healed polymer network.

Figure 1 shows a CT-scan from a subsample of a Tapered Double Cantilever Beam test sample that was allowed to self-heal after breaking. Single microcapsules can be clearly distinguished to study for example capsule size, shape and spatial distribution. Furthermore, the crack surface can be visualized, allowing to study for example tail formation and delamination of microcapsules at this surface.

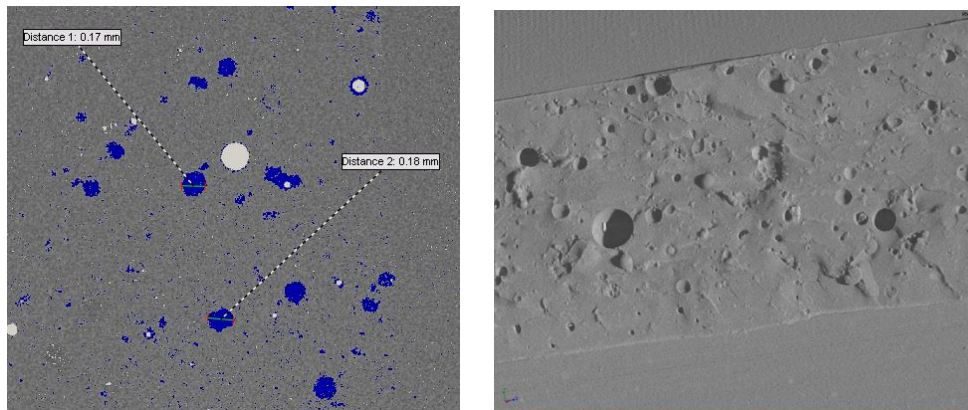


Figure 1: slice through the interior of a self-healing polymer sample (left), 3D rendering of the crack in this sample (right).

4. HECTOR AND EMCT

HECTOR (High Energy CT Optimized for Research) was designed to extend UGCT's imaging capabilities to larger and/or stronger attenuating objects. Furthermore, there was a need to reduce scanning times for monitoring for example dynamic events. An important component of HECTOR is an X-RAY WorX XWT 240-SE microfocus source. This high power directional tube can generate up to 280 W target power to get a high X-ray flux. The focal spot's minimum size of 4 μm ensures that the system is still useful for standard micro-CT scanning. A large 40x40 cm^2 PerkinElmer 1620 CN3 CS flat panel detector allows for a large field-of-view. A rotation stage, specifically chosen to be able to handle heavy loads with extreme precision, was mounted on a vertical stage with a travel of 1m to make helical scanning of long objects (e.g. drill cores) possible [1].

HECTOR's characteristics make this system specially suited to study concrete drill cores (figure). The system will be used to study self-healing geometries and processes in the framework of the SECEMIN research project.

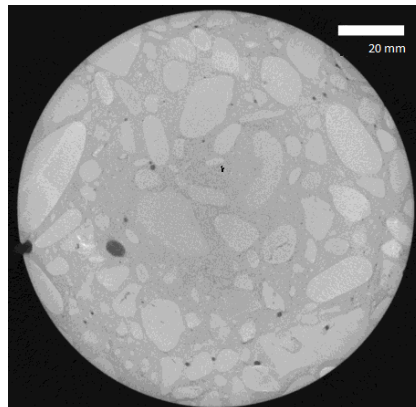


Figure 2 : Reconstruction of a slice of a concrete core with a diameter of 12 cm, scan performed with HECTOR

The EMCT (Environmental Micro CT) scanner was designed to image samples under controlled environmental conditions (temperature, pressure, humidity) or during dynamic experiments (e.g. loading). Therefore, the system is designed having a «rotating X-ray source and detector»-assembly, contrary to conventional XRMCT scanners in which the sample is rotated. Communication, interlocks and power are transmitted over slip ring contacts embedded in the system's granite base. Therefore, the source-detector combination can continuously rotate around the sample which remains stationary with regard to the outside world. This facilitates connecting external equipment (pumps, loading stages, etc.) to the sample during imaging.

The system has a directional X-ray tube with a minimal spot-size of 5 μm and a maximal accelerator voltage and power of 130 kV and 39 W, respectively. Its CMOS detector with CsI scintillator allows for fast CT scans (up to 300 fps), with a sufficiently small angular interval between successive projections.

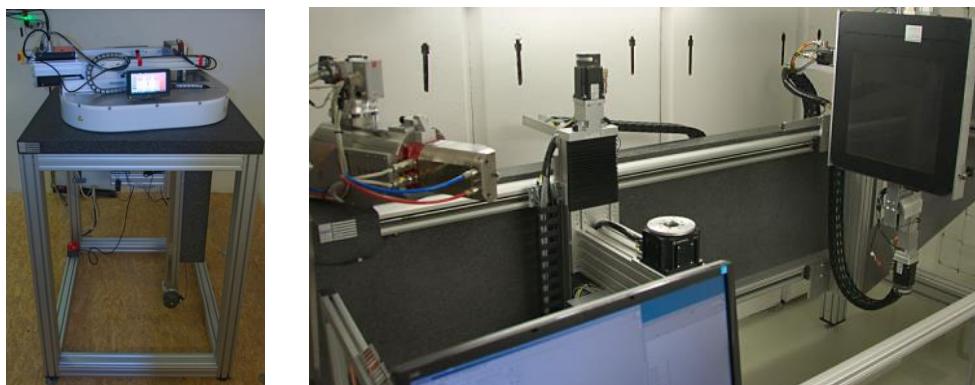


Figure 3: The EMCT scanner (left) and HECTOR (right)

The source and detector are mounted on a linear motorised stage to allow changing the magnification. The goniometer on which this stage is mounted has a bore hole of 190 mm diameter through which the samples can be positioned into the beam. The

EMCT scanner has a vertical stage with 80 cm travel. This will allow helical scanning of long samples, e.g. drill cores. Using a 3D resolution pattern, we have demonstrated that 5 μm spatial resolution can easily be achieved in the reconstructed CT volume.

5. CONCLUSIONS

XRMCT is a powerful imaging technique with great potential to aid characterization of self-healing materials. With the addition of two new XRMCT scanners, UGCT can now accommodate experiments on self-healing concrete and dynamic experiments.

ACKNOWLEDGEMENTS

The Agency for Promotion of Innovation by Science and Technology in Flanders, Belgium (IWT) is acknowledged for the PhD grant to Tom Bultreys. The work presented is part of the Strategic Initiative Materials (SIM) project, supported by the IWT.

REFERENCES

[1] B. Masschaele, M. Dierick, D. Van Loo, M. N. Boone, L. Brabant, E. Pauwels, V. Cnudde and L. Van Hoorebeke (2012). HECTOR: A 240kV micro-CT setup optimized for research. 11th International Conference on X-Ray Microscopy Shanghai.

BIO-INSPIRED MATERIALS

POSTER SESSION

ACTUATED WOUND SENSING, CLOSING AND HEALING IN FLEXIBLE SHEETS USING FUNCTIONAL MACRO CELLS

D. Huston¹, D. Burns¹, J. Razinger¹ and R. Seal¹

¹ School of Engineering, University of Vermont, 33 Colchester Ave., Burlington, VT 05405, USA – e-mail: dryver.huston@uvm.edu; Dylan.Burns@uvm.edu; Jonathan.Razinger@uvm.edu; Robert.Seal@uvm.edu

Keywords: wound, closing, pursestring, functional, cellular

ABSTRACT

This paper describes an examination and demonstration of a flexible sheet system based on a functional macro-scale architecture that detects and localizes cutting damage, closes the wound through mechanical actuation, repairs the cut with healing liquids that solidify in the cut. Following sensing of successful healing, the system deactivates the wound closing and other healing processes. The building block of this system is a functionalized multicellular structure where each cell has the ability to sense through-sheet cut damage, actuate bi-directional in-plane deformation, dispense and cure a healing liquid, and communicate with neighboring cells. The cellular architecture enables varying the type and testing the performance of individual sensing, actuating and healing techniques; along with examining the behavior collective multicellular behavior, such as pursestring wound closing. This system represents a highly simplified mimic of some of the wound healing processes occurring in biological system. One demonstrated variant uses a neoprene skin with embedded subsurface optical sensing, electromechanical in-plane actuation, localized microprocessor control and actuated dispensing of neoprene-specific healing liquids embedded in each cell. Additional techniques presently under investigation are aimed at miniaturizing the cells and enabling a more facile response. These include active solids and constrained gels for in-plane deformation, finer-pitch healing liquid distribution with vascular or wet-sublayer configuration and different spatial gradient collective multicellular healing control.

1. INTRODUCTION

Wound closing is a macroscale healing technique commonly used in biological systems. Wound closing generally alters the mechanical stress and material distribution in the tissue surrounding a wound so as to shrink the size of the open damaged area. The advantages for wound closing are: 1. The contraction reduces the volume and area of the wound to be healed. 2. The closed wound requires less material for a more substantial healing, including subsurface structures. 3. Closing the wound reestablishes the barrier between the interior and the exterior of the system. Tissue swelling along with infilling and circumferential hoop contractions acts to close the wound. Plants, animals and even single-celled creatures routinely close wounds. A surgeon's stitches assist wound closing by exerting tension across the wound. Biological systems use other mechanical techniques, such as 'purse string' tightening.

Self-healing material and structural systems technology has seen considerable development in the past two decades. Much of this activity has addressed the topic of repairing tight cracks through polymer merging or the release of embedded and encapsulated liquid healing agents. Coordination can enhance self-healing performance by making more efficient use, storage and allocation of healing resources [1]. Coordinated self-healing can use virtually all of the techniques described above, while taking advantage of sensing coordination, decision making, actuation and monitoring. Coordination also includes sensing of damage and actuating repair terminating and modulating repair as it progresses, and actively directing construction of new structural forms. This paper examines the related, but relatively unaddressed problem of autonomic wound closing methods. When the damage is moderate to severe, closing the wound as a first step can enable tight crack healing methods to work with greater efficiency and ease. Closing or filling the gap with material compatible to the original material and restoring the smooth flow of stress and strain across the crack.

Wound closing requires shape control. A variety of tools are becoming more readily available that enable controlled altering of the shape of materials. Shape memory materials can return to an original following an extended period of large inelastic deformation, often with the aid of thermal cycling [2]. The heat-induced swelling of intumescent materials can alter the connectivity of structural components and significantly delay or arrest the progress of fires or extreme heat. Dielectric elastomers can induce large deformations under control, but the required geometries and large voltages presently limit the range of applicability. Microstructure-actuated snapping surfaces are another possibility. Compliant arrays of flexure mechanisms can aid integrating shape changing methods into structural systems. Liquid-induced swelling can cause autogenous crack sealing. This requires a material that swells when the liquid penetrates into the crack. Micciché et al. [3] resolve the issue with a water/humidity-induced swelling of a subsurface layer of montmorillite clay layer.

Methods of wound closing in engineered systems include: 1. 2-D Purse String Method – The purse string method acts on planar structures. A tension ring, i.e. knittle, forms around the wound. Inside the knittle swelling induces compression, which closes the wound. Figure 1 shows the concept; 2. 3-D Constrained Layer Swelling – The swelling of material for wound closing is much more effective when the swelling is constrained by stiff layers [4]; 3. 3-D Out-of-Plane Delamination Closing – Delaminations between layers in a material system can be closed by out-of-plane forces perpendicular to the plane of the delamination; 4. Bridging and Stitching Across the Wound – Fibers that bridge and then pull across the gap can be effective at closing the wound [5]; 5. Sliding and Covering – This is an autonomic band-aid technique that slides a prepositioned protective layer across the wound.

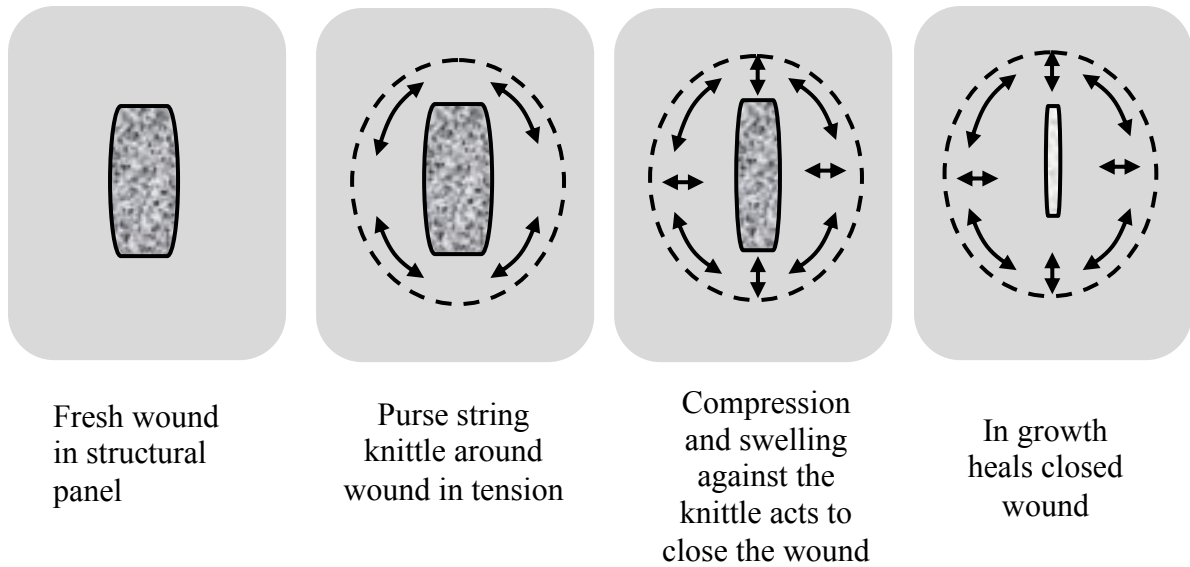


Figure 1: Purse string method of wound closing and healing

2. MATERIALS AND METHODS

Figure 2 shows a test rig and results of a cellular actuated purse string method developed to demonstrate autonomic wound closing through a multistep process of injury sensing with embedded optical sensors, followed by solenoid-actuated wound closing, then the dispensing of a neoprene-specific healing fluid and curing to seal the wound.

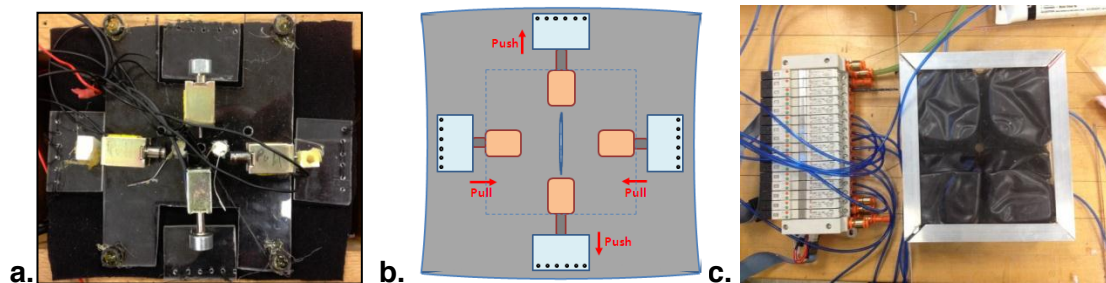


Figure 2 : a. bottom side view of autonomic wound closing mechanism, b. solenoid actuation schematic, and c. cellular pneumatic concept for multi-site repair under development.

3. RESULTS AND DISCUSSION

Figure 3.a shows the results of a finite element analysis of the wound closing system. Figure 3.b shows successful closing and repair of a cut into the neoprene skin. Extending this technique to large regions requires spanning an external skin surface with multiple repair mechanisms.

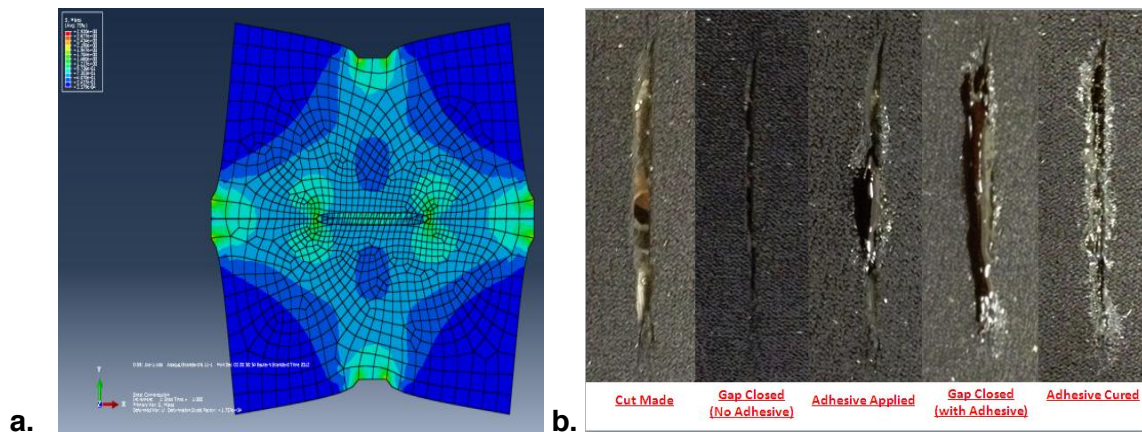


Figure 3: Cellular mechanical wound closing test rig developed at UVM a. Backside sensing and actuation mechanism, b. Conceptual model, c. Numerical model, d. Wounds closed and then healed in neoprene skin, e. Plan for scalable multi-celled system.

4. CONCLUSION

The actuated wound closing then healing method has been demonstrated. The present system is somewhat bulky, but may be miniaturized and packaged in a way to be practical for future applications.

ACKNOWLEDGEMENTS

This research was supported by the US Navy ONR contract N00421-09-1-0008

REFERENCES

- [1] D. A. Hurley, D. R. Huston. Coordinated sensing and active repair for self-healing, *Smart Materials and Structures* (2011) 20, 025010
- [2] E. Choi, S.C. Cho, J.W. Hu, T. Park T, Y.S. Chung. Recovery and Residual Stress of SMA Wires and Applications for Concrete Structures *Smart Materials and Structures* (2010). 19, 094013
- [3] F. Miccichè, H. Fischer, R. Varley, S. van der Zwaag. Moisture induced crack filling in barrier coatings containing montmorillonite as an expandable phase, *Surf. Coat. Technol.* 202 (2008) 3346.
- [4] T.S. Ohnstad, R.A. Monk. Sealing-reaction, layer-effective, stealth liner for synthetic fuel container, US Patent 8,043,676, (2011)
- [5] Y. Kuang, J. Ou. Self-repairing performance of concrete beams strengthened using superelastic sma wires in combination with adhesives released from hollow fibers, *Smart Mater. Struct.* 17 (2008) 025020

DEVELOPMENT OF COHESIVE SELF-HEALING GELS BASED ON SELF-ASSEMBLY OF ORGANIC AND INORGANIC NANOPARTICLES

M. Diba^{1,2}, D. W. P. M. Löwik², J.C. M. van Hest², J. A. Jansen¹, S. C. G. Leeuwenburgh¹

¹ Department of Biomaterials, Radboud University Nijmegen Medical Center, Philips van Leydenlaan 25, 6525 EX Nijmegen, The Netherlands– e-mail: m.diba@dent.umcn.nl; j.jansen@dent.umcn.nl; s.leeuwenburgh@dent.umcn.nl

² Department of Bio-organic Chemistry, Radboud University Nijmegen, Heyendaalseweg 135, 6525 AJ Nijmegen, The Netherlands– e-mail: d.lowik@science.ru.nl; j.vanhest@science.ru.nl

Keywords: Colloidal gel, self-healing, nanoparticles, nanocomposite

ABSTRACT

Noncovalent bonds are often reversible and sensitive to external stimuli. Although noncovalent interactions are inherently weak and generally perceived as inadequate to construct macroscopic materials of sufficient integrity and cohesion, the emergence of nanotechnology has shown that the intrinsic weakness of noncovalent interactions can be compensated by maximizing the number of these bonds that work in concert. In that way, remarkably strong materials can be formed. Colloidal gels are an emerging and particularly attractive class of cohesive hydrogels. These materials allow for “bottom-up” design of functional materials by employing noncovalent interactions between micro- or nanoscale particles as building blocks to assemble into shape-specific bulk materials. In an attempt to explore the feasibility of using electrostatic and hydrophobic interactions between nanoparticles, it was recently observed that colloidal gels made of oppositely charged gelatin nanospheres were surprisingly cohesive, elastic and self-healing. In the current study, we aim to extend this concept towards self-healing colloidal gels by synthesizing organic nanoparticles that exhibit a strong affinity for inorganic nanoparticles using various types of bioinspired derivatization strategies. The organic nanoparticles impart flexibility and resilience to these gels, while the inorganic nanoparticles improve their hardness and rigidity.

1. INTRODUCTION

Generally, functional materials owe their integrity to irreversible covalent bonds. The irreversibility of these covalent bonds renders these materials incapable of self-healing since these bonds cannot be restored after rupture. In contrast, non-covalent bonds are often reversible and more sensitive to external stimuli. Although these noncovalent interactions are inherently weak and generally perceived as inadequate to construct macroscopic materials of sufficient integrity and cohesion, the emergence of nanotechnology has shown that the intrinsic weakness of non-covalent interactions can be compensated by maximizing the number of these bonds that work in concert. In that way, remarkably strong materials can be formed. Still, non-covalent synthetic methodology is only starting to emerge as a research field. In that respect, colloidal gels are an emerging and particularly attractive class of cohesive hydrogels.

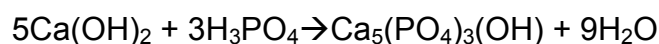
These materials allow for “bottom-up” design of functional materials by employing noncovalent interactions between micro- or nanoscale particles as building blocks to assemble into shape-specific bulk materials. Moreover, biomimetic strategies have shown to be promising approaches for development of advanced functional materials. Bone tissue is a nanostructured inorganic-organic composite and is one of the most striking examples of a self-healing material since it is able to continuously restore its integrity in response to damage. Studies have indicated that the nanostructure of bone as well as non-covalent interactions between its organic and inorganic phases are key factors determining its self-healing properties. The current study aims to develop a self-healing colloidal nanocomposite gel with combining different types of optimized organic and inorganic nanoparticles through mimicking the composition, structure and interactions between different components of bone tissue. Therefore, different types of organic (gelatin) and inorganic (calcium phosphate, bioactive glass and silica) nanoparticles will be synthesized and their surface properties (surface charge, surface chemistry and hydrophobicity) will be modified to obtain composite gels with improved self-healing properties.

2. MATERIALS

Gelatin types A and B, glycine ($\geq 99\%$), and tetraethyl orthosilicate (TEOS; 99.999% trace metals basis) were purchased from Sigma–Aldrich. Calcium hydroxide ($\text{Ca}(\text{OH})_2$, 98+%, extra pure), ammonium hydroxide (NH_4OH ; 25 wt% solution in water), sodium citrate tribasic dihydrate ($\text{Na}_3\text{C}_6\text{H}_5\text{O}_7 \cdot 2\text{H}_2\text{O}$), and Glutaraldehyde (GA, 25 wt% solution in water) were purchased from Acros Organics. Calcium nitrate tetrahydrate ($\text{Ca}(\text{NO}_3)_2 \cdot 4\text{H}_2\text{O}$) was from Merck. Acetone and phosphoric acid (H_3PO_4 , 85%) were purchased from J.T.Baker. All the other reagents were analytical grade.

3. METHODS

A two-step desolvation method was used for fabrication of gelatin nanospheres as described elsewhere [1]. Bioactive silicate glass nanospheres with different calcium contents were synthesized via optimization of the Stöber method [2]. A precipitation method was used for preparation of calcium phosphate nanoparticles [3]. This wet chemical approach is based on a neutralization reaction between ortho-phosphoric acid and calcium hydroxide yielding apatitic nanoparticles, the aspect ratio and size of which can be finetuned by changing reaction parameters such as temperature as shown below:



4. RESULTS

Scanning electron microscopy (SEM) and transmission electron microscopy (TEM) techniques were used to evaluate the size and morphology of the synthesized nanoparticles. Figure 1 shows the SEM micrograph of positively charged gelatin nanospheres. As shown in this figure the particles were spherical and had the average diameter of about 160-170 nm.

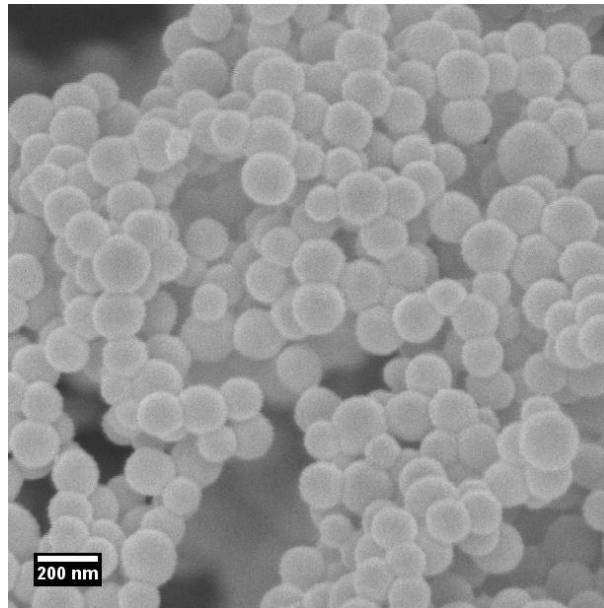


Figure 1: SEM micrograph of gelatin (type A) nanospheres.

In an attempt to explore the feasibility of using electrostatic and hydrophobic interactions between biopolymer nanoparticles, it was recently observed that colloidal gels made of oppositely charged gelatin nanospheres were surprisingly cohesive, elastic and self-healing [1] (as shown in Figure 2).

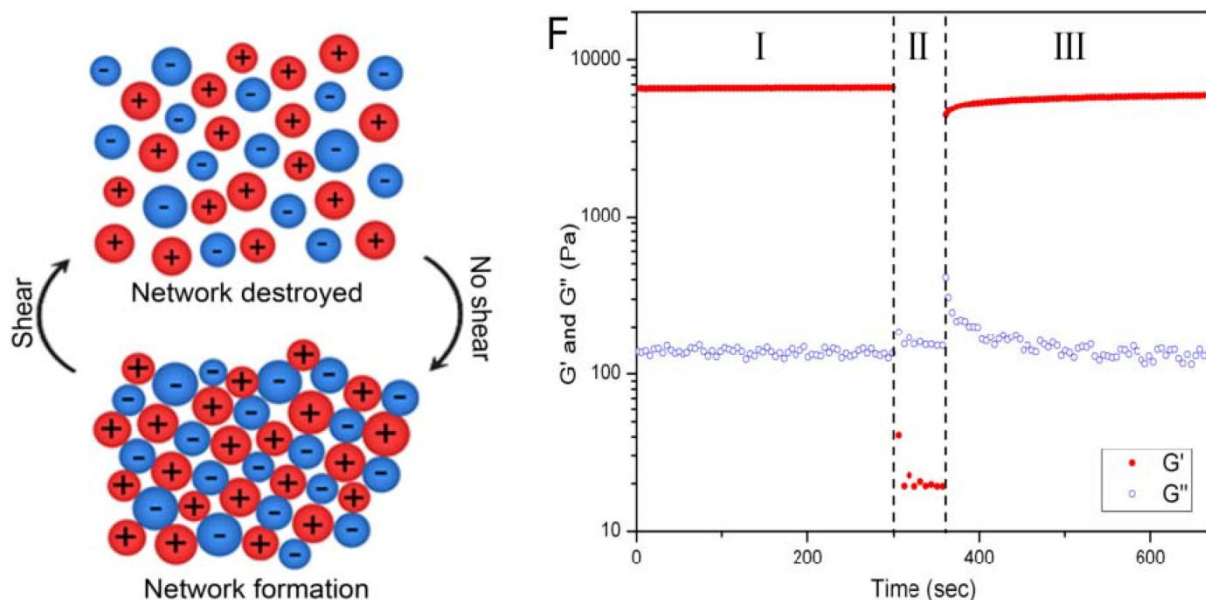


Figure 2: Fast and almost complete recovery of elasticity (G') of colloidal gels made of oppositely charged gelatin nanospheres upon gel network destruction (1000% strain) in phase II.

As shown in Figure 3, calcium phosphate and bioactive silicate glass nanoparticles were synthesized with needle and spherical shapes, respectively.

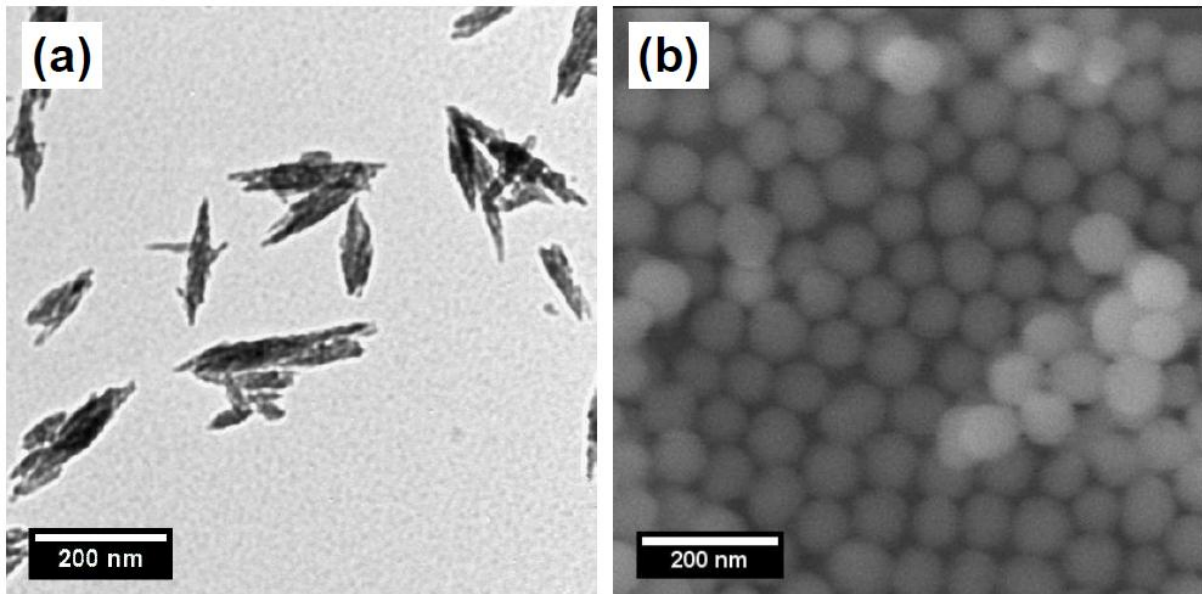


Figure 3: (a) TEM micrograph of calcium phosphate and (b) SEM micrograph of bioactive silicate glass nanoparticles.

Further studies will investigate the effects of these inorganic nanoparticles of different morphology and composition on self-healing properties of composite colloidal gels using techniques such as AFM and optical tweezers (at low solid content) and rheometry (at high solid content).

5. CONCLUSIONS

By combining organic and inorganic nanoparticles, self-healing colloidal gels will be developed in the current project based on optimization of reversible interactions between the nanoparticles. These nanocomposite gels will benefit from the flexibility and resilience of organic matter and hardness and rigidity of inorganic nanoparticles.

ACKNOWLEDGEMENTS

The authors thank AgentschapNL (IOP Self Healing Materials, Project no. SHM012014). The authors would like to thank Prof. Aldo R. Boccaccini for his helpful discussions on the synthesis of bioactive glass nanoparticles.

REFERENCES

- [1] H.A. Wang, M.B. Hansen, D.W.P.M. Lowik, J.C.M. van Hest, Y.B. Li, J.A. Jansen, and S.C.G. Leeuwenburgh, Oppositely Charged Gelatin Nanospheres as Building Blocks for Injectable and Biodegradable Gels, *Advanced Materials* 23 (2011) H119-H124.
- [2] W. Stöber, A. Fink, and E. Bohn, Controlled growth of monodisperse silica spheres in the micron size range, *Journal of Colloid and Interface Science* 26 (1968) 62-69.

[3] R. Kumar, K.H. Prakash, P. Cheang, and K.A. Khor, Temperature driven morphological changes of chemically precipitated hydroxyapatite nanoparticles, *Langmuir* 20 (2004) 5196-5200.

SELF-HEALING BITUMINOUS MATERIALS

POSTER SESSION

FATIGUE AND HEALING PERFORMANCE OF BITUMINOUS BINDERS AND MIXTURES FOR ROAD PAVEMENT – RESULTS OF RE-ROAD PROJECT

W. Van den bergh¹, C. McNally², A. De Keersmaecker¹ and E. Fallon²

¹ Applied Engineering Laboratory for Sustainable Materials, Infrastructure and Building, Artesis University College of Antwerp, Paardenmarkt 92, 2000 Antwerp, Belgium – e-mail: wim.vandenbergh@artesis.be

² School of Civil, Structural & Environmental Engineering, University College Dublin, Newstead, Belfield, Dublin 4, Ireland – e-mail: ciaran.mcnally@ucd.ie

Keywords: bitumen, mastic, asphalt, fatigue, healing, mechanical dynamic testing.

ABSTRACT

An asphalt mixture is believed to be a partial self-healing material. For asphalt pavement design, this characteristic is taken into account as a shift healing factor. Healing during rest periods will result in a longer structural design life for the mixture in situ, compared to the fatigue life determined with a continuous sinusoidal test in the laboratory.

For the FP7 Re-Road project, an extensive research programme was completed in order to increase the recyclability of asphalt mixtures, in particular asphalt mixtures with polymer modified binder. One research task dealt about performance modelling of asphalt pavement containing Reclaimed Asphalt (RA). For this, fatigue and healing tests were performed on virgin and aged binders, mastics and asphalt mixtures.

Bituminous binders and mastics (virgin and aged) were tested using a Dynamic Shear Rheometer (DSR) in oscillation model. The fatigue and healing properties of the asphalt mixtures were determined by means of a dynamic test on compacted asphalt samples. The binders, mastic and asphalt test results show a significant increment in fatigue life when rest periods are taken into account between fatigue cycles.

1. INTRODUCTION

An asphalt mixture is believed to be a partial self-healing material. For asphalt pavement design this characteristic is taken into account as a healing shift factor, representing the effect of rest periods between loadings on the fatigue life. The healing shift factor is mostly determined on asphalt mixtures by applying continuous and discontinuous fatigue tests. However, a standard test method is absent. An overall validated value is still not accepted since the performance of asphalt mixtures differ by bitumen origin, composition, production, climate and traffic history. One can only compare healing properties of different mixtures when identical test conditions (test procedure, temperature, frequency and loading) are selected. That's why a wide range of healing factors are reported: from 1 to more than 100.

For the FP7 Re-Road project an extensive research programme was completed in order to increase the recyclability of asphalt mixtures, in particular asphalt mixtures with polymer modified binder. One of the work packages (WP5) dealt about performance modelling of asphalt pavement containing RA. In this WP5, fatigue and

healing tests were performed on virgin and aged binders, mastics and asphalt mixtures.

2. MATERIALS

The healing and fatigue mechanism can be considered in the asphalt mixture or in its components. Most fatigue and healing tests are performed in binder or asphalt. A compromise is to test mastic or mortar; this is a mixture of the bituminous binder with fine aggregates and filler. The effect of rest periods can be measured on virgin and aged cylindrical mortar specimens [1].

For the asphalt mixture composition, three asphalt mixtures of Stone Mastic Asphalt (SMA) were considered: the reference material (Material I) SMA 11 S with a polymer modified binder and two mixtures with respective 15 m% (Material II) and 30 m% (Material III) Reclaimed Asphalt.

In this study, the fatigue and healing was also evaluated on the binder and the mastic. An asphalt mixture can be considered as a mixture of aggregates with dimensions larger than 0.125 mm, coated with a thin binder film about 5 μm and bound by bituminous mastic. The mastic is defined as the mixture of filler and aggregates with dimensions smaller than 0.125 mm, and the binder. The binder quantity in the mastic is the volume of the binder in the asphalt mixture, decreased with the volume of the binder, that coats the aggregates larger than 0.125 mm with a binder film of 5 μm thickness. For the binder and mastic specimens, the same partial content of aged binder was taken into account as included in the asphalt mixtures e.g. the binder II+RA consists of 36 m% aged binder from RA and 64 m% virgin binder.

3. FATIGUE AND HEALING TESTS ON BINDER AND MASTIC

Bituminous binders and mastics were tested using a dynamic shear rheometer (DSR) in oscillation mode. In this setting, the sample is placed between two parallel plates (diameter 8 mm, gap 2 mm). A Fatigue test is defined as a constant stress-controlled loading signal on the sample until failure. Because of the limitations of DSR-loading signals, a specific healing procedure is developed as a continuous loop of two intervals: a fatigue period during 3 seconds (30 cycles)

In Figure 1, an example is given of the value of G^* (complex shear modulus) in function of time during a healing test (30 cycles at 10 Hz) loading and 9 seconds rest of a binder of Material III. The results show that during loading cycles, the G^* -value decreases and during unloading the cycles G^* -value increases. The recovery of the complex modulus during rest periods is clearly shown.

The fatigue life criterion is defined as the top in the $G^* \times$ number of cycles curve, expressed as the number of loading cycles. The effect of rest periods is not only observed in an increment of G^* -value, but also as the extension of the fatigue life.

In Figure 1 (b), the healing curve and fatigue curve are compared in function of the sample stress: at an equal sample stress rest periods will increase fatigue life or, for an equal fatigue life, rest periods will allow higher sample stresses. The healing shift factor is very high for all binders. Since there is no common applied sample stress between fatigue and healing curve, the factor cannot be quantified in function of sample stress. Quantification can be made as follows: for Binder I at an equal fatigue life (1000 and 10000 cycles) the implementation of rest periods allows increasing the sample stress with 230 kPa.

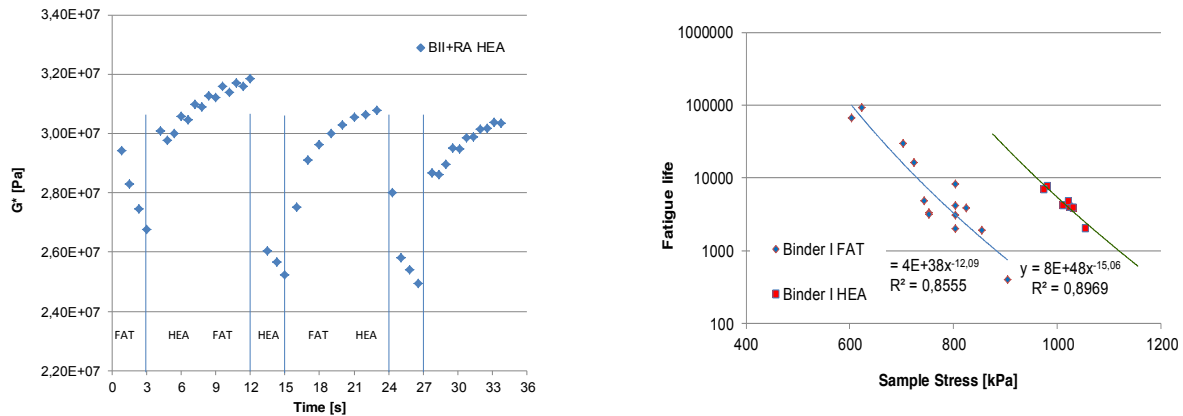


Figure 1: (a) Healing test, (b) fatigue (blue) and healing (red) curve of binder I
 For all binder and mastic types, rest periods increase fatigue life. For Mastic I, rest periods have a positive effect on fatigue life (factor 4.3 – 6.0). When Mastic III is taken, using the binder from RA, a slight increased fatigue life is noticed and healing factor 7.4 (only two tests).

4. FATIGUE AND HEALING TESTS ON ASPHALT

Tests were conducted on SMA samples with RA contents of 0% (Mix I), 15% (Mix II) and 30% (Mix III). The SMA has a maximum particle size of 11.2mm and was compacted using a roller compactor. Slabs with dimension 400mm x 305mm x 100mm were manufactured and the target bulk density was 2391 kg/m³, corresponding to an air voids content of 3%.

After allowing the compacted specimen slabs to cool to ambient temperature for 24 hours, six cylinders of nominal 100mm diameter were cored from the slab. A test specimen of nominal thickness 40 mm was then sliced from the middle of each cylinder using a circular saw.

The specimens were stored in a temperature controlled cabinet, which also contained the testing apparatus, at the test temperature of 10°C. The indirect tensile fatigue and healing tests were conducted using a Cooper Technology Servo-Pneumatic Universal Testing Machine NU-10 apparatus. The specimen was placed in a holding rig with loading strips in the vertical plane. A load was applied to the specimen in the vertical axis, while deformation was measured in the horizontal axis over the centre 40mm of the specimen.

The testing apparatus was controlled using the Cooper Technology Universal Software. This allowed customised fatigue testing profiles to be used and two such profiles were used. For the fatigue test, a loading duration of 0.1s and a test frequency of 10 Hz was used. A haversine waveform was employed and the stress level adjusted to give failure within a reasonable timeframe. For the healing test, a rest period of 0.1 seconds between each loading pulse was introduced to the test profile. The results of the testing programme are presented in Figure 2.

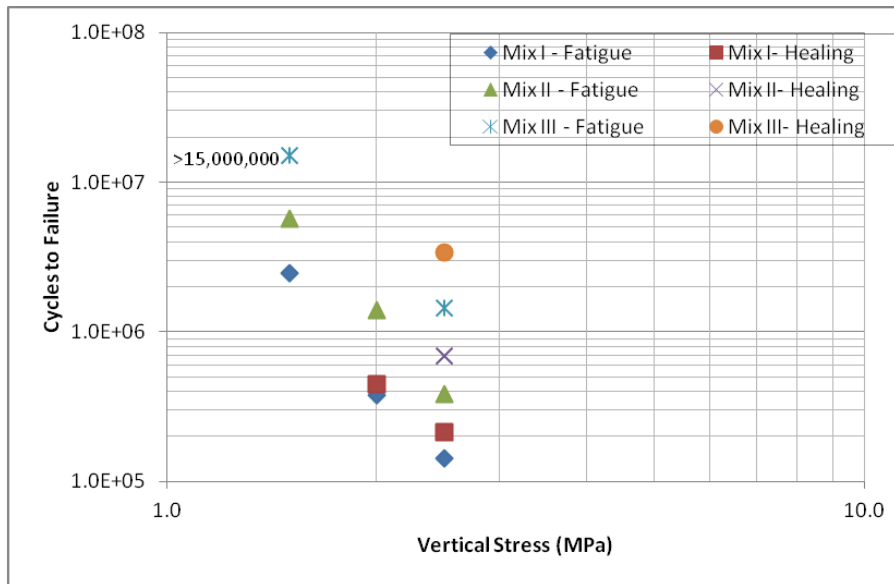


Figure 2: Influence of RA content on fatigue life of asphalt mixtures

It can be seen that the materials tested had a very high resistance to fatigue and that significant numbers of load cycles were required to induce failure. The influence of RA content is very clear in that the addition of RA to the mixture resulted in the fatigue lines moving upwards. Similar observations can be made for the material tested using rest periods. It should however be noted that the number of tests conducted was low due to the long time required per test (several weeks for the more resilient materials). A follow on study using materials less resistant to fatigue is currently being implemented.

5. CONCLUSIONS

The implementation of rest periods after a loading interval will lead to an extended fatigue life and, during the rest periods, an increase of G^* is demonstrated. A DSR allows the possibility of recording this process. It is possible to monitor the healing process during the individual rest periods as during the whole test. The improved fatigue resistance associated with using RA in asphalt mixtures was demonstrated; this will be quantified in later research.

ACKNOWLEDGMENTS

The authors would like to acknowledge the coordinator Bjorn Kalman and other members of the Re-Road project (FP7-project 2008-2013, grant 218747) for providing the materials and funding.

REFERENCES

[1] Van den bergh, W.: The Effect of Ageing on the Fatigue and Healing Properties of Bituminous Mortars, PhD. Thesis, TU Delft, The Netherlands, 2011.

SELF-HEALING CEMENTITIOUS MATERIALS

POSTER SESSION

METHOD TO STUDY THE CURE KINETICS OF POLY(URETHANE) AS HEALING AGENT FOR SELF-HEALING CONCRETE

J.A. Ramos¹, B. Dekeyser², H. Rahier¹

¹ *Physical Chemistry and Polymer Science, Vrije Universiteit Brussel, Pleinlaan 2, B-1050 Brussels, Belgium. e-mail: jramosga@vub.ac.be, hrahier@vub.ac.be*

² *International Development Center, RECTICEL N.V. Damstraat 2, B-9230 Wetteren, Belgium. e-mail: dekeyser.bernard@recticel.com*

Keywords: cementitious material, poly(urethanes), kinetics, dynamic mechanical analysis

ABSTRACT

Poly(urethanes) (PU) can be used as healing agent to heal cracks in self-healing concrete. Studying the reaction kinetics is however difficult as the PU needs environmental moisture to cure. On the other hand the moisture in the concrete could play a role in the reactions. To monitor the reactions a technique where environmental moisture can reach the sample in a comparable way as in cracks is needed. The crack width usually is in the order of 50-500 μm . For this purpose dynamic mechanical analysis (DMA) with parallel plate geometry was proven to be suited. The PU starts as a viscous mixture but gradually becomes stiffer which is measured via the increase in storage modulus. Differences in reaction kinetics between different types of monomers can be observed in this way. The same methodology will be used to study the effect of the cement matrix on the cure behavior of the PU.

1. INTRODUCTION

Concrete is widely used as construction material due to its high strength, durability, availability and versatility. These properties added to the low production cost and recyclability makes concrete the most commonly used building material in the world. However, concrete is a brittle material and susceptible to many sources of damage, caused by freeze/thaw cycles, drying shrinkage, corrosion, external loading (dynamic or static loading), chemical attacks and other environmental conditions. Cracks, one of various types of damage, not only shorten the service life of concrete structures, but also endanger the structural safety [1], leading to large costs of maintenance and repair. The utilization of self-healing technologies could enhance the service life of concrete structures and reduce the demand for crack maintenance and repair.

Autonomous healing of cracks in concrete by encapsulating healing agents into the matrix improves the healing efficiency of concrete. Upon crack appearance, the capsules break and release their content. In some cases healing agents harden in contact with air or environmental moisture, healing the crack. An example involves filling ceramic or glass tubes with poly(urethane) (PU) [2]. PU has the advantage of having a low viscosity, good matrix bonding, a limited reaction time and low cost in comparison with other systems, such as epoxy or cyanoacrylate [3,4]. An additional advantage for using PU comes from the catalytic effect of the cement matrix on the cure behavior of the PU.

In this work, the study of the cure reaction of PU in controlled conditions of environmental moisture and in a comparable way as in cracks was carried out by means of the use of DMA. The effect of the cement matrix on the PU curing was also studied.

2. MATERIALS AND METHODS

A prepolymer of PU kindly supplied by Recticel was used in this study as healing agent. This prepolymer starts foaming and expanding in moist surroundings. A hardened ordinary Portland cement (OPC) paste was used as cementitious matrix. To study the effect of the matrix on the cure kinetics of the PU, different amounts of OPC powder were added to the PU. This mimics the effect of the crack walls, containing some water or hydroxyl groups, on the cure behavior of the PU. The mixtures were vigorously stirred until homogeneous dispersion, to obtain several samples with different weight ratios. Samples with ten OPC:PU ratios were prepared, as shown in table 1.

Table 1: Composition of samples prepared.

OPC (g)	PU (g)
0	100
50	50
75	50
100	50
125	50
150	50
175	50
200	50
225	50
250	50

DMA was carried out with a Perkin-Elmer DMA7 in parallel plates mode to obtain the storage modulus (E') and loss factor ($\tan \delta$). Scans were performed at room temperature ($25^{\circ}\text{C}\pm 1^{\circ}\text{C}$) and at a frequency of 1 Hz for 30 hours. 25 μL of each mixture was placed between the DMA plates, using a piece of open cell foam as spacer to maintain a constant distance between the plates during the experiment. A static force of 200 mN and a dynamic force of 150 mN were used during the measurement to maintain a plate distance of approximately 350 μm . Environmental moisture was controlled by a hand-made reservoir containing a saturated salt solution.

3. RESULTS

Environmental moisture may penetrate into the matrix along the cracks and react with the prepolymer of PU. These conditions were simulated by DMA. Thus, the PU starts as a viscous mixture but gradually becomes stiffer which is measured via the increase in storage modulus. Meanwhile, the loss factor undergoes some changes. The most significant phenomenon is when the gel point is reached and $\tan \delta$ goes through a maximum. Figure 1 shows the evolution of the storage modulus and the loss factor during a measurement for the sample with 125:50 OPC:PU ratio. An

increase in the storage modulus signal is observed during the scan with a noticeable change in the slope around 750 min. A more evident change is observed in the loss factor signal, in which a maximum is clearly distinguished at 750 min. It should be pointed out that the pure prepolymer (without OPC) did not show any of those changes during the measurement, even in longer experiments of 40 hours, meaning that the presence of OPC increases the reaction rate. Figure 1 also shows the lack of variation in probe position remaining almost constant throughout the experiment at a value close to 350 μm .

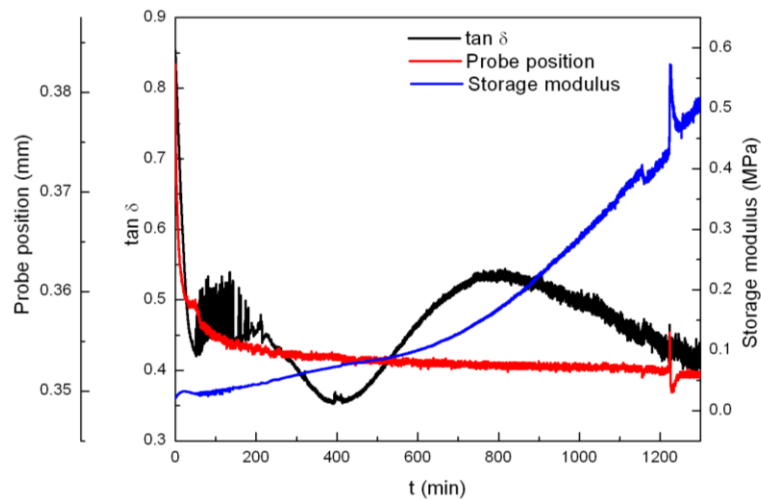


Figure 1: Evolution of probe position, loss factor and storage modulus of 125:50 OPC:PU ratio sample at room temperature.

The addition of higher amounts of cement to PU led to an increase in cure kinetics, turning into a reduced gelation time. Figure 2 shows the variation of the maximum peak of the loss factor signal as a function of the OPC content. The exponential decay curve generated by the addition of OPC is very clear.

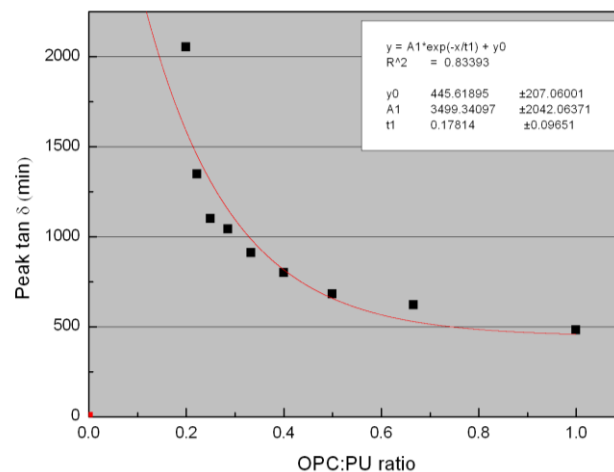


Figure 2: Maximum peak of the loss factor signal versus OPC:PU ratio.

According to the results it appears that the presence of humidity or hydroxyl groups in the cement are the responsible for acceleration of PU cure kinetics. However, the use of other techniques should help to clarify this statement.

4. CONCLUSIONS

The development of a new procedure to measure the cure kinetics of a PU was achieved in this study. Variations in storage modulus as well as in loss factor were recorded by means of DMA. Experimental results showed that an increase in the amount of cementitious material added to PU increased the reaction rate, decreasing the gelation time.

ACKNOWLEDGEMENTS

Financial support from the 'Strategic Initiative Materials' (SIM Flanders) for this study (SBO SECEMIN) is gratefully acknowledged.

REFERENCES

- [1] W. Zhong, W. Yao, Influence of damage degree on self-healing of concrete, *Construction and Building Materials* 22 (2008) 1137–1142.
- [2] K. Van Tittelboom, N. De Belie, F. Lehmann, C.U. Grosse, Acoustic emission analysis for the quantification of autonomous crack healing in concrete, *Construction and Building Materials* 28 (2012) 333–341.
- [3] T.D.P. Thao, T.J.S. Johnson, Q.S. Tong, P.S. Dai, Implementation of self-healing in concrete – proof of concept, *IES J Part A: Civil Struct Eng* 2 (2009) 116–125.
- [4] V.C. Li, Y.M. Lim, Y.W. Chan, Feasibility study of a passive smart self-healing cementitious composite, *Composites Part B* 29B (1998) 819–827.

SELF-HEALING OF THERMAL CRACKS IN SANDWICH PANELS

E. Gruyaert^{1,4}, K. Van Tittelboom^{1,4}, P. De Backer¹, W. Moerman^{2,4},
B. Dekeyser^{3,4} and N. De Belie¹

¹ *Magnel Laboratory for Concrete Research, Ghent University, Technologiepark-Zwijnaarde 904, 9052 Ghent, Belgium – e-mail: elke.gruyaert@ugent.be; kim.vantittelboom@ugent.be; nele.debelie@ugent.be*

² *Willy Naessens Construct, Bedrijvenpark Coupure 15-17, 9700 Oudenaarde, Belgium – e-mail: wim-m@willynaessens.be*

³ *Recticel, Damstraat 2, 9230 Wetteren, Belgium – e-mail: dekeyser.bernard@recticel.com*

⁴ *SIM vzw, Technologiepark 935, 9052 Zwijnaarde, Belgium*

Keywords: sandwich panel, thermal cracking, self-healing, encapsulated water repellent agent, encapsulated polyurethane

ABSTRACT

Sandwich panels are prefabricated, insulated concrete wall elements, which are sensitive to thermal cracking due to their composition (concrete outer cladding – insulation – concrete inner cladding). During hot days, the temperature of the outer concrete layer can rise up to ~ 60°C and the temperature difference between inner and outer layer causes crack formation in the outer concrete layer. Since cracking impairs the durability of concrete (e.g. accelerated corrosion of reinforcement steel by carbonation or chloride ingress), the aim of this research project is to regain impermeability and prevent esthetical damage through incorporation of self-healing capabilities.

At first, different healing agents (polyurethane (PU) and water repellent agent (WRA)) were screened based on their ability to regain impermeability and their behaviour upon reloading of cracked and healed samples. Two types of PU and three types of WRA were then selected to be applied in a real scale test.

For the real-scale test, the different healing agents were encapsulated by glass capsules and embedded in different zones in the outer layer of a sandwich panel (7.59 m x 1.20 m). After about 14 days, the test setup was built and the outer layer of the self-healing sandwich panel was thermally loaded up to temperatures of ~ 60°C for 9 hours per day. The temperature at the inner layer was kept constant at ~ 21°C. Due to the temperature difference, the panel bended, cracking occurred in the outer cladding, capsules broke and the healing agent was released. Some healing agents leaked out of the crack and left stains behind. Adaptation of the capsule volume, viscosity of the healing agent or concrete cover thickness over the capsules could solve this problem. PU and WRA were able to reduce the water permeability of cracks. Cracks treated with WRA remained water tight upon reloading, while PU can lose their bond with the crack surface resulting in an increased water absorption. In future research, more elastic polyurethanes, with a high bond strength to the concrete matrix, will be tested in order to solve this problem.

1. INTRODUCTION

Insulated sandwich panels which are exposed to sun radiation tend to bend because of the temperature difference between inner and outer concrete layer. This principle is schematized in Figure 2 and Figure 3 for a sandwich panel with a 60 mm outer concrete layer, 50 mm PU insulation and 90 mm inner concrete layer (concrete quality C30/37). The temperature of the concrete surface ($\theta_{e,surface}$) is higher than the outside temperature due to radiation.

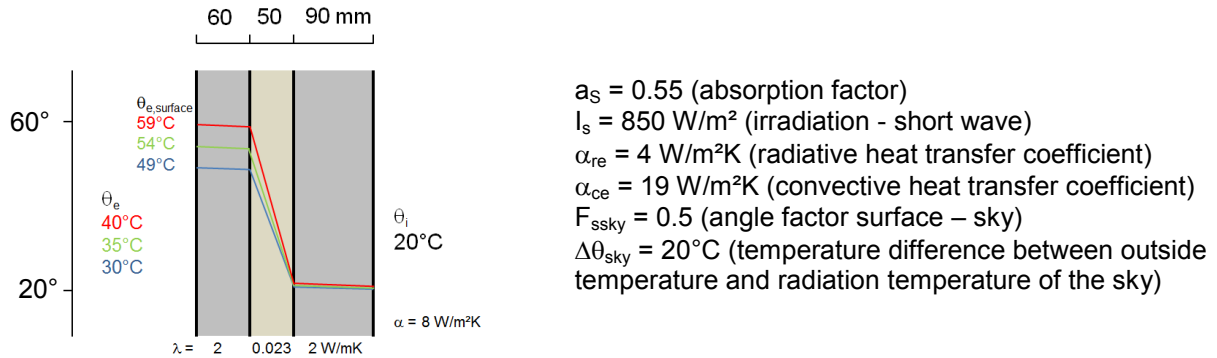


Figure 1: Temperature profile in a sandwich panel – outside temperature (θ_e): 40°C, 35°C or 30°C – inside temperature (θ_i): 20°C

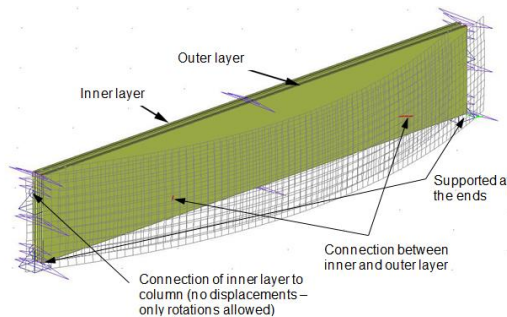


Figure 2: Bending of a sandwich panel under thermal load (simulation with the Scia Engineer software)

Tensile stresses in the outer concrete cladding (e.g. 8.3 MPa for the example given above with an outside temperature of 40°C) lead to cracking of the panels. These cracks impair the durability of the panels and are also unwanted from an aesthetical point of view. Especially after rainfall, the thermal cracks in sandwich panels are visible. In addition to PU healing agents, the use of WRA to eliminate water penetration into the cracks has therefore also been investigated.

2. HEALING AGENTS

The healing agents should be able to reduce the water permeability of the cracked concrete. In order to evaluate this ability, the capillary water absorption of cracked and manually healed specimens (40 x 40 x 60 mm – crack width: 50 – 150 μm after unloading) was compared. Based on the test results, three types of WRA were selected. Also the PU healing agents will be considered in further tests. WRA 1, 2

and 3 are respectively silane based, silane-siloxane based and siloxane-acrylate based agents.

The behavior of the healing agents upon reloading of cracked and healed specimens (40 x 40 x 160 mm) is presented in Figure 3 (WRA 1, 2, 3 and PU1). The cracks treated with WRA grew upon reloading, but the crack faces were impregnated with the WRA. As a consequence, the sorption coefficient remained low. PU bonded to the mortar matrix and filled the crack, so a new crack appeared or the connection between PU and mortar was lost upon reloading. As a consequence, the capillary sorption coefficient increased.

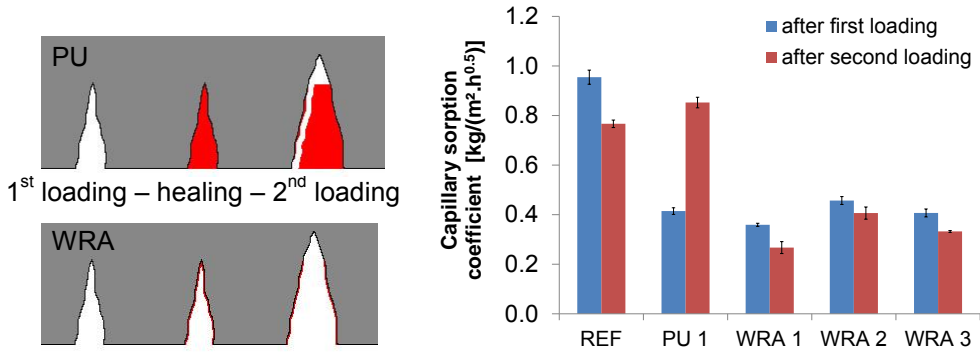


Figure 3: Crack formation during loading and reloading (left) – Capillary sorption coefficient of cracked and healed specimens before (blue) and after (red) reloading (right).

3. SIMULATION OF THERMAL CRACK FORMATION ON LAB-SCALE

In a real scale test set-up in the laboratory, sandwich panels (7.59 m x 1.20 m) made of self-healing concrete, were thermally loaded and the self-healing efficiency of 3 types WRA and 2 types PU (PU 1: one component PU – PU 2: two-component PU) was evaluated. The healing agents were encapsulated by glass capsules (Ø 3 mm) which were placed in zones per healing agent along the length of the panel (Figure 4). The capsules and reinforcement were placed in the mould and concrete was poured. During compaction, the capsules rose and were embedded in the concrete.

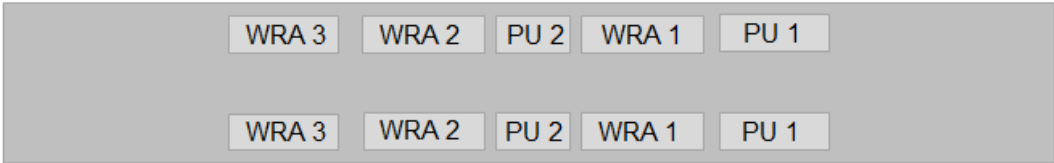


Figure 4 : Position of the capsules in the panel (PU 1: 2 x 95 capsules – PU 2: 2 x 2 x 50 capsules – WRA 1: 2 x 100 capsules – WRA 2: 2 x 100 capsules – WRA 3: 2 x 80 capsules)

After ~ 14 days, the test setup was built (Figure 5) and the outer cladding of the panel was heated until the surface temperature reached ~ 60°C (to simulate an outside temperature of ~ 40°C – see introduction). The inner cladding was exposed to an environment of ~ 21°C. To simulate the day-night effect, the panels were exposed to a thermal cycle of 24 hours (heating for 9 hours per cycle).

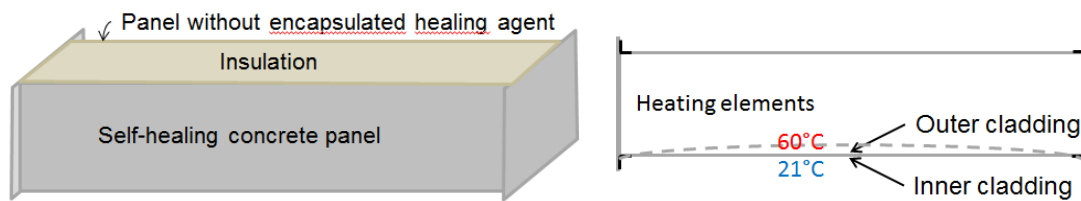


Figure 5: Laboratory test setup (3D view (left) – top view (right))

4. RESULTS

Due to the high temperature differences between inner and outer concrete layer, the panels bended and displaced over ~ 10 mm (measured by LVDTs in the middle of the panels). After the first heating cycle, cracks already appeared and capsules broke. Small cracks of ~ 20 μm , seemed to be enough to trigger breakage of the capsules. However, the early breakage of the capsules was mainly attributed to the small concrete cover on the capsules (~ 2 mm).

Due to the small crack width, the amount of healing agent released from the capsules was too high in comparison to the crack volume. Moreover, because of the high temperature, the viscosity of the healing agents decreased. As a consequence, the healing agent leaked out the crack. PU ran down the crack, leaving behind a long stain, while WRA 1 created dark stains on the surface (Figure 6). The colour difference, measured by a spectrophotometer, between these stains and untreated concrete fades away in wet conditions. No stains were detected in the zones with WRA 2 and WRA 3. In these zones, few cracks were formed and there was no certainty that capsules broke.

The water tightness, measured by the Karsten tube method, could be regained at places where the cracks healed autonomously (PU or WRA), but only for cracks < 100 μm .

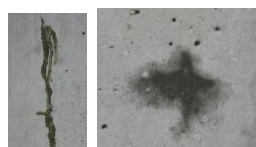


Figure 6: Breakage of capsules due to cracking in a zone containing capsules filled with PU 1 (left) and a zone containing capsules filled with WRA 1 (right).

5. CONCLUSIONS

The natural process of thermal crack creation in sandwich panels could be simulated in the laboratory. Thermal cracks were formed in the outer layer and healing agent was released. The capsules broke in an early stage due to the low concrete cover on the capsules and the healing agent leaked out of the concrete due to the small crack width. Adaptation of the capsule volume, viscosity of the healing agent or concrete cover thickness could solve this problem.

Polyurethanes and water repellent agents were able to reduce the water permeability of cracks. Cracks treated with water repellent agents remained water tight upon reloading, while polyurethanes can lose their bond with the crack surface resulting in an increased water absorption. In future research, more elastic polyurethanes, with a

high bond strength to the concrete matrix, will be tested in order to solve this problem.

ACKNOWLEDGEMENTS

This research under the program SHE (Engineered Self-Healing materials) (project SHEcon: Self-healing Concrete for Structural and Architectural Applications) was performed at the Magnel Laboratory for Concrete Research and funded by SIM (Strategic Initiative Materials in Flanders) and IWT (Agentschap voor Innovatie door Wetenschap en Technologie). The authors would like to thank the foundation for their financial support.

SELF-HEALING CAPACITY OF HARDENED CEMENT SUSPENSIONS WITH HIGH LEVELS OF CEMENT SUBSTITUTION

C. Litina¹ and A. Al-Tabbaa¹

¹ *Engineering Department, University of Cambridge, Trumpington Street, Cambridge CB2 1PZ, UK – e-mail: cl519@cam.ac.uk; aa22@cam.ac.uk*

Keywords: self-healing, cement suspension, compositional variation, supplementary cementitious materials, high water content

ABSTRACT

Aqueous cement suspensions without aggregates have been commonly applied as a remedial technique in structural and geotechnical applications, often comprising part of the permanent infrastructure. These suspensions derive their mechanical characteristics and properties through the same hydration processes and binding chemistry as concrete; thus they are susceptible to the same deleterious environmental factors and inherent properties. This can endanger the long-term functionality of the installation.

Therefore there is a strong incentive of compositional alteration of the basic binder by incorporating supplementary cementitious materials that have been acknowledged to improve the physical properties and enhance the durability characteristics of the hardened matrix. However the latter does not offer a robust long term solution. Therefore a compositional enhancement through biomimetic approach of damage response for the design of high performance cement suspensions is put forward. This study involves two stages, i.e. determination of the autogenous crack sealing behaviour of various optimised blended compositions and the subsequent enhancement of the intrinsic autogenous healing processes through the inclusion of microencapsulated healing agents. Herein the results of this preliminary investigation on the effect of compositional variation on the intrinsic properties of physical response to cracking are presented.

Ternary and quaternary blends of minerals -including Portland cement, slag, MgO and silica fume- are being developed and investigated. Upon cracking and water ingress, the unreacted particles are activated and yield hydration products that crystallize in the crack, sealing it off and recovering mechanical characteristics. The self-healing capacity of the samples is quantified through microscope observation, gas permeability test and three-point flexural bending. The findings on the crack healing efficiency and mechanical recovery of initially cracked specimens confirm the existence of self-healing mechanisms in supplementary cementitious materials.

1. INTRODUCTION

Aqueous cement suspensions often comprise part of the permanent infrastructure. However due to their composition they are susceptible to severe tensile cracking phenomena and environmental deterioration. This can endanger the long-term functionality of the installation. The latter is exacerbated by the remote positioning of these installations. Literature indicates that a common approach to enhance the

durability of cement pastes is to limit the percentage content of Portland cement (PC) and substitute by supplementary material [1–3]. Cementitious materials can display naturally self-healing properties as a result of intricate calcium precipitating processes [4]. However the investigation of the effect of clinker substitution on self-healing properties is limited. Hence, the work presented in this paper focuses on the investigation of the effect of compositional variation on the intrinsic properties of physical response to cracking.

2. MATERIALS

The details of the mixes tested are given in Table 1. Eight different compositions were investigated, denoted A1-A8. Type I Portland cement (52.5N); blast furnace slag (BFS), limestone powder; silica fume; and MgO were used for the preparation of ternary and quaternary blends. The water to binder (total solids) ratio adopted in this design was kept constant ($w/c=0.6$ by weight). This water content is similar to the upper bound water content adopted in relevant studies [5] and common for grouting applications [6].

A series of cylindrical 15mmx30mm and prismatic specimens 40mmx40mmx160mm were cast from each batch using a high shear mixer to ensure homogenisation. Specimens were demoulded after 24hours and water cured at laboratory temperature ($20\pm 1^\circ\text{C}$) until testing. 1- and 28-day-old specimens were considered in order to quantify the effect of the variant consistency and thus the effect of hydration and chemistry of the different mixes on self-healing behaviour.

Table 1: Mixture design proportion by weight

Mix	Components wt (%)					
	PC	BFS	Limestone	Silica fume	MgO	Water
A1	0.50	0.45	0	0	0.05	0.60
A2	0.45	0.45	0	0	0.10	0.60
A3	0.45	0.45	0	0.10	0	0.60
A4	0.45	0.40	0	0.15	0	0.60
A5	0.30	0.40	0.30	0	0	0.60
A6	0.20	0.50	0.30	0	0	0.60
A7	0.10	0.60	0.25	0	0.05	0.60
A8	0.05	0.65	0.20	0	0.10	0.60

3. METHODS

The experiments are divided into two categories; a preliminary phase of characterisation of basic mechanical and rheological properties of fresh and hardened compositions and a subsequent phase of establishing the self-healing potential of these blends. The principle of the latter is to perform mechanical tests aimed at pre-cracking the specimen, followed by a curing period to allow the triggering of self-recovery and then retesting in order to characterise the residual mechanical properties and clarify the self-healing capability. Therefore three-point flexural bending and permeability testing investigations were performed in order to highlight the self-healing phenomenon.

For the determination of the permeability of the hardened specimen the method and apparatus proposed were adopted [7]. Cylindrical specimens prepared for each

composition were removed from water at 1 and 28 days. Half were loaded to 80% of their respective ultimate compressive strength and then set aside for 28 days in water to allow the healing process to take place. The rest of the same batch was used to create the bench mark for the healing efficacy. 10 mm-thick cylindrical disk specimens were cut from the middle of the cylinders. Subsequently, the disk specimens were vacuum-dried until testing time and then placed and sealed on the top of a cell with silica gel sealer to avoid leakage of gas vapour. The values of mass variation with time due to the vaporization of methanol liquid at a constant 40°C water bath temperature were recorded at specific time interval until a steady-state mass loss was reached. The tests were conducted in triplicates.

Mechanical characterisation by means of three-point flexural loading of prismatic specimens was performed. These were allowed to cure for 1 and 28 days- accordingly- and then artificially cracked with a 3-point flexural test fitting until ultimate flexural load was reached and a single crack at the middle of the notch was created. Then the cracked samples were placed in water for 28 days, while care was taken for the crack surfaces to remain in contact; nor force was applied neither renewal of the curing medium. A quasi-static loading speed of 0.02mm/min was selected.

4. RESULTS

The compressive and flexural strengths of the investigated mixes are presented in Figure 1. The basic mechanical behaviour indicates that as the level of cement substitution increases the compressive strength decreases (A1 to A5). Moreover the nature of the supplementary cementitious materials used in each mix seems to also play an important role on the strength gain. At the same levels of cement replacement for BFS the use of MgO yielded higher compressive strength compared to silica fume. Furthermore the use of limestone powder, as a reactivity enhancer of BFS, led to improved strength gain. On the other hand flexural strength does not follow a similar trend, but rather slightly increases with cement substitution fluctuating at 1.5MPa.

The findings on the crack healing efficiency ($\text{Healing efficiency} = E_{\text{healed}}/E_{\text{pristine}}$) and mechanical recovery of initially cracked specimens confirm the existence of self-healing mechanisms in supplementary cementitious materials (Figure 2). Due to the lack of tensile support in the investigated formulations crack control at 28 days did not effectively prohibit the total abruption of the fragments of these specimens. However care was taken for the crack surfaces to remain in contact even after complete abruption. A1 and A2 specimens that had been completely fractured showed partial reattachment however the bond strength was too weak to sustain the specimens in one piece. Virtual reattachment of the two segments could be attributed to the water suction/pressures between the two surfaces. The latter could also explain the dissipation of water/moisture from the crack location to the surrounding surfaces following the load increment. Among specimens produced with the same cement content, the addition of silica fume appeared beneficial for the mechanical recovery. High limestone content (A4) presented the highest self-healing efficiency exhibiting mechanical recovery (fracture stiffness recovery) up to 80% and in fact reaching 30% for samples initially completely separated. So far the presence of MgO has not hindered the manifestation of self-healing properties however a dependency on the content is inferred. Analysis of the precipitated products concentrated in the crack area will give a clearer image of the mechanisms contributing to the healing.

5. CONCLUSIONS

Preliminary results indicate recovery of mechanical properties (tensile strength, stiffness) as well as self-sealing induced permeability reduction of cracked specimen. The quaternary and ternary cementitious composites display autonomous self-healing potential even at high levels of cement substitution. The exact mechanism contributing to the exhibited phenomenon should be confirmed with further observations using SEM of the specimens' microstructure.

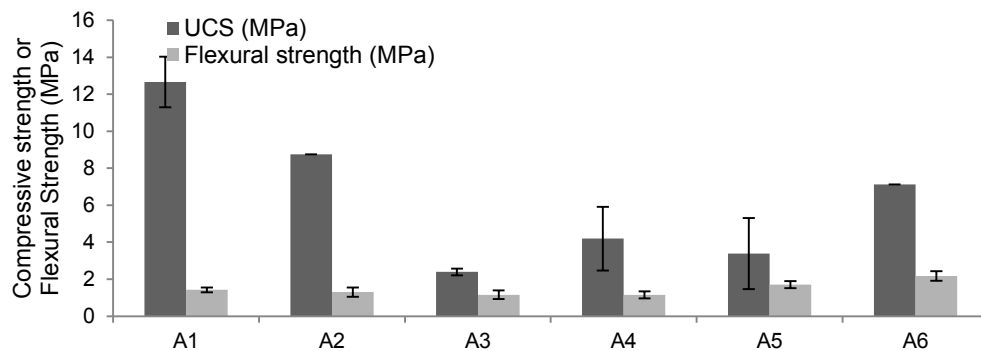


Figure 1: Compressive and flexural strength of different mixes at 28days.

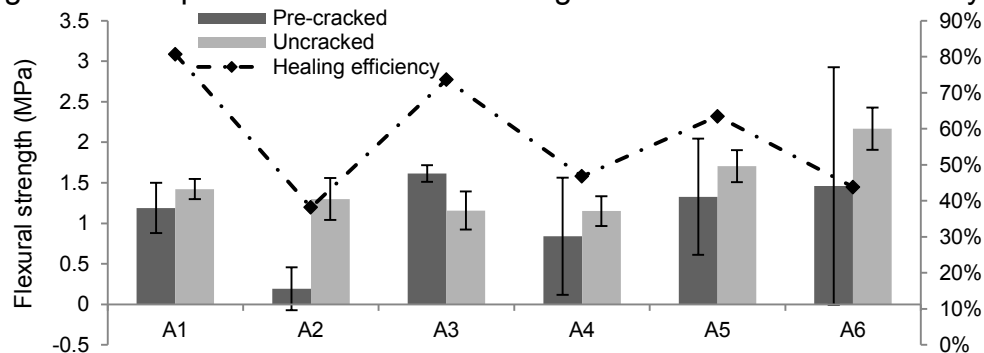


Figure 2: Flexural strength recovery of different mixes after 28days of water curing

ACKNOWLEDGEMENTS

Financial support from the Engineering and Physical Sciences Research Council (EPSRC) and the Hellenic States Scholarship Foundation for the PhD study of the first is gratefully acknowledged.

REFERENCES

- [1] K. Sideris, A. Savva, J. Papayianni, Sulfate resistance and carbonation of plain and blended cements, *Cement and Concrete Composites* 28 (2006) 47–566.
- [2] M. L. Berndt, Strength and permeability of steel fibre reinforced grouts, *Construction and Building Materials* 24 (2010) 1768–1772.
- [3] E. Vintzileou, A. Miltiadou-Fezans, Mechanical properties of three-leaf stone masonry grouted with ternary or hydraulic lime-based grouts, *Engineering Structures* 30 (2008) 2265–2276.

- [4] M. Wu, B. Johannesson, M. Geiker, A review: Self-healing in cementitious materials and engineered cementitious composite as a self-healing material, *Construction and Building Materials* 28 (2012) 571–583.
- [5] R. Lark, C. Joseph, B. Isaacs, D. Gardner, A. D. Jefferson, Experimental investigation of adhesive-based self-healing of cementitious materials, *Magazine of Concrete Research* 62 (2010) 831–843.
- [6] F. Rosquoët, A. Alexis, A. Khelidj, A. Phelipot, Experimental study of cement grout, *Cement and Concrete Research* 33 (2003) 713–722.
- [7] Z. Yang, J. Hollar, X. He, X. Shi, A self-healing cementitious composite using oil core/silica gel shell microcapsules, *Cement and Concrete Composites* 33 (2011) 506–512.

COMBINED PHYSICAL AND BIOLOGICAL GEL-BASED HEALING OF CEMENTITIOUS MATERIALS

M.J. Harbottle¹, J. Zhang¹ and D.R. Gardner¹

¹ Cardiff School of Engineering, Cardiff University, Queen's Buildings, The Parade, Cardiff, CF24 3AA, UK – email: harbottlem@cardiff.ac.uk; zhangj40@cardiff.ac.uk; gardnerdr@cardiff.ac.uk

Keywords: Self-healing cementitious materials, *Sporosarcina pasteurii*, Alginate

ABSTRACT

The outcomes of a preliminary experimental programme into a gel-based healing system that allows immediate healing of cementitious materials followed by longer-term development of robust healing through biological processes are reported. Alginate gels protect and maintain the viability of encapsulated microorganisms and have been used for protection of these and other cargoes in various situations. Soluble alginates form relatively strong, stable gels on contact with cations such as calcium, and can form gels on contact with cementitious materials. Calcium alginate gels were formed both in isolation and in contact with cementitious surfaces and assessed for their ability to protect encapsulated microorganisms (*Sporosarcina pasteurii*) from the harsh cementitious environment and their subsequent ability to generate calcium carbonate within the gel structure via urea biodegradation.

1. INTRODUCTION

Bacterial generation of calcite minerals can create or maintain construction materials such as soils and cementitious substances [1]. In the latter, e.g. mortar or concrete, microbial activity is significantly hindered due to the highly alkaline pH and difficulty in accessing the required nutrients and moisture. Efforts have been made to provide for microbial survival through immobilisation or encapsulation in a range of materials such as polyurethane [2, 3], silica gel [3] or expanded aggregates in conjunction with bacterial spores [4]. There has been some success in sealing (i.e. reducing permeability) materials through generation of calcite, but significant strength regain is often attributable to the immobilising matrix rather than the calcite itself [3].

Alginate gels have found use in protection and delivery of biological payloads such as bacteria [5]. They are formed simply through addition of liquid sodium alginate to a solution of calcium ions. Their ability to support biological payloads in relatively harsh environments has identified them as a potential support matrix in cementitious materials as part of an autonomic system for crack healing and repair. The presence of calcium ions in cementitious materials means alginate could form gels, and so heal or seal flaws, on contact, giving an immediate chemical effect upon crack formation and healing initiation with potential longer term effects through biological action. The potential for alginate to act in this way has been explored in this preliminary study.

2. MATERIALS AND METHODS

Sporosarcina pasteurii (NCIMB, UK; strain NCIMB8221), an aerobic, ureolytic bacterium, was grown in nutrient broth (Oxoid CM001, 13 g/L) amended with urea (20 g/L) for 48 hours at 30°C. Four experiments were performed:

(i) *Optimisation of S. pasteurii survival in alginate beads.* Bacteria were mixed with sodium alginate (2.4, 2.8 and 3.2% w/w) and growth medium (Oxoid CM001 nutrient broth – 3 g/L; urea – 20 g/L; NaHCO₃ – 2.1 g/L; NH₄Cl – 10 g/L). Alginate beads were formed by pipetting 10 µl aliquots into calcium chloride (CaCl₂) solutions in deionised water (1, 3 and 5% w/w). Sets of beads were prepared in triplicate for each combination of alginate and CaCl₂ concentrations. After incubation for 7 days at 30°C, active bacteria were identified by dehydrogenase assay (briefly, incubation for 4 hours at 30°C with 5 mM 5-cyano-2,3-ditolyl tetrazolium chloride (CTC) [6] then imaging on a Nikon LV100D epifluorescence microscope). Average cell counts were taken from ten images.

(ii) *Bacteria survival on mortar surfaces.* Portland cement mortar specimens (27 in total; surface dimensions 44x32 mm; water:cement ratio 0.45, sand:cement ratio 3.0) were cured for 28 days in water and split into 3 equal groups with further curing for 7 days in either air, water or CaCl₂ solution. Each group was sub-divided into 3 triplets (A, B and C) with the following solutions applied to the surface: A - alginate/growth medium; B - alginate/growth medium followed by CaCl₂ solution; C – alginate/growth medium and CaCl₂ solution mixed manually on surface. Optimal concentrations of alginate and CaCl₂ determined in (i) were used, both containing *S. pasteurii*. Following incubation at 30°C for 10 days surfaces were examined using CTC, as above. Cell counts were determined manually using ImageJ software [7]. Surface material was removed by abrasion and examined by x-ray diffraction (XRD).

(iii) *Bacterial strength development in artificial flaws.* 9 mortar beams (mix as above; 25x25x140 mm) with a notch (1mm wide, 10 mm deep) at the mid-point were cured under water for 7 days and divided into 3 equal groups (X, Y and Z) with the following added to the notch: X – alginate/growth medium solution only; Y – alginate/growth medium solution with *S. pasteurii*; Z - alginate/growth medium solution and CaCl₂, both with *S. pasteurii*, placed in alternate layers (0.5 ml aliquots). Again, optimal alginate and CaCl₂ concentrations were used. After incubation at 30°C for 21 days, 3-point bending tests were performed on the beams and surfaces examined microscopically as above.

(iv) *Physical healing from alginate.* 3 mortar beams (75x75x225 mm, mix as above) were fractured in a 3-point bending test, rejoined with sodium alginate solution (1, 2 and 3% w/w) and stored for 24 hours before repeating the bending test.

3. RESULTS AND DISCUSSION

(i) High levels of CaCl₂ (5% or 0.45 M) inhibited cell activity (Table 1), likely due to high salinity, with maximum activity at the median value of 3%. It is unclear why growth was hindered at 1% CaCl₂, though alginate beads did not form in such conditions and so continued bioavailability of CaCl₂ may be an issue. The optimal combination of alginate and CaCl₂ was 2.8% and 3% respectively.

Table 1: Active cell counts in alginate beads (cells per ml sample) – effect of alginate and CaCl₂ content. Presented as average (*n* = 3, standard deviation in brackets).

		Calcium chloride		
		1%	3%	5%
Alginate	2.4%	0 (0)	8.9x10 ⁴ (1.2x10 ⁵)	0 (0)
	2.8%	0 (0)	4.5x10 ⁵ (3.0x10 ⁵)	0 (0)
	3.2%	1.4x10 ⁵ (2.9x10 ⁵)	2.4x10 ⁴ (5.5x10 ⁴)	0 (0)

(ii) Activity of bacteria on mortar surfaces was determined by presence or absence of moisture. The applied alginate solution was, in some cases, found to have flowed off the surface leaving a dry environment. Specimens where it remained had observably moist areas (liquid or gel form). These areas contained amorphous gel layers in which large numbers of cells were embedded (

Figure 1). Counts presented in Table 2 have significant variability due to loss of gel/moisture on certain specimens, which had no detectable active cells present. Little can be inferred as to the effectiveness of the application methods used, but it is clear that alginate gel can support significant numbers of active bacteria on a fresh mortar surface.

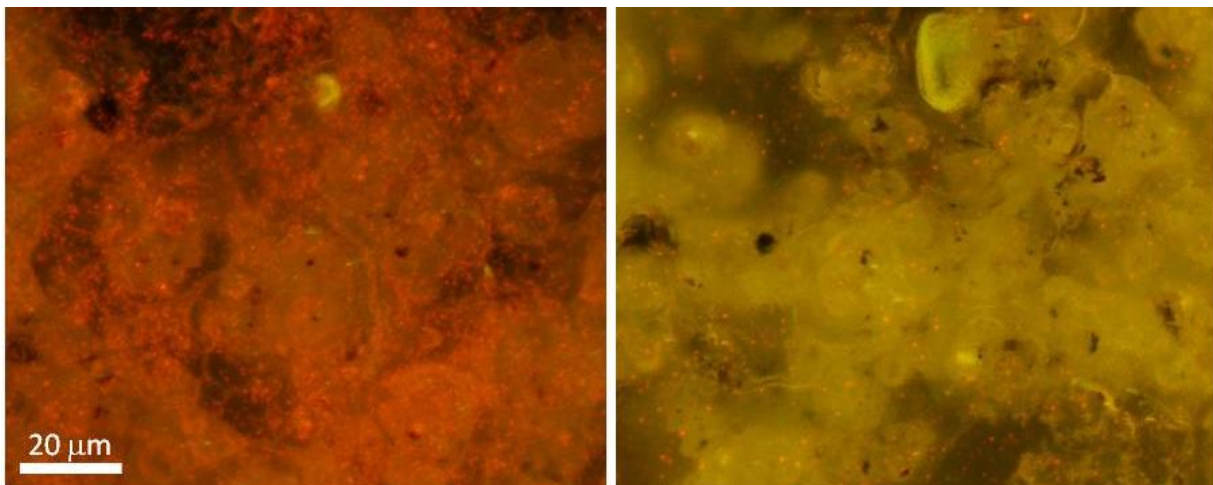


Figure 1: Images of mortar specimen surfaces showing gel and active cells (red).

Table 2: Active cell counts from gel-covered mortar surfaces (cells per mm²). Data presented as average (*n* = 3) with standard deviation in brackets. Data are lower-bound values due to obscuration by gel and counting of large numbers.

		Alginate application method		
		A	B	C
Final curing conditions	Air	7.0x10 ³ (1.2x10 ⁴)	0 (0)	0 (0)
	Water	5.2x10 ⁴ (5.5x10 ⁴)	3.5x10 ³ (3.0x10 ⁴)	0 (0)
	CaCl ₂	2.7x10 ⁴ (3.6x10 ⁴)	2.1x10 ⁴ (2.2x10 ⁴)	0 (0)

(iii) As in (ii) retention of alginate solutions in mortar beam notches was difficult and so no variation in flexural strength was demonstrated (Table 3). Apparently crystalline precipitation was observed on areas of the surface of a number of beams where gel was retained, and only in beams where *S. pasteurii* were present (Figure 2). XRD analysis of this precipitate indicated that it was calcite. Active bacteria were detected infrequently, possibly due to lack of moisture by the time of testing.

Table 3. Flexural strength of beams (kPa) from 3-point bending test.

Alginate application method	Average	Standard deviation
X	2460	80
Y	2389	279
Z	2303	97

(iv) Alginate gels formed a stable bond in fractured mortar beams, but had a relatively weak effect on mechanical performance (Table 4). Only up to 3% of the initial flexural strength was regained with 3% alginate, although the gel was able to support the self-weight of the cracked mortar beam during testing. Although this is relatively insignificant in the case of a fully fractured beam, its behaviour in smaller macroscopic and microscopic cracks may be different.

Table 4: Flexural strength (kPa) of mortar beams and after healing with alginate.

% alginate	Mortar	Alginate-healed
1	1648.4	0
2	1708.8	19.2
3	1651.2	49.8

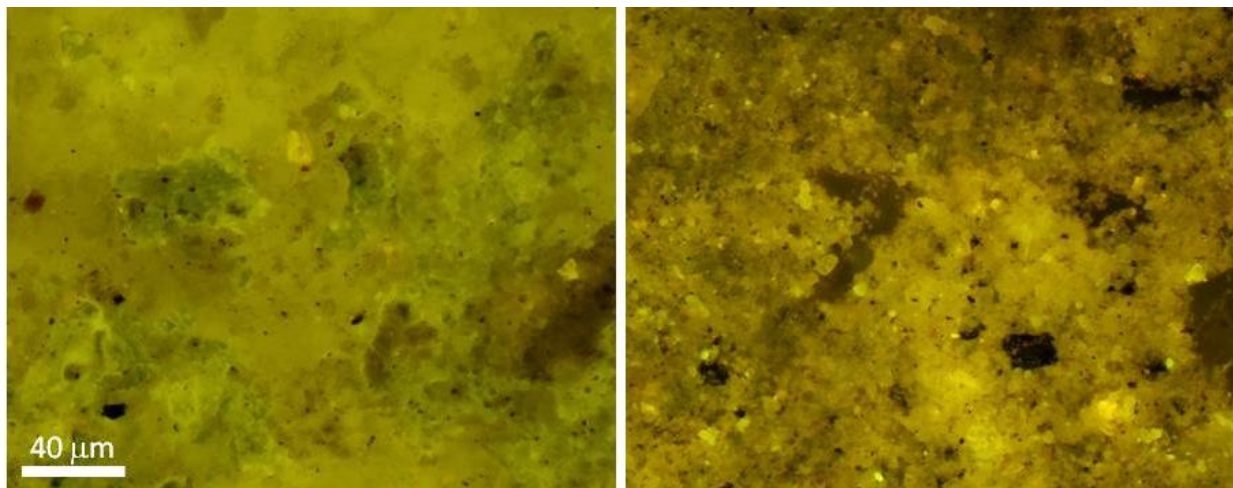


Figure 2: Surface layer development adjacent to notch on mortar beams (group Y, with bacteria, left) and lack of layer development (group X, without bacteria, right).

4. CONCLUSION

This paper reports the preliminary outcomes of an ongoing study, demonstrating that alginate gels optimised for survival of *S. pasteurii* are capable of supporting active cells over several weeks on highly alkaline mortar surfaces. There are indications that calcite precipitation occurs, although strength regain is yet to be demonstrated.

REFERENCES

[1] W. De Muynck, N. De Belie, W. Verstraete, Microbial carbonate precipitation in construction materials: A review, *Ecological Engineering* 36 (2010) 118-136.

- [2] S. Bang, J. Galinat, V. Ramakrishnan, Calcite precipitation induced by polyurethane-immobilized *Bacillus pasteurii*, *Enzyme & Microbial Technology* 28 (2001) 404-409.
- [3] J. Wang, K. Van Tittelboom, N. De Belie, W. Verstraete, Use of silica gel or polyurethane immobilized bacteria for self-healing concrete, *Construction & Building Materials* 26 (2012) 532-540.
- [4] V. Wiktor, H. Jonkers, Quantification of crack-healing in novel bacteria-based self-healing concrete, *Cement & Concrete Composites* 33 (2011) 763-770.
- [5] M. Cassidy, H. Lee, J. Trevors, Environmental applications of immobilized microbial cells: a review, *Journal of Industrial Microbiology* 16 (1996) 79-101.
- [6] G. Rodriguez, D. Phipps, K. Ishiguro, H. Ridgway, Use of a Fluorescent Redox Probe for Direct Visualization of Actively Respiring Bacteria, *Applied & Environmental Microbiology* 58 (1992) 1801-1808.
- [7] C. Schneider, W. Rasband, K. Eliceiri, NIH Image to ImageJ: 25 years of image analysis, *Nature Methods* 9 (2012) 671-675.

A STUDY ON THE STEEL CORROSION PROTECTION OF A MICROCAPSULE BASED SELF-HEALING CEMENTITIOUS SYSTEM BY MEANS OF ELECTROCHEMICAL IMPEDANCE SPECTROSCOPY

B. Dong¹, Y. Wang¹, N. Han¹, F. Xing¹

¹*School of Civil Engineering, Guangdong Province Key Laboratory of Durability for Marine Civil Engineering, Shenzhen University, Shenzhen, P.R.China. 518060 - e-mail: incise@szu.edu.cn; wang.ys1988@gmail.com; nxhan@szu.edu.cn; xingf@szu.edu.cn*

Keywords: Steel reinforced concrete, Chemical trigger, Chemical self-healing, Electrochemical impedance spectroscopy (EIS), Equivalent circuit model

ABSTRACT

Based on microcapsule technology, a new type of self-healing system for cementitious composites is established. The performance of the system was characterized by means of electrochemical impedance spectroscopy of steel bars immersed in a simulated concrete environment. The results demonstrate strong inhibition of chloride-induced corrosion when microcapsules are added to the solution. A novel equivalent circuit model, which takes into account the inductive effect arising from the generation of corrosion products on the steel bar surface, is proposed to explain the protection performance of the microcapsules against steel bar corrosion in a concrete environment.

1. INTRODUCTION

Concrete is a basic material used for modern construction. Due to concrete creep, the humidity change and non-homogeneous settlement of buildings, concrete structures may generate a lot of cracks during service period. These cracks will affect the safety of the buildings and even cause severe accidents [1]. Self-healing technology then has been introduced to repair the cracks in a concrete structure automatically, resulting in an improvement of concrete structure performance [2-3]. An acceptable work that initiates an engineering approach for self-healing cement composite with microcapsules is first developed in Shenzhen University, China. Even so, existing efforts are focusing on the crack repair and mechanical performance recovery. It is not an effective method to deal with the degradation of the concrete structure, which caused by the ions erosion (such as Cl^- , SO_4^{2-} , CO_3^{2-} etc.). For this reason, a chemical trigger mechanism is proposed and a chemical self-healing system with microcapsule inhibitor is designed. And, its protection against steel corrosion is measured by means of electrochemical impedance spectroscopy [4]. A new electrochemical model is proposed to interpret the corrosion-inhibiting performance of the microcapsule system.

2. MATERIALS AND METHODS

For microcapsule fabrication, sodium monofluorophosphate and polysorbate 80 were mixed into sodium monofluorophosphate. And a spray drying method is used to form the microcapsule. With the aim of measuring steel corrosion within a microcapsule-based self-healing cementitious system, a $\Phi 10$ (10 mm diameter) Q235

rebar was prepared. In order to simulate a concrete environment, a saturated $Ca(OH)_2$ solution was prepared with pH=12.5. Different concentrations of $NaCl$ solution were added to the $Ca(OH)_2$ solution to characterize the corrosion behavior of the steel bar with varying microcapsule dosages. The amounts of $NaCl$ and microcapsules used in each sample are listed in Table 1. Electrochemical impedance spectroscopy of the steel bar corrosion was performed with a Potentiostat/Galvanostat (Princeton Applied Research, Model 283). A stainless steel electrode was used as the reference electrode. In order to observe the variation of steel corrosion with time, the tests were repeated at different exposure times.

Table 1: Concentrations of chloride ions and microcapsule dosage for each sample

Sample Number	A	B	C	D	E	F	G	H
chloride ion content (mg/L)	300	3000	6000	300	3000	6000	3000	3000
microcapsule content (g)	0	0	0	25	25	25	15	35

3. RESULTS AND DISCUSSION

For an ideal electrochemical system as illustrated in Figure 2(a), two parallel processes exist: (1) charging/discharging of the electric double layer capacitor with varying potential across the electrodes (non-Faraday process); (2) Faraday’s process (including charge transfer and diffusion) which occurs with a fixed potential across the electrodes. The electrochemical system can thus be represented by the equivalent circuit model shown in Figure 1(b). Based on the above schematic, the electrical circuit model for the idealized electrochemical system can be described by the CDC (Circuit Description Code) $R_s(Q(R_{ct}W))$ (see Figure 1(b), $R_{ct} = Z_{ct}$, $W = Z_D$). Here, Q indicates C_d , the CPE (constant phase element) [5], which is generally attributed to distributed surface reactivity, surface inhomogeneity, roughness or fractal geometry, electrode porosity, and to current and potential distributions associated with electrode geometry. R_{ct} and W are the resistances associated respectively with charge transfer processes and diffusion processes. R_s represents the properties of the electrolyte solution and $(Q(R_{ct}W))$ reflects the reactions at the electrodes. The model can also be re-written as $(Q_1(R_{ct1}W_1))R_s(Q_2(R_{ct2}W_2))$ (see Figure 1(c)). $(Q_1(R_{ct1}W_1))$ and $(Q_2(R_{ct2}W_2))$ represent the functions of the left and right electrodes, respectively [6].

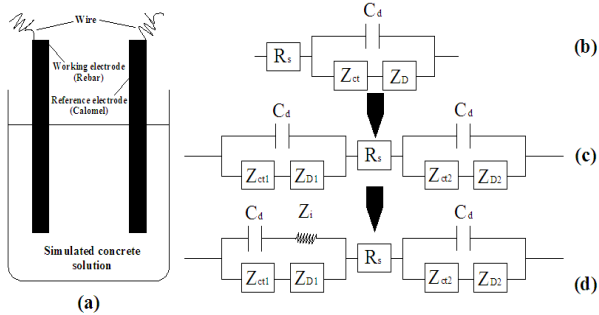


Figure 1: The electrochemical sketch map and equivalent circuit models.

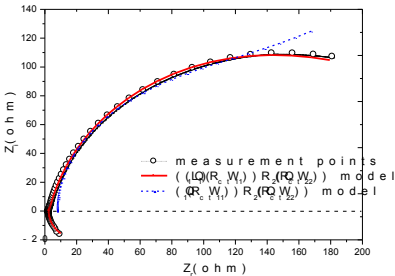
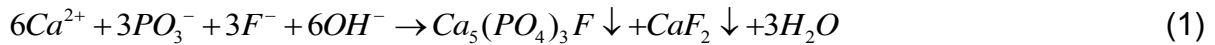


Figure 2: The Nyquist locus for steel corrosion within a microcapsule-based self-healing cementitious system under NaCl solution

In figure 1, R_s is resistance of electrolyte solution; C_d is electric double layer capacitance; Z_{ct} is resistance of charge transferring process and Z_D is resistance of diffusion process (Warburg resistance), where Z_{ct} and Z_D are composed as Z_F (Faraday's process).

For steel corrosion within a microcapsule-based self-healing cementitious system, the process is more complex than the idealized electrochemical system described above. With Cl^- attack, the steel bar rusts and a corrosion product layer will deposit at the surface of the rebar, which results in an inductive effect during EIS measurement. If microcapsules are added into the solution, they will break under the influence of the alkaline environment and the following chemical reaction will then take place:



The reaction products should accumulate on the rebar surface, forming a protective layer against steel corrosion. Correspondingly, a new element must be added to the electrochemical model; the code $((Q_1L_1)(R_{ct1}W_1))R_s(Q_2(R_{ct2}W_2))$ can represent this system, as illustrated in Figure 1(d). In this model, $((Q_1L_1)(R_{ct1}W_1))$ arises from the reaction at the surface of the rebar and $(Q_2(R_{ct2}W_2))$ from the reaction at the reference electrode. The total impedance of this model can be expressed as:

$$Z = \frac{(R_1 + W_1)(1 - \omega^2 Q_1 L_1)^2}{(1 - \omega^2 Q_1 L_1)^2 + (R_1 + W_1)^2} + R_s + \frac{1}{R_2 + W_2} - \left\{ \frac{(R_1 + W_1)^2 (1 - \omega^2 Q_1 L_1)}{(1 - \omega^2 Q_1 L_1)^2 + (R_1 + W_1)^2} Q_1 + \frac{(R_2 + W_2)^2}{1 + \omega^2 (R_2 + W_2)^2 Q_2^2} Q_2 \right\} \omega j \quad (1)$$

Where, $L_1 = Z_i$, represents the inductance impedance; $\omega = 2\pi f$, represents the circular frequency [6]

Experimental measurements of the Nyquist for corrosion of the steel rebar within the microcapsule-based self-healing cementitious system in $NaCl$ solution are shown in Figure 2, along with fits from the equivalent-circuit models $((Q_1L_1)(R_{ct1}W_1))R_s(Q_2(R_{ct2}W_2))$ and $(Q_1(R_{ct1}W_1))R_s(Q_2(R_{ct2}W_2))$. It is clear that the former model, which takes into account reactions at the rebar surface, gives a good fit both to the resistance and reactance loci depending to the frequency. Conversely, the $(Q_1(R_{ct1}W_1))R_s(Q_2(R_{ct2}W_2))$ model gives a poor fit to the experiment results. In particular, the inductive effect arising from steel bar corrosion is manifested in the experimental data by values for the Nyquist locus for $Z'' < 0$ (i.e. in the fourth quadrant of Figure 2); this feature is not captured by $(Q_1(R_{ct1}W_1))R_s(Q_2(R_{ct2}W_2))$. The lack of agreement between $(Q_1(R_{ct1}W_1))R_s(Q_2(R_{ct2}W_2))$ and the experimental results emphasizes that the model doesn't accurately represent the inductive effect caused by steel bar corrosion. Figure 3 shows the Nyquist locus for steel corrosion with different Cl^- concentrations in a simulated concrete environment after a 100-day rusting period. It is clear that the Nyquist curves exhibit a similar trend regardless of the Cl^- concentration. All the loci have values in the fourth quadrant (i.e. $Z'' < 0$, $Z' > 0$) arising from the corrosion of the steel bar. Moreover, the locus shifts towards the left with increasing Cl^- concentration. In addition, Figures 3 show fits from the $((Q_1L_1)(R_{ct1}W_1))R_s(Q_2(R_{ct2}W_2))$ model. The fitted values for the parameter L_1 , which characterizes the inductive effect due to steel bar corrosion. It is found that L_1 increases with the length of the corrosion period and with increasing Cl^- concentration, which is consistent with the interpretation

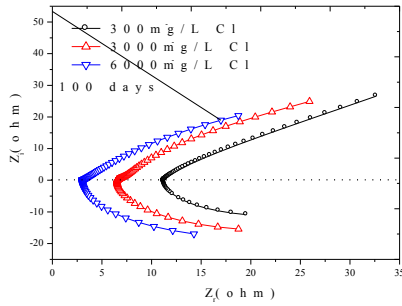


Figure 3: Nyquist locus and $((Q_1L_1)(R_1W_1))R_s((Q_2)(R_2W_2))$ model fit for steel corrosion with different Cl^- concentrations in a simulated concrete environment

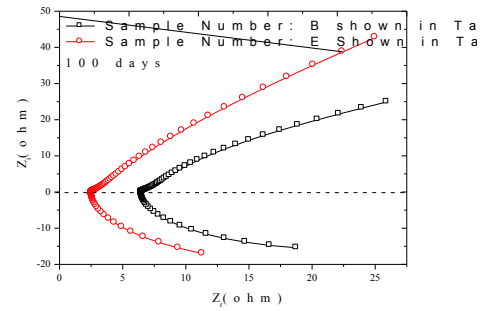


Figure 4: Comparison of Nyquist locus for steel bar corrosion with (E) and without (B) addition of microcapsules

of L_1 as arising from the generation of corrosion products on the surface of the steel bar. This gives support to the physical basis of the $((Q_1L_1)(R_{cf1}W_1))R_s(Q_2(R_{cf2}W_2))$ model and its corresponding parameter L_1 , as an accurate description of the experimental situation. Microcapsules were added to a number of the simulated concrete-rebar systems, and the resulting samples compared with the corresponding no-microcapsule samples to assess the extent to which the microcapsules could protect against corrosion (shown in Figure 4). Regardless of the addition of microcapsules, the electrical inductance feature (Nyquist loci present for $Z_i < 0$) is observed. However, the difference in the L_1 value between the two cases is dramatic: L_1 for that with microcapsule sample (E) is smaller than that for the no-microcapsule sample (B) by roughly four orders of magnitude after 100 days. Since L_1 relates to the amount of corrosion products generated, this clearly demonstrates a strong protective effect of the microcapsules against corrosion of the steel bar by Cl^- ions.

4. CONCLUSION

A new kind of microcapsule has been designed, and its anti-corrosion characteristics is studied in the context of steel bar corrosion triggered by Cl^- ions in a simulated concrete environment with a new electrochemical model, which takes into account the inductive effect caused by the rust layer at the surface of the steel bar. The parameter L_1 in the model is obtained by fitting to experimental data and thus its dependence on the corrosion period, Cl^- concentration are determined. The microcapsule approach is capable of providing excellent protection against steel bar corrosion.

ACKNOWLEDGEMENTS

Financial support of the National Natural Science Foundation of China for this study (Project No.51120185002, No.51272160 and No.50925829) is gratefully acknowledged.

REFERENCES

- [1] S.J. Jaffer, C.M. Hansson. The influence of cracks on chloride-induced corrosion of steel in ordinary Portland cement and high performance concretes subjected to different loading conditions. *Corrosion Science*. 2008, 50(12): 3343-3355
- [2] M. R. Kessler, N. R. Sottos and S. R. White. Self-healing structural composite materials. *Applied Science and Manufacturing*. 2003, 34(8): 743-753
- [3] S.R.White, N.R.Sottos, P.H.Geubelle. Autonomic healing of Polymer Composites. *Nature*. 2001, 409: 794-797
- [4] A.A. Oskuie, T. Shahrabi, A. Shahriari, E. Saebnoori. Electrochemical impedance spectroscopy analysis of X70 pipeline steel stress corrosion cracking in high pH carbonate solution. *Corrosion Science*. 2012, 61: 111-122
- [5] Piotr Zoltowski. On the electrical capacitance of interfaces exhibiting constant phase element behavior. *Electroanalytical Chemistry*. 1998, 433: 149-154
- [6] Shi Meilun. *AC Impedance Spectroscopy Principles and Applications [M]*. Beijing: National Defence Industry Press. 2001

EVALUATION OF A MICROCAPSULE BASED SELF-HEALING SYSTEM FOR CEMENTITIOUS MATERIALS

M. Zhang ¹, N. Han ¹, F. Xing ¹, X. Wang ¹ and E. Schlangen ²

1 Guangdong Provincial Key Laboratory of Durability for Marine Civil Engineering; Shenzhen Durability Centre for Civil Engineering; College of Civil Engineering, Shenzhen University, Shenzhen, P.R. China – e-mail: xingf@szu.edu.cn

2 Faculty of Civil Engineering and GeoSciences, Delft University of Technology, Delft, The Netherlands

Keywords: self-healing, microcapsule, healing effect, mechanical behaviour, permeability

ABSTRACT

An international cooperation research project has been financially supported by China Nature Science Foundation, which consists of three relatively independent, but strategically integrated research sub-programs, aiming at the formation of a self-healing system based on the microcapsule principle for the cementitious composites. In this paper, a self-healing system triggered by physical process (cracking) is introduced. The healing material mainly consists of epoxy like materials. The discussion concerning microcapsule techniques are presented in another paper in this conference. This study mainly focuses on the two healing mechanisms: i.e. the mechanical recovery and the permeability related recovery. The primary test results concerning these healing mechanisms are presented and the healing effects on the relevant properties are further discussed.

1. INTRODUCTION

Self-healing system applied in concrete will have special advantages in comparison with the traditional post-damage repair methods. Since it can self-detect and self-recover the degraded performance, the self-healing system in concrete has been attracting more and more research interests.

In this paper, a self-healing system triggered by physical process (cracking) is introduced. The healing material mainly consists of epoxy like materials. The discussion concerning microcapsule techniques are presented in another paper in this conference. This study mainly focuses on the two healing mechanisms: i.e. the mechanical recovery and the permeability related recovery. The primary test results concerning these healing mechanisms are presented and the healing effects on the relevant properties are further discussed.

2. MATERIALS

Cementitious composites consist of Portland cement, slag, quartz sand, PVA fibre and water. The urea formaldehyde resin was used for the shell of microcapsule, and bisphenol – an epoxy resin E-51 diluted by n-butyl glycidyl ether (BGE) was adopted as the healing-agent inside the microcapsule. A combination of latent curing agent

MC120D and tetraethylene penamine (TEPA) – a type of liquid curing agent functioning at normal temperature was used for curing the healing product.

3. TEST METHODS

Firstly, cement, slag, quartz sand and MC120D were mixed for one minute. Then water and TEPA were added into the mixer. Afterwards, PVA fibre and microcapsule were put in and mixed until a uniform mixture was obtained. Prisms of $40 \times 40 \times 160$ mm were prepared for the mechanical test and cylinders of $\Phi 100 \times 100$ mm were cast for the permeability test. After 60 days one group of specimens were loaded to failure to obtain the compressive strength. Another group of specimens were prepared and tested to obtain the chloride diffusion coefficient by means of RCM method. The rest of specimens were pre-loaded at different stress/strength ratios. Then the specimens were unloaded and put into the curing room for 7 days with a curing temperature of 50°C . Then one group of tests was carried out mechanically to evaluate the healing effect of the mechanical performance. The other one was used for testing the chloride diffusion coefficient with the help of RCM. Then the performance recovery concerning the impermeability could be evaluated accordingly. The healing efficiency was evaluated by using equation (1), where η is the healing efficiency factor; P_{healed} is the performance index after healing and $P_{initial}$ is the performance index before healing:

$$\eta = 100 \times \frac{P_{healed} - P_{initial}}{P_{initial}} \quad (1)$$

4. RESULTS

The healing efficiency regarding the mechanical performance and permeability performance of one group of tests are shown in Figure 1 and Figure 2, respectively. Two types of composites with different contents of microcapsule are evaluated. The major variable in the comparison is the size of used microcapsule, where the pre-loading level and curing condition is kept constant. In general, the increase of the adopted size of microcapsule results in an increase of healing efficiency for both evaluated performance indexes. It is also illustrated that the healing efficiency related to the permeability index is relatively higher than that related to the strength index. One interesting point to be noticed is that too large size of microcapsule could hamper the increase rate of healing efficiency. This might be due that the large microcapsule introduces large voids its self, which need to be filled in by the healing agent when the healing mechanism is excited. Thus less healing agent will be available for the effective healing. As a result the healing efficiency is reduced.

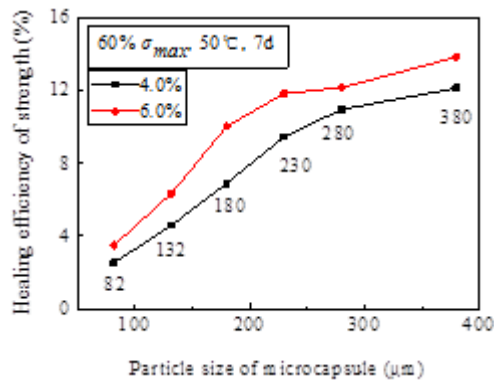


Figure 1: Healing efficiency of strength index with different microcapsule sizes

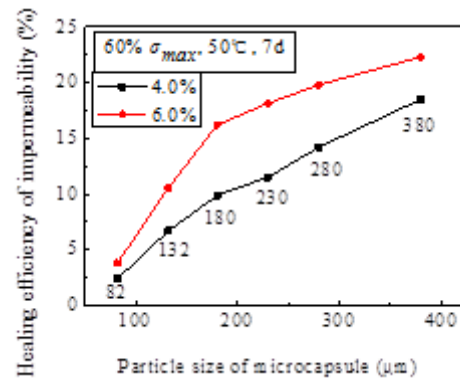


Figure 2: Healing efficiency of permeability index with different microcapsule sizes

The influence of the microcapsule content on the healing efficiency of the strength index and permeability index is illustrated in Figure 3 and 4, respectively. It is shown that the healing efficiency increases proportionally with the content of microcapsule. Again the recovery is more significant for the permeability index than that for the strength index.

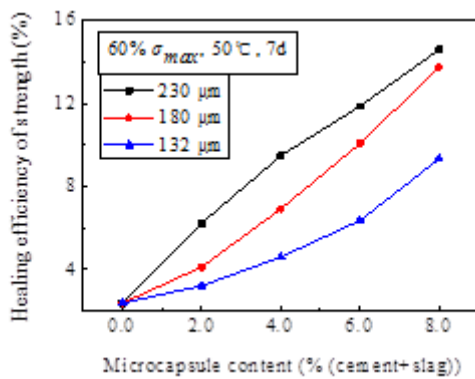


Figure 3 : Healing efficiency of strength index with different microcapsule contents

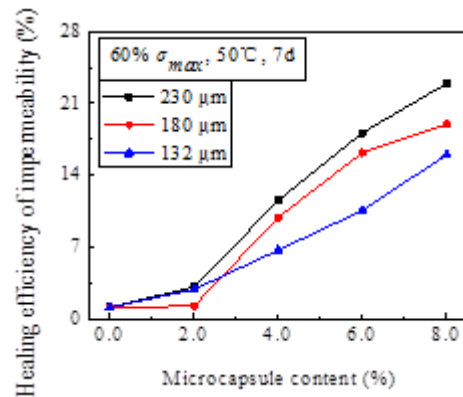


Figure 4 : Healing efficiency of permeability index with different microcapsule contents

Figure 5 and Figure 6 show the influence of pre-load levels on the healing efficiency of the two evaluated performance indexes, respectively. Generally speaking, the higher the pre-load level is the higher the healing efficiency will be. This could be related to the trigger mechanism in this self-healing system. High pre-load level means more cracking, resulting in more participating of microcapsule in the healing process. Thus a high healing efficiency will be realised. At a pre-load level less than 40%, the healing efficiency of the permeability index increases at a high rate. As the pre-load level further goes up the increase rate of healing efficiency will be reduced.

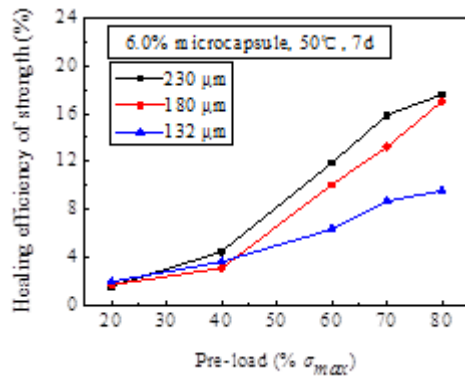


Figure 5 : Healing efficiency of strength index with different pre-load levels

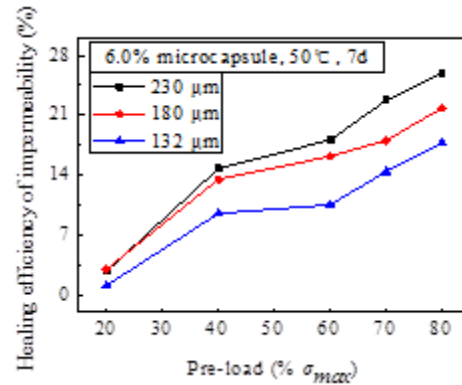


Figure 6 : Healing efficiency of permeability index with different pre-load levels

5. CONCLUSIONS

Microcapsule can be used in cementitious composites to achieve self-healing function. The content and size of microcapsule, as well as the pre-load level, have remarkable influences on the healing efficiency of two performance indexes, namely strength recovery and impermeability recovery.

ACKNOWLEDGEMENTS

Financial support from the NSFC (Project No. 51120185002; No. 51078238, No. 50925829) is gratefully acknowledged.

REFERENCES

- [1] Abrams A. Autogenous Healing of Concrete [J]. Concrete, 1925: 10-50.
- [2] Jeremy L. Day, V. Ramakrishnan, and Sookie S. Bang. Microbiologically Induced Sealant for Concrete Crack Remediation [C]. Proceedings of the 16th ASCE Engineering Mechanics Conference, University of Washington, Seattle. 2003, 93-111.
- [3] Di Shengkui, Li Hui, Du Yong feng, et al. Self-Monitoring and Repairing Based on Crack of Concrete Beam Embedded with SMA [J]. Journal of Building Materials, 2009, 12(1) :27-31.
- [4] Zhang Feier, Yao Lining. Research on Self-repair using hollow-center optical fiber in smart concrete structure [J], Journal of Functional Materials and Devices, 2003, 9(1) : 91-94.
- [5] S.R.White, N.R.Sottos, P.H.Geubelle, J.S.Moore,et al. Autonomic healing of polymer composites[J].Nature. 2001, 409(1):794-817.

PREPARATION AND CHARACTERIZATION OF POLY (UREA-FORMALDEHYDE) WALLED DICYCLOPENTADIENE MICROCAPSULES

W. Xiong¹, G. Zhu¹, J. Tang¹, B. Dong², N. Han², F. Xing², E. Schlangen³

¹Shenzhen Key Laboratory of Special Functional Materials, College of Materials Science and Engineering, Shenzhen University, Shenzhen 518060, PR China-E-mail: gzhu@szu.edu.cn; tjn@szu.edu.cn;

²Department of Civil Engineering, Guangdong Provincial Key Laboratory of Durability for Marine Civil Engineering, Shenzhen University, Shenzhen 518060, PR China

³Delft University of Technology, Faculty of Civil Engineering and Geosciences, Micromechanics Laboratory (MICROLAB), Stevinweg 1, 2628 CN Delft, Netherlands

Keywords: microcapsules, poly (urea-formaldehyde), dicyclopentadiene, self-healing

ABSTRACT

Poly (urea-formaldehyde) (PUF) shelled dicyclopentadiene (DCPD) microcapsules were prepared by *in-situ* polymerization technology for self-healing concrete applications. It's found, during the process, sodium dodecyl benzene sulfonate (SDBS) behaves better in emulsification of DCPD than other surfactant of sodium lauryl sulfate (SLS) and styrene maleic anhydride copolymer (SMA), and the addition of ammonia chloride (NH₄Cl) as PUF curing catalyst accidentally leads to a smooth surface of the microcapsule.

1. INTRODUCTION

Dicyclopentadiene (DCPD) is a monomer would conduct ring-opening-metathesis polymerization (RPMP) on Grubbs' catalyst, and the resulting poly-DCPD was regarded as a good healing agent. In recent years, there are many researchers are interested in preparation of encapsulated PCPD for self-healing propose^[1-3]. The most PCPD microcapsules are poly (urea-formaldehyde) walled, which is formed by an *in situ* condensation polymerization process. It's well known that, for the microcapsule applied in self-healing concrete, epoxy was commonly used as the core materials. However, because of its glutinous attribute, epoxy is difficult to be uniformly emulsified and effectively encapsulated in the *in situ* polymerization of urea formaldehyde. DCPD is a white crystalline solid with a very low melting point at 32.5°C. DCPD at slightly-elevated temperature is oily liquid with low viscosity, so ease to be emulsified in water, accordingly the shape and size of microcapsule were apt to be controlled. In this paper, DCPD was attempted dispersed in water by different surfactants, and the PUF-walled microcapsules were synthesized to reveal the simplicity or easiness of DCPD encapsulation.

2. MATERIALS AND METHODS

2.1 Materials

DCPD and resorcinol were received from Aladdin-reagent, Shanghai, China, and were used as core materials and PUF curing agent respectively. Urea, 37wt%

formaldehyde solution, triethanolamine (TEA), citric acid, ammonium chloride (NH_4Cl) and all of emulsifiers, including SDBS, SLS, SMA, PVA, are purchased from Tianjin Chemical Plant, China, in which triethanolamine and citric acid were employed to adjust pH value, and NH_4Cl was used as PUF curing catalyst. All the chemicals are analytical pure.

2.2 Preparation of microcapsules

5g urea and 10.1g formaldehyde are mixed in 250ml three-neck flask, TEA was added to adjust the pH value to 8-9, then the solution was heated to 70°C and persisted for 1h, PUF prepolymer solution was obtained.

0.1g SDBS, 0.5g PVA (used as emulsion stabilizer^[4]), 17.4g DCPD are added in 100ml deionized water, stirred at rate of 600rpm for emulsification for 30min. PUF prepolymer solution, 0.5g resorcinol and 0.5g ammonium chloride are then added into the emulsion. The pH value of the solution is adjusted to 3-4 by 5% citric acid and the temperature was raised slowly to 60°C and kept for 2h for *in situ* polymerization. After cooling, the solution was filtered, and the residue was rinsed by warm deionized water, dried in succession at 50°C for 12h. The whole process is schematically shown in Fig.1.

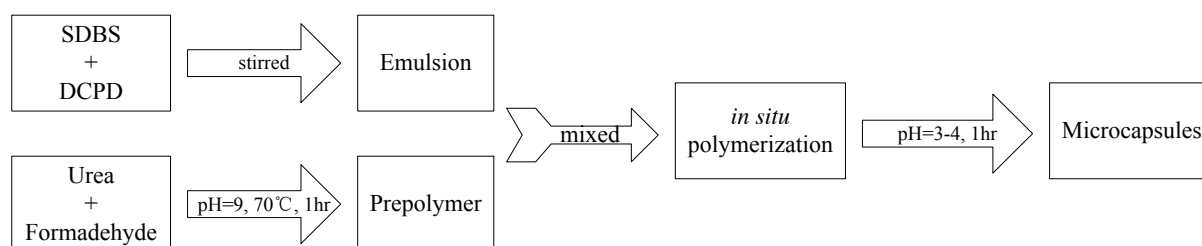


Figure 1: The schematic of preparation of microcapsules

2.3 Characterization of the microcapsules

The morphology of microcapsules was observed under Hitachi SU-20 SEM, by which the particle diameters and shell thickness were also measured. The thermal stability and thermolysis temperature were determined by TA DSC Q200/TGA Q50 thermal analyser. The chemical composition of microcapsules was confirmed by Nicolet 6700 FTIR Spectrometer in 400 to 4000cm^{-1} wave number region.

3. RESULTS AND DISCUSSION

3.1 Effects of different emulsifiers

Fig. 2 (a)-(c) show the OM images of DCPD oil droplet in water emulsified by SDBS, SLS and SMA respectively, and Fig. 2 (d)-(f) show the OM images of corresponding microcapsules. It is clear that the emulsifying effect of monomolecule sulfate surfactants, such as SDBS and SLS, is much better than the polycarboxylate surfactant, SMA.

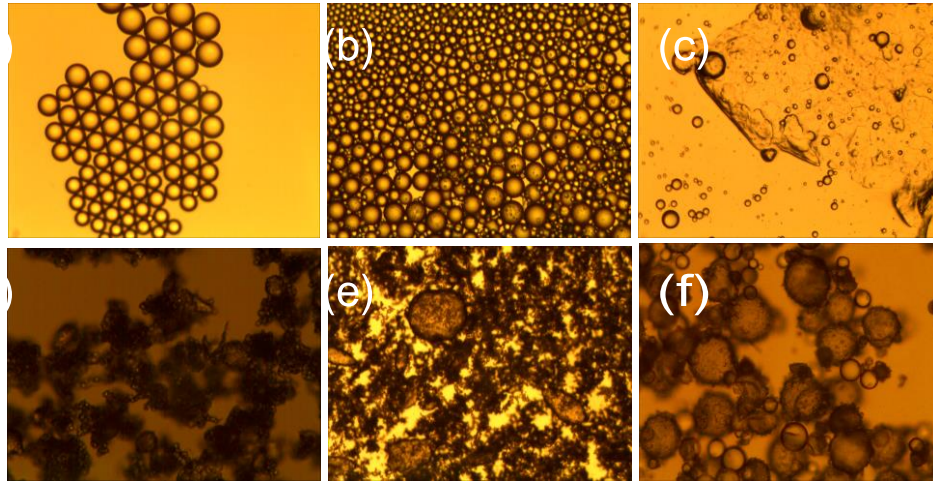


Figure 2: OM images of DCPD oil droplet (200×) emulsified by (a) SDBS, (b) SLS, (c) SMA, and the corresponding PUF/DCPD microcapsules (400×): (d) SDBS, (e) SLS, (f) SMA.

3.2 The influence of NH_4Cl on microencapsulation process

It is well known that NH_4Cl is a curing catalyst commonly used in the cross-linking reaction of PUF resin, but the mechanism is still unknown. Zhou et al regards NH_4Cl promotes the micro-encapsulation reaction comes of the fact it debases pH value^[5]. As there are so much many chemicals can lower pH value, so NH_4Cl is dispensable in the preparation of PUF microcapsules^[6,7]. It's only a curing accelerant. However, in our experiments, it's found NH_4Cl plays an important role in morphology controlling. As shown in Fig. 3 and Fig. 4, the PUF microcapsules synthesized with NH_4Cl presents very smooth surface, meanwhile the microcapsules derived from reaction without NH_4Cl exhibits tough appearance, just like most of PUF microcapsule does. This phenomenon should be brought to the forefront because microcapsule with smooth surface is not appropriate for the application in self-healing concrete.

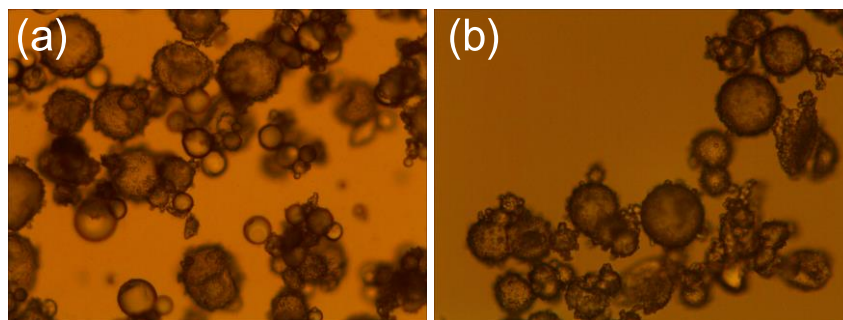


Figure 3: OM images of microcapsules (400×) synthesized (a) with or (b) without NH_4Cl .

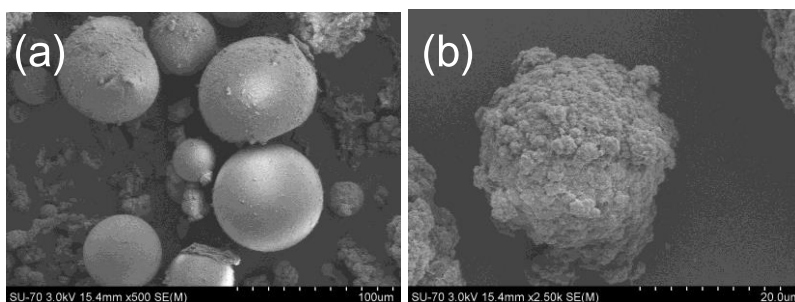


Figure 4: SEM images of microcapsules synthesized (a) with or (b) without NH_4Cl .

3.3 FTIR spectra of microcapsules

On the microcapsule FTIR spectrum, the absorption peaks located at 3060 cm^{-1} and 1630 cm^{-1} belong to of $=\text{CH}$ group, indicating the inner content is DCPD. Existence of the absorption peak of $-\text{NH}$ group at 3240 cm^{-1} and $-\text{OH}$ group at 3500 cm^{-1} affirms the shell of PUF is formed.

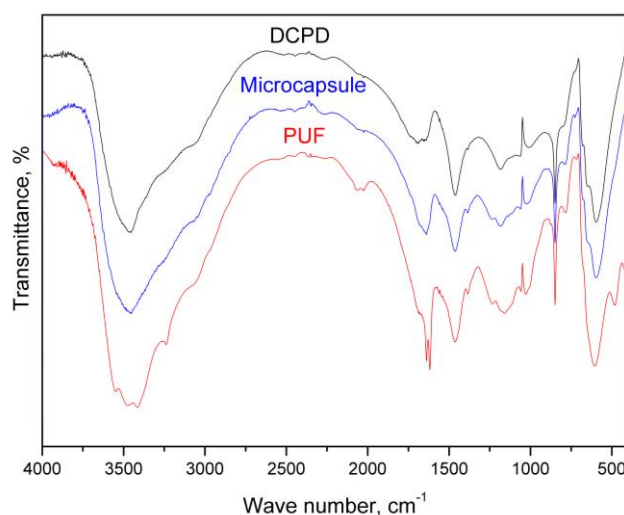


Figure 5: FTIR spectra of the microcapsules and its core and shell materials

4. CONCLUSION

PUF microcapsules filled with DCPD are successfully synthesized. It's found SDBS and SLS are good surfactants for DCPD emulsification in water. Addition of NH_4Cl results smooth surface of microcapsules, brings worry on them to be used in self healing concrete.

ACKNOWLEDGEMENTS

Financial support from the NSFC (Project No. 51120185002 and No. 50925829) is gratefully acknowledged.

REFERENCES

- [1] R. White, N. R. Sottos, P. H. Geubelle, J. S. Moore, M. R. Kessler, S. R. Sriram, E. N. Brown, S. Viswanathan, Autonomic healing of polymer composites, *Nature*, 409 (2001) 794-817.
- [2] Li Yuan, Aijuan Gu, Guozheng Liang, Preparation and properties of poly(urea-formaldehyde) microcapsules filled with epoxy resins, *Materials Chemistry and Physics*, 110 (2008) 417-425.
- [3] Rongguo Wang, Haiyan Li, Honglin Hu, Xiaodong He, Wenbo Liu, Preparation and Characterization of Self-Healing Microcapsules with Poly(urea-formaldehyde) Grafted Epoxy Functional Group Shell, *Journal of Applied Polymer Science*, 113(2009)1501-1506.
- [4] H.H. Noh, J.K. Lee, Microencapsulation of self-healing agents containing a fluorescent dye, *Express polymer letters*, 7(2013) 88-94.
- [5] Chuanjie Fan, Xiaodong Zhou, Influence of operating conditions on the surface morphology of microcapsules prepared by in situ polymerization, *Colloids and Surfaces A: Physicochemical and Engineering Aspects*, 363 (2010) 49-55.
- [6] Li Yuan, Guo-Zheng Liang, Jian-Qiang Xie, Jing Guo, Lan Li, Thermal stability of microencapsulated epoxy resins with poly(urea-formaldehyde)[J]. *Polymer Degradation and Stability*, 91(2006) 2300-2306.
- [7] Haiyan Li, Rongguo Wang , Xiaodong He, Wenbo Liu, Huanying Hao, Preparation and characterization of self-healing poly (urea-formaldehyde) microcapsules. *Proceedings of SPIE*, 2007, International Conference on Smart Materials and Nanotechnology in Engineering, 64232T (November 01, 2007).

PREPARATION OF MONO-SIZED EPOXY/MF MICROCAPSULES IN THE APPEARANCE OF POLYVINYL ALCOHOL AS CO-EMULSIFIER

G. Zhu¹, L. Lü¹, J. Tang¹, B. Dong², N. Han², F. Xing²

¹Shenzhen Key Laboratory of Special Functional Materials, College of Materials Science and Engineering, Shenzhen University, Shenzhen 518060, PR China-E-mail: gzhu@szu.edu.cn; tjn@szu.edu.cn;

²Department of Civil Engineering, Guangdong Provincial Key Laboratory of Durability for Marine Civil Engineering, Shenzhen University, Shenzhen 518060, PR China

Keywords: microcapsule, melamine–formaldehyde resin, epoxy, self-healing, concrete

ABSTRACT

For epoxy microcapsules embedded in concrete as mechanic-triggered self-healing adhesive, globular shape with uniform size is the basic requirement to ensure the solid shell broken and the liquid core released at a designed stress. In this paper, monodispersed melamine–formaldehyde (MF) resin-walled epoxy E-51 microcapsules were successfully fabricated in an in situ polycondensation process, in which a certain amount of polyvinyl alcohol (PVA) solution was added as co-emulsifier to control the microcapsules' shape and size. Detail investigation shows, with the cooperation of PVA, the microcapsule morphologies and size distribution were easy to be adjusted by the parameters such as emulsifying agents, agitation rate, pH value and acidification time.

1. INTRODUCTION

MF is one of cross-linked polyamino resin synthesized from tripolycyanamide by condensation with methanal. As shell material of microcapsule, MF resin is waterproof and thermal tolerant. It is strong enough to remain intact during manufacture and concrete mixing, but also crisp enough to cause leakage of core materials easily when required. It's ideal for the application of self-healing concrete, in which the microcapsules are expected to have optimum mechanical strength and can rupture under a given mechanical load. Theoretically, the mechanical strength of microcapsules is determined by shell's chemical composition, structure, size and thickness. So it is advantageous to prepare MF microcapsules with a narrow size distribution, which may lead to a narrow strength distribution. Moreover, microcapsules with a narrow size distribution can offer many other benefits, including tight control of the release rate of the core material.

2. MATERIALS AND METHODS

2.1 Materials

Bisphenol A type epoxy resin E-51(industrial reagents) was used as core material. Tripolycyanamide (Melamine, AR) and formaldehyde (37wt% aqueous solution, AR) were purchased from Aladdin-reagent, Shanghai, China. Sodium hydroxide (AR) and citric acid (AR) were received from Tianjin Chemical Plant, China, and used as pH

value regulating agents. All of the emulsifiers used, such as polyvinyl alcohol (PVA, MW=1800), sodium dodecyl benzene sulfonate (SDBS), sodium lauryl sulfate (SLS) are analytical pure agents and purchased from Tianjin Chemical Plant, China, but sulfonated copolymer of styrene and maleic anhydride (SMA, Scripset® 520, AR) are from Ashland Inc., USA.

2.2 Preparation of microcapsules

Melamine, equimolar formaldehyde and 100ml water were mixed in a 250ml three-neck flask and agitated at 350rpm till melamine was dissolved, then 10 wt% NaOH solution was added slowly to adjust pH value to 8.5, succeeded by elevation of temperature at 2°C/min to 70°C and keep for 10mins. After cooling, performed MF polymer was obtained.

0.4g emulsifier and 100ml distilled water were poured into an 500ml beaker and mixed, adding 10g epoxy E-51 resin, homogenized at 1000rpm for 30mins, add 2-3 drops of defoamer, latex emulsion of epoxy/water was formed.

Add performed MF polymer into the emulsion, stirred at 350rpm for 10mins. Add 10wt% citric acid solution dropwise to decrease the pH value to 3.5, then drop 0.4wt% PVA solution, meanwhile raise the temperature at 2°C/min to 70°C again and keep for 1hr. The performed MF polymer will cross-linked with each other at the w/o interface. After cooling, vacuum filtration, water rinse and vacuum drying, the products, epoxy/MF Microcapsules, were acquired.

2.3 Characterization of the microcapsules

The morphology of microcapsules was observed under Hitachi SU-20 SEM, by which the particle diameters and shell thickness were also measured. The thermal stability and thermolysis temperature were determined by TA DSC Q200/TGA Q50 thermal analyser. The chemical composition of microcapsules was confirmed by Nicolet 6700 FTIR Spectrometer in 400 to 4000cm⁻¹ wave number region.

3. RESULTS AND DISCUSSION

3.1 Effect of emulsifiers

SMA is an emulsifying agent widely used in the preparation of polyamino resin walled microcapsules. However, in our experiment, it's found the generation of MF prepolymer on SMA-emulsified o/w interface arouses emulsion breaking, leading to a very low encapsulation ratio of epoxy core. SDBS and SLS are unimolecule anionic surfactants. Their stab molecules tend to absorbed on the o/w interface with intensive and highly oriented arrangement, impeding the emergence of demulsification and increasing the efficiency of encapsulation, but the microcapsules have a wide size distribution. PVA can react with formaldehyde to form polyvinyl formal (PVF) in acidic condition. PVF coves on the surface of oil drops and changes the HLB value, making the oil drop size small and uniform. Experimental results shows, SDBS cooperated with PVA has very good effects on shape and size controlling of microcapsule, as showing in Fig. 1.

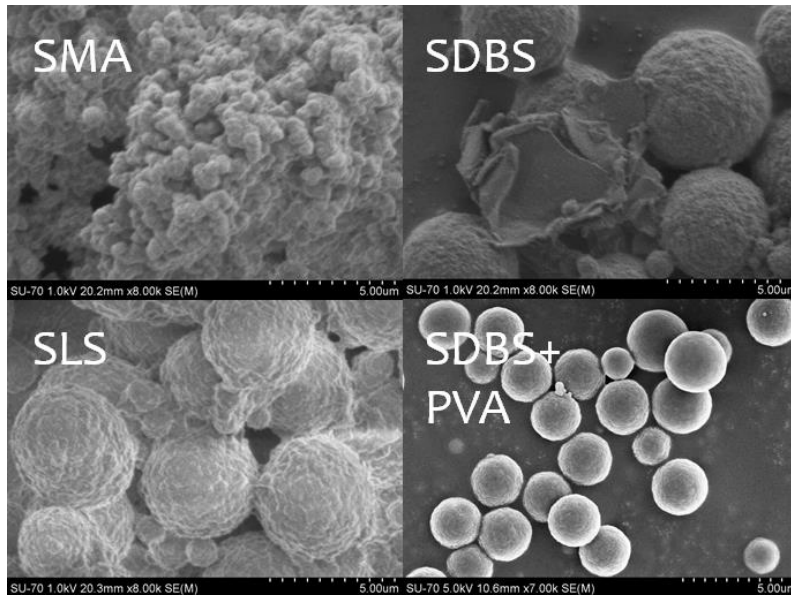


Figure 1: Microcapsules prepared from epoxy/water emulsion with different surfactants

3.2 Effect of pH value and acidification time

During the second period of the *in situ* polymerization of MF, *i.e.*, the cross-linking of performed MF polymer in acid solution, the reaction time and end reaction point (pH value) is very important in microcapsules' morpha controlling. Overlong reaction time will cause partial emulsion drops broken, resulting the microcapsules agglomerate because of the appearance of epoxy resin. Setting end reaction point at higher pH value leading to obtain large-sized microcapsules with rough and loose MF shell, but at lower pH value will arouse wide size distribution. The optimal end reaction point is at 3.5-4 in pH, and the appropriate time is about 1hr. at that condition, the microcapsules received are spheroidal in shape, and with smooth surface and narrow size distribution.

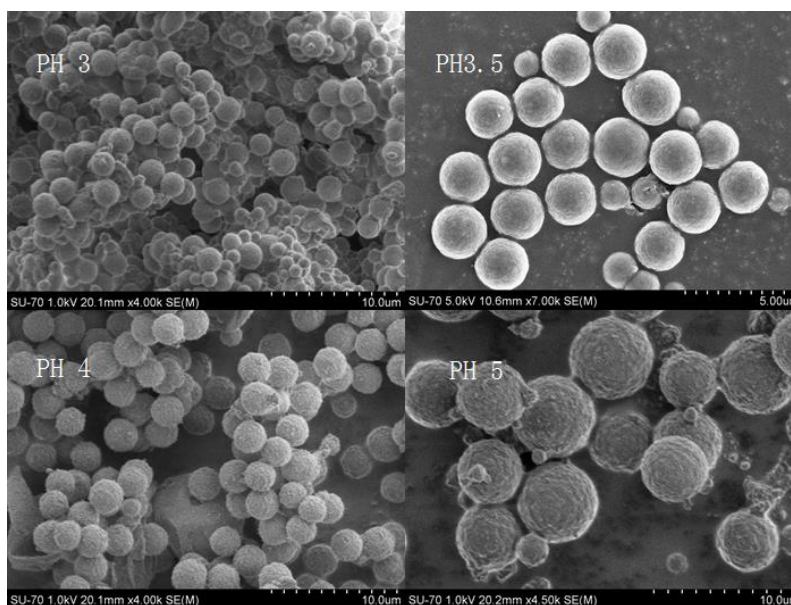


Figure 2: The SEM images of epoxy/MF microcapsules synthesized at different pH values (emulsifier: SDBS+PVA, reaction time: 1hr)

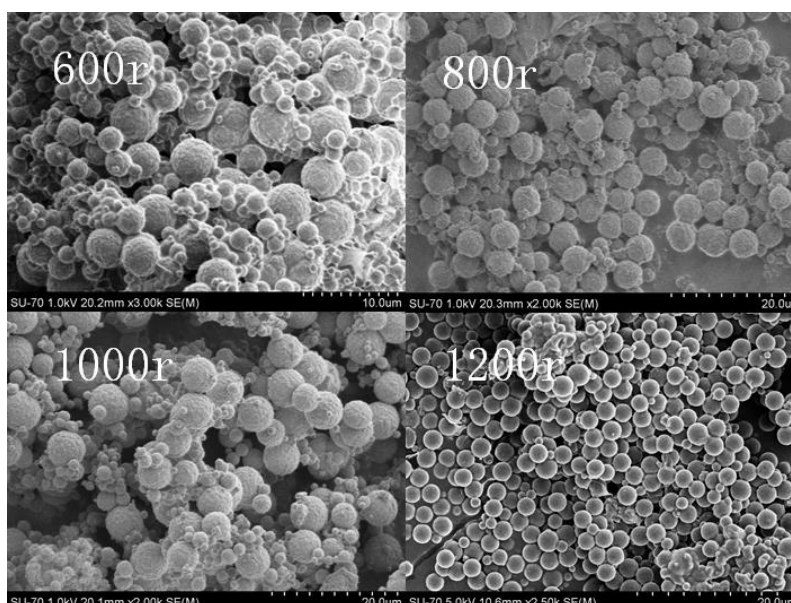


Figure 3: the SEM images of epoxy/MF microcapsules synthesized at different number of agitator per min (emulsifier: SDBS+PVA, reaction time: 1hr, pH value: 3.5)

3.4 Morphological analysis of epoxy/MF microcapsules

Based on the experiments described above, one of the optimal process to obtain mono-sized epoxy/MF microcapsules can be summarized as follows: adding melamine, formaldehyde and water (molar ratio 1:6.3:105) to a three neck flask equipped with stirrer, thermometer and acidimeter, adjusting pH to 9 by 0.1M NaOH solution, heating to 70°C at 2°C/min and keep at that temperature for 10min to obtain MF prepolymer, then dissolving 4g SDBS into 100ml water in a beaker, adding 10g epoxy E-51 as core materials, stirred for 10min to emulsify, then mixed with the MF prepolymer, decreasing pH value to 3.5 by 4wt% citric acid dropwise, pump-injected 100ml 4wt% PVA solution at rate of 3.3ml/min while raising the temperature again to 70°C and keep for 1hr. After standing for 24h, white epoxy/MF microcapsule powders were obtained.

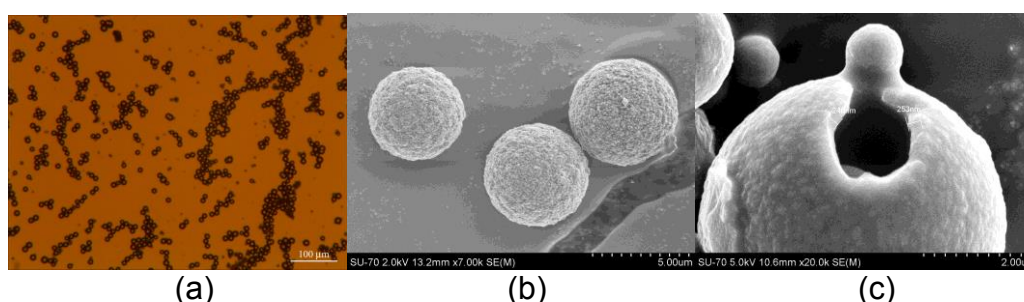


Figure 4: the image of epoxy E-51/MF microcapsules under (a) optical microscopy, (b) and (c) SEM.

Fig. 4 shows the image of the products. It's clear that the shape of microcapsule is perfect sphere. The particle diameters are narrowly centered on 5µm and the shell is

smooth with thickness about 0.2 μ m. Calculation tells us the efficiency of core encapsulation is about 92% and epoxy core content of a microcapsule is about 64%.

3.5 characterization of the epoxy/MF microcapsule

FTIR analysis shows, the spectrum of microcapsules is same with that of pure MF resin, no epoxy absorption peak found, indicating all of the epoxy core materials was successfully encapsulated. TG analysis tells us, the microcapsule pyrolysis goes through 4 stages in turn: (1) lost 2wt% adsorbed water under 100 $^{\circ}$ C, (2) Removal of formaldehyde from MF shell at 173.28 $^{\circ}$ C, (3) epoxy E-51 decomposed at 245.98 $^{\circ}$ C, (4) MF shell decomposed at 370.87 $^{\circ}$ C.

4. CONCLUSION

Monosized epoxy E-51/MF microcapsules can be prepared in the emulsion employing right amount of PVA as co-emulsifier. With cooperation of PVA, the shape, size and surface roughness of microcapsules can be easily controlled by changing emulsifying agents or adjusting agitation rate, pH value and reaction time. In an optimal condition, the microcapsules obtained are dispersed and almost monosized. The shape is perfect sphere. However, it should be noted that the particle size is usually less than 10 μ m. That's too small for application in self-healing concrete. So further work is needed.

ACKNOWLEDGEMENTS

Financial support from the NSFC (Project No. 51120185002 and No. 50925829) is gratefully acknowledged.

SELF-ENCAPSULATION OF EPOXY RESIN BY A CONTROLLED INTERFACE CURING PROCESS IN EPOXY/WATER EMULSION

G. Zhu¹, Y. Zhou¹, Z. Wu¹, J. Tang¹, B. Dong², N. Han² and F. Xing²

¹Shenzhen Key Laboratory of Special Functional Materials, College of Materials Science and Engineering, Shenzhen University, Shenzhen 518060, PR China-E-mail: gzhu@szu.edu.cn; tjn@szu.edu.cn;

²Department of Civil Engineering, Guangdong Provincial Key Laboratory of Durability for Marine Civil Engineering, Shenzhen University, Shenzhen 518060, PR China

Keywords: microcapsule, epoxy, self-healing, emulsion

ABSTRACT

The microcapsules of epoxy E-51 resin encapsulated by cured itself were prepared by interfacial curing reaction, in which ethylenediamine (EDA) was employed as curing agent and sulfonated copolymer of styrene and maleic anhydride (SMA) as emulsifying agent. It's found the morphology of microcapsules strongly depend on reaction time and EDA dosage. Usually, the microcapsules were formed in 20mins, Extension of the time doesn't change the morphology but thicken the shell and strengthen the microcapsules. Large dose of EDA bring about smooth surface of microcapsules. It's believed that this simple process to fabricate epoxy microcapsules is more suitable for the application of self healing concrete, because it is ease to be industrialized and can be produced in large scale.

1. INTRODUCTION

Epoxy resin is widely used in concrete as the crack repairing agent, but so far, there are no epoxy microcapsules are commercially available to be embedded in concrete for self healing propose. The reason may be traced to the glutinous attribute of epoxy, as adhesive materials is difficult to be uniformly emulsified and effectively encapsulated, especially in the *in situ* polymerization of urea formaldehyde as wall materials. In this paper, a novel and simple method is developed to prepare epoxy/epoxy microcapsule based on the idea of core materials partially hardened at the o/w emulsion interface by the diffusion of curing agent from aqueous phase to oil phase.

2. MATERIALS AND METHODS

2.1 Materials

Epoxy resin E-51 was industrial reagent and used without further purification. Ethanediamine and acetone were analytical pure reagents purchased from Aladdin-reagent, Shanghai, China. Sulfonated copolymer of styrene and maleic anhydride (SMA, Scripset® 520, AR) was received from Ashlande Inc., USA.

2.2 Preparation of microcapsules

Add 20g epoxy E-51 and 100ml 3wt% SMA solution into a 250-ml three-necked round-bottomed flask with thermometer and mechanical stirred equipment at room temperature. The mixture was then heated to 50°C, and agitated for at least 30mins at 750rpm for emulsification. After that, elevating temperature to 60°C and increasing agitation rate to 300-400rpm, commence the controlled curing reaction by adding EDA dropwise and slowly. After finished, keep stirring at that temperature for 2hr, then cooling and rest for 24hr, skimming off the solution, rinsing the white powder with acetone, then filtered and air-dried for 24 hr.

2.3 Characterization of the microcapsules

The morphology of microcapsules was observed under Hitachi SU-20 SEM, by which the particle diameters and shell thickness were also measured. The thermal stability and thermolysis temperature were determined by TA DSC Q200/TGA Q50 thermal analyser. The chemical composition of microcapsules was confirmed by Nicolet 6700 FTIR Spectrometer in the wave number range from 400 to 4000cm⁻¹.

3. RESULTS AND DISCUSSION

3.1 The effect of EDA dosage

EDA is a commonly-used hydrosoluble curing agent for epoxy. However, unlike normal curing process, EDA molecules can't contact with epoxy directly in epoxy/water emulsion. They are supposed to diffuse through the o/w interface comprised of SMA. So it's deduced the concentration gradient of EDA plays an important role in the progress.

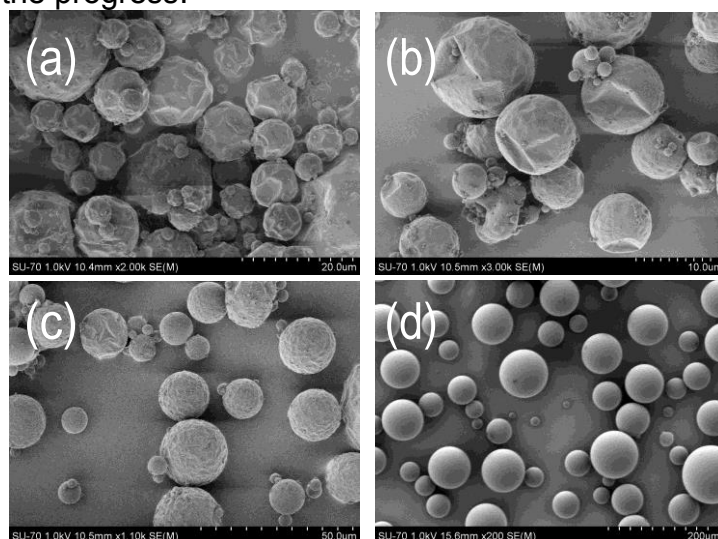


Figure 1: SEM images of the microcapsules synthesized by epoxy reacted for 1hr with different weight ratio of EDA (E-51:EDA): (a) 10:1, (b) 5:1, (c) 4:1, (d) 2:1

Fig.1 clearly shows, with increasing EDA concentration, the microcapsules obtained have better sphericity and more smooth surface. It reveals that small dose of EDA results thin and weak shell, causing the microcapsules were prone to collapse or

crumple in the stirred emulsion. Large dose of EDA not only causes the microcapsules' shell thickened quickly, but also raised the shell's density.

3.2 The effect of reaction time

The shell strength of microcapsules enhanced with curing time. At the beginning, the shell is so thin and soft that was ease to be broken or welded with each other because of collision and convection current, as fig. 1 (a)-(c) shown, but after 20mins, the shell is strong enough to keep its shape.

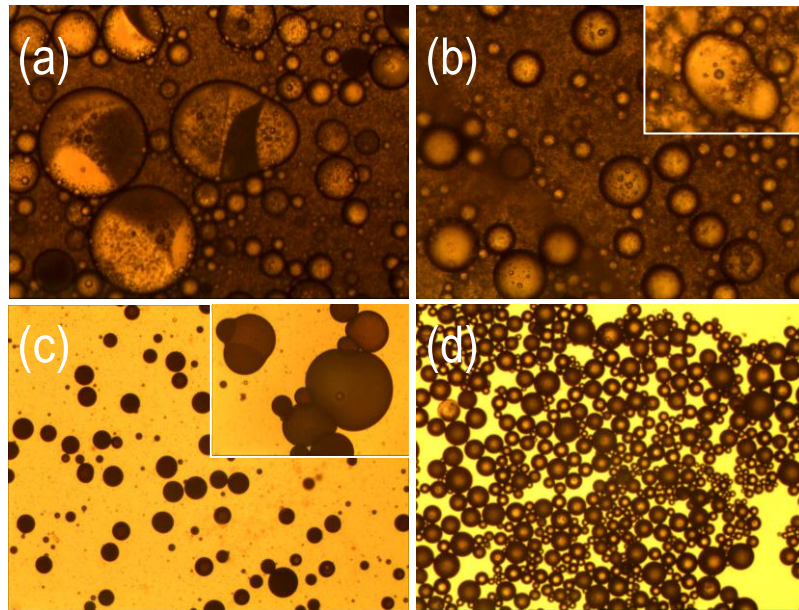


Figure 2: Optical microscope images (100x) of the microcapsules formed at different reaction time (weight ratio of E-51:EDA): (a) 10mins, (b) 15mins, (c) 19mins, (d) 20mins

3.3 Analysis of the microcapsules

Fig.3 shows clearly the shell/core structure of the microcapsule. It has a smooth inner surface, and the shell thickness is $7.78\mu\text{m}$.



Figure 3: SEM images of a broken microcapsule showing its inner structure.

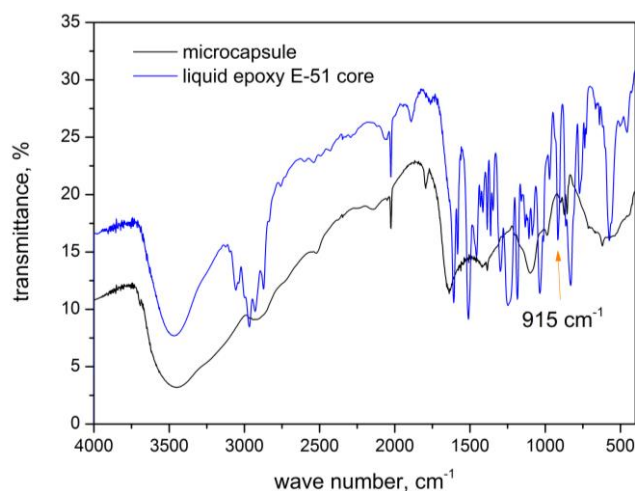


Figure 4: FTIR spectra of epoxy/epoxy microcapsule and the liquid epoxy core.

In FTIR spectrum of microcapsule, the stretching vibration band of epoxy group located at 915cm^{-1} was disappeared, confirmed the shell was composed of completely-cured epoxy E-51 resin.

Thermal analysis indicates the epoxy/epoxy microcapsule is heat-resistant. The pyrolysis temperature is up to 343.44°C .

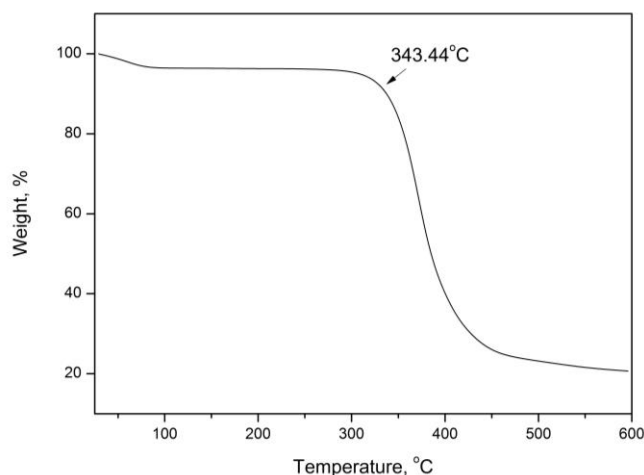


Figure 5: TG curve of epoxy/epoxy microcapsules

4. CONCLUSION

A novel and simple method is developed to prepare epoxy/epoxy microcapsule based on the idea of core materials partially hardened at the o/w emulsion interface by the diffusion of curing agent from aqueous phase to oil phase. The resulting microcapsules are almost consubstantial in shell (solidified epoxy) and core (liquid epoxy), and the size and wall thickness can be adjusted by stirring rate and curing temperature. When weight ratio of EDA to epoxy E-51 is greater than 1:2 and reaction at 60°C lasts over 20mins, the microcapsules obtained will possess perfect spherical shape and smooth surface. We consider this process is easy to be industrialized it's simpler than the traditional *in situ* polymerization methods in which the shell material is different from the epoxy core.

ACKNOWLEDGEMENTS

Financial support from the NSFC (Project No. 51120185002 and No. 50925829) is gratefully acknowledged.

THE EFFECT OF PROCESSING PARAMETERS ON THE FORMATION OF EPOXY/UF RESIN MICROCAPSULES

G. Zhu¹, Z. Wu¹, Y. Zhou¹, J. Tang¹, B. Dong², N. Han², F. Xing²

¹ Shenzhen Key Laboratory of Special Functional Materials, College of Materials Science and Engineering, Shenzhen University, Shenzhen 518060, PR China-E-mail: gzhu@szu.edu.cn; tjn@szu.edu.cn;

² Department of Civil Engineering, Guangdong Provincial Key Laboratory of Durability for Marine Civil Engineering, Shenzhen University, Shenzhen 518060, PR China

Keywords: microcapsule, epoxy, urea formaldehyde resin, self-healing

ABSTRACT

Epoxy E-51/UF resin microcapsules were prepared by traditional two-stepped *in situ* polymerization method and processing parameters affecting the final microcapsules' shape and size were carefully studied in the aim to obtain microcapsule with ideally spherical shape and uniform size. It's found the polycarboxylate surfactant of SMA (styrene-maleic anhydride) is better than the monomolecule sulfate surfactant of SDBS (dodecylbenzenesulphonate) in the emulsification of Epoxy E-51, because the microcapsules from epoxy E-51/SMA emulsion possess good sphericity and clear surface. On the second step of reaction, U/F mole ratio should be controlled in 1.5~2:1 region, and ammonium chloride (NH₄Cl) or m-dihydroxybenzene are strongly recommended to be added to strengthen the shell. For a higher encapsulation ratio, acidification time should be controlled in 2~3h and the end-point pH value of the curing reaction should be controlled at 2~2.5, respectively. The core/shell ratio (weight) is optimal at 2:1 and reaction temperature at 60-65°C.

1. INTRODUCTION

Epoxy encapsulated by urea formaldehyde (UF) resin is a typical repairing agent applied in self-healing concrete. The preparation usually is a traditional *in situ* polymerization process with two steps: first, soluble UF prepolymer forms in an alkaline condition; second, the molecules of UF prepolymer cross-links with each other in an acidic condition to form a hard shell on the emulsified epoxy/water interface. As the polycondensation between urea and formaldehyde is a very complex reaction, so far there are many details on reaction mechanism are still unknown. So it's not surprised that attempts made by many researchers to synthesize epoxy/UF microcapsules with desired shape and size are fail. In order to well understand the formation process and reveal which factor governs microcapsule morphology, the controllable parameters in preparation, such as U/F mole ratio, emulsifying agent, pH value, acidification time, *etc*, were systematically investigated in this paper.

2. MATERIALS AND METHODS

2.1 Materials

Bisphenol A type epoxy resin E-51 was obtained commercially and used without further treatment. Analytically pure urea and 37wt% formaldehyde solution were purchased from Aladdin-reagent, Shanghai, China. Surfactant of SDBS, curing catalyst of ammonium chloride (NH_4Cl), m-dihydroxybenzene (used as chain-extender), triethanolamine and citric acid (both used as pH value regulating agent) were analytical reagents received from Tianjin Chemical Plant, China. SMA (Scripset® 520, AR) were imported from Ashlande Inc., USA.

2.2 Preparation of microcapsules

Urea and formaldehyde solution were mixed in a three-neck flask with U/F mole ratio at 1.5~2:1, adjusting the pH value to 8~9 by triethanolamine. The solution was then heated to 70°C and kept at the temperature for 1h to form UF prepolymer.

Add epoxy E-51, 0.4wt% SMA aqueous solution and 10wt% (of urea) NH_4Cl into a beaker. The mixture was stirred at 800rpm for 20min for emulsification. After cooled to 5°C, the resulting latex was mixed with the UF prepolymer, stirred at 300rpm for 2~3h while regulating pH value at 2.5 by citric acid for acidification. Then elevating the temperature at a very low rate of 1°C/3min to 60°C, commence the curing reaction of UF polymer. After another 2~3h, followed by some post-treatments, such as neutralizing with NaOH, filtering and drying, the final products of E-51/UF microcapsules were obtained.

2.3 Characterization of the microcapsules

The morphology of microcapsules was observed under Keyence VHX-600K stereo optical microscope and Hitachi SU-20 SEM. The thermal stability and thermolysis temperature were determined by TA DSC Q200/TGA Q50 thermal analyser. FTIR analysis was conducted on Nicolet 6700 FTIR Spectrometer.

3. RESULTS AND DISCUSSION

3.1 Effect of surfactants

SMA and SDBS are the two emulsifying agents widely used in the preparation of UF resin walled epoxy microcapsules, but there is an altercation over which one is better. Fig. 1(a) and 1(b) shows the effects on emulsification of epoxy E-51 are almost same. However, the microcapsules obtained from the emulsion emulsified by SMA are more regular in spherical shape and narrower in size distribution. The shells are more compact and smoother, as Fig. 1(c), Fig.1(d) and Fig. 5 shown.

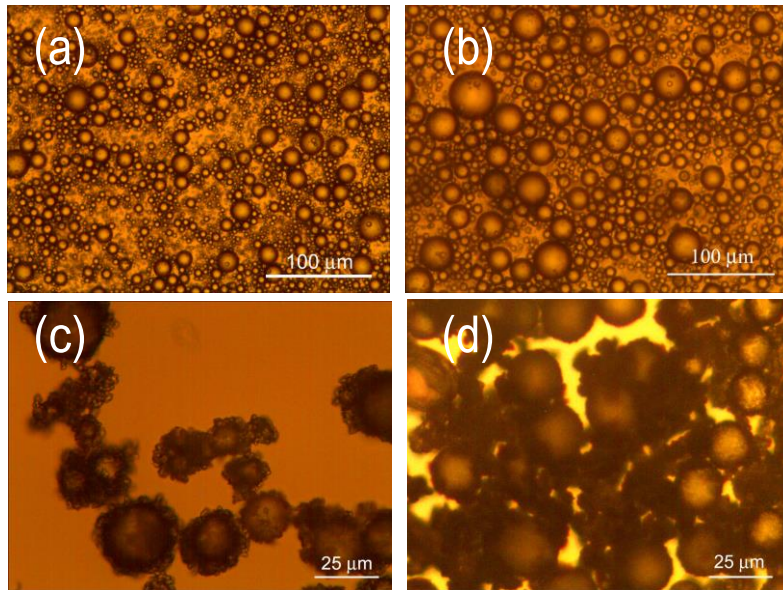


Figure 1: The stereo optical microscope images of epoxy E-51 emulsions [(a) and (b)] and the corresponding microcapsules [(c) and (d)], in which (a) and (c) emulsified by SDBS, (b) and (d) emulsified by SMA.

3.2 Effect of NH_4Cl

Urea reacts with formaldehyde in a complicated way. When the U/F mole ratio locates in 1.5-2:1 region, the UF polymer should be cross-linked, but the degree of crosslinking varies in a large range. In many occasions, the curing process is conducted very slowly, causing the growing microcapsule broken or deformed because the shell is too weak to withstand collision and convection flux. Fig. 2 shows the situation at the very beginning 5mins of the reaction system with U/F mole ratio of 2:1 and pH value of 2.5. It's clear that, the neonatal microcapsule was prone to rupture in flowing solution. It presages the failure of encapsulation or very low encapsulation ratio.

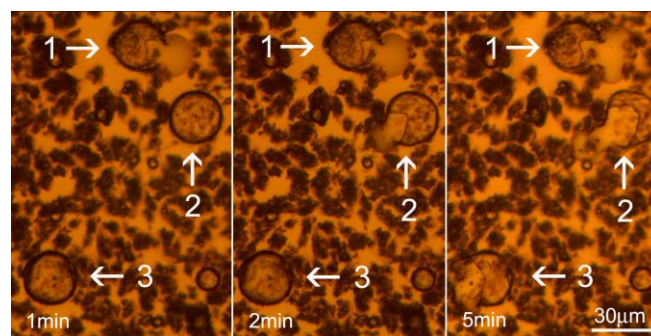


Figure 2: the rupture process of microcapsule shell not strengthened by NH_4Cl

In order to promote the curing reaction, catalyst of NH_4Cl was added. Fig. 3 illustrates the effect. Moreover, the appearance of NH_4Cl changes microcapsule's morphology observably. The microcapsules derived from the reaction with NH_4Cl present a perfect spherical shape and smooth surface (see Fig. 5).

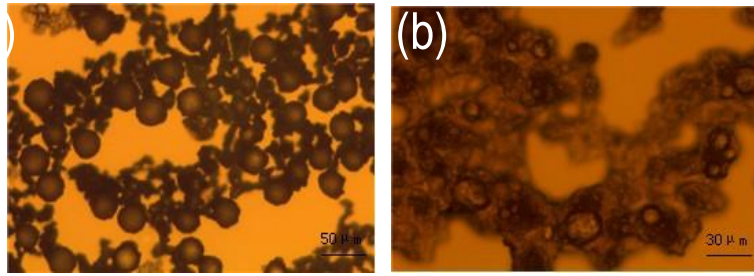


Figure 3: The dried microcapsule powder: (a) with NH_4Cl , (b) without NH_4Cl

3.3 Effect of pH value and acidification time

The formation of epoxy E-51/UF microcapsules is very susceptible to pH value of the reaction end point. At a carefully controlled temperature, a slight fluctuation of pH value will frustrate the encapsulation. In our experiments, the pH value was adjusted or controlled by dilute solution of citric acid added by a precise injection pump.

The acidification time usually should be longer than 1h. Insufficiency in acidification time leads to thin shell of the microcapsules and irregular shape.

As a summary, the optimal processing parameters are as follows:

first step: U/F mole ratio, 1.5-2:1; pH value, 8-9, accurately adjusted by injection of triethanolamine; reaction temperature, 70°C , elevated from room temperature at $1^\circ\text{C}/\text{min}$; reaction time, 1h; agitation rate, 800rpm. The product (UF prepolymer) is transparent viscous solution.

Second step : (1) emulsification of epoxy E-51. core/shell weight ratio, 2:1; emulsifier, 0.4wt% SMA solution + 10wt% (of urea) NH_4Cl ; agitation rate, 800rpm; emulsifying temperature, 45°C ; emulsifying time, 20min; (2) mixture. The emulsion mixed with UF prepolymer solution at 45°C , agitation rate, 300rpm. (3) acidification. pH value, 2.5, accurately adjusted by injection of 0.1M citric acid solution; reaction temperature, 45°C ; reaction time, 2-3h. (4) curing reaction. reaction temperature, 60°C , elevated from 45°C at $1^\circ\text{C}/3\text{min}$, preserved for 2-3h. (5) afterprocessing. neutralized with 0.1M NaOH solution, rinsed with distilled water, filtered, air-dried for 24h.

3.4 Analysis of the microcapsules

On the FTIR spectrum of microcapsule, characteristic peaks of epoxy E-51 in $3000-3100\text{ cm}^{-1}$ and $1600-1450\text{ cm}^{-1}$ become vestigial while peak at 1643 cm^{-1} (allophanyl group) and peak at 3440 cm^{-1} (-NH) are clear indicates epoxy E-51 is enwrapped by UF. The powder has a core/shell structure.

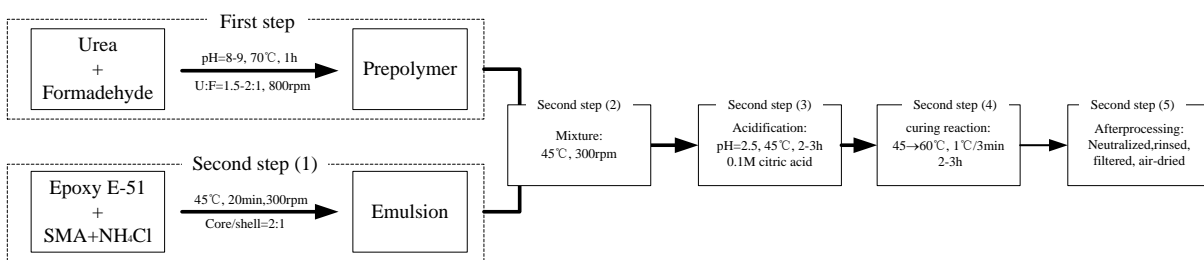


Figure 4: The schematic of the optimal process

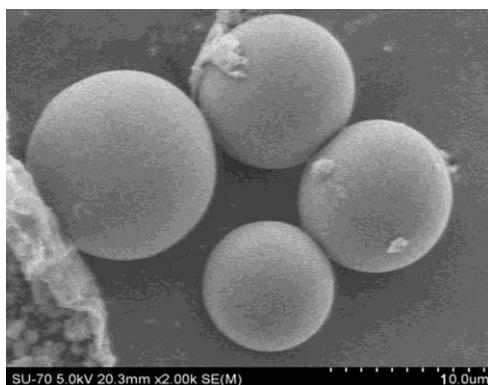


Figure 5: the SEM picture of E-51/UF microcapsules synthesized in optimal process

The TG curve shows, when the microcapsule is heated, epoxy core decomposed at 254.30°C first, then UF shell pyrolyzed at 356.67°C.

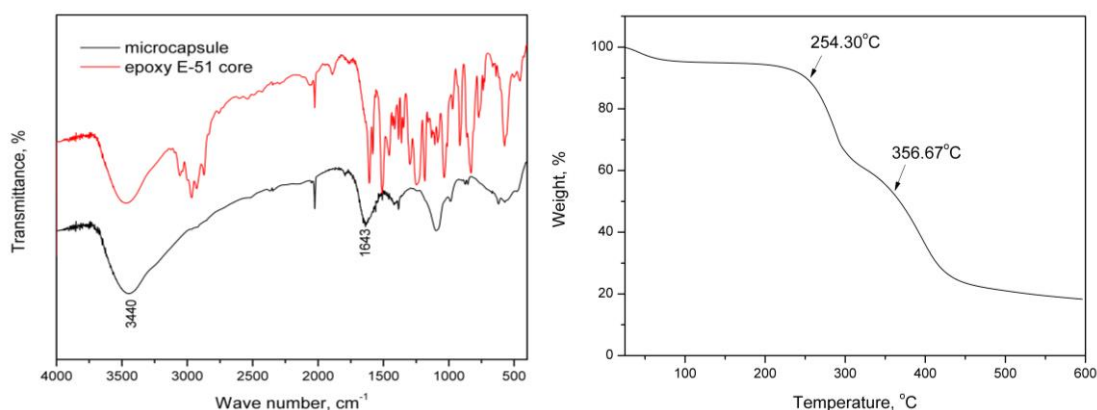


Figure 6: FTIR spectra (left) and TG curve (right) of E-51/UF microcapsules synthesized in optimal process

4. CONCLUSION

Epoxy E-51/UF resin microcapsules were successfully prepared by traditional two-stepped *in situ* polymerization method, and the processing parameters were systematically examined. It's found addition of NH_4Cl promotes the curing reaction greatly and the formation of microcapsule is susceptible to the pH value of the reaction end point. Based on all the experiments, the main processing parameters could be summarized as: pH value at end point controlled at 2.5, acidification time 2-3h, reaction temperature 60 °C, agitation rate 300rpm, U/F mole ratio 1.5-2:1, core/shell weight ratio 2:1.

ACKNOWLEDGEMENTS

Financial support from the NSFC (Project No. 51120185002 and No. 50925829) is gratefully acknowledged.

PRACTICAL APPROACH FOR PRODUCTION OF BACTERIA-BASED AGENT-CONTAINED LIGHT WEIGHT AGGREGATES TO MAKE CONCRETE SELF-HEALING

R.M. Mors¹ and H.M. Jonkers¹

¹ Faculty of Civil Engineering and Geosciences, Materials & Environment section, Delft University of Technology, P.O. Box 5048, 2600 GA Delft, The Netherlands - e-mail: R.M.Mors@tudelft.nl and H.M.Jonkers@tudelft.nl

Keywords: self-healing, concrete, bacteria, agent, LWA

ABSTRACT

A functional experimental concrete system has been developed in our lab, in which a two component bacteria-based healing agent contained in a protective reservoir is included in the concrete mixture. Incorporated bacteria have the potential to produce copious amounts of calcium carbonate based crystals from supplied mineral precursor compounds. Precipitates of the carbonate mineral seal and block occurring cracks. Particles of expanded clay, a type of light weight aggregate (LWA), were chosen as protective reservoir in which the bacteria and precursor compound are contained. Most effective method for intrusion of healing agent in LWA is by vacuum impregnation, a rather expensive process. In this work a more economically feasible in-situ approach is proposed, still gaining the required healing capacity. Prior to mixing LWA are pre-wetted with a warm liquid impregnation solution (80°C) carrying bacterial spores and mineral precursor compounds. This alternative production process is economical and practically more straightforward and functionally additionally beneficial as water-saturated LWA contribute to internal curing. Benefit of the novel approach is the reduced cost of healing agent production and improved practicality directly at a concrete plant, as commonly available equipment can be used. First tests indicate sufficient healing capacity remains after the wet mixing stage and internal drying by cement hydration.

1. INTRODUCTION

Lightweight aggregates (LWA) are used in lightweight concrete structures. Commonly expanded clay aggregates are used. These are also chosen in this research project as LWA to charge with a two component healing agent, consisting of bacteria and nutrients. This 'healing agent' should give the mixture the ability to autonomously block cracks by calcium carbonate production activated by ingress water [1]. In lightweight concrete applications a large fraction of aggregates consists of LWA, therefore a relatively low amount of nutrients need to be included into the LWA to give concrete sufficient healing capacity. Minding ability for in-situ charging of the LWA with commonly available equipment, a method is proposed based on techniques routinely applied in lightweight concrete industry for pre-wetting. In practice often LWA are soaked in water or sprayed for prolonged periods of time until saturation [2]. Saturated particles are necessary when high working pressures are expected, for instance when pumping, to avoid reduction of available water for cement hydration. In other practical cases partial saturation may be sufficient, for instance by supplying absorption water for LWA during the mixing process. Raising

the water temperature can potentially result in more liquid intrusion in LWA [3], helping to evacuate entrapped air in the particles. Another benefit of heating the water for healing agent preparation is that solubility of required bacterial nutrients is higher at elevated temperature, so that concentrations in the intruding liquid are increased. In this case LWA can be soaked in a heated water bath or sprayed with hot nutrient containing liquid before addition to the concrete mixture.

In the EuroLightCon project [4] expanded clay particles have been shown to have different water absorption in wetting state and drying state. The significant hysteresis may have to do with the denser outer shell of the expanded clay particles, creating slow moisture exchange between the inside of LWA and the environment. This inkbottle effect may be beneficial, as the nutrient carrying liquid may remain inside the particles for prolonged period of time, avoiding premature loss to the surrounding cement paste during the mixing stage.

2. MATERIALS AND METHODS

For absorption, expanded clay particles were immersed in warm water saturated with nutrients and suspended bacterial spores. While LWA soak, saturated solution draws into the pores, where nutrients will deposit due to lowered ambient temperature.

In two initial tests 5g LWA (room temperature) were submerged for 15 or 30 minutes in 10mL saturated solution (350g/L calcium lactate) at elevated temperature (80°C), subsequently drained, rinsed 1 minute in a tap water bath (250mL) to remove superficial nutrients and dried in an oven (110°C) or at room temperature. From increase in mass the amount of nutrients deposited inside LWA could be estimated.

For larger scale tests an induction heated mixer was used (Kenwood KM070 series, Cooking Chef Major). Tap water (1.5L) was heated to 80°C under continuous stirring (22rpm) before nutrients were added (350g/L calcium lactate), bacterial spores were dispersed 2 minutes before LWA (1-4mm) were added (2kg). LWA were immersed for 30 minutes, drained and applied wet in the mortar mixture. A 5 gram sample was rinsed in 250mL of tap water for 2 minutes and dried at room temperature for determination of amount of healing agent accumulated inside the LWA.

Mortar prisms were made in triplicate according to the procedure by Wiktor and Jonkers [1], using plain LWA, soaked LWA and two types of vacuum treated LWA. Both types of vacuum treatments were with nutrients according to previous tests [1], but in one case the LWA have been subsequently vacuum impregnated with water and oven dried (110°C) before use. In all cases LWA were wetted before use in the mortar mixture. Furthermore, to test potential effect of LWA-leached calcium lactate on compressive strength, mortar cubes were prepared with varying amounts of calcium lactate. Calcium lactate was dissolved in the mixing water at different ratios by weight of cement (0%, 0.5%, 1%, 4%). Compressive strength tests were executed following European standards (NEN-EN 196-1).

3. RESULTS AND DISCUSSION

After drying, samples of expanded clay showed a mass increase of 6% by weight of LWA for 1 minute rinsing, either dried in the oven or in lab air, and 3.5% wt. for 2 minute rinsing. Content of nutrients is expected to be 3.5-6% by weight of LWA when it is applied to the concrete mixture, which is approximately equal to 3-5%wt. cement.

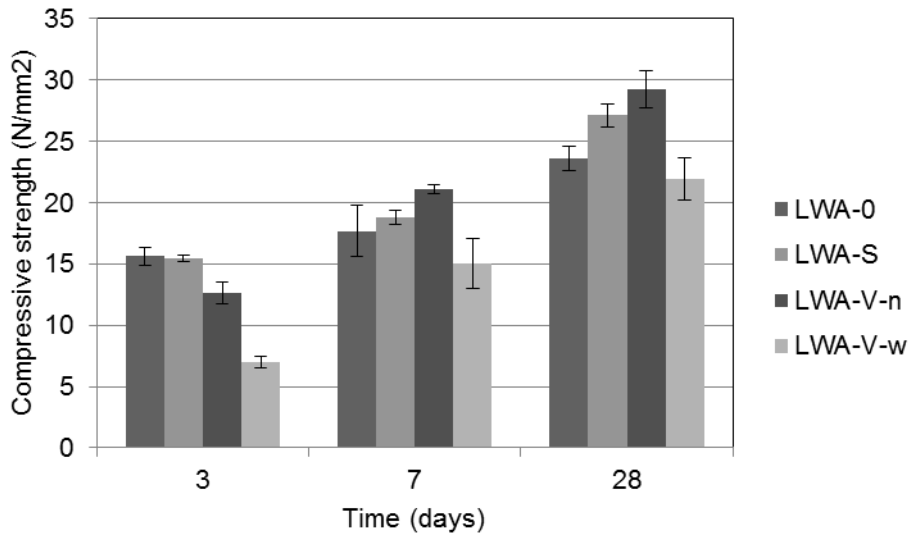


Figure 1: Compressive strength mortars with LWA; 0 = control, S = soaked, V-n = vacuum only nutrients, V-w = vacuum also with water.

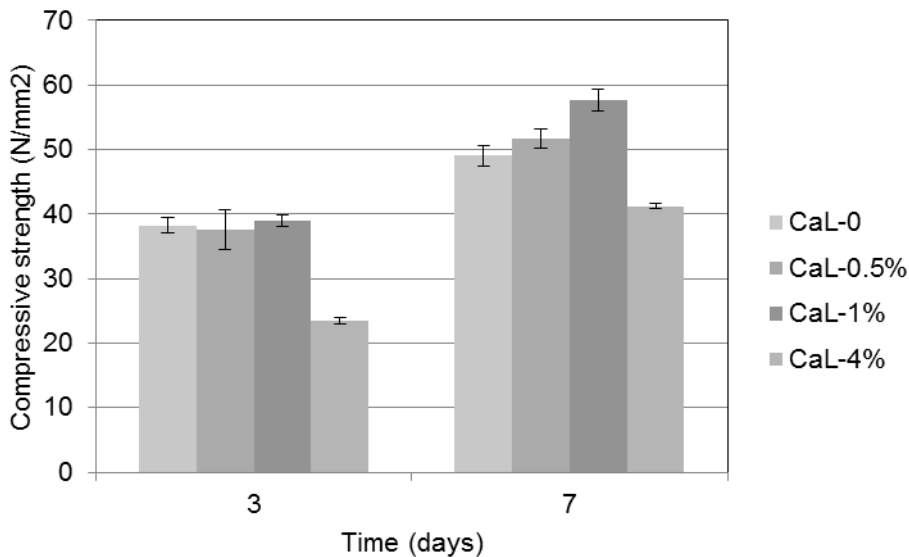


Figure 2: Compressive strength mortars with calcium lactate (%wt. cement).

In case of the oven dried LWA sample, the surface was found notably white of colour, indicating deposition of calcium lactate on LWA surface. This effect was expected, since the solubility is higher at elevated temperature. Calcium lactate was apparently transported with the water, out of the pores during the drying stage, leaving calcium lactate at the surface upon evaporation of the water. In case of drying at room temperature the content of nutrients was the same as the oven dried sample, while the LWA still showed dark colour. Here it is expected that the calcium lactate remained mostly inside the pores, rather than being deposited on the surface. Nutrients at the surface can easily disperse in mixing water. Superficial nutrients are also expected for LWA that have been vacuum impregnated and dried at elevated temperature (LWA-V-w) before use in the concrete mixture. Compressive strength results for specimens made with these LWA show quite different strength development, indicating substantial nutrient loss (Figure 1), since similar decrease in strength is also seen for addition of nutrients at 4%wt. cement (Figure 2).

Internal curing is a process in which water is drawn out of the saturated LWA when cement hydration proceeds [5]. Release of water plus nutrients is also expected for LWA containing healing agent constituents, being embedded in setting concrete. For internal drying, again temperature difference is expected beneficial. Assuming isothermal conditions for lightweight concrete hardening, temperatures are equal to surrounding atmosphere. When applying LWA wet, solubility at a given temperature is expected to be the maximum to be released when the water is drawn from LWA by capillary action. Given a temperature of the saturated solution of 80°C (350g/L) and an atmosphere of 20°C (80g/L), a theoretical nutrient loss of 80/350 is expected during hydration, which is 1/4-1/5 of the total charge. Indication for this shows by comparing compressive strength results in figure 1 and 2. Compressive strength results indeed show relation to an expected loss of nutrients between 0.5 and 1%wt. cement. Still, significance of nutrient loss should be confirmed in future experiments. Although some loss of nutrients from impregnated LWA occurred during the concrete mixing, sufficient amounts seem to remain to serve as healing agent. In practical cases it can be thought of using a heated water bath, instead of a mixer. An alternative pre-wetting process may be to spray appropriate amounts of heated saturated solution onto the LWA in the concrete mixer, before adding the remaining concrete constituents. Since pre-wetting time is limited, the methods proposed may not be appropriate for pumping purposes. For latter application, alternatives may still be vacuum treatment or thermal treatment at the LWA plant.

4. CONCLUSIONS

Practical methods for healing agent preparation for application at the full scale are being considered. The objective is to increase the healing agent production while making use of commonly available equipment. One option is to impregnate larger quantities of LWA with healing agent constituents on-site. Proposed is a method in which dry LWA are immersed in a saturated solution of constituents at elevated temperature, before addition to the concrete mixture. First results indicate that sufficient nutrients remain in the LWA for healing purposes after wet mixing and subsequent concrete setting.

ACKNOWLEDGEMENTS

Financial support from Agentschap NL (grant IOP-SHM01018) for this work is gratefully acknowledged.

REFERENCES

- [1] V. Wiktor, H.M. Jonkers, Quantification of crack-healing in novel bacteria-based self-healing concrete, *Cement and Concrete Composites* 33(7) (2011) 763-770.
- [2] ACI 213R-03, Reported by ACI Committee 213, Guide for Structural Lightweight-Aggregate Concrete, ACI, 2003.
- [3] O.M. Jensen, P. Lura, Techniques and materials for internal water curing of concrete, *Materials and Structures* 39(9) (2006) 817-825.
- [4] CUR H82R20, The effect of the moisture history on the water absorption of lightweight aggregates, ISBN 90 376 0168 5, 2000, 21p.
- [5] P. Lura, Autogenous deformation and internal curing of concrete, Ph.D. thesis, Delft University of Technology, Delft, The Netherlands, 2003.

BACTERIA-BASED SELF-HEALING CONCRETE FOR APPLICATION IN THE MARINE ENVIRONMENT

D. Palin¹, V. Wiktor¹ and H. M. Jonkers¹

¹ Delft University of Technology, Faculty of Civil Engineering & Geosciences, Section of Materials and Environment, Microlab, Stevinweg 1, 2628 CN Delft, The Netherlands – e-mail: d.palin@tudelft.nl

Keywords: Bacteria, self-healing, marine environment, concrete, cracks

ABSTRACT

Marine concrete structures are exposed to one of the most hostile of natural environments. Many physical and chemical phenomena are usually interdependent and mutually reinforcing in the deterioration of marine exposed concrete: expansion and microcracking due to physical effects increases concrete permeability paving the way for harmful chemical interactions between seawater, concrete and embedded steel reinforcement. Early research in self-healing concrete has focused on the autogenous ability of hydrates to heal cracks over time, this form of healing is however restricted to early and small cross sectional crack width reductions, while limited research is available on the autogenous healing of concrete incorporating GBFS (Ground blast furnace slag). A novel approach to self-heal concrete is a bio-inspired technique, where bacteria immobilized in the concrete are activated through crack induced water ingress, forming a mineral healing precipitate [1]. The current study characterises the autogenous healing of blast furnace slag cement (CEM III/B 42.5 N) mortar cubes submerged in both fresh- and synthetic sea- water, as the first step towards developing a bacteria-based self-healing concrete for application in the marine environment.

Compression tests of the mortar cubes showed their strength to be in good agreement with the Norm EN 196-1 [2]. ESEM analysis of the specimens after 54 days submersion revealed two distinctive surface crystal morphologies. Specimens submerged in fresh water displayed rhomboidal surface crystals 10 µm thick, while those specimens submerged in synthetic seawater were covered in a 50 µm carpet of spicules. EDS analysis showed the mineral to be calcium based, suggests the presence of two calcium carbonate polymorphs. FT-IR analysis of the surface precipitates supported observations made by ESEM, as those specimens submerged in fresh- and synthetic sea- water displayed spectra indicative of two calcium carbonate polymorphs, calcite and aragonite respectively. This research provides a valuable reference from where an improved bacteria-based system can later be developed for combating crack-induced deterioration of concrete in the marine environment.

1. INTRODUCTION

Many physical and chemical phenomena are usually interdependent and mutually reinforcing in the deterioration of marine exposed concrete: expansion and microcracking due to physical effects increases concrete permeability paving the way for deleterious chemical interactions between seawater, concrete and embedded

steel reinforcement. Hydraulic minerals such as GBFS are used in the construction of marine concrete structures, as they decrease the pore structure of the concrete slowing chemical ingress. Early research in self-healing concrete has focused on the autogenous ability of hydrates to heal cracks over time, this form of healing is however restricted to early and small cross sectional crack width reductions, while limited information is available on the autogenous healing ability of concrete incorporating GBFS. In this study we have characterised the autogenous healing ability of blast furnace slag cement (CEM III/B 42.5 N) mortar cubes submerged in both fresh water and synthetic seawater (from here on called sea water). This work represents a reference on the way to developing a bacteria-based self-healing concrete for application in the marine environment.

2. MATERIALS

Blast furnace slag cement (CEM III/B 42.5 N LH)(ENCI, The Netherlands) mortar cubes (4 x 4 x 4 cm) were cast with aggregates up to 2 mm in accordance with the European standard EN 196-1 [2]. Tap water and technical grade chemicals were used to produce seawater.

3. METHODS

Mortar cubes were cast, carefully demoulded after 24 hours and tightly sealed in plastic bags for a total curing period of 28 days at room temperature. Cured specimens were then submerged in fresh water and seawater, again at room temperature. Submersion water was changed every two weeks. The mortar cubes were air-dried to prevent damage of the surface precipitates and tested for their compressive strength 2, 7, 28, and 84 days after casting. Environmental Scanning Electron Microscope (ESEM) equipped with Energy Dispersive X-ray spectrometer (EDS) were employed to characterise surface precipitates, while Fourier-Transform Infrared (FT-IR) spectroscopy was also used to analyse precipitates scraped from the dry surface of the specimens 54 days after submersion.

4. RESULTS

Compression tests showed the strength of the specimens to be in good agreement with those from the European Standard EN 196-1 [2]. ESEM analysis of the surface mineral precipitates revealed two distinctive crystal morphologies. Specimens submerged in fresh water displayed rhomboidal crystals 10 μm thick (Figure 1A), while those specimens submerged in seawater were covered in a 50 μm billowing layer of spicules (Figure 1B). EDS analysis showed the minerals to be calcium based, which suggests the presence of two calcium carbonate polymorphs. The FT-IR spectra for specimens submerged in fresh water exhibited characteristic bands of calcite (Figure 2A,C and D): C-O asymmetric stretching vibration (ν_3), C-O out of plane bending (ν_2), and C-O planar bending vibration (ν_4) centred at 1400, 872 and 712 cm^{-1} respectively; while for those in seawater the stretching vibration (ν_1) became apparent at 1083 cm^{-1} (Figure 2B) and the vibration (ν_4) has split at 700 and 712 cm^{-1} (Figure 2D), which are indicative of aragonite.

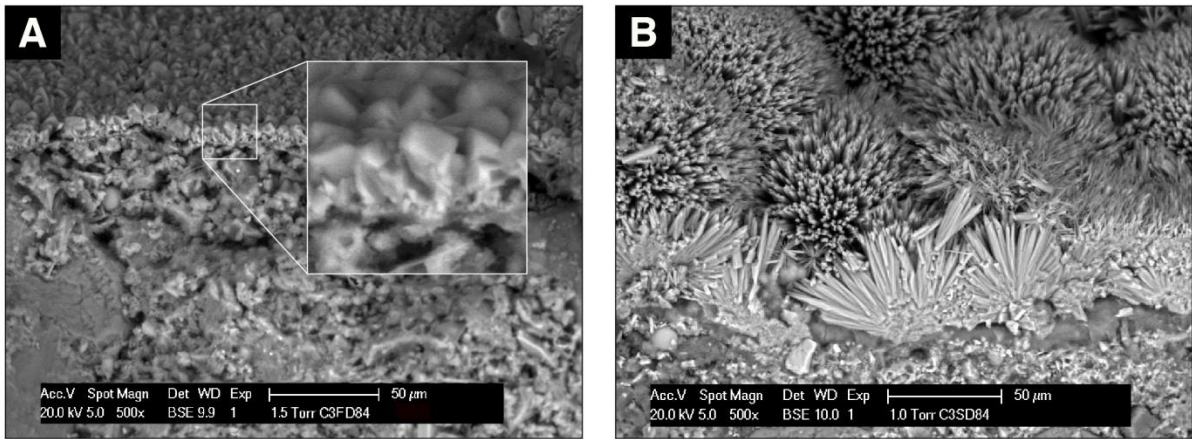


Figure 1: ESEM images showing the respective rhomboidal (A) and spicule (B) surface precipitates of CEM III/B specimens submerged in fresh and sea water.

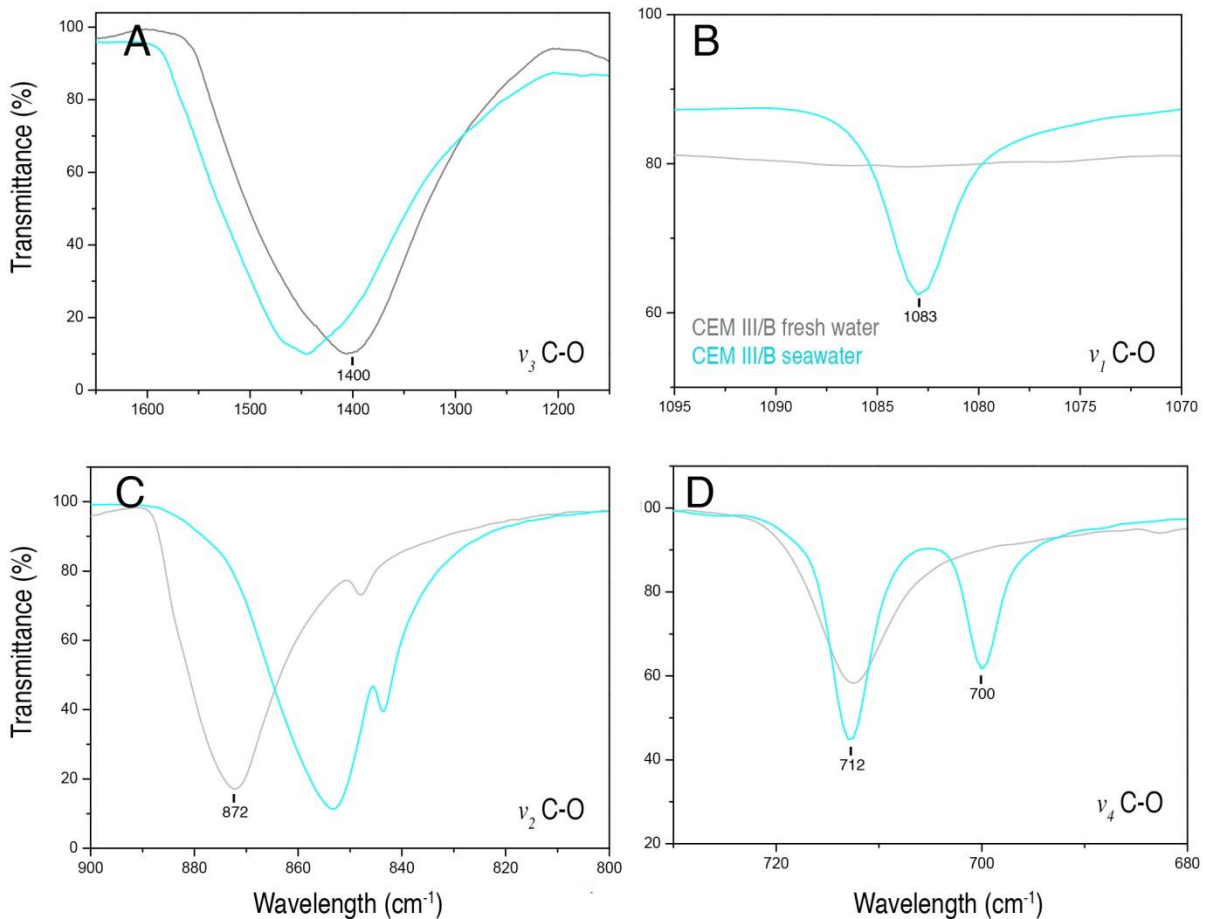


Figure 2: Details of the FT-IR spectra obtained from precipitate produced on the surface of CEM III/B mortar specimens submerged in fresh water are the: C-O asymmetric stretching vibration (ν_3), C-O out of plane bending (ν_2) and C-O planar bending vibration (ν_4) centred at 1400 (A), 872 (C) and 712 (D) cm^{-1} respectively; while the stretching vibration (ν_1) became apparent at 1083 cm^{-1} (B) and the vibration (ν_4) split at 700 and 712 cm^{-1} (D) for those in seawater.

The water-insoluble CaCO_3 observed on the surface of the specimens evolves from a reaction between the calcium ions Ca^{2+} , derived from the concrete and the in-water available carbonates CO_3^{2-} . Whether calcite or aragonite formation develops depends largely on the Mg^{2+} concentration of the solution. Mg^{2+} dissolved in the synthetic seawater is readily adsorbed on to the surface of calcite, inhibiting calcite crystal growth. Dissolved Mg^{2+} is not taken up to any great extent into the aragonite crystal lattice, as a result aragonite crystal growth in seawater is relatively unaffected by the presence of dissolved Mg^{2+} [3]. Variations in precipitate thickness can be explained by the precipitation rate of aragonite to calcite relative to temperature. The experiments presented here were conducted at room temperature and aragonite precipitation rates at $>25^\circ\text{C}$ are much more rapid than those of calcite (up to a factor of 4) [4]. The autogenous healing ability of CEM III/B mortar specimens submerged in fresh- and sea- water has been characterised in terms of the mineral type and amount produced, providing a valuable reference from where an improved bacteria-based system can later be gauged for combating crack induced deterioration of marine concrete.

5. CONCLUSIONS

Specimens submerged in fresh water produced a surface layer of calcite in the order of $10\ \mu\text{m}$, while those submerged in synthetic seawater produced an aragonite layer of $50\ \mu\text{m}$ thick. The difference in polymorph can be attributed to the presence of dissolved Mg^{2+} in the synthetic seawater, which inhibits the more thermodynamically stable calcite, allowing the precipitation of aragonite. The current study has characterised the autogenous healing of blast furnace slag cement mortar cubes submerged in both fresh- and sea- water. This work represents a reference on the way to developing bacteria-based self-healing concrete for application in the marine environment. The next phase will see the design and impregnation of a bacteria-based agent into mortar specimens, with the aim of exerting bacterial control over mineral precipitates for improved healing of concrete in the marine environment.

ACKNOWLEDGEMENTS

We would like to gratefully acknowledged the financial support of the Marie Curie Programme for this work and Mr. Arjan Thijssen for the ESEM images.

REFERENCES

- [1]. H.M. Jonkers, et al., Application of bacteria as self-healing agent for the development of sustainable concrete. *Ecological engineering*, (2010) 36(2): p. 230-235.
- [2] N 196-1, Methods of testing cement – determination of compressive strength (1994).
- [3] R. Berner, The role of magnesium in the crystal growth of calcite and aragonite from sea water. *Geochimica et Cosmochimica Acta*, (1975) 39(4): p. 489-504.
- [4] E.A. Burton, and L.M. Walter, Relative precipitation rates of aragonite and Mg calcite from seawater: Temperature or carbonate ion control? *Geology*, (1987) 15(2): p. 111-114.

BASIC RESEARCH ON THE SELF-HEALING FUNCTIONS OF CONCRETE MIXED WITH FLY ASH

Y. Ishikawa¹

¹ Chigasaki Research Institute, J-Power, 1-9-88 Chigasaki, Chigasaki, Kanagawa, 253-0041 Japan — e-mail : Yoshitaka_Ishikawa@jpower.co.jp

Keywords: fly ash, self-healing, dynamic modulus of elasticity, compression strength, radiographic visualization

ABSTRACT

In recent studies, it has been recognized that concrete deterioration is accelerated by the growth of fine cracks of a few micron meters in width induced by dry shrinkage and/or freezing damage. There have been great expectations for research on concrete that self-heals these fine cracks. Recent research (for example, Taniguchi et al. in the 3rd ISHCM) has developed a "self-healing concrete" which restores the fine cracks due to drying shrinkage and/or freezing damage using fly ash as a mixture material to maintain an intentional hydration reaction inside the concrete for a long period of time. To confirm fly ash's self-healing capacity, we conducted a fundamental test of mortar using fly ash which was deteriorated through an accelerated freeze-thaw cycle until the relative dynamic modulus of elasticity fell to 80% and 60%. The mortar specimens were then cured in water at 40°C and 20°C for 28 days. We have evaluated the self-healing degree of the cured mortar specimens through a strength test, accelerated neutralization test, chloride penetration test, pore size distribution measurement and radiographic visualization. The test results confirmed that fly ash functions effectively as a self-healing material for concrete.

1. INTRODUCTION

There are two main types of techniques for adding self-healing properties to concrete. The first technique is to fill cracks with resin filler, for example. Once resin filler is supplied, cracked open areas are healed by the unreacted filler¹⁾. The second technique is to fill cracks using the hydration reaction of the remaining unreacted components of cement or similar materials. The fact that the pozzolanic reaction of fly ash does not initially occur may possibly give a theoretical advantage to the healing of cracks²⁾. The envisioned self-healing effects take place over a long period of time. In order to apply self-healing concrete to practical usage, however, it is necessary to evaluate its self-healing capabilities in a short period of time before putting in service by conducting various tests such as acceleration tests.

2. MATERIALS AND METHODS

2.1 Overall flow of testing

(1) Two different methods were used to prepare deteriorated test specimens. One was a freeze-thaw method, the other was a compression load method. Under the

compression load method, the degree of deterioration did not advance after repeating a maximum of 10 compressions. This is why we used the freeze-thaw method.

(2) The following tests and measurements were conducted to confirm the self-healing effects of specimens mixed with fly ash. Measurement of the relative dynamic modulus of elasticity, strength test, pore size distribution measurement, accelerated carbonation test, chloride permeability test, and confirmation of healed crack images through radiographic visualization

2.2 Materials used

Mortar specimens (4cm x 4cm x 16cm) were prepared. Table 1 shows the materials used in testing. The fly ash used is a typical type commercially available in Japan as a concrete admixture (Density: 2.23 g/cm³, Blaine specific surface area : 3,670 cm²/g).

Table 1: Materials used

Type	Specifications	Remarks
Cement (C)	Ordinary portland cement	Density: 3.16 g/cm ³
Admixture (FA)	Japanese Industrial Standard, type II fly ash	Density: 2.23 g/cm ³
Fine aggregate (S)	Natural sand from Kakegawa	Density: 2.57 g/cm ³
Water (W)	Public water supply	-

2.3 Mixing conditions

Table 2 shows mortar mixing conditions.

Table 2: Mortar mixing conditions

W/C (%)	FA/(S+FA) Volume (%)	Unit quantity (kg/m ³)				Flow (mm)
		W	C	S	FA	
55.0	10	334	608	1094	105	244

2.4 Specimen preparation and curing conditions

After applying standard curing to specimens at 20°C for 4 weeks, we conducted a few cycles of freeze-thaw testing and created deteriorated specimens, whose relative dynamic modulus elasticity fell to 80% and 60%. After creating deteriorated specimens, we performed curing at the curing temperatures of 20°C and 40°C for curing periods of 1 week, 2 weeks, and 4 weeks. We conducted tests to confirm the properties of the specimens before and after deterioration and after healing.

3. TEST RESULTS

3.1 Relative dynamic modulus of elasticity and strength

For either deterioration degree, the relative dynamic modulus of elasticity and strength tends to recover after post-deterioration curing. The tendency of such recovery is greater at a higher curing temperature and for a lower deterioration degree (60%).

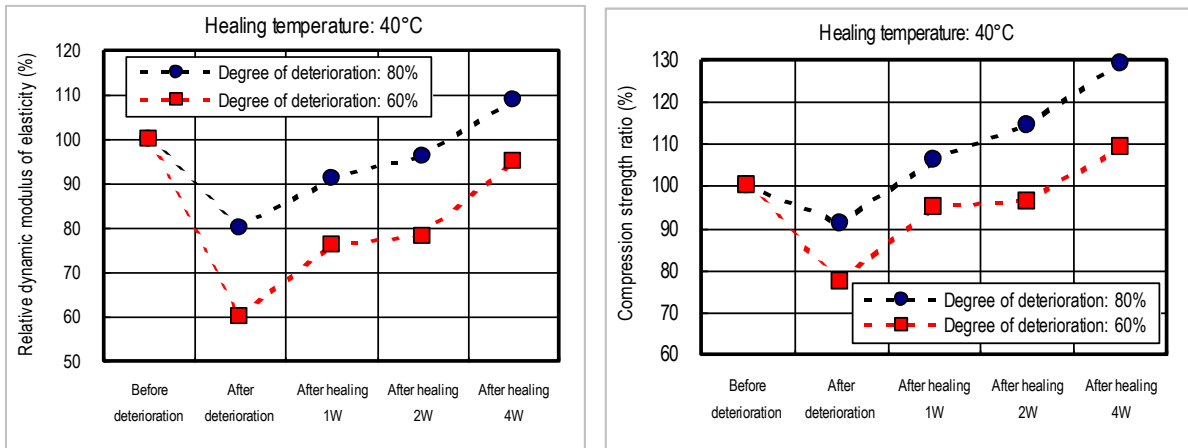


Figure 1: Healing effects in terms of the relative dynamic modulus of elasticity and strength (in case of healing temperature 40°C)

3.2 Confirmation of healing effects by pore size distribution

The peak for the pore diameter of 0.1mm or less shifts toward smaller pore diameters according to the age of the healing material. It was also confirmed that those with a pore diameter of 0.1mm or more were close to pre-deterioration conditions after healing, indicating structural densification.

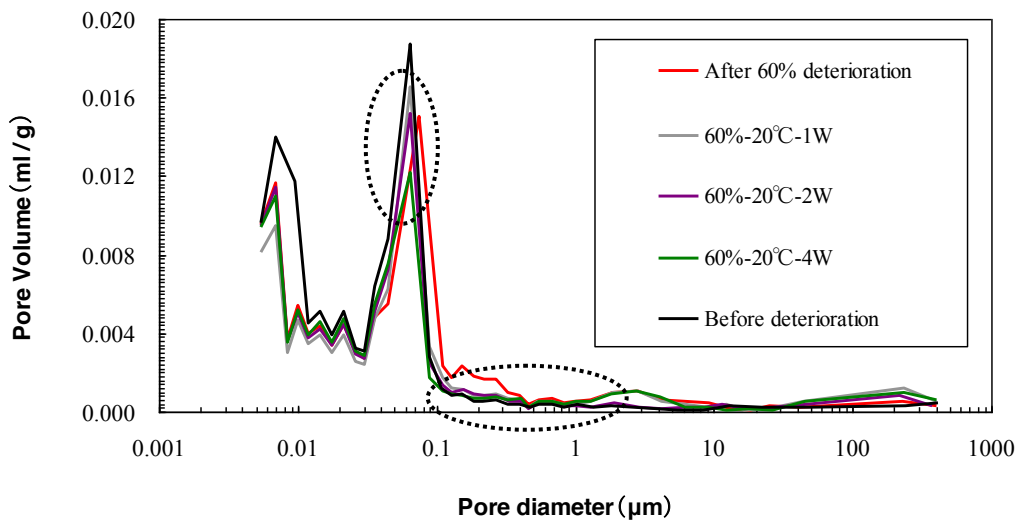


Figure 2: Changes of pore size distribution before and after healing (60% deterioration degree, healing temperature of 20°C)

3.3 Confirmation of healing effects by accelerated carbonation test

The greater the deterioration degree, the faster the carbonation progresses. For either deterioration degree, the carbonation rate coefficient tends to recover after post-deterioration curing. The tendency of such recovery is greater with a higher curing temperature and smaller deterioration degree.

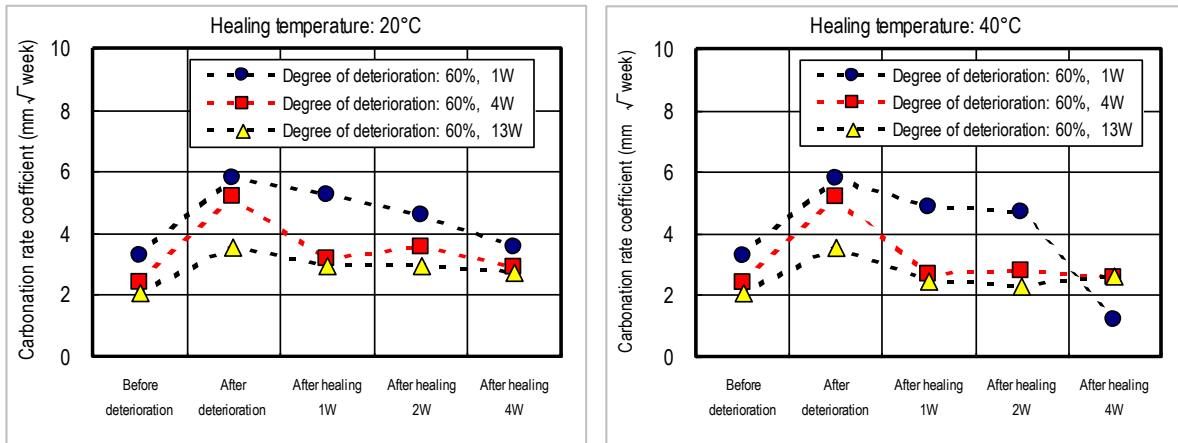


Figure 3: Changes in carbonation rate coefficient (60% deterioration degree)

3.4 Confirmation of healing effects by chloride permeability test

Comparing the chloride ion concentration before and after deterioration, in the place where the depth from the surface is shallow, deterioration does not have significant effects. When the depth exceeds 1cm, chloride ion concentration increases depending on the degree of deterioration. When the depth exceeds 3cm, post-deterioration chloride ion concentration tends to increase. However, the difference between before and after deterioration is not remarkable since the chloride ion concentration value itself is small.

The chloride ion concentration after healing decreases as the healing period gets longer. The healing period has considerable effects on chloride ion concentration when the depth from the surface is up to 2cm.

3.5 Confirmation of healing effects through radiographic visualization test

The observation results of radiographic visualization show clear healing as the healing period gets longer. The 1-week curing case in Photo 1 shows that cracks develop outwardly and in a circle from the center of a specimen and that they are healed as the curing period progresses. Through this experiment, as a result of calculating and digitizing X-ray transmission factors, we confirmed that there is a roughly linear relationship between the X-ray transmission factor and the relative dynamic modulus of elasticity.

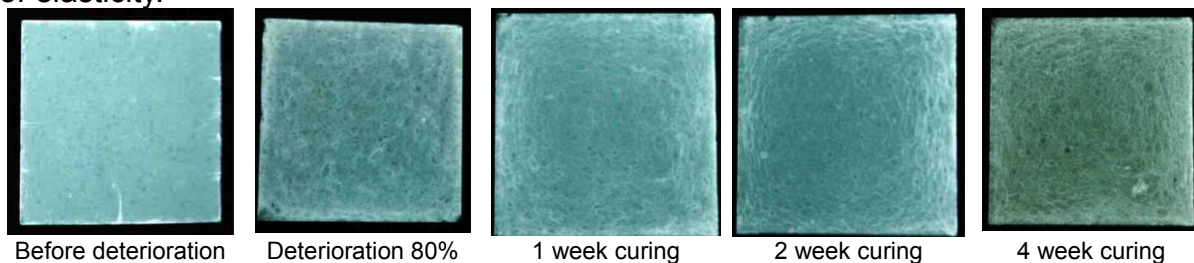


Photo 1: Observation results of radiographic visualization (60% deterioration degree, healing temperature 20°C)

4. CONCLUSION

- (1) We confirmed the self-healing tendency in terms of the relative dynamic modulus of elasticity and strength as a result of post-deterioration healing/curing.
- (2) In the pore size distribution after healing, the peak in segments of pore diameter of 0.1mm or less shifts toward the smaller pore diameter as the healing materials age.
- (3) It was confirmed that the carbonation rate coefficient tends to recover after post-deterioration curing.
- (4) It was confirmed that the chloride ion concentration decreases after post-deterioration curing as the healing period gets longer.
- (5) Based on the observation results of radiographic visualization, we confirmed how cracks are repaired as the healing period gets longer.

ACKNOWLEDGEMENTS

In conducting the tests, we received advice from Professor Yukio Hama of the Muroran Institute of Technology. The observation by radiographic visualization was conducted by Professor Mitsuhiro Takeda of Tohoku Gakuin University.

REFERENCES

- [1] Katsuhata Toshiyuki , Ohhama Yoshihiko and Demura Katsunori, Effect of Polymer-Cement Ratio on Self-Repair Function of Polymer-Modified Mortars Using Epoxy Resins without Hardener, Proceedings of the annual meeting of Architectural Institute of Japan, A-1, July 2000,pp.21-22
- [2] Madoka Taniguchi, Yukio Hama, Osamu Katsura, Takahiro Sagawa and Seung Hyun Na, Self Healing of Frost-damaged Concrete Incorporating Fly Ash, Proceedings of the Third International Conference on Self-Healing Materials, June 2011,pp.48-49

SELF-HEALING MORTAR WITH THERMOPLASTIC POLYMER

L. Bernold¹, and A. Castel¹

¹ *Centre for Infrastructure Engineering and Safety, School of Civil and Environmental Engineering, The University of New South Wales, 2054, Sydney, Australia - e-mail: leonhard.bernold@gmail.com; a.castel@unsw.edu.au.*

Keywords: concrete, thermoplastic polymer, self-healing, cracking, permeability

ABSTRACT

Concrete cracking resulting from mechanical or environmental loading can affect the durability of reinforced concrete structures. In this work the possibility of using thermoplastic polymers to develop a self-healing concrete is investigated. Healing of cracks results from the capacity of thermoplastic polymers to grow together again adding energy by heating the specimens. Several mortars are used in this study including a quantity of thermoplastic polymer ranging between 5 to 15% of the cement mass. Two thermoplastic polymers with softening points of 150°C and 109°C are used.

Mortar mixes with thermoplastic polymer are designed in order to keep a constant workability compared to the reference mortar without thermoplastic polymer. Compressive and tension strength of the mortar are assessed using standard procedures after 28 days. Porosity, water absorption and water permeability of mortars are measured and used as durability criterions.

Two different maximum temperatures below and above the softening points were applied during the heating process in a drying oven. Compressive and tension strength, porosity and water absorption of mortars were measured before and after heating the specimens.

30 mm thick mortar specimens sampled from 50 mm diameter cylinders were used to measure the water permeability. These specimens were cracked (one single crack along the diameter) before starting the heating process. To assess the self-healing capacity of the mortar, permeability was measured before and after cracking and then again after heating the cracked specimens.

Results clearly show the capacity of the mortar for self-healing of cracks if a minimum quantity of thermoplastic polymers of 10% of the cement mass is added in the mix and if the heating temperature is above the polymer softening point. Porosity and water absorption were found lower as well after heating the specimens. With up to 10% of thermoplastic polymers, the mechanical characteristics of the mortar are not modified.

POLYMERIC NANO-MATERIALS FOR CORROSION CONTROL OF STEEL IN CONCRETE

M. Varini¹, D.A. Koleva¹, A.G. Denkova², J.M.C. Mol³, H. Terryn^{3,4}, K. van Breugel¹

¹*Civil Engineering & Geosciences, Materials & Environment, Delft University of Technology, Stevinweg 1, 2628 CN Delft, NL; m.varini@tudelft.nl*

²*Reactor Institute Delft, Delft University of Technology Mekelweg 15, 2629 JB Delft, NL*

³*3mE, Surfaces & Interfaces, Delft University of Technology, Mekelweg 2, 2628CD, Delft, NL*

⁴*Vrije Universiteit Brussel, Electrochemical & Surface Engineering, Pleinlaan 2, B1050, B*

Keywords: concrete, self-healing, corrosion

ABSTRACT

Polymeric nano-materials utilization in reinforced concrete, aiming to deal with steel corrosion was developed in previous works. Promising results were obtained with PEO-*b*-PS nano-formations, both in terms of enhanced bulk matrix properties and improved steel corrosion resistance. Recent research has been focusing on a cheaper and commercially available polymer, Pluronic P123. Pluronic is able to self assemble into micelles and/or vesicles but their sensitivity towards the environmental medium is a drawback: for this reason, a study on Pluronic micelles stability in different solutions has been carried out. A stabilization process against dissociation of micelles was also performed. Both stabilized and non-stabilized micelles were tested in model solutions in terms of their influence on steel corrosion resistance.

1. INTRODUCTION

Steel corrosion in reinforced concrete is a worldwide problem that affects stability and durability of civil structures. Former works developed a novel approach to corrosion control based on nano-formations, able to improve the cement-based bulk matrix characteristics and steel surface properties. The final result was “self-healing” by restoring the environment at the steel/cement paste interface in the event of corrosion. Previously investigated was the addition of PEO₁₁₃-*b*-PS₂₁₈₍₇₆₀₎ micelles and vesicles to plain and reinforced mortar. In their presence (of only 0.006 wt.%), improved bulk matrix properties (reduced permeability, porosity), enhanced chloride binding and “nucleation sites effect” were recorded [1,2]. An improvement was also observed in terms of steel performance in corrosive conditions: electrochemical techniques and surface analysis proved “self-healing” effects on the steel surface in addition to general barrier effects only [2]. Aiming at a cost-effective alternative (PEO-*b*-PS is a high cost material for civil engineering applications), Pluronic P123 formations were recently considered [1], targeting the above discussed superior performance. Pluronic P123 (PEO₂₀ - PPO₇₀ - PEO₂₀) is commercially available and it can self assemble into micelles/vesicles. These are, however, sensitive to ionic strength and chloride content in the medium [1]. Nevertheless, it is possible to tailor their properties in order to gain stability against dissociation and reduce their sensitivity to environmental changes. This paper reports on the stability of Pluronic micelles in model environment and briefly presents preliminary studies on steel electrochemical behaviour in the presence of stabilised and non-stabilised micelles.

2. MATERIALS AND METHODS

Polymeric micelles and stabilization: Aqueous solution of 10 wt% Pluronic P123 (Sigma Aldrich) was prepared by weighting. This stock solution was used to produce a series of 1wt.% and 0.024wt% micelles-containing test solutions with varying pH and Cl-content (pH 3, 5, 7 and 12.7 and 1%, 3.5% and 5% of NaCl). A parallel series of solutions from stabilised micelles were prepared via employing PETA monomer (pentaerythrol tetraacrylate, Sigma Aldrich) as cross-linker, added in a ratio 1:100 according to literature [3]. Polymerization of the cross-linker was achieved with γ radiation; Successful stabilization was proven by Dynamic light scattering (DLS) measurements through dissolving 1 ml of the stabilized solution in 90 ml of ethanol. Except the above test solutions, a series of model pore solutions (cement extract) was produced with analogical micelle concentration, pH and Cl-content variation.

Cement extract and electrochemical set up: Cement extract (CE) was prepared by mixing Ordinary Portland Cement (OPC) CEMI 42.5N and tap water in a ratio of 1 : 1; the suspension was rotated for 24h and then filtered. NaCl was added in 3.5 and 5 wt. % concentration to the CE. Stabilised and non-stabilised micelles (as 1wt.% and 0.024wt%) were added to the CE solutions. Steel corrosion resistance was monitored in these solutions; the difference in behaviour was expected to result from different micelle content, chloride content and possible influence of PETA stabilisation. A general 3-electrode cell arrangement was used, comprising a SCE (saturated calomel electrode) as reference, Ti mesh as counter and the steel plate (low carbon steel St37) of 4 cm² surface area as working electrode. *Impedance spectroscopy* (EIS) was carried out in the frequency range of 50 kHz to 10 mHz by superimposing and AC voltage of 10 mV; *Potential-dynamic polarization* (PDP) was performed in the range of -0.2 to + 1.2 V vs OCP at a scan rate of 0.5 mV/s.

3. RESULTS AND DISCUSSION

DLS measurements were performed on non-stabilized micelles in demi-water and cement extract at varying pH and chloride concentration. For all cases the micelles were added to the relevant solutions in a concentration of 1wt.%. The expected characteristic peak for $PEO_{20}-PPO_{70}-PEO_{20}$ micelles can be clearly observed around 10 nm (Fig.1), which is in agreement with previous reports [1].

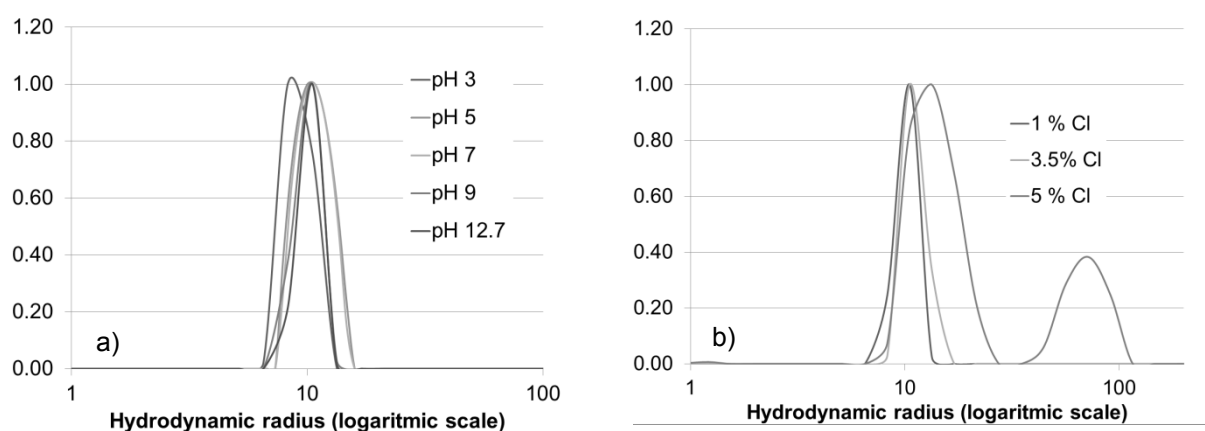


Figure 1: DLS measurements for Pluronic micelles (1%wt) in water at a) different pH and b) at pH 7 and different chloride content

There are no significant modifications of the peaks, as observed within varying pH of the demi-water solutions (Fig.1a). This result was expected to a certain extent since Pluronic is not a pH sensitive polymer [4]. Similar observations hold for the case of CE solutions, despite the complex character and composition of the latter. Non-stabilized micelles were also tested at different pH and chlorides concentrations, since salts are able to modify their properties and therefore to affect the aggregation of PEO-PPO-PEO block copolymers [3]. Chlorides have a “salting – out” effect on the PEO segment (according to the Hoffmeister series, that for this polymer in particular deviates from the original one [5]) and make it “shrink” due to an increase in its hydrophobicity. On the other hand, H^+ and OH^- ions provoke the opposite outcome (although less pronounced [5]), leading to “swelling” of the PEO co-block. The two opposite effects reach balance at more extreme pH (3 and 12.7), while at intermediate values (pH 5 and 7) the influence of chlorides prevails, particularly at the highest concentration (5%), as underlined in the DLS spectrum by a shift of the main peak to higher radius, together with the appearance of a second one (Fig. 1b). The hydrophilic/hydrophobic ratio of the PEO segment is modified due to the pronounced quantity of chlorides in the solution [6] and the micelles tend to transform into a worm – like shape [7]. DLS in CE solutions is an on-going investigation.

Electrochemical tests: $PEO_{20} - PPO_{70} - PEO_{20}$ micelles, both stabilized and not, were added in two different concentrations (1wt.% and 0.024wt%) to CE, containing 3.5wt.% and 5%wt NaCl as corrosion medium.

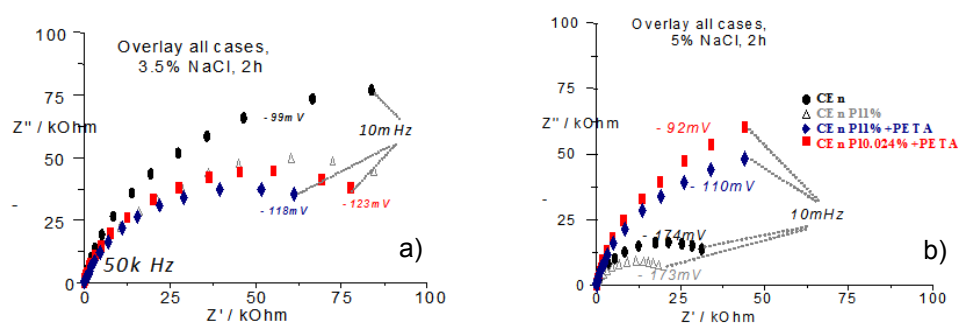


Figure 3: Experimental EIS response (Nyquist) for specimens CE, CE_PL1, CE_Plst1 and CE_Plst0 at a) 3.5 %wt and b) 5% wt chlorides respectively, after 2h of immersion

The steel electrodes were treated (immersed) in the relevant solutions for 2 and 24 h; a series of EIS and PDP measurements were performed in duplicate. The registered OCPs for all specimens show that there was no significant breakdown in steel passivity, since all values were more anodic than -270 mV [8].

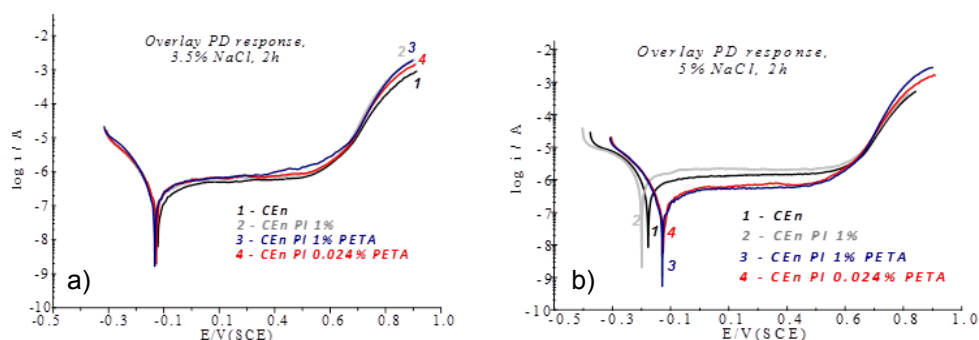


Figure 4: Polarization curves for specimens CE, CE_PL1, CE_PLst1 and CE_PLst0 at a) 3.5%wt and b) 5% wt chlorides respectively, after 2h of immersion

The so far employed Immersion intervals are thus insufficient to claim remarkable variations in corrosion performance and further investigation is on-going. However, even a 2h treatment, results in different behaviour: the EIS response (Fig. 3a) for steel in 3.5wt.% chloride-containing CE and varying micelle concentration did not show any positive effect of the micelles on corrosion resistance. For higher chloride content (5wt.%), the magnitude of impedance increased in the presence of stabilized micelles (Fig.3b), particularly for the cases at lower micelles concentration, whereas the presence of non-stabilised micelles did not improve corrosion resistance. The recorded polarization curves (Fig. 4) support the EIS results: at 3.5 wt.% chloride concentration (Fig.4a) no significant differences were observed. In contrast, steel treated in the 5 wt.% chloride-containing solutions in the presence of both 1 wt% and 0.024wt% stabilised micelles (Fig.4b) showed more anodic corrosion potentials and lower anodic and corrosion current densities, suggesting improvement in steel corrosion performance. The non-stabilised micelles at 1 wt.% did not exert any positive effects.

4. CONCLUSIONS

The Pluronic micelles' behaviour and stability with varying pH and chloride concentration was characterized via DLS analysis. At pH of 7 the effect of chloride prevails, leading to morphological changes. DLS was also employed in order to prove micelles stabilization via cross-linker polymerization. Preliminary electrochemical tests were also performed in cement extract with both stabilized and non stabilized micelles, in order to highlight their possible effect on steel corrosion resistance. The experiments show the positive effect of stabilised micelles. The on-going investigation will clarify the influence of micelle stabilisation and optimum micelle concentration for improved steel electrochemical performance.

REFERENCES

- [1] D. A. Koleva, A. G. Denkova, N. Boshkov, K. van Breugel, Electrochemical performance of steel in cement extract and bulk matrix properties of cement paste in the presence of Pluronic 123 micelles, *J. Mater. Sci.* 48 (2013) 2490 - 2503.
- [2] J. Hu, D. A. Koleva, P. Petrov, K. van Breugel, Polymeric vesicles for corrosion control in reinforced mortar: Electrochemical behaviour, steel surface analysis and bulk matrix properties, *Corrosion Science* 65 (2012) 414 – 430.

- [3] P. Petrov, J. Yuan, K. Yoncheva, A. H. E. Muller, C. B. Tsvetanov, Wormlike Morphology Formation and Stabilization of "Pluronic P123" Micelles by Solubilization of Pentaerythritol Tetraacrylate, *J. Phys. Chem. B* 112 (2008) 8879 – 8883.
- [4] S. Y. Park, Y. Lee, K. Y. Bae, C. Han, T. G. Park, Temperature/pH-Sensitive Hydrogels Prepared from Pluronic Copolymers End-Capped with Carboxylic Acid Groups via an Oligolactide Spacer, *Macromol. Rapid Comm.* 28 (2007) 1172 – 1176.
- [5] Y. Y. Won, A. K. Brannan, H. T. Davis, F. S. Bates, Cryogenic Transmission Electron Microscopy (Cryo-TEM) of Micelles and Vesicles Formed in Water by PEO-Based Block Copolymers, *J. Phys. Chem. B* 106 (2002) 3354 – 3364.
- [6] J. P. Mata, P. R. Majhi, C. Guo, H. Z. Liu, P. Bahadur, Concentration, temperature and salt - induced micellization of a triblock copolymer Pluronic L64 in aqueous media, *Journal of Colloids and Interfaces* 292 (2005) 548 – 556.
- [7] A. G. Denkova, E. Mendes, M. O. Coppens, Non-equilibrium dynamics of block copolymer micelles in solution: recent insights and open questions, *Soft Matter* 6 (2010) 2351 – 2357.
- [8] C. Alonso, M. Castellote, C. Andrade, Chloride threshold dependence of pitting potential of reinforcements, *Electrochim. Acta* 47 (2002) 3469 – 3481.

**SELF-HEALING FIBER-REINFORCED COMPOSITE
MATERIALS**

POSTER SESSION

FLEXIBLE SUPRAMOLECULAR MATRIX BASED SELF-HEALING COMPOSITES

F. Sordo¹, V. Michaud¹

¹ *Laboratory of Polymer and Composite Technology (LTC), Ecole Polytechnique Fédérale de Lausanne (EPFL), CH-1015 Lausanne, Switzerland – e-mail: federica.sordo@epfl.ch; veronique.michaud@epfl.ch*

Keywords: flexible composite, self-healing, supramolecular system, adhesion study, processing

ABSTRACT

Supramolecular polymers gained a great success in the last years as self-healing materials and many different systems have been developed. These polymers combine the advantages of intrinsic and autonomic self-healing systems.

In 2010, Montarnal et al. developed a class of epoxy-based hybrid networks that combine both chemical and supramolecular hydrogen-bonding crosslinks and that are characterized by self-healing properties. These polymers are moreover a priori compatible with composite processing techniques, such as vacuum infusion. For this reason the development of composite materials including the self-healing ability of this type of matrix represent a promising way forward.

In this poster, we will present the development of supramolecular matrix based self-healing composite materials. A supramolecular network with 50% of epoxy crosslinks will be used as matrix material, and glass fibers as reinforcements. In particular, attention will be focused on the set up of the composite processing window, and on the self-healing behavior of the obtained materials themselves as well as at the interface between the matrix and the reinforcement. The latter will be studied through pull-out tests on single fiber model composites.

This PhD research work is part of the SHeMat project "Training Network for Self-Healing Materials: from Concepts to Market", a training and research network funded within the scope of the "Seventh Framework Programme" by the European Commission's "Marie Curie" programme.

1. INTRODUCTION

In 2010 Montarnal *et al.*[1], combined the chemistry of epoxides with supramolecular chemistry, and thus developed an intrinsic hybrid-supramolecular self-healing polymer which network is constituted by both chemical and physical bonds (hydrogen bonds). The aim of this project is to further characterize the self-healing properties of this class of supramolecular polymers and to evaluate their potential as matrices in textile composite materials. The mechanism of interaction of these polymers towards various materials used as reinforcements is analyzed, as well as the possibility of observing healing effects at the interface after fiber debonding.

2. MATERIALS

For this part of the project, the industrial Reverlink HR-NR® produced by Arkema was used as matrix material. The recommended cure cycle is 130°C for 24 hours. The resulting product presents a supramolecular hybrid network composed of 50% of supramolecular hydrogen bonds and 50% of covalent bonds (this composition corresponds to HN-50-HC synthesized by Montarnal *et al.*[1]). A low viscosity epoxy resin (LME 10435, Huntsman) cured for 7 hours at 80°C using a polyamine preparation (LME 10436, Huntsman) as hardener in 100:123 weight ratio, was used to produce a soft epoxy material as material of reference for the interface properties study. 125 µm diameter optical glass fibers (FGN 50/125, Alcatel) were used for the adhesion study. For composite processing, a glass fiber mat and plain glass woven fabric was used.

3. METHODS

The curing process of Reverlink HR-NR® was studied with an AR 2000 ex (TA instruments) rheometer, with 25mm Al parallel plates geometry, using a time sweep method with 1% of applied strain, and 1 Hz.

The sensitivity towards humidity was evaluated by subjecting the material to two different relative humidity environments (22°C-25%RH, climatized room, and 22°C-90%RH obtained using a KNO₃ saturated solution in a dessicator) and measuring the weight percentage of moisture absorption, and in parallel by evaluating the water uptake after samples immersion in distilled water at 23°C (ASTM D570).

The healing properties of Reverlink HR-NR® were evaluated trough tensile tests using a tensile testing machine UTS TestSysteme (Germany) with a 50 N load cell and a constant crosshead displacement rate of 25 mm/min. Dog-bone specimens (ASTM D412) were produced by pouring the liquid unreacted resin in a silicon mold and curing them. The healing of the samples was measured by cutting them with a razor blade in the Gauge length and bringing back the cut surfaces in contact together. The healing efficiency was calculated by comparing the stress at break values of mended samples after different healing times and of virgin samples.

The adhesion properties and the matrix-fiber interface healing behavior after debonding of Reverlink HR-NR® towards glass fibers were evaluated with pull-out tests and SEM analysis. Pull-out samples were realized pouring the resin in cylindrical molds (10mm of diameter and different heights) in which a glass fiber passed through the center and they were tested on a tensile testing machine UTS TestSysteme (Germany) with a 1000 N load cell and a constant crosshead displacement rate of 1 mm/min. While the adhesion properties of the supramolecular polymer were evaluated through a traditional single fiber pull-out test, the healing properties at the interface study was carried out with a partial pull-out of the fiber, followed by a complete pull-out test at different healing times. Pull-out tests using a soft epoxy resin (LME 10435, Huntsman) as polymeric matrix were also performed in order to compare the Reverlink HR-NR® properties. SEM morphological analysis on pull-out specimens was performed using a Philips (FEI) XLF-30 FEG scanning electron microscope. The tensile tests as well as the pull-out tests and the SEM analysis are still in progress. First impregnation trials were performed impregnating 10 layers of glass fiber mat and of glass woven fabrics with Reverlink HR-NR® using a vacuum resin infusion technique (VIP).

4. RESULTS

Figure 1(a) and (b) report the dynamic shear modulus (G' and G'') and the complex viscosity values of Reverlink HR-NR® at 130°C respectively in function of the curing time. The gel time is 194 minutes and the processing window of circa 120 minutes. The same test was performed at different temperatures and using multiple steps curing processes in order to evaluate the best curing process able to reduce the total curing time, maintaining the gel time and processing window values, that are advantageous for a composite processing.

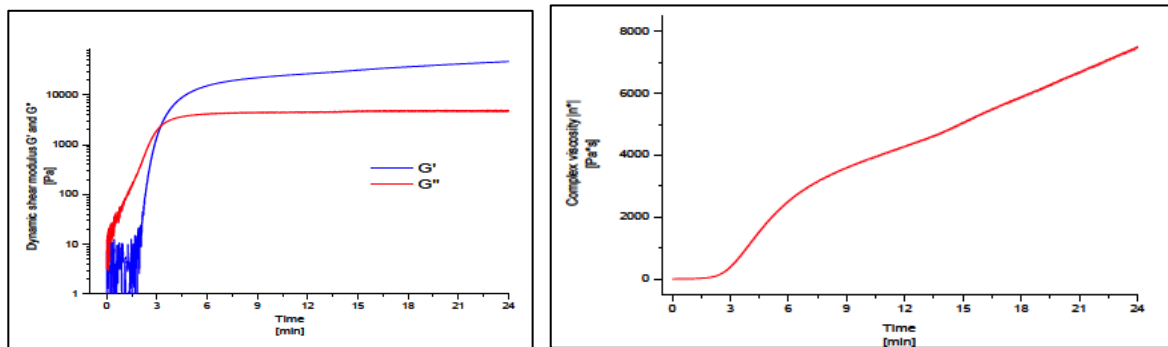


Figure 1 : (a) $\text{Log}G'$ and $\text{Log}G''$ and (b) complex viscosity values in function of curing time at 130°C.

The moisture and water uptake curves reported in Figure 2 show the material sensitivity towards humidity. Consequently it is important to pay attention to the storage conditions as well as at the environmental conditions during tests.

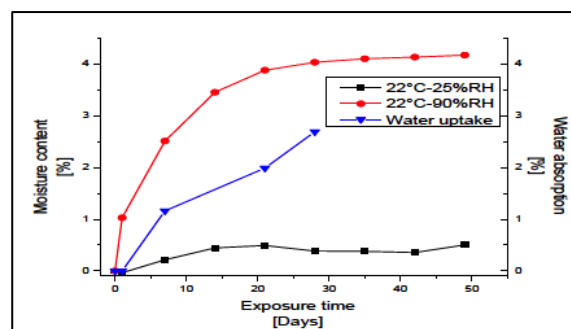


Figure 2: Moisture content and water absorption in weight percentage in function of the exposure time.

Figure 3 presents a SEM image of a pull-out sample. The image clearly shows the good wettability and adhesion of the supramolecular matrix on the glass fiber.

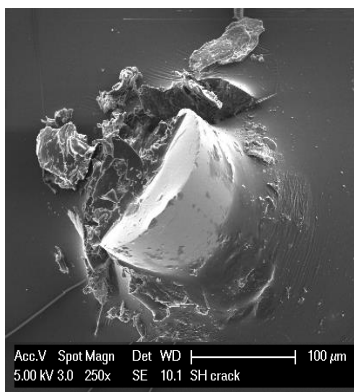


Figure 3 : SEM image of a glass fiber embedded in Reverlink HR-NR®.



Figure 4 : Glass fiber mats impregnated with Reverlink HR-NR®.

Finally, impregnation trials were performed on 10 layers of glass fiber mats and glass woven fabrics using a vacuum infusion technique (VIP). In Figure 4 an example of glass fiber mats impregnated plate is reported, demonstrating the feasibility of the infusion process developed for these materials.

5. CONCLUSIONS

Rheological and vacuum infusion processing analysis showed that Reverlink HR-NR® is a suitable matrix for composite processing, although sensitive to humidity. Self-healing and pull-out tests are still in progress, but from SEM analysis it is possible to already observe a good interaction between the polymeric matrix and glass fiber.

ACKNOWLEDGEMENTS

J.P Disson of Arkema is gratefully acknowledged for providing Reverlink HR-NR® and for technical discussions, as well as F. Tournilhac, L. Leibler and N. Lourero of ESPCI for collaboration.

REFERENCES

[1] D. Montarnal, F. Tournilhac, M. Hidalgo, L. Leibler, Epoxy-based networks combining chemical and supramolecular hydrogen-bonding crosslinks, *Journal of Polymer Science: Part A : Polymer Chemistry* 48 (2010) 1133-1141.

SELF-HEALING OF GFR/ EPOXY COMPOSITE WITH BINARY VASCULAR SYSTEM

S. Vidinejevs, A. Aniskevich

Institute of Polymer Mechanics University of Latvia, 23 Aizkraukles str., Riga, LV-1006, Latvia – e-mail: sergejs.vidinejevs@pmi.lu.lv; andrey.aniskevich@pmi.lu.lv

Keywords: composite, epoxy matrix, self-healing, vascular approach

ABSTRACT

Creation of an ideal self-healing polymer composite material with durable performance could become an alternative to traditional improvement of lightweight constructions. A vascular strategy of the self-healing of the epoxy materials is based on healing agent (HA) delivery to the damage via system of channels formed in the material. The aim of research was to apply the strategy to glass fiber reinforced epoxy composites using binary healing agent and to evaluate its efficiency.

We used a vacuum infusion to make unidirectional laminate specimens laid up from two layers of glass yarns with embedded channels codirectional to reinforcement. The specimens had average size 250×23×1.2 mm. Polytetrafluorethylene tubing (diameter 0.9 mm) was used as preform for channels. Each specimen had 5 channels filled with healing agent — epoxy resin alternated with hardener, and then sealed. These specimens demonstrated the flexural modulus 25.2±2.0 GPa similar within the error to material without channels.

Multiple “local” three-point bending of a specimen was used to cause damage to the matrix and channels across fiber direction. It was performed on the span 20 mm through about each linear 12 mm along specimen. The bending had been terminated when the load decreased by 30 % after reaching a maximum. Released HA components infiltrated into cracks and mixed partially. The triggered self-healing continued 24 h at 50 °C.

Flexural modulus of a specimen was measured in three-point bending on the span 100 mm at a small deflection and was selected as a characteristic of mechanical integrity. Flexural modulus of virgin, damaged, and self-healed specimens was designated as E_v , E_d , E_h , correspondingly. The healing efficiency was evaluated as $\eta = (E_h - E_d) / (E_v - E_d)$ and experimentally ascertained as $\eta \approx 30$ %.

The research results demonstrate the capacity self-healing approach for composite materials.

1. INTRODUCTION

Vascular approach is an important idea for realization of self-healing in epoxy polymers [1, 2]. Self-healing of composites with a vascular system is based on healing agent (HA) delivery to the damage via system of channels formed in the material. The binary system means that resin and hardener are separate components of HA. These components alternate within the channels. The aim of research was to apply the approach to glass fiber reinforced (GFR) epoxy composites and to evaluate its efficiency. In this connection, it was necessary to solve the following tasks:

- to fabricate the self-healing channels which are collinear GFR,
- to evaluate healing efficiency of the composites in consideration of the influence of both retention period of HA and ageing of self-healed specimens.

2. MATERIALS

Series of basic of GFR/ Epoxy Composite plates (250×300 mm) without channels, marked A, and series of the same plates with channels (B, C) were manufactured from Havel Composites CZ s.r.o. commercial products using a vacuum assisted transfer molding. Room temperature curable resin LH289 with hardener H289 (ratio 100:33) was a binder. Two layers of UD glass yarns (500 g/m²) between two restrictive outer layers of plain glass fabric AEROGLOSS (110 g/m²) were manually stacked. In composites B and C, the set of polytetrafluorethylene tubing (external diameter 0.9 mm, TFT20028 Alpha Wire) was located codirectionally to the reinforcement in the middle of the stack. The tubing was used as a removable after curing preform for channels. Specimens, cut out from the plate, had average size 250×23×1.2 mm. In B- and C-specimens, five channels were at a distance of 4 mm from each other. Another epoxy from Nils Malmgren AB, Sweden was used as HA to syringe up the cannels. The recommended stoichiometric proportion of resin 275A to hardener 275B is equal to 100:55 by mass. This ratio is nearer to ideal for alternating channels with HA. The resin with addition of 20 % wt. 4-nonylphenol (Acros Organics) filled up the first channel alternated with hardener filled up the second channel and so on in self-healing C-specimens. Only resin component of HA filled up the channels of reference B-specimens. The filled channels were sealed with epoxy mastic. The C-specimens were kept at room conditions 1- 3 weeks, 2- 3 months, and 5- 6 months before self-healing triggering.

3. METHODS

Method of measuring the mechanical characteristics of the material. Flexural modulus E was selected as a characteristic of mechanical integrity of the material. Load vs. deflection data were measured in three-point bending test at a small deflection (<5 %). All bending experiments were conducted on a Zwick 2.5 universal testing machine with a constant crosshead speed 1.2 mm/min. We calculated E :

$$E = \frac{l^3 \Delta P}{4bh^3 \Delta w} \quad (1)$$

Where $l=100$ mm was the used span, ΔP , b , h , and Δw were the increment of load, the width, the thickness of a specimen, and the increment of deflection, respectively. Specimens had E_{virgin} in the initial state.

Method of damaging of the specimens. The selection of a procedure of doing damage to the C-specimens was essential to start up self-healing and then evaluate healing efficiency. The single local damage [3] triggered effectively self-healing after matrix cracking if a large number of microscopic tubes with HA were presented in a composite. This type of damage could not be acceptable for specimens containing five macroscopic channels. To fracture the matrix across channels direction and release the agents from channels multiple breakages were made through 12 mm along specimen. The breakages were realized using three-point bending loading on the span 20 mm. Each loading had been terminated when the load reached maximum and then dropped for ca. 30 % of this value. The same breakages were

used for reference A- and B-specimens too. Freshly damaged specimens tested on the long span to get $E_{damaged}$.

Method of self-healing. Released HA components infiltrated into cracks then mixed and cured partially thus healing cracks and recovering the stiffness of the C-specimens. These specimens and the reference A- and B-specimens tested two times on the long span to evaluate E_{healed} after repairing in accelerated regime during 24 h at 50 °C and after more than 3 weeks of further ageing at room conditions. A healing efficiency η was defined as a ratio of changes of the modulus [1]

$$\eta = \frac{E_{healed} - E_{damaged}}{E_{virgin} - E_{damaged}} \quad (2)$$

The efficiency value η was determined for both regimes of repairing.

4. RESULTS

The developed procedure for fabrication of the channels using PTFE tubing was approved earlier [4] for epoxy matrix TDCB specimens. The tubing easy combined with vacuum infusion installation to form the channels in GFR/ epoxy composites. Positioned parallel to the unidirectional reinforcement, it was easily and reliably extracted after curing of epoxy resin, without rejects at creation channels. Structural inhomogeneity of a specimen with channels practically did not change its flexural modulus E_{virgin} (Table 1).

Multiple fractures were used to guarantee the matrix cracking. However, both inhomogeneity of damaged specimen and extent of the breakages affected the statistical error of evaluated $E_{damaged}$, E_{healed} , and η . Thus relative error of determination of η for C-specimens reached 25 %. We suppose that the studied self-healing may be attended with 1) the relaxation process which reduces the stresses in the prefracture region and changes the configuration of the crack on the microscopic and submicroscopic levels [5]; 2) continuation of the crosslinking of the macromolecules of matrix. The observed $\eta > 0$ of basic A-specimens and filled with resin B-specimens was due to these processes which were stimulated with elevated temperature at first 24 h of ageing. We believe that HA retained substantially its activity during the storage. Volatility of the value η of C-specimens was of the range equal to η observed for reference A- and B-specimens. We revealed experimentally (Table 1):

- 1) The filled up with HA C-specimens could self-repair to a noticeable degree the matrix thus restore flexural properties of the composite.
- 2) The composite recovery process was continued in time. The efficiency η increased with a further ageing of self-healed specimens.
- 3) There was some reduction of η and further volatility of this value vs. time of storage C-specimens.

Table 1: Flexural modulus and healing efficiency with standard deviations of different series of specimens.

Series of specimens		Number of specimens	E_{virgin} (GPa)	η (%)	
				accelerated regime 24h, 50°C	further ageing >3 weeks, room
A	Without channels	9	24.4±0.6	9±7	10±4
B	Resin in channels	3	25.5±1.6	14±7	15±5
C	HA, kept 1- 3 weeks	13	25.2±2.0	36±6	52±7
	HA, kept 2-3 month	12		22±6	26±7
	HA, kept 5-6 month	6		26±6	32±10

5. CONCLUSIONS

The healing efficiency ca. 30 % was performed experimentally in unidirectional GFR/ epoxy composite using the embedded system of channels with sealed binary healing agent, capable of maintaining the capacity for self-healing for at least six months.

The sequential procedure of flexural damage of the specimen started up partial recovering of the integrity of the composite. The results can be the basis for the use of existing systems of macro-channels in certain composite products for the purposes of self-healing.

ACKNOWLEDGEMENT

The manuscript was prepared within the Project ERDF 2010/0201/2DP/2.1.1.2.0/10/APIA/VIAA/005.

REFERENCES

- [1] B. J. Blaiszik, S. L. Kramer, S. C. Olugebefola, J. S. Moore, N. R. Sottos, S. R. White, Self-Healing Polymers and Composites, Annual Review of Materials Research 40 (2010) 179- 211.
- [2] N. K. Guimard, K. K. Oehlenschlaeger, J. Zhou, S. Hilf, F. G. Schmidt, C. Barner-Kowollik, Current Trends in the Field of Self-Healing Materials, Macromolecular Chemistry and Physics 213 (2012) 131-143.
- [3] J. W. Pang, I. Bond, 'Bleeding composites'—damage detection and self-repair using a biomimetic approach, Composites: Part A 36 (2005) 183- 188.
- [4] S. Vidinejevs, A. Aniskevich, Binary Vascular System in Self-Healing Epoxy Matrix, I. Bond, R. Varley (Eds.), Proceedings of the Third International Conference on Self-Healing Materials, Bath, 2011, p. 139.
- [5] Y. M. Malinskii, V. V. Prokopenko, V. A. Kargin, Investigation of the Self-Healing of Cracks in Polymers. 3. Effect of Medium and Layer Thickness on Self-Healing in Polyvinyl Acetate, Mekhanika Polimerov (1970) 969-972.

Self-Healing of CFRP Composite T-joints

J. Cullinan¹, D. Wass², R. Trask¹ and I. Bond¹

¹ *Advanced Composite Centre for Innovation & Science (ACCIS), Department of Aerospace Engineering, University of Bristol, Bristol, BS8 1TR, United Kingdom – email: Jack.Cullinan@bristol.ac.uk, R.S.Trask@bristol.ac.uk, I.P.Bond@bristol.ac.uk*

² *Wass Research Group, School of Chemistry, University of Bristol, Bristol, BS8 1TS, United Kingdom – email: Duncan.Wass@bristol.ac.uk*

Keywords: Self-Healing, Composite, T-Joint, Vascular, EMAA

ABSTRACT

The effect of the incorporation of self-healing functionality in CFRP composite T-joints has been investigated. Effective self-healing of plain composites using vascular systems and thermoplastic inserts has been demonstrated previously. This work aims to apply these strategies to more complex and industrially relevant composite structures. Three different strategies were examined; vascular networks within the deltoid region, vascular networks within the overlamine region and thermoplastic EMAA inserts placed adjacent to the deltoid. Specimens were loaded under quasi-static and fatigue conditions until damage was incurred, before being healed and re-tested to determine the extent of material recovery.

SELF-HEALING METALLIC AND CERAMIC MATERIALS

POSTER SESSION

A CONCEPTUAL STUDY INTO THE POTENTIAL OF MAX-PHASE CERAMICS FOR SELF-HEALING OF CRACK DAMAGE

A. Farle¹, S. van der Zwaag² and W. G. Sloof¹

¹ Department of Materials Science and Engineering, Delft University of Technology, Mekelweg 2, 2628 CD Delft, The Netherlands – e-mail: A.M.Farle@tudelft.nl; W.G.Sloof@tudelft.nl

² Faculty of Aerospace Engineering, Delft University of Technology, Kluyterweg 1, 2628 HS Delft, The Netherlands – e-mail: S.vanderZwaag@tudelft.nl

Keywords: MAX Phase, crack-healing, high temperature oxidation

ABSTRACT

The reduction of maintenance and replacement work costs is an important driving force in the development of high temperature materials ($T > 800$ °C) that can autonomously heal damage as a result of local cracks. In recent years some potential routes involving the addition of sacrificial particles have been identified, yet these systems have the drawback of reduced initial properties and being capable of healing cracks only once. Hence there is a need for high temperature materials with high initial properties and an ability to heal cracks several times.

Ti₂AlC, being a member of the MAX-Phase ceramics family has shown an unusual ability to heal cracks multiple times through selective oxidation of Al, while maintaining its salient mechanical properties [1]. It is to be expected that other compounds of the M_{n+1}AX_n family, where M is a transition metal, A an element from groups 13 or 14 and X either Carbon or Nitrogen combining characteristics of metals and ceramics, may also show self-healing abilities.

In this work MAX phases known to date (approx. 85) have been evaluated to establish a group of potential compounds expected to be promising applicants of (multiple) crack-healing. To this end, their thermodynamics and material transport at elevated temperatures determining the selective oxidation kinetics and crack filling potential have been considered.

MAX phases with Al and Si are of special interest since the oxides of these A elements have been shown to act successfully as healing agents [2, 3]. While not having been explored, MAX phases which in combination with the oxidation of the M element form a single ternary oxide may also offer attractive self-healing potential.

MAX phases that show an above average potential for self-healing have been identified, in order to guide the experimental research into the wider exploration of MAX phase ceramics for intrinsic high temperature self-healing ceramics.

1. INTRODUCTION

Throughout time materials have been designed and modified in accordance with ‘the damage prevention principle’ [4] meant to delay damage, such as cracks, but not reacting to it. In recent years the research on materials capable of autonomous crack healing has yielded multiple mechanisms, such as addition of sacrificial particles and use of bacteria in concrete. Within the high temperature materials (say >800 °C) a young class of ceramics, the MAX phase ceramics have shown even multiple self-healing potential through selective oxidation. These composites with the nomenclature $M_{n+1}AX_n$, where M is an early transition metal, A an element of the groups IIIA and IVA and X either C and/or N, combine high thermal and electrical conductivity with machinability, corrosion resistance and high stiffness, amongst others.

Based on (multiple) self-healing results achieved with Ti_2AlC a theoretical investigation of further potential compounds is performed to narrow the field of about 85 known MAX phases.

2. POTENTIAL SELF-HEALING MAX PHASES

Generally, healing by selective oxidation relies on the properties of the formed oxide as well as on the reaction kinetics and thermodynamics. Promising healing agents have been shown to be the oxides of the A element, e.g. Al_2O_3 and SiO_2 [1, 5], partially due to higher atom mobility within the layered hexagonal structure.

To limit the scope of the investigation the sum of known compounds is restricted to $M_{n+1}AX_n$ phases with n equals to =1, 2 or 3. No modified compounds such as $Ti_2Al(Si)C$ will be analysed. As the oxidation behaviour of many MAX phase materials has not been investigated yet, thermodynamic and kinetic data is used to evaluate the potential for self-healing such as: Gibbs free energy of oxide formation, atom mobility, coefficient of thermal expansion, etc..

Table 1 : $M_{n+1}AX_n$ (n=1, 2 to 3) Phase Ceramics

MA	Al	Si	Ge	Ga	As	P	S	In	Sn	Tl	Pb	Cd	
Ti	Ti_2AlC Ti_2AlN Ti_3AlC_2 Ti_4AlN_3	Ti_3SiC_2 Ti_4SiC_3 Ti_2SiC Ti_5SiC_4	Ti_2GeC Ti_3GeC_2 Ti_4GeC_3	Ti_2GaC Ti_2GaN Ti_4GaC_3	Ti_2AsC	Ti_2PC	Ti_2SC	Ti_2InC Ti_2InN	Ti_2SnC Ti_3SnC_2 Ti_7SnC_6	Ti_2TlC	Ti_2PbC	Ti_2CdC	25
Cr	Cr_2AlC	Cr_2SiC Cr_3SiC_2	Cr_2GeC	Cr_2GaC Cr_2GaN		Cr_2PC	Cr_2SC						8
V	V_2AlC V_3AlC_2 V_4AlC_3	V_2SiC V_3SiC_2	V_2GeC	V_2GaC V_2GaN	V_2AsC	V_2PC	V_2SC						11
Sc	Sc_2AlC			Sc_2GaC Sc_2GaN				Sc_2InC		Sc_2TlC			5
Nb	Nb_2AlC Nb_4AlC_3	Nb_3SiC_2	Nb_2GeC	Nb_2GaC	Nb_2AsC	Nb_2PC	Nb_2SC	Nb_2InC	Nb_2SnC				10
Mo		Mo_3SiC_2		Mo_2GaC									2
Zr	Zr_2AlC Zr_2AlN	Zr_3SiC_2					Zr_2SC	Zr_2InC Zr_2InN	Zr_2SnC	Zr_2TlC Zr_2TlN	Zr_2PbC		9
Hf	Hf_2AlC Hf_2AlN	Hf_3SiC_2					Hf_2SC	Hf_2InC	Hf_2SnC Hf_2SnN	Hf_2TlC	Hf_2PbC		9
Ta	Ta_2AlC Ta_3AlC_2 Ta_4AlC_3 Ta_6AlC_5	Ta_3SiC_2		Ta_2GaC									6
	19	12	6	12	3	4	6	7	7	5	3	1	85

Firstly, considering future high temperature applications ($T > 800\text{ }^{\circ}\text{C}$), volatile A element oxides can be excluded, such as those of As, P and S with decomposition and boiling temperatures of 315, 173 and $45\text{ }^{\circ}\text{C}$, respectively.

Thermodynamic evaluation of the oxidation sequence is performed by comparison of the Gibbs free energy of oxide formation per mole of O_2 in a temperature interval of 500-1700 K. The healing agent is required to have a lower (more negative) value than the competing M element, to ensure the preferential formation of the A oxide. The Gibbs free energy of formation per mole of O_2 for TiO_2 and its competing A element oxides is shown in

Figure 1. For example the oxidation of TI exhibits much lower reaction energies in the temperature range of 500-1700 K than the formation of TiO_2 , deeming it an unlikely healing agent for Ti containing MAX phases.

The competing oxidation reactions cannot only lead to mixtures (layering) of different oxidation products, but to ternary oxides with possible beneficial attributes. Analysing the Gibbs free energy of oxide formation for possible combinations between the transition metal (M), the A element and oxygen can bear insight into advanced healing agents. An example of such is the ternary oxide ZrSiO_4 , formed between SiO_2 and ZrO_2 .

Furthermore, recovery of initial properties not only depends on the healing agent itself, but on its adhesion to the original matrix. Spallation and stress induced cracking are undesirable effects dependent on lattice orientation and mismatch of thermal expansion coefficients. For example the difference between the thermal expansion coefficient of TiO_2 and that of Ti_2AlC can lead to poor adherence thus reducing the strength recovery [6].

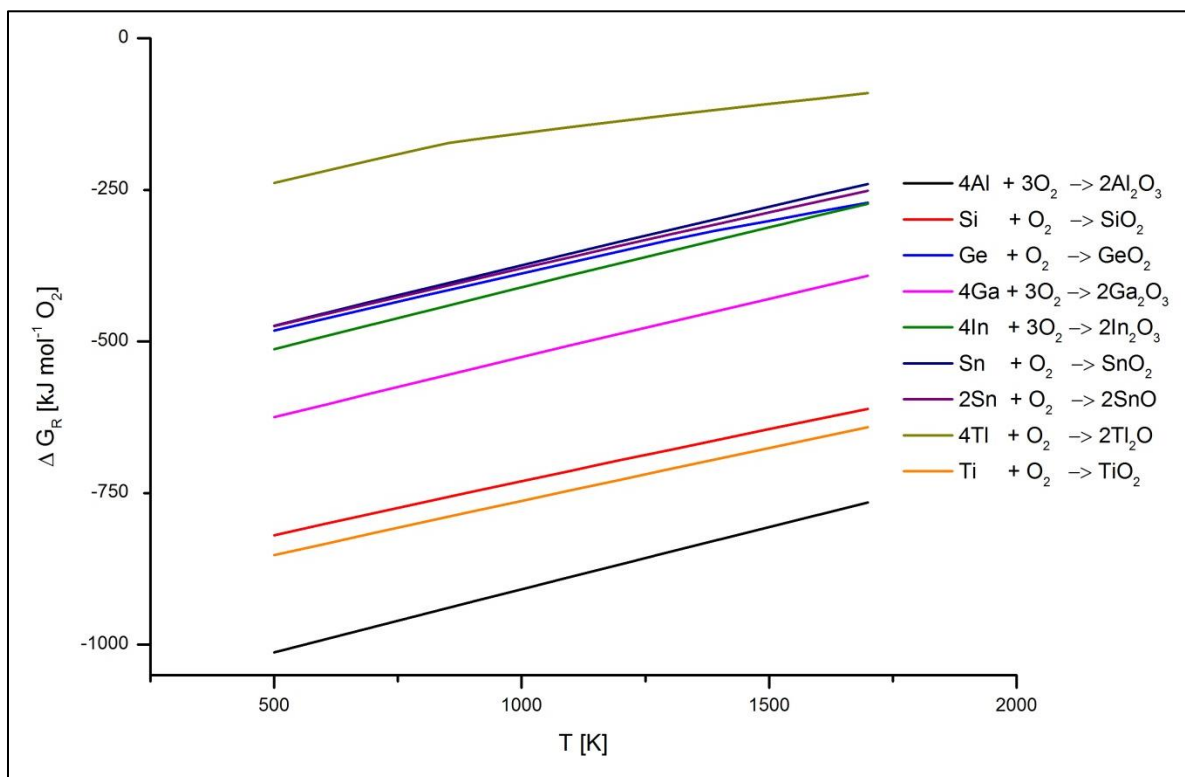


Figure 1 : Gibbs free energy of oxide formation per mole of O_2 for Ti and its associated A group elements

Based on the described factors, MAX phases with Al, Si and Ga show highest potential for crack-healing. A possible ternary oxide with favourable properties is $ZrSiO_4$, which has a low coefficient of thermal expansion and a Gibbs free energy of oxide formation between that of SiO_2 and ZrO_2 . However Zr and Si containing MAX phases have yet to be synthesized. Experimental investigations into the large stable group of Al containing compounds shows great potential for development of self-healing materials.

3. CONCLUSION

Criteria to identify MAX phases that show potential for self-healing have been established, in order to guide the experimental research into the wider exploration of MAX phase ceramics for intrinsic high temperature self-healing ceramics. Thermodynamic and kinetic constraints of selective oxidation, such as Gibbs free energy, diffusivity and thermal expansion are investigated to develop a comprehensive method for the selection of ternary Carbides and Nitrides of the $M_{n+1}AX_n$ group with crack-healing ability. A first evaluation showed that MAX phases with Al, Si and Ga exhibit a high potential for crack-healing.

ACKNOWLEDGEMENTS

Financial support of the European Commissions 'Marie Curie International Training Network for Self-Healing Materials: from Concept to Market' (www.SHeMat.eu), project number 209308, is gratefully acknowledged.

REFERENCES

- [1] Li, S., et al., *Multiple crack healing of a Ti_2AlC ceramic*. Journal of the European Ceramic Society, 2012. 32(8): p. 1813-1820.
- [2] Yang, H.J., et al., *High temperature healing of Ti_2AlC : On the origin of inhomogeneous oxide scale*. Scripta Materialia, 2011. 65(2): p. 135-138.
- [3] Osada, T., et al., *Strength recovery behavior of machined Al_2O_3/SiC nano-composite ceramics by crack-healing*. Journal of the European Ceramic Society, 2007. 27(10): p. 3261-3267.
- [4] Zwaag, S., A.J. Schmets, and G. van der Zaken, *Self healing materials: an alternative approach to 20 centuries of materials science*. 2007: Springer.
- [5] Chu, M.C., et al., *Damage Healing and Strengthening Behaviour in Intelligent Mullite/ SiC Ceramics*. Fatigue & Fracture of Engineering Materials & Structures, 1995. 18(9): p. 1019-1029.
- [6] Song, G.M., et al., *Oxidation-induced crack healing in Ti_3AlC_2 ceramics*. Scripta Materialia, 2008. 58(1): p. 13-16.

METHODOLOGY TO EVALUATE AVAILABILITY OF SELF-HEALING AGENT FOR STRUCTURAL CERAMICS

S. Yoshioka¹, W. Nakao²

¹ Graduated school of Engineering, Yokohama National University, 79-5, Tokiwadai, Hodogaya-ku, Yokohama, 240-8501 Japan – e-mail: yoshioka-shunsuke-tg@ynu.ac.jp

² Faculty of Engineering, Yokohama National University, 79-5, Tokiwadai, Hodogaya-ku, Yokohama, 240-8501 Japan – e-mail: wnakao@ynu.ac.jp

Keywords: Self-healing, Ceramic Matrix Composite, Jet Engine, Oxidation, TG-DTA analysis

ABSTRACT

Simple methodology to evaluate availability of self-healing agent have been established from the investigation on the relationship between oxidation behavior of self-healing agent and self-healing phenomena. The consistency of the established methodology was discussed by comparison in the lower bound of the available temperature range of mullite / TiSi_2 composite. From TG / DTA analysis, the available temperature range for 10 h healing ($T_{\text{H-10h}}^{\text{est}}$) was estimated to be 563 °C. On the other hand, the value of the lower bound of the available temperature range for 10 h healing ($T_{\text{H-10h}}^{\text{exp}}$) was experimentally determined to be 600 °C from strength recovery tests. These values showed a good consistency. Also, the data on 1 h healing of mullite / TiSi_2 and the reference data on alumina / SiC self-healing ceramics exhibited good consistency. Therefore, the proposed methodology is sufficient for evaluating the advanced healing agent.

1. INTRODUCTION

Oxidation induced self-healing ceramics are anticipated to apply the high temperature use with wide temperature range, for example, turbine blades of jet engine. Therefore, it is critical issue to figure out the available temperature range of healing agent. The present study aimed to derive the simple methodology to evaluate availability of self-healing agent by using mullite / TiSi_2 self-healing ceramic. First, the estimated value ($T_{\text{H}}^{\text{est}}$) of lower bound of the available temperature range was evaluated from the TG-DTA analysis of TiSi_2 oxidation. The experimental value ($T_{\text{H}}^{\text{exp}}$) of lower bound of the available temperature range was determined from the strength recovery behavior due to self-healing in mullite / TiSi_2 self-healing ceramic. The consistency of the established methodology was discussed by comparison in these values.

2. OXIDATION BEHAVIOR OF TiSi_2

The value of $T_{\text{H}}^{\text{est}}$ was estimated from the oxidation behavior of TiSi_2 measured by means of TG / DTA analysis. In the analysis, the reaction heat and mass gain were measured for the oxidation of TiSi_2 heating up with the constant heating rate, β . Figure 2(a) shows TG and DTA curves for the oxidation of TiSi_2 particles at the constant heating rate of 40.0 °C / min. At the temperature which DTA curve exhibits a maximum, the TG curve is found to increase significantly. Thus, the oxidation peak temperature, T_{p} , was defined as the on-peak temperature of DTA curve, and

evaluated to be 619 °C when $\beta = 40.0$ °C / min. Similar analyses were conducted for whole condition of β .

Figure 2(b) shows the relationship between T_p and $\ln(\beta/T_p^2)$ for TiSi_2 oxidation with the relationship for the oxidations of the other self-healing agent, where the value of $\ln(\beta/T_p^2)$ as the vertical axis corresponds to the reaction rate constant according to Kissinger-Sunase-Akahira equation [1]. Thus, the righter plot means that arbitrary oxidation rate exhibits at lower temperature. From the figure, it is confirmed that when TiSi_2 is employed as healing agent, the self-healing ceramics must exhibit the available self-healing at lowest temperature compared to the other self-healing ceramics. Osada et al. [2] reported the healing rate, corresponding to the inverse of the minimum healing time to enable to heal the pre-crack in alumina / SiC self-healing ceramic, as functions of the healed temperature, T_H , and the oxygen partial pressure, P_{O_2} , in the surrounded atmosphere as following equation;

$$\frac{1}{t_{H\min}} = 6.95 \times 10^5 \exp\left(\frac{-4.65 \times 10^4}{T_H}\right) P_{O_2}^{0.835}$$

From the equation and the relationship for the SiC oxidation shown in Figure 2(b), the values of $\ln(\beta/T_p^2)$ can be evaluated to be -15.0 and -13.0 as the minimum healing times are 10.0 h and 1.00 h, respectively. Assuming that the self-healing rate can be simply determined from the oxidation rate of the healing agent, one can obtain the value of T_H^{est} for the self-healing ceramic containing the respective healing agent from the relationship of the oxidation of the respective healing agent shown in Figure 2(b), i.e., the values of T_H^{est} for 1.00 and 10.0 h are the equal to the values of T_p at which these relationships intersect with the horizontal lines that $\ln(\beta/T_p^2) = -13.0$ and -15.0, respectively. Consequently, the self-healing ceramics containing TiSi_2 particles as healing agent can be estimated to exhibit T_{H-1h}^{est} of 563 °C and T_{H-10h}^{est} of 577 °C.

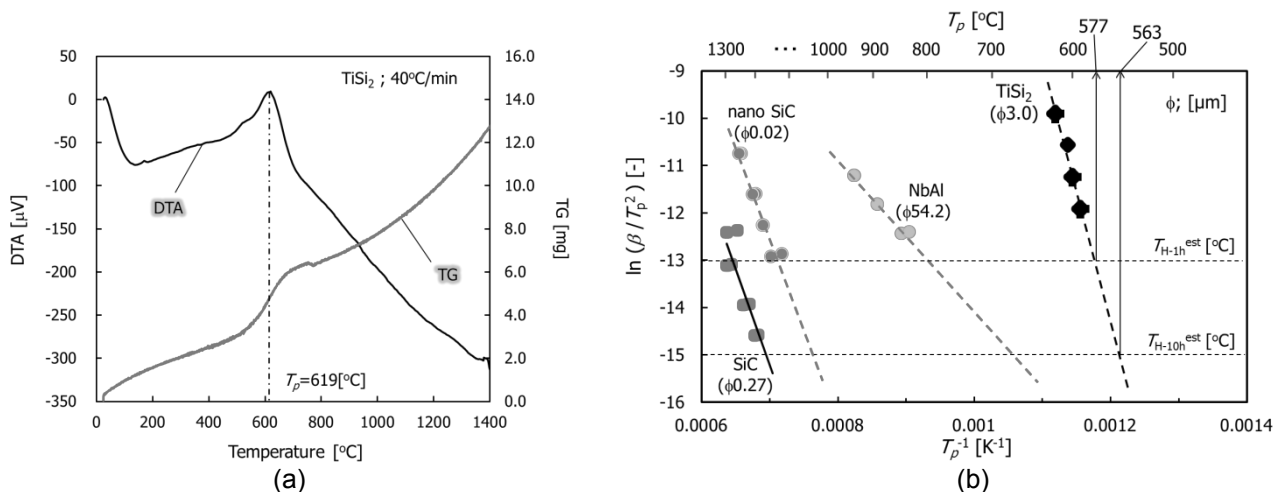


Figure 1 (a) : TG and DTA curves for the oxidation of TiSi_2 at the constant heating rate of $40^\circ\text{C}/\text{min}$, (b) : Kissinger plots of oxidations of TiSi_2 , SiC, nano-SiC and NbAl.

3. STRENGTH RECOVERY BEHAVIOR OF MULLITE/ TiSi_2 COMPOSITE

The lower bound of the available temperature region, T_H^{exp} , was experimentally determined from the strength recovery behavior of mullite/ TiSi_2 composite. The strength recovery rate was evaluated from the strength of the specimen healed at several temperatures (400-1200 °C) for 1 and 10 h after cracked. The value of T_H^{exp}

was determined to be the lowest temperature at which the strength of crack-healed specimen was recovered up to the strength of non-cracked specimen.

The specimen used for strength recovery tests was pressless sintered Mullite matrix composite containing 15 vol% TiSi_2 particles as a self-healing agent. The dimension of the test rectangular bar specimen was $4 \times 3 \times 22 \text{ mm}^3$. The specimens were healed at temperatures from $400 \text{ }^\circ\text{C}$ to $1200 \text{ }^\circ\text{C}$ for 1 and 10 h after cracked at the center of the specimens by a Vickers indentation, where the indentation pre-crack had a surface length of $100 \text{ }\mu\text{m}$. The strength of the specimens were measured by three-point bending with span of 16 mm at room temperature.

Figure 2 shows the strength recovery rate of the mullite / TiSi_2 composites healed at several temperatures for 1 h (open and closed diamonds), with that of alumina / SiC composite (closed square). The mullite / TiSi_2 composites with pre-crack had the strength of $\sim 113 \text{ MPa}$. The composites healed at temperatures between $600 \text{ }^\circ\text{C}$ and $1000 \text{ }^\circ\text{C}$ for 1 h and 10 h had the strength $\sim 183 \text{ MPa}$ and the composite without pre-crack also has almost same strength. Thus, the strength recovery rates of 0 % and 100 % for the mullite / TiSi_2 composites correspond to the 113 MPa and 183 MPa , respectively. Since the strength recovery rates at temperatures below $500 \text{ }^\circ\text{C}$ do not reach 100 %, the value of T_{H-1h}^{exp} was determined to be $600 \text{ }^\circ\text{C}$. Also the value of T_{H-10h}^{exp} was determined to be $600 \text{ }^\circ\text{C}$. No difference between T_{H-1h}^{exp} and T_{H-10h}^{exp} is directly influenced by the small difference between T_{H-1h}^{est} and T_{H-10h}^{est} .

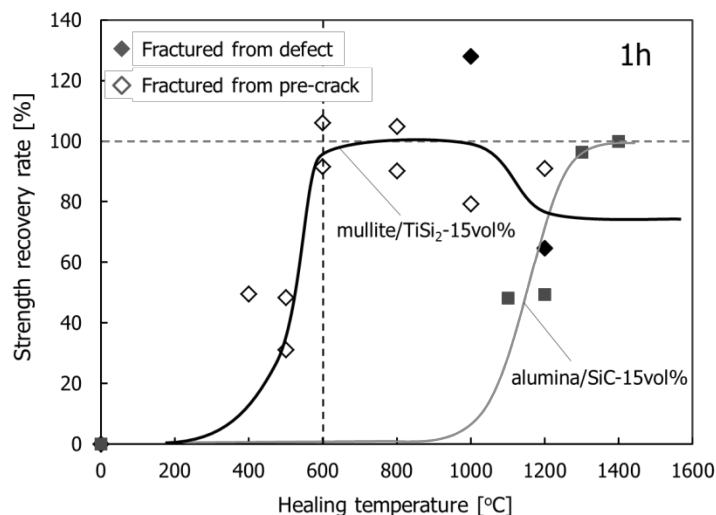


Figure 2 : The strength recovery rate of the mullite / TiSi_2 composites healed at several temperatures for 1h with that of alumina / SiC composite.

4. DISCUSSION

Figure 3 shows the consistency between the values of T_H^{est} and T_H^{exp} for the self-healing in mullite / TiSi_2 composite with some examples [3], [4]. The plots in this figure indicate T_H^{exp} for several self-healing ceramics and the attached bars demonstrate the available temperature range of these ceramics, i.e. the upper and lower bounds of the bars indicate the heat resistance limit-temperature and T_H^{exp} , respectively. The direct proportion line means the value of T_H^{est} is in perfect agreement with the value of T_H^{exp} . Every plot shows good agreement with this line so that one could argue that there is good consistency between estimation and experimental value of lower limit temperature, regardless of self-healing agent and healing time.

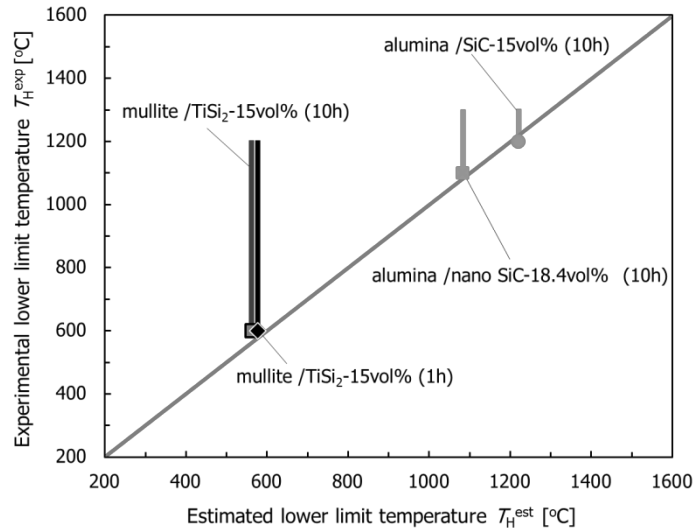


Figure 3: The consistency between the values of T_H^{est} and T_H^{exp} for the self-healing in mullite / TiSi₂ composite with those in alumina / SiC composite and alumina / nanometer-sized SiC composite

5. CONCLUSIONS

The obtained results show that the proposed method is sufficient to evaluate availability of self-healing agent. Therefore, using this method, one can easily estimate whether the new self-healing ceramics containing new healing agent is suitable to the corresponded applications.

ACKNOWLEDGEMENTS

Financial support from the Kumagai Foundation for Science and Technology for this investigation is gratefully acknowledged.

REFERENCES

- [1] T. Akahira, T. Sunose, 1969 Research Report, Chiba Institute of Technology 16 (1971) 246.
- [2] T. Osada, W. Nakao, K. Takahashi, K. Ando, Kinetics of Self-Crack-Healing of Alumina/Silicon Carbide Composite Including Oxygen Partial Pressure Effect, Journal of the American Ceramic Society 92 (2009) 864-869.
- [3] K. Ando, B.S. Kim, S. Kodama, S.P. Liu, K. Takahashi, S. Saito, Fatigue Strength of an Al₂O₃/SiC Composite and a Monolithic Al₂O₃ Subjected to Crack-Healing Treatment, Journal of the Society of Materials Science, 52 (2003) 1464-1470.
- [4] W. Nakao, K. Takahashi, K. Ando, Self-healing of surface cracks in structural ceramics, In: Ghosh S.K. (ed) Self-healing materials, Wiley VCH Verlag GmbH & Co. KGaA, Weinheim, 2009, pp. 183-217.

ENCAPSULATION OF SACRIFICIAL SILICON CONTAINING PARTICLES FOR SH OXIDE CERAMICS VIA A BOEHMITE PRECURSOR ROUTE

A. L. Carabat ¹, S. van der Zwaag ² and W. G. Sloof ¹

¹ Department of Materials Science and Engineering, TU Delft, Mekelweg 2, 2628 CD Delft, The Netherlands – e-mail: a.l.carabat@tudelft.nl; w.g.sloof@tudelft.nl;

² Delft Center for Materials, TU Delft, Kluyverweg 1, 2629 HS Delft, The Netherlands – e-mail: s.vanderzwaag@tudelft.nl

Keywords: ceramic coatings, self-healing particles, encapsulation, alumina shell

ABSTRACT

Easy crack propagation in oxide ceramic coatings limits their application in high temperature environment (e.g. such as engines and gas turbine components) [1]. In order to overcome this problem, incorporation of sacrificial particles into an oxide ceramic coating may be a viable option. Particles of silicon compounds, such as: Si_3N_4 , SiC , MoSi_2 , TaSi_2 and WSi_2 are attractive due to their unique features of producing a reaction product (i.e. SiO_2) which fills the crack and bonds well to the surrounding matrix and exhibit, a relatively low density and melting point above that of the matrix [2]. To achieve a better control of the self-healing process with silicon compound particles a gas tight encapsulation procedure of these particles is a crucial prerequisite in order to avoid premature oxidation in the absence of a local crack. One possible route is the encapsulation of these particles by a sol-gel method [3, 4]. The dispersed healing particles were coated by Al_2O_3 layer prepared from boehmite sols, using two different alumina precursors (salt and alkoxide precursors). The resulted embedded sols were annealed in reducing atmosphere at temperatures above 1200 °C in order to achieve a dense $\alpha\text{-Al}_2\text{O}_3$ microcapsule shell wall. The morphology, structure and composition of the encapsulation are determined with advanced analysis techniques. The thermal stability of the encapsulated healing particles is studied by high temperature exposure in air.

1. INTRODUCTION

Oxide ceramic coatings are promising materials for technological applications which require high temperatures, oxidation resistance and long term stability. The most important factor in the development of these types of materials is the improvement of their mechanical behaviour. The lifetime of oxide ceramic coatings is strongly affected by the crack propagation which limits their application in high-temperature environments (e.g. furnace heating elements, engines and gas turbine components) [1]. A possible route to overcome this critical issue is the incorporation of sacrificial particles into an oxide ceramic coating. Intermetallic particles based on silicon compounds, such as Si_3N_4 , SiC , MoSi_2 , TaSi_2 and WSi_2 are attractive due to their unique features of forming a reaction product, mainly SiO_2 , which fills the crack and bonds well with the surrounding matrix [2].

To have a better control of the self-healing process with silicon based intermetallic compounds an encapsulation process is prerequisite in order to avoid the premature oxidation in the absence of any local crack. One possible way to achieve this is via

inorganic encapsulation of these particles using soft-chemical methods (precipitation or sol-gel).

In this work, an encapsulation process of MoSi_2 particles via boehmite precursor route has been developed.

2. MATERIALS AND METHODS

Aluminium chloride hexahydrate ($\text{AlCl}_3 \cdot 6\text{H}_2\text{O}$, 99% purity, Sigma Aldrich), ammonium hydroxide (NH_4OH , aqueous solution 25%, J.T. Baker Chemical Co) and molybdenum disilicide (MoSi_2 99.5% purity, average particle size $20 \mu\text{m}$, ChemPur) were used as starting materials.

The encapsulation process was performed at room temperature. MoSi_2 particles were firstly dispersed in $\text{AlCl}_3 \cdot 6\text{H}_2\text{O}$ aqueous solution. The obtained suspensions were stirred and ultrasonicated for 30 minutes to break up the agglomerates and to avoid the particles sedimentation. Subsequently, the mixture was hydrolysed by slow addition of NH_4OH under continuous stirring, at room temperature, until the reaction mixture attained a pH value between 5.0 – 6.0. The concentration of $\text{AlCl}_3 \cdot 6\text{H}_2\text{O}$ varied from 0.5 M, 2 M, 3.5 M to 5 M and the molar ratio $\text{AlOOH}/\text{MoSi}_2$ was fixed at 10 : 1. The obtained precipitates were separated by filtration, washed of free chloride and ammonium ions with hot bi-distilled water and dried at $100 \text{ }^\circ\text{C}$ for 2h. The as synthesized samples were then annealed at $1300 \text{ }^\circ\text{C}$ for 2 hours, in a reducing atmosphere (10% H_2 and 90% N_2). The flowchart of the encapsulation process of MoSi_2 particles is shown in Figure 1.

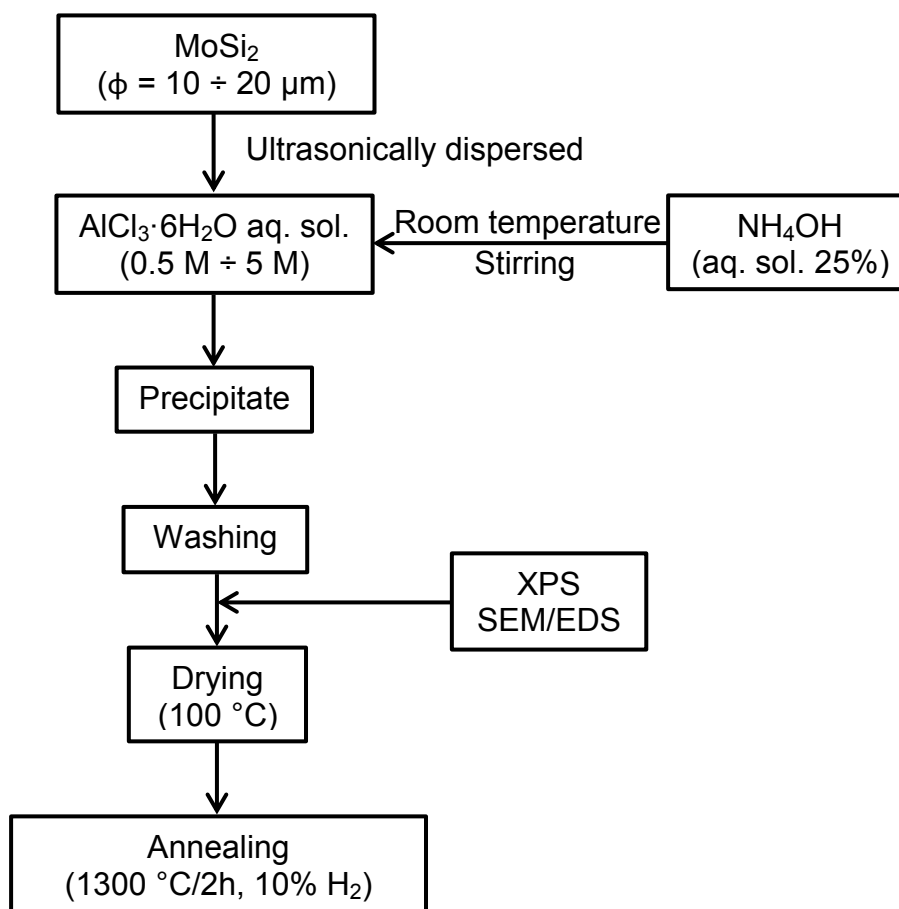


Figure 1: Flowchart of MoSi_2 encapsulation with AlOOH .

3. RESULTS AND DISCUSSION

The morphology of the MoSi₂ healing particles before and after encapsulation was observed by means of scanning electron microscopy (SEM); see Figure 2. The MoSi₂ particles are of irregular shape with sizes in the range of 10 to 20 μm; see Figure 2a. The precipitation of boehmite in a AlCl₃·6H₂O 0.5 M aqueous solution completely covered the surface of MoSi₂ particles; see Figure 2b. Similar observations were made for the other suspensions prepared by using more concentrated solutions of AlCl₃·6H₂O (2 M, 3.5 M and 5 M, respectively).

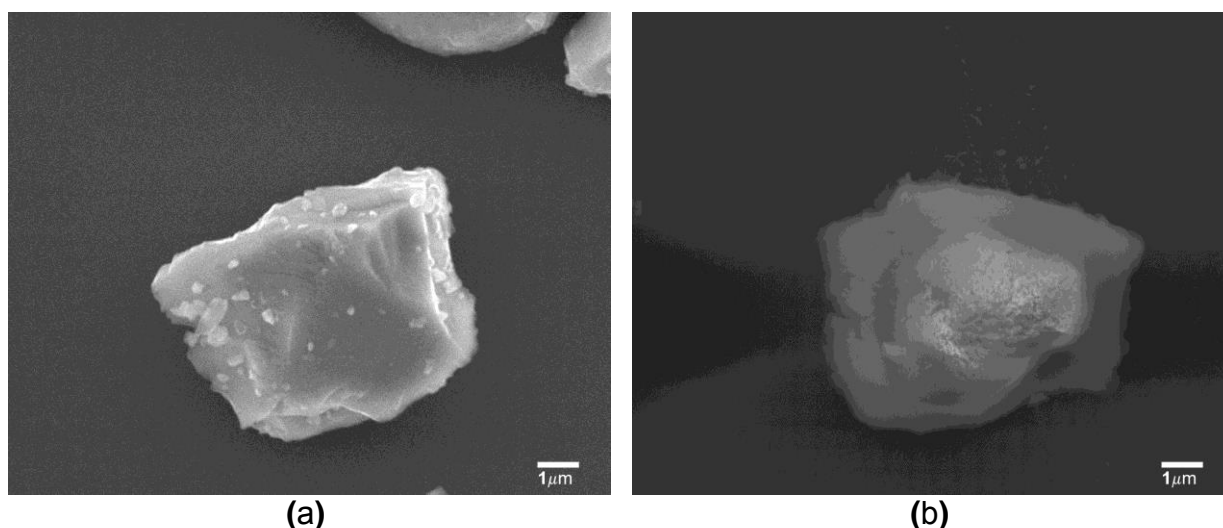


Figure 2: SEM images of uncoated and coated MoSi₂ particles: (a) as received MoSi₂ particles and (b) boehmite coated MoSi₂ particles prepared by using AlCl₃·6H₂O 0.5 M aqueous solution.

Another evidence of boehmite shell formation on the surface of MoSi₂ particles is given by X-ray Photoelectron Spectroscopy (XPS). For all the layers deposited onto the MoSi₂ particles, the O 1s peaks can be described precisely by two components corresponding to OH⁻ and O²⁻, respectively. The curve fitting of the O 1s photoelectron peak was performed using a Gaussian-Lorentzian fitting curve in the binding energy region of 526–538 eV after subtraction of the Shirley type background. The binding energies corresponding to the resolved OH⁻, O²⁻ components of O 1s and Al 2p are summarized in Table 1.

Table 1: Binding energies corresponding to O²⁻, OH⁻ and Al 2p components of the Boehmite shells obtained from the curve fitting of the XPS spectra.

Concentration AlCl ₃ solution	O ²⁻ BE (eV)	OH ⁻ BE (eV)	Al 2p BE (eV)
0.5 M	531.0	532.6	74.0
2.0 M	530.9	532.9	74.0
3.5 M	530.8	532.2	73.9
5.0 M	530.8	532.1	74.0

The binding energies of both components, O²⁻ and OH⁻ present narrow ranges: 530.8 – 531.0 eV and 532.1 – 532.9 eV, respectively. These values for O 1s components are in agreement with the results presented in the literature [5].

As already observed with SEM and confirmed with XPS, the MoSi₂ healing particles are fully covered with boehmite, since no photoelectron peaks corresponding to Mo or Si were detected.

The MoSi₂ particles remained intact during the encapsulation process, as evidenced by X-ray diffraction patterns of the particles before and after encapsulation.

After annealing the boehmite encapsulated MoSi₂ particles in reducing atmosphere (10% H₂ and 90% N₂) at 1300 °C analysis suggests that the boehmite is transformed to the desired α -Al₂O₃ phase.

4. CONCLUSION

MoSi₂ healing particles were successfully encapsulated with boehmite using a soft-chemical method. A closed shell of aluminium oxyhydroxide layer was formed on the surface of MoSi₂ particles after the precipitation process. Annealing the encapsulated particles in a gas mixture of 10% H₂ and 90% N₂ at 1300 °C transformed the boehmite into α -Al₂O₃, while the MoSi₂ core remained intact.

ACKNOWLEDGEMENTS

Financial support from Delft Centre for Materials of Delft University of Technology – DCMat (www.dcmat.tudelft.nl) gratefully acknowledged. The authors are indebted to Ing. R. W. A. Hendrix for the X-ray diffraction analysis, to Ing. J. C. Brouwer for assistance with XPS analysis and annealing experiments, and to Ing. C. Kwakernaak for his advice on the soft-chemical method.

REFERENCES

- [1] M. Backhaus-Ricoult, V. Guerin, A. M. Huntz, V. S. Urbanovich, High-temperature oxidation behavior of high-purity α -, β -, and mixed silicon nitride ceramics, *Journal of the American Ceramic Society*, 85-2 (2002) 385-392.
- [2] X. Fei, Y. Niu, H. Ji, L. Huang, X. Zheng, Oxidation behavior of ZrO₂ reinforced MoSi₂ composite coatings fabricated by vacuum plasma spraying technology, *Journal of Thermal Spray Technology*, 19-5 (2010) 1074-1080.
- [3] A. Taavoni-Gilan, E. Taheri-Nassaj, R. Naghizadeh, H. Akhondi, Properties of sol-gel derived Al₂O₃-15 wt.% ZrO₂ (3 mol% Y₂O₃) nanopowders using two different precursors, *Ceramics International*, 36-3 (2010) 1147-1153.
- [4] X. Lu, M. Zhong, W. Shu, Q. Yu, X. Xiong, R. Wang, Alumina encapsulated SrAl₂O₄:Eu²⁺, Dy³⁺ phosphors, *Powder Technology*, 177-2 (2007) 83-86.
- [5] J. van den Brand, W. G. Sloof, H. Terryn, J. H. W. de Wit, Correlation between hydroxyl fraction and O/Al atomic ratio as determined from XPS spectra of aluminium oxide layers, *Surface and Interface Analysis*, 36-1(2004) 81-88.

OXIDATION INDUCED CRACK HEALING OF $\text{Cr}_2(\text{Al,Si})\text{C}$ MAX PHASE CERAMIC

L. Shen¹, S. B. Li², S. van der Zwaag³ and W. G. Sloof¹

¹ Department of Materials Science and Engineering, Delft University of Technology, Mekelweg 2, 2628 CD Delft, The Netherlands - email: L.Shen@tudelft.nl; W.G.Sloof@tudelft.nl

² Institute of Materials Science and Engineering, School of Mechanical and Electronic Control Engineering, Beijing Jiaotong University, Beijing 100044, China – email: shbli1@bjtu.edu.cn

³ Faculty of Aerospace Engineering, Delft University of Technology, Kluyverweg 1, 2629 HS Delft, The Netherlands - email: S.vanderZwaag@tudelft.nl

Keywords : Cr_2AlC , $\text{Cr}_2(\text{AlSi})\text{C}$, crack healing, oxidation kinetics, microstructure analysis

ABSTRACT

The oxidation crack healing of Cr_2AlC and $\text{Cr}_2(\text{Al,Si})\text{C}$ was studied and compared with known healing of Ti_2AlC . The oxidation induced crack healing of Ti_2AlC is relatively fast and leads to full strength recovery, but the oxidation product contains besides $\alpha\text{-Al}_2\text{O}_3$ also undesired TiO_2 . However, when oxidizing Cr_2AlC only $\alpha\text{-Al}_2\text{O}_3$ is formed, but full crack healing is relatively slow. The efficiency of the oxidation induced crack healing of Cr_2AlC is enhanced if Al is partially replaced by Si atoms.

1. INTRODUCTION

MAX phase materials, such as: Ti_3AlC_2 and Ti_2AlC , are very attractive materials in their own right as they combine desirable metallic and ceramic properties at the same time due to their atomically layered and hexagonal crystal structure. In our earlier studies [1, 2], we demonstrated that these materials possess interesting self-healing properties when exposed to high temperatures in an oxidizing environment. The recovery of mechanical strength is mainly due to the formation of higher strength $\alpha\text{-Al}_2\text{O}_3$, but also some weaker TiO_2 is present in the healed crack.

To avoid the formation of TiO_2 , which is not beneficial for the adhesion between the two fracture surfaces, the crack healing of Cr_2AlC was explored. However, full crack healing of Cr_2AlC was found to be slow compared with that of Ti_2AlC due to the slower oxidation kinetics. To accelerate the oxidation process some of the Al atoms in the Cr_2AlC are to be replaced by Si atoms. Therefore, the oxidation kinetics and the composition of the oxidation product is studied for Ti_2AlC , Cr_2AlC and $\text{Cr}_2(\text{Al,Si})\text{C}$ after isothermal oxidation in synthetic dry air at temperature at 1100 °C. Finally, the crack healing performance and strength recovery of these MAX phases are compared.

2. MATERIALS AND METHODS

The oxidation kinetics of the MAX phase Ti_2AlC , Cr_2AlC and $Cr_2(Al,Si)C$ in N_2 with 20 vol.% O_2 at 1100 °C were determined with thermogravimetry analysis (TGA). The oxidation products were analysed with X-ray microanalysis and X-ray diffractometry.

Crack damage was generated with Knoop indentation in the centre of the samples with dimensions of 3x4x36 mm applying a load of 50 to 1000 N. Next, the cracks were healed at 1100 °C in air for 4 hours.

The strength of the materials before and after oxidation induced crack healing was determined by 3-point bending with a span of 30 mm and cross-head speed of 0.5 mm/min.

3. RESULTS AND DISCUSSION

Cracks in Ti_2AlC can be healed relatively fast at high temperatures in an oxidizing environment. For example, for this MAX phase full crack healing and strength recovery has been observed within 1 hour at 1200 °C [2]. The healing product is mainly composed of $\alpha-Al_2O_3$ and some TiO_2 . Similar experiments with Cr_2AlC and Cr_2AlSiC showed that the crack healing and strength recovery takes much longer time [3]. This is in agreement with the oxidation kinetics observed for these 3 MAX phases; see Figure 1. Partial replacement of Al by Si in the lattice of Cr_2AlC [4] promotes significantly the formation of $\alpha-Al_2O_3$ and thus the crack healing.

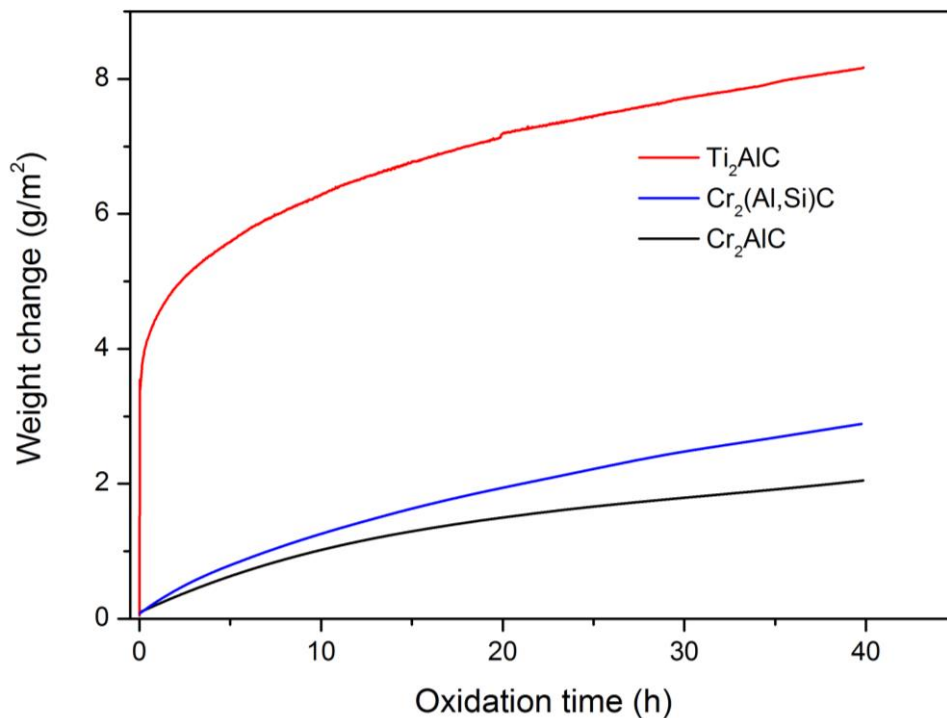


Figure1: Oxidation kinetics of Ti_2AlC , Cr_2AlC and $Cr_2Al(Si)C$ in N_2 with 20 vol.% O_2 at 1100 °C.

Large cracks in Cr_2AlC , as generated with Knoop indentation, were fully healed when sufficient time was allowed for oxidation; see Figure 2. In the example presented here, a crack of about 1 mm length and 2-3 μm width was healed after 100 hours of oxidation in N_2 with 20 vol.% O_2 at 1100 °C. The crack gap is filled with $\alpha\text{-Al}_2\text{O}_3$ and some Cr_2AlC debris as a result of the fracturing. If the crack gap was not fully filled with $\alpha\text{-Al}_2\text{O}_3$ then the strength determined with 3-point bending was lower than the strength of the virginal material [3].

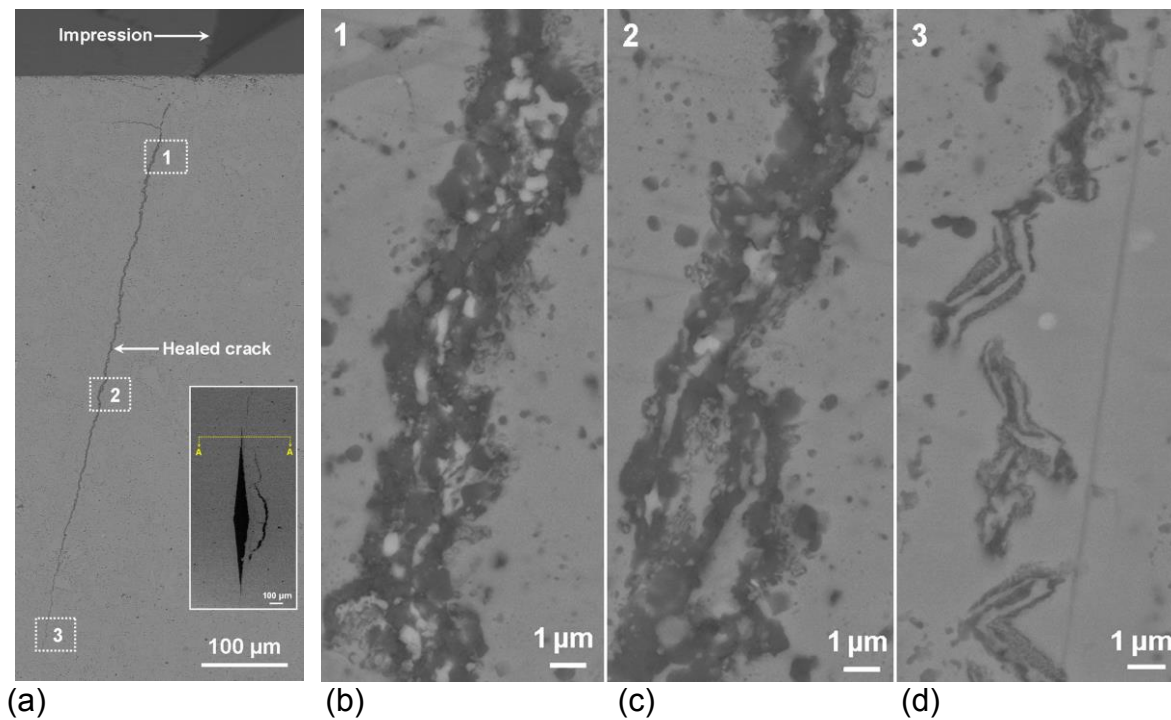


Figure 2: Backscattered electron images of a crack in Cr_2AlC healed at 1100 °C for 100 h in air. (a) A low magnification image of the cross section taken along the A-A direction; see insert (b, c and d) Enlarged images taken from the marked areas denoted as '1', '2' and '3' in (a), respectively.

Since the time for crack healing in practical applications is usually limited, a more efficient healing is required. For Cr_2AlC , this can be realized by partially replacing Al by Si in the MAX phase [4]. Then the time for healing a crack is significantly reduced.

4. CONCLUSIONS

Upon exposure at high temperatures in an oxidizing environment, cracks in Ti_2AlC are fully healed by filling the crack gap with Al_2O_3 and TiO_2 . However, the rutile (TiO_2) formed weakens the adhesion between the two fracture surfaces. Cracks in Cr_2AlC , on the contrary, are healed exclusively with $\alpha\text{-Al}_2\text{O}_3$, but the filling of the crack gap by oxidation proceeds much slower compared with Ti_2AlC . Partial replacement of Al atoms in Cr_2AlC with Si atoms promotes the formation of $\alpha\text{-Al}_2\text{O}_3$ and thus the crack healing.

ACKNOWLEDGEMENTS

Financial support of the German Science Foundation (Deutsche Forschungsgemeinschaft, DFG), in the framework of SPP (Schwerpunktprogramm, 1568) "Design and Generic Principles of Self-Healing Materials" is gratefully acknowledged (cf. <http://www.spp1568.uni-jena.de>).

REFERENCES

- [1] G.M. Song, Y.T. Pei, W.G. Sloof, S.B. Li, J.Th.M. De Hosson, S. van der Zwaag, Oxidation-induced crack healing in Ti_3AlC_2 ceramics, *Scripta Materialia* 58 (2008) 13-16.
- [2] S.B. Li, G.M. Song, K. Kwakernaak, S. van der Zwaag, and W. G. Sloof, 'Multiple Crack Healing of a Ti_2AlC Ceramic', *Journal of the European Ceramic Society*, 32 (2012)1813-20.
- [3] S.B. Li, L. Xiao, G.M. Song, X.M. Wu, W.G. Sloof, and S. van der Zwaag, Oxidation and Crack Healing Behavior of a Fine-grained Cr_2AlC Ceramic, *Journal of the American Ceramic Society*, (2013)1-8.
- [4] W. Yu, S.B. Li, W.G. Sloof, Microstructure and mechanical properties of a $Cr_2Al(Si)C$ solid solution, *Materials Science and Engineering A*, 527 (2010) 5997-6001.

SELF-HEALING EVOLUTION OF OXIDIZED SURFACE OF Al_4SiC_4 AND ITS EFFECT ON MECHANICAL PROPERTIES

X. Huang¹, X. Geng¹, G. Wen^{1,2}, G. Song³, Y. Zhou¹

¹*School of Materials Science and Technology, Harbin Institute of Technology, Harbin 150001, P. R. China-e-mail: swliza@hit.edu.cn; Xingeng@hit.edu.cn; g.wen@hit.edu.cn; yzhou@hit.edu.cn*

²*School of Materials Science and Technology, Harbin Institute of Technology at WeiHai, WeiHai 264209, P. R. China-e-mail: g.wen@hit.edu.cn*

³*Department of Materials Science and Engineering, Delft University of Technology, Mekelweg 2, 2628 CD Delft, The Netherlands-e-mail: songguim@yahoo.com*

Keywords: Al_4SiC_4 , microstructure, self-healing, mechanical testing

ABSTRACT

The recently developed ternary carbide Al_4SiC_4 has attracted extensive attention owing to its lower density (3.03 g/cm^3), higher melt point ($>2000 \text{ }^\circ\text{C}$), excellent self-healing and high temperature mechanical properties. It is a very promising material for high-temperature applications. The self-healing evolution of the surface of Al_4SiC_4 ceramics oxidized at $900\text{-}1400 \text{ }^\circ\text{C}$ for 2-10 hours in air was investigated with X-ray diffraction (XRD) and scanning electron microscopy (SEM). After a heat treatment at 1000°C , nanosized newborn phase, Al_2SiO_5 , with 100 nm in length appeared which kept its existence until to $1200 \text{ }^\circ\text{C}$ for 6 hours. The surface of the specimen heat treated at 1200°C for longer time ($>8 \text{ h}$) or at higher temperatures ($>1200 \text{ }^\circ\text{C}$) was covered with oxidation products consisting primarily of Al_2O_3 as well as some mullite ($3\text{Al}_2\text{O}_3 \cdot 2\text{SiO}_2$). The flexural strength at room temperature increased of 70% ($491.7 \pm 13.2 \text{ MPa}$) for the specimen heat treated at 1000°C for 6 h compared with the polished specimen ($297 \pm 13 \text{ MPa}$).

CRACK-HEALING EFFECT OF Al_2O_3 HYBRID MATERIALS DISPERSED WITH NI NANOPARTICLES VIA THERMAL OXIDATION

D. Maruoka¹ and M. Nanko²

¹ Graduate School of Engineering, Nagaoka University of Technology, 1603-1, Kamitomioka, Nagaoka, Niigata, 940-2188, Japan - e-mail: daisuke@stn.nagaokaut.ac.jp

² Department of Mechanical Engineering, Nagaoka University of Technology, 1603-1, Kamitomioka, Nagaoka, Niigata, 940-2188, Japan - e-mail: nanko@mech.nagaokaut.ac.jp

Keywords: nanocomposite, Al_2O_3 , High-temperature oxidation, bending strength, Diffusion

ABSTRACT

Al_2O_3 hybrid materials dispersed with Ni nano-particles ($\text{Ni}/\text{Al}_2\text{O}_3$) have received great attentions for their excellent mechanical strength and fracture toughness. However, these hybrid materials still have poor fracture toughness in comparison with metallic materials. In the ceramic-based materials, even a small surface crack causes catastrophic failure by a low impact load.

$\text{Ni}/\text{Al}_2\text{O}_3$ have crack-healing function via thermal oxidation as well as SiC-dispersed oxide composites. Recovery of mechanical strength in $\text{Ni}/\text{Al}_2\text{O}_3$ was caused by filling cracks with the oxidation product, NiAl_2O_4 .

NiAl_2O_4 filled in the cracks is developed by the direct oxidation of surface nano-Ni particles and diffusion of Ni ions reacted with surface Al_2O_3 . In order to understand the filling of surface cracks on these hybrid materials, the role of outward diffusion of Ni ions should be investigated.

In the present study, recovery mechanism of mechanical strength was investigated on $\text{Ni}/\text{Al}_2\text{O}_3$ in the point of view on high-temperature oxidation kinetics, in particular, on cation diffusion in the polycrystalline Al_2O_3 matrix.

SURFACE CRACK HEALING OF POLYMER-FILLER DERIVED CERAMICS

L. Schlier¹, N. Travitzky¹, P. Greil¹

¹ *University of Erlangen-Nuernberg, Department of Materials Science (Glass and Ceramics), Martensstr. 5, D-91058 Erlangen, Germany - e-mail: Lorenz.Schlier@ww.uni-erlangen.de; Nahum.Travitzky@ww.uni-erlangen.de; Peter.Greil@ww.uni-erlangen.de*

Keywords: Polymer derived ceramics, surface nitridation, crack healing

ABSTRACT

Healing of surface cracks and pores on the surface of polymer derived Si-O-C ceramics by annealing in nitrogen atmosphere was investigated. Thermodynamic calculations as well as experimental results show Si₃N₄ and Si₂N₂O to be the major condensed reaction products. High mobility of vapour phase reactants SiO(g) and N₂(g) facilitates long range transport and nitride and oxinitride reaction products may fill open pores and cracks. While the filler free Si-O-C system requires annealing temperatures exceeding 1200 °C significantly lower reaction temperatures can be achieved by adding transition metal filler (CrSi₂) which catalyzes nitridation reaction. Maximum crack length and crack opening to be healed were correlated to the penetration depth of nitrogen perpendicular to the surface and specific volume expansion of the nitridation reaction phases. Penetration of nitrogen causes effective reduction of porosity at least near the surface which gave rise for a pronounced improvement of fracture strength of (σ_{heal}/σ_0) \approx 1.5. Removing the surface nitridation reaction layer by grinding and reannealing in nitrogen atmosphere resulted in a complete recovery of the initial modulus of rupture. Since post-fabrication treatment in a reactive atmosphere is independent on the component shape and size formation of a surface reaction zone with reduced porosity and flaws may offer a versatile route for improving properties of bulk polymer-filler derived ceramic components.

THE EFFECT OF GRAIN SIZE ON THE MECHANICAL PROPERTIES AND THE OXIDATION INDUCED CRACK HEALING EFFICIENCY OF Cr₂AlC CERAMIC

X. Duan¹, D. Jia¹, Z. Yang¹, Y. Zhou¹, J. Ouyang¹, W.G. Sloof² and S. van der Zwaag³

¹ Institute for Advanced Ceramics, School of Materials Science and Engineering, Harbin Institute of Technology, Harbin, 150001, China – e-mail: dxmhit@126.com

² Department of Material Science and Engineering, Delft University of Technology, Mekelweg 2, 2628 CD Delft, The Netherlands – e-mail: W.G.Sloof@tudelft.nl

³ Novel Aerospace Materials, Delft University of Technology, Kluyverweg 1, 2629 HS Delft, The Netherlands – e-mail: S.vanderZwaag@tudelft.nl

Keywords: Cr₂AlC ceramic, grain size, mechanical properties, self-healing

ABSTRACT

The Cr₂AlC ternary ceramic compound, which belongs to the MAX phase family, has unique properties, such as high temperature strength, oxidation and corrosion resistance, good electrical and thermal conductivity, and machinability. It has been demonstrated that crack damage in this type of ceramics can be repaired by selective oxidation of the aluminium atoms. The alumina formed in the crack gap has a strong adhesion to the fracture surfaces enabling full strength recovery. However, it was observed that the restoration of the properties upon exposure to high temperature air is very slow, most likely to be due to the slow supply of Al atoms. Given the importance of grain boundaries as a path for rapid element supply to the fracture surface, it is to be expected that the strength and healing efficiency depend on the grain size of the MAX phase material. But this relation has not been demonstrated yet. It is therefore interesting to study the effect of grain size on the oxidation induced crack healing of Cr₂AlC.

In our work, the Cr₂AlC ceramics are produced by reactive hot-press sintering using the chromium, aluminum and graphite powders as the starting materials. The grain size of Cr₂AlC ceramics was controlled by adjusting the sintering temperature and holding time. In this way several materials with an average grain size in the range of 10 to 50 μm were obtained. X-ray diffraction was used to verify the phase compositions of Cr₂AlC ceramics. Crack damage was induced with a Knoop indenter in three point bending samples. The flexural strength and fracture toughness of the initial material before and after healing were determined by three point bending tests and the single edge notch beam technique, respectively. The pre-cracked specimens were healed at 1100 °C in air for various times. From the experimental data the strength recovery was determined as a function of the Cr₂AlC grain size and the observations are used to build a general model for crack healing in MAX phase materials

POSTPONING CRACK NUCLEATION IN SUPERSATURATED XXXX ALUMINIUM ALLOYS

M. Mahdavi Shahri ¹, H. Schut ², S. van der Zwaag ¹ and R. Alderliesten ¹

¹ Delft University of Technology, faculty of Aerospace Engineering, Kluyverweg1 NL- 2629 HS, Delft, The Netherlands- e-mail: M.MahdaviShahri@tudelft.nl; S.vanderZwaag@tudelft.nl; R.C.Alderliesten@tudelft.nl

² Delft University of Technology, faculty of Applied Sciences, Mekelweg 15 NL-2629 JB, Delft, The Netherlands- e-mail: H.Schut@tudelft.nl

Keywords: Fatigue resistance, Aluminium alloys, Dynamic precipitation

ABSTRACT

Recently, a novel strategy to improve the fatigue resistance of aluminium alloys has been proposed, which is based on the spontaneous annihilation of deformation induced damage of aluminium alloys in a supersaturated state. It is proposed that dynamic precipitation in the early stages of crack initiation occurred in the vicinity of defects. Thus, the process can be interpreted as self-healing of fatigue damage.

The objective of the present work is to investigate alternative temperature treatments that can enhance the fatigue resistance through the above self-healing mechanism. The material used is an underaged XXXX aluminum alloy tested under various fatigue conditions, combining load blocks and healing cycles. The underlying healing processes will be analyzed by positron annihilation and other microscopic techniques.

SELF-HEALING COATINGS AND PAINTS

POSTER SESSION

SELF-HEALING COATING HEALED WITH A VISCOELASTIC SUBSTANCE

Y. K. Song¹ and C. M. Chung¹

¹ Department of Chemistry, Yonsei University, Wonju, Gangwon-do 220-710, South Korea – e-mail: ssong-a@yonsei.ac.kr; cmchung@yonsei.ac.kr

Keywords: self-healing, protective coating, capsule type, viscoelastic substance, secondary crack free

ABSTRACT

A protective coating is used to protect surface of a material from various deterioration factors. When cracks form and propagate in the coating, water, chloride ion, and carbon dioxide would penetrate through the cracks. This results in the deterioration of the material, leading to reduction in its serviceability. If the protective coating has self-healing ability, it would effectively protect the materials from the deterioration.

In this work a capsule-type self-healing protective coating has been developed using vegetable oils as healing agent. Healing-agent-loaded microcapsules are embedded in a coating matrix to obtain a self-healing protective coating. Upon damage-induced cracking, the microcapsules are ruptured by the propagating crack fronts, resulting in release of the healing agent into the crack by capillary action. A healing reaction occurs by atmospheric oxygen, generating a viscoelastic substance. The self-healing coating was evaluated as protective coating for steel, and it was demonstrated that our system has good self-healing capability.

In conventional capsule-type self-healing systems, healing reactions generally produce hard solids, so the systems are considered to be vulnerable to regeneration of cracks in the healed region. Furthermore, the regenerated cracks can not be healed because healing agent is consumed in the first healing process. It should be noted that our new system can effectively prevent the coating from regeneration of cracks in the healed region (Figure 1).

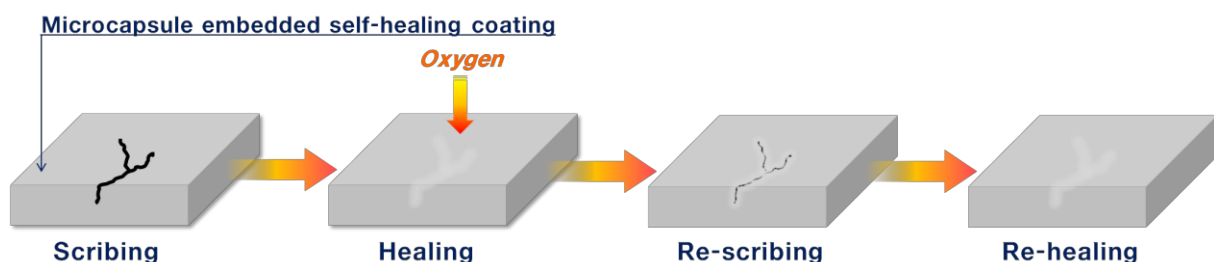


Figure 1: The concept of this study

1. INTRODUCTION

A protective coating is used to protect surface of a material from various deterioration factors. Several reports of microcapsule-type self-healing coatings for metal protection have appeared [1~5]. The conventional extrinsic self-healing coatings have employed healing agents that harden by healing reaction. This type of self-healing systems are limited to single local self-healing event: when the healed region is damaged again, self-healing cannot be repeated due to the depletion of healing agent-filled microcapsule, and the conversion of the released healing agent into a hard solid having no intrinsic self-healing ability. We thought that, if a healing agent has an intrinsic self-healing function after the release and reaction, repeatable self-healing can be accomplished. In this work a novel repeatable self-healing coating has been developed by combination of the extrinsic and intrinsic healing concept, using reactive vegetable oils as healing agent. When vegetable oil-loaded microcapsules are ruptured, the healing agent is released and fills damaged region, generating a viscoelastic substance by oxidation reaction that has intrinsic self-healing ability. It is expected that, if the secondary damage occurs in the healed area, repeated self-healing events would be possible due to the viscoelastic recovery. Although this approach has difficulty in recovery of mechanical property, the recovery of corrosion protection function would be more important than that of mechanical performance in the case of protective coating. In addition to the repeatable self-healing ability, our system also offers the advantages of environment-friendly self-healing because the healing reaction occurs by atmospheric oxygen. This system would be more useful than our previous repeatable self-healing system that only functions in the presence of light [6].

2. MATERIALS

Vegetable oil used as core material was purchased from CJ Cheiljedang. Urea, aqueous formaldehyde solution (37wt%) used as shell materials were purchased from Sigma-Aldrich. Poly(ethylene-*alt*-maleic anhydride) (EMA) used as surfactant was purchased from Sigma-Aldrich. Resorcinol used as chain extender and 1-octanol used as defoamer were purchased from Sigma-Aldrich. Ammonium chloride and sodium hydroxide, used to control the pH of solution, was purchased from Duksan Pharmaceutical. Soy bean oil and olive oil as vegetable oils were purchased from CJ Cheiljedang. Cobalt (II) 2-ethylhexanoate, 65 wt% solution in mineral spirits as dryer was purchased from Sigma-Aldrich. An enamel paint (KCI 7200, white) was purchased from Kunsul Chemical Industrial Co. Silicone sealant (SL 907) was purchased from KCC. All the materials are commercial products and were used without purification.

3. METHODS

A healing agent was prepared by mixing soybean oil, olive oil and the dryer with mass ratio of 1 :0.594 :0.006. The healing agent was coated on a KBr disk and stored under ambient conditions. The reaction of the coating to atmosphere was performed at 20 °C. The conversion was measured by FT-IR spectroscopy.

We have performed microencapsulation of soybean oil using urea-formaldehyde (UF) polymer as shell material. The UF microcapsules were prepared by in situ

polymerization in an oil-in-water emulsion at an agitation rate of 800 rpm. Microcapsules filled with dryer-containing olive oil were prepared in a similar fashion. The enamel paint and microcapsules (soybean oil microcapsules and olive oil microcapsules were mixed with a ratio of 1:0.6) were mixed to give a self-healing coating formulation. A control coating was prepared in a similar fashion using the enamel paint without microcapsule.

Cross scribes were applied manually on the prepared self-healing and control coatings with a cutter blade. The scribed coatings were stored under ambient conditions for 3 day. The scribed specimens were then immersed in 10 wt% NaCl solution for 48 h to evaluate the accelerated corrosion process. After washing with distilled water and removal of residual water, the coating were observed by optical photography. The first scribed and healed region in the coatings was re-scribed and the resultant coatings were kept for 20 min under ambient conditions. The second anticorrosion test was carried out by immersion of the coatings in the NaCl solution and subsequent photography according the method described above.

4. RESULTS

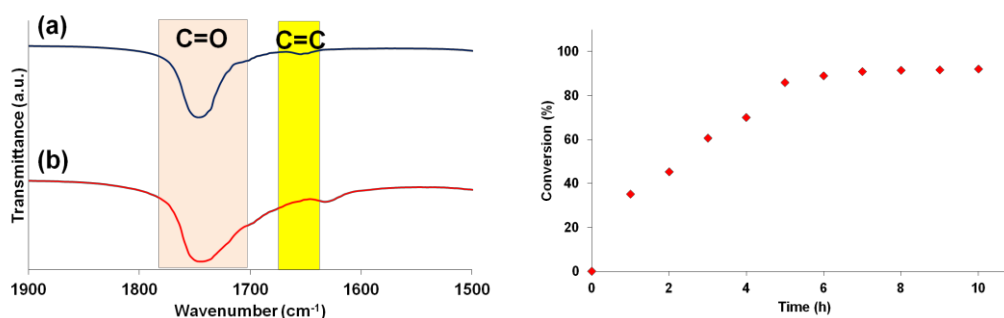


Figure 2 : Infrared spectra of healing agent (left) : (a) before and (b) after oxidation reaction for 10 h. A plot of conversion of C=C vs. oxidation reaction time (right).

The reaction behavior of the soybean oil/olive oil/dryer healing agent was investigated. The healing agent was coated on a KBr disk and stored under ambient conditions to induce oxidation reaction of the soybean oil. The reaction conversion was measured by FT-IR spectroscopy: the ratios of calculated area of the two absorption bands (C=C and C=O as an internal standard) before and after exposure were compared to determine the degree of conversion of the C=C bond using the following formula. The conversion increases with increasing reaction time and 92% conversion was reached after 10 h (Figure 2).

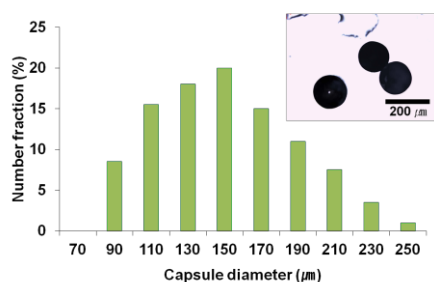


Figure 3 : Size distribution of microcapsules obtained at an agitation rate of 800 rpm. The inset shows the microcapsules.

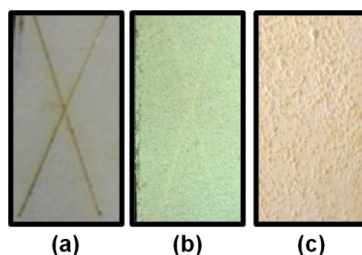


Figure 4 : Photographs of scribed control and self-healing coating samples after immersion in salt water : (a) the control sample after immersion for 48 h. (b) the self-healing sample after immersion for 48 h. (c) the self-healing sample after second scribing of the first scribe region and subsequent immersion for 48 h.

The scribed vegetable oil-based coatings were stored under ambient conditions to induce cross-linking reaction of the released healing agents. Control coatings without microcapsule were also scribed. The scribed and healed self-healing coatings and control coatings were immersed in 10wt% aqueous NaCl solution for 48 h. All control samples corrode, but the self-healing coatings showed no visual evidence of corrosion (Figure 4b). The scribe area in the self-healing coatings was subjected to second scribing to evaluate their repeatable self-healing capability. After 20 min storing under ambient conditions, the coating samples were immersed again in the NaCl solution for 48 h. As shown in Figure 4a, the control coatings showed further corrosion. It is apparent that the vegetable oil-based coatings are nearly free of corrosion despite of the secondary damage (Figure 4c). This result clearly demonstrates the repeatable self-healing capability of the vegetable oil-based coating system. It is considered that the repeatable self-healing can be accomplished based on the viscoelastic property of the cross-linked vegetable oil.

5. CONCLUSIONS

It was successfully demonstrated by anticorrosion test that the vegetable oil-based self-healing coating system has repeatable self-healing capability. This coating system offers the advantages of simple, inexpensive, practical self-healing.

REFERENCES

- [1] M. Huang, J. Yang, Facile microencapsulation of HDI for self-healing anticorrosion coatings, *Journal of Material Chemistry* 21 (2011) 11123-11130.
- [2] C. Suryanarayana, K. C. Rao and D. Kumar, Preparation and characterization of microcapsules containing linseed oil and its use in self-healing coatings, *Progress in Organic Coating* 63 (2008) 72-78.
- [3] R. S. Jadhav, D. G. Hundiwale and P. P. Mahulikar, Synthesis and characterization of phenol-formaldehyde microcapsules containing linseed oil and its use in epoxy for self-healing and anticorrosive coating, *Journal of Applied Polymer Science* 119 (2011) 2911-2916.
- [4] M. Samadzadeh, S. H. Boura, M. Peikari, S. M. Kasiriha and A. Ashrafi, A review on self-healing coatings based on micro/nanocapsules, *Progress in Organic Coatings* 68 (2010) 159-164.
- [5] S. H. Cho, S. R. White and P. V. Braun, Self-healing polymer: Self-healing polymer coatings, *Advanced Materials* 21 (2009) 645-649.

[6] Y. K. Song, C. M. Chung, Repeatability of self-healing of a microcapsule-type protective coating, *Polymer Chemistry* (2013) in press.

CONTROLLED RELEASE OF INHIBITORS FROM COMPOSITE ORGANIC COATINGS: A “GREEN” WAY OF CORROSION PROTECTION

A. Altin¹, A. Erbe¹, H. Ritter² and M. Rohwerder¹

¹ Max-Planck-Institut für Eisenforschung GmbH, Düsseldorf/Germany, e-mail: altin@mpie.de

² Institut für Organische Chemie und Makromolekulare Chemie II, Heinrich-Heine-Universität Düsseldorf, e-mail: h.ritter@uni-duesseldorf.de

Keywords: self-healing, corrosion protection, cyclodextrin, organic coatings, scanning Kelvin probe

ABSTRACT

For many decades chromate based organic conversion coatings were used to protect metal against corrosion. In fact this was the first “self-healing” coating which found a wide application field in the steel, aeronautics and automotive industries. Despite the outstanding self-healing performance of chromate based organic conversion coatings its toxic and carcinogenic properties led to a ban. Hence, there is an urgent need for alternative concepts, which are economically and ecologically viable.

Here we will show that organic composite coatings containing cyclodextrins (CDs) are promising for intelligent corrosion protection. To date, CDs are mainly used for pharmaceutical drug delivery in the human body. They are non-toxic. We successfully complexed different corrosion inhibition agents with CDs and investigated the self-healing properties of coatings containing the resulting complexes. The complexation of inhibitors into the CDs allows the controlled release by electrode potential and pH-change during the corrosion process of the metal. Controlled release and self-healing properties were investigated with a number of different techniques, including Scanning Kelvin probe. Thus, cyclodextrins may develop into a harmless and “green” system for corrosion protection of metals.

A STUDY OF THE TEMPERATURE DEPENDENT HEALING CAPABILITIES OF NEW POLYMERS BASED ON DIELS-ALDER CYCLOADDITION

J. Kötteritzsch¹, M. D. Hager¹, U. S. Schubert¹, R. K. Bose², S. J. Garcia² and S. van der Zwaag²

¹ Laboratory for Organic and Macromolecular Chemistry (IOMC), Friedrich-Schiller-University Jena, Humboldtstr. 10, 07743 Jena, Germany; Jena Center for Soft Matter (JCSM), Friedrich-Schiller-University Jena, Philosophenweg 7, 07743 Jena, Germany – e-mail: julia.koetteritzsch@uni-jena.de; martin.hager@uni-jena.de; ulrich.schubert@uni-jena.de

² Novel Aerospace Materials, Delft University of Technology, Kluyverweg 1, 2629 HS Delft, The Netherlands – e-mail: r.k.bose@tudelft.nl; s.j.garciaespallargas@tudelft.nl; s.vanderzwaag@tudelft.nl

Keywords: copolymerization; crosslinking; Diels-Alder cycloaddition; self-healing polymers; FTIR measurement

ABSTRACT

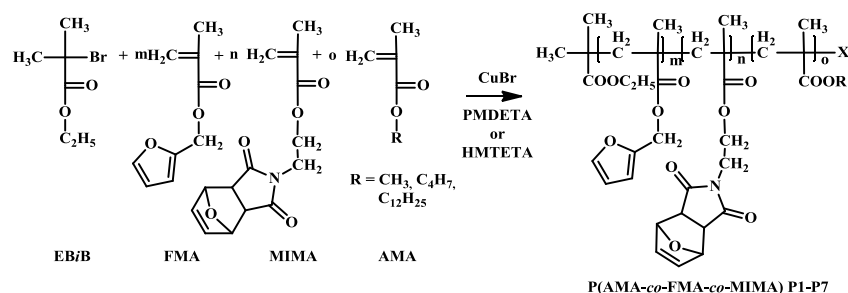
Because of its thermal reversibility, the retro-Diels-Alder (RDA) reaction represents an appealing possibility to produce self-healing polymers with well-defined architectures and tunable properties [1]. However, the polymer architecture for which the Diels-Alder (DA) reaction can best be used to contribute to the healing process is still not well-defined. Therefore, new terpolymers containing moieties for the reversible crosslinking by the DA reaction have been synthesized. These linear polymers are based on a methacrylate backbone containing both functionalities in the side chains and represent a one component self-healing system. As a desirable consequence no separate (low molar mass) crosslinker is necessary to obtain the desired self-healing properties. A protected maleimide is used as functional co-monomer which can be activated after polymerization. Upon the occurrence of local damage the crosslinked material can be heated to a certain temperature, where the retro-Diels-Alder reaction takes place and the material obtains the necessary local mobility for damage closure. Upon cooling to room temperature, the coupling of the two reactive functional groups takes place and the strength of the material is restored. The synthesis of these terpolymers with maleimide methacrylate (MIMA) and furfuryl methacrylate (FMA) as functional units for the DA cycloaddition and different co-monomers in different ratios were achieved by applying the atom transfer radical polymerization (ATRP). Besides the characterization of the obtained polymers by ¹H NMR spectroscopy, SEC, and MALDI-TOF MS, the thermal properties were investigated by TGA and DSC. The damage healing was studied by AFM and SEM. To obtain further details on the healing mechanism at the nanoscale additional temperature dependent FTIR measurements during and after shear flow were made.

1. INTRODUCTION

Self-healing materials are currently in the focus of intensive research. Due to their remarkable ability to heal local mechanical damage such as cracks and scratches, they represent promising candidates for a wide range of applications. The ability for self-healing offers the opportunity to increase the life time of the applied materials which is also associated with less repair events as well as less total replacement of these materials [2]. Therefore, in this project, we synthesized new terpolymers containing functional moieties for the reversible crosslinking by the Diels-Alder reaction which have the ability to heal cracks autonomously after reaching a certain temperature.

2. MATERIALS

The new terpolymers contain MIMA and FMA as functional units for Diels-Alder reactions and different co-monomers in different ratios. As co-monomers methyl methacrylate (MMA, **P1-P3**), butyl methacrylate (BMA, **P4-P6**) and lauryl methacrylate (LMA, **P7**) were used (Scheme 1). The polymers were prepared via ATRP and characterization was carried out using ^1H NMR spectroscopy, SEC, MALDI-TOF MS, TGA and DSC measurements [3].



Scheme 1. Schematic representation of the copolymerization of alkyl methacrylates (AMA), FMA and MIMA by ATRP polymerization.

3. METHODS

The self-healing studies were made using AFM and SEM. AFM measurements were performed in tapping mode with a NTegra Aura (NT-MDT, Moscow, Russia) with commercially available non-contact cantilevers (NSC35, MicroMash). The scratches were performed by using the lithographic mode of the AFM software by dragging the AFM tip at high forces along a line/cross over the surface. Further self-healing experiments and the surface topography were measured using a scanning electron microscope LEO-1450 VP (Variable Pressure) from Carl Zeiss SMT. For this purpose, the crosslinked films were scratched with a hollow needle in a controlled manner to prepare larger scratches, annealed for individual timescales to obtain the different healing states at different temperatures and sputtered with a 10 nm thick gold layer before the measurement. Rheology with *in situ* FTIR was carried out with a ThermoFisher Haake Mars III rheometer coupled to a Nicolet iS10 ATR-FTIR. The rheology with *in situ* FTIR was employed to study the rheology of crosslinking of the polymer followed by reversible heating and cooling cycles to ascertain reversible changes in mechanical properties along with spectroscopic changes in the Diels-Alder adducts in the polymer. These tests allowed following the cyclic and reversibly

occurring Diels-Alder and retro-Diels-Alder reactions. The ratio of the peak height of the furan ring breathing at 1065 cm^{-1} and that of the carbonyl stretch at 1724 cm^{-1} was monitored and used to quantify the healing.

4. RESULTS

The DSC measurements provide highly useful insights into the reversibility capabilities of the copolymers. As depicted in Figure 1 an important precondition for the suitability of self-healing properties of a polymer is the presence of different characteristic transitions during the heating cycles of the DSC measurement. An endothermic peak in the 1st heating curve is expected above 120 °C caused by the energy required for the retro-Diels-Alder reaction and the subsequent evaporation of the furan (protecting group). In addition, the glass transition temperatures (T_g) of the non-crosslinked copolymers should be visible. In the 2nd heating curve the endothermic peak at the T_{RDA} should appear again; however, the area below the curve will be smaller because only the energy of the retro-Diels-Alder reaction is visible; the energy of the evaporation process can not be observed. The appearance of this peak in the 2nd heating curve is a precondition for the later healing process. It depends on the properties of the copolymer, like the co-monomer which causes the flexibility/mobility of the chain and the glass transition temperature.

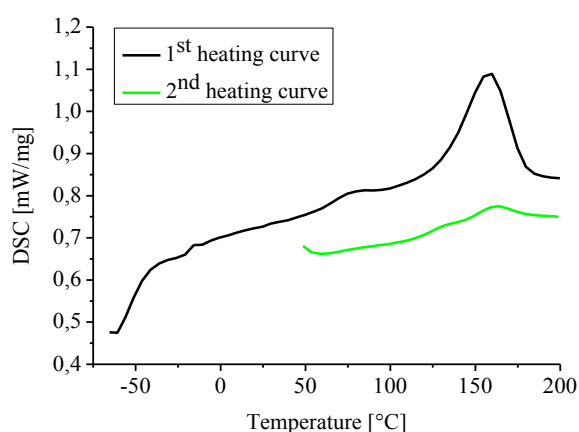


Figure 1: DSC analysis of copolymer **P7**.

The study of the self-healing properties of copolymer **P7** was this time performed by using SEM for visualization (Figure 2). A scratch was created using a hollow needle. Afterwards, the films were annealed for 1 and 3 min at 160 °C , respectively. After only 1 min the scratch was only lightly visible while after 3 min the scratch disappeared completely. Copolymer **P7** has the ability to heal also scratches on a millimeter scale (length).

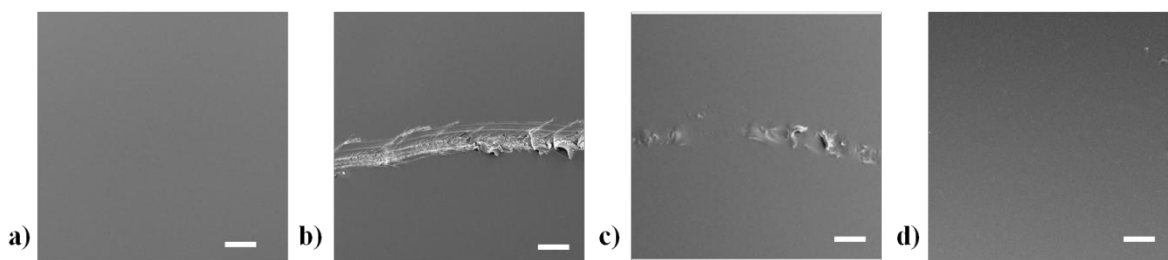


Figure 2: Self-healing experiment of copolymer **P7**. a) Film after crosslinking, b) scratch before annealing, c) scratch after annealing at 160 °C for 1 min and d) scratch after annealing at 160 °C for 3 min (scale bars = 100 μm).

Rheological experiments performed on **P7** at a constant angular strain of 0.1% showed reversible transition of the polymer network indicating flow of the polymer chains which manifest as the healing behavior. Furthermore, quantitative ATR-FTIR showed reversible appearance and disappearance of the furan moiety, as further indication of the Diels-Alder and retro-Diels-Alder reactions as shown in Figure 3.

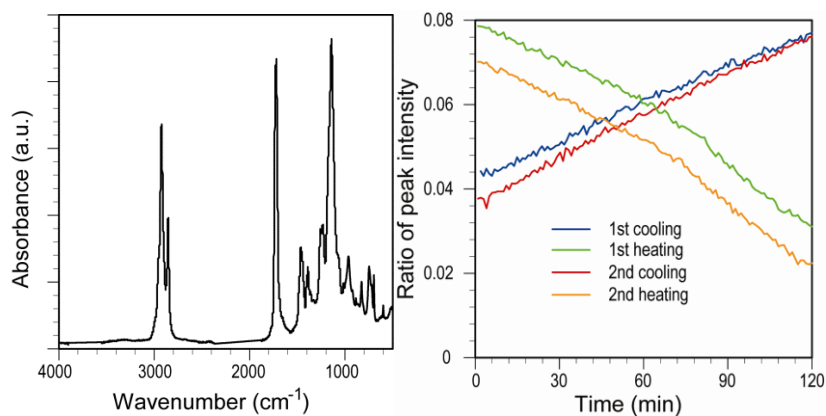


Figure 3: (a) FTIR spectra of the crosslinked polymer prior to the heating and cooling cycles. For quantitative analysis, the peak height ratio of the furan ring breathing at 1065 cm^{-1} to the carbonyl stretch at 1724 cm^{-1} was calculated, and (b) cycling between temperatures of 40 and 160 °C show reversible appearance and disappearance of the furan peak. For each cycle, the temperature was held constant for 120 min.

5. CONCLUSIONS

Well-defined polymers with a methacrylate backbone and the ability to undergo Diels-Alder reactions in the side chain have been produced showing healing behavior at moderate temperatures in the absence of an additional low molar mass crosslinking agent. The copolymer **P7** fulfills all prerequisites for an effective self-healing polymer. Therefore, to the best of our knowledge the described polymers are the first examples for one-component self-healing materials with the complementary Diels-Alder functionalities in the side chain which can reversibly associate and dissociate leading to self-healing behavior.

ACKNOWLEDGEMENTS

Financial support from the Deutsche Forschungsgemeinschaft (SPP 1568) for this study is gratefully acknowledged.

REFERENCES

- [1] S. D. Bergman, F. Wudl, Mendable polymers, *J. Mater. Chem.* 18 (2008) 41-62.
- [2] S. van der Zwaag in *Self healing materials. An alternative approach to 20 centuries of materials science* (Eds.: S. van der Zwaag, A. J. M. Schmets, G. d. van Zaken), Springer, Dordrecht, The Netherlands, (2007) 1-18.
- [3] J. Kötteritzsch, S. Stumpf, S. Hoepfner, J. Vitz, M. D. Hager, U. S. Schubert, One-component intrinsic self-healing coatings based on reversible crosslinking by Diels-Alder-cycloadditions, *Macromol. Chem. Physic.* (2013), DOI: 10.1002/macp.201200712.

SIMULTANEOUS OPTICAL AND ELECTROCHEMICAL MONITORING OF THE PROTECTIVE EFFECT OF FUNCTIONAL SURFACE HEALING AGENTS

C. Mathis¹, S.J. Garcia¹

¹ Novel Aerospace Materials, Faculty of Aerospace Engineering, Delft University of Technology, Kluyverweg 1, 2629 HS Delft, Netherlands – e-mail: c.mathis@student.tudelft.nl; s.j.garciaespallargas@tudelft.nl

Keywords: corrosion protection, capsules, coating, silane, hydrophobicity, optical analysis

ABSTRACT

Encapsulation of reactive agents embedded within a matrix is the most studied concept to develop self-healing materials. The most common approaches employ either a single component with catalyst dispersed in the matrix or a single environment-reactive component for corrosion protection [1].

Recently an approach for corrosion protection based on a single reactive healing agent that combines wetting, reactivity with ambient humidity and the underlying metallic surface, hydrophobicity and densification in time was proposed [2]. Following this idea of using silyl esters, Huang et al. developed a similar system where 1H,1H,2H,2H-perfluorooctyltriethoxysilane (POTS) was used in place of a silyl ester [3]. Despite the good results offered by the octyldimethylsilyl ester and the POTS, there is room for improvement in the design of the healing agents employed for corrosion protection.

The goal of this research is to better understand the wetting, barrier and densification properties of silane based healing agents to be able to develop efficient single reactive healing agents. Therefore a selection of silanes with different chemical backbone structure and surface-reactive end group is evaluated. The barrier properties and the hydrophobicity of the agents is investigated to gain insight into the relationship between chemical structure and final thin film properties. Moreover, in order to evaluate the time dependent corrosion protection performance of the different healing agents a novel optical-electrochemical analysis technique has been developed.

1. INTRODUCTION

Self-healing coatings is a rapidly growing research field. Concepts such as encapsulation of single reactive agents allow the integration of the healing functionality into existing coating technology. The research focuses mainly on new carrier systems, new release concepts, and new **protective** agents. This research aims at investigating the abilities of silane based healing agents to prevent corrosion of an underlying aluminium alloy exposed to a sodium chloride solution. Additionally, a simultaneous optical and electrochemical technique was developed. This technique allowed monitoring the time dependent corrosion protection performance of functional surface healing agents.

2. EXPERIMENTAL

An aluminium alloy AA2024-T3 sheet was employed as a substrate due to its frequent use in the aerospace and automotive industry and for its low corrosion resistance when compared to other aluminium alloys [4].

Several different silane chemistries were chosen as surface healing agents. In this work, three silanes with a trimethoxysilane end group and an alkyl chain of varying lengths of 6, 8 and 10 carbons long for hexyltrimethoxysilane, octyltrimethoxysilane and decyltrimethoxysilane respectively were evaluated. These systems allow a direct correlation between the alkyl chain length and the hydrophobicity and corrosion protection properties.

The metallic samples were cut in small coupons of 2x2cm and grinded using 1000 grit followed by sonication in acetone for 15min and air drying before exposure to the silanes. After the surface treatment a single droplet of 2.5 μ l of undiluted silane was deposited over the substrate using a micro-pipette. The strong wetting capabilities of silanes allowed a rapid coverage. The samples were left at open air to allow hydrolysis and condensation for 24h, leading to the formation of a thin film coating on the metal. The hydrophobicity of the coatings was characterized using a goniometer with 5 μ l drops of ionized water. Finally, corrosion protection was characterized by potentiodynamic polarization scans in a conventional three electrode set-up at a scanning rate of 1mV/s, and by a self-developed corrosion imaging analysis technique for the immersion prior to the potentiodynamic polarization test. The tests were performed under 0.5M NaCl solution in deionized water. The analysis procedure uses image processing software to quantify the number of pits forming during the total immersion time (120 min) followed by the quantification of the corrosion current density by polarization tests.

3. RESULTS

Table 1 shows that the addition of silanes on the surface does not increase the hydrophobicity of the AA2024 in a significant grade. Moreover, the results show a reduction of the contact angle for the longest carbon chain silane (decyltrimethoxysilane (C10)) compared to the other samples.

Table 1: Contact angle (CA) values for the bare substrate and alkyltrimethoxysilanes with three different alkyl chain lengths as indicated by the number of carbons. The values are averages of 4 different measurements and measured between 10 and 30 seconds after deposition of a 5 μ l deionized water drop.

	Bare	C6	C8	C10
CA (°)	83 \pm 1.0	84 \pm 0.6	85 \pm 0.5	77 \pm 0.3

Figure 1 shows the potentiodynamic polarization curves of the four studied samples performed after the first 120min immersion. It can be seen that the hexyltrimethoxysilane, octyltrimethoxysilane and decyltrimethoxysilane coated samples show higher corrosion potentials than the bare aluminium sample, indicating a protective effect. Despite the minor difference in alkyl chain length, the corrosion current density of the octyltrimethoxysilane covered sample shows an increase compared to the other samples and even to the bare aluminium.

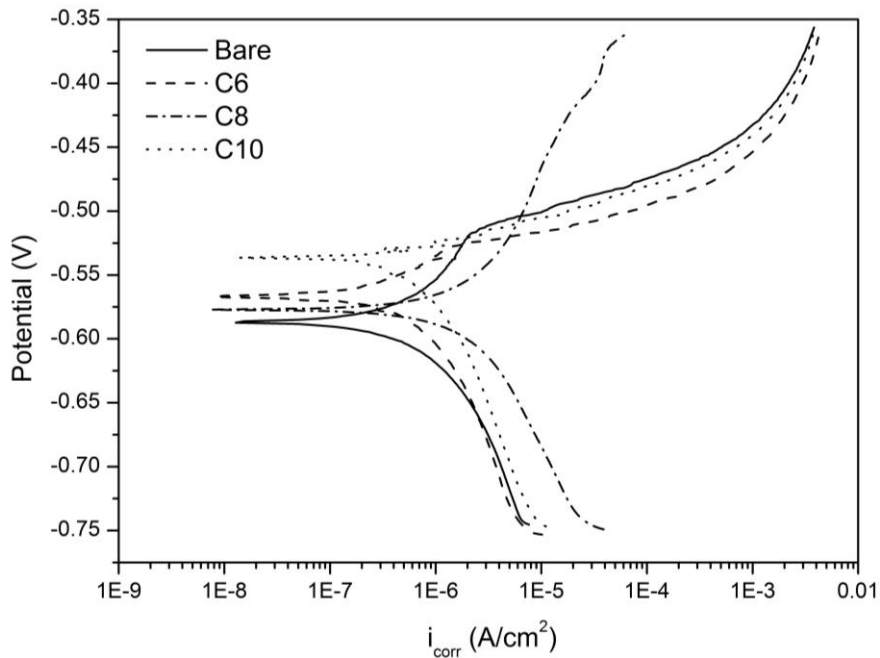


Figure 1: Potentiodynamic polarization scans of the bare aluminium alloy (bare) and the three trimethoxysilanes (C6, C8 and C10) after exposure to a 0.5M NaCl solution for 120min.

Figure 2 shows the optical analysis of the samples immersed in 0.5M NaCl during 120 min prior to the potentiodynamic polarization test. The area covered by pitting (quantified as area of pitting / total exposed area x 100) for hexyltrimethoxysilane and octyltrimethoxysilane is similar and always below that of the reference sample for the same immersion time. Nevertheless, this value is significantly higher when decyltrimethoxysilane is used compared to the other two silanes. This result is in agreement with the potentiodynamic polarization results although more tests need to be performed to confirm the technique works properly.

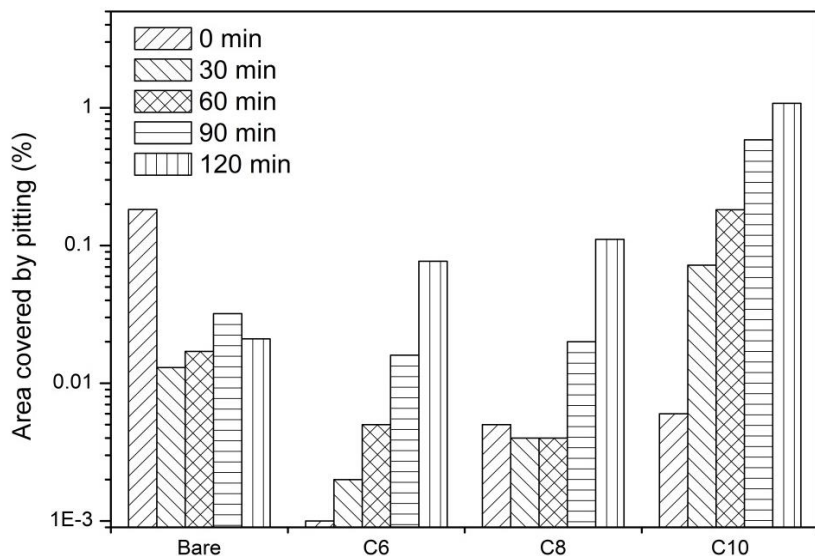


Figure 2: Corrosion image analysis showing the area covered by pitting (quantified as area of pitting / total exposed area x 100) with the exposure time to a 0.5M NaCl solution for the bare sample and the three different silane surface modifications (C6, C8, and C10).

4. CONCLUSIONS

From potentiodynamic polarization scans and optical analysis it was confirmed that the chain length of the silane has a strong influence on the corrosion protection of aluminium substrates. It was found that C6 and C8 show similar protecting results while C10 leads to higher corrosion. Interestingly the contact angles measured with a goniometer showed that the same C10 had the lowest contact angle suggesting a link between the two characteristics. The findings are valuable for the further development of surface reactive healing agents for encapsulated systems. The novel methodology employed to optically monitor corrosion during exposure to a corrosive environment delivered satisfactory preliminary results which are in agreement with the electrochemical analysis. The results open the path to the development of a technique for the simultaneous optical and electrochemical monitoring of corrosion and corrosion protection.

REFERENCES

- [1] S. J. García, H. R. Fischer, and S. van der Zwaag, "A critical appraisal of the potential of self healing polymeric coatings," *Progress in Organic Coatings*, vol. 72, no. 3, pp. 211-221, Nov. 2011.
- [2] S. J. García et al., "Self-healing anticorrosive organic coating based on an encapsulated water reactive silyl ester: Synthesis and proof of concept," *Progress in Organic Coatings*, vol. 70, no. 2–3, pp. 142-149, Feb. 2011.
- [3] M. Huang, H. Zhang, and J. Yang, "Synthesis of organic silane microcapsules for self-healing corrosion resistant polymer coatings," *Corrosion Science*, vol. 65, pp. 561-566, Dec. 2012.
- [4] G. P. Bierwagen and D. E. Tallman, "Choice and measurement of crucial aircraft coatings system properties," *Progress in Organic Coatings*, no. 41, pp. 201-216, 2001.

SELF-HEALING COATINGS FOR TEXTILE

I. De Vilder¹ and M. Vanneste¹

¹ Centexbel, Textile Functionalisation and Surface Modification, Technologiepark 7, 9052 Zwijnaarde, Belgium – e-mail: ivi@centexbel.be

Keywords: self-healing, textile, textile coating, abrasion, test method

ABSTRACT

Self-healing materials have the capability to repair (in an early stage) damage, that would finally lead to material failure. This repair or self-healing occurs with the help of a minor external stimulus or autonomously. Depending on the type of application one or the other is more interesting.

Nature is the major source of inspiration for his type of research: living organisms already possess the property of autonomous repair of damage (wound healing, recovery of broken limbs). Although the phenomenon of self-healing has been recognized in materials throughout history, especially with regards to biological systems, it was only a few years ago that the property of self-healing was seriously considered as a desirable function for man-made materials. As such several research lines have been set up to investigate the possibilities for various application.

Centexbel has looked into the possibilities of a self-healing coating suitable for textiles. In a feasibility study some commercially available products were screened to see their potential as self-healing agents in textile coatings. There was also a need to develop a method enabling to damage the textile coatings in a reproducible way.

In this paper the results obtained will be presented. Eventually a textile coating formulation was developed showing autonomous self-healing properties. It was seen that this coating can also be used on non-textile substrates.

1. INTRODUCTION

The use of self-healing coatings has found a way in multiple industrial branches like automotive, construction,... The introduction of such a self-healing concept into the textile industry can have great benefits. In many cases the textile material gets damaged due to e.g. abrasion, scratches and cuts. The lifetime of a textile material can be prolonged if the repair intervention can be done, automatically and autonomously, at an early stage of the damage formation.

Self-healing can be achieved, among others, via reversible non-covalent crosslink interactions (hydrogen bond formation) in the polymer matrix of the coating.

Functionalised polymers can be used for this purpose. Another type is supramolecular polymers, which are formed by the reversible association of low molecular weight prepolymers. They behave as crosslinked at room temperature (polymer-like viscoelastic behaviour) but show self-healing properties at elevated temperatures due to their liquid-like properties. The effectiveness of such types of self-healing coatings for textile applications was examined.

2. MATERIALS AND METHODS

2.1. Materials

SPH4 SupraB is a supramolecular polymer made by SupraPolix [1].

Bayhydrol U XP 2750 is a hydroxyl functionalized polycarbonate ester-polyurethane made by Bayer Material Science. It is known for its ability to form hydrogen bonds and very high reflow behaviour after dry- or wet-scratching.

Impranil DLC-F is a standard water based polyurethane binder used for textile coatings made by Bayer Material Science.

Fabric: plain woven polyester, 105 g/m².

2.2. Coating of textile

Paste formulations are produced with an IKA-Werke overhead stirrer RW-16 basic.

Labscale samples (A4 format) of the coated material are produced with a Mathis Labdryer type LTF.

2.3. Evaluation of the self-healing properties

2.3.1. Scratch boy

In order to evaluate the self-healing properties of a coating, the coating is damaged and the recovery of the damage is followed over time via microscopy (optic light microscope - episcopic light).

A motorised Pencil Hardness Tester was modified in order to be able to scratch in a reproducible way: the 'Scratch boy' (Figure 1, left). This device enables to scratch at a fixed speed and a set pressure (0N up to 10N), which is not possible when the scratch is done manually.

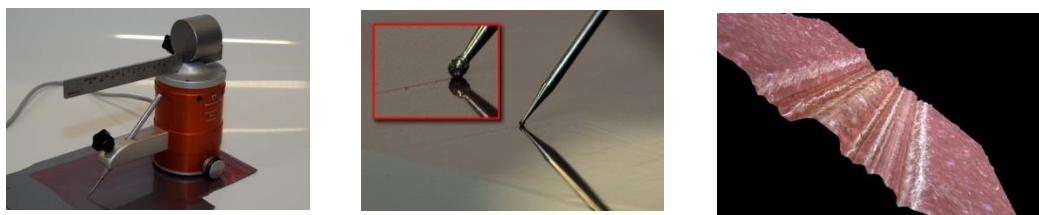


Figure 1: left) Scratch Boy; middle) Diamond wheel point; right) cross-section single scratch

The pencils of the original device are replaced by a diamond wheel point, which is indestructible (Figure 1, middle). Pencils and needles for domestic use are not indestructible, resulting in a variable contact surface, which has an influence on the shape and depth of the damage. Further the device ensures a fixed angle between the coating surface and the wheel point. By placing the diamond wheel point each time at the same manner in the pencil holder identical scratches can be produced, which allows comparison of the healing properties of different samples.

The wheel point resembles a medieval morning star. Several scratches with various depths are made simultaneously. In this way the influence of the depth of the

damage on the self-healing properties can be visualised on a single test piece (Figure 1, right).

2.3.2. Hydrostatic head

Waterproofness is measured with the Textest FX 3000 Hydrostatic head tester according to standard EN 20811 (Textile fabrics – Determination of resistance to water penetration – Hydrostatic pressure test).

3. RESULTS AND DISCUSSION

3.1. SupraB

The SPH4 SupraB polymer beads were dissolved in heated *N,N*-dimethylformamide and the paste was applied onto the polyester fabric via knife coating. Direct coating did not give satisfactory results: during drying of the coating layer (1 min at 80°C and 1 min at 105°C) the polymer started to penetrate the textile. In order to circumvent this problem, the coating layer was applied onto transfer paper and laminated onto the polyester fabric.

The material shows a restorative effect after heating. At elevated temperatures the viscous component becomes predominant and gives the material its flow characteristics. Self-healing occurs at 140°C (Figure 2); at an oven temperature of 100°C no restorative effect was observed.

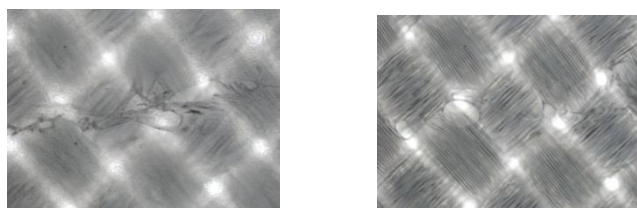


Figure 2: left) initial scratch; right) SupraB after heating to 140°C

This type of self-healing effect is not suitable for textile applications. The flow of the polymeric material, generated upon heating, not only heals the damage, it provokes penetration of the coating material into the textile which can be seen in Figure 2. This results, among others, in a loss of flexibility of the textile, which is not wanted.

3.2. Bayhydrol U XP 2750

After mixing the Bayhydrol with Impranil DLC-F in a ratio of 80/20 a coating layer was produced via direct coating (knife-over-roll) onto the polyester fabric.

In order to evaluate the effect of the self-healing coating on a needle puncture the hydrostatic head was measured (Table 1). After heating the damaged area with a heat gun a slight improvement in waterproofness was observed, which means the puncture has partially repaired.

Table 1 : Hydrostatic head measurements

	Before damage	After damage	After healing
Bayhydrol coating 100 µm	350 cm	18 cm	54 cm

An external stimulus (heating) is needed in order to activate the self-healing which is less attractive in textile applications.

3.3. Self-healing agent

A self-healing agent, based on the formation of hydrogen bonds, is inserted in several types of textile binder materials. Textile materials were coated (knife-over-roll) with these formulations.

No self-healing effect was observed in polyurethane binders, whereas in a certain type of acrylic binder the damage was partially restored. Most of the repair was already observed after 2 days at room temperature; after 1 week no changes were detected anymore.

Small scratches were able to heal completely. On those places where the binder material was completely removed during damaging (bigger scratches), obviously no full self-healing occurred (Figure 3).



Figure 3: left) polyester fabric - initial scratch;
right) polyester fabric - 1 week healing at room temperature

This self-healing functionalised coating system can be applied both on flexible as on hard substrates such as polycarbonate plates (Figure 4).

A basic requirement is flow behaviour of the functionalised binder material at room temperature. If the binder material can close the gap by flowing, additional healing is obtained due to hydrogen bond formation.

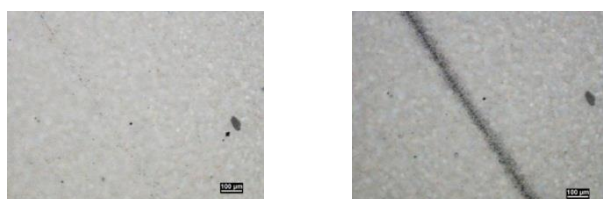


Figure 4: left) PC plate - initial scratch;
right) PC plate - 1 week healing at room temperature

4. CONCLUSION

Self-healing coatings can be implemented in the textile industry. The lifetime of a coated textile can be prolonged if the damaged coating can be healed at an early stage. Centexbel developed an autonomous self-healing coating, based on hydrogen bond formation, which is able to repair small scratches in the coating layer at room temperature. Self-healing coating systems which need external heating as activation

are not recommended for use in textiles as they cause penetration of the coating material in the textile upon heating and tend to change to fabric properties.

REFERENCES

[1] Bosman A. W., Self healing in action, Proceedings of the First International Conference on Self Healing Materials, Noordwijk aan Zee, 2007, pp. 1-6.

UNDERSTANDING THE SELF-REPLENISHING OF HYDROPHOBIC COATINGS FOR FURTHER INDUSTRIAL APPLICATIONS

Y. Zhang¹, A.C.C. Esteves¹, L.G.J. van der Ven^{1,2}, R.A.T.M. van Benthem^{1,3}, G. de With¹

¹ *Laboratory of Materials and Interface Chemistry, Department of Chemical Engineering and Chemistry, Eindhoven University of Technology, Den Dolech 2, 5612AZ Eindhoven, The Netherlands – email: y.zhang3@tue.nl; a.c.c.esteves@tue.nl; r.a.t.m.v.benthem@tue.nl; G.deWith@tue.nl*

² *AkzoNobel, Automotive & Aerospace Coatings, Sassenheim, the Netherlands – email: leo.vandervan@akzonobel.com*

³ *DSM Ahead BV Netherlands, P. O. Box 18, 6160MD Geleen, the Netherlands*

Keywords: Coatings, Self-replenishing, Hydrophobic

ABSTRACT

Hydrophobic materials hold many properties that are desirable in coatings, e.g. water repellency and low-adhesion are essential to achieve an easy-to-clean/ self-cleaning behavior. However, most of the coatings currently available cannot maintain their hydrophobicity upon surface damage or wear, due to the irreversible loss of the low surface energy chemical groups. This damage reduces the service-life time of coatings and limits its implementation on industrial applications.

Therefore, the recovery of surface chemical groups is crucial for extending the service-life of hydrophobic polymeric coatings. One way to achieve this is to introduce a self-healing mechanism which can replenish the low surface energy groups at the surface after the damage. The proof-of-principle was previously reported for a “model” self-replenishing system based on a Poly(urethane) cross-linked soft (low- T_g) network with a small amount of fluorinated dangling chains [1]. In these systems the low surface energy dangling groups can re-orient towards the new air/coating interfaces created upon damaged.

In this poster we report further studies in this model Poly(urethane)-based system which allowed us to clarify key details on the dynamics and kinetics of the self-replenishing mechanism, e.g. the distribution of the dangling chains at the surface and in the bulk [2]. Furthermore, we will also discuss the clear drawbacks identified for the current model system which will restrict its direct industrial applications: 1) weak mechanical properties, e.g. low hardness (due to low T_g) and low solvent resistance. 2) there possibly existed the surface rearrangement due to the presence of hydrophilic ester part in the molecule. So the hysteresis of the coatings were high. 3) the current cross-linking procedure involves high temperature and long curing time.

1. INTRODUCTION

The recovery of surface chemical groups is crucial for extending the service-life of hydrophobic polymeric coatings. One way to achieve this is to introduce a self-healing mechanism which can replenish the low surface energy groups at the surface

after the damage. The proof-of-principle was previously reported for a “model” self-replenishing system based on a Poly(urethane) cross-linked soft (low- T_g) network with a small amount of fluorinated dangling chains [1]. In these systems the low surface energy dangling groups can re-orient towards the new air/coating interfaces created upon damaged.

2. MATERIALS

Several cross-linked polymeric films were prepared according to methods described in the literature [1]. Well-defined polycaprolactone-based oligomer precursors were used to build the cross-linked bulk matrix. The precursors consisted of 3-armed hydroxyl-functionalized polyesters which were synthesized by ring-opening polymerization (ROP) with controlled degree of polymerization(DP) [3]. The low surface-energy polymeric dangling chains consisted of perfluoroalkyl-end capped linear polyesters also prepared by ROP with controlled functionality and DP. Several low surface energy polyurethane films were prepared via reaction of the polyester precursor, dangling chain with the tri-isocyanate, using fixed cross-linking conditions (temperature, solvents and curing time).

3. METHODS

The characterization of the cross-linked films was carried out by Differential Scanning Calorimetry (DSC). Their surface was characterized by X-Ray Photoelectron Spectroscopy (XPS) and dynamic water Contact Angle (CA) measurements.

4. RESULTS

The self-replenishing behavior of the model polymeric coatings was proved by the relatively constant Fluorine to Carbon ratio (F/C ratio) and advancing water contact angle (CA_{adv}) before and after microtoming, which was reported in the literature [1]. However, some drawbacks should also be noticed.

First, all of the studied cross-linked films showed low T_g (below -40°C) (Table 1). For many industrial applications at room temperature, these coatings will function at their rubbery states. Obviously, much lower hardness can be expected compared to its glassy state.

Secondly, with the same binder precursor and same fluorine weight percentage in the initial formulation, the CA_{adv} exhibited the trend to increase with the spacer length of the dangling chain up to DP=16. When the spacer length of the dangling chain increased further, the CA_{adv} showed a significant drop (Figure 1a). However, the F/C ratio obtained by XPS did not indicate significant variance for the dangling chain with different length. The corresponding simulation showed very similar results (Figure 1b) [2]. One possible explanation is the dangling chain with long spacer may adopt a “coiled” configuration exposing more hydrophilic parts of the molecule (Figure 2). This surface rearrangement was confirmed by the significantly lower receding contact angle, which is more sensitive to the hydrophilic groups.

Last but not the least, the current curing method of these polyurethane coatings were carried out at 125°C for 45 minutes in n-methyl pyrrolidone (NMP) via the isocyanate

chemistry. This method will consume a large amount of energy and time if applied in industry.

Table 1: Parameters of the cross-linked films studied [2]

TMP-PCL _x X=	F ₁₇ C ₈ PCL _y Y=	%wt dangling chains	%wt F	T _g (°C)
18	0.0	0.0	0.0	-58
24	0.0	0.0	0.0	-59
36	0.0	0.0	0.0	-59
48	0.0	0.0	0.0	-60
24	16	4.6	0.5	-46
24	16	9.6	1.0	-46
24	16	15.0	1.5	-46
24	16	21.0	2.0	-44
24	16	34.0	3.0	-47
24	8	21.0	2.0	-48
24	12	21.0	2.0	-47
24	16	21.0	2.0	-44
24	22	21.0	2.0	-48
18	8	21.0	2.0	-47
24	8	21.0	2.0	-56
36	8	21.0	2.0	-57
48	8	21.0	2.0	-62

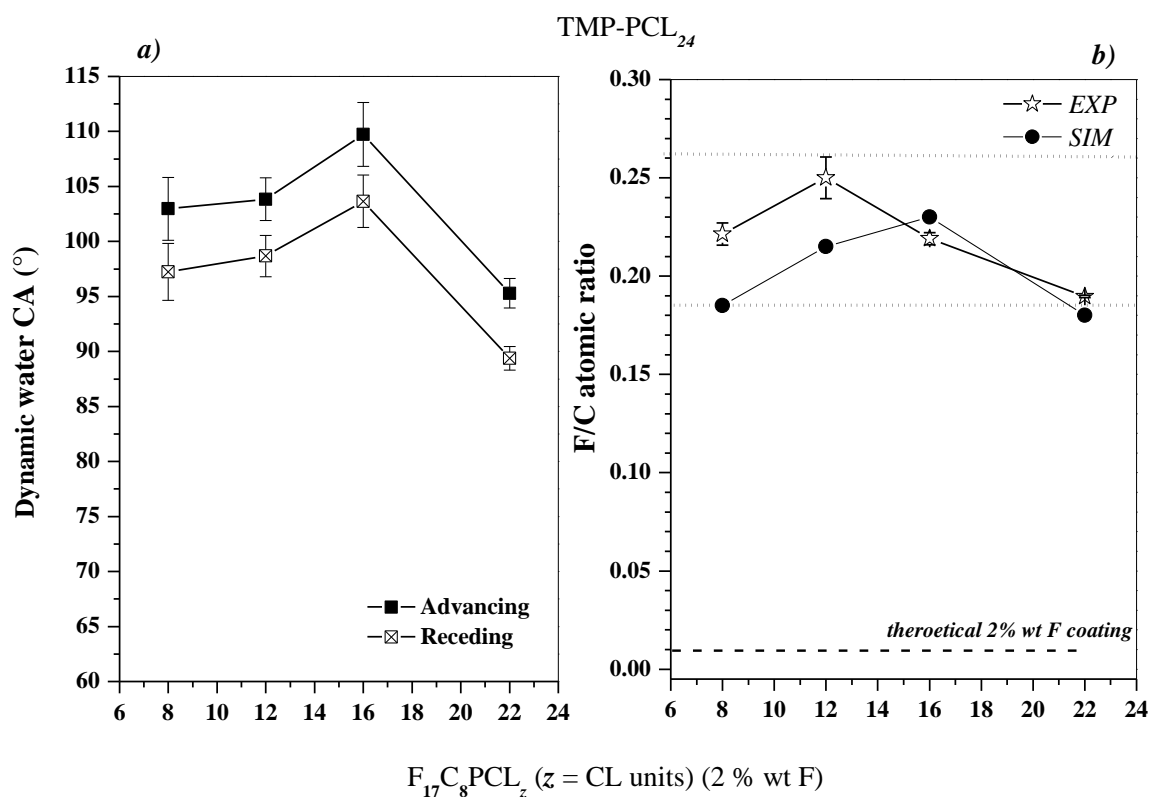


Figure 1: a) Dynamic water contact angles and b) Fluorine/Carbon atomic ratio (F/C) as a function of the length (DP) of the dangling chains (F₁₇C₈PCL_y, y = total CL units), with an overall 2 % wt fluorine in the initial formulation. EXP - determined experimentally by

XPS and SIM - DPD simulation. TMP-PCL24 was used as bulk precursor and $F_{17}C_8PCL16$ as dangling chains (-- dashed lines: F/C theoretical value according to the initial 2% wt of F in the formulation and F/C of Teflon determined by XPS, on a Teflon coated glass substrate) [2].

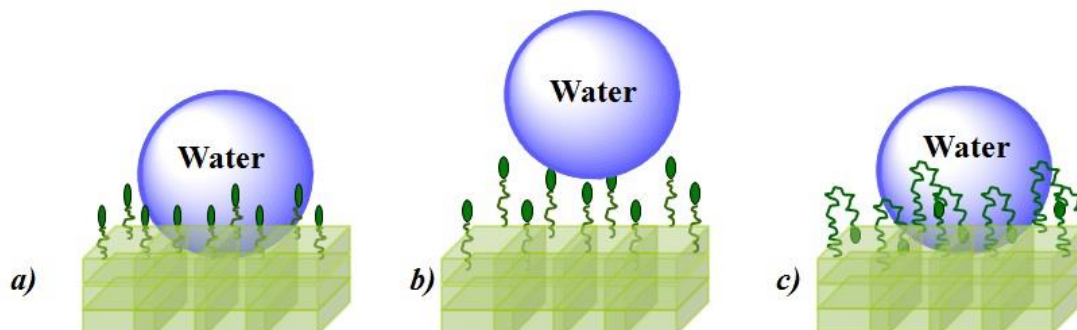


Figure 2: Possible scheme of the configuration of the dangling chains at the air-polymer interface with: a) short polymeric spacer (DP= 8) b) long polymeric spacer (DP = 16) and c) very long polymeric spacer (DP = 22) [2].

5. CONCLUSIONS

According to the results above, several problems identified in the model self-replenishing hydrophobic coating need to be addressed before putting into industrial application. First, the mechanical properties associated to their low glass-transition temperatures should be improved by changing the chemical systems. Secondly, the existence of hydrophilic block in the binder network could probably lead to a surface rearrangement of the dangling chain towards the bulk, which can harm the hydrophobic performance of self-replenishing coatings. Third, it is apparent that the curing method of these coatings by isocyanate chemistry at high temperature and long duration does not fit the trend for high energy-efficiency and eco-friendliness. Therefore, further improvement in the model self-replenishing coating is expected in the future.

ACKNOWLEDGEMENTS

The authors thank Agentschap NL for the financial support (IOP-Self-Healing materials; project # SHM08710).

REFERENCES

- [1] T. Dikic, W. Ming, R. A. T. M. van Benthem, A. C. C. Esteves, G. de With, Self-Replenishing Surfaces, *Advanced Materials* 24 (2012) 3701-3704.
- [2] A. C. C. Esteves, K. Lyakhova, L. G. J. van der Ven, R. A. T. M. Van Benthem, G. de With, Surface segregation of low surface energy polymeric dangling chains in a cross-linked polymer network investigated by a combined experimental-simulation approach, *Macromolecules* (2013), DOI: 10.1021/ma302236w
- [3] T. Dikic, W. Ming, P. C. Thune, R. A. T. M. van Benthem, G. de With, Well-defined Polycaprolactone Precursors for Low Surface-Energy Polyurethane Films *Journal of Polymer Science Part A: Polymer Chemistry* 46 (2008) 218–227.

A REMENDABLE POLYMER NETWORK BASED ON REVERSIBLE COVALENT BONDING FOR COATING APPLICATIONS

G. Scheltjens¹, M. M. Diaz¹, J. Brancart¹, G. Van Assche¹, and B. Van Mele¹

¹ *Research Unit of Physical Chemistry and Polymer Science (FYSC), Vrije Universiteit Brussel, Pleinlaan 2, 1050 Brussels, Belgium – e-mail: gscheltj@vub.ac.be, Maria.Diaz.Acevedo@vub.ac.be, jbrancar@vub.ac.be, gvassche@vub.ac.be, bvmele@vub.ac.be.*

Keywords: Diels-Alder, kinetics, equilibrium, polymer network, gel point

ABSTRACT

An extrinsic self-healing material was synthesized based on the reversible Diels-Alder (DA) reaction between furan and maleimide functional groups, designed for coating applications. At elevated temperatures, the DA/retro-DA equilibrium is shifted towards the initial building blocks. This shift in equilibrium allows a temporary increase in local mobility, which is essential in order to seal any sustained damages to the coating. The actual recovery of initial properties takes place in a subsequent cooling, where recombination of covalent bonds through the exothermic DA reaction occurs.

The advantage of this particular self-healing system lies in its flexible network design. Changing the spacer length in the furan functionalized compound leads to tailor-made properties, such as cross-link density and glass transition temperature (T_g). Based on the T_g analysis performed by differential scanning calorimetry (DSC), a model system was chosen to evaluate the kinetic parameters of the reversible DA reaction by Fourier transform infrared spectroscopy (FTIR).

A methodology to study self-healing properties was developed in a well-defined temperature window based on the kinetics and equilibrium of the reversible networks. In a first step, a maximum sealing temperature of 120 °C was determined to avoid an irreversible homopolymerization of maleimide functional groups [1]. Secondly, the flow behavior at elevated temperatures was characterized by dynamic rheometry. Frequency sweeps were performed in equilibrium conditions at various isothermal temperatures in order to determine the gelation temperature (T_{gel}). It was shown that sealing of microscopic scratches was possible below T_{gel} , leading to the advantage that mechanical properties remain guaranteed during a thermal healing procedure. In addition, the exothermic DA reaction was characterized by Modulated DSC at low temperatures, proving the healing capacity at low temperatures and showing the repeatability of healing procedures.

REFERENCES

[1] G. Scheltjens, M.M. Diaz, J. Brancart, G. Van Assche, B. Van Mele, A Self-healing Polymer Network Based on Reversible Covalent Bonding, *Reactive and Functional Polymers* 73 (2013) 413–420.

SYNTHESIS OF NEW RESINS FOR THE PREPARATION OF UV-CURE SHAPE-MEMORY COATINGS

O. van den Berg^{1,2}, J. Van Damme^{1,2}, F. Du Prez^{1,2}

¹ *Department of Organic Chemistry, Polymer Chemistry Research Group, Ghent University, Krijgslaan 281 S4-bis, B-9000 Ghent, Belgium.*

² *SIM vzw, Technologiepark 935, 9052 Zwijnaarde, Belgium*

Keywords: self-healing, polyester-urethane acrylate, shape-memory

ABSTRACT

In this work the synthesis of novel polyester-urethane acrylates, for use in self-healing UV-cure coatings, is described. Combining telechelic alcohol-functional polyesters and flexible diols of low to medium molecular weight with aliphatic diisocyanates resulted in isocyanate-functional prepolymers that were end-capped with hydroxyl-functional acrylates, yielding acrylated urethane resins of medium molecular weight (15-30 KDa). Introduction of flexible urethane segments into the polyester improved the stability of solutions in isobornylacrylate towards pre-cure phase separation due to crystallization, while the shape-memory characteristics of the final cured materials were retained.

REDOX-RESPONSIVE RELEASE OF SELF-HEALING AGENT FOR ANTICORROSION

L.P. Lv¹, Y. Zhao¹, A. Vimalanandan², M. Rohwerder², K. Landfester, D. Crespy¹

¹ Max Planck Institut für Polymerforschung, Ackermannweg 10, 55128 Mainz, Germany, E-mail: crespy@mpip-mainz.mpg.de

² Max-Planck-Institut für Eisenforschung GmbH, Max-Planck-Str. 1, 40237 Duesseldorf, Germany – e-mail: m.rohwerder@mpie.de

Keywords: capsule, conducting polymer, redox-responsive, self-healing

ABSTRACT

The use of self-healing (SH) materials is a promising approach to hinder corrosion. Extrinsic SH materials based on nanocapsules are good candidates because they can be embedded in coatings without impacting negatively on their structures.

Conducting polymers are applied in various fields due to their high electrical conductivity, good thermal and environmental stabilities [1]. Polyaniline (PANI) is one of the most popular conducting polymers. It has three different oxidation states (Figure 1): the fully reduced leucoemeraldine ($y=1$), the fully oxidized pernigraniline ($y=0$), and the half-oxidized emeraldine ($y=0.5$). Therefore, PANI can also exhibit redox-responsive properties upon electro- or chemical stimuli based on which it has been studied for anticorrosion in metal system [2, 3].

In the present study, we proposed a class of self-healing materials structure based on PANI nanocapsules prepared via miniemulsion polymerization and studied their release behavior upon oxidation or reduction. It was found that the PANI capsules exhibited a release of self-healing agent when reduced by reducing agent. This responsive release behavior after reduction may be due to the chemical structure and morphology change which were investigated by fourier transform infrared spectroscopy (FTIR), ultraviolet–visible spectroscopy (UV-Vis) and scanning electron microscopy (SEM). These conductive nanocontainers are therefore promising for self-healing of corroded metals.

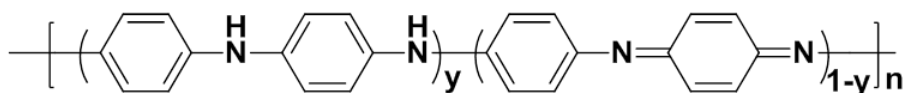


Figure 1: Chemical structure of PANI; the value y dominates the oxidation states.

REFERENCES

- [1] A.G. MacDiarmid, Synthetic Metals: a novel role for organic polymers, *Angewandte Chemie International Edition* 40 (2001) 2581-2590.
- [2] M. Rohwerder, S. Isik-Uppenkamp, C.A. Amarnath, Application of the Kelvin Probe method for screening the interfacial reactivity of conducting polymer based coatings for corrosion protection, *Electrochimica Acta* 56 (2011) 1889-1893.
- [3] M. Rohwerder, Le Minh Duc, A. Michalik, In situ investigation of corrosion localised at the buried interface between metal and conducting polymer based composite coatings, *Electrochimica Acta* 54 (2009) 6075-6081.

SELF-HEALING OF YTTRIUM-DOPED Cr₂AlC MAX PHASE COATINGS DEPOSITED BY HIPIMS

O. Berger¹, C. Leyens¹, S. Heinze¹, M. to Baben², J. M. Schneider²

¹ Technische Universität Dresden, Institute of Materials Science, Chair of Materials Engineering, Helmholtzstraße 7, 01069 Dresden, Germany – e-mail: olena.berger@tu-dresden.de; christoph.leyens@tu-dresden.de; stefan_heinze@kabel.mail.de

² RWTH Aachen University, Chair of Materials Chemistry, D-52074 Aachen, Germany - e-mail: to_baben@mch.rwth-aachen.de; schneider@mch.rwth-aachen.de

Keywords: Cr₂AlC-MAX phase, coating, Yttrium-dotation, oxidation mechanism

ABSTRACT

Self-healing materials allow for a design concept based on damage management where damage that is inflicted during operation can be healed autonomously. It has been shown that the M_{n+1}AX_n phases Ti₃AlC₂, Ti₂AlC and Cr₂AlC exhibit autonomous self-healing behaviour. Cracks are filled and hence healed by oxidation products of the M and A elements in the MAX phase at high operating temperatures. After crack healing the fracture strength is recovered to the level of the virgin material.

Cr₂AlC MAX phase was shown to exhibit excellent erosion resistance and high damage tolerance. The oxide scale forming in the temperature range between 900-1200°C after different oxidation times was studied. The influence of the addition of Y on the rate of oxidation of Cr₂AlC films and on their self-healing behaviour was investigated. The aim of the ongoing research project is to assess the potential of Cr₂AlC MAX phase coatings as autonomous self-healing material by understanding the basic physical and chemical principles governing multiple crack closure to heal erosion damage.

1. INTRODUCTION

The oxidation behaviour of Cr₂AlC has been studied mainly for bulk material so far [1-3] and the oxidation mechanism is not yet fully understood. Interaction with oxygen, especially incorporation of oxygen in the initial stages of oxidation, is essential for the understanding of the oxidation mechanism and improving of the oxidation resistance of this material [4]. Systematic studies of oxygen incorporation into MAX phases are still missing in the literature. Additionally, oxygen dissolution is of importance for the design of self-healing of MAX phases, e.g. [5]. We have focused in this study on the initial stage of the oxidation of the Cr₂AlC-MAX phase synthesized as thin films by High Power Impulse Magnetron Sputtering (HIPIMS) as a new technology, which allows to obtain denser, smoother and better adhesive coatings with determined texture and morphology than other methods. The generally positive impact of reactive-element incorporation on the oxidation resistance of Al₂O₃ and Cr₂O₃ forming high temperature alloys is well known, e.g. [6]. At the present time there are no publications about the influence of yttrium on the oxidation behaviour of Cr₂AlC. In this work we have studied in detail the influence of the yttrium-content on the Cr₂AlC oxidation mechanism and its contribution to self-healing behaviour.

2. MATERIALS AND METHODS

For film preparation by HIPIMS a commercial system (CemeCon AG CC 800-9) and a compound Cr_2AlC target were used. Al_2O_3 -plates were used as substrates. The substrate temperature was maintained at 400°C . These coatings were deposited without doping elements and with addition of Y in the range from 0.1 to 0.3 at.%Y. The coatings were isothermally annealed in the temperature range from 700 to 1200°C in flowing air up to 28h. Our films were characterised by SEM (Zeiss DSM 982 Gemini). Chemical composition analysis was performed by energy dispersive X-ray analysis (EDX) using acceleration voltage of 15kV. The structural analysis was carried out utilizing X-ray diffractometry (Bruker D8 Discover) using $\text{CuK}\alpha$ radiation with area detector VANTEC 2000. Grazing incidence diffraction (GID) method was employed to examine the structure of the thin films. From the characterization results a feedback for improving the synthesis conditions is expected.

3. RESULTS AND DISCUSSION

All deposited films are polycrystalline and consist only of Cr_2AlC . There exists a (110) texture, this means that the (110) and (001) planes are located parallel and perpendicular to the substrate surface, respectively, and the nanolaminates are growing perpendicular to the substrate surface and parallel to (001) plane (Figure 1). From the literature of the oxidation of Al-containing compounds it is known that at low temperatures metastable alumina phases are formed. At high temperatures there is a transformation into the stable α -form. We have found, that in contrast to this, Cr_2AlC forms stable α - Al_2O_3 at all temperatures in the initial phase of oxidation. Probably, oxygen is incorporated in the octahedral interstices of the upper Al-layer leading to formation of Al–O bonds which may act as nucleation sites for Al_2O_3 as described in [4] and shown in Figure 2 [4].

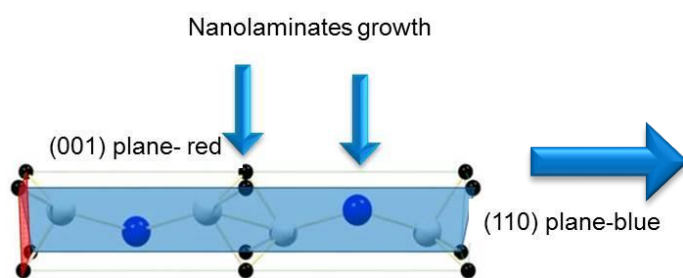


Figure 1: Unit cell of Cr_2AlC with marked position of the (110) and (001) planes.

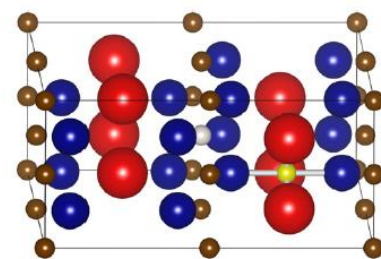


Figure 2: Super cell configurations considered for incorporation of oxygen in M_2AlC : M atoms-blue, Al-red, C-brown, O-yellow, carbon vacancy-white [4].

Preferred orientation (110) of the crystal growth in the MAX-phase thin films is a requirement for epitaxial growth of α -alumina crystals in the initial stage of oxidation at all temperatures.

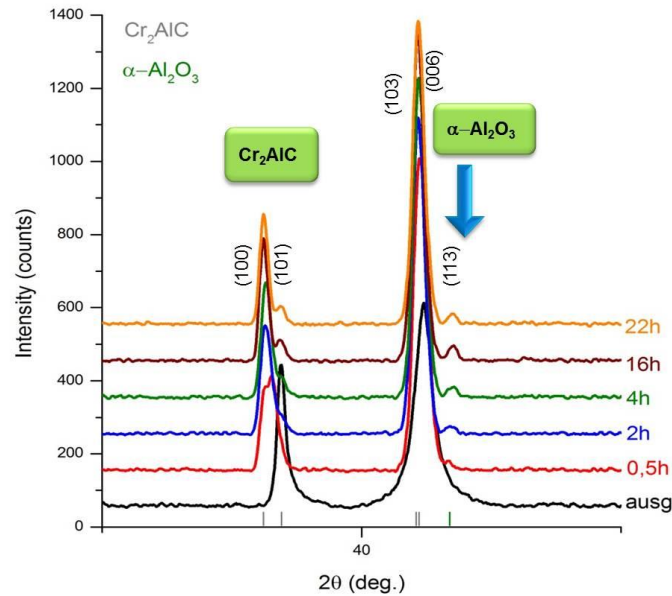


Figure 3: X-Ray diffraction pattern of the as-deposited coatings without Y and after annealing at 700°C for 0.5 - 22h.

We have found, that Y is located in the crystal lattice and does not segregate at the grain boundaries, as shown in [6] and slows down the bulk diffusion of Al-atoms. Oxide growth kinetics is mainly controlled by O anion inward transport. At high temperatures (800-900°C) the oxidation mechanism is changed. The formation and rapid growth of the metastable γ - Al_2O_3 from the α - Al_2O_3 scale for coating without Y was observed. Oxide growth kinetics is mainly controlled by Al cation outward transport caused by the concentration gradient of Al and O in α -alumina grains. As the result, the metastable γ -phase grows in the form of whiskers. The Y-atoms, which are probably located at the places of aluminium atoms at low solubility of Y in the MAX-phase, inhibit the necessary bulk diffusion of Al and Cr atoms and the formation of metastable γ - Al_2O_3 from α - Al_2O_3 scale during oxidation at high temperatures. We have made Vickers indents with 200g load (Figure 4) in order to investigate the influence of 0.3at.%Y on oxidation induced crack-healing in the Cr_2AlC films at 900°C. After annealing at 900°C for 1h the cracks are completely healed by alumina.

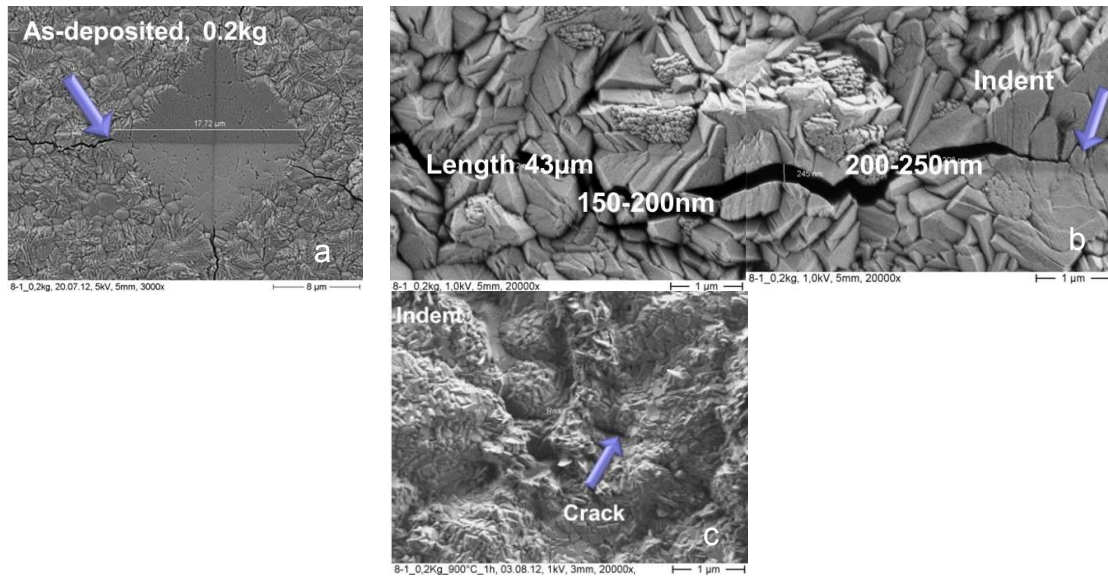


Figure 4: SEM images of the Vickers indents (a) and the crack propagation (b) at the surface of the as-deposited coating, (c) after annealing at 900°C, for 1h in air.

At 1200°C only α -Al₂O₃ is formed. The Al-concentration profile is presented in Figure 5a by the red line. There is an Al-rich area on the surface as a result of the α -alumina formation and an Al-depleted area underneath the surface. An enrichment of Cr occurs (blue line, Figure 5b) also directly beneath the α -alumina area as result of Cr₇C₃ formation. The concentration of Y is presented by the yellow line. Simultaneously, high Al-outward diffusion leads to YAIO₃ formation and an embrittlement of the film.

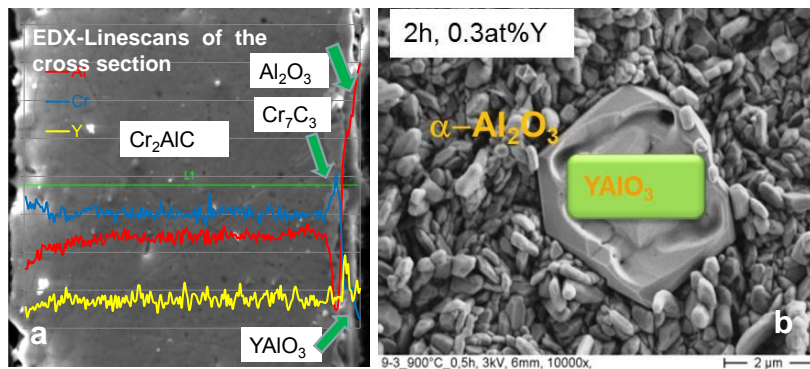


Figure 5: EDX-linescans of the cross section (a) and of the surface (b) of the Cr₂AlC-films with 0.3 at.%Y addition after oxidation at 1200°C for 2h.

Figure 6 shows the influence of 0.2 at.-% Y-addition on the crack healing during oxidation at 1200°C for 2 h.

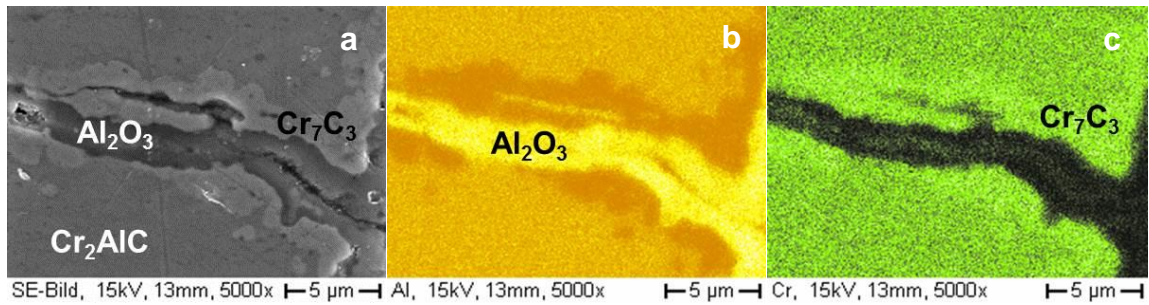


Figure 6: EDX-Mapping of the healed crack filled with alumina after annealing at 1200°C for 2 h of the Cr₂AlC coatings with 0.2 at.-% Y-addition.

4. CONCLUSIONS

In this work, we have determined the optimum Y-content for minimizing oxidation of the Cr₂AlC coatings. Simultaneously, with the same Y-content an optimum self-healing behaviour of cracks was found.

ACKNOWLEDGMENT

Financial support by the Deutsche Forschungsgemeinschaft (DFG) under LE1373/17-1 is greatly acknowledged.

REFERENCES

- [1] W. Tian , P. Wang, Y. Kan and G. Zhang, J. Mater. Science (2008) 1-7.
- [2] D.B. Lee, T.D. Nguyen, J.H. Han and S.W. Park, Corrosion Science 49 (2007) 3926-3934.
- [3] D.B. Lee and S.W. Park, Oxidation of Metals 68 (2007) 211-222.
- [4] M. to Baben, L. Shang, J. Emmerlich and J.M. Schneider, Acta Materialia, 60 (2012) 4810-4818.
- [5] G. M. Song, Y.T. Pei, W. G. Sloof, S. B. Li, J.T.M. de Hosson, S. van der Zwaag, Scripta Mater. 58 (2008) 13-17.
- [6] B.A. Pint, Oxidation of Metals, 45 (1996) 1-37.

SELF-HEALING ADHESION ON POLYMER COATINGS

Y. S. Deshmukh¹, A.C.C. Esteves¹ and G. de With¹

¹ *Laboratory of Materials and Interface Chemistry, Department of Chemical Engineering and Chemistry, Eindhoven University of Technology, Den Dolech 2, 5612AZ Eindhoven, The Netherlands – e-mail: y.s.deshmukh@tue.nl*

Keywords: Coatings, Self-healing Adhesion, Dopamine, Hydrogen Bonds

ABSTRACT

Supramolecular self assembling hydrogen bonded polymeric materials are of great importance due to its practical relevance. Well designed molecules based on these concepts can produce polymeric materials with “responsive” properties like self healing even in coating application. The reversible, non-covalent hydrogen bonding interactions are a recurring design principle for these materials.

Here, we report a concept for repairing mechanical damage at the coating/substrate interface. A dopamine based hydrogen bonded self-healing system was investigated and its use for self-healing adhesion purposes will be discussed. The presence of catechol bonds in the dopamine molecules promotes strong adhesion with the metal surface whereas flexible hydrogen bonding motifs ensure inter/intra molecular hydrogen bonding at the interface with polymer coating. The reversible character of the hydrogen bonds will ensure the repair of the adhesive bonds between the coatings and the substrate upon re-contact at the interface.

1. INTRODUCTION

Polymer coatings are an essential part of our daily life since they can either decorate or protect surfaces from influential aspects of the environment, e.g. from moisture, UV-radiation, chemical attack or mechanical damage. The performance and lifetime of coatings is strongly dependent on the coating materials properties but also on its adhesion to the substrate. Routine handling and usage of coatings typically leads to permanent damage which results in the loss of its protective or decorative functions. Very often, this damage occurs at the primer coating/substrate interface by the rupture of the adhesive chemical bonds, leading to the exposure of the underlying material which becomes vulnerable to further degradation and damage, e.g. corrosion, in the case of metal substrates.

To overcome the occurrence of such damage, extensive research has been performed to introduce self-healing strategies on coatings, which will have the ability to repair the damage, either in an intrinsic or extrinsic way[1,2]^[1]. Many strategies have now been reported to recover “bulk” damage and a few more are now focusing on repairing surface properties[3]^[2] and other functionalities. However, successful healing processes which occur at the coating/substrate interface and repair the adhesion between dissimilar materials have not been reported so far.

In this paper, we report a new strategy for self-healing adhesion, based on dopamine molecules[4] and reversible hydrogen bonds. In our approach we have hydrogen

bonding moieties covalently connected to other molecules strongly attached bonded to a metal substrate, which should provide self healing characteristics at the coating/substrate interface.

2. RESULTS AND DISCUSSION

New molecules having hydrogen bonding moieties and strong metal binding characteristics were designed. The schematic of the molecule having the desired functionalities is presented in the Figure 1.

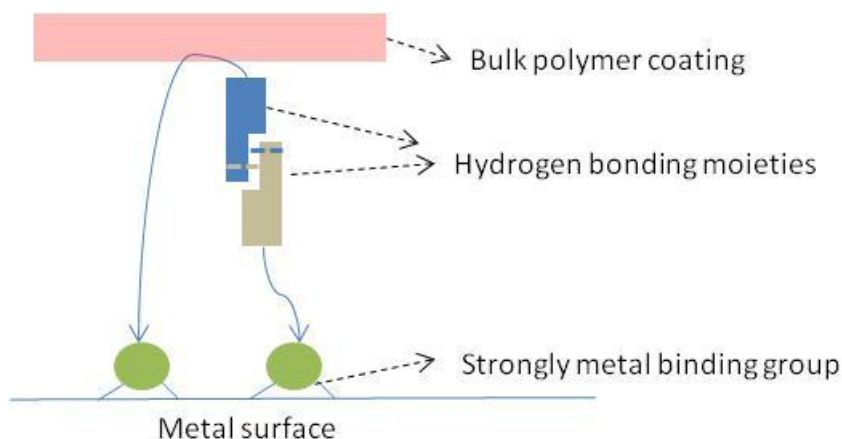


Figure 1: Scheme of a coating having the desired functionalities at interface to provide the self-healing adhesion behavior

The reversible character of the hydrogen bonds will ensure the repair of the adhesive bonds between the coatings and the substrate (bulk polymer coating) upon re-contact at the interface. The scheme of a self healing coating molecule connected via flexible reversible supra-molecular moieties (hydrogen bonding) is presented in Figure 1. The presence of amide moieties at the interface will ensure re-establishment of hydrogen bonding interaction after the mechanical damage.

Figure 2 represents the mechanism of the self-healing adhesion. Figure 2a shows schematically the adhesion before damage and Figure 2b represents the coating after damage, i.e. upon loss of adhesion, represented as a microscopic void. If the flexible reversible supra-molecular moieties from the coating and the substrate re-connect, the adhesion is restored (reversible process from Figure 2b to 2a).

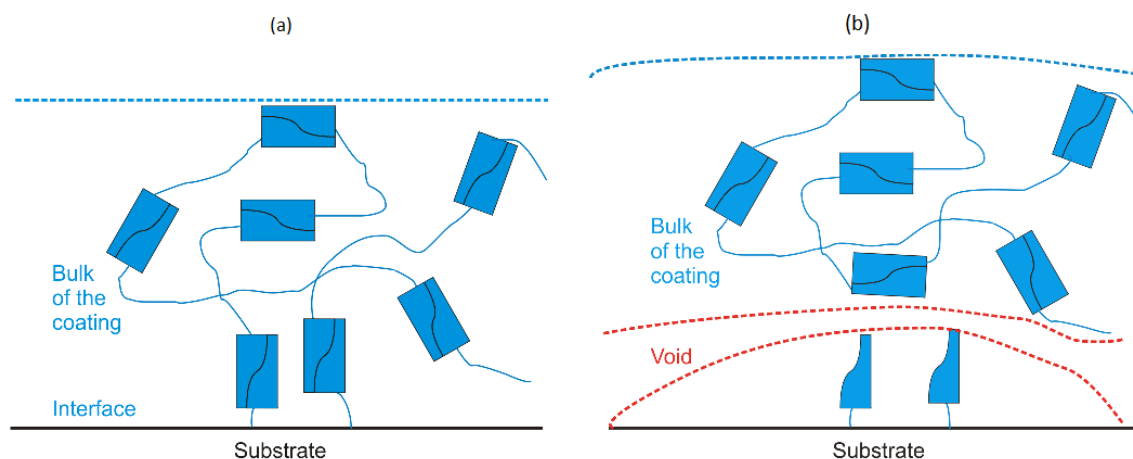


Figure 2: Schematic representation of (a) a coating containing supramolecular moieties connected via supramolecular interactions to a substrate; When stresses in the film are too high, the coating/substrate adhesion can be lost (a \rightarrow b). After the stress is relieved, the adhesion may be restored (b \rightarrow a).

To verify this concept and the recovering from the loss of adhesion, we will make use of a technique known as Johnson-Kendall-Roberts setup (JKR), which is named after its inventors. Two surfaces can be brought in contact and separated in a controlled fashion. Analysis of the contact force and contact area allows quantifying the adhesion between both surfaces. This setup can be used to bring the same surfaces in contact again (re-adhesion). This technique combined with AFM measurements will be used to demonstrate the self healing adhesion concept of the newly designed hydrogen bonded molecules.

3. CONCLUSIONS

We will report a new molecules based on dopamine and supramolecular hydrogen bonding which can be used for preparation of coatings with self-healing adhesion. To rectify the adhesion/re-adhesion of the molecule at the interface, a Johnson-Kendall-Roberts setup will be used. The results will further complimented with AFM measurements.

ACKNOWLEDGMENT

The authors would like to thank SenterNovem / Agentschap NL IOP Self healing materials for providing research funding.

REFERENCES

- [1] A. Dimopoulos, J. L. Wietor, M. Wubbenhorst, S. Napolitano, R. A. T. M. van Benthem, G. de With, R. P. Sijbesma, *Macromolecules*, **2010**, 43, 8664.
- [2] S. van der Zwaag, *Self-healing materials: an alternative approach to 20 centuries of materials science, Vol. 100*, Dordrecht, The Netherlands, **2007**.
- [3] T. Dikic, W. Ming, R. A. T. M. van Benthem, A. C. C. Esteves, G. de With, *Adv. Mater.* **2012**, 24, 3701.
- [4] H. Lee, S. M. Dellatore, W. M. Miller, P. B. Messersmith, *Science* **2007**, 318, 426.

STRESS RELAXATION IN THERMOSETS BY PHOTOREVERSIBLE CROSSLINK EXCHANGE

J. Van Damme¹, O. van den Berg¹ and F. Du Prez¹

¹ Department of Organic Chemistry, Polymer Chemistry Division, Ghent University, Krijgslaan 281 (S4-bis), 9000 Ghent, Belgium – e-mail: jonas.vandamme@ugent.be; otto.vandenberg@ugent.be; filip.duprez@ugent.be

Keywords: coatings, stress relaxation, photoreversible, self-healing

ABSTRACT

Most coating failures are due to stress-related problems. Enabling coating materials to relieve stress can drastically decrease failures and enhance the lifetime of coatings. Stress relaxation can be achieved by reversible exchange of crosslinks. Upon stress (for example due to curing), the reversible crosslinks redistribute and achieve a stress free state. Solar radiation, which is generally available to outdoor coatings, can be used as stimulus for crosslink association (and dissociation) in thermoset coatings. Visible light responsive derivatives are used as photoreversible crosslink in thin thermoset materials, which dimerise photochemically under UV irradiation.

The concept of a novel approach to control MIC corrosion in civil structures

E.J. León¹, D.A. Koleva¹, H.M. Jonkers¹, J.M.C. Mol², H. Terryn^{2,3}, K. van Breugel¹

¹*Civil Engineering and Geosciences, Department Materials & Environment, Delft University of Technology, Stevinweg 1, 2628 CN Delft, The Netherlands; E.LeonFuenmayor-1@tudelft.nl*

²*Faculty 3mE, Department Surfaces & Interfaces, Delft University of Technology, Mekelweg 2, 2628 CD, Delft, The Netherlands*

³*Vrije Universiteit Brussel, Department of Electrochemical and Surface Engineering, Pleinlaan 2, B-1050 Brussels, Belgium*

Keywords: MIC, bio-based coatings, cathodic protection, pulse.

ABSTRACT

Impressed current cathodic protection (CP) based on pulse technology has been proven to be a more efficient and effective alternative of traditional CP for reinforced concrete applications. Essentially, the superiority of pulse CP is in achieving the required steel polarization with otherwise reduced side effects (e.g. influence on bond strength or cement-based bulk matrix properties are minimized); further utilization of lower anodic surface is possible with pulse CP as a result of a better “current throw” at certain frequency and duty cycle of the pulse. The technique has not been tested so far with respect to microbiologically induced corrosion (MIC) and marine applications of steel structures.

This paper will present the concept of recently initiated research for MIC corrosion control through the synergetic action of pulse CP and bio-based coatings. The emphasis is on steel structures for marine applications. An essential part of the expected corrosion control is based on the action of hybrid bio-based coatings, involving competitive microorganisms. The application targets self-healing with respect to MIC and hydrogen-induced damage. Control of anaerobic MIC will be one of the main goals of this research. Extending the application to reinforced concrete and underground pipe-network is also foreseen.

The fundamental mechanisms with respect to MIC corrosion will be defined in parallel to the mechanisms of cathodic polarization when MIC is involved. Clarifying the reasons for steel ennoblement in anaerobic conditions under CP will be achieved and an optimum polarization level will be derived. The first step in this research will be studying the electrochemical behavior of steel in simulated environment as within aerobic, anaerobic and mixed MIC conditions (at open circuit and under cathodic polarization) and the results coupled to steel surface analysis and bacterial viability under conventional and pulse CP.

1. INTRODUCTION

Microbiologically Induced Corrosion (MIC) is a phenomenon where microorganisms initiate or accelerate a corrosion process. It provokes serious damages in various industries and systems which involve the use of natural waters (e.g. oil/gas, shipping, electrical industry) [1]. Conventional cathodic protection (CP) in combination with

coatings, has been used to control steel corrosion, but in most cases, it is necessary to increase the cathodic current density in order to reach protection levels. This is a common problem when MIC is involved due to the “barrier effect” of the bio-film, generated by microorganisms causing MIC. Often, among other phenomena, the bio-film composition i.e. polymeric substances, acts as electrical “insulation” for the cathodic protection. A consequence of increasing the cathodic current density is hydrogen evolution and possibility for hydrogen embrittlement. Pulse cathodic protection has been proven to be more effective than conventional CP in reinforced concrete applications [2-4]. It achieves the required level of polarization by using lower current density, exerts reduced side effects (e.g. bond strength) and enhances positive effects (e.g. Ca-substituted and protective steel product layers). Although known to be applied for underground pipe-networks, the application of pulse CP is to our best knowledge not applied for offshore structures in combination with bio-based coatings, where MIC is involved. A novel approach to solve MIC and hydrogen embrittlement is the synergetic action of pulse CP and hybrid coatings, involving competitive microorganisms that will control the cathodic hydrogen evolution reaction. With this respect it is important to understand the local electrochemical mechanism of microbiologically induced corrosion and the consecutive alterations within cathodic polarization in order to develop more efficient protective alternatives. Therefore this project targets MIC corrosion control through employing self healing hybrid bio-based coatings and pulse CP.

2. MOTIVATION

MIC is a phenomenon affecting properties and service life of civil structures such as carbon steel pipelines (offshore and onshore), bridges, reinforced concrete structures and sewage pipes. Specific environmental conditions can cause different types of MIC, depending on the various microorganisms, as present in the environment. With respect to anaerobic MIC, the most commonly related microorganisms are sulfate reducing bacteria (SRB).

Coatings are the primary protection for corrosion problems in steel structures due to the barrier effect they create by insulating the metal surface from the aggressive environment. A novel solution to control MIC would be a bio based coating that could be used as primer or top coat and act as a barrier on one hand. On the other hand, competitive microorganisms can be involved in the coating and their metabolism will result in self-healing of the interface steel/primer by consuming cathodic and MIC produced hydrogen; additionally the viability of un-wanted microorganisms will be reduced. Sol-gel coatings, containing living cells and oppositely charged poly-electrolytes would be a suitable choice for the above application.

Conventional impressed current CP has been proven of not being able to efficiently deal with MIC due to the above discussed phenomena and those particularly related to steel embrittlement within cathodic polarization. The complexity of the bio-based processes in the presence and absence of cathodic polarization needs in depth investigation, since these determine the electrochemical phenomena, related to the corrosion process itself and/or to CP efficiency respectively.

3. EXPECTED RESULTS

Results to be expected in this work are: to define the fundamental mechanisms with respect to MIC corrosion; to identify the mechanisms of cathodic polarization when MIC is involved; to clarify the reasons for steel ennoblement in anaerobic, aerobic and mixed conditions under CP and to determinate the optimum regime of pulse CP application.

The project targets the formulation of bio-based coatings with the capability to consume cathodic and bio-produced hydrogen and therefore provide the possibility to control the risk of hydrogen embrittlement at a more efficient regime of cathodic polarization. Cost-efficiency is also considered in order to encourage industrial applications

4. SUMMARY AND CONCLUSION

The primary goal of this project is to ensure corrosion control and safe operation within offshore and underground applications (both steel and reinforced concrete) by an integrated approach, combining a novel CP technique based on pulse technology and bio-based, sol-gel coatings for self-healing of hydrogen induced degradation and corrosion damage. The project targets:

- development of a suitable bio-based coating that will control hydrogen formation, absorption/desorption and hydrogen evolution via self-healing mechanisms;
- application of a tailored CP providing larger (or modified) cathodic polarization, so that the cathodic reaction is still effective and not suppressed; using current controlled (instead of the generally applied voltage controlled) regime;
- integration and ensured compatibility of bio-based sol-gel coatings and DC pulse techniques (instead of conventional DC technique), aiming simultaneous corrosion protection, minimised possibility for hydrogen embrittlement and reduced viability of corrosion-inducing microorganisms.

The main outcome(s) of this research will be as follows:

- Formulation of a hybrid, bio-based coating suitable as a primer or top coat for offshore structures (steel), reinforced concrete (underground water mains, sewers) and pipelines (reinforced concrete or steel).
 - Bio-based, sol-gel coating for self-healing of MIC induced damage, simultaneously active to resolve hydrogen-induced damage (as within CP applications). The coating will serve as a matrix (living medium) for competitive microorganisms which consume the cathodic hydrogen (e.g. methanogenes). Alternatively, a sol-gel matrix containing also Gramicidin S producing bacteria can be designed, in order to oppose the SRBs.
 - A hybrid, sol-gel coating containing layer-by-layer deposited bio-polymers on living cells: an approach utilizing bacterial cells and a pair of oppositely charged polyelectrolytes. The low cost of the suggested bio-polymers, compared to others, suggests wider industrial application.

- Bio-based cementitious materials (or mortar/concrete mixtures), containing living organisms of the above defined variety, encapsulated in bio-based polymers. These cement-based materials can be directly applied for new reinforced concrete or as repair materials for existing infrastructure (e.g. underground water mains), where MIC corrosion and/or CP are involved.
- Establishing the optimum regime of pulse CP application in combination with self-healing hybrid coatings: The advantage here with respect to MIC will be reduced viability of the microorganisms (block shaped currents decrease bacterial viability and growth) and reduced hydrogen evolution, while providing the possibility for enhanced cathodic polarization.

REFERENCES

- [1] H. Videla, "Manual of Biocorrosion", New York: Lewis Publishers, 1991.
- [2] D.A. Koleva, JHW de Wit, Ye G, K.van Breugel, Investigation of corrosion and CP in reinforced concrete Part II: Composition and morphology of the surface layers on corroding and cathodically protected steel reinforcement, J. Electrochem. Soc., 154(5), pp.C261-C271 (2007)
- [3] D.A. Koleva, JHW de Wit, K.van Breugel, E.van Westing, Investigation of corrosion and CP in reinforced concrete. Part I: Application of electrochemical techniques, J. Electrochem. Soc., 154(4), pp.P52-P61 (2007)
- [4] D. A. Koleva, Z. Guo, K. van Breugel, J.H.W. de Wit, The beneficial secondary effects of conventional and pulse cathodic protection for reinforced concrete, evidenced by X-ray and microscopic analysis of the steel surface and the steel/cement paste interface, Materials and Corrosion, 60, pp. 704-715 (2009)

**SELF-HEALING THERMOPLASTIC/THERMOSET
POLYMERIC MATERIALS**

POSTER SESSION

INVESTIGATION OF NOVEL CROSSLINKING REACTIONS AS VERSATILE TOOL FOR DESIGNING SELF-HEALING POLYMERS

P. Michael¹, D. Döhler¹, W. H. Binder¹

¹ Institute of Macromolecular and Technical Chemistry, Martin-Luther-University Halle-Wittenberg, Halle (Saale), Germany - Email: philipp.michael@chemie.uni-halle.de

Keywords: self-healing polymers, mechanochemistry, copper(I)-alkyne-azide "click" reaction

ABSTRACT

In recent times the development of self-healing polymeric materials is focused on investigations of fast and efficient crosslinking processes. These should either be able to form new highly branched networks in order to restore thus the initial material properties or to enhance existing materials in view of their thermomechanical and physicochemical properties.

We therefore investigated the copper(I)-catalyzed alkyne-azide "click" cycloaddition reaction (CuAAC) of multivalent polymeric alkynes and azides with respect to crosslinking kinetics, crosslinking efficiencies as well as autocatalytic effects [1-3]. For this purpose a library of several multivalent poly(acrylate)s and poly(isobutylene)s (PIB's) bearing alkyne respectively azide functionalities were synthesized. An efficient network formation could be observed via *in situ* rheology measurements within several hours even at room temperature. Moreover a dependency of the network formation rate on the molecular weight and the functional group densities could be proofed.

Based on these results we expanded the concept of CuAAC to hyperbranched PIB's prepared via living carbocationic inimer (initiator-monomer) type polymerization [4] to study the kinetics and autocatalysis of CuAAC in dependency of branching frequency and to improve the resulting network strand densities and therefore the stiffness of the final crosslinked material.

Beside this we pursue another intrinsic self-healing approach investigating various mechanochemical concepts based on the autonomous activation of a latent catalyst by external force [5]. On this occasion we prepare a polymer based metal-complexes which are able to trigger crosslinking reactions under applied force.

1. INTRODUCTION

Self-healing materials are of great interest for a wide range of applications in material science. Especially the increasing lifetime of polymer compounds lead to the necessity of repairing polymer materials intrinsically, without additional stimulus. Therefore, a fast crosslinking processes based on catalytic reactions acting at room temperature as well as reactive and liquid precursors are required for the development of efficient self-healing concepts.

2. CONCEPT

Thus, the copper(I)-catalyzed alkyne-azide "click" cycloaddition reaction (CuAAC) was chosen and the network formation of multivalent low-molecular weight alkynes as well as of multivalent telechelic or orthogonal functionalized polymeric alkynes and azides were investigated [1-3]. These liquid precursors were encapsulated into melamine-formaldehyde resins and were embedded into a copper(I)-catalyst containing, high molecular weight poly(isobutylene) (PIB) matrix (see Figure 1). The network formations as well as the restoration of mechanical strength were investigated via melt-rheology respectively dynamic mechanical analysis (DMA).

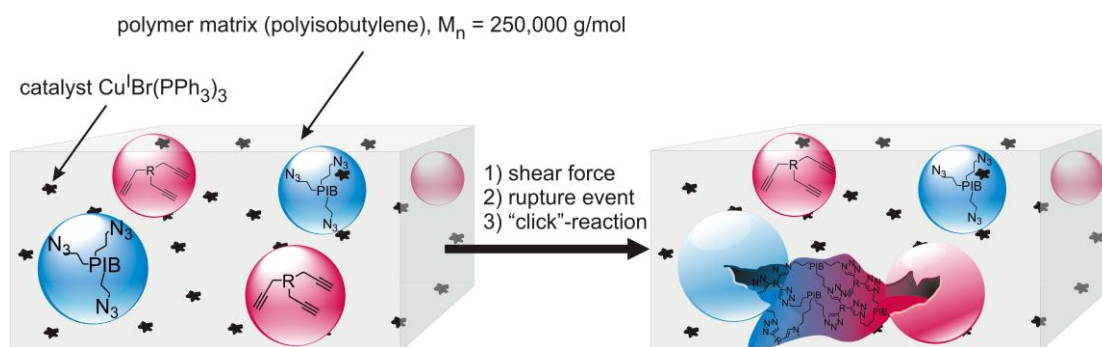
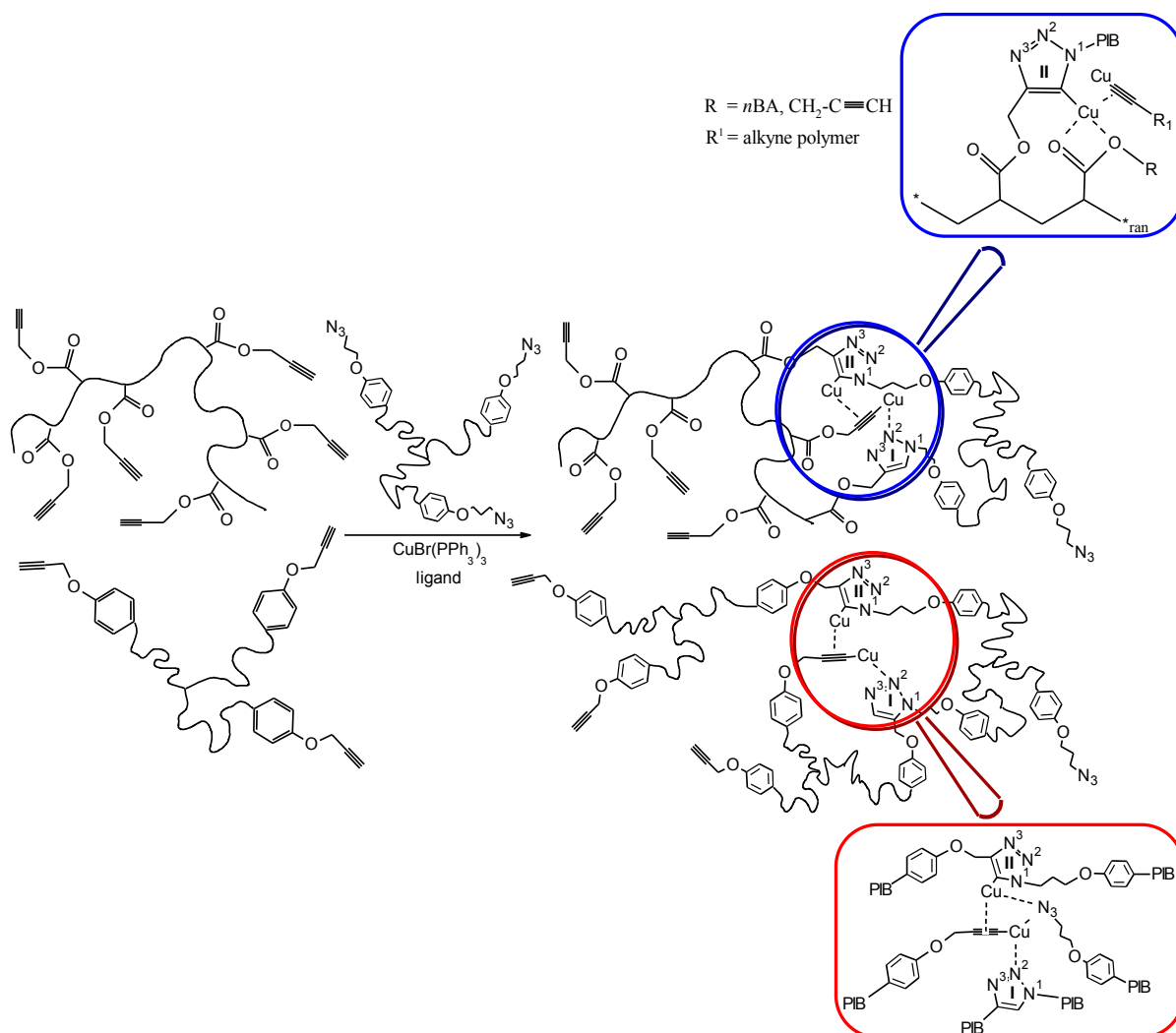


Figure 1: Concept for a shear sensitive self-healing material based on the encapsulation of azide- and alkyne-functionalized compounds embedded in a high-molecular weight PIB matrix containing finely dispersed $\text{Cu}^{\text{I}}\text{Br}(\text{PPh}_3)_3$ as catalyst. Rupture of the capsules and thus release of reactive compounds is induced by shear force resulting in network formation via CuAAC (figure reprinted with permission from [3] Copyright (2011) WILEY-VCH).

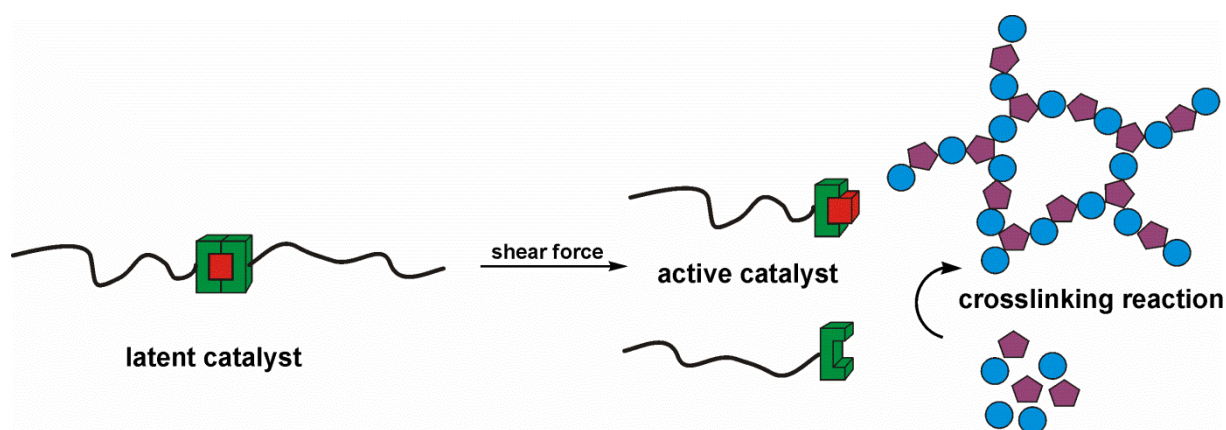
Resulting on these investigations, an efficient network formation depending on the molecular weight and the functional group density could be observed at room temperature via *in situ* rheology measurements within 90 min up to several hours. Polymers with low molecular weight and simultaneously high functional group density show the fastest crosslinking behavior [1].

In order to get a deeper understanding of the crosslinking kinetics and the autocatalytic effects of this reaction, additional melt-rheology, NMR- and IR-spectroscopy as well as differential scanning calorimetry (DSC) measurements were applied in solution and in the bulk state. After screening various reaction conditions, including copper(I) catalysts and different types of polymers for the "click" reaction, like star-shaped azido- and alkyne-telechelic PIB's ($M_n = 5500 - 30000$ g/mol) synthesized via living carbocationic polymerization (LCCP) or random copolymers of propargyl acrylate and *n*-butyl acrylate ($M_n = 7000 - 23400$ g/mol, alkyne content ranging from 2.7 - 14.3 mol% per chain) prepared via nitroxide mediated polymerization (NMP), an auto-acceleration ranging from a factor of 1.6 to 4.3 could be observed. The autocatalytic effect based on the formation of 1,3-triazole rings during the reaction which act as internal ligands within the catalytic process. Moreover, the close special relationship between the neighbored alkyne groups effected the acceleration of the second alkyne addition step according to the proposed mechanism of Fokin et al. [6] (see Scheme 1).



Scheme 1: Proposed mechanism of autocatalysis for crosslinking multivalent poly(acrylate)s and PIB's functionalized with alkyne- respectively azide-groups applying $\text{Cu}^{(I)}\text{Br}(\text{PPh}_3)_3$ and TBTA as catalytic system at 20 °C ((scheme reprinted with permission from [1] Copyright (2012) American Chemical Society)).

Beside this we pursue another intrinsic self-healing approach basing on the mechanochemical activation of latent metal catalysts by external force. On this occasion we prepare a polymer based metal-complexes which are able to trigger crosslinking reactions under applied force (see Scheme 2).



Scheme 2: Schematic concept of a shear force induced mechanochemical scission of a metal complex with polymeric ligands resulting in the activation of a catalyst and triggering of a crosslinking reactions.

REFERENCES

- [1] Döhler, D.; Michael, P.; Binder, W. H.; Autocatalysis in the Room Temperature Copper(I)-Catalyzed Alkyne–Azide “Click” Cycloaddition of Multivalent Poly(acrylate)s and Poly(isobutylene)s; *Macromolecules*; 2012, 45 (8), 3335–3345.
- [2] Schunack, M.; Gragert, M.; Döhler, D.; Michael, P.; Binder, W. H.; Low-Temperature Cu(I)-Catalyzed “Click” Reactions for Self-Healing Polymers; *Macromol. Chem. Phys.*; 2012, 213 (2), 205-214.
- [3] Gragert, M.; Schunack, M.; Binder, W. H.; Azide/Alkyne-“Click”-Reactions of Encapsulated Reagents: Toward Self-Healing Materials; *Macromol. Rapid Commun.*; 2011, 32 (5), 419-425.
- [4] Paulo, C.; Puskas, J. E.; Synthesis of Hyperbranched Polyisobutylenes by Inimer-Type Living Polymerization. 1. Investigation of the Effect of Reaction Conditions; *Macromolecules*; 2001, 34 (4), 734-739.
- [5] Piermattei, A.; Karthikeyan, S.; Sijbesma, R. P.; Activating catalysts with mechanical force; *Nature Chem.*; 2009, 1 (2), 133-137.
- [6] Rodionov, V. O.; Fokin, V. V.; Finn, M. G.; Mechanism of the Ligand-Free CuI-Catalyzed Azide–Alkyne Cycloaddition Reaction; *Angew. Chem. Int. Ed.*; 2005, 44 (15), 2250-2255.

HYPERVELOCITY IMPACT AND OUTGASSING TESTS ON ETHYLENE-CO-METHACRYLIC ACID IONOMERS FOR SPACE APPLICATIONS

L. Castelnovo¹, A. M. Grande¹, L. Di Landro¹, G. Sala¹, C. Giacomuzzo², A. Francesconi²

¹ *Department of Aerospace Science and Technology, Politecnico di Milano, Italy.*

² *Department of Industrial Engineering, Centre of Studies and Activities for Space CISAS "G. Colombo", University of Padua, Italy*

Keywords: ionomer, EMAA, hypervelocity impact, outgassing test

ABSTRACT

The ability of a material to self-repair is particularly important in remote or hostile environment applications, where an external intervention is nearly impossible. For example, the development of self-healing (SH) materials for space applications could dramatically improve spacecraft performances and liability, with significant enhancement of mission duration. A number of copolymeric ionomers have been recognized to present self-healing capability under defined ballistic conditions and have risen considerable interest by researchers. On the other hand, when exposed to a vacuum environment for long period, polymers may exhibit considerable mass reduction due to volatile diffusion and loss; this can significantly affect physical and mechanical properties, thus preventing their employment in space applications.

This work aims to give a preliminary evaluation of possible employment of polyethylene-co-methacrylic acid (EMAA) based ionomers in space environment. The SH capability was studied through hypervelocity impact tests in different experimental configurations, in order to simulate the collision events with micrometeoroids or debris typical of space environment. The healing efficiency was evaluated by leakage tests and by observation of the impact area with a scanning electron microscope.

Thermal outgassing tests were performed to explore the material behaviour in conditions similar to those of space environment. Using a high vacuum chamber, specimens were exposed to a vacuum environment; thermal cycles were also applied to favour the outgassing phenomena. Quite limited mass losses were detected after the tests.

1. INTRODUCTION

In recent years, the amount of space debris has increased significantly and the number of small objects (<1cm), which are difficult to monitor by ground stations, is continuously growing due to space collisions or explosions [5]. Even if small, these objects have a great kinetic energy, so impacts are seriously dangerous for space systems, especially for pressurized systems, such as tanks or habitable modules. In this scenario, it would be very important to employ materials which can self-repair after an impact and avoid any pressure leakage.

The ability to self-heal a damage exhibited by polyethylene-co-methacrylic acid (EMAA) based ionomers has already been discussed in previous works [1-4]. Here the possibility of employ EMAA ionomers in space applications has been investigated, with particular reference to self-healing behavior after hypervelocity impacts. In addition, thermal vacuum outgassing test was also carried out on EMAA ionomer as a first step of a space qualification of the material.

2. MATERIAL AND METHODS

2.1 Materials and sample preparation

A ionomer based on poly-ethylene-co-methacrylic acid copolymer was used. This material, provided by DuPont with the commercial name Surlyn® 8940, has a content of 5.4 mol% of acid groups, 30% of which are neutralized with Na ions. It has a density of 0.95g/cm³ and a melting temperature of 94°C. Flat samples were produced by compression moulding, using an hot press with a moulding temperature of 180°C and a moulding pressure of about 5 bars. These square plates were used as samples both in thermal outgassing test and in hypervelocity impact tests. In these tests different thicknesses were considered from 2 to 5 mm.

2.2 Hypervelocity impact test

Hypervelocity impact tests were carried out using a two-stage Light-Gas Gun (LGG) [6]. Six different test conditions were employed by varying specimen thickness and bullet speed. In all the tests 1.5mm aluminum spheres were used as bullets, while two different velocities were considered, 2 and 4km/s. Samples 2, 3 and 5mm thick were tested.

After the impacts the healing evaluation was performed both by microscope observations of impact zone and by pressure leakage tests. The impact areas of all specimens were observed using an Hitachi TM-3000 scanning electron microscope. To better investigate the healing level, pressure leakage tests were also executed using a specific-designed device developed for this purpose (Figure 1). A pressure gradient of 0.9 bar was applied by a vacuum pump up to more than 15 minutes. When the hole was healed, no appreciable vacuum decay was detected, while non-healed samples showed a vacuum decay within few seconds.



Figure 1: Sketch of the experimental system for leakage test.

2.3 Thermal vacuum outgassing test

Thermal vacuum outgassing test was performed to investigate the possible loss of mass from the material in the form of volatile gases. The test was performed using a thermal vacuum chamber able to perform high vacuum conditions (up to 10⁻⁹ bar) and equipped with two different heat sources: a conductive heat plate and a radiant heating system. Three square plate specimens were tested. All the specimens were cleaned and pre-conditioned at 22±3°C and 55±10% RH, as prescribed by ECSS-Q-ST-70-02 [7].

During the test a pressure of 10⁻⁸ bar was maintained in the chamber for 43 hours (Figure 2). Two thermal cycles at 60°C were applied during the test to promote outgassing: a first cycle performed only by conductive plate and a second cycle performed both by

conductive and radiant heating systems (Figure 3). The temperature was monitored either on the specimen and on the conductive plate. The mass variations were evaluated comparing the weight of each sample before the test, immediately after the test and after two weeks.

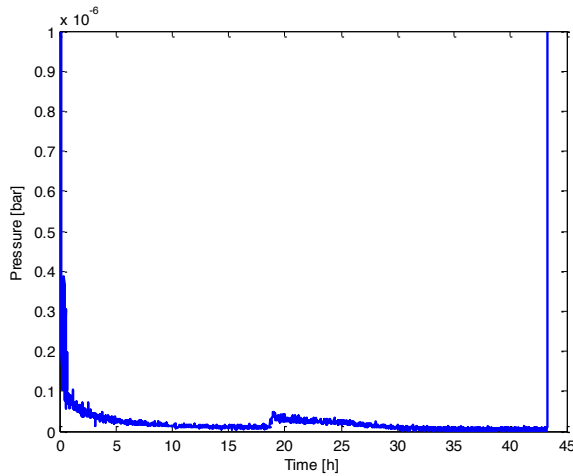


Figure 2: Pressure profile.

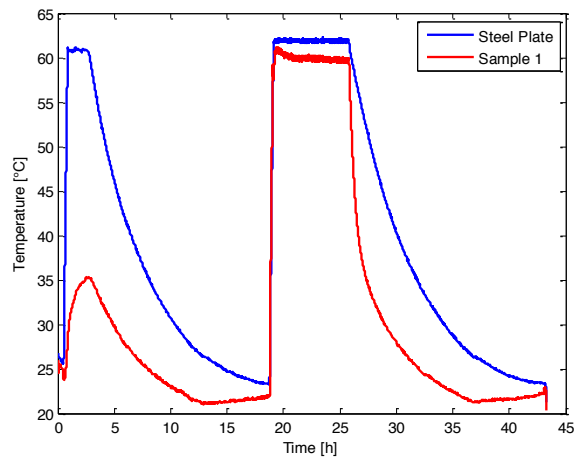


Figure 3: Temperature profile.

3. RESULTS AND DISCUSSION

3.1 Hypervelocity impact test

Hypervelocity impact experiments performed by firing 1.5 mm aluminum spheres proved the healing behavior of EMAA ionomer at the two tested speed ranges; test results are summarized in Table 1. At the lowest projectile velocity, 2 km/s, all samples visually exhibited complete hole closure, but leakage tests showed a loss of pressure of the 3 mm thick specimen. Conversely, at the highest speed, 4 km/s, only the 3 and 5 mm thick samples exhibited complete hole closure.

Table 1: Results of hypervelocity impact test.

Sample ID	Sample thickness [mm]	Bullet velocity [km/s]	Puncture	Visible healing	Leakage test
1	2	1.93	✓	✓	✓
2	3	1.80	✓	✓	✗
3	5	1.64	✗	-	-
4	2	3.90	✓	✗	-
5	3	4.00	✓	✓	✓
6	5	4.10	✓	✓	✓

Morphological analysis after the impact tests showed some debris of the fired aluminum sphere on the bullet entry side of all the specimens, while no residues were detected on the exit side. In every sample the bullet entry zones showed an indented surface, while the exit sides exhibited a clearly defined melted zone of approximately the same diameter as spherical projectile.

3.2 Thermal outgassing test

The results of thermal outgassing test, in terms of weight and mass variations, are reported in Table 2. The test showed that EMAA ionomer considered is not affected by significant outgassing phenomena. The limited mass loss recorded in the two samples immediately after the test is partially due to humidity loss, as confirmed by weight regain exhibited by all samples after storage for two weeks at $22\pm 3^{\circ}\text{C}$ with a relative humidity of $55\pm 10\%$.

Observing the temperature profile it can be noticed that in the first thermal cycle the material didn't reach the target temperature, while in the second cycle immediately reached the target; this is due to the better efficiency of the radiant heating in vacuum compared to conductive heating. Observing the temperature and pressure profiles it can be pointed out that the mass release occurred instantly once the material reached the fixed temperature. This confirms the relevance of thermal cycle in promoting the outgassing and ensures that mass loss was fairly complete at the end of the test.

Table 2: Results of thermal outgassing test.

Sample ID	Weight [g]			Variation	
	Before test	After test	After 2 weeks	After test	After 2 weeks
1	27.730	-	27.719	-	-0.039%
2	30.574	30.544	30.559	-0.098%	-0.049%
3	28.196	28.168	28.180	-0.099%	-0.057%

4. CONCLUSIONS

The self-healing ability of EMAA ionomer was investigated in case of hypervelocity impacts, typical condition of space mission employment. SEM micrographs and de-pressurized air flow tests confirmed the self-repairing behavior for studied material.

Thermal outgassing test showed that the ionomer is not significantly affected by outgassing phenomena. Although extensive testing is needed for a space qualification, these tests provide a first basis for a possible future employment of EMAA ionomers as self-healing materials in space applications.

ACKNOWLEDGEMENTS

The sponsorship of Regione Lombardia - projects STIMA and SMAT - is gratefully acknowledged. The authors wish to thank the company DuPont (Italy) for providing the ionomeric material.

REFERENCES

- [1] Van der Zwaag, S., [Self-healing materials. An alternative approach to 20 centuries of materials science], Springer, Dordrecht, The Netherlands, (2007).
- [2] Kalista S.J., Ward T.C., Oyetunji Z. "Self-healing of poly(ethylene-co-methacrylic acid) copolymers following projectile puncture." *Mech Adv Mater Struct* 2007;14(5):391-397.
- [3] Grande A.M., Coppi S., Di Landro L., Sala G., Giacomuzzo C., Francesconi A., Rahman M.A. "An experimental study of the self-healing behavior of ionomeric systems under ballistic impact tests." *Proc SPIE* 2012;8342.

- [4] Francesconi A., Giacomuzzo C., Grande A.M., Mudric T., Zaccariotto M., Etemadi E., Di Landro L., Galvanetto U. "Comparison of self-healing ionomer to aluminium-alloy bumpers for protecting spacecraft equipment from space debris impacts." *Adv Space Res* 2012; in press.
- [5] Pardini C., Anselmo L. "Physical properties and long term evolution of the debris clouds produced by two catastrophic collisions in Earth orbit." *Advances in Space Research*, 2011; 48: 557-569.
- [6] Angrilli F, Pavarin D, De Cecco M, Francesconi A. "Impact facility based upon high frequency two-stage light-gas gun." *Acta Astronaut* 2003;53(3):185-189.
- [7] European Cooperation for Space Standardization. "Space Product Assurance - Thermal vacuum outgassing test for the screening of space materials." ESA - ESTEC, 2008. ECSS-Q-70-02c.

AUTONOMOUS SELF-HEALING OF POLYMERIC GELS CROSS-LINKED BY DIARYLBIBENZOFURANONE-BASED DYNAMIC COVALENT BONDS

K. Imato¹, T. Kanehara¹, T. Ohishi², A. Takahara^{1,2} and H. Otsuka^{1,2}

¹ Graduate School of Engineering, Kyushu University, 744 Motooka, Nishi-ku, Fukuoka 819-0395, Japan – e-mail: otsuka@ms.ifoc.kyushu-u.ac.jp

² Institute for Materials Chemistry and Engineering, Kyushu University, 744 Motooka, Nishi-ku, Fukuoka 819-0395, Japan – e-mail: otsuka@ms.ifoc.kyushu-u.ac.jp

Keywords: dynamic covalent chemistry, cross-linked polymers, gels

ABSTRACT

Self-healing materials attract a lot of attention because of their ability to repair the internal and external damage, thereby extending the lifetime of the material in numerous applications that we cannot repair easily. Diarylbibenzofuranone (DABBF), which is a novel dynamic covalent bond unit, can reach a state of radically thermodynamic equilibrium under air at room temperature without any stimuli. Furthermore, DABBF and radical species formed from cleaved DABBF are tolerant of oxygen. Here we report that gels cross-linked by DABBF show autonomous self-healing under air at room temperature.

Cross-linked polymers with DABBF as a cross-linker were prepared by polyaddition of tetrahydic DABBF and tolylene-2,4-diisocyanate-terminated poly(propylene glycol) (PPG). To confirm whether or not DABBF units in the cross-linked polymers were a state of equilibrium and could exchange their bonds, de-cross-linking reaction was performed in DMF under air at room temperature by adding excess DABBF. After de-cross-linking for 24 h, a THF-soluble high-molecular-weight component was detected by GPC measurement. It was expected to be linear polymers and/or cross-linked oligomers. ¹H-NMR spectrum of the solution without fractionation after de-cross-linking clearly indicated the presence of soluble PPG, which had constituted a three-dimensional network. In contrast, these results were not observed in the case of the usual cross-linked polymers (control experiment). Consequently, we confirmed that the reorganization of the cross-linked polymers was due to the autonomously exchangeable DABBF units.

The self-healing property of the polymeric gels swollen with DMF was also investigated under air at room temperature. The gels were cut with a razor blade and the cut pieces were brought together immediately without pressing them strongly. After 24 h, self-healing of the contacted samples could be observed and the scars had almost disappeared. This self-healing behavior was also verified from the almost complete recovery of mechanical properties.

1. INTRODUCTION

Polymers with the ability to repair themselves after sustaining damage without external human intervention can extend the lifetimes and improve the inherent safety of the materials. One way to endow polymeric materials with self-healing ability is introducing dynamic bonds into the polymer networks such as hydrogen bonds, ionic bonds, host-guest interaction, and dynamic covalent bonds. Diarylbibenzofuranone (DABBF) can exist as a state of thermodynamic equilibrium of bond breaking and reformation under air at room temperature. In the present research, we employed DABBF as a dynamic covalent bond and demonstrated bond-exchanging property of DABBF in polymer networks. Furthermore, we attempted to prepare autonomously self-healable cross-linked polymer gels by introducing DABBF as a cross-linker [1].

2. MATERIALS

Tetrahydric DABBF (**DABBF-tetraol**) was prepared from 4-hydroxymandelic acid and 2,4-di-*tert*-butylphenol in three steps. Cross-linked polymers with DABBF were synthesized by polyaddition of **DABBF-tetraol** and toluene-2,4-diisocyanate-terminated poly(propylene glycol) (PPG, $M_n = 2400$), in the presence of di-*n*-butyltin dilaurate (catalyst) in 1,4-dioxane. The fluidity of the reaction mixture slowly decreased during the course of the reaction. The reaction mixture finally lost fluidity after 48 h, indicating that polymerization was successful. The samples for self-healing tests were prepared by similar method in DMF and used without purification. A typical cross-linked polymer was also prepared and used as a control sample. It was prepared from tetrahydric bisphenol A and diisocyanate-terminated PPG in a manner outlined for the polymers cross-linked by DABBF.

3. METHODS

To confirm whether or not DABBF units in the cross-linked polymers were a state of equilibrium and could exchange their bonds, de-cross-linking reaction of the polymers was performed in DMF under air at room temperature by adding excess **DABBF-tetraol**.

Self-healing properties of the cross-linked polymer gels were investigated under air at room temperature. DMF was selected as a solvent for the gels, because it prevents the urethane units from hydrogen bonding and it has low volatility. The gel samples were cut with a razor blade to expose fresh surfaces. The fresh surfaces were wetted with a small amount of DMF to contact tightly and then were brought together immediately without pressing them strongly. The in-contact samples were kept at room temperature under air for 24 h.

Tensile tests were performed to quantitatively evaluate the self-healing properties. The healing process of the samples was performed in the dark under saturated vapor pressure of DMF for 3–24 h (healing times). The gels for tensile tests were fabricated into ISO 37-4 specimens (dumbbell shape, 12 mm × 2 mm × 0.6–1 mm) and were fixed at both ends on thin Al plates with glue and adhesion tape. The plates were pulled under air at room temperature at a crosshead speed of 5 mm min⁻¹. The measurements were performed using more than six test pieces for each healing time and three of them were chosen. Average values were determined from these three samples.

4. RESULTS AND DISCUSSION

After de-cross-linking of the polymers cross-linked by DABBF for 24 h, a THF-soluble high-molecular-weight component ($M_n = 28300$) was detected by GPC measurement. It was expected to be linear polymers and/or cross-linked oligomers. Although we tried to perform a detailed analysis by fractionating this component, the cross-linking reaction occurred again after fractionation. However, the $^1\text{H-NMR}$ spectrum of the solution without fractionation after de-cross-linking clearly indicated the presence of soluble PPG, which had constituted a three-dimensional network. In contrast, these results were not observed in the case of the control experiment. Consequently, we confirmed that the above-mentioned reorganization of the cross-linked polymers was due to the autonomously exchangeable DABBF units.

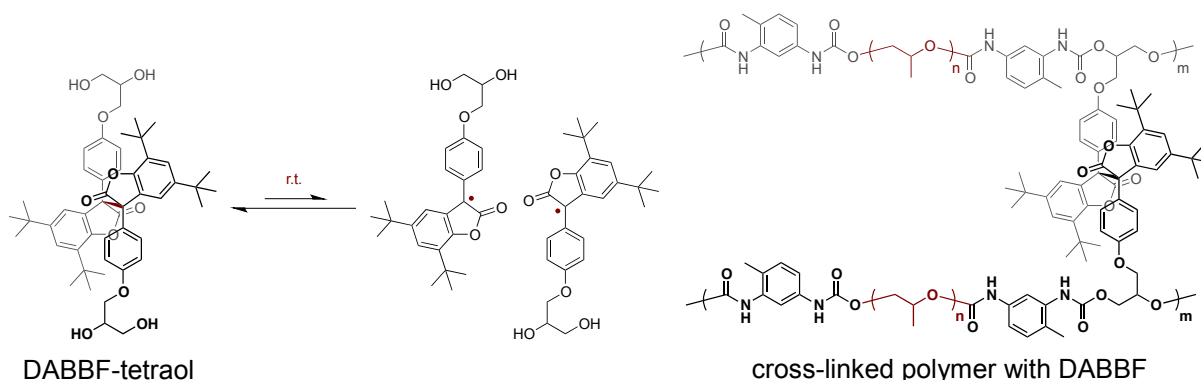


Figure 1: Chemical structures of DABBF-tetraol and of polymers cross-linked by DABBF-tetraol.

Self-healing of the contacted gel samples could be observed and the scars had almost disappeared after healed for 24 h (Figure 2, the gels with and without indigo for better visibility) at room temperature. Even after manually stretching the sample, no failure occurred. A similar self-healing test was performed on the usual chemical gels. These control chemical gels do not possess dynamic covalent bonds. The cut pieces of the control gels could not be coalesced and easily separated into two pieces by manual stretching of the sample. Furthermore, the self-healing behavior of the gels cross-linked by DABBF under air at $0\text{ }^\circ\text{C}$ was not observed, indicating that the self-healing behavior depends on the temperature. In the present system, at room temperature, an autonomously self-healing system was successfully achieved.

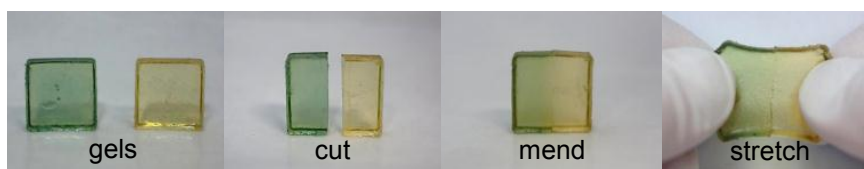


Figure 2: Photographs of self-healing behavior of gels cross-linked by DABBF under air at room temperature; original, cut, mended, and stretched state, respectively, after 24 h.

Figure 3a shows typical stress–strain curves of mended gels cross-linked by DABBF after different healing times. As shown in Figure 3b, longer healing times led to better healing. A recovery of 98% of the original elongation at breaking was possible over

periods of 24 h. An important result is that most of the healed samples did not break at the contacted surface under the tensile testing. This observation indicates that the mechanical strength of the cut samples recovered after being healed for 24 h and a state of equilibrium had been reached. In contrast, the control samples cross-linked by bisphenol A units showed a recovery of less than 5% of the original elongation at breaking even after healing for 120 h.

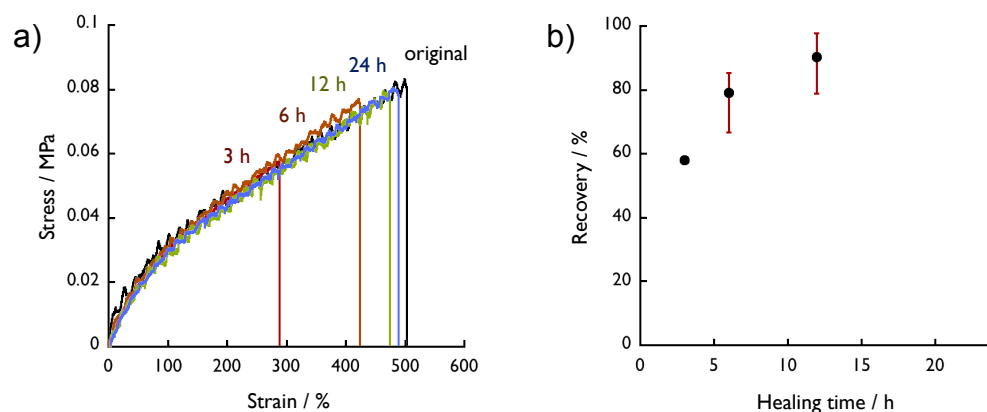


Figure 3: a) Typical stress–strain curves of gels cross-linked by DABBF before and after self-healing measured under air at room temperature. Colored vertical lines correspond to elongation at breaking for given healing times. b) Degree of recovery of healed gels in elongation at breaking depends on healing times. Error bars show maximum and minimum values of three samples.

5. CONCLUSIONS

Cross-linked polymers that contain a DABBF unit, which is a novel dynamic covalent bond unit, were successfully prepared by polyaddition of diisocyanate compounds and a DABBF cross-linker. The autonomous structural transformation and the macroscopic mending of separated gel pieces under mild conditions without any stimuli were accomplished by a dynamic covalent approach.

ACKNOWLEDGEMENTS

The authors gratefully acknowledge the financial support of Funding Program (Green Innovation GR077) for Next Generation World-Leading Researchers from Cabinet Office Government of Japan.

REFERENCES

[1] K. Imato, M. Nishihara, T. Kanehara, Y. Amamoto, A. Takahara, H. Otsuka, Room Temperature Self-healing Chemical Gels Cross-linked by Diarylbibenzofuranone-based Trigger-free Dynamic Covalent Bonds, *Angew. Chem. Int. Ed.* 2012, 51, 1138–1142.

SYNTHESIS OF INTRINSIC SELF-HEALING EPOXY RESINS

B. Di Credico¹, M. Levi¹ and S. Turri¹

¹ *Department of Chemistry, Materials and Chemical Engineering "Giulio Natta", Politecnico di Milano, Piazza Leonardo da Vinci, 20133 Milan, Italy – e-mail: bdicredico@chem.polimi.it, marinella.levi@polimi.it, stefano.turri@polimi.it*

Keywords: Self-healing, Diels-Alder, thermally polymers

ABSTRACT

The thermally reversible Diels-Alder adducts are attractive building blocks for the design of *intrinsic self-healing materials* that do not have an additional healing agent but possess the capability to repair the damage through inherent reversibility of bonding into the polymer matrix.

We report the development of new thermally responsive polymers for self-healing reversible adhesion. Re-mendable epoxy resins were obtained from the DA coupling of multifunctional furans and maleimide monomers. We prepared a new tri-furan macromonomer which reacted with a bismaleimide counterpart giving rise to a DA network following the reaction progress of the non-linear polycondensation by FTIR. Different combinations of di- and tri-functional furans with maleimide were investigated to polymerize in solution or in bulk. The thermal reversibility of the cross-linked networks were analyzed in detail by differential scanning calorimetry and dynamic mechanical analysis. Preliminary studies on the ability of healing of new materials were performed. The relatively large number of DA bonds in the polymers determine satisfactory healing efficiency of the new materials.

1. INTRODUCTION

Over last few decade, self-healing materials have been shown to have useful applications in numerous aerospace, mechanical, electromechanical, and structural subsystems. Self-healing materials are a class of smart materials that have the structurally incorporated ability to repair damage caused by mechanical usage over time. A new potential class of self-healing materials is based on thermally reversible cross-linked polymers, that are capable of healing internal cracks through thermo-reversible covalent bonds formation. These new healable resins have the built-in capability to restore mechanical properties several times through multiple cycles of healing without use of catalyst. This allows multiple damages occurring at the same location to be repaired. The Diels-Alder cycloaddition of furan and maleimide is one of the most attractive reaction to construct thermally mendable crosslinked materials [1] [2].

In this work, we prepared new difuran (2F) and trifuran (3F) macromonomers which was reacted with a bismaleimide (2M) counterpart to form dense DA networks. Different combination of di- and tri-functional furan and maleimide monomers were used to study the DA cycloaddition associated with network formation.

2. MATERIALS AND METHODS

2.1 Preparation of trifuran (3F) and difuran compound (2F)

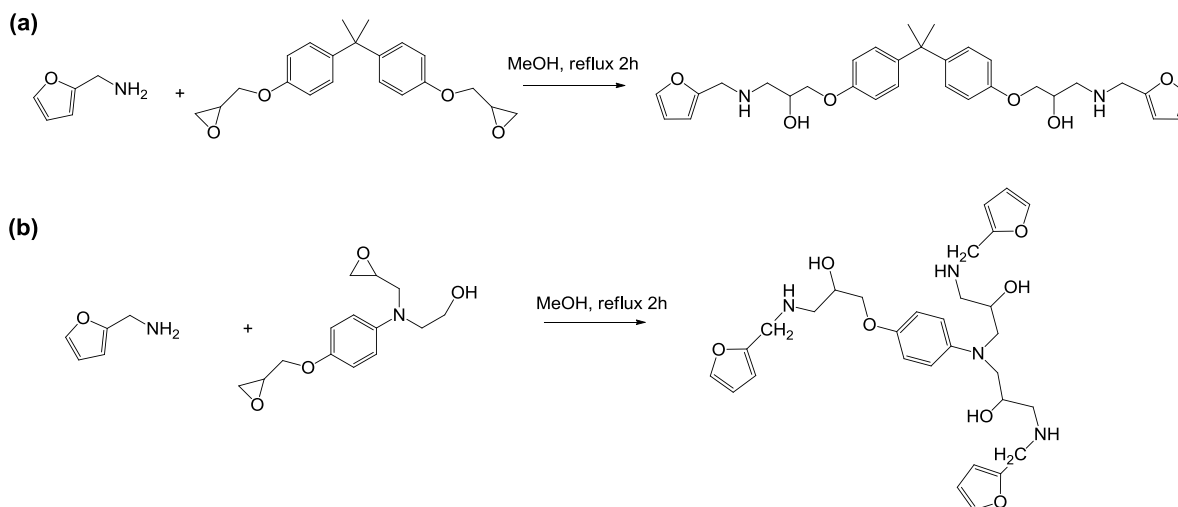
N,N-Diglycidyl-4-glycidyoxyaniline and Bisphenol A diglycidyl ether (DGEBA) was reacted with the furfurylamine in the stoichiometric ratio 1:3 and 1:2 respectively. The reaction was carried in methanol at 85 °C for 3h, using a magnetic stirrer. At the end of the reaction, the products were obtained from drying the sample under vacuum (95-98 % of yield).

2.2 Preparation of new cross-linked polymers: 2M-3F polymer and 2M-2F/3F polymers

1,1'-(Methylenedi-4,1-phenylene)bismaleimide (2M) was dissolved in dichloromethane. Then, the furan compounds (ratio of 2F/3F = 1/1) were added to the mixture and stirred at 50 °C until most of the solvent was evaporated. The resultant homogeneous compounds were poured into a silicone rubber mold and cured at 50 °C for 24h. The solid cross-linked samples were obtained.

3. MATERIALS AND METHODS

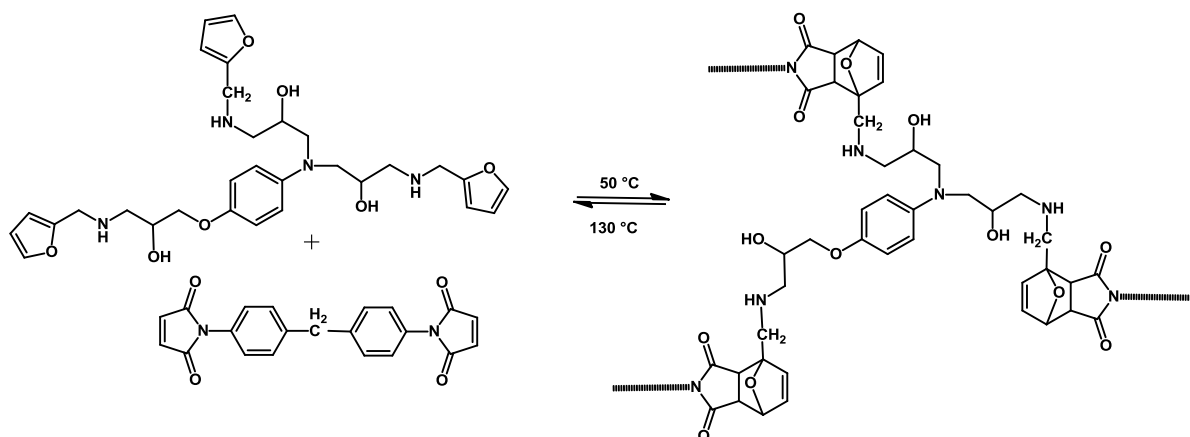
Di- and tri-functional furans were prepared according to the following reactions (Scheme 1).



Scheme 1: Synthesis of (a) difuran and (b) trifuran compounds.

Chemical characterization of furans was performed with FTIR and NMR experiments which supports to the chemical structures of the prepared compounds. The disappearance of absorption peak of oxirane ring in the FTIR spectra demonstrated the complete reaction of the epoxides with the amine groups.

Thus, the new remendable polymers were synthetized. The DA reaction involving 2M took place within a temperature range of 50-70 °C, which change with the structure of the furan compound. The reaction of difuran and maleimide moieties affords a highly cross-linked polymer 2M-3F (Scheme 2).



Scheme 2: Synthesis of 2M-3F cross-linked polymer.

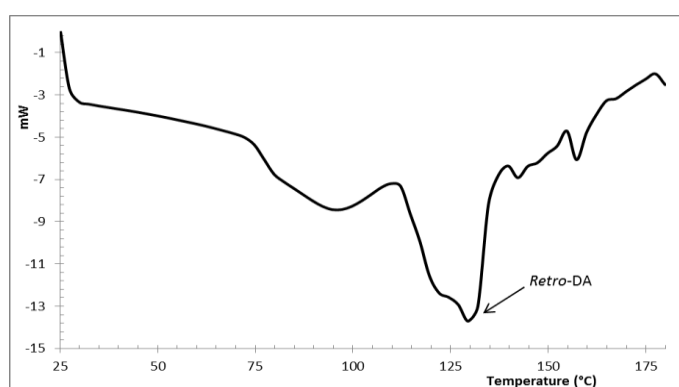


Figure 1: DSC curve of 2M-3F cross-linked polymer (heating rate: 10 °C min⁻¹)

The thermal reversibility in the new polymer 2M-3F was further inspected by performing DSC, applying repeated thermic cycles using a sample of starting 3F and 2M monomers (Figure 2).

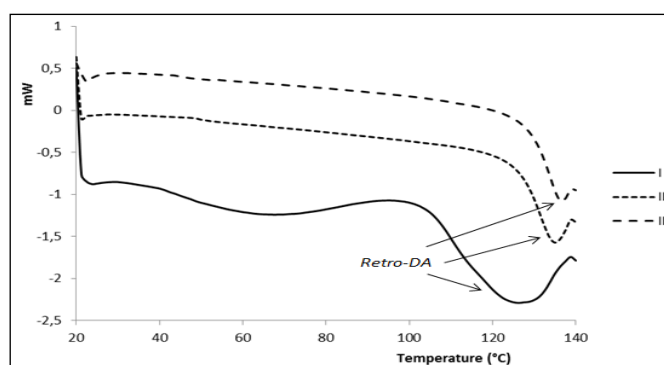
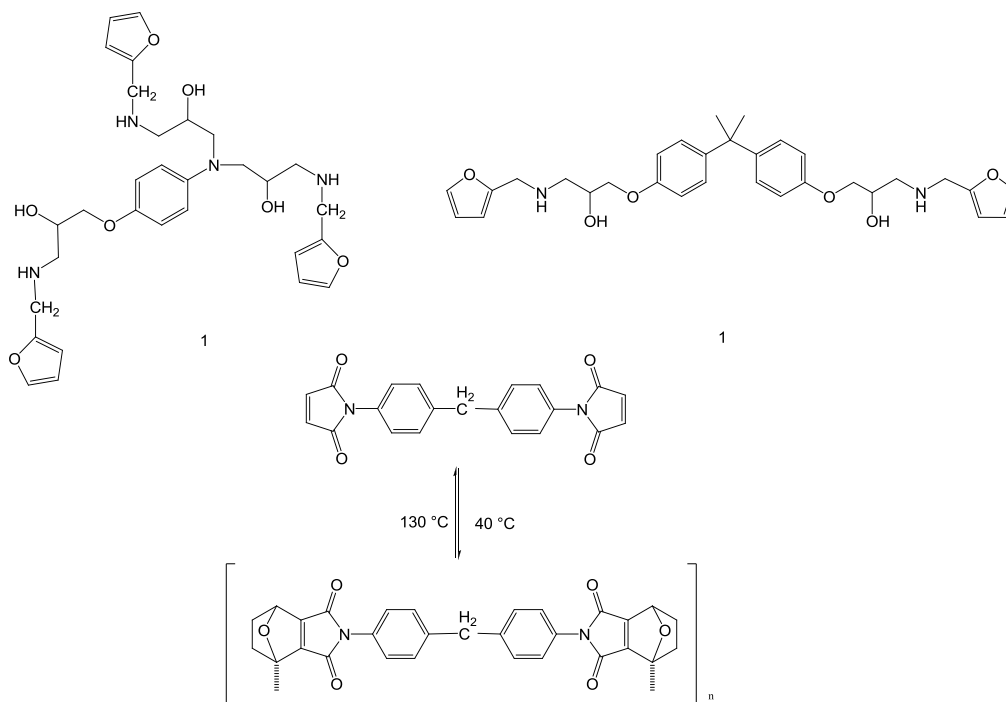


Figure 2: DSC heating traces of 3F/2M crosslinked polymer (heating rate: 10 °C min⁻¹).

The sample of 3F and 2M in an appropriate molar ratio is heated from 20 to 140 °C to allow polymerization (curve I). The endothermic peak observed at 130 °C is attributed at the reverse DA reaction. Consecutive heating of the polymer 2M-3F leads to a disconnected polymer via retro-DA reaction and slow cooling allows the broken

bonds to reconnected via forward DA reaction. It is noted that the endothermic peak of reverse DA reaction increases (curve I and II) in repeated DSC experiments. This trend may be related with the increase of density and better packaging of 2M-3F polymer after heat treatment, as evidenced by gradual increase of the temperature. Finally, maleimide monomer, di- and tri-functional epoxy compounds were used to make polymer 2M-3F/2F (Scheme 3). It was found that the DA crosslinks of this polymer are thermally reversible.



Scheme 3: Synthesis of 2M-3F/2M cross-linked polymer

4. CONCLUSION

We have developed two thermosetting re-mendable highly cross-linked polymers, 2M-3FM and 2M-3F/2F. The systems are highly reversible thanks to remarkable fraction of intermonomer linkages that can be disconnected and reconnected upon specific heat treatment.

The final aim of this study is to implement materials which unify self-healing properties with the typical mechanical characteristics of epoxy resins. Mechanical tests and other experiments which can demonstrate and evaluate the self-healing effect are currently being conducted.

ACKNOWLEDGEMENTS

Special thanks for funding are expressed to ST.I.M.A. "Strutture Ibride per Meccanica e l'Aerospazio" (Project ID 14567), sponsored by Regione Lombardia.

REFERENCES

- [1] X. Chen MAD, K. Ono, A. Mal, H. Shen, S.R. Nutt, K. Sheran, F. Wudl. *Science* 2002;295:1698-1701.
- [2] Gandini A. *Progress in Polymer Science* 2013;38:1-29.

DEVELOPMENT OF NEW SELF-HEALING MATERIALS BASED ON NOVEL DIELS – ALDER REACTIONS

S. Billiet¹, J. Winne² and F. Du Prez¹

¹ Department of Organic Chemistry, Polymer Chemistry Research Group, Ghent University, Krijgslaan 281, S4-bis, B-9000 Ghent, Belgium – e-mail: stijn.billiet@ugent.be; filip.duprez@ugent.be

² Department of Organic Chemistry, Ghent University, Krijgslaan 281, S4-bis, B-9000 Ghent, Belgium – e-mail: johan.winne@ugent.be

Keywords: Thermoset, Intrinsic healing, Diels-Alder

ABSTRACT

In the field of self-healing, Diels-Alder chemistry was introduced by Chen *et al.*^[1] in 2002 with the use of furan-maleimide systems. This approach led to a system that, when heated, could heal multiple times. The obtained temperature range (forward reaction: 60-90°C – backward reaction 90-150°C) is however not ideal. The forward reaction should occur at ambient (or even lower) temperature while the backward reaction should occur higher than usage temperature, which will depend on the desired application. For this reason novel Diels-Alder reactions, that have the desired properties, are being investigated. This work represents the development of those reactions for the synthesis of self-healing thermoset materials. In the first phase, different model reactions on small molecules were investigated to get a detailed description of the reaction speed, reversibility, possible side reactions and temperature range. In the second step, the knowledge of these model reactions was transferred to reversible polymer conjugation. This allowed the complete characterisation of the new systems on polymer level. The final phase of this work focused on the incorporation of the desired functional groups into different monomers. All monomers consisted of the required functional group(s) for the Diels-Alder reaction and the presence of two alcohol functionalities to incorporate them into the polymer backbone. The thermoset materials were then conducted to different qualitative and quantitative tests to determine the unique properties of this Diels-Alder reaction in the field of self-healing.

REFERENCES

[1] X. Chen, M.A. Dam, K. Ono, A. Mal, H. Shen, S.R. Nutt, K. Sheran, F. Wudl, A thermally re-mendable cross-linked polymeric material, *Science* 295 (2002) 1698-1702.

INTERFACIAL POLYMERIZATION AS A TOOL TO MICROENCAPSULATE HIGHLY REACTIVE INGREDIENTS

R. F. A. Teixeira¹, L.T. Nguyen¹, F. E. Du Prez¹

¹ *Department of Organic Chemistry, Polymer Chemistry Research Group, Ghent University, Krijgslaan 281 S4-bis, B-9000 Ghent, Belgium. E-mail: Roberto.Teixeira@UGent.be
SIM vzw, Technologiepark 935, B - 9052 Zwijnaarde, Belgium*

Keywords: self-healing, microcapsules, thermosets, active ingredients, interfacial polymerization

ABSTRACT

The microencapsulation approach already described by White et al is amongst the most studied self-healing concepts in recent years. Microcapsules represent reservoirs of healing agents which are dispersed into materials. Deterioration and weakening of materials lead to the formation of cracks and microcapsules present in the matrix should break (and not debond). Releasing their reactive liquid content, they allow the material to recover its strength [1].

In this project, different synthetic routes for the formation of core-shell structures, well-known in the literature, are applied and adapted to our targeted systems. Emulsification of the active agent into an immiscible phase is realized upon mechanical stirring and shell formation is typically performed by interfacial polymerization of monomers that are present separately in one of the liquid phases.

REFERENCES

[1] R.F.A. Teixeira, X.K.D. Hillewaere, S. Billiet, F.E. Du Prez, to be published in: W.H. Binder (Ed.), *Self-Healing Polymers*, Wiley & Sons Inc., New-York, 2013.

MICROENCAPSULATION OF SELF-HEALING AGENTS VIA POLYCONDENSATION

R. F. A. Teixeira^{1,2}, X. Hillewaere^{1,2}, L.-T. Nguyen^{1,2}, C. Colard^{1,2}, I. Pais³, A. Beirao³,
F. E. Du Prez^{1,2}

¹ Department of Organic Chemistry, Polymer Chemistry Research Group, Ghent University, Krijgslaan 281 S4-bis, B-9000 Ghent, Belgium. E-mail: Roberto.Teixeira@UGent.be

² SIM vzw, Technologiepark 935, B - 9052 Zwijnaarde, Belgium.

³ Devan Micropolis S.A., Parque da Ciencia e Tecnologia, Rua Eng. Frederico Ulrich 2650, 4470 605 Moreira Da Maia, Portugal.

Keywords: self-healing, microcapsules, thermosets, active ingredients, polycondensation

ABSTRACT

Matrixes such as thermoset materials undergo damages over time due to external forces such as cyclic stresses and climate conditions. Microcapsules represent reservoirs of healing agents which are dispersed into materials. Upon crack formation, the microcapsules present in the matrix should break (and not debond) and release their reactive liquid content, allowing the material to recover its strength [1].

The polycondensation approach used within our group is presented with melamine based components to build the microcapsule shell. This controlled and well-known process in industry is described in our particular case for the encapsulation of healing agents such as multi-thiols. Important criteria of the final encapsulated components before their integration into materials, which are discussed, are for instance: the chemical compatibility between the shell and the encapsulated agents, the shell strength and surface properties and the size and concentration of the microcapsules.

REFERENCES

[1] R.F.A. Teixeira, X.K.D. Hillewaere, S. Billiet, F.E. Du Prez, to be published in: W.H. Binder (Ed.), Self-Healing Polymers, Wiley & Sons Inc., New-York, 2013.

THIOL-ISOCYANATE CHEMISTRY FOR AUTONOMOUS SELF-HEALING OF EPOXY RESINS

X. Hillewaere^{1,4}, R. Teixeira^{1,4}, T. Nguyen^{1,4}, T. Bultreys^{2,4}, E. Tsangouri^{3,4} and
F. Du Prez^{1,4}

¹ Department of Organic Chemistry, Polymer Chemistry Research Group, Ghent University, Krijgslaan 281, S4-bis, B-9000 Ghent, Belgium – e-mail: xander.hillewaere@ugent.be; roberto.teixeira@ugent.be; thu.nguyen@ugent.be; filip.duprez@ugent.be

² Centre for X-ray Tomography (UGCT) – Dept. Geology and Soil Science, Ghent University, Krijgslaan 281, 9000 Ghent, Belgium – e-mail: Tom.Bultreys@UGent.be

³ Department of Mechanics of Materials and Constructions, Vrije Universiteit Brussel, Pleinlaan 2, B-1050 Brussels, Belgium – e-mail: etsangou@vub.ac.be

⁴ SIM vzw, Technologiepark Zwijnaarde 935, B-9052 Ghent, Belgium

Keywords: self-healing, thermoset, epoxy, thiol-isocyanate

ABSTRACT

In order to develop better performing and longer lasting epoxy thermosets and composites, novel healing agents were inserted into microcapsules and these were then dispersed in the epoxy matrix. The fast and efficient thiol-isocyanate chemistry was screened by means of kinetic studies and mechanical testing for the potential use as the main network forming reaction during self-healing, leading to the improved healing efficiencies compared to most of the results obtained in literature so far [1]. Furthermore, certain conditions necessary for industrial applicability were met, such as a low toxicity, low cost and stability at both ambient and epoxy processing conditions.

REFERENCES

[1] R.F.A. Teixeira, X.K.D. Hillewaere, S. Billiet, F.E. Du Prez, to be published in: W.H. Binder (Ed.), Self-Healing Polymers, Wiley & Sons Inc., New-York, 2013.

THIOL-MALEIMIDE CHEMISTRY FOR AUTONOMOUS SELF-HEALING OF EPOXY RESINS

X. Hillewaere^{1,3}, S. Billiet¹, R. Teixeira^{1,3}, H. Rahier^{2,3} and F. Du Prez^{1,3}

¹ Department of Organic Chemistry, Polymer Chemistry Research Group, Ghent University, Krijgslaan 281, S4-bis, B-9000 Ghent, Belgium – e-mail: xander.hillewaere@ugent.be; stijn.billiet@ugent.be; roberto.teixeira@ugent.be; filip.duprez@ugent.be

² Department Materials and Chemistry, Physical Chemistry and Polymer Science, Vrije Universiteit Brussel, Pleinlaan 2, B-1050 Brussels, Belgium – e-mail: hrahier@vub.ac.be

³ SIM vzw, Technologiepark Zwijnaarde 935, B-9052 Ghent, Belgium

Keywords: self-healing, thermoset, epoxy, thiol-maleimide

ABSTRACT

In order to develop better performing and longer lasting epoxy thermosets and composites, novel healing agents were inserted into microcapsules and these were then dispersed in the epoxy matrix. The fast and efficient thiol-maleimide chemistry was screened by means of kinetic studies and mechanical testing for the potential use as the main network forming reaction during self-healing, leading to the improved healing efficiencies compared to most of the results obtained in literature so far [1-2]. Furthermore, certain conditions necessary for industrial applicability were met, such as a low toxicity, low cost and stability at both ambient and epoxy processing conditions.

REFERENCES

- [1] R.F.A. Teixeira, X.K.D. Hillewaere, S. Billiet, F.E. Du Prez, to be published in: W.H. Binder (Ed.), *Self-Healing Polymers*, Wiley & Sons Inc., New-York, 2013.
- [2] S. Billiet, W. Van Camp, X.K.D. Hillewaere, H. Rahier, F.E. Du Prez, Development of optimized autonomous self-healing systems for epoxy materials based on maleimide chemistry, *Polymer* 53 (2012) 2320–2326.

SYNTHESIS AND PROPERTIES OF CROSS-LINKED POLYMERS CONTAINING DIARYLBIBENZOFURANONE BY ADMET POLYMERIZATION

T. Ohishi,¹ K. Imato,² T. Kanehara,² A. Takahara,^{1,2} and H. Otsuka^{1,2}

¹Institute for Materials Chemistry and Engineering, Kyushu University, ²Graduate School of Engineering, Kyushu University, 744 Motooka, Nishi-ku, Fukuoka 819-0395, Japan - e-mail: t-ohishi@cstf.kyushu-u.ac.jp

Keywords: dynamic covalent bonds, cross-linked polymers, acyclic diene metathesis polymerization

ABSTRACT

Diarylbibenzofuranone (DABBF) derivatives can be reversibly cleaved to the corresponding arylbenzofuranone (ABF) radicals under mild conditions. We recently reported the synthesis and physicochemical properties of the cross-linked polyurethane containing DABBF unit. The autonomous structural transformation and the macroscopic self-healing of separated gel pieces under air at room temperature without any stimuli were accomplished by a dynamic covalent approach. Since the self-healing property was derived from DABBF units, one can expect the self-healing of DABBF-containing cross-linked polymers with various structures. We here report the acyclic diene metathesis (ADMET) polymerization of multifunctional olefin monomers containing DABBF unit. This is because a low-polarity olefin polymer can be obtained by ADMET polymerization.

The DABBF-diolefin monomer was first polymerized at room temperature in the presence of Grubbs catalyst (2nd generation) in CH₂Cl₂. However, the yield of the obtained polymer was low (29%). Under this condition, it is considered that the ethylene molecules produced during polymerization can not be removed. The polymerization was also performed at 40 °C to give polymers in good yield (83%).

Furthermore, cross-linked polymers were synthesized by ADMET polymerization of DABBF-tetraolefin monomer and copolymerization of DABBF-bifunctional olefin monomer and triolefin monomer. All cross-linked polymers were obtained in good yields. These polymers showed high swelling properties in organic solvents with relatively low polarity.

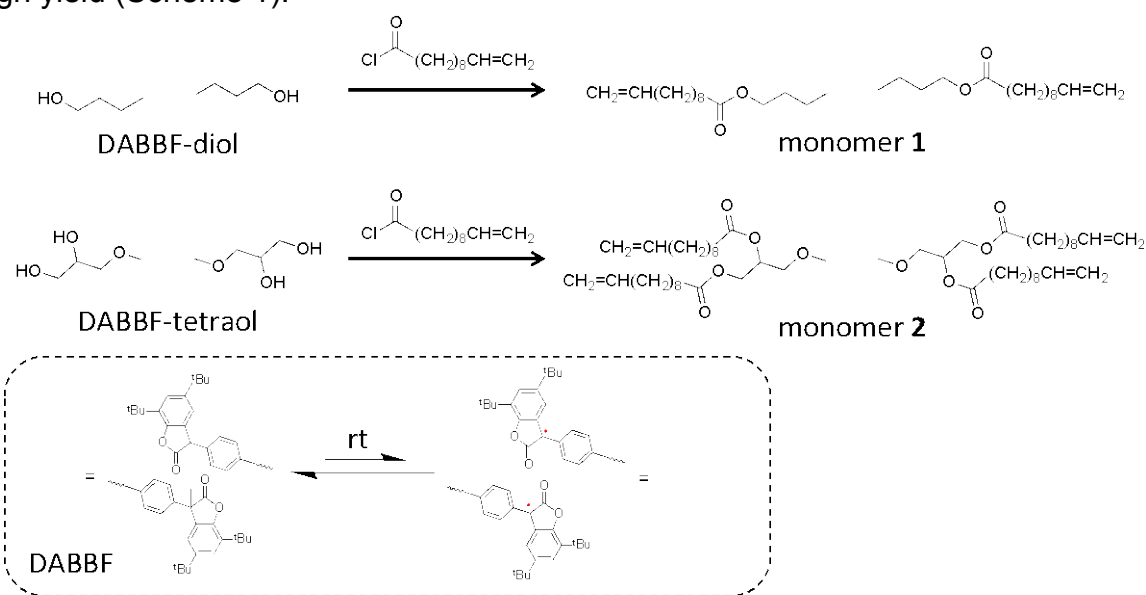
1. INTRODUCTION

A reversible system can repeat the self-healing process for numerous cycles when noncovalent bonds or dynamic covalent bonds are used.¹ Such noncovalent and dynamic covalent bonding² can be reversed under equilibrium controls. Modified by external stimuli or through continuous component exchange, noncovalent and dynamic covalent bonds can be reorganized or reshuffled to cure the system. Diarylbibenzofuranone (DABBF), a dimer of arylbenzofuranone, exists as a state of equilibrium between dissociation and association and its central C-C bond can act as a dynamic covalent bond at room temperature.³ We recently reported the synthesis and physicochemical properties of the cross-linked polyurethane containing DABBF

unit.⁴ The autonomous structural transformation and the macroscopic self-healing of separated gel pieces under air at room temperature without any stimuli were accomplished by a dynamic covalent approach. Since the self-healing property was derived from DABBF units, one can expect the self-healing of DABBF-containing cross-linked polymers with various structures. We here report the acyclic diene metathesis (ADMET) polymerization of multifunctional olefin monomers containing DABBF unit. This is because a low-polarity olefin polymer can be obtained by ADMET polymerization.

2. MATERIALS

Grubbs second-generation catalyst was purchased from Aldrich. Substrates and reagents were purchased from Tokyo chemical industry or Wako pure chemical industries; 4-hydroxymandelic acid monohydrate, 2,4-di-*tert*-butylphenol, methane sulfonic acid, 3-chloro-1-propanol, 3-chloro-1,2-propanediol, di-*tert*-butyl peroxide, 10-undecenoyl chloride, and 1,1,1-tris(4-hydroxyphenyl)ethane were used as supplied. Organic solvents were purchased from Kanto chemical or Wako pure chemical industries at the highest purity and used as supplied. DABBF-diol and DABBF-tetraol were prepared according to the literature.⁴ The olefin groups were then introduced by condensation of **DABBF-diol** and/or **DABBF-tetraol** 10-undecenoyl chloride at room temperature. This reaction gave the monomers **1** or **2** in high yield (Scheme 1).



3. METHODS

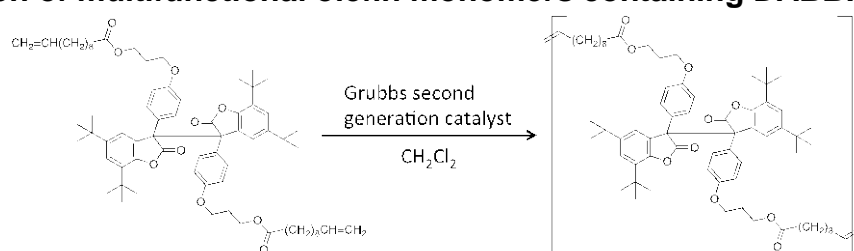
Polymerization: An example of the procedure for the synthesis of polymer containing DABBF unit is as follows. In a nitrogen-filled Schlenk flask, Grubbs second-generation catalyst was added to the solution of monomer **1** in CH_2Cl_2 , which was degassed with three freeze-vacuum-thaw cycles. Then the mixture was heated to 40 °C and stirred for 24 h. The reaction was quenched by adding ethyl vinyl ether using syringe and stirred for 12 h at room temperature. CH_2Cl_2 was added to the reaction mixture and treated with tris(hydroxymethyl)phosphine (THP) in order to remove the residual catalyst. The polymer was purified by reprecipitation from

methanol. ^1H NMR (400 MHz) spectroscopic measurements were carried out at 25 °C with a 400 MHz Bruker spectrometer using tetramethylsilane (TMS) as internal standard in chloroform-*d* (CDCl_3). Gel permeation chromatographic (GPC) measurements were carried out at 40 °C on TOSOH HLC-8220 GPC system equipped with a guard column (TOSOH TSK guard column Super H-L), three columns (TOSOH TSK gel SuperH 6000, 4000, and 2500) and a UV-Vis detector. Tetrahydrofuran (THF) was used as the eluent at a flow rate of 0.6 mL min^{-1} . Polystyrene (PS) standards ($M_n = 4920\text{-}3000000$; $M_w/M_n = 1.02\text{-}1.03$) were used to calibrate the GPC system.

4. RESULTS AND DISCUSSION

• ADMET polymerization of multifunctional olefin monomers containing DABBF

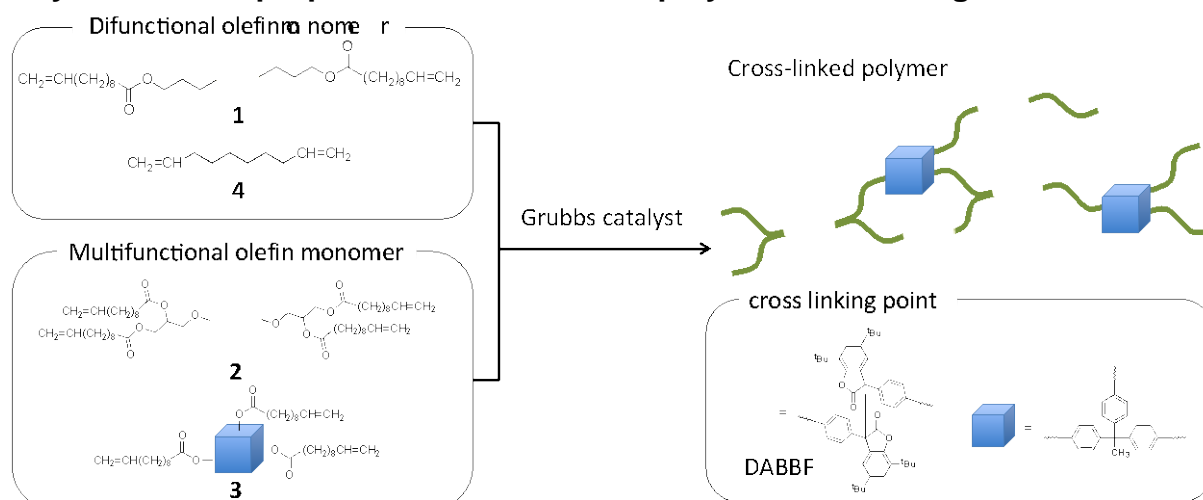
The DABBF-diolefin monomer was first polymerized at room temperature in the presence of Grubbs catalyst (2nd generation) in CH_2Cl_2 . However, the yield of



Scheme 2. Polymerization of 1

the obtained polymer was low (29%). Under this condition, it is considered that the ethylene molecules produced during polymerization can not be removed. The polymerization was also performed at 40 °C to give the corresponding polymers in good yield (83%) (Scheme 2).

• Synthesis and properties of cross-linked polymers containing DABBF



Scheme 3. Synthesis of cross-linked polymer containing DABBF prepared by ADMET polymerization

Diverse types of cross-linked polymers were synthesized by ADMET polymerization of DABBF-tetraolefin monomer and copolymerization of DABBF-bifunctional olefin monomer and triolefin monomer (Scheme 3). The swelling behavior of the cross-linked polymers containing DABBF was investigated in various organic solvents (Table 1). The cross-linked copolymers containing monomer 1 unit, such as poly1-co-poly3 and poly1-co-poly3-co-poly4, did not form a gel in benzene, THF, CHCl_3 , and anisole. These results indicate that cross-linked copolymers containing monomer 1

have low crosslink density. In contrast, the cross-linked copolymers containing monomer **2** unit, such as poly**2**-co-poly**3**, poly**2**-co-poly**4**, and poly**2**-co-poly**3**-co-poly**4**, swelled and absorbed benzene, THF, CHCl₃, and anisole. Accordingly, the swelling properties of these cross-linked copolymer containing DABBF unit are probably dependent on the cross-linked density. Furthermore, poly**2**-co-poly**4** and poly**2**-co-poly**3**-co-poly**4** were formed high viscosity solution in low-polar organic solvent such as CH₂Cl₂. These results imply that swelling behavior of cross-linked copolymers containing DABBF unit depends on polymer main chain polarity and dynamic covalent bond property of DABBF unit.

Table 1. Degree of swelling cross-linking polymer containing DABBF.^a

polymer	Q ^b						
	cyclohexane	benzene	THF	CHCl ₃	anisole	methanol	DMF
poly 1 -co-poly 3	1.65	– ^c	– ^c	– ^c	– ^c	0.514	2.05
poly 1 -co-poly 3 -co-poly 4	1.63	– ^c	– ^c	– ^c	– ^c	0.230	– ^c
poly 2	1.60	5.18	– ^c	– ^c	– ^c	1.05	3.08
poly 2 -co-poly 3	1.19	5.47	9.07	13.6	6.62	0.308	2.20
poly 2 -co-poly 4	5.70	11.2	8.20	14.8	9.71	2.47	5.39
poly 2 -co-poly 3 -co-poly 4	2.28	6.40	9.25	8.57	9.86	1.96	4.74

^a Cross-linked polymer was allowed to swell at room temperature for two days.

^b $Q = \frac{W_{wet} - W_{dry}}{W_{dry}}$ (W_{dry} : Weight of dried cross-linking polymer, W_{wet} : Weight of swollen cross-linking polymer)

^c Polymer was dissolved.

5. CONCLUSIONS

We have demonstrated the synthesis and properties of cross-linked polymers having DABBF prepared by ADMET polymerization. All cross-linked polymers were synthesized by ADMET polymerization of DABBF-tetraolefin monomer and copolymerization of DABBF-bifunctional olefin monomer and triolefin monomer. These polymers showed high swelling properties in organic solvents with relatively low polarity. Furthermore, poly**2**-co-poly**4** and poly**2**-co-poly**3**-co-poly**4** were formed high viscosity solution in low-polar organic solvent. These results imply that swelling behavior of cross-linked copolymers containing DABBF unit depends on polymer main chain polarity and dynamic covalent bond property of DABBF unit.

ACKNOWLEDGEMENTS

The authors gratefully acknowledge the financial support of the Funding Program (Green Innovation GR077) for Next Generation World-Leading Researchers from the Cabinet Office, Government of Japan.

REFERENCES

- [1] Syrett, J. A.; Becer, C. R.; Haddleton, D. M. *Polym. Chem.* 2010, 1, 978–987.
- [2] (a) Rowan, S. J.; Cantrill, S. J.; Cousins, G. R. L.; Sanders, J. K. M.; Stoddart, J. F. *Angew. Chem., Int. Ed.* 2002, 41, 898–952. (b) Corbett, P. T.; Leclaire, J.; Vial, L.; West, K. R.; Wietor, J. L.; Sanders, J. K. M.; Otto, S. *Chem. Rev.* 2006, 106, 3652–3711. (c) Lehn, J. M. *Chem. Soc. Rev.* 2007, 36, 151–160.

[3] Frenette, M.; Maclean, P. D.; Barclay, L. R. C.; Scaiano, J. C. J. *Am. Chem. Soc.*, 2006, 128, 16432-16433.

[4] Imato, K.; Nishihara, M.; Kanehara, T.; Amamoto, Y.; Takahara, A.; Otsuka, H. *Angew. Chem. Int. Ed.*, 2012, 51, 1138-1142.

IMPROVED PRESSURIZED BURST TESTING OF BALLISTIC SELF-HEALING IN IONOMERS

S. J. Kalista, Jr.^{1,2}, R. A. Knepple¹ and C. W. Pillsbury¹

¹ Department of Mechanical Engineering, Union College, 807 Union St, Schenectady, NY 12308 USA – e-mail: kalistas@union.edu, kneppler@garnet.union.edu, pillsbuc@garnet.union.edu

² Macromolecular Science and Engineering, Virginia Tech, Blacksburg, VA 24060 USA – e-mail: skalista@vt.edu

Keywords: ionomers, ballistic self-healing, EMAA, burst testing, healing efficiency

ABSTRACT

The unique ballistic self-healing response expressed by poly(ethylene-co-methacrylic acid) EMAA ionomers holds unique potential for creating new and functional materials with puncture-reversal abilities. While previous testing has allowed some measure of healing ability, these have mostly been limited to qualitative observation (appearance, scar size, etc.). Consequently, no measure of healing efficiency exists for the self-healing of puncture-reversal systems. To fully characterize the healing ability and provide definitive comparisons between chemistries and systems, a method of quantitative benchmarking for puncture-healing efficiency must be developed.

While the previous pressurized burst test provided quantitative data on healed strength, its manual control yielded inaccuracy, reduced safety, and limited testing to relatively low pressures (< 35 bar). A new, automated version of this device has been fully designed and fabricated allowing burst strength to be measured in a secure and electronically-controlled fashion. Following ballistic puncture, samples are sealed within a test chamber. They are then pressurized using an air-over-water intensifier system allowing low air pressures (< 10 bar) to produce ultimate sample loads greater than 130 bar (1885 psi). A precise MATLAB/Simulink control system allows user-definable loading rates with sample pressures accurately recorded during the loading ramp and upon failure at the healed location.

The high ultimate pressures and safeguards built into this device allow measurement of both healed and undamaged films having a range of thicknesses. By comparing burst pressures of healed vs. undamaged films, this device allows the first truly quantitative measurement of healing efficiency (% strength recovery) in ballistic self-healing of ionomers. Further, its use allows continued characterization of the role of various chemistries in the self-healing of ionomers (ionic character, aging, test temperature) and provides a consistent method for measuring healing efficiency in any new and novel puncture-healing systems.

MICROENCAPSULATION OF VARIOUS REACTIVE MONOMERS BY IN SITU POLYMERIZATION

R.P. Ollier¹, M.E. Penoff¹, E.S. Rodriguez¹ and V.A. Alvarez¹

¹ *Composite Materials Group (CoMP), Research Institute of Material Science and Technology (INTEMA) CONICET- National University of Mar del Plata (UNMdP), Solís 7575, 7600 Mar del Plata, Argentina - e-mail: rominaollier@fi.mdp.edu.ar*

Keywords: Self-healing, microcapsules, reactive monomers, synthesis.

ABSTRACT

Advances in the study of composite polymeric materials for structural applications have suggested the possibility of an early elimination of cracks to avoid macroscopic damage of the material. Hence, the concept of self-healing composite materials has been introduced to reduce the maintenance cost and frequency, to increase the life in service and to expand the applications of these materials. One of the most successful and versatile approach consists on embedding an encapsulated healing agent inside the matrix.

One of the key features for the effectiveness of the healing system is the microcapsule design. The release properties depend on the healing agent properties, wall materials, the microencapsulation method, the physico-chemical parameters of the process, the mean particle size and the shell thickness. In order to have a successful self-healing performance, it is important to synthesize microcapsules with rough surface morphology to assure a good adhesion with de polymer matrix, low core material permeability, appropriate diameter and core content, and adequate shell thickness.

The aim of this work was to synthesize poly (urea-formaldehyde) microcapsules filled with different reactive monomers: dicyclopentadiene and two epoxy monomers with different viscosities. This parameter is important for the release properties and the healing performance of the resulting capsules. Microcapsules were prepared by in situ polymerization in oil-in-water emulsion and the best experimental conditions were selected to optimize the subsequent healing efficiency. Several reaction conditions were analyzed, by changing the following parameters: the rate of agitation, the concentration of surfactant and the viscosity of the encapsulated phase. The effect of the addition of nanoclay along the shell was also studied. The final step of filtering and washing the obtained capsules with different solvents was analyzed as well.

1. INTRODUCTION

Microcracking is a critical problem for polymers and polymer composites during their service in structural applications. The ability of self-healing materials to repair cracks is necessary to retain structural integrity. The route based on dispersing microcapsules filled with a healing agent which rupture upon a crack event, mimicking a biological 'bleeding', seems to be very promising due to its versatility. Therefore, the objective of this work was to synthesize and characterize poly (urea-

formaldehyde) microcapsules containing different reactive monomers and to establish the best reaction conditions for each case.

2. MATERIALS

Urea (Anhedra), 40% w/v aqueous solution of formaldehyde (Biopack), ammonium chloride (Timper) and resorcinol (Biopack) were used as shell forming materials. Poly (ethylene-alt-maleic anhydride) (EMA), 1-octanol and dicyclopentadiene were purchased from Sigma-Aldrich. A bisphenol A epoxy resin (Epon 826, epoxy equivalent weight 178 a 186 g/eq) and a bisphenol F epoxy resin (Distraltec (RBF170), epoxy equivalent weight 182.8 g/eq) were also used. Figure 1 shows the chemical structures of the encapsulated monomers.

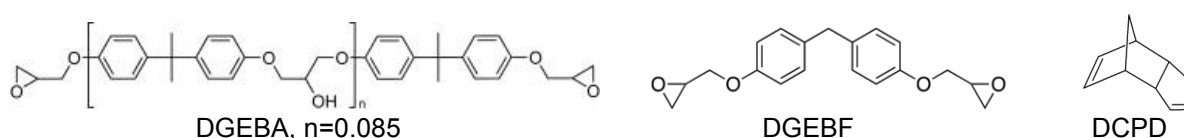


Figure 1: Encapsulated monomers.

3. METHODS

Microcapsules were prepared in oil-in-water emulsion by in situ polymerization [1], as it is shown in Figure 2.

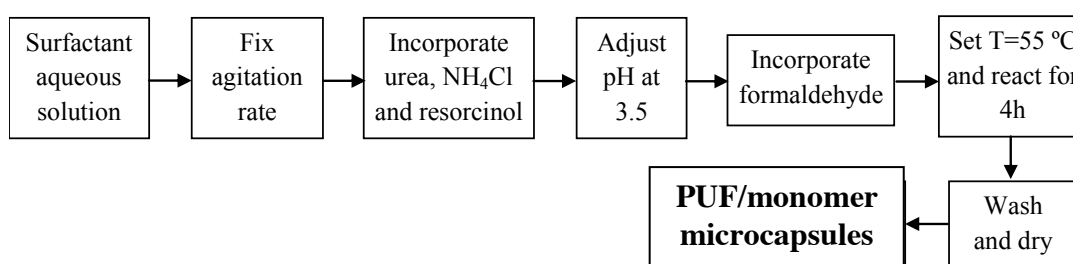


Figure 2: Microencapsulation procedure.

The prepared microcapsules were observed by scanning electron microscopy (JEOL JSM 6460 LV). Surface morphology and microcapsule size were studied. Infrared Spectroscopy (FTIR) spectra were obtained on a Perkin-Elmer Spectrophotometer model Spectrum 100 in attenuated total reflection (ATR) mode. Spectra, averaged over 16 scans, were taken in the range of 4000–600 cm⁻¹ at a resolution of 4 cm⁻¹.

4. RESULTS

Syntheses of microcapsules have been successfully performed for all encapsulated monomers. Regarding PUF/DCPD system, different agitation rates between 300 and 600 rpm previous to the incorporation of formaldehyde were studied; the emulsion was stabilized for 15 min in all cases. At 300 rpm the agitation rate was not enough to stabilize the droplets in the emulsion. The best results were obtained for samples synthesized at 450 rpm. Figure 3 displays the characterization of these capsules.

Spherical and high quality microcapsules with a normal and narrow size distribution were obtained. The measured values of mean diameter and standard deviation of the outer diameter were 282.3 μm and 50.9 μm , respectively. The microcapsule shell has a smooth inner wall and a rough porous morphology on the outer surface (Figure 3b). The presence of DCPD was evidenced by FTIR (Figure 3c).

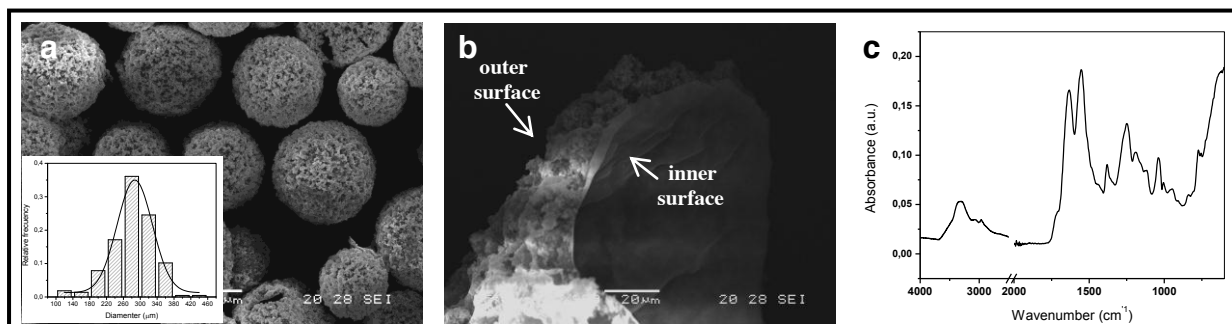


Figure 3: Characterization of PUF/DCPD microcapsules obtained at 450 rpm: a) SEM micrograph, b) SEM micrograph of a broken capsule, c) FTIR spectrum.

As regards PUF/DGEBA systems, higher stirring rates were required to stabilize the emulsion due to the considerably higher viscosity of the epoxy monomer (12400 cP at 25 $^{\circ}\text{C}$) compared with DCPD. The best results were registered at 600 rpm. Different washing solvents were employed: water, ethanol, acetone and ethanol-acetone (80:20). As water and ethanol were unable to remove the excess of epoxy, microcapsules with a smooth wall were observed by SEM (Figure 4a). On the other hand, acetone and ethanol-acetone (80:20) were more suitable for the washing step and a “cleaner” and rougher microcapsule surface can be observed (Figure 4b). The measured values of mean diameter and standard deviation of the outer diameter were 31.3 μm and 6.8 μm , respectively.

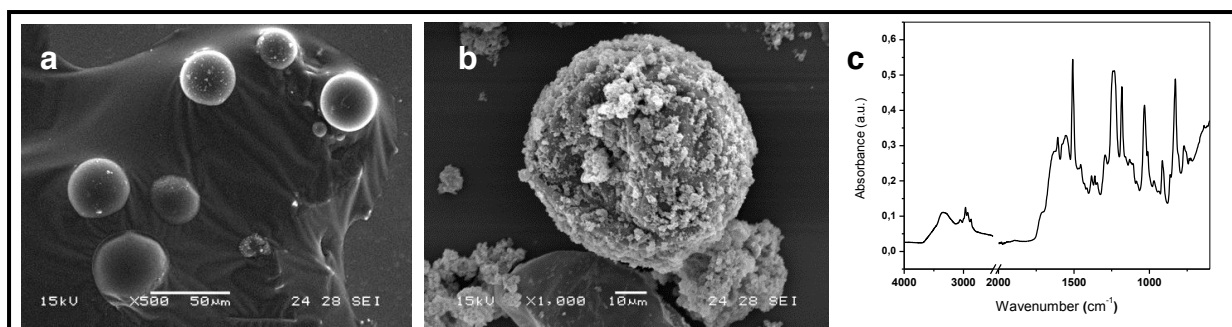


Figure 4: Characterization of PUF/DGEBA microcapsules obtained at 600 rpm: a) SEM micrograph of microcapsules washed with ethanol b) SEM micrograph of microcapsules washed with acetone, c) FTIR spectrum.

Regarding PUF/DGEBF systems, the same agitation rate of 600 rpm was used; this rate was selected owing to the higher viscosity of DGEBF monomer compared with DCPD. However, the viscosity of this epoxy monomer is lower than DGEBA monomer (6170 cP at 25 $^{\circ}\text{C}$), which is an advantage for the release properties of the resulting microcapsules, once they have been embedded in an epoxy matrix and a propagating crack provokes its rupture. In this case, the emulsion was stabilized for 1 h in order to obtain a homogenous distribution of resin droplets. The characterization

is displayed in Figure 5. Once again, different solvents were evaluated in the washing procedure and the best results were observed when microcapsules were washed with acetone. A white free-flowing powder was obtained, but an agglomerated yellow powder was obtained when it was washed with ethanol. The measured values of mean diameter and standard deviation of the outer diameter were 136.9 μm and 22.3 μm , respectively.

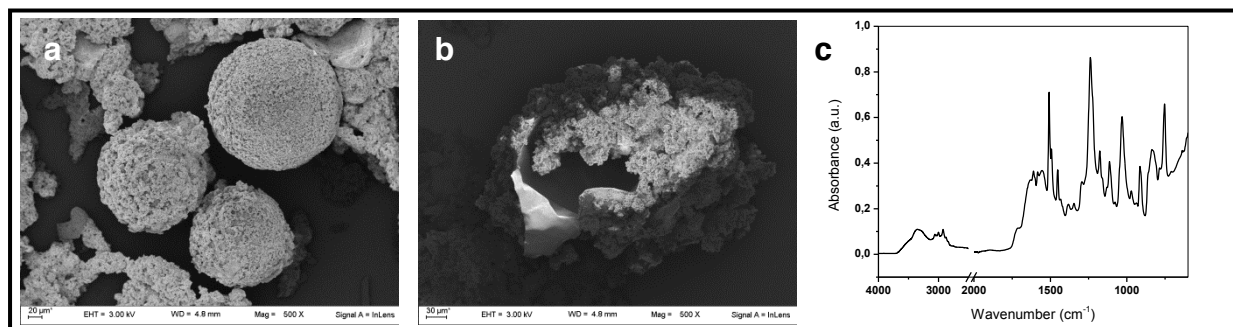


Figure 5: Characterization of PUF/DGEBF microcapsules obtained at 600 rpm: a) SEM micrograph of microcapsules washed with acetone, b) SEM micrograph of a broken capsule, c) FTIR spectrum.

Samples including bentonite were also prepared. The presence of clay was evidenced by FTIR, thermo gravimetric analysis and X-Ray Diffraction (not shown). It was found that the addition of clay did not affect the surface morphology but it changed the thermal behavior of the microcapsules (studied by TGA). Future works regarding the incorporation of the clay on the microcapsules will be carried out.

CONCLUSIONS

Poly (urea-formaldehyde) microcapsules with different encapsulated reactive monomers (dicyclopentadiene and two epoxy monomers: DGEBA and DGEBF) were successfully synthesized. This was evidenced by SEM and FTIR. It was demonstrated that the washing steps have a very important effect on the final morphology and the cleanness of the microcapsules surface. For each case, optimal agitation rate and emulsion stabilization were established according to the monomer properties. Regarding epoxy containing capsules we believe that DGEBF is more suitable for self-healing applications due to its lower viscosity.

Future works regarding the effect of the incorporation of clay in the microcapsules on the barrier properties and rupture behavior once embedded in the epoxy matrix are being carried out.

ACKNOWLEDGEMENTS

Financial support from CONICET, UNMdP and Project FSNano 004 (ANPCyT) is gratefully acknowledged.

REFERENCES

[1] E.N. Brown, N.R.Sottos, S.R. White, Fracture Testing of a Self-Healing Polymer Composite, *Experimental Mechanics* 42 (2002) 372-379.

MECHANICAL PROPERTIES AND BIOCOMPATIBILITY OF POLY(METHYL METHACRYLATE) BONE CEMENT CONTAINING MICROENCAPSULATED TISSUE ADHESIVE

A.B.W. Brochu ^{1,2}, G.A. Evans ¹ and W.M. Reichert ^{1,2}

¹ Department of Biomedical Engineering, Duke University, 136 Hudson Hall Box 90281 Durham, NC, USA – e-mail: abw10@duke.edu; gregory.evans@duke.edu; reichert@duke.edu

² Center for Biomolecular and Tissue Engineering, Duke University, 136 Hudson Hall Box 90281 Durham, NC, USA

Keywords: biomaterial, bone cement, self-healing, microencapsulation, biocompatibility

ABSTRACT

One of the most broadly reported self-healing schemes is that pioneered by White and Sottos et al. in which a polymer matrix is co-embedded with a catalyst and microcapsules containing a reactive healing agent. Although this field has been steadily growing over the past 10 years, little discussion of extension into biomaterials has taken place and none of the existing systems employ materials acceptable for *in vivo* applications. Due to its long history of use, lack of post-polymerization modifications, and susceptibility to fatigue failure, poly(methyl methacrylate) (PMMA) bone cement is an attractive option for the first self-healing biomaterial designed utilizing the aforementioned embedded capsule and catalyst approach.

Interfacial polymerization of a polyurethane prepolymer with 1,4-butanediol was performed to encapsulate 2-octyl cyanoacrylate (OCA), an FDA-approved tissue adhesive, using an oil-in-water emulsion. The compressive, tensile, and fracture toughness properties of commercial PMMA matrices containing various wt% of capsules were investigated. The proliferation and viability of MG63 human osteosarcoma cells following various exposure times to extracts from OCA, capsule-embedded bone cement, and bone cement without capsules were also examined.

Incorporation of greater than 5 wt% capsules reduced the compressive and tensile strengths below commercially-accepted standards for bone cement. Fracture toughness, K, was increased by 13% with the inclusion of 3 wt% capsules but was decreased below the control value with contents of 15 wt% and higher. Additionally, cellular viability and proliferation were similar in cells exposed to media conditioned with commercial and capsule-embedded bone cements, suggesting the addition of capsules to the bone cement does not have a detrimental effect on the toxicity of the material.

1. INTRODUCTION

Numerous implants fail due to fatigue, wear, and environmental cracking following the accumulation of microdamage[1], marking these biomaterials as potential candidates for the introduction of self-healing biomaterials. PMMA bone cement is a space-filling matrix that forms mechanical interlocks between the metallic stem of a total joint replacement and the surrounding boney tissue, serving to transfer loads from the prosthesis to the bone[2]. Over time, microcrack formation within the bone cement matrix can lead to implant loosening and subsequent failure; development of a self-healing PMMA could significantly extend the functional lifetime of the implant.

2. MATERIALS

Unless otherwise specified, materials were obtained from commercial suppliers and used without further purification. OCA was generously donated by Ethicon, Inc. Methyl ethyl ketone, methyl isobutyl ketone, and cyclohexanone were used as solvents and 2,4-toluene diisocyanate and 1,4-butanediol were used to synthesize the polyurethane prepolymer following the protocol outlined by Yang et al. and reported by the authors previously[3, 4]. Pluronic F-68 was used as a surfactant. Para-toluenesulfonic acid was added to the organic phase as a stabilizer for the OCA monomer. Commercially-available Palacos R PMMA bone cement was used for all experiments reported herein.

3. METHODS

Interfacial polymerization of a polyurethane prepolymer with 1,4-butanediol was performed to encapsulate OCA using an oil-in-water emulsion[4]. Capsule-containing PMMA samples were fabricated following ASTM F451 and D638 for compression and tension, respectively. Fracture toughness was investigated using the tapered double-cantilever beam (TDCB) geometry described previously[5]. In all samples, the weight of particles (PMMA powder plus OCA-containing capsules) comprised 67% of the sample. Extracts from OCA and bone cement containing 0 or 10 wt% capsules were prepared in culture medium following the recommendations of ISO 10993. MG63 human osteosarcoma cells were cultured in these extract media to observe the effects on cellular proliferation and viability.

4. RESULTS

The minimum standard for the compressive strength of bone cement is 70 MPa[6]. Compressive tests of capsule-embedded bone cement specimens exceeded this criterion up to 5 wt% or less capsules (Figure 1A). However, a 20% decrease in ultimate compressive strength (UCS) occurred when the capsule content was increased to 10 wt%. Incorporation of more than 10 wt% capsules further decreased the compressive strength until 25 wt% capsules, where compressive strength leveled off. Furthermore, specimens containing 10 wt% or less capsules deformed plastically upon failure whereas specimens with higher capsule content fragmented upon failure (Figures 1B and C). The ultimate tensile strength (UTS) of the capsule-embedded specimens decreased monotonically with increasing wt% capsules, whereas the Young's modulus of capsule-containing samples appeared to drop sharply at 5 wt%

then decreased more slowly thereafter. Cements filled with 5 wt% or less capsules lie above the lower limit of the industry standard.

The inclusion of 3 wt% capsules resulted in a 13% increase in average K while inclusion of 5 wt% and 10 wt% capsules yielded K values approximately equal to that of control samples. Increasing capsule content to 15 and 20 wt% resulted in decreases of 26% and 47%, respectively when compared with capsule-free controls.

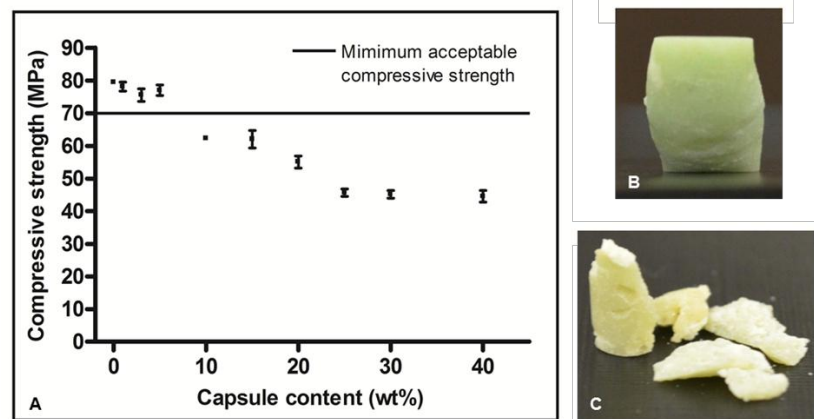


Figure 1: (A) Relationship between capsule content and the ultimate compressive strength of bone cement (average \pm SEM, $n=3$ with 5 replicates per group). Photographs of samples containing (B) 0 wt% and (C) 40 wt% capsules post-compression testing.

The effects of bone cement extract on MG63 proliferation over 24, 48, and 72 h are shown in Figure 2A-C. While proliferation in cells treated with commercial and capsule-embedded (SH) bone cement extracts was significantly reduced with respect to control samples, the addition of capsules did not significantly affect proliferation at 24, 48, or 72 h with respect to samples of bone cement without capsules.

The effects of OCA extract on cellular proliferation over 24, 48, and 72 h are presented in Figure 2D-F. A significant decrease in the proliferation of cells exposed to OCA extract-containing medium diluted to 50% (50% OCA) with respect to control was observed at each time point; the large decrease observed after 48 h suggests the OCA has a delayed effect on proliferation. However, some proliferative recovery is noted after 72 h.

5. CONCLUSIONS

The effects of capsule incorporation on the compressive, tensile, and fracture toughness properties of bone cement showed that inclusion of greater than 10 wt% capsules resulted in the decrease of UCS and UTS below the commercially-required levels; the fracture toughness was improved with the incorporation of 3 wt% capsules but declined as content was increased above 15 wt%. The effects of extract from a capsule-embedded bone cement on the proliferation and viability of MG63 human osteosarcoma cells indicated the addition of capsules did not significantly affect the response of the cells to the PMMA. The effects of both capsule-embedded bone cement and OCA extracts were found to be mediated through dilution of the extract.

Cells also demonstrated the potential to regain proliferative ability with increasing exposure time.

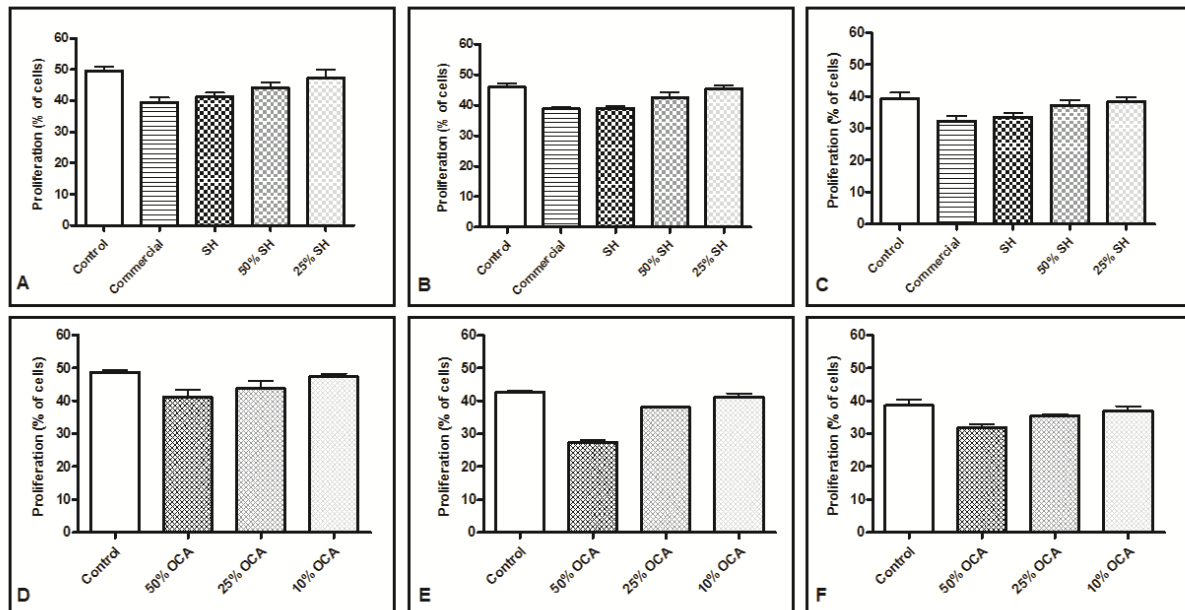


Figure 2: Proliferation of MG63 human osteosarcoma cells in response to growth in extract from (A,B,C) bone cement and (D, E, F) OCA after (A, D) 24, (B, E) 48, and (C, F) 72 h (average \pm SEM, n=4).

ACKNOWLEDGEMENTS

The authors would like to thank Ethicon, Inc. for the generous donation of 2-octyl cyanoacrylate. This research was supported by NIH grants T32-GM8555 (ABWB) and R21 EB 013874-01 (WMR).

REFERENCES

- [1] Brochu, A.B.W., S.L. Craig, and W.M. Reichert, Self-healing biomaterials. *Journal of Biomedical Materials Research Part A*, 96 (2011) 492-506.
- [2] Saha, S. and S. Pal, Mechanical properties of bone cement - a review. *Journal of Biomedical Materials Research*, 18 (1984) 435-462.
- [3] Yang, J.L., et al., Microencapsulation of Isocyanates for Self-Healing Polymers. *Macromolecules*, 41 (2008) 9650-9655.
- [4] Brochu, A.B.W., W.J. Chyan, and W.M. Reichert, Microencapsulation of 2-octylcyanoacrylate tissue adhesive for self-healing acrylic bone cement. *Journal of biomedical materials research. Part B, Applied biomaterials*, 100 (2012) 1764-72.
- [5] Brown, E.N., S.R. White, and N.R. Sottos, Microcapsule induced toughening in a self-healing polymer composite. *Journal of Materials Science*, 39 (2004) 1703-1710.
- [6] Kuehn, K.D., W. Ege, and U. Gopp, Acrylic bone cements: mechanical and physical properties. *Orthopedic Clinics of North America*, 36 (2005) 29-39.

SELF-HEALING BEHAVIOUR ORIGINATED BY DYNAMIC COVALENT BONDS IN DIARYLBIBENZOFURANONE: A DENSITY FUNCTIONAL STUDY

F. L. G. Sobrinho¹ and J. T. Arantes¹

¹ Universidade Federal do ABC, Av. Dos Estados 5001, 09210-580, Santo André, Brazil – e-mail: fernando.lucas@aluno.ufabc.edu.br; jeverson.teodoro@ufabc.edu.br

Keywords: self-healing materials, dynamic covalent bonds, cross-linked polymers, *ab initio* simulation, Density Functional Theory (DFT)

ABSTRACT

The ability to conduct a responsive behaviour of the material regarding external stimulations or environment conditions may lead to prevention and even management of damages that occurred on some applications, as an example surface coating. This is provided on polymeric materials by dynamic bonds, a class of bonds that under equilibrium conditions can break and reform selectively. This dynamic behaviour is achieved by supramolecular interactions (e.g. hydrogen bonding and π - π stacking) and also dynamic covalent bonds.

Both of these types are being studied by different research groups, with a wide range of approaches. Nonetheless, Imato et al. could achieve a unique set of conditions. Using the dimer of arylbenzofuranone (ABF), the diarylbibenzofuranone (DABBF), as cross-linker, the polymer gel synthesized was able to undergo self-healing on mild conditions at room temperature. This cross-linker, in special, was already studied due to the anomalous behaviour and antioxidant character.

In this work, *ab initio* methods were used based on the density functional theory (DFT), aiming a better comprehension of the structural and electronic properties of ABF and DABBF. As a result, the HOMO-LUMO energy difference of the former was 3.74 eV. No studies in the literature were found regarding empirical values. Nonetheless, benzofuran, with a similar structure, has a HOMO-LUMO energy difference of 4.0 eV. Using the dimer of ABF, DABBF, the HOMO-LUMO transition achieved was 3.23 eV. The empirical bond dissociation energy is 1.02 eV, while the calculated was 0.71 eV. Regarding the length of the bond responsible for the dynamic behaviour, values of 1.59 Å and 1.62 Å were obtained, for empirical and computational measures, respectively.

OPTIMIZING CU(I) CATALYSTS ONTO NANOPARTICLES FOR ENHANCED REACTIVITY IN SELF-HEALING POLYMERS

A. Stojanovic¹, A. Shaigan Nya¹, S. Rana¹ and W. H. Binder¹

¹*Institute of Chemistry, Chair of Macromolecular Chemistry, Faculty of Natural Sciences II (Chemistry, Physics and Mathematics), Martin-Luther University Halle-Wittenberg, von Danckelmann-Platz 4, Halle 06120, Germany– e-mail: wolfgang.binder@chemie.uni-halle.de*

Keywords: copper(I) catalyst, nanoparticles, alkyne-azide “click” reaction

ABSTRACT

The concept of self-healing polymers requires fast and efficient crosslinking processes, ideally based on catalytic reactions. Recently, we have developed a click-based concept to enable self-healing properties in polymeric materials, with a focus on fast crosslinking processes. Basically, liquid reagents were encapsulated and thus can be activated by a catalytic system, inherently present within the polymer-matrix. As especially the combination of self-healing properties of nanocomposite-materials in aerospace industry deems valuable in terms of property-optimization, we focus on crosslinking processes under mild conditions, based on the copper(I)-catalyzed alkyne-azide “click” cycloaddition reaction (CuAAC). Thus we have immobilized copper(I) catalysts onto the surface of nanoparticles, on the one hand to increase the stability of the catalyst and to stimulate the self-healing processes, on the other hand to enhance the properties of the polymeric nanocomposites via the presence of the nanoparticles. For this purpose the surface of different types of nanoparticles has been chemically modified, in the subsequent step immobilizing the corresponding Cu(I) catalyst coordinatively onto their surfaces. The prepared immobilized Cu(I) were extensively characterized via TGA, XRD and TEM, furthermore demonstrating and optimizing the activity of the immobilized catalyst for all types of “click”-reactions.

1. INTRODUCTION

Polymers with self-healing [1] or self-repairing properties [2], often including capsule-based concepts [3], mechanophores [2] and supramolecular concepts [4] have gained increasing attention in the past years. In all cases the basic concept of such materials relies on the use of crosslinking processes which enables repair of a mechanically induced damage by subsequent network-formation [5]. Recently, we have developed a click-based concept to enable self-healing properties in polymeric materials, with a focus on fast, “click-chemistry-based” crosslinking processes [6]. Basically, liquid reagents were encapsulated and thus can be activated by a catalytic system, inherently present within the polymer-matrix (see Figure 1).



Figure 1: The self-healing process based on the combination of “click”-crosslinking and encapsulation.

For many applications e.g. in aerospace industry the crosslinking processes under mild conditions are of an especial interest. Hence, we focus on the crosslinking processes based on the copper(I)-catalyzed alkyne-azide “click” cycloaddition reaction (CuAAC). The features of CuAAC such as high efficiency and substrate insensitivity, make this type of reactions suitable for crosslinking processes under moderate condition, both in homogenous and heterogeneous systems [7].

In present work we focus on the immobilization of copper(I) catalysts onto the surface of nanoparticles, with the aim to on the one hand increase the stability of the catalyst and to stimulate the self-healing processes, and on the other hand to enhance the properties of the polymeric nanocomposites via the presence of the nanoparticles.

2. RESULTS AND DISCUSSION

For the purpose of the effective immobilization of Cu(I) onto the surface of nanoparticles the surface of the selected nanoparticles was modified in the multiple-step synthetic route in order to be able to coordinatively bound the corresponding Cu(I) catalyst. The schematic representation of the synthetic route is presented in figure 2. The obtained functionalized nanoparticles have been intensively characterized via TGA, FTIR and EDX.

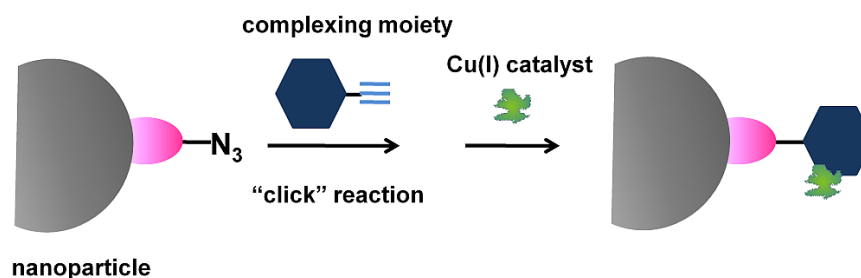


Figure 2: Scheme of the immobilization of Cu(I) catalyst

In the next step the selected Cu(I) catalyst is coordinatively attached to the surface of the nanoparticles. After suitable immobilization of the corresponding Cu(I) catalyst, the amount of the coordinatively bonded Cu(I) was determined and the prepared nanoparticles were extensively characterized via TGA, XRD and TEM. Furthermore

the activity of the immobilized catalyst for all types of "click"-reactions has been investigated.

3. CONCLUSION

Our preliminary results have shown that the selected Cu(I) catalysts can be effectively bounded on the surface of nanoparticles. Furthermore, the concept of the use of immobilized Cu(I) catalyst for the crosslinking processes based on alkyne-azide "click" cycloaddition reaction seems to be very promising.

ACKNOWLEDGEMENT

The research leading to these results has received funding from the European Union Seventh Framework Program (FP7/2007-2013) under grant agreement n° 313978.

REFERENCES

- [1] E. B. Murphy, F. Wudl, The world of smart healable materials, *Progress in Polymer Science* 35 (2010) 223-251.
- [2] M. M. Caruso, D. A. Davis, Q. Shen, S. A. Odom, N. R. Sottos, S. R. White SR, J. S. Moore, Mechanically-Induced Chemical Changes in Polymeric Materials, *Chemical Reviews* 109(2009) 5755-5798.
- [3] M. M. Caruso, B. J. Blaiszik, H. Jin, S. R. Schelkopf, D. S. Stradley, N. R. Sottos, S. R. White SR, J. S. Moore, Robust, Double-Walled Microcapsules for Self-Healing Polymeric Materials, *ACS Applied Materials & Interfaces* 2 (2010) 1195-1199.
- [4] P. Cordier, F. Tournilhac, C. Soulie-Ziakovic, L. Leibler, Self-healing and thermoreversible rubber from supramolecular assembly, *Nature* 451(2008) 977-980.
- [5] W. H. Binder, *Self-Healing Polymers. From Principles to Applications*, Ed., Wiley-VCH: Weinheim, 2013.
- [6] M. Gragert, M. Schunack, W. H. Binder, Azide/Alkyne-"Click"-Reactions of Encapsulated Reagents: Toward Self-Healing Materials, *Macromolecular Rapid Communications* 32 (2011) 419-425.
- [7] W. H. Binder, R. Zirbs, "Click"-Chemistry in Macromolecular Synthesis. *Encyclopedia of Polymer Science and Technology*: John Wiley & Sons, Inc; 2009. p. DOI: 10.1002/0471440264.pst565.

SELF-HEALING SUPRAMOLECULAR MATERIALS

POSTER SESSION

SELF-HEALING METALLOPOLYMERS: DETAILED INVESTIGATION OF THE SELF-HEALING PROPERTIES BY SCRATCH TESTING

S. Bode^{1,2}, R. Bose³, B. Sandmann^{1,2}, M. D. Hager^{1,2}, S. J. Garcia³, S. van der Zwaag³ and U. S. Schubert^{1,2}

¹ Laboratory of Organic and Macromolecular Chemistry (IOMC), Friedrich Schiller University Jena, Humboldtstr. 10, 07743 Jena (Germany), e-mail: ulrich.schubert@uni-jena.de; martin.hager@uni-jena.de

² Jena Center for Soft Matter (JCSM), Friedrich Schiller University Jena, Philosophenweg 7, 07743 Jena (Germany)

³ Novel Aerospace Materials, Delft University of Technology, Kluyverweg 1, 2629 HS Delft, The Netherlands – e-mail: s.vanderzwaag@tudelft.nl

Keywords: Metallopolymers, self-healing polymers, polymer testing, polymer coatings

ABSTRACT

In the last decade several intrinsic self-healing materials have been developed in which the healing mechanism was mainly based on the reversibility of a certain structural element. For this purpose, reversible covalent bonds, e.g., based on the Diels-Alder reaction or weaker non-covalent interactions, e.g., hydrogen bonding, ionic interactions or π - π interactions, have been successfully utilized. In contrast, only few examples describe the self-healing of polymeric materials based on reversible metal-ligand-interactions, although this concept can be observed in nature (e.g., in mussel byssus threads). The directed interaction between a metal ion and corresponding ligands offers the possibility to integrate a reversible unit into a polymer matrix. If metal complexes are used as structural units to promote self-healing, a compromise between the mechanical properties and the self-healing behavior must be found. Typically, the strength of the metal-ligand bond is the key factor for both. However, weaker metal complexes would promote the healing while, at the same time, the mechanical stability is reduced. The analysis of the self-healing capacity and the mechanical properties are central in order to design new functional materials.

The terpyridine ligand was chosen as a model system to study the parameters for the resulting polymer properties. For this purpose, terpyridine containing polymers were synthesized and subsequently crosslinked with different metal salts, which offers the possibility to understand the influence of the crosslinking unit, the cation and the counterion. The resulting polymeric materials were investigated in detail (e.g., by scratch testing) to obtain a better insight into the self-healing behavior of the material.

1. INTRODUCTION

Self-healing materials can be defined as materials which are able to heal local mechanical damage, such as cracks or scratches. The (partial) recovery of the drop in mechanical properties as a result of local damaged sites without major external manipulation represents an intriguing feature of such materials. If the mechanism of healing is not related to an added external component, but is linked to the molecular architecture of the polymer itself, the resulting intrinsic self-healing behavior enables

the ability to design novel materials, which can theoretically heal themselves endlessly, if the right healing mechanism is applied.^[1,2]

In principle, metal-ligand interactions can also be used for intrinsic self-healing, as the reformation of coordinative bonds does not require demanding conditions such as high pressure or the addition of further substances, but it can occur *in-situ* for polymers in a suitable environment.^[3]

The terpyridine moiety, which was used frequently, represents a well investigated polypyridyl-type ligand and the corresponding properties, *e.g.*, the complex stabilities are well-known in literature.^[4] However, the reported values always refer to the solution state and the solid-state behavior of terpyridine metal complexes is still rather unexplored.

Thus, we investigated polymers, which were functionalized by terpyridine moieties and afterwards crosslinked by metal salts. We want to understand the healing mechanism behind and to combine mechanical stability and self-healing properties in metallopolymer coatings.

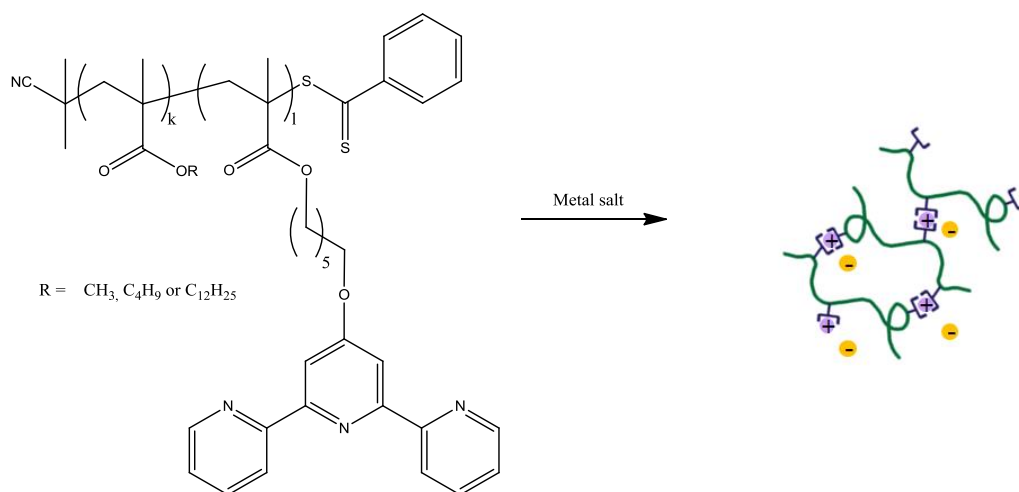
2. RESULTS AND DISCUSSION

Firstly, it is necessary to design the terpyridine containing copolymers. For this purpose, a terpyridine monomer was copolymerized with other monomers (*i.e.* alkyl methacrylates), in order to adjust the amount of the crosslinking units as well as to tune the thermal and mechanical properties of the resulting polymer networks. The RAFT-polymerization technique was used to obtain well-defined polymers with adjustable composition.^[5] For the copolymerization three different methacrylate monomers were used: methyl methacrylate, butyl methacrylate and lauryl methacrylate. The resulting polymers have molar masses (M_n) of about 30,000 g/mol and differ in the glass transition temperature, which indicates the different flexibility/mobility of the polymer backbones. The desired content of terpyridine of 10% could be nearly reached for all polymers. Afterwards the terpyridine containing copolymers were crosslinked by the addition of a metal salt, *i.e.*, iron(II) and cadmium(II) salts (Scheme 1).

To identify the influence of the counterion on the self-healing process different cadmium(II) salts (*i.e.*, the chloride, bromide, iodide, and acetate) were used; these anions differ both in size (from 162 pm to 220 pm) and polarizability.

It could be shown that the polymer networks crosslinked with cadmium acetate shows the best self-healing behavior. The results could be explained by a phase transition, which could be detected by DSC, SWAXS and TMA-measurements. The SWAXS results are depicted in Figure 1.

The self-healing behavior was initially observed by optical microscopy. The healing process of the cadmium acetate crosslinked metallopolymer takes place at temperatures above 70 °C as shown in Figure 2.



Scheme 1: Schematic representation of the synthesis of metallopolymer network.

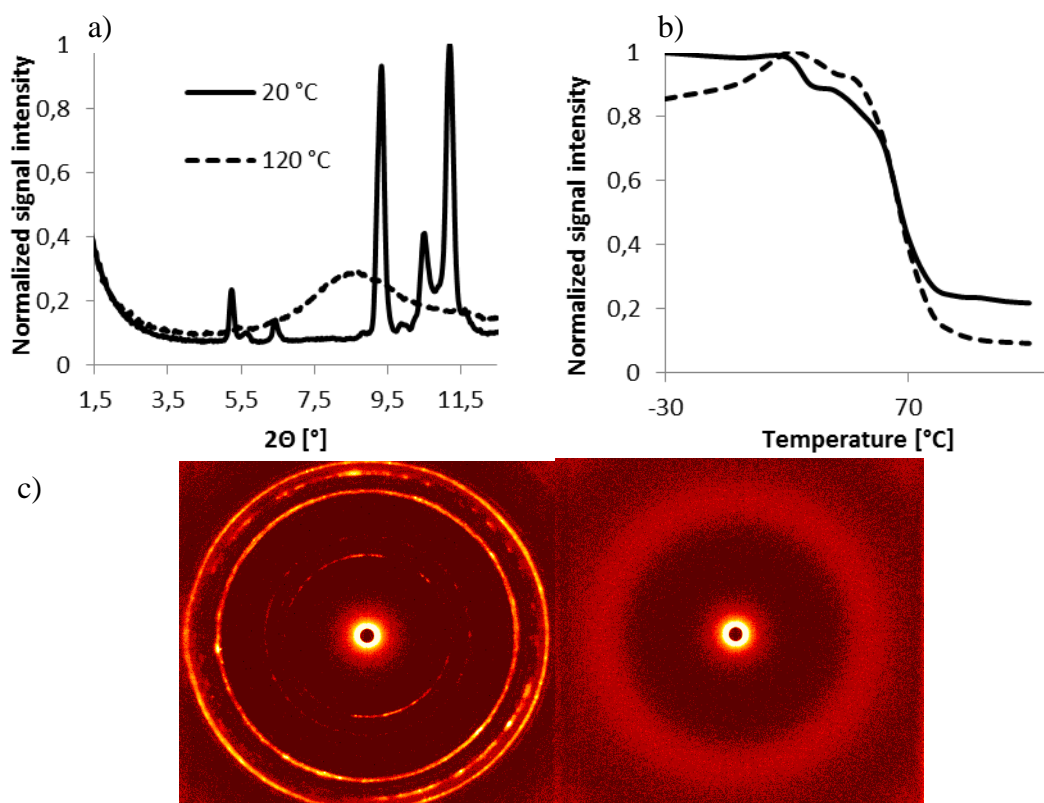


Figure 1: SWAXS results of the cadmium acetate crosslinked metallopolymer: a) SWAXS diagram at 20 °C (solid black line) and at 120 °C (dotted black line), b) signal intensity of the signal at 9.34° (solid black line) and 11.18° (dotted black line) as a function of the temperature, c) SWAXS signal at the 2D-detector at 20 °C (left) 120 °C (right).

It could be noted that the copolymers were also crosslinked by the addition of other metal salts (iron (II) sulfate, cadmium (II) chloride, bromide and iodide), although these new polymers didn't lead to a significant improvement of the healing capabilities.^[6] The results show a strong dependency of the healing efficiency on the cation and anions used during the crosslinking step.

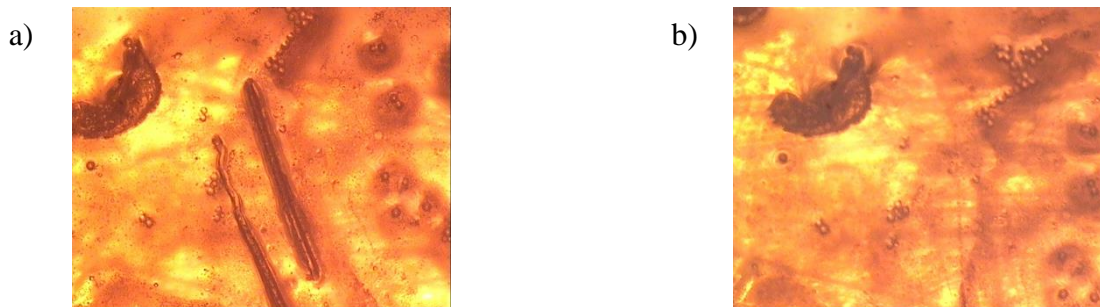


Figure 2: Self-healing experiments of the cadmium acetate crosslinked metallopolymer: a) Scratch and b) Healing after 16 h at 80 °C.

3. CONCLUSIONS

In this study, it could be shown, that metallopolymer networks are able to heal mechanical damage. The influence of the counterion was studied and it could be shown, that a copolymer, which was crosslinked by the addition of cadmium acetate shows the best self-healing behavior. This is based on the transition of the polymer and above 70 °C the acetate moieties exchange. This results in very good self-healing. Further research is being performed to gain a major understanding of the role of the different cations on the healing capabilities.

ACKNOWLEDGEMENTS

The authors thank the Deutsche Forschungsgemeinschaft (DFG, SPP 1568), the Thuringian Ministry for Education, Science and Culture (TMBWK grants #B515-10065, ChaPoNano; #B514-09051, NanoConSens; and #B515-11028, SWAXS-JSCM), the Fond chemischer Industrie (scholarship for S.B.) and the DPI (technology area HTE) for financial support.

REFERENCES

- [1] M. D. Hager, P. Greil, C. Leyens, S. van der Zwaag, U. S. Schubert, Self-healing materials, *Advanced Materials* 22 (2010), 5424-5430.
- [2] U. Lafont, H. van Zeijl, S. van der Zwaag, Influence of Cross-linkers on the Cohesive and Adhesive Self-healing Ability of Polysulfide-Based Thermosets, *Applied Materials and interfaces* 4 (2012) 6280-6288.
- [3] G. R. Whittell, M. D. Hager, U. S. Schubert, I. Manners, Functional soft materials from metallopolymers and metallosupramolecular polymers *Nature Materials* 10 (2011) 176-188.
- [4] A. Wild, A. Winter, F. Schlütter, U. S. Schubert, Advances in the field of π -conjugated 2,2':6',2''-terpyridines *Chemical Society Reviews* 40 (2011) 1459-1511.
- [5] J. Chiefari, Y. K. Chong, F. Ercole, J. Krstina, J. Jeffery, T. P. T. Le, R. T. A. Mayadunne, G. F. Meijs, C. L. Moad, G. Moad, E. Rizzardo, S. H. Thang, Living Free-Radical Polymerization by Reversible Addition-Fragmentation Chain Transfer : The RAFT Process *Macromolecules* 31 (1998) 5559-5562.
- [6] S. Bode, L. Zedler, F. H. Schacher, B. Dietzek, M. Schmitt, J. Popp, M. D. Hager, U. S. Schubert, Self-healing polymer coatings based on crosslinked metallosupramolecular copolymers *Advanced Materials* DOI: 10.1002/adma.201203865.

TOWARDS THE MICROSCOPIC UNDERSTANDING OF SELF-HEALING MECHANISMS

A. R. Brás¹, C. Hövelmann¹, W. Antonius¹, M. Krutyeva¹, A. Radulescu², J. Allgaier¹, W. Pyckhout-Hintzen¹, A. Wischnewski¹ and D. Richter¹

¹Forschungszentrum Jülich, Jülich Centre for Neutron Science JCNS, D52425 Jülich, Germany – e-mail: a.bras@fz-juelich.de; c.hoevermann@fz-juelich.de; w.antonius@fz-juelich.de; m.krutyeva@fz-juelich.de; j.allgaier@fz-juelich.de; w.pyckhout@fz-juelich.de; a.wischnewski@fz-juelich.de; d.richter@fz-juelich.de

²Forschungszentrum Jülich, Jülich Centre for Neutron Science JCNS, Outstation at FRM II, D85747 Garching, Germany – e-mail: a.radulescu@fz-juelich.de

Keywords: Supramolecular polymers, hydrogen bonds, neutron scattering, random phase approximation

ABSTRACT

In the present work we report on a Random Phase Approximation (RPA) which can be applied to multiblock copolymers consisting of supramolecular building blocks and hydrogen-bonded compounds including interactions in solution. These systems are model for the self-healing process due to the hydrogen-bonding interaction between the end-groups. This new analysis allowed to quantitatively access the assembly route with varying concentration.

1. INTRODUCTION

Supramolecular polymers are an increasingly important class of polymers, where designed intermolecular interactions allow a specific tailoring of polymer properties. One of the most recent additions to this field are self-healing polymers, which bases on the hydrogen-bonding interaction of groups on parts of the molecules. Small Angle Neutron Scattering (SANS) measurements were performed on systems as a 50/50 mixture [1] in deuterated toluene, using the complementary end-groups Thy and DAT (Fig. 1) and polypropylene glycol as backbone.

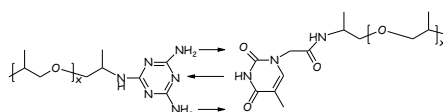


Figure 1: Complementarity between DAT and THY, leading to self-assembly.

Recently [1], Small Angle X-Ray (SAXS) was performed on the same systems in the bulk. It shows the typical behavior of a block copolymer [1] in a 1-phase region. In solution, the same behavior as in an homogenous phase in the respective diagram is expected. More, even though in literature cyclization is possible to occur upon dilution in the formation of supramolecular polymers, the polymers in this study showed, at our experimental conditions, a much smaller fraction of rings as expected by theory (~50 %) [2]. We cannot distinguish rings from linear aggregations within ~10%. In practice, any imbalance of stoichiometries, monofunctional imperfection or disproportion of the building blocks of which the exact molecular weights differ, shifts the equilibrium to unclosed or linear species.

The intriguing question how to quantitatively access the assembly route is tested by an RPA for a *thought* multiblock copolymer consisting of simple blocks and hydrogen-bonded compounds including for the first time interactions between the separate components in solution.

2. METHODS

Experiments were performed at the SANS diffractometer KWS2 @FRM2, Munich.

3. RESULTS

The RPA structure factor for a diblock copolymer, considering no interactions between the blocks ($\chi_{AB}=0$) is [3]:

$$S_{RPA} = \frac{S_{AA}S_{BB} - S_{AB}^2}{S_{AA} + S_{BB} + 2S_{AB}} (\chi = 0) \quad (1)$$

In this work we need to consider a ternary system of a block copolymer in solution. In our terminology, this is a third “component” case with the block as components A, B and the solvent as component C. The number of components is determined by the number of different scattering length densities. Block A is connected to block B leading to the general multiblock copolymer $(AB)_{N_{agg}-1}A$. In addition we have included in the multi-component RPA all possible interactions X_{ij} with $i,j=A,B,C$.

Assuming the complex and solvent as oligomers of the same stiffness as the main blocks, one can express the partial structure factors by a number of monomers noted as n_A , n_B and n_C (polymer, end-groups and solvent, respectively), the volume fractions (ϕ_A , ϕ_B and ϕ_C), the specific monomeric volumes (v_A , v_B and v_C), the form factors are $P_{AA}(Q)$, $P_{BB}(Q)$ and $P_C(Q)$, the Flory-Huggins interaction parameters are χ_{AB} , χ_{BC} and χ_{AC} (χ_{AB} polymer-endgroups, χ_{BC} endgroups-solvent and χ_{AC} polymer-solvent), the different contrasts to the background ($\Delta\rho_A$, $\Delta\rho_B$) and the number of aggregates (N_{agg}): $S_{RPA} = f(N_{agg}, \chi, \Delta\rho, \phi_c)$

In the related polycondensation theory the N_{agg} is defined as ($N_{agg} \approx \text{Sqrt}(K_{ass} \cdot \phi_p)$) [4], K_{ass} being the equilibrium association constant in solution of the system Thy-Thy /DAT-DAT mixture and assumed as a fit parameter of the model. The RPA approach is strictly valid only in the melt state and assumes Gaussian statistics. Deviations therefore are possible especially at high Q but the main information will be independent from this. As a further approximation the non-bonded end-groups at the beginning and end of the multiblock are neglected.

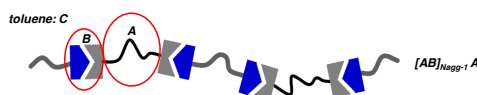


Figure 2: Sketch of the suggested block copolymer structure of the type $(AB)_{n-1}A$.

With N_{agg} one could naively obtain an apparent size of living chain M_w . Assuming Gaussian statistics and monomolecularity as polydispersity in connection with RPA is not manageable, a concentration-dependent overlap or critical concentration can be estimated from published chain dimensions depending on M_w . As the K_{ass} is not known and depends on the specific purity of the experimental system a range of concentrations was selected between 0 and $c^*=\phi_p \approx 10\%$ from the chloroform constant. The used concentration of the mixture of the components A-B were 0.9 to

9% (m/m): Neglecting in a first approximation inter-component interactions, a general model-independent Guinier representation of the low Q data, $\ln I(Q) = \ln I_0(Q) - 1/3Q^2R_g^2$, allows us to qualitatively interpret the data. The range of scattering vectors was restricted to $QR_g \sim 2$ here, for which the Guinier approximation is valid. At $Q=0$ the intercept intensity I_0 is proportional to M_w . Thus for the system Thy-Thy/DAT-DAT mixture, if association occurs, its expected dependence should be $I_0 \approx (\phi_p)^{3/2}$. Similarly, the chain radius of gyration R_g obtained by the same approach should depend on ϕ_p as $R_g \approx (\phi_p)^{1/4}$. The Gaussian statistics assumption seems to be kept upright through the Q^{-2} dependence found even at the lowest dilution. In figure 3 the results from this first analysis are shown, respectively:

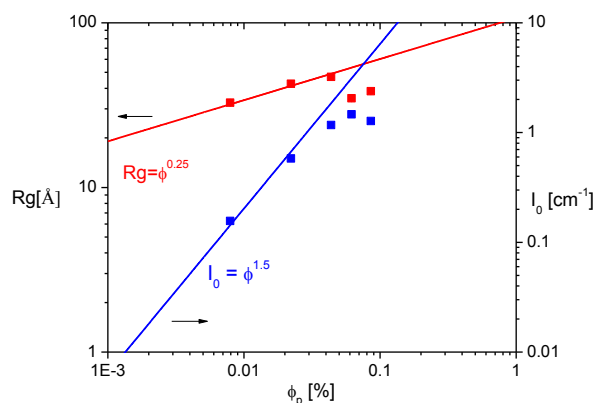


Figure 3: The forward scattering intensity I_0 and R_g follow closely the predictions of a linear association in a multiblock-like chain, proven from the different slopes vs. ϕ_p .

It is evidenced that the above proportionalities are observed only for $\phi_p < 6.0\%$. It indicates that, contrarily to the previous estimations for Chloroform ($K_{ass} = 890 \text{ mol}^{-1}$) [1], c^* is reached at a lower concentration. Hence we are led to the conclusion that in toluene the K_{ass} is higher. As a consequence the full Random Phase Approximation model described before for these supramolecular associating polymers was only applied to the systems with concentrations below $\phi_p < 6.0\%$. The only parameters were the K_{ass} , χ_{AB} and χ_{BC} . Concerning χ_{AC} , i.e. the interaction between PPG-toluene, the estimated value is in accordance to what was found in literature [5] and therefore was kept constant. All values are presented in Table 1. A simultaneous fit to the data was done in order to obtain the most accurate estimate of K_{ass} and also since the interaction parameters should not vary in the different concentrations, too. The respective obtained parameters for all systems are summarized in the table below:

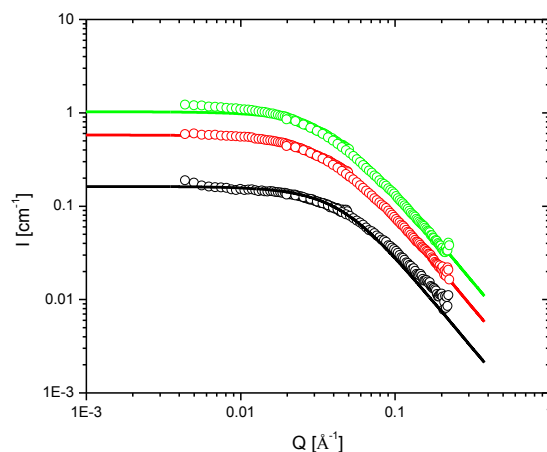


Figure 4: Coherent scattering intensities for the stoichiometric mixture at different concentrations below c^* in toluene at room temperature. The solid lines show a fit to the data with the RPA approximation.

The obtained interaction parameters compare very well to the estimated ones and clearly show that the similarity with block copolymers like suggested [1] is appropriate. The fit to the data is shown in figure 4 as solid lines. The high interactions reflect the different solubilities of the specific components and may well form a basis for the occurrence of a considerable nanostructuring into micelle-like or more compact aggregates by phase-separation or stacking mechanisms at concentrations exceeding highly the investigated concentration range below c^* .

Table 1: Empirical estimations of χ obtained from solubility parameters following the Hansen method [5] compared to the data parameters from the simultaneous fit to the data using the new RPA.

	K_{ass}	χ_{AC}	χ_{AB}	χ_{BC}
Estimation	---	0.34	1.7-4.8	3.8 (Thy)- 4.1 (DAT)
RPA fit	1400 ± 200	0.34	6.38 ± 0.06	4.0 ± 0.01

4. CONCLUSIONS

It can be seen that the used RPA approach very reasonably describes the SANS data. Except for small discrepancies at high Q which can be explained by the finite size of the blocks, the model is superior over the often-used too simple Guinier approach. The intramolecular interaction parameters are of the order or much larger than for typical flexible polymers. Moreover, from the power-law for both zero- Q -scattering and R_g it could be confirmed that a linear conformation of these mixtures is present, and ring-association and collapsed or in se aggregation are absent or can be neglected in very good approximation.

ACKNOWLEDGEMENTS

Prof. Leibler for introducing these polymers to the FZJ group and DFG-SPP1568 for financial support.

REFERENCES

- [1] J. Cortese, C. Soulie-Ziakovic, M. Cloitre, S. Tence-Girault, L. Leibler, Order-Disorder Transition in Supramolecular Polymers, *Journal of the American Chemical Society* 133 (2011) 19672-19675; J. Cortese, C. Soulié-Ziakovic, S. Tencé-Girault, L. Leibler, Suppression of Mesoscopic Order by Complementary Interactions in Supramolecular Polymers, *Journal of the American Chemical Society* 134 (2012) 3671-3674.
- [2] L. Rique-Lurbet, M. Schappacher, A. Deffieux, A New Strategy for the Synthesis of Cyclic Polystyrenes: Principle and Application, *Macromolecules* 27 (1994) 6318-6324; H. Jacobson, W. J. Stockmayer, Intramolecular Reaction in Polycondensations. I. The Theory of Linear Systems, *Journal of Chemical Physics* 18 (1950) 1600-1606.
- [3] http://www.ncnr.nist.gov/staff/hammouda/the_SANS_toolbox.pdf
- [4] L. Bouteiller, Assembly via Hydrogen Bonds of Low Molar Mass Compounds into Supramolecular Polymers, *Advances in Polymer Science* (2007) 207, 79-112.
- [5] D.W. Van Krevelen, *Properties of Polymers*, 3rd ed., Elsevier: Amsterdam, New York, 1990; J.E. Mark; *Polymer data handbook*, Oxford University Press, 1999; S.W. Kuo, H.T. Tsai, Complementary Multiple Hydrogen-Bonding Interactions Increase the Glass Transition Temperatures to PMMA Copolymer Mixtures, *Macromolecules*, 2009, 42, 4701-4711.

A NEW CLASS OF SUPRAMOLECULAR THERMOPLASTIC ELASTOMERS FOR SELF-HEALING COATINGS

M. M. Diaz^{2,4}, L. Voorhaar^{1,4}, T. Perkisas^{3,4}, A. Abakumov³, G. Van Assche², B. Van Mele² and R. Hoogenboom¹

¹ *Supramolecular Chemistry Group, Department of Organic Chemistry, Ghent University Krijgslaan 281 S4, B9000 Ghent, Belgium – e-mail: Lenny.Voorhaar@ugent.be*

² *Department of Materials and Chemistry, Physical Chemistry and Polymer Science, Vrije Universiteit Brussel, Pleinlaan 2, Brussels 1050, Belgium – e-mail: mdiazace@vub.ac.be*

³ *EMAT, University of Antwerp, Groenenborgerlaan 171, B-2020 Antwerp, Belgium – e-mail: Tyche.Perkisas@ua.ac.be*

⁴ *SIM vzw, Technologiepark 935, B - 9052 Zwijnaarde, Belgium*

Keywords: supramolecular polymer, thermoplastic elastomer, coatings, phase separation.

ABSTRACT

A supramolecular material exhibiting self-healing properties was studied in this work. The material is based on the mixture of two ABA-type oligomeric triblock copolymers, the first consisting of positively charged end blocks and the second one of negatively charged ones. Each oligomeric triblock consists of a soft middle block and soft end blocks. When mixed together the resulting material phase-separates in an electrostatically assembled phase with a high glass transition temperature (T_g) and an uncharged phase with a low T_g . The mechanical and physical properties of the resulting thermoplastic elastomer can be tuned by varying the size of the charged blocks, using different polymer architectures and using different monomers. The building block oligomers are synthesized via reversible addition-fragmentation chain transfer (RAFT) polymerization using a bifunctional chain transfer agent and purified by precipitation. Characterization was done by Modulated Differential Scanning Calorimetry (MDSC), Dynamic Mechanical Thermal Analysis (DMTA) and Transmission Electron Microscopy (TEM). The self-healing behaviour of the coating was studied under optical microscope proving self-healing abilities after scratching.

1. INTRODUCTION

Polymers are one of the most widely studied materials for self-healing (SH) applications. Several strategies have been approached in order to achieve materials that exhibit comparable performance to materials used today, with the extra capability of recovering its strength after being damaged. The use of supramolecular interactions as a SH mechanism are advantageous due to their reversible nature and their response to external factors such as temperature and concentration.[1] In addition, non-covalent reversible interactions undergo continuous dynamic exchange that can lead to intrinsic autonomous self-healing materials.[2][3][4]

The material studied in this work is based on ABA-type oligomeric triblock copolymers, consisting of a soft uncharged middle block and soft oppositely charged end blocks. When mixed together, the resulting material will phase-separate in an electrostatically assembled charged phase with a high T_g and an uncharged phase with a low T_g . The electrostatic interaction between the charged blocks will provide the strength of the material, resembling an electrostatic SBS rubber analogue.[5]

Polymers of similar design have been used previously for hydrogels.[6] The mechanical and physical properties can be tuned by varying the size of the charged blocks, using different polymer architectures and using different monomers.

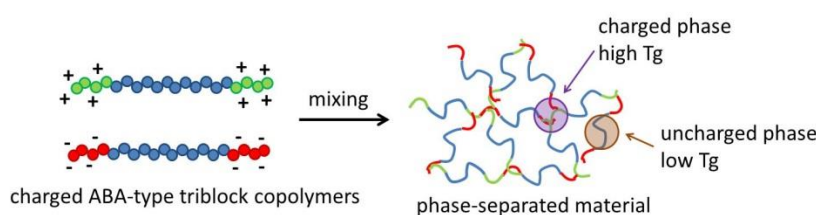


Figure 1: Formation of a phase-separated material by mixing oppositely charged ABA-type triblock copolymers.

2. MATERIALS AND METHODS

The ABA-type triblock copolymers were synthesized via reversible addition-fragmentation chain transfer (RAFT) polymerization using a bifunctional chain transfer agent and purified via precipitation. Molecular weights of the polymers were around 10000 g/mol with PDIs of around 1.2.

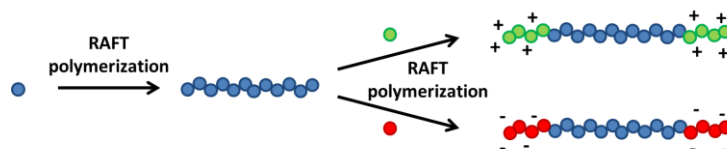


Figure 2: Two-step synthesis of ABA-type triblock copolymers via RAFT polymerization.

Thermal characterization of the materials was done in a TA instruments Q2000 DSC with MDSC option and an RCS cooling. Heat cooling cycles with the following conditions were done: a heating rate of 2°C/min, a period of 80s and amplitude of $\pm 0.4^\circ\text{C}$ was used. Dynamic Mechanical Analysis (DMTA) was done on a TA instruments Q800 at heating rate of 2.5°C/min and frequency of 1Hz.

A FEI Tecnai G2 electron microscope was used in order to study the morphology of the elastomer by Transmission Electron Microscopy (TEM). In order to enhance the contrast of the sample, it was stained in OsO₄ vapors for 12 hours. The sample was also cooled to liquid nitrogen temperatures in order to avoid knock-on damage and heating of the sample by the electron beam.

3. RESULTS AND DISCUSSION

The individual block copolymers were characterized by MDSC to determine their thermal transitions. The observed result is shown in Figure 3(a), the ABA block copolymer exhibits one T_g at -41°C , these means that the two blocks are merged in one phase. The same is observed for the second block copolymer CBC, which also exhibits one T_g at -35°C showing the miscibility of both blocks. The mixing of the two materials results in a material with two glass transitions: a lower glass transition corresponding to the middle common block of both copolymers and a higher

transition resulting from the interaction between the charged blocks. In addition, the result shows that as both types of blocks associate a second phase is generated, giving an indication about the morphology of the mixture.

The thermomechanical characterization of the mixture on DMTA is shown in Figure 3(b). At low temperature around -30°C a maximum in the loss modulus can be observed indicating a glass transition. At this moment the modulus drops and a rubbery plateau is kept until 40°C when the storage modulus starts decreasing again. This last transition is agreement with the results obtained by DSC and show that the obtained material behaves like an elastomer.

Scanning Transmission Electron Microscopy (STEM) was performed upon the sample (see Figure 4). From diffractogram (see inset Figure 4) analysis it was found that the average domain size of the elastomer was nanometer sized, which is in agreement with the DSC measurements.

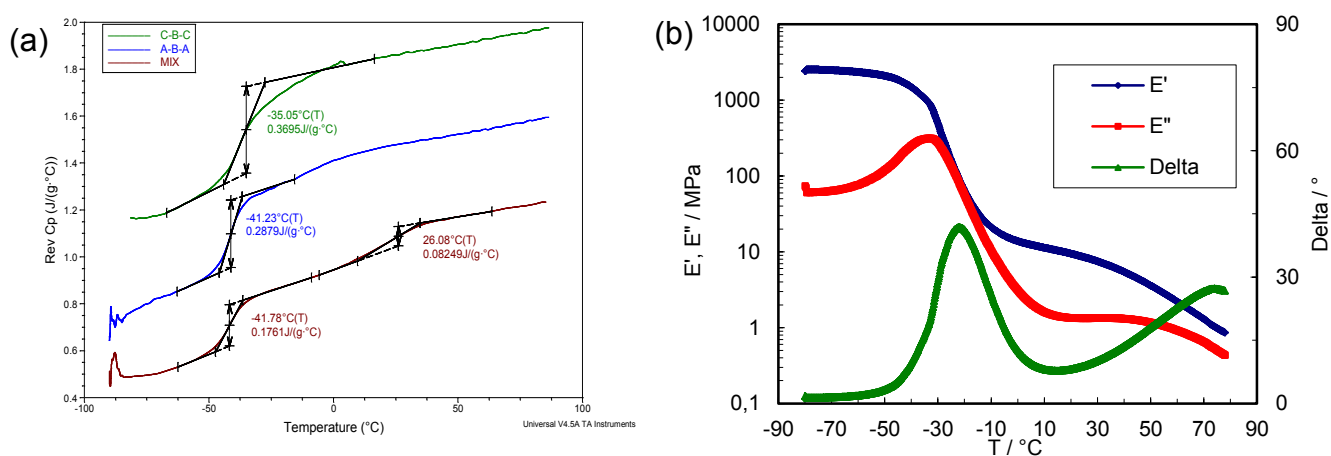


Figure 3: (a) MTDSC of the individual block copolymers and mixture (b) DMTA of the mixture of oligomers.

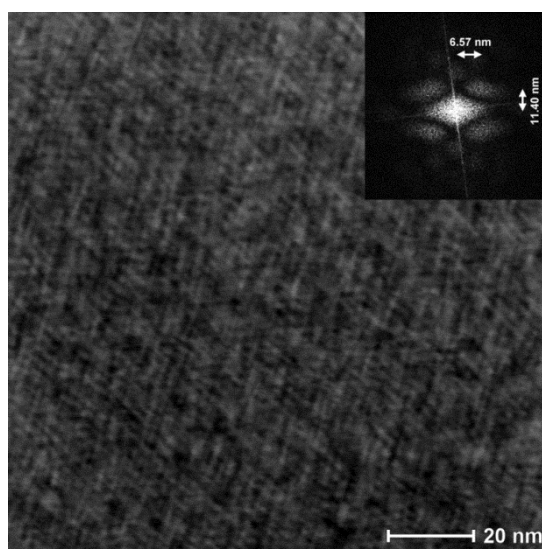


Figure 4: Scanning Transmission Electron Microscopy (STEM) image of the polymer mixture stained with OsO₄ showing separate domains of the charged associated high T_g zones in a soft matrix. The diffractogram (inset) shows evidence of nanometer sized domains.

4. CONCLUSIONS

When the oppositely charged ABA-type triblock copolymers are mixed together, a two-phase system is formed, giving indication of supramolecular interaction. This can be observed in MDSC by the appearance of a second T_g at 26°C and with TEM. DMTA shows the elastomeric properties of the material. Further research to optimize the properties of the material is in progress.

ACKNOWLEDGEMENTS

This work was funded by the Special Research Fund (BOF) of Ghent University and the Strategic Initiative Materials (SIM).

REFERENCES

- [1] W.P.J. Appel, M.M.L. Nieuwenhuizen, E.W. Meijer, Multiple Hydrogen-Bonded Supramolecular Polymers, in: *Supramolecular Polymer Chemistry* (ed A. Harada), (2011) Wiley-VCH Verlag GmbH & Co. KGaA, Weinheim, Germany.
- [2] G.M.L van Gemert, J.W. Peeters, S.H.M. Söntjens, H.M. Janssen, A.W. Bosman, Self-Healing Supramolecular Polymers In Action, *Macromolecular Chemistry and Physics* 213 (2012), 234-242.
- [3] Y.Chen, A.M. Kushner, G.A. Williams, Z. Guan, Multiphase design of autonomic self-healing thermoplastic elastomers, *Nature Chemistry* 4 (2012) 467-472.
- [4] R. Hoogenboom, Hard Autonomous Self-Healing Supramolecular Materials—A Contradiction in Terms? *Angewandte Chemie International Edition* 51 (2012), 11942-11944.
- [5] J.F. Masson, S. Bundalo-Perc, A. Delgado, Glass transitions and mixed phases in block SBS, *Journal of Polymer Science Part B: Polymer Physics* 43 (2005) 276-279.
- [6] J.N. Hunt, K.E. Feldman, N.A. Lynd, J. Deek, L.M. Campos, J.M. Spruell, B.M. Hernandez, E.J. Kramer, C.J. Hawker, Tunable, High Modulus Hydrogels Driven by Ionic Coacervation, *Advanced Materials* 23 (2011), 2327-2331.

MICROVASCULAR SYSTEMS

POSTER SESSION

NOVEL MANUFACTURING METHOD FOR FRP COMPOSITES WITH A MULTIFUNCTIONAL VASCULAR NETWORK

K. Boba¹, C. Heath¹, I.P. Bond¹ R.S.Trask¹ and D.F. Wass²

¹ ACCIS, Department of Aerospace Engineering, University of Bristol, University Walk, Bristol BS8 1TR, UK – email: Kasia.Boba@bristol.ac.uk, I.P.Bond@bristol.ac.uk, R.S.Trask@bristol.ac.uk

² School of Chemistry, University of Bristol, Bristol BS8 1TS, UK – e-mail: Duncan.Wass@bristol.ac.uk

Keywords: vascular network, self-healing, thermal management, pluripotential, Poly(lactic acid)

ABSTRACT

Fibre reinforced polymer composite materials are becoming more widely adopted for high performance industrial applications. The hierarchical nature of these materials offers a unique opportunity to incorporate multi-functionality whilst maintaining their excellent mechanical properties. Ideally, multifunctional composites can be configured to mimic natural biological systems. For example, the fabrication of an embedded array of hollow channels in the form of a vascular network can be utilised to provide a variety of functions, including self-healing, thermal management or sensing and actuation [1].

Previous research has shown that vascular integration into FRP laminates can be achieved through incorporation of material in-situ (hollow glass fibres [2] or polyether ether ketone (PEEK) tubing [1]), or through a “lost-wax” process using solder [3,4]. This study considers a novel manufacturing method for hollow channel fabrication, with the intention of limiting damage to the FRP laminates during post-cure channel manufacture, using Polylactic Acid (PLA) coated Nichrome wires to produce vascular networks running through multiple levels of the FRP ply stack. Low voltage resistive heating of the Nichrome wires enables their removal from the FRP post cure, even in complex shapes. The successful manufacture of an Animalia inspired network design was achieved within a glass fibre reinforced polymer (GFRP) panel. Furthermore, for panels subjected to steady state heating, the branched network displayed far greater cooling potential than the parallel channel design. This suggests the possibility to manufacture more complex networks within FRP laminate structures, facilitating their multi-functionality, namely for thermal management or self-healing applications.

1. INTRODUCTION

The use of biologically inspired networks within composite laminates has been considered for a variety of functions, including but not limited to: sensing, healing and thermal management [1]. Incorporation of multifunctionality can improve the longevity of components, directly through self-healing, or through increasing permissible temperatures of operation through self-cooling. As the temperature of composite components approaches the glass transition temperature of the matrix, thermal stress induced ageing greatly increases [5,6], thus the incentive for integrated cooling.

The in-situ manufacture of biomimetic vasculature within FRP laminates has been considered in some detail, using sacrificial solder or hollow tubing, running parallel to adjacent fibre reinforcement, similar in form to those seen in *Plantae* [3].

This study will look at the concept of multiple bifurcations with hierarchical vascular geometry which is mimetic of the circulatory systems of *Mammalia*, or more broadly of *Animalia*. The key difference is the separation and later coalescence of the introduced fluid flow. As such, this paper considers whether the in-situ manufacture of *Animalia* inspired 3D branched vasculature networks within FRP laminates is possible, and investigates the thermal management capability compared to *Plantae* inspired parallel vasculature. This study should be considered to serve as a proof of concept of the integration of branched vascular architecture into FRP laminates.

2. MATERIALS AND METHODS

Pseudo vascular network was incorporated into composite prepreg using Nichrome wires “dip-coated” in a 10% PLA solution in 1,4-dioxane, which were subsequently removed post-cure. Figure 1 shows the wire dip-coating process used to produce around a 0.25mm PLA coating.

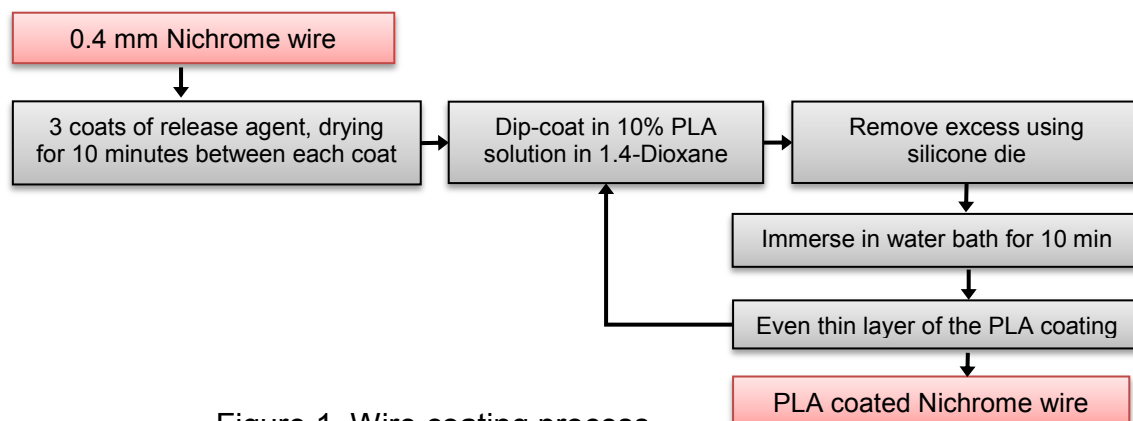


Figure 1. Wire coating process.

The removal of the Nichrome wire was achieved by softening the PLA coating through the effect of resistive heating of the Nichrome. This process significantly decreases the mechanical force needed to withdraw the wire. The remaining PLA can then be removed through injection of chloroform solvent alternated with flushing with water.

E-glass FRP and carbon FRP (CFRP) pre-impregnated with high toughness SE-70 epoxy were used to manufacture two laminated panels with a stacking sequence of (“bottom-up”): [90, +45, -45, -45, +45, 0//0, -45, +45, +45, -45, 90], cured at 70° C for 16 hours.

In order to limit the adverse effect of the incorporation of a network preform, “cut outs” were made into the plies in which the channels will be accommodated, minimising distortion to plies adjacent to the wire inserts.

For the thermal management testing, the panels were heated to temperatures of 50, 60 and 70°C. The cooling system consisted of a peristaltic pump, pumping iced water held at 0°C at a total flow rate of 30 ml/minute. In addition to the temperature profiles, values at locations A-G, (Figure 2A), were logged for every second of the test period. The panel cooling profile was observed using infrared imaging for a 5 minute application of the cooling system.

3. RESULTS AND DISCUSSION

GFRP panels were manufactured with branched and straight channels labelled as GB and GS respectively alongside the control panel with no network labelled as GC. Two further CFRP panels with and without network of straight channels were also manufactured labelled as CS and CC.

Figure 2A (bottom, right) shows the successfully produced sample with incorporated branched network (GB). Example microscopy images of the vasculature pre and post-chloroform injection are showed in Figure 2B, which provide greater insight into the achieved vascular architecture.

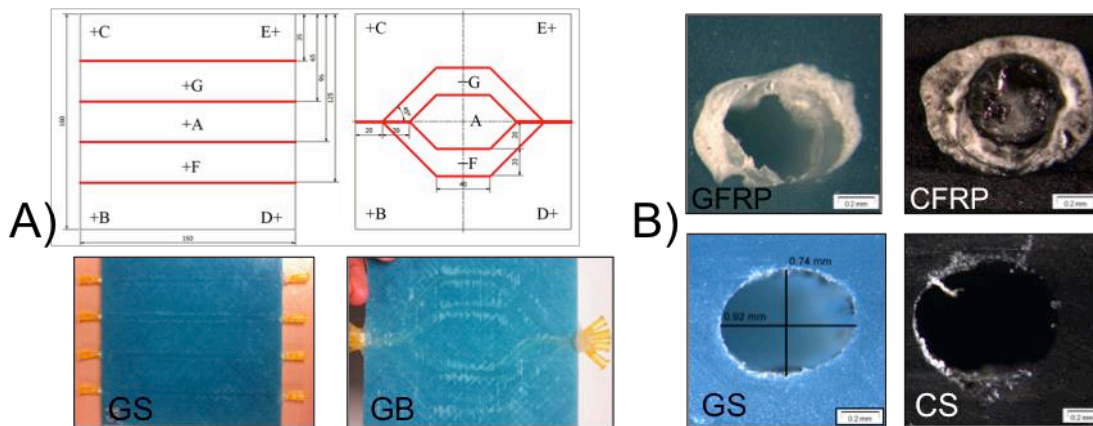
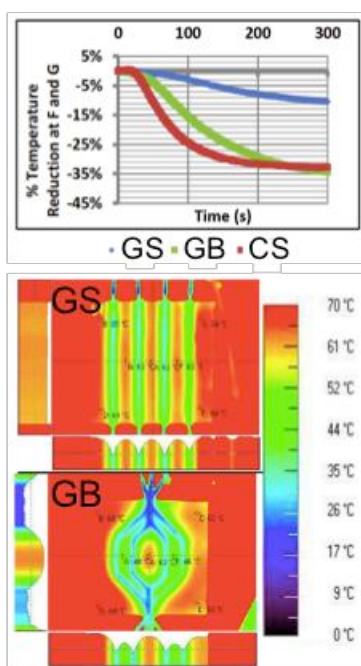


Figure 2: A) *Plantae* (straight) and *Animalia* (branched) inspired vasculature configuration (dimensions in mm). Pictures below show a manufactured laminate with visible vasculature. B) Straight vasculature before and after PLA removal.

Figure 3 shows the thermal imaging for the cooling patterns of the *Animalia* inspired network in panel GB compare to the straight channels in panel GS, with the GFRP laminate starting at an approximate steady state temperature of 70°C



From these it was shown that for the GFRP panels at locations F and G, between vasculature produced significantly greater cooling over the 5 minute test period for the branched network design. This can be observed in Figure 3. This resulted from the increased contact time of the cooling flow, in combination with the reduced panel area per vascular perimeter length in these regions. Both of these factors increase the permissible heat transfer between the composite panel and the cooling flow, thus reducing the temperature at these locations. Despite the larger separation of the vasculature at point A at the centre of the branched panel, greater cooling was also observed at this point than for the equivalent on the straight vasculature panels GS and CS. The temperature changes observed at the corner locations B-E were comparatively minimal for both tested GFRP panels GB and GS, as the separation of these points from the cooling flow was excessive.

Figure 3: Thermal management tests in panels

4. CONCLUSION

This study shows that using anti-symmetric laminate designs, the in-situ manufacture of complex branched networks, with vascular bifurcations, within FRP laminates is possible. It has been shown that provided adequate coating and post-cure processing, Nichrome wires can significantly facilitate the manufacture of hollow vasculature within the laminate structure. For GFRP panels it has been shown that for a particular Animalia inspired branched network, greater cooling can be achieved for the areas bounded by vasculature than for a straight channels. The testing of a CFRP panels with straight vascular channels suggests that even greater cooling could be achieved for a more thermal conductive CFRP panel with an integrated branched vascular network.

REFERENCES

- [1] Pierce. M. R 2010 Microvascular heat transfer analysis in carbon fiber composite materials - Thesis submitted to The School of Engineering, University of Dayton, Ohio
- [2] Williams G, Trask RS and Bond IP 2007 A self-healing sandwich carbon fibre reinforced polymer for aerospace applications *Composites A* 38(6) 1525-1532
- [3] Trask RS and Bond IP 2009 Bioinspired engineering study of Plantae vasculature for self-healing composite structures *Journal of the Royal Society: Interface* 7 921-931
- [4] Norris CJ, Bond IP and Trask RS 2011 The role of embedded bioinspired vasculature on damage formation in self-healing carbon fibre reinforced composites *Composites A* 42 639-648
- [5] Schoepper GA, Tandon GP and Pochiraju KV, *Multiscale Modelling and Simulation of Composite Materials and Structures*, Springer US, 2008, ch.9 p.359-462
- [6] Olugebefola SC, Aragón AM, Hansen CJ, Hamilton AR, Kozola BD, Wu W, Geubelle PH, Lewis JA, Sottos NR, White SR. 2010 Polymer-microvascular network composites. *Journal of Composite Materials* 44(22) 2587-2604

**REGIONAL / NATIONAL / INTERNATIONAL PROJECTS ON
SELF-HEALING MATERIALS**

POSTER SESSION

PRESENTATION OF THE SPANISH PROJECT TRAINER “AUTONOMOUS REGENERATION OF MATERIALS FOR DIFFERENT APPLICATIONS”

F. Castro ¹, M. Casado ¹ and J. Vera ¹

¹ ACCIONA Infraestructuras, Avda. Europa 18, 20108 Alcobendas, Madrid, Spain – e-mail: franciscomanuel.castro.visos@acciona.es; auroramaria.casado.barrasa@acciona.com; jose.vera.agullo@acciona.es

Keywords: self-healing, project, Spain, standardisation, industrial applications

ABSTRACT

Despite of the recent creation of self-healing materials, these materials are gaining notoriety in the last years due to their great value for society and economy.

The first publications regarding this type of materials are dated on 2001. The University of Illinois was the first cutting-edge organization dedicated to self-healing materials research. Later, in 2005 and thanks to the financial support of the Dutch ministry, The Netherlands conducted for six years the Innovation Oriented research Program (IOP) on Self-Healing Materials. This fact reflects the importance of public funding for such ambitious research projects.

The project TRAINER, first project dedicated to deal with self-healing materials in Spain, emerged in 2010 thanks to the support of the Spanish government and the interest of different companies and research organizations for that type of materials.

The challenge of the project TRAINER is not only working on self-healing technologies of 1st and 2nd generation, but also trying to adapt current technologies to provide traditional materials (concrete, polymers, ceramics, asphalts, coatings and steel) with self-healing ability. In order to achieve this goal, different approaches have been proposed: use of microorganisms, expansive agents, PVA fibres, supramolecular polymers, new corrosion inhibitors and zirconia based materials. The standardization and development of test protocols for self-healing materials is, also, another objective to be achieved through the project.

This paper will present the most relevant results achieved to date. In this context, it should be highlighted the development of microcapsules reinforced with sepiolite-based nanoclays, expansive agents based on hydrogels and supramolecular polymers based on hydrazones.

HEALCON – SELF-HEALING CONCRETE TO CREATE DURABLE AND SUSTAINABLE CONCRETE STRUCTURES

N. De Belie ¹

¹ *Magnel Laboratory for Concrete Research, Ghent University, Technologiepark-Zwijnaarde 904, 9052 Ghent, Belgium – e-mail: nele.debelie@ugent.be*

Keywords: concrete, bacteria, polymer, super absorbent polymer

ABSTRACT

Within the theme ‘Self-healing materials for prolonged lifetime’ (NMP.2012.2.1-3) of the Seventh Framework Programme, self-healing concrete is an important topic. The project HEALCON, which deals with self-healing concrete to create durable and sustainable concrete structures, is funded by EU-FP7 and started in January 2013. The coordinator of the project is Prof. Nele De Belie (UGent) and the consortium partners are UGent, Avecom, TU Delft, Acciona, TUM, TTI, VTT, COWI, DTI, CEINNMAT, Devan and Fescon.

Adequate perpetuation of the road, tunnel and bridge network, is crucial to preserving European cohesion and business operations; and around 70% of this infrastructure is made of concrete. In order to guarantee liquid tightness of concrete structures, and enhance durability of elements prone to bending cracks, smart concrete with self-healing properties will be designed.

Thanks to the existing expertise of the consortium in the field of self-healing concrete at a lab-scale, a thoughtful selection of promising techniques is possible.

- For early age cracks, a non-elastic repair material can be proposed, such as calcium carbonate precipitated by bacteria, or new cement hydrates of which the formation is stimulated by the presence of hydrogels.
- For moving cracks under dynamic load, an elastic polymeric healing agent is suggested.

Different healing agents and encapsulation techniques are tested and scaled up. Self-healing efficiency is evaluated in lab-scale tests using purposefully adapted monitoring techniques, and optimized with the help of suitable computer models.

Finally the efficiency is validated in a large scale lab test and implemented in an actual concrete structure. Life-cycle cost analysis will show the impact of the self-healing technologies on economy, society and environment compared to traditional construction methods.

1. INTRODUCTION

Reinforced concrete is designed to crack, but crack widths are limited to 0.2 to 0.4 mm depending on exposure class and type of concrete (reinforced or prestressed). Although these cracks do not impair structural stability, through-going cracks drastically affect liquid tightness. This is a major problem in tunnels and large underground structures, where cement hydration reactions and temperature/shrinkage effects in large concrete segments might result in the

formation of early age cracks. Since liquid-tightness is necessary, expensive preventive measures are taken or repair works are needed right after construction. Furthermore, even if not through-going, cracks will allow faster penetration of aggressive liquids and gases. Certainly in case of chloride containing liquids or in case of high CO₂ concentrations (e.g. in urban environments), there will be a higher risk of reinforcement corrosion, which compromises the long-term durability of the structure. Current practice requires regular inspection, maintenance and repair, to ensure structural safety over the service life of the structure. These practices involve large direct and indirect costs, such as economic losses from traffic jams. Additionally, not all structures are easy to access for inspection and repair.

In their search to overcome these problems, researchers have been inspired by nature. Biological systems such as bones, skin or plants have the capacity to detect damage very quickly and have moreover the unique feature to repair the damage efficiently. It would be an enormous advantage if this concept could be translated to our engineering materials, such as concrete. The application of so-called “self-healing” concrete, which will in an autonomous way repair cracks, could reduce the maintenance costs drastically. Additionally, indirect costs such as due to traffic congestion, can be avoided.

The aim of HEALCON, a project funded by EU-FP7 and coordinated by Prof. Nele De Belie (Ghent University), is to design smart concrete with self-healing properties to create durable and sustainable concrete structures.

2. ENCAPSULATED HEALING AGENTS

Within the HEALCON project, the focus will be on two types of structures and damages where the use of self-healing concrete will have the largest benefit (Figure 1) :

- early age cracking in structures which demand liquid tightness
- bending cracks at concrete structural parts with a high risk of premature reinforcement corrosion.

Depending on the type of damage, another self-healing concept will be envisioned in the project. Early age cracks will be filled with a non-elastic material, while bending cracks in e.g. bridge beams will be filled with an elastic healing material to cope with the opening and closing movement of cracks under a dynamic load. This means that biogenic healing agents as well as polymeric healing agents (hydrogels and elastic healing agents) will be considered. Besides, suitable encapsulation techniques for each of the healing agents will be developed and the effect of the capsules on the fresh concrete properties will be investigated.

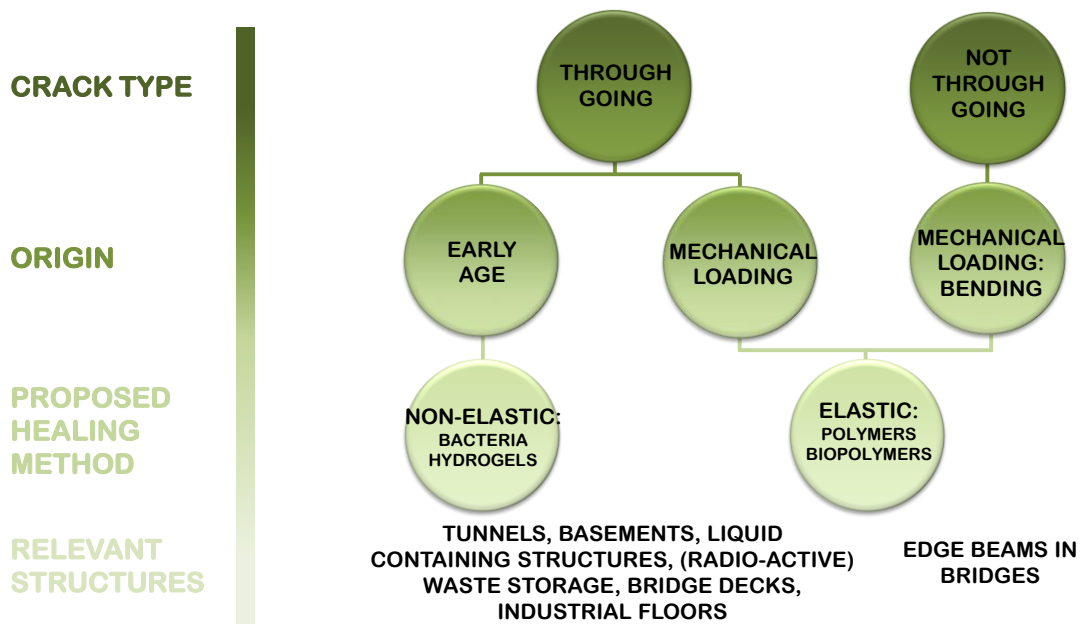


Figure 1: Overview of the self-healing applications envisioned in HEALCON

3. FROM LAB-SCALE TESTS TO FIELD TESTS

The efficiency of the different self-healing mechanisms with regard to mechanical behaviour, liquid-tightness and durability will be firstly quantified at lab-scale. Based on the outcome of these tests and the outcome of the developed computer models, which will simulate the fracturing and self-healing mechanisms, the mechanisms will be scaled to an industrial level. The production of self-healing agents will be upscaled and the developed self-healing methodologies will be experimentally validated in large-scale elements, under conditions close to reality. In the last stage, the new technologies will be demonstrated by their implementation in an actual concrete structure. Furthermore, a life cycle cost (LCC) analysis will be performed for the same structural element as used for the field test / demonstration and the LCC analysis will be supplemented by a life cycle assessment (LCA).

During the laboratory tests as well as during the field tests, non-destructive monitoring techniques will be used to characterize healing.

4. END-USER MARKET NEEDS AND REQUIREMENTS

The technologies developed from the theoretical and laboratory experiments have to be functional and adaptable to engineering design and have to be implemented on real structures. Therefore, an end-user board is established from the beginning of the project to participate in defining technical and application requirements and to form a stakeholder group that will follow the project.

5. PROJECT OVERVIEW

To summarize, Figure 2 gives an overview of the different work packages within the HEALCON project and the interdependencies.

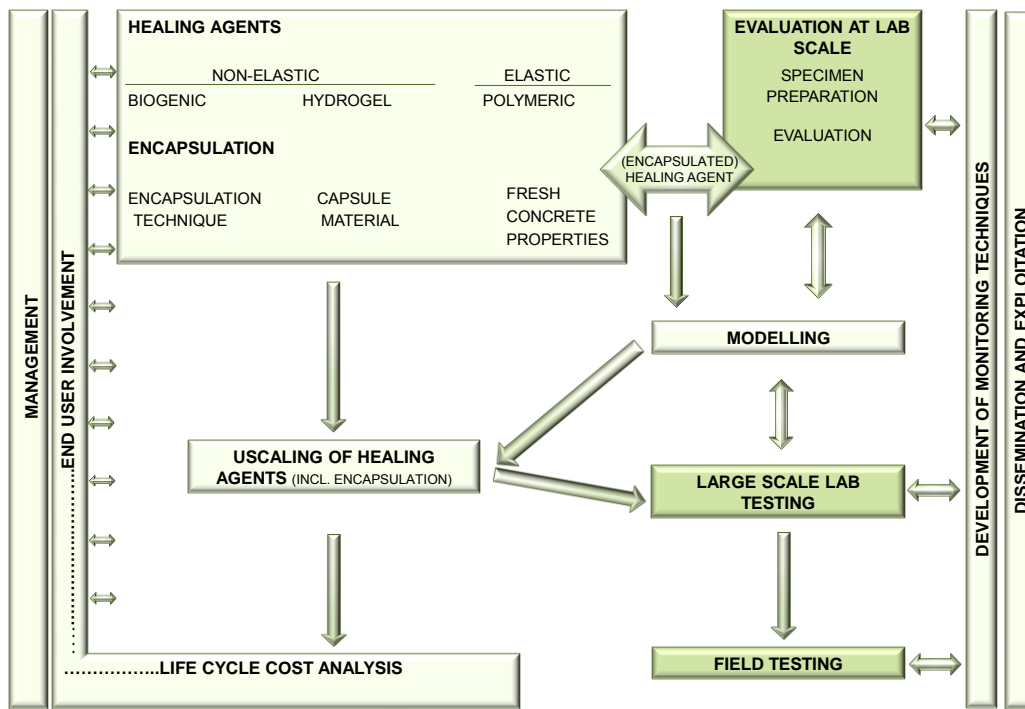


Figure 2: Work packages within HEALCON project and their interdependencies

ACKNOWLEDGEMENTS

The research has received funding from the European Union Seventh Framework Programme (FP7/2007-2013) under grant agreement n° 309451 (HEALCON).

SHE – THE FLEMISH PROGRAM ON ENGINEERED SELF-HEALING MATERIALS

N. De Belie^{1,5}, F. Du Prez^{2,5}, H. Terryn^{3,5}, B. Wallaeyns^{4,5}

¹ *Magnel Laboratory for Concrete Research, Ghent University, Technologiepark-Zwijnaarde 904, 9052 Ghent, Belgium – e-mail: nele.debelie@ugent.be*

² *Polymer Chemistry Research Group, Ghent University, Krijgslaan 281 – S4 bis, 9000 Ghent, Belgium – e-mail: filip.duprez@ugent.be*

³ *Electrochemical and Surface Engineering Research Group, VUB, Pleinlaan 2, 1050 Brussels, Belgium – e-mail: htterr@vub.ac.be*

⁴ *Recticel, Damstraat 2, 9032 Wetteren, Belgium – e-mail: wallaeyns.bart@recticel.com*

⁵ *SIM vzw, Technologiepark 935, 9052 Zwijnaarde, Belgium*

Keywords: self-healing, concrete, polymers, coatings

ABSTRACT

The vision of this program SHE is to develop new and combined smart self-healing concepts, fully resulting in durable and sustainable materials with an expanded life-time of at least 50%. SHE focusses on three different material classes, which cover an important part of the Flemish industry:

- Cementitious and mineral building elements are studied in the strategic basic research project (SBO) 'SECEMIN'. Within this project, a proof-of-concept for self-healing concrete with encapsulated polymeric / bacterial healing agents has already been obtained.
- Polymers and composites are studied in the SBO 'SEPOCOM'. A dual microcapsule approach with a new healing chemistry and novel encapsulation technologies has led to quite promising self-healing results for epoxy resins.
- Coatings are investigated in the SBO 'NAPROM'. Within this project coating demonstrators are developed that combine self-healing polymers and new encapsulated inhibitors for corrosion protection of metals.

To stimulate early valorization, industrial projects are linked to the SBO projects:

- SHEcon (linked to SECEMIN), which aims at structural and architectural applications. The goal of this project is to engineer self-healing concrete to minimize the appearance of cracks in the outer cladding of concrete sandwich panels, in order to maintain the impermeability and mechanical response.
- PUrePAIR (linked to SEPOCOM), which aims at the development of self-healing polyurethane foams and elastomers. The self-healing capacity is obtained by adding especially designed μ capsules with a newly developed chemistry as healing agent.
- SHREC (linked to NAPROM and SEPOCOM), which aims at the development of self-healing coatings that can heal micro- and macroscratches. A series of healing procedures to be tested for a range of commercial coating systems (thermal, UV, self-crosslinking) are being investigated.

The consortium is well balanced to carry out the scientific and technological developments. Research groups of Ghent University, Vrije Universiteit Brussel, University of Antwerp and FLAMAC bring in their expertise. A strong industrial involvement (Recticel, Devan Chemicals, Willy Naessens Construct, Cytec, Bekaert and Arcelor Mittal) ensures the market orientation and exploitation of the results.

SHEMAT - TRAINING NETWORK FOR SELF-HEALING MATERIALS: FROM CONCEPTS TO MARKET

M. Von Tapavicza¹ and A. Nellesen¹

¹ *Fraunhofer Institut UMSICHT, Osterfelderstr. 3, 46047 Oberhausen, Germany – e-mail: max.von-tapavicza@umsicht.fraunhofer.de*

ABSTRACT

The aim of the Marie Curie project SHeMat is the development of self-healing materials, the market implementation for the most promising material concepts and developments as well as the training of young scientists and their knowledge transfer in mutual interaction programs due to the distinct interdisciplinary shape of the project.

The partners intend to address both actual fundamental research in material development as well as the complementary aspects of conceptual process chain analysis from a more industrial perspective. It was decided to restrict the research to self-healing material concepts with an existing sizeable academic development base and a sufficient number of positive findings to ensure a significant possibility of successful conversion to industrial application. The aim is to succeed in bridging the gaps in knowledge and understanding for these promising materials, industrial development of these concepts and technologies is to be expected. This can only be achieved if specific interdisciplinary training is provided to young researchers, to master the concepts, know how to quantify healing, and how to position these materials in the application fields. Finally, it should be made clear that, notwithstanding the industrial oriented approach in this project, the work to be undertaken will always be of the highest scientific/academic character and aims to set a new standard in the development of novel material concepts.

The objects of the project are:

- training and education for junior researchers and a strong support for the interdisciplinarity of the project to ensure technology transfer from laboratory research to industrial application
- promote actual self-healing strategies and concepts that address current materials or engineering limitations to application
- exploit the existing scientific and technological leadership of the partners to deliver viable and advanced solutions for the commercial exploitation of self-healing materials.

BIOMIMETIC MULTI-SCALE DAMAGE IMMUNITY FOR CONSTRUCTION MATERIALS: M4L PROJECT OVERVIEW

R. J. Lark¹, A. Al-Tabbaa² and K. Paine³

¹ Cardiff School of Engineering, Cardiff University, Queen's Buildings, The Parade, Cardiff CF24 3AA, Wales, UK. – e-mail: lark@cardiff.ac.uk

² Department of Engineering, University of Cambridge, Cambridge CB2 1PZ, UK.

³ Dept. of Architecture and Civil Engineering, University of Bath, Bath BA2 7AY, UK.

Keywords: construction materials, self-healing, bio-inspired materials, multi-scale damage

ABSTRACT

This paper presents a vision of a sustainable and resilient built environment that is comprised of materials and structures that continually monitor, regulate, adapt and repair themselves without the need for external intervention. In this way, these self-healing materials and intelligent structures will significantly enhance durability and serviceability, improve safety and reduce maintenance costs. The conglomerate materials that form the basis of the majority of such construction materials (concrete, grouts, mortars, hydraulically bound materials, grouted soils etc), are extremely complex multiphase composites with multi-scale internal structures that exhibit a hierarchy of multi-dimensional, time-dependent damage mechanisms. For example, in cementitious composites nano-scale damage occurs during hydration and the strength development phase, while medium-term damage due to chemical attack also leads to the formation of defects in its structure. Other short-term factors can also produce dislocations at the nano-scale. In time, this nano-damage grows to form micro-cracks which eventually coalesce to form networks of meso-cracks which in turn lead to debonding between the paste and aggregate particles, followed by a discrete number of visible macro-cracks which so often lead to corrosion of the steel reinforcement. Hence, it is evident that to truly achieve a self-healing cementitious composite, a system is needed that can act at both the different time and length scales at which the damage can form. This paper presents a newly funded research project, M4L: Materials for life, that is addressing this complex problem by taking advantage of innovations in allied scientific disciplines to pave the way for the development of a new generation of versatile and robust construction materials.

1. INTRODUCTION

The resilience of building and civil engineering structures is typically associated with the design of individual elements such that they have sufficient capacity or potential to react in an appropriate manner to adverse events. Traditionally this has been achieved by using 'robust' design procedures that focus on defining safety factors for individual adverse events and providing redundancy. As such, construction materials are designed to meet a prescribed specification; material degradation is viewed as inevitable and mitigation necessitates expensive maintenance regimes. More recently, based on a better understanding of microbiological systems, materials that have the ability to adapt and respond to their environment have been developed [1]. This fundamental change facilitates the creation of a wide range of 'smart' materials and intelligent structures, including both autogenous and autonomic self-healing materials and adaptable,

self-sensing and self-repairing structures. Such materials can transform our infrastructure by embedding resilience in the materials and components of these structures so that rather than being defined by individual events, they can evolve over their lifespan.

2. SCOPE AND AIMS

Conglomerate materials, which form the basis of the majority of construction materials (concrete, grouts, mortars, hydraulically bound materials, grouted soils etc), are extremely complex multiphase composites with multi-scale internal structures that exhibit a hierarchy of multi-dimensional, time-dependent damage mechanisms. In cementitious composites *nano-scale damage* occurs at the level of the calcium silicate hydrate (C-S-H) gel during hydration and the strength development phase, while medium-term damage due to chemical attack can also lead to the formation of defects and dislocations in its layered structure. Other short-term factors such as residual stresses that arise during curing and compaction or longer-term physical actions, like repeated cycles of freezing and thawing and fatigue loading, can also produce dislocations between the C-S-H globule-like nanoparticles. In time, all the nano-cracks grow to form dislocations between the C-S-H matrix and other crystals like portlandite within the cement paste (*micro-scale damage*). These micro-cracks eventually coalesce to form networks of meso-cracks. These meso-scale cracks lead to debonding between the aggregate particle and the paste (*meso-scale damage*). Finally the meso-scale network grows to become a discrete number of visible macro-cracks (*macro-scale damage*) which can permit processes leading to corrosion of steel reinforcement. Hence, it is evident that to truly achieve a self-healing cementitious composite a system is needed that can act at both the different time and length scales at which the damage can form.

Similarly, when damaged, higher organisms, including man, use intrinsic immune systems and wound responses to provide a multi-scale response, from a chemical and cellular level through to the macro-scale at which any lesion is bound together and sealed to facilitate the healing process. Inspired by this, the intention is to create construction materials with an inbuilt “immune” system that is responsive to the condition of the material and the onset of damage. This will operate at the nano/micro-scale using micro-encapsulation strategies, at the micro/meso-scale through bacterial healing and at the meso/macro-scale, with fibres, shrinkable polymers and vascular networks (fluid filled micro-scale channels) providing mechanisms to enhance and control the overall physical response. One of the main challenges will be to ensure that, as in the biological systems, these multi-scale healing mechanisms are an appropriate response to the type of damage, are complementary and work synergistically.

3. MATERIALS AND METHODS

While microencapsulation for self-healing materials was pioneered over a decade ago for polymer composites, the development of simple, efficient, cost-effective, environmentally-benign and scalable synthesis techniques without compromising functionality and encapsulation efficiency remains a major challenge. Microencapsulated reactive agents have been considered for applications in building construction materials (fireproofing, antimicrobial protection, temperature control, freeze-thaw resistance) [2] but their application to self-healing is relatively new [3]. Recently, scientists at Cambridge have developed a simple and scalable one-step process, by combining supramolecular host-guest chemistry and a microfluidic droplet platform technology (Figure 1), for the synthesis of highly uniform microcapsules with high cargo loading efficiency, long shelf-life

and easily customizable functionality [4]. Cargos can be chemical, biological, liquid or solid and the capsule shell composition and chemistry can be easily manipulated to suit different stimuli and trigger mechanisms. For example, its porosity, stiffness and strength can be designed to facilitate permanent storage (for crack stress trigger) or controlled on-demand release (for diffusion related sealing) of the cargo; it can be made to disintegrate under electrochemical redox reactions (e.g. corrosion); it can be made to expand/contract in a controlled manner and it can contain separate cargos e.g. catalysts.

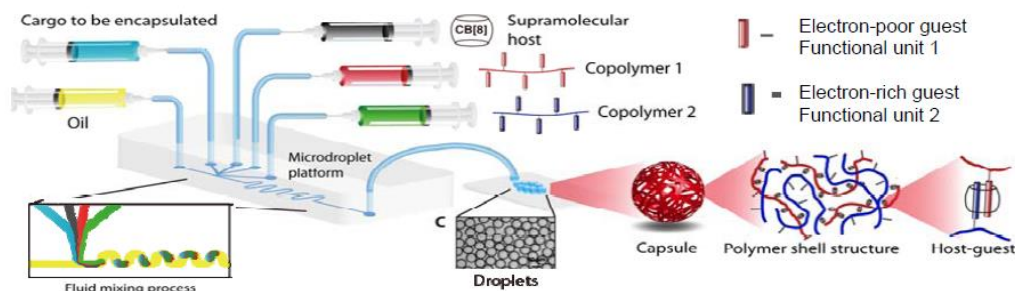


Figure 1: A schematic of the Cambridge microencapsulation synthesis technique [4].

At the meso-scale the use of alkali-resistant spore-forming bacteria from the genus *Bacillus* to heal cementitious materials, ornamental stones and degraded limestone has been the subject of active research since 2000. Bacterial healing utilises the metabolic activity of bacteria and biomineral precursors embedded within the material to form an inorganic material, usually calcium carbonate (CaCO_3) in the form of calcite. It focuses on two major areas – sealing (reducing permeability) of exposed surfaces and cracks to prevent ingress of deleterious chemical species, and healing (strength recovery) of macroscopic and microscopic cracks, re-establishing the ability of the cracked zone to carry load. Bacteria have the capacity to bind Ca ions thanks to charge effects and associated extracellular polymers. Calcite has been commonly derived indirectly from the enzymatic hydrolysis of urea, however this reaction yields ammonia, which is environmentally damaging and urea has limited long-term stability in alkaline conglomerates. Therefore it has been most usefully applied as external treatment and not as a self-healing agent [5]. In light of this the potential of multi-component healing agents that do not yield harmful products when broken down are being investigated [6] with precursors such as calcium lactate, which when driven by metabolic absorption produces CaCO_3 , CO_2 and water, all of which are compatible with cementitious hydrates. However, whilst the potential for bacterial healing has been demonstrated in idealised laboratory conditions the extent of the healing/sealing that is possible and the long-term viability of the *Bacillus* spores is still to be determined.

At the macro-scale construction research has focussed on either developing systems that can heal themselves autonomically (e.g. via glues or resins) or are able to enhance the autogenic healing capacity of many cementitious compounds. A novel technique that is being developed at Cardiff, is to embed shape memory plastic (SMP) tendons into the cementitious matrix with the aim of creating a material system which can either close cracks to a degree whereby they can be healed by one of the in-built healing systems discussed above (Variant I) or prevent them from occurring (Variants II and III) as shown in Figure 2. SMPs often develop relatively low “recovery” or “shrinkage” stresses when undergoing the shape transition under restrained conditions. However, materials in which the shrinkage stress level is sufficient to provide this inbuilt mechanism for closing cracks

have now been identified [7] and the opportunity exists for further development to include manufacture from recycled plastics.

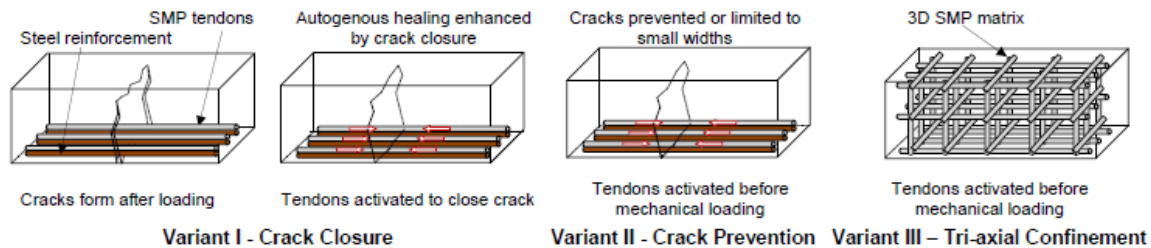


Figure 2: Schematic illustration of concept for composite material system

4. FURTHER STUDY

Inspired by nature, the intention of this project is to develop an interdisciplinary, multi-scale system utilising a range of technologies to promote and enable self-healing of construction materials over various timescales. In particular there is a focus on conglomerate materials such as concrete, grouts, mortars, hydraulically bound materials and grouted soil systems. A range of damage scenarios and structural and geotechnical engineering applications are being addressed including, at the micro-scale, microbiological and chemical healing, focussing on both the methods of delivery (e.g. microencapsulation) and the operation of these systems. At the meso-scale the overall impact and distribution of these microscopic systems are being considered and optimised. At the macro-scale, large-scale healing systems, such as shrinkable polymers and vascular networks are being developed and implemented. Combinations of these systems in different materials and scenarios to give a whole-material response to damage at a range of spatial and temporal scales are being exploited and field-scale tests to address relevant aspects of scale-up, cost, commercialisation as well as full-scale damage scenarios are going to be performed.

ACKNOWLEDGEMENTS

The authors thank their colleagues and co-investigators, D. R. Gardner¹, M. J. Harbottle¹, A.D. Jefferson¹, C. Abell², J.M. Lees², M.L. Oyen², R. Cooper³ and A. Heath³ for their contribution to the project as well as the project's industrial collaborators and the international academic centres whose input will be invaluable. Financial support for this work from the UK EPSRC (Project No. EP/K026631/1) and the project's industrial collaborators is gratefully acknowledged.

REFERENCES

- [1] S. van der Zwaag (Ed.) An alternative approach to 20 centuries of materials science, Springer (2007).
- [2] V.V. Tyagi, S.C. Kaushik, S. Tyagi & T. Akiyama, *Renew. Sust. Energ. Rev.*, 15 (2011) 1373-1391.
- [3] M. Wu, B. Johannesson & M. Geiker, *Constr. Build. Mater.*, 28 (2012) 571-583.
- [4] J. Zhang, R.J. Coulston, S.T. Jones, J. Geng, O.A. Scherman & C. Abell, *Science*, 335 (2012) 690-694.
- [5] H.M. Jonkers, A. Thijssen, G. Muyzer, O. Copuroglu & E. Schlangen, *Ecol. Eng.*, 36 (2010) 230-235.
- [6] S. Birungi, MEng dissertation, University of Bath (2012).

[7] A.D. Jefferson, C. Joseph, R.J. Lark, B. Isaacs, S. Dunn & B. Weager, *Cem. Conc. Res.*, 40(5) (2010) 795-801.

SESSION 10 – SELF-HEALING CEMENTITIOUS MATERIALS

Most recent advances in the field of self-healing cementitious materials

K. Van Tittelboom¹, D. Snoeck¹, J. Wang¹ and N. De Belie¹

¹ *Magnel Laboratory for Concrete Research, Ghent University, Technologiepark-Zwijnaarde 904, 9052 Ghent, Belgium – e-mail: kim.vantittelboom@ugent.be; didier.snoeck@ugent.be; jianyun.wang@ugent.be; nele.debelie@ugent.be*

Keywords: Alternative binders, Fiber reinforcement, Super absorbent polymers, Encapsulated bacteria, Encapsulated liquid polymers.

ABSTRACT

While the Japanese researchers Ohama et al. [1] already mentioned in 1992 that a self-healing effect was noticed when polymer-modified concrete without hardener was made, the real pioneer in the research on self-healing concrete is Carolyn Dry from Illinois. The first time she proposed the use of encapsulated polymers to obtain self-healing concrete dates back to 1994 [2] and based on her publication output, she remained active within this field until 2003 [3, 4]. Within this timeframe, Victor Li started his research on fiber-reinforced self-healing concrete in Michigan [5]. From 2000 onwards other researchers in Japan (Mihashi, Nishiwaki et al.) [6-8], France (Granger et al.) [9], the United Kingdom (Joseph et al.) [10] and the Netherlands (ter Heide et al.) [11] started their research on self-healing cementitious materials. However, it was only in 2007, when the Dutch IOP program on self-healing was granted and the first international conference on self-healing materials was organized in the Netherlands, that self-healing concrete gained world-wide attention and all over the world research groups started working on this topic. One year later, in Belgium or more specifically at the Magnel Laboratory for Concrete Research of Ghent University, research on self-healing concrete started. In this keynote, an overview of the most recent developments within the Magnel Laboratory will be given.

1. INTRODUCTION

Self-healing in cementitious materials can be classified broadly into two groups: (improved) autogenous healing and autonomous healing. (Improved) autogenous healing refers to the recovery process where healing is caused by material components that could also be present when the concrete is not specifically designed for self-healing. The term autonomous healing is used when healing is caused by engineered additions which would otherwise not be found in concrete. In the following paragraphs different approaches of each mechanism will be discussed.

2. (IMPROVED) AUTOGENOUS HEALING

Autogenous crack healing can be mainly attributed to: hydration of unhydrated cement particles and dissolution and subsequent carbonation of calcium hydroxide ($\text{Ca}(\text{OH})_2$). In addition to these mechanisms, swelling of the matrix and blocking of the crack due to debris present in the ingress water or loose concrete particles resulting from cracking, may also cause autogenous healing. While the overall contribution of these mechanisms in autogenous healing remains a matter of debate,

researchers agree that autogenous healing can be improved when the amount of reactive binder agents is increased (Figure 1), crack widths are restricted (Figure 2) or additional water is supplied in the crack region (Figure 3).

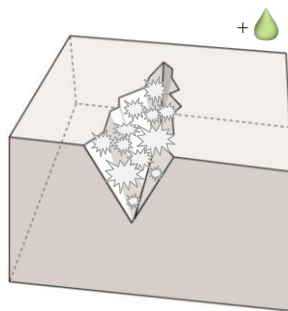


Figure 1. Improved autogenous healing (upon contact with water) due to an increased amount of reactive binder.

While partial cement replacement by blast furnace slag or fly ash, waste products of the steel industry and coal-combusted power stations respectively, results in more environmentally friendly concrete, their use may also cause additional advantages. Their slower reaction rate may result in a higher amount of unhydrated particles and thus an improved possibility for ongoing hydration. However, as the reaction of both binder materials needs to be activated/initiated by $\text{Ca}(\text{OH})_2$, resulting from cement hydration, less $\text{Ca}(\text{OH})_2$ will be available for possible crack healing by carbonation.

Calorimetric measurements on mixes of crushed cement paste and water showed that the cumulative heat production of series in which cement was partly replaced by slag or fly ash was higher compared to series containing only cement. Among both, blast furnace slag resulted in the highest heat production and thus probability of further hydration upon contact with water. This corresponds to the higher crack healing efficiency of slag and fly ash mixes which was noticed when measuring the water permeability over time of cracked samples [12].

For calcium carbonate (CaCO_3) precipitation to occur, both water and carbon dioxide (CO_2) need to be present. Microscopic investigation of the crack width evolution during wetting and drying cycles allowed to study the effect of the mix composition on the amount of autogenous healing by CaCO_3 precipitation. In this experiment, mixes containing only Portland cement proved to have the best healing efficiency. As more $\text{Ca}(\text{OH})_2$ is available within this composition, more $\text{Ca}(\text{OH})_2$ can react with CO_2 from the air to form CaCO_3 crystals within the crack. In addition, it was shown that only cracks below $200\ \mu\text{m}$ could close due to CaCO_3 precipitation at the crack faces [12].

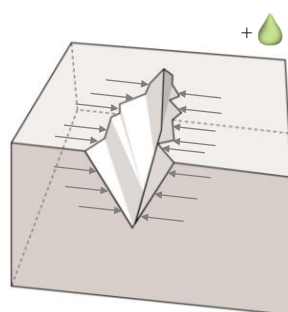


Figure 2. Improved autogenous healing (upon contact with water) due to restriction of the crack width.

This brings us to the second mechanism which can be used to improve autogenous crack healing: restriction of the crack width through the addition of fibers. Fibers are usually added to the concrete mix in order to improve the structural strength, ductility, freeze-thaw resistance, resistance to spalling,... However, it was shown that they can also improve autogenous healing by enhancing multiple crack formation and limiting the crack width.

The efficiency of natural flax fibers and synthetic polyvinylalcohol (PVA) fibers was compared. Measurements of the regain in mechanical properties as well as microscopic investigation of cracked samples subjected to wetting and drying showed that the healing efficiency did not depend on the type of fibers used. However, it was noticed that healing was determined by the initial crack width. Cracks narrower than $30\ \mu\text{m}$ closed completely while cracks with a width between $30\ \mu\text{m}$ and $150\ \mu\text{m}$ only showed partial closure [13].

In both of the afore mentioned approaches (increasing the amount of reactive binder or restricting the crack width), autogenous healing was improved although healing only started at the moment the cracked samples were brought into contact with water. As water is a crucial factor for autogenous healing to occur, autogenous crack healing can be largely improved when additional water is provided. Super absorbent

polymers (SAP) can serve this purpose. SAP are cross-linked polymers which can absorb a disproportional large amount of liquid and swell substantially to form a soft and insoluble gel. SAP particles are currently added to the concrete mix in order to cause internal curing. In addition, SAP particles can result in improved autogenous healing.

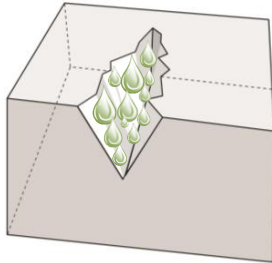


Figure 3. Improved autogenous healing due to additional water supply.

When cracks arise in the concrete matrix, ingress of moisture via the cracks causes the SAP particles to swell, thus leading to a direct physical blocking effect. In addition, SAP will release their water content again during dry periods, improving the reactions leading to autogenous crack healing.

It was noticed that for the types of SAP used in this study (commercial products obtained from BASF), both the mechanical properties and the water tightness were regained after samples were exposed to wetting and drying. Bigger SAP particles ($\pm 500 \mu\text{m}$) seemed to promote self-healing better compared to smaller ones ($\pm 100 \mu\text{m}$). Even without submersion of the samples, just upon exposure to a relative humidity of 90% or even 60%, partial healing of the cracks took place when SAP particles were included [14].

3. AUTONOMOUS HEALING

Autonomous healing of cracks in cementitious materials can be obtained following different approaches. A subdivision can be made based on the type of healing agent used. At one hand bacteria, which precipitate CaCO_3 , can be applied. These bacteria are available, in a dormant state, within the concrete matrix. Once cracks appear and water intrudes into these cracks, the bacteria become active and start to consume the available nutrients resulting in the formation of CaCO_3 crystals which fill the crack. On the other hand, polymer-based, liquid healing agents can be provided in the matrix to cause crack healing. In the latter case, crack formation results in the release of the liquid agent which starts reacting inside the crack and results in this way in crack healing. For each of these approaches, carriers are needed. In the first case the carrier serves as protection mechanism for the bacteria against the high pH in the cementitious matrix. In the second case the main goal of the carrier is to preserve the liquid healing agent until the moment of crack appearance. In both cases an additional function of the carrier is to act as trigger mechanism. At the moment of crack appearance, breakage of the carrier should activate the healing process.

In the approaches mentioned hereafter, *Bacillus sphaericus* (BS) bacteria were used for the precipitation of CaCO_3 crystals. BS is an alkaline spore-forming strain which has a high carbonate production capacity and can precipitate CaCO_3 in alkaline (pH 9-10) environments. However, as the pH in concrete is even higher (pH 12-13) different carriers were investigated in order to protect the bacterial spores.

A first carrier which was used to protect the spores is diatomaceous earth (DE) (Figure 4). DE consists of fossilized remains of diatoms, a type of hard-shelled algae. Some of these algae have a hollow inner structure and can maintain the spores inside, however in most of the cases, the bacteria will be attached to the surface of the diatoms as the surface pores are only between 0.1 and $0.5 \mu\text{m}$. The particles themselves have sizes ranging from 4 - $20 \mu\text{m}$ [15].

Although, most spores were not within the diatoms, an obvious protective effect was noticed upon combination of the spores with DE. While only 5% of nutrient (urea)

decomposition was noticed when bacteria were added to a high pH solution without protection, this percentage increased to more than 70% when the bacteria were previously combined with DE. Moreover, the addition of DE and BS did not have a negative effect on the mechanical properties of the cementitious matrix [15].

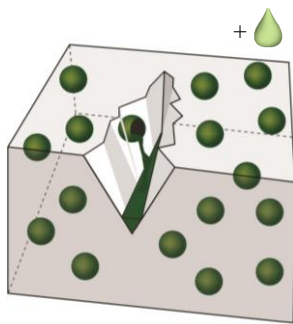


Figure 4. Autonomous healing (upon contact with water) by encapsulated (spherical capsules) bacteria.

While nutrients were already added to the mixing water when making the samples with DE protected spores, more precipitation of CaCO_3 crystals was noted inside the crack when the samples were submerged in a nutrient solution during the time span of healing compared to the submersion in water. Only when the cracked samples were submerged in a nutrient solution, complete filling of the 150-200 μm wide cracks was noted after 40 days. The efficiency of this approach was also proven by a reduced capillary water absorption of cracked samples when DE and BS were included. Here again, an additional beneficial effect was noted when samples were submerged in a nutrient solution instead of water [15].

A spherical carrier which has been used to protect the bacteria are melamine-based microcapsules (Figure 4). The capsules had diameters ranging from 5-10 μm . This type of microcapsules were able to survive the mixing process of cementitious materials. Moreover, after release from the capsules, the bacterial spores were still able to decompose urea and thus to precipitate calcium carbonate. A drawback of this approach, however, is that the addition of nutrients to the mix and the presence of the capsules reduced the mechanical properties of the cementitious matrix. Nevertheless, the matrix porosity was also reduced [16].

The efficiency of this approach was evaluated by means of microscopic investigation of cracked samples. All samples, even when no or empty capsules were added to the mix, showed some crack filling, except those which were stored at a high relative humidity instead of being submerged in water or a nutrient solution. However, while for series without bacteria only cracks with a width up to 250 μm were able to close completely (due to autogenous healing), when bacteria loaded capsules were provided even 1 mm wide cracks were able to heal completely [16].

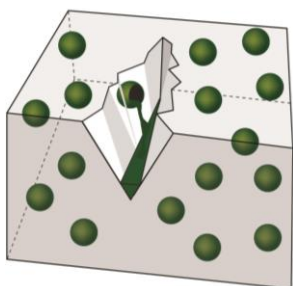


Figure 5. Autonomous healing by encapsulated (spherical capsules) bacteria.

As the bacterial spores need water in order to become active, the previous bacteria-based mechanisms are only activated when samples are submerged periodically or continuously in water or a watery nutrient solution. In order to be able to activate the mechanism in dry state, the bacteria can be incorporated in SAP particles (Figure 5). In this case, the main function of the SAP during crack healing is to facilitate the germination of the spores and bacterial ureolytic activity by supplying water. In addition, the SAP will retain their earlier crack blocking effect due to their swelling reaction and improve autogenous crack healing by providing water for further hydration and CaCO_3 precipitation.

Both the bacterial spores and the nutrients were provided inside the SAP during synthesis of the SAP particles in the laboratory. The bacterial spores were still viable and kept their ureolytic activity after synthesis of the polymers and subsequent processing steps (grinding of the polymer). These bacterially loaded SAP particles were, together with some additional nutrients, added to the mortar mixture upon preparation [16].

After crack formation it was shown that samples with bio-SAP particles, which were subjected to wetting and drying, showed a higher crack healing efficiency in view of the healing rate and maximum healed crack width. In case SAP with spores and nutrients were provided healing ratios of more than 70% were still noticed for cracks with widths until 700 μm [16].

This beneficial effect was only noted for samples subjected to wetting and drying while it was aimed for that healing would now also take place at high or medium relative humidity. The self-synthesized SAP used in this study showed 25 times less water absorption when the relative humidity decreased from 100% (wet state) to 90% and even about 2000 times less when the relative humidity further decreased to 60%. It is thus obvious that the fact that wetting and drying was still needed is caused by the poor behaviour of the specific SAP. Further research therefore aims at the combination of the bacteria with better performing SAP types [16].

While for the bacteria-based approaches mostly spherical capsules or carriers have been used, up to now polymeric agents were mostly embedded inside cylindrical capsules as they have the advantage that the probability of a crack going through is higher. Within the cylindrical capsule-based approach, a subdivision can be made between capsules with one compartment (Figure 6), which are usually filled with one-component healing agents, and capsules with two or more compartments (Figure 7) which are filled with multi-component healing agents.

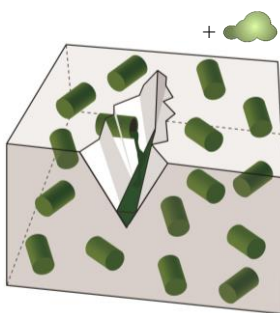


Figure 6. Autonomous healing (upon contact with moisture) by encapsulated (tubular capsules) one-component healing agents.

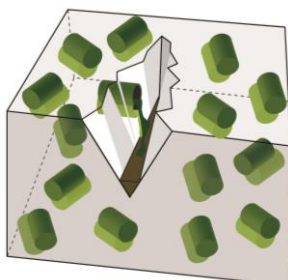


Figure 7. Autonomous healing by encapsulated (tubular capsules) multi-component healing agents.

An example of a one-component healing agent which has been used is cyanoacrylate (Figure 6). This agent is characterized by a very low viscosity and a rapid strength development upon contact with moisture in the air. While this rapid strength development can be seen as an advantage, since crack repair can be done within a few seconds, it was merely experienced as a disadvantage. At first, due to the high reactivity of this agent, hardening of the agent in some cases already occurred within the glass capsules, before capsule breakage. In addition, due to the short reaction time limited outflow of the agent into the crack was noticed. As a result, the obtained strength regain always remained lower than 50% of the original value [17].

The advantage of using a multi-component healing agent is that premature hardening of the agent inside the capsules should not be feared as the reaction only becomes possible when both agents contact each other after capsule breakage (Figure 7). An additional difficulty in this approach, however, is that the different components of the healing agent need to find each other before the reaction can start. As for epoxy resins the mix ratio of the different components is very important in order to have a complete polymerization reaction, multi-component epoxy resins were found not to suit as healing agent inside self-healing concrete [17]. The noticed strength regain always remained lower than 20%. A multi-component

agent which did seem appropriate was a polyurethane-based adhesive.

The polyurethane-based adhesive consists of two components which react upon contact with each other irrespective the mix proportion. One component is a prepolymer of polyurethane, the second component is a mix of accelerator and water. Both components of this agent were embedded inside cylindrical capsules with a

diameter ranging from 2 to 3 mm and made from glass or ceramics. Both materials are very brittle and thus break easily at the moment of crack appearance. To increase the probability that both components contact each other, capsules filled with each of the components were fixed next to each other [18].

Up to 60% of the original strength was regained upon reloading previously cracked samples which contained encapsulated polyurethane. Even when the samples were reloaded for a second time up to 25% of the original strength was regained due to a second healing action. For cracked samples containing encapsulated polyurethane it was possible to reduce the water permeability coefficient with a factor 10^2 to 10^3 when glass capsules were used and even with a factor of 10^3 to 10^4 when ceramic capsules were embedded [18].

4. CONCLUSIONS

Among the earlier mentioned self-healing approaches, those relying on improved autogenous healing are most close to practical application. This is of course because these mechanisms are caused by components which are nowadays already added to the concrete mix for other purposes.

Self-healing by bacteria embedded in DE, microcapsules or SAP is also quite close to practical application as these agents can survive the mixing process and can thus easily be added upon concrete manufacturing. However, some work will have to be dedicated to the reduction of the cost of the bacteria and thus to allow upscaling of the bacteria production. In addition, work is needed to make sure that the decrease in strength due to the presence of the nutrients and carriers, remains limited.

Most work will still be needed to apply the polymer-based self-healing system within a realistic concrete structure. The biggest bottleneck for this approach is to develop a suitable encapsulation material which is flexible enough to survive the mixing process but then becomes brittle enough to break upon crack formation. Also the long term behaviour of the encapsulated liquid healing agent is a topic which needs further attention.

Of course, even when completely ready for application in practice, these self-healing approaches will only be applied in specific types of concrete structures. More exactly those for which the added value due to self-healing is higher compared to the added cost for implementation of the self-healing approach.

For example, for underground structures, such as parking garages and tunnels, additional treatments are already needed before delivery to seal water transporting cracks caused by shrinkage. As in this specific case, water is available within the cracks, the addition of fibers can help to limit the width of the shrinkage cracks and to improve autogenous healing while added SAP particles can help to block the crack immediately and prevent leakage. If a permanent crack barrier is needed (also when the water level goes down) SAP particles can be combined with bacteria to block the crack permanently with CaCO_3 .

For non-water transporting cracks, for example cracks in reinforced bridge ledgers, it will be an advantage when the mechanism does not need water or moisture for its activation. In this case, polymer-based self-healing can be the ideal mechanism to prevent high repair costs. While the use of elastic healing agents holds the advantage of allowing dynamic movements of the healed crack, high modulus healing agents will create a strong bond between the crack faces and possibly allow multiple crack healing as new cracks will appear at another location where the healing agent is not yet exhausted.

While it is not yet clear for which type of structure self-healing will be most promising, we hope that in the near future self-healing will be introduced in at least some of the mentioned applications.

ACKNOWLEDGEMENTS

Financial support from the Research Foundation Flanders (FWO-Vlaanderen) for these studies (Project No's. G.0157.08 and 3.F.0229.02) as well as from the Ghent University Research Fund (BOF) is gratefully acknowledged.

REFERENCES

- [1] Y. Ohama, K. Demura, T. Endo, Strength properties of epoxy-modified mortars without hardener, Proceedings of the 9th International Congress on the Chemistry of Cement, New Delhi, India, 1992, pp. 512-516.
- [2] C. Dry, Matrix cracking repair and filling using active and passive modes for smart timed release of chemicals from fibers into cement matrices, Smart Materials and Structures, 3 (1994) 118-123.
- [3] C. Dry, M. Corsaw, A comparison of bending strength between adhesive and steel reinforced concrete with steel only reinforced concrete, Cement and Concrete Research, 33 (2003) 1723-1727.
- [4] C. Dry, M. Corsaw, E. Bayer, A comparison of internal self repair with resin injection in repair of concrete, Journal of adhesion science and technology, 17 (2003) 79-89.
- [5] V.C. Li, Y.M. Lim, Y.-W. Chan, Feasibility study of a passive smart self-healing cementitious composite, Composites Part B: Engineering, 29 (1998) 819-827.
- [6] Y. Sakai, Y. Kitagawa, T. Fukuta, M. Iiba, Experimental study on enhancement of self-restoration of concrete beams using SMA wire, S.-C. Liu (Ed.), Proceedings of the Conference on Smart Structures and Materials, San Diego, California, 2003, pp. 178-186.
- [7] H. Mihashi, Y. Kaneko, T. Nishiwaki, K. Otsuka, Fundamental study on development of intelligent concrete characterized by self-healing capability for strength, Transactions of the Japan Concrete Institute, 22 (2000) 441-450.
- [8] T. Nishiwaki, H. Mihashi, B.-K. Jang, K. Miura, Development of self-healing system for concrete with selective heating around crack, Journal of Advanced Concrete Technology, 4 (2006) 267-275.
- [9] S. Granger, A. Loukili, G. Pijaudier-Cabot, G. Chanvillard, Mechanical characterization of the self-healing effect of cracks in Ultra High Performance Concrete (UHPC), Proceedings of the 3rd International Conference of Construction Materials, Performance, Innovations and Structural Implications, Vancouver, Canada, 2005.
- [10] C. Joseph, A.D. Jefferson, State of the art report on self-healing materials, in, Cardiff School of Engineering, 2006, pp. 31.
- [11] N. ter Heide, E. Schlangen, K. van Breugel, Experimental study of crack healing of early age cracks, Proceedings of the Knud Hojgaard conference on Advanced Cement-based Materials, Denmark, 2005, pp. 1-11.
- [12] K. Van Tittelboom, E. Gruyaert, H. Rahier, N. De Belie, Influence of mix composition on the extent of autogenous crack healing by continued hydration or calcium carbonate formation, Construction and Building Materials, 37 (2012) 349-359.

- [13] D. Snoeck, N. De Belie, Mechanical and self-healing properties of cementitious composites reinforced with flax and cottinuised flax, and compared with polyvinyl alcohol fibers, *Biosystems Engineering*, 111 (2012) 325-335.
- [14] D. Snoeck, K. Van Tittelboom, S. Steuperaert, P. Dubruel, N. De Belie, Self-healing cementitious materials by the combination of microfibres and superabsorbent polymers, *Journal of Intelligent Material Systems and Structures*, (2012) published online.
- [15] J. Wang, N. De Belie, W. Verstraete, Diatomaceous earth as a protective vehicle for bacteria applied for self-healing concrete, *Journal of Industrial Microbiology & Biotechnology*, 39 (2012) 567-577.
- [16] J. Wang, Self-healing concrete by means of immobilized carbonate precipitating bacteria. PhD in Civil Engineering, Ghent University, 2013, pp. 303.
- [17] K. Van Tittelboom, N. De Belie, Self-healing concrete: suitability of different healing agents, *International Journal of 3R's*, 1 (2010) 12-21.
- [18] K. Van Tittelboom, N. De Belie, D. Van Loo, P. Jacobs, Self-healing efficiency of cementitious materials containing tubular capsules filled with healing agent, *Cement and Concrete Composites*, 33 (2011) 497-505.

NUMERICAL MODELLING OF AUTOGENOUS HEALING AND RECOVERY OF MECHANICAL PROPERTIES IN ULTRA-HIGH PERFORMANCE CONCRETE

B. Hilloulin¹, F. Grondin¹, M. Matallah^{1,2} and A. Loukili²

¹ LUNAM Université, Institut de Recherche en Génie Civil et Mécanique (GeM), UMR-CNRS 6183, Ecole Centrale de Nantes, 1 rue de la Noë, 44321 Nantes, France – e-mail: benoit.hilloulin@ec-nantes.fr; frederic.grondin@ec-nantes.fr; ahmed.loukili@ec-nantes.fr

² RISAM (RISK Assessment & Management), Université de Tlemcen, BP230, Algérie – e-mail: matallah@mail.univ-tlemcen.dz

Keywords: concrete, autogenous healing, finite element method, hydro-chemo-mechanical coupling

ABSTRACT

Cracks, caused by shrinkage or external loading, reduce the durability of concrete structures as aggressive substances can easily enter in the capillary network of the cementitious matrix. Natural 'autogenous' healing ability of concrete by further hydration or precipitation has been studied experimentally for many years. Autogenous healing of concrete by further hydration of residual unhydrated cement particles is triggered by the ingress of water and/or moisture into the crack and leads to a partial recovery of mechanical properties (Young's modulus, tensile strength,...). However, theoretical studies and computer simulations still need to be developed in order to explain macroscopic behaviour of healed specimens and conditions of occurrence of the self-healing phenomenon.

In this study, a hydro-chemo-mechanical model was developed to simulate autogenous healing by further hydration. Firstly, a simulation of a three-point-bending test was performed to represent the initial damaged state before the self-healing process. The volume fraction of the residual cement clinkers at this moment has been calculated with a hydration model. Then, the self-healing phenomenon of concrete beams immersed into water was modelled based on micro-mechanical observations. The diffusion process has been simulated using the Fick's law in order to describe the ingress of water into concrete. The hydration model, based on the Arrhenius law, is then used to simulate the chemical reactions between residual clinkers and water. The mechanical properties of the new formed hydrates are therefore evaluated in order to describe the partial recovery of mechanical properties of healed concrete.

1. INTRODUCTION

Cracks in concrete can heal naturally under favorable conditions. This phenomenon called 'autogenous' healing is the consequence of two main reactions depending on the concrete nature: further hydration for concrete with an important amount of unhydrated cement particles and formation of insoluble calcium carbonate when calcium contained in the cementitious matrix can react with carbon dioxide dissolved in the water filling the crack. Autogenous healing by further hydration has been studied by several researchers. Granger et al. [1] used ultra high performance

cementitious material – UHPC– with a water-to-cement (W/C) ratio close to 0.2 to study the self-healing of cracks with different widths. Mechanical properties of healed and uncracked specimens were compared at different stages (1 week, 3 weeks, 10 weeks, 20 weeks and 40 weeks). However, only few models were developed to describe self-healing of concrete and none of them described the restoration of the mechanical properties.

In this study, a hydro-chemo-mechanical model was developed to simulate autogenous healing by further hydration. The self-healing of a concrete beam was calculated after cracking in a three-point-bending test. The recovery of the cracked concrete beam was obtained by decreasing the local damage value due the fill in of empty space by new hydrates.

2. PROBLEM FORMULATION

First, three-point-bending tests were simulated on a concrete beam to represent the first experimental step corresponding to the creation of the crack, considering an anisotropic description of the damage (eq 1) [2]. Damage is defined through the relationship between the overall stress σ , the total strain ε^e , the plastic strain ε^p and the local initial stiffness C^0 at each point y :

$$\sigma(y) = (1-d)C^0(y) : (\varepsilon(y) - \varepsilon^p(y)) \quad (1)$$

d represents the scalar value of the isotropic damage:

$$d = 1 - \frac{\varepsilon_{d0}}{\varepsilon_{eq}} \exp\left[B_t (\varepsilon_{d0} - \varepsilon_{eq})\right] \quad (2)$$

where B_t represents a damage parameter to control the slope of the strain softening constitutive relation in function of the width h of the element and ε_{d0} the strain threshold. ε^p is computed using a loading function by the normality rule.

To model the autogenous self-healing, external humidity conditions are considered by the arrival of water on the boundary of the beam. The ingress of water, with a speed U , through the damaged material was simulated by using the Fick's law:

$$\frac{\partial U}{\partial T} = D(d) \frac{\partial^2 U}{\partial X^2} - kU \quad (3)$$

where $D(d)$ represents the diffusivity coefficient depending on damage [3].

The local quantity of water inside the beam was then used to activate the hydration process which determined the volume of each component in the microstructure [4]:

$$\tau_i \frac{d\xi_i}{dt} = \tilde{A}(\xi_i) \text{ and } V_k^p(t) = \sum_l^n \left(V_i^0 \frac{n_k^p M_k \rho_c}{n_l^r M_l \rho_k} \right) \xi_l(t) \quad k=1, m \quad (3)$$

where V_i^0 represents the residual clinkers in concrete, V_k^p the new formed hydrates, M the molar mass, ρ the mass density, n the mole number and ξ_i the hydration coefficient of each clinker. The index k represents the products (clinkers), l the reactants and c the cement. \tilde{A} and τ are the normalized affinity and the characteristic time, respectively, used in the Arrhenius law.

The amount of the hydration products created in the damage area fill in the empty space and decreases the local damage value.

3. RESULTS

The constitutive damage parameters used to perform the three-point-bending simulations on a notched beam were adjusted in order to fit the experimental loading curves during the stage of the creation of the crack. The selected Young's modulus is 45 GPa, tensile strength is 5 MPa and Poisson's ratio 0.2. The final crack width was equal to 10 μm . Using the damage state at the end of the first stage representing the crack creation, the healing model was applied to see the influence of the creation of new hydrates on the mechanical behaviour of concrete (fig 1). Because the water diffusion started at the bottom of the beam in the model, the new hydrates were created from the bottom to the top of the beam, and the damage diminution as well.

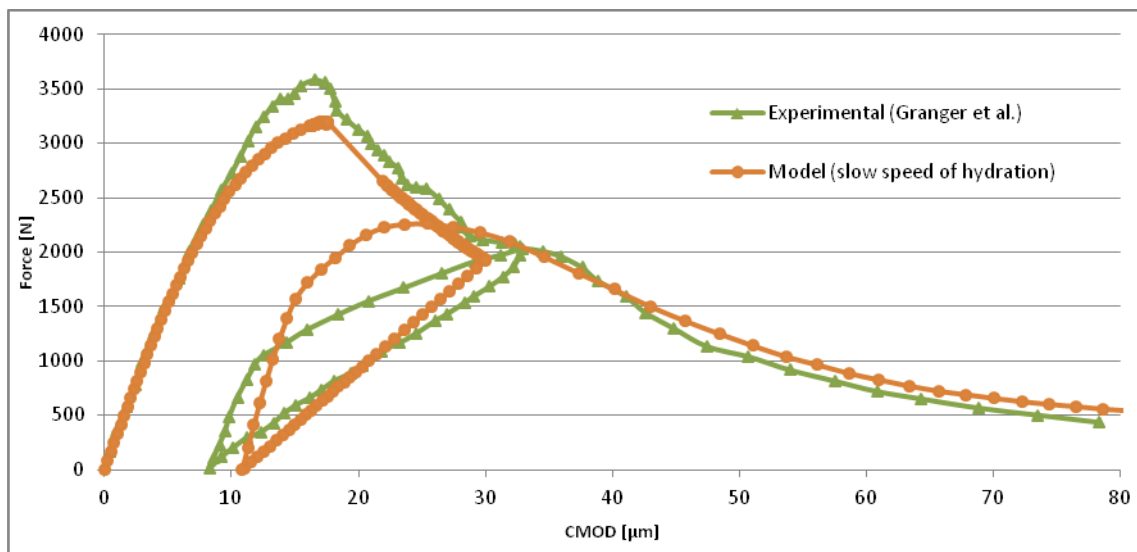


Figure 1: Numerical loading curves before and after healing in comparison with an experimental test (Granger et al., 2007).

The algorithm was applied to different times of healing, considering several speed of hydration and with the possibility to study various mechanical behaviour of the healed zone (fig 2). The simulation of the three-point-bending test after healing revealed that the mechanical behaviour of the healed beam is very sensitive to the kinetic of formation of the new hydrates. For a speed of hydration equal to that observed in concrete at early ages, the healing is almost stopped because the new hydrates are formed at the bottom of the beam and water ingress in the damaged zone is very slow because the diffusivity coefficient is small in undamaged areas. When the kinetic of formation of new hydrates is reduced, the healed zone can be larger over. The difference in the reloading (two slopes in experiments) could be due to different elastic properties and/or kinetic of hydration in the healed area. The elastic response and the maximum bearing load of the beam are affected.

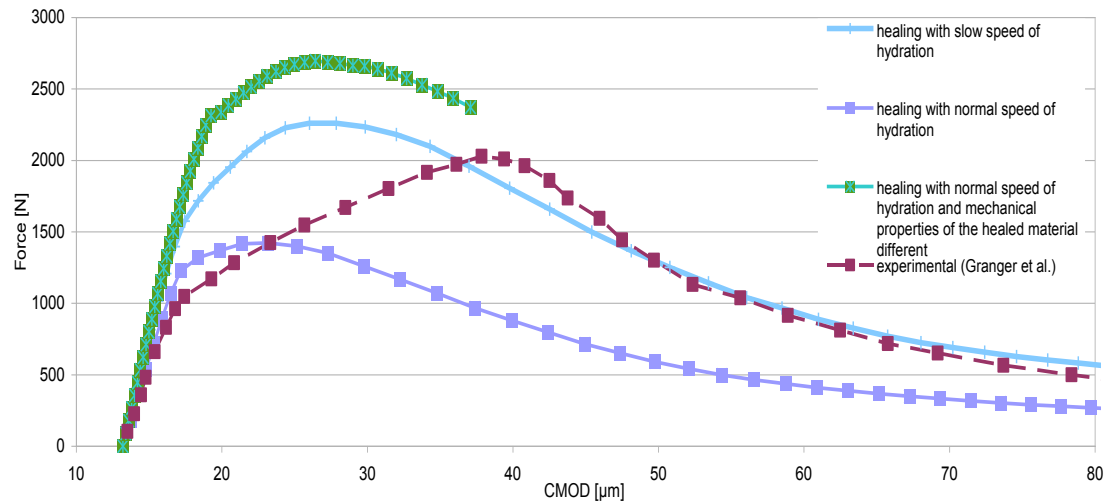


Figure 2: Numerical loading curves after healing with different speed of hydration and with different properties for the new hydrate.

4. CONCLUSIONS

Modelling the autogenous healing in concrete is still a great challenge. A numerical model could help to describe experimental observations and could also help to predict the evolution of mechanical properties of concrete structures during their service life. The speed of formation of the new hydrates in the cracked and damaged concrete seems to play an important role on the speed on healing. However, further investigations are needed to understand the recovery of mechanical properties in concrete structures as well as the occurrence of the self-healing phenomenon. Tests will be made on the influence of the elastic properties of materials in the healed area to obtain the two slopes in the reloading.

ACKNOWLEDGEMENTS

Financial support from the GIS LIRGeC, Région Pays de la Loire (France), for this study is gratefully acknowledged.

REFERENCES

- [1] S. Granger, A. Loukili, G. Pijaudier-Cabot, G. Chanvillard, Experimental characterization of the self-healing of cracks in an ultra high performance cementitious material: Mechanical tests and acoustic emission analysis, *Cement and Concrete Research* 37 (2007) 519-527.
- [2] S. Fichant, C. La Borderie, G. Pijaudier-Cabot, Isotropic and anisotropic descriptions of damage in concrete Structures, *Mechanics of Cohesive-Frictional Materials* 4 (199) 339-359.
- [3] V. Picandet, A. Khelidj, G. Bastian, Effect of axial compressive damage on gas permeability of ordinary and high-performance concrete, *Cement and Concrete Research* 31 (2001) 1525-1532.
- [4] F. Grondin, M. Bouasker, P. Mounanga, A. Khelidj, A. Perronnet, Physico-chemical deformations of solidifying cementitious systems: multiscale modeling, *Materials and Structures* 43 (2010) 151-165.

DEVELOPMENT OF SELF-HEALING GRANULES HAVING SEMI-CAPSULATION EFFECT BY USING CEMENT COMPOUND, CHEMICAL/MINERAL ADMIXTURES & ITS WATERTIGHT PERFORMANCE THROUGH CRACK

V.V. Hung¹, T. Kishi¹, T.H. Ahn¹

¹ Kishi laboratory, Institute of Industrial Science, The university of Tokyo, 4-6-1Komaba, Meguro, Tokyo, Japan – e-mail: vhung@iis.u-tokyo.ac.jp, kishi@iis.u-tokyo.ac.jp, than@iis.u-tokyo.ac.jp

Keywords: concrete, self-healing, granule, watertight, crack

ABSTRACT

Granulation technique, introducing the self-healing ability to concrete, was developed by Koide, 2010 [1] based on the capsulation technology in the food/medicine industry. In this research, self-healing granules, containing cement compounds, chemical and mineral admixtures, were fabricated by a proposed granulation process and the capability of crack-self healing concretes incorporating granules was investigated.

Self-healing granules, which were manufactured in advance by a roller mixer in the laboratory, were added to the concrete mixture as partial sand replacement, at a dosage of 70 kg/m³ concrete.

In order to examine the self-healing performance of the concrete, a water passing test, in which a constant water head of eight centimeters flowing through a static crack of 0.2-0.4mm in width, was conducted for two months. Three different regimes of cured conditions i.e regime one (cured in water at 40°C for one month-short term range), regime two (cured in air at 20°C, relative humidity of 60% for twelve months-long term range) and regime three (cured in water at 40°C for nine months and then in air at 20°C, relative humidity of 60% for three months-long term range) were applied to investigate the self-healing capacity of concrete.

In this study, the capability of crack self-healing concrete was assessed by observing the reduction of water leakage over time, the closing process of surface crack and chemical analysis of deposit products in the crack.

Based on the experimental results, the performance of self-healing concrete, improved by selecting the ingredients of granule and developing suitable method for granulation, will be discussed.

1. INTRODUCTION

One of recent approaches to introduce the self-healing ability to concrete at a normal water/cement ratio was proposed by Ahn and Kishi, 2010 [2]. Some specific mineral and chemical admixtures were added to concrete mixture in form of powder as partial cement replacement. Even though the self-healing performance was promising, there were some disadvantages in this approach, such as the reduction in the workability of fresh concrete and the self-healing efficiency of hardened one. To overcome the

above mentioned drawbacks, the self-healing granules, in which the inner materials containing Portland cements and other additives were coated by cement compound, were used by partial sand replacement in this study.

2. MATERIALS

Self-healing granules were introduced with a target of long term preservation of self-healing capacity in normal water/cement ratio concrete. In this study, the crack self-healing capacity of concrete was attributed by the combined effects of cement hydration reaction, calcite formation and swelling/expansion of cementitious matrix. Apart from the granulation technology to maintain self-healing property for long term, a specific retarder material, which refrained the hydration process of embedded cement during casting concrete, were also investigated (Table 1). After fabrication in the laboratory, the granules were transported to a ready-mixed concrete plant for casting the cylindrical concrete specimen (100mm diameter x 200mm height). Concrete was cast with a water/cement ratio of 49.6% and self-healing granules were incorporated as partial sand replacement at a dosage of 70 kg/m³ concrete (Table 2). After casting, concrete specimens were cured under three different regimes i.e regime one (cured in water at 40°C for one month-short term range), regime two (cured in air at 20°C, relative humidity of 60% for twelve months-long term range) and regime three (cured in water at 40°C for nine months and then in air at 20°C, relative humidity of 60% for three months-long term range).

Table 1 : Ingredients of self-healing granules

Ingredients	Portland cement	Admixtures	Retarder	Water
Percentage (%)	53.8	16.1	21.5	8.6

Table 2 : Mix proportion of concrete

W/C (%)	s/a (%)	G _{max} (mm)	Air (%)	Water	Cement	SH Granule kg/m ³	Sand	Gravel
49.6	51.3	20	4.5	175	353	70	830	869

3. METHODS

After curing, a penetrating crack was induced to the concrete specimen by tensile splitting test. The internal crack was controlled to around 0.2mm by the thickness of Teflon sheet, while the surface crack width was measured by Microscope at three different spots. The average value of those spots was adopted as the surface crack width, ranging from 0.2-0.4mm. In this experiment, a continuous water supply was conducted until 56 days to stimulate the chemical and other reactions in the crack. It was assumed that once crack occurred, the embedded granules were broken. And when water flowed through a crack, not only did the self-healing materials were diffused into crack surface but also the cement hydration products were dissolved in flowing water. Over time, the crack in concrete was healed & the water leakage was stopped, mainly due to the formation of new products by the above mentioned mechanisms.

The self-healing performance of concrete was evaluated by the water passing test, in which the water leakage through a crack under pressure of approximately eight centimeters water head was measured periodically, the crack closing process

observed by microscope, and Thermogravimetry-Differential Thermal Analysis (TG-DTA) of healing product precipitated at the crack.

In order to observe the time dependent permeability of a cracked concrete, the water flow rate was measured and calculated by the formula (1), on the specific days until 56 days subjected to continuous water flow.

$$FR_i = \frac{V_{5min,i}}{t} \tag{1}$$

where: FR_i -water flow rate on i days [cm^3/sec]; $V_{5min,i}$ -volume of water flowing through a crack in five minutes on i days [cm^3]; t -period of testing, in this test $t=300sec$.

Moreover, to assess quantitatively the decreasing flow rate with time, flow relative to initial flow was introduced as in formula (2):

$$RFR_i = \frac{FR_i}{FR_0} \tag{2}$$

where: RFR_i - relative flow rate on i days [%]; FR_i - water flow rate on i days [cm^3/sec]; FR_0 - initial water flow rate on starting day of testing [cm^3/sec].

4. RESULTS

The results showed that there was no significant difference of healing capacity among three curing regimes. The same tendency of reduction in water leakage and healing products deposit on the surface crack was observed with time even though the initial flow rate was relatively different (Figure 1). It could be seen that the water leakage after one day exposed to water flow was just about 10% of initial water flow and then after one week exposure, the water flow was almost stopped during the permeability test as clearly seen in Figure 2.

Moreover, it was found that the crack closing process was mainly observed at the bottom of testing specimen by the substantial amount of white residue forming at crack mouth (Figure 3). A possible reason was that under the effect of flowing water, there was a higher concentration of both calcium and carbonate ions at this area so that facilitating the precipitation of calcite. The findings mentioned above were verified by analyzing the healing products deposited on the surface crack by TG-DTA test. The result showed that the healing products were mainly composed of calcite.

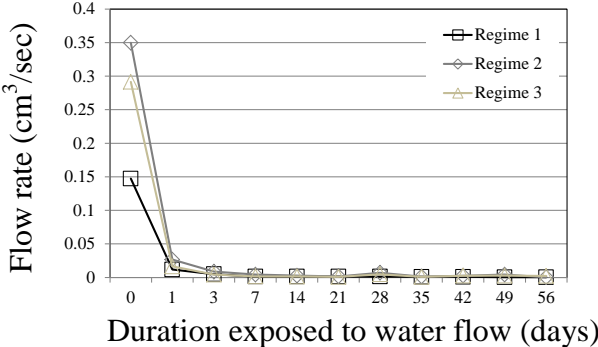


Figure 1: Change of water flow rate with time.

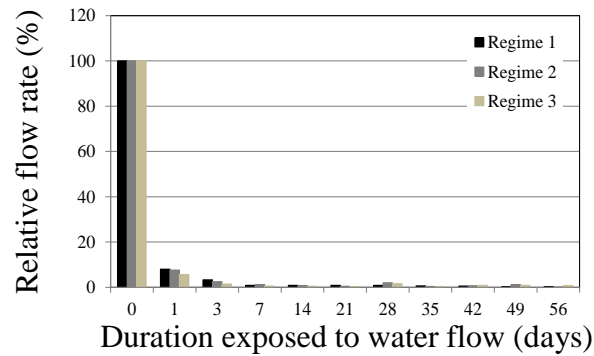


Figure 2: Change of relative flow rate with time.

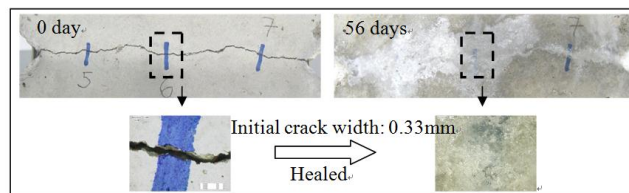


Figure 3: Crack closing process in a typical specimen of regime 1.

5. CONCLUSIONS

Under certain laboratory conditions (static crack of 0.2-0.4mm, continuous water supply), the granulation approach may look promising to maintain the self-healing ability of concrete, with respect to recovery of transport properties, for both short term and long term exposure. Crystalline healing products were gradually formed on the crack surface and thus significantly reduced or completely stopped the water leakage with time. This approach may be suitable for self-healing of underground or water retaining structures where continuous water supply may be expected.

REFERENCES

- [1] Morita, S., Koide, T., Ahn, T.H., and Kishi, T., Evaluation of performance upgrade for the cracked self-healing concrete incorporating capsuled inorganic materials, JCI-TC091A (2010), 183-190 (in Japanese).
- [2] Ahn, T. H., and Kishi, T., Crack self-healing behaviour of cementitious composites incorporating various mineral admixtures", ACT, 8(2) (2010), 171-186

RESISTANCE OF CRACKED CONCRETE HEALED BY MEANS OF POLYURETHANE AGAINST CHLORIDE PENETRATION.

M. Maes¹, K. Van Tittelboom¹ and N. De Belie¹

¹ *Magnel Laboratory for Concrete Research, Ghent University, Technologiepark-Zwijnaarde 904, 9052 Ghent, Belgium – E-mail: mathias.maes@ugent.be; kim.vantittelboom@ugent.be; nele.debelie@ugent.be*

Keywords: Concrete, crack, healing, polyurethane, chlorides

ABSTRACT

A lot of damage is reported for constructions in marine environments. Marine environments are very aggressive, because of the high chloride concentration in sea water. Chlorides affect durability by initiating corrosion of the reinforcement steel. When cracks appear in the concrete structures, chlorides will penetrate faster and will initiate corrosion. A possible solution is self-healing concrete. Self-healing concrete has the ability to recover without external intervention. From the literature concerning self-healing concrete, it is clear that research focuses on the general concept, the mechanical properties and water permeability. Based on the water permeability it is concluded whether harmful substances will penetrate. Specific data on degradation of self-healing concrete in aggressive environments are not available. Nevertheless, these data are important to ensure a good estimation of the service life extension.

In this research, the effect of the healed cracks on the resistance against chlorides was investigated for two concrete types, namely ordinary Portland cement concrete and blast-furnace slag concrete with 50 % cement replacement. Non-steady state migration tests, based on NT Build 492, were performed with uncracked, cracked and healed concrete. In our previous research, autonomous crack healing was obtained by encapsulating polyurethane healing agents. To release the healing agents, realistic cracks were formed by means of a controlled splitting test. In the current work, as a first step, cracks (notches) were manually healed with a two-component healing agent based on polyurethane. These cracks (notches) were formed by means of steel plates with a width of 0.1 and 0.3 mm. The migration tests were performed at constant setup parameters, namely 30 V and 8h. The chloride penetration front was visualized by means of the colorimetric method. By comparing the penetration depths, it seemed that concrete with a healed crack of 0.1 mm can fully regain its resistance against chloride penetration.

1. INTRODUCTION

A lot of damage is reported for constructions in marine environments since these environments are very aggressive, due to the presence of chlorides. A commonly used material for such structures is reinforced concrete. However, chlorides affect the durability of concrete by initiating corrosion of the reinforcement steel. Besides, cracks will facilitate chloride penetration. So, it is important to heal cracks. Since constructions in marine environments mostly have an high economical impact, fast repair of the cracks is desirable. However, repair costs are large and in some cases repair is impossible due to inaccessibility. A possible solution is self-healing concrete. Nevertheless, research on self-healing concrete mainly focuses on the general

concept, the mechanical properties and water permeability. Specific data on degradation of self-healing concrete in aggressive environments are not available. In this paper, the chloride resistance of manually healed concrete is investigated.

2. MATERIALS

Two different concrete mixtures were prepared: one Ordinary Portland Cement (OPC) mixture and one Blast-Furnace Slag (BFS) mixture where the cement replacement level amounts to 50 % (S50).

A two-component polyurethane-based healing agent was used. The first component was a prepolymer of polyurethane which starts foaming in moist surroundings; the second was an accelerator shortening the reaction time. The two components were mixed and injected into the cracks, 24 h before testing, by means of a syringe.

3. METHODS

A non-destructive method was used to generate cracks in concrete conform the method described by Audenaert et al. [1] and Song [2]. They established a notch method to produce an artificial crack in concrete by means of thin steel plates introduced into the fresh specimen. The specimen were cylindrical with a diameter of 100 mm and a height of 50 mm. Varied crack parameters such as crack width, depth and length were obtained by choosing varied sizes of sheets to insert into the concrete. The thin plates used in this research have a preset width of 0.1 mm and 0.3 mm. The crack depth was kept constant at 15 mm for crack widths of 0.1 mm, and at 20 mm for crack widths of 0.3 mm. The crack length was 60 mm.

The resistance to chloride penetration was evaluated experimentally, by means of the rapid chloride migration test as described in NT Build 492 [3]. This method was slightly adopted in order to be able to compare the chloride penetration depths of the different test series. Per concrete mixture, 5 series with at least 6 replicates were tested, namely uncracked, cracked 0.1 mm, cracked 0.3 mm, healed 0.1 mm and healed 0.3 mm. According to the method described in NT Build 492, the applied voltage during the test differs for every measurement, since the penetration depth should be smaller than the specimen height. Because of this, it was not possible to compare the colour change boundaries. Therefore, tests were performed at a constant voltage of 30 V and a constant duration of 8 hours. Afterwards, the chloride penetration was measured by means of the colorimetric method, more specifically by spraying 0.1 M AgNO₃ on both halves of the split specimen.

4. RESULTS

The results show a big difference for the chloride penetration measured at the crack tip of a 0.1 mm crack and a 0.3 mm crack. The wider the crack, the higher the penetration depth measured from the crack tip onwards. Besides, the penetration depth at the crack tips is higher than the penetration depth measured from the exposed surface. In Fig. 1 this relative increase is shown, with the penetration depth at the surface (= crack width 0 mm) as a reference. The increase in penetration depth at the tip of a 0.3 mm crack compared to the penetration from the surface amounts to 30 % and 36 % for OPC and S50 respectively (see Fig. 1).

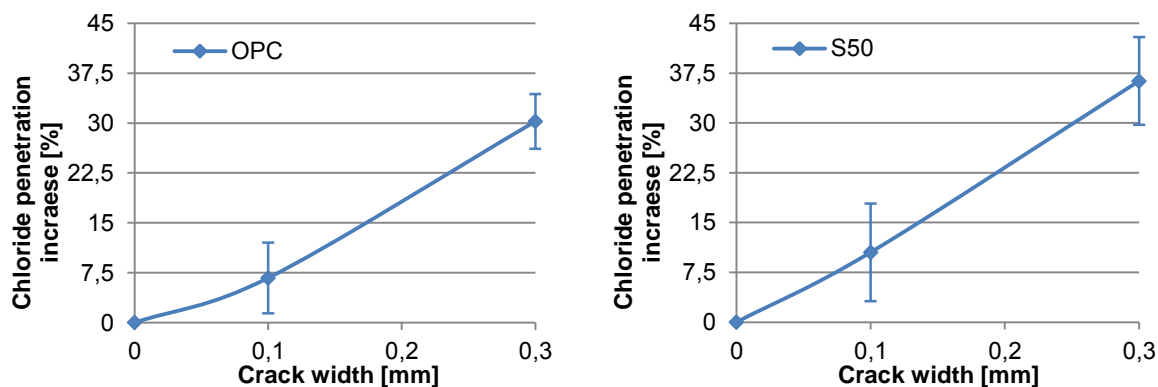


Figure 1: Chloride penetration increase in function of the crack width, for OPC and S50.

It is important to take notice of the fact that chloride penetration from crack tips is higher than from the concrete surface. Considering this, it is important to heal the cracks as quickly as possible.

In this research, the efficiency of polyurethane as a healing agent for self-healing concrete is tested preliminary by means of manual healing of the cracks.

In order to evaluate the healing effect with regard to the resistance against chloride penetration, four healing categories are defined, see Fig. 2: (1) Totally healed (no Cl^- -penetration around the crack), (2) Partially healed (a) (Cl^- -penetration perpendicular to the crack + no Cl^- -penetration at the crack tip), (3) Partially healed (b) (Cl^- -penetration perpendicular to the crack + Cl^- -penetration at the crack tip (< from the surface)) and (4) No effect.

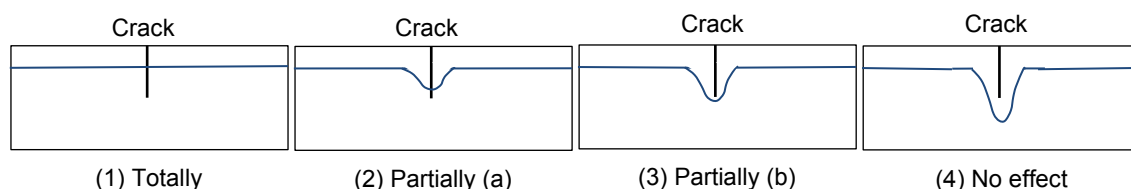


Figure 2: Visual indication of the four categories to evaluate healing based on the chloride penetration depth around the crack.

Table 1 gives an overview of the regained resistance against chloride penetration due to manual healing by means of polyurethane injection. The percentages represent the part of the healed samples belonging to the specific category. To class them, chloride penetration depths were measured and compared.

Table 1: Efficiency of manual crack healing with regard to chloride penetration.

Healing category	OPC		S50	
	0.1 mm	0.3 mm	0.1 mm	0.3 mm
(1) Totally	67 %	34 %	33 %	-
(2) Partially (a)	16 %	33 %	50 %	67 %
(3) Partially (b)	17 %	33 %	17 %	33 %
(4) No effect	-	-	-	-

According to these results, it seems that cracks with width 0.1 mm and depth 15 mm can regain almost full resistance against chloride penetration (categories 1 and 2) in 83 % of the cases. Besides, cracks with width 0.3 mm and depth 20 mm can be healed almost totally in 67 % of the cases. These findings are independent of the concrete mixture. For all samples some positive effect due to the presence of PU in the cracks was measured.

5. CONCLUSIONS

Chloride penetration at the crack tip increases in function of the crack width when the crack width is in the range of 0 mm (= penetration from the surface) until 0.3 mm. A possible solution to repair the cracked concrete is self-healing concrete. Manual healing by means of polyurethane injection shows good results. For cracked concrete with a crack width of 0.1 mm, regardless the composition, 83 % of the samples regained almost full resistance against chloride penetration. In the case that cracks have a width of 0.3 mm, 67 % of the samples regained almost full resistance.

These findings allow for further investigations concerning the resistance against chloride penetration of autonomously healed concrete, with PU as a healing agent. Autonomous crack healing will be obtained by encapsulating the healing agents. To release the healing agents, realistic cracks will be formed by means of a controlled splitting test. After cracking, the specimen will be subjected to a natural diffusion test.

ACKNOWLEDGEMENTS

The research of Mathias Maes is funded by a Ph.D. grant of the Agency for Innovation by Science and Technology (IWT).

REFERENCES

- [1] K. Audenaert, G. De Schutter, and L. Marsavina, The Influence of Cracks in Concrete Structures – Part 1: Experimental Evaluation, Transport Mechanisms in Cracked Concrete, Ghent, 2007, pp. 35-43
- [2] M. Song, Chloride Penetration and Service-Life Prediction of Cracked Self-Compacting Concrete, Doctoral thesis, Department of Structural Engineering, Ghent University, 2012, p. 270.
- [3] NT Build 492, Concrete, Mortar and Cement-based Repair Materials: Chloride Migration Coefficient from Non-Steady State Migration Experiments, Nordtest, Espoo, 1999.

SELF HEALING CAPACITY OF CONCRETE WITH CRYSTALLINE ADDITIVES: NATURAL VS. ACCELERATED EXPOSURE CONDITIONS

V. Krelani ¹ and L. Ferrara ¹

¹ *Department of Civil and Environmental Engineering, Politecnico di Milano Piazza Leonardo da Vinci, 32, 20133, Milano – email: visar.krelani@mail.polimi.it; liberato.ferrara@polimi.it*

Keywords: concrete, self-healing, crystalline additives, natural and accelerated conditioning

ABSTRACT

The presence of cracks may significantly affect the life-cycle of structures, as a results of its influence on the designed structural response vs. persistent or even severe accidental load and exposure conditions, when requested. Repairing damaged concrete in existing structures needs important investments to recover the pristine level of serviceability and extend their designed service life.

In this respect, the ability of cementitious composites to “self-repair” the cracks, because of autogenous or suitably engineered mechanisms, is a challenging opportunity, making concrete more and more attractive in future sustainable developments of civil engineering.

In this study a methodology will be presented to assess the aforementioned capacity, based on three point bending tests on un-cracked and pre-cracked beams, upon exposure to suitable environmental conditions. The paper will focus on the difference between accelerated exposure, in a climate chamber, and “natural conditioning” in air; comparison with immersion in water will also be performed.

1. INTRODUCTION

According to definitions given by design codes, the durability of a structures consists in the capacity of guaranteeing the requested performance, vs. anticipated design actions, all along the service live, without any unplanned maintenance or intervention. The use of materials with “higher quality” may reduce the need for unforeseen maintenance and repair, thus resulting in longer maintenance-free periods and hence, despite the higher construction cost, in a likely lower overall cost of the structure. In the extreme case when “self-healing materials” are applied, i.e. materials which are able to self repair once any kind of damage, anticipated or accidental, occurs, there will be theoretically no need for maintenance and repair, thanks to the materials ability to pristine by itself when requested [1,2].

The “self-healing” mechanisms in cementitious materials are receiving lots of attention by researchers in these last years [2], because of the increasing importance that issues like sustainability are gaining also in the construction industry. Researchers have agreed to make a distinction between “self-sealing”, which is the mere capacity of closing the cracks, and “self-healing”, which is, on its hand, associated to some kind of recovery of mechanical properties, such as stiffness and stress bearing capacity. Summarizing previous studies possible mechanisms of self-healing can be categorized as follows [3]:

- (1) further reaction of unhydrated cement;
- (2) expansion of the concrete in the crack flanks;
- (3) crystallization of calcium carbonate;
- (4) closing of the cracks by spalling-off of loose concrete particles resulting from the cracking.
- (5) closing of the cracks by solid matters in the water (in case of water flow through the cracks).

In the very last decade lot of attention and a huge amount of research work have been dedicated to “engineered” self healing, also in the framework of the sustainability framework addressed in the introduction, along three main fields of research: self healing engineered with fiber reinforcement, mineral-producing bacteria and proprietary chemical admixtures. The latter case will be investigated in this paper, with reference to a crystalline additive, and a methodology will be shown to assess the capacity of the material to recover pristine levels of mechanical properties.

2. EXPERIMENTAL CAMPAIGN

To the aforementioned purpose, two concretes were casted, differing by the presence of the “crystalline” additive: mix-design is shown in Table 1. The employed additive consists of a proprietary mix of silica, cement, sand and other active chemicals, which is added to raw materials during the mixing stage.

Table 1: Mix design of investigated concretes.

	<i>Cement</i> [kg/m ³]	<i>Water</i> [kg/m ³]	<i>Sand</i> [kg/m ³]	<i>Gravel</i> [kg/m ³]	<i>SP</i> [l/m ³]	<i>Additive</i> [kg/m ³]
W/out additive	300	165	975	975	3	0
With additive	300	165	975	975	3	3

66 prismatic specimens, 50 mm thick, 500 mm long and 100 wide were casted. Specimens were kept under a wet towel during the first 72 hours, and then stored in a room at 20°C and 90% RH for 35 days. After this period, specimens were precracked, at to prescribed crack openings, by means of a three point bending test. The crack opening displacement (COD) was measured with the help of clip-gauge, at mid-span specimen intrados (Figure 1).

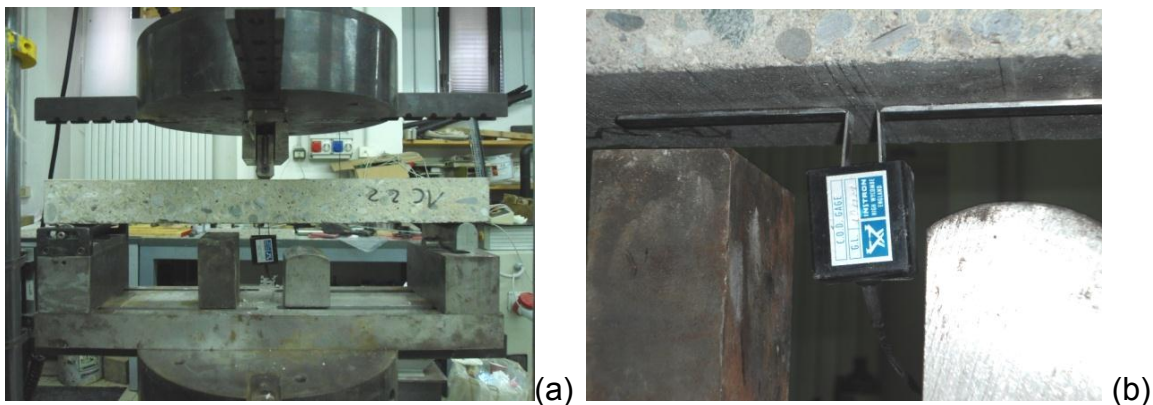


Figure 1: 3-point bending test set-up (a); clip-gauge measuring crack opening (b)

The specimens were divided into two groups and subjected either to natural or accelerated (artificial) conditioning; both groups contained specimens pre-cracked at 130 μm , 270 μm respectively and reference un-cracked specimens.

The accelerated conditioning was performed in a climate chamber, simulating the autumnal season in the northern Italy, Milan. In Figure 2a the temperature cycle is shown, to which specimens were exposed respectively for 1, 2 and 4 weeks (relative humidity was always kept at 95%). On the other hand, natural conditioning consisted either in exposing specimens to open air (in Figure 2b recorded temperatures along the exposure period are shown) or immersing them in water at 20°C; in both cases the duration of the exposure was 4-weeks.

At the end of each prescribed exposure period 3-point bending tests, as in the pre-crack procedure, were performed on the specimens, up to complete failure.

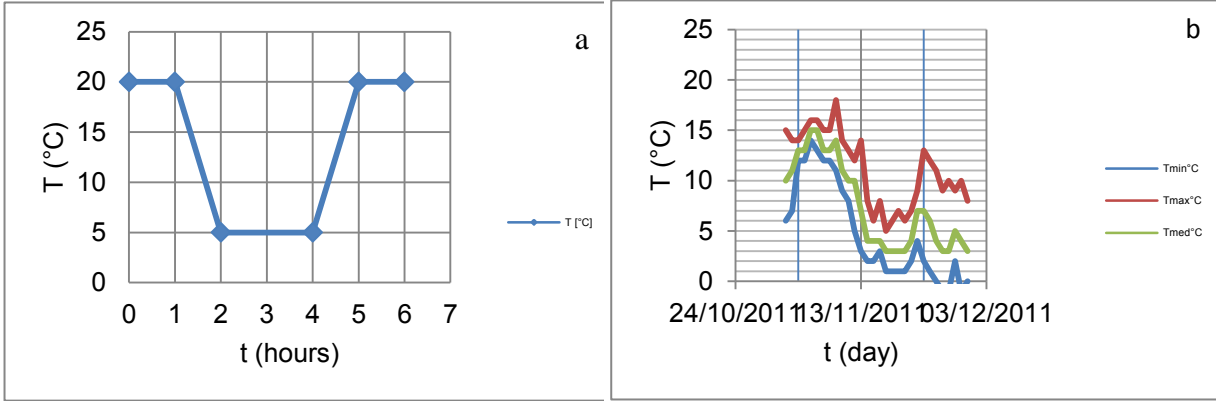


Figure 2: thermal cycle in climate chamber (a); temperatures recorded along the air exposure period (b)

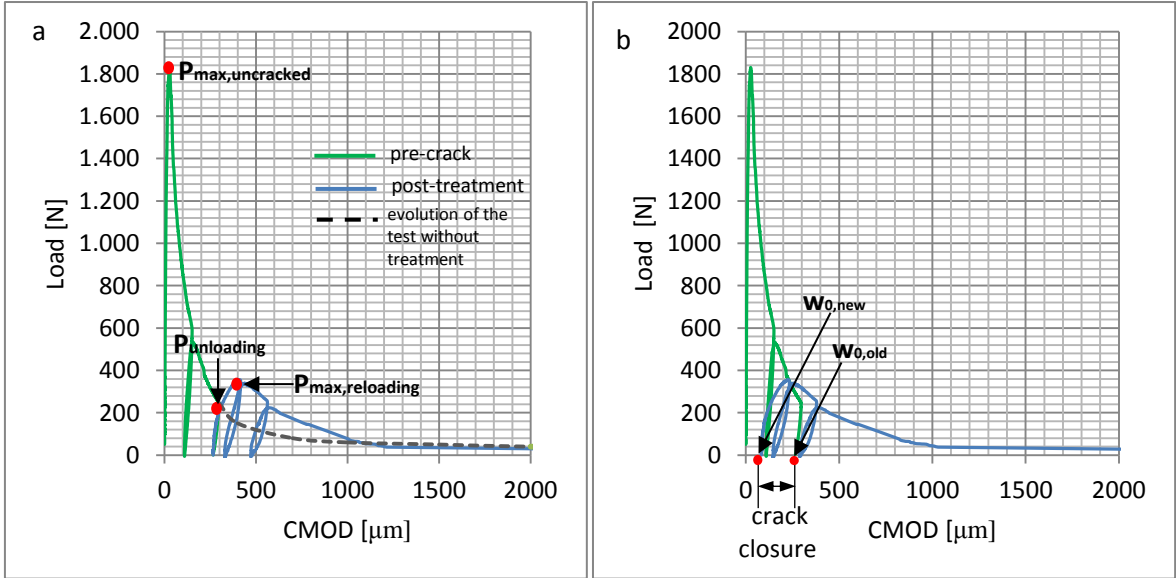


Figure 3: Load-COD curve obtained with 3pb tests from the same specimen before and after “conditioning”: a) principal variables taken into account and b) proposal for crack closure evaluation

3. EXPERIMENTAL RESULTS

Fig.3a shows, for the sake of example, a curve obtained from 3-point bending test on the same specimen in the pre-cracking and in the post-conditioning stage. A recovery of the load bearing capacity, with respect to the unloading value at which pre-cracking was performed in the first stage, is evident. In order to evaluate the crack closure it is necessary to perform a “backward shifting” of the curve obtained after the “conditioning”, originating at the pre-cracking crack opening $w_{0,old}$, until the post-conditioning maximum load, $P_{max,reloding}$, intersects the softening branch recorded during the pre-cracking test (Figure 3b). This makes to curve to be shifted to a new origin, $w_{0,new}$. An Index of Crack Self-Healing (ICSH), is defined as (Figure 4):

$$ICSH = 1 - \frac{W_{0new}}{W_{0old}} \quad (1)$$

4. CONCLUDING REMARKS

The experimental methodology herein proposed allows to provide quantification of crack closure due to self healing in concrete. From preliminary results herein shown, the self healing efficiency in concrete increases with the presence crystalline additive. Furthermore, as expectable, immersion in water leads to higher self healing capacity, mainly for higher crack widths; accelerated conditioning does not seem, at least with reference to present results, to lead to significant improvements with respect to natural exposure conditionings.

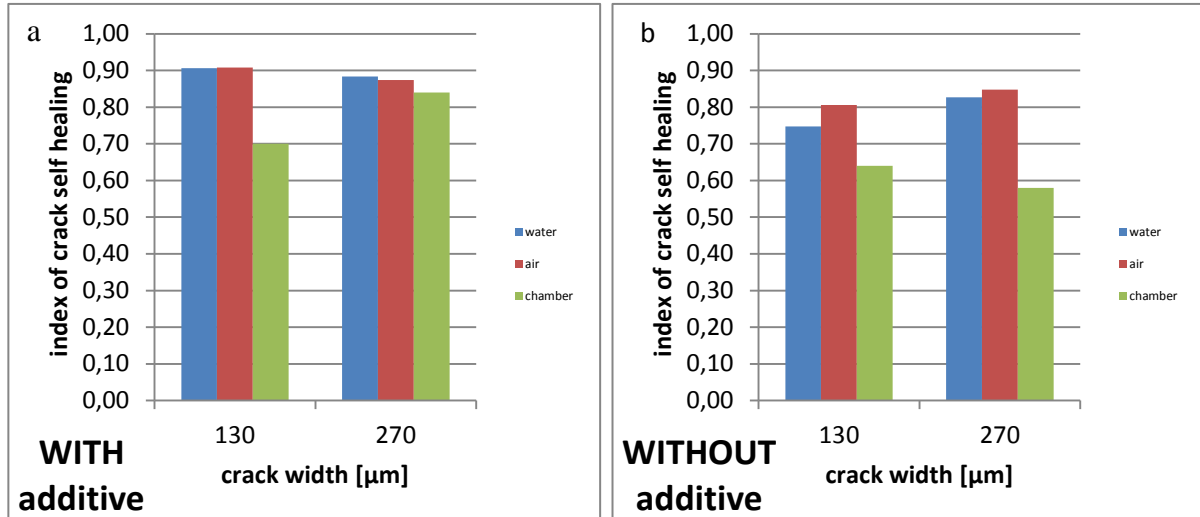


Figure 4: Index of Crack Self-Healing (ICSH), evaluated for concretes without (a) or with (b) crystalline admixture, as a function of crack opening and exposure duration.

ACKNOWLEDGEMENTS

Financial support from the Penetron Italia and to the contribution on the experimental investigation to Ing.Irene Pessina.

REFERENCES

- [1] Van Breugel, K. "Is There a Market for Self-healing Cement-based Materials?" 1st International Conference on self-healing Materials, Noordwijk, Holland, (2007).
- [2] Mihashi, H., Kaneko, Y., Nishiwaki, T. and Otsuka, K. Transactions of the Japan Concrete Institute, **22**, 441–50, (2000).
- [3] Mechterine. V." Towards a durability framework for structural elements and structures made of", Construction and Building Materials, 31 (2012): 94-104.

SESSION 11 – SELF-HEALING SUPRAMOLECULAR POLYMERS

Self-healing supramolecular polymers

F. Tournilhac¹, F. Maes², L. Corté², D. Montarnal¹ and L. Leibler¹

¹ *Matière Molle et Chimie, ESPCI ParisTech CNRS UMR 7167, 10 rue Vauquelin 75005 Paris, France – e-mail: francois.tournilhac@espci.fr*

² *Mines-ParisTech, Centre des Matériaux, CNRS UMR 7633, BP 87, 91003 Evry Cedex, France – e-mail: laurent.corte@mines-paristech.fr*

Keywords: supramolecular rubbers, self-assembling

ABSTRACT

Materials are autonomously self-healing when repair is triggered not by external intervention (heat, light ...) but by the damage itself. Complex composite architectures have been devised by several groups to show essentially this type of behaviour. On the other hand, a simple polymer melt is repeatedly self-healing, by simple re-entanglement of polymer chains. The problem is that even though at short time such a material behaves like an elastic solid, it has sticky surfaces and finally, at long times it flows under the effect of a constraint. Achieving a homogeneous polymer material that can behave like a real elastic solid and can self-repair without external action is therefore a challenge.

Supramolecular chemistry teaches us to control non-covalent interactions between organic molecules, particularly through the use of optimized building blocks capable of establishing several hydrogen bonds in parallel.

On this basis, we will discuss design principles and our endeavours to create novel supramolecular networks with rubbery elasticity, self-healing ability and as little as possible creep. Our strategy was to synthesize assemblies of randomly branched H-bonding oligomers rather than a single molecule. While our materials are non-sticky elastomers, they can be repaired in case of damage, even after a long waiting time, by simply bringing together fractured surfaces.

To understand this paradox, we will show that not only the optimization of hydrogen bonding groups but also the self-assembling ability of the molecular unit as a whole are key parameters which control cohesion, organization and eventually the long lived nonequilibrium state that promotes the self-healing event.

REFERENCES

F. Maes, D. Montarnal, S. Cantournet, F. Tournilhac, L. Corté, L. Leibler, Activation and deactivation of self-healing in supramolecular rubbers, *Soft Matter* 8 (2012) 1681-1687.

UNDERSTANDING THE MOLECULAR MECHANISMS INVOLVED IN THE INTERFACIAL SELF-HEALING OF SUPRAMOLECULAR RUBBERS

R. K. Bose¹, S. J. Garcia¹ and S. van der Zwaag¹

¹ *Novel Aerospace Materials Group, Faculty of Aerospace Engineering, Delft University of Technology, Kluyverweg 1, 2629 HS Delft, The Netherlands – e-mail: r.k.bose@tudelft.nl*

Keywords: supramolecular rubbers, self-healing efficiency, tapered double cantilever beam, rheology

ABSTRACT

Supramolecular rubbers based on 2-aminoethylimidazolidone and fatty acids with epoxy crosslinks have been shown to self-heal via multiple hydrogen bonding sites. In this work, several tools are used to investigate the molecular mechanisms taking place at the interface to understand cohesive healing in these polymers. The quantification of self-healing was performed via a tapered double cantilever beam (TDCB) geometry. The TDCB geometry is especially amenable to studying multiple healing cycles due to the fracture toughness, and subsequently healing efficiencies being independent of crack length. Healing was carried out for multiple fracture-healing cycles and varying fracture testing experimental parameters to track the change in efficiency of interfacial healing. Strain rate and rate of crack closure are both shown to affect the self-healing efficiency.

1. INTRODUCTION

Self-healing in supramolecular rubbers based on 2-aminoethylimidazolidone and fatty acids with epoxy crosslinks has been shown to occur via multiple hydrogen bonding sites [1]. Previous work has shown that these hydrogen bonding systems undergo a “deactivation” of the surfaces under certain conditions [2]. On the other hand, it was also shown that damage or fracture processes can cause “activation” of the surfaces leading to enhanced self-healing upon bringing the fractures surfaces together. Annealing of the fractures surfaces at different temperatures before healing also affects the healing efficiencies. Moreover, surfaces undergo time dependent polymer chain rearrangements which lead to differences in the healing efficiency. In this work, experiments have been designed to further investigate and understand the interfacial molecular mechanisms of these fractured surfaces. Firstly multiple cycles of crack propagation and healing was carried out in a tapered double cantilever (TDCB) setup. The TDCB geometry was chosen due to the independence of fracture toughness on crack length [3], thus providing the advantage of self-healing efficiency that is independent of crack length for multiple healing cycles. Furthermore, rheology in a strain-controlled mode was used to understand the parameters affecting the cohesive strength between fractured surfaces.

2. MATERIALS

Supramolecular rubbers based on 2-aminoethylimidazolidone and fatty acids with epoxy crosslinks (provided by Arkema) were used as the self-healing system under investigation. Modified tapered double cantilever (TDCB) specimens were prepared as described previously [4]. The geometries were shaped out of aluminium and used with 10 x 6 x 2 mm polymer samples inserted in the region of interest. The entire TDCB setup was held inside a rigid aluminum mould to ensure uniform pressure between fractured surfaces during each healing cycle. A sharp 1 mm pre-notch was made on the polymer using a razor blade. For the rheology experiments 20 mm diameter polymer discs with a thickness of 2 mm were used.

3. METHODS

Healing was carried out for five subsequent loading (i.e. fracture) and healing cycles and varying fracture testing experimental parameters to track the change in efficiency of interfacial healing. For the first set of experiments, polymer samples were fractured at different strain rates (5, 10 and 300 mm/min) in a universal tensile testing machine (Zwick, 20 kN) to monitor the relationship between loading and crack propagation. Samples were allowed to heal in the TDCB mould for 1 hour at room temperature between fracture cycles. For these tests, the fractures surfaces were brought together at a fast strain rate of 300 mm/min.

In a separate set of experiments, samples were fractured at a constant strain rate of 10 mm/min but the fractured surfaces were brought together at different speeds (1, 10 and 100 mm/min) in a controlled fashion using the tensile testing machine. This allowed for a study of the mechanism of deactivation and rearrangement of the surface polymer chains. Rheology (ThermoFisher, Haake Mars III) was used to study the viscoelastic behaviour of these polymers. A tack type adhesion testing was carried out in the strain-controlled rheometer to determine cohesive strength between two discs of the same polymer. Two discs of 20 mm diameter and 2 mm thickness were pressed together between parallel plate geometry of a rheometer at 80 °C for 5 minutes. The samples were then separated at a constant strain of 10 mm/min and the force-displacement curves were plotted.

4. RESULTS

Previous work on these polymer films has shown two mechanisms of fracture: cavitation occurring at low strain rates; and brittle fracture which is dominant at high strain rates or low temperatures [2, 5]. Study of the transition from one mechanism to other could provide helpful information regarding healing self-healing. The load vs. displacement behaviour (Figure 1) shows a constant force plateau at 5 and 10 mm/min which corresponds to a steady crack propagation. Whereas, in case of the 100 mm/min loading rate, a markedly different behaviour is observed. The polymer undergoes an initial linear elongation, which rapidly turns into a nucleation and cavitation type of failure. The first signs of cavitation were seen at the displacement value at which the force displacement curve changes slope. Thus, in the TDCB geometry, the polymer has two dissimilar responses under low and high strain rates, which is contradictory to that observed previously [2], and therefore requires further research. However, this strain rate dependence behaviour does provide further

insight into the timescale of the dynamic network formation. Previous work has shown a similar behaviour for other supramolecular polymer networks [6].

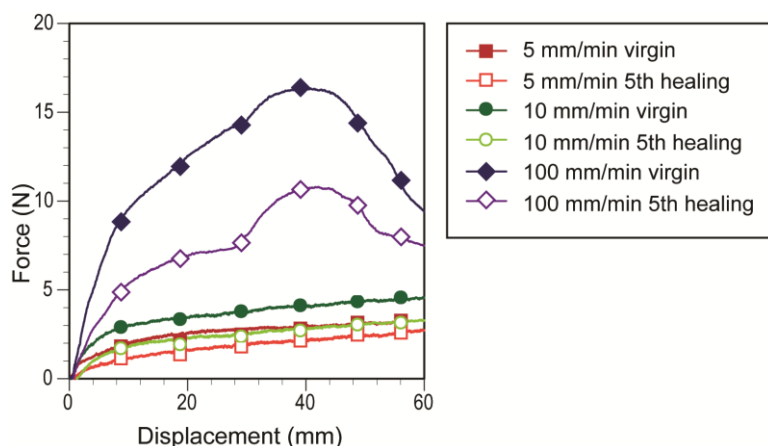


Figure 1: Differences in force displacement curves with different fracture rates indicate two separate mechanisms of fracture.

Since chain relaxation is likely a very important phenomenon at the surface, another set of experiments was performed by varying the rate of crack closure, while keeping loading rate constant. As shown in Figure 2(a) the rate of crack closure also has a major effect in the after healed properties, suggesting a process of polymer chain relaxation at the crack surface plane. This effect can be quantified by plotting healing efficiency as a function of the rate of crack closure as shown in Figure 2(b). The healing efficiency at closure rates of 1-10 mm/min reaches values of 90% while higher closure rates (i.e. 300 mm/min) lead to a clear decrease in healing efficiency, a likely indicator of the time dependent polymer chain relaxation. It is supposed that high crack closure rates do not allow sufficient chain entanglement, leading to a lower bond strength.

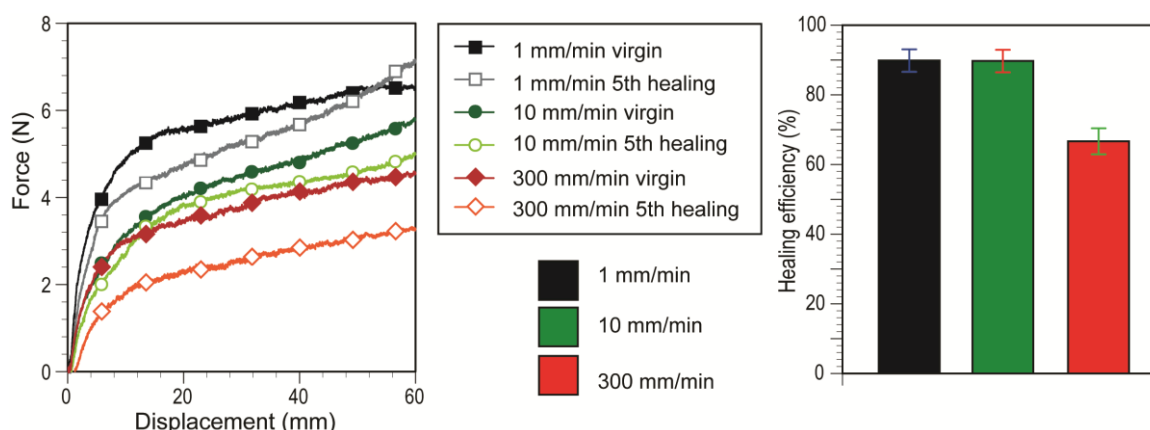


Figure 2: (a) While keeping loading rate constant, different rates of crack closure lead to a difference in the healing phenomena, an indication of the chain relaxations on the surface, and (b) healing efficiency, defined as ratio of force of healed to virgin polymer, is higher for slower rates of crack closure.

5. CONCLUSIONS

As seen in these results, for supramolecular self-healing a study of the interfacial mechanism is necessary and yields interesting information regarding self-healing in these hydrogen bonding networks. Different mechanisms of fracture and crack closure have been observed as function of the rates of loading and crack closure rates. A detailed study of parameters affecting self-healing and the quantification of the fracture energy are expected to yield further information regarding the activation and deactivation of polymer chains on the surface.

ACKNOWLEDGEMENTS

The authors are grateful to Jean-Pierre Disson at Arkema for providing the supramolecular polymers used in this work.

REFERENCES

- [1] Cordier, P., et al., Self-healing and thermoreversible rubber from supramolecular assembly. *Nature*, 2008. 451(7181): p. 977-980.
- [2] Maes, F., et al., Activation and deactivation of self-healing in supramolecular rubbers. *Soft Matter*, 2012. 8(5): p. 1681-1687.
- [3] Brown, E.N., Use of the tapered double-cantilever beam geometry for fracture toughness measurements and its application to the quantification of self-healing. *The Journal of Strain Analysis for Engineering Design*, 2011. 46(3): p. 167-186.
- [4] Brown, E.N., S.R. White, and N.R. Sottos, Microcapsule induced toughening in a self-healing polymer composite. *Journal of Materials Science*, 2004. 39(5): p. 1703-1710.
- [5] Montarnal, D., et al., Synthesis of self-healing supramolecular rubbers from fatty acid derivatives, diethylene triamine, and urea. *Journal of Polymer Science Part A: Polymer Chemistry*, 2008. 46(24): p. 7925-7936.
- [6] Hentschel, J., et al., Self-Healing Supramolecular Block Copolymers. *Angewandte Chemie International Edition*, 2012. 51(42): p. 10561-10565.

ENGINEERING POLY(ISOBUTYLENE) AS SELF-HEALING POLYMER

W. H. Binder¹, A. Stojanovic¹, D. Döhler¹, P. Michael¹, Florian Herbst¹

¹ Institute of Chemistry, Chair of Macromolecular Chemistry, Faculty of Natural Sciences II (Chemistry, Physics and Mathematics), Martin-Luther-University Halle-Wittenberg, von-Danckelmann-Platz 4, Halle (Saale) 06120, Germany – e-mail: wolfgang.binder@chemie.uni-halle.de

Keywords: self healing, autocatalysis, click chemistry, multiple healing, poly(isobutylene)

ABSTRACT

All polymeric materials are subject to thermal, mechanical as well as chemical degradation and destruction during their lifetime. As new materials are designed, the quest for materials with self-healing properties (i.e.: those which can regenerate similar to living matter, especially after mechanical deformation) is increasing, culminating in the need for self-healing polymers after mechano-deformation¹⁻³. We here report on the realization of two different principles of self-healing polymers, based on either dynamic, supramolecular polymers^{4,5}, or via the use of encapsulated reagents^{3,6-8}. Whereas in the first principle either hydrogen-bonded, supramolecular polymers^{5,9} or ionomers^{10,11} are responsible for a restorative force to effect multiple self-healing, reactive liquid polymeric components are embedded into separate capsules in the second concept, subsequently reacting via “click”-reactions after rupture of the capsule by mechanical deformation and destruction. The design of the polymers, their synthesis and the underlying autocatalytic effects to achieve sufficiently fast reactivity and thus self-healing properties are discussed.

1. INTRODUCTION, RESULTS and CONCLUSIONS

Critical for a practical application of self-healing polymers is the need to achieve multiple self-healing cycles thus enabling repeated healing after repeated mechanical deformation has occurred (see Figure 1). Thus the underlying crosslinking reactions should act repeatedly and reversibly, putting supramolecular interactions in the limelight of interest. The current paper concentrates on the use of supramolecular interactions such as ionomers¹⁰⁻¹² and hydrogen bonds^{9,13-15}, both linked to polymers, to achieve reversible self-healing under reasonable time scales. Critical for the design of such processes is a deeper understanding of association dynamics in the melt-state of such polymeric liquids^{9,13}, most of them in the rubbery or partially thermoplastic state. Focus of the current talk is directed towards poly(isobutylenes) as polymers displaying a high chain mobility and high individual segment-dynamics.

Together with crosslinking as well as post-crosslinking reactions and their associated network formation the thermomechanical and physicochemical properties are thus defined. Combined with conventional crosslinking reactions, such as the azide/alkyne-“click”-reaction (CuAAC¹⁶⁻²²) as one of the most prominent “click”-type reactions the kinetics of the CuAAC and the association dynamics of the supramolecular components are discussed, focussing on simple hydrogen bonding systems (such as diaminotriazine/thymine as well as more complex hydrogen bonds (such as the barbituric acid/Hamilton-receptor-moieties).²³⁻²⁵

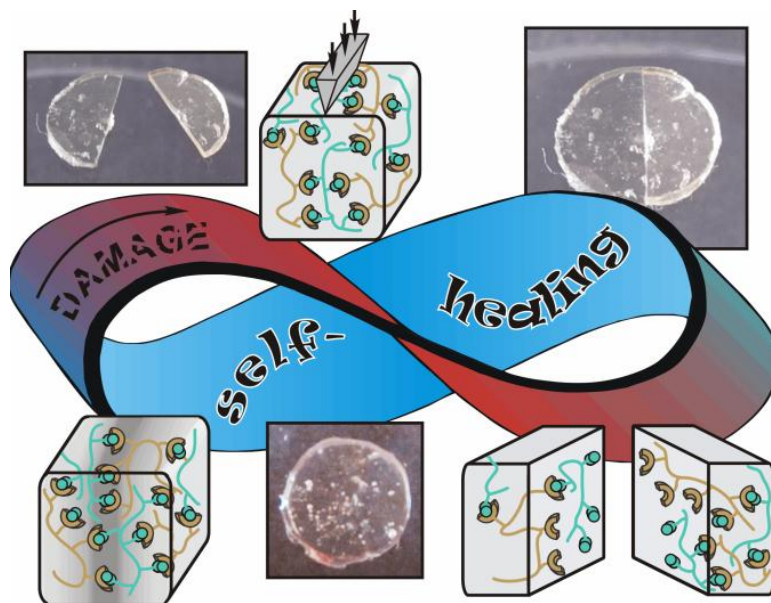


Figure 1: Multiple healing cycles of supramolecular polymers

ACKNOWLEDGEMENTS

We are grateful for the grant DFG BI 1337/8-1 (within the SPP 1568 “Design and Generic Principles of Self-Healing Materials”) and the EU-project IASS for financial support.

REFERENCES

- [1] Self-Healing Polymers. From Principles to Applications.; Binder*, W. H., Ed.; Wiley-VCH: Weinheim, 2013.
- [2] Herbst, F.; Binder*, W. H.: Self-healing polymers via supramolecular, hydrogen bonded networks. In Self Healing Polymers: from Principles to Application; Binder, W. H., Ed.: Weinheim, 2013; pp in press.
- [3] Döhler, D.; Michael, P.; Binder*, W. H.: Principles of Self Healing Polymers. In Self Healing Polymers: from Principle to Application; Binder, W. H., Ed.; Wiley VCH: Weinheim, 2013.
- [4] Herbst, F.; Döhler, D.; Michael, P.; Binder*, W. H.: Self-healing polymers via supramolecular forces. *Macromol. Rapid Commun.* in press 2013, marc.201200675
- [5] Herbst, F.; Seiffert, S.; Binder, W. H.: Dynamic supramolecular poly(isobutylene)s for self-healing materials. *Polymer Chemistry* 2012, 3, 3084-3092.
- [6] Schunack, M.; Gragert, M.; Döhler, D.; Michael, P.; Binder*, W. H.: Low-Temperature Cu(I)-Catalyzed “Click” Reactions for Self-Healing Polymers. *Macromol.Chem. Phys.* 2012, 213, 205-214.
- [7] Döhler, D.; Michael, P.; Binder*, W. H.: Autocatalysis in the Room Temperature Copper(I)-Catalyzed Alkyne–Azide “Click” Cycloaddition of Multivalent Poly(acrylate)s and Poly(isobutylene)s. *Macromolecules* 2012, 45, 3335-3345.
- [8] Gragert, M.; Schunack, M.; Binder*, W. H.: Azide/Alkyne-“Click”-Reactions of Encapsulated Reagents: Toward Self-Healing Materials. *Macromol. Rapid Commun.* 2011, 32, 419-425.
- [9] Hackethal, K.; Herbst, F.; Binder, W. H.: Synthesis and clustering of supramolecular “graft” polymers. *J. Polym. Sci., Part A: Polymer Chem.* 2012, 50, 4494-4506.

- [10] Zare, P.; Stojanovic, A.; Herbst, F.; Akbarzadeh, J.; Peterlik, H.; Binder*, W. H.: Hierarchically Nanostructured Polyisobutylene-Based Ionic Liquids. *Macromolecules* 2012, 45, 2074-2084.
- [11] Zare, P.; Mahrova, M.; Tojo, E.; Stojanovic, A.; Binder, W. H.: Ethylene glycol-based ionic liquids via azide/alkyne click chemistry. *J. Polym. Sci. Part A: Polymer Chemistry* 2013, 51, 190-202.
- [12] Pagano, F.; Gabler, C.; Zare, P.; Mahrova, M.; Dörr, N.; Bayon, R.; Fernandez, X.; Binder, W. H.; Hernaiz, M.; Tojo, E.; Igartua, A.: Dicationic ionic liquids as lubricants. *Proc. I. Mech. Eng., Part J: J. Engineering Tribology* 2012, 226, 952-964.
- [13] Herbst, F.; Schröter, K.; Gunkel, I.; Gröger, S.; Thurn-Albrecht, T.; Balbach, J.; Binder*, W. H.: Aggregation and chain dynamics in supramolecular polymers by dynamic rheology: cluster formation and self aggregation. *Macromolecules* 2010, 43, 10006–10016.
- [14] Binder, W.; Zirbs, R.: Supramolecular Polymers and Networks with Hydrogen Bonds in the Main- and Side-Chain. In *Adv. Polym. Sci.: "Hydrogen Bonded Polymers"*, 2007; pp 1-78.
- [15] Binder, W. H.: Polymeric Ordering by H-bonds. Mimicking Nature by Smart Building Blocks. *Monatsh. Chem. / Chemical Monthly* 2005, 136, 1-19.
- [16] Binder, W. H.; Sachsenhofer, R.: 'Click' Chemistry in Polymer and Materials Science. *Macromol. Rapid Commun.* 2007, 28, 15-54.
- [17] Binder, W. H.; Sachsenhofer, R.: 'Click' Chemistry in Polymer and Material Science: An Update. *Macromol. Rapid Commun.* 2008, 29, 952-981.
- [18] Binder*, W. H.; Herbst, F.: Click chemistry in polymer science. In *McGraw-Hill Yearbook of Science & Technology*; Blumel, D., Ed.; McGraw-Hill: New York, 2011; pp 46-49.
- [19] Binder, W. H.; Zirbs, R.: "'Click'-Chemistry in Macromolecular Synthesis. In *Encyclopedia of Polymer Science and Technology*; John Wiley & Sons, Inc, 2009; pp DOI: 10.1002/0471440264.pst565.
- [20] Binder, W. H.; Sachsenhofer, R.: "Click"-Chemistry in Polymer and Material Science: An Update. *Macromol. Rapid Commun.* 2008, 29, 952-981.
- [21] Binder, W. H.; Sachsenhofer, R.: "Click" Chemistry in Polymer and Materials Science. *Macromol. Rapid Commun.* 2007, 28, 15-54.
- [22] Binder, W. H.; Kluger, C.: Azide/alkyne-"click" reactions: applications in material science and organic synthesis. *Curr. Org. Chem.* 2007, 10, 1791.
- [23] Döhler, D.; Michael, P.; Binder, W. H.: Autocatalysis in the Room Temperature Copper(I)-Catalyzed Alkyne-Azide "Click" Cycloaddition of Multivalent Poly(acrylate)s and Poly(isobutylene)s. *Macromolecules* 2012, 45, 3335-3345.
- [24] Schunack, M.; Gragert, M.; Döhler, D.; Michael, P.; Binder, W. H.: Low-Temperature Cu(I)-Catalyzed "Click" Reactions for Self-Healing Polymers. *Macromol. Chem. Phys.* 2012, 213, 205-214.
- [25] Gragert, M.; Schunack, M.; Binder, W. H.: Azide/Alkyne-"Click"-Reactions of Encapsulated Reagents: Toward Self-Healing Materials. *Macromol. Rapid Commun.* 2011, 32, 419-425.

BINDING CRYSTALLINE SOLIDS AT LOW TEMPERATURES

Z. Chen ¹, Z. Xu ¹, G. Wang ¹, H. Li ², B. Chen ³, X. C. Zeng ² and L. Tan ¹

¹ *Department of Mechanical and Materials Engineering, University of Nebraska, Lincoln, NE, 68588 – e-mail: ltan4@unl.edu*

² *Department of Chemistry, University of Texas, San Antonio, TX, 78249*

³ *Department of Chemistry, University of Nebraska, Lincoln, NE, 68588*

Keywords: supramolecules, crystalline solids, metal-organic frameworks, self-healing

ABSTRACT

Crystalline solids are solid materials whose constituent atoms, molecules, or ions are arranged in a highly regulated fashion. Due to lack of rotational freedom in their stacking, they have been known as fragile materials. Even though some efforts have been dedicated to bind or mend defects/cracks in amorphous materials like concrete or polymers, welding or binding a crystalline solid at ambient or low temperature conditions is quite a challenging task. Mainly, low interface mobility from the atomic or ionic constituents frequently limits interface regroupings.

We recently found that one type of crystalline solid, dubbed metal-organic frameworks (MOFs), shows interfacial binding capability in their solid state. MOFs are molecularly engineered crystals that are mechanically rigid but structurally dynamic and reconfigurable. Unlike traditional studies on surface area and porous structures, our particular interest is placed on surface repairing or regrouping activities. For instance, when defects on bulk MOFs are mended using our process, the solids show a modulus leap from 4 to 12 GPa and hardness from 400 to 1000 MPa. When solids are made as polymer composite, open wounds can be healed at ambient conditions. Moreover, we found that low temperatures down to -56 °C did not appear to restrict this solid binding process, making it outstanding for low temperature healing or binding.

If our results are utilized for many other MOFs that are adopted as catalysts or hydrogen storage/separation materials, we expect their structure integrity can be kept after multiple cycles of packing or extensive uses. Furthermore, the knowledge gained will help people design future crystalline solids or ordered structures that can be assembled, repaired or healed in various engineering applications.

1. INTRODUCTION

Supramolecules are molecularly engineered materials. Rich selections of the molecular building blocks, tunable crystalline packing, easy-to-perform one-pot synthesis, and well-defined structures make them ideal candidates in learning bonding or healing process. It is hoped that, if the bonding mechanisms from these well-defined solids are thoroughly understood, we can engineer many traditional materials as dynamic systems for a variety of important applications, such as solid adhesion, self-healing, cold welding, and polymer blend or mixing. Our work suggests that filling crystalline gaps with small molecules can drive an interfacial

binding between solids. Sufficient mobility from these fillers allows the process to happen at low temperatures.

2. MATERIALS

Cu-MOFs powders and membranes: The crystalline powders were prepared by mechanically crushing as-synthesized Cu-MOFs crystals using a mortar and pestle. The Cu-MOFs membrane (>15 μm in thickness) for nanoindentation tests was obtained by drop-casting a 2.0 wt% water suspension of Cu-MOFs powders onto a piece of Si wafer. The Cu-MOFs membrane ($\sim 25 \mu\text{m}$ in thickness) for three-point bending test, on the other hand, was prepared by drop-casting 5.0 wt% Cu-MOFs powder suspension on a Teflon film. After drying, a freestanding membrane was harvested directly from the Teflon substrate.

Binding Cu-MOFs membranes: The membrane for nanoindentation tests was obtained after dropping 0.2 mL of DEF (>99.0%, TCI America) over crushed MOF powders on glass and let it dry in air. The binding of membrane (freestanding) for three-point bending test was operated by soaking the freestanding piece in DEF for 12 hours.

Binding Cu-MOFs/PDMS composite: Bubble-free fresh PDMS precursor was casted atop a polycarbonate film to form a thin layer with a thickness of 1 mm. Crushed Cu-MOFs powders were then laid on this uncured PDMS surface, letting the solid sink to the bottom of the viscous liquid. Final Cu-MOFs/PDMS composite was received after annealing the mixture in the convection oven at 100 $^{\circ}\text{C}$ for 1 hour.

3. METHODS

Nanoindentation tests were performed using Hystron Bio-Ubi. Quasi-static “trapezoidal” load function tests were selected, with a 5-s loading, 2-s holding, and a final 5-s unloading. Maximum forces were set at 50 or 100 μN . The tip used is a Berkovich tip with a tip radius of 70 nm. In three-point bending tests, samples were placed between two glass slides with a spacing of 3 mm. Then carefully weighted small Si pieces were gradually loaded on top of each sample to investigate the maximum deflection before a failure.

4. RESULTS

Interfacial binding of MOFs is realized at both ambient and low temperature conditions. Taking Cu-MOFs ($\text{Cu}(\text{FMA})(4,4'\text{-Bpe})_{0.5}\cdot 0.5\text{H}_2\text{O}$) as an example. Figure 1A demonstrates how to bind a broken elastic membrane via crushed powders of these MOFs. When the elastic membrane was cut with a blade (Figure 1A-left), the open wound was briefly treated with inert liquid, i.e., diethylformamide (DEF, $(\text{C}_2\text{H}_5)_2\text{NCOH}$). Shortly after, the membrane recovered most of its bendability in ambient conditions (Figure 1A-right). Another freestanding leaf-like structure molded from MOF powders (Figure 1B) was even capable of withholding a high temperature up to 200 $^{\circ}\text{C}$ without a major breakdown. Both microscopic (nanoindentation) and macroscopic experiments (three-point bending) were utilized to evaluate the membrane before and after the DEF treatment (Figure 1C). As the nanoindentation load increased, the physically aggregated membrane behaved rather fragile (upper inset), where failure marks on the loading curve suggest easy and permanent deformations. In contrast, the treated membrane easily deflected with a smooth

loading curve by retaining little residual strain. If we pay closer attention to the crushed pieces of these crystals, they can be loosely dispersed in water with their morphologies remaining intact for extended period of time (Figure 1D). Immediately upon the addition of DEF, dispersed solids bundled together by forming network-like, instead of dense or isolated aggregates, implying certain anisotropy of our process.

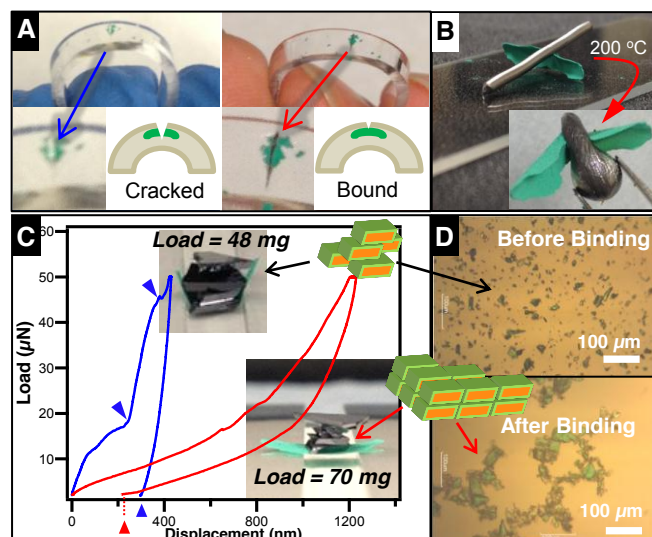


Figure 1: Binding crystalline solids as ambient conditions.

Our AFM scanning on crushed crystals revealed layered structures with individual layer thickness of 0.77 nm, closely matching 0.80 nm of lattice spacing for (200)s (Figure 2A and B). The dynamic changes on this (200) were caught after soaking the sample in water, supported by *in situ* AFM imaging at different times (Figure 2C and D). Right after water covered the crystal surface, many small holes appeared; after 17 minutes, they became deeper and larger (marked by the red ovals and yellow rectangles in Figure 2D), indicating a continuous dissolution of substances from the surfaces into the aqueous medium. When the water-soluble substance was extracted, ¹H-NMR confirmed the existence of fumarate (s, d = 6.7 ppm) as shown in Figure 2E. Collectively, both the AFM and NMR studies have pointed to one fact that the water-soluble fumaric acid or fumarate moieties roll off from (200) surfaces, destabilizing the Cu-MOFs crystal in a continuous manner. A brief comparison in diffraction patterns of crushed solids before and after DEF treatment suggests peak sharpening at (200)s only (Figure 2F). Since the peak intensity or sharpness is indicative to the perfectness of the inter-planar stacking, a sharper (200) peak unambiguously indicates a promoted crystal alignment and structure perfection along [200] direction.

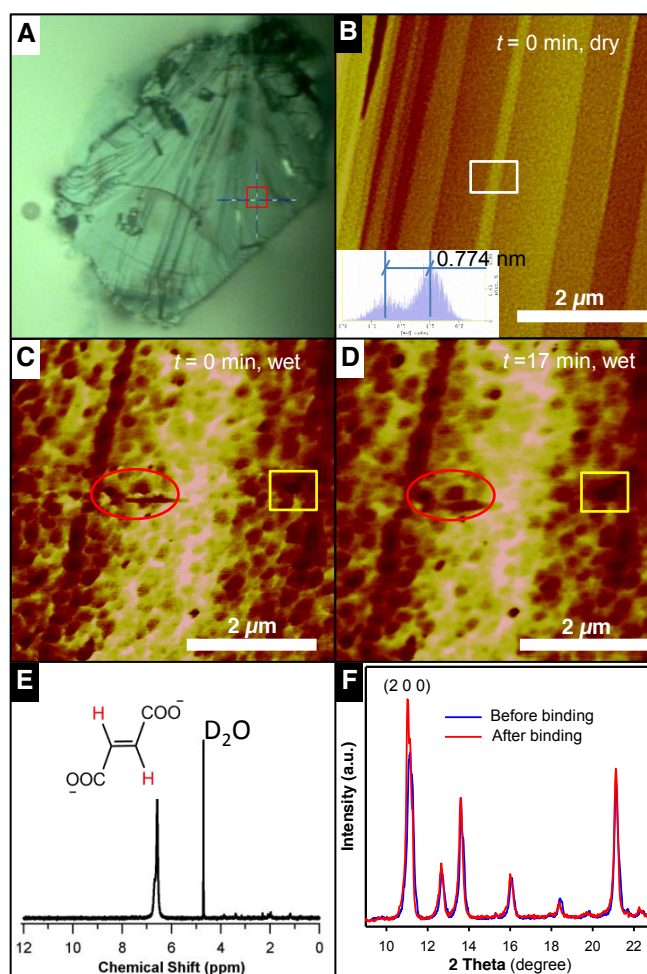


Figure 2: Dynamic properties of the crushed crystalline solids.

If crushed solids or powders can bind, this process might even repair defects on as-synthesized bulk crystals (Figure 3). Unlike mechanical tests for crushed membranes in Figure 1C, neither of our samples here showed permanent deformation. Rather smooth curves were observed in both loading and unloading regions, where the modulus jumped from 4 to 12 GPa and hardness from 400 to 1000 MPa. Since the statistical plot in Figure 3B suggests this as a general trend, we tend to believe this binding process once again is closely resulted from structure transition on surfaces. As revealed in Figure 3C, before the interfacial binding, the Cu-MOFs surface was composed of many small grains with an average size of 10 nm, after the binding the average diameter increased drastically to 30 nm. The XRD patterns (Figure 3D) before and after this transition suggest these growths occur mostly in (200) and (002) planes, where the peak sharpening follow a similar trend as that in the powder case. When crystal grain size increases, the surface area and the surface defect density decrease, rendering less scattering in measurement (Figure 3B, upper corner) and a much-enhanced mechanical performance. We also soaked freshly-made bulk crystals of Cu-MOFs in cold-baths of DEF at various low temperatures (-20, -41, and -56 °C). Average grain size has increased from 15 to 25 nm, accompanied by nearly doubled mechanical properties (Figure 3E). In comparison, soaking at a slight higher temperature of either -20 or -41 °C has tripled the hardness and modulus. While the latter ones are not hugely different from those obtained in the ambient temperature, substantial viscosity increase in DEF at -56 °C

has limited the diffusion of fumarate for reattachment of surface dangling bonds. Nonetheless, these experiments suggest that low temperatures do not restrict the binding between crystalline gaps.

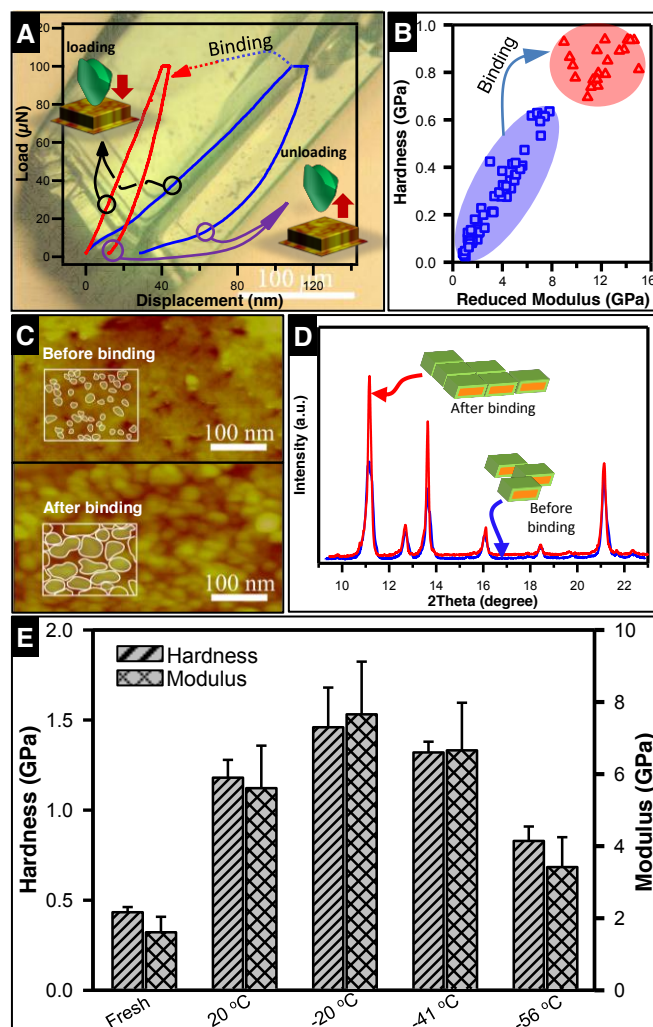


Figure 3: Bulk crystals can heal at ambient and low temperatures.

5. CONCLUSIONS

Crystals of metal-organic frameworks (MOFs) can be mechanically cleaved to reveal defects or dangling bonds, which can be further utilized towards binding at ambient and low temperature conditions. After DEF treatment, solid membranes exhibit greater mechanical resistance, which can potentially be molded into freestanding 3D objects or mend a broken elastic membrane.

ACKNOWLEDGEMENTS

The authors gratefully acknowledge the financial support from the National Science Foundation (CMMI 1068952), Nebraska Center for Energy Science Research, and Layman New Directions (UNL).

METALLOPOLYMERS AS SELF-HEALING MATERIALS

S. Bode,^{1,2} B. Sandmann,^{1,2} **M. D. Hager**,^{1,2} U. S. Schubert^{1,2}

¹ *Laboratory of Organic and Macromolecular Chemistry (IOMC), Friedrich Schiller University Jena, Humboldtstr. 10, 07743 Jena (Germany), e-mail: ulrich.schubert@uni-jena.de; martin.hager@uni-jena.de*

² *Jena Center for Soft Matter (JCSM), Friedrich Schiller University Jena, Philosophenweg 7, 07743 Jena (Germany)*

Keywords: Self-healing supramolecular polymers, metallopolymers, self-healing polymers, ionic interactions

ABSTRACT

Metallopolymers represent an interesting class of supramolecular polymers. Their properties can be tuned by the selection of the attached/incorporated ligand as well as the choice of the corresponding metal ion.[1] In this manner, also reversible interactions, *i.e.* on the one side undirected ionic interactions between positively charged metal complexes and negatively charged counterions as well as on the other side directed ligand-metal interactions can be introduced. These interactions are the basis for the introduction of self-healing properties, comparable to the natural archetype (reversible metal complexes can be found within mussel byssus threads).[2] Different methacrylate-based polymers containing ligands (*i.e.* terpyridine) in the sidechain have been synthesized. These materials have been used for the fabrication of cross-linked metallopolymer networks. The influence of the comonomers, the binding ligand as well as the metal ion on the resulting cross-linked polymer films has been investigated in detail. Additionally the influence of the counter ion on the polymeric films has been studied. The self-healing behavior of these materials was investigated. Lastly, the basic mechanisms behind the self-healing processes within these metallopolymers will be discussed in detail.

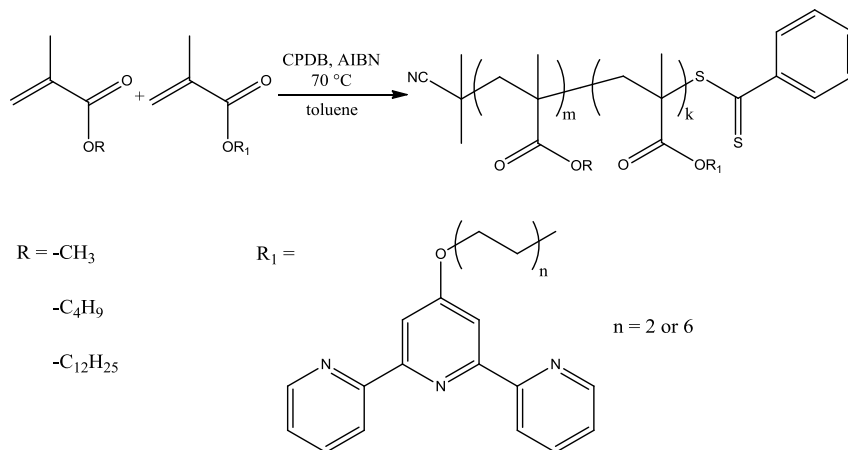
1. INTRODUCTION

Metallopolymers combine typical properties of metals (*e.g.*, conductivity) as well as polymeric properties (*e.g.*, film formation). The resulting properties can be tuned by the choice of the ligands as well as the corresponding metal ions; the nature of the resulting metal complexes influences the polymer properties. The binding strength of the metal complexes can be adjusted: complexes with binding strengths comparable to covalent bonds as well as dynamic and weak complexes can be obtained.

In the context of self-healing materials weaker and more dynamic complexes are preferable. Therefore the required mobility for the self-healing process can be induced easier, *e.g.*, by a decomplexation/rearrangement of the metal complexes.[3] Different copolymers containing terpyridine as binding ligand were synthesized and subsequently crosslinked by different metal ions.[4] The properties of the resulting crosslinked polymer networks have been investigated.

2. MATERIALS AND METHODS

A library of different copolymers (terpyridine containing polymers as well as alkylmethacrylates comonomers) was synthesized using the reversible addition/fragmentation chain transfer (RAFT) polymerization (Scheme 1).



Scheme 1: Schematic representation of the synthesis of the polymer library.

The resulting polymers were characterized by ¹H NMR spectroscopy (composition, ratio of both functional groups), SEC (molar mass as well as molar mass distribution), MALDI-TOF MS (molar mass), TGA and DSC measurements (thermal properties). Moreover the polymers were crosslinked with different metal ions (e.g., iron(II), cadmium (II)). The mechanical properties as well as the self-healing behavior of the polymers were investigated.

3. RESULTS

The synthesized polymers (methyl methacrylate, butyl methacrylate, lauryl methacrylate) feature – as expected – different glass transition temperatures. Therefore the resulting copolymer networks will feature different mobility, which will influence their healing behavior. Subsequently, the linear, soluble polymers were crosslinked by the addition of different metal ions (Fe(II), Cd(II)). Additionally, the counterions have been varied in case of the cadmium(II).

The self-healing of the hard crosslinked films was investigated by an optical microscope. The healing of an iron(II) crosslinked polymer is depicted in Figure 1. A temperature of 100 °C was required for the healing process (if lauryl methacrylate was used as a comonomer). This temperature could only be reduced in the case of cadmium acetate as crosslinking metal salt. The resulting networks could be healed at 80 °C.

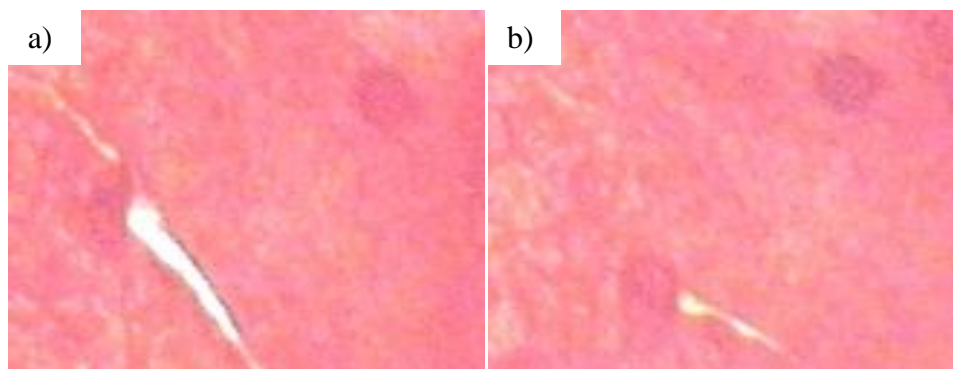


Figure 1: Self-healing of a scratched film (based on iron(II)) a) Scratch and b) healing after 16 h at 100 °C.

The healing of these metallopolymer networks is presumably based on two contributions, which depend on the nature of the metal ion (Figure 2). If weak and dynamic metal complexes are applied, decomplexation and rearrangement of the complexes can induce the required mobility. Additionally, the ionic metal complexes can induce a formation of ionic clusters. The rearrangement of these clusters can also induce the required mobility (also without the opening of the complexes).

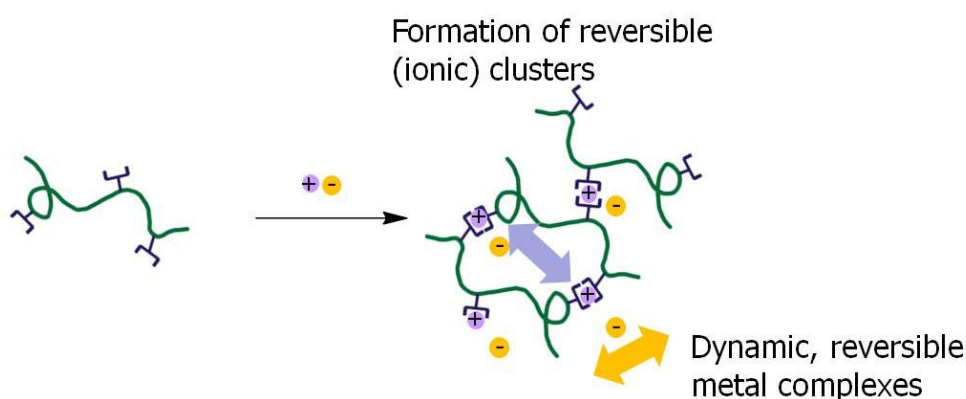


Figure 2: Schematic representation of the self-healing metallopolymer networks.

The healing of the iron(II)-based polymer networks is presumably based on the presence of the described ionic clusters. In contrast, polymer networks based on cadmium(II) acetate feature also dynamic metal complexes due to the acetate counterion, which can lead to bridged metal complexes.

4. CONCLUSIONS

Metallopolymers are interesting candidates for self-healing polymers. The combination of the right ligands with the corresponding counterions can lead to an efficient self-healing of these systems. Both, the cation as well as the anion, have a great influence on the self-healing. The further elucidation of the healing mechanisms within metallopolymers can be used for the design of better self-healing polymers.

ACKNOWLEDGEMENTS

The authors thank the Deutsche Forschungsgemeinschaft (DFG, SPP 1568), the Fond chemischer Industrie (scholarship for S.B.) and the DPI (technology area HTE) for financial support.

REFERENCES

- [1] G. R. Whittell, M. D. Hager, U. S. Schubert, I. Manners, Functional soft materials from metallopolymers and metallosupramolecular polymers, *Nature Materials* 10 (2011) 176-188.
- [2] M. J. Harrington, A. Masic, N. Holten-Andersen, J. H. Waite, P. Fratzl, Iron-clad fibers: A metal-based biological strategy for hard flexible coatings, *Science* 328 (2010), 216-220.
- [3] M. D. Hager, P. Greil, C. Leyens, S. van der Zwaag, U. S. Schubert, Self-healing materials, *Advanced Materials* 22 (2010), 5424-5430.
- [4] S. Bode, L. Zedler, F. H. Schacher, B. Dietzek, M. Schmitt, J. Popp, M. D. Hager, U. S. Schubert, Self-healing polymer coatings based on crosslinked metallosupramolecular copolymers, *Advanced Materials* (2013) DOI: 10.1002/adma.201203865.

SESSION 12 – SELF-HEALING MATERIALS FOR FUNCTIONAL APPLICATIONS

DISSIPATIVE SELF-ASSEMBLY: A NOVEL SELF-HEALING MECHANISM FOR FUNCTIONAL MATERIALS

G. J. M. Koper¹, J. Boekhoven^{1,2}, W.E. Hendriksen¹, R. Eelkema¹, J.H. van Esch¹

¹ Department of Chemical Engineering, TU-Delft, Julianalaan 136, 2628 BL Delft, the Netherlands – e-mail: g.j.m.koper@tudelft.nl

² Currently at: Inst. for BioNanotechnology in Medicine, Northwestern University, Chicago, IL, USA.

Keywords: self-assembly, dissipation, self-healing, functional materials

ABSTRACT

Self-assembled systems formed of micelles or vesicles have frequently been discussed as model systems for self-healing materials because their structure is dictated by thermodynamics and hence they quickly restore upon perturbation. In this aspect, they mimic many natural systems such as biological cells. However, in contrast to most synthetic self-assembling systems the natural systems are not equilibrium processes. Attention is therefore now focusing on dissipative self-assembling systems where energy input is required to sustain the self-assembled state. These systems have the potential to adapt themselves and enter into different self-assembled states depending on the rates of environmental reactions whereas their equilibrium counterparts can only assemble or disassemble depending on the environmental equilibrium condition.

Recently, we have constructed some dissipative self-assembling systems using chemical fuels and presently more examples are being worked on. During this presentation some important aspects of these systems will be discussed in relation to their capabilities of being self-healing.

1. INTRODUCTION

Many functional self-healing materials are synthesized by means of a self-assembly process. Examples are the self-healing rubber of Ludwik Leibler [1], the supramolecular polymers of Bert Meijer [2], the nanofiber forming peptide-amphiphiles of Sam Stupp [3], and the self-healing hydrogels of Takuzo Aida [4]. From a physical point of view, the linear self-assembly process of Stupp's peptide-amphiphiles is the simplest and we shall use it to illustrate some of the important aspects; a cartoon is given in Figure 1a. In addition, it also represents the simplest class of supramolecular polymerizations as reviewed by Alberto Ciferri [5].

The rate of formation of an aggregate of N monomers is given by

$$r_f = k_f x_1^N \quad (1)$$

where x_1 is the mole fraction of monomers and k_f the forward rate constant. The break-up rate of such an aggregate back into monomers is given by

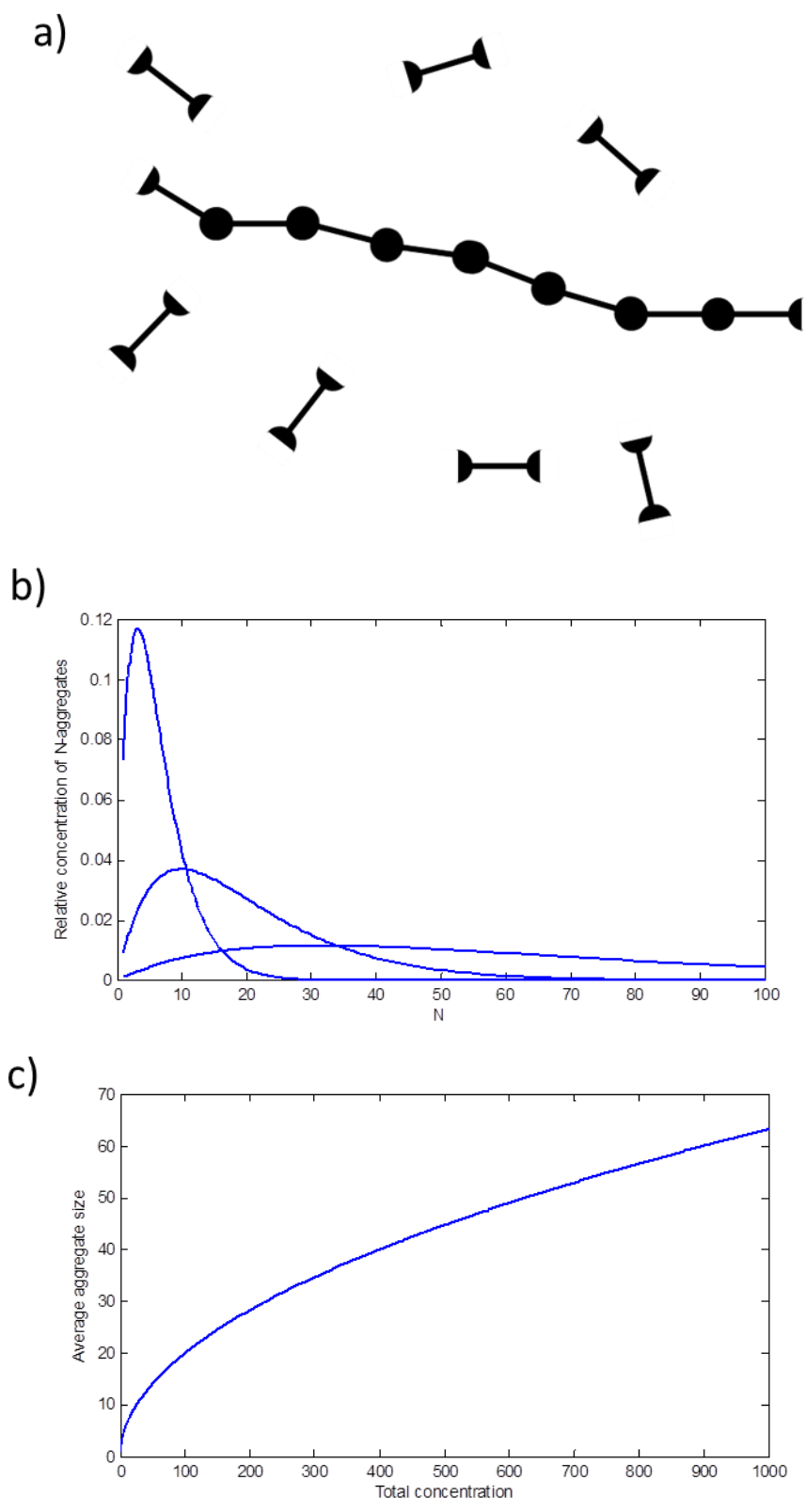


Figure 1: Linear self-assembly of units with binding sites on either side (a), size distribution for total monomer mole fractions 1, 10 and 100 times the cgc (b), and average size (c) as a function of total monomer mole fraction.

$$r_b = k_N \frac{x_N}{N} \quad (2)$$

where x_N is the mole fraction of monomers aggregated into aggregates consisting of N monomers, so called N -aggregates. When we assume equilibrium, the associated equilibrium constant K – per monomer – is defined as

$$K^N = \frac{k_N}{k_1} \quad (3)$$

With a total monomer mole fraction x_t one finds the characteristic, exponentially-tailed size distribution, see Figure 1b, as predicted using the simple mean field model by Cates and Candau [6] with an average degree of polymerization, see Figure 1c, scaling as [7]

$$\langle N \rangle \propto x_t^{1/2} \quad (4)$$

The network structures of Leibler [1] are from a physical point of view much more complex, see Figure 2, as they do not only consist of di-functional units, that are responsible for linear aggregation, but also of tri-functional units with which branching junctions are formed. With these building blocks the resulting structure becomes cross-linked as sketched in Figure 2. A geometrical analysis, not surprisingly, yields a length distribution of the mesh size L that is again exponentially tailed and an average mesh size that scales also algebraically with total mole fraction albeit with an exponent of 0.56 which is slightly larger than the 0.5 for the above described linear case [8]. The case of threefold junctions – as present in Leibler's system – is interesting because the predictions both by Drye and Cates [8] and later by Zilman and Safran [9] indicate the possibility of a phase transition. Experimentally it is indeed found, that crystallization is hampering the synthesis of such systems [1]. Aida's system of clay particles that are interconnected by dendritic binders are – from a physical point of view – a variation of Leibler's system where the average functionality of the branch points is typically larger than 3 and hence the behaviour is less interesting as no phase transitions are to be expected.

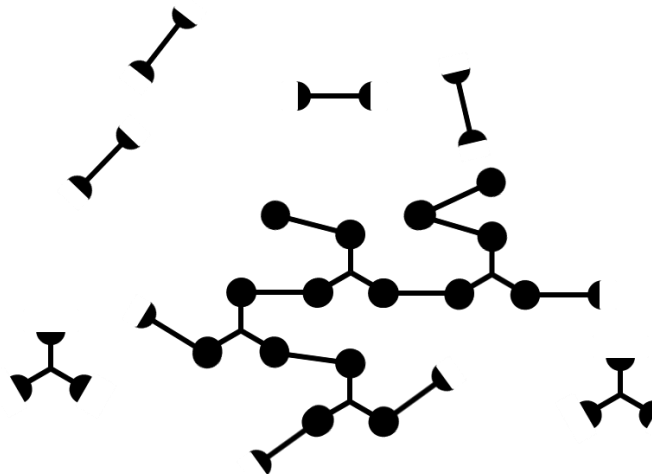


Figure 2: Network assembled from di-functional and tri-functional units.

A crucial aspect of the above described processes is that it is in equilibrium which means that the forward rate r_f (eq.(1)) and the backward rate r_b (eq.(2)) are balanced and this indeed is the condition from which the relation for the equilibrium constant emerges, see eq.(3). It is important to realize that this condition is to be taken literally, meaning that indeed there is a constant exchange of monomers between the aggregates themselves and with their environment where there are only isolated monomers. It is generally accepted, that there are two time scales associated with these aggregates. One is associated with the exchange of single monomers with the aggregates. It is relatively short and fully determined by the diffusion coefficient of the monomer. The slow time scale is associated with the formation process of one complete aggregate and roughly equal to the fast time scale times the average aggregation number. Hence, self-assembly processes are dynamic by nature and not static as sometimes suggested [10]. This dynamic aspect is what makes self-assembling systems an interesting option for self-healing materials. The only disadvantage is that when the system consists of more bulky monomers, the time scales become inherently longer. Therefore, even though self-assembling systems can be tuned by environmental conditions, the response times are relatively long to the extent that some systems do not reach equilibrium at all.

2. A SYNTHETIC DISSIPATIVE SELF-ASSEMBLING SYSTEM

The equilibrium self-assembling systems described above are much less dynamic than their natural counterparts and it is interesting to see why this actually is the case. It is clear that the natural systems are not in equilibrium and require transfer of energy to operate: in biological systems it is often the ATP hydrolysis that conveys the necessary energy [11]. Examples from Nature are networks built from for instance microtubules or compartments such as mitochondria.

To investigate this idea, we chose a synthetic system that has recently been put forward by our group [12,13], see Figure 3. The self-assembly utilizes a low molecular mass hydrogelator, dibenzoyl-(L)-cystine (DBC) in aqueous solution at a pH above its pKa value of 4.5. Under these conditions DBC remains isotropically in solution. Methylation of one of the carboxylic groups results in the formation of fibres and this process can be detected mechanically and optically, using for instance rheometry and turbidity measurements respectively. Crucially, the methylated DBC molecules are chemically unstable and hydrolyse at a pH-dependent rate. Hence, by tuning the pH and the methylation reaction rate the self-assembly dynamics of the gel can be controlled. The methylation reaction is not spontaneous and therefore it is coupled to a reaction that is spontaneous which in the present case is the conversion of dimethyl sulphate (DMS) into monomethyl sulphate (MMS⁻). In actual fact, also the hydrolysis reaction is a coupled reaction that turns the methylated DBC back into DBC itself, see Figure 3a.

Let us now describe the phenomenology of dissipative self-assembly for this system. As soon as fuel is added to the system and the methylation reaction starts, the concentration of self-assembling monomers, the methylated DBC molecules, increases, see Figure 3b. When the critical gelation concentration (c_{gc}) is exceeded the storage modulus starts to increase, see Figure 3c, which indicates that gel formation has started. As soon as the total concentration of monomers – free as well as aggregated – increases, their destruction also sets in by means of the hydrolysis

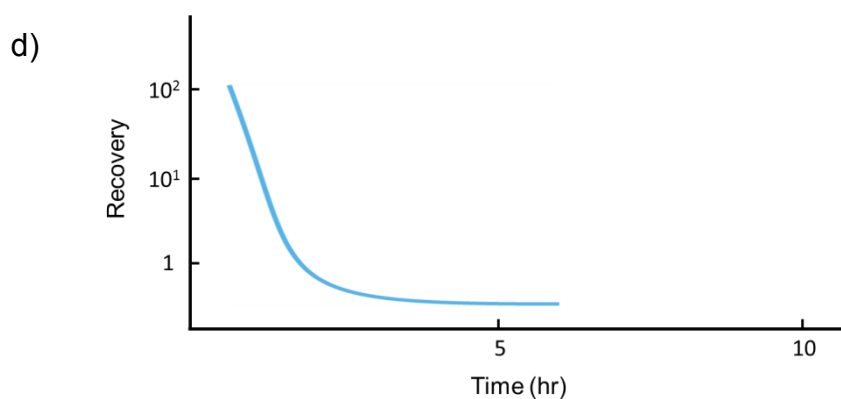
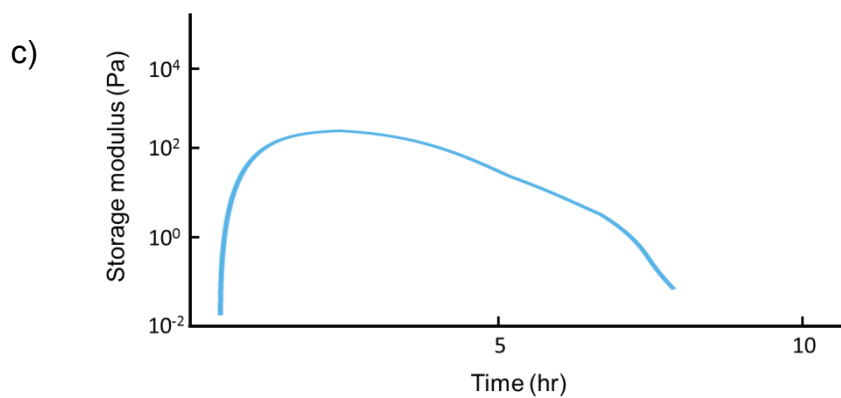
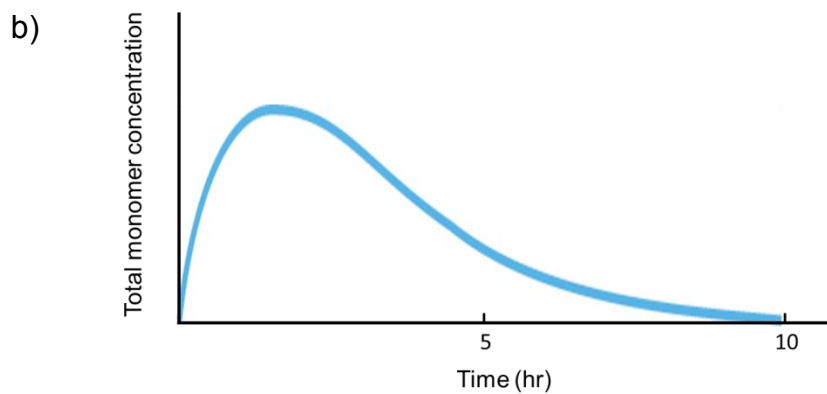
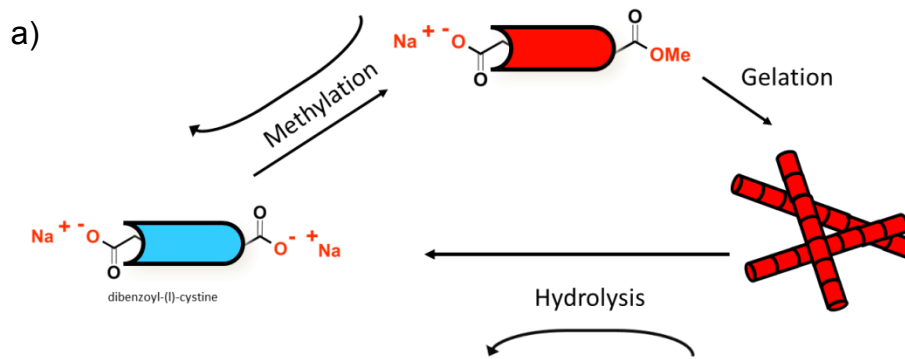


Figure 3: Dissipative self-assembly, schematic of the process (a), total concentration of monomer, the methylated DBC (b), storage modulus of the gelled system (c), and relative recovery after perturbation (d).

reaction. Initially, the formation rate exceeds the destruction rate and the monomer concentration increases resulting in an increasing storage modulus. At the end of the experiment, the destruction rate dominates and the gel breaks down leading to a decreasing storage modulus. In the intermediate regime, where formation and destruction roughly balance, the storage modulus remains reasonably constant. A closer look at the dynamical behaviour of this system reveals, that the maximum in the total monomer concentration occurs before the maximum storage modulus is reached. This most likely is due to the additional time scale associated with fibre formation and break-down and of course the strongly non-linear dependence of gel strength on fibre concentration.

The most interesting question is now, whether this system possesses self-healing properties, that is how does the gel behave after mechanically induced perturbations? Typically, gels formed by self-assembly of low-molecular-mass gelling agents are not capable of self-healing to their original strength, mainly because of the slow assembly and disassembly dynamics of the system at ambient conditions, although exceptions are described [4]. When a gel is subjected to mechanical perturbations the long fibres break into smaller fragments and because of the slow assembly dynamics the fibres are not able to re-assemble and regenerate the former gel properties. The continuous formation and destruction of molecular building blocks in the present out-of-equilibrium system is expected to alleviate this.

In Figure 3d the relative recovery, the ratio of the maximum storage modulus after and before perturbation, of the gels is plotted versus time. As expected, the recovery is very weak in the final regime where break-down of the monomers dominates. In the intermediate regime, where the formation and destruction more or less balance, the recovery is reasonable. The recovery is very good when the formation rate of monomers is dominating.

3. DISCUSSION

The process described here is a non-equilibrium processes in the thermodynamic sense that the associated Gibbs energy change is negative, it runs spontaneously, and that if this Gibbs energy change is not converted to work it is dissipated by the environment in the form of heat [14]. It is therefore that the non-equilibrium form of self-assembly as discussed above is called dissipative self-assembly even though it would in principle still be possible to convert the Gibbs energy change into work which is not immediately lost. In a recent study we evaluated the amount of work that is lost in a dissipative self-assembling system. For the system presented above, the lost work is largely due to the driving reactions, the methylation and the hydrolysis, and amounts to 5.5 W/L solution [15].

Despite the promising result, there are still quite some questions one may ask with regards to this system. In particular, the formation and break-down of the aggregates in relation to the formation and destruction of the monomers is an interesting issue that warrants further investigation. The relation between the structure of the system and its function, its mechanical response, is a classical one. The fact that the structure of the system is dynamical might actually be beneficial in the sense that it allows for a much more detailed study of the behaviour as one may change the structure at experimental time scales.

Dissipative self-assembling systems may find their own fields of application. One of them is surely where long-lived stable moulds are needed. During their life time, the moulds need to be self-healing, but after use they should be easy to discard. In fact, all applications where the constituting materials need to be removed easily after use come within reach which provides a great potential for all applications that need to be running in an environmentally friendly manner.

Other potential applications – not necessarily self-healing – become clear when it is realized that the monomer destruction reaction need not run simultaneously with the monomer destruction reaction. In other words, with a running formation reaction one creates a self-assembling system that remains in place until the destruction reaction is run. Apart from the fact, that the system then acts as an energy store such as a battery where this energy can be reclaimed when the destruction reaction for instance is done electrochemically.

ACKNOWLEDGEMENTS

The authors acknowledge the Netherlands Organisation for Scientific Research (NWO) for financial support.

REFERENCES

- [1] P. Cordier, F. Tournilhac, C. Soulié-Ziakovic, L. Leibler, Self-healing and thermoreversible rubber from supramolecular assembly, *Nature* 451 (2008) 977-980.
- [2] L. Brunsveld, B.J.B. Folmer, E.W. Meijer, R.P. Sijbesma, *Supramolecular Polymers*, *Chem. Rev.* 101 (2001) 4071-4097.
- [3] J.D. Hartgerink, E. Beniash, S.I. Stupp, Self-assembly and mineralization of peptide-amphiphile nanofibers, *Science* 294 (2001) 1684-1688.
- [4] Q. Wang, J.L. Mynar, M. Yoshida, E. Lee, M. Lee, K. Okuro, K. Kinbara, T. Aida, High-water-content mouldable hydrogels by mixing clay and a dendritic molecular binder, *Nature* 463 (2010) 339-343.
- [5] A. Ciferri, *Supramolecular polymerizations*, *Macromol. Rapid Commun.* 23 (2002) 511-529.
- [6] M.E. Cates, S.J. Candau, Statics and dynamics of worm-like surfactant micelles, *J Phys.: Condens. Matter* 2 (1990) 6869-6892.
- [7] J. Israelachvili, *Intermolecular and surface forces: revised third edition*, Academic Press, 2011.
- [8] T.J. Drye, M.E. Cates, Living networks: The role of cross-links in entangled surfactant solutions, *J. Chem. Phys.* 96 (1992) 1367-1375.
- [9] A.G. Zilman, S.A. Safran, Thermodynamics and structure of self-assembled networks, *Phys. Rev. E* 66 (2002) 051107.
- [10] G.M. Whitesides, B. Grzybowski, Self-assembly at all scales, *Science* 295 (2002) 2418-2421.
- [11] T. Hill, *Free energy transduction and biochemical cycle kinetics*, Dover Books on Chemistry Series, Dover Publications, 2004.
- [12] J. Boekhoven, A. M. Brizard, K. N. K. Kowligi, G. J. M. Koper, R. Eelkema, J. H. van Esch, Dissipative self-assembly of a molecular gelator by using a chemical fuel, *Angew. Chemie – Int. Ed.* 49 (2010) 4825-4828.

- [13] J. Boekhoven, Multicomponent and dissipative self-assembly approaches, Ph.D. thesis, Delft University of Technology, 2012.
- [14] A. Bejan, Advanced engineering thermodynamics, John Wiley & Sons, 2006.
- [15] G.J.M. Koper, J. Boekhoven, W.E. Hendriksen, J.H. van Esch, R. Eelkema, I. Pagonabarraga, J.M. Rubí, D. Bedeaux, The lost work in dissipative self-assembly, to appear in Int. J. of Appl. Therm.

SELF-HEALING SHORT-CIRCUITS IN ORGANIC LIGHT-EMITTING DIODES AND SOLAR CELLS

A.J. Oostra¹, K.H.W. van den Bos¹, J. J. Michels² and P.W.M. Blom^{1,3}

¹ Molecular Electronics, Zernike Institute for Advanced Materials, University of Groningen, Nijenborgh 4, 9747AG Groningen, The Netherlands – e-mail: a.j.oostra@rug.nl; karelvdbos@gmail.com; p.w.m.blom@rug.nl

² Holst Centre, High Tech Campus 31, 5656AE Eindhoven, The Netherlands – e-mail: jasper.michels@tno.nl

³ Max Planck Institute for Polymer Research, Ackermannweg 10, 55128 Mainz, Germany – e-mail: blom@mpip-mainz.mpg.de

Keywords: healing, pedot:pss, light-emitting diode, oxidant

ABSTRACT

Organic materials open the way for large-scale applications of Organic Light-Emitting Diodes (OLED) and solar cells (OPV). These materials can be large-scale processed using printing and coating on rigid and flexible substrates. The resulting devices can therefore be fabricated at low cost for various applications.

Production yields suffer, however, from particles which, during processing, become entrapped within the organic multi-layer stack. If these particles are large enough the organic anode is not entirely covered with semiconductor, which may cause a short-circuit since the organic anode, *i.e.* poly(3,4-ethylenedioxythiophene):poly(styrene sulfonate) (PEDOT/PSS), will be in direct contact with the evaporated cathode.

A healing procedure may be helpful here: By treating OLED or OPV device precursors with an oxidizer we may be able to reduce the occurrence of short-circuits in the final device. The purpose of such a treatment is to locally cancel the conductivity of the PEDOT:PSS by oxidation of the electronically conjugated backbone. Subsequent evaporation of the cathode will then no longer lead to short circuits.

In this contribution we present the effect of the treatment with aqueous oxidizer solution (*i.e.* NaClO_(aq)) on various physical properties of highly conductive PEDOT:PSS layers. Layer thickness and conductivity have shown to significantly decrease upon treatment at rates that show a relation with treatment time and NaClO concentration. Interestingly, differences in the trends are observed. The thickness of the PEDOT:PSS follows an exponential decay towards a residual. The decay rate of this trend is proportional to NaClO concentration. In contrast, the conductivity follows a steady decrease until a relatively sudden breakdown occurs. The mechanisms explaining these trends will be highlighted, together with an outlook towards application of the methodology to full device structures.

1. INTRODUCTION

Poly(3,4-ethylenedioxythiophene) (PEDOT), processed as aqueous dispersion, stabilized by poly(styrenesulfonate) (PSS), is the most widely applied transparent organic semiconductor in organic electronics applications, such as organic light emitting diodes (OLEDs) and photovoltaic cells (OPV). Incomplete coverage of the highly conducting PEDOT:PSS anode in organic light-emitting diodes and solar cells is an important manufacturing issue as it induces current leakage paths which reduce both lifetime and efficiency of the fabricated devices. This incomplete coverage of the anode stems from different obstacles, such as, but not limited to, incomplete wetting during printing, or by shadow-effects caused by minor particles entrapped within the organic multi-layer stack. Limiting these problems is not straight-forward, and requires an innovative approach which can eliminate the short-circuits originating from the uncovered PEDOT:PSS, independent of the original manufacturing issue which caused it. One approach is to considerably lower the conductivity of uncovered PEDOT:PSS. This can conveniently be achieved by treating the layer with an oxidizing solution, such as aqueous hypochlorite. In this work the effect of hypochlorite treatment on the layer thickness and conductivity of a state-of-the-art highly conductive (HC) PEDOT:PSS is investigated as a function of exposure time and hypochlorite concentration. A comparison is made between the timescales of loss in thickness and conductivity, while the mechanistic aspects of conductivity disruption are studied within a theoretical framework.

2. MATERIALS

Dispersions of HC PEDOT:PSS containing 1% of an aqueous solution of a polymeric adhesion promoter were supplied by AGFA Gevaert (Mortsel, Belgium). $\text{NaClO}_{(\text{aq})}$ solution was purchased from Sigma-Aldrich and diluted with de-ionized water to concentrations in the range 0.0025% - 5% by weight.

3. METHODS

Treatment with $\text{NaClO}_{(\text{aq})}$ occurred by fully submerging the HC PEDOT:PSS layers in the $\text{NaClO}_{(\text{aq})}$ solutions for durations ranging from zero seconds to 24 hours. The samples were rinsed with de-ionized water for 5 seconds in order to remove excess NaClO from the surface of the layers. In order to measure in-plane conductivity of the treated HC PEDOT:PSS layers five sets of two gold contacts were evaporated on top of the treated and dried HC PEDOT:PSS layer, sufficiently remote from the edges of the substrate. I-V curves were measured using a Keithley 4200 SCS. The thickness of the layers, averaged over at least five different locations, was measured with a Veeco Dektak 6M stylus profilometer.

4. RESULTS

The thickness of the HC PEDOT:PSS layers was found to decrease exponentially with exposure time to $\text{NaClO}_{(\text{aq})}$ to a final residual value of at least ~75% of the initial thickness, the decay rate being a function of NaClO concentration. Even after prolonged treatment (*e.g.* 24 hour treatment in 0.01% $\text{NaClO}_{(\text{aq})}$) the thickness did not decrease beyond this limiting value. The experimental results, together with empirical fits to monoexponential functions are shown in Figure 1. Interestingly, no (significant)

decrease in layer thickness was observed upon treatment with pure water (dark blue symbols in Figure 1).

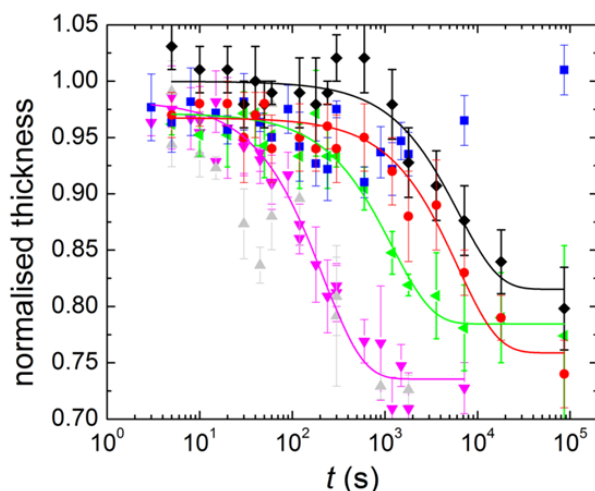


Figure 1: Thickness of HC PEDOT:PSS layers plotted as function of immersion time in $\text{NaClO}_{(\text{aq})}$ solution for various hypochlorite concentrations; light grey: 5 wt%, magenta: 0.5 wt%, green: 0.05 wt%, red: 0.01 wt%, black: 0.005 wt%, blue: 0 wt%; solid lines represent fits to a mono-exponential functions.

The effect of NaClO concentration on the conductivity of the HC PEDOT:PSS* layer is plotted in Figure 2a as a function of exposure time. Similar to the effect on layer thickness, no change in conductivity was observed upon treatment with pure water (blue points). As expected, a pronounced decrease in conductivity was observed when NaClO is present in solution. At sufficiently long treatment times the conductivity eventually dropped below the sensitivity limit of the measurement equipment. Plotting the thickness and conductivity curves corresponding to treatment with 0.01% $\text{NaClO}_{(\text{aq})}$ in the same graph (Figure 2b) shows that the conductivity can be lowered substantially without drastically influencing the layer thickness. Comparison of thickness and conductivity as a function of time also leads to the conclusion that a residual layer consisting of an electrically insulating material remains on the substrate upon treatment of HC PEDOT:PSS with $\text{NaClO}_{(\text{aq})}$.

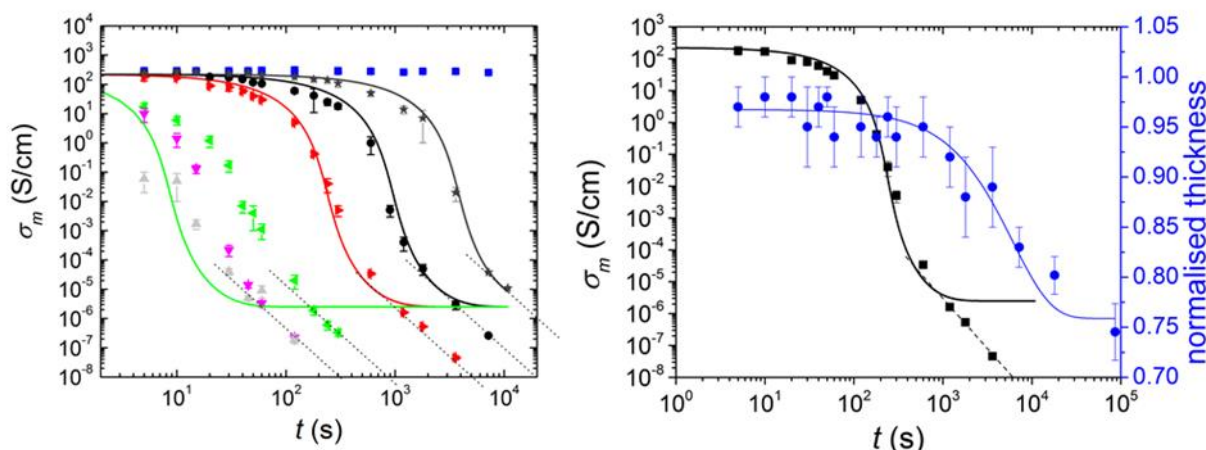


Figure 2: a) Conductivity of HC PEDOT:PSS layers plotted as function of immersion time in $\text{NaClO}_{(\text{aq})}$ solution for various hypochlorite concentrations: from left to right 5

wt%, 0.5 wt%, 0.05 wt%, 0.01 wt%, 0.005 wt%, 0.0025 wt% and blue: 0 wt%; solid lines represent fits to a General Effective Medium (GEM-)reaction model; the thin black lines are guides for the eye; b) Comparison between normalized HC PEDOT:PSS layer thickness (blue) and conductivity (black) as a function of immersion time in 0.01 wt% NaClO_(aq) solution.

The (approach to) overlap of the curves in figure 2a obtained for 0.5 and 5% NaClO_(aq) shows that the influence of concentration diminishes at high NaClO content. The eventual decrease of the conductivity will be controlled by diffusion of NaClO in the HC PEDOT:PSS layer and subsequent reaction with the PEDOT backbone. Using diffusion theory we interpret this observation in terms of a transition from a reaction-limited regime at low hypochlorite concentration to a diffusion-limited regime at high concentration. Experimental evidence for the presence of the reaction limited regime at [NaClO] < 0.01 wt% is provided by the observation that the same conductivity curve is obtained positioning contacts on top or below the treated layer. In order to fundamentally capture the way the conductivity decreases with treatment time, we formulated a model combining an effective medium description of the percolative nature of the charge transport with an effective rate law for the reaction between NaClO and PEDOT [1]. The solid lines in Figure 2a represent the fits to this model. The values of the physical fit parameters allow insight in the morphological features of the PEDOT:PSS blend.

5. CONCLUSIONS

It was shown that the conductivity of PEDOT:PSS can be decreased by ten orders of magnitude without drastically reducing the layer thickness. A residual, electrically insulating, layer remains on the substrate after treatment which, when incorporated in an organic light-emitting diode, may drastically reduce current leakage paths. During treatment with NaClO, one needs to take into account that, depending on concentration, the timescale of conductivity decrease can be diffusion- or reaction-limited. The decrease of the conductivity of PEDOT:PSS by reaction with hypochlorite can be understood in terms of a disruption of percolating current pathways.

ACKNOWLEDGEMENTS

The authors acknowledge the Dutch Ministry of Economic Affairs, Agriculture and Innovation for funding. AGFA Gevaert (Mortsel, Belgium) is acknowledged for supplying the HC PEDOT:PSS dispersions. Dr. T. van Gijseghem (AGFA Gevaert) and Dr. M. M. de Kok (Holst Centre/TNO) are kindly acknowledged for fruitful discussion.

REFERENCES

[1] A.J. Oostra, K.H.W. van den Bos, J.J. Michels and P.W.M. Blom, Disruption of the Electrical Conductivity of Highly Conductive Poly(3,4-ethylenedioxythiophene) :Poly(styrene sulfonate) by Hypochlorite, manuscript submitted for publication (2013).

STIMULATED-HEALING OF PROTON EXCHANGE MEMBRANE FUEL CELL CATALYST

R. Latsuzbaia¹, E. Negro¹, G. J. M. Koper¹

¹ Department of Chemical Engineering, TU Delft, Julianalaan 136, NL-2628BL, Delft - e-mail: G.J.M.Koper@tudelft.nl

Keywords: fuel cell, platinum nanoparticles, self-healing, dissolution, deposition.

ABSTRACT

Platinum nanoparticles, which are used as catalysts in Proton Exchange Membrane Fuel Cells (PEMFC), tend to degrade after long-term operation. We discriminate the following mechanisms of the degradation: poisoning, migration and coalescence, dissolution, and electrochemical Ostwald ripening. There are two ways to tackle this problem. The first option involves formulation of durable catalyst, which can resist harsh fuel cell conditions, and this is the conventional route. The second option is reactivation by dissolution and then redeposition of the catalyst nanoparticles, which is an unprecedented method for platinum catalyst regeneration/stimulated-healing and the one we shall discuss.

Dissolution of platinum can be achieved electrochemically, by potential cycling of the fuel cell electrode impregnated with platinum nanoparticles in oxygen enriched acidic electrolyte according to following reactions [1]:



During the potential cycling, platinum oxides are formed at each positive cycle and subsequently dissolved as platinum ions in the electrolyte on the negative cycle. These cycles are alternated continuously. The partial dissolution of platinum nanoparticles results in a decrease in particles size and oxidation of the poisonous species on the platinum surface. The process of dissolution is monitored in-situ via cyclic voltammetry technique. The concentration of dissolved platinum is measured with Inductively Coupled Plasma Optical Emission Spectroscopy (ICP-OES).

The next step of the regeneration procedure is redeposition of the dissolved platinum back onto the carbon support of the fuel cell electrode. This can be realized by means of electrodeposition. A negative potential is applied to an electrode from where the platinum was dissolved and this results in a reduction of the dissolved platinum ions. Regenerated nanoparticles are characterized by AFM, TEM and XRD. The activity of the catalyst will be checked via voltammetric techniques.

1. INTRODUCTION

Price and durability remain major barriers for full commercialization of Proton Exchange Membrane (PEM) fuel cell technology. The main cause of these obstacles is the degradation of the fuel cell electrodes, and particularly the fuel cell catalyst. Therefore, a stimulated-healing strategy would offer a possibility to prolong the lifetime time of PEM fuel cells and to reduce their operation price.

2. MATERIALS

A fuel cell electrode was employed as a working electrode (WE) for most dissolution studies. The working electrode (20x10 mm) was prepared by spraying catalyst ink (44% Pt, 33% Carbon Black, 23% Nafion®) on carbon paper (Toray TGP-H-060) reaching platinum loading of 0.5 mg cm^{-2} ; then the electrode was dried at $110 \text{ }^{\circ}\text{C}$ for one hour. Commercial JM Hispec 9100 was used to prepare the catalyst ink. Carbon paper of the same dimensions (without catalyst layer) was used as a counter electrode. The carbon paper was chosen as a counter electrode to ensure the dissolution of platinum only from the working electrode. A carbon electrode can be used as a counter electrode instead of platinum because hydrogen evolution is also possible on a carbon surface, however rates are much lower than on platinum [2, 3], for which reason the surface area of the carbon CE during the dissolution experiment should be several times larger than active surface area of the WE. A reversible Hydrogen Electrode (RHE) was used as a reference electrode. For all dissolution experiments 0.1 M HClO_4 and x M HCl ($x = 0, 0.1, 0.3, 0.5\text{M}$) solutions were used as an electrolyte.

The electrodeposition experiments were carried out on Highly Oriented Pyrolytic Graphite (HOPG) in 0.1 M HClO_4 with 1 mM H_2PtCl_6 at room temperature ($21\text{-}22 \text{ }^{\circ}\text{C}$).

3. METHODS

Platinum dissolution experiments were performed in a three-electrode electrochemical cell using the potential cycling technique. The potential was cycled between 0.45 and 1.1 V vs. RHE with a scan rate of 50 mV s^{-1} . The influences of the chloride-ion concentration and of the electrolyte temperature on the dissolution rate of platinum were investigated. ICP-OES was used to determine concentration of dissolved platinum. After 800-1000 cycles the experiments were terminated.

The electrodeposition technique was employed for the redeposition procedure [4]. Platinum deposition was performed in a three-electrode cell on a HOPG working electrode. A platinum wire was used as counter electrode, and a RHE as reference electrode. The particle size and dispersion over the HOPG surface were studied with AFM.

4. RESULTS

The investigations on a possible strategy for a stimulated-healing of fuel cell electrodes have been performed ex-situ in an electrochemical cell using voltammetric techniques. The main aim of the study is optimization of platinum catalyst dissolution and redeposition for the present purpose. Therefore, the project is divided in two parts: dissolution and redeposition studies.

It was reported before that traces of chloride [5], the pH [6], the presence of oxygen [1] and high temperature [6] in the electrolyte accelerate platinum dissolution. However, most of the work has been done under simulated fuel cell conditions with the aim of studying catalyst degradation mechanisms, whereas in our investigations we tried to reach the opposite with the highest possible level of harsh conditions applicable in a fuel cell in order to achieve optimal catalyst dissolution. We studied dissolution of platinum at high chloride concentrations (0.1, 0.25 and 0.5 M HCl in 0.1M HClO_4), at different temperatures. Cyclic voltammetry was used to observe the decay of the electrochemical surface area (ECSA) or hydrogen desorption peak

current of the platinum catalyst, see Figure 1, where both indicate the dissolution of the catalyst.

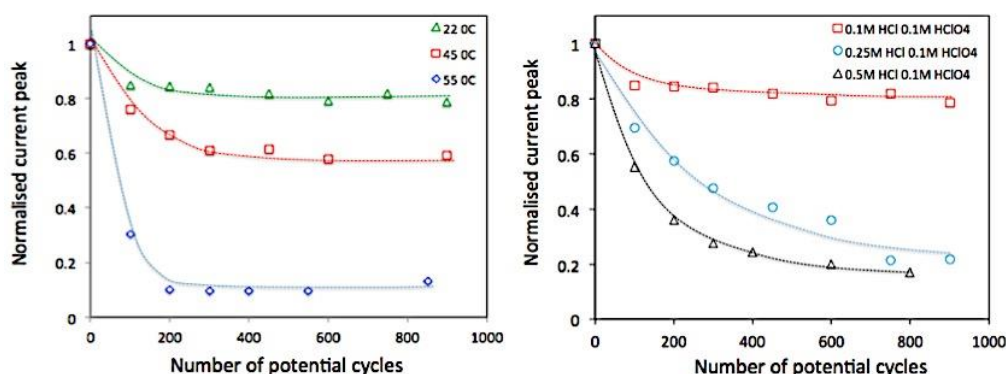


Figure 1: Decay of the hydrogen desorption cathodic peak current.

In our first investigations the fast initial current decay was increasing with increase of chloride concentration up to 0.5 M as well as with increase of temperature up to 55 °C.

During the dissolution experiments in the 0.1M HCl + 0.1M HClO₄ at room temperature about 7.5 % of the platinum catalyst was dissolved, see Figure 2. Further investigations are required to measure the amount of platinum dissolved in harsher conditions.

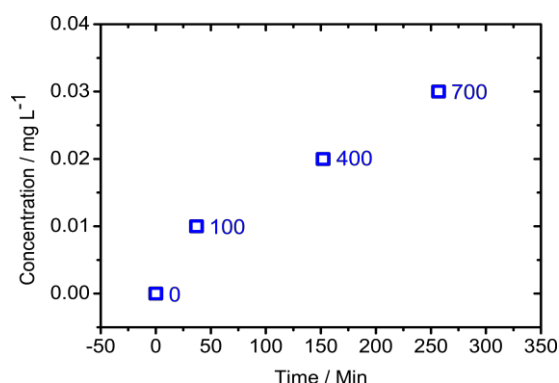


Figure 2: ICP-OES analysis of the platinum dissolution in an electrolyte solution of 0.1M HCl + 0.1M HClO₄, at 22 °C, 0.45-1.1 V potential cycling at 50 mV s⁻¹. Number of cycles: 0, 100, 400, and 700.

Electrodeposition was considered as one of the options for the deposition of dissolved platinum. The HOPG was used as a model support to study the morphology of the electrodeposited particles by AFM. Monodisperse nanoparticles of 30 nm diameter and 8 nm height were deposited and well dispersed on the support, see Figure 3, from the solution of 1mM H₂PtCl₆ and 0.1M HClO₄. Reduction potential of 0.08 V was applied for 0.2 s to deposit the platinum from the electrolyte solution. The procedure still needs to be optimized to get smaller nanoparticles.

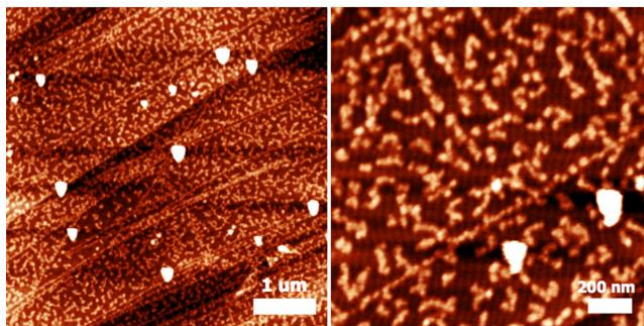


Figure 3: AFM image of platinum nanoparticles electrodeposited 1mM H_2PtCl_6 and 0.1M HClO_4 mixture, cathodic pulse of 0.08V for 0.2 s.

5. CONCLUSIONS

Our first investigations on catalyst dissolution demonstrate that platinum can be dissolved electrochemically at a reasonable rate and that increasing the Cl^- concentration or temperature can increase dissolution rates. The optimum conditions still need to be identified. The dissolved platinum can be redeposited electrochemically resulting in small and monodisperse nanoparticles. As a result, the optimized conditions for both processes could be applied in a real fuel cell setup thus achieving the stimulated-healing of PEMFC catalyst.

ACKNOWLEDGEMENTS

Financial support from IOP Self-Healing Materials (Agentschap NL, Ministry of Economic Affairs) for this study (Project No: SHM1050) is gratefully acknowledged.

REFERENCES

- [1] Matsumoto, M., T. Miyazaki, and H. Imai, Oxygen-Enhanced Dissolution of Platinum in Acidic Electrochemical Environments. *The Journal of Physical Chemistry C*, 2011. 115(22): p. 11163-11169.
- [2] Brennan, M.P.J. and O.R. Brown, Carbon electrodes: Part 1. Hydrogen evolution in acidic solution. *Journal of Applied Electrochemistry*, 1972. 2(1): p. 43-49.
- [3] Sutto, T.E., P.C. Trulove, and H.C. De Long, Direct X-Ray Diffraction Evidence for Imidazolium Intercalation into Graphite from an Ionic Liquid. *Electrochemical and Solid-State Letters*, 2003. 6(3): p. A50-A52.
- [4] Ueda, M., et al., Double-pulse technique as an electrochemical tool for controlling the preparation of metallic nanoparticles. *Electrochimica Acta*, 2002. 48(4): p. 377-386.
- [5] Yadav, A.P., A. Nishikata, and T. Tsuru, Effect of halogen ions on platinum dissolution under potential cycling in 0.5M H_2SO_4 solution. *Electrochimica Acta*, 2007. 52(26): p. 7444-7452.
- [6] Mitsushima, S., et al., Dissolution of platinum in acidic media. *Electrochimica Acta*, 2008. 54(2): p. 455-460.

AUTONOMOUS RESTORATION OF ELECTRICAL INTERFACES

N.R. Sottos^{1,2}, S. Kang¹, A.E. Jones³, O. Okman², J.S. Moore^{2,4}, S.R. White^{2,5}

¹ *Department of Materials Science and Engineering, University of Illinois at Urbana-Champaign, Urbana, IL, 61801, USA. email: n-sottos@illinois.edu*

² *Beckman Institute of Advanced Science and Technology, University of Illinois at Urbana-Champaign, Urbana, IL, 61801, USA*

³ *Department of Mechanical Science and Engineering, University of Illinois at Urbana-Champaign, Urbana, IL, 61801, USA.*

⁴ *Department of Chemistry, University of Illinois at Urbana-Champaign, Urbana, IL, 61801, USA.*

⁵ *Department of Aerospace Engineering, University of Illinois at Urbana-Champaign, Urbana, IL, 61801, USA.*

Keywords: conductivity restoration, microcapsule, carbon black

ABSTRACT

Restoration of electrical interfaces has potential to increase the reliability and safety of high performance batteries. In Li-ion batteries, continued cycling of silicon anodes results in cracking or pulverization of the particles, and ultimately destruction of the conductive network. Here, we consider an approach to increase cycle lifetimes and reliability through restoration of anode conductance via the use of microencapsulated components that form a conductive network when released. In this study, robust microcapsules were prepared with high carbon black loading (up to 20 w/v %) present in liquid core. Increased hydrophobicity of carbon black was achieved through the functionalization of oxidized carbon black with octadecylamine. Upon crushing, functionalized carbon black (FCB) filled microcapsules demonstrated improved particle release compared to unfunctionalized carbon black. The potential for conductance restoration of Si electrodes was first evaluated by crushing FCB microcapsules on electrode line cracks introduced by a fiber removal method, with a maximum recovery of 100% of original conductance. Performance is compared with microencapsulated graphene and carbon nanotubes. In situ recovery of electrode materials is currently in progress.

MULTIPLE HEALING IN MULTI-FUNCTIONAL POLYMER COMPOSITES

U. Lafont^{1,3}, H. van Zeijl² and S. van der Zwaag³

¹ *Material innovation institute, Mekelweg 2, 2600 GA, Delft, The Netherlands – email: U.Lafont@tudelft.nl*

² *DIMES, Electrical Engineering, Mathematics and Computer Science, Delft University of Technology, Mekelweg 4, 2628 CD, Delft, The Netherlands – email: H.W.vanZeijl@tudelft.nl*

³ *Novel Aerospace Materials, Aerospace Engineering, Delft University of Technology, Kluyverweg 1, 2629 HS, Delft, The Netherlands – email: S.vanderZwaag@tudelft.nl*

Keywords: Composite, self-healing, dynamic bonding, adhesion, cohesion, thermal conduction

ABSTRACT

In this work, we investigate the formation of self-healing systems that are able to recover more than once more than one (mechanical or other physical) functionality. To this aim composites were created consisting of a polysulfide thermoset rubber matrix having intrinsic self-healing properties filled with thermally/electrically conductive particles.

The cohesion, adhesion and thermal/electrical conduction recovery of these composites are investigated, monitored and quantified as function of the filler type and content. Moreover, the effects of healing temperature and the intrinsic polymer structure on the kinetics and degree of property recovery are explored.

1. INTRODUCTION

With the introduction of self-healing concepts in material science, materials having the ability to recover their functionality autonomously or upon a mild thermal stimulus did become a reality. To date, self-healing concepts have been applied mainly to structural materials that have to carry mechanical loads or materials that have a protective function against mechanical impact. In this respect, only one functionality (strength) is to be “healed” via the imparted self-healing mechanism. Intrinsic self-healing polymeric materials [1-3] enable the creation of self-healing composites that have the in-built capability of multiple healings at sample locations having failed earlier [4]. This approach is expected to enhance and increase the reliability of composite functionality as a function of the service time and is very promising for opto- and microelectronic applications [5]. In the present work, we investigate the synthesis and characterization of a new type of thermally and/or electrically conductive self-healing composites using a polysulfide rubber thermoset as the matrix [1] and either hexagonal BN or graphite particles as the conductive fillers. The recovery of the functional (electrical and thermal conduction) and mechanical (cohesion and adhesion) properties upon low temperature annealing is described. A very high degree of multiple healing of both mechanical and physical properties was demonstrated for composites containing up to 40% of conductive filler particles.

2. MATERIALS

The composites were produced by mixing an uncured thermoset rubber with sub-micrometre graphite flakes or 5 μm hexagonal BN particles as filler. The amount of the fillers in the composite was varied from 10 to 40 vol%. The synthesis procedure is based on a basic catalysed condensation of epoxy functions with thiols. In a typical procedure, a stoichiometric amount of epoxidized polysulfide Thioplast™ EPS25-aliphatic (640 g/equ.) provided by AkzoNobel BV is mixed with Pentaerythritol tetrakis(3-mercaptopropionate) (~122 g/equ) from Aldrich. 4-dimethylaminopyridine (Aldrich) was used as the catalyst and it was applied at a 1 (wt)% level. Finally, the composites were prepared by adding the fillers to this slurry. After mixing for 2 minutes at 2500 rpm using a high speed mixer, the pastes obtained were poured into a 1 mm thick mould, levelled and cured at 65°C for 2 hours.

3. METHODS

The thermal conductivity of the materials was investigated using the modified transient source technique using a TCi C-Therm apparatus. The adhesive behaviour of the composites was investigated by means of single lap shear tests. To this aim, a known surface of already cured resin (12.5*25 mm, thickness 1 mm) was sandwiched between two identical aluminium 6082-T6 strips (L*W*T = 100*25*2 mm) with an overlap length of ~12.5 mm. The adhesion to the plates was promoted by a 2 h thermal treatment at 65°C. During the thermal treatment the composite and the two parts of the sample were kept in contact using a paper clip. In order to study the adhesion recovery upon thermal healing, the sample ends were repositioned carefully at the end of each lap shear strength test and the thermal treatment was repeated. To investigate the cohesive healing ability, the composites were cut using a fresh razor blade. The cut pieces were put back together and placed between two glass slides. The quantification as function of the healing time of the cohesive healing ability was investigated both at 65 and at 100°C. For this purpose, the samples were taken out from the oven during the healing procedure at different time interval and the evolution of the dimension of the initial cut (width and area) was monitored using a Leica optical microscope. Recovery of electrical contact upon healing was investigated using impedance spectroscopy with an Autolab potentiostat–galvanostat in combination with a frequency response analyser.

4. RESULTS

The composites produced are based on a rubber thermoset that does not exhibit any adhesive or cohesive functionality at room temperature. However, by annealing at 65°C for several minutes the composite materials, irrespective of the filler fraction, shows clear adhesive healing (Figure 1). Moreover, after each failure/healing cycle, the composites are able to regain the same level of adhesion. The adhesive strength varied with the filler type and content. A maximum adhesive strength of 0.4 and 0.5 MPa was achieved for the composite loaded with 30 vol% of graphite and BN, respectively.

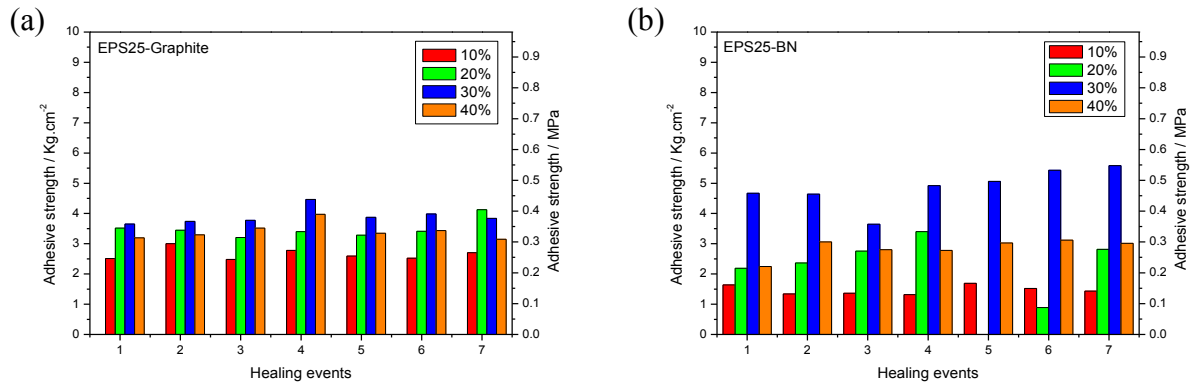


Figure 1: Adhesion as function of the healing events at 65°C for (a) graphite and (b) BN filled composite with different filler content.

In addition to adhesion recovery against an aluminium substrate, the composites also demonstrated a very attractive cohesion recovery behaviour. At lower filler contents (up to 20%) an annealing temperature of 65°C was sufficient to obtain full healing in 10 minutes (Fig 2b), while at higher filler contents (40%) full healing could only be obtained at 100°C (Fig 2a).

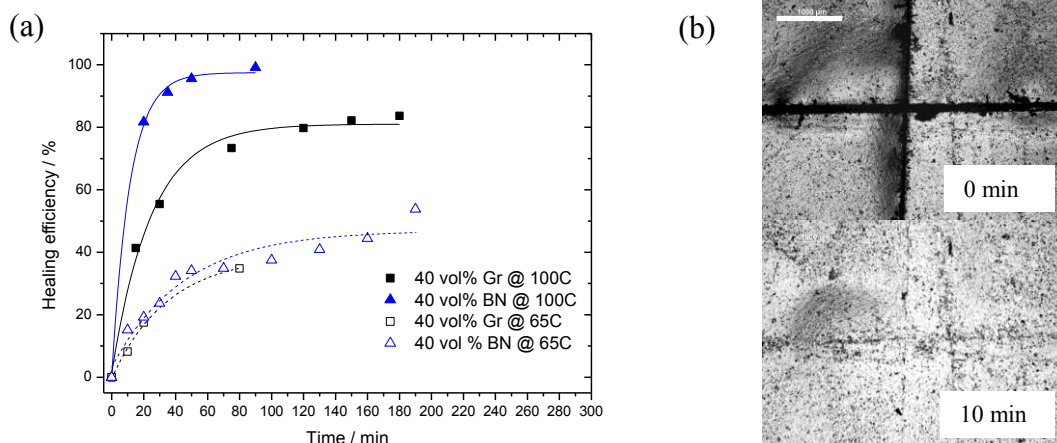


Figure 2: (a) Comparison of the cohesive healing efficiency at 65°C (open symbol/dotted line) and at 100°C (full symbol /full line) of EPS25 and EPS70 composites loaded with 40 vol % of graphite or BN. (b) Micrograph showing the cohesive healing recovery of EPS25-20 vol% graphite composite before and after 10 min healing time at 65°C (scale bar 1 mm).

The healing behaviour is more or less similar for BN fillers as for graphite fillers: the cohesive healing efficiency is 75 and 40% for the composite loaded with 30 and 40 vol% of BN, respectively. If the healing temperature is increased to 100°C, the cohesive healing efficiency and the healing kinetic are increase in almost all cases, leading to 100% efficiency for all BN filled composites.

The thermal conductivity of the composites increased with the filler content. While the pristine polymer has a thermal conductivity of 0.25 W/mK the composites reached values of 2 and 1 W/mK at 40 vol% loading using graphite and BN filler, respectively. The restoration of the thermal conductivity proceeds with the restoration of the mechanical properties. By nature the BN based composites are electrical insulators

whereas the graphite-based composites are electrical conductors. Hence graphite based composites also show an increase in the electrical conductivity with increasing graphite content. The graphite loaded composites showed recovery of both their thermal and electrical conductivity upon restoration of their adhesive or cohesive properties.

5. CONCLUSIONS

Multifunctional healing in functional polymer composites showing a good thermal and/or electrical conductivity can be created by combining a matrix with intrinsic self-healing properties and loading it with conductive fillers. The resulting self-healing response can be tuned as function of the matrix polymeric backbones and the filler type. Fillers enhance the adhesive and conductivity properties of the composites whereas the cohesive response is mainly hampered when the filler content is relatively high. This decrease in cohesion recovery can be tackled by increasing the healing temperature to enhance the system mobility. The self-healing composites are able to restore their interfacial strength values as well as their bulk (thermal and electrical) conductivity even after multiple failure events.

ACKNOWLEDGEMENTS

This research was carried out under project number M71.9.10381 in the framework of the Research Program of the Material innovation institute (M2i) (www.m2i.nl).

REFERENCES

- [1] U. Lafont, H. Van Zeijl, S. Van Der Zwaag, Influence of cross-linkers on the cohesive and adhesive self-healing ability of polysulfide-based thermosets, *ACS Appl. Mater. Interfaces*, 4 (2012) 6280-6288.
- [2] D. Montarnal, M. Capelot, F. Tournilhac, L. Leibler, Silica-Like Malleable Materials from Permanent Organic Networks, *Science*, 334 (2011) 965-968.
- [3] P. Cordier, F. Tournilhac, C. Soulié-Ziakovic, L. Leibler, Self-healing and thermoreversible rubber from supramolecular assembly, *Nature*, 451 (2008) 977-980.
- [4] B.C.K. Tee, C. Wang, R. Allen, Z. Bao, An electrically and mechanically self-healing composite with pressure- and flexion-sensitive properties for electronic skin applications, *Nat Nano*, 7 (2012) 825-832.
- [5] U. Lafont, H.v. Zeijl, S.v.d. Zwaag, Increasing the reliability of solid state lighting systems via self-healing approaches: A review, *Microelectron. Reliab.*, 52 (2012) 71-89.

SESSION 13 – SELF-HEALING POLYMERIC MATERIALS

SELF-HEALING OF THERMOPLASTIC POLYMER BY LIVING POLYMERIZATION

M. Q. Zhang and M. Z. Rong

Key Laboratory for Polymeric Composite and Functional Materials of Ministry of Education, School of Chemistry and Chemical Engineering, Sun Yat-sen (Zhongshan) University, Guangzhou 510275, P. R. China – e-mail: ceszmq@mail.sysu.edu.cn; cesrmz@mail.sysu.edu.cn

Keywords: thermoplastics, self-healing, living polymerization, microcapsules

ABSTRACT

Autonomic self-healing thermosetting polymers or elastomers have been substantially studied, in which polymerization of the healing agents released from pre-embedded capsules serves as the key issue. As for thermoplastics, another major class of polymeric materials, however, researches on their self-healing approaches are less reported.

Here in this work we show the feasibility of a healing chemistry based on living polymerization (that excludes the possibility of chain transfer and termination) for thermoplastics. Monomer-loaded microcapsules are dispersed in a living polymer matrix that contains living chain ends. When the fluidic monomer is released upon cracking, it is easily polymerized at room temperature wherever it meets the matrix. Then, the newly formed macromolecules, which are covalently attached to the interface, fill the interstitial space of cracks and fuse with the matrix into one, offering satisfied healing efficiency. No catalyst is required for resuming chain growth in the system. The repair processes are carried out without the necessity for manual intervention.

Details of the microcapsules preparation, matrix synthesis and types of controlled radical polymerization (atom transfer radical polymerization (ATRP), and reversible addition–fragmentation chain transfer (RAFT)) are discussed. It is hoped that the results would serve as solid basis for the development of self-healing thermoplastic polymers.

1. INTRODUCTION

So far, there are only a few reports on preparation of self-healing thermoplastics. In the authors' lab, a novel approach is proposed, which employs living thermoplastic polymer as the matrix filled with monomer-loaded microcapsules as the healing agent provider. Because the living polymer carrying active end groups is capable of resuming polymerization at room temperature when fresh monomer is supplied, cracks can be covalently re-bonded by the copolymerization product of the released monomer and the matrix. Such self-healing might combine both micron-scale and molecular scale rehabilitations [1]. Considering the versatility of living polymerization and manoeuvrability of microencapsulation techniques, most thermoplastics would thus be converted into self-healing ones accordingly.

2. MATERIALS

Glycidyl methacrylate (GMA, A.R.) used as the core healing agent to be encapsulated was purchased from Tianjin Damao Chemical Co., China. Melamine (M, A.R.) was provided by Shanghai Linfeng Chemical Co., China. Formaldehyde (F, A.R., 37 wt.%) was supplied by Guangzhou Donghong Chemical Co., China. Methyl methacrylate (MMA), used for making the composite's matrix, was purchased from Tianjin Damao Chemical Co., China. It was washed with sodium hydroxide aqueous solution (5 wt.%), thereafter three times with water, dried over magnesium sulphate, and evaporated to dryness in vacuum. The thermally decaying initiator 2,2'-azoisobutyronitrile (AIBN) was recrystallized twice from ethanol. The synthesis of cumyl phenyldithioacetate (CPDA) was undertaken according to the previously reported protocols [2]. It proceeded by a Grignard reaction of benzyl chloride with carbon disulfide and subsequent reaction of the resultant phenyldithioacetic acid with α -methylstyrene, then recrystallized from methanol as orange crystals.

3. RAFT POLYMERIZATION OF MMA AND PREPARATION OF SELF-HEALING PMMA COMPOSITES

Bulk polymerization was conducted in a two-neck flask. MMA (25.0 g, 0.25 mol), CPDA (0.119 g, 4.16×10^{-4} mol) and AIBN (0.068 g, 4.16×10^{-4} mol) were mixed and stirred using a magnetic stirrer. The solution was deoxygenated by purging with argon for 30 min. Considering that CPDA mediated MMA polymerization can be performed at different temperatures from 25 to 45 °C and higher rate of polymerization is achieved at higher temperature, MMA polymerization was conducted at 45 °C for a prescribed time with continuous stirring to accelerate the preparation process of specimens. Samples were taken at regular intervals, and the reaction mixture was chilled and diluted with tetrahydrofuran (THF). The resultant polymer was obtained as a yellow powder after three times of dissolving in THF and precipitating from a 10-fold excess of methanol and finally dried in a vacuum oven at 40 °C for 24 h.

Microcapsules containing GMA was prepared via in-situ polymerization with melamine-formaldehyde resin as the shell material. The details have been reported elsewhere. For making self-healing PMMA composites, the microcapsules have to be compounded with the polymerized MMA. In a typical run, MMA (25.0 g, 0.25 mol), CPDA (0.119 g, 4.16×10^{-4} mol), and AIBN (0.068 g, 4.16×10^{-4} mol) were charged into a two-neck flask and deoxygenated by purging with argon for 30 min. Then, the flask was immersed in an oil bath at a preset temperature of 45 °C. After 22-24 h, a given proportion of GMA-loaded microcapsules (average diameter = 133.4 μm , core content = 77.7 %) were incorporated into the flask under argon atmosphere and stirring. The mixture was then poured into closed silicone rubber moulds and kept for 96 h at ambient temperature to obtain cured specimens..

4. RESULTS

To confirm the living property of PMMA, an intuitional experiment was conducted at ambient temperature. Firstly, CPDA mediated MMA polymerization was carried out in a tube. Then, GMA monomer was poured onto the solidified PMMA surface and polymerization started at ambient temperature in the atmosphere of argon. After completion of the polymerization of GMA monomer, MMA was added. Finally a rod-

like material with sandwich structure was obtained (Figure 1). When the addition order of the monomers is changed, a rod with similar sandwich structure was also produced. The results demonstrate that the CPDA mediated polymerized product of MMA indeed has the capability of re-initiation of polymerization at ambient temperature. When GMA released from broken microcapsules encounters the fractured surface of living PMMA, copolymerization must occur, re-connecting the damaged sites.

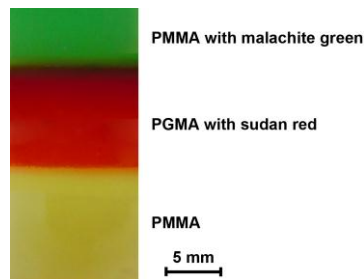


Figure 1: Multilayer sandwich structure formed by successively adding GMA and MMA monomers onto living PMMA. Sudan red and malachite green dye were incorporated for coloring.

Figure 2 shows time dependence of healing efficiency of the self-healing PMMA composites. With a rise in healing time, the healing efficiency increases and eventually reaches the equilibrium of about 100% when the time exceeds 72 h. It means that recovery of impact strength at room temperatures needs at least 72 h. More importantly, the idea of self-healing of thermoplastics via RAFT polymerization proves to be feasible.

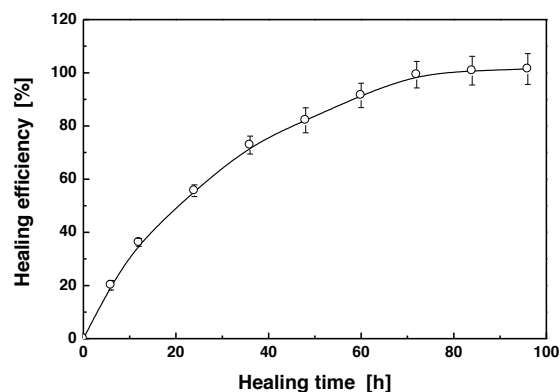


Figure 2: Healing efficiency of PMMA composites containing 15 wt.% GMA-loaded microcapsules as a function of healing time at 25 °C.

5. CONCLUSIONS

The present work proves that RAFT polymerization is applicable to self-healing thermoplastics based on the strategy of microencapsulation. Restoration of impact strength at room temperature without manual intervention is observed in the living PMMA composites filled with GMA-loaded microcapsules.

ACKNOWLEDGEMENTS

The authors thank the support of the Natural Science Foundation of China (Grants: 51273214, 20874117, 51073176 and U0634001), Doctoral Fund of Ministry of Education of China (Grant: 20090171110026), and the Science and Technology Program of Guangdong Province (Grant: 2010B010800021, 2010A011300004).

REFERENCES

- [1] M. Chipara, K. Wooley, Molecular self-healing processes in polymers, *Materials Research Society Symposium Proceedings* 851 (2005) 127-132.
- [2] C. Barner-Kowollik, J. F. Quinn, T. L. U. Nguyen, J. P. A. Heuts, T. P. Davis, Kinetic investigations of reversible addition fragmentation chain transfer polymerizations: cumyl phenyldithioacetate mediated homopolymerizations of styrene and methyl methacrylate, *Macromolecules* 34 (2001) 7849-7857

SYNTHESIS AND CHARACTERISATION OF NOVEL CATALYSTS FOR USE AS SELF-HEALING AGENTS IN EPOXY RESINS

D. T. Everitt¹, T. S. Coope¹, I. P. Bond¹, R. S. Trask¹, D. F. Wass²

¹ *Advanced Composites Centre for Innovation and Science (ACCIS), Department of Aerospace Engineering, University of Bristol, Bristol, BS8 1TR, UK – e-mail: de7812@bristol.ac.uk, Tim.Coope@bristol.ac.uk, I.P.Bond@bristol.ac.uk, R.S.Trask@bristol.ac.uk.*

² *School of Chemistry, University of Bristol, Cantock's Close, Bristol, BS8 1TS, UK – e-mail: Duncan.Wass@bristol.ac.uk.*

Keywords: Self-healing, catalysis.

ABSTRACT

Self-healing polymers typically feature monomer and catalyst either dispersed within a host matrix, or encapsulated within hollow vessels. Unprotected highly active catalysts, sensitive to air and moisture, can readily react with amine cross-linking agents during the cure of reactive prepolymers e.g. epoxy resins. Therefore, catalysts stable to the polymer environment in which they are intended to be used must be developed, in order to remove the requirement for in-situ catalyst encapsulation.

Silver olefin complexes have been shown to be particularly efficient initiators for the curing of epoxy resins. The coordination polymer $\{[Ag(1,7\text{-octadiene})_{1.5}]SbF_6\}_n$, which shall henceforth be referred to as AgOctadiene, is investigated herein for its potential application in self-healing epoxy-based polymers.

Differential scanning calorimetry (DSC) was used to investigate the cure onset temperature of various polymer precursor resins. Tapered double cantilever beam (TDCB) mechanical test specimens were used to investigate thermal activation of the catalyst in the solid state and subsequent healing, results of these tests are presented.

1. INTRODUCTION

Silver olefin complexes have been shown to be particularly efficient initiators for the curing of epoxy resins [1]. AgOctadiene (Figure 1) is investigated for its potential application in self-healing polymer materials. Scope for tuning the behaviour of such coordination polymers through alteration of the ligand is also discussed. 1,7-octadiene was selected as the primary ligand for this study, due to the lability of the Ag-olefin bond and the relative ease of synthesising the quantity required for mechanical testing.

The 'unprotected' silver salt, silver hexafluoroantimonate ($AgSbF_6$), is used as a control initiator.

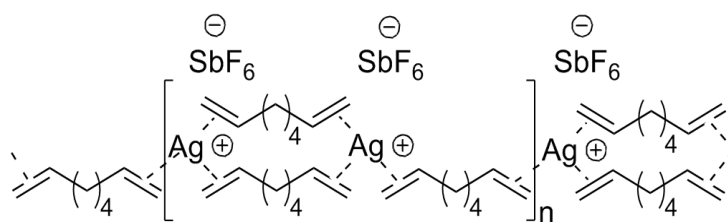


Figure 1: AgOctadiene catalyst.

2. MATERIALS AND METHODS

2.1 Synthesis of $\{Ag(1,7\text{-octadiene})_{1.5}\}n[SbF_6]n$.

To a solution of $AgSbF_6$ (2 g, 5.83 mmol) in Toluene (15 ml), was added 1,7-Octadiene (2 ml, 1.5 g, 13.5 mmol) dropwise in a nitrogen atmosphere. Solution was stirred at room temperature overnight, yielding an off-white precipitate. Product was isolated by filtration and washed with toluene and pentane prior to drying in vacuo. Product was stored in air in an opaque vial. Elemental analysis: calculated (%): C, 28.32; H, 4.16. Found: C, 27.12; H, 3.93. H^1 NMR (300 MHz, Acetone- d_6): δ 1.36-1.47 (m, 4H), 2.04-2.11 (m, 5H), 2.99 (d, 1H), 4.94-5.05 (m, 4H), 5.82-5.96 (m, 2H). C^{13} NMR (75 MHz, Acetone- d_6): δ 29.04 septet), 205.4 (s). FTIR (nujol) (cm^{-1}) 3630, 3547, 2928, 2859, 1593, 1459, 1378, 1037, 964, 728, 663.

2.2 Fracture Testing.

Initial and healed strengths were determined using tapered double cantilever beam (TDCB) test specimens, as developed by Beres *et al.* [2]. This geometry encourages continuous fracture toughness values along the central trench section in order to control crack propagation through the catalyst impregnated epoxy. This also allows for use of small amounts of catalyst. A 30 mm, grooved central section, with a 2 mm diameter crack stopper was used in this study. This arrangement leads to termination of the crack so that healing can occur prior to further testing. The geometry of the TDCB specimens is provided in Figure 2.

Testing was conducted on an Instron 3343 test machine equipped with a 1 kN calibrated load cell at a loading rate of 0.3 mm displacement per minute. Benchmark data for the average failure load of a pure EPON 828 / diethylenetriamine (DETA) test specimen were obtained from previous work by Coope *et al.* [3]. Fracture tests were performed on five specimens and average failure load and displacement values of 68.3 N and 0.58 mm respectively were obtained.

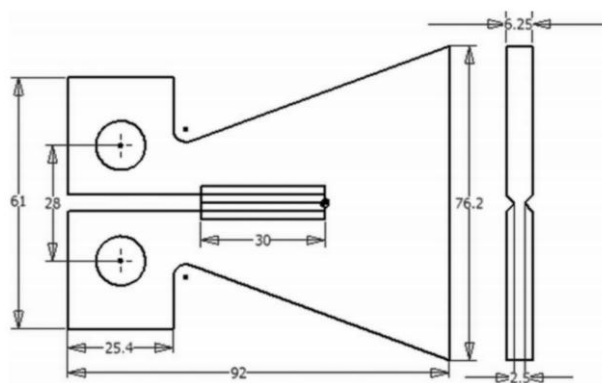


Figure 2: TDCB geometry

3. RESULTS AND DISCUSSION

3.1 Resin Screening.

The effect of dissolved AgSbF_6 upon the cure behaviour of various epoxy resins was investigated using DSC in order to determine which resin would be most appropriate for further analysis.

N,N,N,N-tetraglycidyl-4,4-diaminodiphenyl-methane (TGMDA), triglycidyl-*p*-aminophenol (TGPAP), Poly[(phenyl glycidyl ether)-co-formaldehyde] (DEN 431), and the oligomeric diglycidyl ether bisphenol A (DGEBA) (EPON 828) were investigated. DSC analysis showed a single strong exotherm peak due to the presence of AgSbF_6 in EPON 828, and the solution displayed no evidence of unwanted reactivity. EPON 828 was, therefore, selected as the primary resin for use in this study.

Synthesis of $\{[\text{Ag}(1,7\text{-Octadiene})_{1.5}]\text{SbF}_6\}_n$ proceeded as in Barriau *et al.* [1]. The olefin ligands effectively act as protecting groups for the silver ion, suppressing its reactivity. The onset of thermal curing of AgOctadiene impregnated EPON 828 was determined by DSC to be 96°C . AgSbF_6 initiated curing proceeded at 65°C .

3.2 Healing.

All specimens contained 2.5 pph catalyst dispersed in EPON 828 / DETA (12 pph). Solutions were warmed to 35°C to aid solvation of the catalyst. Catalyst impregnated trenches were cured for 48 hours before being cast into TDCB test specimens. A 2 mm diameter crack stopper was drilled into the end of the trench to discourage complete failure of the specimen. Crack propagation along the trench is encouraged by inserting a sharp notch into the end of the trench. Control specimens containing AgSbF_6 (2.5 pph) were also tested. By comparison of the AgSbF_6 and AgOctadiene results it was possible to investigate the extent to which the presence of the olefin ligands suppressed unwanted reactivity. Monomer delivery occurred by both the use of microencapsulated DGEBA and manual delivery of the resin to the fracture surface. Following monomer delivery, samples were heated for 48 hours to encourage healing. Specimens were then tested again to determine healing efficiency. Results at various temperatures are summarised in Table 1.

Table 1: Summary of healing efficiencies to date

Catalyst: Monomer Delivery: Healing Temperature:	Healing Efficiency (%)								
	AgOctadiene						AgSbF ₆		
	Microcapsules			Manual Delivery			Manual Delivery		
	45°C	60°C	70°C	45°C	60°C	70°C	45°C	60°C	70°C
Specimen 1	-	54.6	73.5	0	12.7	64	0	-	189
Specimen 2	-	85.3	77.2	0	0	38.6	0	-	144
Specimen 3	-	-	99.1	0	0	94.4	0	-	137
Specimen 4	-	-	53.1	-	0	46.9	-	-	-
Mean	0	70	76	0	12.7	61	0	0	157

Table 1 indicates that the TDCB specimens, catalyst loading, and resin delivery method can result in excellent healing. Inconsistency in results is attributed to variability in the dispersion and particle size of the catalyst as well as the delivery of the monomer. Healing values for control specimens are high because the addition of AgSbF₆ appears to significantly reduce the failure loads of pristine samples. This is thought to be due to the highly reactive nature of the unprotected catalyst, which undergoes competing reactions with the amine cross-linking agent, thereby reducing the strength of the resulting thermoset polymer. Also, DSC determined that the onset of thermal curing of EPON 828 due to the presence of AgSbF₆ occurs at 65°C, compared to 96°C for AgOctadiene. A higher healing efficiency is expected from the AgSbF₆ specimens.

4. CONCLUSION

It has been demonstrated through observation, DSC and TDCB mechanical testing, that {[Ag(1,7-Octadiene)_{1.5}]SbF₆}_n is capable of curing epoxy resins both in solution testing and during solid-state mechanical tests.

Thermal activation of both AgSbF₆ and AgOctadiene and subsequent self-healing of catalyst impregnated specimens heated to 70°C for 48 hours has been confirmed through TDCB tests. AgSbF₆ specimens achieved, on average, a 157% recovery in failure load. AgOctadiene specimens on average recovered 68.5% of their failure loads.

The potential for tuning the activation temperature of coordination polymer-based catalysts through alteration of both the ligand and metal will be investigated in future work.

ACKNOWLEDGEMENTS

The authors would like to thank the UK Engineering and Physical Sciences Research Council (EPSRC) [EP/G036772/1] for financial support. We would also like to thank those within ACCIS and the School of Chemistry at the University of Bristol who have encouraged and assisted with this work.

REFERENCES

- [1] E. Barriau, U. Schmidt-Freytag, M. Roth, J. Gehring, N. Simon, F. Wolff-Fabris, V. Altstaedt, M. Do, and D. Arnold, Silver Olefin Complexes: Highly Efficient Initiators for the Electron Beam Curing of Epoxy Resins. *Macromolecules* 41 (2008) 3779-3781.
- [2] W. Beres, A. K. Koul, and R. Thamburaj. A Tapered Double-Cantilever-Beam Specimen Designed for Constant-K Testing at Elevated Temperatures. *Journal of Testing and Evaluation*, 25 (1997) 536–542.
- [3] T. S. Coope, Ulrich F. J. Mayer, D. F. Wass, R. S. Trask, and I. P. Bond. Self-Healing of an Epoxy Resin Using Scandium(III) Triflate as a Catalytic Curing Agent. *Advanced Functional Materials* 21 (2011) 4624–4631.

SELF-HEALING CHEMISTRIES FOR EPOXY RESINS: HAS THE LIMIT BEEN REACHED?

X. Hillewaere^{1,2}, S. Billiet¹, R. Teixeira^{1,2}, T. Nguyen^{1,2} and F. Du Prez^{1,2}

¹ Department of Organic Chemistry, Polymer Chemistry Research Group, Ghent University, Krijgslaan 281, S4-bis, B-9000 Ghent, Belgium – e-mail: xander.hillewaere@ugent.be; stijn.billiet@ugent.be; roberto.teixeira@ugent.be; thu.nguyen@ugent.be; filip.duprez@ugent.be

² SIM vzw, Technologiepark Zwijnaarde 935, B-9052 Ghent, Belgium

Keywords: self-healing, thermoset, epoxy, thiol-isocyanate, thiol-maleimide

ABSTRACT

In order to develop better performing and longer lasting epoxy thermosets and composites, novel healing agents were inserted into microcapsules and these were then dispersed in several types of epoxy resins. Fast and efficient two-compound chemistries were screened by means of kinetic studies and mechanical testing for potential use as the main network forming reaction during self-healing, leading to the improved healing efficiencies compared to most results obtained in literature so far [1-2]. Furthermore, certain conditions necessary for industrial applicability were met, such as low toxicity, low cost and stability at both ambient and epoxy processing conditions.

The mechanical properties of the newly crosslinked products were compared to the original epoxy thermosetting material using both Tapered Double Cantilever Beam and Single Edge Notch Bend tensile tests. In the first step, multifunctional healing agents were manually injected into the broken epoxy matrices and allowed to react while keeping the crack planes into close contact. In a later stage, two types of microcapsules were added to the epoxy matrix to provide the healing agents upon fracture. The self-healing efficiency was determined in accordance to literature [3] and goes up to 140 % after 5 days of healing at room temperature using manual injection. When microcapsules were used to generate a fully autonomous system, a recovery over 50 % was already achieved. This system is currently being fully optimized, taking into account of the factors – such as the viscosity, the ratio of functional groups and the weight fraction of microcapsules – that play a role in the final healed network formation. A more extensive analysis of the mechanical properties of the new material is being performed in collaboration with the project partners.

REFERENCES

- [1] R.F.A. Teixeira, X.K.D. Hillewaere, S. Billiet, F.E. Du Prez, to be published in: W.H. Binder (Ed.), *Self-Healing Polymers*, Wiley & Sons Inc., New-York, 2013.
- [2] S. Billiet, W. Van Camp, X.K.D. Hillewaere, H. Rahier, F.E. Du Prez, Development of optimized autonomous self-healing systems for epoxy materials based on maleimide chemistry, *Polymer* 53 (2012) 2320–2326.
- [3] E.N. Brown, Use of the tapered double-cantilever beam geometry for fracture toughness measurements and its application to the quantification of self-healing, *The Journal of Strain Analysis for Engineering Design* 46 (2011) 167-186.

SELF-HEALING BY MECHANOCHEMICAL ACTIVATION OF A POLYMERIZATION CATALYST

R.T.M. Jakobs¹ and R.P. Sijbesma¹

¹ *Eindhoven University of Technology, Den Dolech, Eindhoven, the Netherlands – e-mail: r.p.sijbesma@tue.nl*

Keywords: self-healing, mechanocatalysis, thermoplastic polymer

ABSTRACT

We have developed a mechanoresponsive catalyst — a catalyst which can be switched between dormant and active states by mechanical deformation. For this purpose, we have synthesized derivatives of the well-known Grubbs metathesis catalysts that are latent due to the presence of two N-heterocyclic carbene ligands. In solution, these catalysts may be switched on by mechanochemical activation with ultrasound. When provided with polymeric ligands and embedded in an semi-crystalline matrix of high molecular weight tetrahydrofuran, the catalyst can be activated by mechanical deformation of a sample, which results in dissociation of one of the ligands. The activated Ruthenium alkylidene species catalyses the ring closing metathesis of a diene. More importantly, this catalyst initiates the polymerization and crosslinking reaction of cyclic dienes such as norbornene derivatives embedded in the polymeric matrix. The system constitutes a novel principle in self-healing materials, since it allows a material to respond to stress by catalyzing a (crosslinking) polymerization reaction – in this way reinforcing the material right at the time and place it is needed when it threatens to fail.

SESSION 14 – SELF-HEALING BITUMINOUS MATERIALS

THE FIRST ENGINEERED SELF-HEALING ASPHALT ROAD; HOW IS IT PERFORMING?

Q. Liu ^{1,2}, E. Schlangen ¹ and G. van Bochove ³

¹ Delft University of Technology, Faculty of Civil Engineering & Geosciences, Section of Materials & Environment - Microlab, Stevinweg 1, 2628 CN Delft, the Netherlands – e-mail: h.e.j.g.schlangen@tudelft.nl

² Wuhan University of Technology, State Key Laboratory of Silicate Materials for Architectures, Luoshi Road 122, Wuhan 430070, China – e-mail: liuqt@whut.edu.cn

³ Breijl-Heijmans.Graafsebaan 3, 5248 JR Rosmalen, the Netherlands – e-mail: gbochove@breijl.nl

Keywords: Asphalt concrete, application, induction heating, steel-wool fibres

ABSTRACT

Porous asphalt shows excellent performance in both noise reduction and water drainage. Although porous asphalt has these great qualities, its service life is much shorter (sometimes only half) compared to dense graded asphalt roads. Ravelling, which is the loss of aggregate particles from the surface layer, is the main damage mechanism of porous asphalt surface wearing courses. In this research, an induction healing approach (namely, activating the healing process of asphalt concrete through induction heating) was developed to enhance the durability of the porous asphalt roads. Steel fibres are added to a porous asphalt mixture to make it electrically conductive and suitable for induction heating. When micro cracks are expected to occur in the asphalt mastic of the pavement, the temperature of the mastic can be increased locally by induction heating of the steel fibres so that porous asphalt concrete can repair itself and close the cracks through the high temperature healing of the bitumen (diffusion and flow). The closure of micro cracks will prevent the formation of macro cracks. In such a way, ravelling can be avoided or delayed in the end.

The healing potential of porous asphalt concrete with steel wool fibre was also evaluated in this research with both cylinder and beam samples. Damaged porous asphalt concrete with steel wool fibre can greatly restore its stiffness, strength and fatigue life with induction heating, which proves that the healing capacity of porous asphalt concrete with steel wool fibre is enhanced by induction heating. The optimal induction heating temperature is 85 °C for porous asphalt concrete to obtain the best healing rate. Reheating does not decrease the healing rate of porous asphalt concrete, which means that heating can be repeated when cracks appear again.

To apply the induction healing technology in real porous asphalt road, a trial section was constructed on Dutch motorway A58 in December 2010. This trial section survived the past three winters perfectly. Experiments were done on the cores drilled from the trial section and the results coincided with those on the laboratory made samples. The field cores showed good particle loss resistance, high strength, good fatigue resistance and high induction healing capacity. Based on the laboratory experiments and field experiences, induction healing can be a very good approach to enhance the durability of porous asphalt pavement.

1. INTRODUCTION

As the skid resistance and noise reduction functions of a porous asphalt surface wearing course can be decreased by ravelling, maintenance is required. In the Netherlands, ravelling is the main cause for maintenance or renewing of the top layer of porous asphalt pavement. To improve the durability of a porous asphalt surface wearing course, ravelling has to be avoided. The objective of this research is to prevent or delay ravelling and by that extend the service life of porous asphalt [1]. To achieve this goal, an induction heating approach (namely, activating the healing process of asphalt concrete through induction heating) is to be used. The schematic diagram of induction heating can be illustrated in Figure 1. Steel fibres are added to a porous asphalt mixture. When micro cracks are expected to occur in the asphalt mastic (or between mastic and stones) of the porous asphalt pavement, the temperature of the mastic can be increased locally by induction heating of the steel fibres via an external source so that porous asphalt concrete can repair itself and close the cracks through the high temperature healing of the bitumen (diffusion and flow). The closure of micro cracks will prevent the formation of macro cracks. In such a way, ravelling can be avoided or delayed eventually. The heating process on the porous asphalt wearing course can be repeated if cracks appear again.

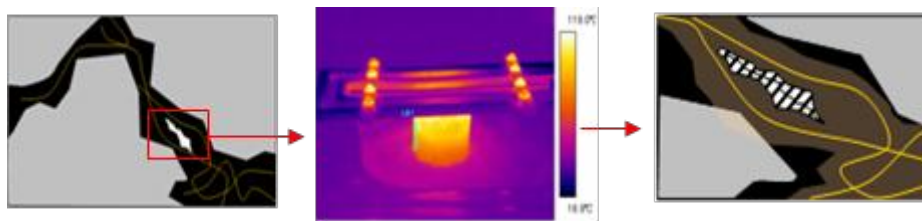


Figure 1: Schematic diagram of induction heating in porous asphalt concrete.

To apply the induction heating technology in real porous asphalt (PA) pavement, a trial section was constructed on Dutch motorway A58. This paper discusses the research performed on specimens taken from the trial section and gives an estimate for the expected service life.

2. TEST METHODS AND RESULTS

To predict the performance of the test section and to get ideas of when and how long to heat the trial section with induction energy, a series of experiments is designed in the laboratory. Cores were drilled from the trial section and beams were prepared with the same materials. Furthermore plates and large beams were cut from part of the trial section to test ravelling resistance and performance in a bridge joint. The mechanical properties of this porous asphalt concrete (Particle loss resistance, indirect tensile strength, water sensitivity, indirect tensile stiffness and fatigue, nano indentation modulus and hardness of the mortar, four point bending fatigue) were studied to predict the performance of the induction healing asphalt test section. The induction healing potential of this material was also investigated. In this paper only a summary of the results can be given. A full overview of the research is given in [1,2]. It was found that it is possible to heat the cores that were taken from the trial section with induction energy. However, the induction heating speed of the cores is not high

enough with the present heating machine to be practical. Either the induction machine or the mix needs optimization. In both there is room for improvement.

Another aspect that was investigated is how to age the materials from the road. It is known that due to ageing the bitumen will oxidize and become stiffer. To predict the long term behaviour it is necessary to check how damage progresses in time and whether healing works at older age. It turned out that the porous asphalt cores that contain steel-wool can be placed in an oven at 85 °C to age them. Ten days in the oven is equivalent to 5 years field aging.

To check the particle loss of the porous asphalt two different type of tests were performed, i.e. the Cantabro tests and the RSAT-test. The Cantabro test were performed on cores from the road with and without steel-wool and with and without ageing. The cores with steel wool showed a much better resistance to particle loss then the plain asphalt cores, also after ageing. This indicates that the fibres also help to improve the mechanical behaviour. In the RSAT (Rotating Surface Abrasion Test) which were conducted at research partner Breijn-Heijmans an asphalt plate is subjected to loading with a wheel with rubber tile, while the plate is rotating (figure 2). In this way abrasion forces are acting on the surface. The test is done on plates with steel-wool with and without ageing. The standard loading-level used in this test for porous asphalt did not result in any damage in the RSAT. With doubling the load level and running for a longer period some damage was obtained in the plates with steel-wool. After some damage was obtained (this means a few stones were released form the surface), the plates were treated with an induction heating until the surface reached 85 °C. The RSAT-tests were then continued and it was found that no more damage was obtained after that, at least for the up to 24 hours that the tests was run after treatment.



Figure 2: RSAT and joint-tester at Breijn-Heijmans.

Part of the trial section was a bridge. Usually there is a standard bridge joint between the road and bridge-deck which is filled with a flexible bituminous materials. In the trial section it was decided to have continuous asphalt surfacing also over the joint. This joint was tested in the joint-tester at Breijn-Heijmans, see figure 2. It turned out that not one single crack occurred in the material, which happens in a standard (porous) asphalt, but due to the steel fibres a multiple crack pattern occurred. Since these cracks were relatively small it turned out to be easy to heal them with induction energy.

The healing potential of the asphalt beams with steel-wool was evaluated in four point bending fatigue tests (figure 4). The healing ratio (fatigue life extension ratio) of

porous asphalt concrete is strain and temperature dependent. Healing is much higher when induction heating is applied on the samples.



Figure 3: Specimen after cracking in joint-tester at Breijn-Heijmans.

The optimal heating temperature is 85 °C. Damage extents affect healing ratio. Heating should not be too early or too late. The stiffness of fatigue damaged beam can recover much more with induction heating. With multiple times induction heating, the fatigue life of porous asphalt beam can be greatly increased as shown in figure 4. Furthermore it was found that ageing doesn't influence the healing of porous asphalt beam very much.

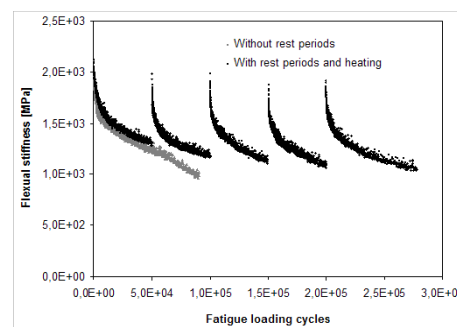
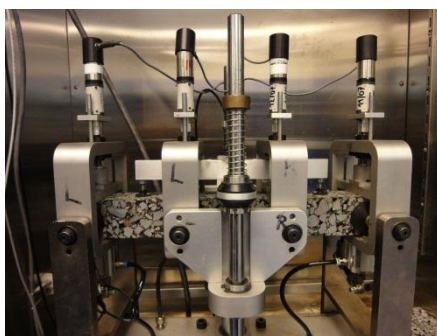


Figure 4: Set-up and results for four point bending fatigue test.

3. CONCLUSIONS

Based on the strength recovery, stiffness recovery, RSAT-tests and fatigue life extension of porous asphalt cores and beams, it is concluded that the healing capacity of porous asphalt concrete is increased by induction heating. Furthermore it has been shown that this self-healing asphalt can also be a great solution for bridge joints in roads. Finally, it can be concluded that the durability of porous asphalt concrete roads will be improved enormously with the induction heating, because of the reinforcement of steel wool and the improvements in the healing capacity. In practice the trial section performs perfect, but it is too early to have a final judgement.

ACKNOWLEDGEMENTS

Financial support from the China Scholarship Council is gratefully acknowledged. Furthermore discussion with Martin van de Ven and Alvaro Garcia and support from Breijn-Heijmans, SGS-Intron and Rijkswaterstaat is highly appreciated.

REFERENCES

- [1] Q. Liu. Induction Healing of Porous Asphalt Concrete. PhD-thesis, Delft University of Technology (2012).
- [2] Liu, Q., García, A., Schlangen, E., van de Ven, M. Induction healing of asphalt mastic and porous asphalt concrete (2011) *Construction and Building Materials*, 25 (9), pp. 3746-3752.

TEMPERATURE INDUCED HEALING IN STRAINED BITUMINOUS MATERIALS OBSERVED BY ATOMIC FORCE MICROSCOPY

S.N. Nahar¹, A.J.M. Schmets¹, A. Scarpas¹ and G. Schitter²

¹*Structural Mechanics, Faculty of Civil Engineering & Geosciences, Delft University of Technology. Stevinweg 1, 2628 CN, Delft, The Netherlands – e-mail: s.n.nahar@tudelft.nl; a.j.m.schmets@tudelft.nl; a.scarpas@tudelft.nl*

²*Automation and Control Institute (ACIN), Vienna University of Technology. Gusshausstrasse 27-29; A-1040 Vienna, Austria – e-mail: schitter@acin.tuwien.ac.at*

Keywords: bitumen, microstructure, atomic force microscope

ABSTRACT

Bitumen is the binder in the composite material named asphalt concrete. Under cyclic mechanical loading of traffic passing over the pavement, eventually damage will initiate in the pavement, leading to eventual structural failure. This damaging process is accelerated by time dependent change of the mechanical properties of asphalt concrete due to ageing mechanisms like oxidation. Bitumen displays spatial heterogeneity at the micrometer scale, which has been observed by atomic force microscopy (AFM). The mechanical properties of the elliptical, microstructural domains of bitumen are distinct from those of the continuous phase. This introduces stiffness discontinuities in the material, which under mechanical loading will concentrate stresses at the interfaces, and thus the locations where early stages of damage will develop.

This work aims at in situ probing of the crack healing of bituminous materials as a function of moderate temperature changes. The bitumen was prepared on a flexible substrate which was mechanically strained to induce damage. AFM measurements of the strained bitumen specimen provides evidence of the crack initiation at the interface and the predominant propagation of cracks through the elliptical domain phases. Healing of these cracks was observed after applying modest amounts of heat to the material. Meanwhile the process was monitored in situ with AFM. With increase of temperature one of the phases starts softening, while the material as a whole remains solid. This allows the phases to rearrange and meanwhile eliminating micro cracks at the interface.

1. INTRODUCTION

When asphalt concrete is mechanical loaded, cracks will easiest form within the bituminous binder that holds together the other components of asphalt, i.e. the fillers and aggregate particles. Bitumen is mechanically speaking the weak link in the asphalt concrete composite. Damage may occur within the bitumen (cohesive damage) or at the interface between the bitumen and the aggregates (adhesive damage). Yet, not much information is available on the damage characteristics of bitumen at the micrometer scale. Though several researchers emphasized on the importance of probing the pre- macro crack regime for improved understanding of the damage process in bituminous materials at the macroscopic level [1, 2].

AFM is a scanning probe technique which measures both topological morphology and the spatial variations of mechanical properties. AFM has been used to probe

bituminous for more than a decade. Various authors have reported that on the micrometer scale bitumen exhibits a two phase morphology at the micrometer scale. AFM measurements of the bitumen microstructure reveals elliptical domains with a corrugated topology in the middle (termed as wrinkling pattern), ordered along the long axis of these domains which are surrounded by a continuous phase [3-5]. The present study focuses on probing with AFM the morphology of early stage cracks at the micrometer scale in bitumen as well as the disappearance of these micro cracks as function of moderate changes of temperature.

2. MATERIALS

Two bitumen samples of penetration grade 70/100 and 160/220, obtained from Q8 have been selected for this study. AFM images were taken in tapping mode using 'Multimode V' from Bruker. All scans were performed in air with RTESP (Bruker) cantilevers with a nominal force constant of 40 N/m and a resonance frequency of 330 kHz. An aluminium tape was used as the primary substrate and an AFM sample puck (12 mm diameter steel disk) was used as a secondary substrate.

3. METHODS

The sample was prepared on a piece of aluminium tape which was adhered to the steel substrate from the adhesive side. An amount of 20mg bitumen was placed on the tape and was heated using a heater plate for 30 seconds at 100°C to obtain a smooth thin and shiny film.

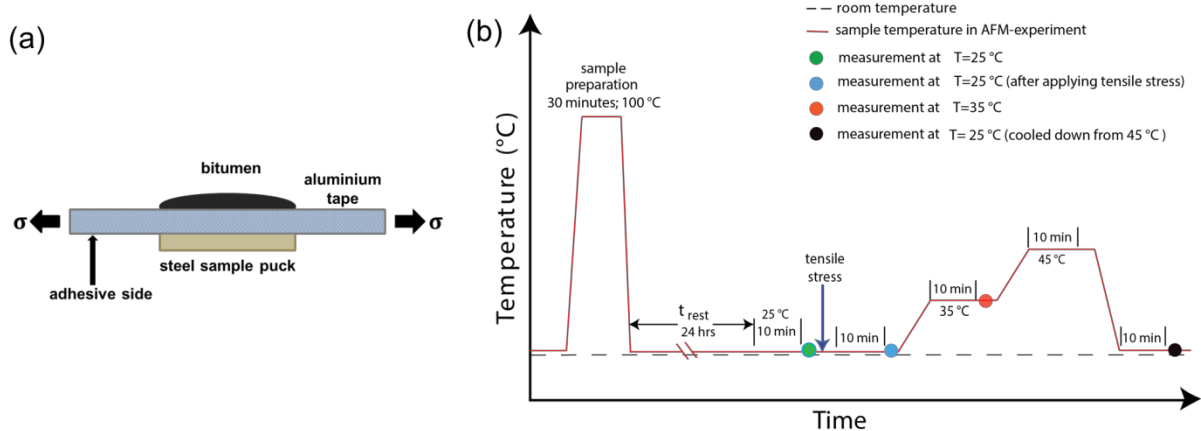


Figure 1: Schematic of (a) sample straining and (b) sample thermal conditioning and imaging protocol.

Two specimens were prepared for each bitumen grade. The samples were thermally conditioned inside an oven at 100°C for 30 minutes as shown in Figure 1b, followed by cooling in ambient air and storage at room temperature for 24 hours. One of these specimen was subjected to damage and a subsequent temperature dependent healing study, while the other sample was used as control. The neat specimen was first imaged by AFM at 25°C. The tape was then strained to initiate damage in the bitumen sample, Figure 1a. Then the strained sample was held for 10 minutes at the measuring temperature of 25°C and then imaged, Figure 1b. Next, the heat conductive aluminum tape was heated to 35°C, and then probed by AFM after 10 minutes of equilibration. The same procedure was followed, but now the temperature

was raised to 45°C, imaged after 10 minutes rest. Finally the sample was cooled down to 25 °C, and imaged again, Figure 1b.

4. RESULTS AND DISCUSSION

For both the bitumen samples (70/100 and 160/220) AFM topography and phase images (30×30 μm) were recorded, for both the neat and mechanically loaded samples, as a function of temperature, Figure 2. The characteristic features observed for the microstructure of the neat material are the presence of elliptical domains and the continuous phase surrounding these domains, Figure 2 a(i) and b(i). The phase images show a significant phase contrast between the domains to the continuous phase and an existence of lamellar phase (tertiary phase) around these domains. The morphology of the microstructure is found to depend on bitumen grade.

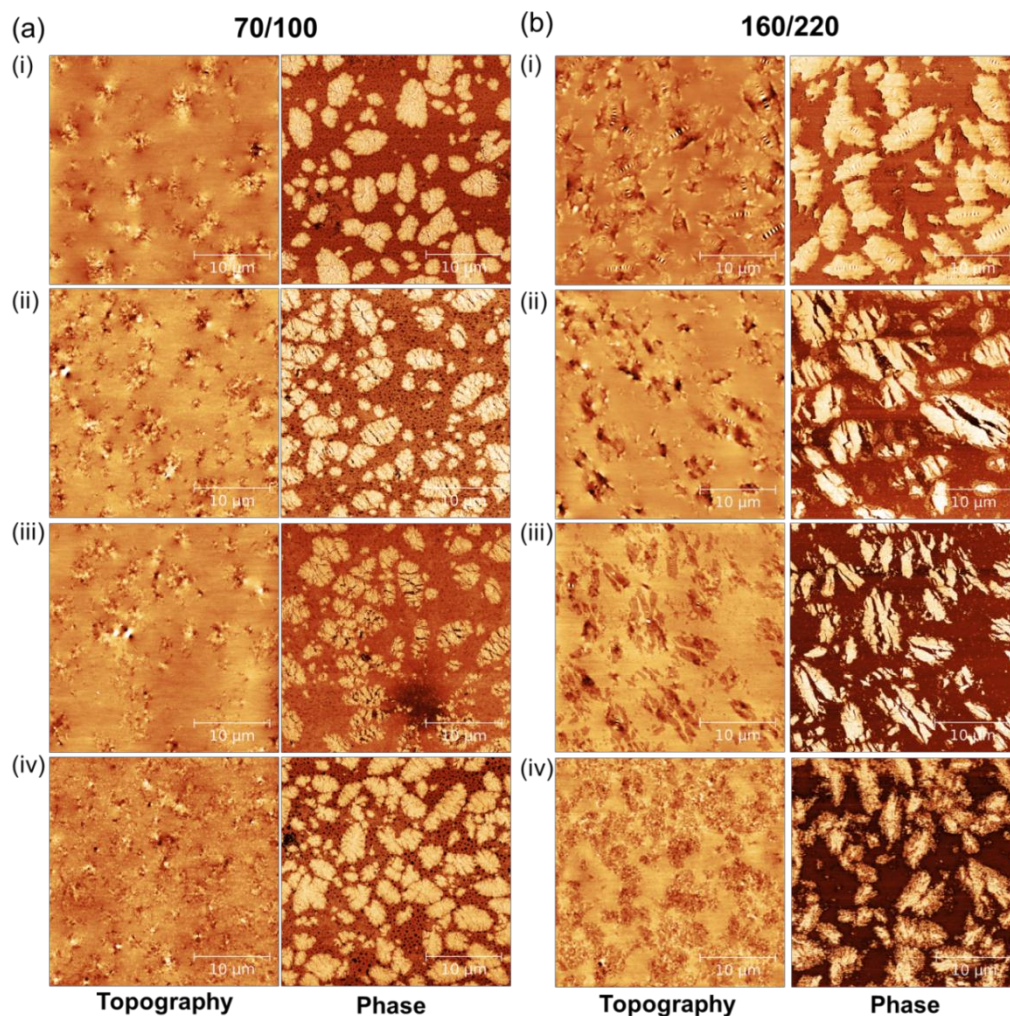


Figure 2: AFM images of a) 70/100 and b) 160/220 bitumen. i) neat sample at 25°C, ii) strained sample at 25°C, iii) same at 35°C, iv) same after cooling to 25°C.

Next, the microstructural response of mechanical loading of bitumen at room temperature is studied. Figure 2 a(ii), b(ii) reveal the impact of loading at the microstructural level. The existence of cracks in elliptical domains is observed. Crack lengths and widths are found to be higher for Q8 160/220 bitumen compared to Q8 70/100. Further, at increasing the temperature from 25 °C to 35 °C, the early cracks

remain visible, Figure 2 a(iii) and b(iii). Though around the edges of the elliptical domains softening is observed, possibly due to increased interfacial energy. Moreover the softened continuous phase tends to push the fragmented domains further apart. This may explain the increase of 'crack widths' within the domains at elevated temperature.

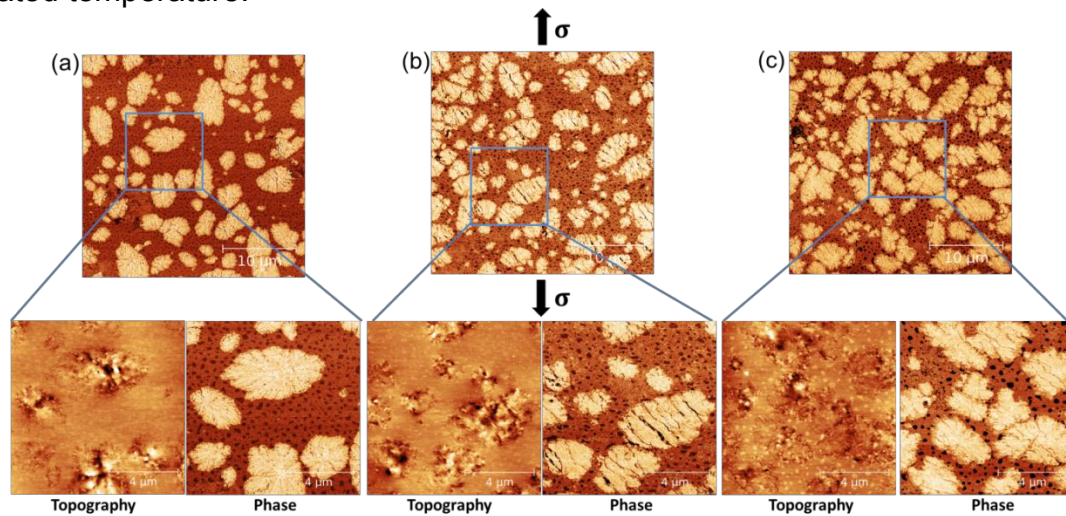


Figure 3: Crack closing observed by AFM of 70/100 bitumen. a) Neat sample at 25°C, b) strained sample at 25°C c) crack closure after cooling from 45°C to 25°C.

At 45°C both material phases have softened and cooling to 25°C, leads to rearrangement of the phases. For 70/100 the earlier observed fragments are pushed together again, allowing for healing by diffusion of molecules across the earlier crack surfaces, Figure 3. For 160/220 the fragments still display gaps at 25°C, so longer times at elevated temperatures would be required to observe the same.

5. CONCLUSIONS

By means of AFM the effect at the microstructural level of mechanical loading of bitumen was shown. Early cracking and fragmenting of domains was observed. Modest thermal changes of only 20°C lead to closing of the gaps between the fragments, allowing for strength recovery by diffusion. Surprisingly, this effect was found to be most pronounced for the harder 70/100 bitumen.

ACKNOWLEDGEMENT

The authors acknowledge the financial support of the Innovation Oriented Research Program (IOP) Self-Healing Materials, contract SHM01056 and Kuwait Petroleum Research & Technology for providing the materials.

REFERENCES

- [1] Jenq YS, Perng JD. Analysis of crack propagation in asphalt concrete using cohesive crack. *Transportation Research record*. 1991(1317):90–99.
- [2] Liang RY, Zhou J. Prediction of fatigue life of asphalt concrete beams. *International Journal of Fatigue*. 1997;19(2):117-124.

- [3] Masson JF, Leblond V, Margeson J. Bitumen morphologies by phase-detection atomic force microscopy. *Journal of Microscopy*. 2006;221(1):17-29.
- [4] Nahar SN, Schmets AJM, Scarpas A, Schitter G. Temperature and thermal history dependence of the microstructure in bituminous materials. *European Polymer Journal*. (accepted manuscript).
- [5] Pauli AT, Grimes RW, Beemer AG, Turner TF, Branthaver JF. Morphology of asphalts, asphalt fractions and model wax-doped asphalts studied by atomic force microscopy. *International Journal of Pavement Engineering*. 2011;12(4):291-309.

SELF-HEALING BITUMEN BY MICROCAPSULES CONTAINING REJUVENATOR

J.F. Su¹, J. Qiu¹ and E. Schlangen¹

¹ *Department of Materials and Environment, Faculty of Civil Engineering & Geosciences, Delft University of Technology, Stevinweg 1, 2628CN Delft, The Netherlands – e-mail: J.Su@tudelft.nl; J.Qiu@tudelft.nl; H.E.J.G.Schlangen@tudelft.nl*

Keywords: Self-healing, Microcapsules, Bitumen, Rejuvenator

ABSTRACT

Preservation and renovation bitumen of pavement is a big problem for the whole world. Traditionally, application rejuvenators is the only one method that can restore the original properties of the pavements. However, some puzzles still restrict its successful usage. Microencapsulation is a promising method to apply rejuvenator in bitumen. These microcapsules can break and leak the oily-liquid rejuvenator into microcracks and self-healing the aged bitumen. The aim of this work was to synthesize and characterize the physicochemical properties of novel microcapsules containing rejuvenator by in-situ polymerization of methanol-melamine-formaldehyde (MMF) prepolymer. A two-step coacervation (TSC) was successfully applied to enhance the thermal stability and compactability of shells with the help of styrene maleic anhydride (SMA) as surfactant. Thermal stability, mechanical stability and interface stability of microcapsules in bitumen were investigated. The results showed that these microcapsules containing rejuvenator survived in melting bitumen and in a violent repeated temperature changes. Mechanical properties indicated that the bitumen had the self-healing ability with the released rejuvenator from microcapsules. Microcapsules containing rejuvenator will be a promising product to realize the smart pavements.

1. INTRODUCTION

The aging problem of bitumen leads to pavement failure, including surface raveling and reflective cracking. It therefore increases the cost of renovating and preserving bituminous pavements. Rejuvenating agents have the ability to reconstitute the binder's chemical composition and they consist of lubricating and extender oils that contain a high proportion of maltene constituents. Rejuvenator can soften the aged binder and provide comprehensive rejuvenation that replenishes the volatiles and dispersing oils while simultaneously promoting adhesion. However, for a rejuvenator to be successfully applied the difficulty in penetrating the pavement surface still remains a significant problem. The method of encapsulating rejuvenators inside the bitumen may be an alternative approach worthy of consideration. In view of the above, the objective of this work was to fabricate microcapsules containing rejuvenator by in situ polymerization using MMF-resin shells and to then investigate their properties in bitumen.

2. MATERIALS

The shell material was commercial prepolymer of melamine-formaldehyde modified by methanol (solid content was 78.0%) purchased from Aonisite Chemical Trade Co., Ltd. (Tianjin, China). The rejuvenator was a commercial product. Styrene maleic anhydride (SMA) copolymer (Scripset[®] 520, Hercules, USA) was applied as dispersant. A small percentage of the anhydride groups have been established with a low molecular weight alcohol and it is fine, off-white, free flowing powder with a faint, aromatic odor. The bitumen used in this study was 70/100 pen obtained from Kuwait Petroleum in a 4.5% by weight. The material used as rejuvenator is dense, aromatic oil obtained from Petroplus Refining Antwerp (800DLA, Belgium).

3. METHODS

The fabrication and investigation methods have been reported in our previous work [1,2]. A thermal absorbing-releasing process was performed to investigate the thermal stability of bitumen/microcapsule composites using a temperature-controlled chest [3]. The state of microcapsules in bitumen could be observed by the fluorescence microscope. Fig.1 shows the testing method of the mechanical properties recovery of bitumen.

4. RESULTS

Fig.2(a) shows the optical morphologies of microcapsules in emulsion fabricated by emulsifying rejuvenator with a stirring rate of 4000 r·min⁻¹. Fig.2(b-c) and Fig.2(d) show the SEM surface morphologies of dried microcapsules with core/shell ratio of 1/1 fabricated by 4000 and 2000 r·min⁻¹ emulsion stirring rates. Their mean sizes are about 10 and 20 μm. The dried microcapsules still keep the regular global shape. There is no adhesion and impurity substance between microcapsules. The shells are compact without holes and cracks. To determine the shell thickness, microcapsules were embedded in epoxy resin as shown in Fig.2(e-f). Microcapsules were uniformly dispersed in epoxy. The cross-section SEM morphologies of a typical single microcapsule are presented in Fig.2(g).

Fig.3 shows the microcapsule states in bitumen with cracks. As shown in Fig.3(a), microcapsules are keeping compact structure in bitumen without defects and microcapsule has the mean size about 10 μm. Microcapsules survived in the bitumen under a temperature of 200 °C. The microcapsules retained their global shape with no cracks or thermal decomposition. These results indicate that these microcapsules can resist the thermal effects of asphalt for common applications

In Fig.3(b,c), microcracks were generated by liquid nitrogen quickly with a width of 10-20 μm. With the cracks propagation, the shell had been split by the tip stress of cracks (Fig.4(d)). Interestingly, it was found that the rejuvenators had rapidly filled the cracks under the capillary action (Fig.3(e)). Then the rejuvenator had permeated through both sides of cracks and the cracks were healed (Fig.3(f)).

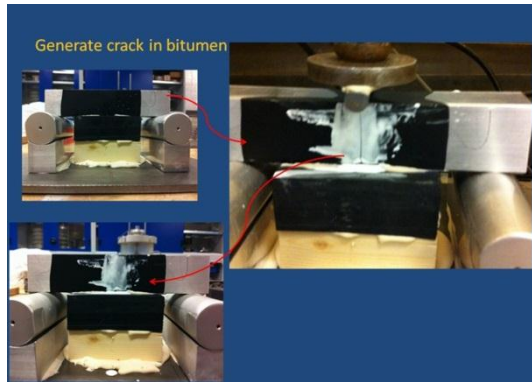


Figure 1: Testing method of the mechanical properties recovery of bitumen

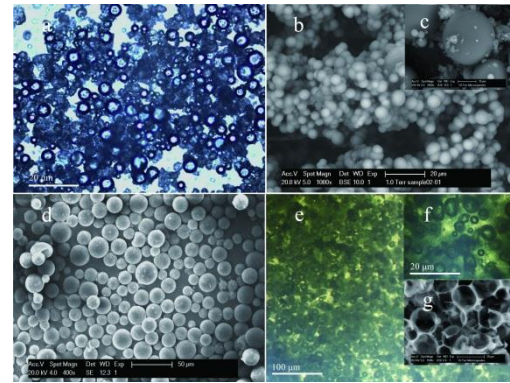


Figure 2: Morphologies of microcapsules containing rejuvenator

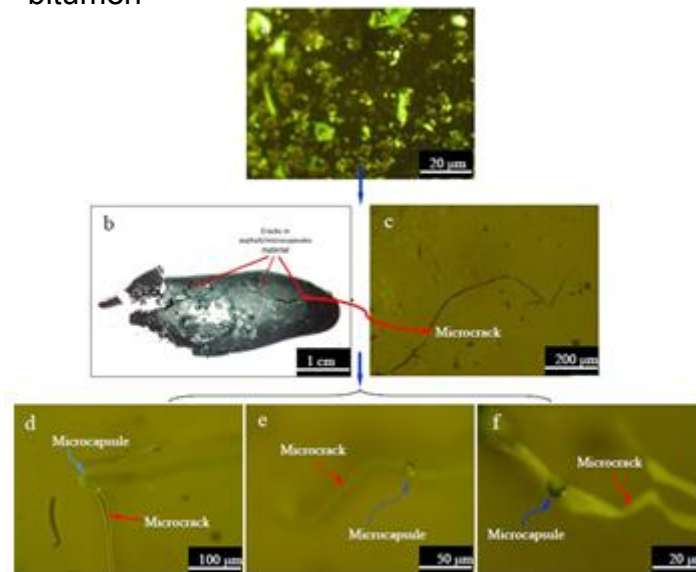


Figure 3: Morphology of bitumen/microcapsules sample treated by liquid nitrogen, (a) cracks appeared in bitumen sample by the low temperature brittleness treatment of liquid nitrogen, (b) original fluorescence microscope morphology of microcapsules in bitumen with cracks, (c-f) fluorescence microscope morphology of microcapsules in bitumen with cracks during 2 h.

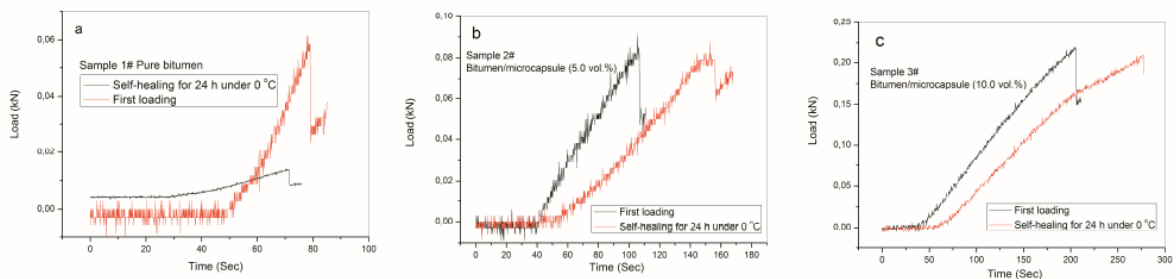


Figure 4: Mechanical test of self-healing bitumen/microcapsule composites under temperature 0 °C for 24 h. (a) pure bitumen, (b) bitumen/microcapsule (vol. 5.0%), (c) bitumen/microcapsule (vol. 10.0%), (d-e) fluorescence microscope morphologies of samples b and c. The microcapsules have a mean size of 20 μm, core/shell weight ratio is 2/1, bitumen and microcapsules mixing temperature is 160 °C.

Fig.4 shows the mechanical test of self-healing bitumen/microcapsule composites under temperature 0 °C for 24 h. It is clear that the bitumen samples with microcapsules (vol.5% and 10%) have a mechanical properties recovery.

5. CONCLUSIONS

Microcapsules had survived in bitumen under temperature of 200 °C, which indicates that these microcapsules can resist the thermal effect of bitumen in application. With the microcracks propagation, the shell had been split by the tip stress of cracks and the rejuvenators had rapidly filled the cracks under the capillary action. Later, the rejuvenator had permeated through both sides of cracks and the cracks were healed. Mechanical properties of bitumen has a recovery. Microcapsules containing rejuvenator will be a promising product to realize the smart pavements.

ACKNOWLEDGEMENTS

The authors acknowledge the financial support from the Delft Centre for Materials (DCMat) in the form of Project IOP Self-Healing Materials SHM1036, “Encapsulated rejuvenator for asphalt”. Dr. Jun-Feng Su also thanks the previous financial support of the National Natural Science Foundation of China (No. 50803045).

REFERENCES

- [1] J.F. Su, E. Schlangen, Synthesis and physicochemical properties of novel high compact microcapsules containing rejuvenator applied in asphalt. *Chemical Engineering Journal*, 198-199 (2012) 289-300.
- [2] J.F. Su, E. Schlangen, J. Qiu, Design and Construction of methylation-melamine-formaldehyde microcapsules containing rejuvenator for asphalt. *Powder Technology*, 235 (2013) 563-571.
- [3] J.F. Su, J. Qiu, E. Schlangen, Stability of self-healing microcapsules containing rejuvenator for bitumen. *Polymer Degradation and Stability*, In Press.

REINTRODUCING THE INTRINSIC SELF-HEALING PROPERTIES IN RECLAIMED ASPHALT BY REJUVENATION

J. Qiu¹, E. Schlangen¹, M.F.C. van de Ven¹ and M. Shirazi²

¹ Faculty of Civil Engineering and Geosciences, Delft University of Technology, Stevinweg 1, 2628 CN Delft, the Netherlands – e-mail: j.qiu@tudelft.nl; h.e.j.g.schlangen@tudelft.nl; m.f.c.vandeven@tudelft.nl

² Latexfalt BV, Hoogewaard 183, 2396 ZG Koudekerk aan den Rijn, the Netherlands – e-mail: morteza.shirazi@latexfalt.com

Keywords: asphalt, self-healing, reclaimed asphalt, rejuvenation

ABSTRACT

Reclaimed Asphalt (RA) is one of the largest fractions of raw materials used in road construction today. Probably over 90% of the total RA in the Netherlands is being reused in new asphalt constructions. RA contains aggregates coated with very hard bitumen (penetration grade of 10-20). During service, the bituminous binder loses its flexibility and its intrinsic self-healing capability because of ageing. These parameters are critical for reconstructing new durable surface layers. Therefore it is very important to reintroduce the flexibility and the intrinsic self-healing capability of the RA. In order to achieve this goal, rejuvenation technology is developed in this paper to re-compound to the aged bitumen in the RA. A preliminary research has been conducted to evaluate the effect of different potential rejuvenators on aged bituminous binders by means of laboratory blending. Two types of laboratory aged bitumen and six types of rejuvenators were developed. The rheological properties were evaluated by using the Dynamic Shear Rheometer (DSR), and the chemical compositions were evaluated using the Infrared Spectrometry (FT-IR). The thermodynamic properties of the blended bitumen were evaluated using the Differential Scanning Calorimetry (DSC) measurements. It is shown that with the blending of the rejuvenator into the laboratory aged bitumen is a physical process, the bitumen can regain its flexibility with a lower complex shear modulus, a higher phase angle and a lower glass transition temperature. A softer rejuvenator shows a higher potential. No significant chemical change can be observed for the rejuvenated bitumen. This research is on-going to investigate the diffusion capabilities of rejuvenators on the field aged reclaimed asphalt and the fatigue and healing evaluation.

1. INTRODUCTION

Typically, RA from surface layer such as reclaimed porous asphalt (RPA) contains high quality aggregates coated with very hard bitumen (penetration grade of 10-20). In practice, the RPA is recycled into base layer with a lower penetration grade bitumen. However, it is not allowed (or very limited amount) to recycle the RA from surface layer into surface layer. One of the main concern is that the currently used technology is not able to restore the intrinsic properties (e.g. flexibility, self-healing capability, etc.) and to guarantee the durability of the recycled porous asphalt. As a result, restoring the intrinsic properties of RPA during recycling process using rejuvenators is of great interest for surface-to-surface recycling. The rejuvenator,

which contains the lost light components of the aged bitumen, can be applied to penetrate and diffuse into the existing RPA to rebalance the material composition. This makes it possible for reconstructing new durable surface layers. In this paper, a preliminary research has been conducted to evaluate different potential rejuvenators on aged bituminous binders.

2. MATERIALS

Table 1 gives the information of the materials used in this paper. Two types of laboratory aged bitumen were produced namely P1 (25 pen.) and P2 (15 pen.) by using RCAT ageing device [1, 2]. A virgin bitumen with a penetration grade of 70/100 is used for comparison. Six types of rejuvenators were developed and provided by Latexfalt B.V. They are either oil type or emulsion type rejuvenators dependent on the area of final application.

3. METHODS

The aged bitumen were blended with different type of rejuvenators with certain dosages at a temperature of 150 °C for further analysis. The rheological properties were conducted using the Dynamic Shear Rheometer (DSR). The chemical compositions were evaluated using the Infrared Spectrometry (FT-IR). The thermodynamic properties of the blended bitumen were evaluated using the Differential Scanning Calorimetry (DSC).

4. RESULTS

Figure 1a gives an example of the complex modulus master curve of P1A2_20 blend (20 part of A2 mixed in 100 part of P1). A log log model was found to be applicable to estimate the rheological properties of a blend between rejuvenators and aged bitumen [3, 4] as shown in Eq. 1.

$$\log \log(|G^*|_{mix}) = a \log \log(|G^*|_a) + b \log \log(|G^*|_b) \quad (1)$$

In order to achieve a rheological properties of a blend similar to a virgin 70/100 penetration bitumen, the amount of rejuvenators used in the blend is dependent on the viscosity of the rejuvenators. As shown in Figure 1b, rejuvenators with a lower viscosity has more potential to rejuvenate the aged bitumen than the ones with a higher viscosity.

Table 1: Materials used in this research

Name	G* @50C 10Hz [Pa]	Type	Notes
Ref	5.2E+04	Virgin bitumen	70/100 pen.
P1	2.1E+05	Aged bitumen	25 pen.
P2	9.4E+05	Aged bitumen	15 pen.
A1	6.1E+02	rejuvenator	Oil type, liquid
A2	1.3E+02	rejuvenator	Oil type, viscous
BM1	8.4E+02	rejuvenator	Emulsion type, on residual
C1	5.0E+03	rejuvenator	Oil type, viscous
CM1	6.3E+01	rejuvenator	Oil type, liquid
D	1.3E+04	rejuvenator	Soft bitumen, 160/220 pen.

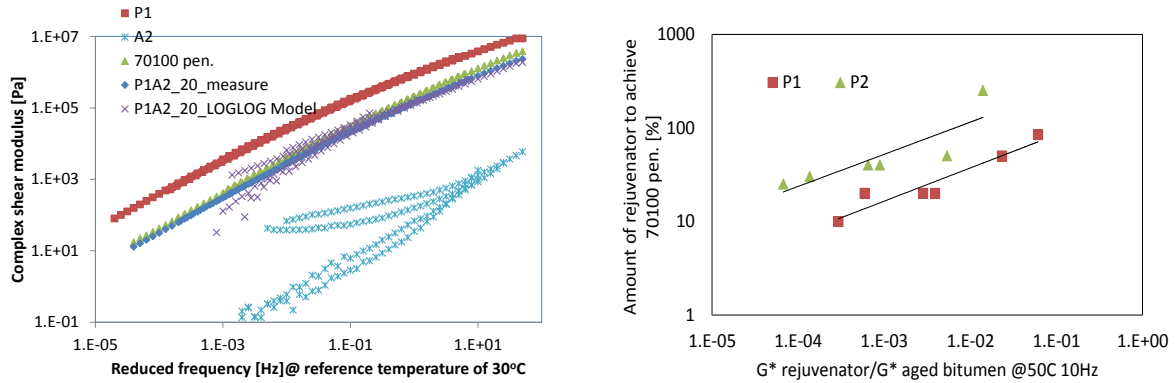


Figure 1: Rheological properties of rejuvenator-aged bitumen blends: (a) Example of master curve of P1A2_20; (b) Amount of rejuvenator to achieve the rheological properties of 70/100 pen. bitumen

Table 2: DSC results of rejuvenator-aged bitumen blends

Samples	Ref	P2	P2A1_10	P2C1_50
Tg (°C)	-22.3	-9.0	-27.0	-24.0

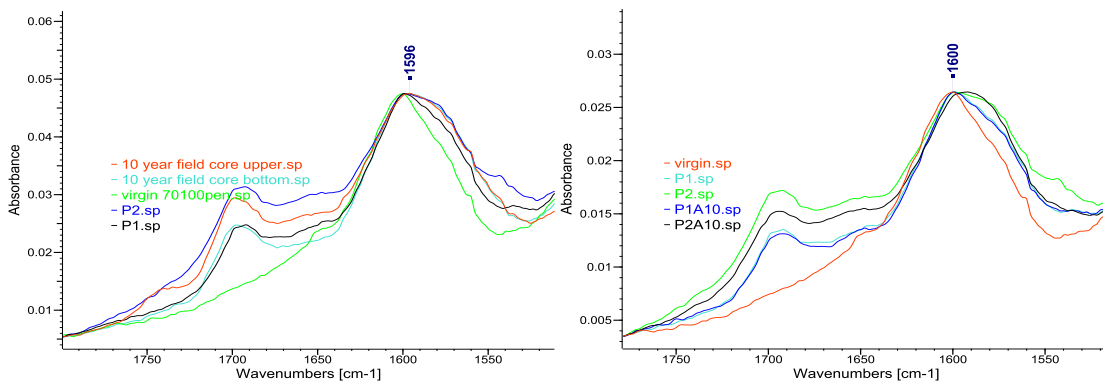


Figure 2: Example of FTIR results: (a) Aged bitumen; (b) Rejuvenator-aged bitumen blends

Table 2 shows the DSC results of the rejuvenator-aged bitumen blends. It can be observed that the lab aged bitumen increases the glass transition temperature. The blending of the rejuvenators into aged bitumen decreases the glass transition temperature to the level of the original bitumen.

As shown in Figure 2a, the FTIR was conducted on lab aged bitumen. It is shown that the lab aged bitumen P1 and P2 are comparable to bitumen extracted from the top part and the bottom part of a 10-year old porous asphalt with regard to the concentration of the carbonyl (C=O) at wavenumber of 1700 cm^{-1} [5]. This is believed to be the representative peak for ageing of bitumen. When mixing with rejuvenators as shown in Figure 2b, the amount of carbonyl in the bitumen samples does not change. This indicates that the blending of rejuvenators into aged bitumen does not alter chemical structure of the aged bitumen but only lower the complex modulus and glass transition temperature of the aged bitumen with soft components.

5. CONCLUSIONS

The blending of the rejuvenator into the laboratory aged bitumen is a physical process, the bitumen can regain its flexibility with a lower complex shear modulus, a higher phase angle and a lower glass transition temperature. A softer rejuvenator shows a higher potential. No significant chemical change can be observed for the rejuvenated bitumen. This research is on-going to investigate the diffusion capabilities of rejuvenators on the field aged reclaimed asphalt and the fatigue and healing evaluation.

ACKNOWLEDGEMENTS

The authors acknowledge the financial support from the Delft Centre for Materials (DCMat) in the form of Project IOP Self-Healing Materials SHM012019, "Reintroducing the Intrinsic Self-healing Properties in Reclaimed (Polymer Modified) Asphalt (RISP2RA)".

REFERENCES

- [1] Hagos, E.T., *The effect of aging on binder properties of porous asphalt concrete*. 2008, Delft University of Technology.
- [2] Van den bergh, W., *The effect of ageing on the fatigue and healing properties of bituminous mortars*. 2011, Delft University of Technology.
- [3] Epps, J.A., et al., *Guidelines for recycling pavement materials*, in *NCHRP Report No. 224*. 1980, TRB, National Research Council: Washington, D.C.
- [4] Lehtimäki, H., *Rejuvenating RAP with light oil products and a new mixing method for hot in-plant recycling*, in *Via Nordica 2012 Congress*. 2012: Reykjavik.
- [5] Jemere, Y., *Development of a laboratory ageing method for bitumen in porous asphalt*. 2010, Delft University of Technology: Delft.

SESSION 15 – SELF-HEALING FIBER-REINFORCED COMPOSITE MATERIALS

SELF-HEALING FIBER REINFORCED COMPOSITES, BEYOND THE CLEVER CONCEPTS?

V. Michaud¹

¹ *Laboratoire de Technologie des Composites et Polymères (LTC), Institut des Matériaux, Ecole Polytechnique Fédérale de Lausanne (EPFL), CH-1015 Lausanne, Switzerland*

Keywords: self-healing materials, polymer composites

ABSTRACT

Composite materials are man-made combinations of several different materials that produce a new material with unique properties, such as improved stiffness and tailored thermal or electrical conductivity. A large part of these materials combine stiffness and light weight, in particular those designed for transport applications. However, many of these materials, in particular based on thermoset matrices, are rather sensitive to damage, that may occur early, sometimes already from process-induced stresses. A recent development path for composites has been to introduce design concepts inspired from nature, that contribute to change the design from “damage prevention” to “damage management”: by introducing an autonomous self-healing ability to man-made materials, it becomes possible to extend their life-time above a certain design value, even if the initial material property is slightly reduced.

In this respect, self-healing composites are a dream for many structural engineers, as one wish that a structure could behave like a biological element that has the ability to detect damage and fix it to a certain extent, by continuously adapting to the changing environment, or by carrying repair fluids to the damaged zone. Due to the presence of reinforcement fibers, the mechanisms of damage in a composite are complex and take place at various scales. The healing system must be designed to act where needed, without further disrupting the structural integrity of the part. As a result, self-healing fiber reinforced composites have been demonstrated to a lesser extent compared to self-healing polymers, and they still pose technical and scientific challenges to reach maturity, and to move from basic laboratory concepts on model systems to practical applications.

The presentation will review current approaches to develop self-healing composites, and attempt to quantify and open to discussion the critical hurdles, from scientific to technical to economical aspects, that should be overcome to bring these materials closer to market applications.

MITIGATING THE EFFECTS OF SPACE DEBRIS ON COMPOSITE STRUCTURES EMBEDDING SELF HEALING AND CARBON NANOTUBE NANOCOMPOSITE MATERIALS

B. Aïssa^{1,2}, D. Therriault³, E. Haddad¹, W. Jamroz¹, K. Tagziria¹, J. Loiseau⁴,
A. Higgins⁴, M. A. Khan⁵ and S. V. Hoa⁵

¹MPB Communications Inc., Department of smart materials and sensors for space mission. Pointe Claire, Quebec, H9R 1E9, Canada.

²Institut National de la Recherche Scientifique, Énergie, Matériaux et Télécommunications, 1650 Boulevard Lionel Boulet, Montreal metropolitan, J3X 1S2, Canada.

³Center for Applied Research on Polymers (CREPEC). Mechanical Engineering Department, Ecole Polytechnique de Montréal, Montreal, Quebec, Canada;

⁴Shock waves physics Laboratory. Department of Mechanical Engineering. McGill University, Montreal, Quebec, H3A 2T5, Canada.

⁵Concordia Center for Composites. Department of Mechanical and Industrial Engineering. Concordia University. Montreal, Quebec, H3G 2M8, Canada.

Keywords: Self healing, space debris, composite structure, carbon nanotubes, hypervelocity impact tests.

ABSTRACT

The presence in space of micrometeoroids and orbital debris, particularly in the lower earth orbit, presents a continuous hazard to orbiting satellites, spacecrafts and the international space station. Space debris includes all non-functional, man-made objects and fragments. As the population of debris continues to grow, the probability of collisions that could lead to potential damage will consequently increase. We report on our recent results obtained on the application of self healing composite materials on impacted composite structures used in space. Self healing materials were blends of microcapsules containing mainly various combinations of a 5-Ethylidene-2-Norbornene (5E2N) and dicyclopentadiene (DCPD) monomers, reacted with ruthenium Grubbs' catalyst.

The self healing materials were then mixed with a resin epoxy and single-walled carbon nanotubes (SWNTs) using vacuum centrifuging technique. The obtained nanocomposites were infused into the layers of woven carbon fibers reinforced polymer (CFRP). The CFRP specimens were then subjected to hypervelocity impact conditions by using an advanced implosion driven-hypervelocity launcher - to simulate the space debris impact- with projectiles of about 4 mm in diameter and velocities up to 9 km/s. Although the microencapsulated self healing materials would not heal the impact's crater zone, we focused mainly on the reparation of potential delaminations developed around the impact-crater over distances much larger than the crater diameter. The different self-healing capabilities were determined and the SWNTs contribution was discussed with respect to the experimental parameters.

1. INTRODUCTION

A major challenge for space missions is that all materials degrade over time and are subject to wear, especially under extreme environments and external solicitations. Impact events are inevitable during the lifetime of a space composite structure, and

once they are damaged they are hardly repairable. More specifically, polymeric composites are susceptible to cracks that may either form on the surface or deep within the material where inspection/detection is often impossible. Materials failure normally starts at the nanoscale level and is then amplified to the micro up to the macro-scale until catastrophic failure occurs. The ideal solution would be to block and eliminate damage as it occurs at the nano/microscale and restore the original material properties.

This work reports on our recent results obtained on the application of self healing composite materials on impacted composite structures used in space. Self healing materials were blends of microcapsules containing mainly various combinations of a 5-Ethylidene-2-Norbornene (5E2N) and dicyclopentadiene (DCPD) monomers, reacted with ruthenium Grubbs' catalyst. The self healing materials were then mixed with a resin epoxy and single-walled carbon nanotubes (SWNTs) using vacuum centrifuging technique.

The obtained nanocomposites were infused into the layers of woven carbon fibers reinforced polymer (CFRP). The CFRP specimens were then subjected to hypervelocity impact conditions -prevailing in the space environment- using an advanced implosion driven-hypervelocity launcher. The fiber Bragg Grating (FBG) sensors were embedded in the composite material providing real-time information about the impact event and the healing process. The different self-healing capabilities were determined and the SWNTs contribution was discussed with respect to the experimental parameters.

2. MATERIALS

Single walled carbon nanotubes (SWNTs) materials have been synthesized by using the developed plasma torch technology (detailed process can be found in the Ref. [1]). In this approach, a carbon containing ethylene (C_2H_4) substance combined with gaseous catalyst based ferrocene ($Fe(C_5H_5)_2$) vapour are injected in an inert gas plasma jet. Figure 1 shows the morphology of the grown SWNTs where the transmission electron microscopy micrographs (TEM) show single nanotubes of 1.2 nm in diameter. The encapsulation of the (5E2N): 5-Ethylidene-2-Norbornene and (DCPD): dicyclopentadiene in poly (melamine urea formaldehyde) microcapsules was achieved following the protocol described in our Ref. [2]. Several batches of microcapsules were produced following the reported process. The size of the microcapsules was mainly controlled by varying the stirring-speed during the synthesis process.

Some samples of the smallest microcapsules synthesized from different batches are shown in Fig. 2. All samples were dried in air for at least 24 hours after their final washing and filtering. The woven CFRP samples containing self-healing demonstrator consists of epoxy used in space for internal structures (Epon 828 resin, with the Epicure 3046 curing agent), and 2 different healing agents (namely, 5E2N, DCPD) prepared as small microcapsules (diameter less than 15 microns) kept within thin shells of poly melamine (urea formaldehyde).

The monomer is homogeneously spread within the epoxy and forms about 10% of the total weight. The Grubbs catalyst was then distributed within the epoxy structure (1 to 2 % of the total weight). Different series of samples specimens were prepared, with and without CNTs.

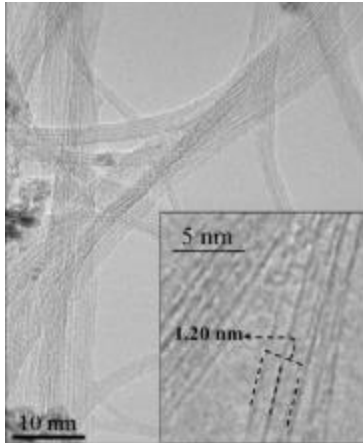


Figure 1: TEM of the as grown SWNTs

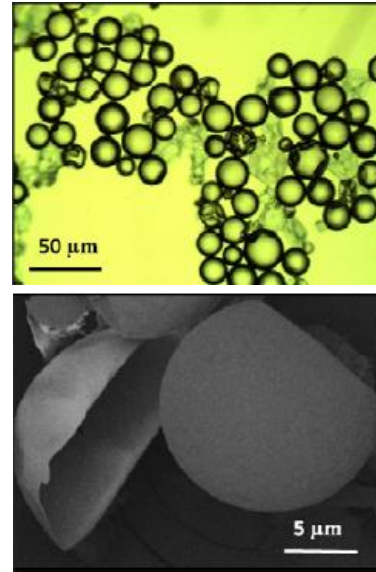


Figure 2: (up): optical image and; (down): scanning electron microscopy (SEM) image of the 5E2N monomer microcapsules.

3. METHODS

After the hypervelocity impact tests (Impact tests were performed with the implosion-Driven Hypervelocity launcher), the crack formed on the CFRP samples reaches a microcapsule and causes its wall rupture, which releases the healing agent monomer (5E2N or DCPD or combination of the two monomers). The FBGs sensors were embedded between the 2nd and 3rd CFRP layer, but concentrated inside a circle surface of 5 cm in diameter (see Fig. 3).

All the fabricated samples are tested under hypervelocity impact test at McGill University (Prof. A. Higgins Lab.) under the same conditions for comparison. To simulate the orbital space debris, small projectiles (3-4 mm-diameters) and velocities up to 9 km/s were employed. The set up of the test is shown in figure 4.

Impacted CFRP samples have been then measured under the flexural “3 point bending test” after the healing process (48 hours and 40° C) to investigate their mechanical properties and to evaluate the self healing capability after impacts event.

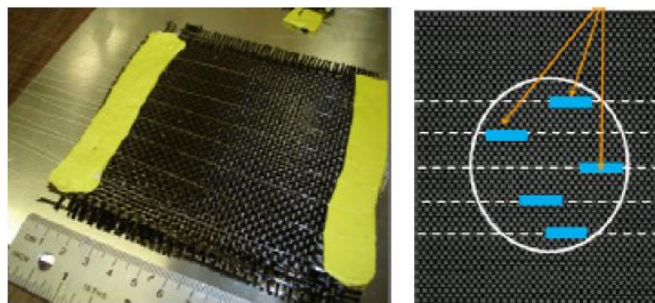


Figure 3: Integration of 4-8 FBGs sensors embedded between 2nd and 3rd CFRP layer and concentrated inside a circle surface of 5 cm-diam.

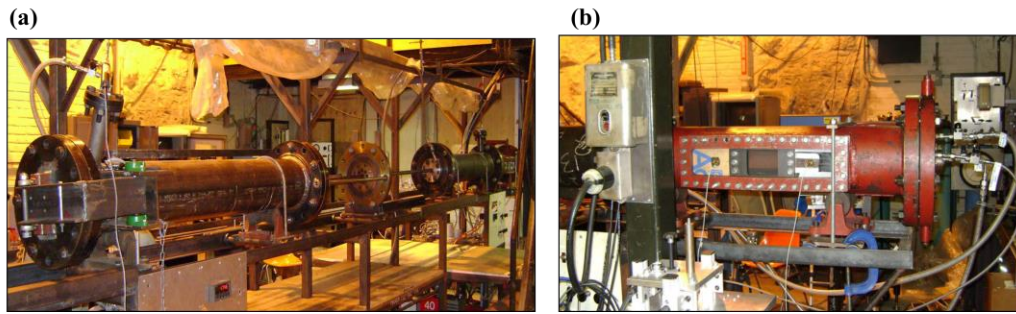


Figure 4: (a) Hypervelocity impact tests Launcher built at McGill University. Launched projectiles to 9 km/s. (b) Section where the CFRP samples are placed.

4. RESULTS AND CONCLUSIONS

When comparing the mechanical recovery to the pristine samples (i.e., containing only epoxy material), we can extract the healing part due exclusively to the self healing materials [3]. In doing so, we conclude the following:

- (i) 31 MPa are due exclusively to the self healing material based on 5E2N, which represents an enhancement in terms of the mechanical strength of about 13 %.
- (ii) When using the DCPD based healing agent, a better healing is obtained (improvement up to 18 % of the mechanical strength).
- (iii) When using a mixture of 50/50 wt. % of DCPD/5E2N healing agent, a slight decrease occurred (From 18 to ~15 %) in terms of the flexural strength, which is due to the incorporation of the 5E2N part (recall that the 5E2N is a linear polymer having lower mechanical strength, its addition to the DCPD slightly decreases somehow the overall mechanical strength of the mixture).
- (iv) A clear improvement is obtained when integrating the SWNT material, even with concentration as low as 0.5 wt. %.
- (v) Then, an enhancement up to 81 MPa in terms of the mechanical recovery is due the healing materials containing 2 wt. % of SWNT, which represents an improvement in the mechanical strength as high as 33 %.

ACKNOWLEDGEMENTS

We acknowledge the financial assistance of the Canadian Space Agency and the constructive advise of Dr. D. Nikanpour and Dr. S. Gendron from CSA, for their support during this work.

REFERENCES

- [1] O. Smiljanic, B.L. Stansfield, J.P. Dodelet, A. Serventi and S. Désilets, Gas-phase synthesis of SWNT by an atmospheric pressure plasma jet, *Chem. Phys. Lett.* 356 (2002) 189-193.
- [2] B. Aïssa, E. Haddad, K. Tagziria, W. Jamroz, Exploring Self Healing of CFRP Laminates Exposed to Hypervelocity Small Pellets Simulating Space Debris, proceedings of 26th Technical Conference/Second Joint US-Canada Conference on Composites, (2012) paper 1066.
- [3] X. Liu, X. Sheng, J.K. Lee, M.R. Kessler, Isothermal cure characterization of dicyclopentadiene, *J. Therm. Anal. Calorim.* 89 (2007) 453-457.

DAMAGE REDIRECTION AND HEALING IN SKIN-STIFFENER DEBONDING SPECIMENS UNDER FATIGUE CONDITIONS

R. Luterbacher¹, I.P. Bond¹ and R.S. Trask¹

¹ *Advanced Centre for Composite Innovation and Science (ACCIS), University of Bristol, Queen's Building, Bristol, BS8 1TR, United Kingdom –e-mail: rafaelluterbachermus@bristol.ac.uk, i.p.bond@bristol.ac.uk, r.s.trask@bristol.ac.uk*

Keywords: Fibre reinforced composite, adhesive joint, self-healing, vascular network, interleaves, delamination.

ABSTRACT

Locally stiffened or 'stringer' - skin composite structures are extensively used for lightweight applications in the aerospace industry. Due to localised stiffening, stress concentrations arise which can initiate damage e.g. debonding or delamination, within the composite structure. Critically, this damage can propagate under fatigue loading compromising the structural integrity of the component. To mitigate against this risk, significant safety margins are used within the design phase, which limit the potential weight savings offered by the application of advanced fibre reinforced composites.

In this study, the potential to redirect propagating cracks away from critical failure paths and into dedicated self-healing zones has been investigated through the use of thermoplastic interleaves (for redirection) and an embedded vascular network (to mitigate the damage). One of the major challenges in employing a vascular network is to ensure the connectivity between the propagating damage and the vasculature.

A self-healing agent (low viscosity epoxy resin) was delivered via the vascular network in order to restore the mechanical performance of the deteriorated structural element. A number of different interleave – vasculature configurations have been investigated, all successfully redirecting the propagating fatigue damage into the vasculature within skin-stiffener debonding specimens. The tensile and fatigue tests performed have shown that these modifications are not detrimental to the mechanical performance in comparison to a baseline configuration. Moreover, the interleave configurations are able to redirect the interfacial damage, between the skin and the stiffener, towards the self-healing functionality embedded within the laminate. During fatigue loading, a notable stiffness loss is observed as the damage propagates. After the healing event, the stiffness in both static and fatigue conditions has been successfully restored.

1. INTRODUCTION

Composite materials are used in lightweight applications, e.g. aerospace industry, for their high specific mechanical properties. One common design concept in the aerospace industry is to use locally stiffened or "stringer"-skin configurations. This design philosophy is efficient as the skin takes the in-plane loads, whereas the stiffening elements provide increased stiffness and a reduction of the effective buckling length. However, due to the localised increment in stiffness, through

thickness stresses arise at the edges of the stiffening element giving rise to delaminations sources, which if untreated, could lead to catastrophic failure in terms of stiffener debonding. The aim of this project is to redirect delaminations within such configurations with the help of interleaves into a vascular network through which a healing agent is injected into the composite.

2. MATERIALS AND METHODS

“Skin/ stringer flange debond specimens” [1] were manufactured using a pre-impregnated E-glass/913 epoxy (Hexcel, UK). The flange was pre-cured, cut to size and co-bonded to the skin. The lay-up for both flange and skin was $[-45_2, 0_2, 45_2, 90_2]_S$. Figure 1 summarizes the specimen set-up and the different configurations studied.

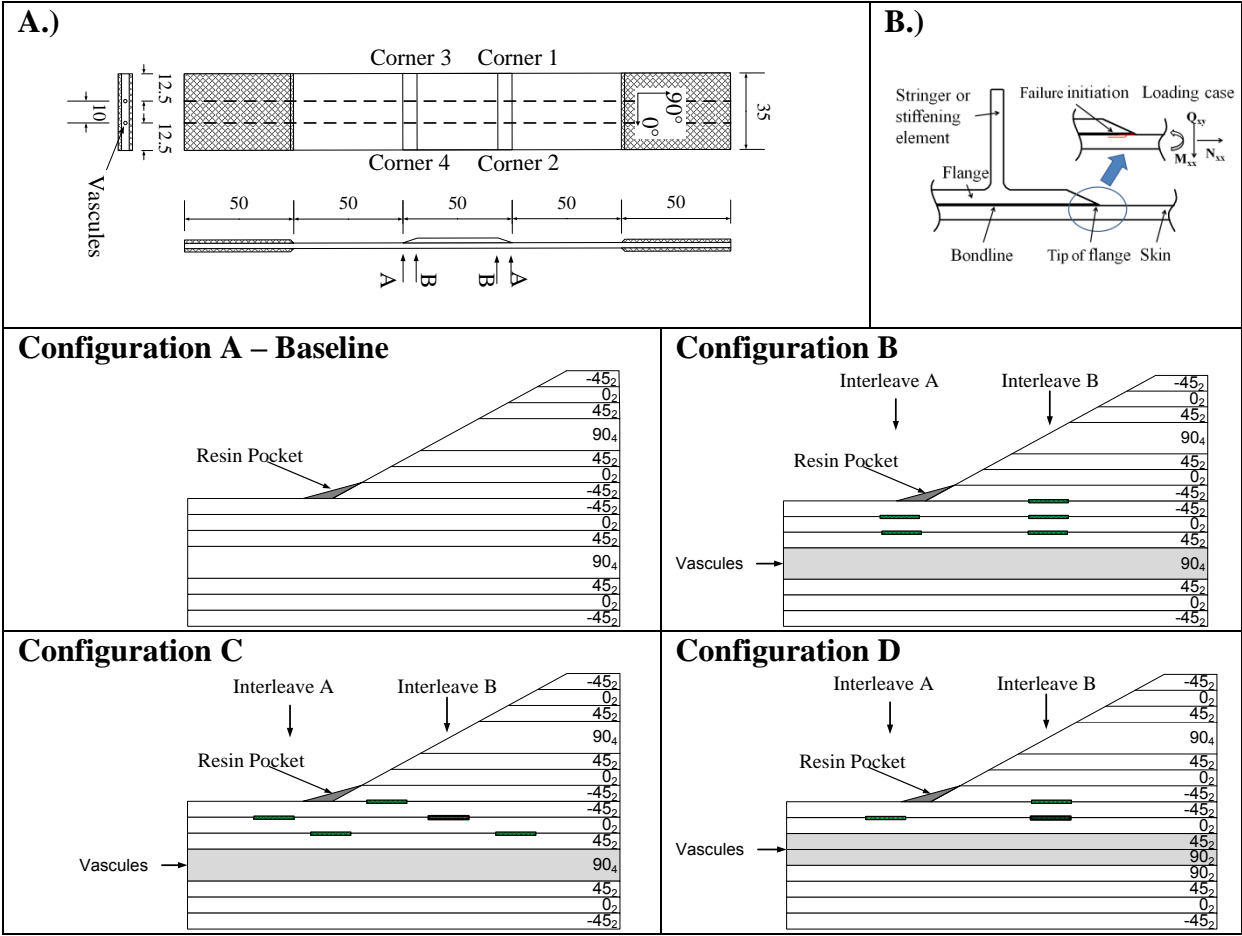


Figure 1: A.) Specimen nominal dimensions (unit: mm) and edge identification. Note vasculures only present for ID B, C and D. B.) Co-bonded skin/stringer configuration with loading

Each specimen of configuration B, C and D contained two vasculures manufactured by removing ply sections and embedding steel wires (diameter 0.56mm) between these cut outs [2]. The selected interleave material was a nominal 50 μm thickness and 3 mm wide polyethylene-co-methacrylic acid (EMAA) film. A commercially available low viscosity resin (Resintech RT151) was used as a healing agent.

In order to assess the influence of the interleaves and the vascular network on the mechanical properties, specimens of the different configurations were tested in static and tensile fatigue loading.

For assessment of the healing performance, the healing agent was injected after 10 000 cycles and then cured at 65°C and then cycled again.

3. RESULTS AND DISCUSSION

Static tensile test results (Figure 2 A) and tensile fatigue test (Figure 2 B) performed at 40% of the ultimate tensile strength ($F_{max}=10kN$, $R=0.1$) show that the introduction of vasculs and interleaves do not alter the global mechanical properties.

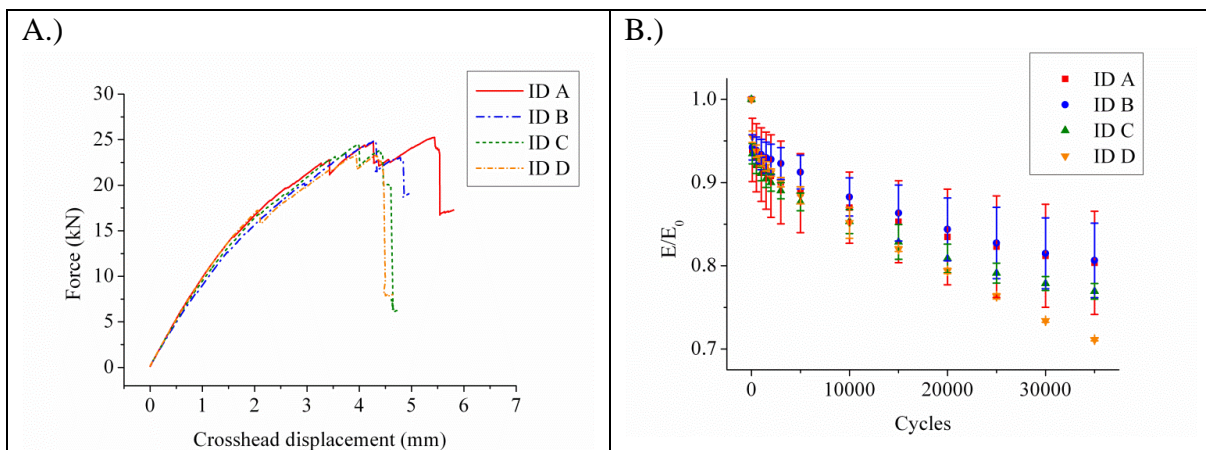


Figure 2: A.) Representative tensile test results for the different tested configurations B.) Stiffness loss as function of cycles for the different tested configurations

After fatigue testing, the damage patterns on the specimen edges were analysed using optical microscopy. Specimens of configuration A (baseline) showed delamination growth along several ply interfaces. However, specimens containing interleaves developed “damage free zones” located inwards from interleave B (refer to

Figure 1). In the observed configurations (total 14 specimens 4 of B, 5 of C, 5 of D), in 96% of all the cases, the delaminations migrate into a lower ply interface when exiting the interleave. In the remaining 4% the delaminations are arrested in the interleave. Our observations suggest that the interleaves enhance the “inherent” tendency of delaminations to migrate into lower plies.

The following mechanism is suggested: as the delaminations are slowed down in the interleave due to the higher toughness [3], [4], the mechanism of ply splitting (migration) overtakes that of propagation and induces the delamination to migrate into the next ply interface within the interleave. In addition, the exit of the delamination accelerates damage growth due to the decrease of fracture toughness [3]. Therefore, the migration along the brittle fibre matrix interface into a lower ply interface is enhanced.

Through this approach, the delaminations have been successfully steered into the interfaces where the vasculs are located. In this way, delaminations propagating along these interfaces will intersect with the vasculs and thus connectivity is assured.

Connectivity between the vasculates and the damage site has been observed by fatigue testing two specimens (one of configuration C and one of configuration D) with red dye penetrant within the vasculates (Ardrox 996PA) (Figure 3 A). From approximately 10 000 cycles onward, connectivity between the damage sites at the corners and the vasculates has been observed in both cases by “bleeding” on the corners. In addition, damage has been visualised in the skin area.

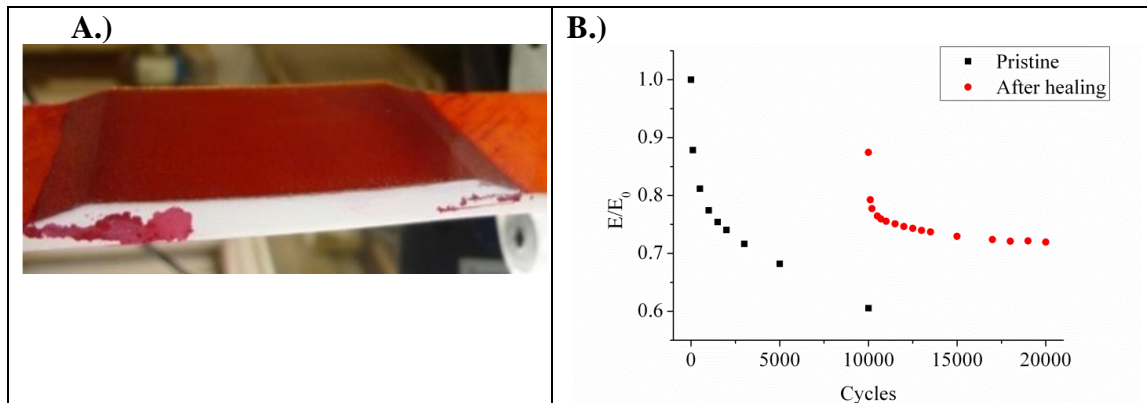


Figure 3: A.) Damage visualisation B.) Stiffness recovery after healing

Figure 3 B shows an example for the healing performance: One specimen of configuration B was cycled for 10 000 cycles resulting in a stiffness loss of 40% as compared to the initial stiffness. The healing agent was injected successfully through both vasculates and cured at 65°C for 1h. A stiffness recovery to 87% of the initial modulus was achieved. After additional cycling of the specimen for 10 000 cycles the stiffness dropped to 72% of the initial stiffness.

4. CONCLUSION

The delamination paths have been steered successfully by the interleaves into the interfaces with vasculates thereby giving the possibility of (1) damage detection and (2) healing. Healing provided partial recovery of the mechanical properties under fatigue conditions.

ACKNOWLEDGEMENTS

The authors would like to acknowledge the Spanish “Fundació la Caixa” and the UK Engineering and Physical Sciences Research Council (EPSRC) for funding for the project.

REFERENCES

- [1] P. J. Minguet and T. K. O’Brien, “Analysis of Test Methods for characterizing skin/stringer debonding failures in reinforced composite panels,” in Composite Materials: Testing and Design (Twelfth volume), 1996, pp. 105–124.
- [2] C. J. Norris, I. P. Bond, and R. S. Trask, “The role of embedded bioinspired vasculature on damage formation in self-healing carbon fibre reinforced composites,”

Composites Part A: Applied Science and Manufacturing, vol. 42, no. 6, pp. 639–648, Jun. 2011.

[3] M. Yasaee, I. P. Bond, R. S. Trask, and E. S. Greenhalgh, “Mode I interfacial toughening through discontinuous interleaves for damage suppression and control,” Composites Part A: Applied Science and Manufacturing, vol. 43, pp. 198–207, 2012.

[4] S. Singh and E. S. Greenhalgh, “Micromechanics of interlaminar fracture in carbon fibre reinforced plastics at multidirectional ply interfaces under static and cyclic loading,” *Plastics, rubber and composites processing and applications*, vol. 27, no. 5, pp. 220–226, 1998.

ADAPTED PROCESSING ROUTES FOR SELF-HEALING FIBRE-REINFORCED COMPOSITES

E. Manfredi¹ and V. Michaud¹

¹ *Laboratoire de technologie des composites et polymères (LTC), Ecole Polytechnique Fédérale de Lausanne (EPFL), Station 12, CH-1015 Lausanne – e-mail: erica.manfredi@epfl.ch; veronique.michaud@epfl.ch*

Keywords: composites, impact, self-healing, X-ray tomography, compaction

ABSTRACT

Fibre-reinforced polymers development has been driven by the need for materials that combine high stiffness and low density, but composites based on thermoset matrices tend to remain sensitive to damage, that may occur early in the matrix. Improved efficiency could be gained by integrating functionalities into the structure, namely a self-healing matrix for repairing low-extent cracks (i.e. barely visible impact damage). Challenges remain to develop an adapted and effective manufacturing methodology to effectively transfer the know-how from self-healing *polymers* to self-healing *composites*.

Vacuum assisted resin infusion moulding (VARIM) is selected as processing technique, since it presents several advantages compared to hand lay-up, including a better quality, uniform part thickness and reproducibility compatible with low-volume industrial applications. The process is firstly optimized for production of thick glass fabric reinforced samples suitable for compression after impact tests and for fast gelation time resin systems such as EPON 862 with DETA as hardener.

Secondly, fabrics are functionalized with capsules containing EPA solvent, taking into account both geometric and capsule strength considerations. On one hand, the fabric type, the dispersion technique and the optimal capsule size are determined through X-ray tomography of fabrics and optical imaging of functionalized fabrics prior to and after processing. The optimal amount of healing agent needed to fill delaminations from small energy impacts is also determined by optical image analysis of impacted samples. In parallel, capsules are characterized for their compression behaviour and bursting strain as a function of the shell type, from pure UF shell to combined UF/PU shells with varying contents of PU. This is then related to their behaviour inside the fabric during the compaction created by the vacuum bagging prior to infusion, to ensure capsule survival during the process.

1. INTRODUCTION

Processing thick and possibly capsule-functionalized fiber reinforcement stackings via vacuum assisted resin infusion moulding (VARIM), preferred to other techniques as hand lay-up [1], is not straightforward and manufacturing parameters need to be adapted. The aim of this study is to find optimal, reproducible and reliable solutions to produce self-healing glass reinforced epoxy materials that could be further mechanically tested through compression after impact experiments.

2. MATERIALS

The composite matrix is a bisphenol F diglycidyl ether resin (Epon 862), cured with diethylentriamine in a 100:12 weight ratio for 24h at room temperature and post-cured for 24h at 35°C. With this cycle, the matrix is undercured (about 71% conversion right after the post-cure treatment [2]), to allow a potential solvent-based healing to further occur. The reinforcement is a standard woven twill 2x2 E-glass with aerial weight of 390 g/cm². 16 layers of fabric with [(+45,-45),(0,90)]_{4s} as stacking sequence are used to achieve a target fiber volume fraction (V_f) of 50%. Urea-formaldehyde shell microcapsules are produced with the established protocol developed by Caruso et al. [3] and sieved to include diameters in the range of 125-250 µm: microcapsule core is a solution of 2.5 vol% of Epon 828 in ethyl phenylacetate (EPA). Overall capsule volume fractions (V_c) are 1.25, 2.5 or 3.75%, corresponding to capsule volume fraction over matrix (V_c^*) of 2.5, 5 and 7.5% respectively.

3. METHODS

The superficial interstice dimensions of the selected fabric are explored by optical microscopy and X-ray micro-computed tomography. Produced capsules are characterized by optical and scanning electron microscopy, thermogravimetric analysis and mechanically tested with a micromechanical compression test. Capsules with diameters in the range of 125-250 µm are manually spread onto the fabric cloths by using a 250 µm sieve.

Prior to manufacturing, the loading-unloading properties of plain and capsule-functionalized fabrics of 100x100 mm are analyzed through a displacement controlled compression test (2 µm/s, pressure 0-8 bar) in a Universal Testing System (Walter & Bai AG, Switzerland) and compared. The pressure range 0.1-1 bar is analyzed since it corresponds to the effect of the pressure difference during VARIM.

Loading data in terms of pressure as a function of V_f are fitted to a simple power law $P=a(V_f)^n$ and fitting parameters a and n are compared. A three zone-fitting is considered.

Further processing of plain and capsule-containing 660x360mm panels is then performed through VARIM and specific manufacturing solutions are optimized to prevent undesired phenomena such as resin viscosity increase and wedge-shaped resin front, that would lead to a poor impregnation. Hence, post-manufacturing verifications allow us to check the composite components and porosity fractions and to validate the processing protocol in the presence and in the absence of capsules.

4. RESULTS

The 125-250 µm fraction of produced capsules (stirring rate of 400 rpm) have a number-length and volume-moment average diameters of 147 and 156 µm respectively, a shell thickness of 200 nm, typical thermal and mechanical behaviours (Figure 1), namely a gradual weight loss at about 100°C and size-dependent bursting forces ranging from 5 to 10 mN, corresponding to a Young's modulus of 3 GPa.

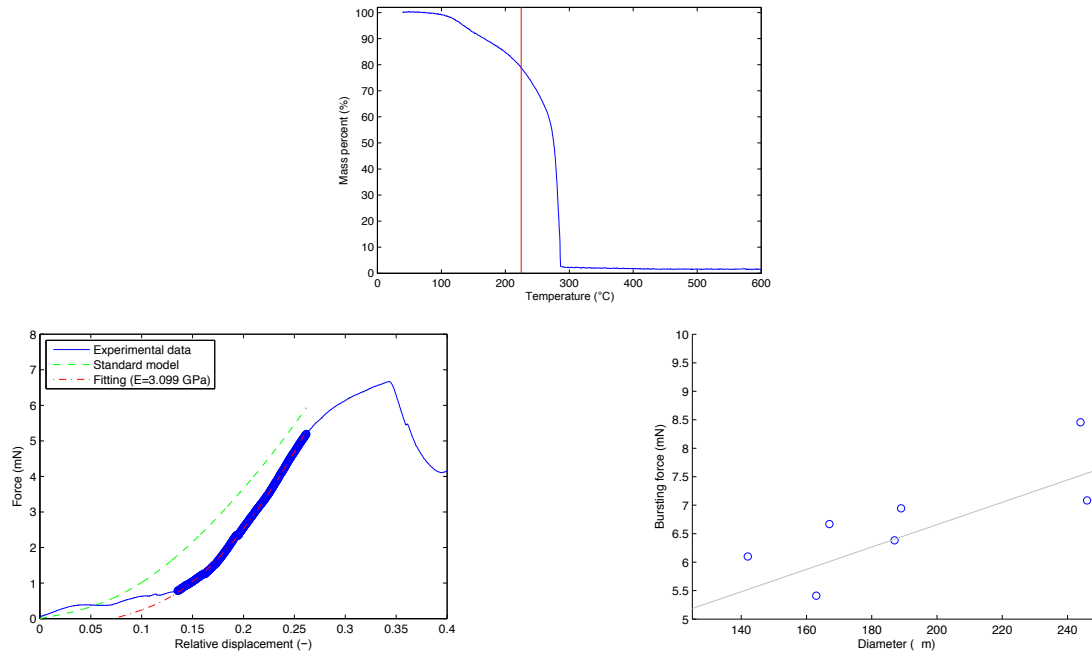


Figure 1: Typical thermal and mechanical behaviour of produced capsules.

Such a diameter range is chosen since both optical imaging and X-ray micro-computed tomography demonstrate interbundle interstices in the range 150-200 μm (width), in which such capsules can thus fit (Figure 2); the yellow area gives a visual indication of the volume –in scale- occupied of 125-250 μm capsules if laying within the interstices and/or onto the fiber bundles.

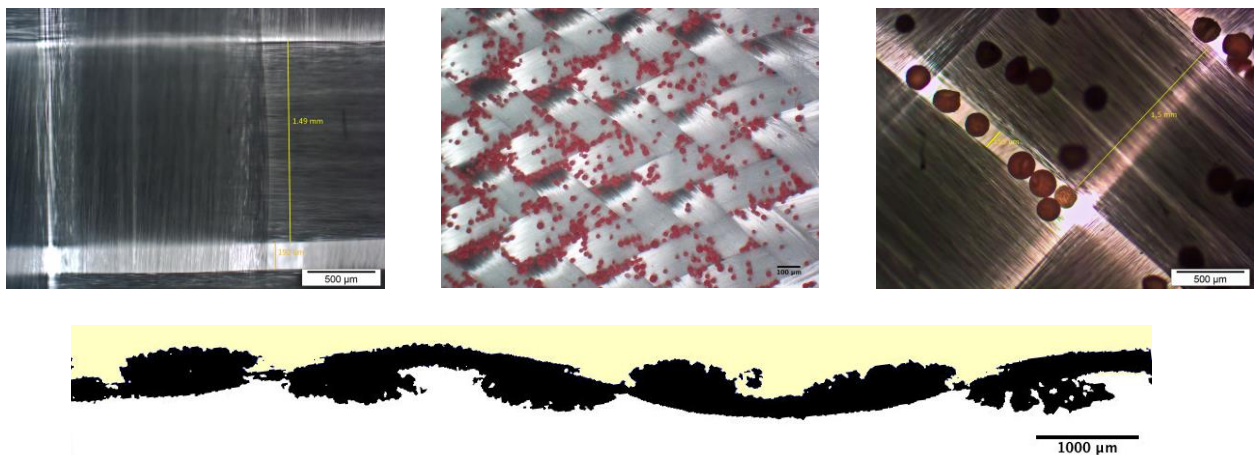


Figure 2: Optical microscopy and X-ray micro-computed tomography images of the plain and capsule-functionalized fabric.

After manually sieving such capsules onto the reinforcement fabrics, their state of dispersion/distribution is visually checked: as expected, it is confirmed that capsules are in general prone to fall down, due to gravity, within the interstices; nevertheless, some of them lay on the top of warp/weft bundles. It is supposed that capsules fitting the interstices keep more protected and safe and do not increase significantly the overall thickness, whereas those onto the bundles would be more responsible for a thickness increase and more susceptible to breakage while the fabric stacking packs. Results of compression tests of plain and capsule-functionalized fabric (Figure 3)

showed that the presence of capsules causes an increase of the overall stack thickness, and that it constitutes an interference for fabric nesting over loading; this phenomenon becomes more significant as the amount of capsules increases. Moreover, the presence of capsules within the interstices is confirmed since the thickness increase (in unloaded conditions) is lower compared to a potential case with all capsules onto the bundles (+0.28 instead 2.35 mm for the 2.5% capsule content). Hence, lower V_f are achievable when processing functionalized instead of plain fabrics, for equal applied pressure. This is proved with post-manufacturing verifications of plain and capsule-containing panels, processed with equal vacuum level (0.9 bar): preliminary results with V_c of 1.25% already showed higher average thickness and lower V_f compared to the plain composite. However, the comparison between expected data (from compression curves) and experimental ones is not straightforward due to the presence of an impregnating fluid in the latter case.

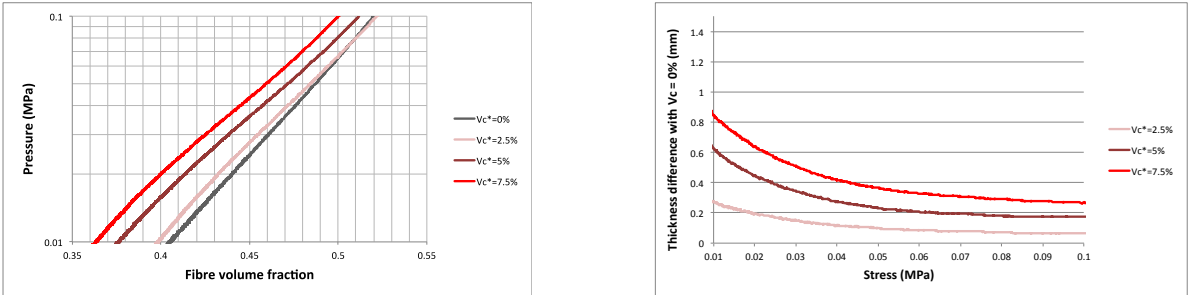


Figure 3: Compressibility of plain and capsule-functionalized fabrics (zoom 0.1-1 bar).

Table 1: Expected and experimental V_f and overall thickness at 0.9 bar pressure.

V_c^* (V_c)	V_f (expected)	V_f (experimental)	Thickness (mm) (expected)	Thickness (mm) (experimental)
0 (0)	0.515	0.462	4.535	5.138
1.25 (2.5)	0.516	0.397	4.562	5.600
2.5 (5)	0.506	on going	4.654	on going
3.75 (7.5)	0.495	on going	4.764	on going

5. CONCLUSIONS

It is shown that manual sieving is an effective and quite reproducible approach to spread microcapsules onto reinforcement fabrics prior to manufacturing. The optimal capsule size is chosen depending on the fabric interstice dimensions. However, the presence of capsules modifies the fabric packing behaviour, thus different processing conditions to obtain equivalent V_f are required.

ACKNOWLEDGEMENTS

Swiss National Science Foundation (FNRS 511482) and S. Neuser are gratefully acknowledged.

REFERENCES

[1] A. J. Patel, N. R. Sottos, E. D. Wetzel, S. R. White, Autonomic healing of low-velocity impact damage in fiber-reinforced composites, Composites Part A: Applied

Science and Manufacturing 41 (2009) 360-368.

[2] S. Neuser, V. Michaud, Effect of aging on the performance of solvent-based self-healing materials, submitted to Polymer Chemistry

[3] M. M. Caruso, D. A. Delafuente, V. Ho, N. R. Sottos, J. S. Moore, S. R. White, Solvent-promoted self-healing epoxy materials, *Macromolecules* 40 (2007) 8830-8832.

SESSION 16 – SELF-HEALING COATING AND PAINTS

LIFE EXTENSION IN PROTECTIVE COATINGS VIA SELF-HEALING TECHNOLOGY

G.O. Wilson ¹

¹ *Autonomic Materials, Inc., Champaign, IL, USA – email: gw@autonomicmaterials.com*

Keywords: Self-healing polymers, corrosion resistance, smart coatings, protective coatings, microencapsulation.

ABSTRACT

As the field of self-healing materials continues to grow, novel self-healing concepts and chemistries are being developed for a variety of applications including coatings. Self-healing functionality is typically considered for incorporation in coatings to solve two basic challenges including restoration of aesthetic properties and restoration of protective function. In this talk I will compare these challenges and discuss the capability of existing technologies to meet them. I will then discuss examples of the development and application of self-healing chemistries to protective coatings and the level of success achieved in autonomic repair of coatings that have been damaged via a variety of mechanisms. These examples will include a range of laboratory and commercial formulations evaluated with a target of real world deployment in the near future.

1. INTRODUCTION

Introduction to the Concept of Self-Healing Materials

Self-Healing materials are a class of smart materials that are capable of repairing themselves, when they are damaged, at ambient temperature, without any external intervention. Self-healing in materials is a bio-mimetic concept modeled after the capability of biological systems to autonomically repair or re-generate after damage. Given the definition of self-healing technology provided above and the biological systems that these technologies are modeled after, not all technologies commonly referred to as self-healing are truly self-healing. Healing technologies can broadly be classified as autonomic and non-autonomic healing technologies. These classifications and representative examples are described below.

Non-Autonomic Healing in Materials

There are many examples of technologies that impart the ability to respond to specific external stimuli such as heat or UV radiation for healing. These technologies harken back to the original examples of crack healing in polymers, which utilized solvents and heat to repair cracks.[3] More recent examples of heat-initiated healing technologies include re-mendable polymers, which have demonstrated crack healing based on Diels–Alder and retro-Diels–Alder reactions at temperatures between 90 °C and 120 °C.[1,2] Other examples of heat-initiated healing technologies include polyurethane resins capable of crack healing when heated above their glass transition temperatures.[2] Oxetane-substituted chitosan polyurethane networks capable of crack healing when exposed to UV light have also been reported.[2]

Another recently reported UV light-initiated healing technology is based on supramolecular materials formed by metal–ligand interactions.[4] Upon exposure to UV light, the metal-ligand functionalities in the material are disengaged facilitating flow of the material to minimize or repair defects. In addition to the external intervention required, the incorporation of molecular functionality included to facilitate the healing response will likely result in an intrinsically less robust material. As such, the majority of these systems are better suited to aesthetic applications in which the damage can be easily observed and addressed, and for which durability is not of the highest priority.

Autonomic Healing in Materials

Technologies that fall under this classification are designed such self-healing occurs at the ambient temperature of the system in its specific application. The most successful approaches to designing systems capable of autonomic healing have been based on the compartmentalization of a healing agent such that damage triggers its release into the site of damage. Once in the site of damage, the healing agent then solidifies through a curing mechanism restoring at least part of the materials' original mechanical properties. Some examples of self-healing concepts capable of autonomic healing include those in which the healing agent is compartmentalized in microcapsules, hollow fibers and microvascular networks.[1,2] Since microcapsules can be easily incorporated into existing commercial polymeric materials, microcapsule-based technologies appear to currently be the most feasible pathway to commercial self-healing applications.

Self-Healing for Corrosion-Resistance and Life Extension in Protective Coatings

A 2002 study by the National Association of Corrosion Engineers (NACE) estimated the direct cost of corrosion to the U.S. economy in 1999 at about 3% of GDP (\$ 276 billion). At the same proportion of GDP, these numbers are estimated to be closer to \$870 billion today and about \$ 2 trillion globally. This challenge has traditionally been met by developing improved coatings via the use of better formulation ingredients (resin, dispersants, corrosion inhibitor etc.) as well as improved formulation techniques. While these efforts often lead to practically improved coatings, they do not address the fact that when the coating is physically damaged, the underlying substrate is exposed to the environment. Once exposed, the substrate rusts and the propagation of rust away from the initial damaged region leads to a loss of adhesion of the coating to the substrate. The loss of adhesion renders the coating incapable of performing its protective function leading to a need for repair or replacement (Figure 1).

Historically, the concept of self-healing was employed in the coating's industry by the use of hexavalent chromium in various coating applications.[5] When a chromated product is exposed to the atmosphere due to damage of the coating, hexavalent chromium slowly leaches out of the film into the damaged region where it is reduced to form a new trivalent chromium oxide layer that restores passivation to the damaged area. Hexavalent chromium compounds are known to be toxic and carcinogenic and are being phased out of most applications. Replacements for this

technology to date however have not been as effective as they have lacked the self-healing functionality of hexavalent chromium.

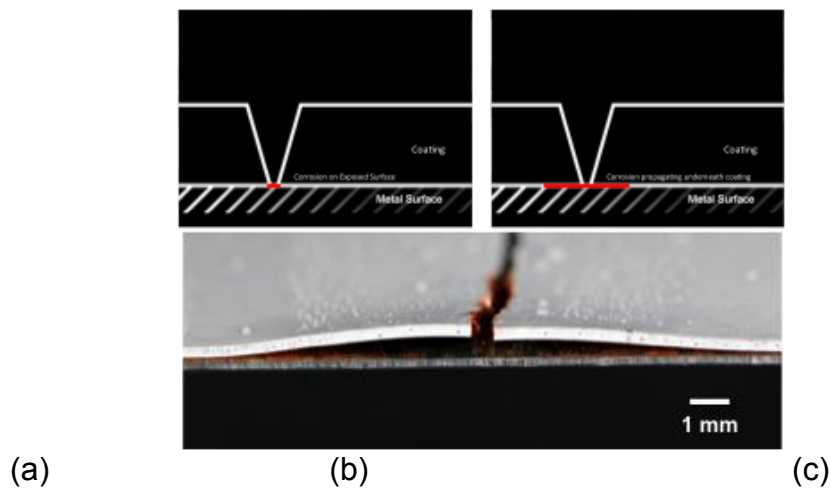


Figure 1: **Traditional Coating.** Schematic demonstrating the effect of damage to a traditional coating. **(a)** The area exposed to the atmosphere is no longer protected and begins to rust. **(b)** Over time the rust propagates underneath the coating, a process known as undercutting. **(c)** Undercutting of a polyurethane mastic coating on the surface of a cold-rolled steel substrate (coating thickness approximately 5 mils).

White and co-workers at the University of Illinois were the first to report the development of a self-healing polymeric material [6]. The original system was based on a common epoxy resin incorporating microcapsules containing dicyclopentadiene (DCPD) and particles of Grubbs' catalyst. Damage in the form of a crack propagating through this material ruptured the microcapsules causing DCPD to be released into the crack plane where upon contact with the catalyst particles a polymerization reaction was initiated [6]. Building on this initial concept for self-healing polymeric materials, several new chemistries have been developed for application in novel self-healing materials for various applications including self-healing coatings [7,8], composites [9] and elastomers [10]. In addition to expanding the scope of potential applications for self-healing materials, these new chemistries utilized more economical raw materials essential for commercialization.

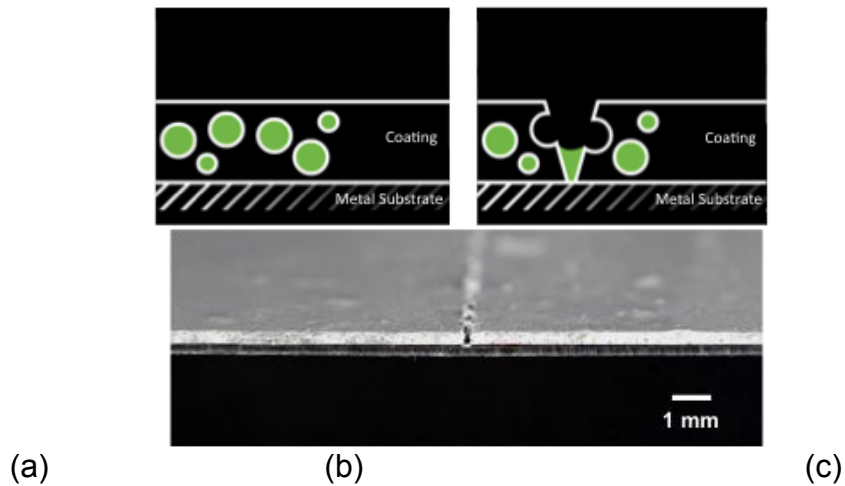


Figure 2: **Traditional Coating with Self-Healing Additive.** Schematic demonstrating the effect of damage to a self-healing coating. **(a)** Microcapsules containing healing agent are mixed in to the coating prior to application on the substrate. **(b)** Damage to the coating ruptures the microcapsules releasing healing agent into the site of damage. **(c)** Polymerized healing agent restores protective function to a polyurethane mastic coating on the surface of a cold-rolled steel substrate, eliminating undercutting (coating thickness approximately 5 mils).

This talk will focus on using similar chemistries for application in the development of self-healing protective coatings. When such coatings are damaged, the microcapsules release a customized healing agent formulation to the site of damage (Figure 2b). Once in the site of damage, the healing agent polymerizes and restores the protective function of the coating thereby preventing undercutting that would have been prevalent in the absence of self-healing functionality (Figure 2c).

Damage Mechanisms and Healing Response

During the talk, I will refer to three categories of damage based on the size of the damage and the amount of healing agent available for delivery. These categories, referred to as internal damage, visible damage and large-scale damage are described in more detail below:

Internal damage: This is damage that occurs deep within the coating film and is usually invisible from the surface. This kind of damage takes the form of multiple micro-cracks that propagate over time to form a network through which the substrate is exposed to the environment. Damage in the form of micro-cracks typically originates from failure at the molecular level due to cycling between temperature extremes, UV-radiation, adverse chemical conditions or repeated impact to the coating. We have successfully demonstrated self-healing systems that facilitate the complete repair of this scale of damage. Cold-rolled steel panels coated with a polyurethane coating containing one of our products and subjected to impact via a gravelometer or an impact tester followed by exposure to an accelerated corrosion test exhibited no rust on the surface of the coating. Since the micro-cracks formed in these coatings as a result of the impact are typically less than 10 μm , there was enough healing agent available to completely heal the cracks. Similarly coated panels excluding the self-healing additive were observed to rust in accelerated

corrosion testing, as the micro-cracks formed in these coatings were incapable of self-healing (Figure 3a).

Visible Damage: This kind of damage typically takes the form of a 50 μm scribe that is often introduced to a coating to evaluate its protective capabilities by measuring creep from scribe after exposure to an accelerated corrosion test. Our observations have been that if the additive microcapsules are at least on the same order of magnitude in size or greater than the width of the scribe, there will be enough healing agent delivered to generate a new barrier at the bottom of the scribe. The new barrier formed protects the substrate from the environment thus preventing rusting that would have otherwise taken place in the absence of the self-healing additive (Figure 3b).

Large-Scale Damage: This is damage that is considered larger than the two forms of damage already discussed. If we consider damage of this scale in the form of a scribe (e.g. $\geq 500 \mu\text{m}$), there will not be enough healing agent to form a barrier that completely covers the bottom of the scribe. In the event of such damage, microcapsules at the edges of the damaged region will be ruptured and the healing agent released will flow to the bottom of the scribe where once polymerized it will seal the edge of the damage. As such, although some part of the scribe will remain exposed and will therefore eventually rust, the rust will be contained to a much smaller area and the self-healing functionality will prevent undercutting and loss of adhesion (Figure 3c).

Once delivered, the healing agent provides protection to the site of damage via a three-step process. The first step is moisture-repulsion. All of our healing agent formulations are designed to be hydrophobic and upon release into the site of damage immediately begin repelling moisture from the substrate thereby providing instantaneous temporary protection. In the next step, as solvents in the formulation begin to evaporate, the polymeric binders mix, coalesce and polymerize to form a gel which hardens over time to form a robust binder capable of providing longer term protection. In the final step, custom additives present in the formulation elevate the formulation from performing simply as binder to performing more like a fully formulated coating with the typical associated benefits.

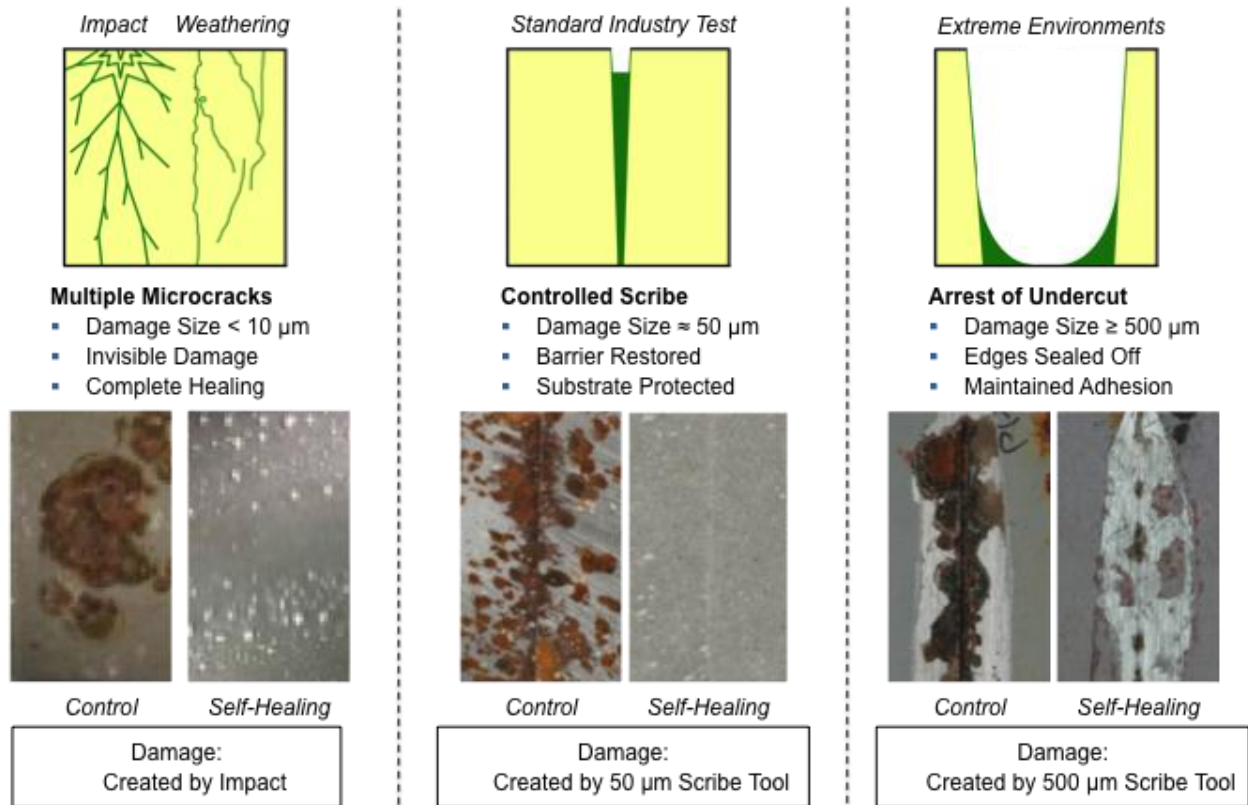


Figure 3: Scales of coating damage and the corresponding self-healing mechanisms. (a) Internal damage. (b) Visible damage. (c) Large-scale damage.

2. MATERIALS AND METHODS

Dual Capsule Systems Based on Vinyl-Terminated PDMS

The two varieties of microcapsules in this dual capsule system are added to the coating formulation at a 1:1 ratio. Damage to the coating resulting in mechanical failure will rupture both sets of microcapsules releasing their contents to the site of damage where they will mix, polymerize and restore the coating's protective function (Figure 4). For the purpose of this paper, this system is referred to as Series 1. Series 1 has demonstrated good performance in a range of coatings including flexible and compliant coatings such as polyurethane and silicone coatings, various powder coatings, epoxies, water and solvent-based direct-to-metal coatings. Demonstrating excellent thermal stability, the self-healing functionality of Series 1 was observed in powder coatings that were cured at temperatures as high as 400 °F.

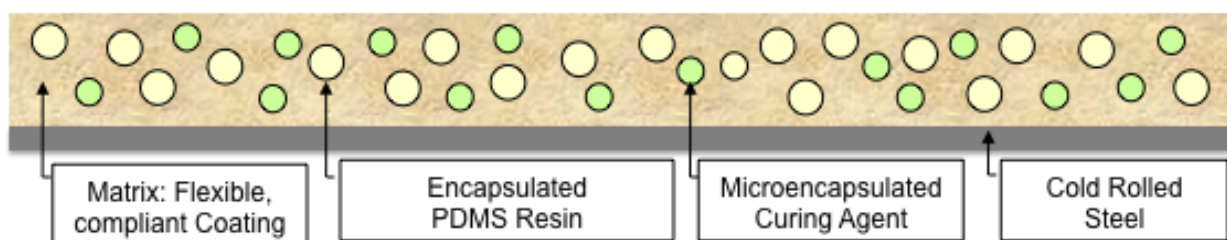


Figure 4: Dual-capsule system based on vinyl-terminated PDMS.

One-Capsule Systems Based on Epoxy Chemistry

The single-capsule concept on which this self-healing system is based is referred to as a solvent-induced healing chemistry and was first demonstrated in polymerized epoxy resins in which it was shown to facilitate greater than a 100% recovery of the original fracture toughness of the material. [11] For the purpose of this paper this system will be referred to this system as Series 2. The resulting microcapsules are formulated into an epoxy coating such that damage to the coating ruptures the microcapsules releasing the healing agent into the site of damage. Once in the site of damage, the solvent elutes out residual curing agent functionality from the polymerized coating matrix, and promotes a reaction with the epoxy resin also delivered to the site of damage. A schematic summarizing the Series 2 self-healing system is shown in Figure 5.

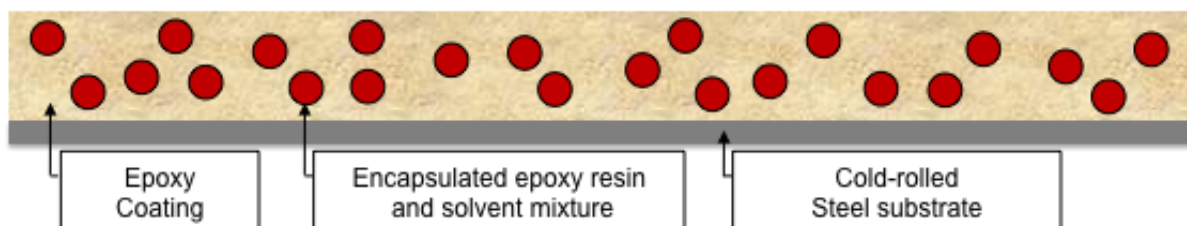


Figure 5: Dual-capsule system based on solvent-induced epoxy healing chemistry.

Microcapsule Preparation

Self-healing systems discussed in this paper are based on microcapsules prepared using previously reported shell walls and procedures. [7,12,13]

Preparation of Coating Formulation and Application

For all results to be discussed, microcapsule-based products were post-added into the coating and mixed in with the help of mechanical stirring maximum stirring rates of 2000 RPM. The resulting formulation was then drawn down on the target substrate using a drawdown bar. The coating was then allowed to cure for the recommended cure time at room temperature (typically 1 to 7 days) after which it was scribed using scribe tools of varying widths. Unless otherwise specified, the samples were then allowed to heal at RT for 24 h prior to accelerated testing (ASTM B117). After exposure to the accelerated test, the samples were then evaluated for corrosion creep or loss of adhesion. For cases in which adhesion loss or corrosion creep from scribe is reported, the measurements were made by measuring from the center of the scribe to edge of the corrosion creep or area of adhesion loss. A total of six equidistant measurements were taken for each scribe and the average recorded.

3. RESULTS AND DISCUSSION

Representative Results from a Dual-Capsule System

An example of the use of Series 1 in an un-pigmented epoxy coating applied on cold-rolled steel (CRS) panels is shown below (Figure 6). The CRS panels were lightly abraded followed by cleaning by wiping with acetone. Un-pigmented systems were

used in the experiments discussed in this paper to observe performance due to restoration of barrier properties alone, excluding the effect of pigments that are typically present in the standard formulation. After exposure to ASTM B117 conditions for 1000 h, the samples were evaluated and the results are summarized in Figure 6. Loss of adhesion around the scribes was evaluated by using ASTM-specified adhesive tape applied along the scribe and rapidly ripped off after about 1 min. This action typically causes areas with adhesion loss to raise up from the steel panel. The area of adhesion loss was outlined immediately and is labeled in Figure 6. While the control sample exhibited significant loss of adhesion, the self-healing sample containing Series 1 at 5 wt% exhibited practically no loss of adhesion for the 186 micron scribe and less than 2 mm of adhesion loss for the 500 micron scribe.

Representative Results from a One-Capsule System

Similar results were observed for Series 2 in a different industrial epoxy coating also applied on CRS panels prepared and cleaned as described above. While the control sample exhibited significant loss of adhesion and corrosion creep from scribe, the corresponding self-healing sample containing 5 wt% Series 2 exhibited no loss of adhesion and minimal corrosion creep for both 186 micron and 500 micron scribes after 1024 h exposure to ASTM B117 conditions. These results represent unprecedented corrosion resistance for coating formulations that do not include any pigment.

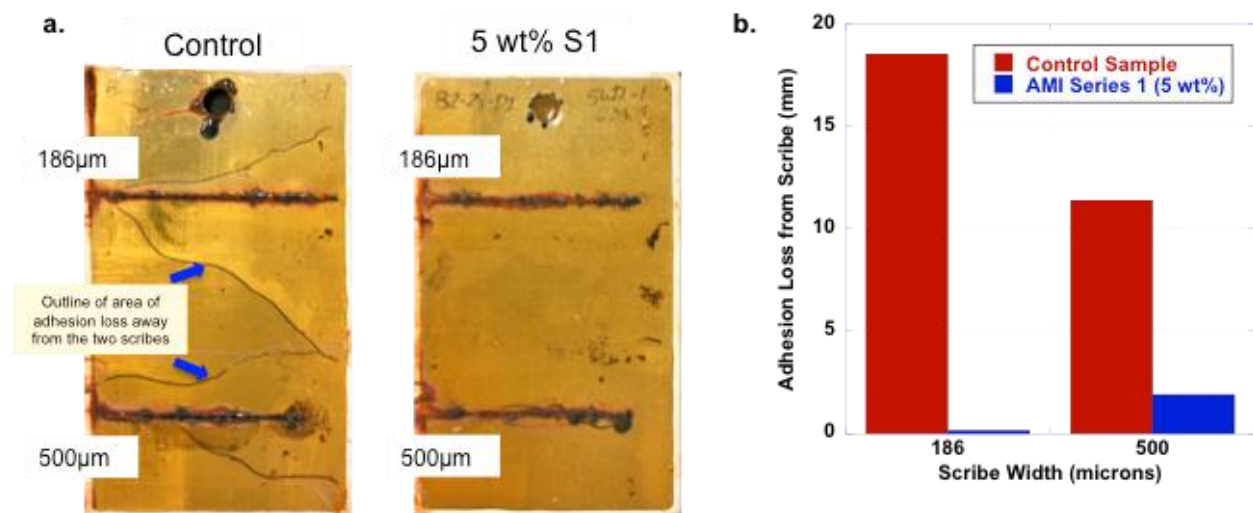


Figure 6: Self-healing performance of Series 1 in an epoxy marine coating.

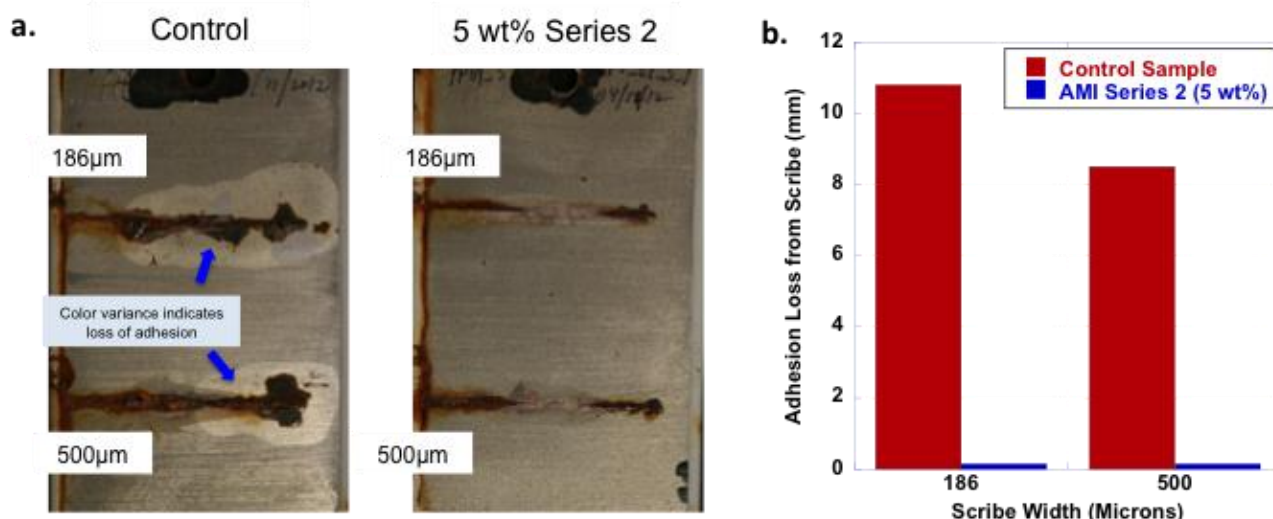


Figure 7: Self-healing performance of Series 2 in an industrial epoxy coating.

4. CONCLUSIONS

In addition to the background provided on the emerging field of self-healing coatings, the results of the self-healing performance due to two different self-healing additives in un-pigmented coatings were discussed. Similar observations have been made in fully pigmented formulations as well. Self-healing additives based on microencapsulation have been demonstrated to improve the corrosion resistance and adhesion of protective coatings damaged via a wide variety of mechanisms. While various pigments and corrosion inhibitors typically used in coating formulations might effectively resist corrosion prior to damage, microcapsule-based self-healing systems present a complementary technology for overall improved corrosion resistance.

REFERENCES

- [1] B.J. Blaiszik, S.L.B. Kramer, S.C. Olugebefola, J.S. Moore, N.R. Sottos, S.R. White, Self-Healing Polymers and Composites, *Annual Review of Materials Research* 40 (2010) 179- 211.
- [2] G.O. Wilson, H.M. Andersson, S.R. White, N.R. Sottos, J.S. Moore, P.V. Braun, S elf-Healing Polymers, *Encyclopedia of Polymer Science and Technology*, Published Online: 2010.
- [3] R.P. Wool, K.M. O' Connor, A Theory of Crack Healing in Polymers, *Journal of Applied Physics* 52 (1981) 5953- 5963.
- [4] M. Burnworth, L. Tang, J.R. Kumpfer, A.J. Duncan, F.L. Beyer, G.L. Fiore, S.J. Rowan, C. Weder, Optically healable supramolecular polymers, *Nature* 472 (2011) 334-338.
- [5] Paint and Coatings, Applications and Corrosion Resistance, in: P.A. Schweitzer (Ed.), CRC Press, Taylor & Francis Group, Boca Raton, 2006.
- [6] S.R. White, N.R. Sottos, P.H. Geubelle, J.S. Moore, M.R. Kessler, S.R. Sriram, E.N. Brown, S.Viswanathan, Autonomic healing of polymer composites, *Nature* 409 (2001) 794-797.
- [7] S. Cho, H.M. Andersson, S.R. White, N.R. Sottos, P.V. Braun, Environmentally stable polydimethylsiloxane-based self-healing of polymers, *Advanced Materials* 18 (2006) 997-1000.

- [8] S. Cho, S.R. White, P.V. Braun, Self-Healing Polymer Coatings, *Advanced Materials* 21 (2009) 645-649.
- [9] M.R. Kessler, N.R. Sottos, S.R. White, Self-healing structural composite materials, *Composites A: Applied Science and Manufacturing*, 34 (2003) 743-753.
- [10] M.W. Keller, S.R. White, N.R. Sottos, A self-healing poly(dimethyl siloxane) elastomer, *Advanced Functional Materials* 17 (2007) 2399-2404.
- [11] M.M. Caruso, B.J. Blaiszik, S.R. White, N.R. Sottos, J.S. Moore, Full recovery of fracture toughness using a nontoxic solvent-based self-healing system, *Advanced Functional Materials* 18 (2008) 1898-1904.
- [12] E.N. Brown, M.R. Kessler, N.R. Sottos, S.R. White, In situ poly(urea-formaldehyde) microencapsulation of dicyclopentadiene, *Journal of Microencapsulation* 20 (2003) 719-730.
- [13] M.M. Caruso, B.J. Blaiszik, H. Jin, S.R. Schelkopf, D.S. Stradley, N.R. Sottos, S.R. White, J.S. Moore, Robust Double-Walled Microcapsules for Self-Healing Polymeric Materials, *Applied Materials and Interfaces* 2 (2010) 1195-1199.

ON THE HEALING MECHANISM OF SOL-GEL DERIVED HYBRID MATERIALS CONTAINING DYNAMIC DI-SULFIDE BONDS

M. AbdolahZadeh¹, A.C.C Esteves², S. van der Zwaag¹ and S.J. Garcia¹

¹ Novel Aerospace Materials Group, Faculty of Aerospace Engineering, Delft University of Technology, Kluyverweg 1, 2629 HS, Delft, The Netherlands – e-mail: m.abdolahzadeh@tudelft.nl; s.vanderzwaag@tudelft.nl; S.J.GarciaEspallargas@tudelft.nl

² Materials and Interface Chemistry Group, Department of Chemical Engineering and Chemistry, Eindhoven University of Technology, Eindhoven, The Netherlands – e-mail: a.c.c.esteves@tue.nl

Keywords: sol-gel, self-healing, Raman spectroscopy, Dynamic mechanical thermal analysis

ABSTRACT

Sol-gel technology is increasingly being used in coatings for corrosion protection and adhesion improvement. So far, the self-healing concept in sol-gel coatings has only been approached from extrinsic healing perspective (i.e. use of nano and micro carriers of corrosion inhibitors) [1]. Despite the benefits of this approach, the damaged area remains open to ambient environment. The implementation of intrinsic healing approaches in sol-gel coatings can thus very well complement current extrinsic ones in order to offer more extended corrosion protection.

In the present work the intrinsic healing sol-gel hybrid systems containing dynamic di-sulfide bonds were developed. The ability of developed systems to restore their cohesion at three different temperatures was evaluated, revealing 70°C as the optimum healing temperature. In order to get a better understanding of the healing mechanisms, dynamic mechanical thermal analysis (DMTA) was complemented by in-situ raman spectroscopy to follow the evolution of the di-sulfide bonds during the healing cycles. Mechanical properties and content of the broken dynamic bonds were found to be the key parameters in the healing performance of the developed systems. Faster healing kinetics at 70°C disclosed the dominating role of the breaking/re-joining of the dynamic di-sulfide bonds in the healing mechanism.

1. INTRODUCTION

Considering the advantageous features of sol-gel chemistry such [2] and the ability of dynamic di-sulfide bonds to be triggered by various stimuli [3], in this work we aim at incorporating dynamic di-sulfide bonds into a cross-linked epoxy matrix through sol-gel chemistry. Upon thermal stimulation, the developed hybrid system is capable of restoring its integrity at moderate temperatures and pressures. The effect of healing temperature on the healing kinetics is presented. Additionally, the healing mechanism is studied using DMTA tests complemented by Raman spectroscopy coupled to a hot-stage.

2. MATERIALS

Hybrid systems were prepared by addition of un-hydrolyzed alkoxy-silanes to the epoxy resin with alkoxy-silane:epoxy resin weight ratio of 1:1. Bis[3-(triethoxysilyl)propyl]tetrasulfide (BS) and (3-Aminopropyl)trimethoxysilane (APS)

were mixed in BS:APS molar ratio of 3:1 and added to the Epikote™ 828 based epoxy resin. The mixture was stirred for 3 h at ambient temperature. Ancamine® 2500 was added as cross-linker with Ancamine:epoxy resin weight ratio of 0.58:1 and the prepared mixture was speed mixed at 2500 rpm for 5 minutes. Pentaerythritol tetrakis(3-mercaptopropionate) (denoted as tetra-thiol) was added in tetra-thiol:epoxy resin weight ratio of 0.56:1 and mixed again for 40 seconds under the same conditions. The resulting mixture was casted using a 600 μm calibrated standard aluminum single blade on Teflon plates and cured for 2 h at 70°C.

3. METHODS

To investigate the cohesive healing, rectangular films of $20 \times 10 \text{ mm}^2$ were cut in two pieces. The cut pieces were put 500 μm apart from each other between two glass plates. The ability of the samples to recover their cohesion under constant pressure of 0.03 MPa was investigated at three different temperatures of 50, 70 and 90°C. The cohesion restoration of the samples was monitored using a Leica DMLM microscope in transmission mode. Assuring a uniform thickness of the samples, the changes in gap area as a function of time (A_t) normalized by initial gap area (A_0) was used for calculation of cohesive healing efficiency of the samples.

To study the healing mechanism of the prepared samples, the changes in the storage (E') and loss modulus (E'') as a function of temperature were monitored using a Perkin Elmer Pyris Diamond DMTA analyzer in the range of 20 to 110°C. Samples were tested in a tensile fixture at frequency of 1 Hz, tension amplitude of 10 μm and at a constant rate of heating of 2°C/min.

Moreover, Raman spectroscopy was performed using a U1000 – High resolution double spectrometer from HORIBA Jobin Yvon, with a 632 nm laser at eight different temperatures in the interval of 20 to 90°C with step of 10°C ($T_1 = 20^\circ\text{C}$, $\Delta T = 10^\circ\text{C}$, $T_8 = 90^\circ\text{C}$). The temperature of the samples was controlled using a Linkam Scientific Instruments THMS600 hot-stage coupled to the Raman set-up.

4. RESULTS

To study the cohesive healing kinetics, temperature triggered healing of the prepared hybrid systems was performed at three different temperatures i.e. 50, 70 and 90°C. The calculated cohesive healing efficiencies of the samples are plotted as a function of healing time in figure 1. It can be seen that by increasing the healing temperature from 50°C to 70°C, samples were able to restore their cohesion at significantly higher rates. After 10 minutes of exposure to 50°C, the cohesive healing efficiency of the sample was slightly over 70% while heating the same sample for 10 minutes at 70°C led to full cohesion recovery. A further increase in healing temperature to 90°C not only did not accelerate the healing process, but also a slight decrease in healing kinetics was observed.

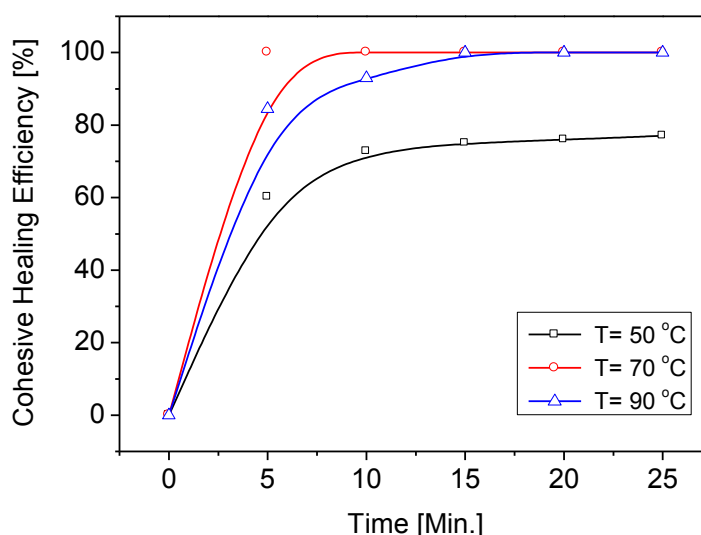


Figure 1: Cohesive healing efficiency versus healing time at three different temperatures.

To further investigate the observed trend, the changes in the storage (E') and loss modulus (E'') of the prepared samples as a function of temperature was measured using DMTA. E' and E'' values at 50, 70 and 90°C were plotted together with cohesive healing efficiency at 10 minutes in figure 2. Figure 2 shows that increasing the temperature from 50 to 70°C lowered the mechanical properties of the hybrid film represented by E' . Furthermore, E'' which is a measure of the viscous phase of the hybrid film showed a decrease by increasing the temperature from 50 to 70°C. Therefore, the faster healing kinetics at 70°C can be attributed to the synergic effect of the reduced mechanical properties and increased chain mobility at 70°C compared to 50°C. A further increase in the temperature to 90°C resulted in higher chain mobility shown by lower E'' . However, the mechanical properties represented by E' remained constant. Although higher chain mobility at 90°C should have increased healing rate compared to 70°C, healing kinetics slightly slowed down. To investigate the obtained results, Raman spectroscopy coupled to a hot-stage was employed to follow the changes in the hybrid film in atomic scale. The content of dynamic disulfide bonds at different temperatures (which are believed to be responsible for temperature triggered healing) was quantified using peak area criteria ($A_{S-S}(T) / A_{\text{internal standard}}(T)$) and plotted in figure 2. The obtained results revealed that the content of di-sulfide bonds at 70°C was at minimum level i.e., a higher proportion of the dynamic bonds were broken at this temperature. The decrease in the content of the dynamic bonds at 70°C compared to 50°C is in line with the faster healing kinetics at 70°C. Additionally, the slight decrease in healing kinetics at 90°C compared to 70°C can be attributed to the lower mobility of the system induced by re-joining of the dynamic di-sulfide bonds at this temperature.

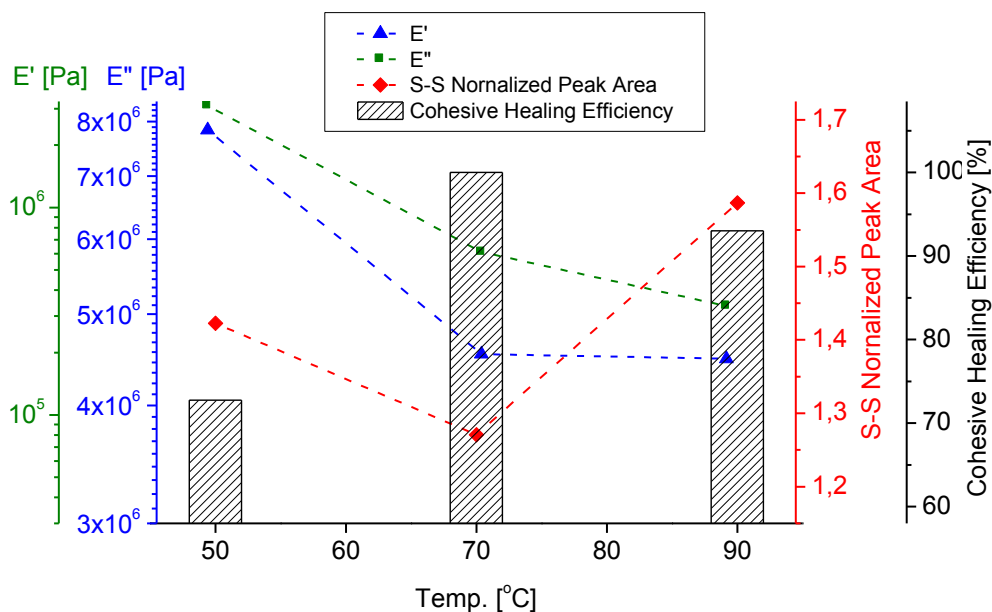


Figure 2. Variations in E' (■), E'' (▲), S-S normalized peak area (◆) and cohesive healing efficiency at t = 10 minutes, versus temperature

5. CONCLUSIONS

Sol-gel based temperature triggered intrinsic healing hybrid systems were developed. Evaluation of the cohesive healing capabilities of the prepared system at three different temperatures revealed 70°C as the optimum healing temperature. Hot-stage Raman spectroscopy together with DMTA results revealed the dominating role of breaking/re-joining of the dynamic di-sulfide bonds in the healing performance of the prepared systems compared to pure viscoelastic behavior.

REFERENCES

- [1] S.J. Garcia, H.R. Fischer, S. van der Zwaag, A critical appraisal of the potential of self-healing polymeric coatings, *Progress in Organic Coatings*, 72 (2011) 211-221.
- [2] Sol-Gel Processing of Hybrid Organic-Inorganic Materials Based on Polysilsesquioxanes in: G. Kickelbick (Ed.) *Hybrid Materials: Synthesis, Characterization, and Applications*, WILEY-VCH, Darmstadt, 2007, pp. 225-254.
- [3] U. Lafont, H. van Zeijl, S.v.d. Zwaag, Influence of cross-linking on the cohesive and adhesive self-healing ability of polysulfide based thermosets, *ACS Applied Materials & Interfaces* (2012).

SURFACE REPAIR: SELF-REPLENISHING FUNCTIONAL POLYMER COATINGS

A.C.C. Esteves¹, K. Lyakhova¹ and G. de With¹

¹ *Laboratory of Materials and Interface Chemistry, Department of Chemical Engineering and Chemistry, Eindhoven University of Technology, Den Dolech 2, 5612AZ Eindhoven, The Netherlands – e-mail: a.c.c.esteves@tue.nl*

Keywords: Coatings, Self-replenishing, Structured-surfaces

ABSTRACT

Previously, we reported a self-replenishing polymer surfaces which recover their low-surface energy (i.e. hydrophobicity), upon surface damage^[1]. Following up, we used a dual experimental-simulation approach to understand in-depth the surface segregation of low surface energy components^[2], the self-healing mechanism involved on the surface recovery and the influence of different parameters (e.g. mobility of the polymer healing components) on the self-replenishing behaviour. Herein we report our further studies on self-replenishing structured-surfaces. The model self-replenishing polymer system was used to develop robust and easy processing hydrophobic surface-structured coatings, which are able to recover the low surface energy groups at new structured surfaces, created after damage.

1. INTRODUCTION

Many efforts have been made towards durable and robust functional surfaces^[3, 4] to face damage and wear, which will always be unavoidable. A rather attracting approach consists in introducing self-repairing mechanisms to prevent early failure or lowering of the materials performance. In the last decade, several strategies have been reported for recovering mechanical properties and bulk damage^[5]. However, little has been done to recover surface properties or functionality^[1], in particular when it depends on the surface structure (topography) as well.

We developed new surface-structured coatings which can self-replenish their surface chemical composition and also self-reproduce the surface structure upon damage. The surface-chemistry repair occurs due to intrinsic elements of the coatings bulk, i.e. low surface energy polymeric dangling chains chemically bonded to a cross-linked polymer matrix^[1]. When damage occurs, the polymeric dangling chains re-orient towards the new air-coating interfaces created, recovering the surface chemical composition. The coatings surface structure is build up by chemically bonding silica nanoparticles to the cross-linked network, which become protuberant at the top-surface. The particles in the bulk allow autonomous reproduction of a new surface roughness every time a surface damage occurs.

2. MATERIALS AND METHODS

The surface-structured coatings were prepared from *all-in-one* dispersions and simple one step chemical methods. The self-replenishing polymer system used was reported before^[1, 2] and consists on Poly(caprolactone)-based precursors with controlled end-functionality and degree of polymerization (DP), which were reacted

with a tri-isocyanate cross-linker, at moderate temperatures and short periods of time. To obtain the low surface energy property, fluorinated dangling chains containing a Poly(caprolactone) spacer with controlled DP and terminal hydroxyl groups, were also inserted in the system, through the reaction with the isocyanate groups of the cross-linker, forming urethane bonds^[1, 2]. To obtain the desired surface structure and chemical composition, several coatings were prepared with SiO₂ nanoparticles, which were synthesized with a specific size, using the well-known Stöber process (\bar{D}_1) (Table 1).

Table 1. Chemical/physical description of the coatings prepared with nanoparticles (DLS average diameter, $\bar{D}_1 = 700$ nm), before intentional surface damage.

Coating with 35 % wt SiO ₂ ^[a]	Overall F content %wt	F/C ratio (XPS)	Advancing Water CA (°) ± 2	Water CA hysteresis (°) ± 2
\bar{D}_1	0	0	83	23
\bar{D}_1	1.5	0.151	135	29
\bar{D}_1	3.0	0.203	147	37

A *all-in-one* mixture containing a small excess of cross-linker (CNO/OH = 1.1) was spread on previously cleaned glass substrates by spin-coating, and finally thermally heated under vacuum, at 80 °C for 30 minutes. Aluminium plates or polymer substrates can also be used for the preparation of these coatings.

3. RESULTS AND DISCUSSION

The surface-morphology of these coatings was investigated by Scanning Electron Microscopy (SEM). In the coatings with 35 % total wt of SiO₂, the nanoparticles were homogeneously distributed through the bulk of the coatings, but also organized on a protuberant layer at the air interface, providing the desired surface roughness (Figure 1a). SEM also showed that the nanoparticles were well embedded in the polymer bulk, the self-healing medium, and that the top particles are covered by a thin polymer layer (Figure 1a). This is an essential requisite for imparting a more hydrophobic character to the coatings surface.

The surface chemical composition of these coatings was investigated by X-Ray Photoelectron Spectroscopy (XPS). For all the coatings, atomic O1s (532.7 eV), C1s (284.8 eV) Si2p (103.3 eV) and F1s (689.1 eV) were present at the surface^[6]. The two last elements identify the presence of silica nanoparticles and fluorinated dangling chains at the top 10 nm layer of the coating, respectively.

These results provide confirmation of the presence of the Fluoroalkyl-dangling chains at the coatings surface, on the thin polymer layer covering the nanoparticles (a take-off angle of 0° was used to probe the surface with a penetration depth of ~ 10 nm). Upon increasing the overall Fluorine (F) concentration up to 3.0 % wt an increase in the F/C ratio was observed (Table 1). All the coatings prepared had a well-aligned layer of protuberant particles at the surface, which was further confirmed by Atomic Force Microscopy (AFM) (Figure 1 b).

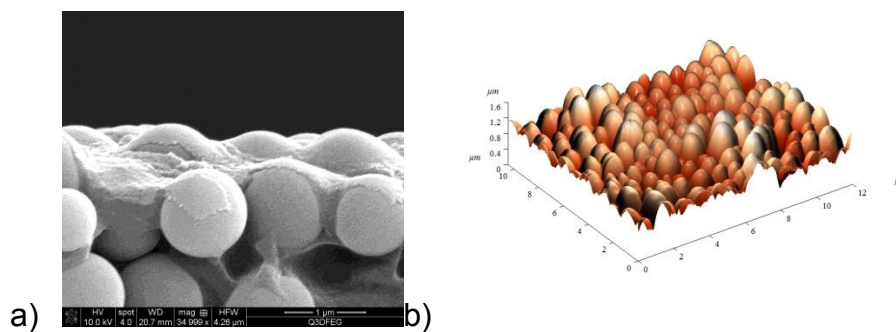


Figure 1. Characterization of the original (non-damaged) surface-structured coatings (with 35% wt of nanoparticles): a) SEM image of the air-interface and b) 3D AFM-height image.

All the advancing water contact angles (θ_{adv}) measured for the structured-coatings (with fluorinated dangling chains) exhibited a $\theta_{adv} > 120^\circ$ (Table 1), which is nearly the max. value that can be achieved on a flat surface with full coverage of low surface energy groups^[7]. As the overall F concentration was increased up to 3.0 wt % the water θ_{adv} increased considerably, up to 147° , which is even close to the superhydrophobic range.

Self-replenishing behaviour

In practical applications these coatings will be inevitably damaged by accidental scratches, sand or dirt rubbing, contact with water, chemicals or animals. To study the self-replenishing effect we tried to inflict a controlled damage at the surface of these coatings, without introducing too many “artifacts”, *e.g.* knife marks, extra roughness, smearing or contamination. A (cryo)microtoming technique was used to cut horizontal slices, plane parallel to the surface, while introducing a minimum of surface cutting effects and knife-originated-roughness. A home-made support was designed to cut plane-parallel slices of 10-30 μm at the top surface. After cut, the coatings were allowed to return to ambient temperature and their morphology was re-analyzed by SEM and AFM (Figure 3).

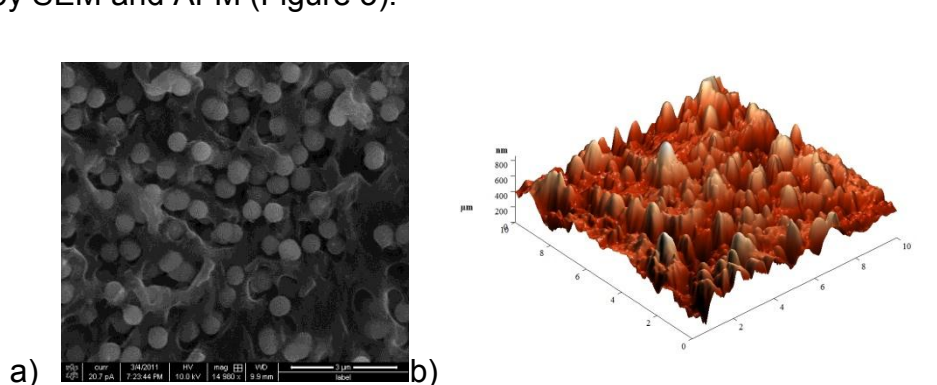


Figure 3. Characterization of a coating with 35 wt % of nanoparticles, after controlled damage (through Cryo-microtoming): a) SEM image of the air-interface and b) 3D AFM-height image.

For all of the damaged coatings, SEM revealed a new layer of protuberant particles at the new top surface (Figure 3a). This new surface structure results from the SiO_2

nanoparticles, initially homogeneously distributed and chemically bonded in the bulk polymer network. Furthermore, the polymer layer which contains the low surface-energy groups is also present at the new surface providing a recovery of the surface chemical composition (confirmed by the F/C ratio determined by XPS). AFM analyses of the new coatings surface have also shown a newly-reproduced topography created by the nanoparticles, previously buried in the polymer bulk (Figure 3b).

The water θ_{adv} measured on the new surfaces (after damage) were comparable with the original coatings (non-damaged), e.g. for a structured-coating with an initial $\theta_{adv} = 104^\circ \pm 2^\circ$ a final $\theta_{adv} = 106^\circ \pm 2^\circ$ was measured on the microtomed surface. These results clearly confirm the self-healing ability of the coatings prepared, which can recover their surface chemical composition and reproduce a new surface structure upon damage.

4. CONCLUSION

Surface-structured coatings which can replenish their surface chemical composition on a rough surface are reported^[8]. The chemical composition recovery is provided by the self-replenishing polymer system used^[1], which embeds the roughness inducing components, i.e. silica nanoparticles. The surface structure reproduction is inherent to the surface damage, via the nanoparticles homogeneously distributed and chemically bonded to the cross-linked polymer bulk.

ACKNOWLEDGEMENTS

This work was supported by Agentschap NL, IOP Self-healing program: SHM01053.

REFERENCES

- [1] T. Dikic, W. Ming, R. A. T. M. van Benthem, A. C. C. Esteves, G. de With, Self-replenishing surfaces, *Adv. Mater.*, 24 (2012) 3701.
- [2] A. C. C. Esteves, K. Lyakhova, L. G. J. van der Ven, R. A. T. M. van Benthem, G. de With, Surface segregation of low surface energy polymeric dangling chains in a cross-linked polymer network investigated by a combined experimental–simulation approach, *Macromolecules*, 46 (2013) 1993.
- [3] L. Boinovich, A. M. Emelyanenko, A. S. Pashinin, Analysis of long-term durability of superhydrophobic properties under continuous contact with water, *Appl. Mater. Interf.*, 2 (2010) 1754.
- [4] Y. Yu, Z.-H. Zhao, Q.-S. Zheng, Mechanical and superhydrophobic stabilities of two scale surfacial structure of Lotus leaves, *Langmuir*, 23 (2007) 8212.
- [5] D. Y. Wu, S. Meure, D. Solomon, Self-healing materials: a review of recent developments, *Prog. Polym. Sci.*, 33 (2008) 479.
- [6] J. F. Moulder, W. F. Stickle, P. E. Sobol, K. D. Bomben, *Handbook of X-Ray Photoelectron Spectroscopy*, Perkin-Elmer Corporation, Minesota, USA
- [7] R. E. Johnson, R. H. Dettre, *Contact angle, wettability and adhesion*, Vol. 43, *Advances in Chemistry Series*, ACS, Washington DC, (1964).
- [8] A. C. C. Esteves, K. Lyakhova, L. G. J. van der Ven, R. A. T. M. van Benthem, G. de With, Self-replenishing of structured-surfaces revealed by a combined experimental-simulation approach, (2013) *in preparation*.

SiO₂ MESOPOROUS THIN FILMS AS NANOCONTAINERS FOR CORROSION INHIBITORS IN SELF-HEALING ANTICORROSION COATINGS

I. Recloux¹ and M-G. Olivier¹

¹ *Materials Science Department, University of Mons, Place du Parc, 23, 7000 Mons, Belgium – e-mail: isaline.recloux@umons.ac.be; marjorie.olivier@umons.ac.be*

Keywords: sol-gel coating, mesoporosity, inhibitor, release, active corrosion protection

ABSTRACT

Among the different alternative surface treatments developed in view of the coming prohibition of chromates in aeronautic applications, sol-gel coatings show very promising properties. These layers provide a barrier against aggressive environments. Moreover, their performance can be improved by introducing inhibitive agents in the coating. However, the direct introduction of corrosion inhibitors in the sol-gel compromises their barrier properties. Nanocontainers are consequently used for the storage of inhibitive agents and dispersed in the sol-gel matrix to avoid direct interactions between components. In case of scratch or when stimulated by external action, nanocontainers release active compounds which form a protective layer healing the defect.

In this work, a mesoporous sol-gel thin film synthesized through “Evaporation Induced Self Assembly” process was used as nanocontainer for 2024 aluminium protection. The mesoporosity developed through the layer was employed to host organic corrosion inhibitors inside the film and consequently to offer an active corrosion protection.

Morphology of the layer was characterized using transmission electron microscopy (TEM) and adsorption porosimetry. High specific surface area and well-organized pores are obtained, providing high-load ability for active species. Incorporation of corrosion inhibitors in the mesoporosity was checked using qualitative and quantitative analyses. Kinetics of active agents release was studied by UV/visible spectroscopy. Successful incorporation in the sol-gel matrix and possible release of corrosion inhibitors were observed. The self-healing properties were underlined by immersion test in aggressive sodium chloride solution.

1. INTRODUCTION

Sol-gel coatings have attracted much attention in the field of anticorrosive protective layers for 2024 aluminum alloys since they are able to offer efficient barrier against aggressive corrosive species. A lot of researches also aim at improving sol-gel coatings performance by introducing corrosion inhibitors inside the matrix. The idea is to benefit from their local protection to heal the sol-gel film in case of damage.

Different means can be used to incorporate corrosion inhibitors. The active agent can be directly added into the silica network during the synthesis, which is a very attractive route as the material can then be processed in one step. However, the solubility of the compound in the sol may limit the amount of inhibitor. Another problem is that the active compound can interfere with the hydrolysis and

condensation reactions, modify the final sol-gel properties and reduce the inhibitor efficiency. As the result, barrier properties of the sol-gel film are weakened by direct addition [1]. Other means of loading include the use of intermediate nanocontainers, such as nanoclays or polyelectrolytes, which are themselves dispersed in the sol. However, with this latter method, it is difficult to ensure a homogeneous dispersion of the active compound and a good compatibility within the matrix.

In this work, in order to overcome these problems, incorporation of corrosion inhibitors was achieved by adsorption onto a silica mesoporous sol-gel thin film. In this way, amount of active agent is only limited by the porous volume of the film and the compound is available in case of corrosion processes. The use of the direct inner porosity of the layer also allows avoiding dispersion and compatibility problems observed with intermediate nanocontainers.

2. MATERIALS AND METHODS

2.1. Synthesis of the mesoporous film and characterization

Mesoporous films were synthesized through “Evaporation Induced Self-Assembly” process using P123 block copolymer from Pluronic family as templating agent, ethanol as solvent and tetraorthosilicate (TEOS) as precursor. In molar ratio, the composition of the sol was 1 TEOS: 0.005 P123: 6 H₂O: 0.001 HCl: 9 EtOH. Films were prepared by dip coating with a withdrawal rate fixed at 60 mm/min and aged under controlled atmosphere (70% RH and 25°C) during 24 h to get reproducible mesoporous structures. Synthesis was inspired by work of Alberius and al. [2] to get a cubic structure which provides more accessible porosity from the surface. Polished silicon substrates and quartz resonator were used according to characterization techniques (respectively, TEM imaging and adsorption porosimetry). After ageing, the film mesostructure was stabilized at 150°C during 30 min and then treated under UV/ozone illumination to remove P123 and create mesoporosity. Elimination of the templating agent is generally achieved by calcination step at temperature higher than 250°C but this process was here avoided due to its incompatibility with aluminum substrates.

Mesoporous films were characterized by transmission electron microscopy (TEM) and adsorption porosimetry based on quartz crystal microbalance analyser (QCM). The principle consists in using a QCM to measure water vapor adsorption and desorption quantities for different water partial pressures. QCM is indeed able to accurately detect very tiny mass changes (about 10⁻⁸ g/Hz) by measuring variations of frequency. These adsorption and desorption isotherms provide characteristics of the pore network.

2.2. Corrosion inhibitor loading

Mesoporous films were immersed in a highly concentrated benzotriazole (BTA) solution (20g/l in ethanol) for 24 h at room temperature. Films were then dried in a desiccator to remove solvent from the porosity. Presence of BTA within the film was checked through adsorption porosimetry. Molecules adsorbed on pore surface indeed decrease the volume accessible for water vapor. UV/visible absorption spectroscopy was also used to quantify the amount of active agent loaded inside the

film. All these analyses were performed before and after wiping off the surface with ethanol to differentiate molecules adsorbed on the film surface and inside the porosity.

2.3. Corrosive tests

2024 aluminum alloy panels were degreased in a commercial bath of TURCO[®] 4215[™] NC-LT and the same procedure of mesoporous sol-gel deposition (see section 2.1.) was achieved on these substrates. However, for this test, a second sol-gel layer was added on the mesoporous thin film to heal the entrance of pores and avoid the direct release of BTA in the aggressive environment. Samples covered in this way were immersed in 0.05 M NaCl for several days and evolution of corrosion was observed.

3. RESULTS AND DISCUSSION

Mesoporous films present high optical quality and homogeneous thickness (about 300 nm). As observed in TEM images (Figure 1), the film structure is still present after UV/ozone treatment showing that the silica matrix does not collapse when P123 leaves the film. Pores are well-ordered and their size is comprised between 5 and 7 nm in agreement with previous work [2].

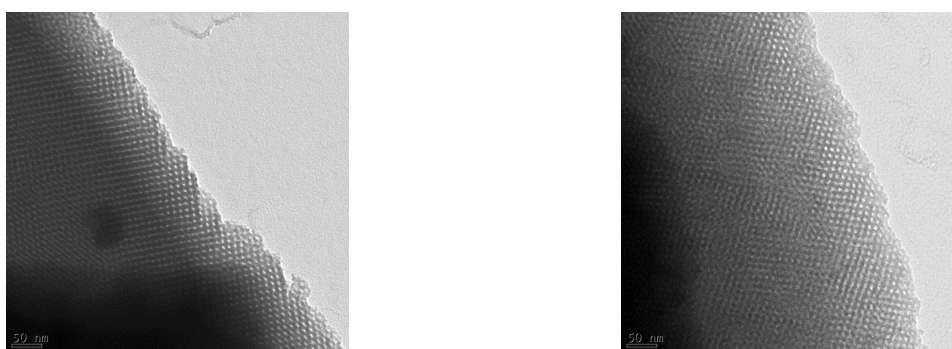


Figure 1: TEM images of mesostructured film before UV/ozone treatment (left) and mesoporous film after UV/ozone treatment (right).

Adsorption porosimetry was also achieved to get more information on accessibility to porous structure.

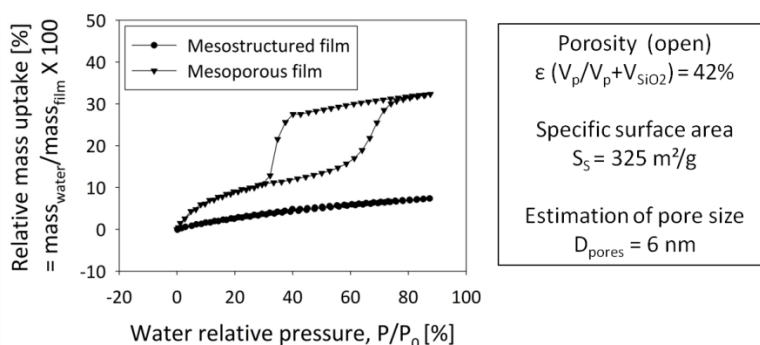


Figure 2: Adsorption and desorption isotherms of water vapor on mesostructured and mesoporous films

Adsorption and desorption isotherms are superimposed for the mesostructured film (Figure 2). The P123 is still present in the porosity and the amount of adsorbed water is low. In opposition, for the film treated under UV/ozone, a hysteresis loop appears due to the capillary condensation of water inside mesopores. Films treated under UV/ozone illumination present high surface specific area and high pore volume. Moreover, this treatment does not affect mechanical properties of 2024 aluminium substrates [3].

Adsorption porosimetry was also used to estimate the loading efficiency by observing variations in water uptake and in total open pore volume (Figure 3). Just after loading, mesoporosity is no longer accessible for water molecules due to the presence of benzotriazole crystals on the film surface. After the wiping step, these molecules are removed and a reduction of the porosity can be observed in comparison with the mesoporous film. This decrease can be assigned to the adsorbed BTA molecules on the surface of mesopores. The hysteresis loop is also slightly shifted towards higher water relative pressure due to the hydrophobicity provided by BTA molecules.

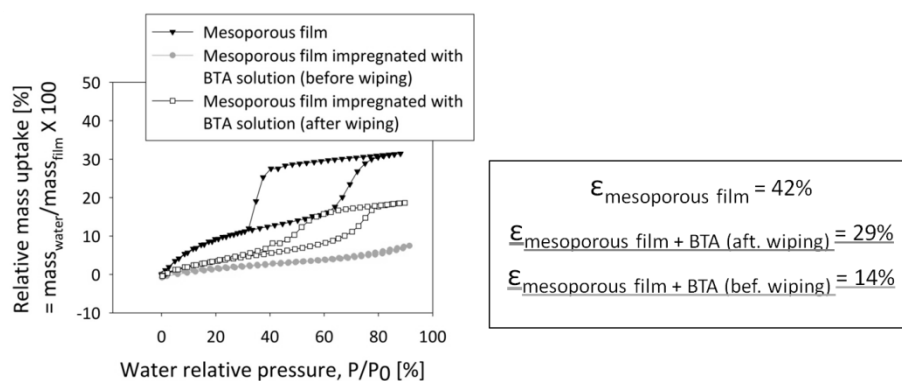


Figure 3: Variations of water uptake during adsorption and desorption isotherms according to the presence of inhibitive molecules inside the porosity

Two different techniques were used to determine the BTA loading capacity of the mesoporous film (Table 1).

Table 1: Comparison of BTA loading capacities obtained by QCM analyser and UV/visible spectroscopy

	QCM analyser		UV/visible
	mg (BTA)/ g (film)	mol (BTA)/ cm ² (film)	mol (BTA)/cm ² (film)
Total (before wiping)	846	6.10 ⁻⁷	3.10 ⁻⁷
In pore (after wiping)	142	9.10 ⁻⁸	7.10 ⁻⁸

Variations in frequency measured by the QCM analyzer before and after immersion in the inhibitive solution were converted into BTA mass uptake. Impregnated mesoporous films were also immersed in distilled water at neutral pH (volume of 20 ml) for several days to obtain the complete release of BTA. UV absorption of the

solution at 256 nm (maximum of absorption of the molecule) was converted into BTA concentration. These values were compared with the theoretical maximum loading capacity of the film (3.10^{-7} mol BTA/cm² film), assuming that all the pores are completely filled with benzotriazole molecules (molar volume 87.6 cm³/mol). The experimental loading is approximately one-third of the theoretical loading.

Finally, the benefit of BTA incorporation inside the film was highlighted by samples immersion in aggressive environment. Photographs taken after 7 days of immersion show the inhibiting effect of loaded mesoporous films when compared with empty films or bare aluminum. In presence of BTA, the surface only presents some pits while a considerable amount of pits and white deposits are observed for non impregnated films and bare aluminum.

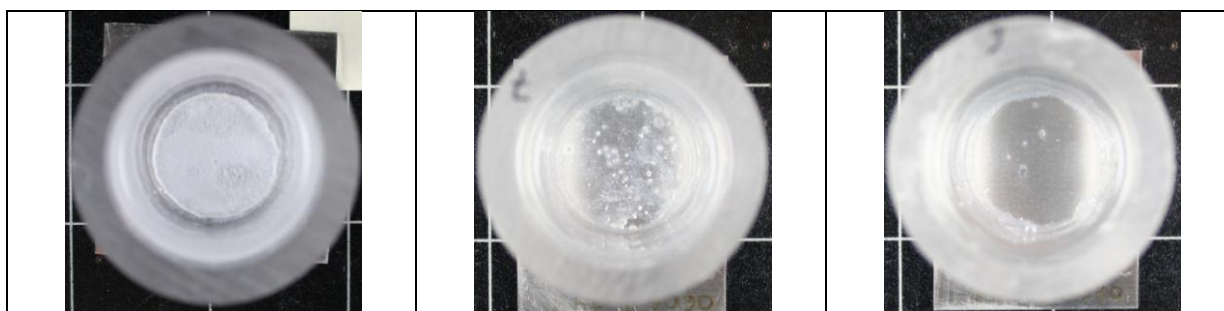


Figure 4: Photographs of samples immersed in NaCl 0.05M during 7 days; bare 2024 AA (left), 2024 AA covered with non impregnated mesoporous film (center) and 2024 AA covered with mesoporous film loaded with BTA (right).

4. CONCLUSIONS

SiO₂ mesoporous films were synthesized and incorporation of BTA was possible into the porosity. Mesostructure is regular, reproducible and present cubic arrangement. Pores are consequently accessible from the film surface. The choice of P123 as templating agent allows getting pore size (6 nm) compatible with the dimension of BTA molecules (diameter 0.6 nm). The loading content of BTA was found to be 14% in weight and reaches 30% of the theoretical maximum loading. First corrosion tests achieved with a second sol-gel layer to seal the entrance of pores are very promising in terms of self-healing behaviour. However, it would be interesting to create stronger interactions between active compound and silica matrix to avoid direct release in the solution and to obtain pH-controlled release.

ACKNOWLEDGEMENTS

Isaline Recloux wishes to thank the FRIA (Fonds pour la Formation à la Recherche dans l'Industrie et l'Agriculture) for funding and Sonaca company for providing 2024 aluminum.

REFERENCES

- [1] W. Trabelsi, P. Cecilio, M. G. S. Ferreira, M. F. Montemor, Electrochemical assessment of the self-healing properties of Ce-doped silane solutions for the pre-treatment of galvanised steel substrates, *Prog. Org. Coat.* 54 (2005) 276-284.
- [2] P. C. A. Alberius, K. L. Frindell, R. C. Hayward, E. J. Kramer, G. D. Stucky, B. F. Chmelka, General Predictive Syntheses of Cubic, Hexagonal, and Lamellar Silica and Titania Mesostructured Thin Films, *Chem. Mater.* 14 (2002) 3284-3294.
- [3] I. Recloux, M. Debliquy, A. Baroni, Y. Paint, A. Lanzutti, L. Fedrizzi, M-G. Olivier, Optimization of synthesis parameters of mesoporous silica sol-gel thin films for application on 2024 aluminium alloy substrates, submitted in *Applied Surface Science*.

SESSION 17 – SELF-HEALING METALLIC AND CERAMIC MATERIALS

INCREASING THE RELIABILITY OF CERAMICS COMPONENTS USING SELF-CRACK-HEALING

K. Ando ¹, W. Nakao ¹

¹ *Department of Energy and Chemical Engineering, Yokohama National University, Tokiwadai Hodogayaku Yokohama-city 204, 8501 Japan – e-mail: andokoto@ynu.ac.jp*

Keywords: structural ceramics, material design, self-crack-healing, high temperature strength, reliability of components

ABSTRACT

Structural ceramics are superior in high temperature strength and anticipated as leading materials for next generation energy machine. However, ceramics have disadvantage of brittleness, sensitive to flaw and low reliability. To overcome the disadvantages, the present authors proposed a new technology for the through life reliability guarantee concept. 1) Materials design with excellent self-crack-healing ability. 2) Through life reliability management process of ceramic components using self-crack-healing ability, proof test and compressive stress introduction. In this paper, each process is introduced.

1. INTRODUCTION

Structural ceramics are superior in high temperature strength and critical heat-proof temperature compared to that of metallic material. Structural ceramics are a leading candidate material for high-temperature apparatuses such as gas-turbines. However, the fracture toughness of ceramics is lower compared to metallic material, thus they are sensitive to flaw, and the following three problems occurred. (1) Cracks occur by the usual machining process, which lowers the component reliability considerably. In order to prevent this, precise polishing is required in the final stage, which is time-consuming, and costly. (2) Crack sizes of about 10~30 μm in depth affect the reliability. The nondestructive inspection technology for detecting the cracks is yet still undeveloped. (3) There is a possibility that a crack will initiate in the components while they are being used at higher temperatures.

To overcome these problems, authors developed four technologies. (a) Induce a self-crack-healing ability, so that all surface cracks can be healed. (b) Improve the fracture toughness of the material by fiber reinforcement. (c) Conduct a proof test to prevent use of a low reliability member containing inner flaw. (d) Introduce compressive residual stress to increase fracture resistance.

There are three advantages using a self-crack-healing technology. (A) If the self-healing of the surface crack which exists is carried out after an efficient machine operation is performed, then there is a great advantage in fabrication efficiency and fabrication cost. (B) Since all surface cracks are healed, reliability improves greatly. (C) It is great advantageous that a crack which occurs during service can be healed and completely recover the strength by the self-crack-healing ability. From the above ideas, the self-crack-healing behaviors of ceramics were investigated by Ando and co-worker. Silicon nitride, alumina, mullite, SiC, AlN and ZrO₂ with the excellent self-

crack-healing ability have been developed [1]. In this paper, outline of the self-crack-healing behavior of ceramics and through life reliability managements of ceramics components were introduced.

2. CONCEPT FOR MATERIALS DEVELOPMENT

2.1. Nano-composite material

Our nano-composite materials are defined as the following specificity [2]. (a) Nano-size SiC particles are added to the material, preventing grain growth of the matrix in the sintering process, and increasing the bending strength through grain refinement: For example, in the case of an alumina, bending strength can be increased from about 400 MPa to 700~1000 MPa [2]. (b) SiC particles of nano-size 15-30 vol% added to the material, and induce a self-crack-healing ability. (c) SiC particles of nano-size are distributed not only in the grain boundaries of an alumina, but in individual grains and increases the critical heat-proof temperature by about 300 K [2].

2.1. Multi-composite material

A multi-composite material is a material which combines nano-sized SiC particles and SiC whiskers in the proportion of 20-30 vol%, and has excellent self-crack-healing ability, fracture toughness, high temperature strength [3]. The nano-sized SiC particles mainly contribute to increase strength and self-crack-healing rate and the SiC whiskers mainly contribute to increase fracture toughness and high temperature strength. The proportion fraction of SiC particles to SiC whiskers is determined by taking into consideration the self-crack-healing ability and fracture toughness requirements [4]. For example, the room-temperature bending strength and fracture toughness of Alumina/SiC(p)15% and Alumina/SiC(p)10%/SiC(w)20% are 850 MPa, 980 MPa and $3.2 \text{ MPam}^{1/2}$, $5.0 \text{ MPam}^{1/2}$, respectively.

The material with a self-crack-healing ability described in this paper has all of the following attributes. (A) The material itself detects an occurrence of a crack and begins crack-healing activities. (B) If surface crack were introduced which reduce 50-90 % strength of a material, the material heals the crack completely, and the strength of the material is completely recovered. (C) The strength of a crack-healed zone is equivalent to or higher than that of a base material up to about 1673 K [1].

3. BASIC SELF-CRACK-HEALING BEHAVIORS

3.1 Mechanism of crack healing

The crack healing of ceramics developed by the authors is caused by the following oxidation reaction of SiC.



A schematic diagram of the self-crack-healing mechanism is shown in Figure 1. To achieve the complete strength recovery by self-crack-healing, following three conditions are necessary. (1) The healing substance has to fill the crack completely. This condition is achieved by the about 80% volume increase of SiO₂ compared to

SiC. (2) The healing substance has to be welded to base material completely. This condition is attained by the huge exothermic heat of 943 kJ. The heat melts matrix and a healing substance and makes the mixture. (3) The strength of a crack-healed zone has to exhibit equivalent or higher strength than that of a base material up to about 1673 K. This condition is attained by forming the crystalline phase SiO_2 in Equation (1).

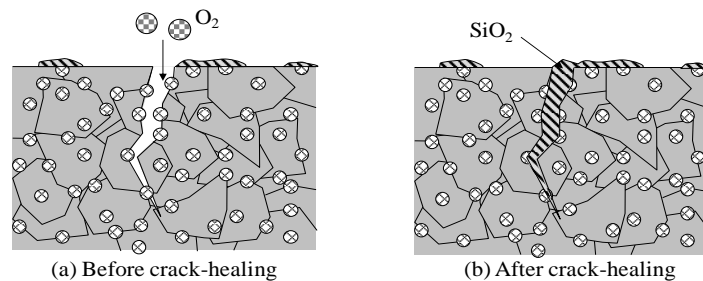


Figure 1: A schematic diagram of the self-healing mechanism.

We used JIS three-point bending-test specimens except for the bending span of 16 mm to evaluate the bending strength (σ_B) of a crack-healed specimen. We introduced the crack into the central part of the test specimen. The crack is a semi-elliptical crack 100 μm in surface length and 45 μm in depth (hereafter called a standard crack). We used the shorter bending span than standard (40 mm) to evaluate the strength of crack-healed zone and to prevent the specimen to break into small pieces by reducing elastic energy at fracture.

3.2 Oxygen partial pressure and temperature dependency of crack-healing behavior

The most basic crack-healing behavior test results were shown in Figure 2 [5]. The bending strengths (σ_B) of an as-received test specimen are about 650 MPa. By the standard crack, the σ_B was reduced to 180 MPa. However, by the crack healing carried out in air at 1573 K for 1 h, the σ_B was improved up to about 800 MPa. The σ_B of a crack-healed specimen is larger than the σ_B of an as-received specimen. The reason is that even the smooth specimens have minute cracks on the surface and the cracks were healed completely. The crack-healed zone exhibit higher strength than base material, thus quite many samples fractured outside the crack-healed zone as shown in Figure 3. However, by the crack healing in a vacuum, N_2 gas, and argon gas, the σ_B recovered to at most 350 MPa. The recovery of σ_B is insufficient. The slight increase of σ_B by this heat treatment occurred because the tensile residual-stress of the crack tip was removed. Similar crack healing and strength recovery behaviors were reported in mullite [5], Al_2O_3 [6] and Si_3N_4 [7-8].

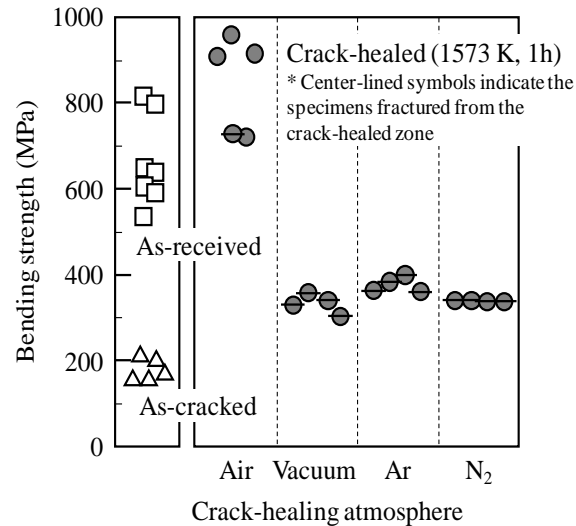


Figure 2: Effect of atmosphere on crack healing behavior.

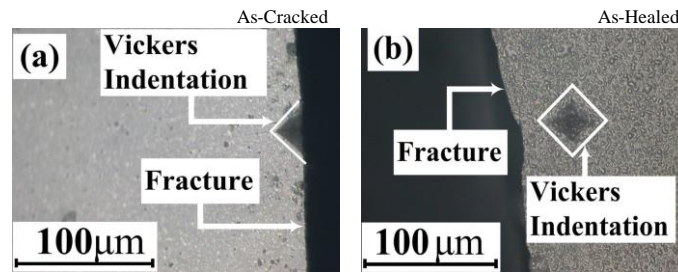


Figure 3: Fracture initiation and crack path.

The crack-healing behavior is greatly dependent on healing temperature, material, oxygen partial pressure and crack size (mainly in depth). The influence of oxygen partial pressure on crack-healing behavior is shown in Figure 4, in $\text{Al}_2\text{O}_3/\text{SiC}$ composite materials [9]. By the crack-healing carried out at 1673 K, in air, the crack healed completely in about 20 min. When the oxygen partial pressures were 5000 and 50 Pa, the crack healed completely in about 1 h and 70 h, respectively. Moreover, the test specimen which healed in thin oxygen showed a bending strength equivalent to a matrix division up to 1673 K. It is said that the oxygen partial pressure in the exhaust gas of a gas-turbine or a vehicle is about 8-10 kPa, which is approximately half in air atmosphere. So it is anticipated that the surface crack can be healed in oxygen partial pressure in the exhaust gas of a gas-turbine or a vehicle.

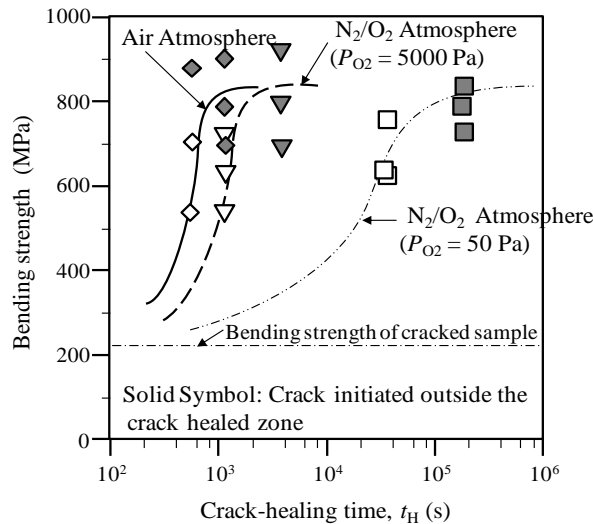


Figure 4: Effect of oxygen partial pressure on crack healing behavior.

The influence of temperature and time on crack-healing behavior in air was conducted on various materials, systematically. By similar experiments as shown in Figure 4, we found the shortest time t_{HM} which can heal a crack completely from a certain temperature T_{HL} . The relationship between $1/t_{HM}$ and $1/T_{HL}$ can be shown by the Arrhenius equation as follows [10].

$$\frac{1}{t_{HM}} = Q_0 \exp\left(\frac{-Q_H}{RT_{HL}}\right) \quad (2)$$

The activation-energy (Q_H) and proportional moduli (Q_0) of each material were calculated and the result is shown in Table 1. Equation (2) is applicable for standard crack in $t_{HM} = 1\sim 300$ h and in air condition. If crack were deeper than the standard crack, and oxygen partial pressure were lower than that of air, the necessary time for the complete crack-healing became longer.

Table 1. Activation energy & proportional constant.

Material	Activation Energy Q_H (Kj/mol)	Proportional Coefficient Q_0 (1/hour)
Si ₃ N ₄ /SiC	277	4.2×10^{11}
Si ₃ N ₄	150	5.3×10^4
Al ₂ O ₃ /SiC	334	1.7×10^{11}
Mullite/SiC	413	4.7×10^3

3.3 Crack-healing behavior of heavily machined ceramics

In general, crack can be introduced by machining processes such as polishing and lapping. The crack-healing behavior of machined specimens was investigated systematically by the authors.

Figure 5 shows the strength recovery behavior of heavily machined Al₂O₃/20 vol.% SiC whiskers [11]. A semicircular groove was made at the center of the smooth specimens by using a diamond-coated ball-drill as shown in Figure 5. The cut depth

by one pass (d_c) during machining of the semicircular groove was $d_c = 5\sim 15\ \mu\text{m}$. The cut depth is 0.5 mm. The local fracture stresses (σ_{LF}) considering the stress concentration factor of the semicircular groove ($\alpha = 1.2$) were evaluated.

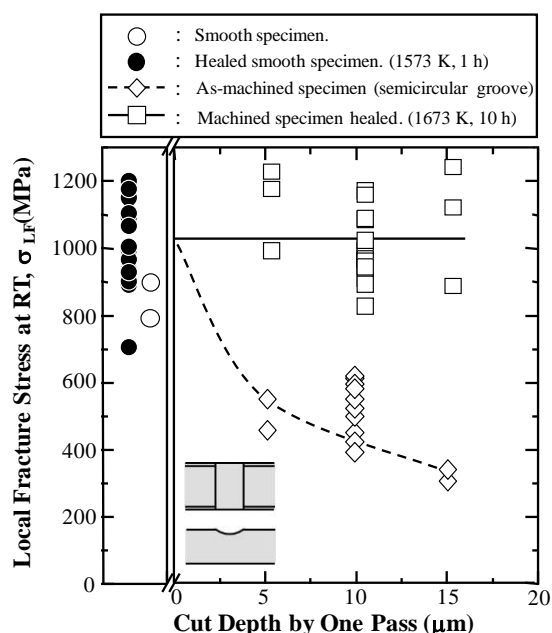


Figure 5: Strength recovery behavior of heavily-machined components.

The open triangle symbols show the local fracture stress (σ_{LF}) of the as-machined specimen. The σ_{LF} of the as-machined specimens decreased with increasing d_c . It was found by SEM images of the fracture surface that as-machined specimens always fractured from the surface long cracks of 20~50 μm in depth caused by machining. The open square symbols in Figure 5 show the σ_{LF} of the machined specimen healed at 1673 K for 10 h in air. The σ_{LF} of these specimens increased significantly by crack healing. The σ_{LF} of the machined specimens was almost equal to the fracture stress of the healed smooth specimens (solid circles). Thus, the surface cracks introduced by the machining process were healed. Therefore, it was concluded that crack healing could be an effective method for improving the structural integrity of heavily machined alumina and reducing machining costs.

4. HIGH TEMPERATURE STRENGTH OF CRACK-HEALED SPECIMENS

The temperature dependency of the σ_B of a crack-healed specimen is shown in Figure 6 [1]. Each test specimen was crack healed by an optimum condition after a standard crack was introduced. As shown in the figure, a newly developed SiC and Si₃N₄ exhibit excellent critical heat-proof temperature of a crack-healed zone of about 1673 K, and we examined its usage [12]. The large improvement in such a critical heat-proof temperature was attained by the crystallization of a grain boundary and a crack-healing substance. In addition, most test specimens fractured from the base material below to the critical heat-proof temperature among the materials of Figure 6, except the commercial SiC. This implied that the crack-healing zone had sufficient bending strength up to 1673 K.

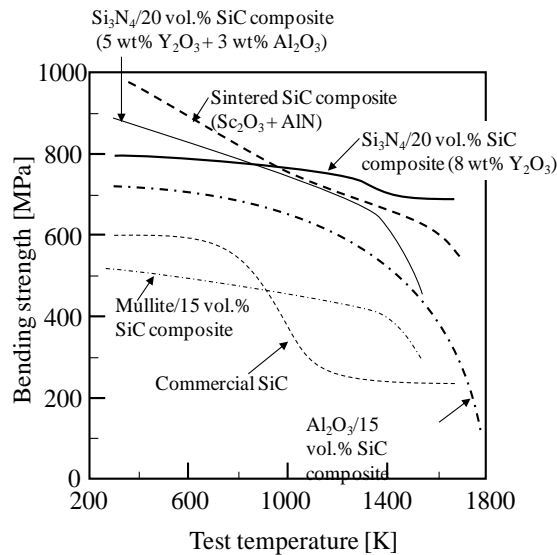


Figure 6: Temperature dependency of strength of a healed sample.

5. CRACK-HEALING BEHAVIOR DURING SERVICE

If the crack could be healed under even service conditions, and the components recover the strength completely, the reliability and lifetime of ceramic components could be increased. The crack-healing behaviors under constant or cyclic stress have been systematically studied for $\text{Si}_3\text{N}_4/\text{SiC}$ [13-14], Mullite/SiC [15-16], $\text{Al}_2\text{O}_3/\text{SiC}$ [17], and SiC [18].

To take advantage of the crack-healing ability during service, it is essential to determine the threshold stress for crack-healing under the stress a crack can be completely healed.

The standard crack was introduced on the bending test specimens. After introducing the pre-cracks, crack-healing tests under cyclic or constant stress were carried out. Figure 7 shows the crack-healing process [13]. Crack-healing was carried out under cyclic ($\sigma_{\max,ap}$) or constant (σ_{ap}) bending stresses at a healing temperature (T_h) for a prescribed healing time (t_h). After the crack-healing process, the bending strengths of the specimens were measured at room temperature or at healing temperature in air.

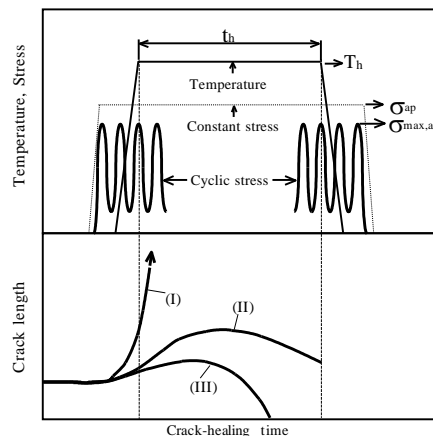


Figure 7: Crack healing method under stress and crack behavior.

Figure 8 shows the results of the bending tests on specimens crack-healed at 1473 K for 5 h under constant stress in $P_{O_2} = 500$ Pa [19]. The material studied was a Si_3N_4 which contained 20 wt% SiC particles and 8 wt% Y_2O_3 as a sintering additive.

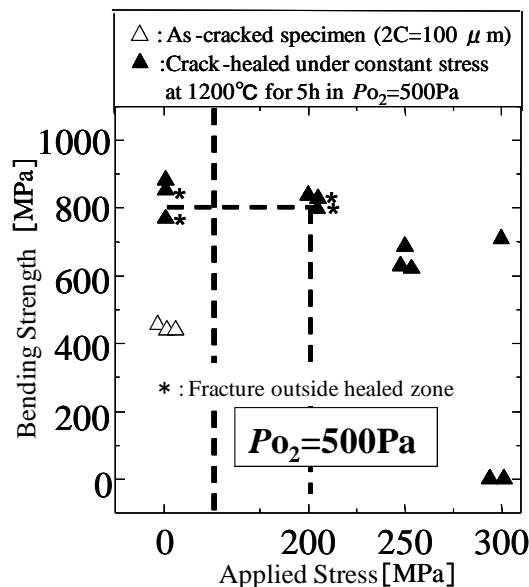


Figure 8: Crack healing and strength recovery behavior under stress.

The asterisks indicate specimens that fractured outside the crack-healed zone, suggesting that the pre-cracks were healed completely. The threshold stresses for crack-healing were defined as the maximum stresses below which specimens recovered their strengths completely and most specimens fractured outside the crack-healed zone even at healing temperature. From Figure 8, the threshold stress was determined to be 200 MPa. Similar crack-healing test under cyclic stress under various P_{O_2} was carried out. If P_{O_2} is higher than 800 Pa, the threshold stress is independent on the P_{O_2} , the threshold stress was found to be 250 MPa. In all materials developed, the threshold stress under cyclic test exhibited higher one than that of under constant stress. From above test results, the Si_3N_4 tested is able to recover the strength completely even under service conditions, i.e., with an applied stress below $\sigma_{app.} = 200$ MPa and an oxygen partial pressure over $P_{O_2} = 500$ Pa.

The threshold stress for crack healing under constant or cyclic stress as a function of the bending strength of pre-cracked specimens were investigated systematically [2]. The threshold stress is almost proportional to the bending strength of pre-cracked specimens, and the proportional constants for the relationship between the threshold stress and bending strength of pre-cracked specimens is 64% for constant stress and 76% for cyclic stress.

6. EFFECT OF SHOT PEENING ON THE RELIABILITY OF CERAMICS COMPONENT

By shot peening, compressive residual stress can be introduced. The value of the compressive residual stress introduced is dependent on peening method and material. The maximum compressive residual stress introduced in Si_3N_4 and ZrO_2 were about 900 MPa and 1200 MPa, respectively. These compressive residual stresses increase apparent fracture toughness and contact strength and fatigue

strength considerably. In conclusion, the compressive residual stress increases reliability of ceramics components, considerably [20].

7. A PROOF TEST THEORY

Oxygen is necessary for crack-healing, and thus embedded flaws such as pores and abnormally large grains cannot be healed. These facts suggest the importance of a proof test for higher reliability. Ando et al. have proposed a theory to evaluate the temperature dependence of a guaranteed (minimum) fracture stress (σ_G) of a proof-tested sample based on nonlinear fracture mechanics [21]. If proof test were carried out at room temperature, the σ_G can be expressed as Eq. (3) with regard to room temperature and high temperature materials constant:

$$\sigma_G = \frac{2\sigma_0^T}{\pi} \arccos \left\{ \left(\frac{K_{IC}^T}{K_{IC}^R} \right)^2 \left(\frac{\sigma_0^R}{\sigma_0^T} \right)^2 \left\{ \sec \left(\frac{\pi \sigma_p^R}{2\sigma_0^R} \right) - 1 \right\} + 1 \right\}^{-1} \quad (3)$$

where K_{IC} , σ_0 and σ_p^R are the plane strain fracture toughness, the strength of plain specimen (intrinsic bending strength) and the proof test stress at room temperature, respectively, and the superscript R and T indicate the value at room temperature and elevated temperature T , respectively. By obtaining the temperature dependence of K_{IC} and σ_0 , one can estimate σ_G .

To evaluate the validation of the proof test theory, fracture tests were made using $\text{Si}_3\text{N}_4/\text{SiC}$ [21], coil spring made of Si_3N_4 [22] and $\text{Al}_2\text{O}_3/\text{SiC}$ [23]. $\text{Al}_2\text{O}_3/\text{SiC}$ was sintered at relatively low temperature to introduce many embedded flaws such as pores and cracks. The results obtained was shown in Figure 9, where the measured σ_{Fmin} is plotted as a function of the evaluated σ_G [23]. N in the figure denotes the number of samples used to obtain σ_{Fmin} . Four solid diamonds indicate the data on the ceramic coil spring. All σ_{Fmin} showed good agreement with σ_G . From this figure, it can be concluded that Equation (3) can be applied to $\text{Al}_2\text{O}_3/\text{SiC}$, Si_3N_4 , and even to a coil spring.

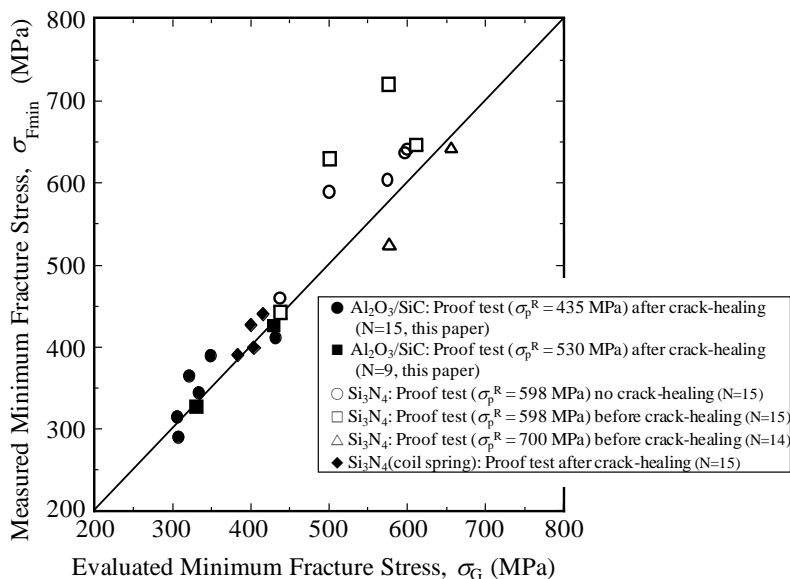


Figure 9: Correlation between σ_G and σ_{Fmin} .

8. FLOW CHART OF THROUGH LIFE RELIABILITY MANAGERMENTS

All processes were explained above sentence, thus in this sentence, only flow chart was shown in Figure 10.

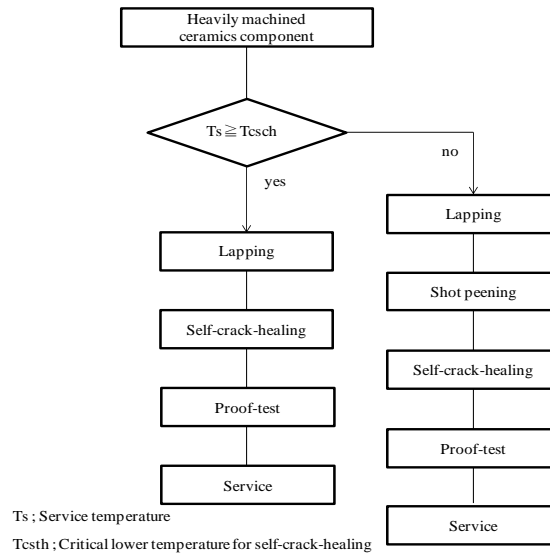


Figure 10: Flow chart for the through-life reliability increase using self-healing ability.

9. CONCLUSION

In this paper, basic self-crack-healing behavior of ceramics and application to increasing reliability were shown. In conclusion, the crack-healing ability of structural ceramics is a very useful technology for higher structural integrity and for reducing the machining and non-destructive inspection costs.

ACKNOWLEDGEMENT

The author shows sincerely thanks to Prof. K. Takahashi, Associ. Prof. W. Nakao and Assist. Prof. T. Osada of Yokohama National Univ. for their creative and active joint researches, and Miss K. Iwanaka for making revised Figures.

REFERENCES

- [1] W. Nakao, K. Takahashi, K. Ando, Self-healing of surface Cracks in Structural Ceramics, in: S.K. Ghosh (Ed.), Self-healing Materials: Fundamentals, Design Strategies, and Applications, WILEY-VCH Verlag GmbH & Co. KGaA, Weinheim, 2010, pp. 183-217.
- [2] Nakao, K. Takahashi, K. Ando, Threshold stress during crack-healing treatment of structural ceramics having the crack-healing ability, Material Letters 61 (2007) 2711-2713.
- [3] K. Ando, B.S. Kim, M.C. Chu, S. Saito, K. Takahashi, Crack-healing and Mechanical Behaviour of Al₂O₃/SiC Composites at Elevated Temperature, Fatigue and Fracture of Engineering Materials and Structures 27 (2004) 533-541.
- [4] W. Nakao, T. Osada, K. Yamane, K. Takahashi, K. Ando, Crack-healing Mechanism by Alumina/ SiC particles/ SiC Whiskers Multi-Composite, Journal of the Japan Institute of Metals 69 (2005) 663-666.
- [5] M.C. Chu, S. Sato, Y. Kobayashi, K. Ando, Damage Healing and Strengthening Behavior in Mullite/SiC Ceramics, Fatigue & Fracture of Materials & Structures 18 (1995) 1019-1029.

- [6] I.A. Chou, H.M. Chan, M.P. Harmer, Effect of annealing environment on the crack healing and mechanical behavior of silicon carbide-reinforced alumina nanocomposites, *Journal of the American Ceramic Society* 81 (1998) 1203-1208.
- [7] K. Ando, T. Ikeda, S. Sato, F. Yao, Y. Kobayashi, A preliminary study on crack healing behaviour of $\text{Si}_3\text{N}_4/\text{SiC}$ composite ceramics, *Fatigue & Fracture of Engineering Materials & Structures* 21 (1998) 119-122.
- [8] Y.S. Jung, W. Nakao, K. Takahashi, K. Ando, S. Saito, Crack-Healing Behavior of $\text{Si}_3\text{N}_4/\text{SiC}$ Composite under Low Oxygen Partial Pressure, *Journal of the Society of Materials Science, Japan* 57 (2008) 1132-1137.
- [9] T. Osada, W. Nakao, K. Takahashi, K. Ando, Kinetics of self-crack-healing of alumina/silicon carbide composite including oxygen partial pressure effect, *Journal of the American Ceramic Society* 92 (2009) 864-869.
- [10] K. Ando, K. Takahashi, W. Nakao, Self-crack-healing behavior of structural ceramics, In: T.Y. Tseng, H.S. Nalwa (Eds.), *Handbook of Nanoceramics and Their Based Nanodevices*, American Scientific Publishers, Valencia, 2009, 1-26.
- [11] T. Osada, W. Nakao, K. Takahashi, K. Ando, S. Saito, Strength recovery behavior of machined alumina/SiC whisker composite by crack-healing, *Journal of the Ceramic Society of Japan* 115 (2007) 278-284.
- [12] S.K. Lee, K. Ando, Y.W. Kim, Effect of heat treatments on the crack-healing and static fatigue behavior of silicon carbide sintered with Sc_2O_3 and AlN , *Journal of the American Ceramic Society* 88 (2005) 3478-3482.
- [13] K. Ando, K. Takahashi, S. Nakayama, S. Saito, Crack-Healing Behavior of $\text{Si}_3\text{N}_4/\text{SiC}$ Ceramics under Cyclic Stress and Resultant Fatigue Strength at the Healing Temperature, *Journal of the American Ceramic Society* 85 (2002) 2268-2272.
- [14] K. Takahashi, K. Ando, H. Murase, S. Nakayama, S. Saito, Threshold stress for crack-healing of $\text{Si}_3\text{N}_4/\text{SiC}$ and resultant cyclic fatigue strength at the healing temperature, *Journal of the American Ceramic Society* 88 (2005) 645-651.
- [15] K. Ando, K. Furusawa, M.C. Chu, T. Hanagata, K. Tuji, S. Sato, Crack-healing behavior under stress of mullite/silicon carbide ceramics and the resultant fatigue strength, *Journal of the American Ceramic Society* 84 (2001) 2073-2078.
- [16] K. Takahashi, K. Ando, H. Murase, S. Nakayama, S. Saito, Threshold stress for crack-healing of $\text{Si}_3\text{N}_4/\text{SiC}$ and resultant cyclic fatigue strength at the healing temperature, *Journal of the American Ceramic Society* 88 (2005) 645-651.
- [17] W. Nakao, M. Ono, S.K. Lee, K. Takahashi, K. Ando, Critical crack-healing condition for SiC whisker reinforced alumina under stress, *Journal of the European Ceramic Society* 25 (2005) 3649-3655.
- [18] S.K. Lee, W. Ishida, S.Y. Lee, K.W. Nam, K. Ando, Crack-healing behavior and resultant strength properties of silicon carbide ceramic, *Journal of the European Ceramic Society* 25 (2005) 569-576.
- [19] K. Takahashi, Y.S. Jung, Y. Nagoshi, K. Ando, Crack-healing behavior of $\text{Si}_3\text{N}_4/\text{SiC}$ composite under stress and low oxygen pressure, *Materials Science and Engineering A* 527 (2010) 3343-3348.
- [20] K. Takahashi, Y. Nishio, Y. Kimura, K. Ando, Improvement of strength and reliability of ceramics by shot peening and crack healing, *Journal of the European Ceramic Society* 30 (2010) 3047-3052.
- [21] K. Ando, Y. Shirai, M. Nakatani, Y. Kobayashi, S. Sato, (Crack-healing + proof test): a new methodology to guarantee the structural integrity of a ceramics component, *Journal of the European Ceramic Society* 22 (2002) 121-128.
- [22] M. Nakatani, S. Sato, Y. Kobayashi, K. Ando, A study on crack-healing + proof test to guarantee the structural integrity of ceramic coil springs, *Journal of High Pressure Institute of Japan* 43 (2005) 85-91.
- [23] M. Ono, W. Nakao, K. Takahashi, M. Nakatani, K. Ando, A new methodology to guarantee the structural integrity of $\text{Al}_2\text{O}_3/\text{SiC}$ composite using crack healing and a proof test, *Fatigue & Fracture of Engineering Materials & Structures* 30 (2007) 599-607.

MECHANISM FOR ABNORMAL THERMAL SHOCK BEHAVIOR OF MAX CERAMICS

S. Li¹ and Y. Zhou¹

¹ Center of Materials Science and Engineering, School of Mechanical and Electronic Control Engineering, Beijing Jiaotong University, Beijing 100044, China. - e-mail: shbli1@bjtu.edu.cn; yzhou@bjtu.edu.cn

Keywords: MAX ceramics, self-healing, abnormal thermal shock behavior, mechanism

ABSTRACT

Ceramics should possess a good thermal shock resistance when subjected to sudden changes of temperature (thermal shock). However, most ceramic materials are susceptible to thermal shock with catastrophic drops in mechanical properties, limiting their wide applications.

Recently, it has been found that some layered ternary carbides and nitrides (also called MAX phases, M denotes an early transition metal, A is a mostly IIIA or IVA group element, and X is either C or N) exhibit abnormal thermal shock behaviour. The residual strength of the as-quenched MAX phases gradually decreases without catastrophic failure with increasing quenching temperatures and then unbelievably increases after quenching at certain temperatures, not like other ceramics showing catastrophic drops in mechanical properties. Although the abnormal thermal shock behaviour has been found in some MAX phases over 15 years, yet the real mechanism is not entirely clear. Up to now, several mechanisms have been proposed for the abnormal behaviour. However, the above mentioned mechanisms are speculative and have never been directly confirmed by experiment evidence.

To reveal the main mechanism for the unusual thermal shock behaviour, we chose a Cr₂AlC ceramic as a representative member of the MAX phases and performed thermal shock test in a quenching temperature range of 800-1300 °C. The main mechanism for the abnormal thermal shock should be attributed to crack healing, i.e. the thermal shock induced cracks are instantly healed by the formation of reactants well adhering to the crack faces during quenching.

SELF HEALING BY CU PRECIPITATION IN DEFORMED FE-CU-B-N-C

S. Zhang¹, G. Langelaan¹, H. Schut¹, E. Brück¹, S. van der Zwaag² and N.H. van Dijk¹

¹ Faculty of Applied Sciences, Delft University of Technology, Mekelweg 15, 2629JB Delft, The Netherlands – e-mail: S.Zhang-1@tudelft.nl; G.Langelaan@tudelft.nl;

H.Schut@tudelft.nl; E.H.Bruck@tudelft.nl; N.H.vanDijk@tudelft.nl,

² Faculty of Aerospace Engineering, Delft University of Technology, Kluyverweg 1, 2629 HS Delft, The Netherlands – e-mail: S.vanderZwaag@tudelft.nl

Keywords: Self-healing, Cu precipitation, deformation-induced defects, carbon addition, positron annihilation spectroscopy

ABSTRACT

Steels are among the most widely used construction materials as their mechanical properties can be tuned over a very wide range of desired combinations of strength formability and other properties. However, when exposed for long times to high temperatures steel components can exhibit premature and low-ductility creep fracture, which arises from the formation, growth and coalescence of (initially) nanoscale pores. Self-healing of such defects is regarded as a promising new approach to enhance the component lifetime. In principle, it could be achieved by nanoscale precipitation on the creep cavity surface preventing further growth. Earlier work has shown that Cu may be a suitable alloying element to induce such a healing behaviour in stainless steels.

In the present work the high temperature precipitation behaviour of Cu on deformation induced defects is studied for a number of high-purity Fe-Cu-B-N-C alloys using positron annihilation spectroscopy (PAS) and hardness tests. Samples with 0% and 8% cold pre-strain are utilized to study the influence of prior tensile deformation on the precipitation kinetics of copper. The time evolution of the *S-W* points derived from Coincidence Doppler Broadening spectra indicates that deformation-induced defects enhance the Cu precipitation kinetics. A clear reduction in open volume defects is accompanied by a strong increase of Cu signature during the initial stage of aging, demonstrating the self-healing potential in the Fe-Cu-B-N-C alloy. A comparison between the hardness behaviour of Fe-Cu, Fe-Cu-B-N, and Fe-Cu-B-N-C indicates the added carbon counteracts the acceleration of Cu precipitation caused by the addition of B and N.

1. INTRODUCTION

Self-healing is a promising new approach to extend the lifetime of steel components operating at high temperatures. Recently, Shinya and coworkers have demonstrated that creep damage can be self-healed in austenitic stainless steels [1,2]. The enhanced creep resistance is proposed to be due to the formation of nano-size precipitates and the surface segregation of solute atoms (i.e. copper, boron) on cavities, which fill the defects and prevent further growth of the creep cavities. In our previous work, the influence of deformation-induced defects on copper precipitation

during aging was studied in Fe-Cu and Fe-Cu-B-N model alloys to evaluate the self-healing potential of Fe alloys with Cu, B and N added [3,4]. It was demonstrated that in deformed Fe-Cu-B-N, the addition of B and N accelerated the formation of spherical nanoscale Cu precipitates and strongly reduced the Cu precipitation along dislocations during thermal aging at 550 °C. Carbon, the primary alloying element in steel, is widely used to improve the mechanical properties of the steel. It is desirable to investigate the influence of carbon on the self-healing behavior and the Cu precipitation kinetics.

2. MATERIALS

The chemical composition of the studied Fe-Cu-B-N-C alloy produced by Goodfellow is shown in Table 1. Dog-bone shaped samples with a thickness of 0.5 mm were machined by spark erosion from the rolled sheet material. The samples were solution treated at 800 °C for 3 h in evacuated silica tubes filled with 200 mbar ultrahigh purity argon, and subsequently quenched into water at room temperature. The Fe-Cu-B-N-C alloy samples were studied in two conditions: with and without an applied pre-strain of 8%. The pre-strain was applied at room temperature by tensile deformation using a 2 kN microtensile tester (Deben).

Table 1: The chemical composition of Fe-Cu-B-N-C alloy (in wt.%) with balance iron. The Ce concentration amounts to the nominal concentration.

Cu	B	N	C	S	Ce
1.00	0.050	0.019	0.087	0.002	0.015

3. METHODS

The coincidence Doppler broadening (CDB) measurements were carried out by using a sandwich of two samples with a ^{22}Na positron source in between. Recording of $>10^6$ annihilation events results in a distribution of the energy difference. By measuring the Doppler shift in the energy of the two 511 keV annihilation γ -rays, one obtains the information on the momentum distribution of the electrons involved in the annihilation process. The overall energy resolution was about 1 keV at 511 keV (full width at half maximum, FWHM), corresponding to a momentum resolution of $4 \times 10^{-3} m_0 c$ (FWHM) with m_0 the electron rest mass and c the light speed. The samples were heated to a fixed temperature of 550 °C in a vacuum furnace ($< 5 \times 10^{-5}$ Pa) in separate aging steps. The CDB spectra were recorded between the heat treatments. Vickers microhardness testing was carried out using a load of 500 g on samples that were aged at 550 °C for 0-96 h in a vacuum chamber ($< 5 \times 10^{-5}$ Pa).

4. RESULTS

In order to clarify the Cu precipitation kinetics and the evolution of defects, we evaluate the evolution of two parameters (S and W) derived from the Doppler broadening spectrum during aging up to 96 h. The S parameter reflects the annihilation with valence electrons and is calculated as the ratio of the counts in a

fixed low-momentum interval ($|p_L| < 3.1 \times 10^{-3} m_0 c$). Similarly, the W parameter is obtained from the contribution of annihilations with high momentum core electrons ($9.2 \times 10^{-3} m_0 c < |p_L| < 24.3 \times 10^{-3} m_0 c$) [3]. The copper precipitates can be regarded as a potential well for positrons and result in a high W parameter. Figure 1 shows the evolution of the S - W points for the as-quenched and the 8% deformed samples. All S - W points are normalized to those for annealed pure iron ($S_{Fe} = 0.4609$, $W_{Fe} = 0.1198$). For the as-quenched Fe-Cu-B-N-C alloy, the W parameter is comparable to that of annealed pure iron. The relatively high S value for the sample with 8% pre-strain is due to the deformation-induced defects (such as dislocations). During the initial aging stage, the S - W points shift toward the Cu position for both the 0% and 8% pre-strain samples. The data points approach the value of the annealed pure Cu after an aging time of 2-4 h for the Fe-Cu-B-N-C alloy without deformation and 1-2 h for the Fe-Cu-B-N-C alloy with 8% pre-strain. A comparison of the time evolution of the S - W points for the undeformed and deformed samples indicates that the deformation-induced defects accelerate the Cu precipitation kinetics. For longer aging times, a shift in S - W points is observed toward a high S and low W position which is attributed to the misfit between the copper precipitates and the matrix.

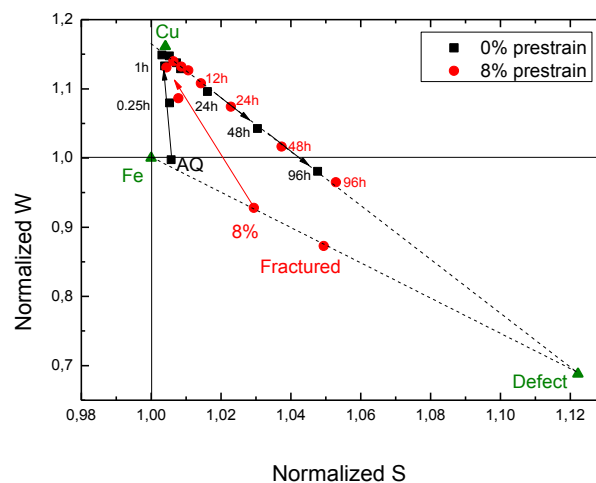


Figure 1 : Time evolution of the S and W parameters for the as-quenched Fe-Cu-B-N-C alloy with 0% and 8% pre-strain.

In Figure 2, the Vickers hardness is shown as a function of the aging time for the Fe-Cu-B-N-C alloy. For comparison the data for the Fe-Cu and Fe-Cu-B-N alloys are also shown [3]. For the samples without pre-deformation, the behaviour of Fe-Cu-B-N-C is close to that of the Fe-Cu alloy, i.e. the hardness gradually increases and reaches the peak hardness at about 6 h, followed by a continuous decrease (Figure 2a). For the shortest annealing time of 0.1 h, the hardness of the Fe-Cu-B-N alloy increases sharply to 130 HV_{0.5}, a much higher level than observed for the Fe-Cu and Fe-Cu-B-N-C alloys. Subsequently, the age-hardening kinetics of the Fe-Cu-B-N alloy is slightly slower, compared to that of the Fe-Cu-B-N-C alloy. For the deformed samples, the addition of trace elements does not noticeably change the age-hardening behaviour for copper precipitation. In the initial aging stage the hardness decreases due to the recovery of dislocations, subsequently it rises with increasing aging time till reaching a peak age and finally decreases again in the over-aged stage. The peak aging time for the Fe-Cu and Fe-Cu-B-N-C alloys is 6 h

while the Fe-Cu-B-N alloy reaches the aging peak within 4 h, as shown in Figure 2b. Thus addition of carbon counteracts the effect of boron and nitrogen on the Cu precipitation.

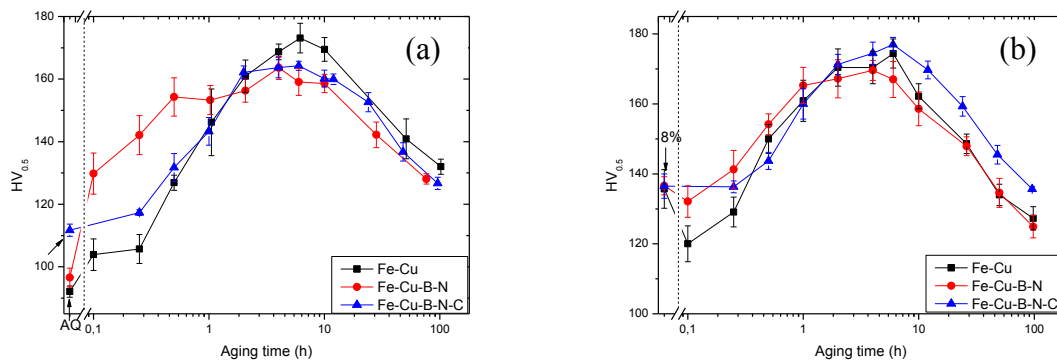


Figure 2 : Vickers Hardness $HV_{0.5}$ as a function of aging time at $550\text{ }^{\circ}\text{C}$ of Fe-Cu, Fe-Cu-B-N, and Fe-Cu-B-N-C alloys (a) without deformation, and (b) with 8% pre-strain (data for the Fe-Cu and Fe-Cu-B-N alloys from Ref. [3]).

5. CONCLUSIONS

The isothermal copper precipitation in high-purity Fe-Cu-B-N-C alloy with 0% and 8% pre-strain was studied as a function of the aging time at $550\text{ }^{\circ}\text{C}$. Self-healing of nano-size defects is demonstrated. In the *S-W* plots, the deformed alloy exhibits a sharp reduction in open-volume defects accompanied with a strong copper signature during the initial aging stage. This is explained by the closure of open volume defects by copper precipitation. The Cu precipitation in the Fe-Cu-B-N-C alloy is comparable to that in the Fe-Cu alloy, which is due to the incorporation of boron and nitrogen in carbides.

ACKNOWLEDGEMENTS

This research was financially supported by the innovation-oriented research program (IOP) on self-healing materials of the Dutch Ministry of Economic Affairs, Agriculture and Innovation (IOP project SHM01017).

REFERENCES

- [1] K. Laha, J. Kyono, N. Shinya, An advanced creep cavitation resistance Cu-containing 18Cr-12Ni-Nb austenitic stainless steel, *Scripta Materialia* 56 (2007) 915-918.
- [2] K. Laha, J. Kyono, N. Shinya, Some chemical and microstructural factors influencing creep cavitation resistance of austenitic stainless, *Philosophical Magazine* 87 (2007) 2483-2505.
- [3] S. M. He, N. H. van Dijk, H. Schut, E. R. Peekstok, S. van der Zwaag, Thermally activated precipitation at deformation-induced defects in Fe-Cu and Fe-Cu-B-N alloys studied by positron annihilation spectroscopy, *Physical Review B* (2010) 094103.
- [4] S. M. He, N. H. van Dijk, M. Paladugu, H. Schut, J. Kohlbrecher, F. D. Tichelaar, S. van der Zwaag, In situ determination of aging precipitation in deformed Fe-Cu and Fe-Cu-B-N alloys by time-resolved small-angle neutron scattering, *Physical Review B* (2010) 174111.

SELF-HEALING BEHAVIOR OF FIBER-REINFORCED SELF-HEALING CERAMICS

S. Sugiyama¹, W. Nakao¹

¹ *Yokohama National University, 79-5 Tokiwadai, Hodogaya-ku, Yokohama, 240-8501 Japan*
– e-mail: sugiyama-saho-yp@ynu.ac.jp; wnakao@ynu.ac.jp

Keywords: Structural ceramics, Fiber reinforced ceramics, Mechanical reliability, oxidation induced self-healing, autonomic self-healing

ABSTRACT

The alumina fiber reinforced alumina containing the interlayer of SiC as healing agent was found to have self-healing ability for the delimitation of the fiber/matrix interface. Main crack in the composite is branched to fiber/matrix interface when the main crack reached the interface, because the interlayer has lower strength than those of the fiber and matrix. The surface of the branched crack consists of the healing agent so that self-healing reaction which is the high temperature oxidation of the healing agent effectively acted to the re-bonding of the branched crack. Therefore, it was found that the developed composite can completely recover the degraded strength during the shorter time than the ordinary SiC particles dispersed self-healing ceramics.

1. INTRODUCTION

Fiber-reinforced self-healing ceramic (shFRC) is most candidates of the advanced turbine blade materials. Turbine blades need to stand high temperature environment, high temperature oxidation, and crush of foreign object with high speed. In spite of its excellent refractoriness and oxidation resistance, ceramic turbine blades have not been realized yet, because ordinary ceramics cannot stand overloading, including to the foreign objective damage (FOD). The proposed shFRC has a high resistance to foreign object impact damage, as shown in Figure 1. As the shFRC has weak interlayer at the fiber/ matrix interface, cracks can be branched along the interlayer when cracks propagate to the interlayer. Further crack propagation leads to the friction at the fiber/matrix interface. Therefore, the shFRC can stand excessive loads by high fracture energy due to the friction at the branched crack surfaces. Moreover, the high temperature oxidation of the interlayer acting as healing agent can re-bond the branched crack surfaces, because the crack allows the surrounding atmosphere flow into the crack surface and react with the healing agent. The branched crack is no longer playing as most severe defect, and thereby, the shFRC can survive the repeated overload, such as FOD.

In the present study, the above materials concept was demonstrated by using continuous alumina fiber reinforced alumina with SiC interlayer.

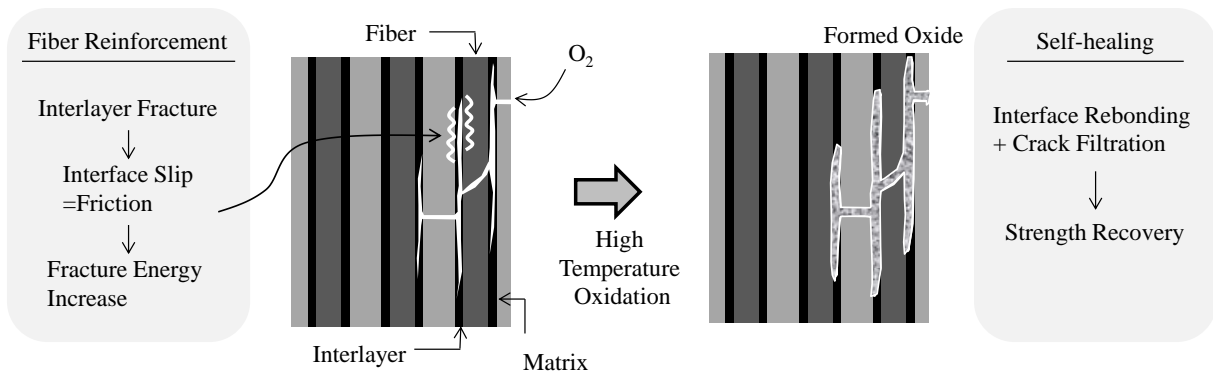


Figure 1: Schematics of the developed continuous fiber reinforced ceramics having self-healing ability and the mechanism of the function combined fiber reinforcement and self-healing

2. MATERIAL AND SAMPLE PREPARATION

For typical sample of shFRC, alumina fiber/ alumina composite with SiC interlayer was prepared in this study. The used alumina fiber (NITIVY CO.,LTD. S-640D) is filaments bundle with diameter of 0.3 mm. Fine alumina (Sumitomo Chemical Co., Ltd. AKP-50, $\phi 0.23 \mu\text{m}$) and SiC (IBIDEN CO., LTD. Ultrafine, $\phi 0.35 \mu\text{m}$) powders were used as matrix and interlayer, which plays role in healing agent.

Figure 2(a) shows the procedure of sample preparation of shFRC. The whole of the coating and figuration were subjected by using the fiber winding apparatus as shown in Figure 2(b). Prior to the interlayer coating, the alumina fine particles were filled with the voids of alumina fiber bundle by letting the fiber bundle pass through alumina slurry. By using similar slurry coating, the SiC interlayer was formed on the alumina fiber bundle. After letting the SiC coated fiber bundle pass through alumina slurry, the fiber bundle was figured by winding on 50 mm x 50 mm x 6 mm stainless plate. The figured fiber bundle lamination was sintered at 1300 °C for 1h in Ar.

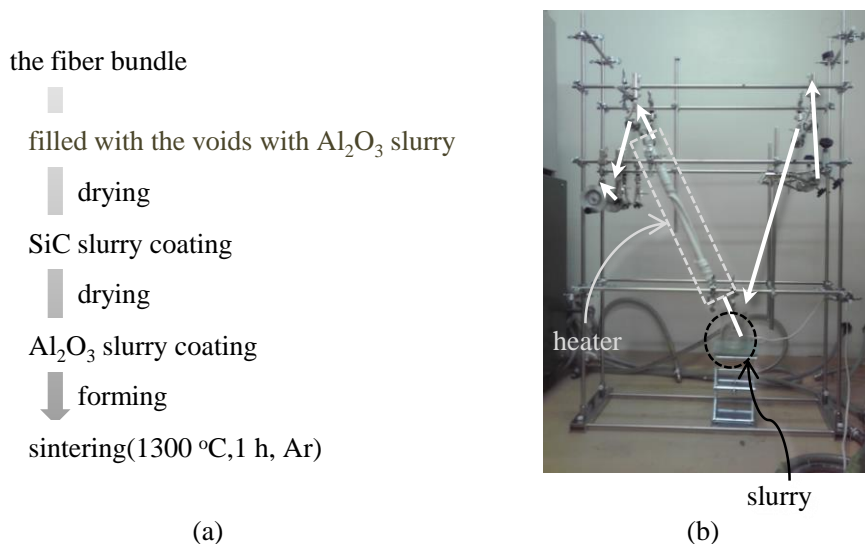


Figure 2: (a) procedure of sample preparation of shFRC
(b) Photograph of the experimental apparatus of wire winding process

Figure 3 shows cross-sectional microscopy of the prepared shFRC. It is found that the shFRC had the SiC interlayer thickness of $\sim 60 \mu\text{m}$ and the mean fiber distance of $** \text{mm}$. Thus, the fiber content was evaluated to be 58 %. Furthermore, the relative density of the shFRC was found to have 78 % from the Archimedes measurement.

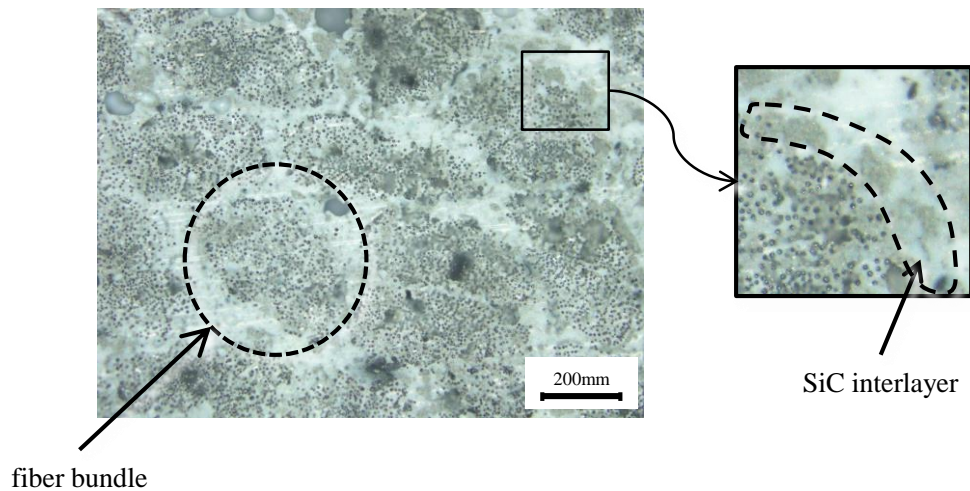


Figure 3: microscopic photograph of cross-section surface of specimen

3. MECHANICAL PROPERTIES

Mechanical properties and self-healing ability of shFRC were investigated from three-point bending using 3 mm x 4 mm x 50 mm rectangular specimen with a V-shaped notch whose depth is 1 mm.

Figure 4 shows stress-strain curves of "virgin" V-notched shFRC and the V-notched shFRC healed at 1000 °C for several time in the air after pre-loading. Black solid line indicates the stress-strain curve of "virgin" shFRC. The bending stress increases linearly as the bending strain increases below the strain which the stress shows a maximum. Above that, the stress drops but the shFRC did not fracture. This behavior implies that the crack introduced and propagated from the tip of the V-shaped notch and then branching along the interlayer when the crack reached to fiber bundle. The branching crack was observed in Figure 5(a). Therefore, the whole self-healed shFRCs had the branching crack before self-healing. Although the shFRC healed for 1 h had lower maximum stress and gradient of primary part of stress-strain curve than those of "virgin" shFRC, the shFRCs healed above 5 h had same or more than maximum stress, and the gradient for the shFRC healed for 50 h reached the same value of "virgin" specimen. In other words, the self-healing of the shFRC can recover the degraded strength and stiffness for 5 h and 50 h, respectively. Figure 5(b) shows the fracture initiation of the shFRC healed at 1000 °C for 50 h. Since the fracture initiation change from the pre-introduced branching crack, the self-healing was found to enable to re-bond the crack surface completely. Moreover, all stress-strain curves revealed that the shFRC had large deformation ability after self-healing.

Similar self-healing behavior was investigated for 1200 °C healing. In 1200 °C healing, the complete strength and stiffness recoveries can be attained within only 1 h.

From the obtained self-healing behaviors, it was found that the shFRC has superior self-healing ability to the ordinary SiC particles dispersed self-healing ceramic. From the previous research [1], SiC dispersed alumina composite was reported to enable to heal semi-elliptical surface crack having surface length of 100m for 100h @ 1000 °C and for 10h @ 1200 °C. Therefore, it is confirmed that the shFRC can effectually heal

the crack, because the shFRC entices cracks into propagating to the interlayer constituting of the healing agent.

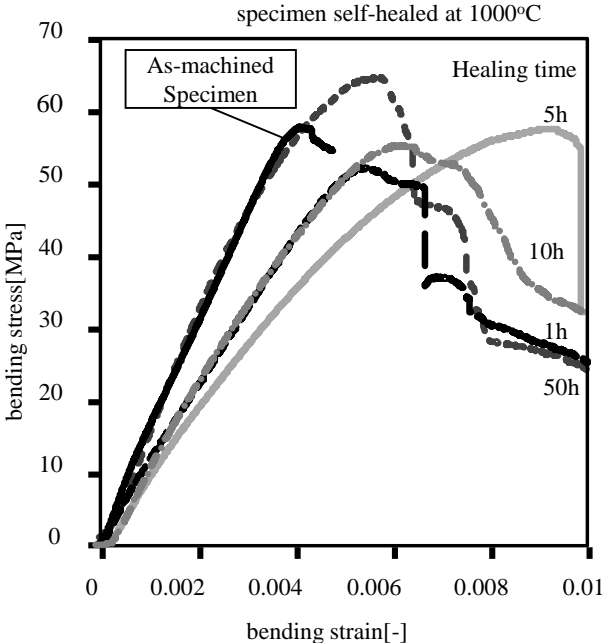


Figure 4: Load-displacement curves of the developed fiber reinforced self-healing ceramics applied by three-point bending with span of 30 mm

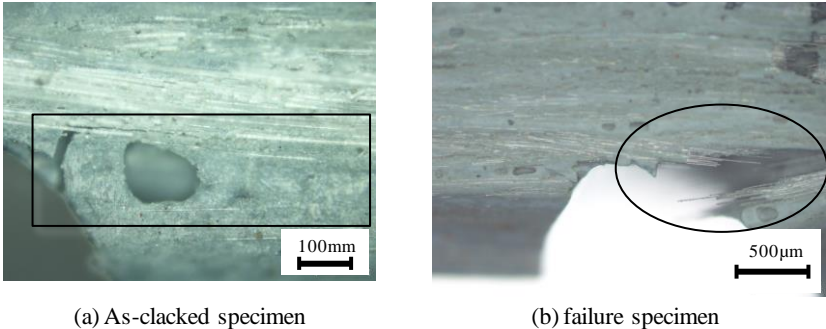


Figure 5: Microscopic photograph of the clack near the notch in specimen

4. SUMMARY

In this study, the alumina fiber reinforced alumina containing the interlayer of SiC as healing agent was found to have self-healing ability for the delimitation of the fiber/matrix interface. it was also found that the developed composite can completely recover the degraded strength during the shorter time than the ordinary SiC particles dispersed self-healing ceramics.

REFERENCES

[1] K. Ando, B.S. Kim, S. Kodama, K. Takahashi, S. Saito, Development of the alumina ceramics which have the excellent crack-healing ability and a heat-resistant limit, Materials and processing conference 115 (2003-11) pp. 75-76.

SESSION 18 – MICROVASCULAR SYSTEMS

COMPOSITE 3D VASCULARIZATION BY USING SACRIFICIAL ELECTROSPUN SUB-MICROMETRIC FIBRES

C. Gualandi ^{1,2}, A. Zucchelli ², M. F. Osorio ² and M. L. Focarete ¹

¹ *Department of Chemistry "G. Ciamician" and National Consortium of Materials Science and Technology (INSTM, Bologna RU), University of Bologna, via Selmi 2, 40126 Bologna, Italy – e-mail: c.gualandi@unibo.it; marialetizia.focarete@unibo.it*

² *Advanced Applications in Mechanical Engineering and Materials Technology Interdepartmental Center for Industrial Research, (CIRI MAM) and Department of Mechanical Engineering (DIEM), University of Bologna, Viale Risorgimento 2, 40136, Bologna, Italy – e-mail: a.zucchelli@unibo.it; marina.f.osorio@gmail.com*

Keywords: vascularization, electrospinning, sub-micrometric fibres, composite material

ABSTRACT

The creation of an extensive vasculature in composite structures is a challenge. The Bond and White groups are pioneers of different methods to achieve composite vascularisation, all of them based on the removal of sacrificial micro-fibres previously embedded in a polymer matrix.

We propose the use of electrospinning to produce sacrificial sub-micrometric fibres. Advantages derived by the use of this technique are: (i) the collection of fibres in form of a non-woven mat that can be easily embedded in a polymer matrix; (ii) the intrinsic morphology of the non-woven mat that resembles the blood vascular network of living system; (iii) the control of fibre diameters from hundreds of nanometers to few micrometers; (iv) the control of fibre spatial arrangement.

Here we present, as a proof of concept, the use of water soluble poly(ethylene oxide) electrospun fibres that can be easily embedded in a low-temperature thermoset polymer matrix and subsequently removed by simply immersing the composite in water. Fibres with different diameters can be used for generating vessels with different diameters. Moreover, non-woven mats either with a random fibre arrangement or with aligned fibres can be used to generate a biomimetic vasculature and unidirectional vessels, respectively. High-temperature thermoset polymer matrix can be similarly vascularized by a smart choice of electrospun fibre material.

1. INTRODUCTION

The complexity in fabricating composites possessing a 3D network of interconnected channel containing healing substances is a real and practical limitation to the exploitation of this type of smart materials. Different methods have been proposed to achieve micro-vascularization of composite materials [1-3]. Here we use electrospun non-woven membranes made of sub-micrometric fibres that, once impregnated in the polymer matrix, can be removed by water dissolution. We present vascularized polymer matrices fabricated by using Polyethylene oxide (PEO) fibres either randomly oriented or aligned in a preferential direction.

2. MATERIALS AND METHODS

2.1 Materials.

PEO ($M_v \sim 4 \times 10^5$ g/mol) and Rhodamine B were purchased by Sigma-Aldrich. A bicomponent epoxy resin Elan-tech® EC 157/W 61 was supplied by Elantas (Italy).

Electrospun mesh preparation

Electrospun non-wovens were produced by using a previously described electrospinning apparatus [4,5]. PEO was dissolved in MilliQ water at a concentration of 7% w/V and the solution was electrospun by using the following conditions: needle-to-collector distance = 20 cm, applied voltage = 18 kV and flow rate = 0.9 ml/h.

2.2 Composite fabrication

Epoxy matrix was prepared by mixing at RT the pre-polymer and the curing agent at a ratio 100/17 by weight, according to manufacturer instructions. The mixture was degassed under vacuum. To produce composite films the electrospun membrane was placed on a PTFE film and the uncured mixture was gently poured on it to get a complete impregnation. The excess of uncured resin was eliminated by using filter paper. The impregnated electrospun membrane was maintained at 40°C for 24, and 120°C for 2h.

2.3 Characterization techniques

SEM observations were carried out by using a Philips 515 SEM at an accelerating voltage of 15 kV, on samples sputter-coated with gold. The distribution of fiber diameters in electrospun non-woven samples was determined through the measurement of about 250 fibres. SEM was also performed on composites before and after water immersion (composite sections obtained by fracturing in liquid nitrogen). After water treatment, the possibility to fill the empty channels of vascularized composites was investigated by immersing the latter in a pink aqueous solution of Rhodamine (0.007% w/V) overnight under stirring.

3. RESULTS AND DISCUSSION

Electrospun non-woven membranes of PEO composed of fibre with diameter distribution $300 \div 50$ nm are shown in Figure 1.

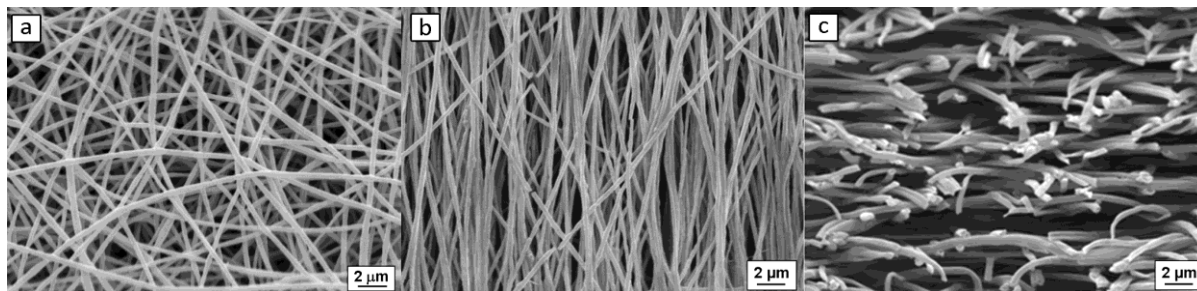


Figure 1: a) PEO random fibres; b) PEO aligned fibres; c) section of electrospun membrane.

The successful incorporation of PEO random fibres in the thermosetting matrix is shown in Figure 2, together with the image of the same composite after water immersion overnight. The section of composite before water treatment was characterized by the presence of fibres and holes, the latter as a consequence of fibre debonding and pulling out during the fracture. After water treatment the section of the matrix displayed many holes and channels as a consequence of the dissolution of fibres oriented perpendicular and parallel to the section, respectively.

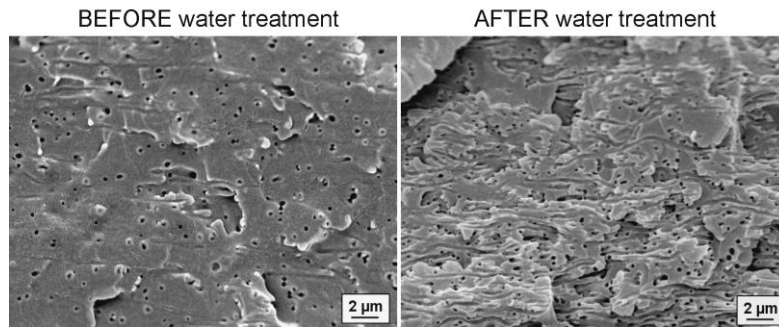


Figure 2: SEM images of composite sections filled with PEO random fibres before and after water immersion.

The incorporation of non-woven membranes made of aligned fibres generated, after fibre dissolution, unidirectional empty channels within the matrix (Figure 3).

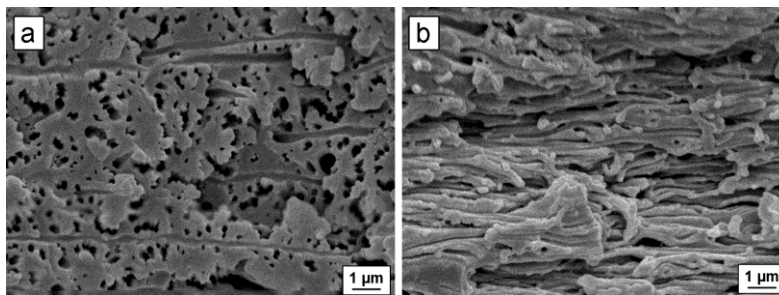


Figure 3: SEM images of composite sections filled with PEO aligned fibres after water immersion: a) section transversal to fibre direction and b) section parallel to fibre direction.

The capability of filling the empty channels with a liquid solution was verified by immersing the composite in a coloured water solution. Pictures in Figure 4 were acquired before and after immersion in Rhodamine B water solution.

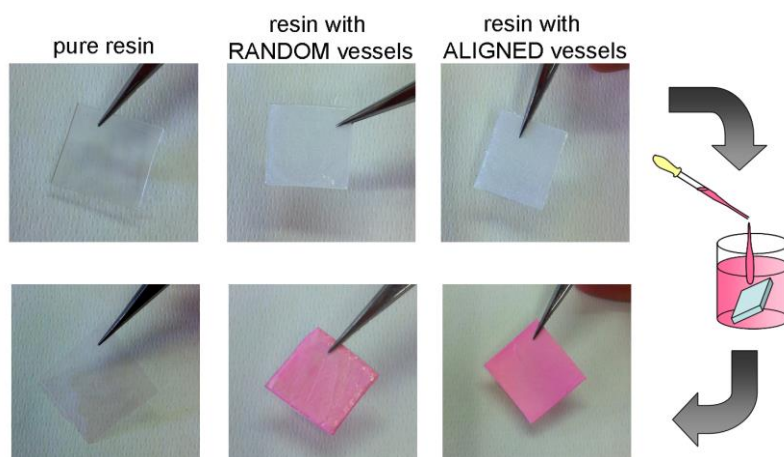


Figure 4: Coloured vascularized matrix after immersion in Rhodamine B water solution

4. CONCLUSION

In this work we demonstrated the possibility to easily generate a vascularized sub-micrometric structure inside a polymer matrix by using non-woven electrospun membranes impregnated in the polymer matrix and subsequently removed by water immersion. We also demonstrated that the empty and branched vessels, whose orientation can be governed during electrospun process, can be filled with a liquid substance.

ACKNOWLEDGEMENTS

The authors gratefully acknowledge Italian Ministry of University and Research for the financial support.

REFERENCES

- [1] K. S. Toohey, N. R. Sottos, J. A. Lewis, J. S. Moore, S. R. White, Self-healing materials with microvascular networks, *Nature Materials* 6 (2007) 581-585.
- [2] C. J. Norris, G. J. Meadway, M. J. O'Sullivan, I. P. Bond, R. S. Trask, Self-healing fibre reinforced composites via a bioinspired vasculature, *Advanced Functional Materials* 21 (2011) 3624-3633.
- [3] A. P. Esser-Kahn, P. R. Thakre, H. Dong, J. F. Patrick, V. K. Vlasko-Vlasov, N. R. Sottos, J. S. Moore, S. R. White, Three-dimensional microvascular fiber-reinforced composites, *Advanced Materials* 23 (2011) 3654–3658
- [4] E. Saino, M. L. Focarete, C. Gualandi, E. Emanuele, A. I. Cornaglia, M. Imbriani, L. Visai, Effect of electrospun fiber diameter and alignment on macrophage activation and secretion of proinflammatory cytokines and chemokines, *Biomacromolecules* 12 (2011) 1900-1911.
- [5] A. Zucchelli, D. Fabiani, C. Gualandi, M. L. Focarete, An innovative and versatile approach to design highly porous, patterned, nanofibrous polymeric materials, *J Mater Sci* 44 (2009) 4969–4975.

AUTONOMIC REGENERATION OF LARGE DAMAGE VOLUMES

B.P. Krull^{1,5}, W.A. Santa Cruz^{2,5}, R.C.R. Gergely^{3,5}, S.R. White^{4,5}, J.S. Moore^{2,5},
N.R. Sottos^{1,5}

¹ *Department of Materials Science and Engineering, University of Illinois at Urbana-Champaign, Urbana, IL, 61801, USA – email: krull3@illinois.edu*

² *Department of Chemistry, University of Illinois at Urbana-Champaign, Urbana, IL, 61801, USA.*

³ *Department of Theoretical and Applied Mechanics, University of Illinois at Urbana-Champaign, Urbana, IL 61801, USA.*

⁴ *Department of Aerospace Engineering, University of Illinois at Urbana-Champaign, Urbana, IL, 61801, USA.*

⁵ *Beckman Institute of Advanced Science and Technology, University of Illinois at Urbana-Champaign, Urbana, IL, 61801, USA – email: n-sottos@illinois.edu*

Keywords: self-healing, large damage volume, regeneration, microvascular, polymer network gel

ABSTRACT

Bioinspired microvascular networks possess the ability to deliver a renewable supply of healing agents to damaged materials. Damage recovery has been successful primarily in high surface area to volume ratio configurations such as delaminations or thin surface coatings. Self-healing of large, open damage volumes presents a significant challenge.

Here we implement vascular delivery of a new bi-phase healing chemistry to regenerate large damage volumes in 3mm thick epoxy sheets with embedded microvascular channels. Damage is introduced through the thickness of the sample by excising a cylindrical volume of material of varying size. Similar to many two-part commercial resins, the bi-phase resin system consists of two separate fluid components. As a damage event occurs, the bi-phase resin components enter the injury region via the vascular networks. The viscosity of the combined resin system rapidly increases and a cross-linked polymer gel forms. Additional bi-phase resin continues to deposit and gel in the damage area until the injury is filled with a soft gel. After the entire damage volume has been recovered, the gel undergoes a second polymerization reaction to form a structural solid.

The bi-phase resin system can be formulated to possess independent control of gelation and polymerization kinetics, a 1:1 stoichiometric mixing ratio, and a viscosity below 100 cps. These desirable design parameters assist in microvascular delivery of the system, making it possible to recover damage diameters in excess of 6mm.

INTEGRATED FLUID RESERVOIRS FOR MICROVASCULAR HEALING IN SANDWICH COMPOSITE MATERIALS

J. Tye ¹, C. Hansen ¹

¹ *Advanced Composite Materials and Textile Research Laboratory, University of Massachusetts Lowell, 1 University Ave, Lowell MA 01854, USA – email: Christopher_Hansen@uml.edu*

Keywords: microvascular, sacrificial fibers, sandwich composites, damage sensing

ABSTRACT

Microvasculature is a pervasive architectural feature in biological systems because fluid transport enables many critical biological functions, including healing of tissue damage. In engineering contexts, embedded microvascular networks permit self-healing of greater damage volumes and multiple damage events due to improved access to healing agents. To date, these healing agents have been supplied by reservoirs external to the material structure, which add complexity and parasitic mass. Here, we address this shortcoming by integration of healing fluid reservoirs into honeycomb core sandwich composites that autonomously transport healing fluids via microvascular pathways to damage sites.

The microvascular networks are fabricated via sacrificial fibers, which were pioneered by Esser-Kahn *et al.* (2011). This work utilizes the same polylactide and tin oxalate catalyst fiber chemistry, which depolymerizes *in situ* at 200°C. We improve the fiber treatment and evacuation process by direct filament extrusion rather than the previous chemical swelling technique. Filaments are extruded at rapid rates (>10 m/s) using a single-screw extruder, thereby speeding fiber manufacture while reducing cost and eliminating chemical waste. Isothermal thermogravimetric analysis indicates improved filament decomposition kinetics, which we attribute to improved catalyst dispersion within the filament.

Sacrificial fibers are successfully woven into the textile face sheets and the resulting microvascular pathways permit transport of healing fluids between the core and the face sheet networks. Fluids are successfully infiltrated into and recovered from the honeycomb compartments, with demonstrated recovery efficiencies greater than 95%. Fluids can be initially pressurized via compressible air and sealed into internal fluid reservoirs to successfully provide a passive mechanism to transport healing agents from the core cell reservoirs to incident damage sites. The repeatability is shown to be dependent on the structural orientation of the damage and the fluid reservoirs.

SELF-HEALING IN WOVEN COMPOSITE LAMINATES VIA BIOINSPIRED MICROVASCULAR NETWORKS

J.F. Patrick^{1,5}, K.R. Hart^{2,5}, B.P. Krull^{3,5}, J.S. Moore^{4,5}, N.R. Sottos^{3,5}, S.R. White^{2,5}

¹ Department of Civil and Environmental Engineering, University of Illinois at Urbana-Champaign, Urbana, IL, 61801, USA – e-mail: jpatric2@illinois.edu

² Department of Aerospace Engineering, University of Illinois at Urbana-Champaign, Urbana, IL, 61801, USA.

³ Department of Materials Science and Engineering, University of Illinois at Urbana-Champaign, Urbana, IL, 61801, USA.

⁴ Department of Chemistry, University of Illinois at Urbana-Champaign, Urbana, IL, 61801, USA.

⁵ Beckman Institute of Advanced Science and Technology, University of Illinois at Urbana-Champaign, Urbana, IL, 61801, USA – email: n-sottos@illinois.edu; swhite@illinois.edu

Keywords: self-healing, fiber-reinforced composites, microvascular, mode-I interlaminar delamination

ABSTRACT

The introduction of microvascular features to a structural material imparts multifunctional capabilities in otherwise quiescent, mechanical support by means of simple fluid circulation. Biomimetic microvascular networks have been created in fiber-reinforced composites via thermal depolymerization of interwoven sacrificial fibers providing added functionality. Thermal regulation, chemical reaction, magnetic field modulation, and conductivity accession have already been demonstrated.

Here we develop a microvascular-based self-healing strategy for improvement in the damage resilience of fiber reinforced composite materials. Specifically, we have investigated healing a woven E-glass composite laminate after Mode-I interply delamination in a Double Cantilever Beam (DCB) geometry. A two-part healing chemistry based on a commercially available thermoset epoxy formulation is employed to rebond the fractured interface. Both components are initially sequestered in separate channels of a vascularized DCB specimen. Upon loading and subsequent crack propagation through the network, the healing agents are released and polymerize on contact to create new polymer material in the crack plane.

An attractive feature of this system is the renewable supply of healing agents leading to the repair of macro-scale delaminations over three consecutive heal cycles. Furthermore, the polymerization reaction occurs at room temperature under non-stoichiometric conditions, enabling practical *in-situ* healing. Through repeated mechanical testing of the healed DCB specimens, we have demonstrated a significant recovery (>100%) of the virgin mode-I fracture resistance for this latest class of self-healing polymer composite materials.

SESSION 19 – SELF-HEALING METALLIC AND CERAMIC MATERIALS

KINETIC MODEL FOR SELF-CRACK-HEALING IN CERAMICS AND POSSIBILITY OF TURBINE BLADE APPLICATIONS

T. Osada¹

¹ Cooperative Research and Development Center, Yokohama National University, 79-5, Tokiwadai, Hodogaya, Yokohama, 240-8501, Japan – e-mail: tosada@ynu.ac.jp

Keywords: Ceramics, Self-crack-healing, Kinetics, Combustion gas, Turbine blade

ABSTRACT

Self-crack-healing behaviors in alumina/ silicon carbide (SiC) nanocomposites (agent diameter of 270 nm) having the semi-elliptical surface crack were investigated at various healing temperatures T_H and oxygen partial pressures p_{O_2} in standard pressure. The results showed the complete strength recovery was attained by heating at test temperature ranging between 1000°C to 1550°C in p_{O_2} above active to passive transition $p_{O_2}^T$. Furthermore, the minimum crack-healing time for complete strength recovery t_H^{Min} increased as decreasing p_{O_2} within the p_{O_2} ranging above $p_{O_2}^T$. Based on the obtained results, the kinetics model for complete strength recovery by self-healing was proposed. Using the model, the t_H^{Min} in various p_{O_2} for alumina/ SiC nanocomposites (agent diameter of 20 nm) were estimated. From the estimation, the possibilities of the self-crack-healing of two types of alumina/SiC composites in combustion gas atmosphere of aircraft engine and of turbine blade applications will be discussed.

1. INTRODUCTION

Self-crack-healing is one of the most valuable phenomena to overcome the reliability decrease of brittle ceramics that are caused by non-acceptable cracking in service. The reason is that the self-crack-healing automatically attains complete recovery of damaged strength through the passive oxidation of SiC triggered by cracking itself [1]. This feature allow the self-healing ceramics to be an attractive candidate for next-generation high temperature material which can be used as gas turbine components. i.e., turbine blade and vane in aircraft engine.

In this study, we proposed the kinetics model for self-crack-healing in alumina/ SiC nanocomposites. Meanwhile, the combustion gas temperature and gas compositions within the ranging from high pressure turbine HPT to low pressure turbine LPT blade and vane in aircraft engine, CF6 were calculated by Chemical Equilibrium with Applications developed by NASA [2]. From the findings, minimum healing time in combustion atmosphere of aircraft engine were estimated.

2. EXPERIMENTAL AND ANALYSIS METHOD

Alumina/ 15 vol.% SiC nanocomposites (agent diameter of 270 nm) were used. The semi-elliptical surface crack with surface length of 100 μ m and aspect ratio of 0.9 was introduced by Vickers indentation method at the specimen. The cracked specimen

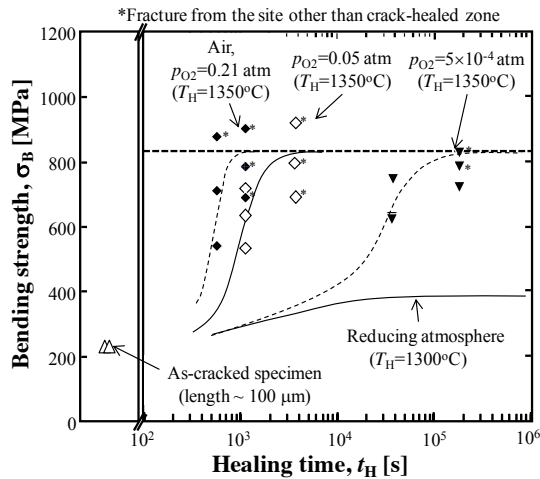


Figure 1: Strength recovery behavior in alumina/SiC composite (270nm).

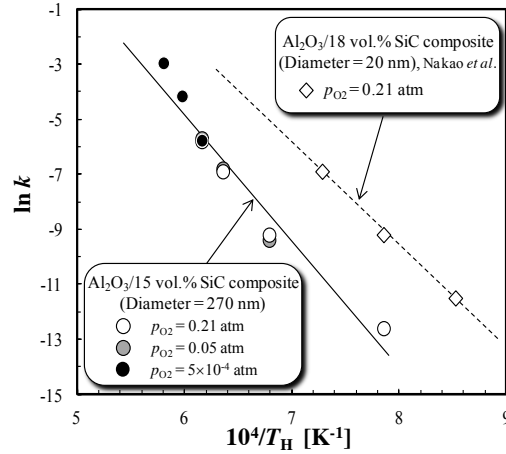


Figure 2: Arrhenius plot showing relationship between k and $1/T_H$.

were conducted to heating at the healing temperature of $1000^{\circ}\text{C} - 1550^{\circ}\text{C}$ for $6 \times 10^2 - 1.8 \times 10^5$ s in various oxygen partial pressure, p_{O_2} , of 5×10^{-4} atm and 0.05 atm controlled by passing N_2/O_2 mixture gas through the furnace. Moreover, by passing the N_2 gas that was deoxidized by reacting with heated graphite, the specimen were subjected to reducing atmosphere. The strength recovery was investigated by the fracture test performed on three-point loading system with a span of 16 mm.

Temperature, pressure and gas compositions at blade and vane from 1st stage HPT to last stage LPT were estimated on the basis of chemical thermodynamics. For analysis, CF6 engine having 2 stage HPT and 5 stage LPT as illustrated in figure 3 was used. Temperature and gas compositions after combustion of the mixture gas of compressed air and fuel (JET-A1, $\text{C}_{12}\text{H}_{23}$) were estimated using NASA-CEA program [2], considering the chemical equilibrium of various gas species. In the calculation, the air-fuel ratios A/F were varied from 4 to 80. The used Mach number was 0.8. All the turbine blade and vane were not cooled by compressed air.

3. RESULTS AND DISCUSSION

3.1 KINETICS FOR SELF-CRACK-HEALING

Figure 1 shows the strength recovery behaviors of alumina/15 vol% SiC composite (270nm) at 1350°C in various p_{O_2} above the active to passive transition $p_{\text{O}_2}^{\text{T}}$ reported by Hinze and Graham [3]. The behaviors at 1300°C in reducing atmosphere corresponding to the active oxidation condition are also shown in the figure. The complete strength recoveries can be attained only by the passive oxidation:



Meanwhile, The crack-healing was not attained by active oxidation: $\text{SiC}(s) + \text{O}_2(g) = \text{SiO}(g) + \text{CO}(s)$, below the $p_{\text{O}_2}^{\text{T}}$. Meanwhile, the minimum healing time for the complete strength recovery t_H^{min} increased with decreasing p_{O_2} . Thus, the strength recovery rate $v_H (=1/t_H^{\text{min}})$ can be given by

$$v_H = \frac{1}{t_H^{\text{min}}} = k (a_{\text{SiC}} a_{\text{O}_2}^{3/2})^n \quad (2)$$

where a_{SiC} and a_{O_2} are the activity of SiC and O_2 , respectively. Since SiC is a solid phase, $a_{\text{SiC}} = 1$. a_{O_2} can be expressed by ration of p_{O_2} to standard pressure $P^{\circ} (=1$

atm). n is a temperature independent constant and has reported to be 0.557 [1]. Meanwhile, the k is the rate constant for strength recovery as given by :

$$k = A_H \cdot \exp\left(\frac{-Q_H}{RT_H}\right) \quad (3)$$

where A_H , Q_H , R are the frequency factor, activation energy for self-crack-healing and gas constant. Thus, kinetic equation for strength recovery can be given by

$$v_H = k \left(\frac{p_{O_2}}{P^\circ}\right)^{3n/2} = A_H \cdot \exp\left(\frac{-Q_H}{RT_H}\right) \left(\frac{p_{O_2}}{P^\circ}\right)^{3n/2} \quad (4)$$

Figure 2 shows the Arrhenius plot showing relationship between k and $1/T_H$. The data for nanocomposite (20 nm) [4] together with nanocomposite (270 nm) were shown in the figure, assuming that the n in both nanocomposites are same value. As shown in the figure, $\ln k$ showed in good agreement with Arrhenius' law. From the intercept and slope of the straight line fitting the data plots, the values of A_H and Q_H can be determined to be $1.04 \times 10^{10} \text{ s}^{-1}$ and 387 kJ/mol, respectively, for alumina/SiC nanocomposites (270 nm) and to be $4.87 \times 10^8 \text{ s}^{-1}$ and 308 kJ/mol, respectively, for alumina/SiC nanocomposites (20 nm). The obtained A_H for the healing by the argon with a diameter 20 nm exhibited about 21 times larger than that with a diameter of 270 nm. This is mainly due to the fact that the specific surface area of SiC increases with decreasing agend diameter, leading to the rapid oxidation of SiC.

3.2 COMBUSTION GAS PROPERTIES

Figure 3 (a) shows the gas temperature and pressure at the compressor and turbine part. Temperature T_i and pressure P_i at i th stage compressor vane or blade in CF6 engine were calculated based on adiabatic compression and stagnation as follows:

$$T_i = T_o \left(\frac{A_o}{A_i}\right)^{\gamma-1} \left\{1 + \left(\frac{\gamma-1}{2}\right) M^2\right\}, \quad P_i = P_o \left(\frac{A_o}{A_i}\right)^\gamma \left\{1 + \left(\frac{\gamma-1}{2}\right) M^2\right\}^{\gamma/(\gamma-1)} \quad (5) \text{ and } (6),$$

respectively, where T_o and P_o are inlet temperature and pressure, and correspond to 273.15 K and 1 atm, respectively. γ is the ration of specific heat at constant pressure C_p and volume C_v of chemically equilburume air, and almost equal 1.38. A_o and A_i are throat area of compressor inlet and i th stage compressor vane or blade, respectively. Thus, the gas temperature and pressure of compressed air can be calculated to be 755.8 K and 27.1 atm at last stage of compressor, respectively.

From the ontained compressed air properties and A/F values, T_1 at the 1st stage vane in turbine part after combustion, corresponding to TIT, can be calculated using

NASA-CEA program. Wen A/F =39.7, TIT was estimated to be 1500°C. The T_i and P_i in turbine part were also shown in figure 4 (a). As shown in the figure, gas temperature and pressure in the turbine part decreased with increasing the distance from fan blade by adiabatic expansiton.

Figure 3 (b) shows the gas compositions at compressor and turbine parts calculated from several T_i and P_i , when A/F = 39.7. As shown in the figure, x_{O_2} were calculated to be approximately 0.108 at all points in the turbine part. The value showed significantly higher than the active to passive transition $p_{O_2}^T$ discussed above.

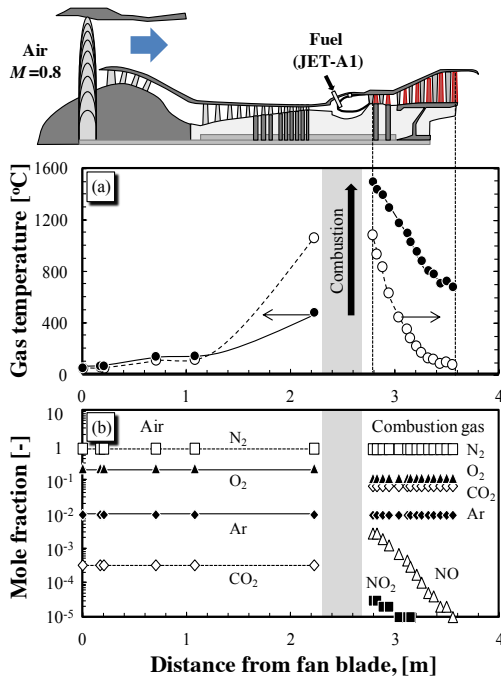


Figure 3: Temperature, pressure and compositions estimated in CF6 engine.

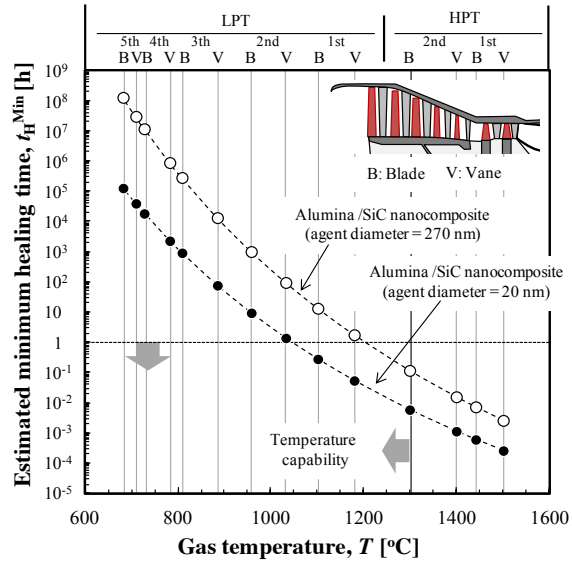


Figure 4: Minimum healing time estimated at turbine blades and vanes.

3.3 POSSIBILITY OF TURBINE BLADE APPLICATIONS

It can be expected that the minimum healing time varies depending on T_i , P_i and x_{O_2} . Assuming that the combustion gas is the ideal gas, the p_{O_2} can be given by

$$p_{O_2} = x_{O_2} P_i \quad (7)$$

Thus, strength recovery rate by self-healing of semi-elliptical surface crack with a length of 100 μm initiated at the i th stage turbine vane and blade of the alumina/SiC composites can be estimated as follows:

$$v_H = \frac{1}{t_H^{min}} = A_H \cdot \exp\left(\frac{-Q_H}{RT_i}\right) \left(\frac{x_{O_2} P_i}{P^\circ}\right)^{3n/2} \quad (8)$$

Figure 4 shows the minimum healing time estimated from 1st stage HPT vane to 5th stage LPT blade for two types of nanocomposites. As shown in figure, t_H^{Min} decrease with increasing gas temperature and pressure. On the other hand, the temperature capability of the alumina/SiC nanocomposite has reported to be approximately 1300°C [4]. Assuming that it is required to completely heal the crack within 1 hour for self-healing in service, it can be confirmed that self-healing can be attained at 2nd stage HPT blade for nanocomposite (270nm), and at 2nd stage HPT blade, 1st stage LPT vane and blade for nanocomposite (20 nm), respectively.

4. CONCLUSIONS

Kinetic study for self-crack-healing and estimation of combustion gas properties indicated that self-crack-healing ceramics can be expected to be used as turbine blade and vane. The finding obtained here will also make a large contribution to the design gas turbine materials with self-healing.

ACKNOWLEDGEMENTS

This work was supported by Grant-in-Aid for Young Scientist (B) of JSPS KAKENHI Grant Number 12019456. The author shows sincerely thanks to Prof. K.Takahashi, Associ. Prof. W.Nakao and Emeritus Prof. K. Ando of Yokohama National University.

REFERENCES

- [1] T.Osada, W.Nakao, K. Takahashi and K. Ando, Kinetics of self-crack-healing of alumina/silicon carbide composite including oxygen partial pressure effect, *Journal of the American Ceramic Society*, 92 (2009) 864-869.
- [2] NASA-Chemical Equilibrium with Application, National Aeronautics and Space Administration, <<http://www.grc.nasa.gov/WWW/CEAWeb/ceaHome.htm>>
- [3] J. W. Hinze and H.C. Graham, The active oxidation of Si and SiC in viscous gas-flow regime, *Journal of Electrochemical Society*, 123 (1976) 1066-1077.
- [4] W.Nakao, Y. Tsutagawa, K. Ando, Enhancement of in-situ self-crack-healing efficient temperature region by SiC nano-sizing, *Journal of Intelligent Material Systems*, 19 (2008) 407-410.

HEALING PARTICLES IN SELF-HEALING THERMAL BARRIER COATINGS

Z. Derelioglu¹, Sathiskumar. A. Ponnusami², S. Turteltaub², S. van der Zwaag² and W.G. Sloof¹

¹ Department of Materials Science and Engineering, Delft University of Technology, Rotterdamseweg 137, 2628 AL Delft, The Netherlands – e-mail: z.derelioglu@tudelft.nl; w.g.sloof@tudelft.nl

² Faculty of Aerospace Engineering, Delft University of Technology, Kluyverweg 1, 2629 HS Delft, The Netherlands – e-mail: s.anusuyaponnusami@tudelft.nl; s.r.turteltaub@tudelft.nl; s.vanderzwaag@tudelft.nl

Keywords: selective oxidation, encapsulation, ceramic coatings, fracture mechanics, thermal stress, finite element simulations

ABSTRACT

Crack healing in ceramic thermal barrier coatings (TBCs) may be realized by embedding Mo-Si based particles in the thermal barrier coating. Upon cracking, these particles are exposed to oxygen that permeates through the top layer and the crack gap is filled with SiO₂ which is produced from oxidation at high temperature. Due to its amorphous characteristics and expanding oxide volume, SiO₂ is able to fill a significant portion of the crack. Simultaneously, Mo forms a volatile oxide (MoO₃) that may leave the coating through the crack path and subsequently through pores, thereby compensating for the volume increase upon oxidation. The present work combines an experimental and modelling approach to develop and characterize the healing particles in the TBC system. In particular, two issues have been addressed, namely (i) the manufacturing of the healing particles that are to be embedded in the coating and (ii) the characterization of damage in TBC systems in order to identify the optimal properties of the healing particles.

1. INTRODUCTION

Thermal barrier coatings (TBC) deposited by air plasma spraying onto hot components in gas turbine engines ultimately fail by the development of cracks that cause delamination [1,2]. These cracks nucleate and grow upon thermal cycling due to thermal stresses that originate from the mismatch in thermal expansion coefficients of the distinct layers that compose the TBC system. Healing of these cracks during service will extend the lifetime of the engine components and reduce maintenance costs.

The healing particles can be encapsulated to prevent premature formation of SiO₂ during operation. Selective oxidation of Mo(Si_{1-x}Al_x)₂, prior to embedding the particles, may be an easy and cost-effective method to realize the desired encapsulation. Next, knowledge of the damage mechanisms in TBCs is essential in order to design a particle-based healing system. In particular, it is important to embed healing particles in regions where cracks are likely to initiate. Furthermore, the size and number of healing particles in these critical regions must be optimized with the purpose of developing an efficient and robust self-healing system.

2. MATERIALS AND METHODS

Oxidation of $\text{Mo}(\text{Si}_{1-x}\text{Al}_x)_2$ healing particles may generate particles consisting of a shell of alumina ($\alpha\text{-Al}_2\text{O}_3$) with a core of Mo-Si. Since Al has a very high affinity to oxygen, it tends to oxidize first amongst Mo and Si. For the application, on hand design of these particles is prerequisite. The thickness of the alumina shell δ depends on the size d and composition x of the original spherical particle considering that all Al is consumed by selective oxidation according to:

$$= d \left(\left(1 + \frac{xM_s \rho_p}{M_p \rho_s} \right)^{1/3} - 1 \right),$$

where M_p and M_s denote the molecular weights, ρ_p and ρ_s the densities of the particle and the shell, respectively.

In order to understand the failure mechanisms under thermal loading, three-dimensional finite element analyses (FEA) have been carried out on macroscopic specimen and microscopic Representative Volume Elements (RVEs) of a TBC. The effect of the substrate on the microscopic RVE is taken into account through macroscopic displacements imposed as boundary conditions at the microscale. These displacements are obtained from the macroscopic analysis, where a finite element model of a macroscopic specimen is employed with two layers, one representing the homogenized TBC and the other representing the substrate as shown in Figure 1a.

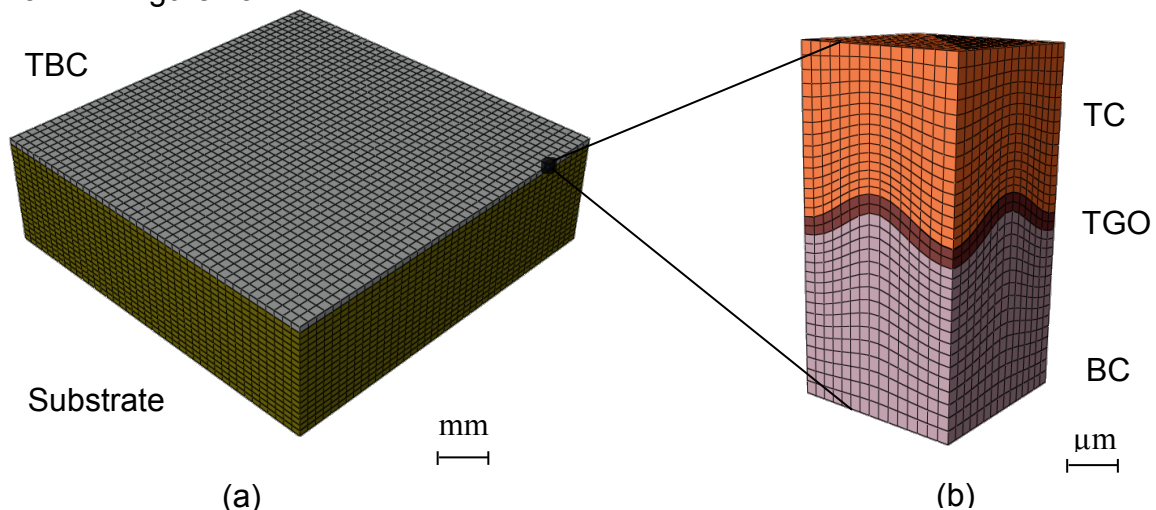


Figure 1: Finite element model of TBC system representing the Bond Coat (BC), Thermally Grown Oxide (TGO) and the Top Coat (TC): (a) coated substrate (macroscale), (b) volume element in TBC (microscale)

The microscopic finite element model of the TBC system is shown in Figure 1b. The RVE consists of three layers of the TBC system representing the Bond Coat (BC), Thermally Grown Oxide (TGO) and the Top Coat (TC). In this study, the interfaces between the layers (TC/TGO and TGO/BC) are modelled as a double-sinusoidal surface. Interface irregularities are known to be one of the key drivers for crack initiation in this inhomogeneous system [2] since they allow large in-plane compressive stresses (generated during cooling) to eventually produce out-of-plane tensile stresses.

3. RESULTS AND DISCUSSION

The explicit relation between the alumina shell thickness δ and the diameter d of the healing particle is displayed in Figure 2 for different fractions x of Al.

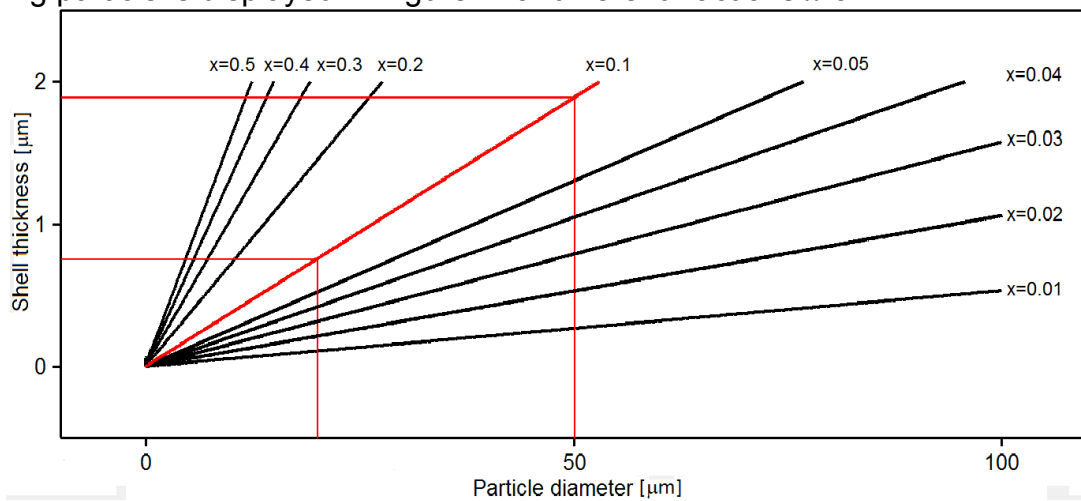


Figure 2: Relationship between the alumina shell thickness and the size of $\text{Mo}(\text{Si}_{1-x}\text{Al}_x)_2$ spherical healing particle for different compositions.

When applying a TBC with plasma spraying, the size of the healing particle should be within 20 to 50 μm due to manufacturing constraints. Correspondingly, if the Al fraction x equals 0.1, then the thickness of the alumina shell will be in the range of 0.8 and 1.9 μm ; cf. Figure 2.

In order to simulate the fracture in the TBC, cohesive elements at the microscale are being used. Both macro and micro specimens are subjected to the same thermal load consisting of a temperature change of 1000 $^\circ\text{C}$. The FEA results corresponding to RVEs near the edge and the middle of the macroscopic specimen coated with a TBC are shown in Figure 3. Red color indicates the regions that are cracked, whereas the blue colored portions are intact.

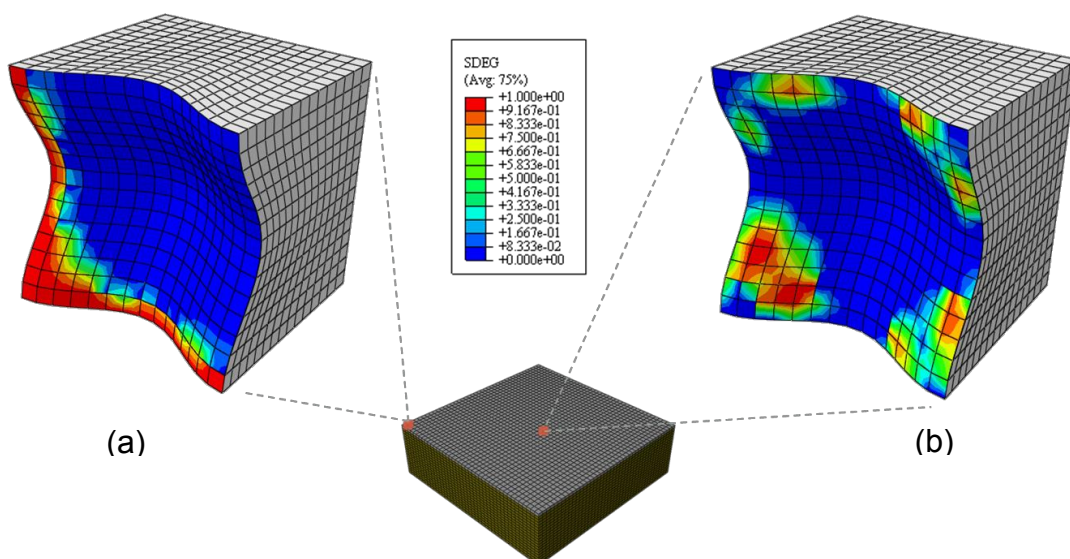


Figure 3: Typical crack pattern in TC/TGO interface of an RVE (a) near the edge of specimen, (b) in the interior of specimen

For points near the edge of the macroscopic specimen, delamination cracks initiate at the free edge as may be observed in Figure 3a. On the other hand, for the RVE in the interior of the macroscopic specimen, cracks initiate at valleys of the TC/TGO interface as shown in Figure 3b. This study will help to identify the critical regions where the healing particles can be embedded.

4. CONCLUSION

Encapsulated Mo-Si healing particles with an α -Al₂O₃ shell of about 1 μ m embedded in matrix of a TBC prepared by plasma spraying may be realized by selective oxidation of Mo(Si_{1-x}Al_x)₂ with x of 0.1.

The finite element simulations of the crack damage in a TBC system due to thermal loading indicate that the healing particles should be placed preferentially close to the TC/TGO interface particularly, if the surface roughness is large.

ACKNOWLEDGEMENTS

Financial support from the Netherlands Innovation Oriented Program (IOP) on Self Healing Materials, grant number SHM01021, is gratefully acknowledged.

REFERENCES

- [1] Gell, M., Jordan E.H., and Padture, N.P., "Thermal Barrier Coatings for Gas-Turbine Engine Applications", *Science*, vol. 296, pp. 280-284, 2002
- [2] Hille, T.S., Nijdam, T.J., Suiker, A.S.J., Turteltaub, S. and Sloof, W.G., Damage growth triggered by interface irregularities in thermal barrier coatings, *Acta Materialia*, vol. 57 (9), pp. 2624-2630, 2009

SELF-HEALING AND HIGH-TEMPERATURE OXIDATION OF NANO-NI DISPERSED Al_2O_3 HYBRID MATERIALS

M. Nanko¹ and D. Maruoka²

¹ Department of Mechanical Engineering, Nagaoka University of Technology, Nagaoka, Niigata, 940-2188, Japan – e-mail: nanko@mech.nagaokaut.ac.jp

² Graduate School of Engineering, Nagaoka University of Technology, Nagaoka, Niigata, 940-2188, Japan – e-mail: daisuke@stn.nagaokaut.ac.jp

Keywords: ceramics, self-healing, high-temperature oxidation, nickel, alumina

ABSTRACT

Al_2O_3 hybrid materials dispersed with Ni nano-particles (referred to as Ni/ Al_2O_3) have excellent mechanical properties with crack-healing function via a thermal oxidation process. In using Ni/ Al_2O_3 at high temperatures in oxidizing atmosphere, nano-Ni particles dispersed in Al_2O_3 matrix are oxidized with Al_2O_3 matrix into NiAl_2O_4 . An oxidized zone consisting of NiAl_2O_4 grains and Al_2O_3 matrix is developed and grown from the surface mainly via inward diffusion of oxide ions at grain boundaries. At the same time, Ni ions are diffused at the grain boundaries from the inside to the surface to form an NiAl_2O_4 layer, which fills cracks for self-healing. Because oxidation of Ni nano-particles means disappearance of metallic Ni in Al_2O_3 matrix, high-temperature oxidation of Ni/ Al_2O_3 may degrade their self-healing performance. In order to use Ni/ Al_2O_3 in high-temperature structural applications, kinetics on high-temperature oxidation and self-healing of Ni/ Al_2O_3 were discussed in the present report. Effects of dopants such as Y_2O_3 and SiO_2 on high-temperature oxidation and self-healing are also described.

CRACK HEALING IN Al_2O_3 COMPOSITE MATERIALS USING Ti_2AlC AS REPAIR FILLER

B.J. Pedimonte¹, G.P. Bei¹, T. Fey¹ and P. Greil¹

¹ *University of Erlangen-Nuernberg, Department of Materials Science (Glass and Ceramics), Martensstr. 5, D-91058 Erlangen, Germany - e-mail: Guoping.Bei@ww.uni-erlangen.de; Joana.Pedimonte@ww.uni-erlangen.de; Tobias.Fey@ww.uni-erlangen.de; Peter.Greil@ww.uni-erlangen.de*

Keywords: ceramics, crack healing, repair filler, strength recovery

ABSTRACT

Oxide ceramics such as Al_2O_3 may undergo crack-healing when exposed to temperatures exceeding 1400°C . In order to reduce healing temperature repair fillers based on nanolaminate MAX-phase in the system Ti-Al-C were dispersed in Al_2O_3 matrix. In contrast to solid-state sintering process requiring high activation energy, oxidation reaction of repair filler facilitates filling of disrupted cracks with oxidation product at significant lower temperatures.

Al_2O_3 -MAX phase composites, loaded with 10-20 vol% Ti_2AlC were fabricated by pressureless sintering at 1400°C . Cracks were prepared by indentation. Strength recovery was analyzed after annealing at various temperatures ($600 - 1000^\circ\text{C}$) and times (1 - 10h). Critical conditions to achieve crack healing were derived from microstructure and fracture surface analyses.

ELECTRODEPOSITED ZINC-NANOCOMPOSITE-COATINGS AND MULTI-COMPONENT-COATINGS FOR SMART CORROSION PROTECTION

T. H. Tran¹, A. Vimalanandan¹, D. Crespy², J. Fickert², K. Landfester², J. Kron³, G. Schottner³, K. Egly³, G. SEXTL³, M. Jobmann⁴, B. Paulke⁴, F. Börner⁴, M. Rohwerder¹

¹ Max-Planck-Institut für Eisenforschung GmbH, Max-Planck Str. 1, 40237 Düsseldorf, Germany – e-mail: tran@mpie.de; vimalanandan@mpie.de, rohwerder@mpie.de,

² Max-Planck-Institute for Polymer Research, Ackermannweg 10, 55128 Mainz, Germany – e-mail: crespy@mpip-mainz.mpg.de;

³ Fraunhofer Institut für Silicatforschung ISC, Neunerplatz 2, 97082 Würzburg, Germany – e-mail: johanna.kron@isc.fraunhofer.de; gerhard.schottner@isc.fraunhofer.de; karine.egly@isc.fraunhofer.de, gerhard.sextl@isc.fraunhofer.de

⁴ Fraunhofer Institut für angewandte Polymerforschung IAP, Geiselbergstraße 69, 14476 Potsdam-Golm, Germany – e-mail: monika.jobmann@iap.fraunhofer.de; paulke@iap.fraunhofer.de; frank.boerner@iap.fraunhofer.de

Keywords: galvanized steel, inhibitors, nanocomposite coating, nano-carrier, self-healing, smart corrosion protection,

ABSTRACT

Corrosion is one of the main factors for the deterioration of technical components, especially for metallic ones. Therefore the development of smart corrosion protection systems for metallic components is of utmost importance. In this work, two concepts for smart corrosion protection are shown.

Smart corrosion protection stands for a targeted delivery of corrosion inhibitors to a corrosion site when this starts to actively corrode, and only then. In the meanwhile, the inhibitors should be safely stored inside the coating, if possible even for decades. Storing them inside protective zinc coatings seems to be the ideal choice. For that purpose, surface modified mesoporous silicon based nano-carriers filled with corrosion inhibitors were incorporated into zinc coatings. Mesoporous silicon based nano-spheres are used as nano-carriers because of their high stability and insolubility at acidic electrodeposition conditions of the galvanizing bath and their solubility at higher pH. The idea is that they are released when zinc is corroding and then slowly release their content by dissolving at the higher pH, especially at the cut edge. It will be shown by Scanning Kelvin Probe (SKP) measurements at the cut edge that a slow but steady passivation of the surface under corrosive conditions can thus be achieved.

After corrosion inhibition the next step is real site selective self-healing by forming a protective polymeric barrier film isolating the inhibited metal surface from aggressive and corrosive media. For that purpose a 2-component layer system consisting of a zinc coating with incorporated surface modified nano capsules filled with catalyst and an organic top coating with embedded nano capsules filled with healing agents is used. By contact of healing agent and catalyst a ROMP (ring opening metathesis polymerization) is initiated which leads to the formation of a thin polymer film that seals off the defect and stops the further corrosion.

PLENARY SESSION – SELF-HEALING POLYMERIC MATERIALS

AUTONOMIC SELF-HEALING AND MATERIALS REGENERATION

J.S. Moore¹, N. R. Sottos¹, S. R. White¹

¹ Beckman Institute for Advanced Science and Technology, University of Illinois at Urbana-Champaign, Urbana, IL, 61801, USA – e-mail: jsmoore@illinois.edu

ABSTRACT

We have previously demonstrated efficient and repeated self-healing of microcrack damage in polymers using capsule and vascular modalities for delivery of repair agents. More recently these concepts have been extended to the repair of damage in fiber reinforced composites and the restoration of electrical conductivity in circuits. While microcrack healing extends the lifetimes of devices that are limited by fatigue damage, the autonomic repair of damage from isolated, energetically intense events such as impact or blast loadings is an unsolved problem. The resulting defective regions are of macroscopic dimensions, characterized by both significant mass losses and high crack densities. Extension of previously developed self-healing concepts to the repair of damage following blast and impact loadings motivates concepts in synthetic materials regeneration. Synthetic materials regeneration aims to restore lost functionality by autonomic processes that mimic biological *growth* of tissue and appendages. A robust, autonomic regeneration process must first transfer sufficient healing fluid to span the voids in the damaged zone. Delivery of large quantities of healing fluids is achievable using vascular networks that are integrated into composites; however, the gap-filling process must also contend with environmental forces, minimally gravity, but also other factors such as wind, variable temperature, moisture and oxygen. After filling the voids, the fluid must then transform into a structural solid that has high strength and stiffness. To fill voids from puncture damage, we are developing novel *gap-filling fluids* that transform from a liquid, to a gel-like scaffold, to a mechanically strong solid polymer. Surface tension between the liquid healing agent and the damaged solid, as well as the fluid's time dependent viscosity are physicochemical parameters critical to the success of the filling process. Characterization data on filling prototypical voids created in vascularized polymeric specimens will be presented, including the scaffold-forming chemistry, its transformation to a structural solid and the evolving mechanical properties.

SESSION 20 – SELF-HEALING CEMENTITIOUS MATERIALS

BIO-HEALING FOR MICRO-CRACK TREATMENT IN CEMENTITIOUS MATERIALS: TOWARD A QUANTITATIVE ASSESSMENT OF BACTERIAL EFFICIENCY

J. Ducasse-Lapeyrousse^{1,2,3}, R. Gagné¹, C. Lors^{2,3} and D. Damidot^{2,3}

¹ Research Center on Concrete Infrastructures (CRIB), University of Sherbrooke, Department of Civil Engineering, Québec, Canada

E-mail: Jean.Ducasse-Lapeyrousse@USherbrooke.ca; Richard.Gagne@USherbrooke.ca

² École Nationale Supérieure des Mines de Douai, LGCE-GCE, Douai, France

E-mail : christine.lors@mines-douai.fr; denis.damidot@mines-douai.fr

³ Université Lille Nord de France, Lille, France

Keywords: mortar, bio-healing, self-healing, *Bacillus cohnii*, calcium lactate

ABSTRACT

Bio-healing is a promising approach to enhancing natural self-healing and thus completely heal large micro-cracks ($> 200 \mu\text{m}$) in cementitious materials. The aim of this research is to better understand bio-healing of cementitious materials in order to accelerate the healing kinetics and maximize sealing efficiency of large micro-cracks. The bio-healing approach generally consists in soaking micro-cracks in a culture medium containing a bacterial strain. However, it is difficult to precisely assess the efficiency of the bacterial-mediated precipitation in the bio-healing process with respect to the impacts of natural self-healing and precipitation induced by the culture medium. The aim of this work is to study the healing of well-defined micro-cracks on mortars subjected to more and more complex healing mechanisms. First, cracked mortars were subjected to natural self-healing, then to a precursor solution (calcium lactate), and finally, to a culture medium containing a bacterial strain. However, before this last step, an important part of this study focused on assessing the growth kinetics of a bacterial strain: *Bacillus cohnii*. Mortars specimens ($W/C = 0.485$) were submitted to controlled cracking at 28 days (under sustained load) using a mechanical expansive core. Two micro-crack categories were created ($100 \pm 5 \mu\text{m}$ and $195 \pm 30 \mu\text{m}$). The healing kinetics was evaluated from air-flow measurements that were used to compute the evolution, over time, of the apparent crack opening (1, 3 and 6 months of conservation at 23°C and 100% R.H.) Overall, self-healing was faster and more complete when cracks were soaked in calcium lactate solutions compared to natural healing. Thus, precursor solutions significantly improved the healing kinetics of the larger micro-cracks ($> 150 \mu\text{m}$). On the other hand, the optimum growth conditions for *Bacillus cohnii* were evaluated at different nutrient concentrations and pH values. Finally, a method was developed in order to evaluate the bacterial activity semi-quantitatively.

1. INTRODUCTION

Bio-healing is a promising approach to enhancing natural self-healing and thus completely heal large micro-cracks ($> 200 \mu\text{m}$) in cementitious materials. One bio-healing approach consists in soaking micro-cracks in a culture medium containing a bacterial strain. Bio-healing proceeds from a combination of several mechanisms that include: 1- precipitation of calcium carbonate and cementitious hydrates by natural

self-healing [1]; 2- precipitation of specific reaction products formed by the precursor solution [2]; 3- precipitation of products formed by the bio-healing process (calcium carbonates and other specific products formed by the bacterial activity in the crack) [3]. The development and optimization of bio-healing approaches require a better understanding of the individual contribution of these mechanisms and their combined effects on the precipitation of healing products in cracks.

The first part of the experimental program aimed at studying the mechanisms and kinetics of natural self-healing in mortar samples, as well as the impact of calcium lactate, a precursor solution containing calcium ions in order to enhance calcite formation. The second part aimed at evaluating the optimum growth conditions of a bacterial strain, *Bacillus cohnii*, involved in bio-healing at different pH values and in the presence of calcium lactate. This inoculated culture medium would be later injected into cracks formed in mortar samples.

2. MATERIALS AND METHODS

The kinetics of natural self-healing was evaluated according to a procedure developed by Gagné et al. [4]. Air-flow measurements through a crack were used to calculate an effective crack opening (W_{ef}). The evolution of the effective crack opening is used to assess self-healing evolution over time. Mortar specimens ($W/C = 0,485$) were submitted to controlled cracking at 28 days (under sustained load) using a mechanical expansive core [4]. Two micro-crack categories were created ($100 \pm 5 \mu\text{m}$ and $195 \pm 30 \mu\text{m}$). Samples cracked under sustained deformation, were stored in a fog room at 23°C and 100% R.H. for 1, 3 and 6 months.

Three test conditions were used with the cracked mortars samples: 1- natural self-healing (no culture medium injected in the crack); 2- calcium lactate impregnation in the crack. Crack impregnation was achieved by submerging the mortar samples for 24 hours in a solution containing calcium lactate close to its solubility level (79 g/L).

The studied strain, *Bacillus cohnii*, was provided by the German Collection of Microorganisms and Cell Cultures (DSMZ, Germany). This bacteria was cultured in the growth medium recommended by DSMZ, Nutrient Broth (NB) medium (3 g/L at $\text{pH}=9.7$). The growth kinetics of this bacterial strain was also measured at different initial pH values equal to 7.5, 8.0, 9.5, 10.5, and 11.5, to assess the impact of mortar alkalinity on bacterial activity. The bacterial growth was indirectly evaluated by biological oxygen demand (B.O.D.), using the Oxitop[®] system. The system uses gas pressure measurements over a bacterial suspension placed in a sealed container. The vacuum created by the oxygen consumption is used to compute the B.O.D. expressed in mg of O_2 per litre of solution. The B.O.D. was monitored during 6 days at 30°C under continuous agitation.

The effect of calcium lactate on bacterial growth was also investigated: 9.7 g/L of calcium lactate was added to the Nutrient Broth (NB) medium. The impact of a source of nitrogen (NH_4Cl) was also checked. The bacterial growth and the lactate concentration were monitored during 36 days at 30°C under continuous agitation.

3. RESULTS AND DISCUSSION

It appears that natural self-healing is systematically faster during the first month (Figure 1-A). After 6 months, natural healing is more advanced for small cracks ($100 \pm 5 \mu\text{m}$) leading to an apparent effective opening of 50%. For large cracks ($195 \pm 30 \mu\text{m}$), effective opening is only reduced by 30%. These results are similar to those obtained by Gagné and Argouges [4]. The main product formed in cracks is calcite. Influence of the precursor (calcium lactate) on healing kinetics is shown in Figure 1-B. The healing is faster and more complete for large cracks. On the other hand, the healing of small cracks was not influenced by the precursor.

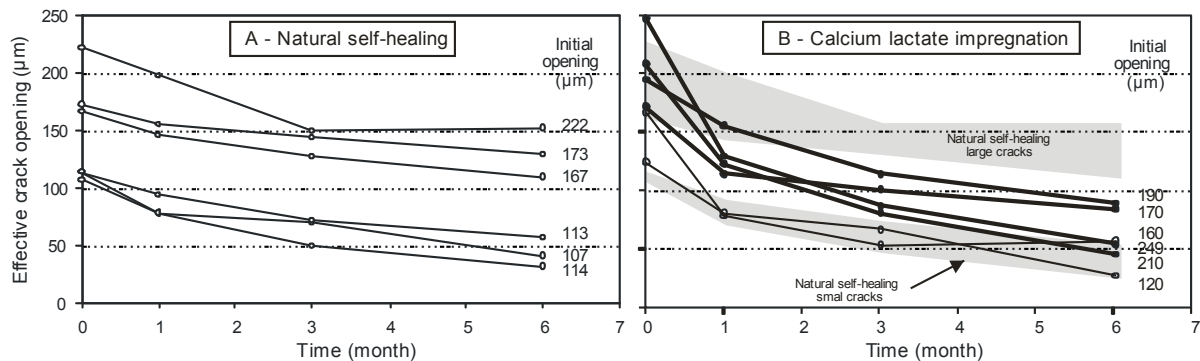


Figure 1: Evolution of the effective crack opening: (A) Natural self-healing; (B) Calcium lactate impregnation in the cracks

Using bacteria appears to be one of the most promising ways of improving healing capacity in cementitious materials. Figure 2 shows the bacterial activity in the NB medium at initial pH values ranging between 7.5 and 11.5. The bacterial activity, monitored by using the Oxitop system, showed that *Bacillus cohnii* grows rapidly in pH values between 7.5 and 10.5, which are the pH of a carbonated or leached concrete surface. No significant activity is noticed at a pH value of 11.5.

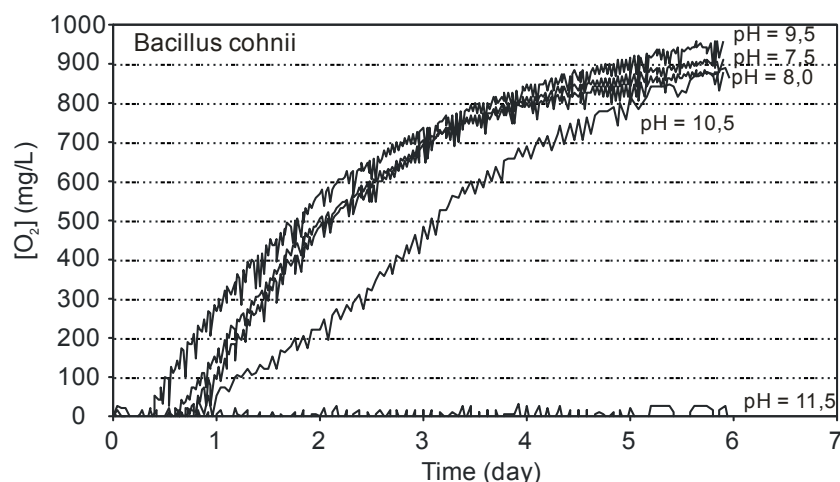


Figure 2: Oxygen consumption of *Bacillus cohnii* in NB medium at different pH

The bacterial growth was also observed in media containing calcium lactate in addition to NB. Moreover, a decrease in the lactate concentration was observed,

indicating that the bacteria can use lactate as a nutrient (Figure 3). The lactate disappears in less than 20 days. However, it is important to notice that no significant bacterial activity is observed in the medium containing only calcium lactate without others nutrients. *Bacillus cohnii* seems to be unable to decompose lactate without the presence of other nutrients. The nitrogen source added (NH_4Cl) does not impact the calcium lactate consumption nor the bacterial growth.

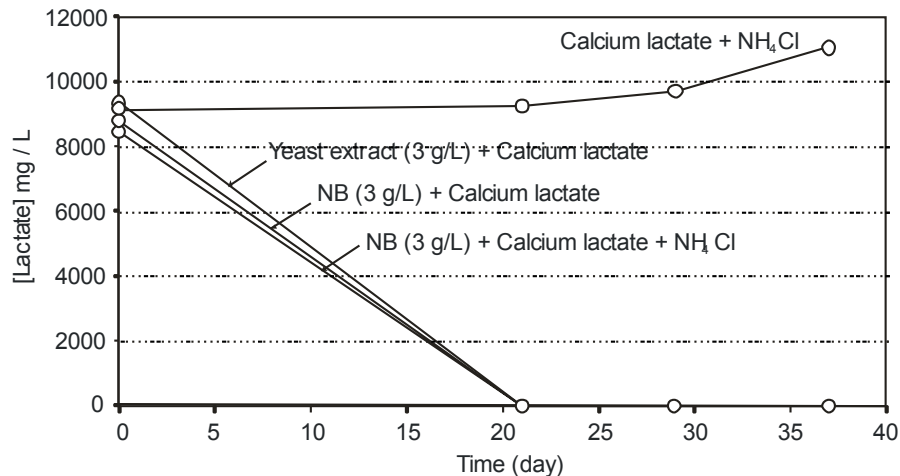


Figure 3: Evolution of the lactate concentration by *Bacillus cohnii* growth in different media

4. CONCLUSION

Self-healing naturally occurs in cracked cementitious materials. The most important effect is observed for small cracks ($\approx 100 \mu\text{m}$). The use of a calcite precursor, containing calcium, such as calcium lactate, significantly improves the healing of large cracks, even in the absence of bacteria. However, calcite mediated precipitation by bacteria is expected to enhance crack healing even further. Amongst possible bacterial strains, *Bacillus cohnii* shows an interesting potential. It has been demonstrated that it can grow in pH values ranging from 7.5 to 10.5 and that calcium lactate can be one of its nutrient. However, *Bacillus cohnii* is unable to decompose lactate without the presence of other nutrients such as Nutrient Broth (NB) medium. These results are a first step toward the development of a bacterial repair technique. The next step will be to inject the cracks with bacterial media in order to evaluate the additional improvement of healing thanks to the microbiological activity leading to the formation of greater amounts of calcite.

REFERENCES

- [1] C. Edvardsen, Water penetrability and autogenous healing of separation cracks in concrete, *ACI Materials Journal* 96-M56 (1999) 448-454
- [2] H. Jonkers, A. Thijssen, G. Muyzer, O. Copuroglu, E. Schlangen, Application of bacteria as self-healing agent for the development of sustainable concrete, *Ecological Engineering* 36 (2010) 230-235
- [3] W. De Muynck, N. De Belie, W. Verstraete, Microbial carbonate precipitation in construction materials : A review, *Ecological Engineering* 36 (2010) 118-136
- [4] R. Gagné, M. Argouges, A study of the natural self-healing of mortars using air-flow measurements, *Materials & Structures* 45(11) (2012) 1625-1638

POTENTIAL OF BACTERIA-BASED REPAIR SOLUTION AS HEALING AGENT FOR POROUS NETWORK CONCRETE

V. Wiktor, S. Sangadji, H.M. Jonkers and E. Schlangen

Delft University of Technology, Faculty of Civil Engineering & Geosciences, Section of Materials & Environment - Microlab, Stevinweg 1, 2628 CN Delft, the Netherlands

Keywords: concrete, self-healing, cracks, bacteria-based system, porous network.

ABSTRACT

Bacterially induced calcium carbonate precipitation has received considerable attention for its potential application in enforcing or repairing construction material. The mechanism of bacterially mediated calcite precipitation in those studies is primarily based on the enzymatic hydrolysis of urea. Besides calcite precipitation, this reaction mechanism leads also to the production of ammonium ions which may result in excessive environmental pressure.

More recently, bacterially mediated calcite precipitation thanks to metabolic conversion of calcium lactate has been successfully applied in self-healing concrete. This concept is also now considered for the development of bio-based repair system for concrete structures.

The bio-based repair system as presented in this paper is a liquid-based system which transports the bio-based agent into concrete. This paper presents the recent advances on the development of the bacteria-based repair system and especially its possible application as healing agent in porous network concrete.

To assess the repair capacity of the system the bacteria-based solution is injected into porous cores, and the production of the biomineral in time is monitored by X-ray micro-tomography. In parallel, water permeability testing is conducted before and after the injection of the bacteria-based solution to determine the sealing efficiency of the system. The precipitate is analyzed with FTIR and thermal analysis for identification and quantification. Finally, at the end of the healing period, polished sections of injected specimens are observed with ESEM/EDS to analyze and locate precipitated biominerals.

FTIR results coupled with thermal analysis and ESEM observations showed that CaCO_3 has been formed in pores after 21 days, with increased amount after 28 days. Moreover, the evidence that CaCO_3 precipitation was indeed mediated by bacteria has been found with observations of bacteria imprints on Ca-based minerals.

It can be concluded that the bacteria-based repair system can successfully be injected as healing agent into porous network concrete.

1. INTRODUCTION

Porous network concrete, a novel concept of self-healing concrete which imitates bone morphology, has recently been developed [1]. This concrete is composed of a porous core surrounded by a concrete structure. Upon crack formation, the healing agent (chemical-, bio-, or cement-based) can easily be distributed through the porous network to the crack location.

This paper investigates the possible application of bacteria-based repair system as healing agent for porous network concrete.

2. MATERIALS

2.1. Bacteria-based system

The bacteria-based system is a liquid-based system which transports a bio-based agent into concrete. The bio-based agent consists of concrete compatible bacteria and feed which produces calcite-based minerals resulting in decreased porosity. The preparation and composition of solutions (solution A&B) is as described by Wiktor and Jonkers [2].

2.2. Porous core

The goal of this study is to investigate the feasibility of injecting a bacteria-based solution into porous network concrete. Therefore, several parameters are tested and due to the high number of specimens required, the experiment is conducted only on the porous core used in porous network concrete. Porous cores are prepared as described by Sangadji and Schlangen [1]. The porous cores are then cut in smaller specimen of 3cm high.

3. METHODS

The experiment is designed over 5 series as shown in Figure 1. Tests are performed 3, 7, 14, 21 and 28 days after injection and 2 replicates are used per time and series except for series D (only 28 days is tested).

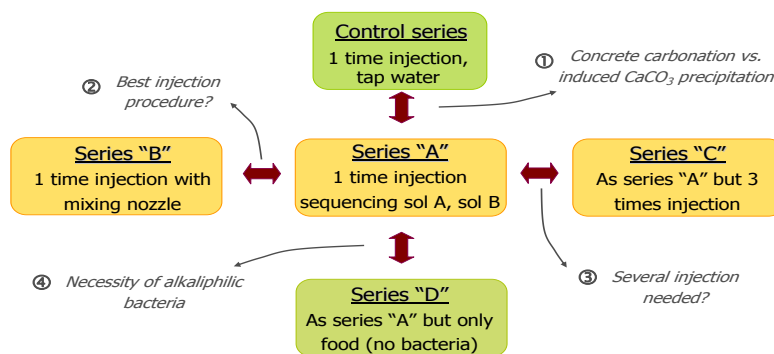


Figure 1: Experimental approach of the study

To assess the repair capacity of the system the bacteria-based solution is injected into porous cores, and the production of biominerals in time is monitored by X-ray micro-tomography. In parallel, water permeability test is conducted before and after the injection of the bacteria-based solution at regular time interval to determine the sealing efficiency of the system. When possible, sampling of the mineral is performed by gently scrapping the surface of the core and FTIR analysis is performed for identification. Finally, at the end of the healing period, polished sections of injected specimens are observed with ESEM/EDS to analyze and locate biominerals.

4. RESULTS

The results for water permeability test showed sparse data and no significant difference is observed between the series. However, the specimens are very porous, and based on theoretical calculations the maximum volume of CaCO_3 which can be formed in these conditions is less than 1% of the total porosity. This explains why the water permeability test results are not relevant in the present case.

Processing of CT-scan data showed that 3 days after injection ~6% of the material volume corresponds to new material. This percentage decreases to ~2% after 7 days and stays constant until 28 days. Even though bacteria start to grow within the first 24h, they cannot yet produce that high volume of CaCO_3 . This means that after 3 days mainly the solution that has been injected into the porous core is detected with this technique. With time the solution dries out so that its volume decreases. As a conclusion, it is very hard to distinguish between food (organic precipitates) and converted food (biominerals) with CT-scan analysis.

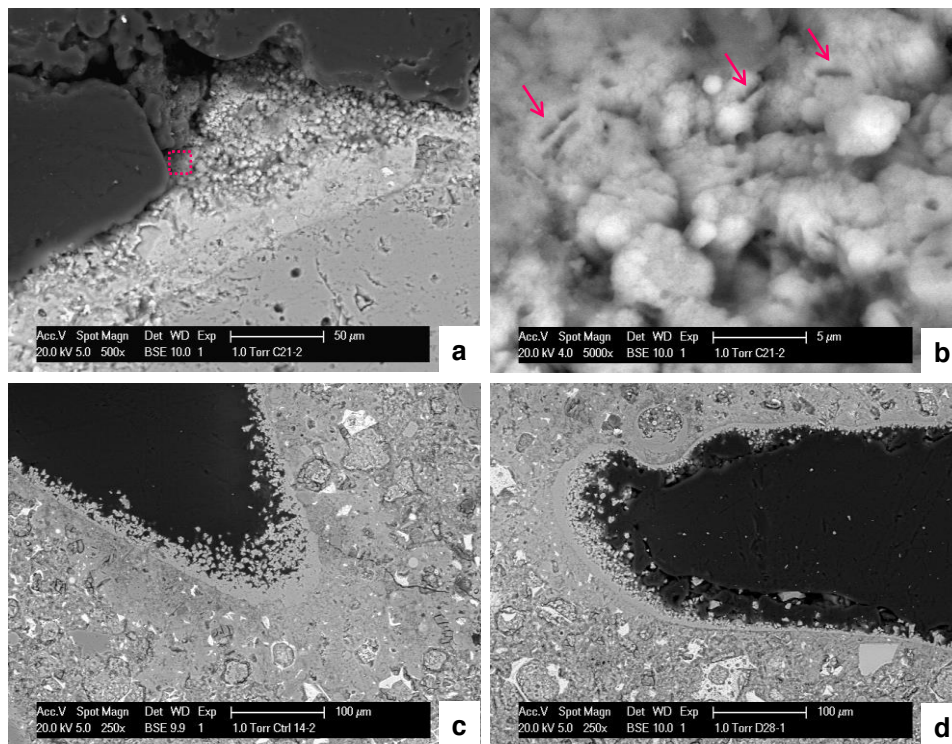


Figure 2: ESEM pictures of polished sections – (a) Series “C” at 21 days: Ca-based mineral at the surface of cement matrix, (b) zoom in of (a), bacteria imprints in Ca-based minerals (pink arrows), (c) control series at 14 days, (d) series “D” at 28 days.

Observations of polished sections with stereomicroscope and ESEM showed that for series containing food (A, B, C and D) the bonding between the epoxy and the specimen is not good (Figure 2a). Considering that during the preparation of the polished sections the grinding was performed with water and that each specimen has been in contact with the grinding paper and water for 45 min, it can be concluded that the food dissolved resulting in holes what then appears as bad bonding between epoxy and the matrix. However, this “de-bonding” can serve as indicator of the presence of food, and help to locate CaCO_3 formed due conversion of food by bacteria.

For series “A”, small Ca-based crystals are observed 21 days after injection. After 28 days less debonding and more Ca-based crystals are noticed suggesting that their formation could be due to bacterial activity.

Similar observations are made for series “B”, and FTIR and DSC/TG analysis on precipitate scrapped from the edge of the specimen at 21 days showed that the precipitate is composed in majority of Ca-lactate, and to a lower extent (~10%) of Calcium carbonate which strongly suggest that bacteria are active at 21 days. However it seems that less crystals are formed in series “B” compared to series “A”.

Observations for series “C” showed similar results as in series “A” but with a more pronounced debonding. This is explained by the fact that 3 injections have been made for series “C” compared to 1 for series “A” resulting in more food. Bacteria imprints are observed in different locations at 21 and 28 days (Figure 2a, b) and FTIR analysis confirmed the presence of CaCO_3 in the scrapped precipitate. This constitutes the evidence that bacteria are already active at 21 days leading to the formation of CaCO_3 .

Finally, the observations at 28 days of series “D” were similar to the control specimen besides some debonding, which is explained by the presence of the food (Figure 2c, d). This also means that in this case no bacteria induced CaCO_3 formation is noticed and therefore, alkaliphilic bacteria are an essential part of the system.

5. CONCLUSIONS

CT-scan results pointed out that this technique is not appropriate for this type of experiment as it is really hard to distinguish between food which has been initially injected and food which has been converted in CaCO_3 .

However, FTIR results coupled with thermal analysis and ESEM observations showed that CaCO_3 has been formed in pores after 21 days, with increased amount after 28 days. Moreover, evidence that CaCO_3 precipitation was indeed mediated by bacteria has been found with observations of bacteria imprints on Ca-based minerals. Finally, multiple injections of the solutions in sequence appear to be most efficient for CaCO_3 precipitation.

It can be concluded that the bacteria-based repair system can successfully be injected as healing agent into porous network concrete. Nevertheless, the system needs to be further optimized in order to increase the CaCO_3 formation capacity and the crack healing efficiency should be assessed by injection into porous network concrete beams.

ACKNOWLEDGEMENTS

Authors would like to thank the Technology Foundation STW for the financial support for the project 11342 and the Ministry of National Education, the Government of the Republic of Indonesia for its financial support in the form of scholarship for S. Sangadji.

REFERENCES

[1] S. Sangadji, E. Schlangen, Self-healing of Concrete Structures - Novel approach using porous network concrete. *Journal of Advanced Concrete Technology*. 10 (2012) 185-194.

[2] V. Wiktor, H.M. Jonkers, Application of bacteria-based repair system to damaged concrete structures, Proceedings of the 2nd International Workshop on Structural Life Management of Underground Structures, Daejeon, 2012, pp. 31-34.

IMPROVEMENT ON BACTERIA-INDUCED CALCIUM MINERALIZATION ABILITY OF *BACILLUS PSEUDOFIRMUS* BY AN INTEGRATED HIGH-THROUGHPUT SCREENING STRATEGY

J.L. Zhang¹, X. Deng¹, X. Feng², N. X. Han², H. M. Jonkers³

¹Institute of Eco-environmental Science, College of Life Science, Shenzhen University, Shenzhen, P.R. China

²Guangdong Provincial Key Laboratory of Durability for Marine Civil Engineering; Shenzhen Durability Centre for Civil Engineering; College of Civil Engineering, Shenzhen University, Shenzhen, P.R. China

³Faculty of Civil Engineering and GeoSciences, Delft University of Technology, Delft, The Netherlands

Keywords: biomineralization, *Bacillus pseudofirmus*, UV-induced Mutation, High throughput screening,

ABSTRACT

The CaCO₃-mineralizing bacteria from different taxonomic groups have shown potential in restoration of construction material such as concretes, cements and stony materials. However, these strains are far from the demand of practical application due to some shortages, including the low mineralizing capacity.

In this work, an integrated high-throughput screening (HTS) strategy was developed in an attempt to screen enhanced CaCO₃-producing mutants of *Bacillus pseudofirmus*. The isolates, mutagenized by ultraviolet radiation (UV), were cultivated in the suitable media containing calcium ion by using 96-deep-well microliter plates. The residual calcium in supernatants from micro-cultivation plates was determined by O-Cresolphthalein Complexone method to evaluate the CaCO₃-producing activity. On the other hand, the activity of carbonic anhydrase of the isolates, which is responsible for the formation of CO₃²⁻, was also monitored to further evidence the bacteria-induced calcium mineralization process.

As a result, the mutant strain B388 with the highest calcium mineralizing capability (92.67%, 11.1% higher than that of the original strain) was obtained from about 3000 isolates. It is proved that this novel HTS strategy is a promising procedure for selecting high efficient calcium mineralizing microorganisms.

1. INTRODUCTION

Self-healing of concrete by microorganisms has been proved to be a promising strategy during the recent years [1, 2, 3, 4]. Although protective vehicles were necessary for the effectiveness of bacterial self-healing process [1, 3, 4], the calcium mineralizing activity of the self-healing microorganism itself was also crucial. The aim of this work, therefore, was to improve CaCO₃-producing capability of a previously used bacterial strain in our group.

2. MATERIALS

Strain *Bacillus pseudofirmus* DSM8715 was provided by Dr. H. M. Jonkers(Delft University of Technology, Delft, Netherlands); Calcium standard concentrate, O-cresolphthalein complexone(OCPC) and 8-Hydroxyquinoline were purchased from Sigma-Aldrich (St. Louis, MO);3-(cyclohexylamino)-1-propanesulfonic acid (CAPS) was purchased from Ameresco(Solon,OH) ; 2-Amino-2-methyl-1-propanol(AMP) and L-sodium lactate was purchased from Aladdin(shanghai).

3. METHODS

The UV-mutagenesis of strain DSM 8715

Strain DSM8715 was grown overnight on LB Agar plates containing 1% Na₂CO₃ at 30°C. After washed twice with 1% Na₂CO₃, the cells were resuspended in the same buffer and diluted to about 10⁸ cells/ml which was detected with bacterial microscopic counting method. Then the bacterial suspension were exposed to UV-light for 16 min which resulted in a death rate of 92%. The UV-treated cell suspension was cultivated in the LB broth containing 1% Na₂CO₃ for 6 h and then gradiently diluted and spread on LB agar plates. After 48 h cultivation at 30°C, single colonies formed and were respectively transferred onto the LB agar in the wells of 96-well microplates(Corning Inc.; Corning, NY). The inoculated microplates(plate 1) were cultivated for 24 h at 30°C and then preserved at 4°C for further tests.

The screening of high-efficiency calcium mineraling mutant isolates

The O-Cresolphthalein Complexone(OCPC) method^[6] was applied to evaluate the CaCO₃-producing activity of all mutant isolates.The high throughput screening strategy was introduced in the selection of mutant isolates.Cultures in the above microplate(plate 1) were respectively transferred into the ASWM4 medium(L-sodium lactate(60%) 15ml, yeast extract 1g, NaNO₃ 2g, MgCl₂ 0.1g, KH₂PO₄ 0.02g, CAPS 23g, artificial sea water^[5] without MgCl₂ and NaHCO₃ 1L, pH=10.5) in a 96-deep-well microplate(plate 2) using a multi-channel pipettor and precultivated for 36 h. 10μL culture of each well was then transferred into another 96-deep-well microplate(plate 3) and cultivated for 7 d. The culture from plate 3 was centrifugated (6000×g, 5 min) and 3.75μL supernatant of each well was transferred into corresponding well of another 96-well microplate(plate 4) with 300μL calcium assay reagents(25 mg/L OCPC and 0.5 g/L 8-Hydroxyquinoline in a buffer containing 45g/L AMP) added into each well. The mixtures were gently agitated and further incubated at 30°C for 10 min. Light absorbance of each well was measured at 575 nm on a 96-well plate spectrometers (SpectraMax 190, Molecular Devices, Corp.). Standard curve was obtained by using Ca²⁺ at following concentrations(mM): 0, 0.25, 0.5, 1, 2, 3,4 and 8. Calcium mineralizing activity was calculated using the following equation:

$$R = (C_0 - C) / C_0 \times 100\%$$

R, the calcium mineralizing ratio;

C, the residual calcium concentration after 7-day cultivation;

C₀, the initial calcium concentration;

4. RESULTS

Considering that the measurement of calcium ion in supernatant might be easy and highly efficient, the reduction of free calcium ions in the medium was determined to indirectly assess the yield of CaCO_3 during the experiment. ASWM4 was a newly designed medium for the calcium mineralizing assay. Artificial sea water and high pH were used in an attempt to mimic the coastal concrete environment. The results showed that strain DSM8715 was able to resist the high salinity and induce the

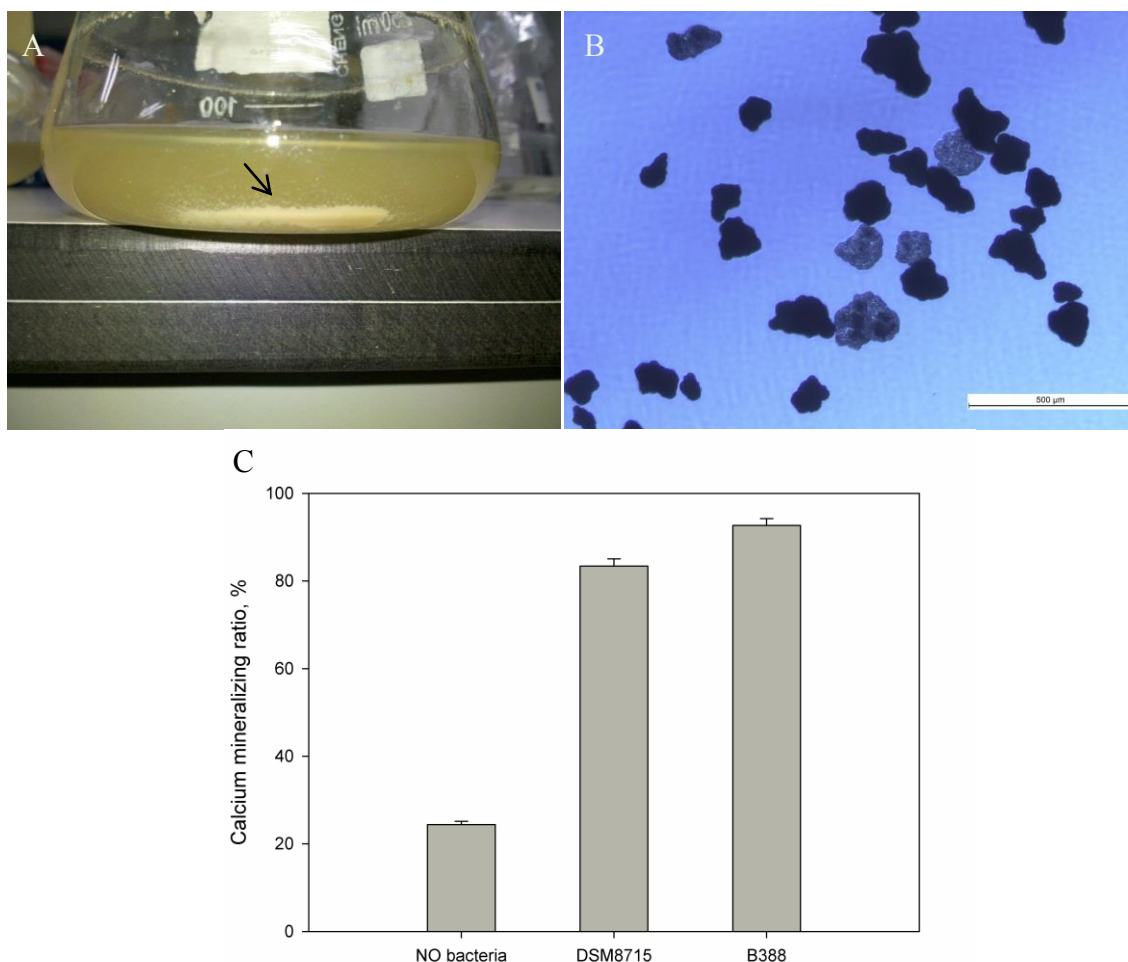


Figure 1: CaCO_3 production by strain DSM8715 and B388.

A, The CaCO_3 particles produced by strain DSM8715 in a flask; B, Optical photomicrograph of the CaCO_3 particles produced by strain DSM8715; C, the calcium mineralizing ratio of strain DSM8715 and B388 after 7-day incubation.

formation of CaCO_3 particles in ASWM4 liquid medium (Fig. 1, A and B). The calcium mineralizing ratio of DSM8715 was remarkably higher than that of the control (no bacterial strain) (Fig. 1, C).

The established high-throughput screening method was used to select *Bacillus pseudofirmus* mutants with high CaCO_3 -producing activity. Totally 3000 single colonies were obtained and among them the calcium mineralizing activity of one mutant strain designated as B-388 reached 92.67%, displaying 11.11% increase compared with that of the original strain DSM8715, which was 83.4%. Comparatively, the calcium mineralizing ratio of the medium ASWM4 without bacterial induction was

only 24.39%. It might be due to the high pH value of the medium. CO₂ in the air reacted with OH⁻ in the medium and resulted in the formation of CO₃²⁻, which further reacted with Ca²⁺ to form insoluble CaCO₃.

5. CONCLUSIONS

In summary, a simple and easy HTS strategy was developed for the screening of CaCO₃-producing microorganisms after UV-irradiation treatment. The efficiency of this procedure depended on the high-throughput characteristics of each step in the screening process, especially for bacteria cultivation, culture centrifugation and Ca determination. By using this novel method, more than 3000 strains were evaluated in 3 weeks and one strain (B-388) with 11% improvement of calcium mineralizing activity was achieved, proving that this method is a rapid and reliable way to screen high efficient CaCO₃-producing microorganisms.

ACKNOWLEDGEMENTS

Financial support of the National Natural Science Foundation of China for this study (Project No.51120185002 and No.50925829) is gratefully acknowledged.

REFERENCES

- [1] J. Y. Wang, N. De Belie, W. Verstraete. Diatomaceous earth as a protective vehicle for bacteria applied for self-healing concrete, *Journal of industrial microbiology & biotechnology*, 39 (2012) 567-577.
- [2] H.M. Jonkers, A. Thijssen, G. Muyzer, O. Copuroglu, E. Schlangen. Application of bacteria as self-healing agent for the development of sustainable concrete, *Ecological engineering*, 36 (2010) 230-235.
- [3] V. Wiktor, H. M. Jonkers, Quantification of crack-healing in novel bacteria-based self-healing concrete, *Cement & Concrete Composites*, 33 (2011) 763–770
- [4] H.M. Jonkers. Bacteria-based self-healing concrete. *Heron*, 56(2011) 1.
- [5] D. R. Kester, I. W. Duedall, D. N. Connors. Preparation of artificial seawater, *Limnology and Oceanography*, 12 (1967) 176-179.
- [6] E.S. Bagainski, Calcium estimation by OCPC method, *Anal Biochem*, 18 (1973) 521

POTENTIAL OF SOIL BACTERIA FROM THE *COMARCA LAGUNERA*, NORTH-EAST MEXICO FOR BIOCONCRETE DEVELOPMENT

R. Narayanasamy¹, A. Alvarado², J. Sanchez Medrano¹, J. Betancourt Hernandez¹
and N. Balagurusamy²

¹ Facultad de Ingeniería, Ciencias y Arquitectura, Universidad Juárez del Estado de Durango, Av. Universidad S/N Fracc. Filadelfia, C.P. 35010, Apdo. Postal 36 –B, Gómez Palacio, Durango, México. e-mail: naraya@ujed.mx; jesus_ocl@hotmail.com; jbetancourth@ujed.mx

² Laboratorio de Biorremediación, Escuela de Ciencias Biológicas, Universidad Autónoma de Coahuila, Carretera Torreón- Matamoros km 7.5, C.P.27000, Torreón, Coahuila, México. e-mail: ale.alv89@gmail.com; bnagamani@uadec.edu.mx

Keywords: concrete, cement mortar, bacteria, self-healing, compressive strength

ABSTRACT

Sustainability or environment friendly green technology is based on the use of agents of biological origin that can mimic nature in their process applications. The production and use of conventional Portland cement is significant contributor to emission of greenhouse gases and the resultant global warming. Microbial induced carbonate precipitation (MICP) is an emerging technology to minimize the environmental problems, to improve the concrete qualities, and more importantly as a self-healing agent.

This study was aimed at isolation, selection and evaluation of urease producing bacterial strains from the soils of *Comarca Lagunera* of North-East Mexico. Carbonate precipitation is achieved by urease enzyme, which catalyzes the hydrolysis of urea to CO₂ and ammonia, resulting in an increase of the pH and carbonate precipitation.

Out of twenty four bacterial strains isolated, six were selected based on their urease activity and were denoted as ACRN1 to ACRN6. All strains recorded their maximum growth after 24 h and death phase after three days. ACRN4 showed the highest biomass production at 35°C, while ACRN6 recorded the least growth rate. Initially the ACRN4, ACRN5 and ACRN6 were evaluated for their potential in increasing the compressive strength of cement mortar by varying the cell concentrations and were observed that addition of bacteria at 10⁵ cells significantly increased the compressive strength around 35%.

However, concrete specimens were prepared with ACRN4 at same concentration, in the presence and absence of water reducing additives showed an increase of 4% and a decrease of 6.64% in their compressive strength on 14th day, and a decrease of 6% and 7.6% on 28th day, with and without additive respectively. Scanning electron microscopic and X-ray diffraction studies are in progress to understand the phenomenon observed.

1. INTRODUCTION

Recent interest in the term "sustainability" involves use of environment friendly green technology, which involves the use of an agent of biological origin. Existing biological principles and advances in knowledge on microbial induced carbonate precipitation (MICP) offer opportunities to use natural stable systems to meet these challenges. Recent studies reveal that the addition of bacteria like *Bacillus pasteurii*, *Bacillus sphaericus*, *Shewanella* sp., *Bacillus pseudofirmus*, *B. Cohnii* and *Bacillus Subtilis* promoted self healing of the cracks in concrete since they are capable of carbonate precipitation [1]. This study was focused to evaluate the behavior of bacterial strains on the bio concrete.

2. MATERIALS & METHODS

Ordinary Portland cement, gravel and sand available in the local market were used for this study. Distilled water was used for the isolation of bacterial strains. Locally available potable water (tap water) was used for the preparation of mortar cubes and concrete cylinders. Out of 24 bacterial strains from the soils of *Comarca Laguna* of North-East Mexico which has the ability to produce Urease were isolated, evaluated and the best six (ACRN1 to ACRN6) were selected based on their urease activity for the mortar and concrete preparation. Bacterial strains were multiplied in the urea medium and harvested after 48 hrs. were used to prepare mortar cubes and concrete cylinders.

2.1 Cement Mortar Cubes preparation and Compressive Strength Testing

- a) Three cubes of dimensions 50 x 50 x 50 mm for each bacterial strain and three cubes without bacteria (Control) were cast. Bacterial strains ACRN 4, ACRN 5 and ACRN 6 were added at a cell concentration of 10^8 per ml of water to prepare the cement mortar. The compressive strength was determined after 28 days of curing.
- b) Mortar cubes were prepared by adding bacteria ACRN 4 (higher compressive strength compared to other strains) at different cell concentrations (10^4 , 10^5 , 10^6 , 10^7 y 10^8 per ml of water) to the water used for preparing the cement mortar. The tap water was used for the dilutions of the bacteria cells and was used directly for the preparation of mortar samples. After 24 hrs. of casting, all the specimens with or without cells were demolded and were cured under water in the moist curing cabinet. The compressive strength was determined after 7, 14, 21 and 28 days.

2.2 Concrete cylinder preparation and Compressive Strength Testing

Cement, coarse aggregate and fine aggregate were mixed properly to obtain a concrete of strength, $fc' 200 \text{ kg/cm}^2$. A total of 60 concrete cylinders of dimensions 150 mm diameter with 300 mm height were prepared by adding bacteria ACRN 4 at its optimum concentration (identified from the mortar cube samples) of 10^5 per ml of water to the water used for preparing the concrete. After 24 hrs. of casting, all the specimens with or without bacteria were demolded and were cured under water in the moist curing cabinet. The compressive strength of the cylinders was determined after 3, 7, 14 and 28 days.

2.3 SEM analysis of Concrete Cylinder specimens

The broken concrete cylinder samples (with / without bacteria) collected after compressive strength testing were thinned down to small pieces and were coated with carbon prior to SEM examination. The prepared samples were examined in ESEM (Fei –Quanta 600 ESEM™) with Tungsten Filament (W) with high vacuum mode to take the microphotographs.

3. RESULTS & DISCUSSION

Compared to control, the mortar cubes prepared with bacterial strain ACRN 4 with 10^8 cells per ml of water showed higher compressive strength of 21.92 % after 28 days (Table 1). From the compressive strength results of the mortar cubes prepared with 10^8 , 10^7 , 10^6 , 10^5 and 10^4 cells per ml of mixing water, it was found that the optimum cell concentration of the bacterial strain ACRN 4 was 10^5 cells per ml (Figure 1) with an increase of 18.83% compared to the control after 28 days, which is almost similar to the results reported earlier [2].

Table 1: Effect of added bacteria strains on Compressive strength of Mortar cubes

Treatments	28 day Compressive Strength of Mortar (Kg/cm ²)					
	Specimen #1		Specimen # 2		Specimen #3	
		Increase (%)		Increase (%)		Increase (%)
Control(without bacteria)	187	-	184	-	185	-
With ACRN 6	219	17.11	169	-8.15	180	-2.78
With ACRN 5	201	7.48	191	3.8	196	5.95
With ACRN 4	228	21.92	201	9.24	203	9.73

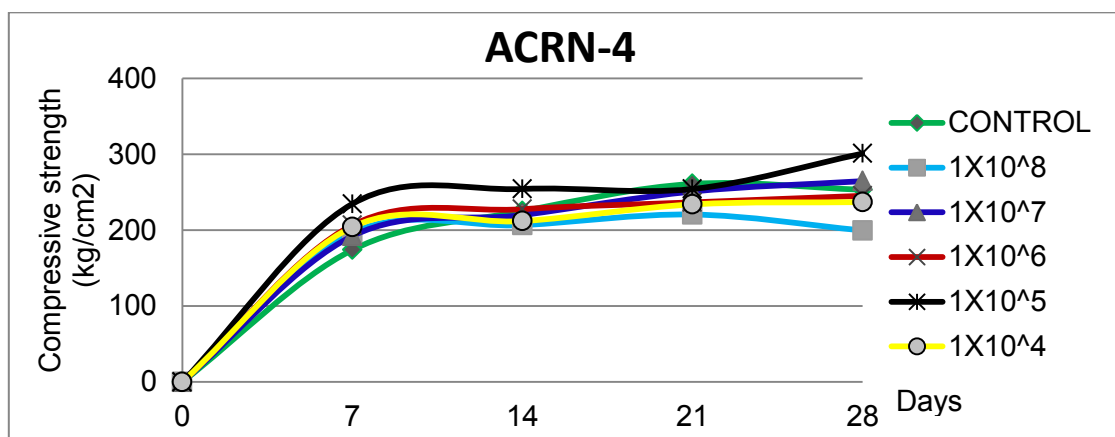


Figure 1: Compressive strength of Cement mortar cubes in relation to different cell concentrations of bacterial strain ACRN 4.

The addition of ACRN 4 strain at a concentration of 10^5 cells per ml of water in concrete cylinders resulted in higher compressive strength (4.11% increase) after 14 days of curing compared with the control specimens. The cylinders prepared with bacteria added with admixture showed lower compressive strength (7.60 % decrease) after 28 days of curing period. But the cylinders prepared with admixture only showed higher compressive strength (8.57% increase) after 28 days of curing

period (Figure 2). The prepared broken samples of concrete cylinders, control one and with bacteria and admixture were examined (Figure 3). Figure 3(b) revealed the formation of calcite crystals with well-formed rhombohedral shape as reported [3]. SEM image (Figure 3(c)) showed the presence of microorganisms on the surface of the concrete cylinder sample prepared with bacteria and admixture.

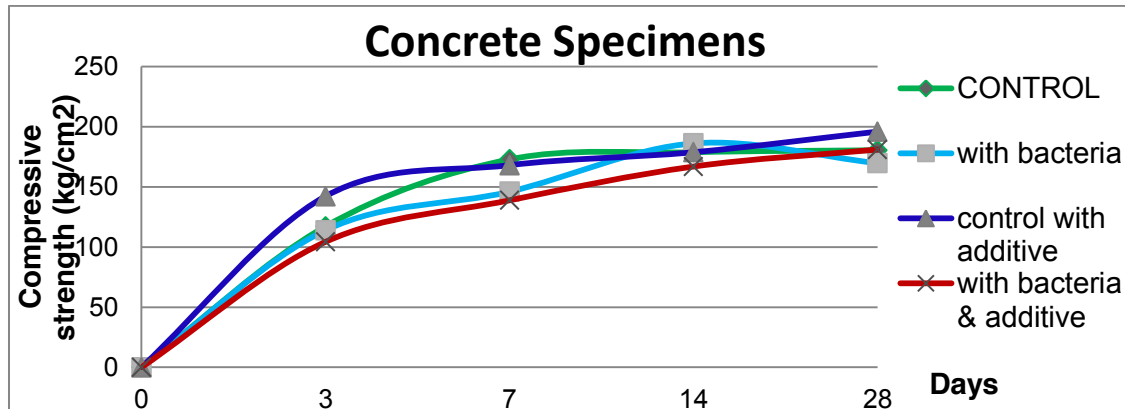


Figure 2: Compressive strength of Concrete Cylinders in relation to bacteria

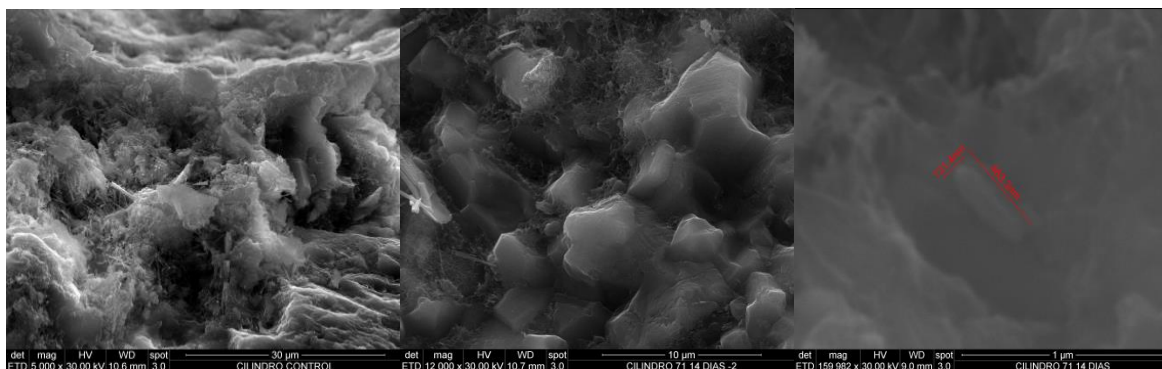


Figure 3: SEM images of Concrete Cylinder Samples (a) control (b) & (c) with bacteria and additive

4. CONCLUSION

Ureolytic bacteria that can form calcites are isolated from the soils of Laguna region. Cell density (ACRN 4) of 10^5 per ml of water was found to be optimum concentration, which increased the compressive strength of concrete cylinders. SEM studies confirmed the formation of calcite crystals and the presence of bacteria on the surface of the broken samples of concrete cylinder.

ACKNOWLEDGEMENTS

Authors gratefully acknowledge the help of M.C. Juan Fernando de la Rosa, CIDT, Peñoles, Toraon in SEM analysis.

REFERENCES

- [1] W. De Muynck, N. De Belie, W. Verstraete, Microbial carbonate precipitation in construction materials: A review, *Ecological Engineering* 36 (2009) 118 – 136.
- [2] M. Biswas, S. Majumdar, T. Chowdhury, B. Chattopadhyay, S. Mandal, U. Halder, S. Yamasaki, Bioremediation: a unique protein from a novel bacterium BKH1, ushering a new hope in concrete technology, *Enzyme and Microbial Technology* 46 (2010) 581- 587.
- [3] J. Dick, W. de Windt, B. de Graef, H. Saveyn, P. Van der Meeren, N. de Belie & W. Verstraete, Bio- deposition of a calcium carbonate layer on degraded limestone by *Bacillus* species, *Biodegradation* (2006) 17: 357-367.

HYDROGEL ENCAPSULATED BACTERIAL SPORES FOR SELF-HEALING CONCRETE: PROOF OF CONCEPT

J.Y. Wang^{1,2}, S. Van Vlierberghe³, P. Dubruel³, W. Verstraete² and N. De Belie¹

¹Magnel Laboratory for Concrete Research, Ghent University, Technologiepark-Zwijnaarde 904, 9052 Ghent, Belgium – e-mail: jianyun.wang@ugent.be; nele.debelie@ugent.be

²Laboratory of Microbial Ecology and Technology (LabMET), Ghent University, Coupure Links 653, 9000 Ghent, Belgium – e-mail: willy.verstraete@ugent.be

³Polymer Chemistry and Biomaterials Group, Ghent University, Krijgslaan 281,S4-bis, 9000 Ghent, Belgium – e-mail: sandra.vanvlierberghe@ugent.be; peter.dubruel@ugent.be

Keywords: self-healing, concrete, hydrogel, bacterial spores, microbial CaCO₃

ABSTRACT

Self-healing concrete is regarded as a promising solution to reduce the high maintenance and repair cost of concrete infrastructure. Due to the limited autogenous healing capacity of concrete as such, additives are needed to enhance its self-healing properties. Among various strategies, microbial-based self-healing has gained increasing attention because of its distinct features including environmental friendliness, long-term viability and low cost. Within the framework of this strategy, bacteria and the relevant bio-reagents are pre-added into the concrete during the casting and are expected to play their role (heal cracks) when cracking occurs. Due to the high alkalinity and small pore sizes of concrete, bacteria cannot be added directly, and hence an immobilization process is required prior to incorporation into concrete.

In the present work, a bio-compatible hydrogel was evaluated as the carrier to encapsulate an efficient carbonate precipitating bacteria, *Bacillus sphaericus*, which was selected based on previous research. As proof of concept, the activity of bacterial spores after immobilization, the carbonatogenesis of the hydrogel encapsulated spores, the influence of the bio-agents on the hydrogel swelling properties, and the crack healing efficiency were investigated. Interestingly, no significant viability loss was observed after the immobilization process. The precipitation of CaCO₃ in/on the hydrogel matrix by the encapsulated spores was demonstrated by thermogravimetric analysis (TGA). The swelling capacity of the hydrogel was slightly increased after incorporation of the bio-agents. In addition, the specimens combined with the bio-hydrogels showed an obvious superiority in crack healing efficiency, both with respect to the healing rate as well as the maximum healed crack width. A maximum crack width of about 0.5mm can be healed in the specimens containing bio-hydrogels within 7d, while no crack healing was observed in the reference specimens.

The feasibility of using hydrogel immobilized bacteria for self-healing concrete is therefore demonstrated.

1. INTRODUCTION

Hydrogels are hydrophilic gels which have high water absorption capacity and can retain large amount of water or aqueous solution in the network without dissolving. The water absorbed would be gradually released to the exposing environments. There would be three benefits to use hydrogel for encapsulation of bacterial spores for

self-healing: 1) Hydrogel can protect bacterial spores during the mixing and hydration stage; 2) Swollen hydrogel can be used as the water reservoir for spores germination and bacterial activity when cracking occurs; 3) The precipitated microbial CaCO₃ can restrain the re-opening of the cracks due to long exposure to dry environment.

2. MATERIALS

Bacillus sphaericus LMG 22557 (Belgian coordinated collection of microorganisms, Ghent) was used in this study. MBS medium [1] was used to cultivate *B. sphaericus* spores. The hydrogel used was synthesized based on the commercial Pluronic®F-127 (Sigma Aldrich) which is a tri-block copolymer and has a polymer chain of polyethylene oxide — polypropylene oxide — polyethylene oxide ((PEO)-(PPO)-(PEO)) units.

3. METHODS

Bacterial spores suspension (10⁹ cells/mL) and/or the bio-reagents (yeast extract, urea, etc) were first mixed with a 20% w/w polymer solution (modified Pluronic®F-127). Then the initiator (Irgacure 2959) was also added to the solution. The mixture was degassed and mixed for 5min, which was subsequently subjected to UV radiation for 1h and a gel sheet was formed. The hydrogel sheet was then subjected to freeze grinding (IKA Yellowline A10 Analytical Grinder) and freeze drying (Christ Alpha 2-4 LSC, Germany) to obtain the dry powders.

The viability was evaluated by the amount of urea decomposed by the hydrogel immobilized spores, which was tested by TAN method [2]. Both pure (H) and blended hydrogels (with different combinations of spores (S), urea (U) and yeast extract (Y)) were tested. Thermogravimetric analysis (TGA) was used to demonstrate the formation of CaCO₃ in/on the hydrogels.

Five kinds of mortar prisms (30 mm x 30 mm x 360 mm) with a reinforcement ($\Phi = 6$ mm, L = 660 mm) in the center were made. The composition is shown in Table 1. The amount shown in the table is for one batch of the specimens, which also need 450g cement (OPC CEM I 52.5N) and 1350g sand (DIN EN 196-1 Standard sand). The last column shows whether bacteria were present (Y) or not (N). Urea and Ca-nitrate in the third and fourth column were added to the mortar matrix.

Multiple cracks were created in the prisms after 28d by means of a uniaxial tensile test. The cracked specimens were then subjected to the wet – dry cycles (1h in water and 11h exposure to 60%RH). The crack healing efficiency was evaluated by the decrease of crack widths monitored by light microscope (Leica S8 APO, Switzerland).

Table 1: Composition of the specimens

Type	Water (g)	Urea (g)	Ca(NO ₃) ₂ .4H ₂ O (g)	Yeast extract (g)	Hydrogel(g)	Spores
R	225	0	0	0	0	N
N	214	18	36	3.84	0	N
m-H	214	18	36	3.84	9 (H)	N
m-HYUC	214	18	36	3.84	22.5(HYUC)	N
m-HSYUC	214	18	36	3.84	22.5(HSYUC)	Y

4. RESULTS

After encapsulation and the subsequent treatments (grinding and drying), spores were still viable and kept high ureolytic activity. As shown in Fig.1, only limited amount (about 1~2g/L) of urea was decomposed after 1d and 2d in the media containing the hydrogels without spores inside. While in the media with bio-hydrogels, around 14~16g/L urea was decomposed in the first 24 hours. This was lower than that of free spores (about 18g/L urea decomposed in 1d). Yet, after 2 days, urea in the media with free or immobilized spores, was all completely decomposed. The subsequent grinding and drying had very limited negative effect on the immobilized spores.

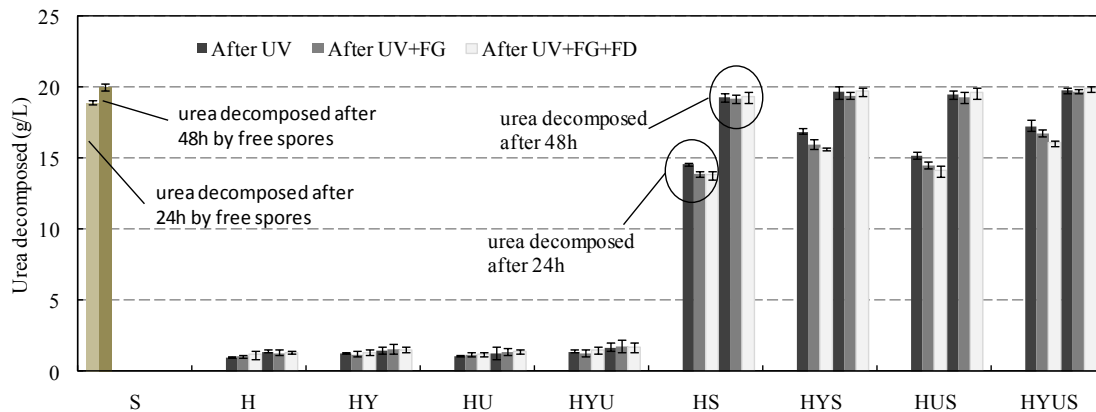


Figure 1: Urea decomposed in the media with the addition of different hydrogels (with or without encapsulated spores)

TGA results demonstrated the presence of CaCO_3 precipitation in the bio-hydrogels. CaCO_3 decomposes into CaO and CO_2 in the temperature range of 650~800°C and this causes weight loss. As shown in Fig.2, the samples from pure hydrogel (H, data not shown) and the ones with bio-reagents (HYUC) had no weight loss at 650~800°C; while the hydrogels with encapsulated bacterial spores (HSYUC) had distinct weight loss at the range of 650~800°C. The weight loss percentage was about 26%.

The swelling capacity of the hydrogel was slightly increased after incorporation of the bio-agents (Fig.3). No significant difference in swelling properties was observed in de-ionized water or filtered cement slurry. The swelling and re-swelling properties of the hydrogels (pure and blended) were also equivalent.

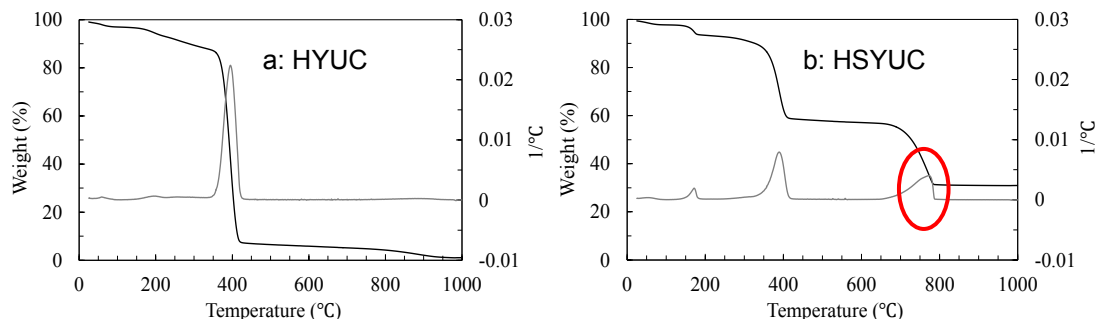


Figure 2: TGA graphs of samples from the hydrogels (encapsulated with only bio-agents (HYUC), and with both bio-agents and spores (HSYUC)) after immersion in water

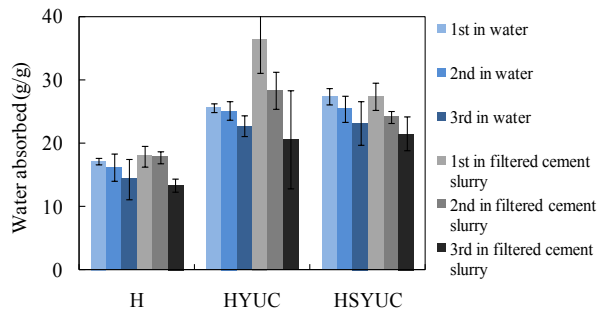


Figure. 3: Swelling properties of hydrogels de-ionized water and filtered cement slurry

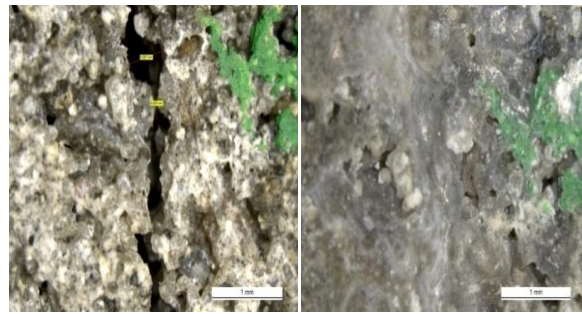


Figure 5 Healed crack (within 7d) in the in specimens with bio-hydrogels

The specimens with the bio-hydrogels showed an obvious superiority in crack healing efficiency, both with respect to the healing ratio (Fig.4) and the maximum healed crack width (data not shown). A maximum crack width of about 0.5mm can be healed in the specimens containing bio-hydrogels within 7d (Fig.5), while no crack healing was observed in the reference specimens.

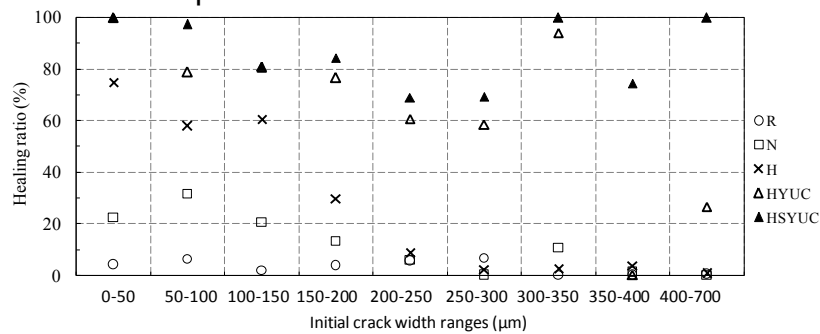


Figure 4: Average crack healing ratio in different ranges of crack widths of the specimens

5. CONCLUSIONS

It was demonstrated that hydrogel encapsulated spores have high viability and have great potential to be used for enhancing the self-healing capacity of the concrete.

ACKNOWLEDGEMENTS

Financial support from the Research Foundation Flanders (FWO-Vlaanderen) (Project No. G.0157.08) and Ghent University (a BOF grant) is gratefully acknowledged

REFERENCES

- [1] Kalfon, A., et al. (1983) Growth, sporulation and larvicidal activity of bacillus-sphaericus, European Journal of Applied Microbiology and Biotechnology, 18, 168-173.
- [2] Ivanov, V.M., et al. (2005) Chromaticity characteristics of $NH_2Hg_2I_3$ and I_2 : Molecular iodine as a test form alternative to Nessler's reagent, Journal of Analytical Chemistry, 60, 629-632.

MICROBIALLY MEDIATED CARBONATION OF MARINE ALKALINE MINERALS: POTENTIAL FOR CONCRETE CRACK HEALING

H. M. Jonkers¹, D. Palin¹, P. Flink¹ and A. Thijssen¹

¹ Faculty of Civil Engineering and Geosciences, Materials & Environment section, Delft University of Technology, P.O. Box 5048, 2600 GA Delft, The Netherlands - E-mail: h.m.jonkers@tudelft.nl and d.palin@tudelft.nl

Keywords: self-healing, marine concrete, bacteria, serpentinization, expansive minerals

ABSTRACT

Concrete constructions in the marine environment suffer from chemical attack of sea salts which can induce damage to both the concrete matrix and embedded steel reinforcement. For example, ingress of sulfate and chloride ions can respectively result in detrimental ettringite formation and enhanced corrosion of the steel rebars. The first degradation mechanism is due to development of expansive minerals within the concrete matrix, a process where increased internal pressure can result in crack formation. Cracking dramatically increases matrix porosity further enhancing the ingress rate of detrimental chemicals. However, with controlled mineral expansion comes the possibility of an employable mechanism for autonomous sealing of cracks. In this research project our aim is to study the potential for carbon dioxide-producing bacteria to act as an agent to control expansive carbonation reactions following serpentinization (hydration reactions) of alkaline precursor minerals in marine concrete. Early experimental results showed that seawater derived magnesium ions and carbon dioxide molecules show high potential for self-healing due to the formation of crack-filling expansive minerals. Environmental scanning electron microscopy combined with X-ray element analysis revealed that dolomite ($\text{CaMg}(\text{CO}_3)_2$) formation via intermediate conversion of brucite ($\text{Mg}(\text{OH})_2$) is the mechanism underlying this process. Several previously documented studies have reported that dolomite formation, analogous to delayed ettringite formation, can be detrimental to concrete as it can in fact induce crack formation due to increased internal stresses. In this project our aim is to control expansive mineral formation by bacterial CO_2 production channelling the process for healing- but not for causing cracks in concrete constructions in the marine environment.

1. INTRODUCTION

Autonogenous crack-healing in concrete has certain limitations as was e.g. observed in an early study by Edvardsen [1] and appears commonly limited to crack widths of maximally up to 0.2mm. In order to enhance crack-healing several mechanisms have been tested in a number of studies, varying from increased cement content, mineral (expansive) additives, organic polymers and limestone-producing bacteria [2]. In these systems autonomous crack-healing up to 0.5mm crack width has been observed [3]. As most documented studies focussed on crack-healing of concrete specimens and structures in freshwater environments, limited information is available of crack-healing in marine environments. Due to the presence of much higher concentrations of (interfering) sea salt compounds such as sulphate molecules and

magnesium ions, processes as secondary cement particle hydration and calcium carbonate mineral formation may differ substantially in fresh- and seawater. The objective of this study therefore was to investigate if and how the presence of typical seawater salts influence inorganic mineral formation on the surface of concrete specimens and furthermore if the presence of metabolically active bacteria might influence this process. While both mineral formation on the surface of both Portland cement and blast furnace slag cement was investigated, only results of Portland cement based specimens are presented in this study.

2. MATERIALS AND METHODS

Mineral formation on mortar specimens surface as well as autogenous crack-healing was compared between freshwater and sea water incubated specimens. Mineral formation was assessed by Environmental Scanning Electron Microscopy (ESEM) combined with X-ray element (EDAX) analysis. Crack-healing was quantified observing surface crack closure using light microscopy. Mortar specimens were prepared according to the following recipe: 294g sand (0.125-0.25mm), 154g sand (0.25-0.5mm), 392g sand (0.5-1mm), 560g sand (1-2mm), 850g CEMI 42.5N and 360ml tapwater, thus with a water cement ratio of 0.42. Small 1.5cm cubes were cut out of larger specimens after 10 days curing. Sets of these small cubes were subsequently cured for 7 and 21 days by submersion in respectively tapwater and artificial seawater at room temperature. Artificial seawater was prepared by amending 1L tapwater with KCl (0.8g), $\text{CaCl}_2 \cdot 2\text{H}_2\text{O}$ (1.5g), NaCl (27.35g), $\text{MgSO}_4 \cdot 7\text{H}_2\text{O}$ (6.9g) and $\text{MgCl}_2 \cdot 6\text{H}_2\text{O}$ (5.1g). Mineral formation on surfaces of these specimens were compared to those who were not water cured (kept in either air or preserved in 96% ethanol). Steel bar reinforced mortar prisms (16x4x4cm), cracked under tension after 28 days curing, were also further incubated in either tapwater or artificial seawater and analysed for surface crack-closure after 0, 28 and 63 days incubation.

3. RESULTS AND DISCUSSION

Mineral formation on surfaces of mortar cubes incubated in respectively fresh and artificial seawater appeared strikingly different both in terms of quantity and type of mineral formed (Figure 1). While moderate amounts of small calcium carbonate based minerals were formed on the surface of tapwater incubated specimens, substantial and dense layers of brucite, dolomite- and calcium carbonate based minerals appeared on surfaces of seawater incubated specimens.

The small calcium carbonate minerals formed on tapwater incubated specimens were likely formed due to carbonation of the cement paste resulting in conversion of Potlandite into calcium carbonate according to: $\text{Ca}(\text{OH})_2 + \text{CO}_2 \rightarrow \text{CaCO}_3 + \text{H}_2\text{O}$

EDAX analysis indicated that the substantially thicker layer of minerals formed on the surface of seawater incubated specimens consisted of brucite ($\text{Mg}(\text{OH})_2$) minerals and dolomite ($\text{MgCa}(\text{CO}_3)_2$) minerals visible in Fig 1B. Interestingly, a sequence of mineral formation, from brucite to dolomite, with concomitant expansion of reaction products appeared visible. This apparent sequential process can be explained by a reaction of seawater derived magnesium ions reacting with hydroxide ions leaching from the concrete matrix to form brucite: $\text{Mg}^{2+} + 2\text{OH}^- \rightarrow \text{Mg}(\text{OH})_2$, followed by reaction with seawater derived calcium ions and carbon dioxide molecules:

$2\text{Mg}(\text{OH})_2 + \text{Ca}^{2+} + 2\text{CO}_2 \rightarrow \text{CaMg}(\text{CO}_3)_2 + \text{Mg}^{2+} + 2\text{H}_2\text{O}$. The expanding mineral reaction results in more efficient crack healing in seawater than in freshwater as was

also visible in crack-healing of mortar prisms incubated in both types of water (Figure 2). During 56 days of curing, seawater incubated specimens showed higher autogenous crack-healing rates than tapwater incubated specimens.

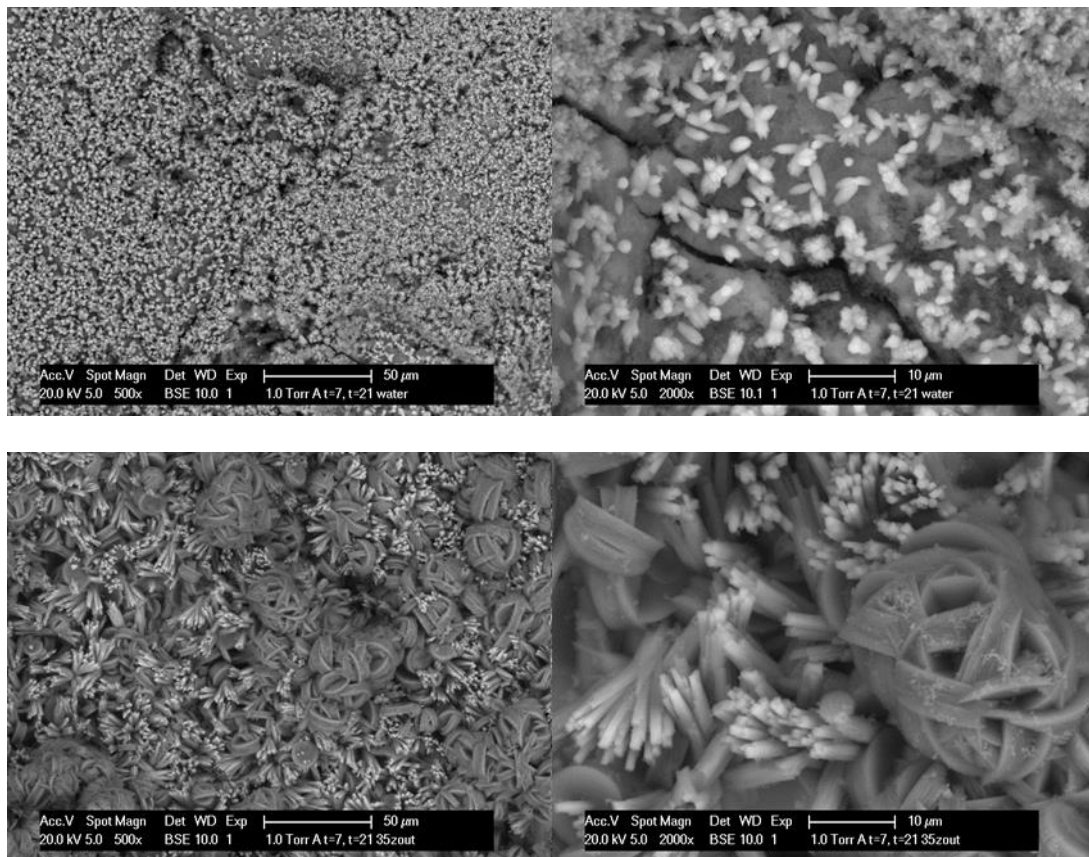


Figure 1: Specimens (10 days cured, 21 days incubated) in tapwater (top image, left: 500x magnification, right: 2000x magnification), showing formation of small calcium carbonate minerals, and seawater (bottom image, same magnifications), showing formation of larger brucite minerals (ball-shaped structures) and dolomite minerals (needle shaped structures).

4. CONCLUSIONS

The results of this study indicate that autogenous crack-healing is higher in seawater than in freshwater incubated mortar specimens. The difference can be explained by type of mineral formation, which is predominantly calcium carbonate in freshwater and eventually dolomite in seawater. As the later mineral formation involves more seawater derived molecules (magnesium and carbon dioxide) its reaction is more expansive thus resulting in potentially higher autogenous crack-sealing capacity. Our on-going research currently focusses on the role of microbial metabolic CO_2 production as this process could exert a control on brucite to dolomite formation.

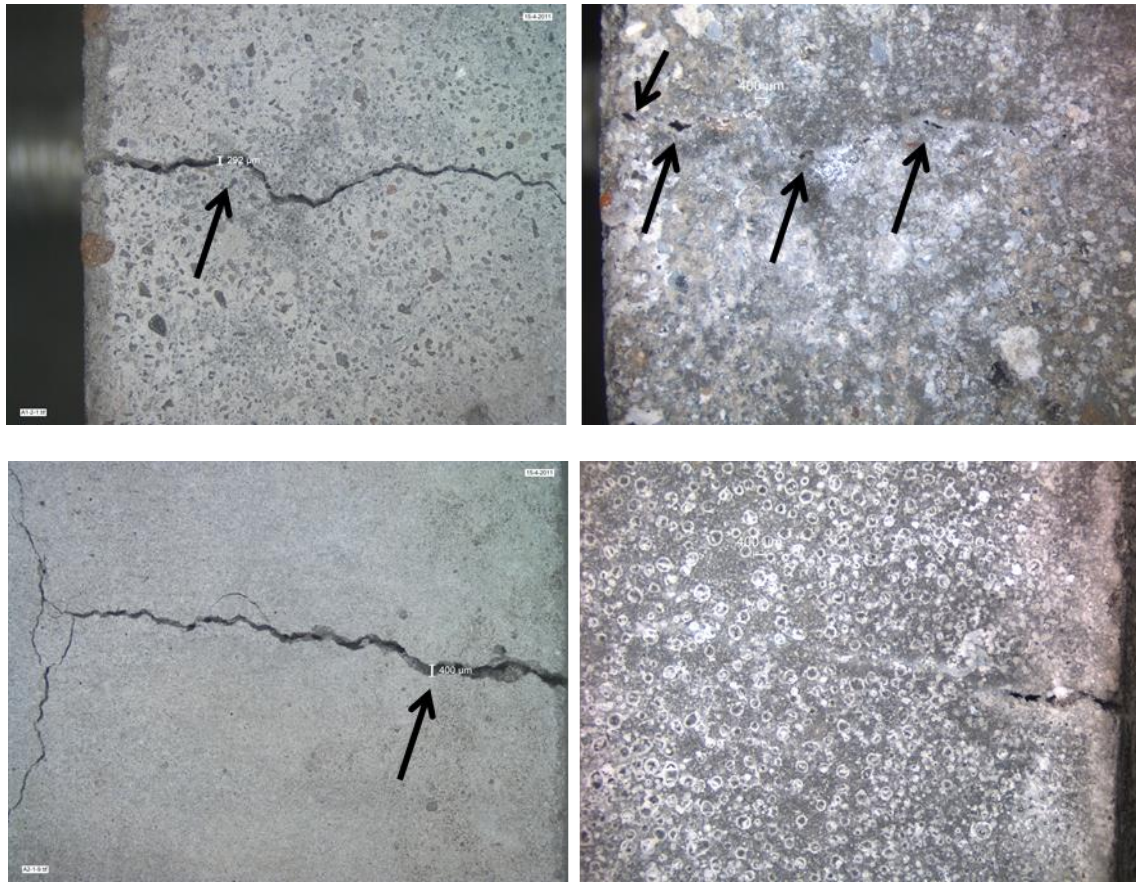


Figure 2: Autogenous crack-healing of mortar specimens incubated in fresh water (top image, left picture: crack induced after 28 days curing, crack width at arrow: 292 μm , right picture: imperfect crack closure (arrows) after 63 days incubation) and seawater (bottom image, left picture: crack induced after 28 days curing, crack width at arrow: 400 μm , right picture: crack closure up to 400 μm crack width after 63 days incubation)

This is important as unrestricted internal dolomite formation in concrete could potentially result in crack formation or crack extension due to the expansive reaction comparable to harmful secondary ettringite formation.

ACKNOWLEDGEMENTS

Financial support from the Delft Centre for Materials (DCMat: www.dcmat.tudelft.nl), and the EU Marie Curie SHeMat program for this work is gratefully acknowledged.

REFERENCES

- [1] Edvardsen, C. (1999) Water permeability and autogenous healing of cracks in concrete. *ACI Materials Journal*, 96(4), (1999) pp.448-454.
- [2] Schlangen, E. and Joseph, C. (2008) Self-healing processes in concrete. In SK Ghosh (Ed.), *Self-healing materials: fundamentals, design strategies and applications*. Weinheim, Wiley-vch. (2008) pp. 141-182.

[3] Wiktor, V. and Jonkers, H.M. (2011) Quantification of crack-healing in novel bacteria-based self-healing concrete. *Cement and Concrete Composites* 33 (2011) 763-770.

SESSION 21 – SELF-HEALING POLYMERIC MATERIALS

SELF-HEALING PMMA BIOMATERIALS

S.R. White^{1,4}, A.S. Gladman^{2,4}, A.-D. Celestine^{1,4}, J.S. Moore^{3,4}, N.R. Sottos^{2,4}

¹ Department of Aerospace Engineering, University of Illinois at Urbana-Champaign, Urbana, IL, 61801, USA – email: celesti1@illinois.edu, swhite@illinois.edu.

² Department of Materials Science and Engineering, University of Illinois at Urbana-Champaign, Urbana, IL, 61801, USA. n-sottos@illinois.edu

³ Department of Chemistry, University of Illinois at Urbana-Champaign, Urbana, IL, 61801, USA – email: jsmoore@illinois.edu

⁴ Beckman Institute of Advanced Science and Technology, University of Illinois at Urbana-Champaign, Urbana, IL, 61801.

Keywords: self-healing, bone cement, PMMA, thermoplastic

ABSTRACT

Inspired by living systems, self-healing polymers and composites are designed to autonomously repair damage whenever and wherever it occurs, thus providing a means to significantly extend the service life and reliability of structural materials. Capsule-based approaches to self-healing have been demonstrated in a variety of polymers and composites nearly all of which are relegated to thermosetting, structural systems. Autonomic-healing of thermoplastics remains a significant challenge for this class of materials at room temperature conditions. Of particular importance is the subset of PMMA thermoplastics used in biomedical applications for bone cement and dental implants.

Here we demonstrate a self-healing bone cement using a capsule-based approach for use in medical implants. Knee and hip replacement surgeries are increasingly common, but are typically limited to a 10-year lifetime due to aseptic loosening exacerbated by fatigue damage in the cement material. Self-healing of the bone cement could significantly extend the lifetime of implants and reduce the need for revision surgeries.

A self-healing bone cement is formulated using medical grade bone cement in which microcapsules (ca. 100 μm) of encapsulated healing agent(s) are dispersed. Two different healing approaches are presented including a dual-capsule free radical reaction chemistry and single capsule solvent chemistry. Fracture toughness evaluation is carried out for virgin and self-healed specimens following established protocols. The effect of capsule concentration and healing conditions on self-healing performance are elucidated.

NOVEL POROUS WALL VASCULAR NETWORKS FOR REPEATED SELF-HEALING

I. P. S. Qamar¹, R. S. Trask¹, T. S. Coope¹ and I. P. Bond¹

¹ *Advanced Composites Centre for Innovation and Science (ACCIS), Department of Aerospace Engineering, University of Bristol, University Walk, Bristol, BS8 1TR, UK – e-mail: Isabel.qamar@bristol.ac.uk; r.s.trask@bristol.ac.uk; tim.coope@bristol.ac.uk; i.p.bond@bristol.ac.uk*

Keywords: Self-healing, polymer composite, vascular network

ABSTRACT

A key limitation in the vascular self-healing systems to date has been the inability to achieve repeated healing for an infinite number of cycles due to fracture of the fluid-carrying vessel, which ultimately restricts and then terminates the transportation of the healing agent throughout the structure.

In order to overcome this limitation, a novel concept employing a porous thermoplastic network integrated within a fibre-reinforced composite laminate has been utilised. This approach does not require the fracture of the healing network architecture, but rather promotes the adhesive failure between the network and the surrounding host matrix material; thus exposing a series of radial pores and permitting the secretion of the liquid healing agent into the damage crack plane.

In this study holes of varying diameter have been introduced into PTFE tubes to create a porous vascular network (for the release of a healing potential), which in turn are embedded within a carbon fibre reinforced epoxy composite laminate. A microfluidics investigation into the effect of the shape and size of the pores on volume flow rate of a designated healing system has been undertaken. Mechanical characterisation of the crack-vascule interaction through a fracture mechanics (Mode I, Mode II and Mixed-Mode) assessment has indicated that moderate crack arrest occurs at the location of each vascule resulting in a controlled fracture process; a desirable attribute for self-healing composites. On arrival of a propagating crack to the external wall of the network, adhesive failure between the epoxy matrix and circumference of the network occurs which exposes the radial pores and allows the healing agent to permeate out into the damage area without fracture of the network.

The experimental characterisation of this system is on-going with self-healing trials imminent. These studies will investigate the integration of a low viscosity healing system into the network and the secretion of the healing agent through the pores into the crack plane. Mode I, Mode II and Mixed-Mode fracture toughness tests will be undertaken to determine the full potential of this approach to accomplish repeated self-healing in fibre reinforced composite laminates.

The role of clusters on the healing efficiency of a modified Zn based ionomer

J.M. Vega ^{1,2}, S. van der Zwaag ² and S.J. Garcia ²

¹ *Materials innovation institute, Mekelweg 2, 2600 GA, Delft, The Netherlands. – e-mail: j.m.vegavega@tudelft.nl*

² *Novel Aerospace Materials Group, Faculty of Aerospace Engineering, Delft University of Technology, Kluyverweg 1, 2629 HS Delft, The Netherlands – e-mail: s.vanderzwaag@tudelft.nl; s.j.garciaespallargas@tudelft.nl*

Keywords: EMAA, ionomer, WAXS, scratch healing.

ABSTRACT

Poly(ethylene-co-methacrylic acid) (EMAA) ionomers have shown healing capabilities in both ballistic and static tests. In previous studies it was shown that the degree of crosslinking (clusters) affects (positively or negatively) the healing under impact tests. Moreover, it has also been reported that the modification of the ionomers by additives leads to different healing behaviours under static puncture tests. Despite the preliminary tests the effect of the additives on the ionomers was not clarified.

In this work we use scratch healing and WAXS to gain a major understanding of the effect of additives in ionomers. Several blends of a semi-crystalline ionomer partially neutralized with zinc (EMAA-Zn) with adipic acid were prepared.

Temperature assisted healing (well below the melting temperature) of artificial scratches in the surface of modified and unmodified EMAA-Zn ionomers was performed. A confocal microscope was employed for the healing quantification and measurements of Young modulus. Wide Angle X Ray diffraction (WAXS) was employed to track the effect of the additive in the polymer structure.

The results show a strong influence of the additive on the clusters leading to a clear increase of the healing efficiency when clusters disappear.

1. INTRODUCTION

Ionomers are partially neutralized polymers with their bulk properties governed by ionic interactions within discrete regions of the polymer structure [1]. The ionic interactions are obtained by the partial neutralization of the precursor polymer using monovalent and divalent cations. The presence of the cations leads to strong Coulombic interactions between the ion pairs yielding ionic aggregates, namely clusters, which act as multifunctional “electrostatic” crosslinks [2]. As a result, a supramolecular network of physical (reversible) crosslinks (clusters) is formed affecting the final properties (viscoelastic behaviour, absorption of solvents, etc.). Earlier work has shown that the ionomers have a good self healing behaviour for ballistic impact [3], which could be tuned by addition of cluster modifiers [4]. The present work concerns a more detailed study into the role of adipic acid on cluster formation and low temperature scratch healing efficiency.

2. MATERIALS

A commercial Zn based semi-crystalline poly(ethylene-co-methacrylic acid) ionomer (EMAA-Zn) was used for this study as a precursor. The EMAA-Zn contains 3.5 mol% methacrylic acid, out of which 71 % have been neutralized with Zn^{2+} ions. This polymer has two characteristic transition temperatures, the first one around 44 °C, linked with the clusters and semicrystals, and the second one at 97 °C linked to the melt of the main crystalline structure. Adipic acid (AA) was used as chemical modifier of the ionomer system. The blends were prepared in a DSM mini-extruder with twin screw configuration at 150 °C. The ionomer was dried overnight at 80 °C before blending with the adipic acid. Five EMAA-Zn / adipic acid blends were prepared containing 1, 3, 6, 10 and 20 wt% of adipic acid.

Two types of specimens were prepared by compression moulding using a hot press: (i) coated galvanized steel plates for scratch healing tests and (ii) free standing films for general characterization. During the compression moulding, the polymer blends were located between two fresh Kapton[®] sheets (or one Kapton sheet and the galvanized steel substrate). Compression was performed at 0.67MPa and 130 °C during 5 minutes. The hot press and, thus the samples, were water-cooled to room temperature before releasing the pressure. The thickness of both coatings and free-standing films was around $160 \pm 10 \mu m$ as measured by a PosiTector[®] 6000 thickness meter.

3. METHODS

A microscratch tester (MST) from CSM Instruments was used to perform controlled scratches at 2N constant load on the polymer surface of the coated galvanized specimens. This same instrument was used to obtain the Young modulus (E) by indentation mode (load of 0.5N).

For the quantification of the subsequent scratch healing (i.e. viscoelastic recovery) upon exposure to 70 °C, a laser scanning confocal microscope Olympus OLS 3100 (software LEXT OLS 6.0.11) using a 20x objective was employed. After the initial scratch, the specimens were placed in a pre-heated circulating hot air furnace operating at 70 °C for 30 min.

The analysis consisted in following the evolution of the scratch profiles (healing) by taking 3D images before and after the heat treatment. In order to analyse the viscoelastic recovery (healing efficiency), the empty volume (V) of the scratch was measured before and after heating and corrected by the surface area of the measured region. The healing efficiency was quantified using equation 1:

$$Healing(\%) = 100 - \left(\frac{V / A_{A.H.}}{V / A_{B.H.}} \right) 100 \quad \text{Equation 1}$$

where V/A is the volume/area ratio after healing (A.H.) and before healing (B.H.). The V/A values were averaged amongst 4 different sections along the scratch.

WAXS measurements were carried out using a Bruker D8 Discover X-ray diffractometer equipped with the 2-dimensional Hi-Star Area Detector and Cross Coupled Göbel Mirrors. The measurements were performed in transmission mode at room temperature using monochromatic Cu $K\alpha 1$ radiation and a sample to detector face of 30 cm.

4. RESULTS

Figure 1 shows the healing efficiency and E as a function of the adipic acid content. From the plot it can clearly be seen that there is a strong influence of both parameters with the adipic acid content, especially in terms of healing efficiency. Healing efficiency increases dramatically with the adipic acid content until around 7% after which the healing remains constant independently of the adipic acid content. At the same time small additions of adipic acid (<5%) do not lead to an increase in healing. Nevertheless an addition of about 6% shows a dramatic increase of up to 55%. At the same time the elastic modulus shows a continuous decrease with adipic acid levels which saturates from about 10%. These results show a clear link between the decrease in Young modulus and the increase in healing efficiency for this system.

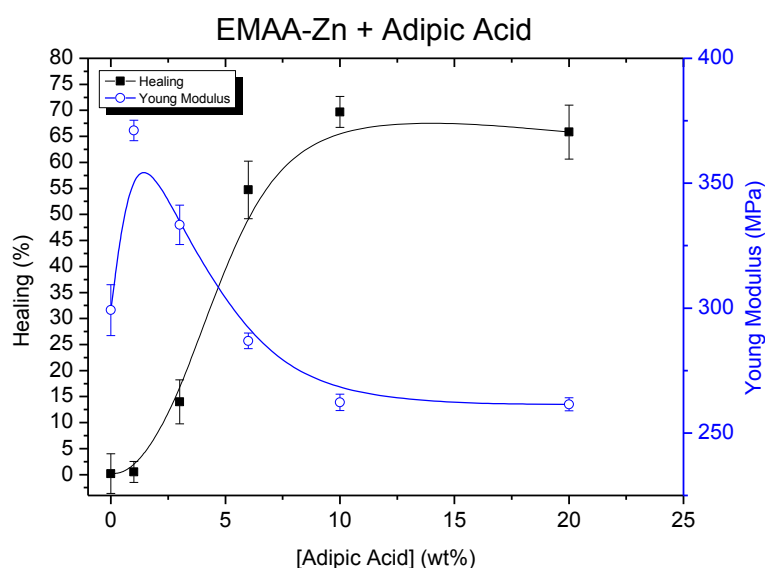


Figure 1: Variation of the healing efficiency (%) and Young modulus of the polymer blends with varying amounts of adipic acid content in the blend.

In order to understand the effect of the additive in the polymer structure, WAXS measurements were performed at room temperature (Figure 2). The EMAA-Zn ionomer shows a reflection at 5 (2θ) related to the clusters. The reflections at higher values are related with the main crystalline structure. The addition of 1% of adipic acid decreases the intensity related with cluster reflection although the cluster signal is still visible. This trend is kept for all the blends until 6% of adipic is added and the peak related to the cluster is not visible anymore. It results evident that the disappearance of the clusters occur at the same concentration of adipic acid at which the healing efficiency is boosted up to its maximum constant value.

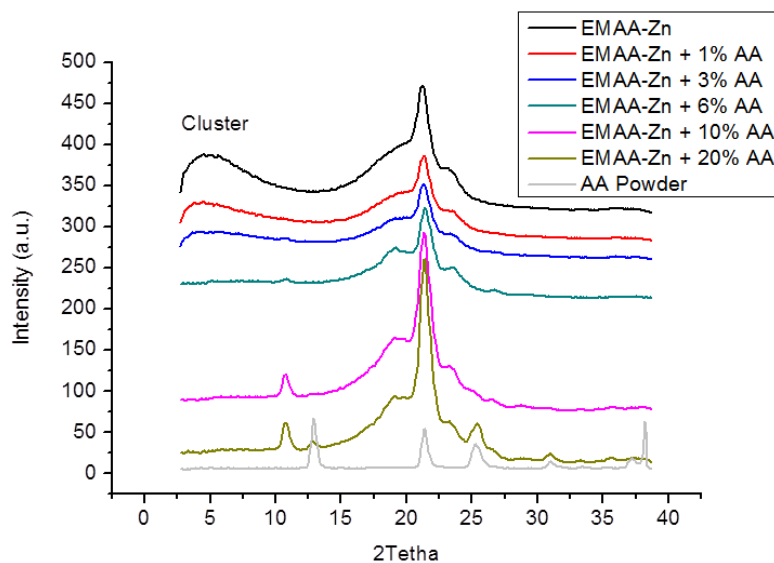


Figure 2: WAXS patterns for EMAA-Zn ionomer and its blends with different content of adipic acid.

5. CONCLUSIONS

In this work it was demonstrated that the addition of adipic acid leads to a suppression of the clusters formation in EMAA-Zn ionomers. Rather surprisingly the scratch healing efficiency increased with the disappearance of detectable clusters by WAXS. The suppression of clusters leads to a modest reduction of the Young modulus.

ACKNOWLEDGEMENTS

This research was carried out under projects M41.6.10400 and M41.6.12456 in the framework of the Research Program of the Materials Innovation Institute M2i (www.m2i.nl).

REFERENCES

- [1] A. Eisenberg and M. Rinaudo, Polyelectrolytes and ionomers, *Polymer Bulletin* 24 (1990) 671-671.
- [2] A. Eisenberg, B. Hird, and R.B. Moore, A new multiplet-cluster model for the morphology of random ionomers, *Macromolecules* 23 (1990) 4098-4107.
- [3] S.J. Kalista and T.C. Ward, Thermal characteristics of the self-healing response in poly (ethylene-co-methacrylic acid) copolymers, *Journal of the Royal Society Interface* 4 (2007) 405-411.
- [4] R.J. Varley, S. Shen, and S. van der Zwaag, The effect of cluster plasticisation on the self healing behaviour of ionomers, *Polymer* 51 (2010) 679-686.

OLEFIN METATHESIS FOR EFFECTIVE POLYMER HEALING VIA DYNAMIC EXCHANGE OF STRONG CARBON-CARBON BONDS

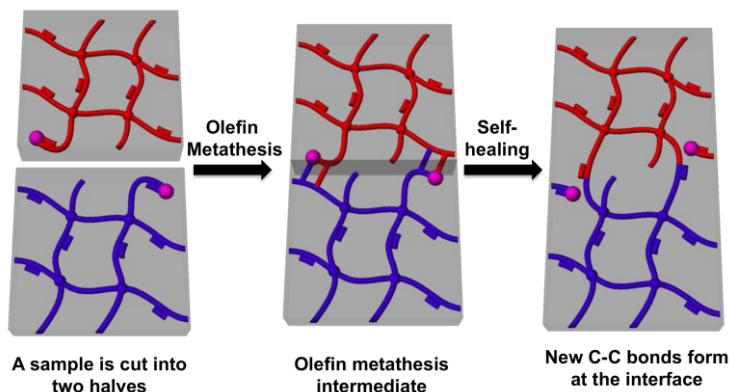
Y. Lu¹ and Z. Guan¹

¹ Department of Chemistry, 1102 Natural Sciences 2, University of California, Irvine, CA 92697, USA – e-mail: zguan@uci.edu

Keywords: Self-healing, dynamic covalent exchange, olefin metathesis, elastomer

ABSTRACT

Introducing self-healing capability into materials would greatly improve their safety feature, lifetime, and energy efficiency. A significant amount of efforts has been devoted to this field in recent years and several groups have reported different self-healing polymer designs through the incorporation of encapsulated monomers, dynamic non-covalent bonding, and reversible or irreversible covalent bonds into polymers. Most dynamic covalent bonds used for self-healing applications involve heteroatoms in dynamic exchange reactions. In addition, most of those self-healing systems require specially designed monomers or polymers to serve the purpose. It is highly desirable to develop a simple strategy for effective polymer healing through dynamic exchange of strong C–C bond under ambient conditions. In principle, reversible carbon-carbon (C–C) bond formation may offer the possibility of designing stronger self-healing materials because of the high stability of C–C bonds. Recently, my laboratory has demonstrated transition-metal catalyzed olefin metathesis as a simple, effective method for healing polymers via dynamic exchange of strong carbon-carbon bonds (*J. Am. Chem. Soc.* **2012**, *134*, 14226). By introducing a very low level of the Grubbs' second-generation Ru metathesis catalyst into cross-linked polybutadiene (PBD) network, the material self-heals effectively at various conditions under moderate pressures. In sharp contrast, catalyst-free control samples with identical network topology and cross-linking density show minimal healing. The healing efficiency of the materials was carefully investigated under different concentrations of the Ru catalyst, compression pressure and temperature. It was demonstrated for the first time that a bulk polymer could effectively heal via dynamic covalent bond formation at sub-ambient temperature. The Ru-loaded PBD samples not only heal well with themselves but also with control samples without any catalyst. The simplicity and effectiveness of this self-healing approach make it potentially applicable to a wide range of olefin-containing polymers.



GAP-FILLING FLUIDS FOR MATERIALS REGENERATION

W. A. Santa Cruz^{1,5}, B.P. Krull^{2,5}, R.C.R. Gergely^{3,5}, N.R. Sottos^{2,5}, S.R. White^{4,5},
J.S. Moore^{1,5}

¹ *Department of Chemistry, University of Illinois at Urbana-Champaign, Urbana, IL, 61801, USA – email: turchyn@illinois.edu*

² *Department of Materials Science and Engineering, University of Illinois at Urbana-Champaign, Urbana, IL, 61801, USA.*

³ *Department of Theoretical and Applied Mechanics, University of Illinois at Urbana-Champaign, Urbana, IL 61801, USA.*

⁴ *Department of Aerospace Engineering, University of Illinois at Urbana-Champaign, Urbana, IL, 61801, USA.*

⁵ *Beckman Institute of Advanced Science and Technology, University of Illinois at Urbana-Champaign, Urbana, IL, 61801, USA – email: jsmoore@illinois.edu*

Keywords: self-healing, large damage volume, regeneration, polymer network gel, free radical polymerization

ABSTRACT

Robust schemes for autonomic regeneration present challenging problems that demand new concepts in healing agents. The challenges arise from the interplay of mass transport and the forces, both intrinsic (e.g. surface tension) and extrinsic (e.g. gravity), that act upon liquid healing agents as they traverse the zone of regeneration. We demonstrate a cross-linked polymer gel as a synthetic scaffold for large damage volume regeneration and subsequent in situ post-polymerization for recovery of mechanical properties. The bi-phase chemical resin undergoes two independent autonomic transformations that are tunable and chemically compatible. In contrast to high viscosity epoxies, the resin begins as a two-component, low viscosity sol state. The scaffold material forms by acid-catalyzed gelation of an aldehyde cross-linker and functionalized oligomer in liquid monomer. The second transformation, occurring after gel formation, is a free-radical polymerization of the gel monomer “solvent” for several orders of magnitude increase in modulus. Each phase, gelation and polymerization, can be independently adjusted to accommodate multiple healing configurations. Preliminary results suggest that careful timing of these chemical changes make it possible to fill large damage volumes with restorative materials without loss of healing agent.

Unlike photopolymerizations or high temperatures required in other curing systems, the bi-phase resin cures autonomously and under ambient conditions. The room temperature cure is accomplished using the promoted decomposition of a peroxide initiator with a metal-salt. Although oxygen inhibition is a common problem with free-radical polymerization, thiol-ene chemistry has shown great effectiveness in ambient cures. The combination of the gel scaffold with post-polymerization defines a new type of healing chemistry and further expands the healing capability of microvascular composites.

SESSION 22 – SELF-HEALING COATINGS AND PAINTS

ONE-COMPONENT INTRINSIC SELF-HEALING POLYMER FOR COATINGS BASED ON REVERSIBLE CROSSLINKING BY DIELS-ALDER-CYCLOADDITIONS

J. Kötteritzsch¹, M. D. Hager¹, U. S. Schubert¹

¹ Laboratory for Organic and Macromolecular Chemistry (IOMC), Friedrich-Schiller-University Jena, Humboldtstr. 10, 07743 Jena, Germany; Jena Center for Soft Matter (JCSM), Friedrich-Schiller-University Jena, Philosophenweg 7, 07743 Jena, Germany
e-mail: martin.hager@uni-jena.de; ulrich.schubert@uni-jena.de

Keywords: polymer coating, Diels-Alder cycloaddition, self-healing polymers, reversible covalent bonds

ABSTRACT

Self-healing can be achieved in polymer coatings by the incorporation of extrinsic materials, i.e. a healing agent is embedded into the coating (e.g., within capsules). In contrast the polymeric coating itself can feature the ability for healing – for instance if reversible covalent bonds are introduced into the polymer network. The Diels-Alder reaction is one prominent example to obtain reversibility within self-healing/mendable materials.

In this context, a novel acrylic-based one-component polymer system has been synthesized, which contains both binding units for the Diels-Alder reaction (i.e. the maleimide and the furan moiety) as well as comonomers to tune the mechanical as well as thermal properties. The ATRP (atom transfer radical polymerization) of maleimide methacrylate (MIMA), furfuryl methacrylate (FMA) as well as of different alkylmethacrylates was utilized to synthesize well-defined functional terpolymers, which could be crosslinked subsequently via thermal treatment. The mechanical and thermal properties of these polymers have been investigated in detail. Moreover, the healing ability of these polymer coatings was studied. The influence of the crosslinking density, the kind of the comonomer and the healing temperature was investigated in detail. An efficient healing of these coatings could be observed. Additionally first attempts to tune the healing temperature of these coatings have been performed. The comonomers can also influence the required temperature for the retro-Diels-Alder reaction.

1. INTRODUCTION

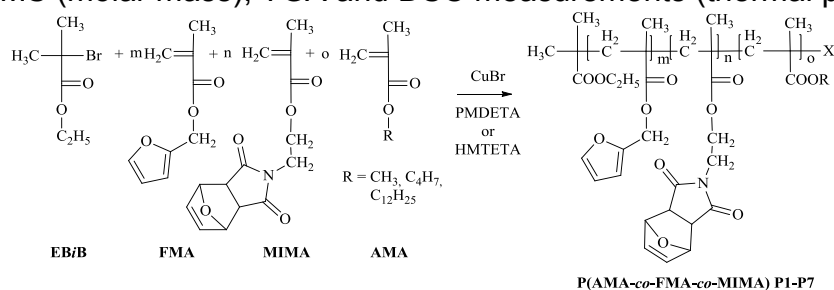
In recent years several approaches have been investigated in order to obtain self-healing polymer coatings.[1] These materials are of particular interest because coatings are particular prone to damage. Moreover polymer coatings fulfill different functionalities: the protection of the underlying material (e.g., polymeric coating on metals) as well as an aesthetic function. In contrast to embedded healing agents (i.e. capsule approach) intrinsic self-healing would allow a continuous healing.[1]

The utilization of reversible chemical bonds (non-covalent as well as covalent bonds) allows the design of intrinsic self-healing materials. One of the most prominent examples of self-healing polymers based on reversible covalent bonds is the Diels-Alder reaction. The cycloaddition has been successfully applied for bulk materials [2] as well as coatings [3].

Currently, all systems are based either on monofunctional polymers, which are crosslinked by low molar mass crosslinkers or on polymeric networks based on multifunctional monomers (*i.e.* polymerization by cycloaddition). Therefore, a multifunctional polymer bearing both functionalities – the furan as well as the maleimide – have been synthesized. The self-healing of these polymers was investigated.[4]

2. MATERIALS AND METHODS

A library of different terpolymers have been synthesized by the atom transfer radical polymerization (ATRP). [4] All polymers (see Scheme 1) contain the maleimide monomer (MIMA), furfuryl methacrylate (FMA) as well as different alkyl methacrylates (methylmethacrylate - **P1-P3**, butylmethacrylate - **P4-P6**, laurylmethacrylate - **P7**). The resulting copolymers were characterized by ¹H NMR spectroscopy (composition, ratio of both functional groups), SEC (molar mass as well as molar mass distribution), MALDI-TOF MS (molar mass), TGA and DSC measurements (thermal properties).



Scheme 1: Schematic representation of the copolymerization of alkyl methacrylates (AMA), FMA and MIMA by ATRP polymerization.

Films of these polymeric materials were obtained by thermal treatment of the soluble linear polymers. After cleavage of the furan protecting group of the MIMA a crosslinked polymer film was obtained. These films were insoluble in common organic solvents.

The self-healing of these coatings was investigated by scratch healing experiments. Self-healing on the nanoscopic level was investigated by AFM measurements (tapping mode with non-contact cantilevers; scratches were applied by dragging the AFM tip in the surface). Moreover, microscopic scratches were applied by a knife in a controlled manner. The healing of these scratches was investigated by SEM.

3. RESULTS

The controlled radical polymerization ATRP could be successfully applied for the synthesis of well-defined terpolymers with relatively narrow molar mass distributions. Polymers with molar masses between 5,000 and 15,000 g/mol could be obtained. The content of both functional groups was determined by NMR spectroscopy. **P1-P3** featured a content between 12 and 79%, **P4-P6** between 6 and 73%; **P7** 19%.

Subsequently, the thermal properties of the polymers were investigated. The TGA measurements (Figure 1, right) revealed on the one side the thermal stability of the polymers, on the other hand the mass loss around 130 °C corresponds to the furan from the protecting group. In addition DSC measurements were performed to investigate the thermal properties (Figure 1, left). **P7** showed an endothermic peak in

the 1st heating curve (120 °C), which corresponds to the retro-Diels-Alder reaction as well as the evaporation energy of the released furan. The glass transition temperatures (T_g) of the non-crosslinked copolymers could also be observed. In the 2nd heating curve the endothermic peak caused by the retro-Diels-Alder reaction could also be observed. However, the peak was much smaller, because no additional furan is released. Additionally not all functional groups combine upon cooling after the first cycle.

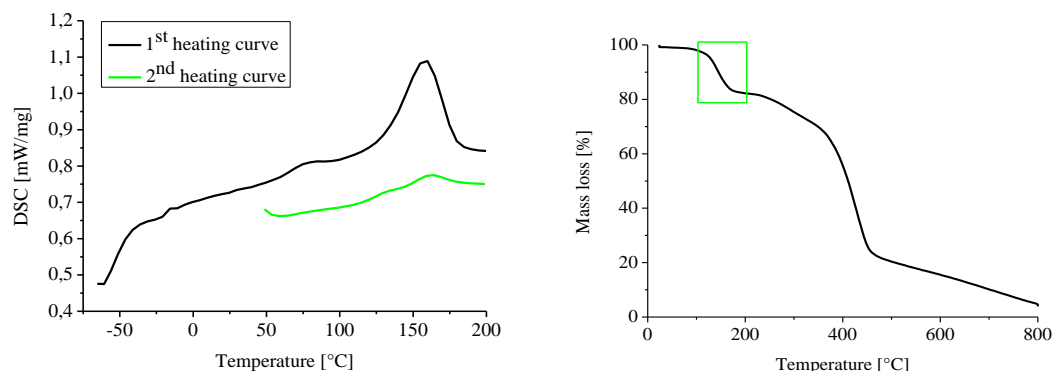


Figure 1: DSC analysis of copolymer **P7** (left); TGA of copolymer **P6** (right).

All polymers of the polymer library were investigated in scratch healing experiments. Coatings based on **P1-P3**, which contain methylmethacrylate as comonomer, could not be healed after being scratched. The mobility of the polymer chains is not sufficient due to the high glass transition temperature. In contrast, poly(butylmethacrylate) features a lower T_g . Therefore polymer coatings, based on butylmethacrylate as comonomer (**P4-P6**), could be healed, if the scratches were on the nanoscopic level.

A further lowering of the T_g could be obtained by the incorporation of laurylmethacrylate as comonomer (**P7**). The scratch healing of this material was investigated by SEM (Figure 2). The applied scratch was annealed at elevated temperature (160 °C). A beginning of the healing process could already be noticed after 1 min; the healing was complete after 3 min.

The usage of the unpolar lauryl methacrylate causes a slight increase in the retro-Diels-Alder temperature. However, the usage of more polar comonomers (e.g., OEGMA) did not lead to a significant decrease of the retro-Diels-Alder reaction.

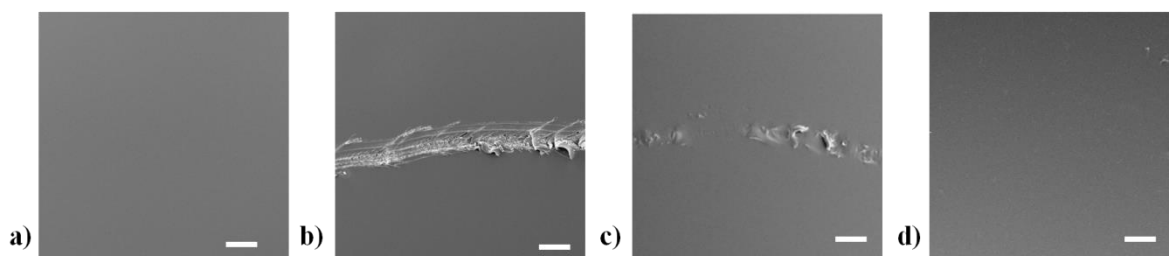


Figure 2: Investigation of the scratch healing of copolymer **P7**. a) Crosslinked film, b) scratch c) scratch after annealing at 160 °C for 1 min and d) scratch after annealing at 160 °C for 3 min (scale bars = 100 μ m).

4. CONCLUSIONS

A library of one-component intrinsic self-healing polymers was synthesized. These polymers are solution-processable and hard coatings can be formed by thermal treatment of preformed polymer films. The addition of low-molar mass crosslinkers is not required in contrast to many other examples described in the literature. Moreover, the thermal properties, and as a consequence, the mobility of the polymer chains within the network, can be tuned by the corresponding comonomer (alkylmethacrylates). The terpolymer based on lauryl methacrylate revealed the best self-healing properties. Scratches could be healed at elevated temperatures (160 °C) within a few minutes.

ACKNOWLEDGEMENTS

Financial support from the Deutsche Forschungsgemeinschaft (SPP 1568) for this study is gratefully acknowledged.

REFERENCES

- [1] S. J. García, H. R. Fischer, S. van der Zwaag, A critical appraisal of the potential of self healing polymeric coatings, *Progress in Organic Coatings* 72 (2011) 211-221.
- [2] S. D. Bergman, F. Wudl, Mendable polymers, *Journal of Materials Chemistry* 18 (2008) 41-62.
- [3] M. Wouters, E. Craenmehr, K. Tempelaars, H. Fischer, N. Stroeks, J. van Zanten, Preparation and properties of a novel remendable coating concept, *Progress in Organic Coatings* 64 (2009) 156-162.
- [4] J. Kötteritzsch, S. Stumpf, S. Hoepfener, J. Vitz, M. D. Hager, U. S. Schubert, One-component intrinsic self-healing coatings based on reversible crosslinking by Diels-Alder-cycloadditions, *Macromolecular Chemistry and Physics* (2013), DOI: 10.1002/macp.201200712.

REGENERATIVE POLYMERIC COATINGS

R. Gergely¹, B. Krull², W. A. Santa Cruz³, J. Moore^{3,4}, N. Sottos^{2,4}, S. White^{4,5}

¹ Department of Mechanical Science and Engineering, University of Illinois at Urbana-Champaign, 1206 W. Green Street, Urbana, Illinois, 61801, USA – e-mail: gergely2@illinois.edu

² Department of Materials Science and Engineering, University of Illinois at Urbana-Champaign, 1304 W. Green Street, Urbana, Illinois 61801, USA – e-mail: krull3@illinois.edu; n-sottos@illinois.edu

³ Department of Chemistry, University of Illinois at Urbana-Champaign, 505 South Mathews Avenue, Urbana, Illinois, 61801, USA – e-mail: turchyn@illinois.edu; jsmoore@illinois.edu

⁴ Beckman Institute for Advanced Science, University of Illinois at Urbana-Champaign, 405 N Mathews Avenue, Urbana, Illinois 61801, USA

⁵ Department of Aerospace Engineering, University of Illinois at Urbana-Champaign, 104 South Wright Street, Urbana, Illinois 61801, USA – e-mail: swhite@illinois.edu

Keywords: coating, regeneration, polymer, vascular, valve

ABSTRACT

Autonomic healing of coatings has been previously demonstrated using both capsule-based and vascular network approaches. However, healing in both systems has been limited to small damage volumes resulting from scratches or cracks. In this work, we demonstrate a system capable of regenerating a protective coating after large scale damage, for multiple cycles. Our bio-mimetic design incorporates pressure sensitive valves which open upon coating removal to release liquid (uncured) monomer onto the vascularized substrate whereby exposure to UV light polymerizes the monomer to form a protective barrier (coating).

Results are presented summarizing coating regeneration performance as characterized by hardness recovery and resistance to abrasion. The evolution of coating formation is captured through optical microscopy. Multiple damage and regeneration cycles are demonstrated through repeated delivery of coating materials through the vascular substrate. Results from both *ex-situ* and *in-situ* regeneration tests are discussed. Specimens incorporating arrays of pressure valves for regeneration of larger scale damage are also presented.

The autonomic flow valves are characterized by flow rate measurements as well as optical inspection. The influence of coating formulation, vascular pressurization, and environmental temperature are presented. The feasibility of using the sun as a source of UV light for curing the regenerated coating as well as the importance of valves as a mechanism for preventing backflow and channel blockage is discussed.

By restoring their protective function autonomously, regenerative coatings could significantly increase the service life of coated substrates. Future design challenges such as the reduction of valve footprint, improved adhesion between the substrate and coating, and manufacturing scalability will be discussed.

SELF CRACK HEALING INDUCED BY HIGH TEMPERATURE OXIDATION IN SiN/SiC NANO-LAMINATED FILM

M. Nakatani¹, J. Nishimura², S. Hanaki¹ and H. Uchida¹

¹ Department of Mechanical Engineering, University of Hyogo, Syosya 2167, Himeji, Japan
e-mail: nakatani@eng.u-hyogo.ac.jp; hanaki@eng.u-hyogo.ac.jp; uchida@eng.u-hyogo.ac.jp

² Graduate Student, Department of Mechanical Engineering, University of Hyogo, Syosya 2167, Himeji, Japan

Keywords: Self healing, Crack, Thin film, High temperature oxidation, Deposition

ABSTRACT

In bulk, Si₃N₄ reinforced by dispersing SiC particle has superior self crack healing ability at high temperature. In consideration with this fact, SiN/SiC nano-laminated film is expected to exhibit the self crack healing at high temperature. In this study, we investigated the self crack healing behavior of the SiN/SiC nano-laminated film including its factors such as heating temperature, heating time.

The films were deposited on the silicon wafer using an ion beam assisted deposition technique. The SiN/SiC nano-laminated films with four layers were fabricated by alternative deposition of SiN and SiC. Total film thickness is approximately 1 μm. After the deposition, a pre-crack was introduced using a Vickers indentation. Then, the cracked film was heated using an electric furnace at temperatures ranging from 873 K to 1473 K in the air. The heating time was changed from 1 h to 72 h.

The crack on SiN monolayer film was almost not healed at the temperature less than 1273 K. On the other hand, in the case of SiN/SiC nano-laminated film, crack healing occurred at even 873 K. SiO₂ was observed along the healed crack. These results indicate that SiC layer contributes to crack healing significantly. However, the crack with large opening was not healed. These results indicate that SiN/SiC nano-laminated film has an ability to heal initial small crack.

The crack healing became remarkable with an increase in heating temperature and time. This result is corresponding with the tendency observed in bulk. However, at 1473 K, though the crack was healed perfectly, the laminate structure disappeared and the overall film was subjected to oxidation. This suggested that there is an upper limitation of temperature for in-situ self crack healing.

1. INTRODUCTION

Bulk silicon nitride (Si₃N₄) ceramics reinforced by silicon carbide (SiC) nanoparticles exhibits a self-crack-healing behavior at high temperature [1-2]. When a cracked ceramic is heated at high temperature in air, the SiC particles exposed on the crack plane thermochemically react to form silicon dioxide (SiO₂). As this reaction proceeds, the crack is filled by SiO₂ because the volume of SiO₂ is larger than that of SiC. Other research groups have reported that an Al₂O₃/TiC composite coating fabricated by plasma spraying also exhibits self crack healing by oxidation [3]. However, there are very few reports on self-healing micromaterials.

On the basis of the above reports, carbide composite thin films may also exhibit a self-crack-healing ability at high temperatures. The purpose of this study is to

fabricate SiN/SiC nano-laminated thin films with a self crack healing ability and investigate the influence of heating temperature and time on the self crack healing behavior.

2. EXPERIMENTAL PROCEDURES

The SiN/SiC nano-laminated films were deposited on Si(100) substrates by an ion beam assisted deposition [4]. The substrates were cleaned by successive rinsing in ultrasonic baths of acetone. After cleaning, the Si substrates were fixed on a water-cooled holder. After setting the substrates, the chamber was evacuated to a base pressure of 1×10^{-3} Pa.

The SiN/SiC nano-laminated films were fabricated with alternating layers of SiN and SiC. The deposition conditions for the layers are shown in Table 1. The SiN layer was obtained by electron-beam evaporation of pure silicon and simultaneous bombardment by a nitrogen-ion beam. The SiC layer was deposited by the electron-beam evaporation of silicon and simultaneous bombardment by an argon-ion beam under an ethylene atmosphere [5]. The fabricated nano-laminated film consisted of four layers with the top layer being SiN. The bilayer thickness was fixed to 500 nm and the bilayer ratio of SiN to SiC was 1. The SiN monolayer films were also fabricated to compare their properties with that of the SiN/SiC nano-laminated film. The total thickness of all the films was 0.9–1.2 μm .

A small artificial crack was introduced using a Vickers micro-indenter. The crack length was 10–15 μm . The cracked films were heated using an electric furnace in an air atmosphere. In this study, the self-crack-healing behavior of the nano-laminated films was systematically investigated by changing the heating temperature (873–1473 K) and time (24–96 h). The films were observed by field emission type scanning electron microscope (FE-SEM) every 24 h.

3. RESULTS AND DISCUSSION

Figure 1 shows the FE-SEM images of the crack after heating the samples at a temperature of 1073 K for 24 h. In the case of the SiN monolayer film, the crack was poorly healed after heating, as shown in Figure 1(a), respectively. On the other hand, the cracks in the SiN/SiC nanolaminated films were healed, as shown in Figure 1(b). In bulk, when Si_3N_4 and SiC are heated in air, oxidation occurs by the following chemical reactions:

Table 1: Deposition conditions.

	SiN	SiC
Arc voltage (V)	80	
Ion beam	Nitrogen	Argon
Gas flow rate (sccm)	4.0	1.5
Acceleration voltage (keV)	2.0	0.3
Acceleration current (mA)	14.0	15.0
Atmosphere gas	-	Acetylene
Vapor rate (nm/s)	0.2	0.1



The theoretical volume expansions caused by these reactions are calculated to be approximately 80% and 69%, respectively. These volume expansions results in crack healing. However, the crack healing in the SiN films did not almost occur, while it was observed in SiN/SiC nanolaminated films. This suggests that the activation energy of oxidation in SiC is lower than that in SiN [6]. Therefore, it can be concluded that the SiC layer is the major contributing factor to crack healing in the SiN/SiC nanolaminated films.

The influence of the heating temperature on the self-crack-healing behavior was investigated. The heating temperature was varied from 873 to 1473 K and the heating time was fixed at 24 h. Figure 2 shows the FE-SEM images of crack after heating. Slight crack healing occurred at 873 K. Crack healing improved with an increase in the heating temperature, and heating at 1273 K perfectly healed the crack. However, at 1473 K, the laminated structure disappeared because of oxidation even though the crack was healed. This suggests that the SiN/SiC nanolaminated cannot use cyclically for self-healing material once the film is heated at temperature over 1473 K.

The influence of heating time on the self crack healing behavior was also investigated. The heating time was varied from 24 to 96 h at temperatures of 873 K.

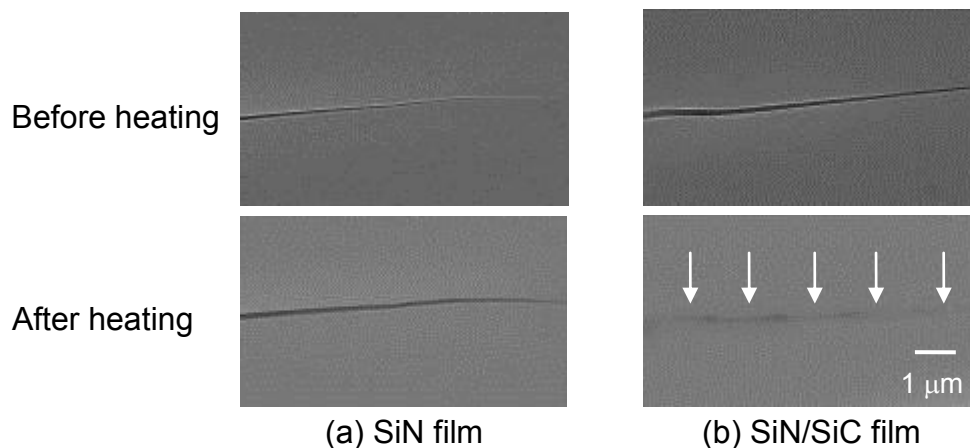


Figure: 1 FE-SEM images of crack tip before and after heating. The upper and below images indicate crack before and after heating respectively.

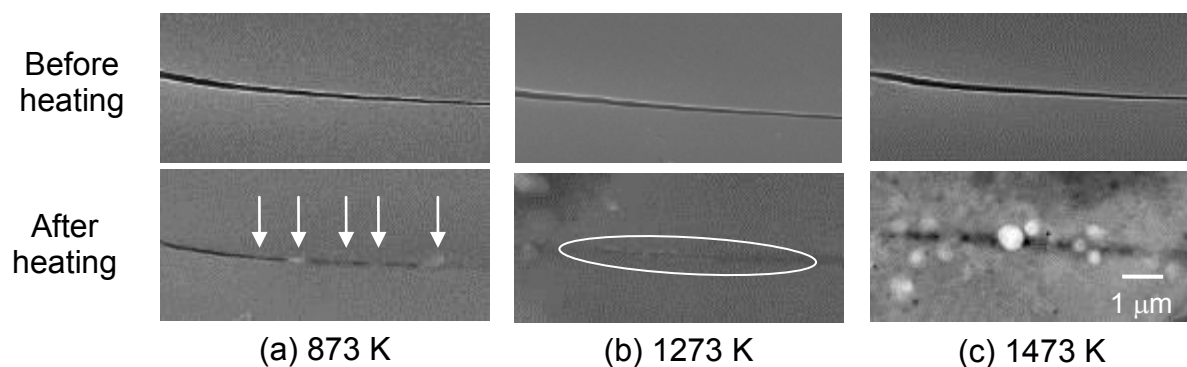


Figure 2: Influence on heating temperature on the crack healing. The upper and below images indicate crack before and after heating respectively.

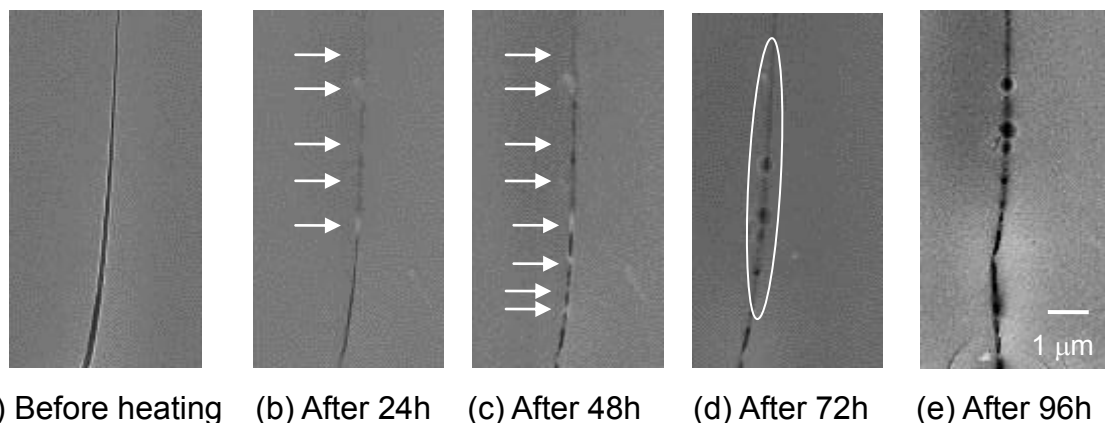


Figure 3: Influence on heating time on the crack healing in SiN/SiC film.

Figure 3 shows the FE-SEM images of the cracks after heating. The crack healing improved with an increase in the heating time. However, the crack healing stopped after heating for 72 h despite the crack did not heal perfectly.

4. CONCLUSION

In this study, the self-crack-healing ability of SiN/SiC nano-laminated thin film under high temperature environment was investigated. In SiN monolayer film, cracks were poorly healed because the size of the crack opening increased significantly during heating. On the other hand, SiN/SiC nano-laminated films exhibited a superior self-crack-healing ability. Crack healing was promoted by an increase in the heating temperature and time. However, at temperatures over 1473 K, the laminated structure disappeared and the film was subjected to oxidation overall.

ACKNOWLEDGEMENTS

The authors acknowledge financial support from JSPS KAKENHI Grant Number 23656091.

REFERENCES

- [1] K. Houjou, K. Ando, S.-P. Liu, S. Sato, Crack-healing and oxidation behavior of silicon nitride ceramics, *Journal of the European Ceramic Society* 24 (2004) 2329–2338.
- [2] Y.-S. Jung, Y. Guo, W. Nakao, K. Takahashi, K. Ando, S. Saito, Crack-healing behaviour and resultant high-temperature fatigue strength of machined Si₃N₄/SiC composite ceramic, *Fatigue and Fracture of Engineering Materials and Structures* 31 (2008) 2–11.
- [3] J.-F. Gao, J.-P. Suo, Proposal of self-healing coatings for nuclear fusion applications, *Surface and Coating Technology* 204 (2010) 3876–3881.
- [4] J. K. Hirvonen, Ion beam assisted thin film deposition, *Material Science Report* 6 (1991) 215–274.
- [5] Z.-G. He, S. Inoue, G. Carter, H. Kheyrandish, J. S. Colligon, Ion-beam-assisted deposition of Si-carbide films, *Thin Solid Films*, 260 (1995) 32–37.
- [6] L. Ogbuji, E.J. Opila, A comparison of the oxidation-kinetics of SiC and Si₃N₄, *Journal of the Electrochemical Society* 142 (1995) 925-930.

PROTECTIVE COATINGS WITH MULTI-LEVEL SELF-HEALING PROPERTIES

M.L. Zheludkevich¹, J.Tedim¹, M.G.S. Ferreira¹

¹ *Department of Materials and Ceramic Engineering, CICECO, Universidade de Aveiro, 3810-193 Aveiro, Portugal*

Keywords: coating, self-healing, corrosion, nanocontainer, inhibitor, nanotrap

ABSTRACT

The new active anticorrosion coating systems are currently under dynamic development because of continuously growing demands of different industries such as aeronautics and car manufacturing. Recently, a new concept of multi-level self-healing based on “smart” nanocontainers was introduced. In the present work we briefly overview various active protection mechanisms achieved via utilization of nanoreservoirs with different healing agents such as corrosion inhibitors, monomers, and water repellents. The specific focus is given to the coating systems containing layered double hydroxides. Layered double hydroxide (LDH) nanocontainers are among the most interesting systems since they confer the delivery of inhibitors on demand under action of corrosion-relevant triggers such as the presence of corrosive anions or local change of pH. The additional active functionality of LDHs is possibility to trap aggressive ions preventing their interaction with coated metallic substrates.

In this paper, we report both the use of LDH based nanocontainers and nanotraps as well as nanostructured LDH-container layers directly formed on metallic surfaces as a result of conversion reaction.

The LDH nanocontainers are prepared by co-precipitation methods followed by anion-exchange used for loading nanocontainers with corrosion inhibiting species. The release kinetics of inhibitors was studied under action of two different triggers namely pH and concentration of aggressive anions. The polymer coatings with LDH nanocontainers confer significant self-healing ability and provide improvement in long-term performance on both the galvanized steel and aluminum alloys.

The LDH container layer loaded with vanadate ions also provides an efficient active corrosion protection and can be used as a functional layer in self-healing coating systems. This simple methodology is easy to implement at an industrial level as it does not require exotic conditions, being also environmentally friendly.

NOVEL TYPES OF SELF-HEALING COATINGS FOR CORROSION PROTECTION OF METAL SUBSTRATES

O. van den Berg^{1,2}, J. Van Damme^{1,2}, F. Du Prez^{1,2}

¹ Department of Organic Chemistry, Polymer Chemistry Research Group, Ghent University, Krijgslaan 281 S4-bis, B-9000 Ghent, Belgium.

² SIM vzw, Technologiepark 935, 9052 Zwijnaarde, Belgium

Keywords: self-healing, polyester-urethane acrylate, shape-memory

ABSTRACT

In this work a new concept for simultaneous healing of barrier properties, passivation of the metallic substrate and the esthetic qualities of coatings is discussed. Using strain-recovering (shape-memory) materials, low-viscous UV-cure coating formulations were prepared with either amorphous or semi-crystalline switching units.



Figure 1. Example of an amorphous shape-recovery coating after scratching and recovery

These formulations were successfully applied onto metallic and polymeric substrates to yield coatings that are able to recover from large defects (up to ~ 1 mm in width). Full closure of the defects was observed, similar to the work recently published [1] by Rodriguez et al., however, without the addition of linear, non-functionalized polymer.

REFERENCES

[1] E.D. Rodriguez, X. Luo, P.T. Mather, Linear/Network Poly(ϵ -caprolactone) Blends Exhibiting Shape Memory Assisted Self-Healing (SMASH), ACS Applied Materials & Interfaces 3 (2011) 152-161.

SELF-HEALING COATINGS UTILIZING A SHAPE MEMORY EFFECT

P. T. Mather¹, X. Luo¹, S. M. Kowalski¹, and E. D. Rodriguez¹

¹ *Syracuse Biomaterials Institute, Syracuse University, 318 Bowne Hall, Syracuse, NY USA –
e-mail: ptmather@syr.edu; luoxiaof@gmail.com; smkowals@syr.edu;
erikarodriguez06@gmail.com*

Keywords: shape memory polymer, self-healing coating, corrosion, optical coatings

ABSTRACT

Self-healing (SH) coatings are desired for the reduction or repair of corrosion cause by mechanical damage. SH coatings, particularly clear coatings, are also sought for the facile or autonomous repair of mechanical damage to optical lenses. In this report we will present and compare two distinct approaches to self-healing coatings that share in common the use of a shape memory effect but differ dramatically in process and microstructure.

Our first approach is that of an immiscible blend prepared by a combination of electrospinning and spin-coating. The coatings feature a phase-separated morphology with electrospun thermoplastic poly(ϵ -caprolactone) (PCL) fibers randomly distributed in a shape memory epoxy matrix. Mechanical damage to the coating can be self-healed via heating, which simultaneously triggers two events: (1) the shape recovery of the matrix to bring the crack surfaces in spatial proximity, and (2) the melting and flow of the PCL fibers to rebond the crack. In controlled healing experiments, damaged coatings not only heal structurally, but also functionally by almost completely restoring the corrosion resistance.

Comparison will be made to our second approach involving a transparent blend of linear acrylate copolymer with a crosslinked acrylate copolymer network. Shape memory assisted self-healing enabled crack closure and linear polymer chain diffusion to rebond damaged surfaces. Coatings on glass were prepared by mold-filling and UV-cure, followed by asymmetric demolding that yielded a coating on one glass surface. Coating with a range of composition were prepared in this manner and subjected to scratch damage and subsequent heat-induced recovery. We found that an optimum glass transition temperature exists for maximum healing efficiency.

PLENARY SESSION – MODELLING AND NUMERICAL ANALYSIS TOOLS

STRAIN RECOVERY AND SELF-HEALING IN DUAL CROSS-LINKED NANOPARTICLE NETWORKS

B. Iyer¹, V. Yashin¹, T. Kowalewski², K. Matyjaszewski² and A. C. Balazs¹

¹ *Chemical Engineering Department, University of Pittsburgh, 3700 O'Hara St., Pittsburgh, Pennsylvania 15261, USA – e-mail: bav16@pitt.edu; vvy1@pitt.edu; balazs@pitt.edu*

² *Department of Chemistry, Carnegie Mellon University, 4400 Fifth Ave., Pittsburgh, Pennsylvania 15213, USA – e-mail: tomek@andrew.cmu.edu, km3b@andrew.cmu.edu*

Keywords: computer simulations, nanoparticle networks, self-healing materials, mechanical recovery

ABSTRACT

Via computational modeling, we investigate the mechanism of strain recovery in dual cross-linked polymer grafted nanoparticle (PGN) networks. The individual nanoparticles are composed of a rigid spherical core and a corona of grafted polymers that encompass reactive end groups. With the overlap of the coronas on adjacent particles, the reactive end groups form permanent or labile bonds, and thus form a “dual cross-linked” network. We consider the strain recovery of the material after it is allowed to relax from the application of a tensile force. Notably, the existing labile bonds can break and new bonds can form in the course of deformation. Hence, a damaged material could be “rejuvenated” both in terms of the recovery of strain and the number of bonds, if the relaxation occurs over a sufficiently longtime. We show that this rejuvenation depends on the fraction of permanent bonds and strength of labile bonds. Specifically, we show that while an increase in the labile bond energy leads to formation of a tough material, it also leads to delayed strain recovery. Further, we show that an increase in the fraction of permanent bonds yields improved recovery even after multiple stretch-relaxation cycles.

1. INTRODUCTION

The functionalization of nanoparticles with polymeric chains permits these particles to be cross-linked into extensive networks that can exhibit remarkable mechanical properties [1]. “Dual cross-links”, which combine both “permanent” and labile bonds, are known to significantly improve the mechanical properties of polymer gel networks [2]. Here, we use a computational model to study how the dual cross-links affect the elastic and inelastic behavior of polymer grafted nanoparticle (PGN) hybrid materials that are stretched and relaxed (by gradually decreasing the applied force). Simulating the response of these networked PGNs to the application and gradual removal of an applied force is challenging because all the relevant length and time scales should be captured in one specific model. Namely, the model must span a range of architectural features and temporal events. Our recently developed approach [3] encompasses the following components: 1) the essential structural features of the polymer grafted nanoparticles, 2) the interactions between the coated particles, 3) the kinetics of bond formation and rupture between the reactive groups on the polymer chains that form the coating, and 4) the resulting global response of a macroscopic sample to an applied tensile force.

Building on this multi-component model, we now formulate a procedure for applying a strain-controlled tensile deformation to the material and then a force-controlled release of that deformation. Via this protocol, we specifically determine how the energies of the labile bonds, and the amount of “permanent” bonds in the network affect the recovery of the materials properties and self-healing of the sample after loading and unloading. We also determine how the material behaves after multiple cycles of this strain-controlled deformation and stress-controlled relaxation. Below, we first detail our hybrid, multi-component model.

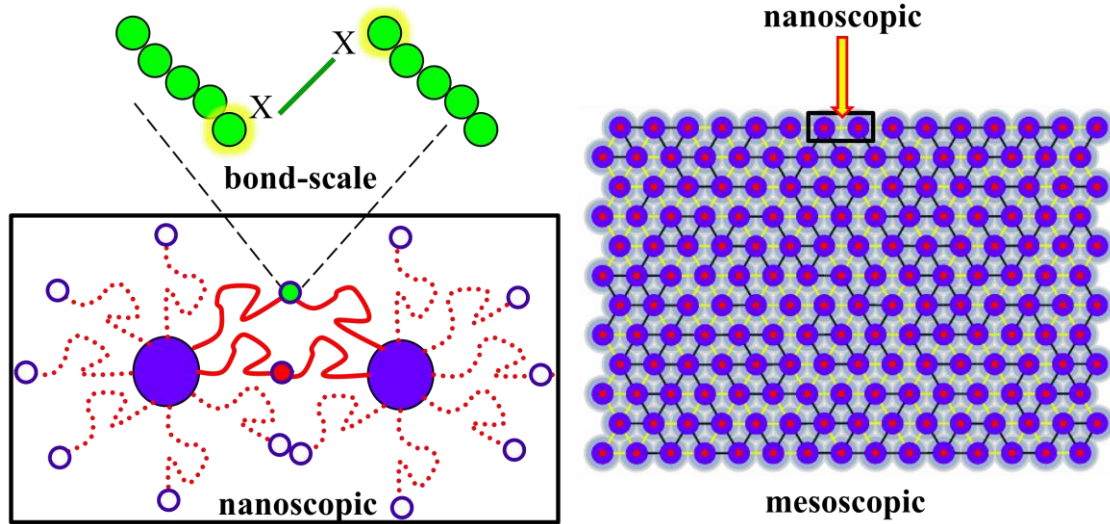


Figure 1: Multiscale interactions in a network of dual cross-linked PGNs.

2. METHODOLOGY

Our system consists of a swollen network of cross-linked polymer-grafted spherical nanoparticles (PGNs), which are cross-linked by a combination of “permanent” and labile bonds to form an extended network (see Fig. 1). The center-to-center separation between these coated particles is R . The interaction between two such PGNs is modeled through a sum of interaction potentials, which is given by $U_{int} = U_{rep} + U_{coh} + U_{link}$. The first term characterizes the repulsive interactions between the coated nanoparticles and is given by [3,4]:

$$\frac{U_{rep}(R)}{k_B T} = \frac{5}{8} f^{3/2} \times \begin{cases} -\ln(R/\sigma) + (1 + f^{1/2}/2)^{-1} & , R \leq \sigma \\ (1 + f^{1/2}/2)^{-1} (\sigma/R) \exp[-f^{1/2}(R - \sigma)/2\sigma] & , R > \sigma \end{cases} \quad (1)$$

Here, f is the number of arms, and $\sigma = 2(1+q)(1+2f^{-1/2})^{-1}$ is the range of the potential, which is related to the diameter of the last blob in the Daoud-Cotton (DC) model [5,6]. The second term in the potential describes the attractive cohesive interaction between the coated particles and is chosen to have the form:

$$U_{coh}(R) = -C \{1 + \exp[(R - A)/B]\}^{-1} \quad (2)$$

where, C is an energy scale, and A and B are length scales [7].

The final term in the potential, U_{link} , describes the attractive interaction between particles that are linked by the bonded polymer arms. The attractive force acting between the two bonded particles is given by the following equation [3]:

$$F_{link}(r) = N_b \kappa(r) r \quad (3)$$

where, N_b is the number of bonds formed between the given pair of particles, and $\kappa(r)$ is the spring constant, which increases progressively with the chain end-to-end distance $r = R - 2$ [3]. The stiffening of the chain is described by the following equation obtained for a worm-like chain [8]:

$$\kappa(r) = \kappa_0 \{1 + 2[1 - r^2(2L)^{-2}]^{-2}\} \quad (4)$$

In the above equation, $2L$ is the contour length of the chain formed by bonding two corona arms of length L .

The number of polymer cross-links, N_b , formed between two PGNs by the bonding of the polymer arms depends on the extent of overlap between the coronas of the nanoparticles, and on the kinetics of bond formation and rupture [3]. The set of bonded arms are referred to as a link; in other words, each link in the network corresponds to multiple re-formable bonds. At the individual bond level, we use the Bell model [9] to describe the rupture and re-formation of bonds due to thermal fluctuations. The rupture rate, k_r , increases exponentially with the applied force $k_r = k_{0r} \exp(\gamma_0 F)$, where $k_{0r} = \nu \exp(-U_0/k_B T)$ is the rupture rate in the zero force limit. The formation rate, k_{0f} , is assumed to be a constant. We note that it is only the labile bonds that can reform after breaking; the permanent bonds can only break. The evolution equation for the number of bonds can be written as [3]:

$$\frac{dN_b}{dt} = -k_r(R)N_b + P_c(R)k_{0f}[N_{max}(R) - N_b]^2 \quad (5)$$

where $N_{max}(R)$ is the maximum number of chain ends that could be found in the overlap volume and $P_c(R)$ is the probability of contact of two chain ends [3].

The dynamics of the system is assumed to be in the overdamped regime; hence, the motion of each particle described by the equation $d\mathbf{x}/dt = \mu \mathbf{F}_{tot}$, where μ is the mobility and \mathbf{F}_{tot} is the total force on the polymer grafted particle. The total force acting on a particle can be written as $\mathbf{F}_{tot} = -\partial U_{int}/\partial \mathbf{x} + \mathbf{F}_{ext}$, where \mathbf{F}_{ext} is the external force acting on the edge particles of the particle array (see Fig 1). This equation is solved numerically in two steps since the polymer spring force (within the expression for F_{tot}) in the dynamic equation depends on the number of bonds between particles and consequently, on the evolution of the chemical kinetics given by eq. (5). In the first step, we determine the number of bonds at any given time, $N_b(t)$, by evolving numerically the unsteady state kinetics, eq. (5), through an explicit Euler scheme with a time step of $10^{-2}T_0$, where T_0 is the unit of time in the simulation. Note that the numerical evolution of eq. (5) yields a real number, whereas the number of bonds $N_b(t)$ should take discrete integer values. In order to determine the integer value, we compare the fractional part of the numerical result, $\{N_b(t)\}$, with a random number ξ

distributed uniformly between 0 and 1. If $\{N_b(t)\} < \xi$, then we truncate the result; otherwise, we increment the integer part of the result by 1. In the second step, we use this value for the number of bonds to calculate the spring force (see eq. (3)) in the dynamic equation and integrate numerically the resulting equation using a fourth-order Runge-Kutta algorithm with a time step of $10^{-2}T_0$.

Each sample considered here is composed of $N_{PGN} = 180$ particles, which are initially arranged in 12 rows, with 15 particles in each row (see Fig. 1). To quantify the mechanical properties and strain recovery, eight independent runs are performed on samples at each set of model parameters. The strain ε is calculated as the ratio of the extension of the sample to its length in the undeformed state. Via our computer simulations, we employed a three-step procedure to study the strain recovery of the material (see Fig 2a). In the first step, the sample is subjected to a strain-controlled tensile deformation by pulling the left edge of the sample at a constant velocity of $v = 0.001$, which corresponds to roughly 3.55 nm/s, until the desired maximal value of strain, ε_{\max} , is reached. The values of ε_{\max} are chosen to not exceed the strain at break. The external tensile force F acting on the left edge of the sample is recorded as a function of ε during the first step. In the second step, the force F is relaxed to zero at a constant rate over $10^4 T_0$ time steps, and the strain ε is recorded (force-controlled strain relaxation). The inelastic component of the deformation is characterized by the residual strain, ε_0 , which is recorded at the moment of time when $F = 0$. Finally, in the third step of the procedure, the relaxation of the residual strain at zero external force is tracked over some period of time. To elucidate the mechanism of strain recovery, the samples are subjected to either single or multiple cycles of the stretching and relaxation procedure.

3. RESULTS AND DISCUSSION

Using the model described above, we determine how the key parameters of the system affect the strain recovery in dual cross-linked networks of PGNs, which are subjected to tensile loading and unloading. We begin by analyzing the effects of varying the energy of the labile bonds, $U_0^{(l)}$, on the mechanical response of the material; here, the average number of permanent bonds between a pair of neighboring PGNs was initially set to $P = 1$ (i.e., during the initial generation of the sample).

A. Effect of varying the bond energy of the labile bonds

To obtain insight into the role that the bond energy of the labile bonds plays in the strain recovery process, we consider the deformation of samples with $U_0^{(l)} = 33, 37$ and $39 k_B T$. As indicated in Figure 2a, at $0 \leq t \leq 2.5 \times 10^4 T_0$, the samples were stretched at a constant strain rate until the strain reaches the maximal value $\varepsilon_{\max} = 0.53$. Then, at $t > 2.5 \times 10^4 T_0$, the force F was released at a constant release rate such that $F = 0$ at $t = 3.5 \times 10^4 T_0$. We use the term “recovery” for the relaxation processes that occur after $F = 0$ is reached. From these simulations, we obtain the set of plots in Figure 2, which shows the strain ε (Fig 2a) and number of labile bonds per particle $N_b^{(l)}/N_{PGN}$ (Fig 2b) as a function of time t .

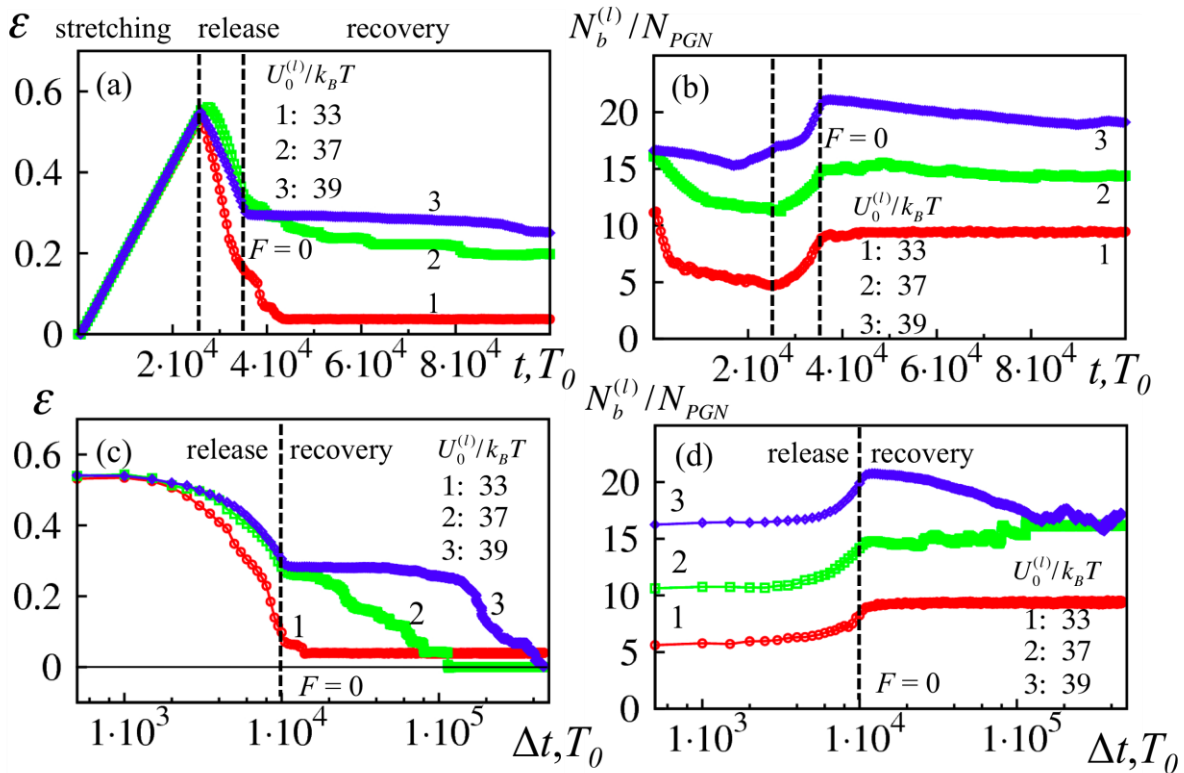


Figure 2: Response of the network to tensile strain applied at a constant velocity and a subsequent controlled, linear decrease of the force. After $F = 0$, the sample continues to undergo recovery. (a) Strain (ε) versus time (t). (b) Number of labile bonds per particle ($N_b^{(l)}/N_{PGN}$) versus time (t). (c) (ε)-(Δt) curves. (d) ($N_b^{(l)}/N_{PGN}$)-(Δt) curves during release and recovery. The plots are from a single simulation run.

Figure 2 clearly shows that the behavior of the dual cross-linked PGNs depends strongly on the strength of the labile bonds. In particular, Figure 2a indicates that some part of this deformation is inelastic since the samples exhibit residual strain upon release of the external load; the residual strain is considerably lower in the sample having the weaker labile bonds than in the other two samples (compare curve 1 with curves 2 and 3 in Figure 2a). Additionally, Figure 2a shows that the recovery of the residual strain in the unloaded samples at $t > 3.5 \times 10^4 T_0$ becomes remarkably slow as the energy of labile bonds increases from $U_0^{(l)} = 33 k_B T$ (curve 1) to 37 and $39 k_B T$ (curves 2 and 3, respectively).

During the course of the deformation, the rupture of stressed labile bonds occurs simultaneously with the formation of new bonds within the overlapped coronas. Figure 2b shows that $N_b^{(l)}/N_{PGN}$ drops during the initial stretching of a sample, and this decrease slows down even though the stretching continues. The latter behavior indicates that the rupture of stressed bonds is balanced by bond formation. Further, Figure 2b shows that owing to the bond formation, the labile bonds are restored in the samples during the release of force ($N_b^{(l)}/N_{PGN}$ increases at $2.5 \times 10^4 T_0 < t < 3.5 \times 10^4 T_0$), thus, clearly indicating that the material is capable of self-healing. Figure 2b indicates that during the strain controlled stretching there is greater number of the labile bonds in the samples with higher $U_0^{(l)}$.

The relaxation of strain and of the labile bonds continues in the system after the tensile force is released and the system reaches the $F=0$ state. To highlight this behavior, we specifically focus on the time frame around $F=0$ in Figures 2c and 2d. Note that Figure 2c and 2d shows the behavior of the system during the release of force and recovery ($t > 2.5 \times 10^4 T_0$), as well as the dynamics of recovery at longer times (up to $5 \times 10^5 T_0$). From the latter plots, we clearly see that the rate and extent of recovery depend on the energy of the labile bonds. In the system having the weaker labile bonds ($U_0^{(l)} = 33 k_B T$), the recovery occurs during $\sim 1 \times 10^4 T_0$ (see Figure 2c). The residual strain, however, is not recovered completely and remains about 4% in this case. Additionally, the number of labile bonds is lower than its initial value (as can be seen by comparing curve 1 at $t=0$ in Figure 2b and late times in Figure 2d). In contrast, at the labile bond energies of $U_0^{(l)} = 37$ and $39 k_B T$, the recovery is markedly slower than in the case of weaker bonds and takes about $1 \times 10^5 T_0$ and $5 \times 10^5 T_0$, respectively (see Figure 2c). Furthermore, in these cases, the strain and the number of labile bonds exhibit a complete recovery that occurs in two distinct stages, as can be seen from curves 2 and 3 in Figures 2c and 2d, respectively. At the first stage the number of labile bonds relax close to the initial one (i.e., to the one before deformation) while in the second stage strain recovery happens around a constant value of $N_b^{(l)}/N_{PGN}$.

Recovery of the residual strain and the labile bonds at $F=0$ and beyond occurs through local rearrangements of the PGNs. The motion of these nanoparticles relative to each other is limited by the rate of breakage of the labile bonds. Note that the labile bonds break less often as the bond energy is increased. Therefore, the rate of recovery decreases with an increase in $U_0^{(l)}$. Notably, $U_0^{(l)}$ also controls the degradation of the cross-linked system in the course of deformation [3]. An increase in the energy of labile bonds from 33 to $37 k_B T$ and higher prevents the formation of large voids, which cannot be healed during recovery. Hence, complete strain recovery is observed at $U_0^{(l)} = 37$ and $39 k_B T$.

B. Effect of varying the fraction of permanent bonds

Permanent bonds form an elastic skeleton in the dual cross-linked nanoparticle network; the presence of these bonds can lead to notable improvements in the toughness of the material [3]. We anticipate that the permanent bonds between the PGNs will also play an important role in the strain recovery within the sample. To test this hypothesis, we vary the average number of permanent bonds between two particles over the range $1 \leq P \leq 2$, while fixing the labile bond energy at $U_0^{(l)} = 37 k_B T$.

As in the previous section, we examine the behavior of dual cross-linked PGNs that were strained to the maximum extension of $\varepsilon_{\max} = 0.53$, and then subjected to the force-controlled relaxation during the period of time $10^4 T_0$, followed by the recovery process. We can obtain insight into the effect of permanent bonds by examining snapshots from simulations of samples in the process of recovery, i.e., after the force in the sample is released. Figures 3a and 3b show the nanoparticles and the labile bonds in the samples at $P=1$ and $P=2$, respectively, at $\Delta t = 1.5 \times 10^4 T_0$ and $7.5 \times 10^4 T_0$. Figure 3a reveals that at $P=1$, there are a number of voids of various sizes distributed throughout the sample during recovery. In contrast, Figure 3b shows

that upon unloading all the voids are healed by $\Delta t = 7.5 \times 10^4 T_0$ due to the increase in the number of permanent bonds from $P = 1$ to $P = 2$.

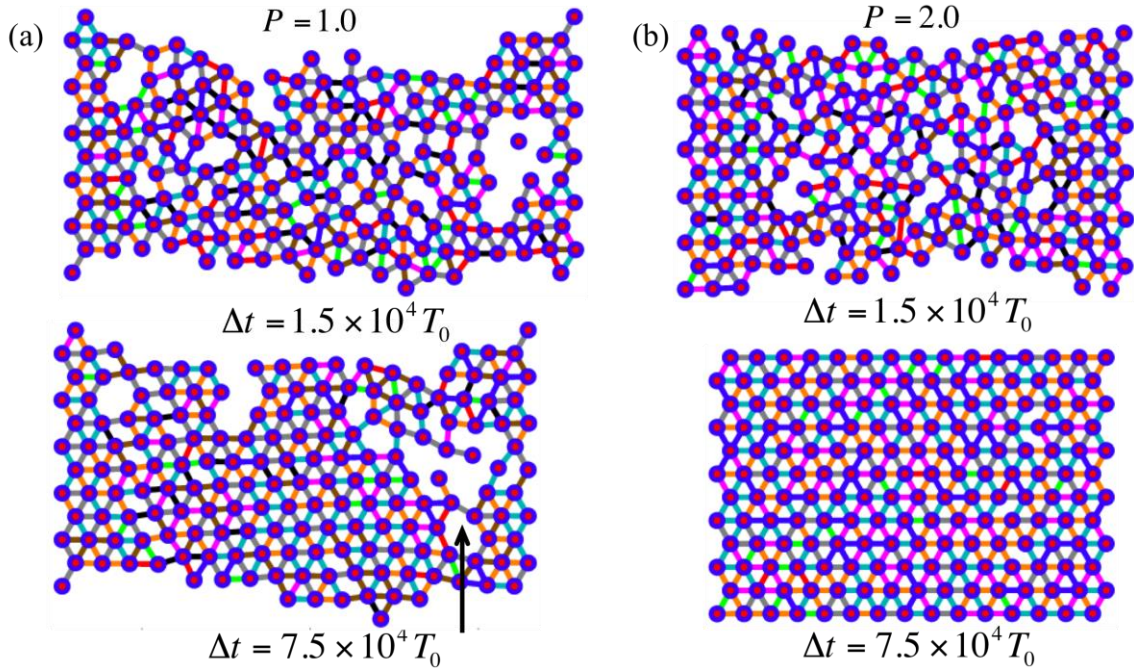


Figure 3: Snap shots of the sample during recovery (a) $P = 1$ (b) $P = 2$

C. Effect of applying multiple cycles of stretching and relaxation

In the above studies, we showed that the structure of the sample could be recovered (rejuvenated) after the forces were released, and that the extent of healing depends on the fraction of the permanent bonds in the network. We now examine the recovery process for systems subjected to multiple cycles of strain and relaxation.

We quantify the influence of P on the properties of materials undergoing multiple deformations by calculating the hysteresis ΔW , which is defined as the area confined within a force-strain loop. Figure 4 shows the material properties of samples that are subjected to repeated deformations where the maximal strain, ε_{\max} , is increased incrementally with each subsequent cycle. Namely, $\varepsilon_{\max} = 0.1$ in the first cycle and $\varepsilon_{\max} = 0.53$ in the fifth cycle. As above, the consecutive cycles of strain-controlled tensile deformation are followed by the force-controlled relaxation during $10^4 T_0$ and the samples are allowed to recover during the time $5 \times 10^4 T_0$ before the next cycle. Figure 4a shows the force-strain curves for five consecutive cycles at the fraction of permanent bonds of $P = 2$. The curves correspond to a single simulation run at $U_0^{(l)} = 37 k_B T$. While the residual strain increases with an increase in ε_{\max} , the healing of the sample is complete; that is, the strain eventually goes back to $\varepsilon = 0$. However, the recovery is incomplete in the $P = 1$ sample for strain values $\varepsilon_{\max} > 0.31$ and results in modified behavior during the consecutive cycle (see Figure 3a and Figure 4b). In contrast, the sample having more permanent bonds (at $P = 2$) recovers completely after each cycle (Figure 4a).

Figure 4b shows that the average hysteresis ΔW (obtained from 8 simulations) increases with an increase in the maximal strain for all samples at $\varepsilon_{\max} < 0.42$. Furthermore, while the hysteresis of the samples at $P=2$ is slightly lower than that at $P=1$ at $\varepsilon_{\max} < 0.42$ and continues to increase for increasing strains, the hysteresis for the $P=1$ samples levels off at $\varepsilon_{\max} > 0.31$. The results indicate that there is higher energy loss with increasing extents of maximum strain due to, in particular, the increase in the residual strain. In addition, at $\varepsilon_{\max} \leq 0.31$, the energy loss is higher at $P=1$ than that at $P=2$. Beyond the latter strain, the deterioration of the sample that occurs at $P=1$ leads to a reduction in ΔW (see curve 1 in Figure 4b). Thus, an increase in the fraction of permanent bonds is seen to improve recovery.

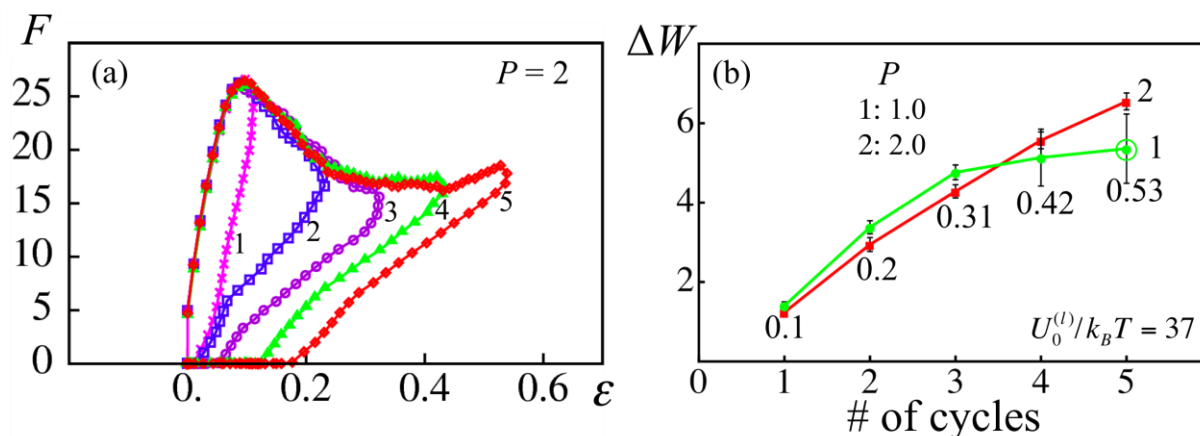


Figure 4: Effect of strain-relaxation cycles on recovery. (a) Force(F)-strain(ε) curves for repeated cycles at $P=2.0$. (b) Hysteresis, ΔW , as a function of number of cycles at $P=1$ and 2. Open circles indicate conditions when one of the samples fracture.

4. CONCLUSION

We examined the strain recovery and healing characteristics of dual cross-linked PGN networks via a hybrid computational model that integrates the kinetics of individual bond rupture/formation with the nano- and meso-scopic structure of the system. Our findings showed that an increase in the energy of the labile bonds led to a decrease in the residual strain within the material. The increase in $U_0^{(l)}$ did, however, also lead to an increase in the time scale needed for recovery; this is due to the decrease in the rate of bond breakage with increasing $U_0^{(l)}$. These results highlight a competition between the extent and rate of recovery with increasing energies for the labile bonds. For, the studies considered here, the value $U_0^{(l)} = 37k_B T$ led to an optimal compromise, with the relaxed sample returning to $\varepsilon=0$ on timescales that lay between the $U_0^{(l)} = 33k_B T$ and $U_0^{(l)} = 39k_B T$ extremes.

By examining snapshots from the simulations, we found that the $P=2$ networks displayed a more pronounced relaxation of voids within the samples and hence, greater healing than the $P=1$ materials. We also examined the extent of healing and recovery that occurs after the PGN networks were subjected to multiple cycles of stretching and relaxation. Using the hysteresis, ΔW , as a measure of the extent of damage recovery, we found that the $P=1$ materials showed progressive deterioration with consecutive cycles of stretching and relaxation. In contrast, at a higher amount of permanent cross-links ($P=2$), the networks recovered completely

after consecutive cycles of stretching and relaxation. Thus, introduction of additional permanent cross-links to the dual cross-linked PGN networks can prevent the effects of pre-stressing by healing defects that were created during deformation unlike filled rubber and thermoplastic elastomers [10].

In summary, these results indicate that the dual cross-linking strategy provides an effective means of designing self-healing PGN networks. The results of these computer simulations reveal how choices in the materials parameters, such as the energy of the labile bonds and fraction of permanent bonds, affect the final mechanical performance of the material.

REFERENCES

- [1] K. E. Mueggenburg, X. M. Lin, R. H. Goldsmith, H. M. Jaeger, Elastic membrane of close-packed nanoparticle arrays, *Nature Materials* 6 (2007) 656-660.
- [2] J. P. Gong, Y. Katsuyama, T. Kurokawa, Y. Osada, Double-network hydrogels with extremely High mechanical strength, *Advanced Materials* 15 (2003) 1155-1158.
- [3] B. V. S. Iyer, I. G. Salib, V. V. Yashin, T. Kowalewski, K. Matyjaszewski, A. C. Balazs, Modeling the response of dual cross-linked nanoparticle networks to mechanical deformation, *Soft Matter* 9 (2013) 109-121.
- [4] C. N. Likos, H. Löwen, M. Watzlawek, B. Abbas, O. Jucknischke, J. Allgaier, D. Richter, Star polymers viewed as ultrasoft colloidal particles, *Physical Review Letters* 80 (1998) 4450-4453.
- [5] A. Jusufi, M. Watzlawek, H. Löwen, Effective interaction between star polymers, *Macromolecules* 32 (1999) 4470-4473.
- [6] M. Daoud, J. P. Cotton, Star shaped polymers: a model for the conformation and its concentration dependence, *J. Phys (Paris)* 43 (1982) 531-538.
- [7] F. Lo Verso, C. N. Likos, L. Reatto, Star polymers with tunable attractions: cluster formation, phase separation, reentrant crystallization, *Progress in Colloid Polymer Science* 133 (2006) 78-87.
- [8] A. V. Dobrynin, Y. J. Carrillo, Universality in nonlinear elasticity of biological and polymeric networks and gels, *Macromolecules* 44 (2011) 140-146.
- [9] G. Diezemann, A. Janshoff, Dynamic force spectroscopy: analysis of reversible bond-breaking dynamics, *Journal of Chemical Physics* 129 (2008) 0849041-10.
- [10] J. E. Mark, B. Erman and F.R. Eirick (Eds.), *Science and technology of rubber*, 2nd ed., Academic Press, San Diego, 1994.

SESSION 23 – SELF-HEALING CEMENTITIOUS MATERIALS

CRACK SELF-HEALING EFFECT ON PERFORMANCE OF REINFORCED CONCRETE MEMBERS SUBJECTED TO WATER SUPPLY AND CYCLIC LOADING

P. V. Truong¹, T. Kishi² and M. Kayondo¹

¹Kishi Laboratory, Institute of Industrial Science, The University of Tokyo, 4-6-1 Komaba, Meguro-ku, Tokyo, Japan – email: phuong80@yahoo.com; email: kayondo@iis.u-tokyo.ac.jp

²Institute of Industrial Science, the University of Tokyo, 4-6-1 Komaba, Meguro-ku, Tokyo, Japan, – email: kishi@iis.u-tokyo.ac.jp

Keywords: self-healing, crack, additives, cyclic loading, fatigue life

ABSTRACT

Self-healing concrete (SHC) can heal itself from cracks and other minor imperfections and thus prolong the life of the material itself and structure. In plain and reinforced concrete structures, fatigue is one of the major causes of both material and structural failures. Under the moving load due to traffic, it is not only the relatively simple opening and closing action in the transverse direction to the crack plane but also the severe reversed shear displacement along the crack plane. This accelerates the deterioration on the shear transfer mechanism at the crack surface. Although the shear transfer between two cracks accelerates the rupture of crack surface, a lot of crushed powders and fragments are produced in the crack. Even in this severe situation it is expected for self-healing concrete that crushed powders and fragments would bring the healing effect to cracks and then water leakage through cracks would reduce. When cracks form, the release of effective components from the SHA (Self-healing additives) would be promoted. Under cyclic loading, not only opening-closing action, but also reversed shear transfer are repeated and then the release of effective components from SHA would be accelerated. To verify this interesting scenario several SHA were applied to specimens of structural reinforced members subjected to cyclic loading in a series of tests. In this study, flexural fatigue tests were conducted for three different types of Self-healing concrete (SHC) and the effect of self-healing at fracture process zone (FPZ) and cracks area on structural performance is examined. The experimental results indicate that one of SHC shows remarkable effect not only on water sealing in water pass tests but also prolongation of fatigue life in flexural tests.

1. INTRODUCTION

Cracks in concrete may accelerate the rate of chemical deterioration and reinforcement corrosion that affect the durability of infrastructures. Self-healing concrete is one of the modern smart concretes, which can heal the cracks by itself. These are the results of moisture interaction with un-hydrated cement clinker in the crack under some special situations [1].

The man-made self-healing ability of concrete (autonomic healing) which replaces a part of cement or sand by self-healing additives was introduced by many researches [1],[2]. From the water leakage tests of previous studies [1]-[3], the performance of new type self-healing additives showed remarkable decrease in crack width (crack width is smaller than 0.2mm, water passes through the cracks all the time).

In this research, crack self-healing effect on performance of reinforced concrete members subjected to water supply and cyclic loading is studied.

2. EXPERIMENTAL PROGRAM

The materials used in this study included the basic concrete materials (sand, cement aggregates) and self-healing additives that were manufactured in the laboratory, plus other concrete admixtures. Concrete was ready-mix from concrete plant and cast at the same time for all specimens. The mix proportions are shown in Table 1.

For the purpose of investigation, 14 specimen of 100×100×900mm were considered. To avoid the un-hydrated cements inside concrete specimens, which may disturb the result, all the specimens were cured under 40 Celsius degree hot water to make sure almost all the hydration process is finished [4]. After 1 month curing, 3 cracks with crack spacing 110mm were induced in the compressive zone of beam. Holes were induced for crack holding during test. The detail of specimen is shown in Figure 1. After initial cracks were induced at the top of specimens, cracks were kept open and curing done for two weeks.

Table 1: Mix proportions

Series	W/C	S/A	Fiber	Water	Cement	SHA	other	Sand	Gravel
	(%)	(%)	(kg/m ³)						
NC	49.6	51.3	0.65	175	353	-	-	900	869
SH30-LRA	49.6	51.3	0.65	175	353	240	60	600	869
SH10-G-S	49.6	51.3	0.65	175	353	123	-	777	869
SH27-LC	49.6	51.3	0.65	175	353	SHS 865.78		SHG 799.8	
Remarks	SH: self-healing; LRA: low reaction activation; LC: low heat cement; 30 is 30% of aggregate is replaced by self-healing additives; S: Swelling material based; SHS; SHG: self-healing additives + sand and gravel								

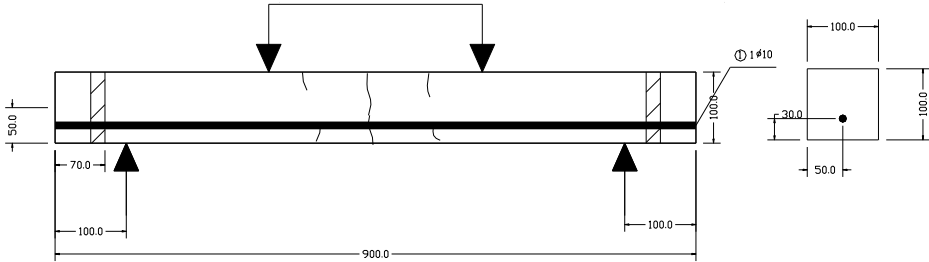


Figure 1: Profile of specimens

To investigate the degradation of flexural stiffness of concrete, a low reinforcement ratio was designed to ensure the failure stage is the same in all specimens. Ultimate capacity of the four types of concretes is the same; value 20kN is taken as the ultimate load. Mid span displacement of 4 mm was taken as the service criteria to quantify the life span of concrete member subjected to flexural loading in stress level 65% and 85% of ultimate capacity

3. EXPERIMENTAL RESULTS AND DISCUSSIONS

Because all the specimens are cured under hot water, it is assumed that almost all the hydration process in concrete is completed. Response of normal concrete in dry and wet condition under static flexural tests is shown in Figure 2a. The response of specimens in wet condition showed smaller flexural stiffness than normal concrete in dry condition. This can be explained as the reduction of compressive and tensile strength of concrete when it is wet.

The static flexural responses of SHC are shown in Figures 2 (b, c and d). Flexural stiffness recovery of SHC was found after curing. In case SH30-LRA and SH27-LC, the flexural stiffness of specimens under wet test was even larger than the specimen under dry test. It can be explained as the process of curing; the specimens were put up side down and bended on opposite direction to keep the crack open during curing period by bolt anchors.

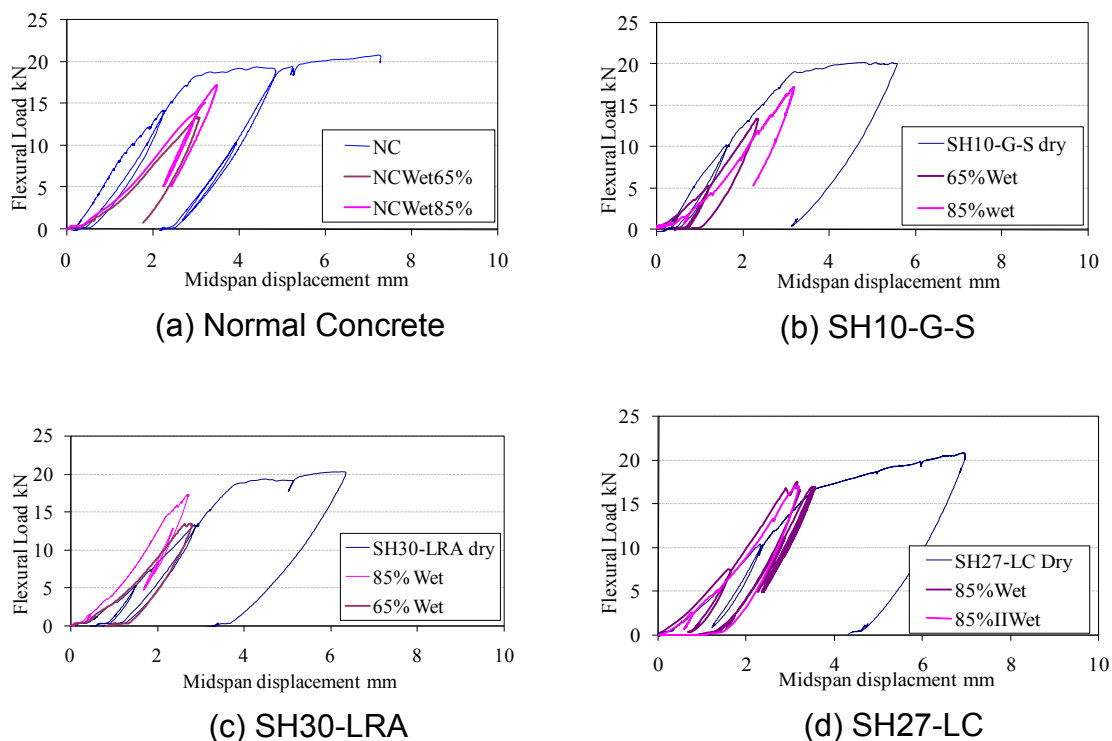


Figure 2: Response of concrete specimens in dry and wet condition

When the crack is opened, the SH products are activated and fill the cracks and harden after two weeks. After the bolt anchors on both sides of specimens were released, due to the existence of SH products on the cracks, the cracks could not close completely. In dry conditions, the damage was large in first stage due to the appearance of new cracks. It was observed from experimental results that from cycle 60000, the degeneration of stiffness was almost stopped (Figure 3a). The possible change was the plastic deformation of steel bar. Figure 3b shows the broken particles flushed out after test. The initial crack induced before tests are nearby the ink line. After the test, the initial cracks penetrated to the bottom of the specimens, gray color indicated the broken particles of concrete which was washed out by water. White color may be the self-healing products that formed after curing and one part of them were washed out by water. Therefore, SHC is expected to reduce the effect of water

into RC members by creating a self-healing solid layer; reducing the smoothness of crack surface, and then prolong the flexural fatigue endurance of RC structures. The results of the fatigue test are generally expressed in terms of S-N curves. The linear regression of specimens is shown in Figure 3c. SHC shows different level of improvement in comparison with normal concrete in wet condition. SH27-LC showed longer and stable flexural fatigue endurance than normal concrete.

The relationship between load and mid span displacement is shown in Figure 3a.

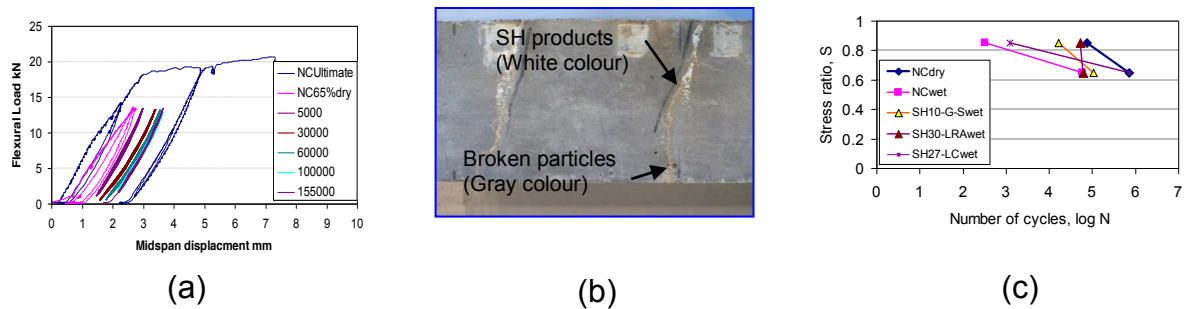


Figure 3: Cyclic load result, flushing effect and S-N curves

4. CONCLUSIONS

- Water is found to accelerate the degradation of concrete under flexural fatigue loading. Washing out of crushed particles was observed.
- The increase of flexural stiffness of SH30-LRA and SH27-LC were observed at the first cycle after curing.
- Self-healing additives may make flexural fatigue endurance of concrete member become longer than that of normal concrete in wet condition.

ACKNOWLEDGEMENTS

The authors wish to express their most sincere gratitude to Dr. Tae-Ho Ahn, IIS, The University of Tokyo, and Dr. Yuichi Otabe and Mr. Takao Koide, Sumitomo-Osaka Cement Corp. for the supply of self-healing agents, and the members of KISHI laboratory, IIS, The University of Tokyo for their help in the experiments.

REFERENCES

- [1] T. Kishi, T. Ahn, A. Hosoda, S. Suzuki, and H. Takaoka: Self-healing behaviour by cementitious recrystallization of cracked concrete incorporating expansive agent, First International Conference on Self-Healing Materials, Noordwijk, the Netherlands. 2007
- [2] T. Ahn and T. Kishi: Crack Self-healing Behaviour of Cementitious Composites Incorporating Various Mineral Admixtures. Journal of Advanced Concrete Technology Vol. 8, No. 26, June 2010, pp.171-184
- [3] T. Viet Phuong, Effect of expansive agent/ lightweight aggregate combination and self-healing technology on fatigue behaviour of RC. Doctoral Thesis, Sep, 2011
- [4] Heritage "Thermal Acceleration of Portland Cement Concretes Using Direct Electronic Curing," ACI Materials Journal, January-February, 2000, pp. 37-40.

INVESTIGATING SELF-HEALING CAPACITY OF MICRO-CRACKED ECC WITH DIFFERENT VOLUME OF FLY ASH

Z. Zhang¹ and S. Qian¹

¹ School of Transportation, Southeast University, Sipailou 2, 210096 Nanjing, P R China, – e-mail: yujian168971681@126.com; sqian@seu.edu.cn

Keywords: micro-cracked ECC, self-healing, fly ash, capillary water sorption test

ABSTRACT

Crack is called the intrinsic flaw of concrete that is inevitable for concrete infrastructures during their service life. The presence of crack offer aggressive agent access to pass through, which has a direct impact on durability, therefore resulting in shortened service life. Nevertheless, the influence of crack on the durability can be greatly minimized when crack width is controlled within certain limits. Engineered Cementitious Composite (ECC) is a new class of HPFRCC micro-mechanically designed to achieve high tensile strain capacity of 3-5%, while maintaining very tight crack width. In this paper, we attempt to investigate the self-healing capacity of micro-cracked ECC by capillary water sorption test. Three ECC mix proportions with different volume of fly ash are used in this research. Before water curing the specimens are pre-loaded at 28 days so as to produce micro-cracks. The micro-cracked specimens are then cured under water for another 30 and 60 days, respectively, before water sorption test is conducted. It is found that water absorbed by cracks of the pre-loaded specimens reduces with increasing curing age, which suggests that self-healing products accumulate within the cracks over time. Subsequent ESEM observations also confirm the above findings. Most pronounced self-healing behavior is revealed for the mixture with highest fly ash content, which also shows smallest crack width. The crack width reduces with increasing volume of fly ash, denoting better capacity of crack width control. With excellent crack width control and self-healing behavior, ECC can be an ideal material for durable concrete infrastructure.

1. INTRODUCTION

Concrete cracking is a result of the combined effects of mechanical loading conditions and environmental exposure, which is inevitable for concrete infrastructures during their service life. The presence of crack offer aggressive agent access to pass through, and has a direct impact on durability, thus decreases the service life. In this paper, we attempt to investigate the self-healing capacity of ECC with different fly ash content.

2. MATERIALS

Table 1 lists a set of ECC mixtures used for this study. The fly ash-to-cement ratios are 1.2, 2.2 and 4.0, while water-to-cementitious material ratio (w/cm) and silica sand-to-cementitious material ratio (s/cm) are fixed at 0.25 and 0.36, respectively.

Table 1: ECC mixture proportions

Mixture ID	Cement (c)	Fly ash (FA/c)	Silica sand (s/cm)	Water (w/cm)	Water reducer	PVA fiber(by volume)
M1	1.0	1.2	0.36	0.25	0.03	0.02
M2	1.0	2.2	0.36	0.25	0.03	0.02
M3	1.0	4.0	0.36	0.25	0.03	0.02

From each mixture beam specimens of 355 by 75 by 50 mm were prepared for water sorption test. All specimens were demolded at the age of 24 h, and cured under $95 \pm 5\%$ RH, 20°C for 27 days. At 28 days, except for the control specimens, all other ECC beams were loaded until final failure via four-point bending test. The cracked specimens were then cut for subsequent water curing and sorption test. For each mixture, a series of virgin specimens were left un-cracked as control.

3. METHODS

Self-healing capacity of the cracked specimens was evaluated by the normalized crack water absorption. The crack water absorption is defined as water sorption of cracked specimens minus that of the control specimen. The crack water absorption is then normalized by water absorbed by cracked specimens before water curing. A lower normalized crack water absorption denotes better self-healing capacity.

During the capillary water sorption test, specimens were dried and then side surfaces were coated with silicone. Afterwards, specimens were weighed and the cracked surface was brought into contact with water. At regular time intervals, the increase in mass, due to water sorption, was determined.

4. RESULTS

The crack number and width for the specimens of each mixture are shown in Table 2. As shown in Table 2, the crack width of specimens for M3 is much tighter; meanwhile, the crack number in the specimens of M3 is much more compared with that of the M1 and M2. This trend is similar to what Yang et al 2007 has observed in high volume fly ash ECC, which is a result of increased frictional bond due to high compactness of fly ash within the fiber interface zone [1].

Table 2: Crack information of specimens for capillary water sorption test

Specimens No.	M1.1/M2.1/ M3.1	M1.2/M2.2/ M3.2	M1.3/M2.3/ M3.3	M1.4/M2.4/ M3.4
Crack width (μm)	0	60	80	90
	0	30	60	90
	0	20	20	13
Crack number	0	1	1	2
	0	2	2	3
	0	2	7	7

*M1.1-1.4, M2.1-2.4, M3.1-3.4 mean the specimens No. of M1, M2, M3, respectively.

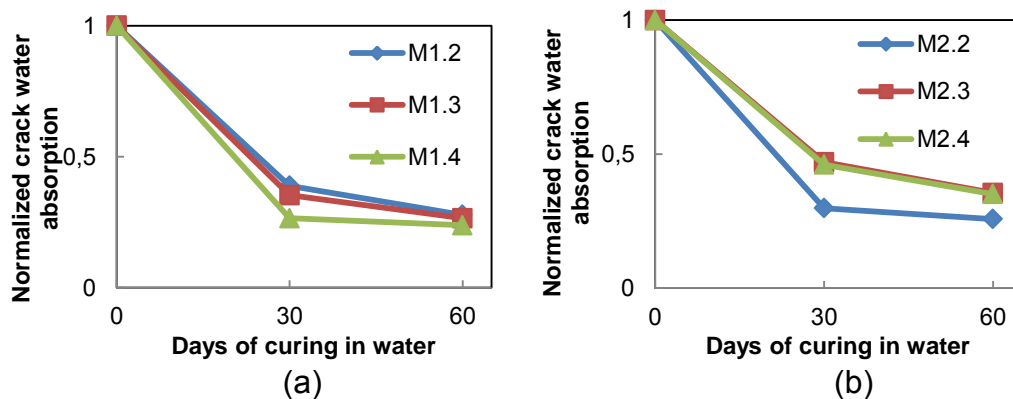
Figure 1 shows normalized crack water absorption for each mixture undergoes self-healing process. After water-curing for 30 days, the normalized crack water absorption for M2 scheme is larger than that of M1. There is no factor of crack width influence on self-healing effect, because the crack width for M1 and M2 scheme is so close that the crack width factor can be neglected. There it seems that increasing fly ash content is detrimental to self-healing capacity with the same crack width. The low cement content will influence the amount of hydration products which is necessary for the pozzolanic reaction of fly ash. The comparison between M3 and M1, M2 shows the opposite trend. The normalized crack water absorption of specimens for M3 scheme reduces to 0.23, which is lower than M1 and M2. One possible explanation is that crack width of M3 is much tighter than that of M1 and M2 as shown in Table 2, and the tight crack is beneficial to self-healing behavior as demonstrated in previous studies. Compared with the benefits of tighter crack width for M3 scheme, the negative effect brought by increasing fly ash content is diminished.

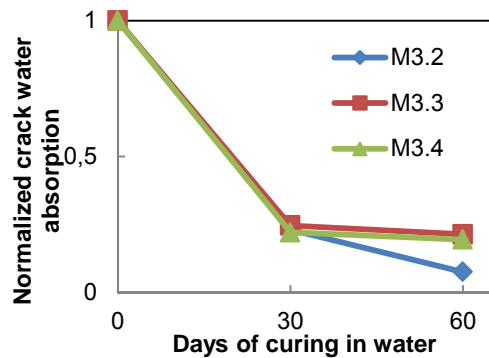
Figure 2 shows the self-healing products in ECC crack under ESEM. In order to investigate the chemical nature of the self-healing products, specimens were examined using EDS. Table 3 suggests that the main healing product may consist of calcium carbonate and C-S-H. Therefore, the correct combination of cement and fly ash is critical for robust self-healing behavior.

Table 3: EDS element analysis of self-healing product

Element	C	O	Al	Si	Ca	Fe
At %	15.96	56.17	4.06	9.13	12.55	1.16

*Elements with less than 1 atomic percent concentration not shown.





(c)

Figure 1: Normalized crack water absorption

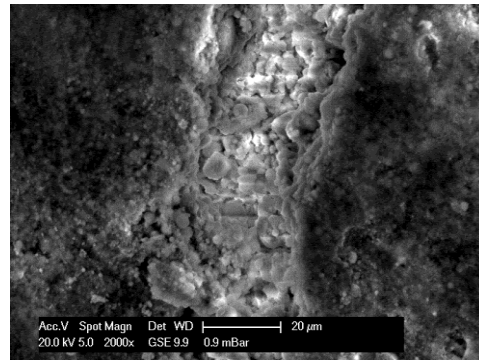


Figure 2: ESEM image of self-healing products in ECC crack

5. CONCLUSIONS

From this paper, it can be concluded that the self-healing capacity of ECC with the highest fly ash content is the best. The main self-healing product is calcium carbonate and C-S-H, denoting fly ash participate the self-healing process.

ACKNOWLEDGEMENTS

The National Natural Science Foundation of China (No.51008071, 51278097), the Natural Science Foundation of Jiangsu Province (No.BK2010413), Teaching Research Excellence Grant for Young Faculty Member at Southeast University, Jiangsu Top Talents in Six Major Fields (2011-JZ-011), Jiangsu Provincial Graduate Student Scientific Research Innovation Plan Projects(No.CXLX_0136) & Student Research Training Program at Southeast University (T12211020).

REFERENCES

[1] Yang, EH, Yang, YZ and Li, VC. Use of High Volumes of Fly Ash to Improve ECC Mechanical Properties and Material Greenness, ACI Materials Journal, (2007), pp.303-311.

EXPERIMENTAL STUDY ON EVALUATION OF SELF-HEALING CAPABILITY OF FRCCS COMPRISING DIFFERENT COMPONENTS

T. Nishiwaki¹, M. Yamada¹, T. Kikuta¹, S. Kwon¹ and H. Mihashi¹

¹ Department of Architecture and Building Science, Graduate School of Engineering, Tohoku University, Aramaki Aoba 6-6-11-1205, Aoba, Sendai, Miyagi 980-8579, Japan – e-mail: ty@archi.tohoku.ac.jp

Keywords: FRCC, self-healing, reinforcing fiber, limestone, calcium carbonate

ABSTRACT

Fiber reinforced cementitious composite (FRCC) has a great capability for self-healing of cracks. Concrete cracks with a sufficiently small crack width (below 0.1 mm) can be closed and self-healed by crystallization of calcium carbonate in the presence of moisture, even in the case of ordinary concrete. Such precipitation is caused by reaction of calcium ions and dissolved carbon dioxide. FRCC can accelerate the self-healing process mainly due to two characteristics, i.e., crack widths can be restricted to be narrow, and fibers bridging cracks can act as a core for precipitating chemical products. Previous research by the authors showed that some types of reinforcing fibers with polar groups, such as polyvinyl alcohol (PVA) with a hydroxy group, can induce a greater precipitation volume for calcium carbonate crystals around themselves than fibers without polarity, such as polypropylene (PP).

In this study, a fundamental experiment was performed in order to specify the FRCC component materials that can enhance the self-healing effect. FRCCs with different types of reinforcing fibers (PVA and PP), aggregates, and admixtures (silica sand, limestone sand, and limestone powder) were subjected to the precipitation test—the volume of the precipitated calcium carbonate crystals around each fiber and on the crack surface of FRCC specimens was measured in order to estimate the self-healing capability. Specimens with a crack surface were immersed for 7 days in a small water tank. The results showed that limestone sand and powder did not strongly affect the quantity of crystal precipitation around the exposed fiber; however, they enhanced the crystal precipitation area on the crack surface (flank). A large amount of precipitated crystal on the crack surface might enhance the self-healing function of FRCCs.

1. INTRODUCTION

Fiber reinforced cementitious composite (FRCC) has a great capability for crack self-healing because of its crack width control [1]. For FRCC with synthetic fibers, one of the main mechanisms for self-healing is precipitation of calcium carbonate in the crack. The authors previously revealed that fibers act not only to control the crack width but also as the cores of chemical precipitation sites [2]. In particular, synthetic fibers with high polarity can promote effective precipitation of self-healing products [3]. Therefore, the self-healing capability of FRCC depends on the characteristics of the employed fibers, i.e., FRCC with high polarity fibers such as polyvinyl alcohol (PVA) has greater self-healing capability than that with no polarity fibers such as polypropylene (PP) because the fiber polarity can attract calcium ions and accelerate

calcite precipitation. Moreover, enough providing of calcium ion from mortar matrices is expected to enhance precipitation of calcium carbonate. In this study, FRCCs with different types of reinforcing fibers and limestone aggregates/admixtures were subjected to the precipitation test in order to estimate their self-healing capabilities.

2. EXPERIMENTAL PROGRAM

The volume of precipitated calcium carbonate crystals around each fiber exposed from the crack surface of FRCC immersed in curing water was observed and measured in order to estimate the self-healing potential. Table 1 shows the materials employed, and Table 2 shows the testing series and mix proportions of the specimens. Limestone sand and powder were employed instead of silica sand as the calcium source. Figure 1 shows the geometry of the employed specimen and a schematic diagram of the testing procedures. After standard curing for 7 days, the notched cuboid specimens (40 mm × 40 mm × 160 mm with 12 mm notch depth) were subjected to a three-point bending test until they separated into two pieces. One of the specimen halves was cut to a 30 mm height and immersed in a small water tank (150 cc). The thickness of the precipitated crystal was measured by microscopic observation. Phenolphthalein was sprayed onto the crack surface (flank) in order to recognize the area of calcium carbonate precipitation. The area was calculated by microscopic observation.

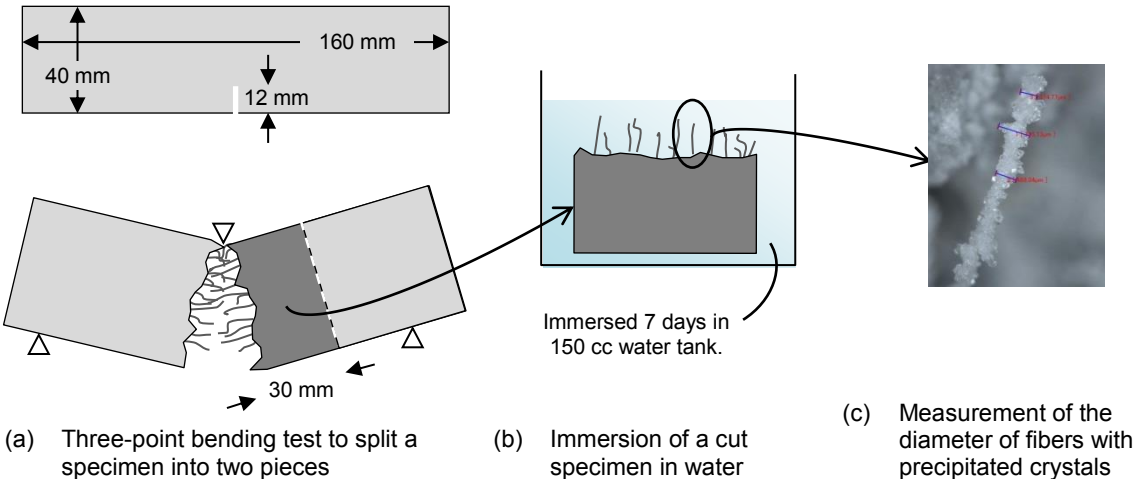


Figure 1: Testing procedure

Table 1: Materials employed

Material	Symbol	Properties
Cement	C	High early strength Portland cement, Density: 3.14 g/cm ³
Silica fume	SF	Density: 2.20 g/cm ³
Aggregate (Admixture)	S (SS)	Silica sand #5, Density: 2.61 g/cm ³ , Diameter: ~500 μm
	(LS)	Limestone sand, Density: 2.71 g/cm ³ , Diameter: ~500 μm
	(4K)	Limestone powder (4K), Specific surface: 4800 cm ² /g
	(7K)	Limestone powder (7K), Specific surface: 6730 cm ² /g
Reinforcing fiber	PVA	Polyvinyl alcohol, Length: 6 mm, Nominal diameter: 37 μm
	PP	Polypropylene, Length: 6 mm, Nominal diameter: 11 μm
Super plasticizer	SP	Polycarboxylic acid ether system, Density: 1.05 g/cm ³

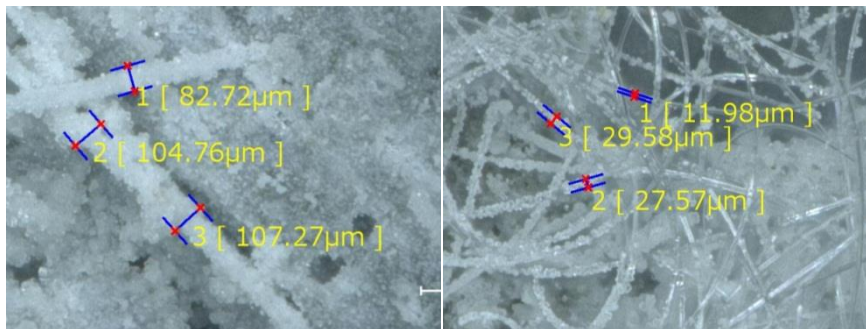
Table 2: Testing series and mix proportion

Series	W/B	S/B	Vf (vol.%)	Type of fiber	Aggregate (Admixture)	σ_c (N/mm ²)	σ_b (N/mm ²)
NF	45	45	-	-	Silica sand	70.9	3.18
PVA-SS			2	PVA	Silica sand	66.0	7.86
PVA-LS					Limestone sand	78.1	7.27
PVA-4K					Limestone powder 4K	92.4	6.21
PVA-7K					Limestone powder 7K	75.6	8.12
PP-SS			PP	Silica sand	55.4	5.62	
PP-LS				Limestone sand	38.4	4.86	
PP-4K				Limestone powder 4K	47.2	3.67	
PP-7K				Limestone powder 7K	59.8	5.47	

*B: Binder, Vf: Volume fraction of fiber, σ_c : Compressive strength, σ_b : Bending strength

3. RESULTS AND DISCUSSION

Figure 2 shows typical measurement examples by microscopic observation for both the PVA and PP series. In the PVA series, thick precipitation was confirmed on all the exposed fibers; on the other hand, in the PP series, some fibers had no precipitation. In particular, when PP fibers repelled and interrupted water contact during immersion in the water tank (Figure 3), no precipitation was observed on both the PP fiber surface and the crack flank. Figure 4 shows the microscopic photos and summarized precipitation thickness on the fibers and precipitated area on the crack surface. Limestone sand and powders slightly affected the precipitation thickness around fibers; however, they strongly affected the precipitated area on the crack surfaces. A larger specific surface of limestone meant a greater precipitated area obtained. The calcium distribution on the crack surface accelerated additional calcite crystal precipitation on the crack surface. In other words, a better self-healing effect might be induced by using limestone to provide additional calcium.



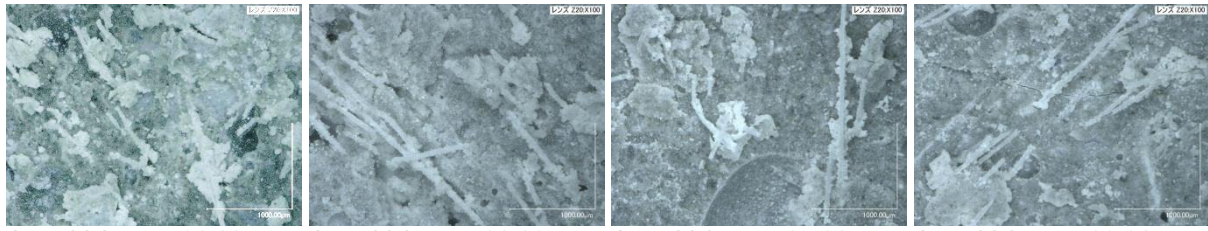
(a) PVA series

(b) PP series

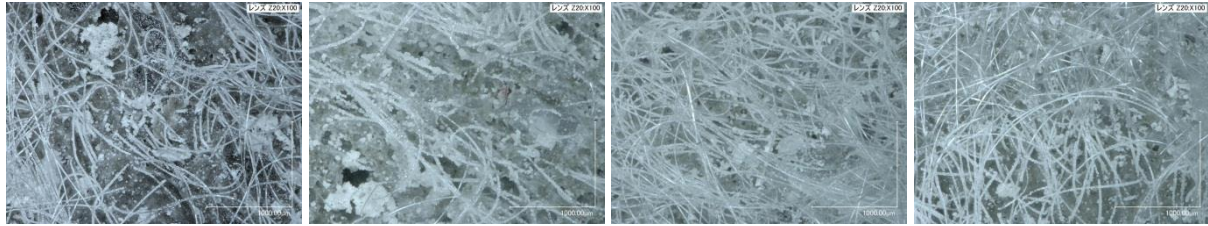
Figure 2: Testing procedures



Figure 3: Repelling of PP fiber surface



Avg. thickness: 36.23 μm Avg. thickness: 30.09 μm Avg. thickness: 34.32 μm Avg. thickness: 29.61 μm
 Precipitated area: 56.16% Precipitated area: 65.02% Precipitated area: 90.75% Precipitated area: 91.41%
 (a) PVA-SS (b) PVA-LS (c) PVA-4K (d) PVA-7K



Ave. thickness: 6.85 μm Ave. thickness: 9.73 μm Ave. thickness: 5.48 μm Ave. thickness: 8.25 μm
 (e) PP-SS (f) PP-LS (g) PP-4K (h) PP-7K

Figure 4: Testing procedures

4. CONCLUSIONS

In this study, fundamental experiments were performed on FRCC with different components to confirm the enhanced self-healing effects. The results showed that limestone sand and powder did not strongly affect the quantity of crystal precipitation around the exposed fiber. On the other hand, they enhanced the crystal precipitation area on the crack surface (flank). Using limestone additive as the calcium provider may be a promising approach; a large amount of precipitated crystals on the crack surface may make the self-healing function of FRCCs more effective.

ACKNOWLEDGMENTS

This research was partially supported by a Grant-in-Aid for Young Scientists (A) from the Ministry of Education, Culture, Sports, Science and Technology of Japan (#23686078, 2011-2014).

REFERENCES

- [1] V.C. Li, Y.M. Lim, Y.-W. Chan, Feasibility Study of a Passive Smart Self-Healing Cementitious Composite, *Composites Part B*, 29B (1998) 819-827
- [2] D. Homma, H. Mihashi, T. Nishiwaki, Self-healing Capability of Fibre Reinforced Cementitious Composites, *Journal of Advanced Concrete Technology*, Vol. 7, No. 2 (2009) 217-228
- [3] T. Nishiwaki, M. Koda, M. Yamada, H. Mihashi, T. Kikuta, Experimental Study on Self-Healing Capability of FRCC Using Different Types of Synthetic Fibers, *Journal of Advanced Concrete Technology*, Vol. 10 (2012) 195-206

DESIGN OF POLYMERIC CAPSULES FOR AUTONOMOUS HEALING OF CRACKS IN CEMENTITIOUS MATERIALS

B. Hilloulin¹, K. Van Tittelboom², E. Gruyaert², A. Loukili¹ and N. De Belie²

¹ L'UNAM Université, Institut de Recherche en Génie Civil et Mécanique (GeM), UMR-CNRS 6183, Ecole Centrale de Nantes, Nantes, France – e-mail: benoit.hilloulin@ec-nantes.fr; ahmed.loukili@ec-nantes.fr

² Magnel Laboratory for Concrete Research, Ghent University, Technologiepark-Zwijnaarde 904, 9052 Ghent, Belgium – e-mail: kim.vantittelboom@ugent.be; elke.gruyaert@ugent.be; nele.debelie@ugent.be

Keywords: concrete, autonomous healing, polymeric capsules, concrete mixing process

ABSTRACT

Now, most of the capsules used to contain polymeric healing agents in self-healing concrete, are made of glass. However, glass capsules cannot be mixed in concrete and are therefore placed manually into the moulds during concrete casting in laboratory tests. This represents a major drawback for an eventual industrialisation.

In this study, polymeric capsules were designed to meet three requirements: breakage upon crack appearance, compatibility with the polymeric healing agent and survival during concrete mixing. Three different polymers with a low glass transition temperature (T_g) were selected (PLA – PS – P(MMA-n-BMA)). These polymers are brittle at 20°C, and consequently have the possibility to break upon crack appearance, but are rubbery above their glass transition temperature and, consequently, can survive mixing upon heating.

Differential Scanning Calorimetry and Dynamic Mechanical Analysis were performed to define the glass transition temperature of the selected polymers and to quantify the evolution of their mechanical properties with increasing temperature.

Concrete mixing tests were performed both at 20°C and at a temperature above the T_g of the capsules. Mixing at increased temperature was done by previously heating the capsules and the concrete components. The survival rates increased drastically when the capsules and the concrete components were heated. Even capsules with a thin wall (thickness 0.4 mm) resisted a 2 minute concrete mixing process, whereas none of them survived at 20°C.

In addition, the compatibility of the capsules with a two-component polyurethane healing agent was studied. The pre-polymer hardened after some days.

This research revealed that suitable design of polymeric capsules can help to meet the requirements for self-healing concrete even though further research is needed before a possible use in industry.

1. INTRODUCTION

Encapsulation of polymer-based healing agents is a very effective method to obtain autonomous healing of concrete cracks. However, up to now, capsules used to store the healing agent cannot resist the concrete mixing process, which is a major drawback on the way of a possible industrialization. Therefore, in this project, we attempt to create polymeric capsules which are able to survive the concrete mixing process without any particular protection, and to break upon crack appearance without human intervention.

2. MATERIALS

Polymeric hollow tubes with a length of 5 cm, inner diameters between 1 mm and 4 mm and outer diameter between 2 mm and 7 mm, were extruded from polymers which are brittle at room temperature and have a relatively low glass transition temperature (T_g): Poly(lactic acid) (PLA), Polystyrene (PS) and Poly(methyl methacrylate/n-butyl methacrylate) (P(MMA-n-BMA)). In order to study the possibility of capsule breakage with crack appearance, mortar specimens containing capsules were prepared. First, a layer of 10 mm mortar with a W/C ratio of 0.4 was poured into 40 mm x 40 mm x 160 mm moulds. Two steel reinforcing bars with a diameter of 2 mm were placed on top of the mortar layer to avoid premature failure during crack formation. Two to four capsules were positioned in the middle of the specimen where the crack was presumed to appear. Some capsules which survived mixing were embedded, as well as 'new' capsules which were not mixed previously. Then the moulds were filled completely with mortar. The specimens were demoulded one day after casting.

3. METHODS

In order to prove the efficiency of adjusting the brittleness of polymeric capsules with temperature, mixing tests have been performed in a 20L planetary mixer to compare the resistance of non-heated and heated capsules. Hollow tubes with a length of 5 cm were used as capsules. After sealing one end, capsules were filled with water mixed with red dye, and finally sealed at the other end. For the concrete mixing test with heated capsules, capsules were heated in an oven during 20 to 40 minutes before the mixing test. The mixing processes are summarized in Figure 1.

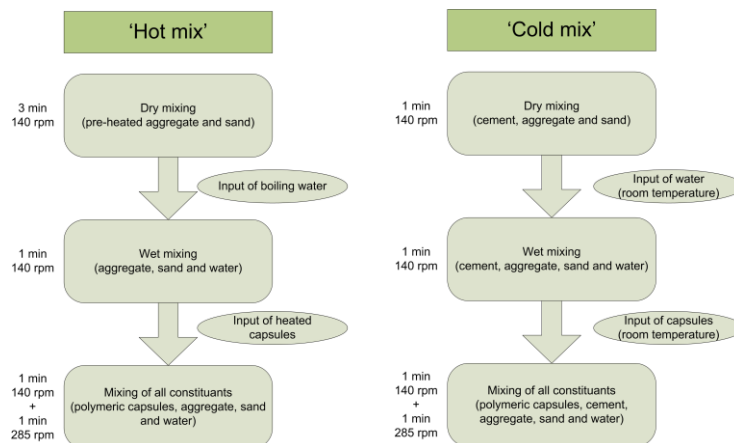


Figure 1: Mixing processes to study the resistance of the polymeric capsules

When the mortar samples, described in section 2, were 28 days old, three-point-bending tests were performed following 2 successive methods. The first method was used to see if the capsules break when a crack is created and its width increases at a speed of 0.001 mm/s until 0.4 mm (measured by linear variable differential transformer (LVDT)). Capsule breakage was expected and some pictures were taken when leaching dye of the broken capsules was detected. In the second method the mortar sample was completely broken to see whether the capsules break at higher crack width or whether they slip in the matrix.

4. RESULTS

Almost all polymeric capsules survived the concrete mixing process while they were heated above their T_g . The differences between 'hot' and 'cold' mixes are detailed in Figure 2. The improvement in survival ratio after heated is assumed to be caused by the more flexible behavior of the capsules above their T_g . Even the very small PLA capsules with a wall thickness around 0.4 - 0.5 mm survived the mixing process whereas none survived the cold mixing process.

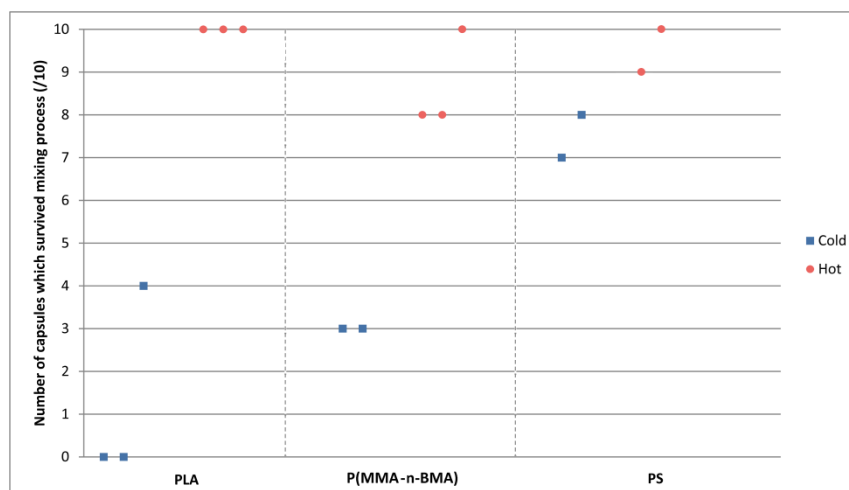


Figure 2: Survival ratios of the polymeric capsules during mixing

Some P(MMA/n-BMA) capsules broke when cracks of 0.4 mm were created. For two specimens with incorporated deformed capsules, which previously survived the hot mixing process, some capsules broke and released the water they initially contained as illustrated in Figure 3a. For 2 other specimens with capsules which previously resisted the concrete mixing process but which were not deformed, capsule breakage was observed. The crack width at which the capsules broke was deduced from the graphs representing the load in function of the crack width measured by the LVDT. When a sudden drop in the curve was observed (as illustrated in Figure 3b) and the sound of capsule breakage was heard, the capsules were supposed to be broken. Three capsules broke when the crack width was around 0.15 mm, which corresponds to a relatively small crack. Therefore, if the healing agent could be encapsulated by these capsules, healing of cracks with a width of around 0.15 mm could be possible.

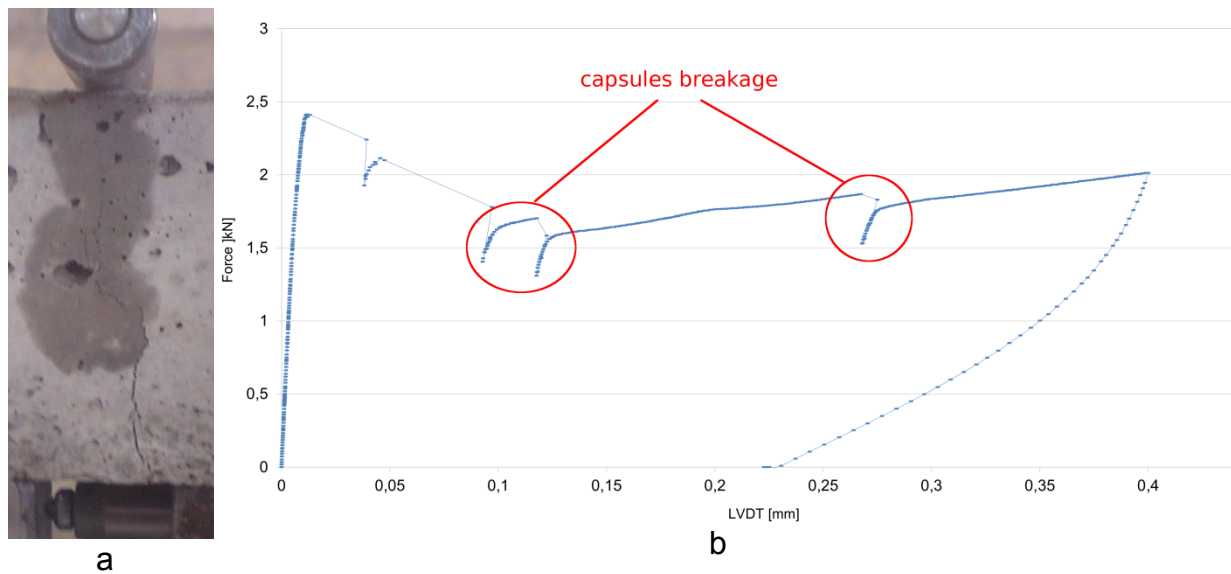


Figure 3: Breakage of P(MMA-n-BMA) capsules with visible water release (a) and sudden drop in the load curve (b).

However, none of the PS and PLA capsules broke when cracks with a width of 0.4 mm were created. No drops were observed in the load curves and no water marks were observed. During the second test (complete breakage of sample), the PS capsules broke without visible. PLA capsules also broke during the second test, but most of them broke just before specimen failure at crack widths larger than 1 mm. A plastic deformation of the capsules was observed. Moreover, some small capsules were pulled out when the two parts of the specimens were disconnected. This indicates that there is no sufficient bond between the PLA capsules and the cementitious matrix.

5. CONCLUSIONS

The use of polymeric capsules to obtain self-healing properties in concrete seems promising but still needs further investigation. In this study, brittle thermoplastics which can resist the concrete mixing process through heating, and break with crack appearance at room temperature have been extruded. Even if the three polymers studied are known for their brittleness, only one type of capsules broke with the creation of crack with a width smaller than 0.4 mm. Therefore the brittleness of the material is a very sensitive parameter to design capsules for self-healing concrete.

SESSION 24 – MODELLING AND NUMERICAL ANALYSIS TOOLS

MACROSCOPIC MODELLING OF SELF-HEALING THERMOSET MATERIALS

J. Mergheim¹, P. Steinmann¹

¹ Chair of Applied Mechanics, University of Erlangen Nuremberg, Egerlandstr. 5, 91058 Erlangen, Germany – e-mail: julia.mergheim@itm.uni-erlangen.de, paul.steinmann@itm.uni-erlangen.de

Keywords: thermoset materials, continuum modelling, self-healing model, damage model, finite element simulation

ABSTRACT

The present contribution introduces a phenomenological model for self-healing polymers. Self-healing polymers are a promising class of materials which mimic nature by its capability to autonomously heal micro-cracks. Self-healing in the here considered system is accomplished by integrating microcapsules filled with a healing agent and a dispersed catalyst into the material. Propagating microcracks break the capsules which release the healing agent in the microcracks where it polymerizes with the catalyst into a solid material closing the crack and 'healing' the material.

The present modelling approach is attached to the macroscopic scale, and thus, the microscopic effects of crack propagation and healing are described by means of continuous damage and healing variables. The basic concept of continuum damage mechanics is that microstructural defects are represented by means of a continuous damage variable. The damage variable evolves when a certain failure limit is exceeded and describes the degradation of the material. In isotropic-elastic damage models a scalar damage variable is defined, that reduces the elastic properties, ranging from 0 (undamaged state) to 1 (fully damaged state). Since healing of the material, i.e. the recovery of material stiffness or integrity at a material point, is directly related to the curing process of the healing agent in microcracks, the evolution of the healing variable is based the evolution of the mechanical properties during the process of cure. In contrast to existing damage-healing models, the healing variable is not merely introduced as an 'opposite variable' to the damage variable, but it defines the amount of newly emerging material (due to polymerization), equipped with its own strain energy density. This strain energy density takes into account that the curing process of the healing material only increases the stiffness, but not its stress or strain energy unless the strain state is changed.

The model is implemented and its capabilities are studied by means of numerical examples.

1. INTRODUCTION

A phenomenological thermodynamically consistent damage-healing model for self-healing polymers with integrated healing agents is introduced. The initiation and propagation of microcracks is modelled by means of continuum damage mechanics and also the healing process is described from a macroscopic point of view. Suitable

internal damage and healing variables are introduced, whereby the latter takes into account the similarity of healing events and curing processes.

2. DAMAGE AND HEALING MODEL

For an isotropic material scalar damage and healing variables are introduced which describe degradation and healing of the material in a homogenized manner. The damage variable ranges from $d=0$ for the original material to $d=1$ when the material is completely degraded. Healing affects only the damaged part of the material: microcracks and voids are filled with a polymer liquid that polymerizes to a solid with time. This process is described by a healing variable ranging from $h=0$ when healing starts to $h=d$ when all cracks are filled with fully cured healing agent. To describe damage within the healed material an additional damage variable δ is introduced: $\delta=1$ if the healed material is fully damaged and $\delta=0$ if no further damage in the healed material is observed.

The damage process reduces the load-carrying capacity of the original material. The healed cross-section, on the other hand, carries load, but the healed material can experience and response only to strains that are applied after the initiation of the healing process. To take that into account an additive decomposition of the strain-energy density into an elastic-damage part and a healing-redamage part is proposed

$$\Psi(\boldsymbol{\varepsilon}, d, \delta, t) = [1-d] \Psi^{el}(\boldsymbol{\varepsilon}) + [1-\delta] \Psi^h(\boldsymbol{\varepsilon}, t) \quad (1.1)$$

Thereby, $\boldsymbol{\varepsilon}$ is the linear strain tensor, Ψ^{el} the standard elastic energy and Ψ^h the strain energy of the healing material, which is defined as

$$\Psi^h(\boldsymbol{\varepsilon}, t) = \frac{1}{2} \int_{s=0}^{s=t} [\boldsymbol{\varepsilon}(t) - \boldsymbol{\varepsilon}(s)] : \frac{dh}{ds} \mathbb{C} : [\boldsymbol{\varepsilon}(t) - \boldsymbol{\varepsilon}(s)] ds, \quad (1.2)$$

whereby \mathbb{C} denotes the elasticity tensor and dh/ds the total derivative of h with respect to the time variable s . Evaluation of the Clausius-Duhem inequality with the proposed strain energy density results in the following definition of the stresses

$$\boldsymbol{\sigma} = [1-d] \mathbb{C} : \boldsymbol{\varepsilon} + [1-\delta] \boldsymbol{\sigma}^h, \quad (1.3)$$

whereby the healing stress is defined by the rate equation

$$\dot{\boldsymbol{\sigma}}^h(t) = h(t) \mathbb{C} : \dot{\boldsymbol{\varepsilon}}(t). \quad (1.4)$$

This rate equation ensures that only the stiffness is increased during healing but not the stress, if the strain rate is zero.

To describe the onset and evolution of damage, a damage condition is introduced that depends on the elastic energy Ψ^{el} and a suitable damage threshold r^d

$$\Phi^d(\Psi^{el}, d, h) = \Psi^{el} - r^d(d, h) \leq 0. \quad (1.5)$$

Damage increases only if $\Phi^d = 0$, for $\Phi^d < 0$ the damage rate is zero $\dot{d} = 0$. For a damaging material the damage threshold increases monotonically. Since healing reverses the damage process to some extent the damage threshold has to be affected by the healing process. To ensure that the healed material behaves similar as the original one, the healing h variable decreases the damage threshold r^d in the same way as it is increased by d . Here, damage hardening is described by a logarithmic function

$$r^d(d, h) = r_0^d - \frac{1}{B} \ln(1-d+h), \quad (1.6)$$

with the initial damage threshold r_0^d and the material parameter B . A similar damage threshold is defined for δ , but it depends on the elastic healing energy Ψ^h .

The model is completed by an evolution equation for the healing variable. The similarity between healing and curing is once more exploited: healing starts at time t^c when a certain amount of damage exists and an exponential evolution of the healing variable in time is assumed, following the experimental findings concerning the stiffness increase during the curing process

$$h(t) = \int_{s=t^c}^t d(s)\eta_h \exp(-\eta_h[t-s]) ds, \quad (1.7)$$

whereby the parameter η_h defines how fast the healing progresses. The healing process should finally recover the stiffness of the original material. We consider the tangent modulus, that defines the relation between the stress and strain rate, by taking the time derivative of equation (1.3)

$$\dot{\sigma} = [1-d]\mathcal{C} : \dot{\epsilon} - \dot{d}\mathcal{C} : \epsilon + [1-\delta]h\mathcal{C} : \dot{\epsilon} - \dot{\delta}\sigma^h \quad (1.8)$$

For elastic loading or unloading, i.e. $\dot{d} = \dot{\delta} = 0$ the elastic modulus $\mathcal{C}_e = [1-d + [1-\delta]h]\mathcal{C}$ is obtained. Obviously, the completely healed material with $h=d$, $\delta=0$ has the same stiffness as the original one. Identical material behaviour is assumed for the original and the fully healed material. However, the introduction of different strain energy densities and different damage conditions is possible and straightforward.

3. RESULTS

The damage-healing-redamage model is discussed in a one-dimensional setting to point out the influence of material parameters, strain history and possible rest times between loading cycles. A certain unidirectional strain history is prescribed to one material point and the evolution of the stress is analysed.

In figure 1 the stress responses for a prescribed strain history are given. The material is loaded up to failure by prescribing a linearly increasing strain, then the strain is reduced to zero and a recovery time of various length follows to allow the material to heal, afterwards the strain is increased again, compare Fig. 1, top. The same figure, bottom, shows the stress response for a material without self-healing capacities. The first increase in strain leads to a linear increase in stress. When the damage threshold is reached the material stiffness decreases and an exponential softening of the stress curve follows. During unloading and reloading the stress remains close to zero since the material is almost completely damaged. In Fig. 2 stress-time and stress-strain diagrams for the same strain history are given, but now the material starts to heal when the critical energy threshold is exceeded and the rest time between unloading and loading is varied. The material recovers a part of its stiffness that depends on the recovery time. For the case with a rest time of only 600s the stiffness reaches approx. 1/7 of its original value, a recovery time of 60000s is enough to achieve the original properties. Further predictions of the damage-healing-redamage model are discussed in [1].

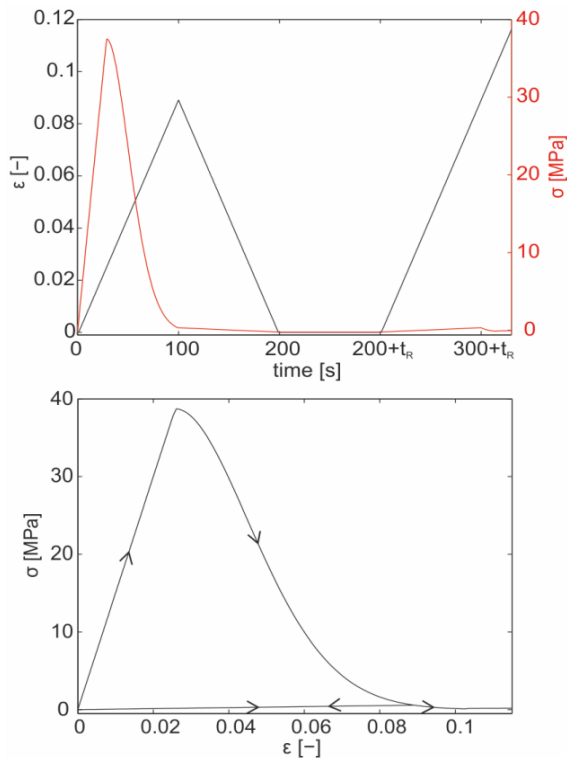


Figure 1: strain-history and stress-time-response (top), stress-strain-response (bottom) for damage without selfhealing

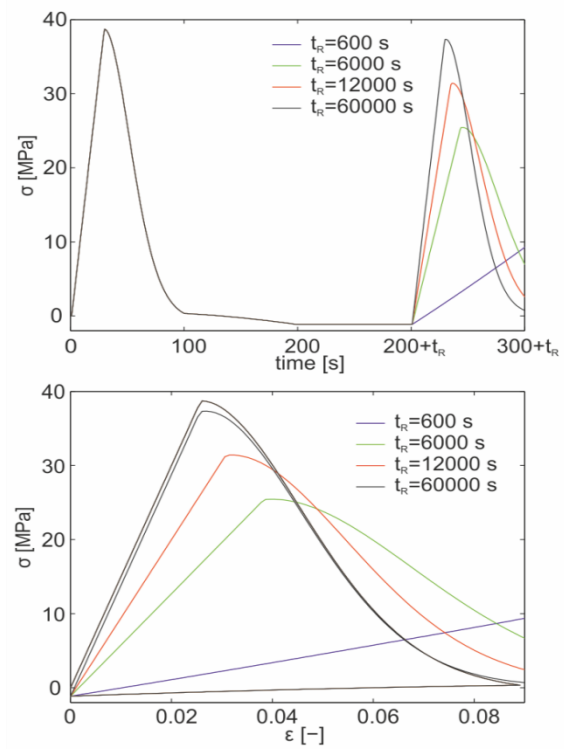


Figure 2: stress-time-response (top), stress-strain-response (bottom) for damage and selfhealing, comparison of various recovery times

4. CONCLUSIONS

A continuum model for damaging and self-healing thermosetting materials is introduced. The model is based on the macroscale such that the occurrence of failure and healing is described by means of internal damage and healing variables. A thermodynamic consistent damage model is extended towards the modelling of self-healing and redamaging. Thereby, a rate equation for the healing dependent stress is formulated to account for the similarity between healing and curing. This ensures that healing does not change the stress state unless the strain state is varied and, additionally, that the model is thermodynamically consistent. The characteristics and possibilities of the model are illustrated by means of a one-dimensional example. It is highlighted that the model predicts the expected stiffness recovery and regeneration of failure properties during healing.

ACKNOWLEDGEMENTS

Financial support of the Bavarian Academy of Sciences and Humanities is gratefully acknowledged.

REFERENCES

[1] Mergheim J, Steinmann P. Phenomenological modelling of self-healing polymers based on integrated healing agents. *Computational Mechanics*: DOI 10.1007/s00466-013-0840-0 (2013)

MODELLING OF SELF-HEALING SURFACE STRUCTURED COATINGS

K. Lyakhova¹, A.C.C. Esteves¹ and G. de With¹

¹ *Laboratory of Materials and Interface Chemistry, Department of Chemical Engineering and Chemistry, Eindhoven University of Technology, Den Dolech 2, 5612AZ Eindhoven, The Netherlands – e-mail: k.lyakhova@tue.nl*

Keywords: Self-healing polymer coatings, simulation, mesoscopic modeling, hydrophobic coating, low-surface energy component.

ABSTRACT

For many current engineering applications the performance of materials depends strongly on the surface properties of the top layer. In many cases a hydrophobic/superhydrophobic top surface is desired (for example for easy-to-clean/self-cleaning applications). The durability of coatings will be substantially extended if the layer which provides the hydrophobic/superhydrophobic property will have ability to self-heal.

Previously, hydrophobic coatings with a self-healing surface were reported by our group. These coatings can recover a sufficiently high concentration of the low-surface-energy groups at the air/polymer interface. The bulk material serves as reservoir of the low-surface energy component (fluorinated polymer dangling chains). A mechanism of self-replenishing involves the reorientation of the dangling chains which carry the fluorinated group. Silica particles were incorporated into the polymer system in order to introduce the surface roughness leading eventually to higher contact angles of the polymer coating. Our goal is to create a model of the a self-healing superhydrophobic coating.

In this work we use the mesoscopic modelling technique (dissipative particle dynamics) in order to study several aspects of these polymer/particle coating: 1) the segregation of the low surface energy groups at the top surface of the coating.; 2) the self-healing response of the system and 3) the dynamics and distribution of crosslinks in the polymer system in presence of relatively large silica particles. For these studies we considered the distribution of the low surface energy groups in a confined geometry at the interfaces available. The minimal thickness of the polymer layer which provides self-healing ability was also calculated.

All the relevant parameters (crosslinking conditions, polymer precursor and dangling chain length and distance between particles) were changed systematically. The simulations give a valuable insight into the details of microstructures and dynamics and guide experiments towards the choice of the system with the maximal self-healing efficiency.

1. INTRODUCTION

The surface properties of polymeric materials are generally determined by the chemical groups present at their surface. The preferential location of the low surface energy chemical groups at the surface is crucial for the low-adhesion properties

which are of high interest for various engineering fields. Controlling the surface segregation of such chemical groups, would allow maintaining the materials properties at high performance level all through its service lifetime. Previously the self-healing mechanism for the low-surface energy coatings was proposed and well studied within our group [1,2]. Introducing the surface roughness allows transition from hydrophobic to super hydrophobic surfaces. We use a combined experimental/simulation approach to study surface structured low-surface energy coatings.

2. METHOD

Modelling of self-healing low-surface energy surface structured coatings was performed using the coarse grained simulation method. Dissipative Particle Dynamics (DPD). This method is a coarse grained of-lattice simulation technique which involves movement of coarse grained particles (beads) in the box with discrete timestep. Beads represent fluid regions as well as parts of molecules. Beads interact with simplified repulsive pair-potential. This method was chosen in order to reach the time-scales and length-scales of interest. The traditionally used DPD simulation method was modified in order to allow the formation of chemical crosslinks. The presence of silica particles was modelled by introducing to the simulation system a wall which consists of immobile beads. Also the spherical particles consisting of large amount of beads (~ 32000) were introduced to the simulation box. The system was parameterized using relevant experimental data. In previous work we have obtained a very good agreement between experiment and simulation results and can rely on the simulation parameters.

The molecular model of the system is shown in Figure 1. The caprolactone (CL) unit was chosen as a minimal volume corresponding to the single bead. The crosslinking was realized by making beads CL-H and CR reactive. During crosslinking process the permanent bonds between these two beads can form. The beads which model Silica particle also can interact with crossliker and can form a permanent bond (mimicking the presence of OH groups at the particle surface).

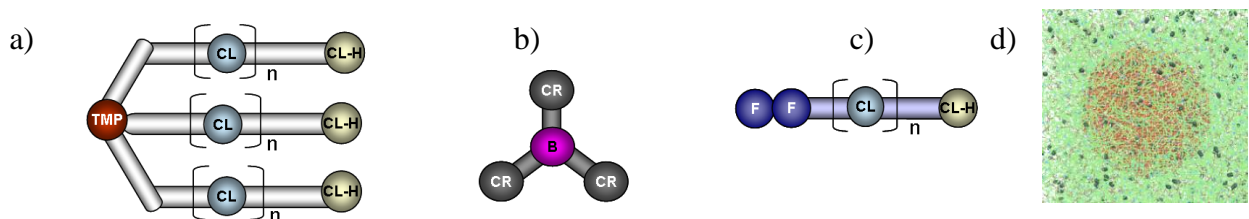


Figure 1: Coarse grained model used in DPD simulations. a) Model of polymer precursor (TMP-PCL_{3n}); b) model of crosslinker (tri-isocyanate), c) – model of fluorinated dangling chain (F₁₇C₈-PCL_n), d) model of silica particle incorporated in polymer coating.

3. RESULTS AND DISCUSSION

As the Silica particles used in experiment are ~ 700 nm in diameter (in contrast to a typical length scale of polymer ~ 1 nm) in our simulation we present a particle surface as a flat substrate consisting of immobile particles. A free polymer surface is

modelled by placing a layer of 'void' beads on a top of polymer coating. In this way the two interfaces are created : a polymer/particle and a polymer/air interface. The concentration of fluorine per layer in z-coordinate was calculated and summarized in fluorine profiles. First polymer coating was equilibrated and crosslinked (see Figure 2a). Then the damage of polymer layer was modelled by replacing the part of simulation box by 'void' component. Depth of damage was varied (see Figure 2 b,c) The segregation of the low-surface energy groups at the newly formed interface was studied. The profiles are shown in Figure 2d. We found that there exists a critical polymer thickness at which bulk of polymer coating does not contain sufficient

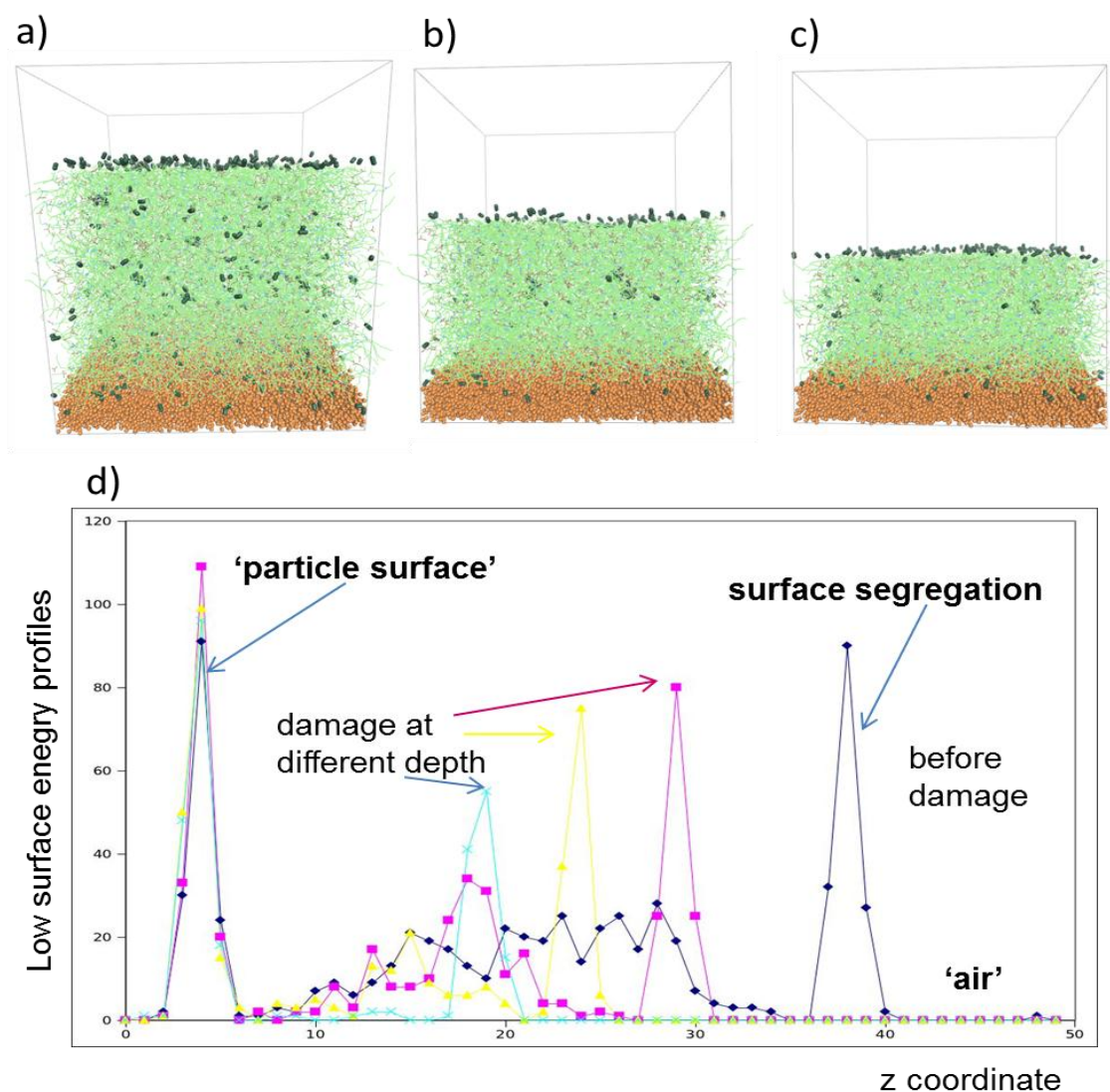


Figure 2. a) Simulation of the surface supported polymer film with one free surface before damage. The fluorinated beads are shown in dark green and are increased for visualisation purposes; b) and c) simulation of surface supported film after damage(different depth of cuts); d) profile of the low surface energy groups as function of z coordinates before and after damage.

concentration of the low surface energy groups and self-healing is not realized. In our previous study on self-healing coatings we have shown that the depletion layer is formed just below the interface layer enriched by the low-surface energy groups. We found that the depth of the depletion layer is not dependent of dangling chain length.

In the supported polymer film fluorinated groups are segregated at the two interfaces: polymer-air and polymer-particle interface and the region of the low fluorine concentration is doubled. We found that at thickness of polymer film ~ 10 nm no self-healing observed. This imposes a restriction on the concentration of particles in composite system.

Further the self-healing behavior of the system was studied starting from the bulk material. The bulk material is modeled as a polymer film sandwiched between the two particle surfaces. Similar to the previous approach first the model system was crosslinked and equilibrated. After this pretreatment the part of simulation box was replaced by 'void' component creating a new polymer/air interface.

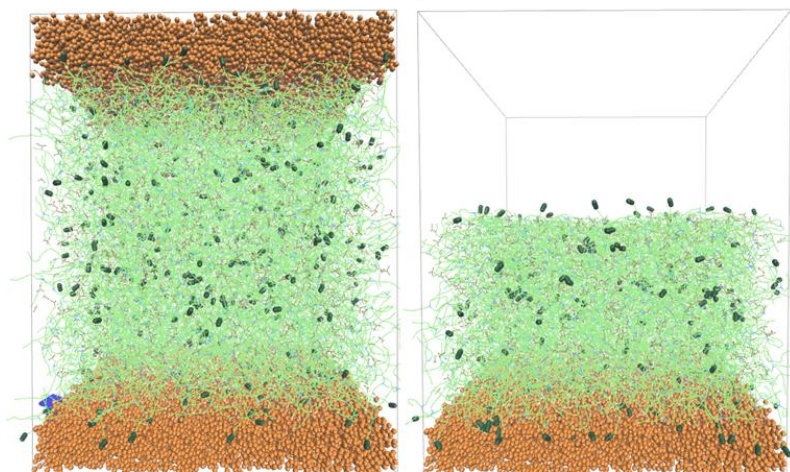


Figure 3. Simulation of the sandwiched polymer film before (left) and after (right) damage. Fluorinated beads are shown in dark green and are increased for visualisation purposes. The 'void' component is not shown.

4. CONCLUSIONS

Self healing ability of the polymer system containing dangling chains was studied. The segregation of the low-surface energy groups in the presence of Silica particles was modelled. We found that there exists a critical polymer layer at which the surface properties of the system are not healed.

ACKNOWLEDGEMENTS

Financial support from the IOP-Self Healing Materials (Project SHM01053) is gratefully acknowledged.

REFERENCES

- [1] T. Dikic, W. Ming, R. A. T. M. van Benthem, A. C. C. Esteves, G. de With, *Adv. Mater.* 2012, 24, 3701-3704.
- [2] A. C. C. Esteves, K. Lyakhova, L. G. J. van der Ven, R. A. T. M. van Benthem, G. de With, Surface Segregation of Low Surface Energy Polymeric Dangling Chains in a Cross-Linked Polymer Network Investigated by Combined Experimental-Simulation Approach, *Macromolecules*, 2013, 46 (5), pp 1993–2002.

A COHESIVE ELEMENTS BASED MODEL TO DESCRIBE FRACTURE AND COHESIVE HEALING IN ELASTOMERS

A. Baldi ¹, **A. M. Grande** ¹, R. K. Bose ², A. Airoidi ¹, S. J. Garcia ²,
L. Di Landro ¹, S. van der Zwaag ²

¹ *Dipartimento di Scienze e Tecnologie Aerospaziali, Politecnico di Milano, via La Masa 34, 20156, Milano, Italy - e-mail: baldi@aero.polimi.it; grande@aero.polimi.it; alessandro.airoidi@polimi.it; luca.dilandro@polimi.it*

² *Novel Aerospace Materials, Delft University of Technology, Kluyverweg 1, 2629 HS Delft, The Netherlands - e-mail: r.k.bose@tudelft.nl; s.j.garciaespallargas@tudelft.nl; s.vanderzwaag@tudelft.nl*

Keywords: explicit finite element analyses, cohesive elements, elastomer

ABSTRACT

Several polymeric systems with intrinsic Self-Healing (SH) capabilities have been reported in literature. Many of them showed healing upon contact across the crack interface. Different parameters such as contact time, temperature, pressure or chemical activity determine the degree of healing obtained.

In this work, a numerical simulation of the healing efficiency as a function of the environment is proposed based on the use of cohesive elements in a finite element model. Cohesive elements are commonly used to model interlaminar fracture mechanisms in composite materials. In this work, they are adopted to simulate both failure and subsequent healing by a specific SH elastomeric system.

The SH elastomeric system is initially characterised by means of the identification of its conventional mechanical properties. From these results, a hyperelastic constitutive model is selected. At the same time, a model simulating fracture mechanics and healing mechanics is established and validated using a cohesive failure model in a commercial explicit finite element code. Finally, the two models are combined to evaluate the capability of the proposed numerical approach to simulate: (i) the restoration of contact of the two separated sides of the material during their re-joining, and (ii) the restoration of the mechanical properties of the elastomeric system. This later stage is directly linked to the healing efficiency. While the model does not yet capture all features of healing, it offers attractive features worth further exploring also for other SH systems.

1. INTRODUCTION

Damage propagation in elastomeric materials plays a fundamental role in many applications (e.g. seals, vibration absorbers, tyres) and the implementation of SH concepts to rubbers can extend the lifetime of structures manufactured with this innovative approach [1-3].

In this context, experimental and numerical results for the crack propagation and subsequent healing of a commercial supramolecular SH rubber are presented.

2. MATERIALS

The SH rubber Reverlink[®] grade HR, provided by Arkema in the non-cured version, was used. The supplied elastomer is characterized by a density and a glass transition temperature of 1.09 g/cm³ and 10±5 °C, respectively (producer datasheet). Uncured polymer was cast into a rectangular PTFE mould and subsequently cured in oven at 120 °C for 24 hours producing samples of typical dimensions 100x40x1 mm.

3. METHODS

Tensile and relaxation tests were performed using rectangular samples at different strain rates and strain levels, respectively. Obtained results were employed to calibrate a visco-hyperelastic model for the following numerical simulation.

Regarding damage, the energy necessary to extend a fracture plane is a material property that can be measured using different approaches (Figure 1), each providing a simple way to evaluate the failure behaviour of rubbery materials [4,5]. In this work, both tensile and tear samples were employed.

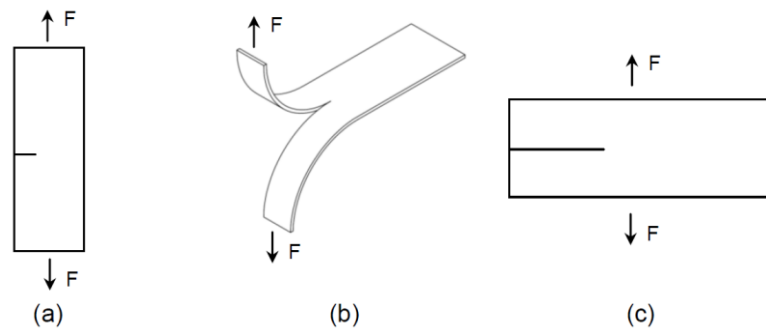


Figure 1: Tensile (A), Trouser tear (B) and pure shear test specimens (C).

The fracture propagation process experienced by the specimen in the tensile test schematically reported in Figure 1-(A) has been simulated by adopting a cohesive zone modelling approach in an explicit FE code. In order to overcome the typical problems related to the introduction in the FE scheme of high initial penalty stiffness values K_n for the conventional cohesive elements, which are characterised by infinitesimal or zero thickness, the cohesive zone model has been implemented in finite thickness solid elements with reduced integration scheme [6].

The specimen was modelled using solid elements with reduced integration scheme endowed with a visco-hyperelastic material model. In particular, a Marlow hyperelastic material model has been calibrated and integrated with a three-element Prony series.

Cohesive fracture processes along the crack propagation path has been described by means of the relative displacement ($\Delta = \mathbf{S}^+ - \mathbf{S}^-$) between the mid-point of the surface of the adjacent solid elements, which are sketched in Figure 2-(A). The components of the relative displacement vector, Δ , can be associated to the three possible modes of fracture opening, as indicated in Equation (1).

$$\Delta_I = \begin{cases} \Delta_z & \text{if } \Delta_z > 0 \\ 0 & \text{if } \Delta_z \leq 0 \end{cases} ; \Delta_{II} = \Delta_x ; \Delta_{III} = \Delta_y \quad (1)$$

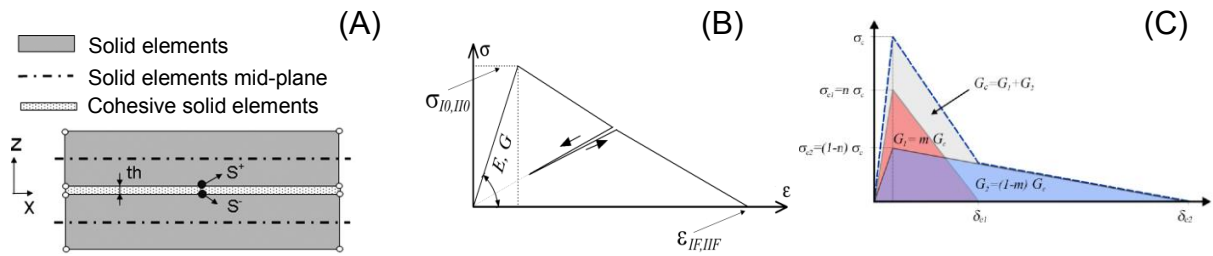


Figure 2: Scheme of the modelling technique (A), bi-linear response (B) and two superimposed bi-linear responses (C) adopted in the cohesive elements.

A scalar damage variable d is introduced in the cohesive elements to obtain the bi-linear response that has been reported in Figure 2-(B). The onset and evolution of such a damage variable can be tuned to model the strength and the toughness of the material at the location of the crack. To accomplish such an objective, the links between the critical energy release rates and the energy dissipated in the damage process are exploited [6]. For mode I opening, the link is expressed by Equation (2).

$$\int_0^{\infty} \sigma_{zz} d\Delta_I = t_k \int_0^{\infty} \sigma_{zz} d\varepsilon_{zz} = G_{Ic} \quad (2)$$

A separate material model can be used in the simulation of the healing process by simply introducing a relation between the duration of the process, the applied pressure and the mechanical properties recovered through the healing mechanism. The recovery of the mechanical properties can be obtained by reducing the value of damage parameter.

The simplest law that can model both strength and toughness in the cohesive layer is the bi-linear one shown in Figure 2-(B). Nevertheless, the shape of the response after the maximum stress may have a noticeable impact in the case of a non-negligible length of the process zone at the crack tip. This happens in the case of bridging phenomena and requires a special shape of the cohesive response. The requirement response can be obtained by using two superimposed cohesive elements, as shown in Figure 2-(C) [7].

4. RESULTS

In the model of the tensile test shown in Figure 3-(A), the strength of the cohesive layer was taken by considering the maximum stress obtained in a tensile test on an unnotched specimen. In the first round of analyses, the viscoelastic behaviour of the elastomer was neglected and a bi-linear cohesive law was used. The toughness attributed to the cohesive element had been derived from a standard tear test (Figure 1-(A)). Numerical results showed that an unstable propagation process was obtained, whereas a progressive crack propagation was apparent in the experiments. The quantitative and qualitative discrepancies between numerical and experimental responses remained unacceptable even if toughness was significantly increased (Figure 3-(B)). Correlation was improved with the introduction of viscoelastic behaviour and of a tri-linear cohesive response defined by adopting two superimposed cohesive elements. In the response presented in Figure 3-(B), the maximum loads are captured by the numerical model. The progressive crack

propagation is represented and the displacement at failure tends to be close to the experimental results. The peculiar shape in the crack region during the failure of the specimen is qualitatively modelled, as can be seen by comparing Figure 3-(A) and Figure 3-(C).

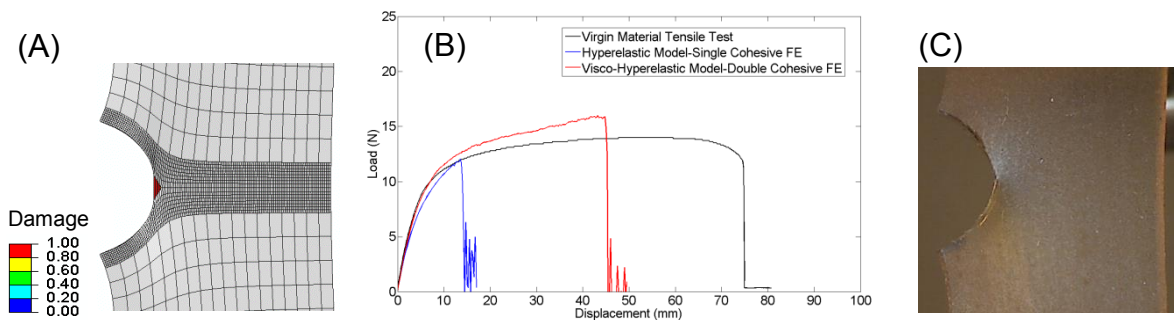


Figure 3: FE Model of the tensile test (A), numerical vs. experimental response correlation (B) experimental evidence (C)

5. CONCLUSIONS

The obtained results show that the fracture process in a healed supramolecular rubber can be modelled using a cohesive zone approach implemented in an explicit finite element code. The importance of properly representing the visco-hyperelastic behaviour and the strain softening response in the cohesive law has been outlined. Such aspects complicate the identification of material parameters, which could be obtained by means of optimization procedures. The numerical approach could represent a valuable tool for the identification of the healing effect in elastomers, overcoming the limitation of data reduction techniques applied to standard tests. Moreover, the material model could be used for simulation of healing process under externally applied load and to predict the mechanical properties of healed elastomeric layers in real-world applications.

REFERENCES

- [1] P.Cordier, F.Tournilhac, C.Soulié-Ziakovic, L.Leibler. Self-healing and thermoreversible rubber from supramolecular assembly, *Nature*, 451 (2008) 977-980.
- [2] M. W. Keller, S. R. White, N. R. Sottos. A Self-Healing Poly(Dimethyl Siloxane) Elastomer, *Advanced Functional Materials*, 17 (2007) 2399-2404.
- [3] D. Montarnal, F. Tournilhac, M. Hidalgo, L.Leibler. Epoxy-based networks combining chemical and supramolecular hydrogen-bonding crosslinks, *Journal of Polymer Science Part A: Polymer Chemistry*, 48 (2010) 1133-1141.
- [4] R. S. Rivlin, A. G. Thomas. Rupture of rubber. I. Characteristic energy for tearing, *Journal of Polymer Science*, 10 (1953) 291-318.
- [5] G. J. Lake. Fracture mechanics and its application to failure in rubber articles. *Rubber Chemistry and Technology*, 76 (2003) 567-591.
- [6] A.Airoldi, G.Sala, P.Bettini, A.Baldi, An efficient approach for modeling interlaminar damage in composite laminates with explicit FE codes, *J. Reinf. Plast. Comp.*, (2013), doi: 10.1177 /0731684412473004, *in press*.
- [7] A.Airoldi, C.G.Davila, Identification of Material Parameters for Modelling Delamination in the Presence of Fibre Bridging, *Composite Structures* 94(2012) 3240-3249.

COMPUTATIONAL PREDICTIONS OF MECHANOCHEMICALLY BASED SELF-REINFORCING ELASTOMERS

M. Silberstein¹

¹ *Department of Mechanical and Aerospace Engineering, Cornell University, Upson Hall, 14853 Ithaca, NY, USA – e-mail: ms2682@cornell.edu*

Keywords: mechanophore, elastomer, crosslinking, modeling, polymer

ABSTRACT

Mechanically-induced reactivity is a promising means for designing self-reinforcing and self-healing materials. Mechanically sensitive chemical groups termed mechanophores can be covalently linked into polymers in order to trigger specific chemical reactions upon mechanical loading (Hickenboth et. al. 2007). Experimental groups are developing mechanophore-based schemes to trigger crosslinking within polymers when mechanical reinforcement is needed (Black et. al. 2011, Diesendruck et. al. 2013). Beyond the mechanophore chemistry many issues remain unsettled from a design perspective. What deformation history is required to trigger chemical response? Over what time scales will the reinforcing reaction occur? What do these time scales depend on? How much crosslinking produces a significant change in mechanical behavior? What is a desirable mechanical property change from a structural performance perspective? Theoretical and computational approaches can address some of these questions and accelerate design of self-reinforcing polymers. Previously we developed a microstructurally-based continuum model for the opto-mechanical response of a mechanophore-linked elastomer (Silberstein et. al, submitted). This model was specified to spiropyran-linked polymethacrylate, where spiropyran is a fluorescent mechanophore and polymethacrylate is a viscous elastomer. Comparison with corresponding uniaxial tensile experimental data showed that the model provides a reasonable lower bound to the material behavior. Here we extend this model to predict behavior for an elastomer with a chemically active mechanophore. The mechanical stress caused by macroscopic deformation is transferred by the polymer chain segments to force on the mechanophores. This force modifies the mechanophore energetics according to Bell theory promoting the mechanophore reaction (Bell 1978). The mechanophore reaction then catalyzes a crosslinking reaction, assigned as either instantaneous or time delayed. The crosslinking change in turn modifies both the local force distribution on the mechanophores and the macroscopic stress. Initial crosslinking density, mechanophore inclusion density, and mechanophore energetics are studied parametrically. Optimal conditions for demonstrating self-reinforcing elastomers are identified.

SESSION 25 – SELF-HEALING SUPRAMOLECULAR MATERIALS

MULTIPHASE DESIGN OF AUTONOMIC SELF-HEALING THERMOPLASTIC ELASTOMERS

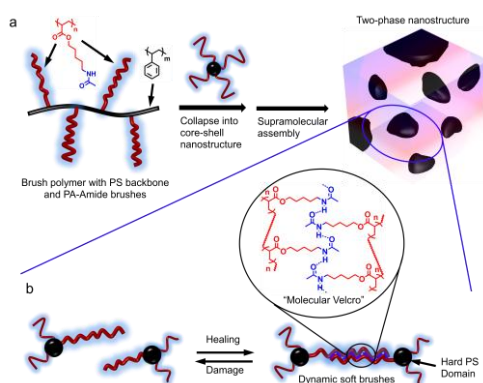
Y. Chen¹, A. M. Kushner¹, G. A. Williams¹, J. Hentschel¹ and Z. Guan¹

¹ Department of Chemistry, 1102 Natural Sciences 2, University of California, Irvine, CA 92697, USA – e-mail: zguan@uci.edu

Keywords: Self-healing, thermoplastic elastomer, multiphase material, supramolecular, brush copolymer

ABSTRACT

The development of polymers that can spontaneously repair themselves after mechanical damage would significantly improve the safety, lifetime, energy efficiency, and environmental impact of manmade materials. Most approaches to self-healing materials either require the input of external energy, or need healing agents, solvent or plasticizer. Despite intense research in this area, the synthesis of a stiff material with intrinsic self-healing ability remains a key challenge. Our laboratory has recently succeeded in a design of multiphase supramolecular thermoplastic elastomers that combine high modulus and toughness with spontaneous healing capability. In one design, H-bonding brush polymers (HBPs) self-assemble into hard-soft microphase-separated system, combining the enhanced stiffness and toughness of hybrid polymers with the self-healing capacity of dynamic supramolecular assemblies [1]. In another design, supramolecular ABA triblock copolymers formed by dimerization of 2-ureido-4-pyrimidone (UPy) end-functionalized polystyrene-*b*-poly(*n*-butylacrylate) (PS-*b*-PBA) AB diblock copolymers are synthesized, resulting in a self-healing material that combines the advantageous mechanical properties of thermoplastic elastomers and the dynamic self-healing features of supramolecular materials [2]. In contrast to previous self-healing polymers, our systems spontaneously self-heals as a single-component solid material at ambient conditions without the need of any external stimulus, healing agent, plasticizer, or solvent.



REFERENCES

- [1] Y. Chen, A.M. Kushner, G.A. Williams, Z. Guan, Multiphase design of autonomic self-healing thermoplastic elastomers, *Nature Chemistry* 4 (2012) 467-472.
- [2] J. Hentschel, A.M. Kushner, J. Ziller, Z. Guan, Self-Healing Supramolecular Block Copolymers, *Angewandte Chemie International Edition* 51 (2012) 10561-10565.

SELF-HEALING PROCESSES IN IONOMERIC ELASTOMERS

N. Hohlbein¹, T. Pelzer¹, J. Nothacker¹, M. von Tapavicza^{1,2}, A. Nellesen²
H. Datta¹, **A. M. Schmidt**¹

¹ *University of Cologne, Chemistry Department, Luxemburger Str. 116, D-50939 Cologne, Germany – e-mail: annette.schmidt@uni-koeln.de*

² *Fraunhofer UMSICHT, Osterfelder Str. 3, D-46047 Oberhausen, Germany*

Keywords: self-healing elastomers, ionomers, dynamic bonds, rheology

ABSTRACT

The use of dynamic bonds in self-healing polymeric systems allows restoring of the chemical structure and mechanical properties multiple times. In this respect, the use of ionomers represents a promising approach. The strong interaction between ionic moieties within a non-polar matrix leads to microphase separation and a behavior similar to covalent crosslinks in a thermally reversible network. The implementation and parameter optimization, however, requires a profound understanding of the structure-property relationships.

Motivated by recent findings on the excellent self-healing behavior of ionomeric NBR-based systems, we report on an ionomer model system designed to explore the thermal and viscoelastic properties of these materials by varying the ionic content, neutralization degree and nature of counter-ions.

The dynamic mechanical properties of the materials are investigated by rheological oscillation measurements in dependence on the ionic content and the nature of cation.

The temperature-reversible formation of ionic cross-links, an essential feature for the ability of extrinsic self-healing by thermal activation, is shown to be possible by incorporation of magnetic nanoparticles. The transfer of the basic results to NBR elastomers is successfully demonstrated.

1. INTRODUCTION

Environmental stress and weathering may lead to micro- and macro-cracks in elastomers resulting in a catastrophic failure of the material performance, especially when the device material is difficult to access and hence difficult and expensive to repair. This raised the scientific interest in self-healing elastomers towards more reliable and durable materials. Up to now, many concepts have been successfully developed on autonomous self-healing thermo- and duroplasts e. g. microcapsule and fiber approaches [1,2], but their transfer to elastomers is still a challenge due to their drastic processing and working conditions. In addition, the reversibility of the healing processes in such systems is limited, while the use of dynamic bonds allows to rearrange the chemical structure and to restore mechanical properties multiple times.

Non-covalent intermolecular bonds based on π - π stacking, hydrogen bonds, or metal-ligand interactions thus open pathways to unique, structurally dynamic materials that

may be designed to be sensitive to a wide range of stimuli [3]. When properly designed, they show great potential as self-healing systems, and within this class of materials, ionomers represent a promising approach toward novel self-healing elastomers [4,5]. As such, a properly designed system requires a highly viscous flow at low strain conditions, while it shall behave like an elastomer under working conditions. Based on these material requirements, we developed an ionomer model system with a flexible polymer backbone including only ionic crosslinks [6,7]. Dynamic mechanical and thermal properties of the model ionomers are studied in dependence of the ionic content and the nature of the counter ions. As an additional feature, magnetic nanoparticles are incorporated in order to allow for a local heating effect in an oscillating electromagnetic field (OEMF) as an external trigger for self-healing.

2. MATERIALS

The model system is based on copolymers of n-butylacrylate and a varying fraction of t-butylacrylate prepared by Atom Transfer Radical Polymerization (ATRP). The polymers show an adjustable molecular weight up to 80.000 g/mol and a narrow molecular weight distribution (PDI: 1.08- 1.2). After selective hydrolysis of the t-butyl groups, carboxylic acid moieties are formed that are neutralized with basic sodium, zinc or cobalt salts to produce the corresponding ionomer. Similarly, carboxylated NBR (XNBR) is transferred to ionomeric elastomers. For composites that allow a local heating activation, cobalt, magnetite and cobalt-ferrite nanoparticles are incorporated in different contents into the model copolymer and NBR matrices, respectively.

3. METHODS

^1H - and ^{13}C nuclear magnetic resonance (NMR) and respective 2D methods are employed to elucidate the copolymer composition and sequence structure. The degree of neutralization and the specific metal coordination are detected by infrared spectroscopy (FT ATR-IR). Differential scanning calorimetry (DSC) is used to detect the glass transition temperature of the polymer matrix T_g and the transition temperature of ionic aggregates T_i with a heating rate of $10\text{ K}\cdot\text{min}^{-1}$, while small-angle X-ray scattering (SAXS) measurements are performed for the superstructure of the copolymers. The dynamic shear storage (G') and loss (G'') moduli are measured by oscillatory rheometry using parallel plates of diameter 40 mm and a gap of 1.0 mm. The measurements are performed on homogeneous polymer samples with a frequency sweep from 3.14 to 628 rad/s at $25\text{ }^\circ\text{C}$ with 2% strain level. Thermorheology is used to study the influence of temperature on dynamic properties in the range of $20 - 90\text{ }^\circ\text{C}$ at a heating rate of $10\text{ K}\cdot\text{min}^{-1}$. The magnetic heating behavior of ionomeric composite samples is investigated using a high frequency generator equipped with a water-cooled copper induction coil, operated at 247 kHz with a magnetic field amplitude of $31.5\text{ kA}\cdot\text{m}^{-1}$. The sample temperature is recorded with an optic temperature sensor. Tensile testing is carried out using 15 mm x 2 mm pressed sample stripes and an elongation rate of 500 mm/ min.

4. RESULTS AND DISCUSSION

All methods indicate a successful formation of model ionomers with predetermined structure by using the employed synthetic pathway. As well SAXS as DSC experiments indicate an influence of the nature of the cation on the phase separation, increasing in order $\text{Co}^{2+} < \text{Zn}^{2+} < \text{Na}^+$.

All model ionomers show a qualitative similar dynamic mechanical behavior in oscillatory rheology. At low frequencies, the shear loss (G'') modulus is dominant, indicating a prevailing viscous behavior. With increasing frequency, the shear storage (G') modulus increases, and a G''/G' cross-over to a dominating elastic behavior is observed at a frequency that depends on the ion content and the nature of the counter ion. The loss angle $\tan\delta$ defined as the ration of G'' and G' serves as a significant value to describe the frequency-dependent viscoelastic behavior of the employed systems (Fig. 1, left). Temperature-dependent rheology experiments reveal a shift of the crossover point to higher frequencies with increasing temperature, and a shift of the ionic transition (indicated by a strong increase of $\tan\delta$) to higher temperatures with increasing frequency (Fig. 1, right).

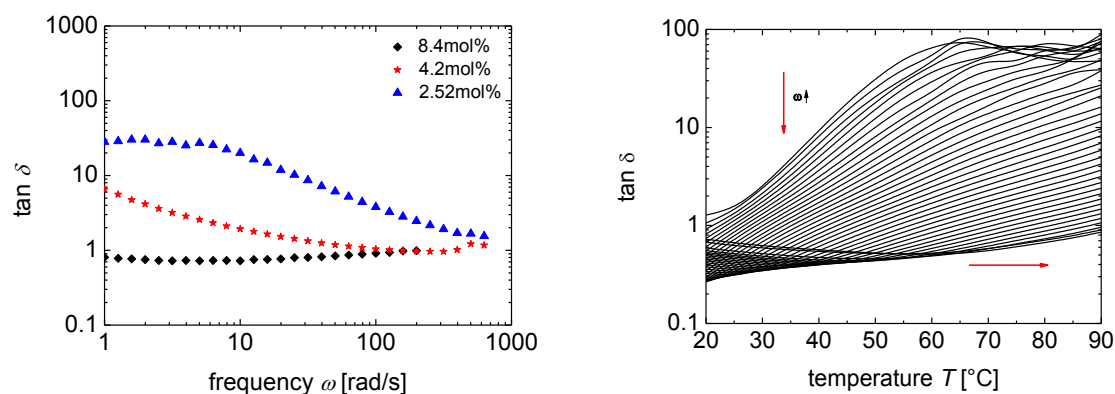


Figure 1: Frequency dependency of the loss angle $\tan\delta$ for Co^{2+} -based ionomers with different ionic content (left), and temperature dependence of $\tan\delta$ for a Zn^{2+} based ionomer (right).

By incorporation of magnetic nanoparticles into the ionomer matrix, a local heating effect is possible employing an alternating magnetic field that is correlated to the particle content (Fig. 2, left). The temperature effect accelerates the healing effect of the materials, and a transfer of the concept to XNBR systems is successfully shown. We have demonstrated a dependence of the self-healing efficiency on the healing temperature, and the impact of the external magnetic field is evident (Fig. 2, right). Tensile tests show a nearly 100% recovery of the original breaking elongation of ZN-HNBR healed at 55°C.

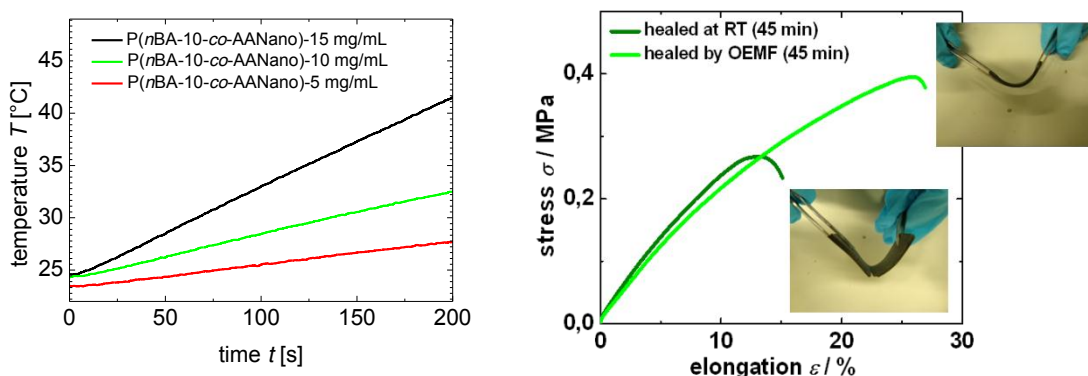


Figure 2: Magnetic heating profiles for magnetic ionomer composites with varying particle content (left), and tensile profiles of a Co@Zn-HNBR (0.5 wt%) healed at RT with and without magnetic field application, respectively (right).

5. CONCLUSIONS

The self-healing behavior of ionomeric elastomers is of high interest for prospective applications, and a profound understanding of their structure-property correlation is required for the optimization of the effect. The presented ionomer model system clearly shows the relationship between the dynamic and thermal properties, the nature of the cation and the ionic content. It is further shown that the ionic aggregates can be stimulated by different heating methods. Local heating in alternating magnetic fields is a selective and effective activation mode as well in the model systems as in NBR matrices, and correlates to the content of incorporated magnetic nanoparticles. A proof of concept for self-healing MNP filled elastomers is demonstrated.

ACKNOWLEDGEMENTS

We gratefully acknowledge the DFG (SPP 1568, “Design and Generic Principles of Self-healing Materials”) for financial support, and Dr. Wim Pyckhout-Hintzen at the Forschungszentrum Jülich for SAXS measurements.

REFERENCES

- [1] S. R. White, N. R. Sottos, P. H. Geubelle, J. S. Moore, M. R. Kessler, S. R. Sriram, E. N. Brown, S. Viswanathan, *Nature* 409 (2001) 794-797.
- [2] C. Dry, *Composite Structures* 35 (1996) 263- 269.
- [3] L. Leibler, *Macromolecules* Vol. 13 No.6 (1980) 1602- 1617.
- [4] N. Hohlbein, M. von Tapavicza, A. Nellesen, A. M. Schmidt, in: W. H. Binder (Ed.), *Self-Healing Polymers: from Principles to Applications*, Wiley-VCH, 2013, pp. 323-342.
- [5] A. Eisenberg, M. Rinaudo, *Polymer Bulletin* 24 (1990) 671.
- [6] M. von Tapavicza, A. Nellesen, J. Bertling, A. M. Schmidt, *Proceedings of the Third International Conference on Self-Healing Materials*, Bath, 2011.
- [7] N. Hohlbein, T. Pelzer, M. von Tapavicza, H. Datta, A. M. Schmidt, *Proceedings of the Makromolekulares Kolloquium*, Freiburg, 2013.

SELF-HEALING SUPRAMOLECULAR POLYMER NANOCOMPOSITES

Z. Liu¹, N. A. M. Besseling¹, E. Mendes¹ and S. J. Picken¹

¹ Chemical engineering Department, Delft University of Technology, Julianalaan 136, 2628 BL Delft, The Netherlands – e-mail: zhen.liu@tudelft.nl

Keywords: Polyborosiloxane (PBS), hydrogen-bonding, self-healing

ABSTRACT

Polyborosiloxanes (*PBSs*) are viscoelastic, transparent, colourless, self-healable polymer matrices, synthesized by reacting linear polydimethylsiloxanes (*PDMSs*) with boric acid (*BA*) above 150°C. *BA* takes part not only in cleaving the *PDMS* chains, but also contributes boronic-acid like moieties to the cleaved chain ends, which provide supramolecular self-healing capabilities. *PBSs* can be regarded as supramolecular elastomers, owing to the reversible cross links formed by the abundant hydroxyl groups. Therefore they are able to recover both the microscopic and macroscopic fractures intrinsically via hydrogen-bonds. Additionally, a glass transition temperature (T_g) as low as -90°C ensures chain mobility to *PBSs* molecules to heal cracks autonomously without extra heat supply. Compared to traditional carbon-based polymeric materials, *PBSs* provide a higher resistance to heat and light owing to the siloxane backbone. Upon increasing the degree of modification, *PBSs* get stronger on the one hand. However, *PBSs* also become less adhesive and start suffering from brittle fracture. Interestingly, the addition of nano-clay (*Cloisite 30B*) solves this problem. It does not make *PBSs* more brittle as it does in traditional thermal plastics. Instead, it renders *PBSs* ductile but strong. Comparing to *PBSs*, the *PBSs/Cloisite 30B* nanocomposites even exhibit an additional filler-induced mechanical relaxation at high frequency. This phenomenon implies that *PBSs/Cloisite 30B* nanocomposites can be applicable as self-healing shock absorber. Further investigations will be focusing on characterization of the self-healing capacity, on strengthening the composites and on tuning the position of the filler-induced rheological response.

Upon applying other (nano-sized) reinforcements, *PBSs* can be endowed with wide variety of targeted functionalities, for instance, stiffness by nano-clay; thermal conductivity by graphite or boron nitride; piezoelectric properties by lead zirconate titanate (*PZT*), etc. The presence of particles is also advantageous for the adhesive properties of the composites, because particles lower the number of hydrogen-bonds by, either isolating molecules or forming particle-molecule interaction.

1. INTRODUCTION

Polyborosiloxanes (*PBSs*) were invented during the World War II in the U.S.. The goal was to look for synthetic rubber compounds to solve the shortage of natural rubber. However, *PBSs*, possessing reversible physical cross-links, were born accidentally, and served the world for decades under the names, Silly Putty, bouncing putty¹, Solid-liquid², dilatant compound³, etc.

In the field of self-healing materials, two main mechanisms exist, encapsulated systems and intrinsic systems. One ‘family’ relies on the implanted capsules, which contain healing agents. Upon loading, capsules may break and the released healing agent in order to close local cracks. In intrinsic systems, the cross-links among molecules are physically reversible. So in principle, the intermolecular disconnection due to fractures can reconnect autonomously whenever it appears. PBSs constitute an important contribution to the intrinsic self-healing family, as they are outstanding self-healing matrices, which have the potential to deliver abundant self-healing composites by adding functional filler particles. For instance, nano-clay increases the stiffness of PBSs; graphite and boron nitride give rise to thermal conductivity; lead zirconate titanate (*PZT*) enhances piezoelectric property, etc.

This paper will present the characterization of the lab-synthesized *PBSs*, the properties of *PBSs*/filler composites, and efforts to quantify the self-healing capabilities of *PBSs* and their composites.

2. MATERIALS AND METHODS

Trimethylsiloxy terminated polydimethylsiloxanes (*PDMSs*) and boric acid (*BA*) are heated at 200°C to produce the viscoelastic *PBSs*. The siloxane backbone of *PDMS* cleaves in the presence of *BA*, which leads to a $-\text{SiOB}(\text{OH})_2$ structure at the new chain ends. n-Hexane is used to dissolve the products, in order to filter out unreacted *BA* and other unexpected side-products.

Nano-sized clay platelets (*Cloisite 30B*), graphite, and lead zirconate titanate (*PZT*) give rise respectively to stiffness, thermal conductivity, and piezoelectric properties. Brabender blander is used to mix the filler particle with *PBSs* matrix, in order to prepare the *PBSs* composites.

Fourier transform infrared (*FTIR*) spectroscopy is used to characterise the cleavage of the siloxane backbone, generation of Si–O–B linkages, and the presence of *BA* as impurity. By means of a TA AR-G2 rheometer, the self-healing capacity of *PBSs* matrices was also quantified in the plate-plate geometry.

3. RESULTS AND DISCUSSION

Figure 1 shows the *FTIR* spectra of pure *PDMSs* that have been held at 240°C for different durations. The absorption bands correspond to specific chemical groups, for instance, peaks in the range of 1020–1090 cm^{-1} present the vibrations of the siloxane backbone⁴. Other bands⁵ correlated to our research assign to, $-\text{Si}(\text{CH}_3)_2$ at 880 cm^{-1} and 1260 cm^{-1} , $-\text{CH}_3$ at 2905 cm^{-1} , and $-(\text{CH}_3)_2$ at 2960 cm^{-1} , etc. Upon heating, the spectra of pure *PDMSs* do not change with time, except for a slight decrease of the band corresponding to the siloxane backbone. This implies *PDMSs* are quite resistant at 240°C, besides a minor degree of backbone cleavage, due to residual water molecules.

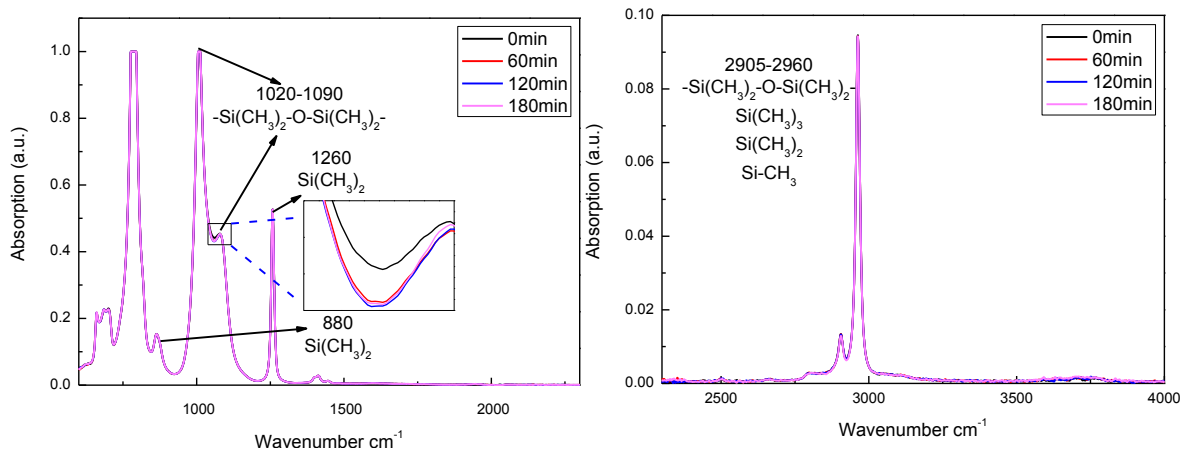


Figure 1: FTIR spectra of the pure PDMSs heated at 240°C

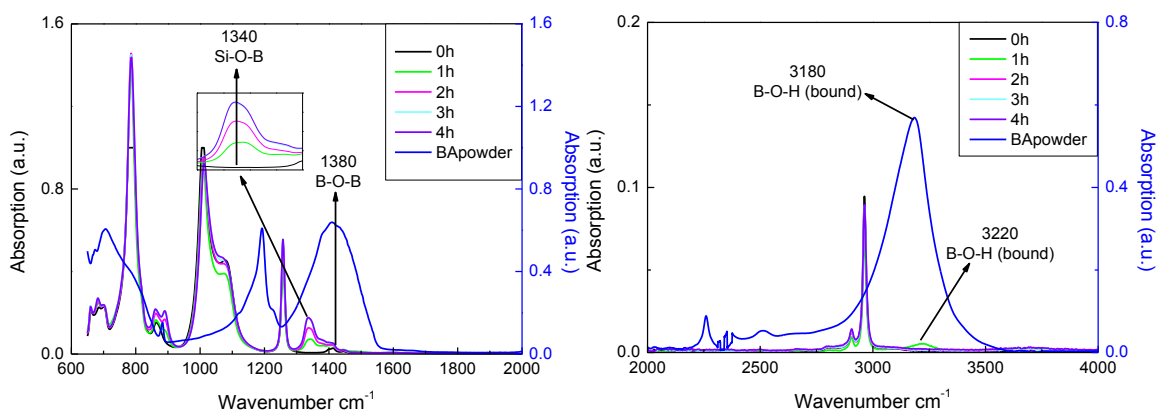


Figure 2: FTIR spectra of a mixture of *PDMSs* and *BA* reacted at 200°C for different reaction times

Boric acid (*BA*) plays a crucial role in the cleavage of polydimethylsiloxanes (*PDMSs*) backbone. In the presence of *BA*, *PDMSs* undergo backbone cleavage in a less rigid condition (above 150°C⁶⁻⁸). Polyborosiloxanes (*PBSs*) were synthesized by mixing *PDMSs* and *BA* at a weight ratio of 10:1 at 200°C in this work. To observe the change in the molecular structure of *PDMSs*, *FTIR* spectroscopy was applied on samples with various reaction times. Figure 2 introduces three relevant new bands. At 1340 cm^{-1} , a peak appears and grows as the reaction continues, which is assigned to the Si-O-B linkage. Its appearance signifies that *BA* has connected to the siloxane backbone. Bands around 1380 cm^{-1} and at 3180 cm^{-1} correlate with the B-O-B and the bound B-O-H structures in the crystalline boric acid. The absence of B-O-B assigned band in our *PBSs* indicates that our reaction procedure does not involve significant boric acids polymerization, Hence no big, branched molecule is produced. The B-O-H assigned band exists in *PBSs* in the early stages (1h), but vanishes later. The reason is, the B-O-H structure in *BA* crystals dissociates and is consumed during the reaction.

We have designed an approach to quantify the self-healing capacity using the rheometer, where we program the rheometer to perform cyclic pulling and squeezing. By measuring the normal force of each step, the self-healing behaviour can be roughly quantified. Pure *PDMSs* served as reference (in black) and experiments were

run at two operation temperatures (Figure 3). In both cases, the normal force vs. gap (sample deformation, in μm) plot of the 2nd pulling step (in pink) is well overlapping with the 1st pulling step (in red) after resting, which indicates the deformed *PBSs* have healed cohesively and autonomously. Additionally, an increase in healing temperature shortens the healing time.

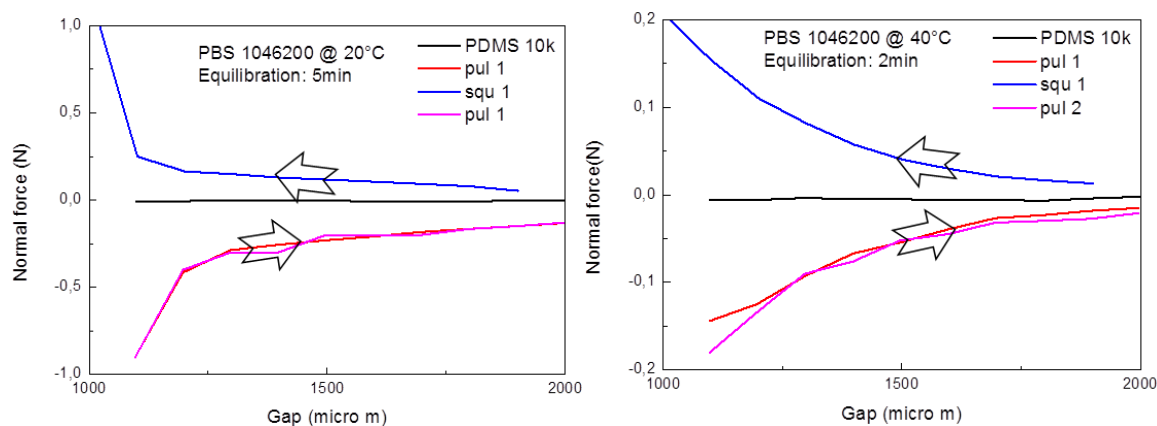


Figure 3: Quantification of the self-healing capacity.

4. CONCLUSIONS

Formation of the Si–O–B moieties in polyborosiloxanes (*PBSs*) has been demonstrated by *FTIR*. Together with the absence of B–O–B, we announce that the intention of producing a class of supramolecular self-healing materials has been accomplished. A cyclic pulling and squeezing experiment has proved that *PBSs* are capable of self-healing, intrinsically and autonomously.

ACKNOWLEDGEMENTS

Financial support from the Innovation Oriented research Programs (IOP) for this study (Project No. TCOC42) is gratefully acknowledged.

REFERENCES

- [1] Juhász, A.; Tasnádi, P.; Fábry, L. *Physics Education* 1984, 19, 302–304.
- [2] Goertz, M. P.; Zhu, X. Y.; Houston, J. E. *Journal of Polymer Science: Part B: Polymer Physics* 2009, 47, 1285–1290.
- [3] Hailemariam, H.; Mulugeta, G. *Tectonophysics* 1998, 294, 131–141.
- [4] Voronkov, M. G. *The Siloxane Bond*; Consultants Bureau, 1978.
- [5] Willis, R. F.; Shaw, R. F. *Journal of Colloid and Interface Science* 1969, 31, 397–423.
- [6] Wright, J. G. E. *Process for making puttylike elastic plastic, siloxane derivative composition containing zinc hydroxide*. 1944.
- [7] McGregor, R. R.; Warrick, E. L. *Treating dimethyl silicone polymer with boric oxide*. 1943.
- [8] Zinchenko, G. A.; Mileshekevich, V. P.; Kozlova, N. V. *Polymer Science U.S.S.R.* 1981, 23, 1421–1429.
- [9] Meyers, M. A.; Chawla, K. K. *Mechanical behaviour of materials*, 1999, 98-103.

SYNTHESIS AND MECHANICAL ANALYSIS OF TRANSIENT-COVALENT DOUBLE NETWORKS

C. H. Hövelmann¹, B. Gold¹, A. Brás¹, J. Allgaier¹, W. Pyckhout-Hintzen¹,
A. Wischnewski¹ and D. Richter¹

¹ JCNS : Jülich Centre for Neutron Science, Forschungszentrum Jülich, Wilhelm-Johnen-Straße, 52428 Jülich, Germany – email : c.hoevelmann@fz-juelich.de; b.gold@fz-juelich.de; a.bras@fz-juelich.de; j.allgaier@fz-juelich.de; w.pyckhout@fz-juelich.de; a.wischnewski@fz-juelich.de, d.richter@fz-juelich.de

Keywords: self-healing, network, elastomer, hydrogen bond

ABSTRACT

Nature uses a combination of dynamic hydrogen bonds and static covalent bonds in e.g. the muscle sarcomer to achieve toughness in otherwise elastic materials. The dynamic bonds can open when a force is applied, thereby providing a stress-relieve mechanism to prevent rupturing of the covalent links. Upon release of external force the hydrogen bond network can heal to restore the former properties. To mimic these astonishing effects we envisioned a similar combination in elastomeric compounds by creating a dual network of hydrogen bonded and covalently linked polyisoprene.

We synthesized a number of dual networks by first modifying polyisoprene with hydrogen bond forming urazole groups to form supramolecular networks with a cross-linking density between 0 and 15 mol%. In a second step covalent crosslinks were added by hydrosilylation with a bissilane linker.

Linear rheological analysis of the transient network showed a dissipation mechanism extrapolated to be on the order of 0.01 - 0.10 s at ambient temperature. In combination with neutron scattering, which provides unrivalled and first insights on the chain level, the self-healing properties of these novel semi-transient networks are studied on the molecular level in static and dynamic deformation through a selective labelling of chains. Understanding of the self-healing mechanism in these mixed covalent and transient systems will allow the development of new polymeric materials with advanced functionality.

1. INTRODUCTION

The combination of dynamic and static bonds can lead to improved material properties. This unique design is credited with the unusual combination of strength, toughness and elasticity that is found in muscle proteins [1]. We envisioned to mimic this properties by constructing a twice crosslinked elastomeric network consisting of transient links by H-bonding urazole connections and permanent links via a covalent connection by hydrosilylation crosslinking.

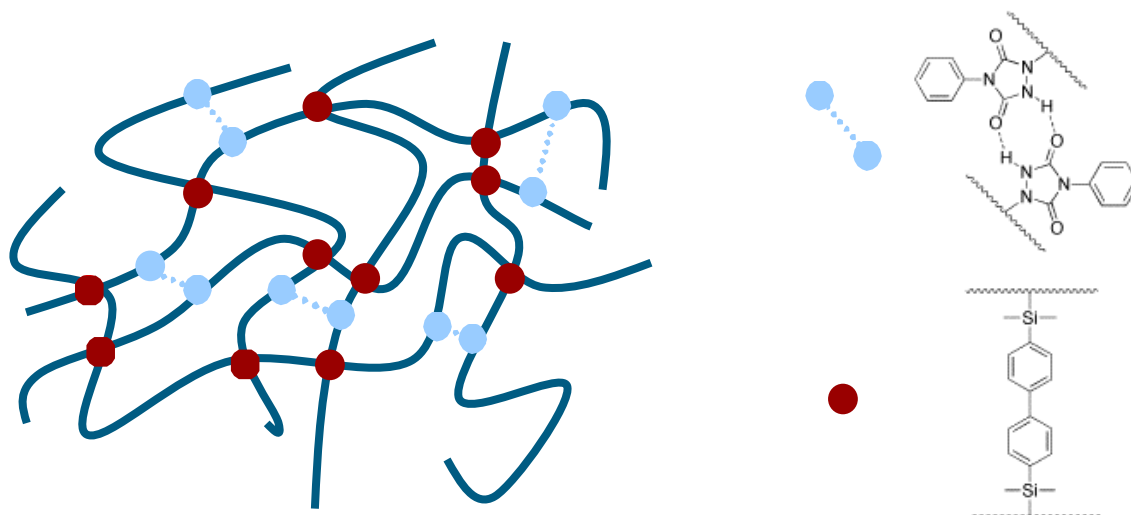


Figure 1: Elastomeric double networks with transient and covalent crosslinks.

2. MATERIALS

Polyisoprene and polybutadiene were synthesized by standard anionic polymerization techniques using *t*-butyl lithium as initiator and cyclohexane as a solvent with a molecular mass of $M=100K$ and a PDI of 1.02. The urazole functionalization was performed according to known literature procedures [2] by reacting a THF solution of the polydiene with 4-Phenyl-1,2,4-triazoline-3,5-dione to give a number of functionalized polyisoprenes with 1,2,4,8 and 15% of the monomer units functionalized. These transient networks were further crosslinked by hydrosilylation with a 4,4'-bis(dimethylsilane)biphenyl linker using 0.1mol% of Karstedt's catalyst at 95°C. This final crosslinking was performed in bulk state in a teflon mold to obtain 15x60x1 mm elastomer films that were used in all further investigations.

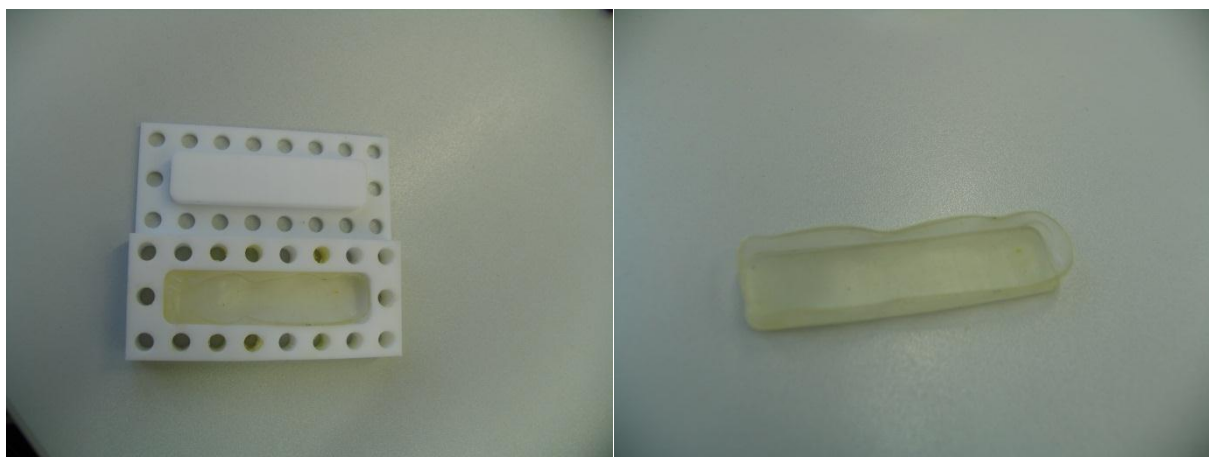


Figure 2: Teflon mold (left) and polyisoprene double network (right)

3. METHODS

The rheological and mechanical experiments on the uncrosslinked and crosslinked networks respectively were conducted using an Advanced Rheometric System

(ARES, Rheom. Sci. Instrum.), equipped with a 2K-FRT transducer using a parallel plate geometry for the dynamical modulus $G^*(\omega)$ in the temperature range of -40 to $+25^\circ\text{C}$ and frequency range between 0.01 and 100 rad/s, and a tensile testing tool for the measurement of the normal stress as a function of the travelled distance at ambient temperature. The normal force was recorded as a function of time during the extension to $\pm 100\%$.

4. RESULTS

We synthesized a number of polydiene transient-covalent double networks by combination of an ene-reaction for the urazole functionalization and hydrosilylation for the covalent crosslinking. Rheological experiments were performed both on the transient and the double networks. To investigate the dissipation of the H-bonds step-shear as well as oscillatory shear experiments were performed on the urazole functionalized polyisoprene. The transient network component is evidenced from a pronounced new loss peak in $G''(\omega)$ and corroborated from the time dependence in a separate step-shear and subsequent relaxation at the temperature of -20°C as is shown to avoid the onset of thermorheological complex behavior. The increase of the storage modulus as well as the slowing down of the dynamics compared to the unmodified polymer points at an additional elastic contribution from the H-bonds.

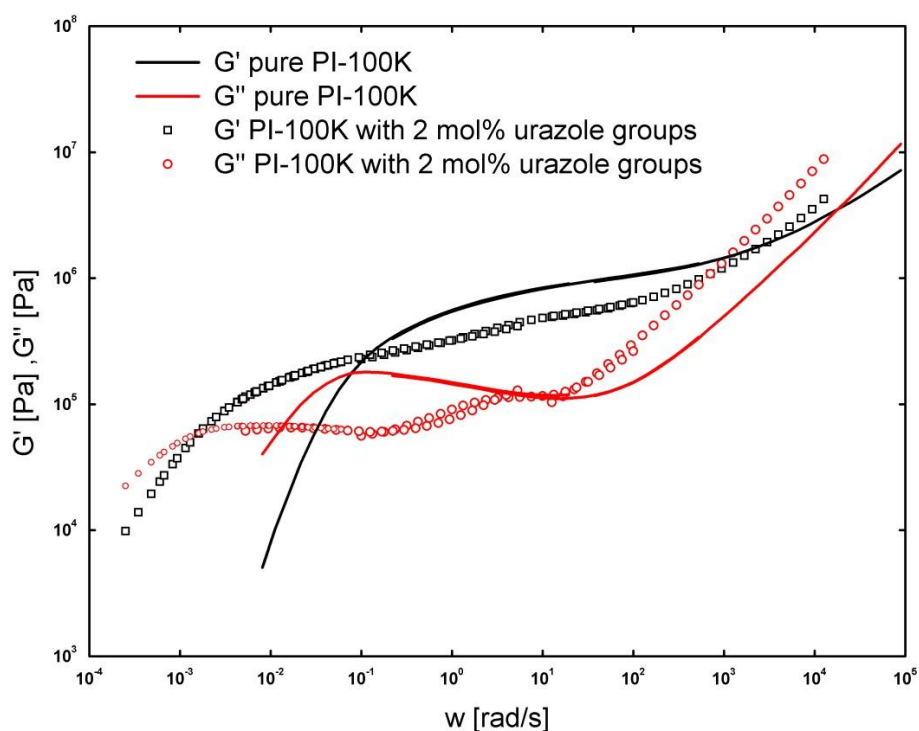


Figure 3: Shear modulus of polyisoprene with 2% urazole functionalization.

The evaluation of the stress-strain data on the crosslinked networks with and without supramolecular functionalization was limited to the lowest strains where Hookean behavior i.e. $\sigma = E \varepsilon$ should prevail. The increase of the Young modulus E reflects the additional networking and compares well to the increase in the high frequency plateau of the storage modulus $G'(\omega)$.

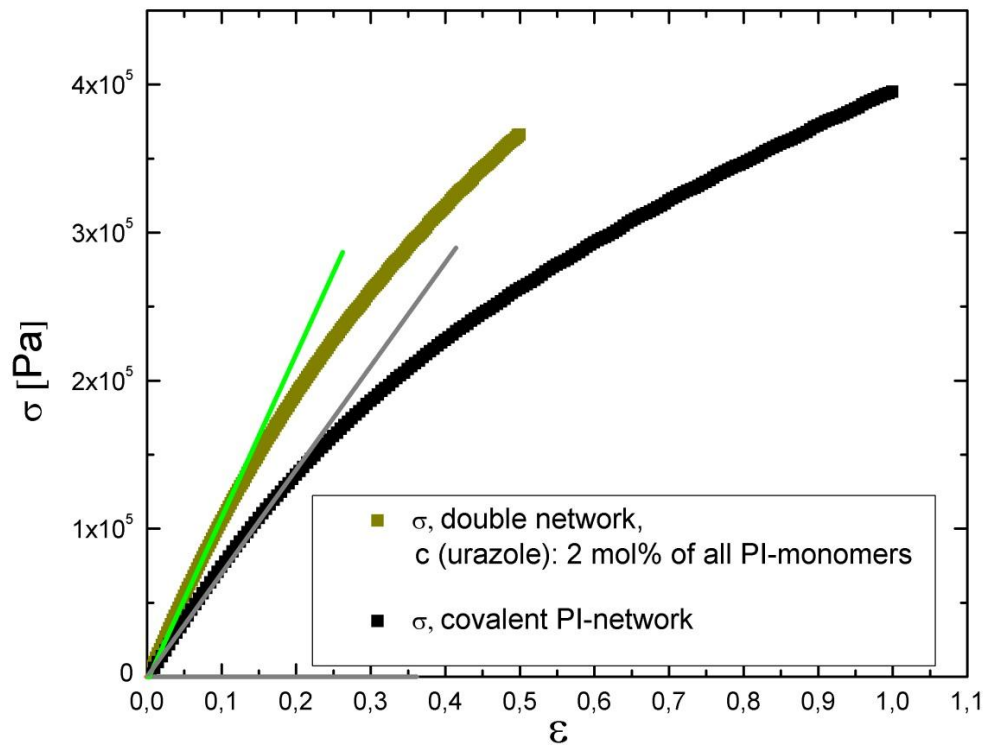


Figure 4: Stress-strain experiment on a double network compared to the corresponding covalent crosslinked network.

5. CONCLUSIONS

We synthesized a new elastomeric material that combines transient and covalent crosslinks. Preliminary rheological experiments show a dissipation of the H-bonds in the transient networks. Stress-strain experiments show the contribution of the transient bonds to the Young modulus of the compound. Both can be combined to achieve new adaptive systems for dynamical applications.

REFERENCES

- [1] R. J. Wojtecki, M. A. Meador, S. J. Rowan, Using the dynamic bond to access macroscopically responsive structurally dynamic polymers, *Nature Mater.* 10 (2011) 14-27
- [2] R. Stadler, J. Burgert, Influence of hydrogen bonding on the properties of elastomers and elastomeric blends, *Makromol. Chem.* 187 (1986) 1681-1690

SESSION 26 – SELF-HEALING FIBER-REINFORCED COMPOSITE MATERIALS

COMPARTMENTED FIBRES: THE CONCEPT OF MULTIPLE SELF-HEALING IN ADVANCED FIBRE COMPOSITES

M. Prajer¹, X Wu¹, S. J. García¹ and S. van der Zwaag¹

¹ *Novel Aerospace Materials Group, Faculty of Aerospace Engineering, Technical University of Delft, Kluyverweg 1, 2629 HS, Delft, The Netherlands – e-mail: S.vanderZwaag@tudelft.nl*

Keywords: self-healing, polymer composites, compartmented fibres, multiple release

ABSTRACT

Polymers reinforced with high performance fibres are successfully replacing metal alloys in lightweight aircraft structures. A critical factor in structural design is the resistance of a structure to progressive damage which develops during its service time. The brittle nature of matrix cracking is the main source of composite failure initiating ply delamination and fibre to matrix debonding.

Bio-inspired autonomous healing systems, embedded in a polymer matrix, are being developed to improve the fracture resistance of structural composites [1, 2, 3]. An exemplary system can consist of fibres with individual compartments, i.e. compartmented fibres, which are filled with a healing liquid. The healing agent is distributed within the fibre in the form of long elongated compartments of ellipsoidal shape with high aspect ratio. The fibres are designed to release the liquid healing agent at multiple specific microcrack sites developed in the polymer matrix as a result of structural loading during its life-time.

The advantage of such a fibre as a healing agent carrier is obvious - compartmented fibres enable multiple local healing events. Neither is the whole healing agent consumed in the first damage/healing event (as for hollow fibres) nor is the functionality of remaining compartments affected by the healing event (compared to vascular networks).

Compartmented fibres were spun from an oil/water emulsion of a healing agent in an aqueous solution of sodium alginate. The retention of the liquid healing agent (*ortho*-dichlorobenzene) in a solid fibre was provided by the coagulation of the alginate polymer during fibre formation.

Spun fibres were embedded in polymethylmethacrylate, pre-cracked in 3 point bending and allowed a certain period of time to self-heal before they were loaded again. Computed micro-tomography was used to visualise damage and healing sites. Test samples with the new fibres located at the likely damage sites were able to recover, (in part) their mechanical properties.

The concept of multiple release of healing agent from a compartmented fibre into the surrounding polymer matrix was demonstrated successfully.

1. INTRODUCTION

Multi-compartmented fibres were spun from an oil in water emulsion of a healing agent in an aqueous solution of sodium alginate [4]. The emulsion was extruded through a spinneret into a coagulation bath where the fibre solidification and liquid retention took place as a result of the ion exchange reaction (sodium alginate is a natural polysaccharide able to cross-link with bivalent ions such as Ca^{2+} and form a three-dimensional network). In this work alginate fibres containing 1,2-dichlorobenzene as a healing agent for polymethylmethacrylate (PMMA) resin were prepared. Spun fibres were embedded in a PMMA resin and compression moulded. Three-point bending test combined with computed μ -tomography was used to prove that compartmented fibres are able of distributed multiple-healing of the surrounding polymer matrix.

2. MATERIALS AND SAMPLE PREPARATION

2.1 Materials

Sodium alginate (ALG), σ -dichlorobenzene (DCB), Poly(ethylene-maleic-*alt*-anhydride) (PEMA) and Calcium chloride hexahydrate were purchased from Sigma-Aldrich, The Netherlands.

2.2 Spin dope preparation and fibre spinning

Sodium alginate was dissolved in de-ionized water and a 6 wt.% solution was prepared. PEMA 2.5 wt.% solution was prepared by dissolving the copolymer in water at 70°C/60 min. Appropriate amounts of PEMA solution were mixed with the sodium alginate solution using a high speed mixer at 2500 rpm for 2.5 min. After that the mixture was continuously stirred with a three-blade stirrer and the DCB was slowly injected. The emulsification took place at 300 rpm for 5 and 10 min, depending on the desired morphology of the emulsion. The composition of the final emulsion was as follows: the DCB/ALG ratio was 1/4 and the PEMA/DCB ratio was 1/50. Fibres with small and large compartments were spun using a plunger based lab scale spinning line in a conventional wet spinning process. A spinneret containing one capillary of 0.25 mm diameter and 2 mm length was used. The extrusion rate was 38 $\mu\text{l}/\text{min}$. and the take up speed was 1.3 m/min. The coagulation bath was 0.8 m long and contained a 0.45 M solution of $\text{CaCl}_2 \cdot 6\text{H}_2\text{O}$. Fibres were wound onto a pre-heated (40°C) plastic bobbin.

2.3 Composites

As spun compartmented fibres were unidirectionally aligned and embedded in a thin layer of castable polymethylmethacrylate (PMMA) on top of 3 mm thick extruded sheet of PMMA. The thickness of the layer containing the fibres was 300 μm . Beams for three point bending test were cut from the sheets. Compartmented fibres were placed on the tension side of the beam.

3. METHODS

3.1 Three point bending

Composite beams were tested in three-point bending (*off-axis* geometry). Composites were pre-strained up to $\varepsilon = 4\%$ to crack open the compartments and allowed to heal after the test. After the healing period the samples were bended again, this time in a different normal plane (i.e. *off-axis*), and up to the strain of $\varepsilon = 7\%$ (ultimate failure). X-ray micro-computed tomography was used to observe compartments crack opening and the release of the healing agent into the surrounding polymer matrix. Samples were X-ray scanned before bending, after the first and after the second bending test.

3.2 Computed μ -tomography (μ -CT)

Compartment crack opening and healing agent release was measured with Phoenix Nanotom X-ray tomography scanner, using 100 kV radiation. The contrast of the encapsulated healing agent was enhanced with 1,2-dibromobenzene (density of 1.956 g/cm^3). The samples were rotated along their longitudinal axis and three X-ray attenuation images were recorded and averaged every 0.5° . The image reconstruction was done using the Phoenix reconstruction software package. The resolution of the X-ray tomography scan was $(3\mu\text{m})^3$ per voxel. The final rendering of the 3D tomography of the cracked compartments was completed with Volume Graphics 2 software.

4. RESULTS

Computed μ -tomography is a powerful non-destructive testing method which was used to qualitatively investigate the release of healing agent from compartmented fibres embedded in polymer matrix after the flexural test of polymer composites.

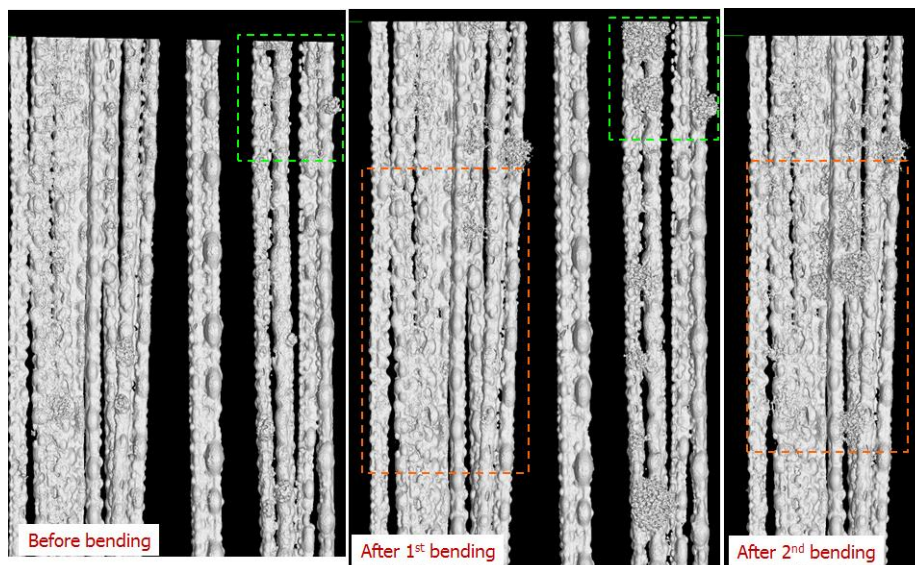


Figure 1: Morphology of compartmented fibres embedded in a polymer matrix before and after successive flexural tests reconstructed with computed μ -tomography.

Figure 1 shows the compartment opening and healing agent release into the polymer matrix before and after successive flexural tests. Release of healing agent is manifested from the formation of local cauliflower like structures. Pre-cracked composites were allowed to heal for one week prior to subsequent secondary *off-axis* loading. The images shown are viewed from the tension side of the composite beam. It can be seen from Figure 1 that new compartments are opened when the fibre is more strained and new healing agent is delivered into the neighbouring matrix. The compartmented fibre responds to the damage progressively.

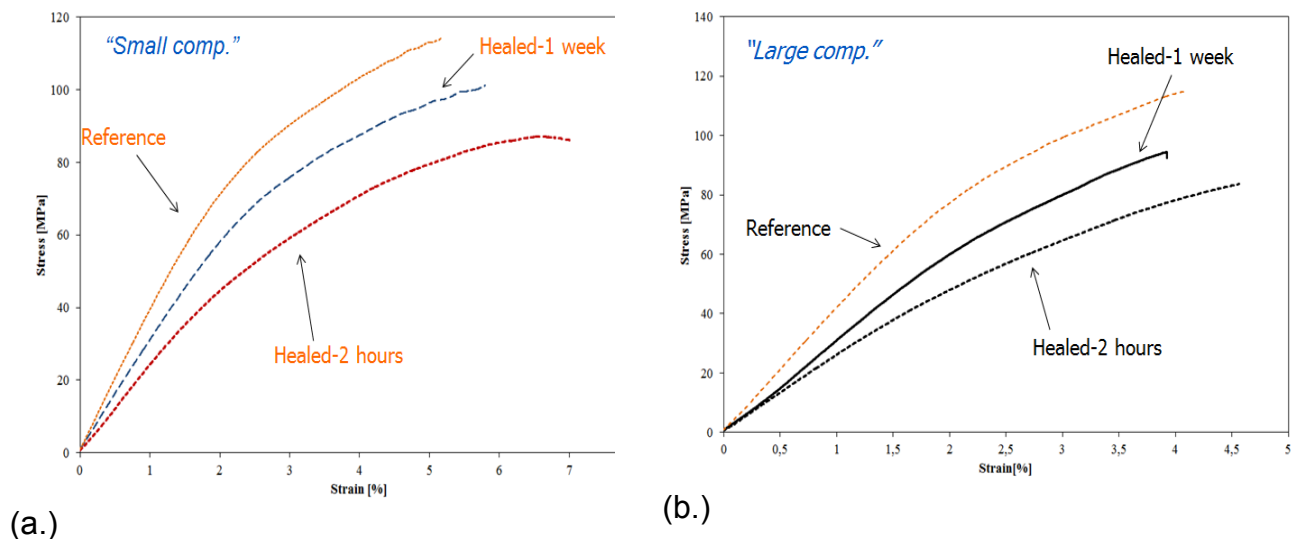


Figure 2: Stress-strain curves of pre-damaged/healed beams with embedded compartmented fibres; fibres with small (a) and large (b) compartments.

Stress-strain curves of pre-damaged/healed composites containing compartmented fibres with small (Figure 2a.) and large (Figure 2b.) compartments show partial recovery of flexural strength after one week of healing. Composites with small compartments showed strength of 101.6 ± 5.26 and 89.67 ± 5.78 MPa after one week and two hours of healing, respectively. Composites containing compartmented fibres with the morphology of large compartments showed flexural strength of 95 ± 8 MPa after one week of healing. Their strength after two hours of healing was only 86 ± 4 MPa.

5. CONCLUSIONS

Micro-computed tomography combined with off-axis flexural test proved that compartmented fibres enable multiple local healing in fibre reinforced polymer composites. All the tested model composites were able to partially recover their mechanical properties. The concept of multiple release of healing agent from a fibrous carrier was demonstrated successfully.

REFERENCES

[1] T. C. Mauldin, M. R. Kessler, Self-healing polymers and composites, *International Materials Reviews*, 55 (2010) 317-346.

- [2] S. M. Bleay, C. B. Loader, V. J. Hawyes, L. Humberstone, P. T. Curtis, A smart repair system for polymer matrix composites, *Composites Part A*, 32 (2001), 1767-1776.
- [3] R. S. Trask, I. P. Bond, Bio-inspired engineering study of *Plantae* vasculae for self-healing composite structures, *Journal of the Royal Society Interface*, 7 (2010) 921-931.
- [4] S. D. Mookhoek, H. R. Fischer, S.van der Zwaag, Alginate fibres containing discrete liquid filled vacuoles for controlled delivery of healing agents in fibre reinforced composites, *Composites Part A*, 43 (2012), 2176-2182.

METAL TRIFLATES AS CATALYTIC CURING AGENTS IN SELF-HEALING FIBRE REINFORCED POLYMER COMPOSITE MATERIALS

T. Coope¹, I. Bond¹, R. Trask¹ and D. Wass²

¹ *Advanced Composites Centre for Innovation and Science (ACCIS), Department of Aerospace Engineering, University of Bristol, Queen's Building, University Walk, Bristol, BS8 1TR, UK – e-mail: Tim.Coope@bristol.ac.uk; I.P.Bond@bristol.ac.uk; R.S.Trask@bristol.ac.uk*

² *School of Chemistry, University of Bristol, Cantock's Close, Bristol, BS8 1TS, UK – e-mail: Duncan.Wass@bristol.ac.uk*

Keywords: fibre reinforced polymer, self-healing, scandium triflate, ring-opening polymerisation, double cantilever beam

ABSTRACT

High performance, damage tolerant fibre reinforced polymer (FRP) composite materials are currently required to demonstrate no propagation of any sub-surface structural micro-cracking when under service load, thereby encouraging overdesign and limiting the inherent lightweight nature of such a material. By incorporating self-healing functionalities, in-situ autonomous repair can be initiated in the event of damage to maintain structural integrity while ultimately realising lighter and more sustainable structures. We have demonstrated metal triflate initiated ring opening polymerisation (ROP) of epoxide resin [1] in FRPs to restore >99% of the host matrix fracture toughness after damage under Mode I tests.

Optimising the polymer composition via differential scanning calorimetry (DSC) identified the key parameters to achieve autonomous curing under ambient conditions. Initial and self-healed performance was evaluated using FRP E-glass double cantilever beam (DCB) coupon mechanical test specimens with embedded microvascular channels for self-healing agent delivery. Full recovery of fracture toughness (>99%) was demonstrated while achieving the following requirements: low cost, low toxicity, autonomous curing, autonomous delivery, usability, manufacturing processability and applicability to existing aerospace and automotive maintenance programs.

Brittle and ductile cohesive failure mechanisms resulted from inclusion of a solvent (ethyl phenylacetate) within the healing agent under low (10 wt%) and medium (25 wt%) concentrations. Therefore, the failure mechanism can be adapted as the solvent acts as a plasticiser in the self-healing agent. This was further confirmed by imaging fracture plane surfaces via scanning electron microscopy (SEM). The adhesive repair was typically ~100 µm in thickness, comparable to damage voids present in impact damaged FRP composite materials.

1. INTRODUCTION

Micro-cracking in FRP materials can ultimately lead to catastrophic failure by rapid propagation throughout the laminated structure. For example, this damage can occur between stacked laminae, manifest itself as fibre-resin interfacial debonding or arise from manufacturing defects, causing stress concentrations which lead to the onset of

premature component failure. In this research the focus has been on the implementation of previously developed self-healing agents (SHAs) by Coope et al., [1] to achieve a self-healing FRP material using typical industrial composite manufacturing techniques.

2. MATERIALS

Solid-state, metal triflate, catalysts stable to air and moisture were used as curing agents for the polymerisation of an oligomeric diglycidyl ether bisphenol A (EPON 828) epoxy resin. Two catalysts, scandium(III) triflate (Sc) and aluminium(III) triflate (Al) were considered. Polymer formulations containing 10 wt% (E10) and 25 wt% (E25) of a non-toxic solvent, ethyl phenylacetate (EPA) (added to reduce viscosity), were investigated for their effect on mechanical performance recovery. The thermal reactivity of these materials were evaluation using differential scanning calorimetry (DSC), a TA Instruments Q200 DSC was used to study non-isothermal curing via dynamic scans. Samples were heated from 0 to 250 °C at a heating rate of 10 °C/min under a flow rate of 50 mL/min of nitrogen as the purge gas.

E-glass/epoxy (Hexply 913, Hexcel Composites) unidirectional (UD) plates (300 mm x 220 mm x 3.8 mm) were manufactured using hand lay-up (28 ply). Cure was undertaken according to the manufacturer's recommendations of 125 °C for 1 hour and a pressure of 700 kPa. Stainless steel wire (ca. 0.5 mm in diameter) pre-coated with PTFE release agent was placed parallel to the fibre direction in pre-cut 0.5 mm channels (equal to the thickness of 4 plies) centred on the mid-plane. Release film (15 µm thickness) was placed from the laminate edge to 25 mm before the start of the vasculature. Cured composite plates were cut into DCB coupon specimens using a water-cooled diamond grit saw (195 mm x 20 mm x 3.8 mm). Piano hinges were bonded in place using Hexcel Redux 810 adhesive onto grit-blasted surfaces as preparation for mechanical testing.

3. METHODS

An Instron 3343 fitted with a 1kN load cell was used to initiate and propagate Mode I crack opening. Double cantilever beam (DCB) E-glass composite test specimens fixed via attached piano hinges were loaded at a displacement rate of 2 mm/min in accordance with ASTM 5528-01 [2, 3]. Cracks were propagated for 75 mm from the point of initiation and crack length recorded with a video camera.

Specimens were healed after initial fracture using the prescribed healing agent, delivery method and cure temperature (Table 1). SHAs were delivered via the edge-located vasculature using 26 gauge hypodermic needles. Healed specimens were re-tested as outlined above for initial fracture.

4. RESULTS

The results revealed the two achievable resultant failure mechanisms, ductile and brittle, by incorporating EPA solvent at certain prescribed loadings. Therefore, self-healed specimens containing 25 wt% EPA with respect to EPON 828 failed in a way that is comparable to the initial composite fracture under Mode I testing. Equally, curing temperature variance (45 °C, 80 °C and ambient temperature) maintained this

failure methodology, with higher healing efficiencies being achieved for samples healed at higher temperatures and/or with a higher catalyst loading (Figure 1).

Table 1. Specimen derivatives used to demonstrate self-healing performance.

Designation	Monomer Solution ^{a)}	Catalyst	Catalyst Loading [pph] ^{b)}	Healing Temperature [°C]		
				45	80	RT
E10 Sc (M)	E10	Sc(OTf) ₃	3.125 (M)	X	X	X
E10 Al (M)		Al(OTf) ₃	3.125 (M)	X		
E25 Sc (M)	E25	Sc(OTf) ₃	3.125 (M)	X	X	X
E25 Sc (H)			6.25 (H)	X		X
E25 Sc (L)			1.5625 (L)	X		
AUTO E25 Sc (M)		3.125 (M)	X			
E25 Al (M)		Al(OTf) ₃	3.125 (M)	X		
E25 DETA		DETA	12			X

^{a)} **E10**: 90 wt% EPON 828, 10 wt% Ethyl phenylacetate (EPA); **E25**: 75 wt% EPON 828, 25 wt% EPA. ^{b)} (L) = low loading, (M) = medium loading, (H) = high loading

A 26% minimum healing efficiency increase was observed for implementing these SHAs compared with the commercial-based EPON 828/DETA system (Figure 1). E25 Sc healed test specimens achieved a minimum healing efficiency of 129% via the injection of a pre-mixed solution at 45 °C, demonstrating full recovery of fracture toughness. Ultimately, autonomous curing was one of the main objectives for this self-healing system. Thus, curing at ambient temperature provided a minimum healing efficiency of 113% for this same system. A modest increase of 30% healing efficiency resulted from healing at 80 °C when compared with healing at low temperature. The highest healing efficiency was achieved by introducing a higher catalyst concentration to E25 Sc cured at 45 °C. This resulted in a 176% load recovery and a 352% fracture toughness recovery. Furthermore, an autonomous delivery method facilitated by infusion of separate Sc(OTf)₃-EPA and EPON 828 solutions via parallel vasculature achieved a 100% load recovery and 88% fracture toughness.

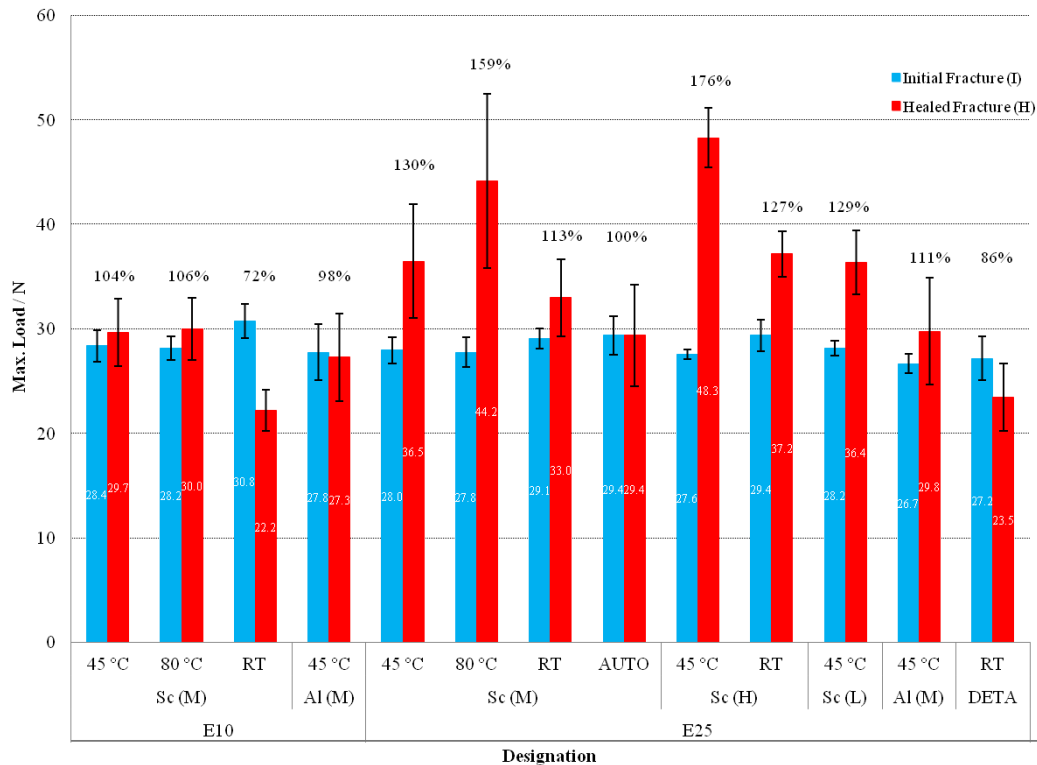


Figure 1: Healing performance for maximum load

5. CONCLUSIONS

Evaluation of self-healing agents using a fibre-reinforced polymer (FRP) double cantilever beam (DCB) geometry demonstrated full recovery of material properties under Mode I test. A cohesive failure of self-healed polymer, containing variable solvent concentrations, resulted in either a brittle or ductile fracture mechanism. This research further demonstrates the applicability and tailorability of the underpinning chemistry in this self-healing system and how it is not limited by the delivery mechanism (i.e. microcapsules, hollow glass fibres (HGF) or microvascular channels) or the end-user application.

ACKNOWLEDGEMENTS

The authors would like to acknowledge the UK Engineering and Physical Sciences Research Council (EPSRC) [EP/G036772/1] and the UK Ministry of Defence/Defence Science and Technology Laboratory for funding this research.

REFERENCES

- [1] T. S. Coope, U. F. J. Mayer, D. F. Wass, R. S. Trask, I. P. Bond, Self-Healing of an Epoxy Resin Using Scandium(III) Triflate as a Catalytic Curing Agent, *Adv. Funct. Mat.* 21 (2011) 4624-4631.
- [2] ASTM International, Test Method Designation: D5528-01.
- [3] C. J. Norris, R. S. Trask, I. P. Bond, Interactions between propagating cracks and bioinspired self-healing vasculature embedded in glass fibre reinforced composites, *Compos. Sci. Technol.* 71 (2011) 847-853.

MATRIX DAMAGE HEALING IN FIBRE REINFORCED COMPOSITE MATERIALS CONTAINING WOVEN-IN SHAPE MEMORY ALLOY WIRES

T.C. Bor¹, L.L. Warnet¹ and R. Akkerman¹

¹ Chair of Production Technology, University of Twente, Drienerlolaan 5, 7522 NB Enschede, The Netherlands – e-mail: t.c.bor@utwente.nl; l.warnet@utwente.nl; r.akkerman@utwente.nl

Keywords: self-healing composite, shape memory alloy

ABSTRACT

Continuous fiber reinforced composite materials are susceptible to delamination upon impact. Shape Memory Alloy (SMA) wires can be used to assist the healing of damage employing various known or new healing methodologies. Upon a local heating stimulus the contracting action of pre-strained wires, oriented parallel to the out-of-plane direction of the composite material, can be utilized to compress a delaminated region.

In this work the healing behavior of a continuous fibre reinforced thermoplastic model material is studied with woven-in SMA wires. The thermoplastic character of the matrix material allows for welding/healing of delaminated regions under the generated compressive stress when the material is in a soft state at elevated temperatures.

The requirements for optimum matrix healing at the delaminated interface are studied as a function of temperature and local stress state for different SMA wire distributions and volume fractions. The progress of interface healing is based on a reptation model for the interface mobility of polymer chains of the thermoplastic matrix.

The healing process is critically dependent on the thermal and mechanical properties of both the thermoplastic matrix material and the shape memory alloy wires. The developed compressive stresses in the out-of-plane direction depend on the weave pattern of the SMA wires employed. Additional stresses develop in the in-plane directions upon heating due to the undulating character of the weave patterns of the SMA wires. Requirements for optimum healing conditions with assistance of 3D woven SMA wires are provided.

1. INTRODUCTION

Advanced continuous fibre reinforced composite materials are increasingly being used for structural applications where long term reliability of the mechanical and other properties is of prime importance. However, during the lifetime of a composite structure, relatively minor events like low energy impact can cause local damage, such as small matrix cracks and delaminations. In-situ (self) healing of the damage would definitely enlarge the lifetime, reliability and robustness of structural composite materials as well as prevent costly repairs.

In this work Shape Memory Alloy (SMA) wires are employed to compress delaminated regions in continuous fibre reinforced composite materials at elevated temperatures. In this way an intimate contact zone at the faces of the delaminated regions can be formed stimulating the thermal reptation process, where polymer chains of one side of the delamination interdiffuse with those across the interface providing new strength. The application of SMA wires to assist damage healing has been studied before both theoretically and experimentally employing straight wires oriented in the out-of-plane direction. Such a configuration requires special attention to the bonding between the wires and the matrix of the composite material to maintain proper force transfer. A possible alternative is the use of woven-in SMA wires. The undulating and continuous character of the wire distribution ensures good force transfer from the wires to the composite material without the risk of debonding/slippage at the wire-matrix interface. An example of a model system with a symmetric distribution of SMA wires is shown in Fig. 1 for a $[0\ 90]_s$ lay-up of plies with uni-directional fibers.

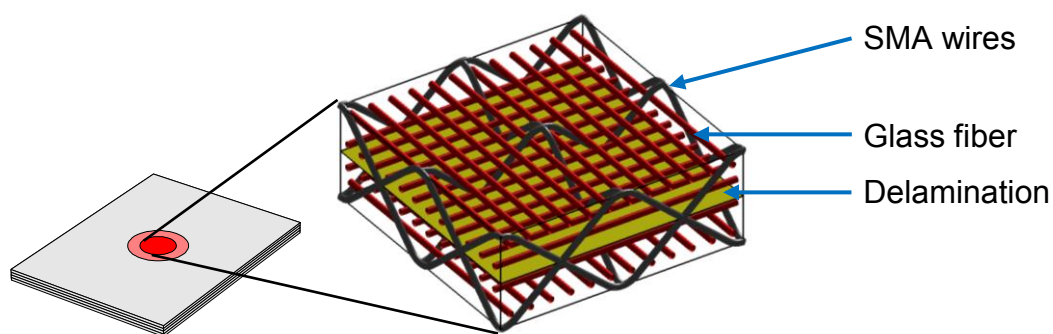


Figure 1: Schematic distribution of SMA wires in a continuous fibre reinforced thermoplastic composite material with a $[0\ 90]_s$ lay-up of UD glass fibers. The area in the centre of the composite material denotes a delaminated region.

2. MODEL

The response of the continuous fiber reinforced model composite material with woven-in SMA wires is determined in a similar fashion as reported recently for straight SMA wires oriented in the out-of-plane direction [1]. The composite material contains an amorphous matrix characterized by glass transition temperature T_g . The constitutive behaviour of the SMA wires has been modeled according to the work of Popov and Lagoudas [2], incorporating the shape memory effect and pseudo-elasticity. The mechanical response of the composite material to the compressive action of the wires can be determined from the effective in-plane and out-of-plane properties of the composite material along with proper boundary conditions. Here, it is assumed that only a small portion of the composite material is heated up for a healing treatment and since the rest of the composite material remains at ambient temperature, the in-plane strain of the heated region is zero.

3. RESULTS

The effective stiffness and thermal expansion coefficient of the composite material in a direction parallel to the SMA wires can be determined as a function of the angle ϕ between the wires and the plane of the composite material. It is assumed that the wire density is sufficiently large to impose homogeneous deformation in the in-plane

and out-of-plane directions. The angle equals 0° for wires oriented in the plane of the composite material and 90° for wires oriented in the out-of-plane direction. Results are shown in Fig. 2 for temperatures sufficiently below and above T_g of the amorphous thermoplastic matrix material [1]. The fiber volume fraction of the glass fibers equals 50%.

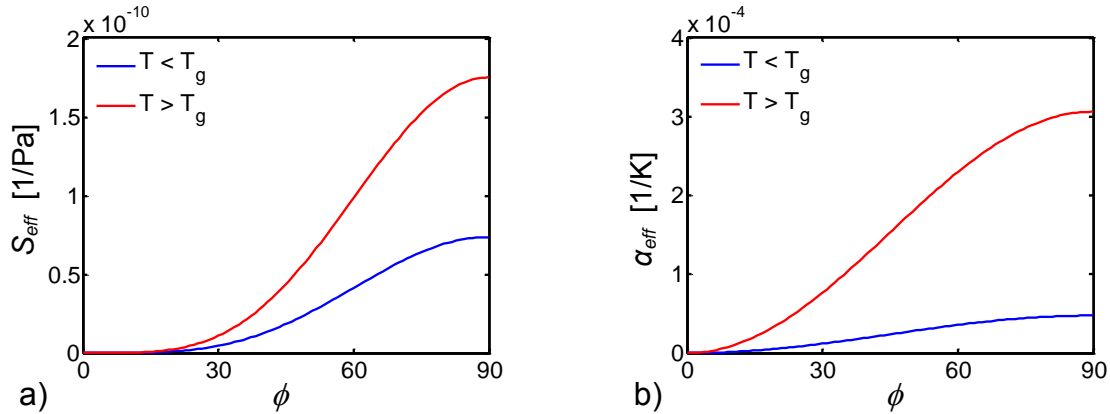


Figure 2 : Effective compliance and linear thermal expansion coefficient of the $[0\ 90]_s$ continuous glass fibre reinforced composite material with a thermoplastic matrix material in a direction parallel to the SMA wires below T_g (blue) and above T_g (red) versus the angle of the SMA wires.

The compliance of the composite material in a direction parallel to the SMA wires is strongly dependent on the SMA wire orientation. For $\phi = 0^\circ$, the wires are oriented in the plane of the composite material and, as in-plane deformation is suppressed by the adjacent composite material (see above), the effective composite material compliance equals zero. The more the wires are oriented in the out-of-plane direction, the more the compliance increases and reaches the maximum value at $\phi = 90^\circ$. A similar behavior is observed for the linear thermal expansion coefficient. Subsequently, the behavior of the continuous fibre reinforced composite model system has been studied during a healing treatment as a function of T_g , the fraction of SMA wires, f_{SMA} , the wire orientation ϕ and the level of prestrain of the SMA wires. Here, wires are either not prestrained (fully detwinned) or prestrained to a value of 5% (fully twinned) which also indicates the maximum extent of the shape memory effect [2]. The other thermo-mechanical properties of the SMA wires employed can be found in [1]. The healing treatment comprises heating to the healing temperature $T_g + 25\text{ K}$, holding the composite material for a sufficiently long time to allow interdiffusion of the polymer chains and cooling down to room temperature.

In previous work [1] it was shown that under certain conditions a mild compressive stress of -1 MPa can be exerted by the SMA wires in the out-of-plane direction at the healing temperature and a stress free state can be obtained after healing. In this way thermal healing can be accomplished without the occurrence of residual stresses after cooling to room temperature. Here, the same approach is followed to determine the optimal fraction of SMA wires f_{SMA} as a function of the SMA wire angle for a range of glass transition temperatures. The results are shown in Fig. 3 for non-prestrained SMA wires (a) and fully prestrained SMA wires (b).

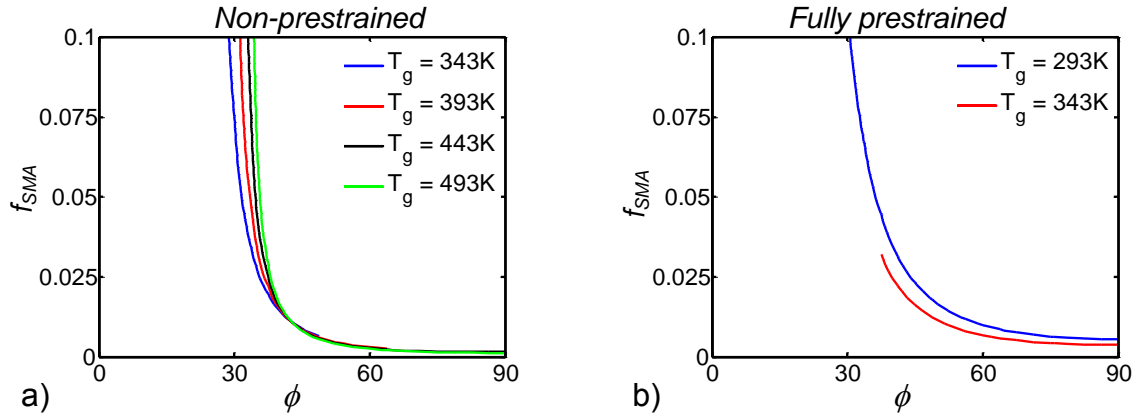


Figure 3 : Required volume fraction of SMA wires at different orientation angles ϕ for optimum healing conditions without residual stresses after cooling to room temperature for (a) non-prestrained SMA wires and (b) fully prestrained SMA wires.

At $\phi = 90^\circ$ optimal healing conditions occur for fully prestrained SMA wires only at relatively low glass transition temperatures, whereas for non-prestrained SMA wires a wide temperature range is possible [1]. Low fractions of SMA wires are sufficient for high angles ϕ . However, the more the wire orientation deviates from 90° , the less effective the exerted force can be used to compress the composite material in the out-of-plane direction, requiring higher fractions of SMA wires to obtain the -1 MPa compressive stress at the healing temperature. The relatively stiff response of the composite material at small angles ϕ (see Fig. 2a) enhances this effect. Especially below 45° , f_{SMA} increases so strongly, that the application of SMA wires renders impractical. Similar results have been obtained if the SMA wires were replaced for wires made of carbon, steel, glass or aramide as will be presented in a future publication.

4. CONCLUSIONS

Woven-in shape memory alloy wires can be employed to exert sufficient compressive stresses to assist thermal healing of delamination damage in continuous fibre reinforced composite materials upon a thermal healing treatment. If the angle of the woven-in SMA wires with the plane of the composite material is too small, the required amount of SMA wires becomes impractically large.

REFERENCES

- [1] T.C. Bor, L. Warnet, R. Akkerman, A. de Boer, Modeling of stress development during thermal damage healing in fiber-reinforced composite materials containing embedded shape memory alloy wires, *J. Comp. Mat.* 44, 22 (2010) 2547-2572.
- [2] P. Popov, D.C. Lagoudas, A 3-D constitutive model for shape memory alloys incorporating pseudoelasticity and detwinning of self-accomodated martensite, *Int. J. of Plasticity*, 23 (2007) 1679-1720.

SELF-HEALING OF IMPACT DAMAGE IN 3D MICROVASCULAR COMPOSITES

K.R. Hart^{1,4}, E.D. Wetzel², N.R. Sottos^{3,4}, and S.R. White^{1,4}

¹ Department of Aerospace Engineering, University of Illinois at Urbana-Champaign, 104 S. Wright St., Champaign, IL, 61820, USA. – e-mail: hart22@illinois.edu; swhite@illinois.edu

² US Army Research Laboratory, Weapons and Materials Research Directorate, Aberdeen Proving Ground, MD, 21005, USA. – e-mail: eric.d.wetzel2.civ@mail.mil

³ Department of Materials Science and Engineering, University of Illinois at Urbana-Champaign, 1304 W. Green St., Urbana, IL, 61801, USA. – e-mail: n-sottos@illinois.edu

⁴ Beckman Institute for Advanced Science and Technology, University of Illinois at Urbana-Champaign, 405 N. Mathews Ave., Urbana, IL, 61801, USA.

Keywords: Self-healing, fiber-reinforced composite, microvascular, impact

ABSTRACT

Fiber-reinforced composites are susceptible to micro- and macro-scale damage due to a number of different damage modes including out-of-plane impact events. Transverse impact damage causes a reduction in material stiffness and strength by introducing interlaminar delaminations and intralaminar transverse cracking and is one of the most limiting design considerations preventing widespread acceptance of composites in structural applications. To combat reductions in material properties, microvascular based self-healing composites have been explored as a means to repair damage in the host material after an impact event.

Here we report on a vascularized 3D fiber-reinforced composite capable of recovering mechanical properties following an impact event. Vascular networks are fabricated by inserting nylon monofilament in the composite preform before resin infusion and subsequently removing them manually after composite processing. Vascularized composites are then sectioned into flexure specimens and impacted across the sample width using a cylindrical impact tup to introduce damage. After impact damage, the samples are allowed to heal and mechanical properties are evaluated using a four point flexure-after-impact (FAI) protocol.

Prior to impact, two-part epoxy based healing agents are injected into the isolated, embedded networks, individually sequestering the two components. During impact, damage bridges isolated channels and provides a pathway for mixing of the healing agents. Results of autonomic healing tests are compared with control tests in which pre-mixed healing agents are pumped after impact through the entire network(s).

TOUGHENING OF SHAPE MEMORY ALLOY EMBEDDED COMPOSITES

F. Barrie¹ and M. V. Manuel¹

¹ *Materials Science and Engineering, University of Florida, 152 Rhines Hall, Gainesville, FL, 32611 USA – e-mail: fbarrie@ufl.edu, mmanuel@mse.ufl.edu*

Keywords: NiTi, J-integral, Multifunctional composites, Transformation toughening, Fracture toughness

ABSTRACT

Shape memory alloys (SMAs) are a class of materials that are being increasingly used within self-healing research and have been successfully implemented in self-healing polymers and metals. The SMAs are specifically used for their inherent ability to recover their shape after deformation due to reversible thermo-elastic martensitic phase transformations. While the addition of SMAs as reinforcements to a matrix primarily serves to facilitate crack closure, a subsequent result is increased fracture toughness of self-healing metal and polymer matrix composite systems. Self-healing systems with increased fracture toughness can be used longer in their intended application prior to failure and healing. The motivation of this study is SMA reinforced metal matrix systems. Manuel *et al.* developed a self-healing SnBi matrix that was embedded with uni-directional SMA wires. Research has continued utilizing more structurally relevant metal matrices. Because the constituent composite materials were capable of inelastic deformation, J-integral fracture toughness experiments were performed on composites embedded with nickel-titanium SMAs. The SMA reinforcements were in the austenite and martensite phases to evaluate the effect of the martensitic phase transformation and detwinning processes during the composite deformation. The fracture toughness results will be presented. Relevant toughening mechanisms will be discussed yielding a better understanding of the SMA contribution to composite toughness and what this means for SMA reinforced self-healing materials. This project was supported by a NASA Office of the Chief Technologist's Space Technology Research Opportunity – Early Career Faculty grant number NNX12AQ42G and the University of Florida NASA Florida Space Grant Consortium.

THERMOPLASTIC FIBRE STITCHING: A NEW SELF-HEALING METHOD FOR CARBON-EPOXY COMPOSITES

K. Pingkarawat¹, C.H. Wang¹, R.J. Varley² and A.P. Mouritz¹

¹ Sir Lawrence Wackett Aerospace Research Centre, School of Aerospace, Mechanical and Manufacturing Engineering, RMIT University, GPO Box 2476, Melbourne, Victoria 3001, Australia - e-mail: s3249363@student.rmit.edu.au; adrian.mouritz@rmit.edu.au; chun.wang@rmit.edu.au

² CSIRO Materials Science and Engineering, Private Bag 33, Clayton South MDC, Victoria 3169, Australia – e-mail : Russell.Varley@csiro. au

Keywords: Delamination, Stitching, Self-healing, Mendable polymer, Fracture toughness

ABSTRACT

This paper presents an investigation into the delamination toughening and self-healing properties of carbon-epoxy laminates using through-thickness stitches of mendable thermoplastic (poly[ethylene-co-(methacrylic acid)]). The effect of increasing stitch density on the improvement to the interlaminar fracture toughness and healing of mode I delamination cracks generated under static and fatigue interlaminar loads is determined. The self-healing and delamination toughening mechanisms of the mendable stitches are identified.

1. INTRODUCTION

A new type of self-healing polymer composite material was recently developed that synergistically combines high interlaminar fracture toughness (to resist delamination crack growth) with high healing efficacy (for in-situ repair and toughening of delaminations). Yang et al. [1] developed this self-healing composite by reinforcing conventional carbon-epoxy laminates in the through-thickness direction with mendable polymer stitches. The stitches consist of poly(ethylene-co-(methacrylic acid)) (EMAA) filament, which can heal cracks via a condensation reaction with the epoxy matrix phase which generates high pressure microbubbles that force the mendable polymer into open cracks [2].

The present study extends the work by Yang et al. [1] by investigating the influence of EMAA stitch density on the synergistic combination of delamination toughening and healing properties. The focus is to quantify the effect of increasing stitch density on the healing efficiency of delamination cracks generated by mode I static or fatigue cracks. The efficacy of the stitched composites to restore the mode I interlaminar fracture toughness and delamination fatigue resistance is determined for multiple healing operations.

2. MATERIALS AND METHODS

Mode I static and fatigue delamination tests were performed on unstitched and stitched carbon fibre-epoxy composites. The uncured prepreg stack was manually stitched through-the-thickness with EMAA filament. The stitch areal density along the

laminatamid-plane was 0.25, 1, 1.6 and 4 stitches/cm². The architecture of the EMAA filaments in the laminate material was the same for each stitch density (Figure 1). The unstitched and stitched composites were cured and consolidated inside an autoclave at 120°C and 620 kPa for one hour. The interlaminar fracture toughness properties were measured using the double cantilever beam (DCB) test under mode I static and fatigue loading. Static DCB tests were performed at a crack opening displacement rate of 2 mm/min. Fatigue DCB tests were performed at a cyclic loading frequency of 10 Hz and R ratio of 0.1. After static and fatigue testing, the stitched specimens were healed by heating at 150°C for one hour followed by compaction at a pressure of 20 kPa for ten minutes. Further details are given by Pingkarawat et al. [3,4].

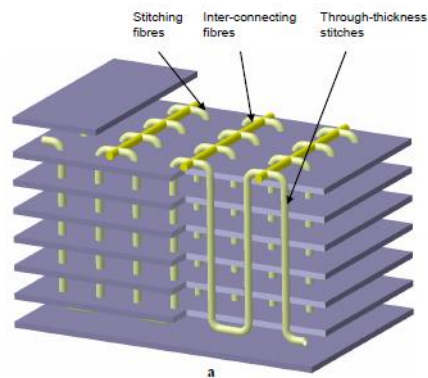


Figure 1 : Architecture of the EMAA stitches in the self-healing carbon fibre-epoxy composite [1].

3. RESULTS AND DISCUSSION

3.1 Static Delamination Fracture Properties of Mendable Stitched Composites

Figure 2 shows the effects of stitch density and number of healing operations on the mode I interlaminar fracture toughness of the carbon-epoxy composite. Stitching increased the delamination resistance of the laminate before healing. The fracture toughness was increased by the stitches bridging the delamination crack, The bridging stitches generated traction loads which resisted crack opening, thereby increasing the interlaminar fracture toughness. The bridging traction load generated by the stitches increases with their volume content, and this accounts for the interlaminar fracture toughness increasing rapidly with stitch content.

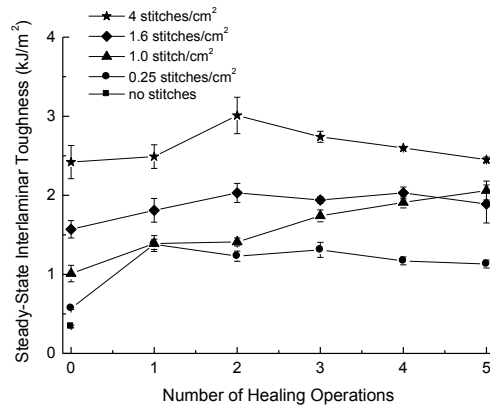


Figure 2 : Effects of EMAA stitch density and number of healing operations on the mode I interlaminar fracture toughness.

After self-healing by heating the delaminated DCB specimens to 150°C, the interlaminar fracture toughness of the stitched composites was fully and/or more than fully recovered and this was retained for multiple healing cycles (Figure 2). Recovery to the interlaminar fracture toughness was achieved by the EMAA flowing from the stitches into the delamination crack during the healing process. Healing was activated by heating the stitched composites, which caused acid functional groups along the EMAA polymer chains to react with hydroxyl groups in the epoxy matrix phase of the composite with tertiary amine groups acted as the catalyst. Meure et al. [2] found that the acid-hydroxyl reaction generates volatiles (mostly water) that phase separate into high-pressure microbubbles within the EMAA, which is a molten insoluble phase at the healing temperature of 150°C. Due to this reaction process, the molten EMAA stitches had a high internal gas pressure which forced them into the delamination and thereby healed the crack. The interlaminar fracture toughness was restored by the formation of a crack bridging traction zone generated by the EMAA stitches (which refused during healing) as well as the presence of a thin film of EMMA healing agent along the crack plane.

3.2 Fatigue Delamination Properties of Mendable Stitched Composites

Figure 3 presents Paris curves of delamination crack growth rate plotted against cyclic stress intensity range for the composites with the lowest and highest stitch contents. Curves are shown for laminates in their original condition and after one or multiple healing operations. The figure shows that the EMAA stitches were able to restore the delamination fatigue resistance of the laminate after healing, and the efficacy of the healing process did not change significantly with number of healing operations. The stitches restored the interlaminar fatigue resistance by flowing into the delamination crack during healing via the same healing process as mode I static loading, and then forming a bridging traction zone during repeated fatigue crack growth.

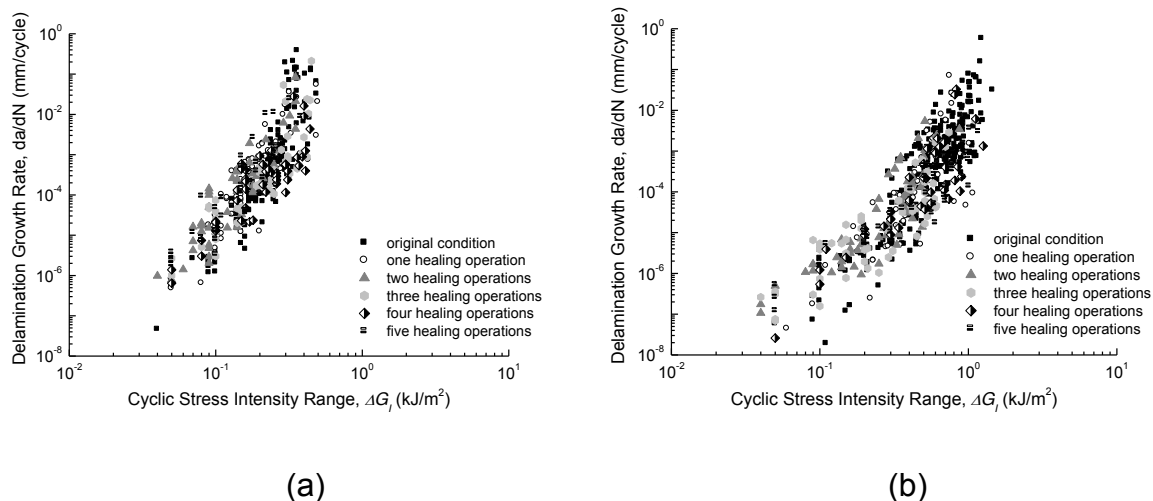


Figure 3: Effect of number of healing operations on the fatigue crack growth rate of the (a) lightly stitched (0.25 stitches/cm²) and (b) heavily stitched (4 stitches/cm²) laminates.

4. CONCLUSION

This study has shown that EMAA stitching is an effective interlaminar toughening method for restricting mode I delamination crack growth under mode I static and fatigue loading in mendable composites, which thereby reduces the amount of damage that must be repaired via the healing process. The fracture toughness and fatigue resistance increased with the stitch density due to the increase in traction load arising from a greater number of stitches within the crack bridging zone. In-situ repair of static and fatigue delaminations occurred by the healing agent flowing from the stitches into open cracks under a pressure delivery mechanism unique to EMAA. This healing process fully restored the mode I interlaminar fracture toughness and fatigue resistance of the stitched composite, and these properties were maintained for multiple healing cycles.

REFERENCES

- [1] T. Yang, C.H. Wang, J. Zhang, S. He, A.P. Mouritz, Toughening and self-healing of epoxy matrix laminates using mendable polymer stitching, *Composites Science and Technology*, 72, (2012), 1396-1401.
- [2] S. Meure, D.Y. Wu, S. Furman, Polyethylene-co-methacrylic acid healing agents for mendable epoxy resins, *Acta Materialia*, 57, (2009), 4312-4320.
- [3] K. Pingkarawat, C.H. Wang, R.J. Varley, A.P. Mouritz, Self-healing of delamination cracks in mendable epoxy matrix laminates using poly(ethylene-co-(methacrylic acid)) thermoplastic, *Composites Part A: Applied Science and Manufacturing*, 43, (2012), 1301-1307.
- [4] K. Pingkarawat, C.H. Wang, R.J. Varley, A.P. Mouritz, Self-healing of delamination fatigue cracks in carbon fibre-epoxy laminate using mendable thermoplastic, *Journal of Materials Science*, 47, (2012), 4449-4456.

SESSION 27 – SELF-HEALING POLYMERIC MATERIALS

POLYMER COMPOSITE LAYER WITH DAMAGE INDICATION ABILITY

O. Strekalova¹, S. Vidinejevs¹, and A. Aniskevich¹

¹ *Institute of Polymer Mechanics, University of Latvia, 23 Aizkraukles street, LV-1006, Riga, Latvia – e-mail: ostrekalova@pmi.lv, sergejs.vidinejevs@pmi.lv, andrey.aniskevich@pmi.lv*

Keywords: damage visualization, microcapsule, “bruise”, epoxy, fiber reinforced composite

ABSTRACT

Bio-inspired “bruisable” polymer composite layer is the solution in structural health monitoring processes which will allow minimise time of inspection and simplify the process of monitoring.

The aim of the study was to develop polymer composite layer with damage indication ability. Visualization of damaged place is provided by colour changing in the place of definite load. Colour changing mechanism is provided by chemical reaction between encapsulated leuco dye and particles of dye developer. After definite load shell of a capsule bursts and chemical reaction is possible. So damage visibility is provided like a “bruise” in the human body.

As a result of work the following issues have been solved. Layer of glass fabric epoxy composite with visualization capability provided by mixture of components (microcapsules of leuco dye, polymer adhesive, and particles of dye developer) was worked out. The optimal ratio of mixture components was found. Specimens with different component concentrations were tested by quasi-static compression tests. An intensity of the colored response was estimated by digital image analysis. As a result components ratio was found as 6/3/2.

Composite with damage indication ability was manufactured via the vacuum assisted resin transfer molding process.

The method of sensitivity control of damage indication layer with protective coating was developed. Relation of threshold level of the impact visualization vs. coating thickness was estimated by series of quasi-static experiments and further processing of the data (compilation and analysis of quasi-static compression tests data, digital image analysis data with parameters of specimens).

Present damage indication method simplifies limited in time inspection of big surfaces. Wind turbine blades and boat hulls are just only some examples of the use of this layer.

1. INTRODUCTION

Nowadays fibre-reinforced composites with epoxy matrix are widely used in many applications in engineering and construction. Unfortunately, internal damage of such material is not always visible. Non-destructive testing methods for fiber reinforced composites with epoxy matrix are very costly and usually are related to the use complex equipment. The use of the self-monitoring material can be the optimal way to implement a structural health monitoring [1].

The aim of the study was to develop polymer composite layer with damage indication ability. For the implementation of this layer, it was decided to use fabric, epoxy binder and a leuco dye ink.

To achieve the aim, following issues have been defined: to select components for the damage indication layer, to find optimal ratio of components, to develop the method of manufacture and the method of sensitivity control of damage indication layer.

2. MATERIALS

As a carcass of damage indicating layer nylon fabric was used. For the colour changing function three components were selected: water emulsions of microencapsulated leuco day, dye developer and epoxy-modified polyurethane acrylic polymer. The main task of damage indicator is to visualize the damaged place. It is provided by colour changing in the place of definite load. Colour changing mechanism is provided by chemical reaction between encapsulated leuco dye and particles of dye developer, accordingly after definite load shell bursts and chemical reaction is possible. So damage visibility is provided like a "bruise" in the human body. Epoxy-modified polyurethane acrylic polymer was used to isolate encapsulated leuco day and dye developer from the alkaline environment of hardener. The ratio of 1st and 2nd components was 2/1 and it was known. To define the ratio of 3rd component, mixtures with different ratio of 3rd component were prepared and tested. In the present study specimens with matrix of epoxy resin were used.

3. METHODS

Nylon fabric pieces were homogeneously impregnated with mixture of water emulsions of microencapsulated leuco day, dye developer and epoxy-modified polyurethane acrylic polymer, using components concentrations from 6/3/0.2 to 6/3/4 respectively. After impregnation the fabrics were dried until full removal of the water basis. Dried fabrics were exposed to the ultra-violet irradiation for 30 min from each side. This operation provides the polymerization of components. Thereby the colour providing agents were isolated from the alkaline amines of the hardener.

Damage indicating fabric pieces (prepregs) with different 3rd component concentration were tested by quasi-static compression tests. After each load, photo of specimen was taken. Using digital image analysis for photo processing, an intensity of the colored response was estimated [2]. Therefore, the prepreg with the most intensive visual response to the specific load was selected.

Protective epoxy coatings with different thickness were used to control sensitivity of damage indication layer. Specimens of composite with different thickness of protective coatings were made using vacuum assisted resin transfer molding process. Then these specimens were tested by compression test. In this way experimental models with protective epoxy coating from 0 till 4.5 mm were tested. Specimens with define protective coating were subjected to load, exceeding the threshold load of visual response. Visual response was estimated using digital image analysis, as described before.

4. RESULTS

In the result of the study, the layer with damage indication ability was worked out. For the selected components, it was experimentally determined that the most intensive

colored response under load was obtained using ratio of the components 6/3/2. It was possible to control the sensitivity of damage indication layer using additional protective epoxy coating. The correlations between integral colour response B and indentation load P for the defined protective epoxy coating thickness were established after series of the experiments. Intersection of the linear trend of the second section and abscissa axis was defined as a threshold P^* of visualization of the load. For several points photos of specimens and visual response after the load are presented in Figure 1.

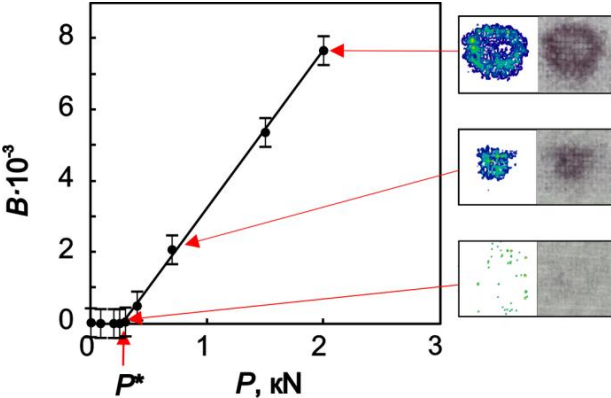


Figure 1: The correlation between integral colour response B and indentation load P for the protective epoxy coating thickness $d = 1.26 \pm 0.05$ mm. Photos of specimens and visual response after the load for three points are shown.

Summarizing data of tested specimens with different thickness of protective epoxy coating, the correlation between the threshold P^* of visualization of the load and protective epoxy coating thickness d was established (Figure 2).

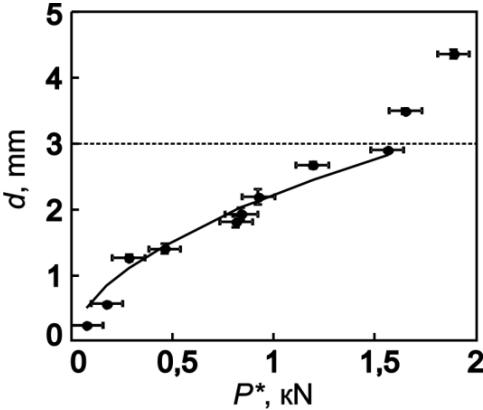


Figure 2: The correlation between the threshold P^* of visualization of the load and protective epoxy coating thickness d . For $d > 3$ mm, an irreversible deformation was detected.

During the experiments the irreversible deformation of protective epoxy coatings $3 < d < 4.5$ mm was detected. Besides the visual response, an indentation on the surface of the protective epoxy coatings was visible.

Polymer composite layer with damage indication ability was tested on real objects. Directly after manufacturing prepreg with damage indication ability was placed on building safety helmet (Figure 3).



Figure 3: Building safety helmet with damage indicating strips.

Keeping helmet at room conditions (18 - 22°C) for 4 months, adhesion and damage indication ability of strips are still working.

5. CONCLUSIONS

In the present study, a model of polymer composite layer with damage indication ability was developed. Present layer can be placed into the composite during assembling or placed on the finished production. Damage visualization function is preserved for a long time. In the result, it is possible to vary the sensitivity threshold of damage indicating layer.

Present results permit to produce self-monitoring fibre-reinforced composites with improved visual response to impact damage. Use of this material guaranties visual response appearance after specific load and gives opportunity timely replace the damaged part.

ACKNOWLEDGEMENTS

Material support from the Papierfabrik August Koehler AG for this study is acknowledged.

Financial support from the ERDF Project No. 2012/0201/2DP/2.1.1.2.0/10/APIA/VIAA/005 "Support to international cooperation projects on the physicomechanical investigation of polymer composite materials" for this paper is acknowledged.

REFERENCES

- [1] S. Vidinejevs, O. Strekalova, and A. Aniskevich, Development of a composite with an inherent function of visualization of a mechanical action, *Mechanics of Composite Materials*, Vol. 49, No. 1, March, 77-84 (2013).
- [2] S. Vidinejevs, A. Aniskevich, A. Gregor, M. Sjöberg, G. Alvarez, Smart polymeric coatings for damage visualization in substrate materials, *Journal of Intelligent Material Systems and Structures*, Vol. 23, 1371-1377 (2012).

IONIC AGING AND THE SHELF-LIFE OF BALLISTIC SELF-HEALING IN IONOMERS

S. J. Kalista, Jr.^{1,2}, J. R. Pflug³ and R. J. Varley⁴

¹ Department of Mechanical Engineering, Union College, 807 Union St, Schenectady, NY 12308, USA – e-mail: kalistas@union.edu

² Macromolecular Science and Engineering, Virginia Tech, Blacksburg, VA 24060 USA – e-mail: skalista@vt.edu

³ Department of Physics and Engineering, Washington and Lee University, 204 W Washington St, Lexington, VA 24450 USA – e-mail: pflugj10@mail.wlu.edu

⁴ CSIRO Materials Science and Engineering, Private Bag 33, Clayton South, Victoria 3169, Australia – e-mail: Russell.Varley@csiro.au

Keywords: ionomers, ballistic self-healing, EMAA, aging, shelf-life

ABSTRACT

Poly(ethylene-*co*-methacrylic acid) (EMAA) copolymers and ionomers possess the unique ability to autonomously self-heal following ballistic puncture. Given this response, these materials hold significant potential for use in a range of applications including fuel tanks, pressurized environments or containment applications. While the mechanism has previously been assumed the result ionic content, it has been shown that hydrogen-bonding within the non-ionic precursor copolymer produces the same response. However, given changes in morphology upon aging, the self-healing ability may diminish with time.

A range of EMAA copolymers and ionomers having zero, moderate, and high ionic content were examined using various characterization techniques including FTIR, DSC, DMA, tensile, and ballistic puncture testing. Puncture tests below the order-disorder transition, T_i (~40°C), showed moderate ionic content the most successful in self-healing with neither non- nor high ionic varieties successful at very low temperatures. Above T_i , all varieties were successful, with moderate and highly ionic materials healing into the melt state. Overall, ballistic healing persisted over a wide range from -50°C to 130°C. By correlating this response with standard characterization methods, it was determined that the increased rigidity of ionic clusters inhibited the necessary elastomeric nature of the healing response at low temperatures, yet provided the strength to maintain elasticity into the melt state.

However, success of the healing response was shown to be dependent on age post melt processing. Physically, ionic and hydrogen-bonded domains present in EMAA materials appear to order with age when held below T_i . Ballistic tests on these materials over several months showed a clear loss in self-healing response in the most ionic varieties, while those less ionic varieties remained consistently successful. Ultimately, this suggests a shelf-life for self-healing in the most ionic materials, which provides further understanding of the healing mechanism and must be considered in future studies or prospective commercial applications.

RECENT DEVELOPMENTS IN MICROENCAPSULATION OF SELF-HEALING AGENTS

R. F. A. Teixeira¹, L. Nguyen¹, F. E. Du Prez¹

¹ *Department of Organic Chemistry, Polymer Chemistry Research Group, Ghent University, Krijgslaan 281 S4-bis, B-9000 Ghent, Belgium. E-mail: Roberto.Teixeira@UGent.be
SIM vzw, Technologiepark 935, B - 9052 Zwijnaarde, Belgium.*

Keywords: self-healing, microcapsules, thermosets, active ingredients, interfacial polymerization

ABSTRACT

Microcapsules represent reservoirs of healing agents that are dispersed into materials. Matrixes such as thermoset materials undergo damages over time due to external forces such as cyclic stresses and climate conditions. This can eventually lead to the formation of cracks, thereby deteriorating and weakening the materials. Upon crack formation, the microcapsules present in the matrix should break (and not debond) and release their reactive liquid content, allowing the material to recover its strength [1]. The development of self-healing materials has gained considerable attention over the last decade. This is driven by the replacement of heavy materials by lightweight high performance materials. The application fields include building and construction, automotive and aerospace, industrial applications, wind energy and marine applications.

Our research aims at the encapsulation of newly developed self-healing agents. Different synthetic routes for the formation of core-shell structures, well known in literature, are applied and adapted to our targeted systems. Emulsification of the active agent into an immiscible phase is realized upon mechanical stirring and shell formation is typically performed by interfacial polymerization of two monomers present separately in one of the liquid phase, or by dispersion polycondensation of a precondensate onto the droplet surface.

In self-healing composites, for capsules to rupture in a reliable fashion, they must have an effective embedded modulus lower than that of the surrounding polymer matrix. Typical compositions used for the shell material are poly(urea-formaldehyde) (PUF), poly(melamine-formaldehyde) (PMF), poly(melamine-urea-formaldehyde) (PMUF), polyurethane (PU) and acrylates.

This study not only demonstrates the interdependency of many parameters controlling the encapsulation process such as pH, temperature, ionic strength, stirring speed, and in general the concentration of each component but also discusses the complexity of having a reactive core system, such as multi-thiols. Moreover, new encapsulation strategies for the encapsulation of reactive ingredients, beyond the classical approaches, will be discussed.

REFERENCES

[1] R.F.A. Teixeira, X.K.D. Hillewaere, S. Billiet, F.E. Du Prez, to be published in: W.H. Binder (Ed.), *Self-Healing Polymers*, Wiley & Sons Inc., New-York, 2013.

A GENERIC METHODOLOGY TO STUDY SELF-HEALING PROPERTIES OF THERMO-REVERSIBLE POLYMER NETWORKS

B. Van Mele¹, G. Scheltjens¹, M. M. Diaz¹, J. Brancart¹ and G. Van Assche¹

¹ *Research Unit of Physical Chemistry and Polymer Science (FYSC), Vrije Universiteit Brussel, Pleinlaan 2, 1050 Brussels, Belgium – e-mail: bvmele@vub.ac.be, gscheltj@vub.ac.be, Maria.Diaz.Acevedo@vub.ac.be, jbrancar@vub.ac.be, gvassche@vub.ac.be.*

Keywords: Diels-Alder, kinetics, equilibrium, polymer network, gel point

ABSTRACT

Based on the reversible Diels-Alder (DA) reaction between furan and maleimide functional groups, an extrinsic self-healing material was synthesized for coating applications [1]. At elevated temperatures, the DA/retro-DA equilibrium is shifted towards the initial building blocks. This shift in equilibrium allows a temporary increase in local mobility, which is essential to seal damage. The recovery of initial properties takes place in a subsequent cooling by recombination of covalent bonds through the exothermic DA reaction.

Changing the spacer length in the furan functionalized compound leads to a flexible network design and tailor-made network properties with a variable cross-link density and glass transition temperature [1]. Based on these systems, a generic methodology was developed to study the self-healing properties of thermo-reversible networks.

The effect of temperature on kinetics and equilibrium of the reversible DA/retro-DA reaction, and also the effect of diffusion-control was measured (and modeled) by means of Fourier transform infrared spectroscopy, microcalorimetry and Modulated DSC. Both elastomeric and thermosetting reversible networks were investigated.

A maximum sealing temperature was determined to avoid unwanted side-reactions. In case of the DA networks studied, an irreversible homopolymerization of maleimide functional groups occurs above 120 °C. The flow behavior at elevated temperatures was characterized by dynamic rheometry in order to determine the gelation temperature (T_{gel}) of the reversible networks. It was shown that sealing of microscopic scratches is possible below T_{gel} , leading to the advantage for coatings that sufficient mechanical properties remain guaranteed during a thermal sealing/healing procedure. At low temperatures, the exothermic DA reaction was characterized by microcalorimetry and Modulated DSC proving the healing capacity of the networks and showing the repeatability of sealing/healing cycles in an acceptable temperature window. The mechanical properties in this temperature window were studied with dynamic mechanical analysis.

REFERENCES

[1] G. Scheltjens, M.M. Diaz, J. Brancart, G. Van Assche, B. Van Mele, A Self-healing Polymer Network Based on Reversible Covalent Bonding, Reactive and Functional Polymers (2012) available online.

CAPSULE-BASED SELF-HEALING EPOXY SYSTEMS USING DIELS-ALDER REACTIONS

G.R. Palmese¹, P.A. Pratama¹, A.M. Peterson¹ and M. Sharifi¹

¹ Department of Chemical and Biological Engineering, Drexel University, Philadelphia, PA 19104, USA – e-mail: palmese@coe.drexel.edu

Keywords: epoxy, Diels-Alder, solvent, capsule, self-healing

ABSTRACT

We present recent results on the use of Diels-Alder reversible reactions for the design of self-healing polymer systems. Previous work has shown that solutions of maleimide functional monomers can be used to heal cracks of furan functionalized epoxy networks. Two topics will be discussed. First, the results of an investigation regarding the influence of solvent selection and maleimide type as well as concentration on healing efficiency, and second, our progress encapsulating solutions containing maleimide-based healing agents to create capsule-based self-healing systems that rely on Diels-Alder chemistry.

The effects of maleimide healing agent structure, concentration, and solvent type on the effectiveness of solution-based healing agents for a furan-functionalized epoxy-amine thermoset were investigated. These factors were found to influence healing behavior by affecting two mechanisms: (1) Diels-Alder bonding across the crack surfaces and (2) mechanical interlocking promoted by solvent-induced swelling. Aliphatic and aromatic maleimides with varying functionality were studied. The solvents evaluated were toluene, dimethyl formamide (DMF), and phenyl acetate. The maleimide healing agent structure and concentration were found to affect the degree of Diels-Alder interfacial bonding, while solvent selection was found to influence both healing mechanisms.

A urea-formaldehyde (UF) encapsulation technique was used to encapsulate phenyl acetate – maleimide solutions. The resulting capsules were found to be thermally stable up to 90°C. It was not possible to encapsulate DMF solutions, and solutions using toluene resulted in low capsule yield. Phenyl acetate – maleimide capsules were incorporated into a furan functional epoxy creating a material system that heals autonomously. Compact tension specimens prepared with 10 wt.% capsules showed 75% strength recovery 24 hours after first fracture at ambient temperature. This compares favorably with the direct injection of healing solution into the crack. The new capsule healing system based on Diels-Alder chemistry also provides the opportunity for repeated healing cycles.

SESSION 28 – ADVANCED CHARACTERIZATION METHODS FOR SELF-HEALING

ASSESSMENT OF SELF-HEALING CAPABILITIES, A ROUTE TOWARDS STANDARDIZATION

S. S. Lucas¹, A. Nellesen¹ and M. v. Tapavicza¹

¹ Fraunhofer Institute for Environmental, Safety and Energy Technology UMSICHT, Osterfelder Straße 3, 46047 Oberhausen, Germany, – e-mail: sandra.lucas@umsicht.fraunhofer.de; anke.nellesen@umsicht.fraunhofer.de; max.von-tapavicza@umsicht.fraunhofer.de

Keywords: self-healing, quantification, polymers, composites, testing

ABSTRACT

In the last decade, an increasing attention has been given to the development of repairing capabilities in materials, with an emphasis in specific strategies that can promote self-healing, with or without external triggers. Self-healing has opened several new possibilities, especially in applications where long-term reliability is demanded and either maintenance or replace of these materials is difficult to perform.

Depending on the material class, different approaches in order to achieve self-healing, can be adopted. This led to distinct evaluation methods of the self-healing efficiency, depending on the material and its final use. One of the new challenges in self-repairing materials lays in the establishment of a common testing procedure for different materials classes, such as ceramics, concrete, polymers and composites. Normalized procedures can conduct to a standardization of the healing evaluation, which will set a common ground towards a better understanding of the concept and its quantification.

The assessment of self-healing capabilities is one of the major goals in the SHeMat project. SHeMat is a Training Network for Self-Healing Materials funded within the scope of the Seventh Framework Programme by the European Commission's Marie Curie programme. The focus of this work will be the development of a standard procedure and its applicability to the specific materials developed within the project. The comparative analysis of the results will act as a support to establish a common base for the definition of self-healing as a quantifiable characteristic. This discussion covers the work that has been conducted so far in the SHeMat project and possible future directions.

1. INTRODUCTION

The assessment of self-healing capabilities in materials depends not only of the specific type of material but also on the healing process by itself. Self-healing process can be divided into three different types depending on how the capability is developed: by physical or chemical interactions working autonomously or triggered by external stimulation. The strategy adopted to evaluate the self-healing capabilities must therefore consider the way that this property is developed. Healing can refer to a wide range of properties and can be evaluated considering the tensile strength, strength recovery or the fracture behaviour, among others. This assessment also depends on the repairing mechanism: if it is based on a microencapsulated healing

agent, an additive or if it is caused by an external stimulus (temperature, electrical or magnetic field) [1].

2. ASSESSMENT OF SELF-HEALING IN MATERIALS

2.1. MACROSCOPIC APPROACH

Several authors try to develop and adopt a standard quantification formula to assess self-healing capabilities, with the goal of setting a common ground that allow comparisons between different works. The evaluation of the stress–strain response under both quasi-static and high loading rate deformation conditions in polymers is fundamental to understand the deformation history of the material over the initial loading cycles. For quasi-static fracture conditions, healing efficiency is defined in terms of the recovery of fracture toughness. Healing evaluation starts with a virgin fracture test of an undamaged tapered double cantilever beam (TDCB, Figure 1). Prior to testing, a pre-crack was created with a fresh razor blade into the centre groove of the specimen. The damage is introduced to sharpen the crack-tip, while loading increased until the crack propagates along the centreline of the sample until failure. The crack is then closed and allowed to heal at room temperature (without any external intervention). After healing, the sample is loaded again until failure [2].

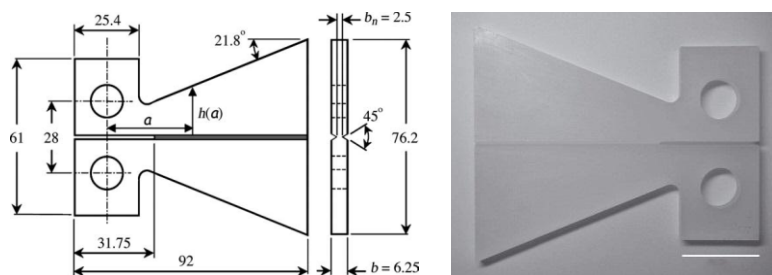


Figure 1: example of a TDCB sample.

Static fracture tests evaluate the changes in the crack growth and the absolute fatigue life of the healed material [3]. The fatigue response of the self-healing material is dependent of a wide number of factors, such as stress intensity, healing periods, among others. With this assessment method, it is possible to evaluate the recovery after the induced damage caused by cyclic loading [4]. The healing efficiency λ , can be determined by the correlation between the fatigue life-extension (Equation 1).

$$\lambda = \frac{N_{healed} - N_{control}}{N_{control}} \quad \text{Equation 1}$$

Where N_{healed} stands for the total number of cycles until the failure of the healed sample and $N_{control}$ the total number of cycles until the failure of a non-healed sample. For elastomeric self-healing material, the fracture toughness protocol with the TDCB-sample configuration may not be the most suitable model to evaluate the healing performance, since elastomers can fail through fracture and fatigue processes. [5]. Instead of evaluating the fracture toughness, it should be assessed the tear strength recovery. For this purpose, some authors developed a specific rectangular specimen (Figure 2).

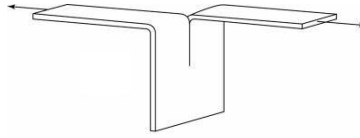


Figure 2: example of a rectangular sample.

Healing efficiency η , can be defined as the recovery of the tear strength of the healed sample (T_{healed}) compared to the non-damaged one (T_{virgin}), according to Equation 2.

$$\eta = \frac{T_{\text{healed}}}{T_{\text{virgin}}} \quad \text{Equation 2}$$

Depending on the material and the properties under evaluation, the technique and the self-healing quantification method change, becoming difficult to compare performances and establish standards.

The main challenge remained in the development of a suitable method to evaluate the healing efficiency. Until recently, the focus has been the macroscale evaluation of the healing properties, usually with a complete separation of the material during the tests. However, this is not enough to provide a comprehensive evaluation of what happen inside the material when the first microcracks start to develop. To achieve a quantitative evaluation for the relationship between the material structure and the self-healing properties of the system an extra emphasis on in situ microscopic measurements is essential.

2.2. MICRO AND NANOSCALE EVALUATION

One of the most important causes for material failure during service is the development of multiple microcracks. The propagation of these cracks lead to severe damage, the leading cause for loss of performance. Mechanical testing of materials with microindentation techniques has become widely accepted as a viable tool. It is even regulated recently, by international standards [6]. This technique can be easily applied to hard materials however, its application to softer materials need to be considered more carefully [7]. Instrument calibration, strain effects, and material heterogeneity are examples of possible complications that arise when small volumes of polymers are tested. However, with a proper setup planning it is possible to test these materials and obtain reliable data from this technique [8].



Figure 3: Equipment for microcutting, inside the UMSICHT ESEM (left) image of a healed cut, elastomer sample (right)

These data, when complemented with the macroscopic bulk methods, retrieve important information regarding the micro and nanoscale self-healing of polymers.

The analysis of the damaged surface morphology can provide essential information concerning the evolution of the healing reaction and crack propagation. This analysis can be performed with an environmental scanning electron microscope (ESEM) (Figure 3). The self-healing process can be studied by inducing mechanical damage through micromachining, followed by imaging of the repair process.

This can be an important tool to produce and analyse the damage in a material surface. This technique as evolved in recent years, can now be used to characterize several mechanical properties (elastic modulus, flexural strength, compression, etc.).

3. CONCLUSIONS

The macroscale evaluation by itself is not sufficient to establish standard parameters for the self-healing quantification in materials. Using microscopic evaluation techniques it will be possible to relate the behaviour of a single static defect to the self-healing ability, rather than an evaluation by a collective behaviour of defects. One obstacle that has delayed the implementation of the microscopic self-healing evaluation concerns to the very small volume of the samples. Considering the nonhomogeneous composition of some materials, sampling can be challenging. The preliminary tests, conducted at Fraunhofer UMSICHT proved the viability of this technique, however further improvements need to be done, so that it can be accepted as a standard method.

Microindentation technique can be used in several different classes of materials to measure numerous materials properties. This can be a useful step towards the standardization of the self-healing quantification process. Establishing a standard is one key step for the industrialization of self-healing materials.

ACKNOWLEDGEMENTS

Financial support for this study from the European Commission, through the SHeMat project, Grant agreement n°: 290308, is gratefully acknowledged.

REFERENCES

- [1] B. Aïssa, D. Therriault, E. Haddad, W. Jamroz, Self-Healing Materials Systems: Overview of Major Approaches and Recent Developed Technologies, *Advances in Materials Science and Engineering* 2012 (2012) 1–17.
- [2] E.N. Brown, N.R. Sottos, S.R. White, Fracture testing of a self-healing polymer composite, *EXP MECH* 42 (2002) 372–379.
- [3] H. Jin, G.M. Miller, N.R. Sottos, S.R. White, Fracture and fatigue response of a self-healing epoxy adhesive, *Polymer* 52 (2011) 1628–1634.
- [4] D.Y. Wu, S. Meure, D. Solomon, Self-healing polymeric materials: A review of recent developments, *Progress in Polymer Science* 33 (2008) 479–522.
- [5] M. Keller; S.R White; N.R Sottos, *An Elastomeric Self-Healing Material* (2006).
- [6] D. Lucca, K. Herrmann, M. Klopstein, Nanoindentation: Measuring methods and applications, *CIRP Annals - Manufacturing Technology* 59 (2010) 803–819.
- [7] M.R. VanLandingham, J.S. Villarrubia, W.F. Guthrie, G.F. Meyers, Nanoindentation of polymers: an overview, *Macromol. Symp.* 167 (2001) 15–44.
- [8] Bruker Nano Surfaces, *Modern-Trends-in-Atomic-Force-Microscopy-of-Polymers* (2006).

INVESTIGATION OF THE FRACTURE CRACKING BEHAVIOR OF SELF-HEALING SYSTEMS BY USE OF OPTICAL AND ACOUSTIC EXPERIMENTAL METHODS

E. Tsangouri¹, K. Van Tittelboom², X. K. D. Hillewaere³, D. Van Hemelrijck¹
N. De Belie² and F. E. Du Prez³

¹ Department of Mechanics of Materials and Constructions, Faculty of Engineering Sciences, Vrije Universiteit Brussel, Pleinlaan 2, B-1050 Brussels, Belgium & SIM vzw - program SHE, Technologiepark 935, B - 9052 Zwijnaarde, Belgium – e-mail: etsangou@vub.ac.be; dvhemelr@vub.ac.be

² Magnel Laboratory for Concrete Research, Ghent University, Technologiepark-Zwijnaarde 904, 9052 Ghent, Belgium & SIM vzw - program SHE, Technologiepark 935, B - 9052 Zwijnaarde, Belgium – e-mail: kim.vantittelboom@ugent.be; nele.debelie@ugent.be & SIM program SHE vzw, Technologiepark 935, B - 9052 Zwijnaarde, Belgium

³ Department of Organic Chemistry, Polymer Chemistry Research Group, Ghent University, Krijgslaan 281 S4-bis, B-9000 Ghent, Belgium & SIM vzw - program SHE, Technologiepark 935, B - 9052 Zwijnaarde, Belgium – e-mail: xander.hillewaere@ugent.be; filip.duprez@ugent.be

Keywords: self-healing, mechanical characterization, Digital Image Correlation, Acoustic Emission, NDT methods, cracking deformations, fracture parameters

ABSTRACT

Nowadays the self-healing process efficiency in loaded structural materials is evaluated by studying the damage mechanisms. Based on fracture mechanics theories, the resistance to damage and the cracking recovery can be an indication of healing performance.

Experimentally, the cracking behavior is quantified by measuring the fracture energy of the material during cracking and the fracture process zone area at which the damage is expanded. In literature, damage detection at loading stage of testing and damage recovery due to healing mechanisms at the reloading stage is monitored by application of several experimental (Non-) Destructive Methods.

In this study, the Fracture Process Zone (FPZ) in different heterogeneous materials (polymer and cementitious composites) is visualized in strain and deformation (crack opening-close-reopening) profiles of the crack tip area by application of Digital Image Correlation (DIC) and the fracture energy released in different stages of cracking is quantified and located by Acoustic Emission (AE). The combination of the aforementioned optical and acoustic techniques can confirm the recovery of cracked specimens in which healing mechanisms are applied.

1. INTRODUCTION

Cracking phenomena in structural materials are liable for degradation of the mechanical properties in local areas and generally decrease of service life of the construction. Healing approach upgrading the mechanical response of these materials, pursues to reclose the cracked region and restrain damage. As a matter of fact, the supervision and evaluation of the healing response conforms to study the

cracking stages (loading- crack formation, curing- crack closure, reloading- crack re-opening differently due to healing) of an experimental configuration.

Two different experimental healing system arrangements are examined by the use of advanced optical and acoustic methods and a critical review of their potentials at healing efficiency evaluation is done. In more details, tubular capsules filled with healing agent are embedded into concrete beams and tested to form cracks under three and four point bending [2]. Additionally, manually injected healing agent is applied on polymer resin beams and tested under pin loading [1]. The response of both material systems under two stages of loading (loading- crack formation, reloading- crack reopening after healing) is monitored by Digital Image Correlation (DIC), Acoustic Emission (AE) and a microscope device.

2. METHODS OF TESTING

Digital Image Correlation is an optical deformation and strain measuring method well-established in fracture mechanics experiments in recent years. The DIC system consists of 2 cameras (-CCD) and a data acquisition system and requires a random speckle pattern attached to the material. A number of images are captured by cameras and via a digitizing board, the analog signal is converted into an integer gray level intensity value for each pixel of the image. The grey scale images of an object during loading are compared by image correlation software which calculates the displacement of regions in each image relatively to the reference image. Then, the strains are derived from the displacement gradients [3].

Acoustic Emission is an acoustic Non- Destructive technique applied to monitor the fracture process when samples undergo deformation. The AE system consists of sensors attached to the surface of the material, a pre-amplifier that receives the dynamic motion caused by an AE event and a display and analysis software that reports the AE characteristics and locates the AE events position at the tested specimen [4].

Microscope device is the crucial tool to visualize fracture surfaces and quantify crack opening and closure phenomena. The length, width and orientation of cracking and the volume of fracture process zone is scanned by Leica MZ 12₅ while a digital camera Leica DFC295 fixed to the microscope captured and stored the images.

Crack Mouth Opening Device calibrated to 10 mm width, and attached on the specimen at the two sides of the pre-crack groove measures accurately the crack opening of the crack for mode I of fracture (3 point bending and TDCB pin loading).

3. EXPERIMENTAL SET-UP

A series of six pre- notched concrete beams prepared, cured for 14 days, and tested and re-tested after 1 day of curing according to the RILEM TC 50-FMC protocol in order to determinate the fracture characteristics during cracking. CMOD device is attached at the two sides of the notch groove to measure the crack opening during the two stages of loading. DIC cameras watching one of the side surfaces of the beam are visualizing the displacement and strain profiles around the pre- crack notch and across the height of the beam. A group of eight AE sensors are attached to the surfaces of the beam surrounding the pre-crack region and monitor the AE activity.

Another series of six concrete beams, are reinforced by two steel bars, prepared, cured for 14 days, and tested under four point bending to determinate the healing response in the case of multiple cracking fracture. DIC cameras watching

perpendicular the side of the beam visualize the profiles of deformations as described above and AE sensors, on a configuration similar to the of the previous tests, monitor fracture events during the two stages of loading (loading- curing 1 day- reloading). Finally, pin loading applied on TDCB resin samples, prepared following White's protocol and tested under displacement control evaluate the healing efficiency, by measuring during testing the load response, the mode I crack opening by the use of CMOD attached to the edge of clampers of the specimen, and the strain concentration around the crack tip indicated by area of increased strain at the DIC profiles. The varied maximum load, crack opening and mode of crack fracture are analyzed at loading (formation and propagation of crack) and reloading stage (reopen of the sample after 5 days of curing).

4. RESULTS

The figures that follow present the different testing set-ups and the analysis obtained by the use of DIC, AE and microscope for unreinforced concrete beams, reinforced concrete beams and resin polymer beams respectively. It is proved that the characterization of the healing efficiency of embedded healing agent into concrete systems can be done only if tests of notched beams under three point bending are combined with tests on beams with more realistic cracking formation under four point bending. Furthermore, the loading response of TDCB specimens can be critically reviewed by visualizing the strain profiles during testing in order to correlate the final mechanical behavior with the fracture mode of the cracking. In any case, the combination of an optical and acoustic advanced technique forms a powerful, accurate and promising experimental set-up that can fully characterize the healing efficiency of encapsulated healing systems.

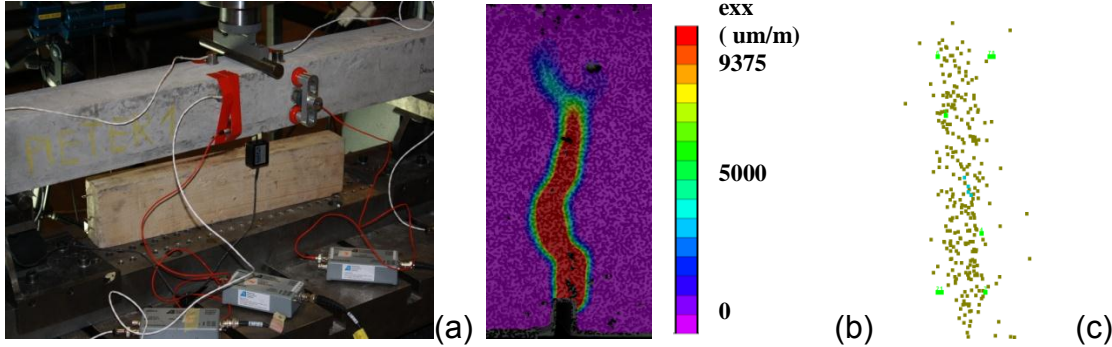


Figure 1: (a) experimental set-up of 3-point bending test, (b) fracture process around cracking visualized by DIC, (c) AE events of crack formation and capsule breakage.

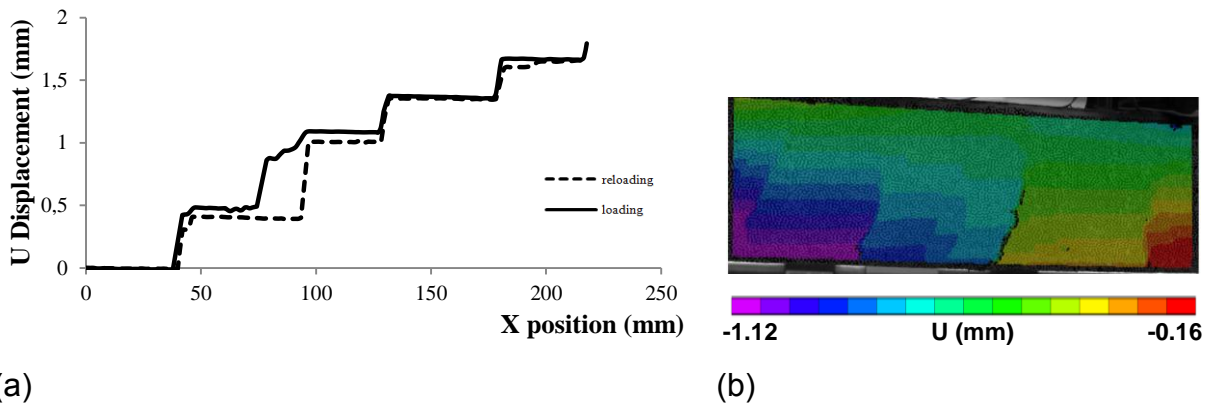


Figure 2: (a) Crack opening of beams tested under 4- point bending at loading and reloading stage in which crack healing is observed, (b) profiles of deformation measuring crack opening.

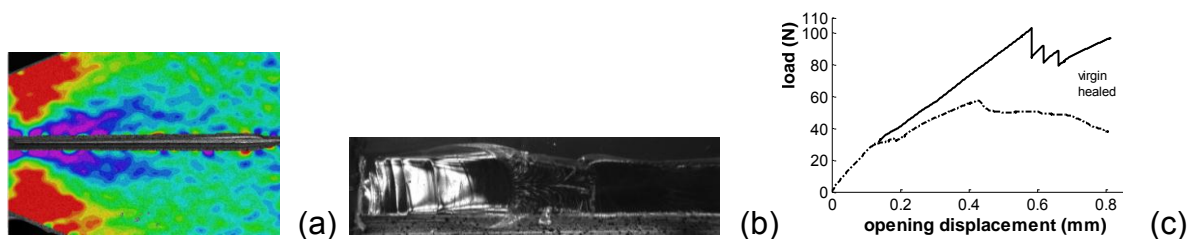


Figure 3: (a) TDCB strain profile pointing out the tip of cracking during propagation, (b) Microscope view of the side groove indicating thickness increase anomalies, (c) loading response of TDCB specimen in case of manually healed systems.

ACKNOWLEDGEMENTS

Financial support from the SIM research program (Strategic Initiative Materials) for this study is gratefully acknowledged.

REFERENCES

- [1] S. Billiet, W. Van Camp, X. Hillewaere, H. Rahier, F. Du Prez, Development of optimized autonomous self-healing systems for epoxy materials based on maleimide chemistry, *Polymer* 53 (2012) 2320- 2326
- [2] K. Van Tittelboom, N. De Belie, D. Van Loo, and P. Jacobs, Self-healing efficiency of cementitious materials containing tubular capsules filled with healing agent, *Cement and Concrete Composites* 33 (2011) 497-505, 2011
- [3] M.A. Sutton, J. Ortu, H.W. Schreier, *Image Correlation for Shape, Motion and Deformation Measurements* (2009) USA
- [4] D. Soulioti, N.M. Barkoula, N.M. Barkoula, A. Paipetis, T.E. Matikas, T. Shiotani, D.G. Aggelis, Acoustic emission behavior of steel fibre reinforced concrete under bending, *Construction and Building Materials* (2009) 23 3532–3536

MICROSTRUCTURE EVOLUTION OF Cr₂AlC CERAMIC BEFORE AND AFTER OXIDATION INDUCED CRACK HEALING

J. Rao¹, D. Jia¹, X. Duan¹, Z. Yang¹, Y. Zhou¹, J. Ouyang¹, W.G. Sloof² and S. van der Zwaag³

¹ Institute for Advanced Ceramics, Harbin Institute of Technology, Harbin, 150001, China – e-mail: jrcrao@hit.edu.cn

² Department of Material Science and Engineering, Delft University of Technology, Mekelweg 2, 2628 CD Delft, The Netherlands – e-mail: W.G.Sloof@tudelft.nl

³ Novel Aerospace Materials, Delft University of Technology, Kluyverweg 1, 2629 HS Delft, The Netherlands – e-mail: S.vanderZwaag@tudelft.nl

Keywords: Cr₂AlC ceramic, self-healing, SEM, TEM

ABSTRACT

Ternary Cr₂AlC composites have good properties like other MAX phases, such as high temperature strength, oxidation and corrosion resistance, good electrical and thermal conductivity, and machinability. In present work, Cr₂AlC ceramic is produced by reactive hot-press sintering with the starting materials of chromium, aluminium and graphite powders. Crack damage was induced with a Knoop indenter in three point bending samples. The pre-cracked specimens were healed at 1100 °C in air for various times. XRD, SEM, TEM as well as SAD, EDS, HAADF techniques were used to characterize the phase constitution and microstructure evolution of Cr₂AlC ceramic before and after oxidation induced crack healing. The mechanism of atom diffusion and crack healing effect in Cr₂AlC will be uncovered through intensive study of the oxidation of aluminium and chromium.

UNRAVELLING THE CORROSION PROTECTION MECHANISM OF SILYL ESTER BY COMBINED ELECTROCHEMISTRY AND X-RAY COMPUTED TOMOGRAPHY

S.J. Garcia¹, X. Wu¹

¹ Novel Aerospace Materials Group, Faculty of Aerospace Engineering, Delft University of Technology, Kluyverweg 1, 2629 HS, Delft, The Netherlands – e-mail: S.J.GarciaEspallargas@tudelft.nl ; Xiaomin.Wu@tudelft.nl

Keywords: silyl ester, delamination, coating, x-ray tomography, impedance

ABSTRACT

Recently, encapsulated silyl esters have been shown to act as efficient healing agents for self-healing anticorrosive coatings. While the positive protective effects were irrefutable, the actual protection mechanism has not been clarified yet. In this study, x-ray computed μ -tomography and electrochemical impedance spectroscopy have been employed to unravel the protection mechanisms for a coated AA7050 aluminium alloy.

The results show that the employed silyl ester protects the damaged coating-metal system by delaying the delamination initiation and growth kinetics while at the same time decreasing the underfilm pit area growth. The study also shows the potential of x-ray computed μ -tomography to follow the delamination front line and underfilm pits in coated metallic samples. The combination with EIS led to a major understanding of both EIS plots and the protection mechanisms offered by the silyl ester used.

1. INTRODUCTION

In the search of ideal self-healing systems using the microencapsulation route for corrosion protection, efforts have been recently put into the design of healing agents that do not require reacting with a second agent present in the coating matrix (i.e. second capsule or catalyst) but rather with species available in the environment (e.g. O₂, H₂O) [1]. In this direction previous studies have proposed the use of oils [2], silanes [3, 4] and silyl esters [5, 6]. In particular, the silyl ester concept, independently of the first chemistry used and published, involves a multifunctional action concept based on wetting, adhesion, hydrophobicity, reaction with humidity and metal surface, and time-dependent densification. At the same time, the oil linked to the silane group protects the silane from early reaction in the capsule proposing thus a multi-action agent. The first results with an encapsulated silyl ester showed by means of general [5] and local electrochemical techniques [6] long time corrosion protection of coated AA2024-T3 under immersion in mild NaCl solutions. In these previous studies, it was suggested that the main corrosion protection mechanism was due to the partial restoration of the barrier protection at a hand-made scratch.

In this study we combined two non-destructive techniques (x-ray computed micro-tomography and electrochemical impedance spectroscopy) to try to unravel the corrosion protection mechanism of silyl esters for high strength aluminium alloys. X-ray tomography was capable of quantifying underfilm corrosion processes (i.e. pit and delamination growth) supporting the impedance results.

2. MATERIALS

Hollow square tubes with rounded corners were machined from a hot rolled AA7050-T74. The tubes were 30mm long with an outer surface of 5×5mm² at cross section and 6mm diameter rounded corners. The inner diameter of the tube was 4mm. The tubes were abraded with Scotch Brite-3M “Clean N Finish grade A-VFN” followed by alkaline pretreatment in 2M NaOH for 10 seconds, rinsing with water and drying with pressurized air. The tubes were then dip-coated in an epoxy-amine bath to form a homogeneous coating, and allowed to cure at room temperature for one day followed by a 2h post-curing at 80°C. The dry thickness of the coatings was 100±10µm. After curing, a controlled 10mm long scratch was performed on one of the flat outer surfaces of each sample (Figure 1 schematically shows the longitudinal view and cross-section of the tubes).

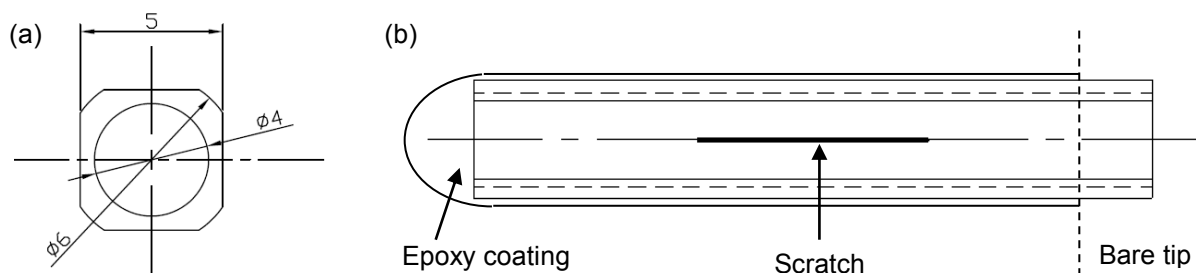


Figure 1: Cross-section of the square tube with round corners (a); longitudinal view of the coated and scratched tubes (b). Units in mm.

Prior to the start of the immersion tests, the scratch on one of the two samples was manually covered with liquid octyldimethylsilyloleate (silyl ester) synthesized as presented in [5]. The two samples (protected with silyl ester, and non-protected one) were then exposed overnight to ambient conditions before immersion and evaluation procedure started.

3. METHODS

The tube samples were exposed to a cycle of X-ray μ -tomography imaging + immersion in 0.05M NaCl distilled water solution + evaluation by electrochemical impedance spectroscopy. The procedure was repeated for 19 days combining thus two non-destructive techniques. For the micro tomography tests a Phoenix Nanotom S micro-CT scanner was employed using an X-ray radiation of 75kV and 90µÅ. Image reconstruction was performed using the Phoenix reconstruction software package. The electrochemical impedance spectroscopy tests (EIS) were performed using a potentiostat-galvanostat Autolab-PGSTAT302N with frequency response analyzer and traditional three electrode set-up was employed using Ag/AgCl, KCl (saturated) as the reference electrode, platinum gauze as the counter electrode and the coated squared tubes as the working electrodes.

4. RESULTS

Image analysis to obtain delamination area, surface pit area, and pits volume was completed using Volume Graphics Studio MAX 2.0. Two layers were taken for the analysis depending on the quantification of the delamination or the pit area formation. The layer for delamination analysis was placed (in the computing software) 25 μm above the estimated metal surface, while for the pit analysis the layer was placed 25 μm below the same metal surface. The position of these layers was selected based on the limit of detection of the device and image optimization. This approach disregards very superficial pits at initiation stage as well as pits that go into the material less than 25 μm , although it detects the general trend of corrosion (delamination and pits) of the metallic surface.

In Figure 2 it can be seen that there is a change in corrosion behaviour when adding the silyl ester to one of the scratched samples. The fitting of the delamination curves shows linear trends in both samples although with different slopes (delamination growth kinetics). It is clear from Figure 2 that the addition of silyl ester delays the delamination initiation time (from one day after immersion to 12 days) as well as restrains the delamination growth (three times slower growth kinetics when using silyl ester; from 0.92 to 0.34 mm^2/day). This result suggests that one of the most relevant mechanisms of protection offered by the silyl ester is by prevention and delay of delamination. Moreover the results also confirmed (not shown here) that the silyl ester delayed pit formation and underfilm pit growth kinetics significantly. The results were confirmed by the EIS tests.

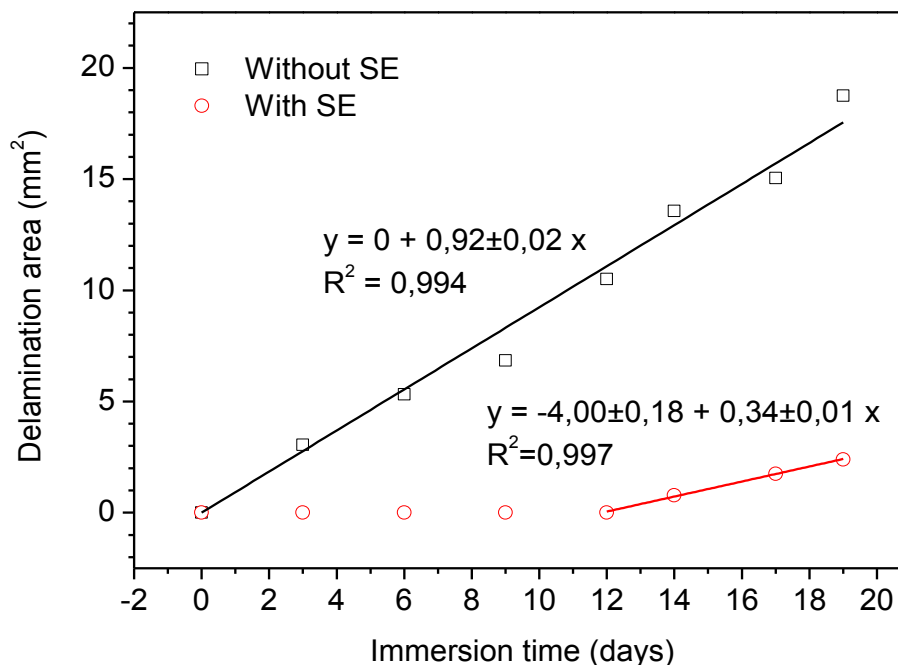


Figure 2: Evolution of delamination area with immersion time for non-protected (black-square) and protected with silyl ester (red circle). Plot includes regression.

5. CONCLUSIONS

This work highlights the potential of using combined tomography and electrochemical tools to gain major understanding of underfilm corrosion processes (pitting and delamination) and their inhibition. It is foreseen that the approach here employed will be of importance for the field of self-healing anticorrosive coatings and paints as more quantified information can be obtained from the approach here presented. Moreover, the combination of tomography and EIS allows also a direct link between the trend changes in EIS and corrosion phenomena such as pitting and delamination. The results confirmed that the silyl ester reduced delamination initiation and growth kinetics while decreasing underfilm pit area growth. Pit area growth followed different kinetics for the protected with silyl ester and the non-protected sample. These results confirm the potential use of silyl esters and related chemistries to reduce general degradation by a combined effect of barrier and coating-metal interface restoration.

REFERENCES

- [1] S.J. Garcia, H.R. Fischer, S. van der Zwaag, A critical appraisal of the potential of self-healing polymeric coatings, *Progress in Organic Coatings*, 72 (2011) 211-221.
- [2] A. Kumar, L.D. Stephenson, J.N. Murray, Self-healing coatings for steel, *Progress in Organic Coatings*, 55 (2006) 244.
- [3] M. Wiesener, R. Regenspürger, M. Pilz, D. Shchukin, A. Latnikova, J. Yang, G. Grundmeier, In-situ contact angle studies of the release of water displacing agents from capsule filled organic coatings, *Surface & Coatings Technology*, 206 (2012) 4481.
- [4] M. Huang, H. Zhang, J. Yang, Synthesis of organic silane microcapsules for self-healing corrosion resistant polymer coatings, *Corrosion Science*, 65 (2012) 561.
- [5] S.J. García, H.R. Fischer, P.A. White, J. Mardel, Y. González-García, J.M.C. Mol, A.E. Hughes, Self-healing anticorrosive organic coating based on an encapsulated water reactive Silyl Ester: synthesis and proof of concept, *Progress in Organic Coatings*, 70 (2011) 142-149.
- [6] Y. González-García, S.J. García, A.E. Hughes, J.M.C. Mol, A combined redox-competition and negative-feedback SECM study of self-healing anticorrosive coatings, *Electrochemistry Communications*, 13 (2011) 1094–1097.

CHARACTERIZATION OF DISTRIBUTED DAMAGE AND SELF-HEALING IN CEMENTITIOUS MATERIALS BASED ON TIME-DEPENDENT 3-D X-RAY COMPUTED MICROTOMOGRAPHY (MICRO-CT)

S. Fan¹ and M. Li¹

¹*Department of Civil & Environmental Engineering, University of Houston, 4800 Calhoun Road, Houston, TX 77204 – e-mail: sfan@uh.edu; moli@uh.edu.*

Keywords: x-ray computed microtomography, nondestructive, damage, self-healing, engineered cementitious composites,

ABSTRACT

Concrete cracking is inevitable, and can be the result of one or a combination of factors such as dry shrinkage, thermal contraction, fatigue, and embedded steel corrosion. The presence of cracks leads to further deterioration, service life reduction of concrete infrastructure, and frequent maintenance and repairs. These challenges can be potentially addressed with innovative self-healing cementitious materials, which can autogenously regain material transport properties as well as mechanical characteristics after the damage self-healing process.

For the development of self-healing cementitious materials, it is crucial to precisely characterize the extent and quality of self-healing due to a variety of factors. X-ray computed microtomography (Micro-CT) was adopted in this study to derive three-dimensional tomographic data of micro-cracks before and after healing in engineered cementitious composite (ECC) materials. This method is a non-destructive visualizing technique that allows digitalization and monitoring of the interior characteristics of solid objects. ECC specimens were pre-damaged under bending to form multiple micro-cracks, and then exposed to wet-dry cycles to allow potential self-healing to occur. Micro-CT was then employed to build 3-D tomography models of the samples. The 3-D microcrack geometry, width and area were quantified. The extent of self-healing was then determined. The results were further combined with scanning electron microscopy (SEM) and energy-dispersive X-ray spectroscopy (EDX) to characterize crystalline and chemical properties of the self-healing products.

This study showed that Micro-CT is a suitable advanced technique to directly quantify self-healing potential in solid materials. The Micro-CT results revealed that self-healing extent of ECC is strongly influenced by crack width. For a bending crack with surface crack width of 30 μm , 55.3% of the crack volume was healed after 5 wet-dry cycles. For a bending crack with surface crack width of 100 μm , only 7% of the crack volume was healed after 5 wet-dry cycles. Hence, controlling microcrack width to under 30 μm is a necessary condition for achieving early, robust self-healing in ECC.

1. INTRODUCTION

Self-healing cementitious materials, which can autogenously recover transport properties as well as mechanical capacity after cracking, can greatly extend service life of civil infrastructure with minimum repairs. Engineered cementitious composites, or ECC, shows great potential of developing robust self-healing cementitious materials because of its unique and inherent cracking control capacity [1]. ECC

features a strain-hardening behavior accompanied by multiple micro-cracking, which is in contrast with the localized cracking or fracture in conventional concrete materials. As a result, the micro-crack width in ECC during strain-hardening is independent of steel reinforcement ratio, applied deformation and member geometry, offering one of the most important prerequisites for self-healing. Self-healing in ECC has been studied in terms of recovery of transport properties and tensile stress-strain relation under various environmental exposure conditions [2-5].

Self-healing characterization techniques for ECC and concrete materials include: water permeability and signal transmission tests to characterize transport properties, ultrasonic echoing and dynamic modulus measurement to characterize both transport and mechanical properties, as well as destructive tests such as bending, compressive, uniaxial tension and stiffness measurements. Additionally, analysis techniques of self-healing products include SEM and AEM (analytical electron microscopy) imaging, EDX and XRD (X-ray diffraction) chemical analysis, and nano-indentation. These methods have been effective to characterize self-healing in cementitious materials at the bulk composite material level, or to analyze self-healing products present at the sample surface. However, until now collecting full data on the 3-D microstructure of cementitious materials is still a difficult task. This paper focuses on the nondestructive and 3-D characterization of distributed damage and self-healing in ECC through Micro-CT. For the first time, the self-healing extent of 3-D bending cracks within ECC was directly and accurately quantified.

2. MATERIALS AND SPECIMEN PREPARATION

ECC specimens were prepared using the mixture proportion in Table 1. The fresh ECC mixture was cast into a series of coupon specimens with dimensions of $300 \times 76.2 \times 12.5$ mm. The specimens were covered with plastic sheets and cured in laboratory air with a temperature of $20 \pm 1^\circ\text{C}$ and relative humidity of $45\% \pm 5$. At the age of 45 days, the specimens were tested under four-point bending until failure. A number of microcracks with width ranging from 20 to $120\mu\text{m}$ were generated at the tensile side of the specimen. After unloading, the crack patterns of the specimens were examined under an optical microscope. Two $10 \times 10 \times 11$ mm cubic samples with different average crack width were selected and cut from the tensile side of coupon specimens. Sample A contains 4 similar-size microcracks with average surface crack width of $30\mu\text{m}$; Sample B contains 3 similar-size microcracks with average surface crack width of $100\mu\text{m}$. The two samples were then exposed to 5 wet-dry cycles to allow potential self-healing to occur. For each cycle, the samples were first submersed into water at 20°C for 24h, and then naturally dried in ambient air at $20 \pm 1^\circ\text{C}$ and $45\% \pm 5$ RH for 24h. Micro-CT was conducted on the samples before and after self-healing to build 3-D tomography models.

Table 1: ECC mixture proportion

Mix	W/(C+F)	Cement	Sand	Fly ash	Superplasticizer	Fiber
		Kg/m ³	Kg/m ³	Kg/m ³	Kg/m ³	Vol-%
ECC	0.21	461	370	1015	2.8	2

3. X-RAY COMPUTED MICROTOMOGRAPHY CHARACTERIZATION RESULTS

The principle of X-ray computed tomography is based on the 3D computed reconstruction of a sample from 2D projections acquired at different angles around its axis of rotation. Figure 1(a) shows one of the raw 2D images of sample B before self-healing, which was converted into binary images and then the final images of ROI (region of interest) after the air pores were removed. Figure 2 shows the 3D image of sample B after reconstruction that combines all the 2D images.

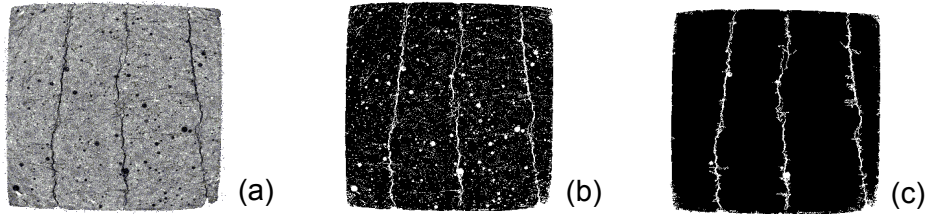


Figure 1: 2D images of slice 1652 for sample B before self-healing: (a) raw images built from tomography data set; (b) binary image; (c) final processed image of ROI

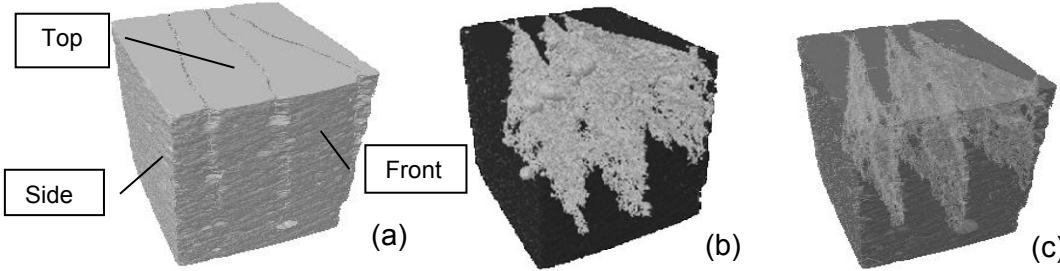


Figure 2: 3D images model for sample B: (a) original reconstructed 3D image before self-healing; (b) final processed image of ROI before self-healing ; (c) final processed image of ROI after self-healing

Sample A has an average surface crack width of 30 μ m; its average crack width along the crack depth is 15 μ m. After 5 water/air cycles the total crack volume decreased by 55.3%. Sample B has an average surface crack width of 100 μ m; its average crack width along the crack depth is 55 μ m. Only 7.5% of the total crack volume was healed, which is not as significant as sample A. Figure 3 shows the crack area and normalized crack width as a function of crack depth before and after self-healing. It was obvious that sample B, due to its larger initial crack width, has much less extent of self-healing. Figure 4 shows the extent of self-healing along the crack depth in two single microcracks in sample A.

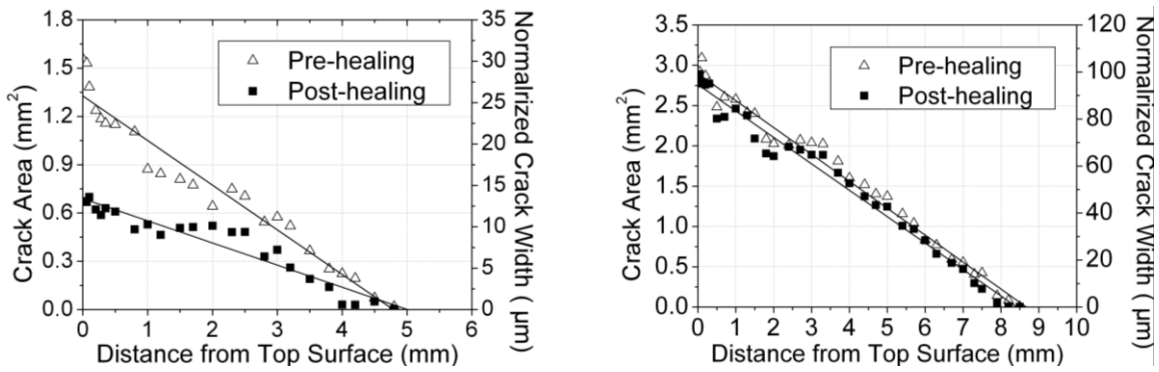


Figure 3: Self-healing extent of micro-cracks within sample A (left) and B (right)

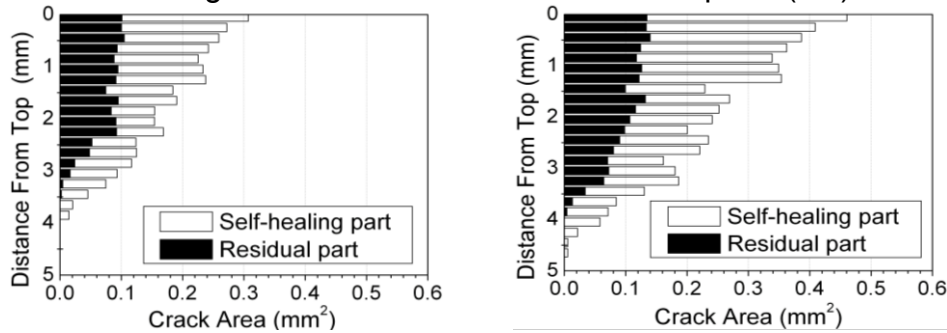


Figure 4: Crack area of sample A before and after self-healing: crack #1 (left); crack #2 (right)

4. CONCLUSIONS

Micro-CT is an effective non-destructive technique to directly characterize self-healing extent in three dimensions. This is extremely important when the cracks do not have a uniform geometry along their depth, such as bending cracks, so that self-healing characterization from the surface is not sufficient. Furthermore, compared to other techniques that provide bulk information of the self-healing extent, Micro-CT can offer direct measurement of each crack. Based on the Micro-CT results, we found that the extent of self-healing strongly depends on the initial crack width, which must be controlled to be very tight for achieving early and robust self-healing. Self-healing extent also depends on crack depth. The microcracks close to the surface tend to heal sooner because it takes time for water or carbon dioxide to transport through the micro-cracks to react with unhydrated cement or calcium hydrate to form self-healing products (i.e. C-S-H and calcium carbonate). The crystalline and chemical properties of the self-healing products were studied with SEM and EDS, and will be reported in a separate paper.

ACKNOWLEDGEMENTS

The authors gratefully acknowledge Dr. Roberto Fajardo and Dr. James Schmitz at the Micro-CT core facility at the University of Texas Health Science Center.

REFERENCES

- [1] V.C. Li, On engineered cementitious composites (ECC) — a review of the materials and its applications, *Journal of Advanced Concrete Technology*, 1, (2003) 215–230.
- [2] Y. Yang, M.D. Lepech, E. Yang and V.C. Li, Autogenous healing of engineered cementitious composites under wet-dry cycles, *Cement and Concrete Research*, 39, (2009) 382-390.
- [3] M. Li and V.C. Li, Cracking and healing of engineered cementitious composites under chloride environment, *ACI Materials Journal*, 108(3), (2011) 333-340.
- [4] L.L. Kan, H.S. Shi, A.R. Sakulich and V.C. Li, Self-healing characterization of engineered cementitious composite materials, *ACI Materials Journal*, 107(6), (2010) 617-624.
- [5] E.N. Herbert and V.C. Li, "Self-healing of engineered cementitious composites in the natural environment", in *Proc., Sixth Int'l Workshop on High Performance Fiber Reinforced Cement Composites (HPFRCC6)*, 2011, pp. 148-155.